

CONTRACT REPORT NO. AJA-6424

STUDY OF  
SHOCK ISOLATION FOR HARDENED STRUCTURES

Contract Number DA-49-129-ENG-532

June 17, 1966

Prepared for  
The Office of the Chief of Engineers  
Washington, D. C.

By

Agbabian-Jacobsen Associates  
8939 South Sepulveda Boulevard  
Los Angeles, California 90045



ERRATA in Study of Shock Isolation for Hardened Structures.

- Page 69 - In Figure 3.13 change shock radius scale  $r_p$   
to span from  $10^{-2}$  to  $10^3$
- Page 97 - In equation (3.19) delete  $(\times 10^{-3})$
- Page 99 - Delete  $(\times 10^{-3})$ , change  $a_{hz}$  to  $a_{vz}$
- Page 293 - Equality sign missing in last expression
- Page 328 - Parenthesis missing under root sign of equation (5.42)
- Page 688 - Figure E-3, parenthesis missing in expression for  $k'$ .



## FOREWORD

This is the final report to the Office of the Chief of Engineers, Department of the Army, under Contract DA-49-129-ENG-532. The purpose of this study was to prepare a comprehensive report on the design of shock isolation systems for hardened structures to be used by engineers engaged in the planning and design of installations required to resist the effects of nuclear weapons. The engineering approach to the preparation of definitive designs and to the evaluation of requirements for shock isolation systems is adopted.

Methods and procedures available in reports on government sponsored research and in the generally available engineering literature have been used freely; in addition, the recommended design procedures, in compliance with the contract Work Statement, have been developed in sufficient detail so that this report may be used without extensive reference to other sources.

This report is the result of the work of the engineering staff of Agbabian-Jacobsen Associates. John Karagozian acted as Project Engineer.

The principal authors of the report are:

L. S. Jacobsen  
M. S. Agbabian  
John Karagozian  
J. A. Malthan  
D. W. Bareis  
R. J. Brandt

Major contributions to the work were also made by R. D. Ewing and C. F. Bagge. The entire final manuscript was typed by Mrs. Grayce Jones.

Acknowledgment is made to the engineering staff of the Office of the Chief of Engineers, notably to Mr. Norman G. Hansen, technical monitor, for his advice and assistance, and to Messrs. G. Crowe and J. Healy for their very thorough review of the manuscript and numerous excellent suggestions.



## ABSTRACT

The design of shock isolation systems for equipment and personnel platforms within aboveground and underground hardened structures is explained in this report by the use of both the shock spectra and the velocity pulse techniques. Ground motions are explained and their pertinent quantities are defined; the effect of the structure supporting the shock isolation system is considered; and methods are presented to obtain the response of practical isolation systems. Design procedures are outlined with frequent use of numerical examples; and tolerance levels are summarized, so that the calculated responses of designed systems may remain within acceptable limits. The report also gives a descriptive account of almost all the major shock isolation systems that have been installed at various military facilities.

## PUBLICATION REVIEW

This report has been reviewed and is approved.





## CONTENTS

	<u>Page</u>
SECTION 1. INTRODUCTION	1
1.1 Scope	1
1.2 Objective	1
1.3 General Requirements and Procedures	2
SECTION 2. ELEMENTARY CONCEPTS OF SHOCK ISOLATION	6
2.1 Introduction	6
2.2 Single-Mass-One-Degree-of-Freedom Undamped System	8
2.3 Two-Mass Systems	12
2.4 Shock-Spectra Envelope	18
2.5 Relationship of Simple Pulses to Shock Spectra	32
2.6 Response Analysis Using a Waveform as the Input	38
2.7 Texts on Principals of Shock Isolation	44
SECTION 3. GROUND MOTIONS	45
3.1 Introduction	45
3.2 Times of Arrival of Ground Disturbances	47
3.3 Blast Wave Travel Time	66
3.4 Generation of Seismic Waves by a "Moving Line" Load on the Surface of an Elastic Half Space	73
3.5 Ground Motion Quantities	81
3.6 Waveforms to Describe Ground Motions	110
3.7 Ground Motions in Terms of Shock Spectra	140

CONTENTS (continued)

SECTION 4.. STRUCTURAL ENCLOSURES	156
4.1 Introduction	156
4.2 Aboveground Structures	158
4.3 Partially Buried Structures	230
4.4 Shallow Buried Structures	234
4.5 Deep Buried Cavity Liners	244
SECTION 5. SHOCK ISOLATION SYSTEMS	249
5.1 Introduction	249
5.2 Symmetrical Spring Systems	250
5.3 Near Symmetrical Systems	277
5.4 Base Mounted Spring Mass Systems	288
5.5 The Symmetrical Pendulum Systems	300
5.6 High C. G. Pendulum System	323
5.7 Low C. G. Pendulum System	331
5.8 Effect of Damping	352
5.9 Hard Mounted Systems	363
5.10 Arrangement of Springs	374
5.11 Component Isolation Versus Platform Isolation	378
SECTION 6. SPRINGS	380
6.1 Introduction	380
6.2 Mechanical Springs	381
6.3 Pneumatic Springs	450
6.4 Liquid Springs	464





## SECTION 1: INTRODUCTION

### 1.1 Scope

The purpose of this report is to provide design and analysis procedures for shock isolation systems placed inside hardened structures. The procedures are intended for the use of engineers in the planning, design and analysis of installations to resist the effects of nuclear weapons.

The need and requirements for shock isolation systems can be defined and definitive designs for such systems can be prepared through well-outlined procedures based on principles of engineering mechanics, experimental data, and methods of translating engineering analyses into the practical design of isolation systems. Theoretical considerations based on research and the available data from nuclear and non-nuclear tests will therefore serve as the starting point for developing design procedures. Many approximations and simplifications, however, will be made in order to move out of the domain of research and to achieve the main purpose of the report - the development of procedures by which engineering decisions can be made within the degree of accuracy required for the design of shock isolation systems for hardened structures. The scope of this report will be governed by this consideration.

For the use of this report as a design guide, the reader is expected to have a basic background in engineering mechanics and some knowledge of the fundamentals of nuclear weapon effects and protective construction. For those who do not have this background the report will be useful by providing data and procedures that give the bases for evaluating the scope and effort involved in design of shock isolation systems in protective structures.

### 1.2 Objective

An introductory treatment of the subject of shock isolation must consider four distinct and interacting factors: air blast effects, ground motion effects, dynamic response, and damage levels of equipment and personnel.

The objective of this report is to discuss these factors and to develop methods of design and analysis for shock isolation systems in hardened structures.

### 1.3 General Requirements and Procedures

Equipment and personnel within a protective structure may experience a severe shock resulting from the sudden motion of the structure. Failure of equipment and injury to personnel may occur even though the structure will maintain its integrity under the applied loads. The loads to be considered are those resulting from the explosion of nuclear weapons and they may be due to direct air blast impingement on the structure or to induced ground motions.

If the equipment is "hard-mounted" (i.e., attached directly to the structure), it must be ruggedly constructed. Equipment which does not have the required ruggedness should be "soft-mounted", i.e., supported by shock isolation devices which allow the structure to move relative to the equipment and which transmit accelerations much smaller than those the structure receives. Shock isolation thus involves the protection of equipment by isolators interposed between it and the supporting structure.

Personnel housed inside a protective structure must be protected from injury due to the shock motion of the structure. Impact injury may result from loss of balance even at low shock levels. Therefore, a shock isolated platform may be required for adequate protection of personnel when the structure is subjected to nuclear weapon effects.

Shock isolation systems in hardened facilities may be grouped somewhat generally into four classes as follows:

- a. To support entire multi-floor structures often used to house personnel and equipment
- b. To support floors or platforms within structures
- c. To support missiles in their launching structure, either in the launching position or in a position from which they are elevated to the launching position
- d. To support various individual items of equipment.

Mechanical devices for shock isolation consist of helical springs, pendulums, beams, pneumatic and liquid springs, alone or in combination, depending on specific requirements.

All input motions to shock isolated systems are associated with motions of their supports. The support motions depend on numerous factors:

- a. Motion characteristics of the structural element which constitutes the "support"
- b. Magnitude of weapon yield
- c. Type of burst (air, surface, buried)
- d. Distance of structure from ground zero
- e. Depth of structure below ground surface
- f. Seismic properties of ground
- g. Interaction of ground with structure
- h. Interaction of blast wave and structure in structures exposed directly to blast wave.

A consideration of all the above factors in determining the motion of the supports of a shock isolated system is necessary, but it is seldom achieved in a direct manner. Ordinarily the structural configuration and properties are known and the weapon yield and the distance or the overpressure are specified. The magnitude of the yield determines the duration of the blast wave and the ground motion characteristics. The influence of the factors f and g often must be estimated or inferred from field tests or from simplified soil dynamics calculations.

The general procedure in developing a shock isolation system is outlined in the following steps.

As a first step, for below ground structures the characteristics of the soil or rock environment and the ground motions corresponding to nuclear attack conditions of interest must be known. For above ground structures the interaction of the air blast with the exposed structure results in a complex loading profile that must be calculated. In the usual case, the engineer starts with a knowledge of the yield of the nuclear weapon, the distance of the structure from the weapon or the design overpressure, the physical characteristics of the soil or rock and a conceptual design of the structure. All parameters of interest such as air blast pressure-time

histories and soil displacements, velocities, and accelerations, must be estimated. These parameters are referred to in the literature as the free-field environment. ("Free-field" in general refers to the air medium as well as to the ground.)

The second step is to evaluate the influence of the structure that is interposed between the free-field and the equipment or personnel to be protected.

In the third step the survival requirements of the equipment and personnel must be defined - the degree of structural damage that may be tolerated; the tolerance on performance degradation; the possible need for the equipment to continue to perform during the attack period, or the period during which its service may be interrupted. These operational conditions must then be translated into parameters that define the response characteristics in terms of the physical behavior of an isolation system under shock - a tolerance limit on peak accelerations at well-defined natural frequencies, and maximum relative displacements between the structure and the isolated equipment or platform.

The fourth step is to obtain the dynamic response of the isolation system to motions of the structure. Occasionally steps one, two and four must be combined, because the interaction among the free-field, the structure, and isolation system cannot be readily defined and the analysis must consider the situation as a total system.

The fifth step is a comparison of the results of the fourth step with the tolerance limits set forth in the third step. The design is, of course, revised until the prescribed conditions are met.

There is a sixth step that is most desirable but often ends up as a compromise - experimental verification of the design under nuclear attack or under conditions simulating the combined environment of ground shock and air blast induced motions. A compromise is necessary in the simulation of the various parameters because seismic disturbances in a given soil for a given weapon yield, the effect of soil-structure interaction, and, for above ground structures, air blast-structure interaction can seldom be simulated in a satisfactory manner.



Finally, it is very important to introduce into the design the ability of the system to survive within a range of input values in the vicinity of the parameters that are accepted as criteria. Survival within a range of input values is necessary because of many uncertainties in input, response and tolerance. The specific reasons will become evident in the sections of the report covering these topics.

## SECTION 2: ELEMENTARY CONCEPTS OF SHOCK ISOLATION

### 2.1 Introduction

Design procedures for shock isolation systems are based on basic concepts that use simple mathematical models from which the dynamic response characteristics of the system are obtained. In this section a brief introduction is given to the method of representing by a mathematical model an internal system attached to the protective structure, depicting the system in terms of characteristics that are susceptible to mathematical analysis. Another model, defining a simple relationship between the structure and the internal system, is devised by assuming that each unit can be lumped into a single mass allowing the structure-equipment interaction to be treated as a two-mass problem.

These simple concepts will introduce the basic mathematical relationships from which may be developed two powerful techniques for analysis - the shock spectra technique and the dynamic analysis for ground motions expressed in terms of a time-dependent function. The techniques in this section will be used when applying input motions (given in Section 3) to problems ranging from very simple to complex shock isolation systems (given in Section 5) mounted in various types of structures (given in Section 4).

Figure 2.1a shows an equipment supported on a slab or beam inside a structure. When the structure is subjected to shock in the vertical direction, the slab tends to deflect as indicated by the dotted line. A mathematical model such as shown in Figure 2.1b describes the equipment and the flexible slab as a two-mass system subjected to an input at the support points of the slab. The equipment may or may not be supported on isolator springs. If it is mounted directly to the slab,  $k_2$  and  $c_2$  represent the stiffness and damping characteristics of the equipment mount consisting usually of bolts and structural elements. If isolators are used, the simple model makes  $k_2$  and  $c_2$  characteristics of the isolator device.

For a shock applied in the horizontal direction, the slab may be assumed to be rigid, and the mathematical model of Figure 2.1c would be

a reasonably accurate model for computing equipment response, the shock being applied directly at the base of the equipment due to rigid body motion of the slab and the enclosing structure. If the slab of Figure 2.1a happens to be the roof of an aboveground structure and the equipment is mounted to the ceiling, the relatively flexible support of the equipment will be subjected to the direct effect of air blast forces, and the equipment response will depend both on the slab deformations due to rigid body motion of the structure and to slab responses due to air blast forces applied directly to the roof slab.

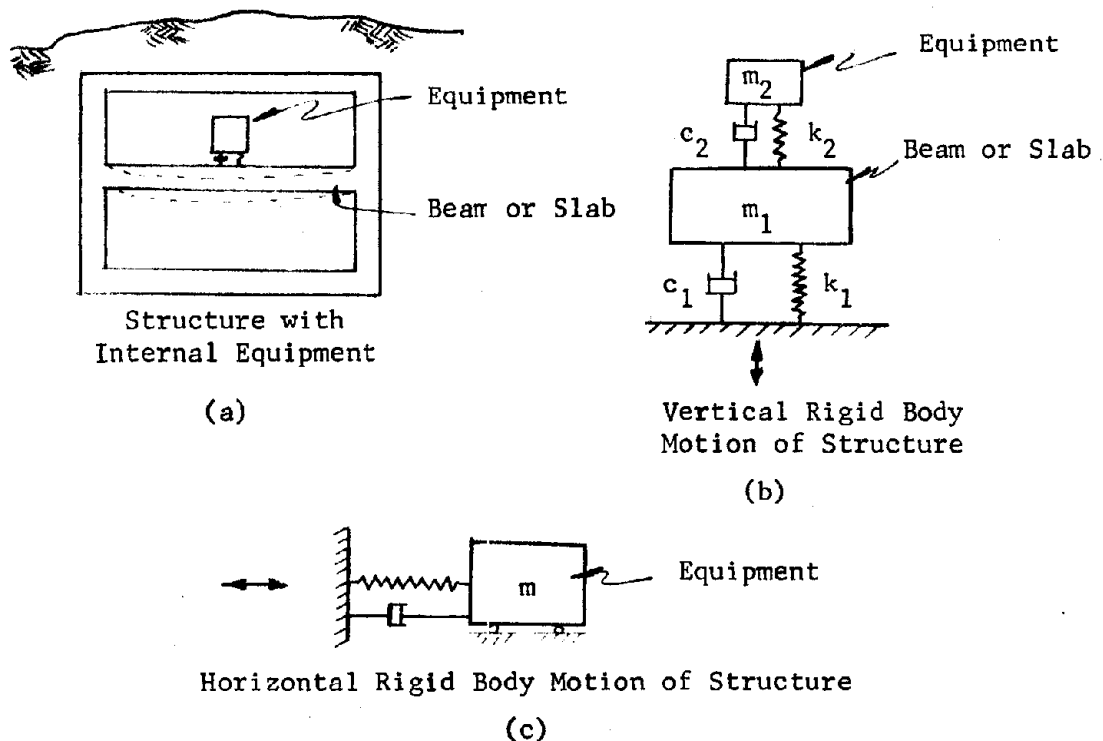


FIGURE 2.1

The examples of Figure 2.1, a single-mass-one-degree-of-freedom system and a two-mass system, represent appropriate models for equipments mounted directly to a structure element not directly exposed to the air blast force. Some systems, of course, are more complex and require more degrees of freedom to define their response characteristics. These more complex systems will be discussed in Section 5.

## 2.2 Single-Mass-One-Degree-of-Freedom Undamped System

The response of an undamped one-degree-of-freedom system is of primary importance because a great deal of reliable ground motion data is based on the response of single-degree-of-freedom reed gages designed to cover the frequency of interest and mounted in buried canisters exposed to nuclear weapon detonations. This data has been extrapolated for other soil conditions and used as criteria for response motions of equipments or platforms attached to the structure.

The equation of equilibrium of a single-degree-of-freedom (SDOF) system is written as

$$m\ddot{x} = -k(x - x_s) = -ky \quad (2.1)$$

where  $y$  is the relative displacement between support and equipment (change in length of spring),  $x_s$  is the support displacement and  $x$  is the absolute mass displacement. (See Figure 2.2.)

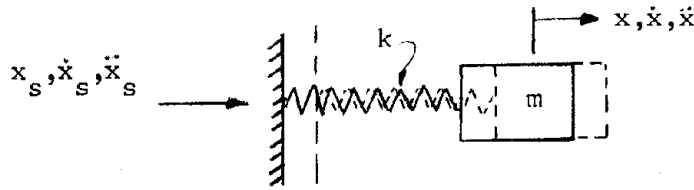


FIGURE 2.2: TYPICAL SDOF UNDAMPED SYSTEM

Equation (2.1) may be rewritten in the form

$$m\ddot{y} + ky = -m\ddot{x}_s \quad (2.2)$$

or by placing  $\omega^2 = k/m$ , the natural frequency of the system, it becomes

$$\ddot{y} + \omega^2 y = -\ddot{x}_s \quad (2.3)$$

It is concluded from this fundamental relationship that

$$|\omega^2 y| = \ddot{y} + \ddot{x}_s = \ddot{x} \quad (2.4)$$

which is the absolute value of the acceleration of the equipment mass. We

define the maximum amplification factor as

$$\frac{|\omega^2 y|_{\max}}{|\ddot{x}_s|_{\max}} = \frac{|\ddot{y} + \ddot{x}_s|_{\max}}{|\ddot{x}_s|_{\max}} = \frac{|\ddot{x}|_{\max}}{|\ddot{x}_s|_{\max}} \quad (2.5)$$

A shock spectrum for this simple system is obtained by plotting  $\omega^2 y$  or the ratio given by Equation (2.5) as a function of the frequency  $\omega$  (or  $\frac{\omega}{2\pi}$ ) of the system.

As an example illustrating the method, we consider a horizontal velocity shock,  $\dot{x}_s$ , equal to an instantaneous step velocity. The solution of Equation (2.1) by the standard methods for solving such differential equations, is

$$x = \dot{x}_s \left( t - \frac{1}{\omega} \sin \omega t \right) \quad (2.6)$$

The relative deflection is

$$y = \frac{\dot{x}_s}{\omega} \sin \omega t \quad (2.7)$$

giving

$$y_{\max} = \frac{\dot{x}_s}{\omega}$$

The maximum absolute acceleration is

$$\ddot{x}_{\max} = \omega^2 y_{\max} = \omega \dot{x}_s \quad (2.8)$$

and the relative velocity is

$$\dot{y}_{\max} = \dot{x}_s = \omega y_{\max} = \frac{\ddot{x}_{\max}}{\omega} \quad (2.9)$$

In Figure 2.3, on a special coordinate system are plotted the maximum relative displacement, maximum absolute acceleration, and maximum relative velocity for a particular value of  $\dot{x}_s$ . (The velocity coordinate is the true relative velocity for a step velocity pulse and a reasonable approximation for other input pulse shapes. Because in the general case it is only an approximation to the relative velocity, the name "pseudo-velocity" has been given to the quantity obtained by the relationships of Equation (2.9).) The three primitive quantities of motion are then assumed to be simply related and they are plotted on a special four-scaled logarithmic

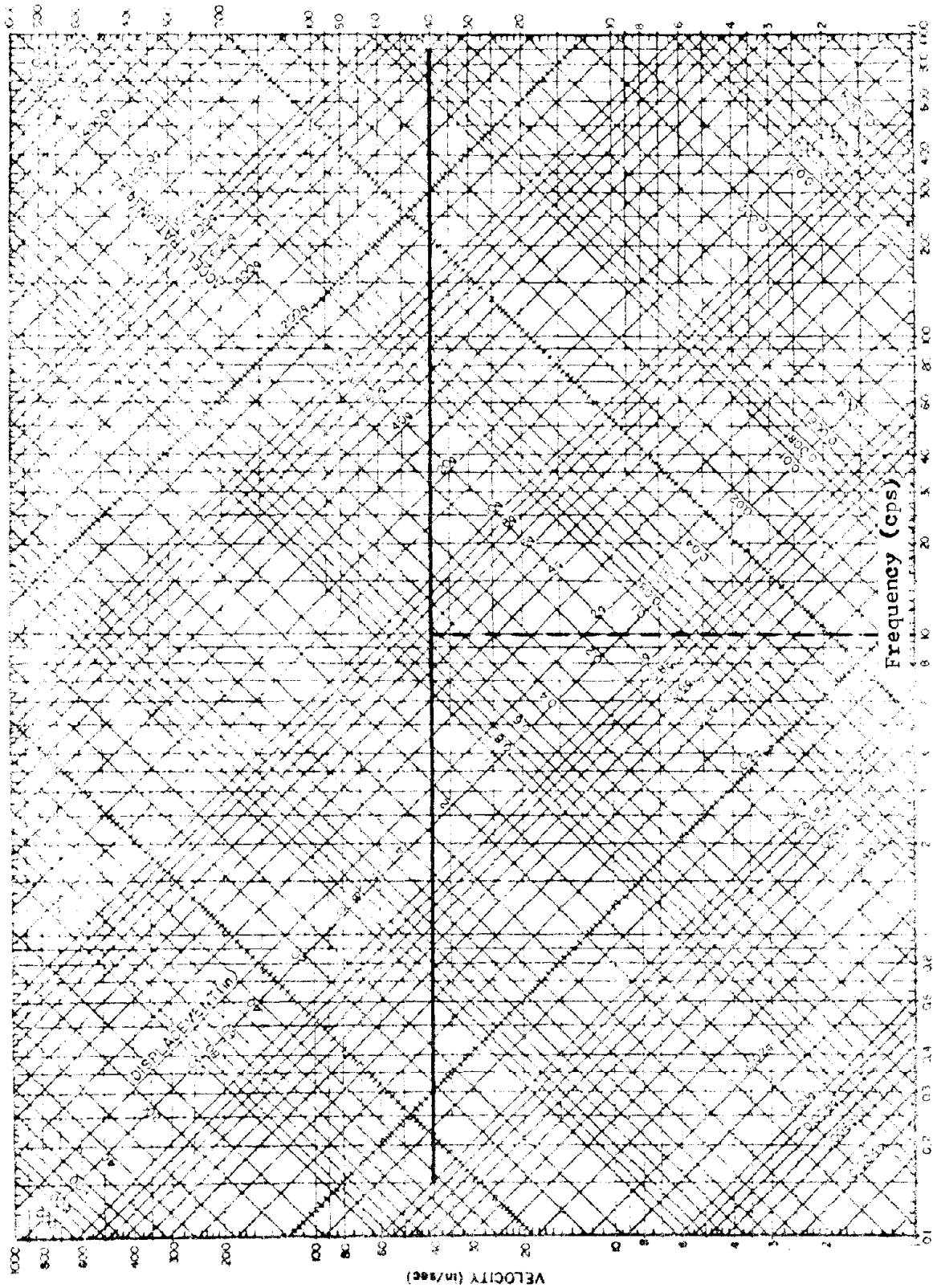


FIGURE 2.3: TYPICAL SHOCK SPECTRA FOR A STEP VELOCITY PULSE

coordinate system. The frequency  $f$  of the responsive system is the abscissa, the maximum velocity of the motion is the ordinate, the maximum displacement coordinate is taken in a direction normal to straight lines with positive slopes of unity, and the maximum acceleration coordinate is in a direction normal to straight lines with negative slopes of unity. Thus any point  $P$  in the coordinate system automatically obeys the relation:

$$(\ddot{x}g)_{\max} = 2\pi f(\dot{y})_{\max} = 4\pi^2 f^2 (y)_{\max}$$

where

- $\ddot{x}$  = peak absolute acceleration in g's
- $\dot{y}$  = peak relative pseudo-velocity in inches per second
- $y$  = peak relative displacement in inches.

This shock spectrum serves to define the motion of the mass  $m$ . Such spectra are particularly useful when the ground motion cannot be defined analytically. It should be noted that the maximum force applied to the spring  $k$  as a consequence of the shock is  $m|\ddot{x}|_{\max}$  where  $|\ddot{x}|_{\max}$  is determined from Figure 2.3. Correspondingly, the maximum deflection,  $y_{\max}$ , of the spring  $k$  is also determined from the same figure. For example, if a single-degree-of-freedom-system has a frequency of 10 cps and the step-velocity ( $\dot{x}_s$ ) is 40 in/sec, the peak response is read directly from Figure 2.3,  $|\ddot{x}|_{\max} = 6.5g$  and  $y_{\max} = 0.65$  inches. Thus, shock spectra supply necessary information for the strength design of supports for rigid mounted equipment and also for the design of springs for shock mounts to limit the maximum acceleration delivered to the mass of the equipment. The use of shock spectra is further discussed in Section 2.4.

Damping is normally neglected when the peak response for spring design is the major consideration. When systems need to be shock isolated to very low acceleration levels, damping may introduce a significant increase in acceleration response. Also when the time to completely damp out the motion is important, then the damping in the system cannot be ignored. Section 5, Shock Isolation Systems, will cover this situation.

### 2.3 Two-Mass Systems

In Subsection 2.2 the single-degree-of-freedom system was described and the interpretation of the shock response spectrum for this system was given. Many internal systems can be approximated by a two-mass system, the second mass being the item to be isolated from the shock, and the first mass being a flexible structural element on which the item is supported. (Figure 2.4)

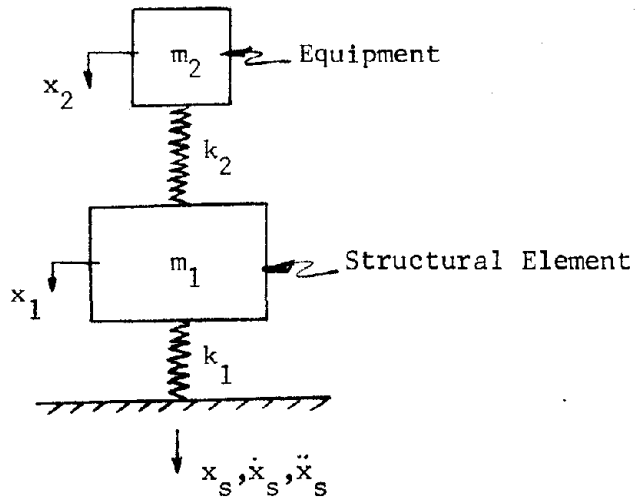


FIGURE 2.4: TWO-MASS SYSTEM

The equations of motion for a two-mass system are

$$m_1 \ddot{x}_1 + (k_1 + k_2)x_1 - k_2 x_2 = k_1 x_s \quad (2.10)$$

$$m_2 \ddot{x}_2 + k_2 x_2 - k_2 x_1 = 0 \quad (2.11)$$

where  $\ddot{x}_1$ ,  $x_1$ ,  $\ddot{x}_2$ ,  $x_2$  are the absolute motions of the two masses.

Introducing a coordinate transformation,

$$y_1 = x_1 - x_s \quad \ddot{y}_1 = \ddot{x}_1 - \ddot{x}_s \quad (2.12)$$

$$y_2 = x_2 - x_s \quad \ddot{y}_2 = \ddot{x}_2 - \ddot{x}_s$$

Equations (2.10) and (2.11) can be rewritten in terms of the relative displacements ( $y_1$  and  $y_2$ ) and relative accelerations ( $\ddot{y}_1$  and  $\ddot{y}_2$ ) and the



ground acceleration  $\ddot{x}_s$

$$m_1 \ddot{y}_1 + (k_1 + k_2)y_1 - k_2 y_2 = -m_1 \ddot{x}_s \quad (2.13)$$

$$m_2 \ddot{y}_2 + k_2 y_2 - k_2 y_1 = -m_2 \ddot{x}_s \quad (2.14)$$

or

$$[m] (\ddot{y}) + [k] (y) = - [m] (\ddot{x}_s) \quad (2.15)$$

in matrix notation (see Appendix A).

The solution to these two simultaneous differential equations is covered by the general case of  $n$  simultaneous differential equations which is given in Appendix A; it is presented in a form that is suited for electronic computer solutions. In this subsection, however, some simple concepts will be presented based on approximations that will lead to the calculation of peak responses for mass  $m_2$  when the response of mass  $m_1$  to a support motion input is known, the latter being readily calculated by the principles applicable to a single-degree-of-freedom system.

For illustration of the basic relationships, let it be assumed that the support input is a step velocity pulse. If the mass  $m_2$  is assumed small relative to  $m_1$ , the motion of  $m_1$  becomes independent of the motion of  $m_2$ , simplifying the analysis considerably.

Considering first the mass  $m_1$ , for which the equation of equilibrium is written as

$$m_1 \ddot{x}_1 = k_1(x_s - x_1) \quad (2.16)$$

and the step-velocity shock input

$$\dot{x}_s(t) = \dot{x}_s \text{ (constant)} \quad (2.17)$$

we write, as in Equation (2.16),

$$x_1 = \dot{x}_s \left( t - \frac{1}{\omega_1} \sin \omega_1 t \right) \quad (2.18)$$

The differential equation of motion for the mass  $m_2$  is

$$m_2 \ddot{x}_2 = k_2(x_1 - x_2) \quad (2.19)$$

Applying the initial conditions  $x_2 = \dot{x}_2 = 0$ , when  $t=0$ , the displacement of

mass  $m_2$  is obtained from the solution of Equation (2.19) and using Equation (2.18) as:

$$x_2 = \dot{x}_s t - \frac{\dot{x}_s}{\omega_2 \left[ 1 - (\omega_2/\omega_1)^2 \right]} \sin \omega_2 t - \frac{\dot{x}_s}{\omega_1 \left[ 1 - (\omega_1/\omega_2)^2 \right]} \sin \omega_1 t \quad (2.20)$$

The displacement  $x_2$  is thus comprised of two harmonic terms of different frequencies and different amplitudes, superimposed upon the displacement  $x_s = \dot{x}_s t$  of the support, all three terms being directly proportional to the velocity change  $\dot{x}_s$ .

The acceleration experienced by the mass  $m_2$  may now be determined by double differentiation of Equation (2.20), with respect to time, and by considering  $\dot{x}_s$  a constant to give:

$$\ddot{x}_2 = \frac{\dot{x}_s \omega_2}{1 - (\omega_2/\omega_1)^2} \left[ \sin \omega_2 t - (\omega_2/\omega_1) \sin \omega_1 t \right] \quad (2.21)$$

Since the system is undamped, its motion continues indefinitely. The term within the parentheses of Equation (2.21) cannot exceed the maximum value of

$$(1 + \omega_2/\omega_1).$$

The maximum acceleration of the mass  $m_2$  may then be written:

$$|\ddot{x}_2|_{\max} = \frac{\dot{x}_s \omega_2}{|1 - (\omega_2/\omega_1)^2|} + \frac{\dot{x}_s \omega_1}{|1 - (\omega_1/\omega_2)^2|} \quad (2.22)$$

but by Equation (2.8)  $\dot{x}_s \omega_2$  and  $\dot{x}_s \omega_1$  are, respectively, the peak acceleration responses of the two masses  $m_2$  and  $m_1$  when each mass is subjected independently to a step velocity shock  $\dot{x}_s$ . Equation (2.22) may be written more conveniently in the form:

$$|\ddot{x}_2|_{\max} = \left| \frac{\omega_2^2}{\omega_2^2 - \omega_1^2} \right| A_1 + \left| \frac{\omega_1^2}{\omega_1^2 - \omega_2^2} \right| A_2 \quad (2.23)$$

where  $A_1 = \dot{x}_s \omega_1$  and  $A_2 = \dot{x}_s \omega_2$

$$\omega_1 = \sqrt{k_1/m_1} \quad \text{and} \quad \omega_2 = \sqrt{k_2/m_2}$$

The Equation (2.23) reduces further to

$$|\ddot{x}_2|_{\max} = \left| \frac{\omega_2}{\omega_1 - \omega_2} \right| A_1 \quad (2.24)$$

Although the above synthesis was based on a step-velocity pulse input, the form of Equation (2.23) is also applicable for use with shock spectra of other types of input pulses (see Reference 2.1) based on the following important consideration. If the shock spectrum were known for a single-degree-of-freedom system, the peak response acceleration of the equipment could then be expressed in terms of the response acceleration  $A_1$  and  $A_2$  corresponding to the two respective natural frequencies  $\omega_1$  and  $\omega_2$ . Therefore, the shock spectra technique may be applied directly to a two-mass system when  $m_1 \gg m_2$ . This will be further developed in Sub-section 2.4.2. Some limiting cases can be obtained from the above equation. If the equipment is "soft-mounted" and  $\omega_2 \ll \omega_1$ , so that  $\omega_2^2$  is negligible compared to  $\omega_1^2$ , then  $|\ddot{x}_2|_{\max} \approx A_2$ , the response at frequency  $\omega_2$ . In this case, the structural element is essentially rigid and participates only in the rigid body motion of the structure.

If the equipment is "hard-mounted", then the attenuating effect is due primarily to the structural element to which it is attached. In the extreme case if  $\omega_1 \ll \omega_2$ , then  $|\ddot{x}_2|_{\max} \approx A_1$ , the structural element will act essentially as the shock mounting for the equipment.

The following example will show the relationship between the response spectrum of mass  $m_2$  and the shock spectrum for a specific step velocity pulse input.

#### Example 2.1

Let  $\dot{x}_s = 40$  in/sec and  $m_2 = m_1/10$ . From Equation (2.9), for a single-degree-of-freedom system, the response velocity,  $\dot{y}_{\max}$ , is equal to  $\dot{x}_s$ . In Figure 2.5, this response is plotted as a horizontal line at  $\dot{y}_{\max} = 40$  in/sec.

In the same figure are also plotted three curves depicting the response of mass  $m_2$  when the natural frequency of mass  $m_1$  is 3 cps, 15 cps, and 150 cps, respectively. These curves are based on the exact solutions

Example 2.1 (continued)

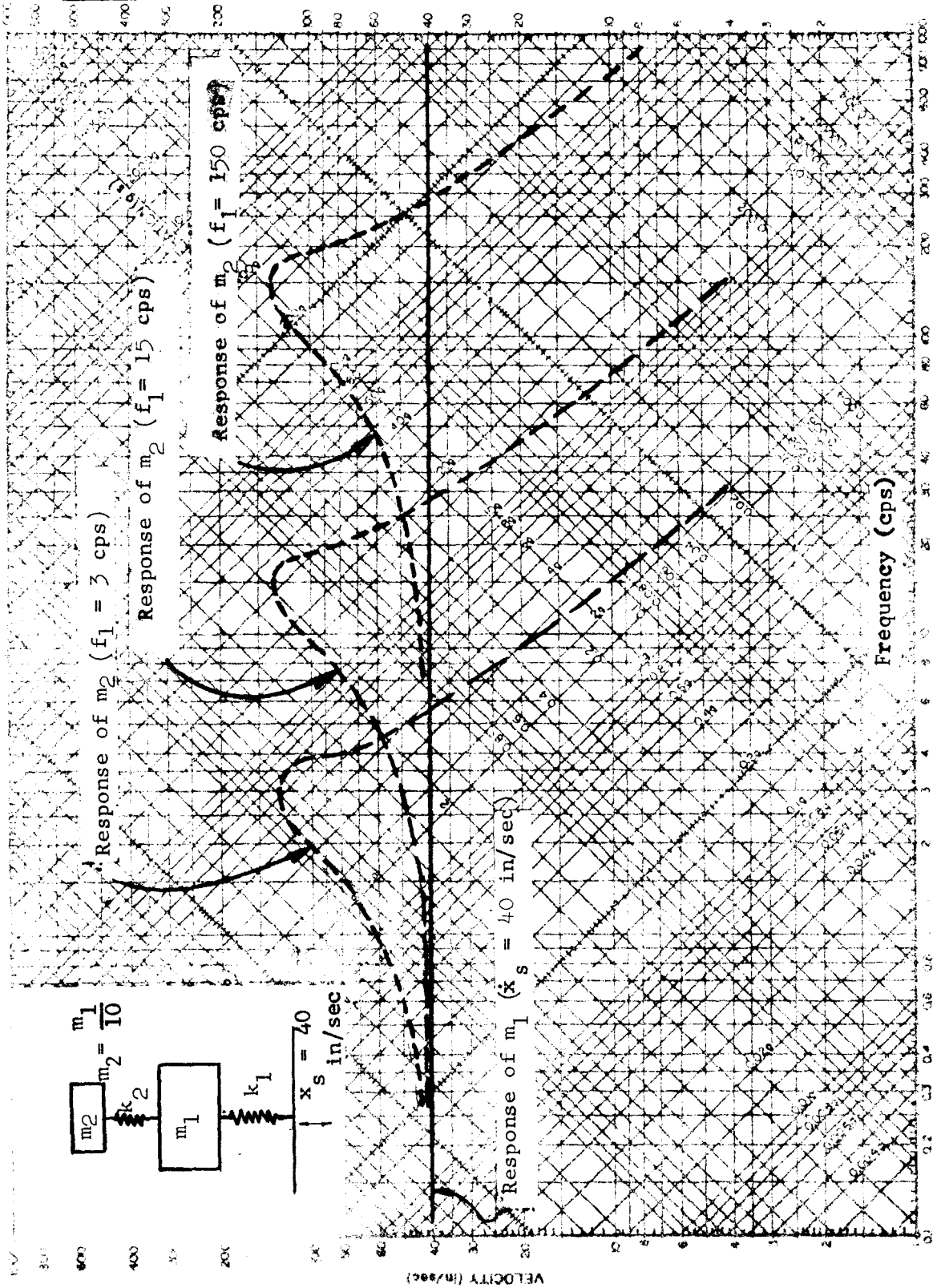


FIGURE 2.5: RESPONSE SPECTRUM FOR A VELOCITY STEP-PULSE ON A 2-MASS SYSTEM:  $m_2 = m_1/10$

Example 2.1 (continued)

given in Reference 2.2 and show peaks of approximately 135 in/sec.

We consider the intermediate condition ( $f_1 = 15$  cps). If mass  $m_2$  has a natural frequency of  $f_2 = 5$  cps, the curve in Figure 2.5 gives a peak acceleration of  $\ddot{x}_2 = 5g$ . Direct calculation by Equation (2.23) will give:

$$A_1 = \dot{x}_s \omega_1 = \frac{40 \times 2\pi \times 15}{386} = 9.76 \text{ g}$$

$$A_2 = \dot{x}_s \omega_2 = \frac{9.76}{3} \text{ g} = 3.25 \text{ g}$$

and

$$\begin{aligned} |\ddot{x}_2|_{\max} &= \left| \frac{5^2}{5^2 - 15^2} \right| 9.76 \text{ g} + \left| \frac{15^2}{15^2 - 5^2} \right| 3.25 \text{ g} = 1.22 \text{ g} + 3.66 \text{ g} \\ &= 4.88 \text{ g} \approx 5 \text{ g} \end{aligned}$$

Other points on the curves of Figure 2.5 may be similarly compared. There will be a large discrepancy between Equation (2.23) and the response curves of Figure 2.3 as  $\omega_1 \rightarrow \omega_2$ .

Equation (2.23) shows that when  $\omega_1 = \omega_2$ , the peak response acceleration of  $m_2$  becomes infinite when damping is neglected. This condition, however, will be achieved only after an infinitely long time, as shown below:

For the region in which  $\omega_2/\omega_1 \rightarrow 1$ , Equation (2.21) may be rewritten in the form

$$\ddot{x}_2 = \frac{\dot{x}_s \omega_2}{1 - (\omega_2/\omega_1)^2} 2 \sin\left(\frac{\omega_2 - \omega_1}{2} t\right) \cos\left(\frac{\omega_2 + \omega_1}{2} t\right) \quad (2.25)$$

since  $\omega_2 \approx \omega_1$

$$\sin \frac{\omega_2 - \omega_1}{2} t \approx \frac{\omega_2 - \omega_1}{2} t \text{ and } \cos \frac{\omega_2 + \omega_1}{2} t \approx \cos \omega_1 t \quad (2.26)$$

Equation (2.21) then becomes

$$\ddot{x}_2 = - \frac{\dot{x}_s \omega_1 \omega_2 t \cos \omega_1 t}{1 + (\omega_2/\omega_1)} \quad (2.27)$$

The acceleration  $\ddot{x}_2$  of the mass  $m_2$  thus increases continuously as time  $t$  increases, and the infinite transmissibility indicated by Equation (2.23)

### Example 2.1 (continued)

for  $\omega_2 = \omega_1$  occurs only after an infinitely long time.

It is also apparent from the physical concept of this condition that the vibration of the mass  $m_2$  must continue indefinitely if the infinite acceleration  $\ddot{x}_2$  is to be reached. This cannot occur, because no energy will be added after the initial sudden velocity change, and the amplitude  $x_1$  therefore must inevitably decrease as the initial energy is dissipated. The maximum acceleration  $\ddot{x}_2$  which is ultimately reached by a system subjected to a shock represents a balance between the excitation tendency and the operating energy dissipation tendency to decrease the amplitude of mass  $m_1$ . The mathematics required to determine such results in general form is very laborious, and the methods of Appendix A must be used for a general solution. In Reference 2.1, amplification factors for two-mass systems are given for various values of damping ratios.

In designing shock isolation systems, it is most important to avoid situations in which  $\omega_1$  approaches  $\omega_2$ . For practical situations, when the input is not given explicitly as a velocity pulse, the above method may be used for approximate results, observing that the maximum acceleration experienced by the equipment is reduced by the flexible structural member only if the natural frequency of the equipment is at least two times as high as the natural frequency of the member. The maximum acceleration will continue to decrease as the equipment becomes more rigid; and it is influenced but little by the degree of damping in the isolator provided that the damping is small. On the other hand, a flexible member is likely to enhance the peak accelerations of a "soft-mounted" equipment.

### 2.4 Shock Spectra Envelope

A shock spectrum is a plot of the maximum response of a single-degree-of-freedom vibrational system to one specific disturbance. The independent coordinate of the plot is the natural frequency of the responsive system and the dependent coordinate usually is either the relative displacement, the pseudo velocity, or the absolute acceleration of the mass of the system.

Consequently, a spectrum does not describe the response except in regard to the maximum value of one or more of the three primitive quantities determining motions. The times of the occurrences of the maxima are practically never given, because they are very sensitive to the precise shape of the disturbance. Attention is called to the fact that the maxima of the three primitive quantities often do not occur simultaneously, even for a simple harmonic motion response, and that for many disturbances the time occurrence of the maxima may be far apart.

In the analysis of ground shock effects due to nuclear weapons, a shock spectra envelope is defined as an upper bound which hopefully envelopes the response motions to the ground disturbances at a given site. As a result of many studies and evaluation of test data, shock spectra have been considered to be a very acceptable way, due to limited knowledge of free-field motions, for defining upper bounds of ground motions for a given set of weapon effects and site conditions. Shock spectra are used as design criteria, and if a time-history input is necessary, a pulse (or a set of pulses) whose shock spectrum generally falls within a prescribed shock spectra envelope may be used as a basis for determining a more specific history of the response of particular shock isolation systems.

2.4.1 Shock spectra for elastic systems. The response spectrum corresponding to a step-velocity pulse does not give a realistic picture of the response characteristics of a system subjected to ground motion, and it must be modified in accordance with the requirements of the real conditions observed during tests with nuclear weapons. This modification applies particularly to the extreme left and right ends of the horizontal line spectrum shown in Figure 2.5. The inference to be drawn from the left end of the spectrum is that the relative displacement increases without limit as the natural frequency approaches zero. Actually, the maximum relative displacement reaches a definite limit which can be described by bending the left end of the spectrum down along a diagonal line representing the maximum ground displacement, as indicated in Figure 2.6. Correspondingly, the sudden change in velocity depicted by Figure 2.5 suggests that the acceleration of the responding system increases without limit as its natural

frequency increases. Actually, the velocity change occurs, not instantaneously but over a relatively short time interval, resulting in a finite upper limit to the acceleration. This is reflected on the spectrum by bending the right end down along a diagonal line representing an envelope bound on maximum absolute acceleration.

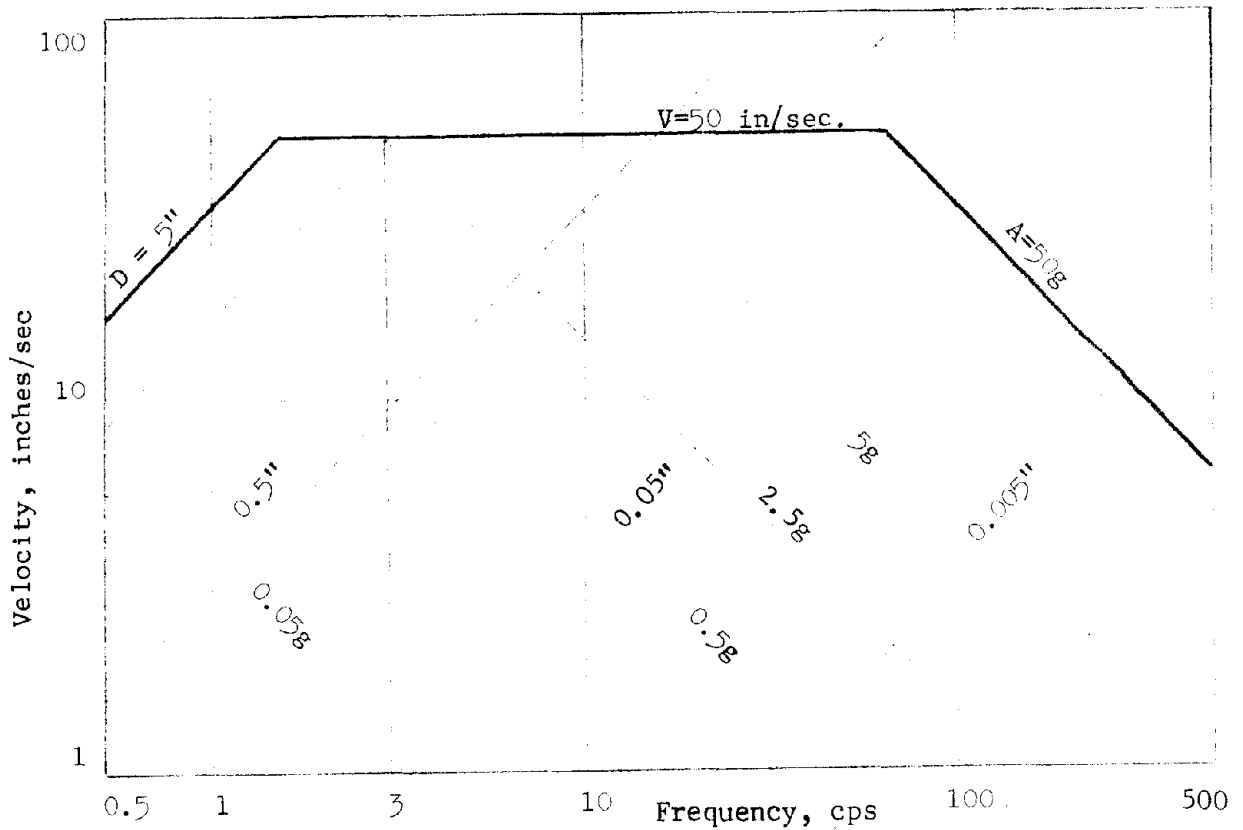


FIGURE 2.6: TYPICAL SHOCK SPECTRA

Shock spectra envelopes giving upper bound displacement, velocity, and acceleration values resulting from free-field motions due to nuclear blasts have been recommended based on field measurements and studies involving response of SDOF systems to many types of simple and complex pulse shapes. The parameters considered are: weapon yield, air, surface or buried burst, local maximum overpressure, depth of burial of the facility and soil characteristics. (See Section 3 for specific relationships).



We now consider a shock spectra envelope as it is usually defined for ground motions due to weapon effects. In the low frequency region, the relative response displacement,  $D$ , is set equal to the ground displacement,  $d$ , as a maximum. In the high frequency region, the response acceleration,  $A$ , when set equal to  $2a$ , will usually bound the response in this region. Also in the mid-frequency region, a constant pseudo-velocity,  $V$ , equal to  $1.5v$  will usually bound the response. The values  $d$ ,  $v$ , and  $a$  are the peak ground displacement, velocity, and acceleration, respectively.

For an example of the use of this shock spectra envelope, assume that Figure 2.6 defines an envelope which will bound the shock spectrum for a ground motion for a given weapon yield and overpressure region and that an isolator is to be designed to protect the equipment. (The structure is assumed to move as a rigid body with the free-field of the ground.)

It is assumed in this example that tests and calculations have shown that the equipment can withstand loads equal to 2.5 times the dead weight loads; that is, the equipment will withstand 2.5 g. Entering Figure 2.6 on the diagonal line representing a maximum acceleration of 2.5 g, the required natural frequency on the horizontal scale is 3 cps as determined from the intersection of the spectrum with the diagonal line representing 2.5 g. For an isolator having a natural frequency of 3 cps, the maximum deflection of the isolator in response to the ground motion is approximately 2.75 in. as read from the intersection of the spectra envelope with the horizontal line representing a velocity change of 50 in/sec. The design of the isolator must be such as to permit this deflection.

Many studies of ground motions due to earthquakes and nuclear weapon effects (References 2.3 and 2.4) have generally verified that the method of plotting the spectra envelope described above provides a nominal but reasonable bound on the response motions. If the ground displacement has a half cyclic characteristic, then SDOF systems with periods of vibration close to the ground displacement duration will have amplified response amplitudes which exceed the above envelope due to resonance. If the ground motion has some oscillatory components, the specific shock spectrum may

exceed the above specified envelope in the frequency regions which coincide with the ground motion oscillatory components. The recommendations in Section 3.7 will modify the shock spectra envelope factors given in the previous paragraph to account for these two effects.

Finally, in this introductory discussion of the concept of shock spectra envelope, a comparative discussion is given on the shock spectra envelope for direct air blast pressure impingement on aboveground structures and ground motions. Let us consider the response spectrum for a parabolic velocity pulse input as shown in Figure 2.7 (from Reference 2.4). The equation of motion for a support input is compared with the equation of motion for a force applied to the mass itself.

(1) Support input:  $\ddot{y} + \omega y = -\ddot{x}_s$

(2) Force input :  $\ddot{x} + \omega x = P/m$

The two equations are identical in form, and the shock spectrum for case (2) will be similar to the spectrum for case (1) if the forcing function  $P/m$  (an acceleration) has a shape similar to the acceleration input  $\ddot{x}_s$  in case (1).

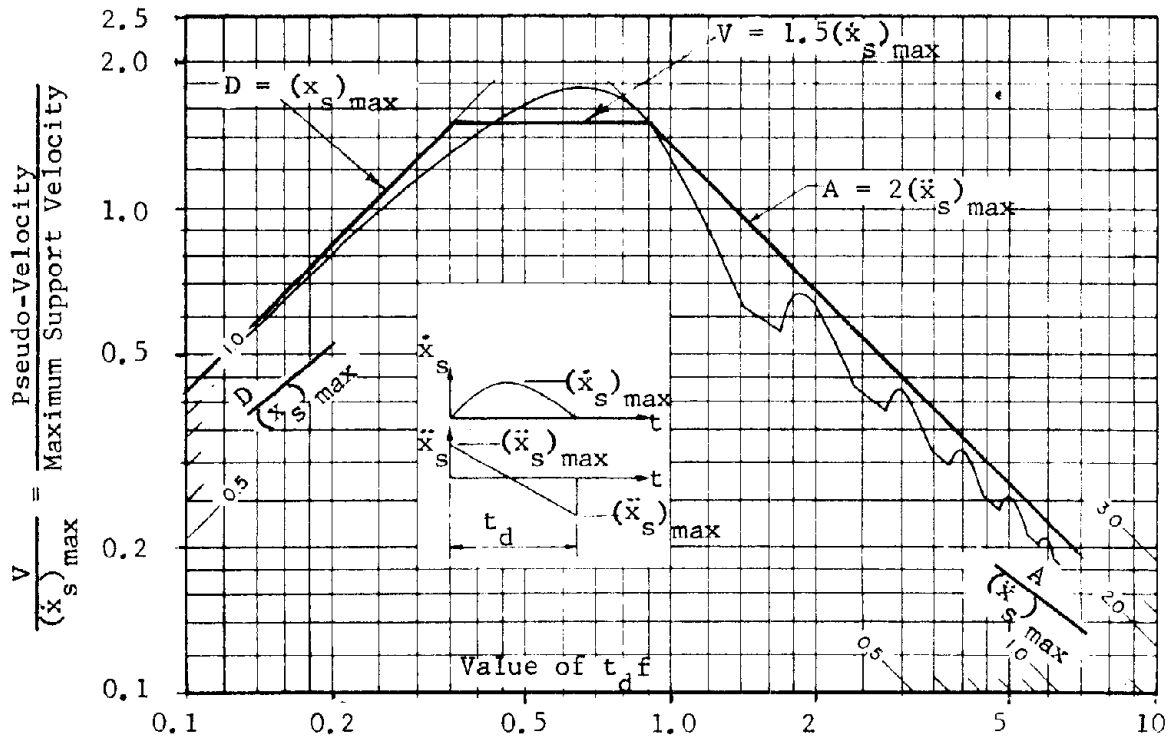


FIGURE 2.7: DEFORMATION SPECTRUM FOR UNDAMPED ELASTIC SYSTEMS SUBJECTED TO A PARABOLIC VELOCITY PULSE (REFERENCE 2.4)

The acceleration pulse,  $\ddot{x}_s$ , in the insert of Figure 2.7 is noted to have a triangular shape with an instantaneous rise time. Air blast forces applied to aboveground structures are also idealized to triangular pulses. Therefore, the spectrum shown in Figure 2.7 can be considered as a good approximation to the spectrum for the air blast loading applied to an SDOF system. Figure 2.7 shows that the shock spectra envelope defined by the three straight lines,  $D = (\dot{x}_s)_{\max}$ ,  $V = 1.5 (\ddot{x}_s)_{\max}$ ,  $A = 2.0 (\ddot{x}_s)_{\max}$ , will also be an adequate approximation for direct air blast loading on structural elements, assumed to be SDOF systems. Section 4 takes advantage of this approximation in deriving shock spectra envelopes for air blast induced loadings.

**2.4.2 Shock spectra for two-mass systems.** An approximate rule may be developed for the upper bound of the peak response for mass,  $m_2$ , in a two-mass system ( $m_1 \gg m_2$ ), if a shock spectrum or spectrum envelope is given for mass,  $m_1$ , when the latter is acting alone as a single-degree-of-freedom system. This approach was developed in Section 2.3 for a step velocity pulse input and Equation (2.23) was derived for computing the maximum absolute acceleration of mass,  $m_2$ , from a given shock spectra envelope, irrespective of the input function. Equation (2.23) rewritten in terms of natural frequencies is:

$$(\ddot{x}_2)_{\max} = \left| \frac{f_2^2}{f_2^2 - f_1^2} \right| A_1 + \left| \frac{f_1^2}{f_1^2 - f_2^2} \right| A_2 \quad (2.28)$$

Figure 2.8 shows a typical shock spectra envelope based on the amplification factors given in Section 2.4.1. Let us consider the three values of frequency  $f_1$ ; 1.5 cps, 15 cps, and 150 cps. From Equation (2.28) we can then calculate a shock spectrum of  $m_2$  for given values of  $f_1$ . The three frequencies, 1.5, 15, and 150 cps, represent specific cases of mass and stiffness characteristics of  $m_1$  for which the response spectra of  $m_2$  are obtained as shown in Figure 2.8. It is again noted that for frequencies of  $f_2$  approaching  $f_1$  a resonant condition exists and the amplified response indicated in this region, i.e.,  $f_1/2 < f_2 < 2f_1$ , may be overly conservative for damped systems.

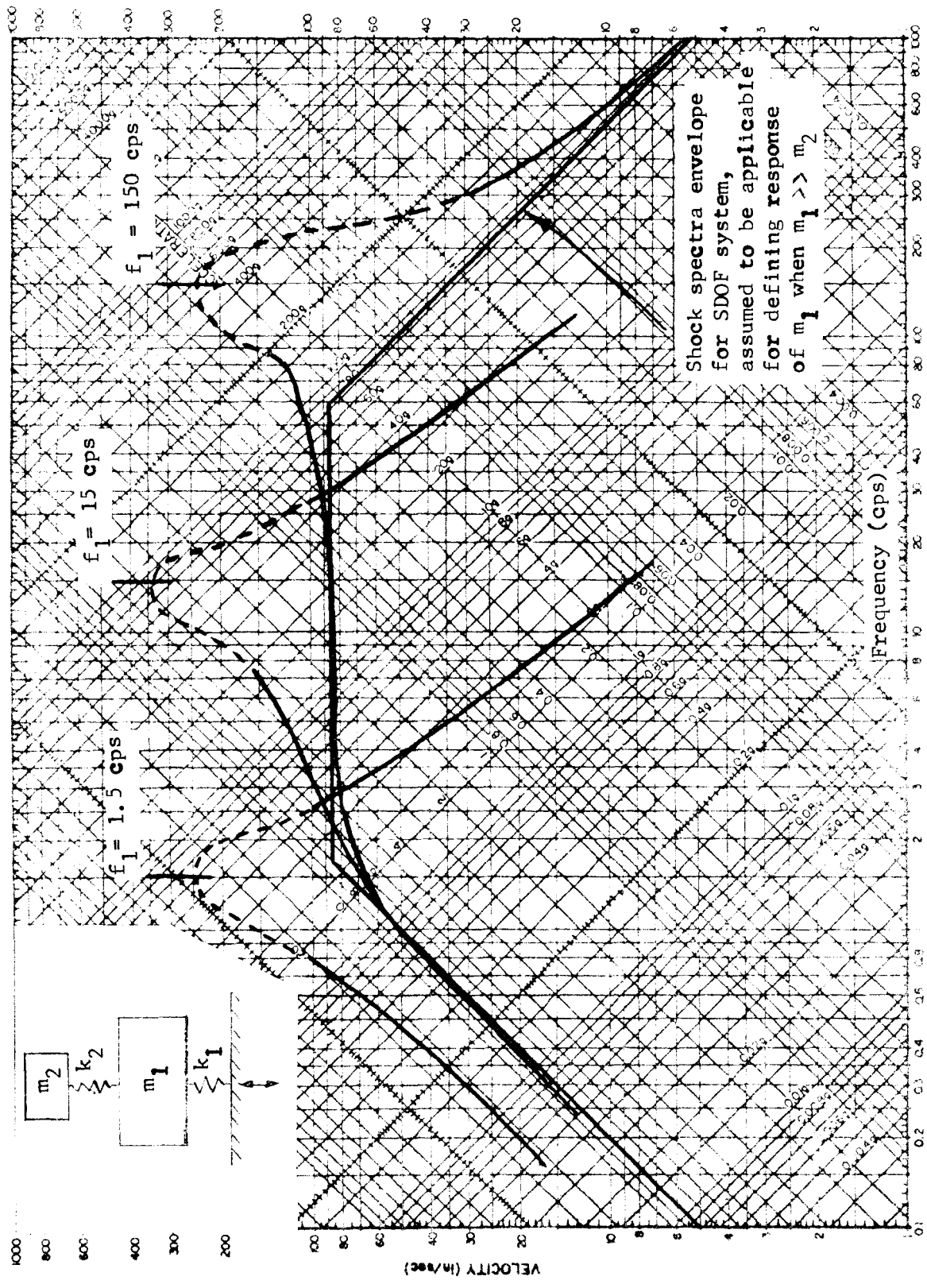


FIGURE 2.8: RESPONSE SPECTRUMS FOR A 2-MASS SYSTEM

An alternate procedure, in lieu of the spectrum derived from Equation (2.28), is to construct a response envelope using amplification factors similar to those used for one-mass systems thus bounding the response spectra of the second mass  $m_2$ . This method has been suggested in Reference 2.5, and the procedure is as follows:

- (a) From the shock spectra envelope used for defining the peak response of  $m_1$ , compute the response values,  $y_1$ ,  $\dot{y}_1$ ,  $\ddot{x}_1$  at the frequency  $f_1 = \frac{1}{2\pi} \sqrt{k_1/m_1}$  (maximum intensities are implied in this discussion). The absolute peak motions of  $m_1$  are then:

$$\begin{aligned}x_1 &= x_s + y_1 \\ \dot{x}_1 &= \dot{x}_s + \dot{y}_1 \\ \ddot{x}_1 &= \ddot{x}_1 \text{ (response spectrum calculates absolute} \\ &\quad \text{acceleration)}\end{aligned}$$

These relationships were discussed in Section 2.2.

- (b) We now assume that the absolute motions calculated in (a) are the peak intensities of a complex pulse input to  $m_2$ , and a shock spectra envelope for  $m_2$  may be defined by the three straight lines:

$$\begin{aligned}D' &= x_1 = x_s + y_1 \\ V' &= 1.5 \dot{x}_1 = 1.5 (\dot{x}_s + \dot{y}_1) \\ A' &= 2.0 \ddot{x}_1 = 2.0 \ddot{x}_1\end{aligned}$$

based on the amplification factors recommended in Section 2.4.1.

In Figure 2.9, the above rules are applied for three cases,  $f_1 = 1.5$  cps, 15 cps, and 150 cps, respectively. For the intermediate case, ( $f_1 = 15$  cps) for example,  $y_1$ ,  $\dot{y}_1$ , and  $\ddot{x}_1$  are 0.9 in, 85 in/sec and 20 g respectively. The shock spectrum for mass  $m_2$  when mass  $m_1$  has a natural frequency  $f_1 = 15$  cps is then obtained as:

$$\begin{aligned}D' &= x_s + y_1 = 8 + 0.9 = 8.9 \text{ in} \\ V' &= 1.5 \left[ 85 + (2/3) 85 \right] = 210 \text{ in/sec} \\ A' &= 2 \times 20 \text{ g} = 40 \text{ g}\end{aligned}$$

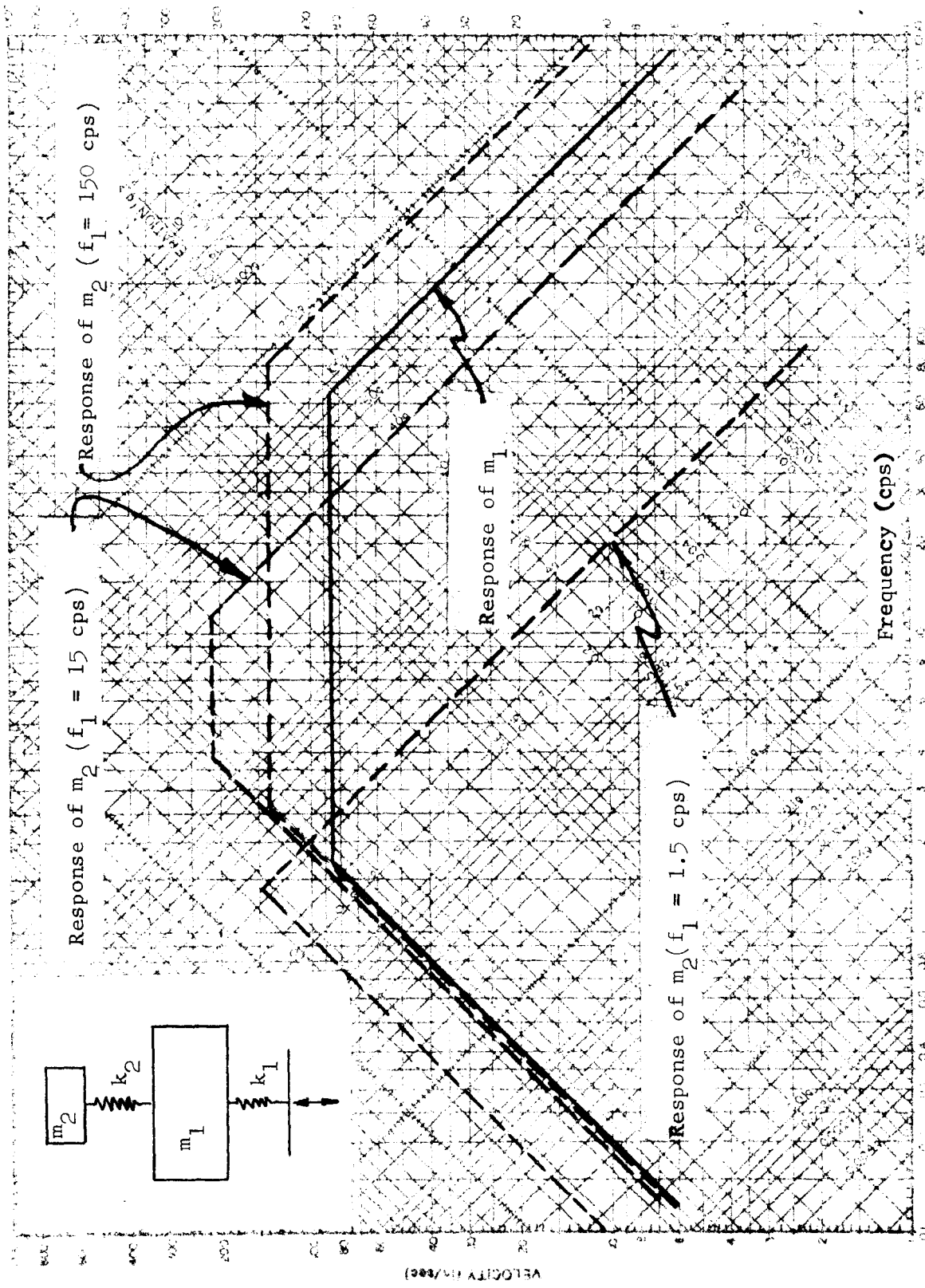


FIGURE 2.9: SHOCK SPECTRA ENVELOPE FOR A 2-MASS SYSTEM

The response spectra bounds for mass,  $m_2$ , are shown in Figure 2.9 with these peak values.

Also, for  $f_1 = 1.5$  cps, from Figure 2.9,

$$D' = 8 + 8 = 16 \text{ inches}$$

$$V' = 1.5 \left[ 75 + (2/3) 85 \right] = 225 \text{ in/sec}$$

$$A' = 2 \times 1.6 \text{ g} = 3.2 \text{ g}$$

It is seen here for  $f_1 = 1.5$  cps that the response displacements of  $m_2$  are amplified by a factor of 2 (which closely bounds the spectrum in Figure 2.8). It may therefore be concluded that two low frequency systems should not be used in series. Also, the trapezoid in this case has degenerated to a triangle with a limiting peak pseudo-velocity of 145 in/sec at the intersection of the constant displacement and acceleration lines. Of course, the apex of the triangle is the region of possible resonance between the two masses ( $f_2 \approx f_1 = 1.5$  cps) and the value of  $V'$  can be in error due to a hump at the resonant region which the shock spectrum does not account for.

For  $f_1 = 150$  cps,

$$D' = 8 + 0.04 \approx 8 \text{ in}$$

$$V' = 1.5 \left[ 37 + (2/3) 85 \right] = 140 \text{ in/sec}$$

$$A' = 2 \times 90 \text{ g} = 180 \text{ g}$$

In this case the response accelerations of mass,  $m_2$ , are amplified by a factor of 2 in the high frequency region, but the relatively stiff spring of the  $(m_1, k_1)$  system has negligible effect on the displacements of a low-frequency  $(m_2, k_2)$  system; this envelope in the high frequency region bounds the spectrum in Figure 2.8 and will be conservative when  $f_2 \gg f_1$ , since  $\ddot{x}_2$  approaches  $\ddot{x}_1$  for  $f_2 \gg f_1$ . For all practical purposes, if mass,  $m_2$ , is "soft-mounted" ( $k_2 \ll k_1$ ), the first mass acts as an integral part of the structural enclosure, transmitting the ground motion directly to the "soft-mounted" system without any amplification.

The shock spectra envelope for two-mass systems will be used in several examples given in Section 4 in which mass,  $m_1$ , represents a flexible support structure and mass,  $m_2$ , is the mounted item.

2.4.3 Shock spectra for elastic-plastic systems. The shock spectra envelope defined in Section 2.4.1 is applicable for a spring-mass system that remains elastic. Many real situations exist where the flexible element will yield plastically to many times the yield deflection before the element fails; therefore it is feasible (and economical) to utilize the energy dissipation capability of the material in the plastic region. If the input is specified as a time-history velocity pulse (or acceleration or displacement pulse) the elastic-plastic response can be determined by the methods which are given in later sections of this report. It would also be desirable, however, to estimate conservatively the peak response by deriving a spectral bound for an elastic-plastic system as a function of the amount of yielding. This approach was taken in References 2.4 and 2.5, and the results and design rules are summarized in this section.

The characteristic of the flexible (or spring) element is idealized to an initial straight line, elastic portion, followed by a plastic region which increases in deformation without increase in load, (see Figure 2.10).

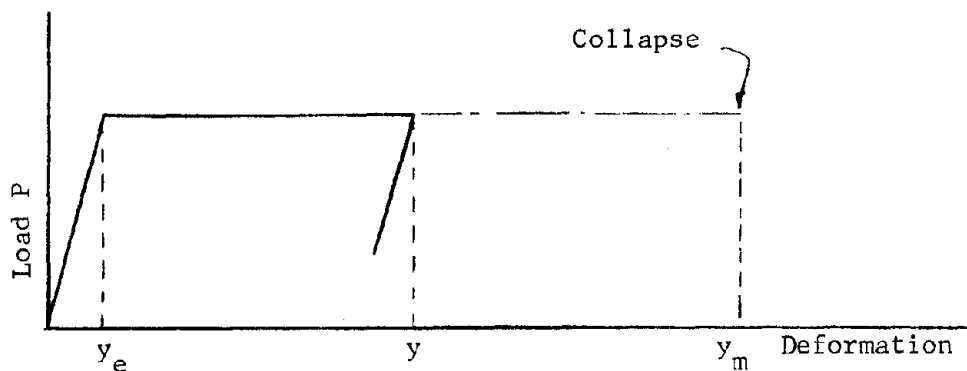


FIGURE 2.10

An important parameter is the ductility factor ( $\mu$ ) which is defined as the ratio of the total transient deflection ( $y$ ) to the yield deflection ( $y_e$ ):

$$\mu = \frac{y}{y_e} \quad (2.29)$$



Because the failure or collapse of many structural elements is governed by the amount of yielding capability prior to failure, we write

$$\mu_{\text{failure}} = \frac{y_m}{y_e} \quad (2.30)$$

where  $y_m$  = total deflection at failure of the element.

For example, it is known that steel beams in flexure can yield to a  $\mu \approx 50$  before failure. Therefore, the designer must insist on a  $\mu$  of less than 50 in the design of a supporting steel beam spring element.

Reference 2.4 reports the results of a parametric study where response spectrums were derived for a single-degree-of-freedom system with elastic-plastic spring characteristics. Input pulses with and without ground recovery were used. First the response of the elastic system was computed as a function of the frequency parameter. Then the maximum responses of elastic-plastic systems were computed for a range of ductility ratios of 1 through 10. Figure 2.11 is taken from Reference 2.4 for one of the input pulses considered and is representative of the relationship between elastic response ( $\mu = 1$ ) and yielding response ( $1 < \mu < 10$ ). Definite conclusions can be made concerning the low frequency response and the high frequency response but the transition region (intermediate frequency region) does not show a simple relationship between the peak ground velocity and the peak response pseudo-velocity.

#### Low Frequency Region

For any given input pulse, the maximum total relative response displacement cannot be greater than the maximum support displacement. This holds true for both elastic and elastic-plastic springs. Considering the response of a range of elastic-plastic systems with different amounts of plastic yielding, to the same input pulse, the relative amounts of elastic and plastic deformation must vary as shown in Figure 2.12. The total deformation is constant and the elastic portion is reduced by the factor  $\frac{1}{\mu}$ . This expected behavior is shown in the low frequency range of Figure 2.11 where it can be seen that the values of  $y_e/x_s$  vary approximately as  $\frac{1}{\mu}$ .

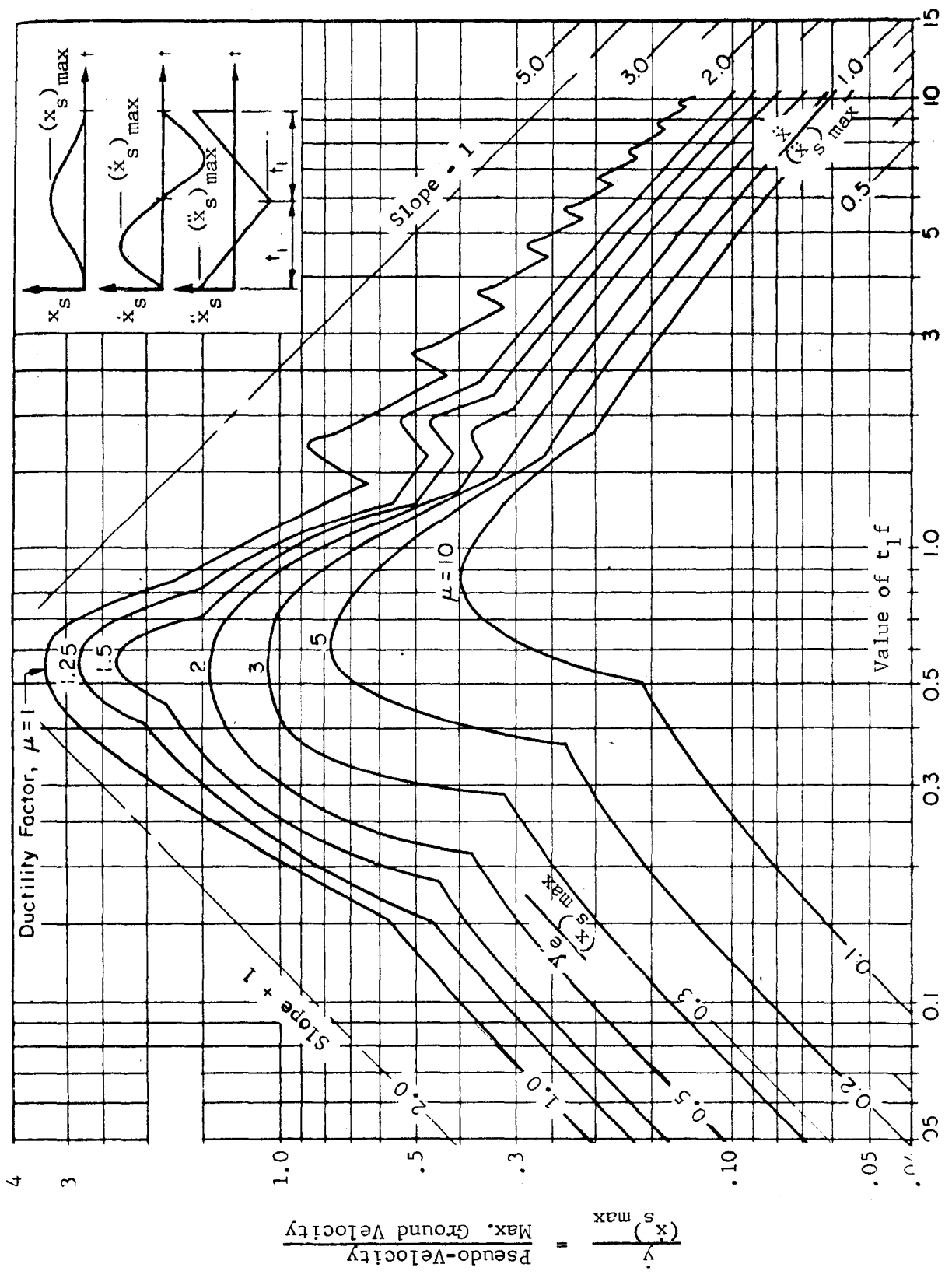


FIGURE 2.11: RESPONSE SPECTRA FOR ELASTIC-PLASTIC SYSTEMS (REFERENCE 2.4)

In Figure 2.12 the yield deflection ( $y_e$ ) for  $\mu = 2$  is one-half the yield deflection for  $\mu = 1$  for the same total deflection, and in general

$$(y_e)_\mu = \frac{1}{\mu} y_e \quad (2.31)$$

Since acceleration response in the elastic range is proportional to stiffness times displacement, the acceleration in the low frequency region will be reduced by  $\frac{1}{\mu}$ , as beyond  $y_e$  the stiffness is zero for the elastic-plastic system. The plastic behavior (in the low frequency region) becomes an asset for the designer in reducing acceleration but the total displacement response which governs rattle space requirements remains the same for all values of  $\mu$ .

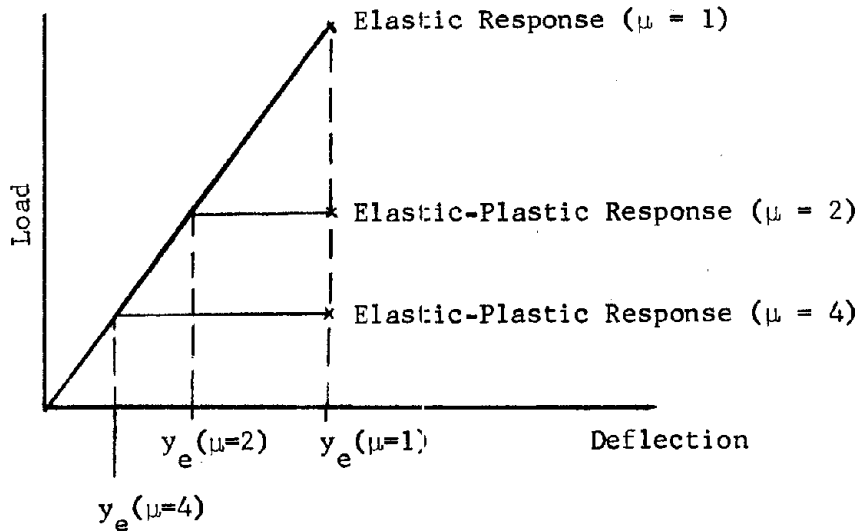


FIGURE 2.12

### High Frequency Region

In the high frequency region the bound on the maximum acceleration response ( $A$ ) for  $\mu = 1$  is  $2(\ddot{x}_s)_{\max}$  where  $(\ddot{x}_s)_{\max}$  is the peak ground acceleration. As  $\mu$  increases, the bound on the response acceleration approaches the ground acceleration, i. e.,  $A \rightarrow (\ddot{x}_s)_{\max}$  as  $\mu$  increases. The total displacement is not constant as  $\mu$  increases. For a shock spectrum with a maximum elastic response acceleration equal to  $2 \ddot{x}_s \max$  the reduction factor,  $C$ , (Reference 2.3) for elastic-plastic response acceleration is given by the approximation:

$$C = \frac{\mu}{2\mu - 1} \quad (2.32)$$

### Intermediate Frequency Region

The form of the input significantly affects the response in this region. The pseudo-velocity response is attenuated by the factor  $\frac{1}{\mu}$  and in some cases the reduction will be greater if the elastic response spectrum ( $\mu = 1$ ) has a high amplification factor, i.e., the ratio  $\frac{V}{(\ddot{x}_s)_{\max}}$  is greater than 1.5. For design purposes the reduction factor  $\frac{1}{\mu}$  has been recommended by Reference 2.3 for the peak pseudo-velocity in the elastic-plastic case.

The above conclusions are shown in Figure 2.13. The smooth curves are taken from Reference 2.4 relating the elastic-plastic response spectrum to the elastic spectrum. If the three regions are defined by straight lines the relationship between the two spectra are shown as dashed lines in the figure.

### 2.5 Relationship of Simple Pulses to Shock Spectra

It was already mentioned that a shock spectrum or spectra envelope does not give information about the times of occurrences of any of the maximum primitive response quantities: displacement, velocity and acceleration. Moreover, it is important to understand that for a definite shock input or pulse train a unique response spectrum always can be computed, but that a response spectrum does not define a unique pulse shape; it may be related even precisely to numerous, differently shaped, shock inputs since it gives only maximum response values.

The waveform parameters that may be predicted by current techniques described in Section 3 are:

- (a) peak ground acceleration ( $a_{\max}$ )
- (b) peak ground velocity ( $v_{\max}$ )
- (c) peak ground displacement ( $d_{\max}$ )
- (d) velocity rise time ( $t_r$ )

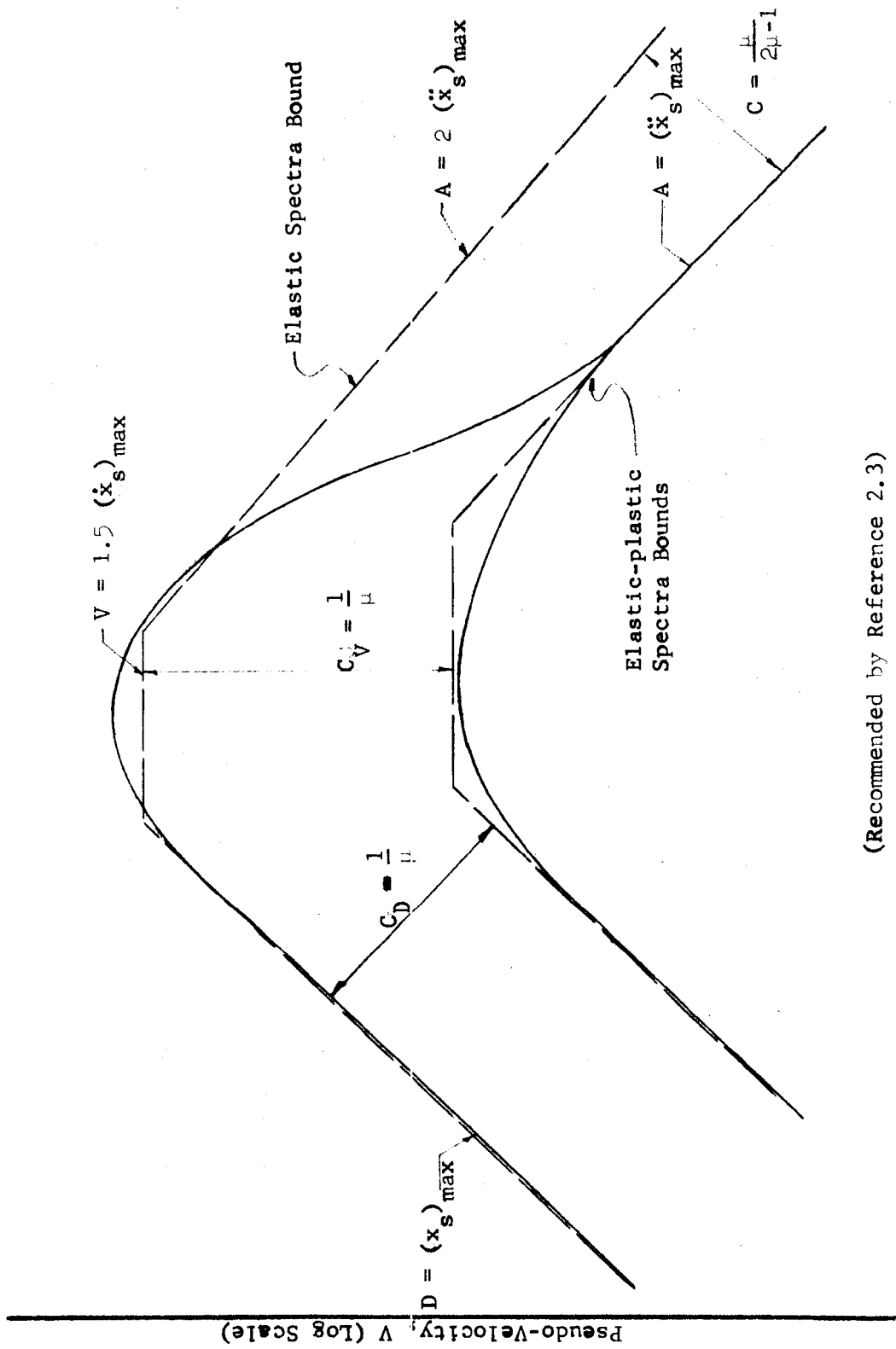


FIGURE 2.13: ELASTIC-PLASTIC SHOCK SPECTRA RELATIONSHIP TO ELASTIC SHOCK SPECTRA

- (e) positive velocity phase duration ( $t^+$ )
- (f) permanent displacement ( $d_p$ )

The confidence placed in each of the predictions varies widely. One further parameter not predictable by current methods, but which has been shown to be important to system response, is the total pulse duration ( $t_d$ ).

In most cases, the magnitudes of these parameters are fixed by such factors as weapon yield, range, seismic velocity, and depth of burial, i.e., the same factors that define the shock spectra. Thus, the waveform in which the designer is interested must be described in terms of these parameters. The effect of variations in these parameters on the response of shock isolation systems, i.e., the effect of pulse duration,  $t_d$ , or shape, as well as phasing of horizontal and vertical components, can be investigated for a given system when they are considered to be important.

Pulse shapes as functions of the above parameters are defined in Section 3. In Sections 4 and 5 conditions requiring dynamic analyses using waveforms as inputs are discussed. A simple pulse will be used here to illustrate how the pulse can be related to the given shock spectra envelope. Moreover the response spectrum for this input pulse will be derived and compared with the given shock spectra.

A ground disturbance,  $d$ , described by a half sine wave of duration  $t_d$  is shown in Figure 2.14.

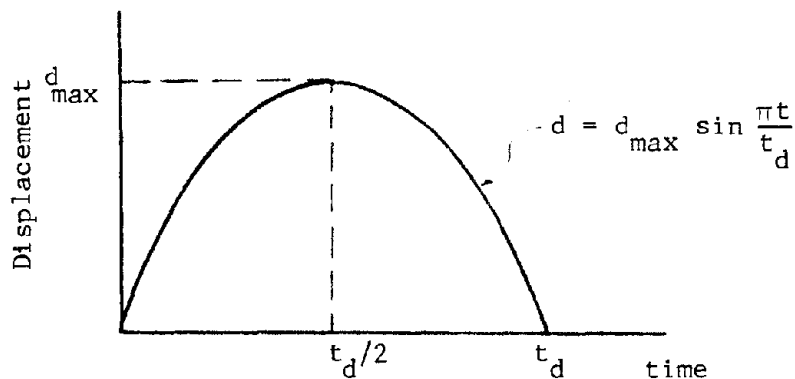


FIGURE 2.14: HALF SINE WAVE GROUND MOTION

The maximum ground displacement ( $d_{\max}$ ) and the time duration ( $t_d$ ) are the only two parameters necessary to define this pulse. The maximum displacement can be assumed to be the response displacement ( $D$ ), defined by the shock spectra, and the time to reach maximum displacement ( $t_d/2$ ) is taken to be the positive phase duration of the velocity ( $t^+$ ). In this particular example the time duration can easily be determined by taking the first derivative of the displacement function and equating the coefficient to the peak ground velocity.

$$v = \frac{\pi d_{\max}}{t_d} \cos \frac{\pi t}{t_d} = v_{\max} \cos \frac{\pi t}{t_d} \quad (2.33)$$

therefore

$$t_d = \frac{\pi d_{\max}}{v_{\max}} \quad (2.34)$$

and  $v_{\max}$  is usually considered to be two-thirds of the peak shock spectra velocity ( $V$ ).

For shock spectra of a linear system, meaning a system with a linear restoring force and linear or viscous damping force, the magnitudes of the specific disturbance and the response maxima are linearly related, and only the shape of the specific disturbance is involved. The maximum relative displacement  $D$  of an undamped responsive system with respect to the ground can be plotted as the ratio  $D/d$  against the ratio of the duration  $t_d$  of the disturbance to the natural period  $T$  of the system. (See Figure 2.15 which is taken from Reference 2.6.)

It is noted that for extremely short durations of the disturbance with respect to the responsive system's period, or for slow systems - the relative displacement ratio is near unity, i.e., the system hardly moves, but if the period ratio  $t_d/T$  is near 0.7 a maximum of relative displacement ratio is obtained. As  $t_d/T$  increases the relative displacement will decrease and be less than unity for values of  $t_d/T$  greater than 1.1. Near the period ratios 2, 3, 4, etc., local bumps or maxima will occur as indicated.

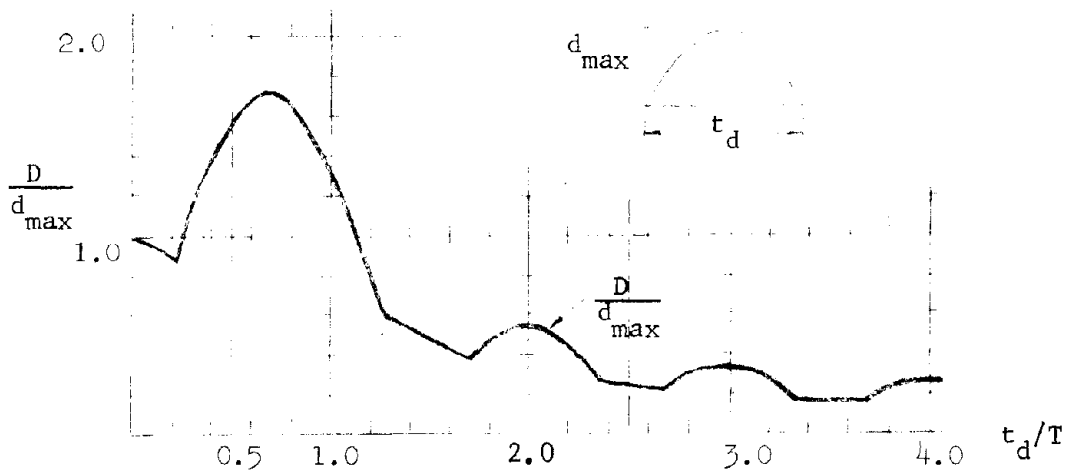


FIGURE 2.15

The parameters of the shock spectra of Figure 2.6 will be used to see how the shock spectrum for this pulse compares with the given shock spectra envelope.

$$d_{\max} = D = 5 \text{ inches}$$

$$v_{\max} = \frac{2}{3} V = \frac{2}{3} \times 50 = 33.4 \text{ in/sec}$$

$$t_d = \frac{\pi \times 5}{33.4} = 0.5 \text{ sec.}$$

Figure 2.16 shows the given shock spectra with the spectrum for the response to the half sine pulse superimposed upon it. This shows that the response for the half sine pulse exceeds the given shock spectra in the frequency region above 0.5 cps due to a partial resonance condition. Therefore if this pulse were considered to be a good representation of the ground motion the designer would have to accept the amplified response in this region.

Input waveforms will be discussed in greater detail in Section 3.



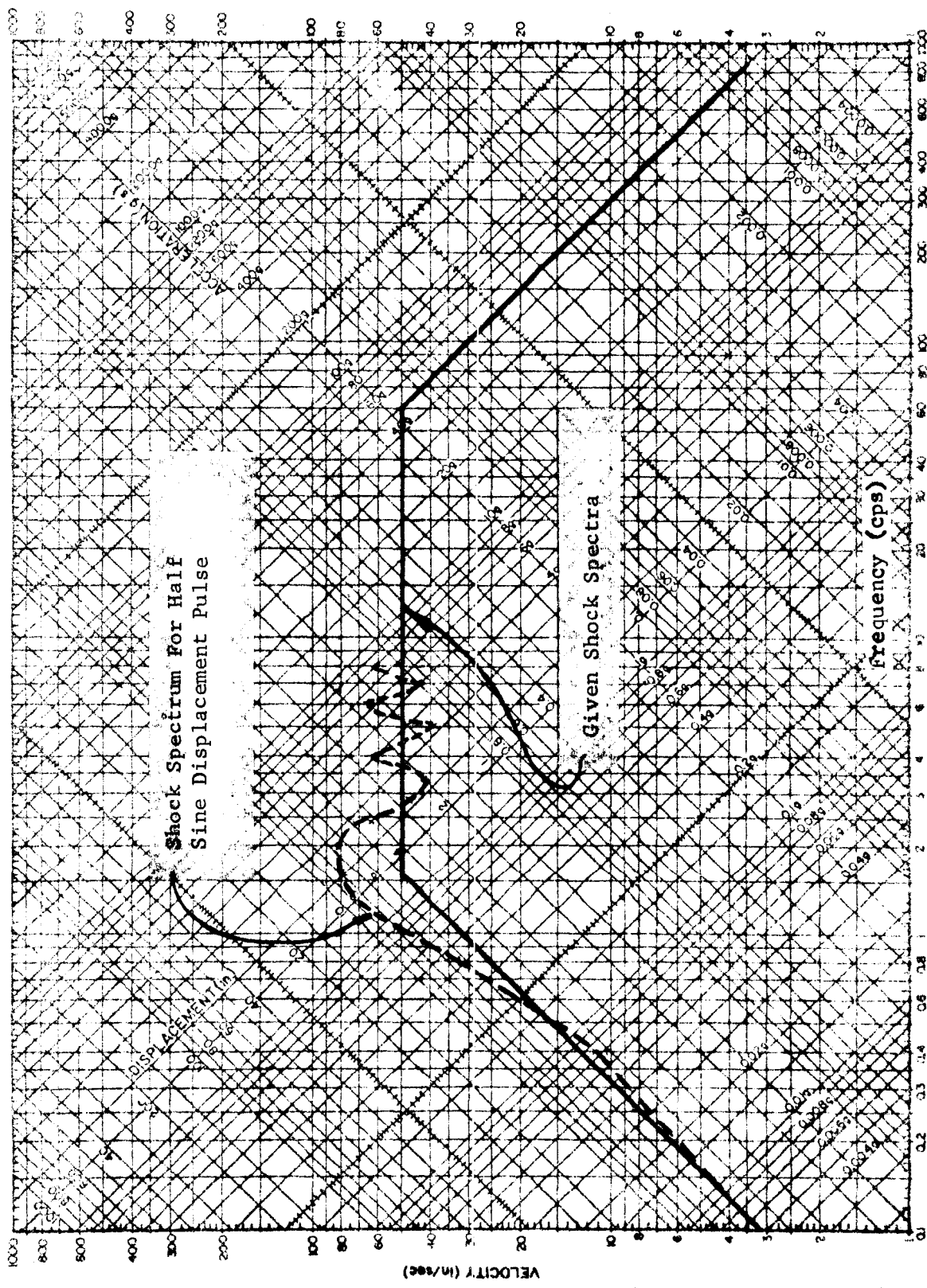


FIGURE 2.16: COMPARISON OF GIVEN SHOCK SPECTRA AND SHOCK SPECTRUM FOR HALF SINE DISPLACEMENT PULSE

## 2.6 Response Analysis Using a Waveform as the Input

The response of a simple system subjected to the indefinite type of input and resulting in the form of a shock response spectra has been described in the previous sections. In some cases a time-history response may be necessary to gain sufficient confidence in the design. For example, a single mass may be supported eccentrically, so that for a simultaneous horizontal and vertical input its response acceleration and required rattlespace can only be determined by computing its time-history response. Examples of real situations with numerical examples for complex systems will be given in Section 5, Shock Isolation Systems. A numerical integration technique which is applicable to a computer solution of a multi-degree-of-freedom system will be illustrated in this section by taking a single-degree-of-freedom system and applying a time-history input to the support thus obtaining the time-history response.

Starting with the single-degree-of-freedom system described in Section 2.2 with viscous damping included and using the same notation as in Section 2.2, Equation (2.2) can be rewritten in the following form (see Figure 2.17):

$$m\ddot{x}_s + ky + c\dot{y} = -m \frac{d(\dot{y})}{dt} \quad (2.35)$$

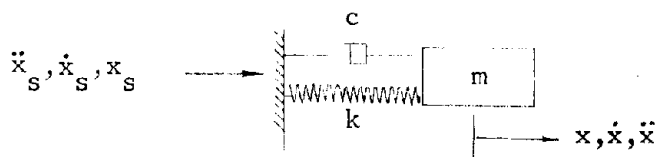


FIGURE 2.17

Multiplying both sides by  $dt$  and integrating between corresponding values of  $t$  and  $y$ :

$$\int_{t_1}^{t_2} (m\ddot{x}_s + ky + c\dot{y}) dt = \int_{\dot{y}_1}^{\dot{y}_2} -m d(\dot{y}) \quad (2.36)$$

the impulse and momentum relationship is obtained:

$$\int_{t_1}^{t_2} F dt = -m (\dot{y}_2 - \dot{y}_1) \quad (2.37)$$

where  $F = (m\ddot{x}_s + ky + c\dot{y})$  is the systemic force during the time interval  $t_2 - t_1$ . For small intervals of time the area under the force-time curve can be approximated by:

$$\int_{t_1}^{t_2} F dt = \frac{F_1 + F_2}{2} \Delta t \quad (2.38)$$

We now can relate the response at time  $t_2$  to the response at time  $t_1$ . This permits a stepwise process in calculating the time-history response wherein the calculated values at the end of one time interval are used as initial conditions for the next time interval.

The response relative acceleration  $\ddot{y}$ , velocity  $\dot{y}$  and displacement  $y$  can also be related between time intervals by the same averaging technique in deriving Equation 2.38. Thus,

$$\dot{y}_2 = \frac{2}{\Delta t} (y_2 - y_1) - \dot{y}_1 \quad (2.39)$$

and

$$\ddot{y}_2 = \frac{2}{\Delta t} (\dot{y}_2 - \dot{y}_1) - \ddot{y}_1 \quad (2.40)$$

Making the proper substitutions into Equation (2.37), the following expression is obtained for computing the relative displacement ( $y_2$ ) at time  $t_2$  with respect to the known response at time  $t_1$

$$\left(\frac{4m}{\Delta t} + 2c + k \Delta t\right) y_2 = \left(\frac{4m}{\Delta t} + 2c - k \Delta t\right) y_1 + 4m \dot{y}_1 - 2m (\ddot{x}_{s2} - \ddot{x}_{s1}) \quad (2.41)$$

The accuracy obtained depends on the time interval chosen. The shape of the forcing function and the natural period of the system should be considered when a time interval is selected for computation. Usually an interval equal to  $\frac{1}{10}$  of the natural period will provide sufficient accuracy for most purposes.

The above method is a direct approach requiring only one step solution per time increment; iterations or corrections are not made. Although Equation 2.41 uses the input in the form of a velocity pulse, other forms for specifying input, e.g., acceleration time-history, may be used without any great advantage of one method over another.

A brief description of the  $\beta$ -Method (an iterative numerical integration method) is now presented since it is widely used in solving civil engineering dynamic problems. It is more accurate than the one step method presented above because of the iterative nature of the procedure (Reference 2.7).

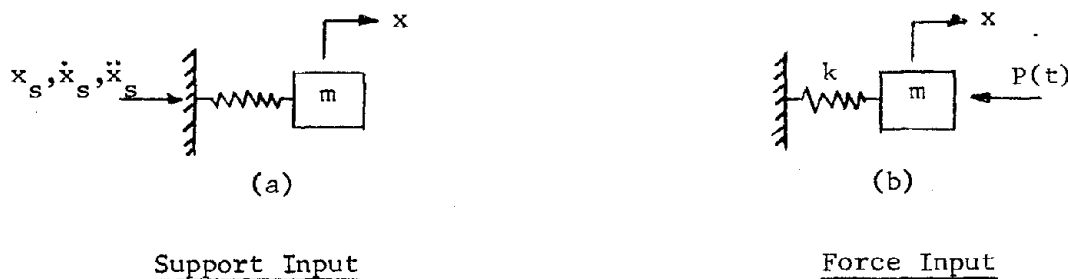


FIGURE 2.18

Figure 2.18 shows the two typical conditions for (a) input at the support and (b) force applied to the mass. If relative motions are considered in case (a), then the equations of motion are of the same form for the two cases.

$$(a) \quad m\ddot{y} + ky = -m\ddot{x}_s(t)$$

$$(b) \quad m\ddot{x} + kx = P(t)$$

The generalized form of the integration equations are:

(The subscripts refer to time period, 1 and 2, respectively.)

$$\ddot{y}_2 = \frac{-m\ddot{x}_s(t) - ky_2}{m} \quad \ddot{x}_2 = \frac{P(t) - kx_2}{m} \quad (2.42)$$

$$\dot{y}_2 = \dot{y}_1 + \frac{\Delta t}{2} (\ddot{y}_1 + \ddot{y}_2) \quad \dot{x}_2 = \dot{x}_1 + \frac{\Delta t}{2} (\ddot{x}_1 + \ddot{x}_2) \quad (2.43)$$

$$\begin{aligned} y_2 = y_1 + \Delta t \dot{y}_1 + (\Delta t)^2 (1/2 - \beta) \ddot{y}_1 & \quad x_2 = x_1 + \Delta t \dot{x}_1 + (\Delta t)^2 (1/2 - \beta) \ddot{x}_1 \\ + (\Delta t)^2 \beta \ddot{y}_2 & \quad + (\Delta t)^2 \beta \ddot{x}_2 \end{aligned} \quad (2.44)$$

In the above equations the parameter  $\beta$  must be chosen and it is associated with the acceleration-time curve. The  $\beta$  value equal to 1/6 assumes a linear variation in acceleration over the chosen time interval. This value has been widely used in solving structural dynamic problems. The reader is referred to References 2.7 and 2.8 for a complete discussion of the proper value of  $\beta$  for specific applications.

The equations are solved by successive approximation over each time interval. The steps are:

- (a) Assume  $\ddot{y}_2$  (a first guess of  $y_2 = y_1$  is usually assumed)
- (b) Compute  $\dot{y}_2$  from Equation (2.43)
- (c) Compute  $y_2$  from Equation (2.44)
- (d) Compute  $\ddot{y}_2$  from Equation (2.42)
- (e) Compare  $\ddot{y}_2$  from step (d) with assumed value in step (a). Use step (d) computed value of  $\ddot{y}_2$  as new assumed value and repeat steps (b) through (d) until the computed value for  $\ddot{y}_2$  agrees with the assumed value of  $\ddot{y}_2$  to the desired occupancy.

The above methods (and similar but more accurate numerical integration methods) can be used in computing the response of multi-degree-of-freedom systems. A predictor-corrector method is described in Appendix C. Instead of one equation, such as Equation (2.41), a set of simultaneous equations are solved for the stepwise response. The numerical integration method is very laborious if a slide rule or desk calculator are the only tools available, but with high speed electronic computers this form of solution is feasible. Although Equation (2.41) is for a constant spring

rate,  $k$ , over the whole range of response, a non-linear (elastic or hysteretic) spring can be averaged for each time interval in the same way as the load function was averaged over each time interval. The following example illustrates this technique using the one step method.

Example 2.2

Given:  $f = 1$  cps  
 $m = 1$  lb. sec<sup>2</sup>/in  
 $c = 2$  lb. sec/in  
 $k = 39.4$  lb/in

and the velocity pulse shown in Figure 2.19

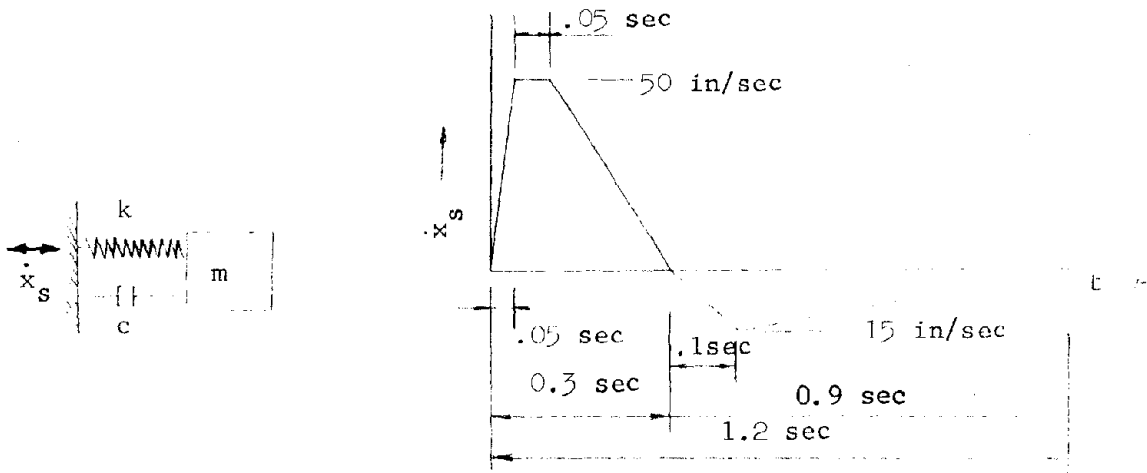


FIGURE 2.19

Substitute the above constants into Equation (2.41).

Use  $\Delta t = .05$  sec for the first two time steps and

$\Delta t = .1$  sec thereafter

Steps (1 and 2)  $y_2 = .9541 y_1 + .0465 \dot{y}_1 - .0233 (\dot{x}_{s2} - \dot{x}_{s1})$

Steps (3,4,---)  $y_2 = .8356 y_1 + .0834 \dot{y}_1 - .0417 (\dot{x}_{s2} - \dot{x}_{s1})$

$$\dot{y}_2 = \frac{2}{\Delta t} (y_2 - y_1) - \dot{y}_1$$

Table 2.1 gives the response values for 13 steps and Figure 2.20 is a plot of the relative displacement and velocity of the mass.

Example 2.2 (Continued)

TABLE 2.1

STEP	TIME INTERVAL	$\dot{x}_{s2} - \dot{x}_{s1}$	$y_1$	$\dot{y}_1$	$y_2$	$\dot{y}_2$
1	.05	50	0	0	- 1.1650	- 46.6000
2	.05	0	- 1.1650	- 46.6000	- 3.2784	- 37.9360
3	.10	- 25	- 3.2784	- 37.9360	- 4.8607	+ 6.2900
4	.10	- 25	- 4.8607	+ 6.2900	- 2.4946	+ 41.0320
5	.10	- 15	- 2.4946	+ 41.0320	+ 1.9631	+ 48.1220
6	.10	+ 1.8750	+ 1.9631	+ 48.1220	+ 5.5755	+ 24.1260
7	.10	+ 1.8750	+ 5.5755	+ 24.1260	+ 6.5928	- 3.7800
8	.10	+ 1.8750	+ 6.5928	- 3.7800	+ 5.1156	- 25.7640
9	.10	+ 1.8750	+ 5.1156	- 25.7640	+ 2.0477	- 35.5940
10	.10	+ 1.8750	+ 2.0477	- 35.5940	- 1.3356	- 32.0720
11	.10	+ 1.8750	- 1.3356	- 32.0720	- 3.8689	- 18.5940
12	.10	+ 1.8750	- 3.8689	- 18.5940	- 4.8616	- 1.2600
13	.10	+ 1.8750	- 4.8616	- 1.2600	- 4.2454	+ 13.5840

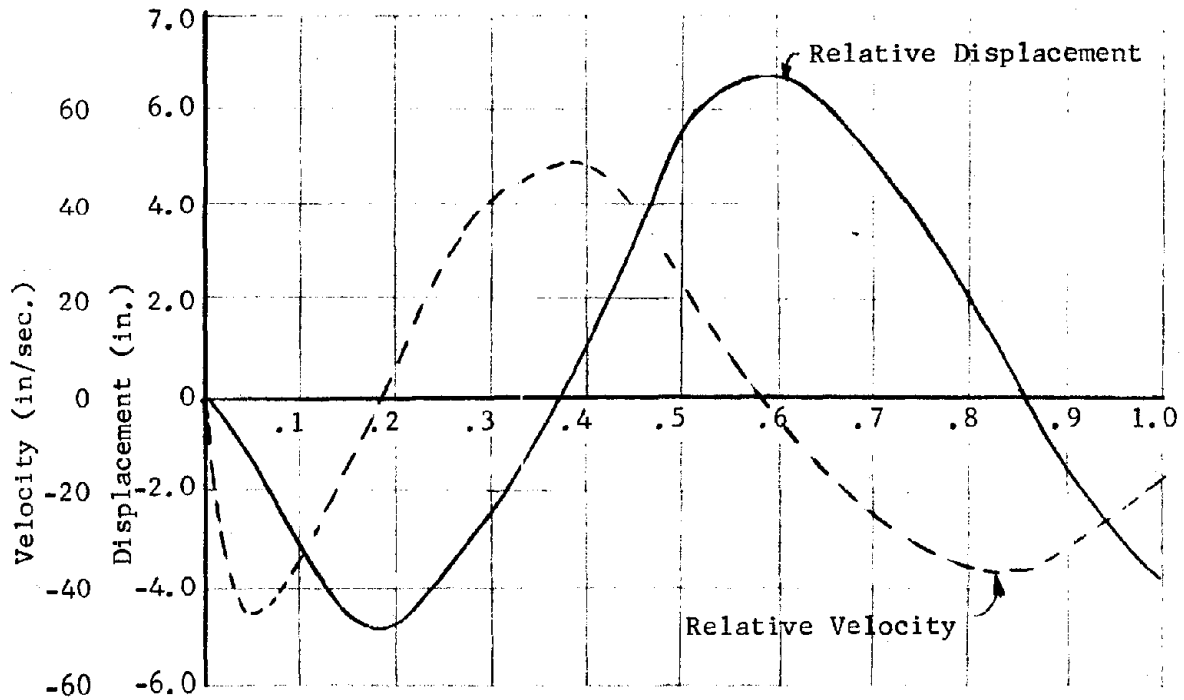


FIGURE 2.20

## 2.7 Texts on Principles of Shock Isolation

In Section 2 only some of the basic concepts on shock isolation have been included. These concepts are developed further in subsequent sections and are applied to the design and analysis of systems that must survive the air blast and ground induced motions. Section 3 covers the ground motions resulting from weapon effects. The air blast characteristics are based on the work by Brode (Reference 2.9) and applied in the report by direct reference. Section 4 considers the structure response to both the air blast impingement and ground motion in arriving at a resultant motion to equipment or platforms attached to the structure. Shock isolation system design and analysis methods are discussed in Section 5 and the types of spring isolators used in shock isolation systems are covered in Section 6. The reader should consult texts on principles of shock isolation and vibrations for additional background. References 2.6, 2.10 and 2.11 are particularly recommended.



## SECTION 3: GROUND MOTIONS

### 3.1 Introduction

Structures located on or extending to the surface will experience loadings due to the air borne shock wave as well as to seismic or ground borne disturbances coming through its foundations, but a fully buried structure will receive only seismic disturbances.

Our knowledge of air borne or shock wave overpressures for different types of nuclear weapon bursts, yields, times and locations from ground zero is relatively precise. The corresponding particle or wind velocities and the reflection pressures may be obtained from numerous references (cf Ref 3.1 and 3.4). This section relates only to ground motions.

Seismic disturbances emanate from the initial, almost instantaneous and almost point pressure source located above or below ground zero as well as from an expanding, relatively narrow, and intense air pressure ring load, coincident with the moving air shock wave front and followed by a less intense air pressure area load. The "point" pressure at ground zero initiates a direct seismic wave disturbance that may be reflected and refracted by underlying strata before it arrives at the structure, but the expanding narrow and intense ring load on the surface will continue, as it expands, to generate or induce seismic waves of diminishing intensity. Since the propagational velocity of the expanding ring loading gradually approaches the acoustic value in air it is certain that the initial direct seismic wave generated by the "point" load from ground zero as well as the ring load induced seismic wave will outrun the air shock front if the effective seismic velocities of the ground are significantly higher than the air shock wave's terminal velocity of about 1100 fps. In fact outrunning occurs whenever the near surface seismic velocity is greater than the velocity of the air blast front. Since seismic motions attenuate more rapidly with distance from ground zero than the overpressure, the air blast and the induced seismic waves will be of primary concern at large distances. At closer in regions where only buried facilities are feasible the direct

seismic disturbances will gain in importance.

There are three basic ground motion characteristics that must be known in order to define adequately the input motions to shock isolated systems: (a) the times of arrival of air borne and seismic waves from which the phasing of the various loading phenomena may be determined; (b) the peak intensities of the dynamic stresses and motions associated with the various sources of excitations, and (c) the time-dependent functions defining the buildup and decay of stresses and motions.

Ideally, a general solution giving the values of all three sets of data would be the most consistent and unified method by which the ground motion characteristics could be defined. Only partial progress has been made, however, along these lines, and solutions are available only for idealized conditions that do not correspond well with the real situation in a rock or soil medium. The results are not, therefore, applicable directly to the design of shock isolation systems. The approach that will be taken in this report is semi-empirical. Mathematical elegance is sacrificed where warranted in order to arrive at results for which fairly adequate substantiation exists from field test data. Also, rather than seeking a general solution that gives the complete time history and intensities of stresses and motions of ground environment, three separate and more or less independent methods will be used to arrive at the three basic sets of data, which, briefly stated, are the times of arrival, peak intensities, and waveforms of the ground motions and associated stresses. The justification for this simpler approach is the fact that empirical data may be used for each set of data without affecting the other two, thereby making the best use of the limited amount of information available from tests. The resulting inconsistency in the mathematical techniques for the three areas of interest is more than offset by achieving results that are consistent with test observations in real media.

This section will, therefore, be developed in three parts: by principles of wave propagation the times of arrival of airborne and seismic waves will be obtained; by using simple empirical relationships and test data the peak intensities of displacement, velocity, accelerations, and stress will be calculated; and by intuitive reasoning and test data, simple

mathematical relationships, depicting the ground motion time history, will be given. The most useful part of this section, 3.5, dealing explicitly with numerical values of ground motion, can be readily understood.

In other sections of the report, the use of these parameters in calculating the motion of the enclosing structure and in obtaining the response of shock isolation systems will be explained.

For some practical purposes of ground motion application to design problems it may not be necessary to read Subsections 3.2, 3.3, and 3.4 since these sections have been included so as to provide a deeper understanding of the phenomena than normally can be expected of people whose practical design duties do not warrant the effort required to have comprehensive understanding.

### 3.2 Times of Arrival of Ground Disturbances

3.2.1 Multiple seismic waves. An understanding of seismic wave propagation is necessary for assessing the input motions and to gain insight as to the arrival sequence or phasing of the initially upward motion of seismic origin and the initially downward motion of air pressure origin. Some facilities are very sensitive to initially upward accelerations. A secondary purpose of the study is to show that the effect of a multilayering system, exhibiting seismic velocity increases with depth, is to channel or to redirect nearly all the half space energy flux to the surface, thereby reducing the dispersive attenuation of dilatational and shear waves to one of two dimensions rather than of three. The following terminology will be used:

- a. Direct seismic waves originate instantaneously at ground zero GZ or near the edge of crater, they propagate entirely through the ground to the station in question, suffering reflections and refractions at material interfaces.
- b. Induced seismic waves originate continuously at the leading edge of the expanding ring load of the air pressure, they propagate entirely through the ground to the station in question, suffering reflections and refractions at material interfaces.

- c. Dilatational or push-pull seismic waves involve periodic changes in the volume of the half space material through which they propagate.
- d. Distortional or shear seismic waves involve only distortion of the half space material through which they propagate. Their displacements are transverse to their direction of propagation.
- e. Surface or Rayleigh seismic waves involve dilatation as well as distortion of the half space material through which they propagate relatively close to the surface. They exhibit elliptical displacements in vertical planes.

Due to the fact that many facilities are very sensitive to initially upward impulsive motions and such motions will result from refracted-reflected phenomena in stratified half spaces, it is of importance to determine whether or not these upward motions will arrive at a specific location before the arrival of blast overpressure. If this occurs the seismic waves are spoken of as outrunning the overpressure, and phasing of the two motions will be required.

A very rough qualitative idea of the multiple possibilities of seismic waves arriving at various locations in a stratified half space can be obtained by considering Figure 3.1 in which four facilities have been located. A more quantitative treatment of seismic wave travel will then follow.

In Figure 3.1, the symbols are defined as:

- $T_n$  = transmitted or refracted wave from layer n
- $R_{n-m}$  = reflected wave from interface n - m
- $TR_{n-m}$  = critically refracted-reflected wave through interface n, m
- p = overpressure wave

This schematic diagram does not include either shear wave or Rayleigh wave generation at interfaces or near the surface. Four facilities, differently located with respect to ground zero and surface are shown with a few of their seismic ray paths indicated. Depending on geological stratification and on the yield of a nuclear burst, the direct\* and/or the blast front induced seismic waves may outrun the expanding blast wave front. A very rough qualitative tabulation of possible waves at the four facilities

---

\* Direct seismic waves will also be referred to as crater induced.

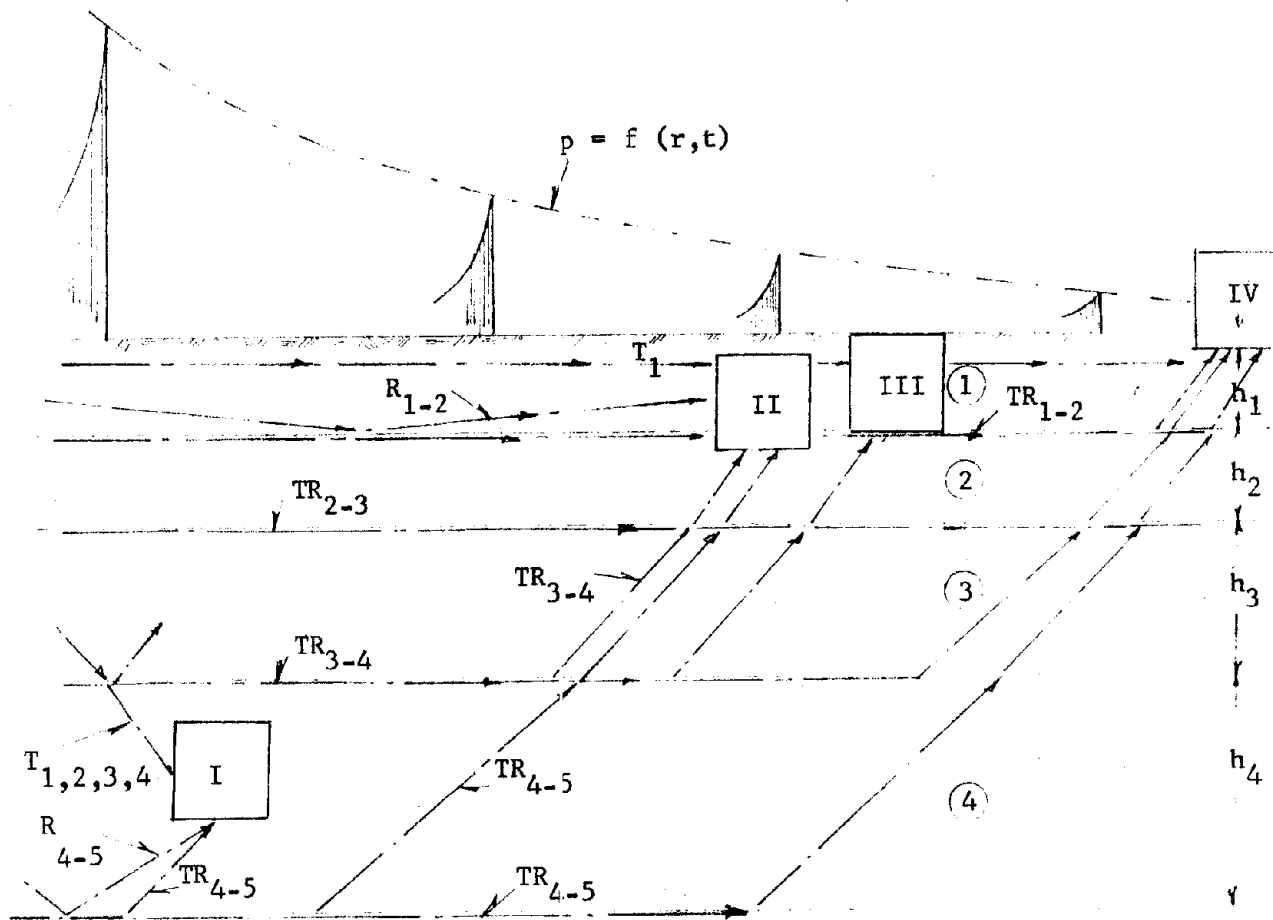


FIGURE 3.1

is shown in Table 3.1. The indicated degree of importance is relative with respect to each facility and category of generation, moreover, it will depend on the quantitative aspects of the stratification.

### 3.2.2 Generation of Seismic Waves by a "Stationary Point" Source on the Surface of an Elastic Half Space

3.2.2.1 Types of seismic waves generated. A suddenly applied, normal, point load will cause rupture or cratering at its point of application on the surface and thereby generate displacement disturbances in the surrounding unruptured elastic half space. Dilatational or volumetric change types of elastic waves as well as shear or purely distortional change types of elastic

Table 3.1  
Multiple Seismic Waves Arriving at Four Facilities

Facility	Type of Wave	Crater Induced	Degree of Importance	Blast Front Induced
I Deep close in	T <sub>1,2,3,4</sub>	down - radial	High	down - radial
	R <sub>4-5</sub>	up - radial	Low	up - radial
	TR <sub>4-5</sub>	up - radial	Medium	up - radial
II Shallow burial	T <sub>1</sub>	radial	High	down - radial
	R <sub>1-2</sub>	radial - up	Medium	down - radial
	R <sub>2-3</sub>	radial - up	Medium low	radial - up
	R <sub>3-4</sub>	up - radial	Low	up - radial
	R <sub>4-5</sub>	up - radial	Very low	up - radial
	TR <sub>1-2</sub>	radial - down	High	radial - down
	TR <sub>2-3</sub>	up - radial	Medium	up - radial
	TR <sub>3-4</sub>	up - radial	Medium low	up - radial
III Flush with ground	T <sub>1</sub>	radial	Medium high	down - radial
	R <sub>1-2</sub>	radial - up	Medium low	radial - up
	R <sub>2-3</sub>	radial - up	Low	radial - up
	R <sub>3-4</sub>	up - radial	Very low	up - radial
	R <sub>4-5</sub>	up - radial	Negligible	up - radial
	TR <sub>1-2</sub>	radial	Medium high	radial - down
	TR <sub>2-3</sub>	up - radial	Medium low	up - radial
	TR <sub>3-4</sub>	up - radial	Low	up - radial
	TR <sub>4-5</sub>	up - radial	Very low	up - radial
	P	none	Very high	down
IV Above ground	T <sub>1</sub>	radial	Low	radial - up
	R <sub>1-2</sub>	radial - up	Very low	radial - up
	R <sub>2-3</sub>	up - radial	Negligible	up - radial
	R <sub>3-4</sub>	up - radial	Negligible	up - radial
	R <sub>4-5</sub>	up - radial	Negligible	up - radial
	TR <sub>1-2</sub>	up - radial	Low	up - radial
	TR <sub>2-3</sub>	up - radial	Very low	up - radial
	TR <sub>3-4</sub>	up - radial	Negligible	up - radial
	TR <sub>4-5</sub>	up - radial	Negligible	up - radial
	P	none	Very high	radial - down

waves will then radiate away from the rupturing region into the half space. Seismic waves generated by a stationary point source are idealized cases of direct seismic waves from ground zero of a nuclear detonation.

Due to the fact that the degree of confinement of the elastic material in the half space is a function of its nearness to the free surface, the dilatational and shear waves will experience changes in environment as they approach the surface. Demanding that normal forces as well as shear forces must vanish at the unloaded surface of the elastic half space, Lord Rayleigh in 1887 demonstrated that it is essential to have waves of a different type from dilatational and shear waves. These waves are propagated over the surface, and they penetrate only a small distance into the half space. They are similar in type to waves produced on a smooth surface of a pond by an object falling into the water. Since these Rayleigh waves may be considered two dimensional they will attenuate less with distance than three dimensional waves, and therefore they will gain in relative importance with respect to the former as the distance from the stationary point source increases.

It will be shown later that the three dimensional dispersion of dilatational and shear waves in a layered half space is greatly modified by the seismic velocity properties of the layers. Since in general the seismic velocities increase with depth, the effect is to refract the seismic energy in such a way that travel paths initially downwards will be bent upwards and reach the surface at various distances from their point of origin. This phenomenon therefore tends to make the seismic phenomena of importance two dimensional or quasi-two dimensional in explosion dynamics.

### 3.2.2.2 Seismic propagational velocities.

Let  $E$  = modulus of elasticity of medium  
 $\nu$  = Poisson's ratio of medium  
 $G$  = modulus of shear of medium  
 $\rho$  = mass density of medium  
 $c$  = seismic velocity of dilatational waves  
 $c_s$  = seismic velocity of shear waves  
 $c_R$  = seismic velocity of Rayleigh waves

The propagational speed of the dilatational or axial wave in an elastic rod is given by  $(E/\rho)^{1/2}$ , but in an elastic space it is:

$$c = \left[ \frac{2(1-\nu)}{1-2\nu} \right]^{1/2} \sqrt{G/\rho} = \left[ \frac{1-\nu}{(1+\nu)(1-2\nu)} \right]^{1/2} \sqrt{E/\rho} \quad (3.1)$$

$$= \begin{cases} 1.055 \\ 1.095 \\ 1.161 \end{cases} \sqrt{E/\rho} \quad \text{for } \nu = \begin{cases} 0.20 \\ 0.25 \\ 0.30 \end{cases}$$

In other words, the spatial "confinement" will increase the speed  $c$  from 6 to 16 percent. Unlike the dilatational wave the distortional or shear wave has the same propagational speed in one, two or three dimensions, namely  $c_s = (G/\rho)^{1/2}$ . The propagational speed of the Rayleigh surface wave is given by  $c_R = 0.919 c_s$  for  $\nu = 0.25$ . Moreover, it can be shown that the ratio of the horizontal to the vertical displacement of the Rayleigh waves is constant and equal to 0.681 for  $\nu = 0.25$ .

**3.2.2.3 Reflection and refraction.** In general an incident wave at a boundary, of either the dilatational or the shear type, will produce a pair of reflected and a pair of refracted waves. Each pair will consist of a dilatational wave and a shear wave. The angle of incidence together with the four constants of wave velocities in the two media adjacent to the boundary will determine the two angles of reflection and the two angles of refraction as well as the amplitude relationships of the four generated waves. The boundaries between half space media are considered to be infinitely thin, slip free, horizontal planes, and two boundary conditions arise:

- a. Free boundary, i.e. second medium a vacuum or air.
- b. Interface boundary between two media.

Two angle of incidence situations, relating to interface boundaries, are possible:

- a. Ordinary refraction-reflection (angle of incidence  $\neq$  critical).
- b. Critical refraction-reflection (angle of incidence = critical).

Referring to Figure 3.2 let  $c_1$  and  $c_{s1}$  be dilatational and shear wave speeds in medium (a), while  $c_2$  and  $c_{s2}$  relate to similar speeds in medium (b).



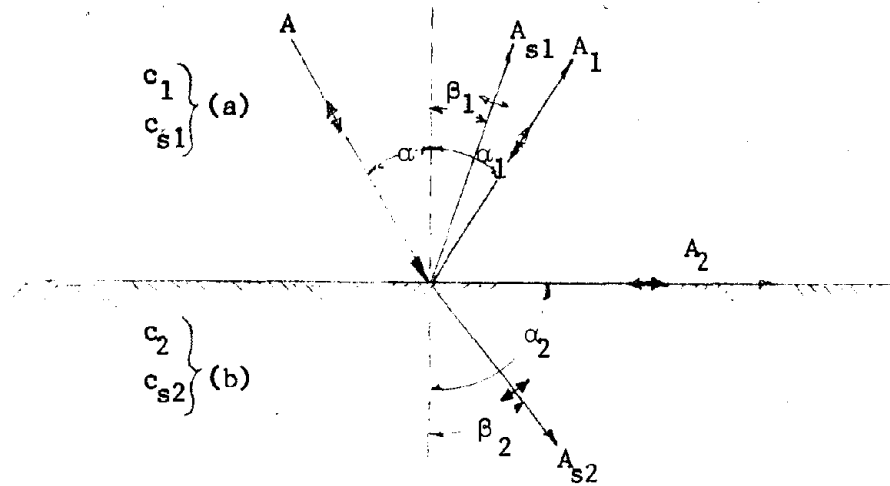


FIGURE 3.2 DILATATIONAL WAVE CRITICAL REFRACTION-REFLECTION

For a dilatational wave of amplitude  $A$  incident at angle  $\alpha$  the relationships are:

$$\frac{\sin \alpha}{c_1} = \frac{\sin \alpha_1}{c_1} = \frac{\sin \beta_1}{c_{s1}} = \frac{\sin \alpha_2}{c_2} = \frac{\sin \beta_2}{c_{s2}} \quad (3.2)$$

where  $\alpha_1$  and  $\alpha_2$  are the angles of reflection and refraction of the dilatational components respectively and  $\beta_1$  and  $\beta_2$  are similar angles for the shear components.

When  $\alpha_2 = 90^\circ$  criticality occurs, then if

$$c_1 = 1000 \text{ fps}, \quad c_{s1} = 633 \text{ fps}$$

$$c_2 = 2000 \text{ fps}, \quad c_{s2} = 1267 \text{ fps}$$

$$\frac{\sin \alpha}{1000} = \frac{\sin \alpha_2}{2000} = \frac{1}{2000}; \quad \text{Criticality occurs when } \alpha = 30^\circ$$

$$\frac{\sin \alpha}{1000} = \frac{\sin \beta_1}{633}; \quad \sin \beta_1 = 0.3165 \quad \beta_1 = 18\frac{1}{2}^\circ$$

$$\frac{\sin \alpha}{1000} = \frac{\sin \beta_2}{1267}; \quad \sin \beta_2 = 0.633 \quad \beta_2 = 39^\circ$$

Consequently for  $c_1/c_2 = 0.5$  the critical angle of incidence for the dilatational wave is  $30^\circ$ .

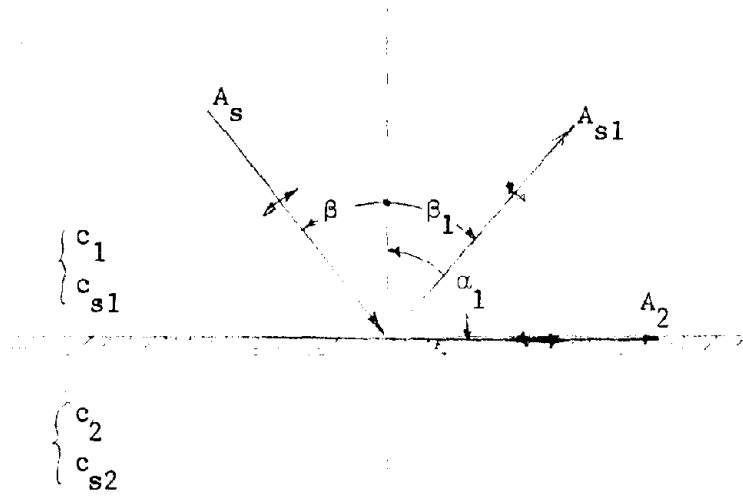


FIGURE 3.3 SHEAR WAVE CRITICAL REFRACTION-REFLECTION

Referring to Figure 3.3, consider a shear wave of amplitude  $A_s$  incident at angle  $\beta$ . Then

$$\frac{\sin \beta}{c_{s1}} = \frac{\sin \beta_1}{c_{s1}} = \frac{\sin \alpha_1}{c_1} = \frac{\sin \alpha_2}{c_2} = \frac{\sin \beta_2}{c_{s2}} \quad (3.3)$$

When  $\alpha_1 = 90^\circ$  criticality occurs, then if

$$c_1 = 1000 \text{ fps}, \quad c_{s1} = 633 \text{ fps}$$

$$c_2 = 2000 \text{ fps}, \quad c_{s2} = 1267 \text{ fps}$$

It is seen that  $\beta = \beta_1$ , and

$$\frac{\sin \beta}{633} = \frac{\sin \alpha_1}{1000} = \frac{1}{1000};$$

This means that  $\beta = 39^\circ$ . Since

$$\frac{\sin \beta}{633} = \frac{\sin \alpha_2}{2000} = \frac{\sin \beta_2}{1267},$$

$\alpha_2$  and  $\beta_2$  are not real. Therefore, total reflection of the shear wave for  $c_{s1}/c_{s2} = 0.5$  will occur when  $\beta = 39^\circ$ .

For angles of incidence larger than the criticals the reflection-refraction phenomena become rather involved.

The critical situation, especially for the incident dilatational wave, is of considerable interest in a study of input motions.

3.2.2.4 Simplified dilatational wave travel for layered space.

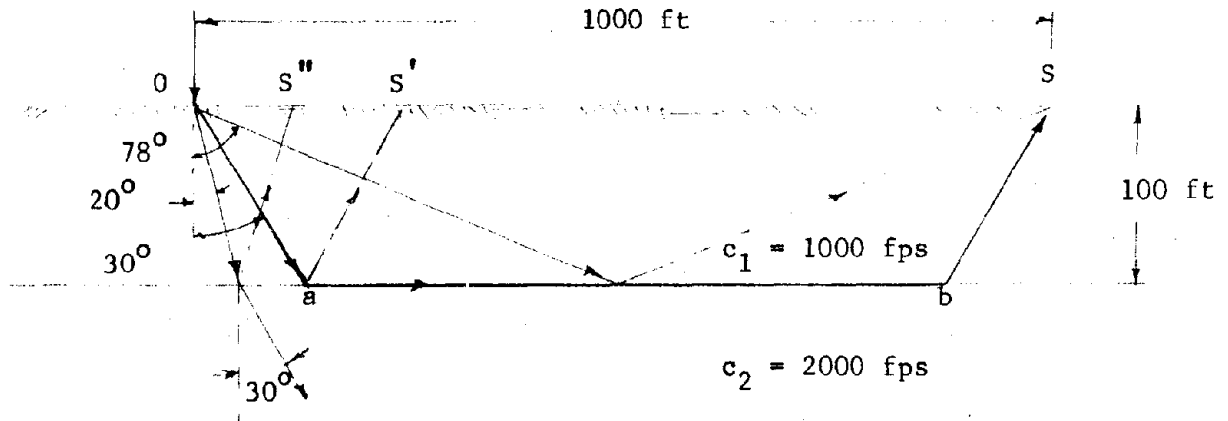


FIGURE 3.4

Figure 3.4 shows a two layered space. At time  $t = 0$  a disturbance occurs at point 0. If surface waves are neglected the direct wave arrives at station S, 1000 feet away from C, in 1 second. The first reflected wave, at incidence angle of  $78^\circ$ , will arrive at S in  $(1000/\cos 78^\circ)/1000 = 1.02$  seconds. At the critical incidence of  $30^\circ$  the first reflected wave will reach the surface at S' in  $2 (100/\cos 30^\circ)/1000 = 0.231$  seconds. But the critically refracted wave, a layer-interface-wave, will travel from a to b with the speed of the lower medium, or 2000 fps. The distance a b is  $1000 - 200 \tan 30^\circ = 984$  ft. Accordingly the arrival time at S of the critically refracted wave, following the path 0 a b S, will be

$$0.231 + 984/2000 = 0.231 + 0.492 = 0.723 \text{ seconds}$$

or 0.277 seconds ahead of the direct wave from 0 to S.

For smaller angles of incidence than the critical, say for  $20^\circ$ , the first reflected wave will reach the surface at S'' in 0.213 seconds, and its refracted part, entering into the 2000 fps. medium, will not reach the surface unless it is reflected from a lower layer.

The capability of an underlying, faster stratum to transmit a wave disturbance to station S ahead of the direct wave is of considerable importance in a study of input motions since it governs outrunning and consequent phasing of disturbances.

Wave travel curves in two layer space may be plotted as shown in Figure 3.5.

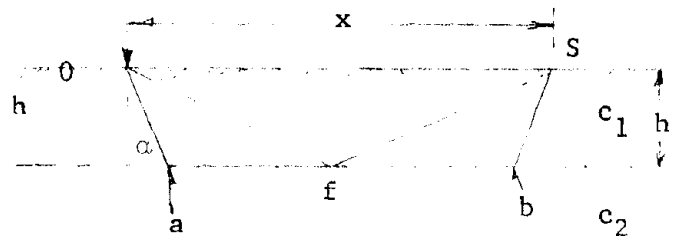


FIGURE 3.5

Waves are sent out at O and arrive primarily by three paths at location S, x feet distant from O:

direct wave, O to S, requiring  $x/c_1$  or  $t_d$  seconds

first reflected, Ofs, requiring  $\frac{1}{c_1} \sqrt{x^2 + 4h^2}$  or  $t_r$  seconds

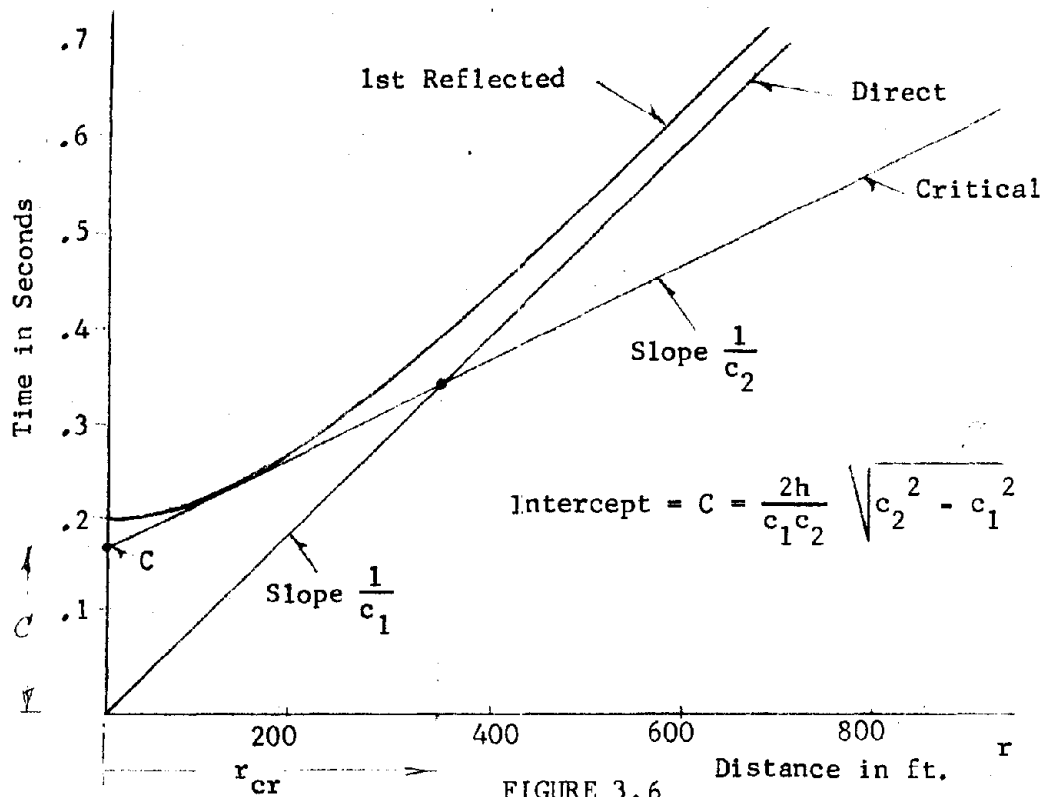
critical, OabS, requiring  $\frac{2h}{c_1 c_2} \sqrt{c_2^2 - c_1^2} + \frac{x}{c_2} = t_{cr}$  seconds

Example 3.1

Let  $c_1 = 1000$  fps     $c_2 = 2000$  fps     $h = 100$  ft.     $x = 450$  ft.

Figure 3.6 shows the seismic wave travel diagram for Example 3.1.

Example 3.1 (continued)



The critical distance  $r_{cr}$  is the distance at which the direct wave traveling at velocity  $c_1$  and the critical refracted-reflected wave arrive simultaneously, it is given by

$$r_{cr} = 2h \sqrt{\frac{c_2 + c_1}{c_2 - c_1}} \approx 350 \text{ ft.} \quad (3.4)$$

The critical travel time from 0 to S is

$$t_{cr} = \frac{2h}{c_1 c_2} \sqrt{c_2^2 - c_1^2} + \frac{x}{c_2} = 0.4 \text{ sec} \quad (3.5)$$

this wave therefore arrives at the target S ahead of the direct wave as is seen from Figure 3.6.

Example 3.2

Figure 3.7 shows a multilayered half space in which critically refracted wave travels occur and in which the intercept constants  $C_1, C_2, C_3,$  and  $C_4$  are given by:

Example 3.2 (continued)

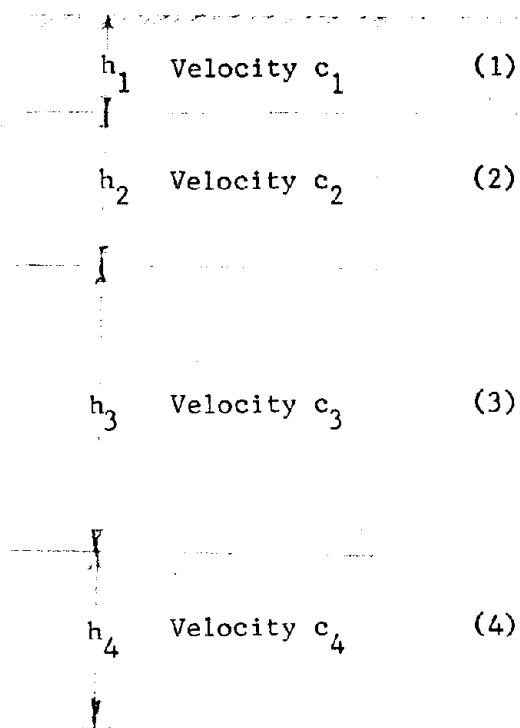


FIGURE 3.7

$$\begin{aligned}
 c_0 &= 0 \\
 c_1 &= 2h_1 \frac{\sqrt{c_2^2 - c_1^2}}{c_2 c_1} \\
 c_2 &= 2h_1 \frac{\sqrt{c_3^2 - c_1^2}}{c_3 c_1} + 2h_2 \frac{\sqrt{c_3^2 - c_2^2}}{c_3 c_2} \\
 c_3 &= 2h_1 \frac{\sqrt{c_4^2 - c_1^2}}{c_4 c_1} + 2h_2 \frac{\sqrt{c_4^2 - c_2^2}}{c_4 c_2} + 2h_3 \frac{\sqrt{c_4^2 - c_3^2}}{c_4 c_3} \\
 c_4 &= 2h_1 \frac{\sqrt{c_5^2 - c_1^2}}{c_5 c_1} + 2h_2 \frac{\sqrt{c_5^2 - c_2^2}}{c_5 c_2} + 2h_3 \frac{\sqrt{c_5^2 - c_3^2}}{c_5 c_3} + 2h_4 \frac{\sqrt{c_5^2 - c_4^2}}{c_5 c_4}
 \end{aligned} \tag{3.6}$$

Example 3.2 (continued)

The distances at which the slope changes will occur (i.e. the distance at which the direct wave traveling in layer 1 and a critical-refracted wave will arrive simultaneously at the target S) are expressed by:

$$\begin{aligned} (r_{cr})_1 &= \frac{C_1 - 0}{1/c_1 - 1/c_2} ; & (r_{cr})_3 &= \frac{C_3 - C_2}{1/c_3 - 1/c_4} \\ (r_{cr})_2 &= \frac{C_2 - C_1}{1/c_2 - 1/c_3} ; & (r_{cr})_4 &= \frac{C_4 - C_3}{1/c_4 - 1/c_5} \end{aligned} \quad (3.7)$$

The procedure for constructing Figure 3.8 is to calculate the C intercepts and plot them along the time axis. Then from each intercept  $C_i$  draw the corresponding slope  $1/c_{i+1}$ , noting that the intercept  $C_0$  acts as the origin. The slopes will then intersect at the abscissas  $r_{cr}$ . The analytical expressions for  $r_{cr}$  are superfluous if accurate drafting is done.

The wave travel diagram for this 5 layered space is shown in Figure 3.8.

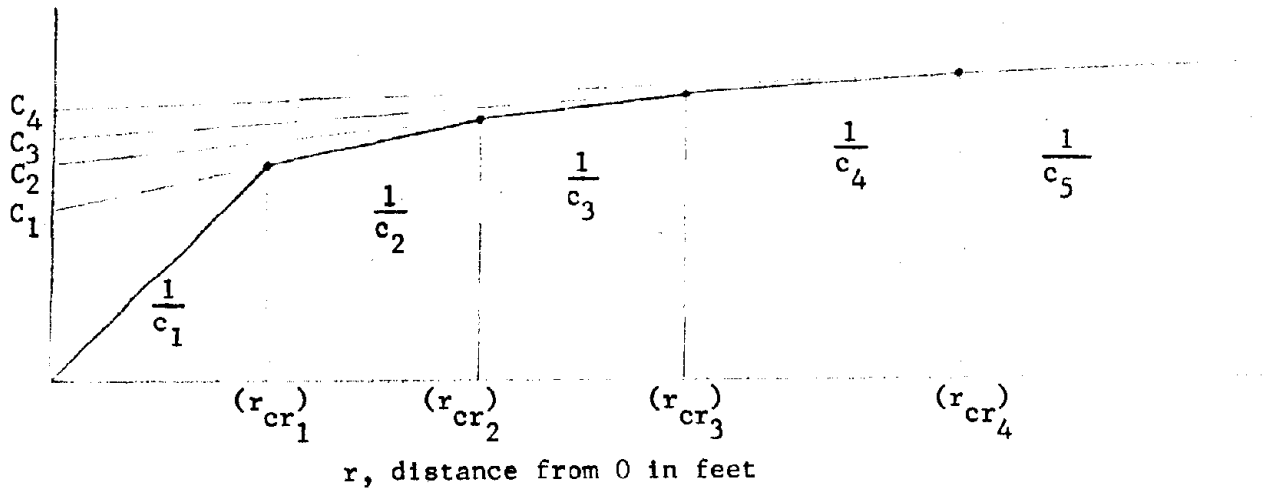


FIGURE 3.8

Example 3.3

Another example is given in Figure 3.9 for a seven layered medium with uniform seismic velocity increases from 1000 fps at the first layer to 7000 fps at the seventh layer. The method of obtaining the curve for the blast front will be given in Subsection 3.3.

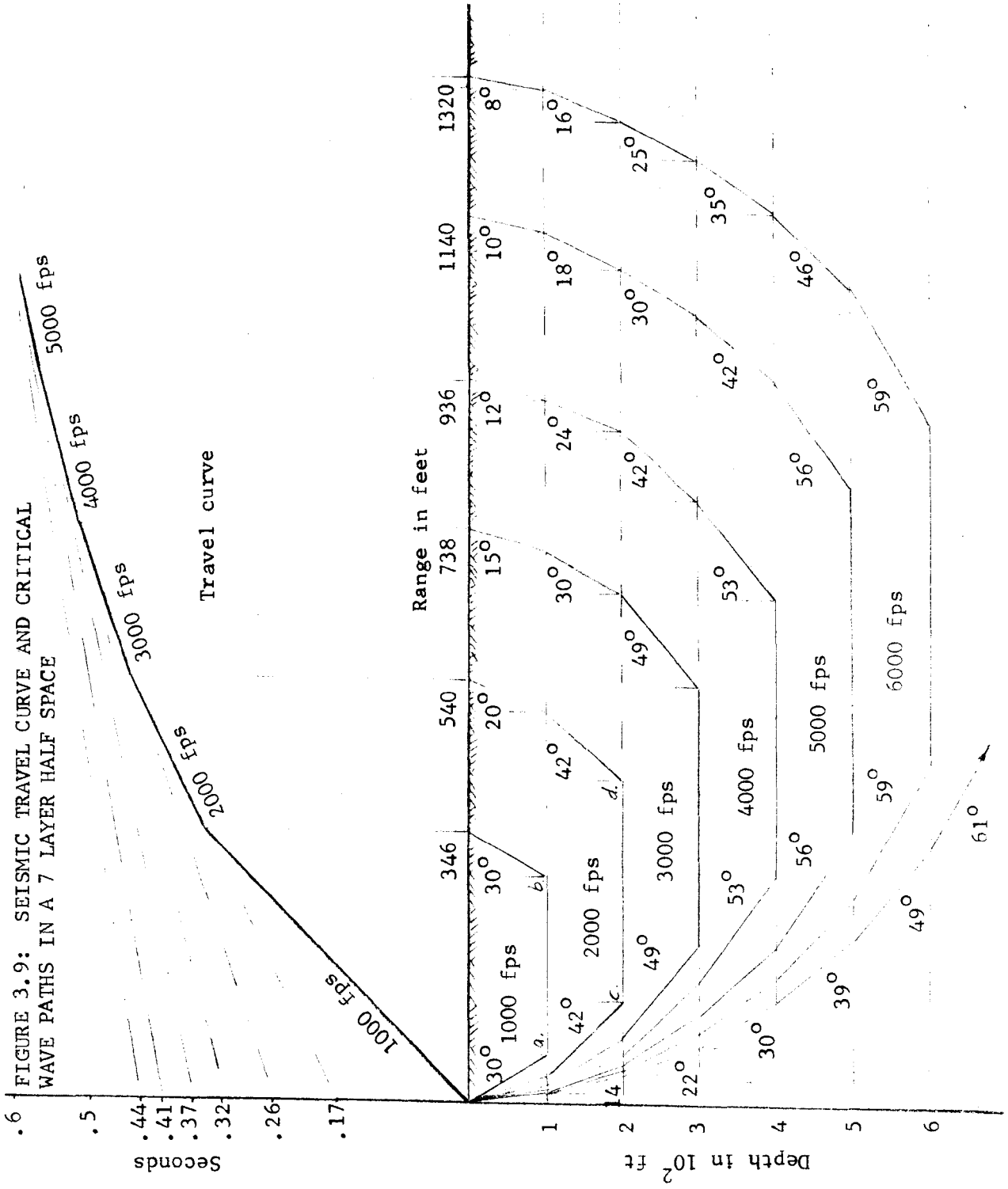


FIGURE 3.9: SEISMIC TRAVEL CURVE AND CRITICAL WAVE PATHS IN A 7 LAYER HALF SPACE

Seconds  
 .6  
 .5  
 .44  
 .41  
 .37  
 .32  
 .26  
 .17



### Example 3.3 (continued)

The critical angles indicated in the path diagram of this numerical example are given completely by the seismic velocities and the  $r_{cr}$  values

Layer (1)  $\sin \alpha_1 = c_1/c_2 = 0.5$ ;  $\sin \alpha_2 = c_1/c_3 = 0.33$ ;  $\sin \alpha_3 = c_1/c_4 = 0.25$ ; etc.

Layer (2)  $\sin \alpha_2 = c_2/c_3 = 0.67$ ;  $\sin \alpha_3 = c_2/c_4 = 0.50$ ;  $\sin \alpha_4 = c_2/c_5 = 0.40$ ; etc.

Layer (3)  $\sin \alpha_3 = c_3/c_4 = 0.75$ ;  $\sin \alpha_4 = c_3/c_5 = 0.60$ ;  $\sin \alpha_5 = c_3/c_6 = 0.50$ ; etc.

Layer (4)  $\sin \alpha_4 = c_4/c_5 = 0.80$ ;  $\sin \alpha_5 = c_4/c_6 = 0.67$ ;  $\sin \alpha_6 = c_4/c_7 = 0.57$ ; etc.

Layer (5)  $\sin \alpha_5 = c_5/c_6 = 0.83$ ;  $\sin \alpha_6 = c_5/c_7 = 0.72$ ;

Layer (6)  $\sin \alpha_6 = c_6/c_7 = 0.86$

The procedure for constructing Figure 3.9 is to draw the distance - time diagram first, then to calculate the  $\alpha$  values for the various layers and then to combine the distance - time diagram with the distance - depth diagram as follows:

For the top stratum the critical angle  $\alpha_1$  is  $30^\circ$ , lay it off from the origin to depth 100' and from  $(r_{cr})_1 = 346'$  to depth 100' as shown; the distance a to b is then the distance the critically refracted wave travels with the speed of 2000 fps. Similarly for the second stratum, lay off angle  $\alpha_2$  or  $20^\circ$  to the 100 ft level and angle  $\alpha_3$  or  $42^\circ$  to the 200 ft level as shown. The critically refracted wave travels from c to d at 3000 fps.

Figure 3.9 shows clearly that a large part of the energy radiated to the half space from point zero will be directed to the surface within a circular area of approximately 1500 ft radius.

The seismic energy flux per unit area comprising a dilatational and a shear component is very involved, and a qualitative discussion of it is beyond the scope of this study. The important aspect of the above presentation is the fact that a half space whose seismic velocities increase with depths will direct a very large part of vibrational energy generated at ground zero to the surface within a relatively small area.

So as to get an idea of the outrunning and phasing phenomenon in variously layered soils the following eight examples have been worked out.

Examples 3.4 - 3.11

Soil A is homogeneous with		$c = 1,000$ fps
B is 11 layered, $\Delta h = 100'$	, $1,000 < c < 11,000$	
C is 6 layered, $\Delta h = 200'$	, $1,500 < c < 11,000$	
D is 4 layered, $\Delta h = 300'$	, $2,000 < c < 10,667$	
E is 3 layered, $\Delta h = 400'$	, $2,500 < c < 10,250$	
F is 3 layered, $\Delta h = 500'$	, $3,000 < c < 11,000$	
G is 2 layered, $\Delta h = 1000'$	, $5,000 < c < 11,000$	
H is homogeneous with		$c = 11,000$

Table 3.2 shows the seismic velocity values of six of these half spaces. The values have been chosen so as to obtain an idea of the effect of averaging seismic velocities over two or more layers.

Figures 3.10a and 3.10b are identical wave travel curves plotted to different scales. These curves show that averaging seismic velocities of the 11 layered space may give rather different results.

It should be noted that the travel curves of Figure 3.9 and 3.10 relate to specific geophysical stratifications. Thus if a 100 ft layer with  $c = 1000$  fps is underlain by an infinitely deep layer with  $c = 10,000$  fps the applicable travel curve cannot be inferred from Figures 3.10a and 3.10b. It would in this case be necessary to compute the applicable intercept from Equation (3.6) namely

$$C_1 = \frac{2 h_1}{c_1 c_2} \sqrt{c_2^2 - c_1^2} = \frac{200}{10^3 \times 10^4} \sqrt{10^8 - 10^6} = 2 \times 10^{-4} \text{ seconds}$$

and the two applicable slopes of  $10^{-3}$  and  $10^{-4}$  sec/ft. respectively.

Use of Figures 3.10a and 3.10b will be made later in conjunction with blast wave front travel curves so as to ascertain at what location and at what time seismically generated waves will outrun the blast wave front.

Table 3.2 Showing Seismic Properties  
of Six Multilayered Soils

Depth	Soil B	Soil C	Soil D	Soil E	Soil F	Soil G
	1000 fps					
100	—————	1500 fps				
	2000		2000 fps			
200	—————	—————		2500 fps		
	3000				3000 fps	
300	—————	3500	—————			
	4000					
400	—————	—————		—————		
	5000		5000			
500	—————	5500			—————	5000 fps
	6000					
600	—————	—————	—————	6500		
	7000					
700	—————	7500				
	8000		8000		8000	
800	—————	—————		—————		
	9000					
900	—————	9500	—————			
	10,000					
1000	—————	—————		10,250	—————	—————
	11,000	11,000	10,667		11,000	11,000

Seismic Wave Travel Curves for  
8 Different Half Spaces

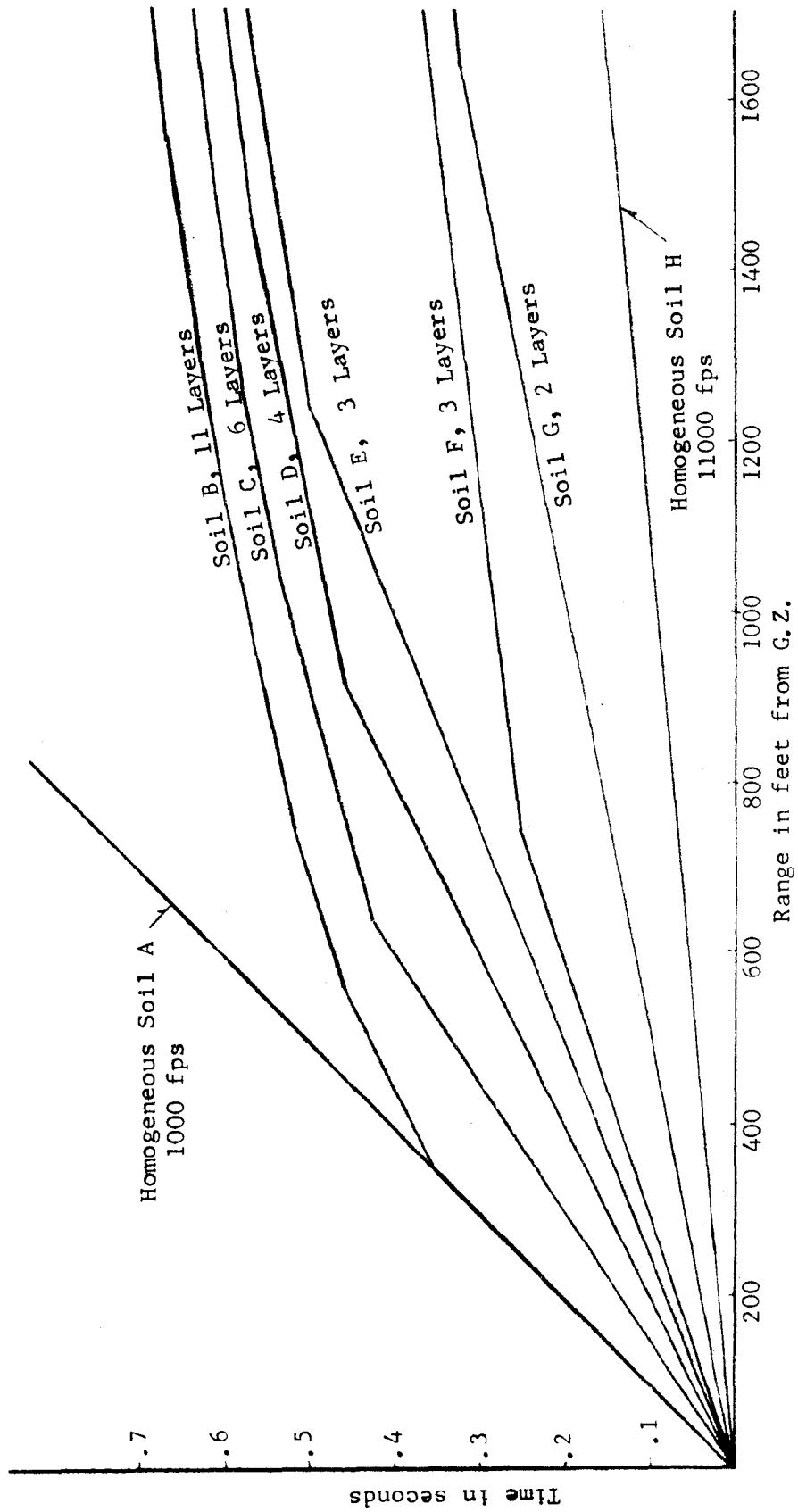
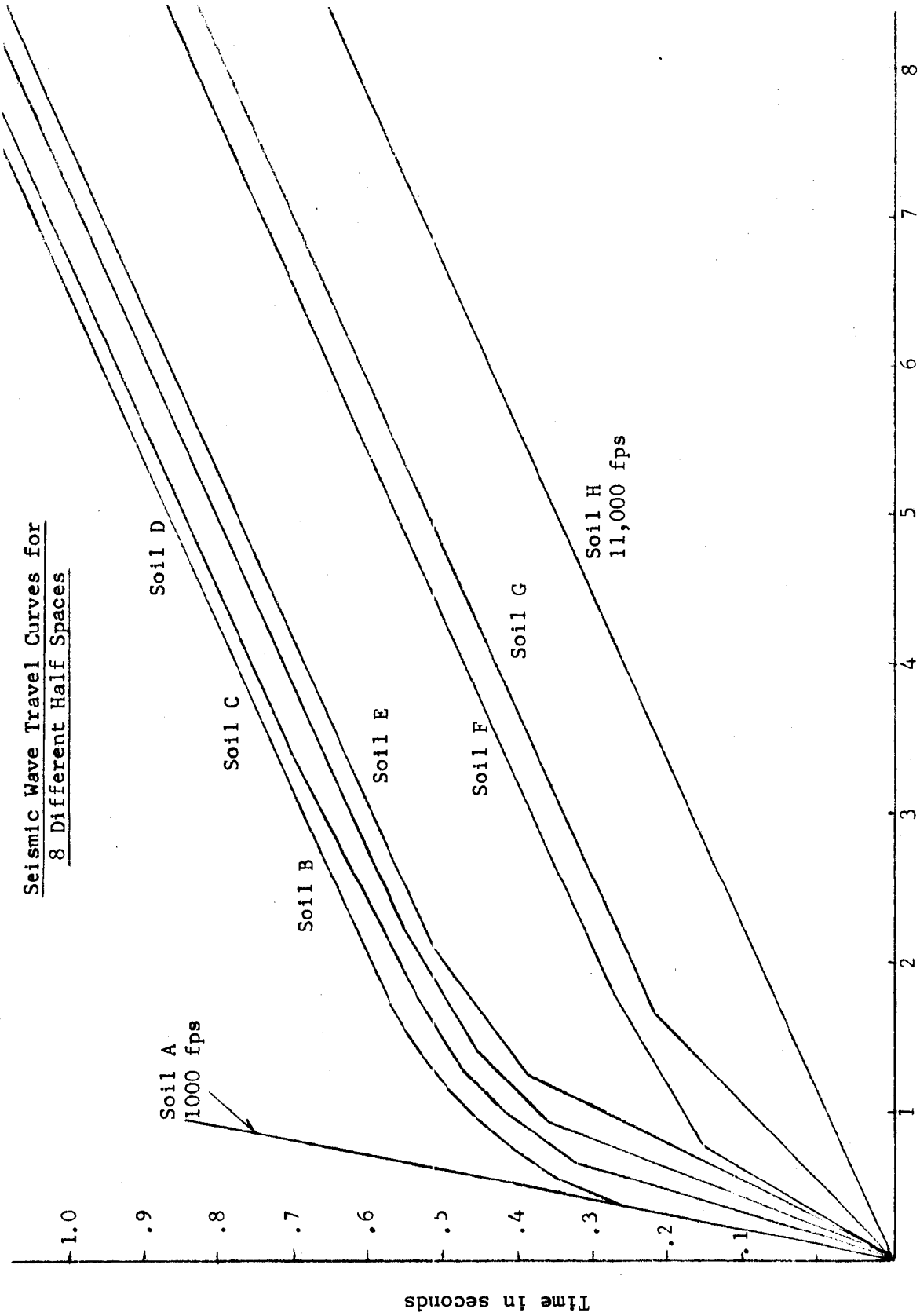


FIGURE 3.10a

Seismic Wave Travel Curves for  
8 Different Half Spaces



Range in kft from G.Z.  
FIGURE 3.10b

### 3.3 Blast Wave Travel Time

3.3.1 Basic relationships. The theoretical work of Brode (Reference 3.1) as well as a limited amount of experimental data constitute a basis on which the following empirical relationships have been developed. The coefficients are not constants over the entire range of scaling, but within some indicated ranges, see Figures 3.11 and 3.12, they may be treated as such.

- Let  $W$  = yield in MT  
 $t_s$  = arrival time in seconds  
 $r_p$  = distance from G.Z. to blast front in feet  
 $p_{so}$  = overpressure at  $r_p$  in psi

then assuming a single exponent representation over the six order range of  $W$  from 1 KT to  $10^3$  MT, it is found that

$$r_p = 6 \times 10^3 W^{\frac{1}{6}} t_s^{\frac{1}{2}} = 4.3 \times 10^4 W^{\frac{1}{3}} p_{so}^{-\frac{1}{2}} \text{ ft} \quad (3.8)$$

$$p_{so} = 51.4 W^{\frac{1}{3}} t_s^{-1} = 1.85 \times 10^9 W^{\frac{2}{3}} r_p^{-2} \text{ psi} \quad (3.9)$$

Figure 3.11 shows on log log paper the linearized plot of Equations (3.8 and 3.9) as well as the theoretical curve due to Brode. It is seen that the two plots coincide only at the two specific points

$$(1) \quad r_p = \left\{ \begin{array}{l} 192 \text{ ft (1 KT)} \\ 1920 \text{ " (1 MT)} \\ 19200 \text{ " (10}^3\text{ MT)} \end{array} \right\} \text{ with } p_{so} = 500 \text{ psi}$$

$$(2) \quad r_p = \left\{ \begin{array}{l} 3770 \text{ ft (1 KT)} \\ 37,700 \text{ " (1 MT)} \\ 377,000 \text{ " (10}^3\text{ MT)} \end{array} \right\} \text{ with } p_{so} = 1.3 \text{ psi}$$

So as to show the effect of the linearization of Equations (3.8 and 3.9) on the overpressure, a correction curve, giving the overpressure due to Brode  $(p_{so})_B$  divided by the linearized overpressure  $(p_{so})_L$  is presented in Figure 3.12. Thus, if at the yield of 1 MT a linearized overpressure of 100 psi is obtained, the correction factor is about 0.75, meaning that the pressure by the Brode analysis will be only 75 psi. If the  $(p_{so})_L$  for 1 KT is 100 psi, the correction factor is 1.1 and  $(p_{so})_B = 110$  psi.

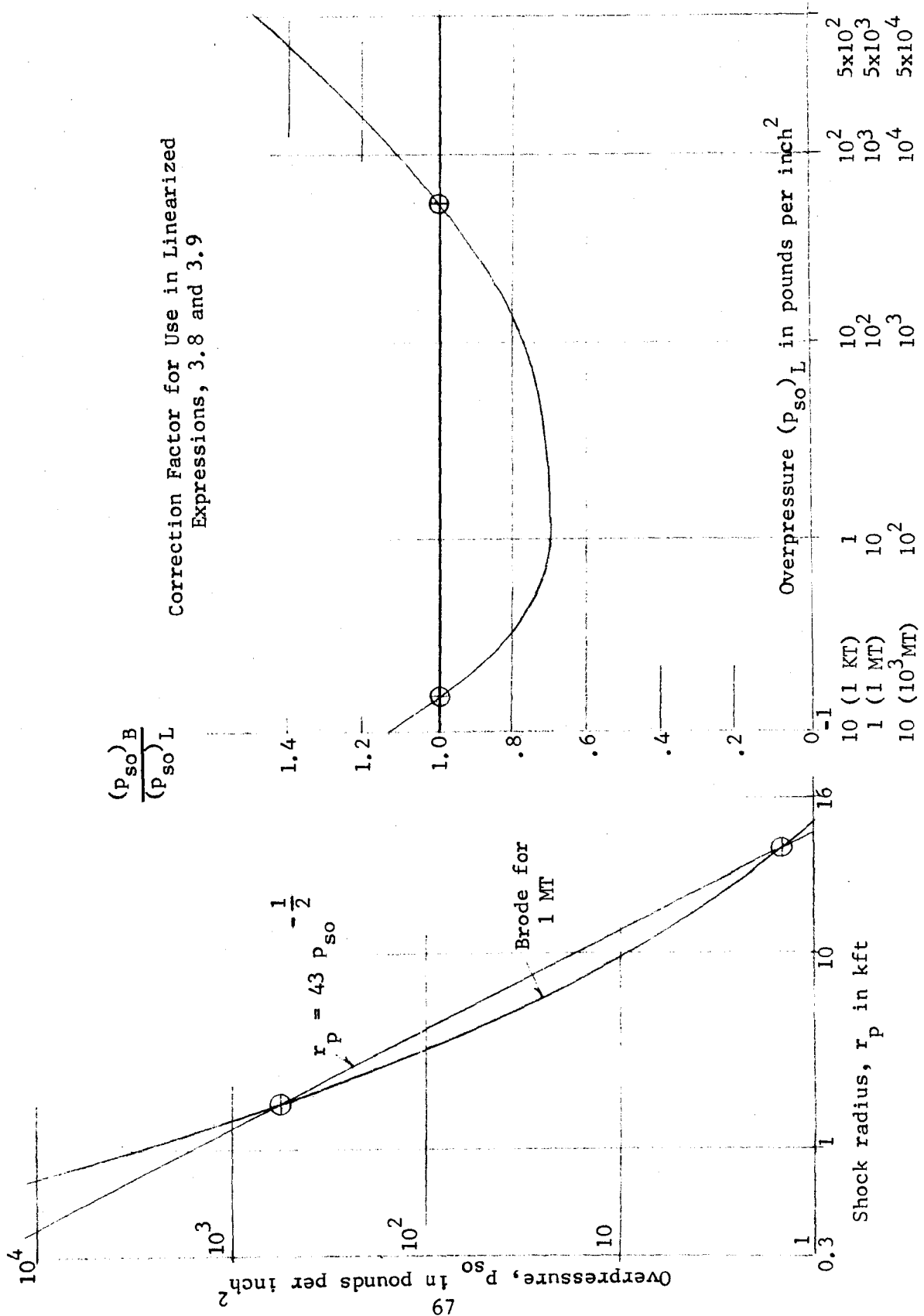


FIGURE 3.11

Correction Factor for Use in Linearized Expressions, 3.8 and 3.9

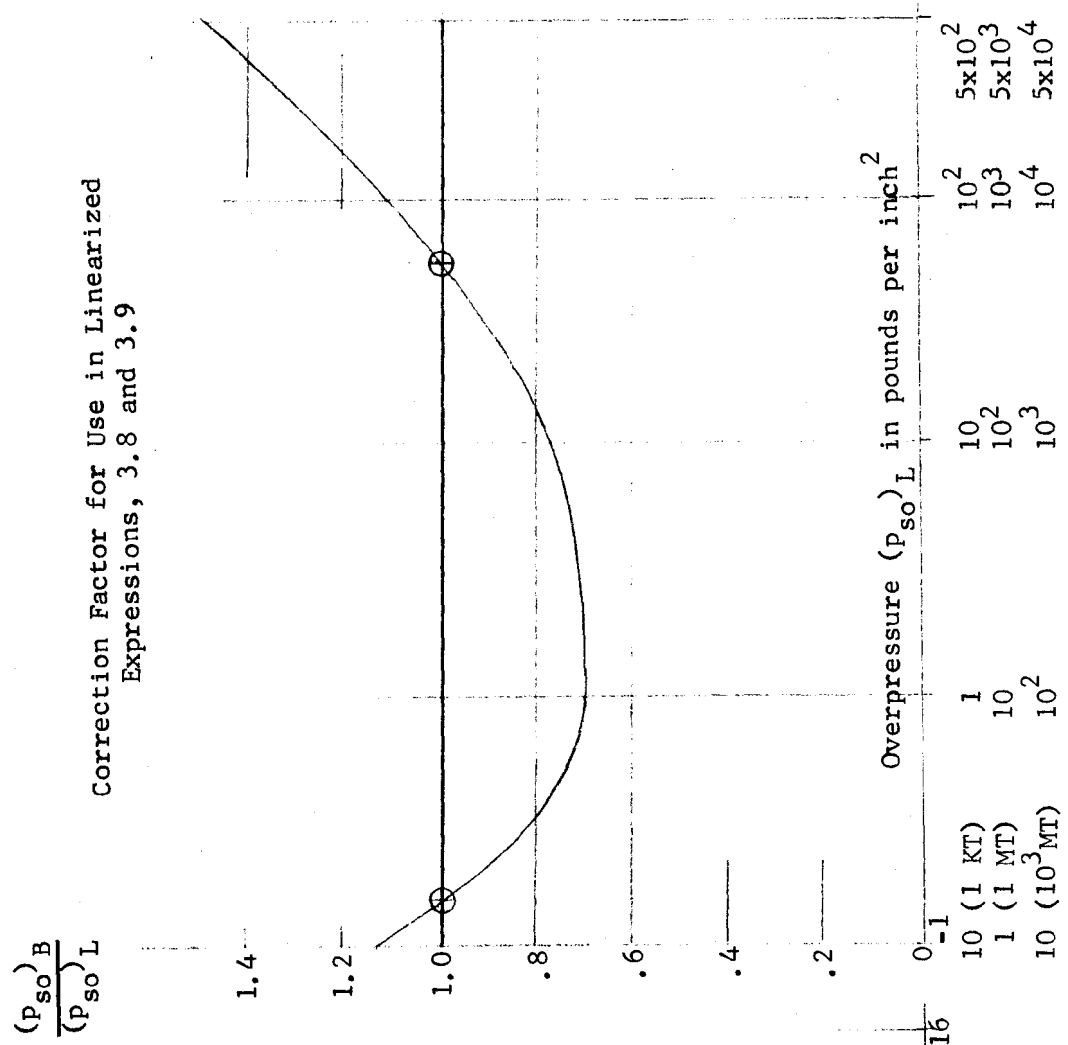


FIGURE 3.12

Figure 3.13 shows six linear log-log plots of  $r_p$ ,  $t_s$ , and  $p_{so}$  for the three yields, 1 KT, 1 MT, and  $10^3$  MT. The linearity approximation for the 1 MT yield may be compared with the curve labeled Brode. The linearity constant of  $6 \times 10^3$  for a 1 MT yield is precise at two times only, namely at  $t = 0.103$  seconds and at  $t = 39$  seconds.

The logarithmic linearizations employed in representing the relationships of  $r_p$ ,  $p_{so}$ ,  $t_s$ , and  $W$  are sufficiently accurate for many purposes and give a clearer appreciation of the situation than the actually non-linear logarithmic relationships given by References 3.1.

The use of Figure 3.13 is indicated by the dotted lines and the arrows pointing toward the  $r_p$  and  $p_{so}$  coordinates. Thus for a 1 MT burst with arrival time  $t_s$  of  $10^{-1}$  seconds, the  $r_p$  is about 1900 ft and the overpressure is about 500 psi. For a 1 KT with arrival time  $t_s$  of  $10^{-2}$  seconds the  $r_p$  is about 190 ft and the overpressure is about 50 psi.

If rather complete knowledge is available or assumed in regard to the magnitude of  $W$ , its point of burst, and the properties of the cratering material, use of the curves given by the above references will lead to results that are without doubt in better agreement with reality than is obtainable from the simplified expressions that will be used for illustrative purposes in all the following subsections.

3.3.2 Use of blast travel curves for stationary or GZ source. A replot using linear coordinates of the  $r_p$ ,  $t_s$  relationship for the 1 KT yield of Figure 3.13 is shown in Figure 3.14 for three downscaled constants of:  $5 \times 10^3$ ,  $6 \times 10^3$ , and  $7 \times 10^3$ , giving:

$$r_p = \left\{ \begin{array}{l} 7 \times 10^3 \\ 6 \times 10^3 \\ 5 \times 10^3 \end{array} \right\} (10^{-3})^{1/6} t^{1/2} = \left\{ \begin{array}{l} 1580 \\ 1900 \\ 2220 \end{array} \right\} t^{1/2} \text{ feet}$$

The reason for plotting the three curves is to show the effect of a reasonable spread in the constant  $6 \times 10^3 W^{1/6}$ .

If the 6 layer soil (C) is assumed, the outrunning distance  $r_o$  (measured from G.Z.) at the surface can be obtained simply by superposing Figure 3.10a on Figure 3.14 in such a manner that the origin, 0, of Figure 3.10a coincides with the origin of Figure 3.14. The soil (C) curve then



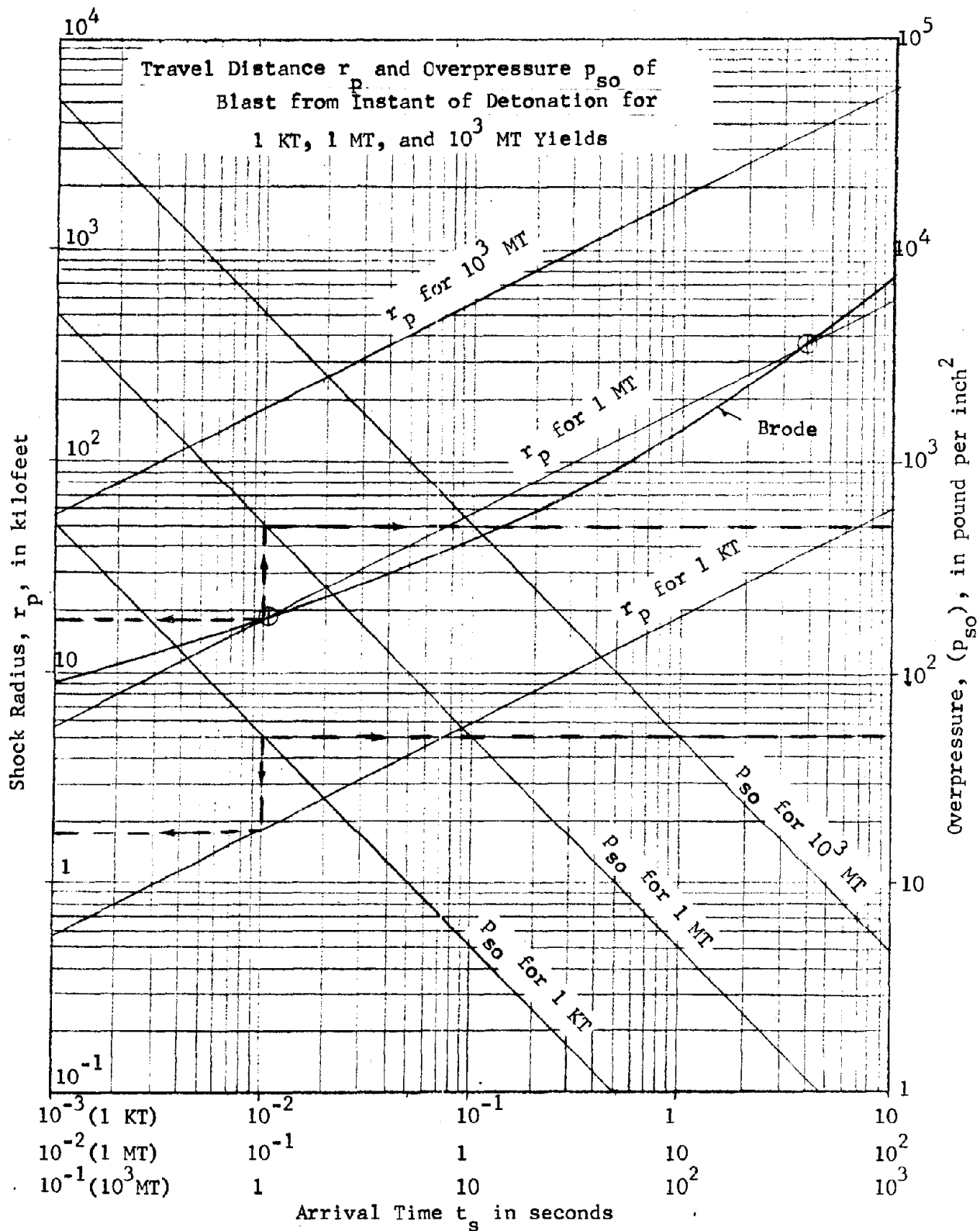


FIGURE 3.13

Three Blast Front Travel Curves for a 1 KT Burst  
Indicating a Spread of Estimated Uncertainty

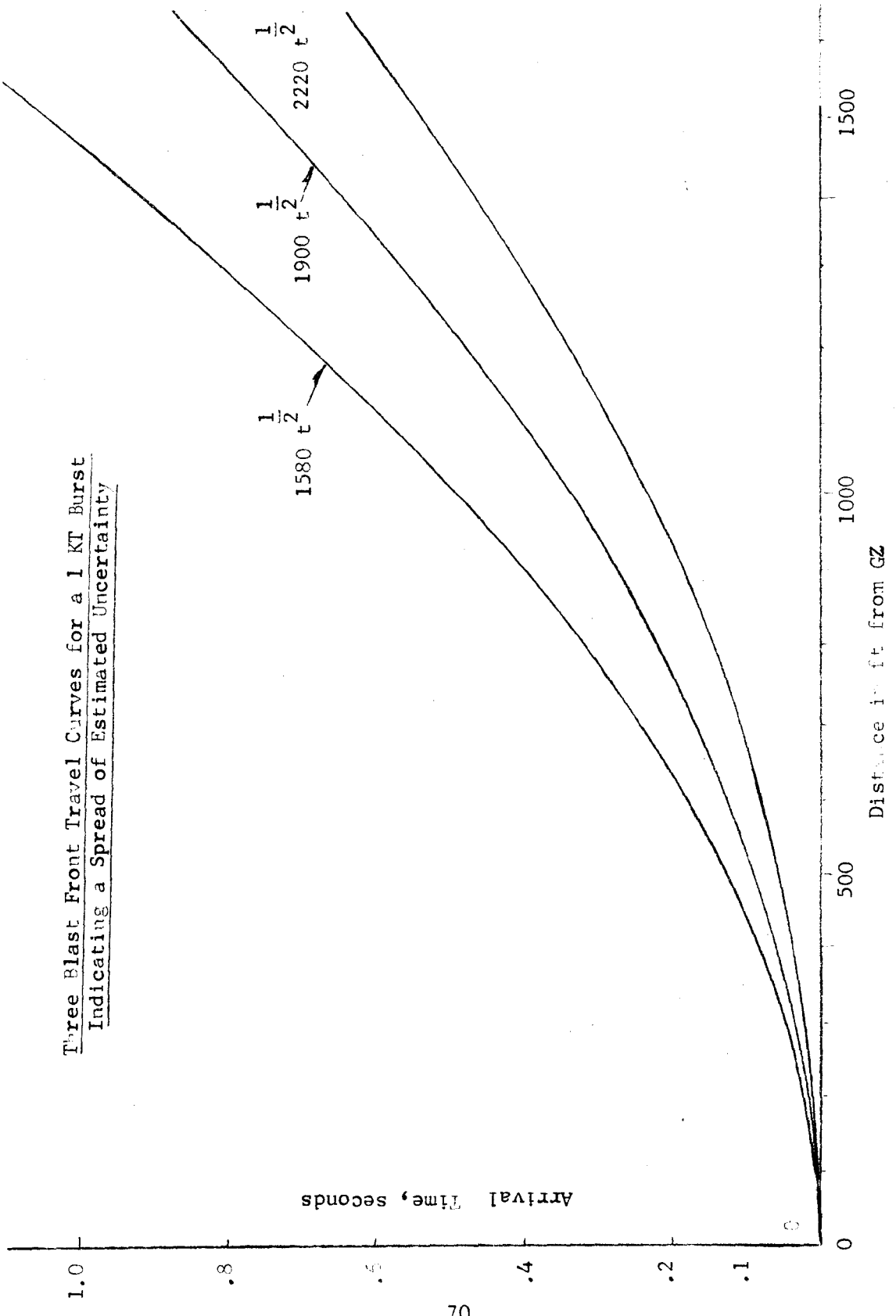


FIGURE 3.14

is found to intersect the three blast travel curves at the respective distances 1050, 1340, and 1630 feet from G.Z. giving outrunning distance spread of

$$r_o = 1340 \pm 290 \text{ feet}$$

to which correspond overpressures computed by Equation (3.9)

$$p_{so} = 1.85 \times 10^9 (10^{-3})^{2/3} r_p^{-2}$$

$$= 1.85 \times 10^7 r_p^{-2} = \begin{cases} 16.8 \\ 10.3 \\ 7.0 \end{cases} \text{ psi}$$

The conclusion can be made that uncertainty will exist in the surface outrunning distance even if the seismic wave travel curve is precisely known. If a three layer soil (E) is assumed, the outrunning distances from G.Z. are 800, 1200, and 1520 ft respectively for the three assumed constants in the blast travel curves, and the corresponding overpressures amount to 29, 13 and 8 psi respectively.

Figure 3.15 is also taken from Figure 3.13, but it uses only the constant  $6 \times 10^3 W^{1/6}$  as referred to 1 MT. Thus for superposition of the 10 MT curve of Figure 3.15 with the seismic wave travel curve for the 6 layered soil (C), of Figure 3.10b, surface outrunning will be found to occur at 6400 ft. from G.Z., and for the three layered soil (E), of Figure 3.10b, at 5800 ft. from G.Z. The corresponding overpressures are given by Equation (3.9) for the 10 MT burst

$$p_{so} = 8.6 \times 10^9 \times r_p^{-2} \text{ psi}$$

or 210 psi for soil (C) and 256 psi for soil (E).

It should be pointed out that the curves 3.10a and 3.10b relate only to seismic wave travel emanating from a point source located at the surface to a station on the surface. Since a surface burst creates a crater of considerable dimensions it cannot be considered a point source located precisely on the surface. For buried stations, and for estimated depths of the source point the diagrams shown in Figures 3.8 and 3.9 will indicate how the seismic travel curves may be modified to take into account depth of location.

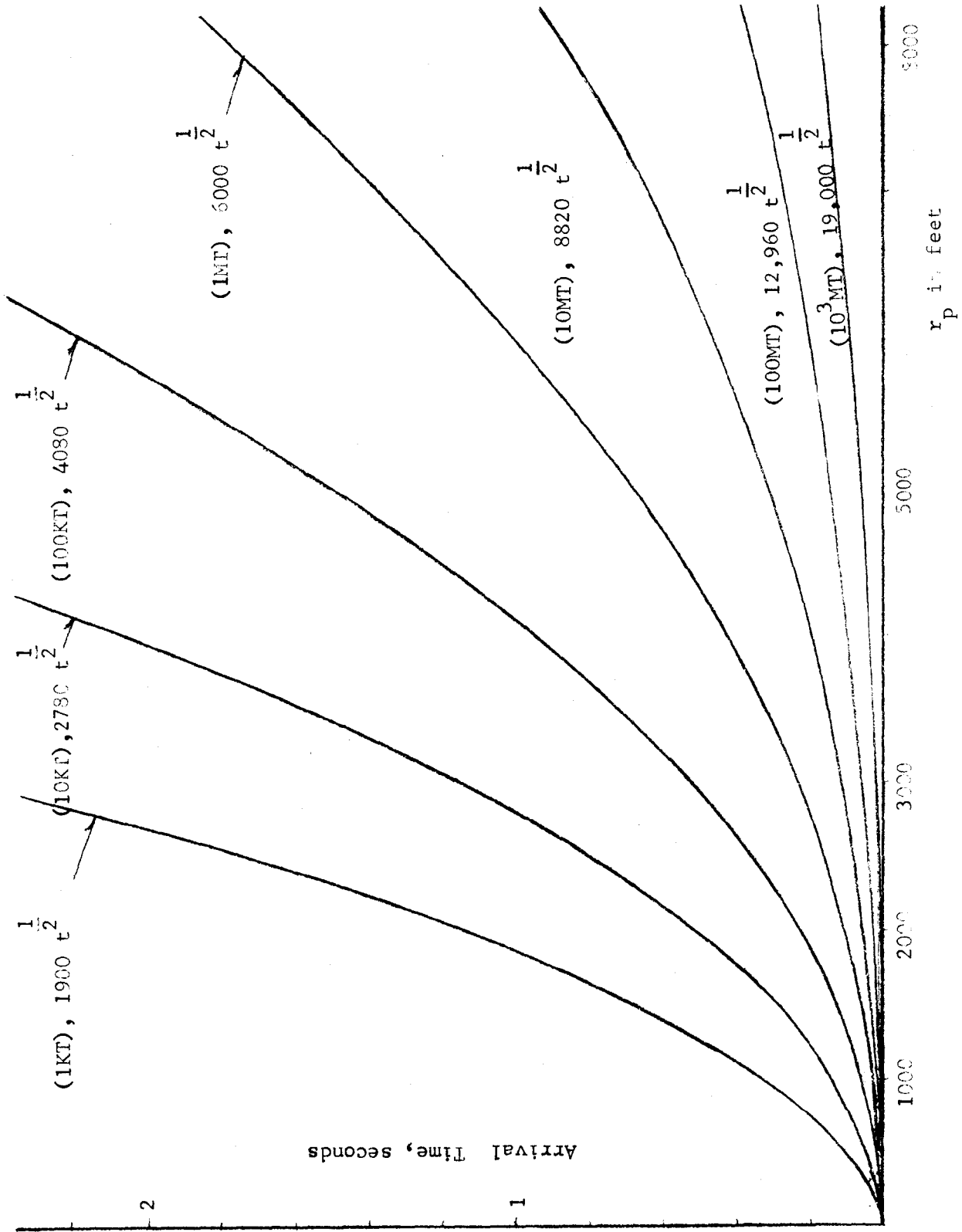


FIGURE 3.15

### 3.4 Generation of Seismic Waves by a "Moving Line" Load on the Surface of an Elastic Half Space

The two dimensional problem is a simplification of the radially expanding circular line load but it gives a sufficiently accurate idea of the situation. The moving line then corresponds to the front of the air blast, inducing seismic waves as it propagates on the ground surface.

It will be assumed that the deformations are elastic and that the seismic velocities are unaffected by the dynamic stress level.

Three regimes will be considered

- a. Superseismic, i.e. line velocity  $U > c > c_s$
- b. Transseismic, i.e.  $c > U > c_s$
- c. Subseismic, i.e.  $c > c_s > U$

For a homogeneous elastic half space, and for a slowly decreasing velocity  $U$  of the loading line, the dilatational and the shear wave fronts will appear as straight, inclined lines. Let  $c = 2000$  fps and  
 $c_s = 1250$  fps

The 5 diagrams shown in Figure 3.16 are self explanatory. Thus, in the superseismic case no disturbance is felt at stations  $S$  and  $S'$ . In the first case the dilatational wave front will arrive at  $S$  simultaneously with blast wave front but the shear wave front lags behind. In the third transseismic case the shear wave front arrives simultaneously with blast wave front at  $S$  but the dilatational front has already passed through  $S$  and  $S'$ . In the subseismic case both wave fronts are "outrunning" the loading line front.

In all cases it is seen that an object of appreciable size and buried in the half space will experience differential loadings due to the finite travel times of disturbances in the elastic medium of the half space.

A combination of the critical path diagram and a wave front traveling at constant speed is shown in Figure 3.17 for a two layer half space.

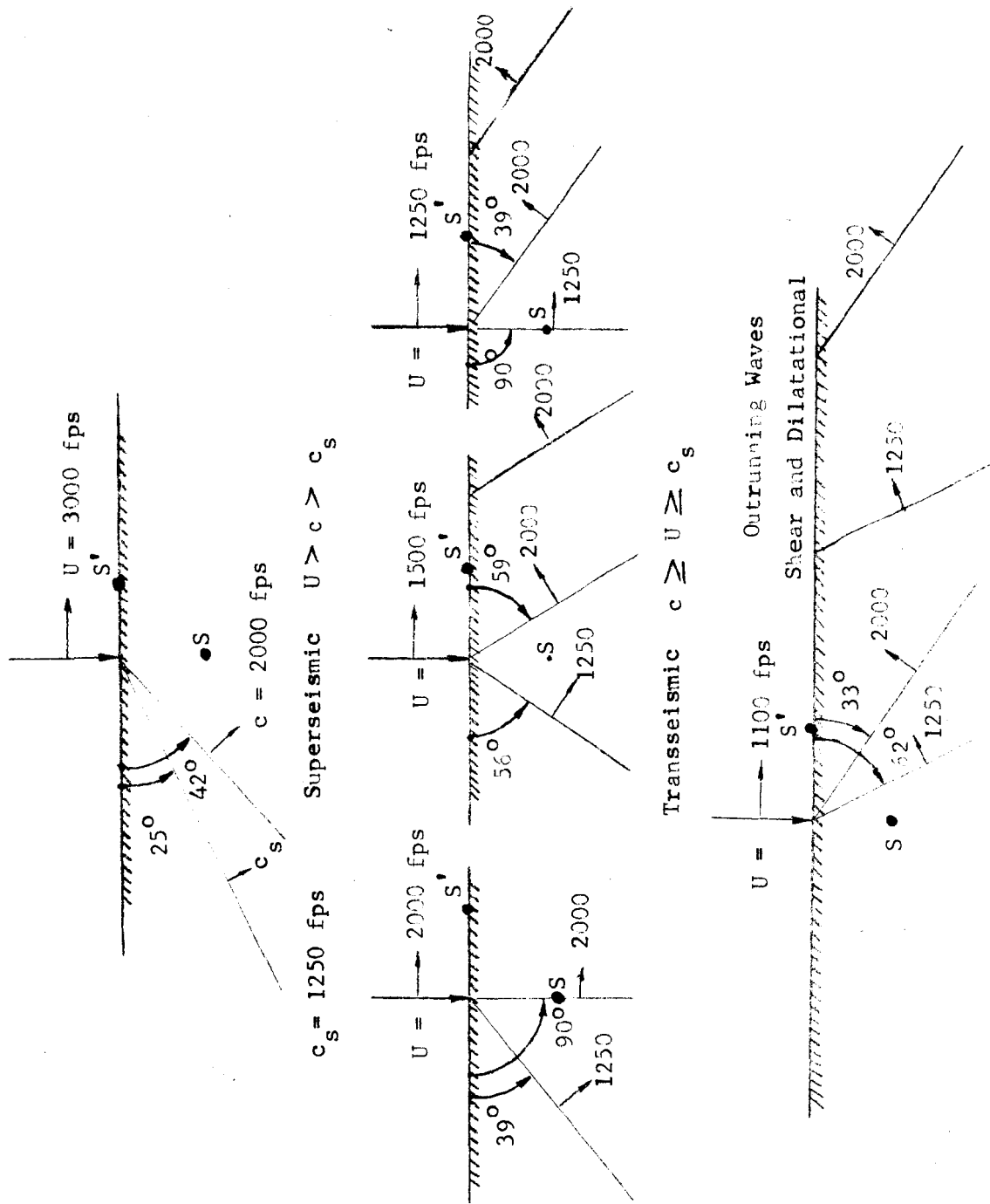


FIGURE 3.16

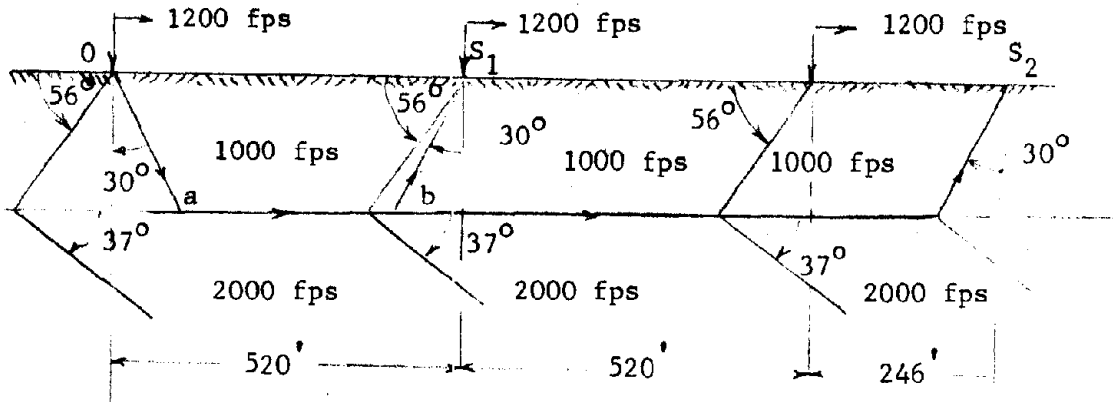


FIGURE 3.17

Assume that the traveling wave front in Figure 3.17 is located at 0 at time zero and that its constant speed of 1200 fps is superseismic with respect to the top layer's dilatational speed of 1000 fps, but not with respect to the second layer's speed of 2000 fps. Accordingly a direct, i.e., a horizontal, disturbance in the upper layer will always lag behind the line load as shown by the wave front; its angle of  $56^\circ$  is determined by the arcsine of  $1000/1200$ . Since a critical refraction angle of  $30^\circ$  for dilatational waves corresponds to the arcsine of  $c_1/c_2$ , part of the disturbance originating at  $t = 0$  will travel along the critical path  $0abS_1$  by which it will arrive at  $S_1$  in the time

$$t_o = \frac{2h}{c_1 c_2} \sqrt{c_2^2 - c_1^2} + \frac{x_o}{c_2}$$

Equating this time to the travel time of the line loading,  $x_o/U$ , it is found that

$$x_o = \frac{2h}{c_1} \sqrt{c_2^2 - c_1^2} \frac{U}{c_2 - U} \quad (3.10)$$

If  $h = 100$  ft,  $c_1 = 1000$  fps,  $c_2 = 2000$  fps,  $U = 1200$  fps

$$x_o = 520 \text{ ft and } t_o = 520/1200 = 0.433 \text{ sec.}$$

Therefore the disturbance following the critical path will begin to outrun the traveling line load in 0.433 seconds. Moreover when  $t = 2 t_0 = 0.866$  sec. the line load will have moved an additional 520 ft. and the corresponding critical path disturbance initiated at 0 will emerge at  $S_2$  or 1286 ft. from 0, i.e., 246 ft. ahead of the line load.

Example 3.12

As an illustration of the use of blast travel curves for a moving origin, the six layered soil (C) will be investigated for surface outrunning due to blast front induced seismic waves. Assume a 1 KT burst, then from Equation (3.9) and (3.10) the blast travel curve will be given by

$$r_p = 1900 t^{1/2} \text{ ft.}; \text{ and } p_{so} = 1.85 \times 10^7 r_p^{-2}$$

This curve, similar to the middle one in Figure 3.14, is drawn in Figure 3.18. Then six translated replots of the soil (C) curve from Figure 3.10a have been superposed on the blast travel curve, beginning with the one at the origin 0. The following table gives the results:

<u>origin at</u>	<u>outrun at</u>	<u>by way of</u>	<u>overpressure</u>
0 ft	1340 ft	4-5 layer	10.3 psi
200	1320	3-4 layer	10.6 psi
400	1300	2-3 layer	10.9 psi
600	1312	1-2 layer	10.9 psi
800	1290	1 layer	11.1 psi
1100	1100	1 layer	15.3 psi

It is seen that due to the sudden slope change in the seismic travel curve from layer 1 to 2, and the more gradual slope changes for deeper layers, all the paths outrunning at the surface through deeper layers will occur within a small variation of  $r_0$ , so small that for practical purposes  $r_0$  may be considered invariant.

The horizontal push-pull wave through layer 1 will have a minimum outrunning distance when the slope of the blast travel curve is the same as the slope of the first layer travel curve. This occurs when  $r_0 \approx 1100$  feet.

For larger yields the curves in Figure 3.10b can be superposed on those of Figure 3.15 to give minimum outrunning distances.



Example 3.12 (continued)

Combinations of Blast Front and Seismic Wave Travel Curve  
for a 1 KT Burst and for 6 Layered Soil C  
(Moving Point Generation)

Blast Front for 1 KT  
( $1900 t^{1/2}$ )

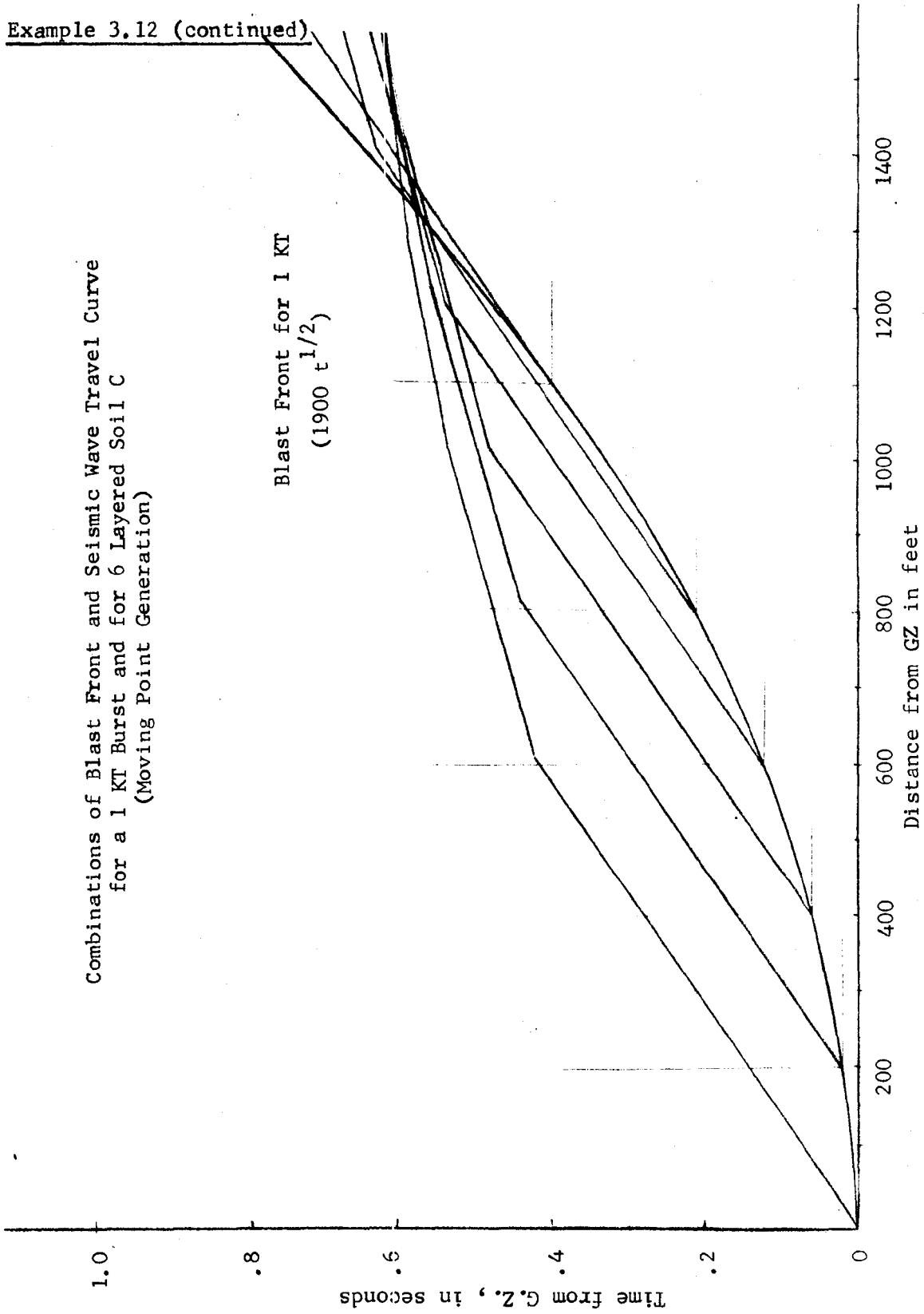


FIGURE 3.18

Example 3.13

As a second example consider a burst of 1 MT occurring at the surface of soil C. Equation (3.9) then gives  $r_p = 6000 t^{1/2}$  and this curve, plotted in Figure 3.19 to the same scale as the curve for soil C, Figure 3.10b, is then superposed on Figure 3.15. The following translated distances of superposition give the corresponding outrunning distances.

Translated distance	0	500	1000	1500	2000	3000	4000 ft.
Outrunning distance	6200	6050	5900	5870	5850	6050	6500 ft.

The smallest distance of 5850 ft. results from the wave generated at  $r_p = 2000$  ft, but for all practical purposes the one generated at G.Z. may be considered the first to outrun in Soil C.

3.4.1 Outrunning or phasing of shocks. In view of the preceding discussions in Sections 3.3.1 - 3.3.3, it is apparent that a precise determination of the distance at which the disturbance will arrive simultaneously with the blast front involves specific knowledge of the seismic properties of the ground as well as reliable knowledge of the magnitude and type of the nuclear burst. For these reasons it is difficult to predict the phasing of the seismic, initially upwards shocks with the downward slap due to the blast front. Consequently rather arbitrary phasings are usually assumed, ranging from leads and lags up to one third of the duration  $D_p^+$  of the positive phase of the overpressure.

A few pointers are given by Reference 3.2 in regard to the overpressure  $p_{so}'$  at which outrunning or zero phasing of the G.Z. induced motion will occur in a homogeneous soil of seismic velocity  $c$ . The information relates to the range of overpressures from 200 psi upwards and is:

$$p_{so}' \approx \left[ \frac{c}{280 \text{ fps}} \right]^2 \quad \text{for } c \geq 4000 \text{ fps} \quad (3.11)$$

Thus, for a soil with  $c = 5000$  fps, outrunning will occur at 318 psi which corresponds to a blast front radius, Equation (3.8), of

$$r_o = r_p \approx 4.3 \times 10^4 W^{\frac{1}{3}} p_{so}'^{-\frac{1}{2}} = 2.4 \times 10^3 W^{\frac{1}{3}}$$

Therefore if  $W = 10$  MT,  $r_o = 5160$  ft.

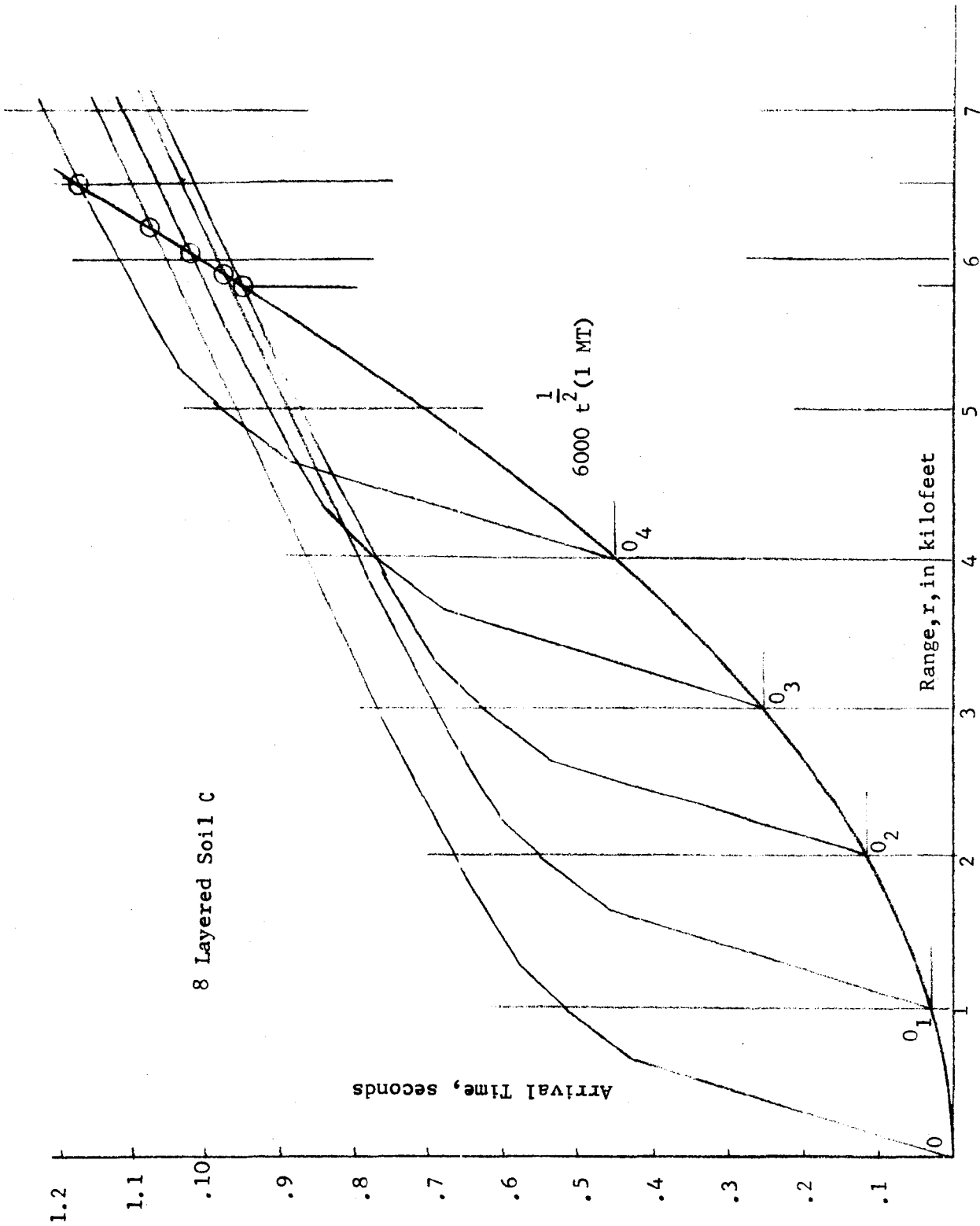


FIGURE 3.19

Since soils are seldom homogeneous, and since an equivalent seismic velocity for several layers is almost impossible to estimate, the above calculations become very imprecise for actual soil conditions.

Only minor seismic effects are transmitted ahead of the blast front by the dilatational waves, but major seismic effects will result when the shear waves are outrunning the blast front. Thus at the 300 psi overpressure level the shear wave velocity,  $c_s$ , will have to be approximately 5000 fps which means that the dilatational wave velocity must be close to 10,000 fps. Therefore this situation will seldom occur in ordinary soils.

At the 1000 psi overpressure level dilatational outrunning will occur if

$$c \approx 280 \sqrt{1000} = 9,200 \text{ fps}$$

and if  $c \approx 18,000$  fps, shear wave outrunning will take place. This requires a very hard rock medium.

The phasing or time differential  $\Delta t$  between the outrunning seismic wave and the blast front at a target located at distance,  $r_p$ , from G.Z. is given approximately by Reference 3.7 and reads

$$\Delta t \approx 0.024 W^{-1/2} \left[ \left( \frac{r_p}{1000} \right)^{2.5} - \left( \frac{r_o}{1000} \right)^{2.5} \right] - \frac{r_p - r_o}{c} \text{ seconds} \quad (3.12)$$

Thus if  $W = 10$  MT;  $r_o = 5,160$  ft; and  $r_p = 8,000$  ft.

$$\Delta t \approx 0.011 (8^{2.5} - 5.16^{2.5}) - \frac{2840}{c} = 1.34 - \frac{2840}{5000} = 0.77 \text{ sec.}$$

The dilatational wave therefore will arrive 0.77 seconds ahead of the blast. The corresponding overpressure at 8000 ft. will be

$$\begin{aligned} P_{so} &= 1.85 \times 10^9 W^{2/3} R^{-2} \\ &= 4.65 \times 10^9 R^{-2} = 72.7 \text{ psi} \end{aligned}$$

The shear wave in a medium with  $c_s \approx 5000$  fps, i.e., with  $c \approx 10,000$  fps also will have  $\Delta t = 0.77$  sec. The duration of the positive phase of the overpressure for a 10 MT burst is found from Brode's Figure 24 in Reference 3.1 to be about 2.15 seconds. Accordingly the numerical example will have a phasing time of about one third of the positive overpressure duration.

## 3.5 Ground Motion Quantities

3.5.1 Motion of free-field particles. The propagational velocities of seismic disturbances in elastic half spaces are independent of the stress levels, but in real half spaces or soils the moduli of elasticity vary with stress and thereby make the propagational speeds variant even within each stratum. If the moduli usually decrease with stress, the propagational speeds are reduced and the seismic wave travel curves therefore will overestimate the distances traveled.

The intensities of seismic disturbances generated and propagated in layered elastic half spaces are amenable to closed form solutions by a very involved rational analysis. In real half spaces or soils, especially near the surface as well as further down for high stress levels, the behavior of the media, is far from elastic, making a rational approach very difficult. Accordingly the knowledge of seismic intensities stems almost wholly from empirical data.

Since nearly all field tests relate to small scale events, many of which were carried out by high explosives, H. E., the accumulated body of empirical knowledge must be normalized or referred to scaled parameters. The conversion factors for relating free field motions resulting from H E tests to those from nuclear tests are very uncertain, being in the order of 20 percent, and similarly the conversion factors from fully contained bursts to surface bursts, which are in the order of 2 to 5 percent, are also open to serious question. Accordingly a relatively large uncertainty is present in normalizing a great deal of the test data.

The free field motion of a particle located in or on the surface of a half space is completely defined by its radial, tangential, and circumferential components of either an acceleration, or a velocity, or a displacement time record. However, such a record is invariably complicated and difficult to describe and normalize. Therefore only the most pertinent measurements are considered, namely the peak acceleration, peak velocity and peak displacement. If these three quantities are known then it is assumed that the free field intensity is defined sufficiently well for practical purposes, in other words, the time element defining the shape of the motion is left out.

3.5.1.1 Compatibility criterion. A necessary criterion for the relationship or compatibility of peak acceleration  $a$ , peak velocity  $v$ , and peak displacement  $d$  will now be stated, namely

$$a d \geq v^2 \quad (3.13)$$

A simple demonstration of this necessary but not sufficient criterion for compatibility of  $a$ ,  $v$ , and  $d$  can be shown as follows:

Assume a symmetrical triangular velocity pulse of peak value  $v$  and duration  $\tau$  as shown in Figure 3.20.

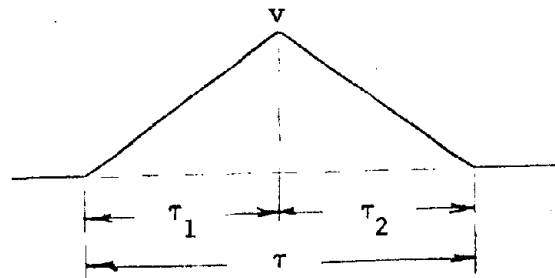


FIGURE 3.20

Since  $\tau_1 = \tau_2 = \tau/2$  the slopes or accelerations are constants with values of  $\pm 2v/\tau$  and the final displacement is a peak value and equal to  $v\tau/2$ . Accordingly

$$a d = \left| \frac{2v}{\tau} \right| \cdot \left| \frac{v\tau}{2} \right| = v^2$$

Now if  $\tau_1 \neq \tau_2$  then the peak acceleration corresponding to the smaller value of  $\tau$  will be larger than  $2v/\tau$  while the peak displacement remains  $v\tau/2$ . Therefore if  $\tau_1 \neq \tau_2$

$$a d = \left| \frac{v}{\tau_1} \right| \cdot \left| \frac{v\tau}{2} \right| > v^2$$

It may therefore be said that even the smallest imaginable asymmetry or skewness of the triangular velocity pulse will make

$$a d > v^2$$

The same reasoning can be applied to differently shaped but symmetrical velocity pulses, and the general observation can be made that  $a$ ,  $v$ , and  $d$  are not compatible unless  $a d > v^2$ . In nearly all field tests this inequality is considerable.

The following types of free field ground motions will be discussed briefly:

1. directly transmitted ground motion, including outrunning of blast front
2. air blast induced motion
  - a. superseismic or air shock wave
  - b. subseismic air shock wave, outrunning ground shock

3.5.2 Directly transmitted ground motions. Using the results of the contained nuclear explosive tests in tuff from Rainier Shot of Operation Plumbob as a basis for extrapolation, Newmark, Reference 3.7 found that the maximum peak radial acceleration,  $a_r$ , can be represented by

$$a_r = 2300 \text{ g} \left( \frac{W}{1 \text{ KT}} \right) \left( \frac{100 \text{ ft}}{R} \right)^4$$

where  $R$  = radial distance from C.Z. Furthermore, taking into account the  $a$ ,  $v$ , and  $d$  compatibility criterion as well as results from other sources, the following expression has been devised:

$$a_r = 1600 \text{ g} \left( \frac{W}{1 \text{ KT}} \right)^{5/6} \left( \frac{100 \text{ ft}}{R} \right)^{3.5}$$

Employing the highly conjectural equivalence or conversion factor of 5 percent to convert from a fully contained explosion to a surface explosion, and relating the yield to an MT basis and the distance,  $R$ , to kilofeet, it is found that for Rainier tuff:

$$a_r = 13 \text{ g} \left( \frac{W}{1 \text{ MT}} \right)^{5/6} \left( \frac{1000 \text{ ft}}{R} \right)^{3.5}$$

or

$$a_r = 13 W^{5/6} R^{-3.5} \text{ g's}$$

It is to be kept in mind that the above expression is for a particular medium, a tuff, with a seismic dilatational velocity,  $c$ , of about 6000 fps. Elementary considerations indicate that the particle acceleration in a medium should be proportional to  $c^2$ . Making this assumption Newmark Reference 3.7 found that the representation of peak values of radial acceleration, velocity, and displacement on a log-log plot with distance, or with scaled slant range  $R$ , requires a bi-linear plot in which the linearity

transition occurs at the scaled slant range of 2.5 kilofeet, i.e.  
 $R = 2.5 W^{1/3}$  with  $W$  expressed in MT. Using  $c$  in kilofeet per second the representation is

$$\begin{aligned} \text{For } R \leq 2.5 W^{1/3} \quad & \text{kilofeet} \\ a_r &= 0.4 W^{5/6} R^{-3.5} c^2 \text{ in g's} \\ v_r &= 12 W^{5/6} R^{-2.5} c \text{ in inches/sec} \\ d_r &= 4 W^{5/6} R^{-1.5} \text{ in inches} \end{aligned} \tag{3.14a}$$

But for  $R \geq 2.5 W^{1/3}$  kilofeet a slower rate of attenuation must be used, namely

$$\begin{aligned} a_r &= 0.081 W^{1/4} R^{-1.75} c^2 \text{ in g's} \\ v_r &= 4.8 W^{1/2} R^{-1.5} c \text{ in inches/sec} \\ d_r &= 3.2 W^{3/4} R^{-1.25} \text{ in inches} \end{aligned} \tag{3.14b}$$

These relations of  $a_r$ ,  $v_r$ , and  $d_r$  satisfy the compatibility relationships, Equation (3.14) so that for the close in representation (Equations 3.14a)

$$1.6 g W^{5/3} R^{-5} c^2 = 620 W^{5/3} R^{-5} c^2 > 144 W^{5/3} R^{-5} c^2$$

and for the further out representation (Equations 3.14b)

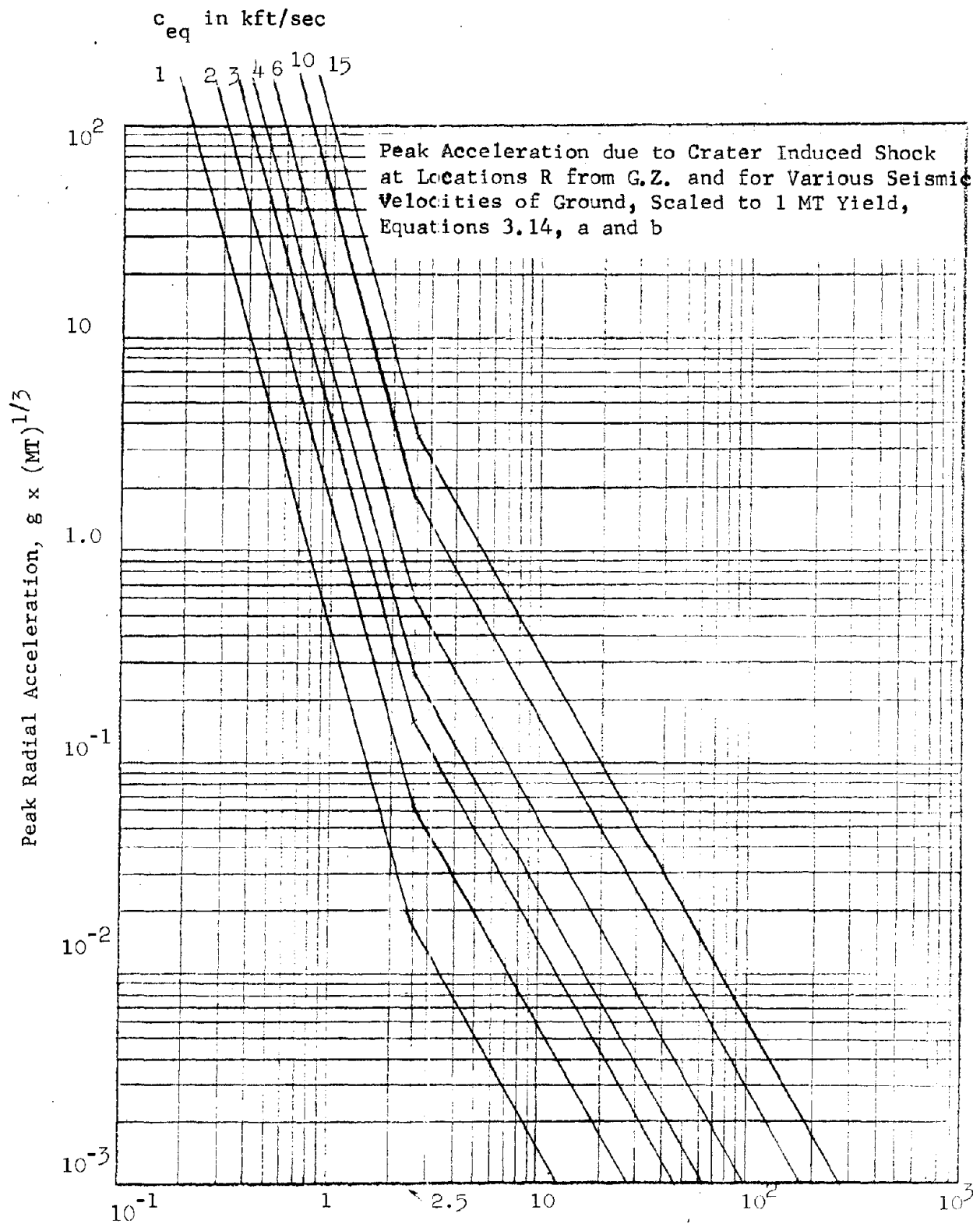
$$0.26 g W R^{-3} c^2 = 100 W R^{-3} c^2 > 23 W R^{-3} c^2$$

In both cases the left side to right side ratio of the inequality is 4.3, indicating that considerable asymmetry is present in the velocity-time relationship or that peakedness is present in the acceleration-time relationship.

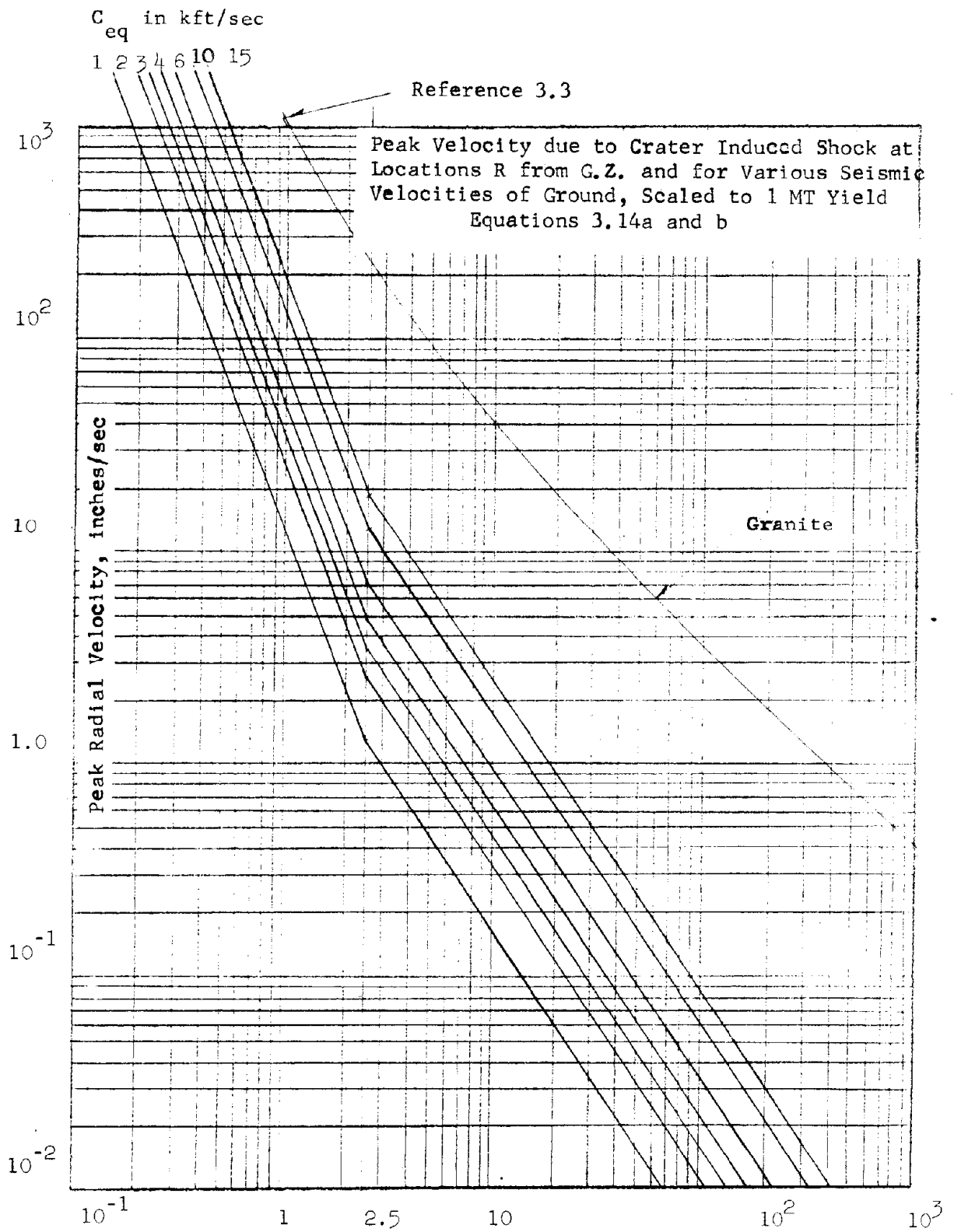
The above relationships of  $a_r, v_r, d_r$  with  $R$  are plotted in Figures 3.21, 3.22, and 3.23.

**3.5.2.1 Comparison of expressions.** It is of interest to compare Newmark's representation with recently published results by Stanford Research Institute (SRI), Reference 3.3. Since the SRI data relates to contained shots the use of conversion factors will be required. Moreover, most of the SRI reported data was obtained from small detonations.





$R = \text{Slant Range, k ft}/(MT)^{1/3}$   
FIGURE 3.21



$R = \text{Slant Range, k ft}/(\text{MT})^{1/3}$

FIGURE 3.22

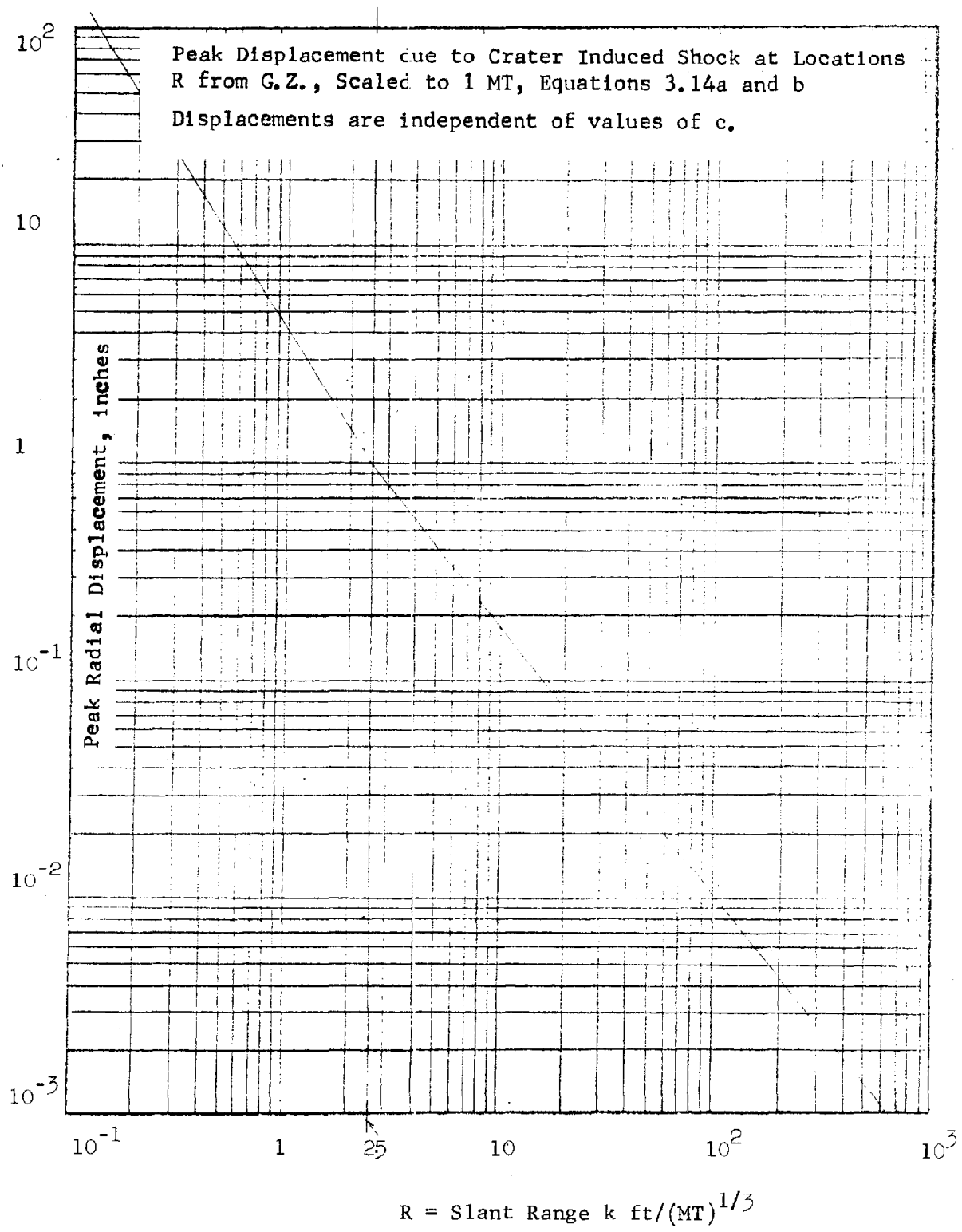


FIGURE 3.23

Figures 3.24 and 3.25 show the SRI results for four media replotted from the reference to the same scale as the Newmark expressions. Confining the attention to the tuff found at Nevada Test Site, i.e. Rainier tuff, and assigning the seismic velocity value of 6 kft/sec to this medium, it is found that at the transitional slant range of  $2.5 W^{1/3}$  kft the results are:

	<u>Newmark</u>		<u>SRI</u>	
$a_r$	0.6 g	(Fig. 3.21)	-	
$v_r$	7.2 in/sec	(Fig. 3.22)	75 in/sec	(Fig. 3.24)
$d_r$	1.0 inches	(Fig. 3.23)	8.0 inches	(Fig. 3.25)

Since Newmark's representations (Equations 3.14a,b) give identical values of  $a_r$ ,  $v_r$  and  $d_r$  at  $R = 2.5$  kft., the scaling relationship of yield, which is  $W^{1/3}$ , offers two possibilities of inferring the value of the (surface shot)/(contained shot) equivalence yield factor, namely, either by scaling up Newmark's results or by scaling down the SRI results. Let the equivalence factor be denoted by  $\alpha$ , then a yield of  $\alpha$  MT(contained) produces the same effect as 1 MT on the surface. Scaling up Newmark's results, Figure 3.22, to give the SRI value of 75 inches/sec it is seen that the slant range must be reduced from 2.5 kft to about 1 kft. The yield must then be increased from 1 MT to  $(2.5/1)^3$  MT or 15.6 MT from which  $\alpha$  is inferred to be  $1/15.6$  or 0.064. By scaling down the SRI results, to give the Newmark velocity value of 7.2 inches/sec, Figure 3.24, the slant range must be increased to about 14 kft. The yield must therefore be reduced to  $(\frac{2.5}{14})^3$  MT or to 0.0057 MT from which  $\alpha$  is inferred to be 0.0057. This seemingly poor agreement of  $\alpha$  with 0.064 is not unexpected, considering the small scale tests from which the curves have been drawn.

A similar scaling up of Newmark's displacements gives an  $\alpha$  value of 0.018, and a scaling down of SRI data gives  $\alpha = 0.021$ , an almost perfect agreement considering the sensitivity of  $\alpha$  with the third power of  $R$ .

In spite of the relatively unsatisfactory agreement between the Newmark expressions and the SRI reference it is recommended that the curves in Figures 3.21, 3.22 and 3.23 be used for determining peak free field intensities of directly transmitted ground motions originating from GZ of a

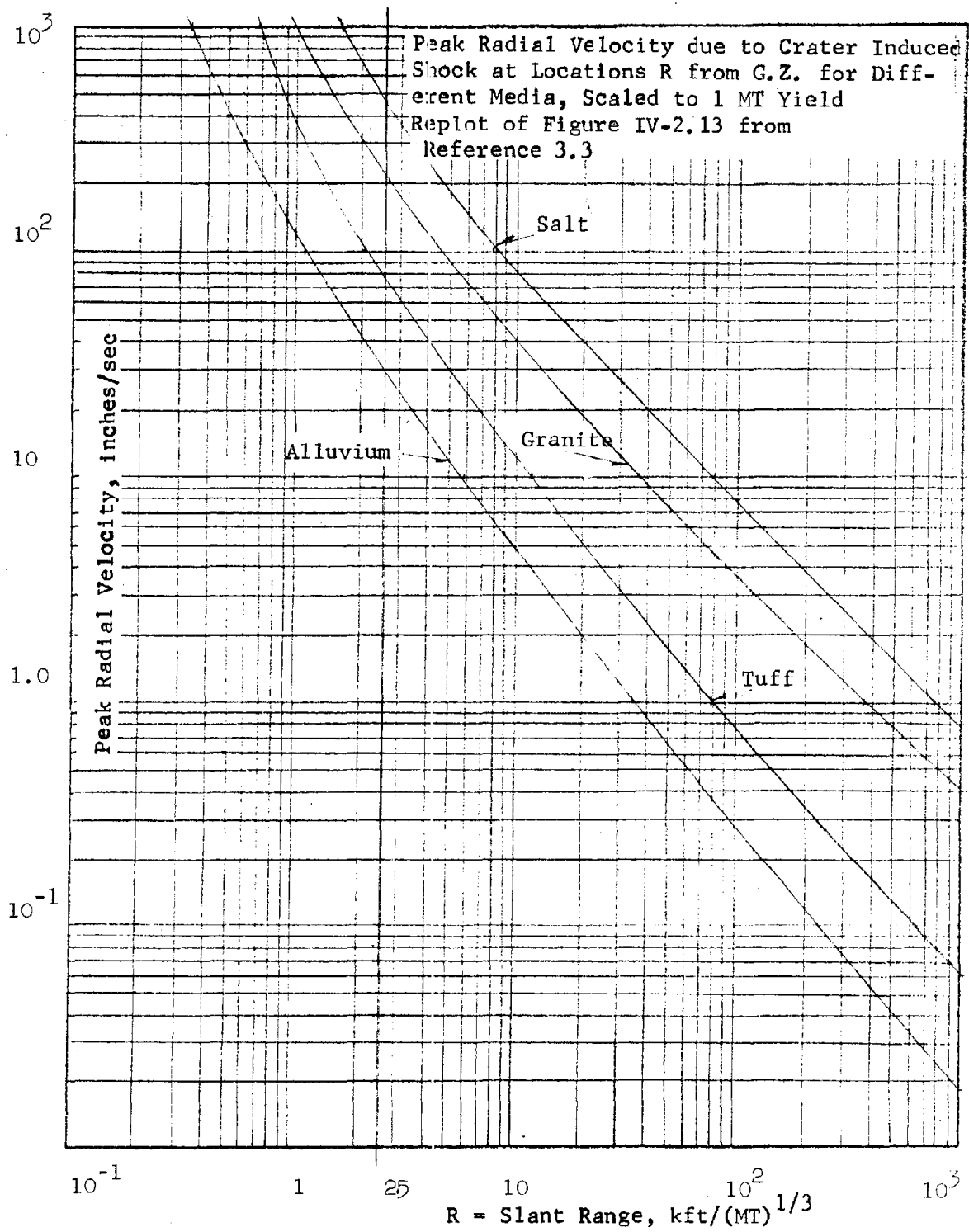


FIGURE 3.24

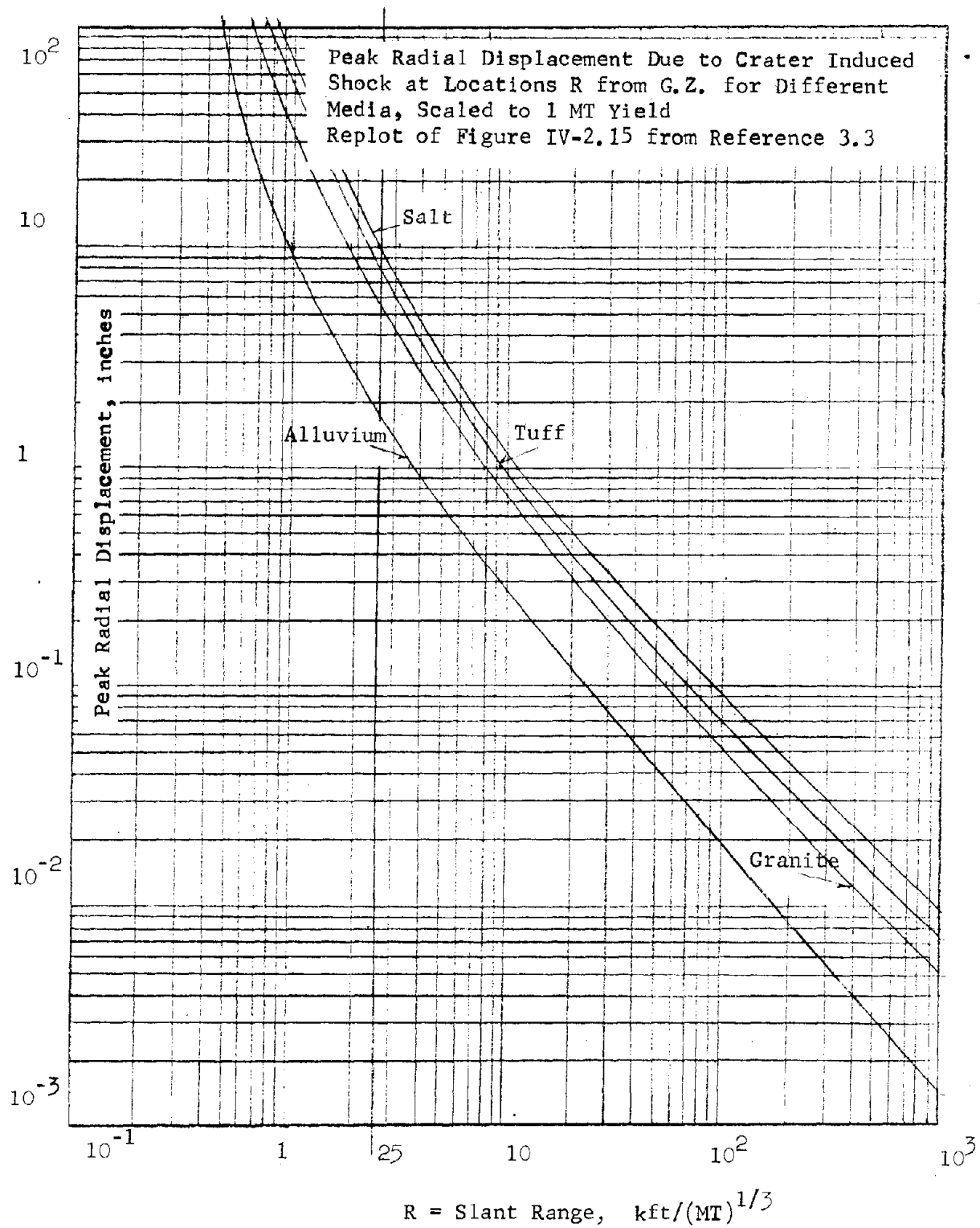


FIGURE 3.25

surface burst. Some caution should be sounded in regard to applying the curves to outrunning at the surface where the free field is considerably modified by the medium's inability to act in tension. Since the curves 3.21 and 3.22 relate to soils which have a single seismic velocity, the surface layering commonly found may also modify the intensities considerably. In short, Figures 3.21, 3.22, and 3.23 cannot be expected to give much more accuracy than the correct order of magnitude of free field intensity.

3.5.3 Air blast induced ground motions. These motions originate continually at the air blast front as initially downward disturbances. They are very sensitive to the near surface elasto-plastic and/or elasto-locking properties of the soil.

3.5.3.1 Superseismic or direct downward slap from blast front. The descending compressional wave due to the traveling blast front is referred to as the direct downward slap, and it is by all counts the most important disturbance occurring near the surface at overpressure levels below 1000 psi.

A simplified one dimensional theory of the dynamic vertical displacements has been developed in Reference 3.2. It is based on the inelastic behavior of soil and involves the consideration of a linearized stress strain curve as shown in Figure 3.26. The initial tangent modulus of deformation  $M_i$  is assumed to govern the propagational velocity  $c_i$  of the initial part of the wave front, i.e.

$$c_i^2 = \frac{M_i}{\rho} \quad (3.15)$$

The peak strain or the peak of the wave front is propagated at a lower velocity  $c_p$  given by

$$c_p^2 = \frac{M_p}{\rho} \quad (3.16)$$

and the unloading strain part of the disturbance has a velocity related to  $M_r$ .

where  $M_p$  = Secant Modulus of the loading curve to the peak stress value  
 $M_r$  = Secant Modulus of the unloading curve

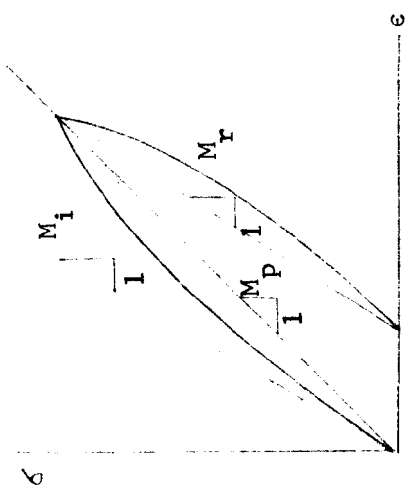


FIGURE 3.26

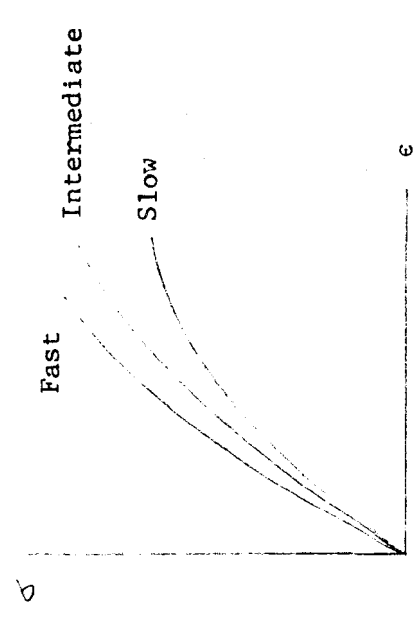


FIGURE 3.28

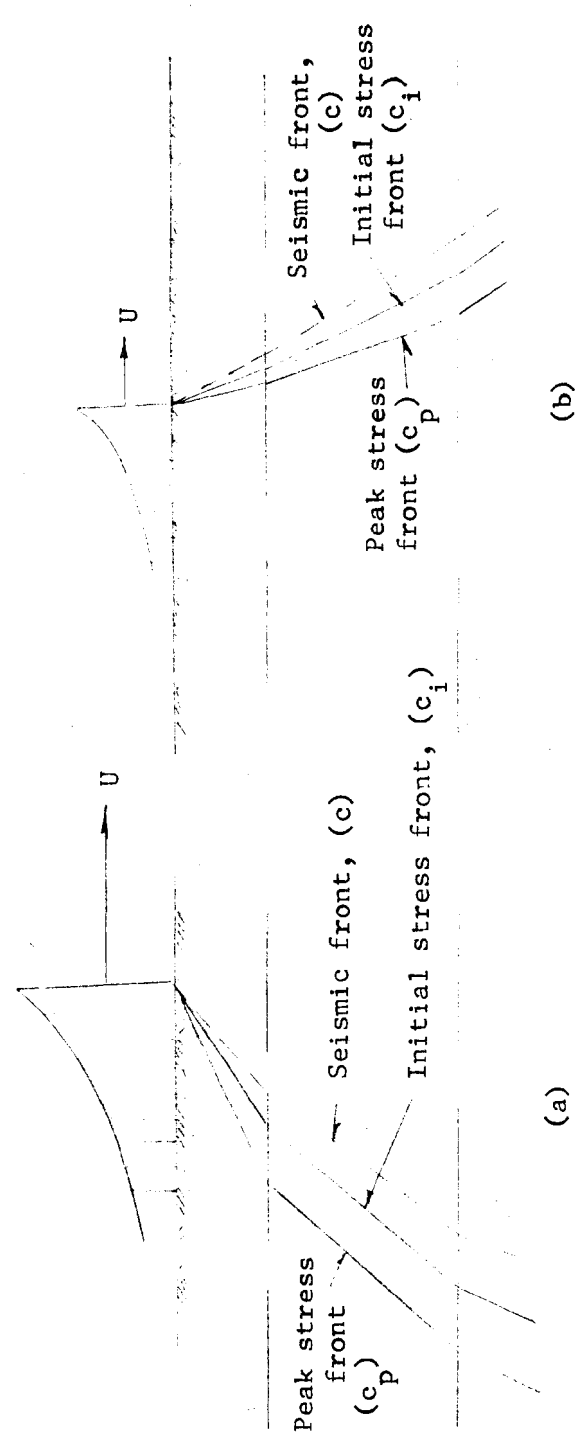


FIGURE 3.27



Figures 3.27a and b show the two stress wave fronts in a layered medium for the comparatively close in situation where  $U$  is superseismic, and for the farther out where  $U$  is subseismic with respect to the dilatational wave velocity,  $c$ .

The problem of assigning meaningful values to  $c_i$  and  $c_p$  is complicated by the fact that the stress strain curve of most soils is affected by the rate of loading as indicated schematically in Figure 3.28. Stanley D. Wilson and Earl A. Sibley in Reference 3.5, show, on a semi-logarithmic plot, Figure 3.29, the experimentally obtained tangent moduli of deformation of a Playa silt when the medium is loaded in two confined conditions characterized by the lateral to axial stress ratio,  $\gamma$ . The scatter for slow and for fast loading was considerable, but the slow loading results fell primarily in the left half of the band, the fast loading results fell to the right, and the medium loading along the median of the band. When the medium is vibrated in the two confined conditions a somewhat small range of results is obtained. Finally for the situation where the modulus is computed from a seismic velocity survey the discontinuous curve is obtained. The numerical range of the modulus is seen to be very large, at the surface from 6,000 to 60,000 psi, and at the 200 ft. level from 15,000 to 200,000 psi. To these moduli correspond computed propagational velocity ranges of 500 to 1500 fps at the surface, and 780-2800 fps at the 200 ft. level for a soil weighing 115 pounds per cubic foot. Since the degree of saturation as well as the overburden stress will also affect the moduli, only a general conclusion can be made, namely that:

$$M_{\text{seismic}} > M_{\text{vibrational}} > M_{\text{static}}$$

and from this it follows that the seismic velocity  $c$  will be larger than the initial stress front velocity,  $c_i$ ; and  $c_i$  will be larger than the peak stress front velocity,  $c_p$ . Moreover,  $c_p$  may be assumed to be about equal to the velocity computed for the vibrational tests; it is definitely larger than the nominal velocity computed from the  $M$  values of the essentially static tests.

Reference 3.2 in Figure 3.30 shows a suggested variation of  $c_i$  and  $c_p$  with depth and the resulting arrival times of these two wave fronts at

FIGURE 3.29 SUMMARY OF LABORATORY TEST RESULTS REFERENCE 3.5

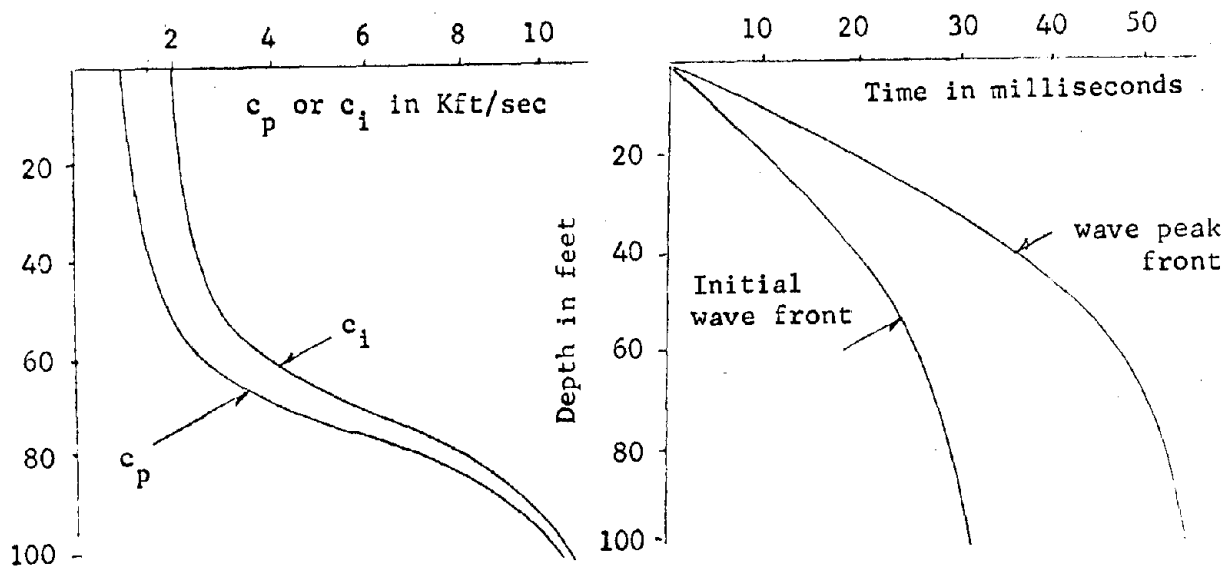
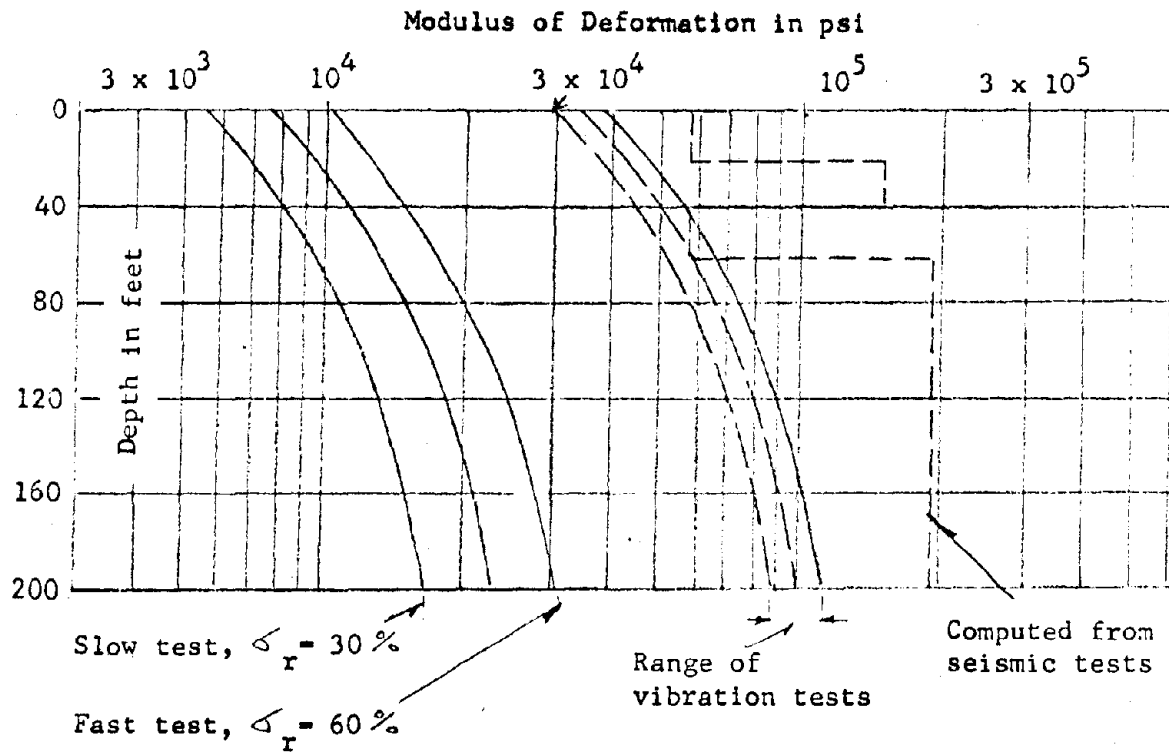


FIGURE 3.30

the various depths. It is seen that at depths greater than 100 ft., the propagational velocities are about equal and the wave fronts will occur a constant time interval apart, about 20 milliseconds. Due to this phenomenon of different values of  $c_i$  and  $c_p$  near the surface, the extremely steep front of the blast wave at the surface will become considerably less steep below the surface; eventually it will approach a rise time of about 20 milliseconds. This in turn means that the particle accelerations and velocities below the surface will be greatly reduced with respect to their surface magnitudes.

Attenuation of the vertical stress with depth has been formulated empirically in Reference 3.2 as a result of both the spatial dispersion and the inelastic behavior of the medium. It is described by an empirical attenuation factor  $\alpha_z$  so that the peak vertical stress  $\sigma'_z$  at a level  $z$  below the surface is given by

$$\sigma'_z = \alpha_z p_{so}$$

in which

$$\alpha_z = \frac{1}{1 + \frac{z}{L_w}} \quad (3.17)$$

and

$$L_w = 2300 p_{so}^{-\frac{1}{2}} W^{\frac{1}{3}} \text{ ft with } W \text{ expressed in MT}$$

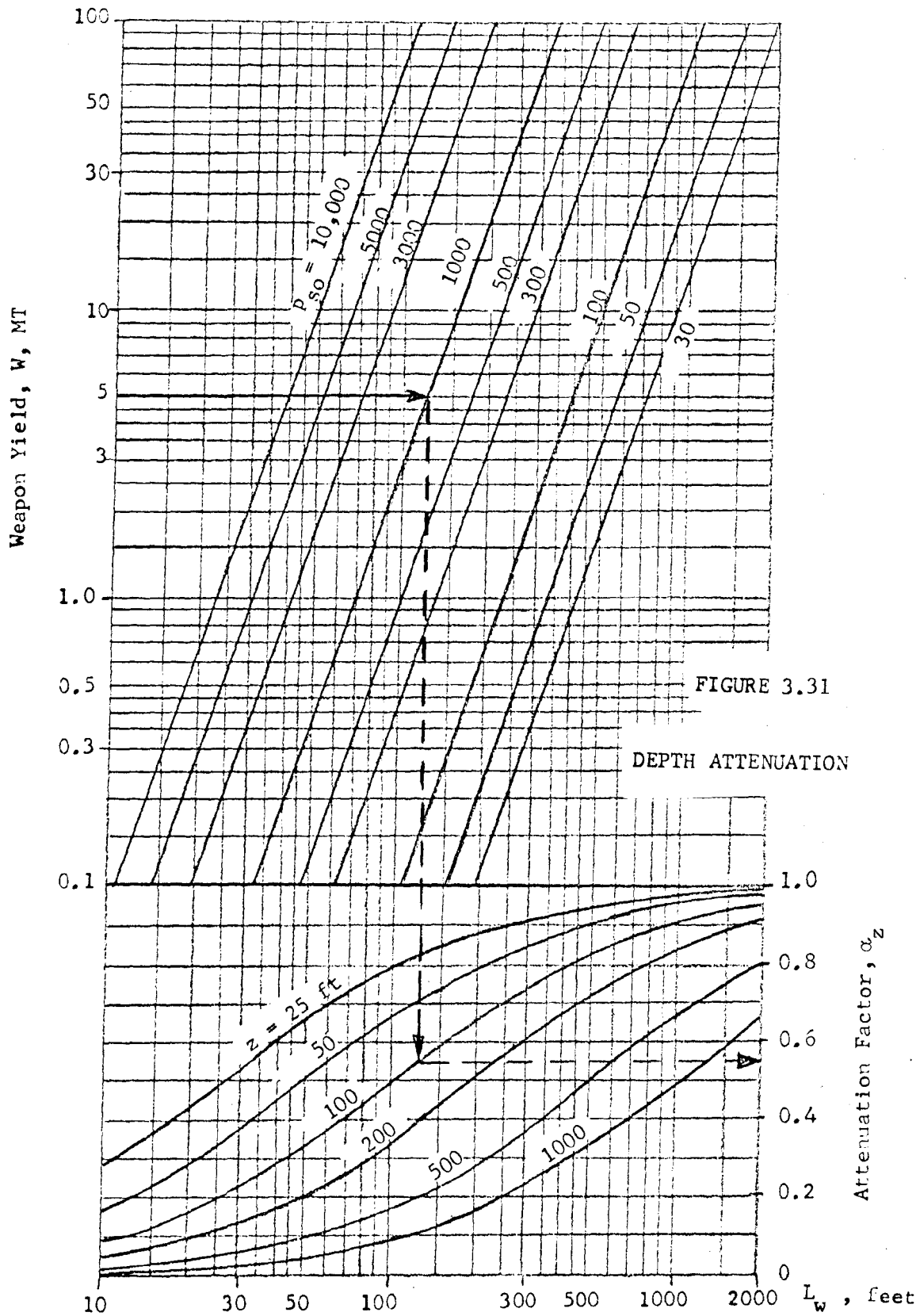
Reference 3.2 also gives Figure 3.31 from which  $\alpha_z$  can be found for any depth up to 2000 ft, at a given yield and overpressure.

It is obvious that many parameters will enter into the problem of free field intensities due to blast wave slap on layered soils, and even by expending considerable effort it is at best possible to be certain only of the order of magnitude. The following expressions from Reference 3.2 are therefore presented only as a rough means of obtaining, with small effort, an idea of the magnitudes of the free field motions. They represent the considered judgment of the authors of the reference.

The recommended expressions for  $a_v$ ,  $v_v$  and  $d_v$  are:

Peak downward acceleration at the surface

$$a_{vs} = 1.5 p_{so} c_p^{-1} \quad \text{in g's} \quad (3.18)$$



Peak downward acceleration at depth z

$$a_{vz} = 5 \times 10^{-3} p_{so} z^{-1} \alpha_z \text{ in g's} \quad (3.19)$$

with

$$p_{so} \text{ in psi; } c_p \text{ in kft/sec, taken at the surface; and } z \text{ in kft.}$$

The peak horizontal acceleration is commonly assumed to be equal to the peak vertical acceleration.

It is seen that  $a_{vz}$  is not equal to  $a_{vs}$  at zero depth. This is caused by a very rapid attenuation of acceleration, mainly due to  $c_i > c_p$  and a consequent rise time increase that occurs in a very thin layer near the surface. The rise time of stress for a depth z is given by

$$t_r = \int_0^z \frac{dz}{(c_p)_z} - \int_0^z \frac{dz}{(c_i)_z}$$

If  $c_p$  and  $c_i$  are constant from the surface to depth, z, the rise time is simply

$$t_r = \frac{z}{c_p} - \frac{z}{c_i} \quad (3.20)$$

Peak downward velocity at the surface and at depth z

$$v_{vz} = 0.5 p_{so} c_p^{-1} \alpha_z \text{ inches/sec.} \quad (3.21)$$

The peak horizontal velocity is commonly taken at 2/3 of  $v_{vz}$ .

For preliminary estimates of ground displacements the following expressions from Reference 3.2 may be used for a homogeneous soil weighing 115 pcf.

The peak downward elastic displacement at the surface is expressed by

$$d_{vse} = 0.9 p_{so}^{1/2} c_r^{-1} W^{1/3} \text{ inches} \quad (3.22)$$

in which  $c_r$  is an average seismic velocity defined by

$$c_r^2 = M_r / \rho, \text{ see Figure 3.26}$$

The approximate downward residual displacement at the surface as related to tests at the Nevada Test Site (N.T.S.) is given by

$$d_{vsr} \approx \frac{p_{so} - 40}{30} c_o^{-2} \text{ inches} \quad (3.23)$$

in which

$c_o$  is the surface seismic velocity in kft/sec.

At N.T.S. the use of  $c_o = 1$  kft/sec gives an upper bound to the surface residual displacements, moreover this means that no residual displacement at the surface will occur for  $p_{so} \leq 40$  psi, and also that the total peak displacement at the surface is  $d_{vse} + d_{vsr}$ .

The approximate value of the residual downward displacement at a depth, z, is expressed by

$$d_{vzr} \approx d_{vsr} \left(1 - \frac{z^*}{100 \text{ ft}}\right) \text{ inches} \quad (3.24)$$

with

$$\begin{aligned} z^* &= z \text{ ft for } 0 \leq z \leq 100 \text{ ft} \\ z^* &= 100 \text{ ft for } z > 100 \text{ ft} \end{aligned}$$

This means that no residual relative displacements will occur below 100 ft.

The approximate value of the downward elastic component of the relative displacement between the surface and a point at depth, z, is expressed by

$$\Delta d_{vze} \approx \left\{ \begin{array}{l} 4.8 \\ 2.4 \end{array} \right\} \times 10^{-2} p_{so} c_r^{-2} \frac{z^*}{100} \text{ inches} \quad (3.25)$$

The two numerical values given in the parentheses reflect the uncertainty of this expression.

A reasonable estimate of the maximum vertical displacement at a point, z, is

$$(d_{vz})_{\max} \approx d_{vse} - \Delta d_{vze} + d_{vzr} \quad (3.26)$$

It should be remembered that expressions (3.22) - (3.26) are based on the N.T.S. limited number of experiments and on a soil density of 115 pcf. A correction for soils of density,  $\rho$ , can be made by multiplying all  $c$  values by  $\sqrt{\rho/115}$ .

Horizontal displacements are not obtainable by the one dimensional theory. Currently two dimensional models are being studied by several investigators. Until more information becomes available it is suggested that

$$\frac{d_h}{d_v} \text{ be taken as } \frac{1}{3} \quad (3.27)$$

The above equations will usually lead to conservative estimates of the ground displacement since the soil stiffness increases significantly with depth. This will decrease the vertical displacements near the surface. Appendix E discusses an alternate static procedure for estimating the ground displacements accounting for increase in stiffness of the soil with depth. Subsection 3.5.4 outlines a more accurate procedure for calculating displacements on an incremental basis.

Example 3.14

Assume a 10 MT yield and  $p_{so} = 300$  psi; moreover let  $\rho g = 115$  pcf  
 $c = 2.5$ ;  $c_i = 2.0$ ,  $c_p = c_o = 1.0$ ,  $c_r = 1.5$  kft/sec =  $\frac{1}{2} (c_i + c_p)$

Then from Equation (3.17) the attenuation is

$$L_w = 2300 \times 300^{-1/2} 10^{1/3} = 2300 \times \frac{2.16}{17.3} = 287 \text{ ft.}$$

$$\alpha_z = \frac{287}{287 + z}$$

Giving:

$z =$	10	30	60	100	200	500	ft
$\alpha_z =$	.965	.905	.827	.741	.589	.364	

Peak vertical acceleration at the surface, downward from Equation (3.18) is

$$a_{vs} = 450 \times 1^{-1} = 450 \text{ in g units}$$

Peak vertical acceleration at  $z$  ft. below the surface from Equation (3.19) is

$$\begin{aligned} a_{vz} &= 5 \times 10^{-3} p_{so} z^{-1} \alpha_z \text{ in g units} \\ &= 1.5 \frac{\alpha_z}{z} \end{aligned}$$

Giving

$z =$	10	30	60	100	200	500	ft
$a_{hz} =$	145g	45g	21g	11g	4.4g	1.1g	

Note that the acceleration decreases from 450g to 145g in the top 10 feet of soil.

Example 3.14 (continued)

Peak vertical velocity at z ft. below surface from Equation (3.21) is

$$v_z = 150 \times 1^{-1} \alpha_z \text{ in/sec}$$

Giving

z	=	0	10	30	60	100	200	500	ft.
$v_{vz}$	=	150	145	136	126	111	88	54	in/sec
$v_{hz}$	=	100	97	91	84	74	59	30	in/sec

Peak vertical elastic displacement at surface, downward, from Equation (3.22) is

$$d_{vse} = 0.9 \times 17.3 \times 2.2^{-1} \times 10^{1/3} = 15.3 \text{ inches}$$

Approximate residual downward displacement at the surface from Equation (3.23) is

$$d_{vsr} = \frac{P_{so}^{-40}}{30} c_o^{-2}$$

$$d_{vsr} = 8.7 \text{ inches}$$

Accordingly

$$(d_{vs})_{\max} = d_{vse} + d_{vsr} = 15.3 + 8.7 = 24 \text{ in.}$$

Approximate residual downward displacement at depth z from Equation (3.24) is

$$d_{vzr} = d_{vsr} \left(1 - \frac{z^*}{100 \text{ ft}}\right) \text{ inches}$$

Giving

$z^*$	=	9	10	30	60	100	200	500	ft
$d_{vzr}$	=	8.7	7.8	6.1	3.5	0	0	0	inches

Using the average coefficient of  $3.6 \times 10^{-2}$  in Equation (3.25), the approximate downward elastic relative displacement between the surface and at depth z is

$$\Delta d_{vze} = 10.8 c_r^{-2} \frac{z^*}{100} = 4.8 \frac{z^*}{100} \text{ inches}$$

Giving

$z^*$	=	10	30	60	100	200	500	ft
$\Delta d_{vze}$	=	0.48	1.44	2.90	4.8	4.8	4.8	inches



Example 3.14 (continued)

Approximate peak downward displacement at depth,  $z$ , according to Equation (3.26) is

$$(d_{vz})_{\max} = d_{vse} - \Delta d_{vze} + d_{vzr} = 15.3 - \Delta d_{vze} + d_{vzr}$$

Giving

$z$	=	0	10	30	60	100	200	500	ft
$d_{vse} - \Delta d_{vze}$	=	15.3	14.8	13.9	12.4	10.5	10.5	10.5	inches
$d_{vzr}$	=	8.7	7.8	6.1	3.5	0	0	0	inches
$(d_{vz})_{\max}$	=	24.0	22.6	20.0	15.9	10.5	10.5	10.5	inches

Figure 3.32 shows plots of the ground motion quantities for Example 3.14.

3.5.3.2 Subseismic air shock wave, outrunning of ground shock. As the moving blast front expands it continues to send out seismic disturbances which may outrun the blast front or arrive at a buried facility before any other disturbance if the layered medium's seismic velocities increase with depth. The intensities and shapes of these outrunning motions are very complicated and not well defined. In fact, the field records are extremely difficult to interpret and describe in general by empirical means.

It may be assumed that the intensities of these motions will be comparatively low with respect to those resulting from the GZ disturbance and from those due to the direct slap of the blast. They might be neglected except for the fact that they tend to be alternating in character and to have a large upward component. Consequently they may excite appreciable responses in shock mounted equipment whose frequencies are within their periodic content. For want of a better description these disturbances are sometimes referred to as being of random character. At the present time the field records of these motions are under study so as to obtain better quantitative ideas of their upper bounds in terms of seismic and blast parameters.

These motions are discussed in Subsection 3.6.2.3 in terms of idealized triangular waveforms and in Section 3.7.4 in terms of shock spectra.

Example 3.14 (continued)

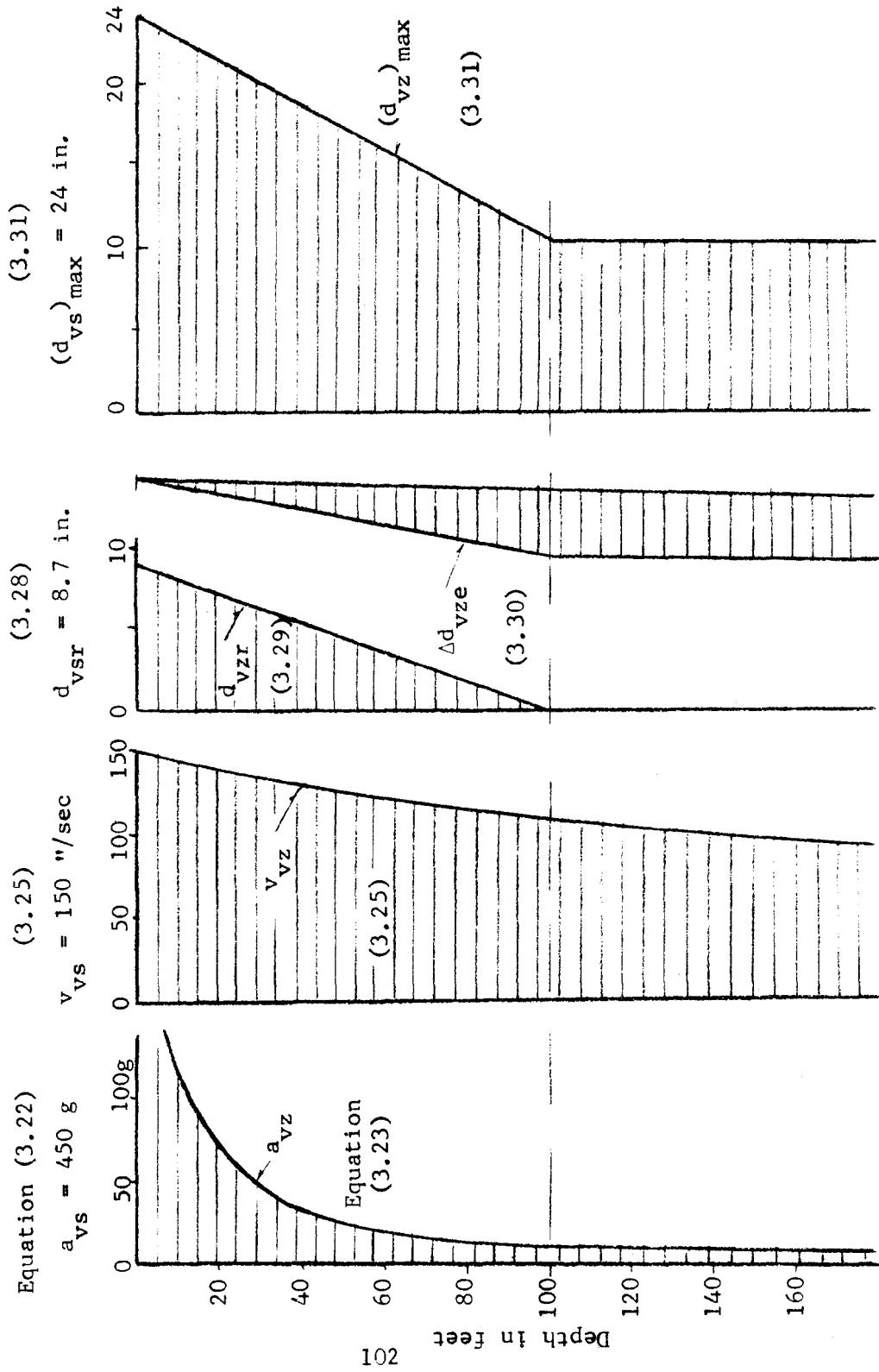


FIGURE 3.32: SHOWING PRELIMINARY ESTIMATES OF GROUND MOTIONS OF EXAMPLE 3.14

### 3.5.4 Discussion of vertical dynamic stress and displacement conditions.

One-dimensional soil model. So as to obtain an idea of the behavior of the one-dimensional model of a soil acted upon by an instantaneously applied and subsequently decaying surface pressure Figure 3.33 has been drawn. It shows a superseismic case with a blast wave of constant velocity  $U = 1.05 c_1$ , and with a corresponding overpressure peak  $p_{so}$  traveling over the point P located at the depth h below the surface. At the instant shown the blast front is at the arbitrary location  $O'$ . Reckoning time from the instant when the overpressure peak was at O, the initial and peak wave fronts are as indicated, and accordingly at time  $t_1 = (O' - O)/U$  the initial wave front has just reached the point, P, the peak wave front has just arrived at the location, Q. The stress in the soil is plotted horizontally in the vertical diagram as a function of depth. It is clear that the stress at  $O''$  must be equal to the local overpressure, and that the peak of the stress attenuated from  $p_{so}$  to  $\sigma'_z$  will be located at Q when the initial wave front has just reached point P at the depth h.

The lower diagram is a time plot of the vertical stress at point P, plotted vertically; the time scale beginning at  $t_1$  runs from right to left. The peak vertical stress  $p_{so}$  has been attenuated to  $\sigma'_z$  due to the wave having traveled the vertical distance h-z; the peak occurs at the approximate time  $t_1 + \frac{h}{c_p} - \frac{h}{c_i}$ .

#### Example 3.15

Assume a 5 MT burst and a 300 psi overpressure level.

Overpressure-time relations. The local variation of pressure with time can be obtained from Brode's curves, Figures 24 and 26 of Reference 3.1. From Figure 24 it is found that the positive duration  $D_p^+$  is 1.0 sec for a 1 MT burst;  $D_p^+$  is therefore  $1.0 \times (5)^{1/3} = 1.7$  sec for a 5 MT burst. From Figure 26 of the reference an interpolation between the 200 and 500 psi curves for  $\Delta p_s$  gives values of  $\Delta p/\Delta p_s$  for the normalized times  $(t - t_s)/D_p^+$

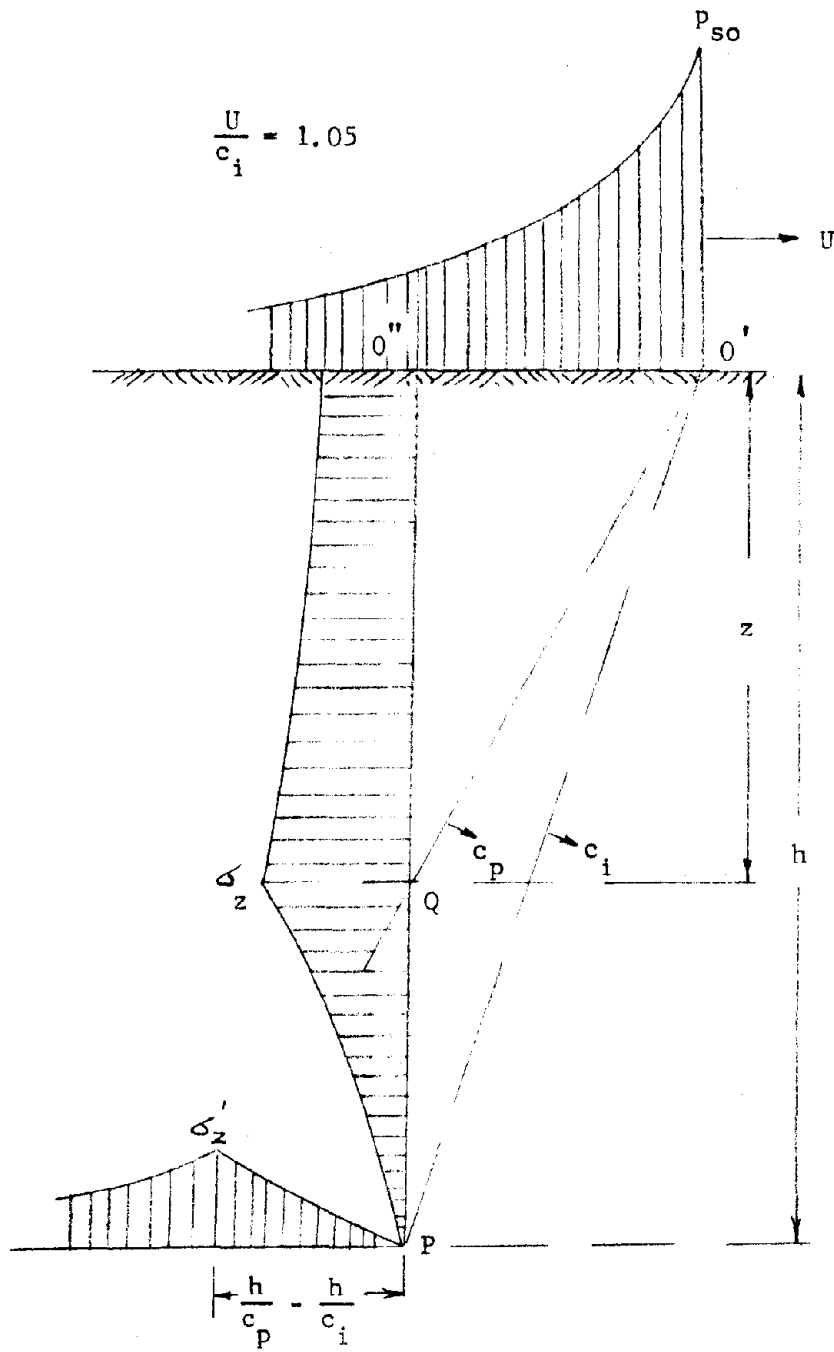


FIGURE 3.33

Example 3.15 (continued)

$(t - t_s)/D_p^+$	=	0	.025	.050	.100	.150	.200	.250	
$\Delta p/\Delta p_s$	=	1.0	0.60	0.43	0.28	0.20	0.15	0.13	
$\Delta p$	=	300	180	130	84	60	45	39	psi
$t - t_s$	=	0	43	85	170	255	340	430	ms.

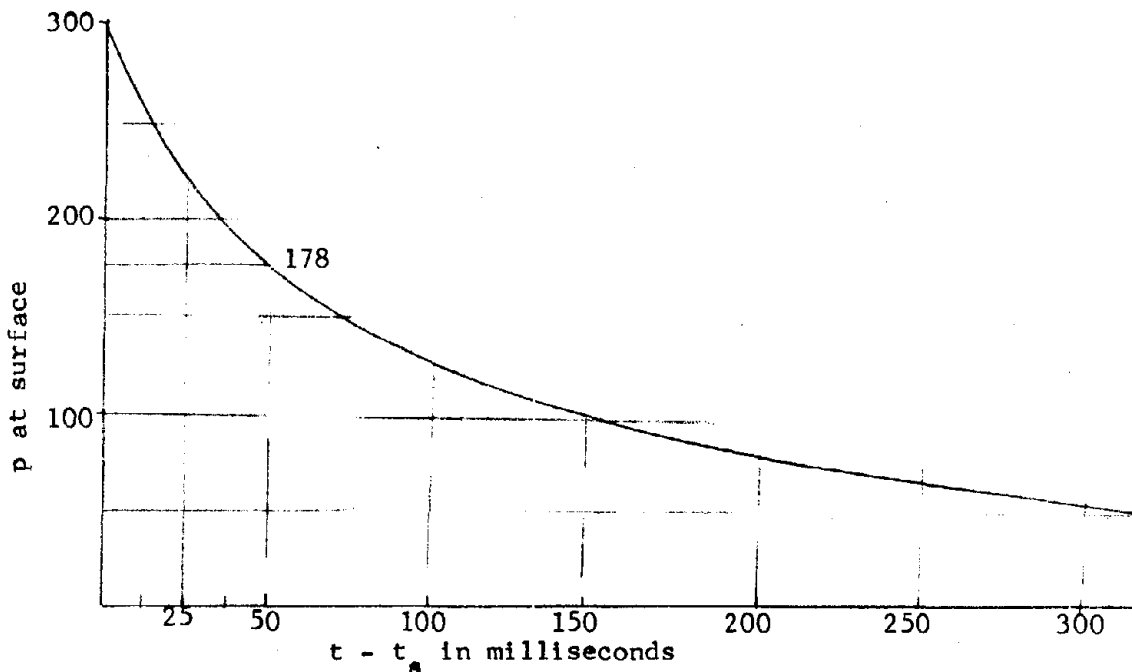


FIGURE 3.34

Figure 3.34 shows a plot of the overpressure  $\Delta p = p_{s0}$  against the actual time  $t = t - t_s$  reckoned from the instant the blast front passes over point P.

Soil constants. A specialized study of vertical stress and displacement cannot be made unless the site exploration has been carried out to give specific values of the propagational velocities  $c_i$  and  $c_p$  as shown in Figure 3.30. If it is assumed for simplicity that  $c_i = 2$  kft/sec and  $c_p = 1.5$  kft/sec then the locations of the two wave fronts with time may readily be computed.

Example 3.15 (continued)

Stress distribution with location and time. Being guided by Figure 3.33, it is possible to construct the stress distribution with depth for various locations and times of the blast front as shown in Figure 3.35. The stress distribution with depth is assumed to be linear with a zero value of stress at the wavefront and having the depth-attenuated value,  $\alpha_z$ , at the wave peak; the stress at the surface is equal to the time-attenuated overpressure as given by Figure 3.34.

Since  $L_w = 2300 p_{so}^{-1/2} W^{1/3} = 220$  ft, the peak vertical stress variation with depth  $z$  is expressed by

$$\alpha_z = \frac{p_{so}}{1 + \frac{z}{220}} \quad (3.28)$$

The numbers shown in parentheses in Figure 3.35 relate to time instants in milliseconds from the arrival of air blast front at the surface. Moreover, the stress distribution extending from the surface to 800 ft depth is close to uniform and approximately equal to 55 psi when the time is 400 milliseconds. It is seen that as time goes on the initial wave front and the peak wave front will occur further apart due to the simplifying assumption of the  $c_i$  and  $c_p$  being constant. This assumption of course is untenable at low stresses and at great depths.

Calculation of vertical displacement. The displacement is the summation of the strains  $\epsilon_z$  over the depth, using average values of  $\epsilon_z$  over arbitrary increments  $\Delta_z$  of depth. The increments of displacement  $\Delta d$ , Reference 3.2, are computed for:

Increasing strain or stress from

$$\epsilon_z = \frac{\sigma_{vz}}{\rho c_p^2} \quad (3.29)$$

$$\Delta d = \epsilon_z \Delta z$$

Decreasing strain or stress from

$$\epsilon_z' = \frac{\sigma_{vz} (1-k_p) + k_p \alpha_z p_{so}}{\rho c_p^2} \quad (3.30)$$

$$\Delta d = \epsilon_z' \Delta z$$

Example 3.15 (continued)

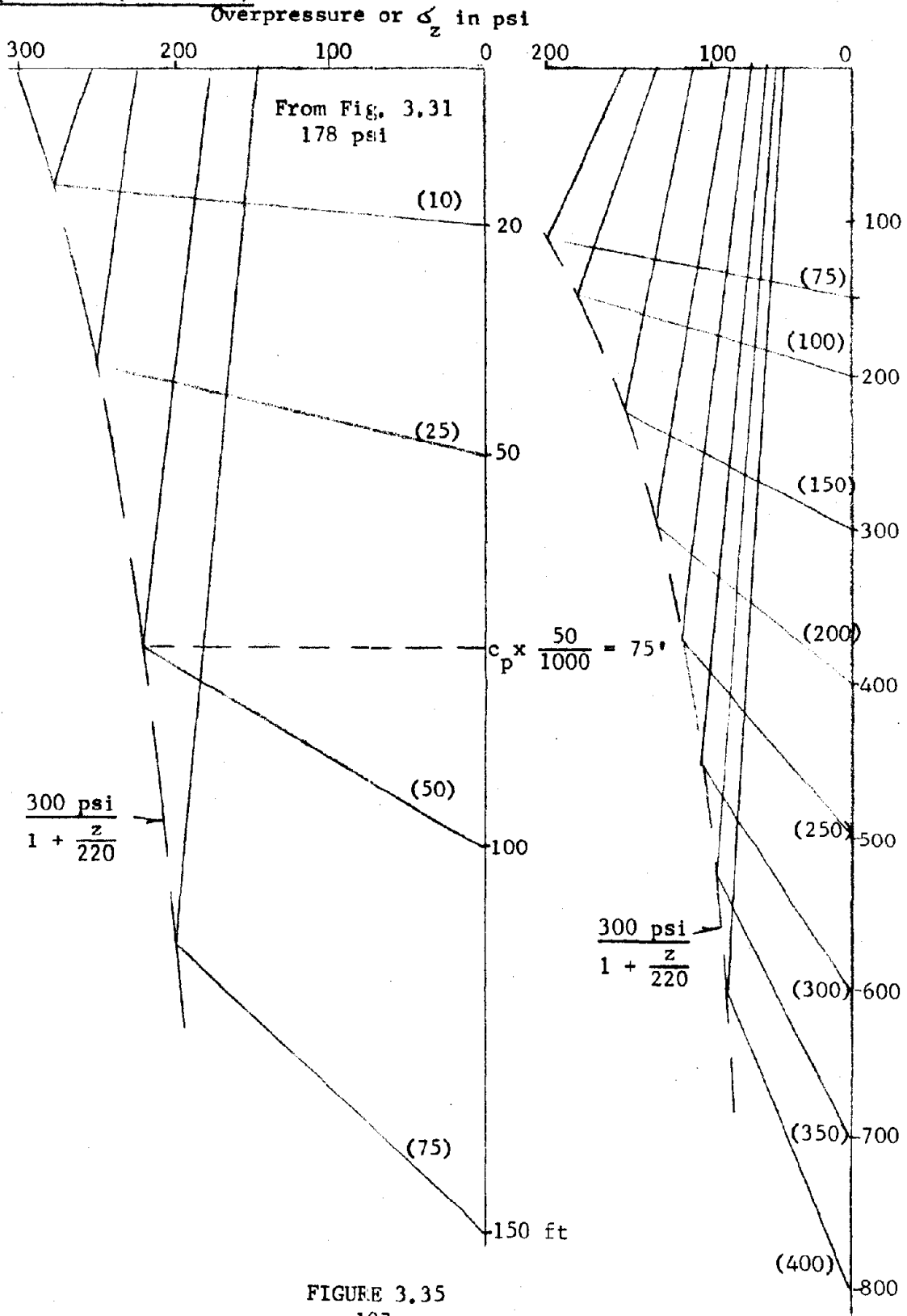


FIGURE 3.35  
107

Example 3.15 (continued)

in which

$$k_p = \frac{\epsilon_{zr}}{\epsilon_{zp}} = \text{residual strain/peak strain}$$

for  $z \leq 100$  ft,  $k_p = 0.3$  (compressible overburden)

$z \geq 100$  ft,  $k_p = 0$  (sound rock)

The  $k_p$  is taken equal to 0.3 since the overstress ratio exceeds three for nearly the full depth of  $z^* = 100$  ft. to "sound" rock.

To find the peak displacement at a given depth a displacement-time curve must be constructed. For each instant of time it is necessary to:

Determine stress versus depth, Figure 3.34

Determine increment of displacement  $\Delta d$  in each  $\Delta z$ , using the appropriate relation for either increasing or decreasing stress.

The displacement at a location  $z$  is then equal to the sum of all displacements occurring below the location. This provides one point on the displacement-time curve at location  $z$ . Repetition of this at additional instants of time will provide data for a complete displacement-time curve at location  $z$ . Figure 3.35 shows such a complete displacement-time curve extending from the surface to 800 ft. depth.

Calculation of vertical residual displacement. The residual displacement  $d_r$  is obtained from the curve of attenuated peak stress with depth and from the soil properties.

Thus,

$$\epsilon_{zr} = \frac{k_p \alpha_z p_{so}}{\rho c_p^2} \quad (3.31)$$
$$\Delta d_r = \epsilon_{zr} \Delta z$$

The residual displacement at depth,  $z$ , is then the sum of the increments occurring below that depth. The relative residual displacement between the surface and  $z = 100$  ft. is the difference between the surface curve and the 100 ft. depth curve; it is shown in Figures 3.36 and 3.37, taken from Reference 3.2.

It is apparent that very little elastic rebound occurs in the soil.



Example 3.15 (continued)

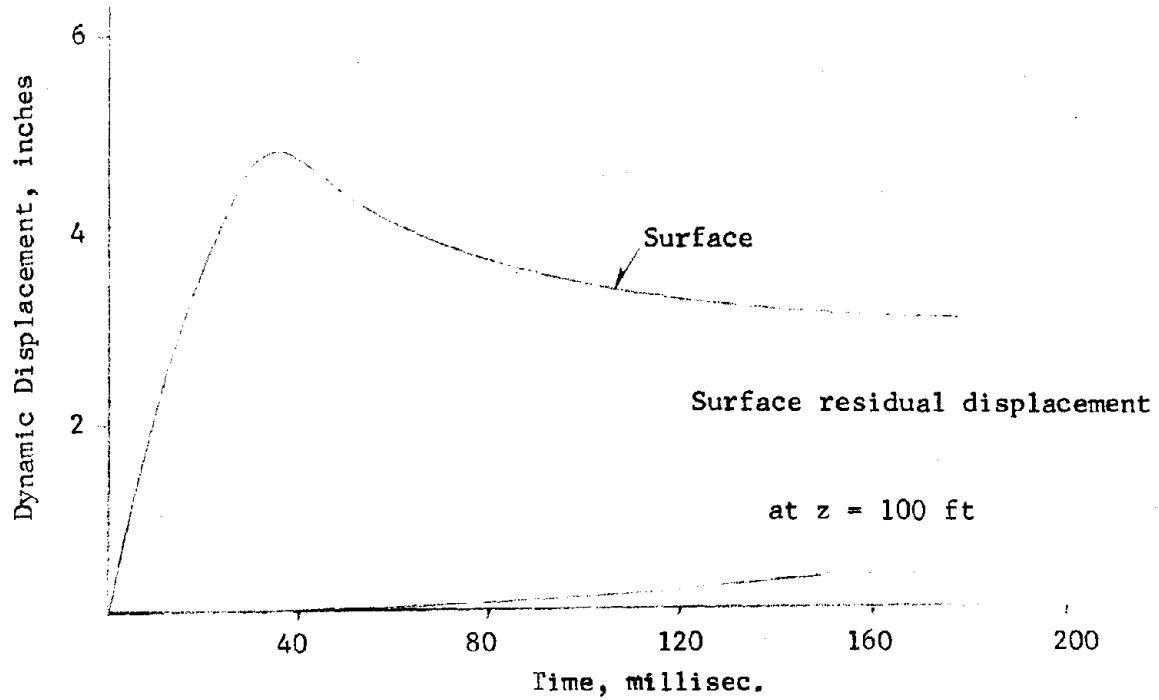


FIGURE 3.36

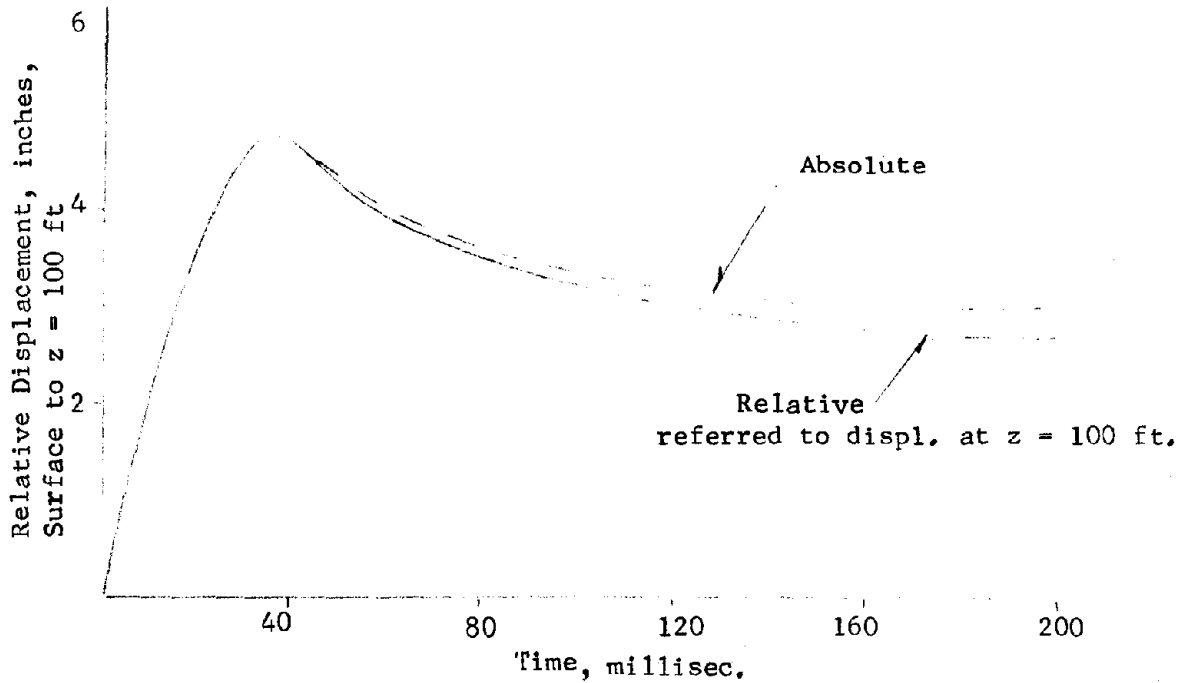


FIGURE 3.37

### 3.6 Waveforms to Describe Ground Motions

In Sections 3.1 - 3.4 the ground motions were discussed qualitatively and methods were given for estimating arrival times of different pulses at various distances from ground zero. Seismic waves induced by the expanding pressure front along the ground surface, and seismic waves that are directly induced at ground zero were both considered for a contact surface burst. In Figure 3.38 the regions where the crater induced motions and air blast induced motions are significant are shown schematically. The ground motions in region (1) may be a combination of the two motions if the crater induced motions arrive simultaneously with the air blast induced motions. In region (2) the air blast induced motions are negligible compared to the crater induced motion, and in region (3) the predominant motion is due to the air blast.

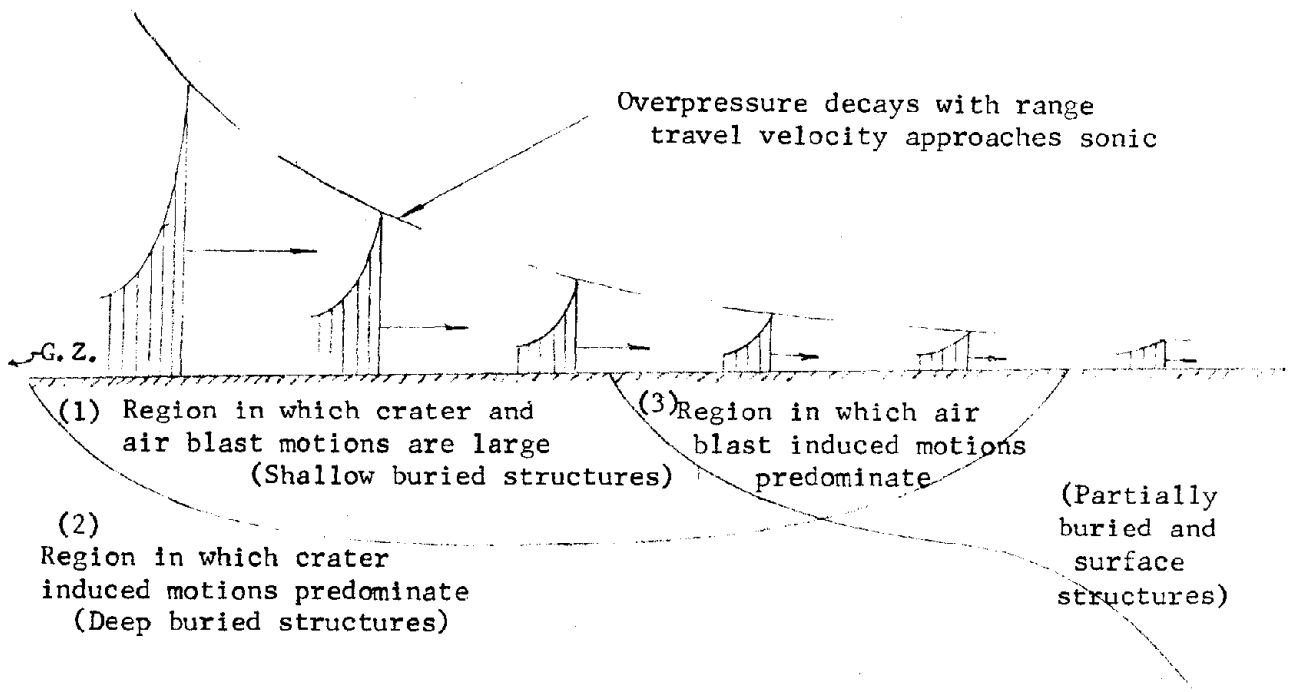


FIGURE 3.38

The peak intensities of ground motion in these regions may be obtained by the empirical relationships of Subsection 3.5. In Subsection 3.7 the peak responses to these motions will be given in terms of shock spectra.

Waveforms of input motions that result in spectra bounded by the shock spectra envelope of Subsection 3.7 can be derived. It must be kept in mind that in general it is possible to devise many different pulses whose peak responses will fall within the shock spectra envelope.

3.6.1 Combination of waveforms (phasing). Figure 3.38 indicates the three regions where either air blast induced ground motions or crater induced ground motions (or both) are predominant. The waveforms and phasings (including phasing of horizontal and vertical components) will depend on the characteristics of the region.

a. Region (1): Crater and air blast induced motion on shallow buried structure. In this region the air blast shock front (in free air) is superseismic with respect to the top layers of the soil media and an outrunning condition is not very probable. The arrival time charts in Subsection 3.2 - 3.4 define radial distances from ground zero when critically refracted-reflected waves in the soil media arrive before the air blast shock front. At close distances to ground zero the two effects that must be considered are the air blast pulse and the G.Z. induced pulse. The oscillatory pulse either lags or is engulfed by the crater induced pulse as it reaches the structure; usually it will not appear as a separate pulse.

A structure in soft soil near the ground surface underlain by very hard material (rock or shale) may feel the simultaneous or near simultaneous effects of the air blast pulse and the crater induced pulse (see Figure 3.36). If the arrival times of the two pulses are approximately the same then the two waveforms should be applied to the structure (or equipment support points if the structure moves with the free field) either in or out of phase. Judgment must be used in determining the amount of phasing. For example in Figure 3.39 the seismic velocity of the rock is estimated to vary between 8 kfps and 12 kfps.

If the average seismic velocity of 10 kfps gives a simultaneous arrival of the two pulses, then it must be assumed that the crater induced pulse can lead (+  $\Delta t$ ) or lag (-  $\Delta t$ ) the air blast induced pulse by

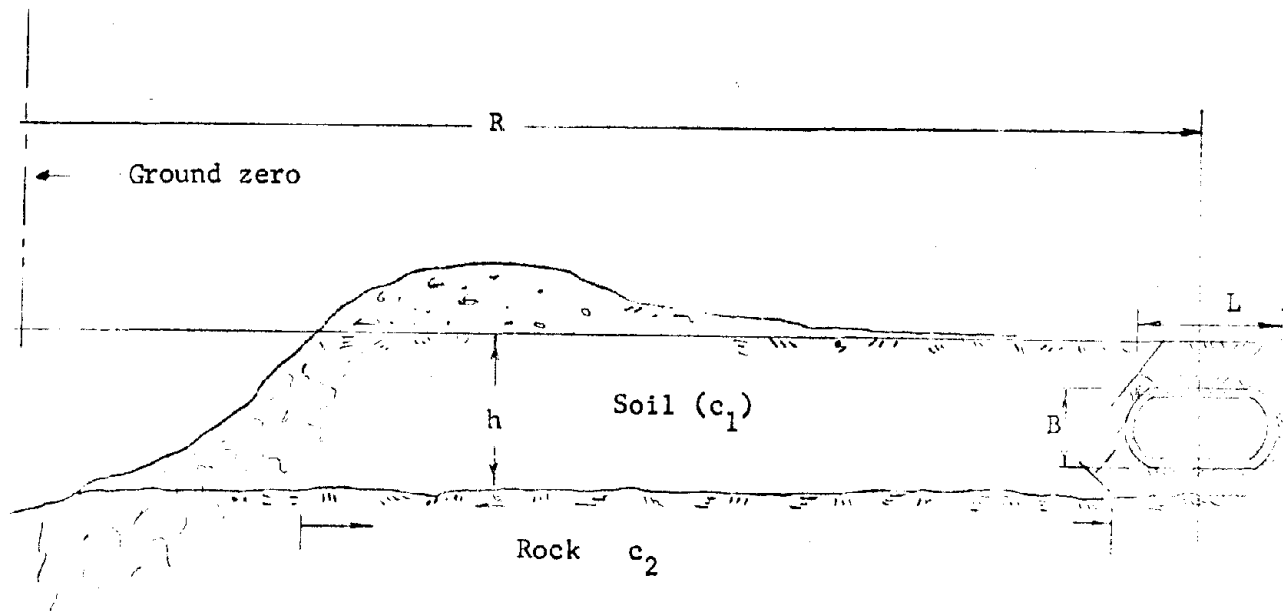


FIGURE 3.39

$$- \Delta t = R \left( \frac{1}{8} - \frac{1}{10} \right) = \frac{R}{40} \text{ milliseconds}$$

$$+ \Delta t = R \left( \frac{1}{10} - \frac{1}{12} \right) = \frac{R}{60} \text{ milliseconds}$$

If 8 kfps seismic velocity gives a simultaneous arrival then it might be assumed that the crater induced pulse can lead or be in phase with the air blast induced pulse.

In addition to the phasing of the two pulses, each pulse will induce a horizontal and a vertical motion of the structure which may be out of phase. Time phasing of the horizontal and vertical components must be arbitrarily estimated when the structure is assumed to move with the ground. The lead or lag of the horizontal component will not exceed the transit time across the longest dimension  $L$  of the structure.

$$\Delta t = \pm \frac{L}{c_1}$$

b. Region (2): Crater induced motions on deeply buried structures.

In this region it is customary to assume that the velocity pulses are triangular with complete return, see Figure 3.40. Equations (3.14a) and (3.14b) may be used for obtaining the maximum velocity  $V_{\max}$  of Figure 3.40.

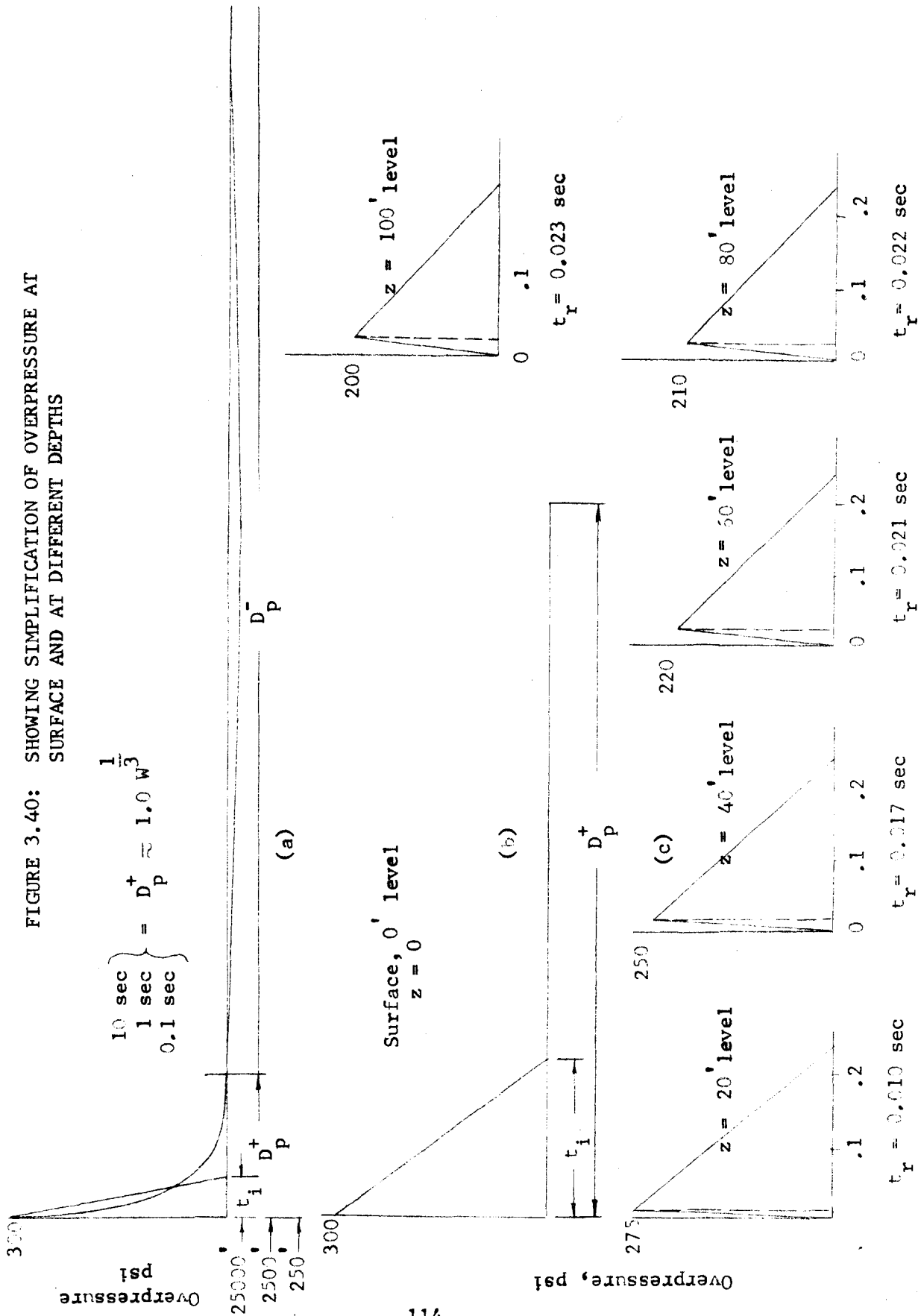
c. Region (3): Crater induced motions are negligible. The air blast shock front velocity may be superseismic with respect to the surface soil layer but subseismic with respect to lower soil layers. The blast slap component and the oscillatory component of the ground motions may both be important, and phasing should be considered. This is described in Subsection 3.6.2.3. The crater induced motions are assumed to have attenuated to a negligible amount.

3.6.2 Specific waveforms. Many trial cases have shown that the shape of a velocity pulse, be it a sine, a parabolic, a square, or a trapezoidal function of time, does not significantly affect the response of most systems. The time duration ( $t_d$ ) and a cyclic nature of the pulse, however, are the two major factors that affect the response of soft shock isolation systems. For a satisfactory design of a shock isolation system, a group of pulses may therefore have to be used in order to vary these critical parameters so as to determine the sensitivity of the system's response to these variations. Rather than attempting to develop a unique pulse for a given design requirement it is more expedient to estimate the range of values of the significant parameters of assumed pulse shapes for given soil characteristics, burial depth, and peak intensities of ground motions. Waveforms and their significant parameters are defined and illustrated in the following sections.

3.6.2.1 Waveforms due to blast slap. Figure 3.40 has been drawn in order to get a comprehensive picture of the time elements involved in the peak intensities already expressed in Subsection 3.5 by Equations (3.18) to (3.22). Diagram (a) shows the overpressure time relationship, for the positive overpressure Duration  $D_p^+$  and for the specific overpressure of 300 psi, Reference 3.1. The corresponding distances to ground zero and the values of  $D_p^+$  are indicated for a  $10^3$  MT, 1 MT, and 1 KT burst. The positive impulses  $I_p$  ascribable to the overpressures are expressed by

$$I_p = 1.8 p_{so}^{\frac{1}{2}} W^{\frac{1}{3}} = \begin{cases} 312 \text{ psi-sec for } 10^3 \text{ MT burst} \\ 31.2 \text{ psi-sec for } 1 \text{ MT} \\ 3.12 \text{ psi-sec for } 1 \text{ KT} \end{cases} \quad (3.32)$$

FIGURE 3.40: SHOWING SIMPLIFICATION OF OVERPRESSURE AT SURFACE AND AT DIFFERENT DEPTHS



and the corresponding time values  $t_i$  of a triangular pressure distribution giving an equivalent impulse are expressed by:

$$t_i = 3.7 p_{so}^{-\frac{1}{2}} W^{\frac{1}{3}} = \begin{cases} 2.1 & \text{seconds for } 10^3 \text{ MT burst} \\ 0.21 & \text{seconds for } 1 \text{ MT} \\ 0.021 & \text{seconds for } 1 \text{ KT} \end{cases} \quad (3.33)$$

The time duration of the negative overpressure  $D_p$  is very long compared to  $D_p^+$ ; it is from 8 to 12 times  $D_p^+$ . Moreover, the peak value of the negative overpressure is very small compared to that of the positive. The negative overpressure phase is therefore usually neglected and diagram (b) shows the equivalent triangular representation of the surface pressure.

It is seen that the pressure rise time in diagram (b) is zero. Below the surface, due to different travel velocities  $c_i > c_p$  of the initial and the peak pressure fronts, the peak front will lag behind the initial front, Equation (3.20) by the rise time

$$t_r = \frac{z}{c_p} - \frac{z}{c_i}$$

Moreover, the peak pressure will attenuate in accordance with Equation (3.17) as it descends into the medium. This situation is shown in diagrams (c) for increasing depths in the ground. The actual data relate to the numerical values in Section 3.5.3.1.

Figure 3.41 shows a linearized overpressure-time curve for given depths as well as a linearized velocity-time curve. Since according to Equation (3.21) the peak velocity is proportional to the overpressure, the triangular velocity distribution is considered to have for its maximum the attenuated value of  $v_{max}$ . The velocity rise time  $t_r$  and the positive velocity pulse duration  $t^+$  must then be adjusted by the fact that the values of  $a_{vz}$ ,  $v_{vz}$ , and  $(d_{vz})_{max}$ , (based on impulse considerations and given by Equations (3.19), (3.21) and (3.26)) must be made compatible with the triangular velocity-time diagram itself. This gives:

$$t_r = \frac{v_{vz}}{a_{vz}} \quad (3.34)$$

$$t^+ = \frac{2 d_{vz}}{v_{vz}} \quad (3.35)$$

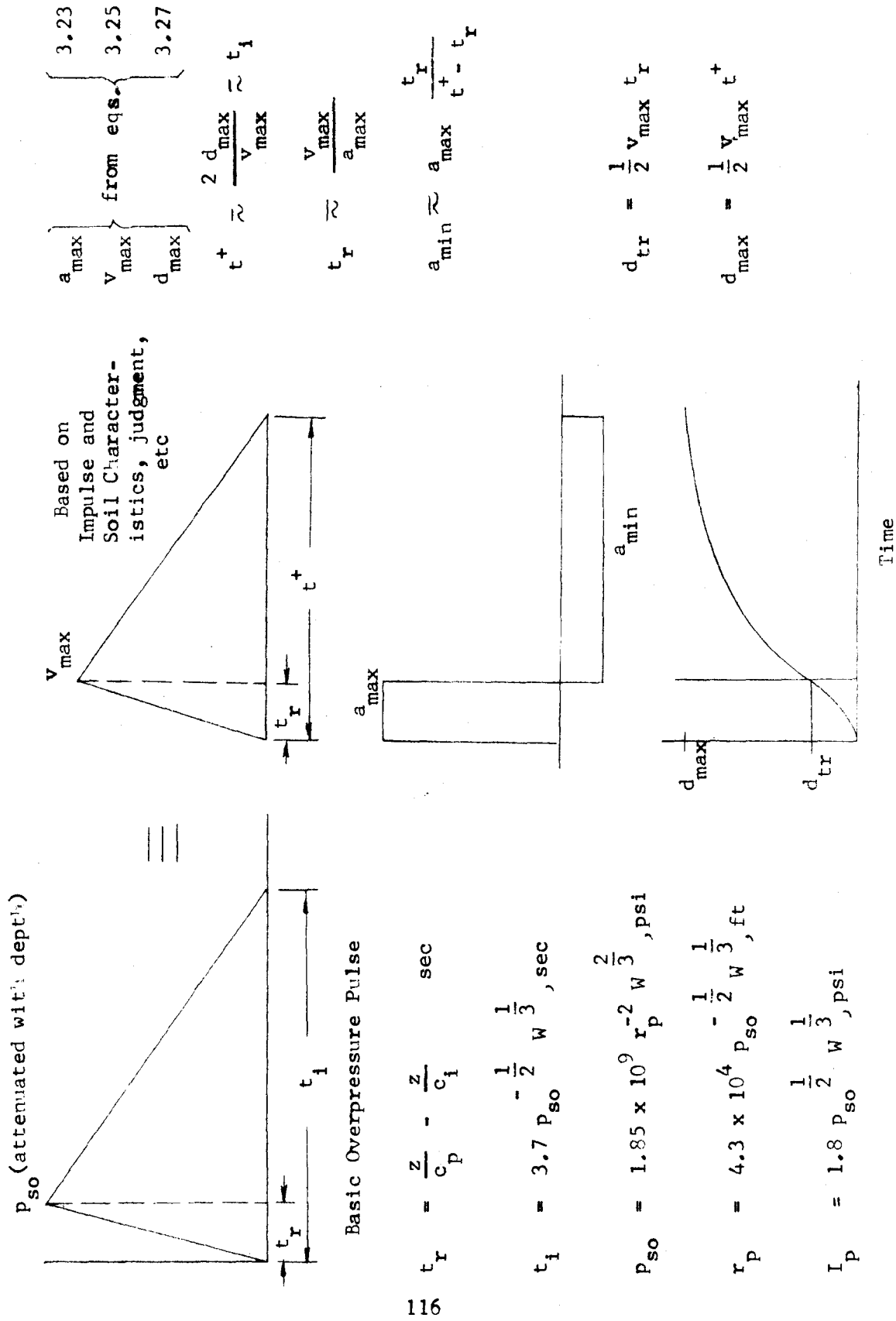


FIGURE 3.41: BASIC VELOCITY PULSE WITH NO RETURN



The corresponding acceleration-time and displacement-time diagrams have also been drawn in Figure 3.41 for the case of the basic velocity pulse with zero return of displacement.

Figure 3.42 shows in the first diagram the triangular, basic velocity pulse and indicates that  $D_p^+$  is very much longer than  $t^+$ . Just what happens when  $t$  is longer than  $t^+$  is not well known, but it is obvious that in all cases where elastic action occurs the displacement must eventually be reduced to zero. Therefore in the second diagram, representing the displacement, common sense assumptions have been made about the return displacement time, one of which reduces it parabolically from  $d_{\max}$  to zero in the time interval  $2 t^+$  and the other in the time interval  $3 t^+$ . The corresponding linear velocity diagrams and block acceleration diagrams are shown for a complete return velocity pulse.

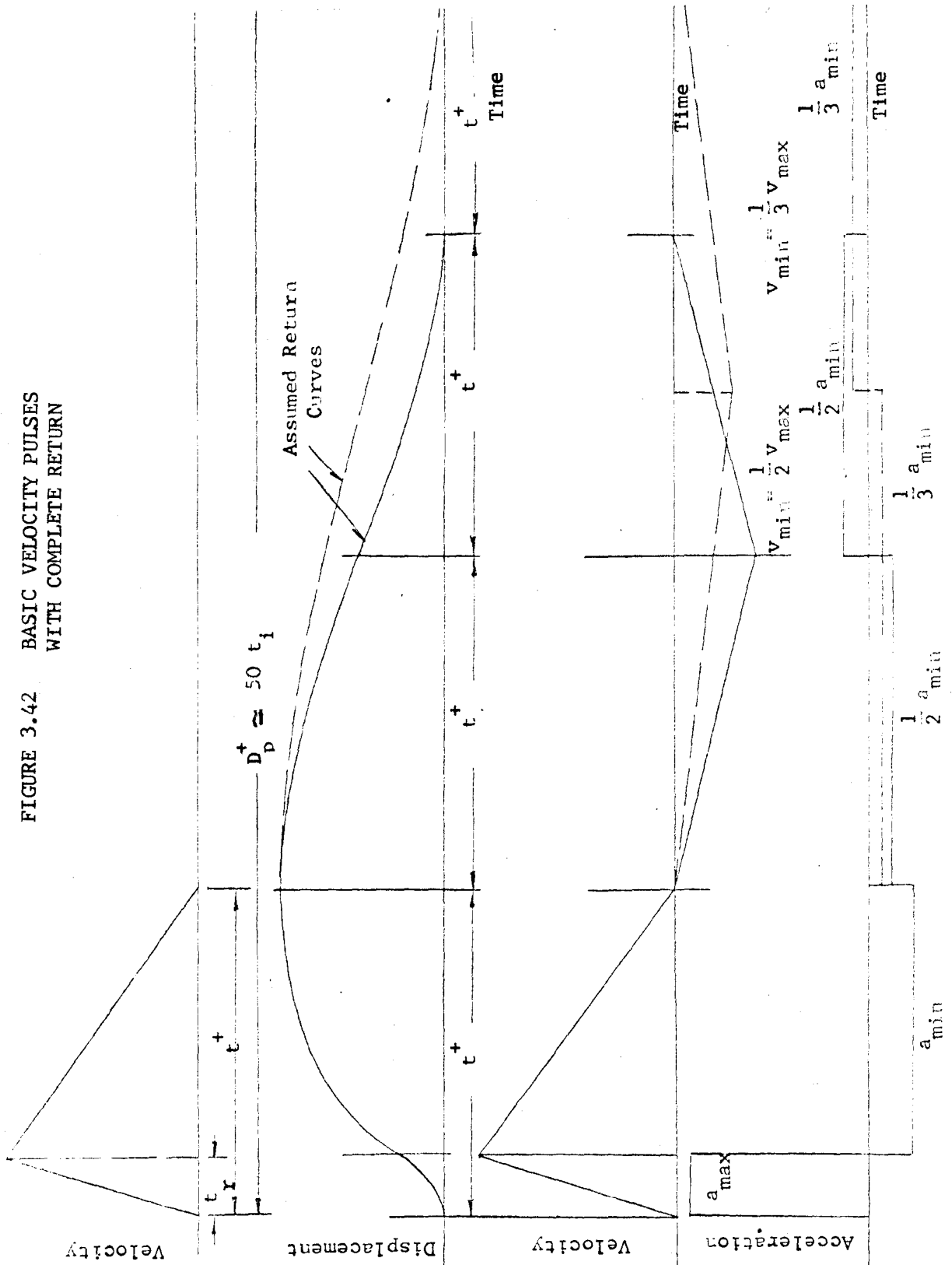
Since the behavior of the soil is not linear and will exhibit permanent displacements Figure 3.43 shows the velocity and displacement pulses for:

Full return	$d \rightarrow 0$
Partial return	$d \rightarrow \frac{1}{6} d_{\max}$
Partial return	$d \rightarrow \frac{2}{3} d_{\max}$
No return	$d = d_{\max}$

It is seen that all the triangular velocity pulses correspond to parabolic displacement pulses having slope continuity and to block acceleration pulses. For many applications the slope discontinuities in the velocity pulses are acceptable, but in some instances, especially when excitations of high frequency components are of importance, the assumed velocity pulses should possess slope continuity. This can be accomplished by resorting to employ several types of velocity waveforms.

As previously stated, since the shape of the pulse is not very important, either a sine function or a parabolic function may be used. Henceforth combinations of sine functions are used to define the assumed waveforms.

FIGURE 3.42 BASIC VELOCITY PULSES WITH COMPLETE RETURN



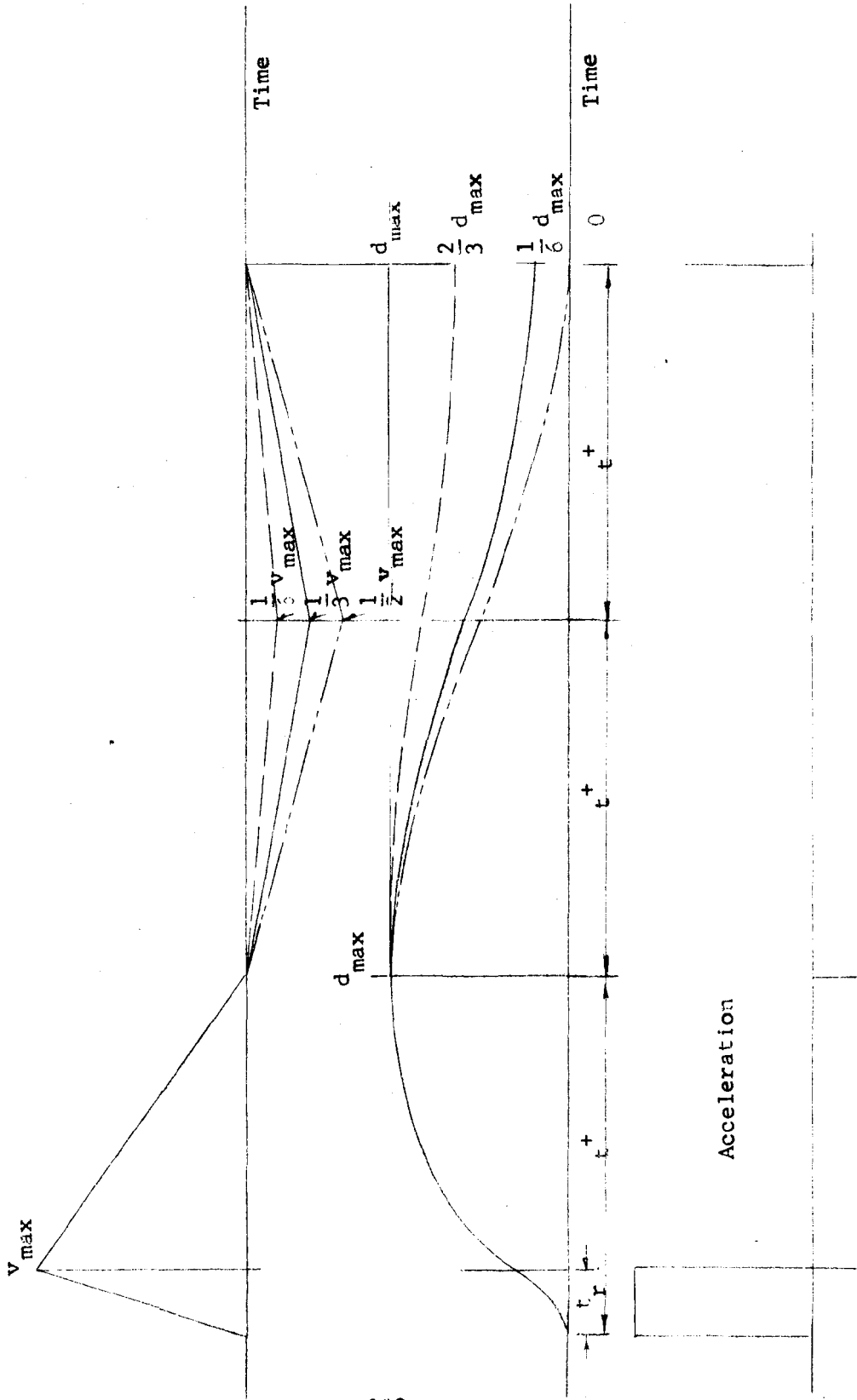


FIGURE 3.43: BASIC VELOCITY PULSES WITH PARTIAL RETURN

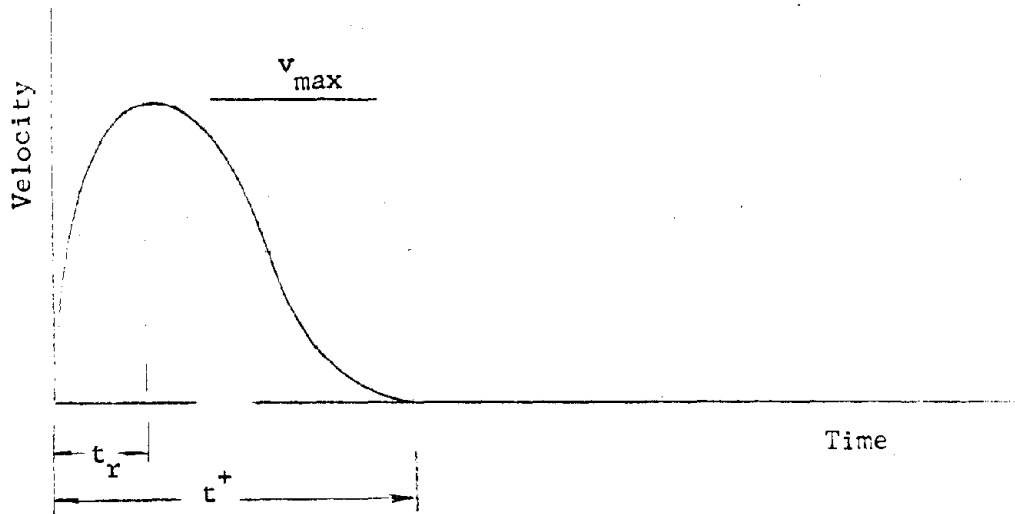


FIGURE 3.44

Figure 3.44 represents a typical pulse and is defined by the following functions:

$$v = v_{\max} \sin \frac{\pi t}{2 t_r} ; \quad 0 \leq t \leq t_r \quad (3.36)$$

$$v = 0.5 v_{\max} \left[ 1 - \cos \pi \left( \frac{t - t^+}{t^+ - t_r} \right) \right] \quad t_r \leq t \leq t^+$$

The velocity pulse is therefore defined in terms of the rise time,  $t_r$ , and the positive phase duration,  $t^+$ . The rise time is easily calculated since the initial slope of the velocity pulse is equal to the peak acceleration,

$$a_{\max} = \dot{v}_{t=0} = \frac{\pi v_{\max}}{2 t_r} \quad (3.37)$$

giving

$$t_r = \frac{\pi}{2} \left( \frac{v_{\max}}{a_{\max}} \right)$$

The positive phase duration,  $t^+$ , cannot be taken as the overpressure positive phase duration since the analytic expression assumed for the velocity pulse is different from that of the overpressure pulse. The positive phase duration for the assumed shape of the velocity pulse can be calculated by equating the area under the velocity pulse to the peak ground

displacement,  $d_{\max}$ .

$$d_{\max} = \int_0^{t_r} v_{\max} \sin \frac{\pi}{2} \frac{t}{t_r} dt + \int_{t_r}^{t^+} 0.5 v_{\max} \left[ 1 - \cos \pi \left( \frac{t - t^+}{t^+ - t_r} \right) \right] dt$$

which yields for  $t^+$  the expression

$$t^+ = \frac{2 d_{\max}}{v_{\max}} - \frac{t_r}{\pi} (4 - \pi) = \frac{2 d_{\max}}{v_{\max}} - 0.27 t_r \quad (3.38)$$

Equation (3.38) is consistent with the peak intensities given by Equations (3.19), (3.21) and (3.26).

It is instructive at this point to show the acceleration and displacement pulse, see Figure 3.45.

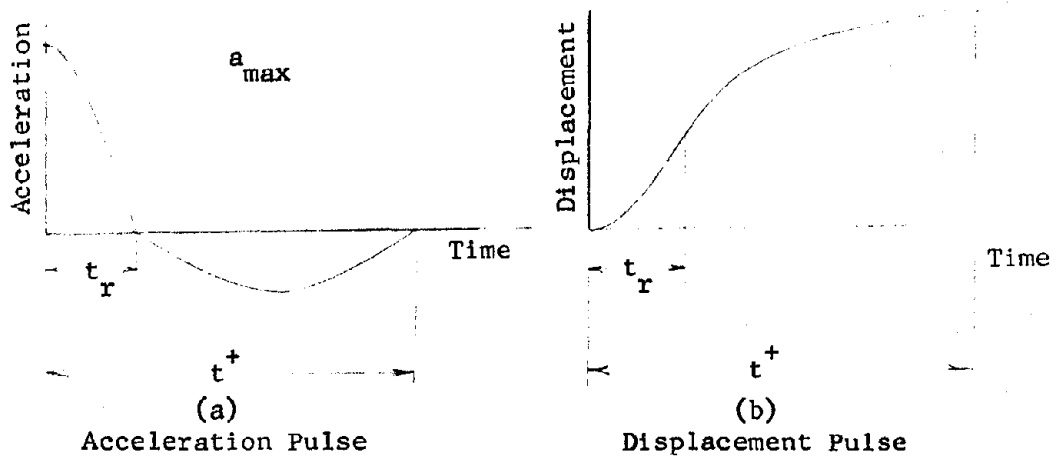


FIGURE 3.45

Mathematically, the maximum acceleration will occur instantaneously, or practically during the initial rise of the velocity pulse (Figure 3.45a); this is expected from the nature of the overpressure pulse. The displacement pulse (Figure 3.45b) rises to a peak value of  $(v_{\max}/2)(t^+ + 0.27 t_r)$  at the termination of the positive velocity pulse. In most real situations there will be some ground recovery, and the amount will depend upon the type of soil and ground motion intensities. At very low overpressures and regions near the surface (Region 3 of Figure 3.38) the motion will

be essentially elastic (full ground recovery). The same is also true for deeply buried structures where the medium is a firm rock that behaves elastically. In Region 1, of Figure 3.38, the soil behavior may be approximated by an elastic-plastic stress-strain relationship, and some permanent deformation can be expected (on the order of 1/6 to 1/3 the peak displacement).

The ground recovery is very important in the design of soft isolation systems, because, if the ground displacement resembles a half cycle pulse of duration,  $t_d$ , then the response may be significantly amplified if  $t_d$  is close to the half period,  $T/2$ , of the isolation system. Unfortunately, the recovering ground displacement during the time  $(t_d - t^+)$  cannot be computed with satisfactory confidence. Judgment places the duration of this motion from 2 to 4 times the positive phase duration,  $t^+$ , of the velocity pulse. Thus, it can be assumed that  $t_d$  falls between the limits

$$2\frac{1}{2} t^+ < t_d < 5\frac{1}{2} t^+ \quad (3.39)$$

Figure 3.45 will have to be modified to account for the recovering displacement of the soil. This can be done by adding a negative velocity pulse following the end of the positive velocity pulse, see Figure 3.46.

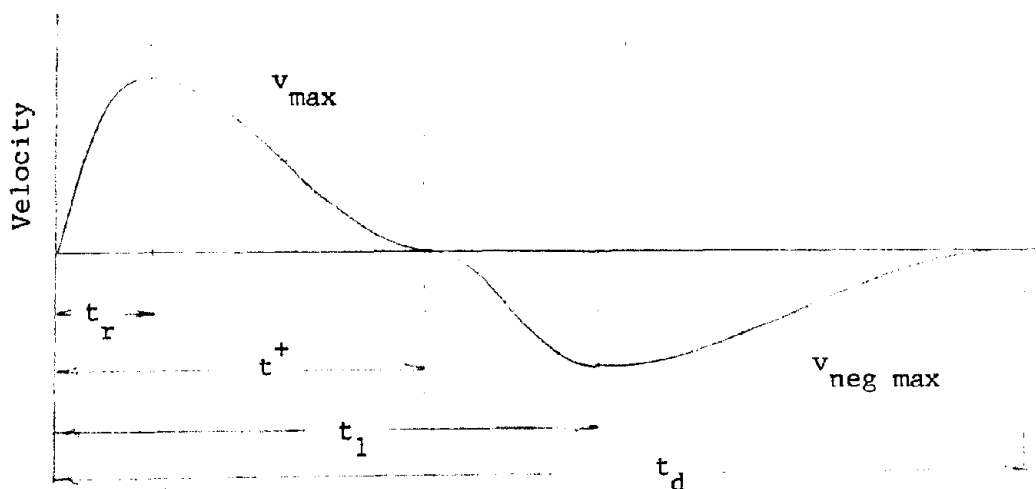


FIGURE 3.46

The precise shape of this negative pulse is not too important, but its time duration,  $t_d$ , and maximum negative velocity,  $v_{neg\ max}$ , will

determine the amount of recovery. Limits on  $t_d$  have been defined by Equation (3.39). The negative velocity peak will be less than  $v_{\max}$  and may vary between  $0.25 v_{\max}$  and  $0.5 v_{\max}$ .

$$v_{\text{neg max}} = \begin{cases} 0.25 v_{\max} \\ 0.5 v_{\max} \end{cases} \quad (3.40)$$

For 100 percent ground recovery the area under the negative velocity pulse is equal to the area under the positive pulse. This gives all the conditions necessary to define a pulse with or without ground recovery provided that a definite shape, such as a trigonometric, is adopted.

The positive portion of the pulse has been defined in terms of a sine (or versed sine) function, Equations (3.36 - 3.38). We can similarly define the negative portion in terms of sine functions and stipulate that the area of the negative portion of the velocity pulse must be equal to the recovery displacement.

$$d^- = \beta d^+ \quad (3.41)$$

where

$d^+$  = peak positive displacement

$d^-$  = recovery displacement

$\beta$  = ratio of recovery displacement to positive displacement  
(i.e. if the ground has 100 percent ground recovery  
 $\beta = 1.0$ )

The velocity pulse between  $t^+$  and  $t_1$  (the time to reach peak negative velocity) may be defined by the following equation:

$$v = -0.5 v_{\text{neg}} \left[ 1 - \cos \pi \left( \frac{t - t^+}{t_1 - t^+} \right) \right] \quad (3.42)$$

and the portion between  $t_1$  and  $t_d$  by:

$$v = -0.5 v_{\text{neg}} \left[ 1 - \cos \pi \left( \frac{t - t_d}{t_d - t_1} \right) \right] \quad (3.43)$$

The terms in the above two equations have all been defined except for the time,  $t_1$ . A reasonable assumption is to let the ratio

$$\left( \frac{t_1 - t^+}{t^+ - t_r} \right)$$

be proportional to the ratio

$$\left( \frac{v_{\text{neg max}}}{v_{\text{max}}} \right).$$

Then

$$t_1 = \left( \frac{v_{\text{neg max}}}{v_{\text{max}}} \right) (t^+ - t_r) + t^+ \quad (3.44)$$

and the area under the velocity pulse Equations (3.42 and 3.43) will define  $t_d$  or  $v_{\text{neg}}$ , whichever is assumed to be the dependent variable. Finally we write:

$$d^- = v_{\text{neg}} \left( \frac{t_d - t^+}{2} \right) \quad (3.45)$$

#### Example 3.16

Given: At a specified burial depth the peak ground motions due to the air blast are:

$$\begin{aligned} a_{\text{max}} &= 50 \text{ g} \\ v_{\text{max}} &= 67 \text{ in/sec} \\ d_{\text{max}} &= 10 \text{ inches} \end{aligned}$$

the permanent residual displacement is estimated to be 25 percent of the peak transient displacement.

From Equation (3.37) the rise time is calculated:

$$t_t = \frac{3.14}{2} \left( \frac{67}{50 \times 386} \right) = 0.0053 \text{ sec}$$

The positive phase duration is calculated from Equation (3.38)

$$\begin{aligned} t^+ &= 2 \left( \frac{10}{67} \right) - \frac{0.0053}{3.14} (4 - 3.14) \\ &= 0.3 - .0015 = 0.2985 \approx 0.3 \text{ sec} \end{aligned}$$



Example 3.16 (continued)

Assume that  $t_d = 4 t^+$  from assumption of Equation (3.39)

$$t_d = 1.2 \text{ sec.}$$

From Equation (3.40)

$$d^- = 0.75 d^+ = 7.5 \text{ inches}$$

Equations (3.44) and (3.45) establish  $v_{\text{neg}}$  and  $t_1$

$$v_{\text{neg}} = \frac{2 (7.5)}{1.2 - 0.3} = 16.7 \text{ in/sec}$$

$$t_1 = \left( \frac{16.7}{67} \right) (0.3) + 0.3 = 0.375 \text{ sec.}$$

Figure 3.47 shows the waveform for the given example. It is desirable to vary the negative portion of this pulse and use two or more pulses.

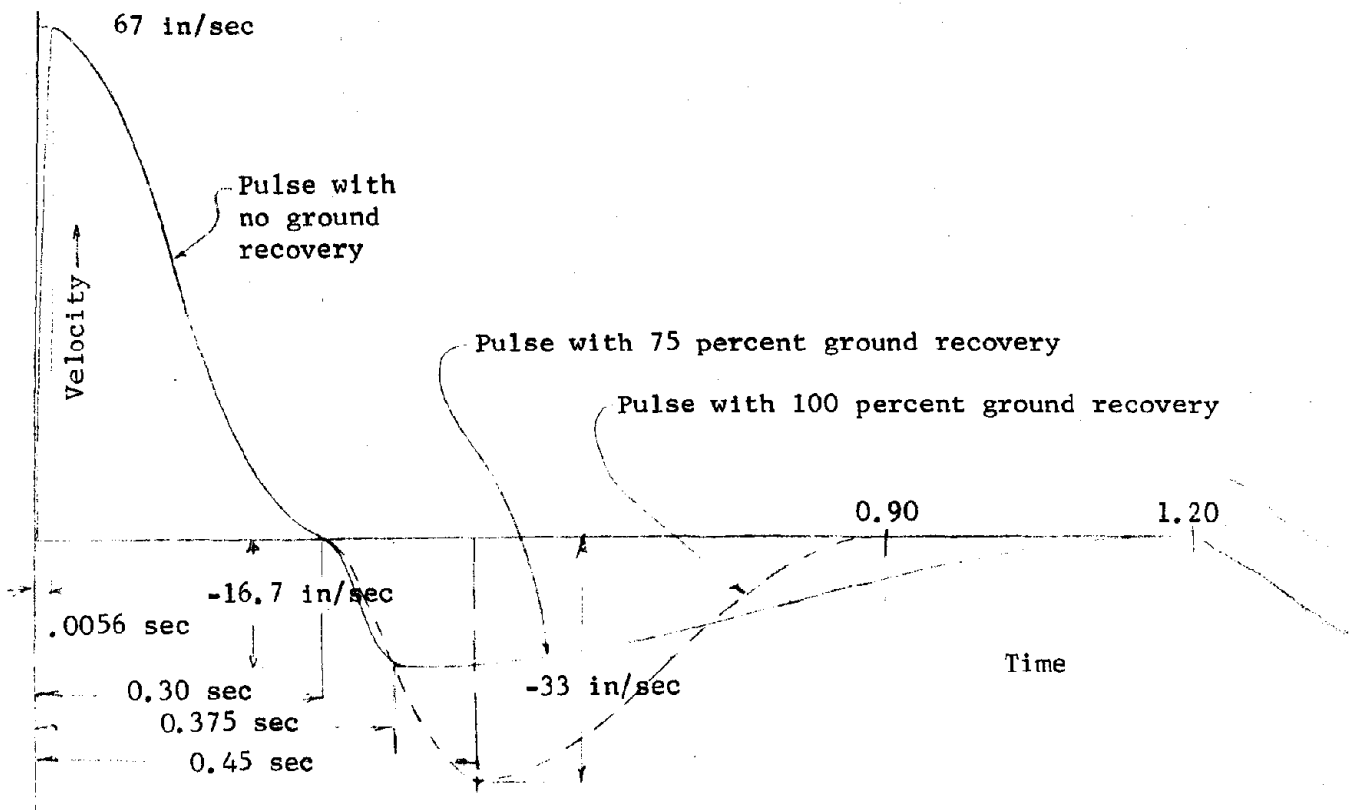


FIGURE 3.47

Example 3.16 (continued)

For example another pulse that might be considered feasible should have full ground recovery and a time duration of  $3 t_d$  (this would be applicable for a firm soil that remains essentially elastic during the specified ground motion). The negative portion of the pulse is then defined by the following parameters.

$$v_{\text{neg}} = \frac{2 (10)}{0.9 - 0.3} = 33.3 \text{ in/sec}$$

$$t_1 = \left( \frac{33.3}{67} \right) (0.3) + 0.3 = 0.45 \text{ sec}$$

This pulse is shown in dashed lines in Figure 3.47. To bound the possible real situation a pulse with positive phase only could be used as an extreme condition simulating a soil that is fully plastic (no displacement recovery).

3.6.2.2 Crater or G.Z. induced waveforms. A contact surface burst will generate seismic disturbances and propagate stress wave from ground zero. Empirical relationships have been derived (see Section 3.5) relating peak displacement, velocity and acceleration to radial distance, weapon size and seismic properties of the media. The arrival time at any specified distance can also be estimated if the seismic properties of the media are known.

Relatively little is known about the shape of the G.Z. induced waveforms in comparison with the knowledge of waveforms due to the blast front. Until more evidence is available, Reference 3.2 suggests that the duration of the velocity pulse be taken as one half of the transit time,  $t_t$ , from G.Z. to the station at the radial distance,  $R$ . If the station is located near the surface in comparison with  $R$ , the transit time, see Equation (3.5), is given by

$$t_t = \begin{cases} \frac{R}{c_1} & \text{for homogeneous soil} \\ \frac{2 h_1}{c_1 c_2} \sqrt{c_2^2 - c_1^2} + \frac{R}{c_2} & \text{for two layer soil} \\ \frac{2 h_1}{c_1 c_2} \sqrt{c_2^2 - c_1^2} + \frac{2 h_2}{c_2 c_3} \sqrt{c_3^2 - c_2^2} + \frac{R}{c_3} & \text{for three layer soil} \end{cases}$$

A linear velocity-time diagram for the G.Z. generated motion is shown in Figure 3.48. The rise time,  $t_r$ , is taken equal to  $1/6 t_t$  and the duration,  $t^+$ , of the positive velocity is taken equal to  $1/2 t_t$ . The maximum velocity is assumed to be given by Equation (3.14a) or by (3.14b). Since in most cases some return of the displacement takes place, the time for this to happen must be estimated or assumed. Figure 3.48 shows two such estimates of return time for complete returns, namely  $2/3 t_t$  and  $t_t$ . The corresponding block acceleration and parabolic displacement diagrams are also shown.

An alternate waveform which has a smooth transition from the positive to the negative velocity is shown in Figure 3.49.

The equations defining the pulse of Figure 3.49 are:

$$v = v_{\max} \sin \frac{\pi t}{2 t_r} \quad \text{for } 0 \leq t \leq t_r$$

$$v = \left( \frac{v_{\max} + v_{\text{neg max}}}{2} \right) \left[ 1 - \cos \pi \left( \frac{t - \tau_1 - t_r}{\tau_1} \right) \right] - v_{\text{neg}} \quad (3.46)$$

for  $t_r \leq t \leq (t_r + \tau_1)$

$$v = \frac{v_{\text{neg max}}}{2} \left[ 1 - \cos \pi \left( \frac{t - t_d}{t_d - \tau_1 - t_r} \right) \right]$$

for  $(t_r + \tau_1) \leq t \leq (t_d)$

The critical time parameters are derived in terms of the peak intensities (for 100 percent ground recovery).

$$t_r = \frac{\pi}{2} \frac{v_{\max}}{a_{\max}} \quad (3.47)$$

$$\tau_0 = \frac{1}{\pi} \tau_1 \arccos \left( \frac{-v_{\max} + v_{\text{neg max}}}{v_{\max} + v_{\text{neg max}}} \right) \quad (3.48)$$

$$\tau_1 \sin \frac{\pi \tau_0}{\tau_1} = \frac{\pi}{v_{\max} - v_{\text{neg max}}} \left[ d_{\max} - \frac{2}{\pi} v_{\max} t_r - \left( \frac{v_{\max} - v_{\text{neg max}}}{2} \right) \tau_0 \right] \quad (3.49)$$

$$\tau_2 = \frac{2}{v_{\text{neg}}} \left[ \frac{2}{\pi} v_{\max} t_r + \frac{1}{2} (v_{\max} - v_{\text{neg max}}) \tau_1 \right] \quad (3.50)$$

G. Z. Seismic Wave Pulse with Complete Return

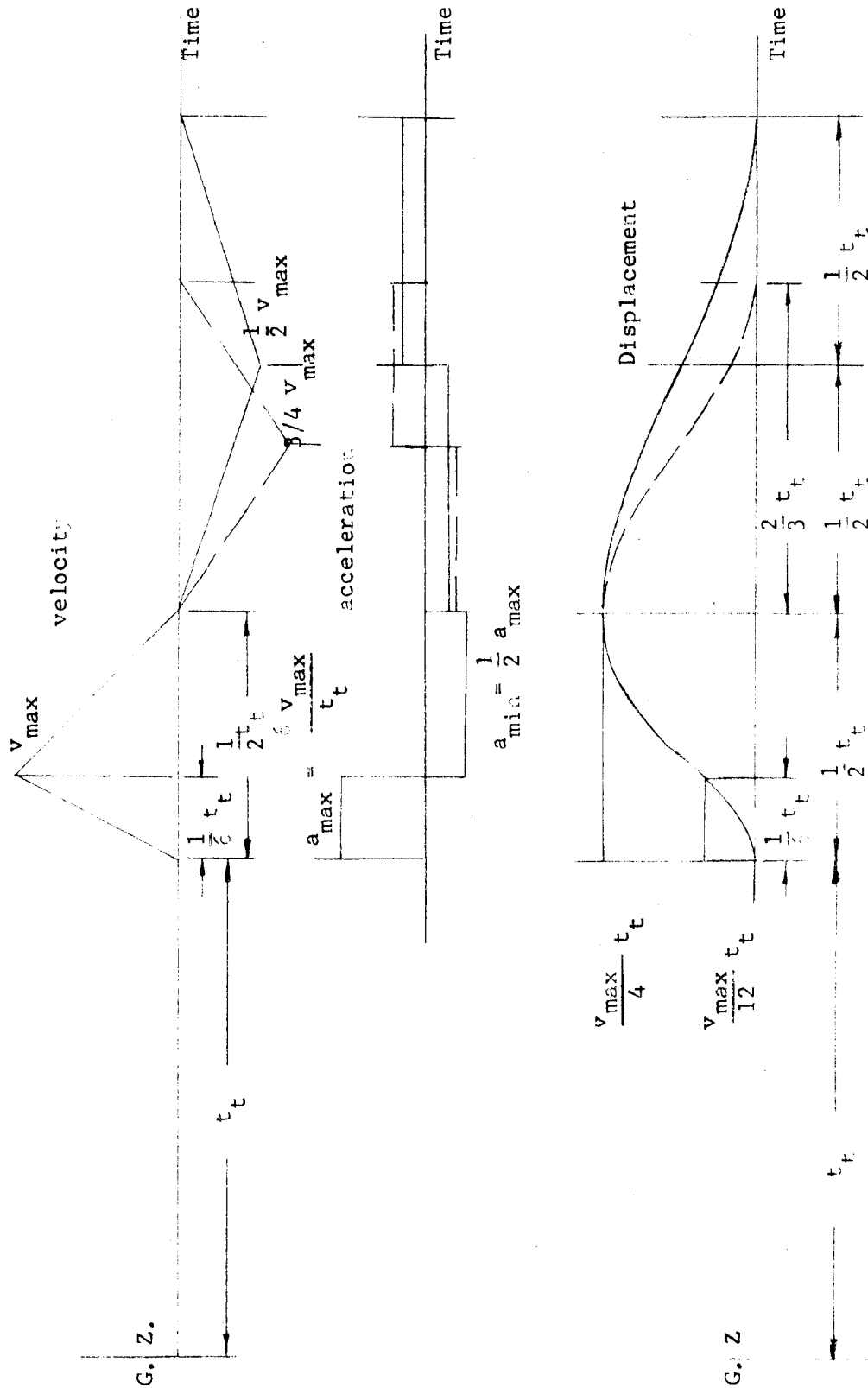


FIGURE 3.48

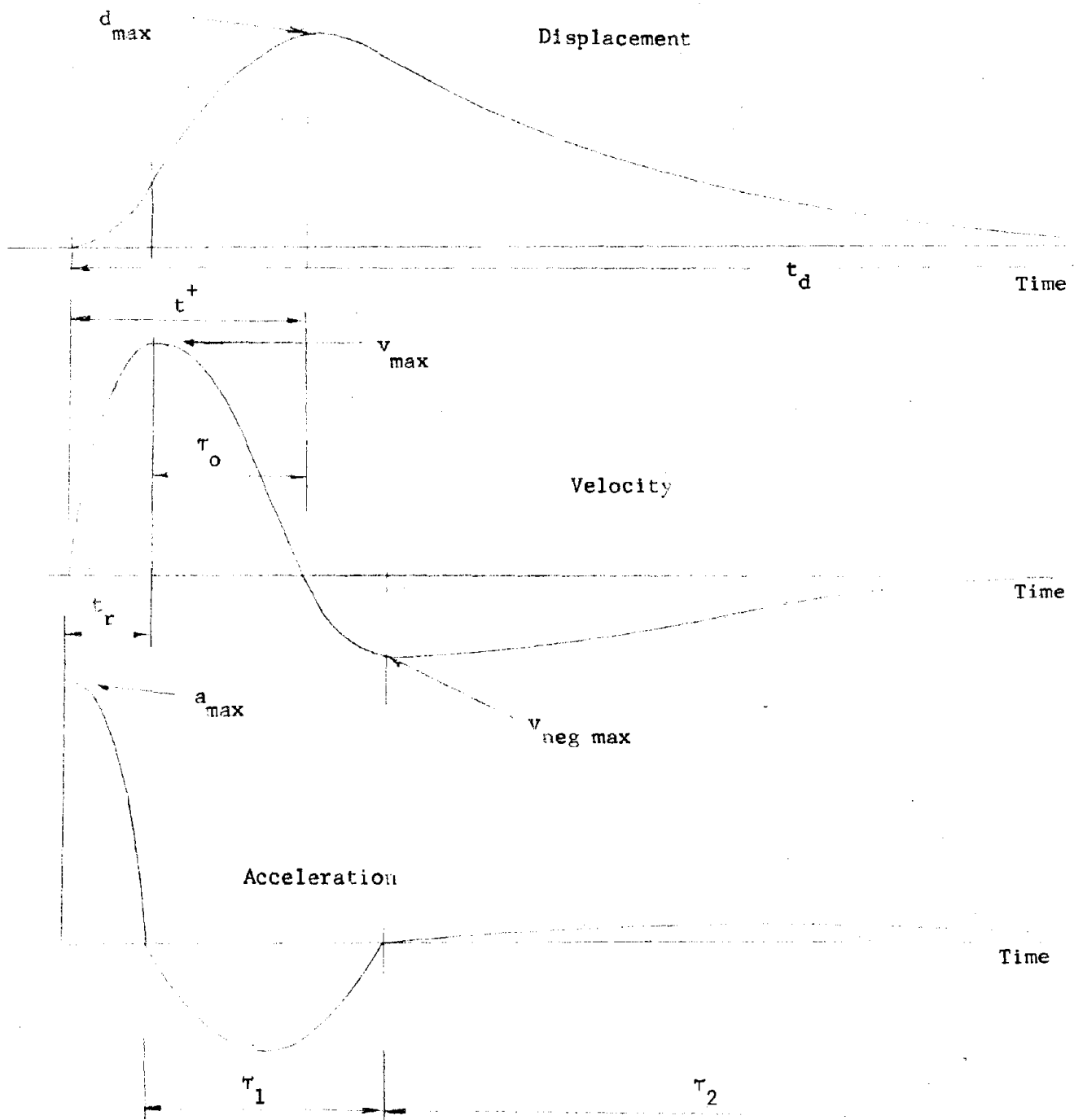


FIGURE 3.49

For partial ground recovery the time  $\tau_2$  must be decreased until the recovery displacement (area under negative velocity pulse) reaches the estimated value.

Example 3.17

An example will illustrate the use of the above equations in deriving a waveform with 100 percent ground recovery given:

$$\begin{aligned}d_{\max} &= 5 \text{ inches} \\v_{\max} &= 50 \text{ inches/sec} \\a_{\max} &= 50 \text{ g} \\t^+ &= 0.18 \text{ sec}\end{aligned}$$

assume that the critical time parameters are from Equations (3.47 - 3.50)

$$t_r = \frac{\pi}{2} \left( \frac{50}{50 \times 386} \right) = 0.004 \text{ sec}$$

$$\tau_o = \frac{\tau_1}{\pi} \arccos \left( \frac{-50 + 20}{50 + 20} \right) = \frac{\tau_1}{\pi} (.65 \pi) = .65 \tau_1$$

$$\tau_1 \sin .65 \pi = \frac{3.14}{50 - 20} \left[ 5 - \frac{2}{3.14} (50) .004 - 15 (.65 \tau_1) \right]$$

Solving for  $\tau_1$  and  $\tau_2$

$$\tau_1 = 0.27 \text{ sec.}$$

$$\tau_2 = \frac{2}{20} \left[ \frac{2}{3.14} (50) .004 + \frac{1}{2} (50 - 20) 0.27 \right] = 0.42 \text{ sec.}$$

Summing up the above time parameters gives:

$$t_d = 0.694 \text{ sec}$$

which is about 4 times the positive phase duration ( $t^+ = 0.18 \text{ sec}$ )

Figure 3.50 shows the above derived pulse.

Example 3.17 (continued)

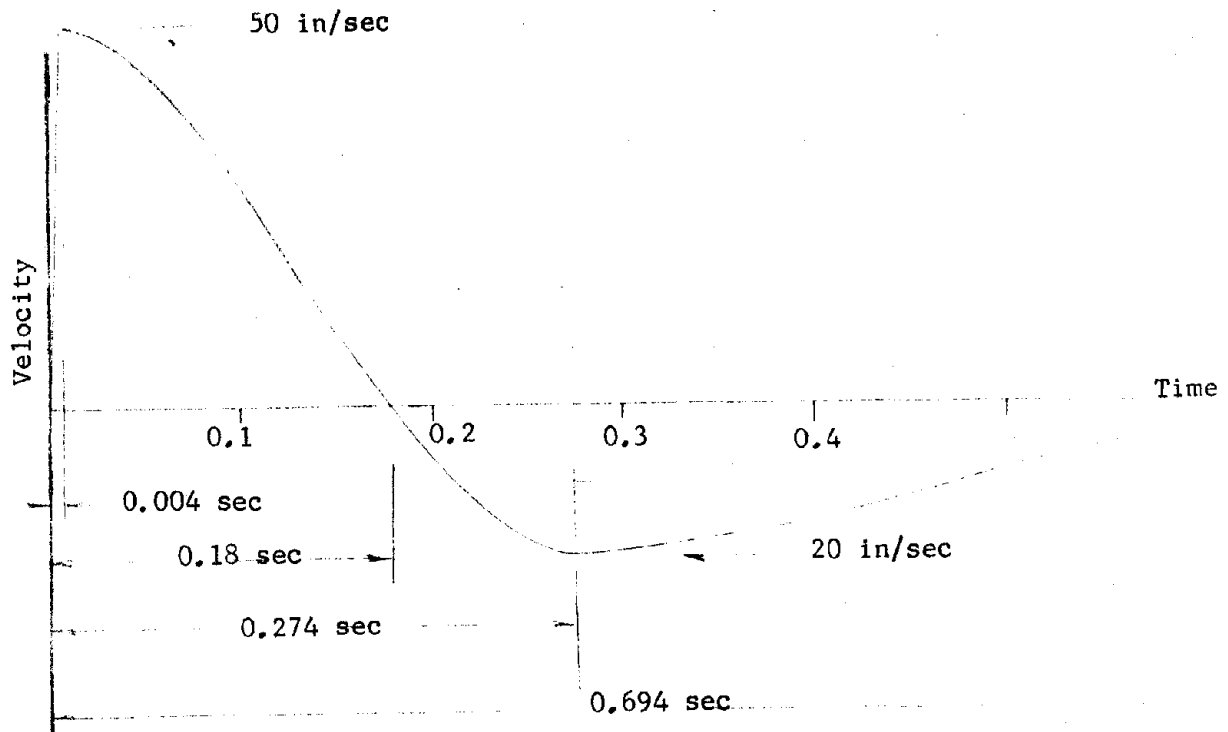


FIGURE 3.50

3.6.2.3 Alternating waveforms generated by the outrunning ground disturbance. Observation of many test results at NTS and at Eniwetoc has indicated that a train of alternating vertical velocity waves is brought into existence when outrunning motion begins, Reference 3.3. The records in Figure 3.52 relate to the Tumbler Shot I and depict the observed vertical particle velocity at stations 4, 5, 6, and 7 that are located at increasing distances from G.Z. The records obtained at the closer in stations 1, 2, and 3, where no outrunning had occurred, showed only the typical vertical velocity waveform associated with the overpressure. This type of motion is indicated in an idealized form in Figure 3.51 and will be referred to as Type I waveform. Its characteristic time is the duration of the positive overpressure,  $D_p^+$ .

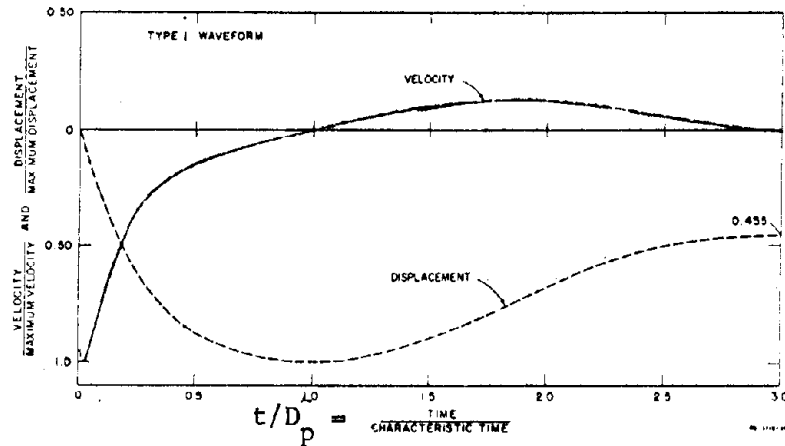


FIGURE 3.51: TYPE I (SUPERSEISMIC AIRBLAST)  
VERTICAL PARTICLE VELOCITY WAVEFORM AND ITS DISPLACEMENT

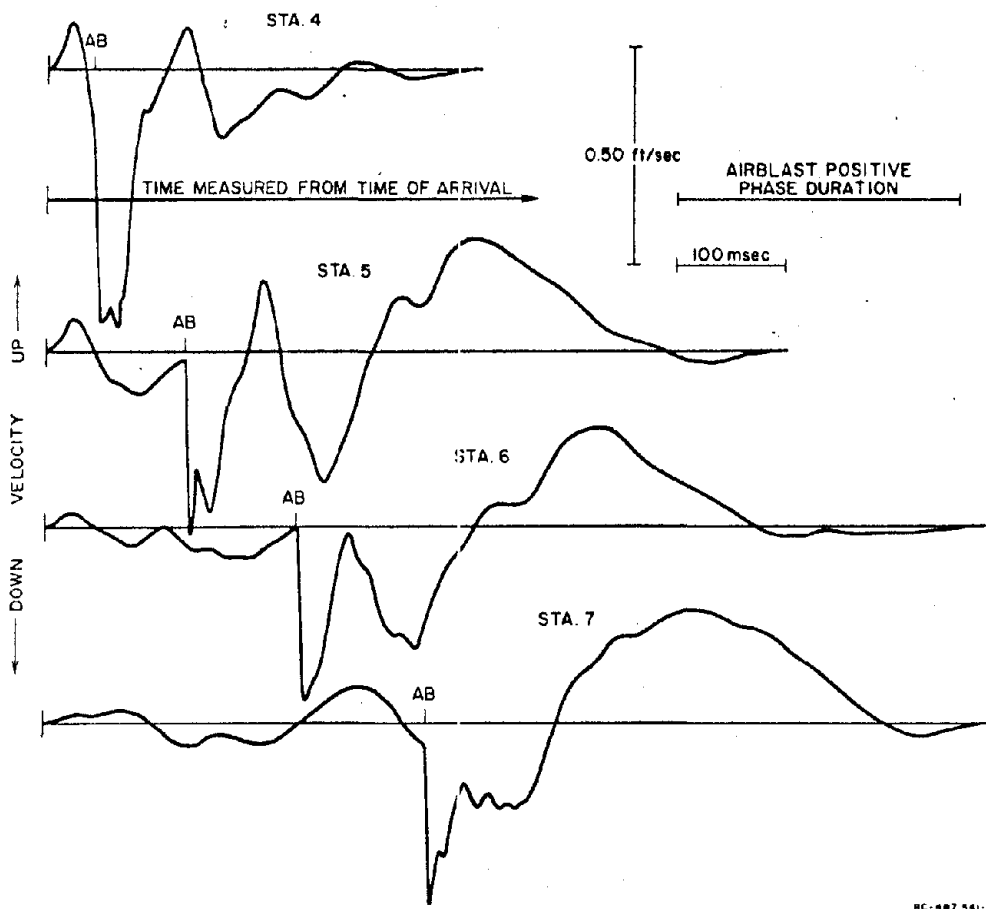
Referring to Figure 3.52 it is clearly seen that Type I or air blast induced motion arrives at the four times marked by AB. Moreover, at Station 7 three half waves precede the arrival of the air blast and at least two half waves follow it. Also note that the initial velocity at all stations is upward.

F. M. Sauer of Stanford Research Institute, References 3.3 and 3.8, appears to have been the first to recognize a regularity in the alternating outrunning seismic wave. By studying a number of field records he discerned and normalized an average wave shape from about one dozen observations and called it Type II wave form; this wave is depicted in an idealized form in Figure 3.53. The idealization excludes high frequency components; moreover, it is based on the assumption that it produces no residual displacement i.e. the sum of the five velocity-time areas is zero. Sauer also observed that the wave's characteristic duration,  $D_2$ , does not appear to scale with the one third power of the yield as the duration,  $D_p^+$ , does, but tentatively it may be related to the difference between a station's range,  $R$ , and the smaller range,  $r_0$ , at which outrunning begins. Thus

$$D_2 \approx 0.10 + \frac{R - r_0}{4000} \quad \text{in seconds} \quad (3.51)$$

if  $R$  and  $r_0$  are given in feet. Consequently the initial value of  $D_2$  will





RC-407,541-8

FIG. 3. 52 ILLUSTRATION OF DEVELOPMENT OF OUTFRACING GROUND MOTION-TUMBLER SHOT 1

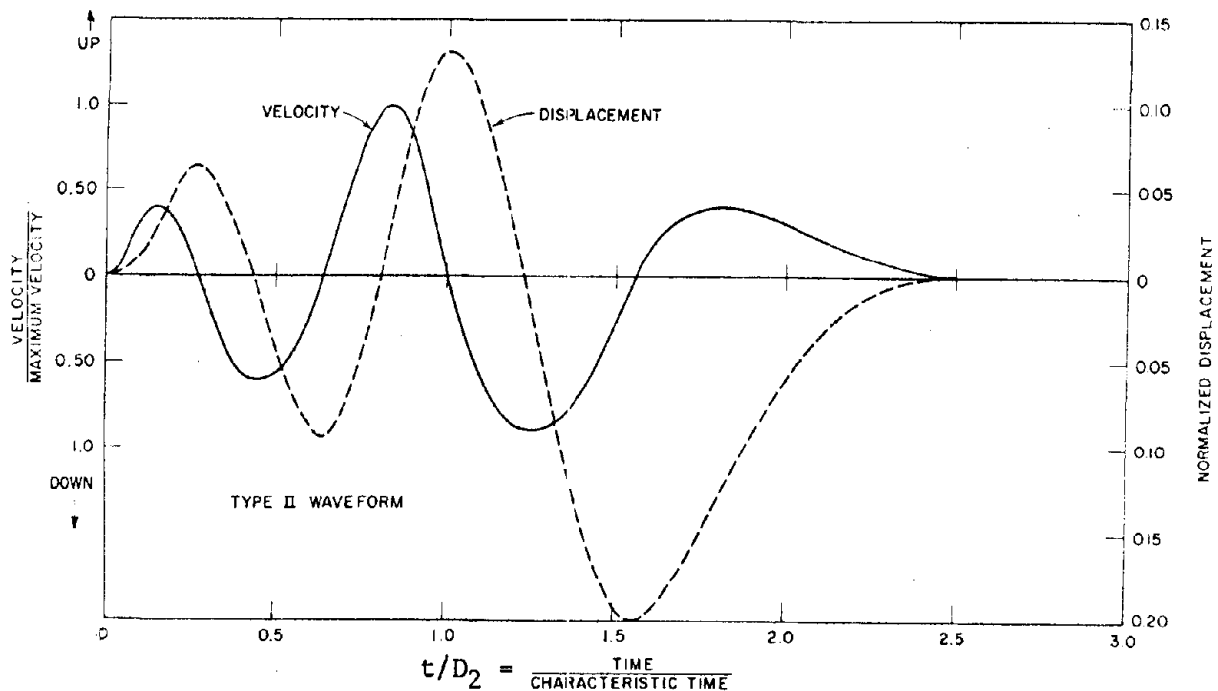


FIG. 3. 53 TYPE II (OUTRACING GROUND MOTION) VERTICAL PARTICLE VELOCITY WAVEFORM AND ITS DISPLACEMENT

increase linearly with  $(R - r_0)$ . The phasing between Type I and Type II waveforms may be determined when seismic and air blast wave travel curves are known, but their relative amplitudes may be only roughly estimated, Reference 3.8. Simple superposition of the two waveforms is theoretically not admissible but it nevertheless leads to a reasonably close approximation of the observed outrunning ground motion, see Figure 3.54 a, b, c, d.

The data presented in Figure 3.54a shows the motion at the surface for the Tumbler I event, a one kiloton detonation, and in Figure 3.54b it shows the motion at the 30 foot level for the EPG-4 event, a much larger yield detonation. It should be noted that the onset of the air blast is clearly seen only in Figure 3.54a, indicating that the attenuation of Type I waveform with depth is considerable. Figures 3.54c and 3.54d show two additional comparisons of observed and idealized Type II waveform.

A semi-quantitative set of six time plots of idealized Types I and II vertical velocity waveforms for a 1 MT burst is shown in Figure 3.55 for stations located at the indicated ranges from G.Z.. The quantitative time scales begin when the first motion arrives at a station. The characteristic time,  $D_p^+$ , of Type I waveform is constant and equal to 1.0 second but the characteristic time,  $D_2$ , of Type II waveform is seen to increase with range from 0.127 sec to 0.375 sec. The relative amplitudes of the two types of waveforms are not quantitative; their maximum peaks have been drawn arbitrarily equal at each station, and they have been assumed to decrease inversely with the square of the range,  $R$ .

The alternating characteristic of the Type II waveform, together with the fact that the corresponding, initial velocity pulse is upward may be of considerable importance even if the peak value of the velocity is smaller than for the Type I waveform. Thus the alternating nature of the motion may lead to quasi-resonance response, and the initially upward velocity, occurring before the advent of the air pressure front, may be large enough to lift covers off their seats if they are not adequately tied down, e.g., the sliding cover of a launch silo.

In order to give a semi-quantitative idea of the outrunning ground shock Figure 3.55 has been drawn. The data relate to Example 3.13 in which a 1 MT burst occurs on the surface of the specific, 6 layered soil denoted

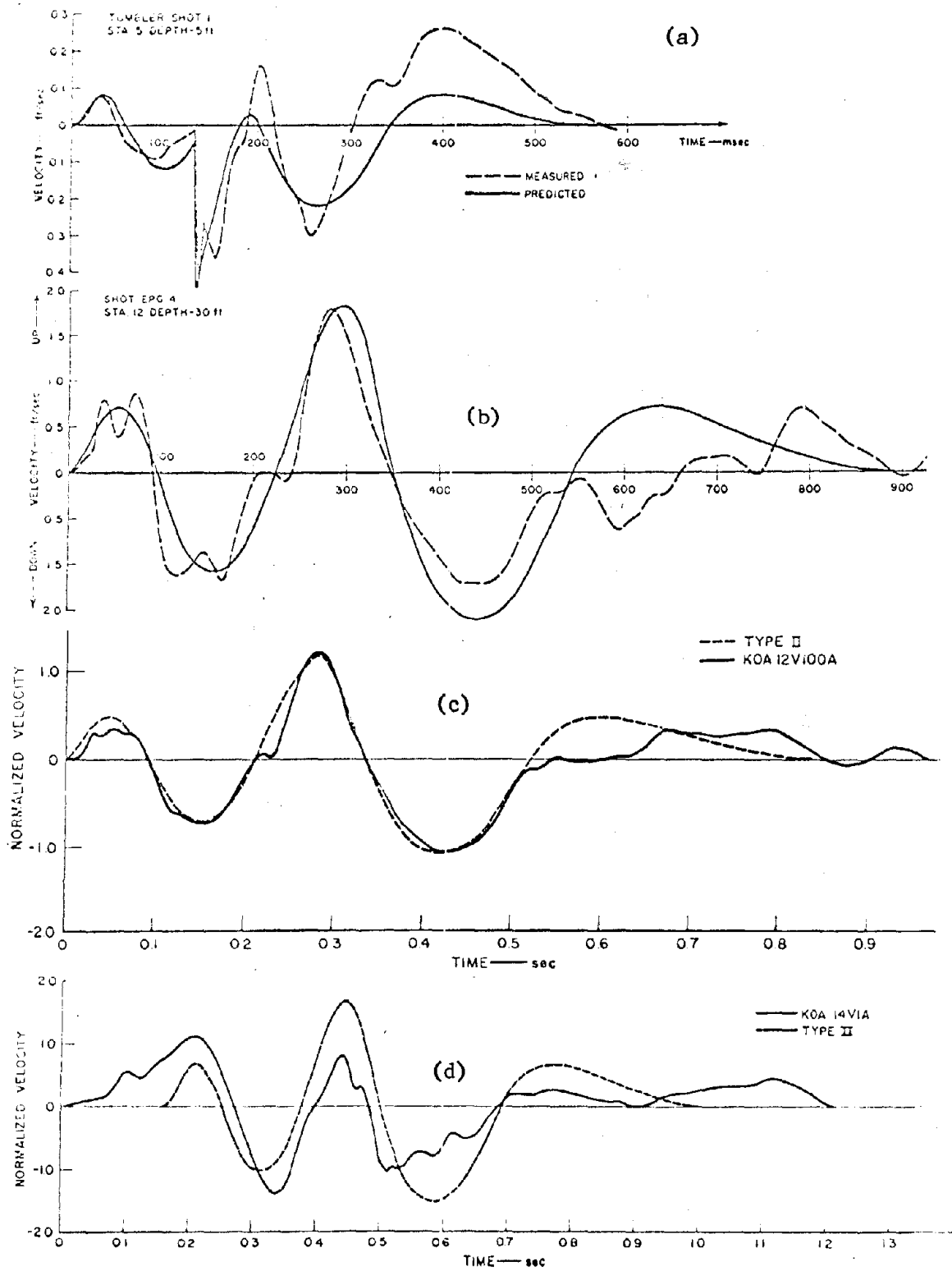
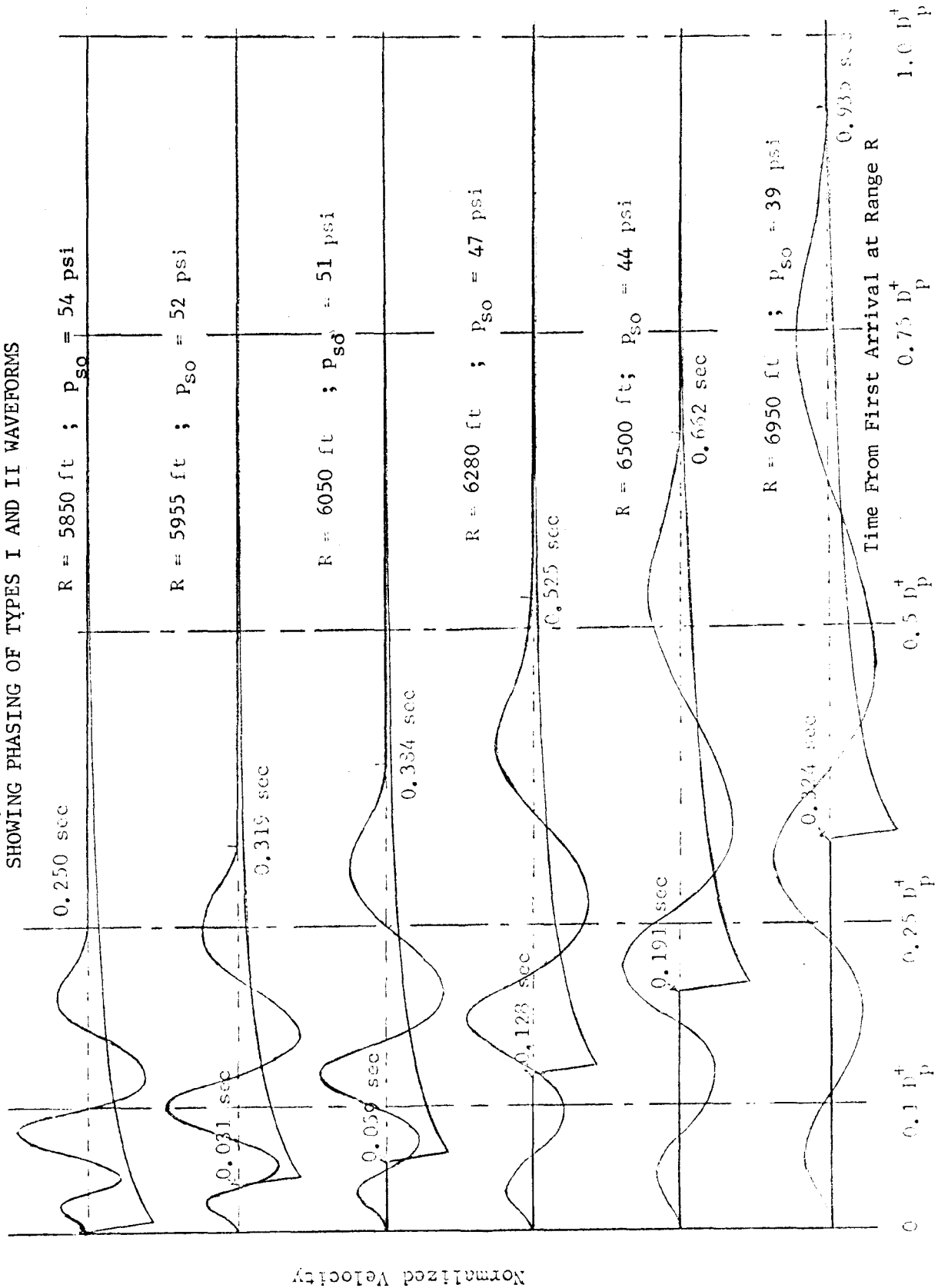


FIGURE 3.54: COMPARISON OF PREDICTED AND OBSERVED OUTFRACING GROUND MOTION

FIGURE 3.55: 1 MT, SOIL C OUTRUNNING AT 5850 FT FROM G.Z.  
SHOWING PHASING OF TYPES I AND II WAVEFORMS



by C. In this example outrunning begins at the distance of 5850 feet where the overpressure is 54 psi.

Since the S.R.I. analysis was based on the relatively few field tests carried out on unconfined bursts before the test ban, only the shape and duration of the alternating motion is given; its magnitude has not been related to bomb yield, distance, and seismic properties of ground. However in many of the tests analyzed by S.R.I. the peak values of Type I and Type II motions were of the same order of magnitude. The six diagrams of Figure 3.55 arbitrarily show equal peak velocity amplitudes of the two types of motion. It should be noted that the six phasing times  $t_{\phi}$  range between  $t_{\phi} = 0$ , at  $r_o = R = 5850$  ft, with  $p_{so} = 54$  psi, and  $t_{\phi} = 0.324$  sec, at  $R = 6950$  ft, with  $p_{so} = 39$  psi.

If outrunning begins at  $r_o$ ,  $t_o$  and  $(p_{so})_o$ , and if the facility is located at  $R$ , then, as already stated, the intensity of the outrunning seismic Type II motion at  $r_o$  is neither well understood nor quantitatively defined. Therefore it is customary for a design criterion bluntly to assume that the alternating Type II motion can be replaced by a fraction  $m$  of the systematic Type I motion occurring at the outrunning distance  $r_o$  and depending in magnitude on  $(p_{so})_o$  so that:

$$(p'_{so})_o \approx m (p_{so})_o \quad (3.52)$$

Under these circumstances the outrunning seismic motion at  $R$  may be thought of as related to a seismically attenuated equivalent negative overpressure  $(p'_{so})_f$  of the same duration as the positive overpressure and which is given by

$$(p'_{so})_R \approx m (p_{so})_o \left(\frac{r_o}{R}\right)^n \quad (3.53)$$

in this expression the exponent,  $n$ , may be taken as 2.5 if  $(r_o + R)/2$  is less than  $2.5 W^{1/3}$  kilofeet, and for  $(r_o + R)/2$  greater than  $2.5 W^{1/3}$  kilofeet,  $n$  may be taken as 1.5. Since the calculations are very rough, sufficient accuracy for engineering purposes may be obtained by assuming that  $n = 2$ .

Which means that the  $p_{so}$  equivalent attenuation in the seismic medium is the same as the one in air. Accordingly, for  $n = 2$ , the equivalent negative

overpressure at R becomes

$$(p'_{so})_R = m (p_{so})_R \quad (3.54)$$

Since the value of  $m$  is problematic, a parametric study should be made, and it is believed that a variation of  $m$  from unity to  $1/3$  is a reasonable range.

3.6.2.4 Triangular replacement of alternating waveforms. Figure 3.56 shows six phased diagrams of an idealized, triangularly shaped Type I downward motion and of a bluntly assumed triangular shaped (Type I) upward motion for the specific 1 MT yield and for the specific soil C in which out-running begins at  $r_o = 5720$  feet. A fraction of  $m = 2/3$  has been assumed; consequently at  $r_o = R = 5720$ ;  $t_\phi = 0$ ;  $(p_{so})_R = 57$  psi; and  $(p'_{so})_R = 38$  psi, it can be concluded from Equation (3.21) that the peak velocities at the surface will be

$$v_I = \frac{57}{2 c_p} \text{ in/sec} \quad \text{for the initially downward component}$$

$$v_I' = \frac{38}{2 c_p} \text{ in/sec} \quad \text{for the initially upward component}$$

If  $c_p = 1.5$  kilofeet per second

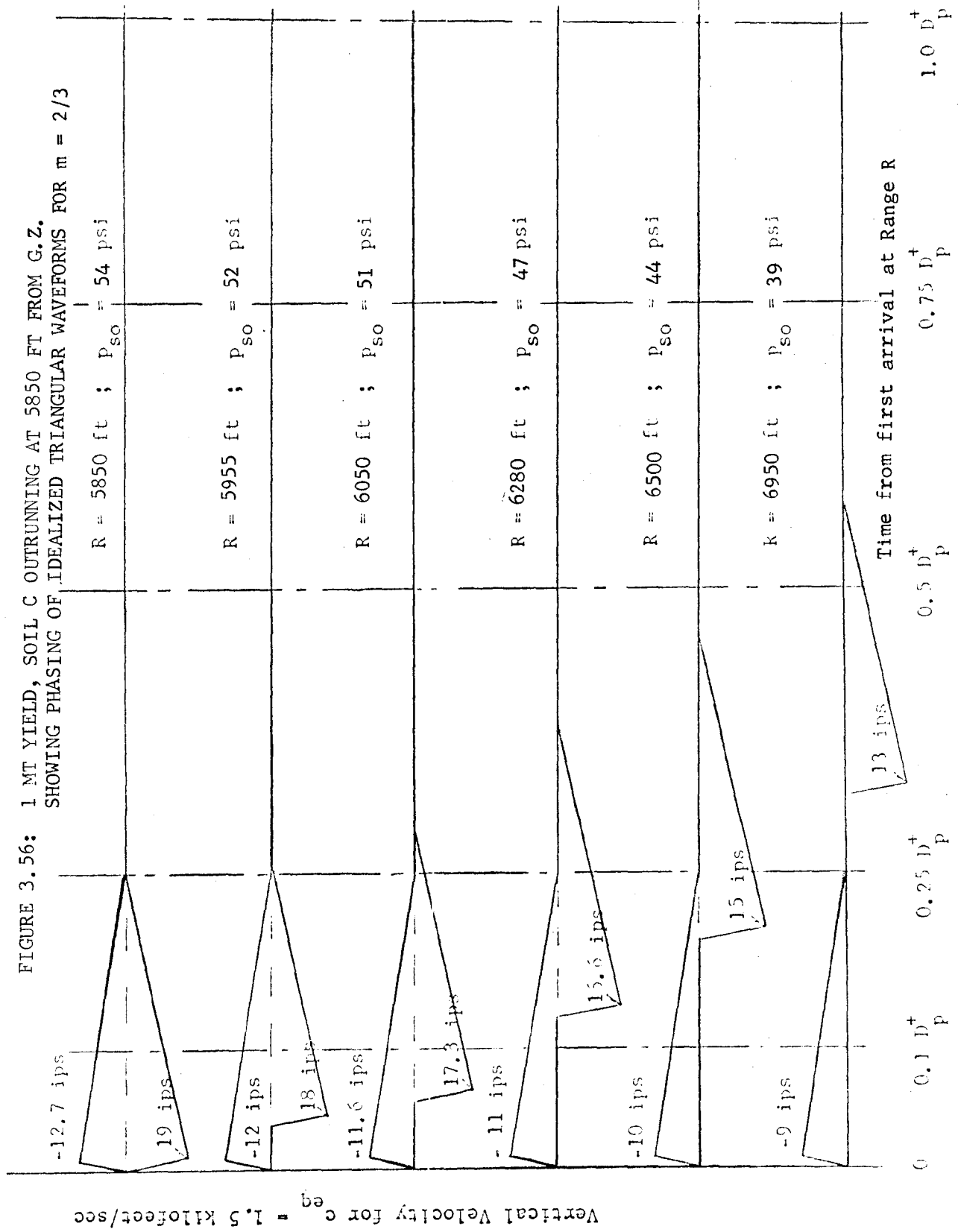
$$v_I = 19 \text{ in/sec, and } v_I' = -12.7 \text{ in/sec}$$

at  $R = 6820$  ft;  $t_\phi = 0.324$  sec;  $(p_{so})_R = 40$  psi; and  $(p'_{so})_R = 27$  psi

$$v_I = 13 \text{ in/sec, and } v_I' = -9 \text{ in/sec}$$

The idealization of the Type II waveform to a triangular shape, of the same duration as the idealized Type I but of somewhat smaller intensity, is of course highly debatable, especially since at the most only one complete alternation will result. This idealization is shown in Figure 3.56. A different point of view will be represented under Subsection 3.7.4 in terms of spectra.

FIGURE 3.56: 1 MT YIELD, SOIL C OUTRUNNING AT 5850 FT FROM G.Z.  
 SHOWING PHASING OF IDEALIZED TRIANGULAR WAVEFORMS FOR  $m = 2/3$



Vertical Velocity for  $c_{eq} = 1.5$  kilofeet/sec

### 3.7 Ground Motions in Terms of Shock Spectra

In the published literature, shock spectra have been widely accepted as a form of input, but it must be remembered that they predict the upper bound on the peak response of a mass - spring system to inputs at the support points of the system.

The interpretation and use of shock spectra is given in Section 2. It was explained that the shock spectra envelope can be plotted in terms of three straight lines; a line parallel to the constant displacement coordinates in the low frequency region, a line parallel to the constant velocity coordinates in the mid-frequency region, and a line parallel to the constant acceleration coordinates in the high frequency region. The response displacement,  $D$ , in the low frequency region approaches the peak ground displacement,  $d_{\max}$ , and the response acceleration,  $A$ , in the high frequency region approaches twice the peak ground acceleration,  $a_{\max}$ . In the mid-frequency region significant amplification of the response may be expected as it is very sensitive to the nature of the input waveform and to damping in the system.

3.7.1 Spectral amplification factors for shock pulses. The spectral amplification factors recommended in Reference 3.6 are:

$$\begin{aligned} A &= 2 a \\ V &= 1.5 v \\ D &= d \end{aligned} \tag{3.55}$$

and the relationship between horizontal and vertical components is given as

$$\begin{aligned} a_h &= a_v \\ v_h &= 2/3 v_v \\ d_h &= 1/3 d_v \end{aligned} \tag{3.56}$$

These factors have been widely used as design criteria. In a situation where the air blast slap produces the primary ground motion, they will adequately envelop any single-degree-of-freedom system's response except possibly in the frequency region where the constant displacement line intersects the constant velocity line.



3.7.2 Spectral amplification factors for outrunning pulses. In an outrunning condition, i.e., the air blast induced ground disturbance outruns the surface wave, pulses occurring ahead of or in phase with the air blast slap induced motion may be random or oscillatory in nature. The response to alternating pulses may also be expressed in terms of spectral amplification factors which in some cases may exceed those given above. However, alternating motion amplification factors should be used cautiously due to meager test data for the shape and magnitude of the outrunning pulse. Accordingly the same amplification factors often may be used for both the primary pulse and the oscillatory or random pulse (secondary pulse). It has been suggested in Reference 3.7 that the peak values of the oscillatory or random component may be related to the primary pulse as follows:

$$\begin{aligned}d_{\text{outrunning}} &= 0.3 d_v \\v_{\text{outrunning}} &= 0.6 v_v \\a_{\text{outrunning}} &= 1.0 a_v\end{aligned}\tag{3.57}$$

3.7.3 Spectral amplification factors for resultant pulses. Horizontal components of outrunning motions are assumed to be equal to the vertical components. The peak ground motions intensities due to the air blast slap and outrunning are then combined in the following approximate manner:

$$\begin{aligned}d_{\text{result}} &= d + d_{\text{outrunning}} \\v_{\text{result}} &= \sqrt{v^2 + v_{\text{outrunning}}^2} \\a_{\text{result}} &= \sqrt{a^2 + a_{\text{outrunning}}^2}\end{aligned}\tag{3.58}$$

The total peak motions can be expressed roughly in terms of the air blast slap motion for which empirical relationships have been given in Section 3.5. Thus Reference 3.7 recommends that

	<u>Vertical</u>	<u>Horizontal</u>	
$d_{\text{result}}$	$1.3 d_v$	$0.6 d_v$	
$v_{\text{result}}$	$1.2 v_v$	$0.9 v_v$	(3.59)
$a_{\text{result}}$	$1.4 a_v$	$1.4 a_v$	

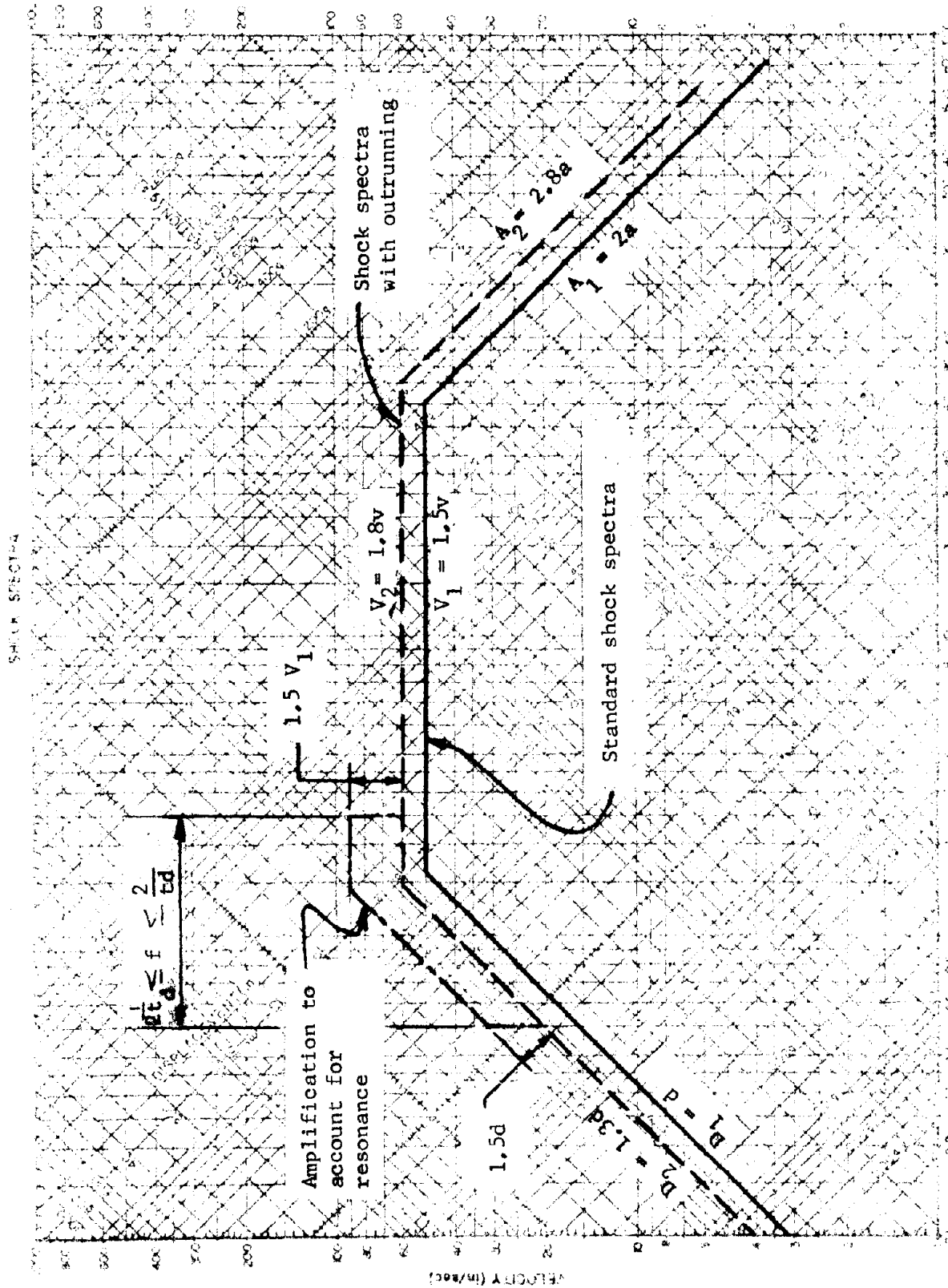


FIGURE 3.57: SHOCK SPECTRA AMPLIFICATION FACTORS (VERTICAL)

Using the same amplification factors as recommended for the simple pulse case, the shock spectra envelope is then defined by:

	<u>Vertical</u>	<u>Horizontal</u>	
D	1.3 d <sub>v</sub>	0.6 d <sub>v</sub>	
V	1.3 v <sub>v</sub>	1.35 v <sub>v</sub>	(3.60)
A	2.3 a <sub>v</sub>	2.8 a <sub>v</sub>	

The peak response magnitudes (for the primary motion) sometimes must be further modified in the frequency region

$$\frac{2}{t_d} \leq f \leq \frac{1}{2t_d} \quad (3.61)$$

due to a partial resonance condition. This was illustrated in Section 2 where the spectrum for a half sine displacement pulse showed a response amplification in this region. Unfortunately the total time duration,  $t_d$ , is one of the parameters that is not easily determined. The time to reach maximum displacement, i.e., the positive phase duration of the velocity pulse,  $t^+$ , can be calculated, and  $t_d$  is usually estimated to be 2 to 4 times  $t^+$ . When the frequency region bounded by Equation (3.61) is determined approximately and when it is found that a shock isolation system frequency falls in this region, a rough estimate of the response amplification bound may be made by multiplying the spectra bound of Equation (3.72) by 1.5 for this region only. This increased response can often be avoided by designing the shock isolation system to have a frequency less than  $1/(2t_d)$ , but when this is not practical, a more accurate response of the system may be obtained by a pulse analysis. For approximate methods, the above amplification factors may be used, and they are summarized in Figure 3.57.

3.7.4 Spectral amplifications due to combinations of Type I and Type II waveforms. In Reference 3.8 shock spectra have been computed by analog methods for linear, and for bi-linear oscillators with and without damping as well as with hysteretic energy absorption. The velocity inputs to the oscillators comprise 27 combinations of Type I and Type II waveforms of durations  $T_I$  and  $T_{II}$  as well as specified input ratios of amplitude, duration, and phasing of the two parent types. A discussion of the results of the 27 combinations follows.

3.7.4.1 Linear systems. Figures 3.59 and 3.60 show plots against  $T/T_I$  or  $T/D_p^+$  of the undamped velocity spectra when a linear oscillator of period  $T$  is subjected to the  $27 + 2$  inputs.

It is seen that the two normalized types of motion shown in Figure 3.58 are not using quite the same normalized duration, Type I having 3 time units and Type II having only 2.5 units; the reason for this is not stated in the Reference. Only three phasings were employed and they are denoted by:

- "Leading": when time unit 0 of Type I coincides with time unit 1 of Type II waveform
- "Central": when time units 1 of both motions coincide
- "Lagging": when time unit 3 of Type I coincides with time unit 1 of Type II waveform

Adjacent to the plots of the Type I and Type II normalized waveforms on Figure 3.58 are located the spectra labeled (1) and (29) that relate to a pure Type I and to a pure Type II input respectively. Two spectra are shown on each of these plots, corresponding to a normalized unit peak velocity and to a normalized half unit peak velocity.

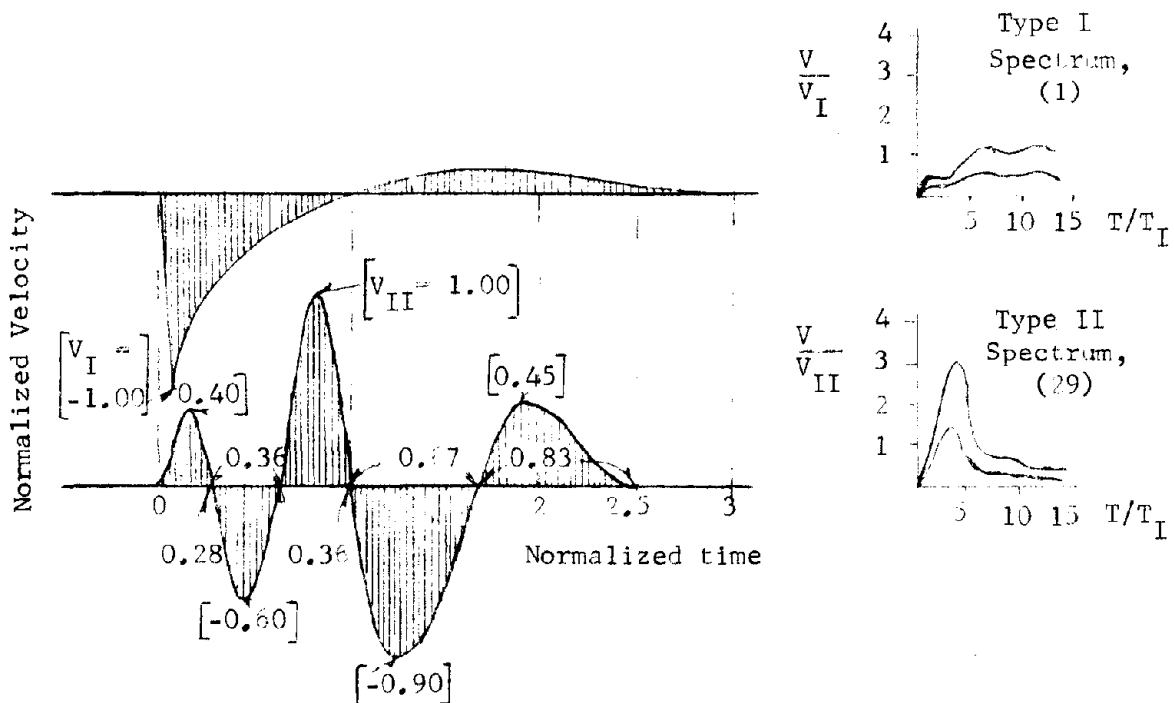


FIGURE 3.58

Let us begin by examining the quasi periodic Type II motion. The five alternating half cycles have durations varying from 0.28 to 0.82 normalized time units, and their amplitudes vary from 0.4 to 1.0 normalized velocity units. If it is assumed that the first three half cycles of an average duration of a normalized time unit of  $1/3$  are in effective resonance with the undamped, linear oscillator, the oscillator's response for the three half cycles of unit amplitude will have an amplification of  $3 \times \pi/2$ . If the three half cycles' average amplitude of  $(0.4 + 0.6 + 1.0)/3 = 2/3$  is used as a correction factor, the oscillator's amplification will be close to  $\pi$ . The peak of the corresponding spectrum (29) is seen to occur near the normalized time coordinate 4, and to be about 3.1 for the unit peak velocity; consequently it is in fair agreement with the computed spectrum.

The spectrum labeled (1) shows an upper amplification value of about 1.3 for  $T/T_I \approx 12$ . If a triangular waveform of normalized duration 1 were to replace the Type I waveform, an upper amplification bound for the response spectrum would be less than two; accordingly the value of 1.3 seems to be reasonable.

The 27 spectra, shown in Figures 3.59 - 3.60 and labeled consecutively (2) to (28) relate to the  $3 \times 3 \times 3$  combinations of three phasings "leading", "central", and "lagging", the three relative durations, and three relative amplitudes of Type I and Type II waveforms  $V_I = 2 V_{II}$ ,  $V_I = V_{II}$ , and  $2 V_I = V_{II}$ . The envelopes, i.e. the upper and lower amplification bounds have been shown on the right and below. They are marked by hatching the areas between them to show:

- a) the effect of relative duration
- b) the effect of phasing
- c) the effect of phasing, relative duration, and relative amplitude

Whatever general observations can be made from these 27 combinations are not very precise, but the following seem to be indicated:

- a) Possible variations of phasing, relative duration and relative amplitude will give a maximum spectral amplification spread from 0.5 to 4.2 for  $T/T_I \approx 4$ .

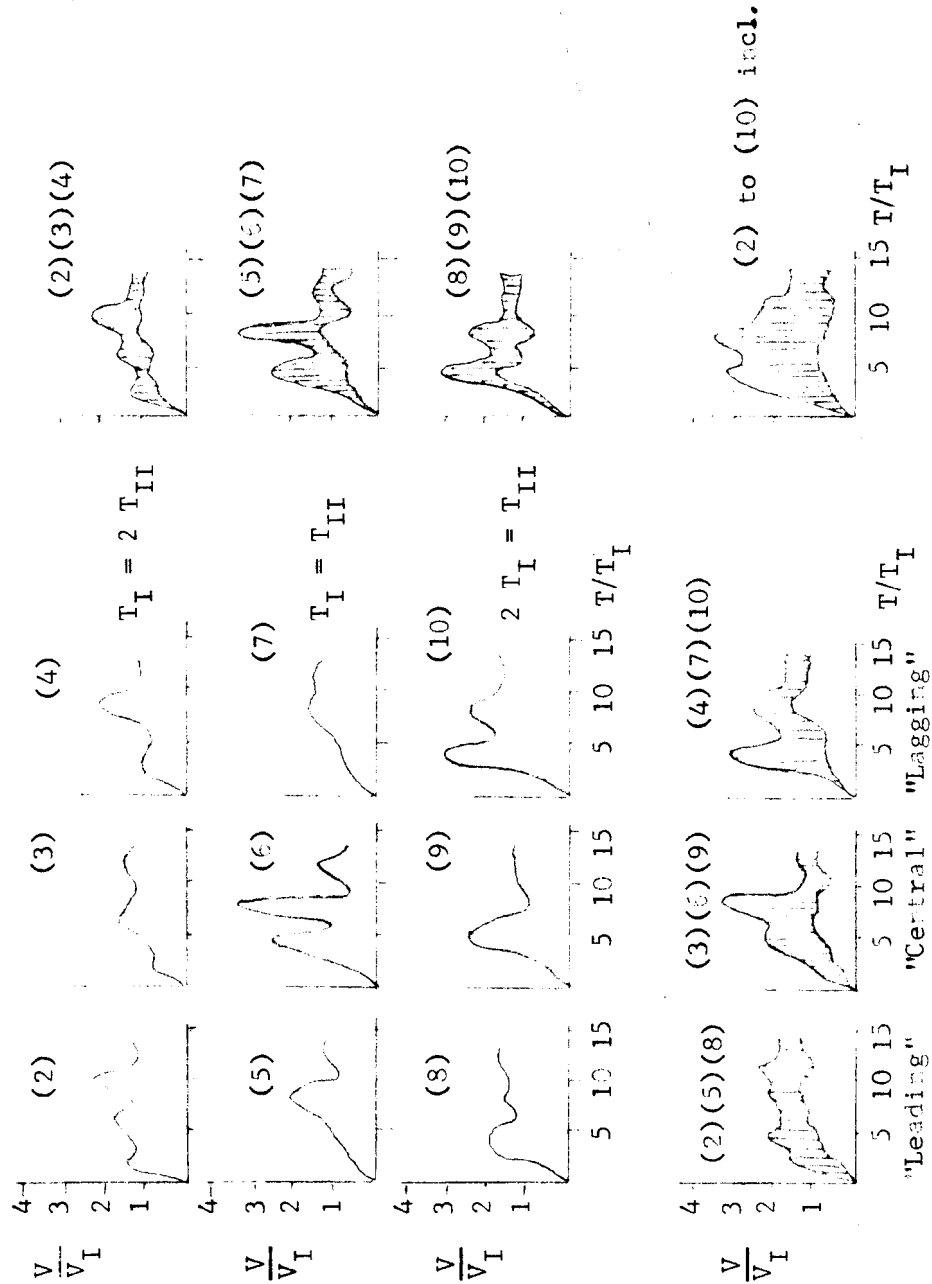


FIGURE 3.59a: LINEAR SPECTRA FOR COMBINATIONS OF TYPES I AND II MOTIONS WITH  $V_I = 2 V_{II}$

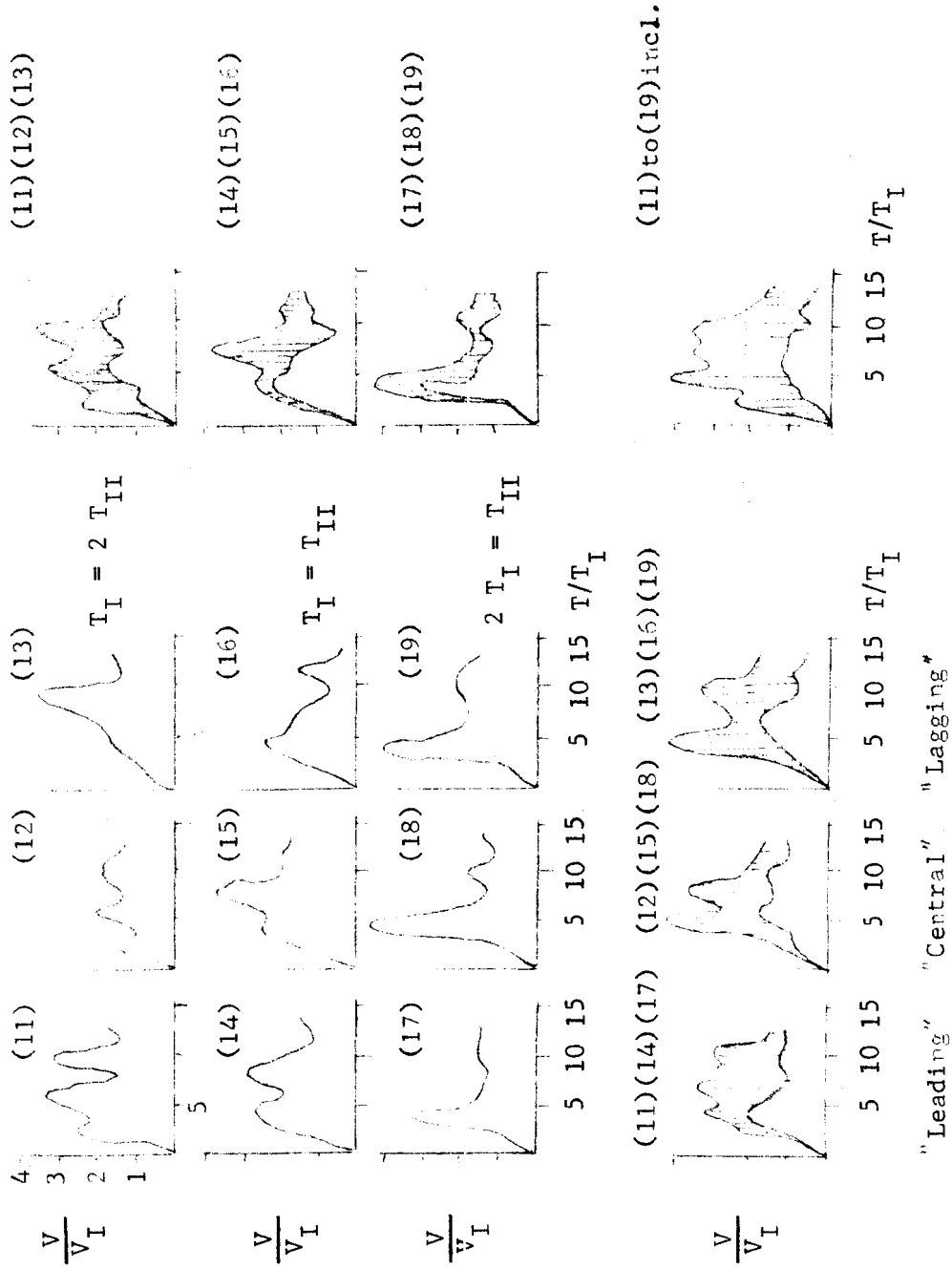


FIGURE 3.59b: LINEAR SPECTRA FOR COMBINATIONS OF TYPES I AND II MOTIONS WITH  $V_I = V_{II}$

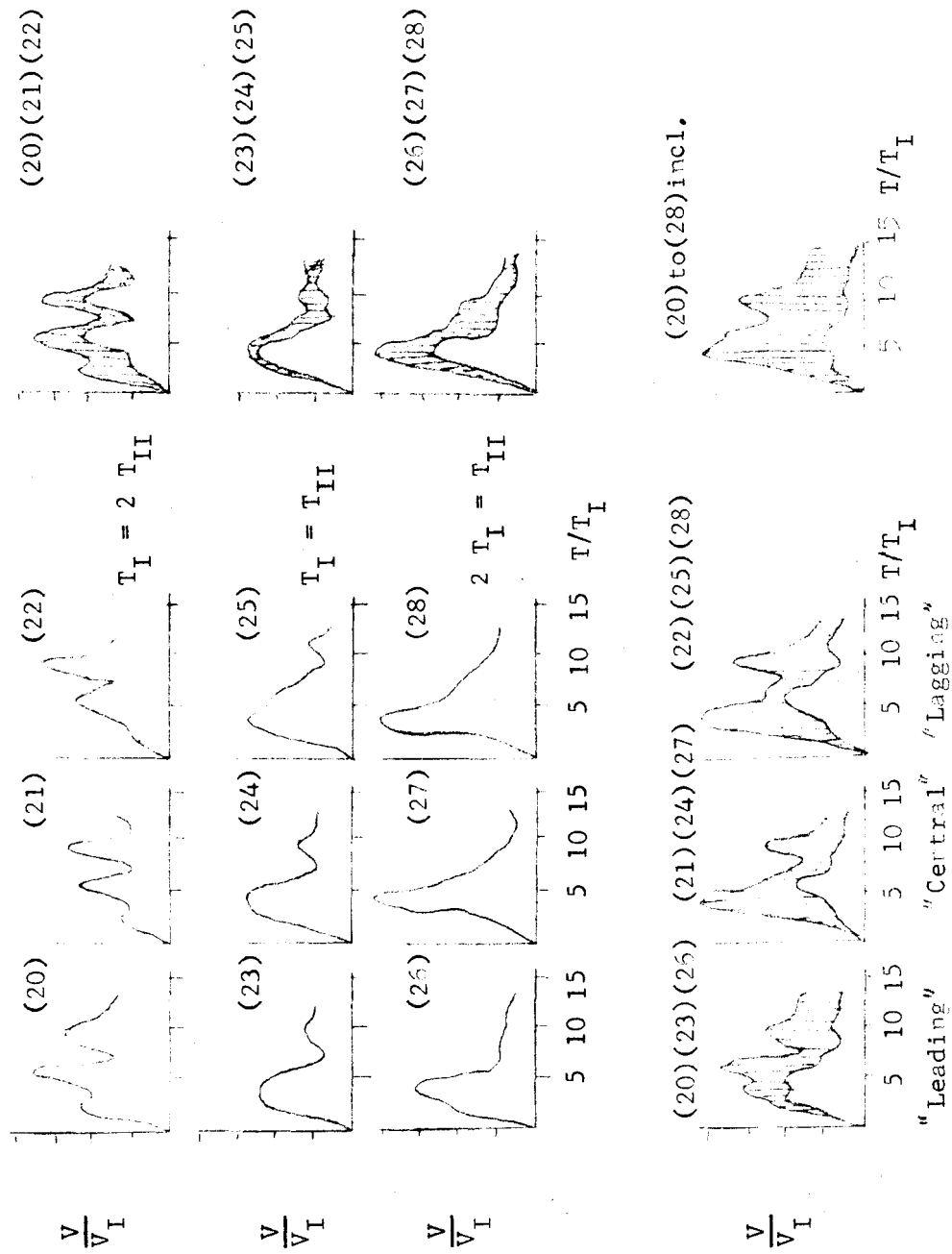


FIGURE 3.60: LINEAR SPECTRA COMBINATIONS OF TYPES I AND II MOTIONS WITH  $2 V_I = V_{II}$



- b) Possible variations of relative duration will give a maximum spectral amplification spread from 1.0 to 4.2 for  $T/T_I = 4$ .
- c) Possible variations of phasing will give a maximum spectral amplification spread from 1.0 to 3.0 for  $T/T_I = 4$ .

In view of the above general observations the following conclusions are made:

Peak velocity magnifications of 3.3, 4.2, and 4.2 are reached for the three velocity amplitude ratios of  $V_I/V_{II}$  equal to 2, 1, and 1/2 respectively, moreover, duration effects due to  $T_I/T_{II}$  equal to 2, 1, and 1/2 are slightly more important in producing peak velocity magnifications than effects due to "leading", "central", and "lagging" phasings.

For weapon effects in the one megaton class,  $D_p^+ / T_I$  is about one second for an overpressure range of 30 to 1000 psi. Referring to Figure 3.61, which shows on a large scale the envelope of the 27 velocity spectra as well as the spectra for the two pure motions, it is seen that systems having natural periods falling in the range of about one half to one thirteenth of a second will experience velocity amplifications greater than two, and systems having natural periods within the range of one third to one tenth of a second will have undamped velocity spectra upper bounds of about 4.

Since the envelope includes all the 27 combinations of the three variables, amplitude, timing, and phasing, and since the relative magnitudes of these variables have been arbitrarily selected, the reality of the data is open to question. It seems plausible however, that for systems with a natural period range of one half to one tenth of a second the velocity amplification factor may be assumed close to 3.

The dotted curve in Figure 3.61 shows the envelope of the 27 spectra for linear systems with 10 percent of critical viscous damping, indicating that a maximum amplification of about 2.5 occurs when  $D_p^+ / T$  is between 5 and 6.

The first 29 diagrams of Figure 3.62 depict the velocity inputs of the two parent waveforms Type I and Type II and of the 27 combinations of them as previously discussed. The inputs 30 to 34 relate to five records obtained from actual events.

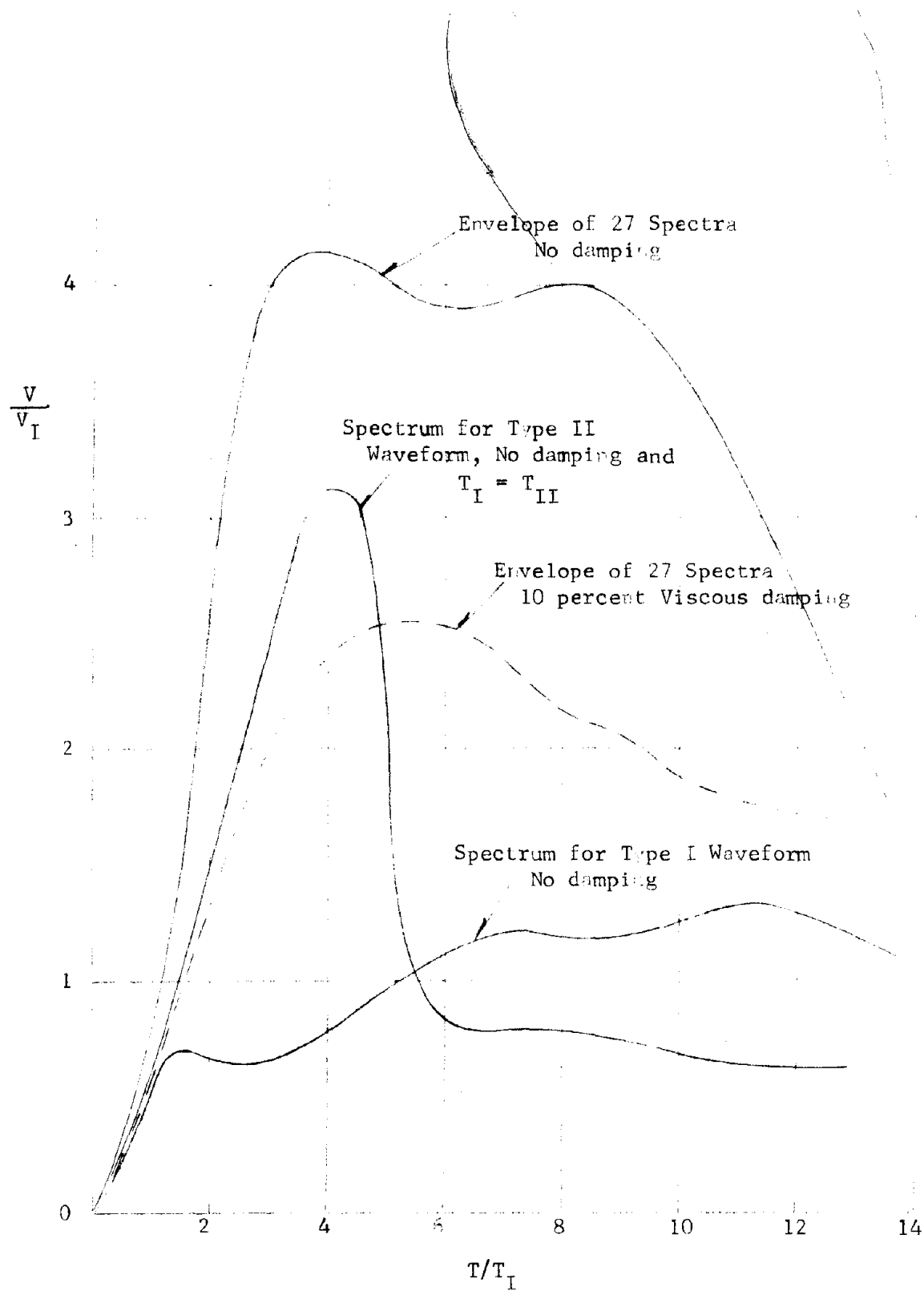


FIGURE 3.61: SUMMARY OF SPECTRA FOR 27 COMBINATIONS OF TYPE I AND TYPE II WAVEFORMS ACTING ON LINEAR SYSTEMS

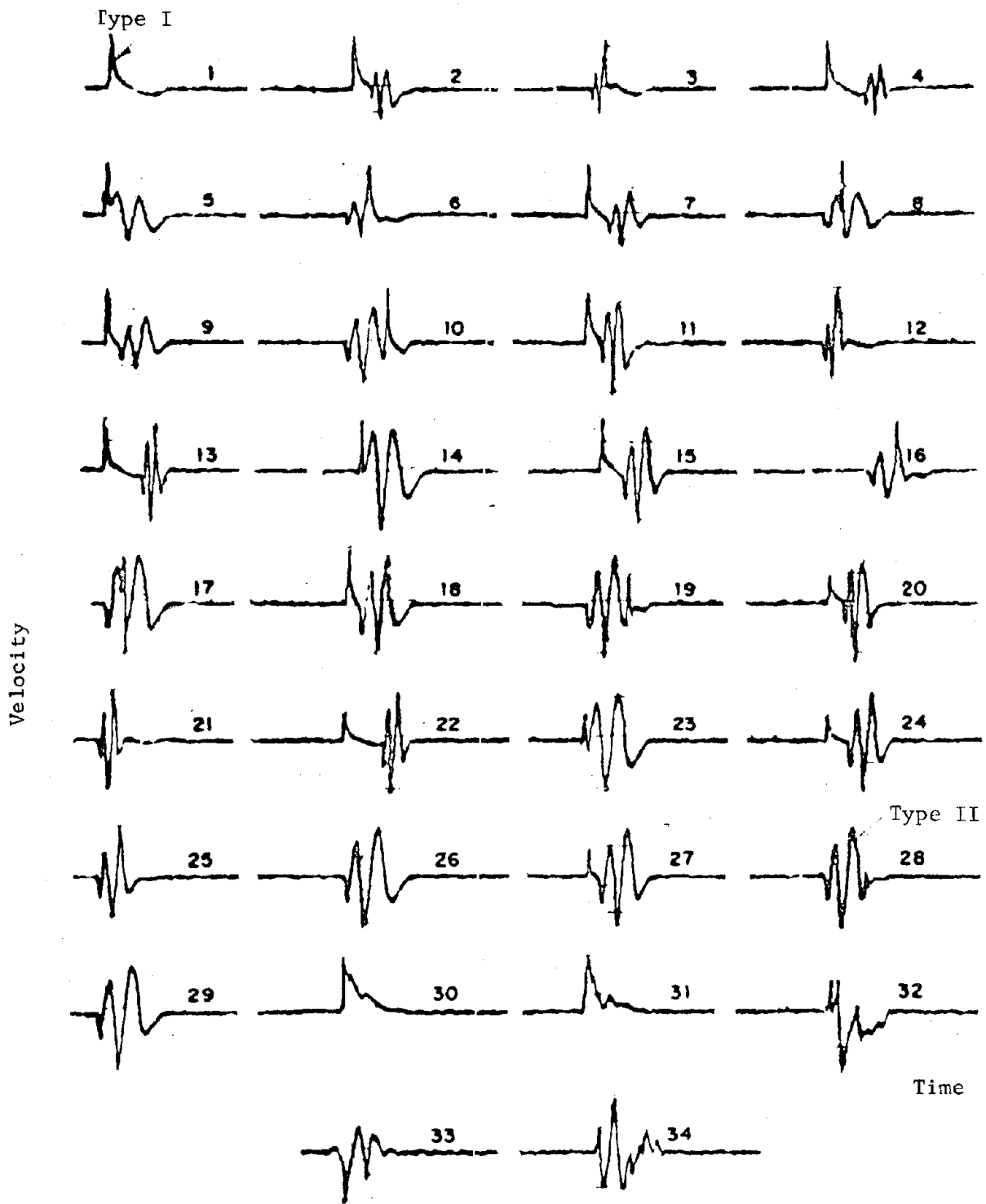


FIGURE 3.62: VELOCITY WAVEFORMS USED AS INPUTS IN LINEAR AND IN BILINEAR SYSTEMS ANALYSIS (REFERENCE 3.8)

Example 3.18

Find the spectral values for a frictionless linear system with  $T = 2.5$  seconds or  $\omega = 2.5$  radians/second which is exposed to pure Type I, pure Type II, and a combination of Types I and II motions, defined by:

Amplitude:  $V_I = 100$  inches/sec,  $V_{II} = 50$  inches/sec

Duration:  $D_p^+ = T_I = 0.25$  seconds  $T_{II} = 0.50$  seconds

Phasing: "Leading", "Central", and "Lagging"

For the ratio  $T/T_I = 10$  Figure 3.61 gives

For pure Type I motion  $V/V_I \approx 1.25$ ,

Accordingly  $V_{max} = 125$  in/sec,  $A_{max} = 2.5 \times 125 = 313$  in/sec<sup>2</sup> = 0.81 g and

$$D_{max} = \frac{125}{2.5} = 50 \text{ inches}$$

For pure Type II motion Figure 3.61 gives  $V/V_I \approx 0.70$  or  $V/V_{II} \approx 0.35$

Accordingly  $V_{max} = 35$  in/sec,  $A_{max} = 2.5 \times 35 = 88$  in/sec<sup>2</sup> = 0.23 g, and

$$D_{max} = \frac{35}{2.5} = 14 \text{ inches}$$

For combinations of Type I and Type II motions, the ratios  $V_I/V_{II} = 2$  and  $T_I/T_{II} = \frac{1}{2}$  must be used. If the alternating motion is "leading", or "central", or "lagging" Figure 3.58, Spectrum 8, 9, or 10 must be used respectively, giving:

for "leading"  $V/V_I \approx 1.45$  or  $V_{max} = 145$  in/sec;  $A_{max} = 0.94g$ ;  $D_{max} = 58$  inches

" "central"  $\approx 1.25$  = 125 " ; = 0.81g ; = 50 "

" "lagging"  $\approx 1.70$  = 170 " ; = 1.10g = 68 "

Example 3.19

Assume that all 27 combinations of Types I and II motion are possible, i.e.

Amplitude	$V_I = 100$ inches/sec	$V_{II} =$	}	50 inches/sec 100 " 200 " 0.50 seconds
Duration	$T_I = 0.25$ seconds	$T_{II} =$	}	0.25 " 0.125 "

Example 3.19 (continued)

Phasing "Leading", "Central" and "Lagging"

Then for the ratio  $T/T_I = 10$ , Figure 3.61 gives an upper envelope for the undamped spectra of  $V/V_I \approx 3.6$ , to which corresponds

$$V_{\max} = 360 \text{ in/sec} ; A_{\max} = 2.3g ; \text{ and } D_{\max} = 144 \text{ inches}$$

If a 10 percent viscous damping is assumed in the system, Figure 3.61 gives an upper envelope of  $V/V_I \approx 1.85$ , to which corresponds

$$V_{\max} = 185 \text{ in/sec} ; A_{\max} = 1.2g ; \text{ and } D_{\max} = 74 \text{ inches}$$

It can be concluded that a reasonable amount of damping is of considerable value in reducing the transmitted velocity, acceleration and relative displacement to a shock mounted system.

3.7.4.2 Systems with nonlinearities and damping. G. N. Bycroft in Reference 3.8 also obtained spectra corresponding to Figure 3.62 inputs for systems with

- Bilinear stiffness and viscous damping
- Hysteretic stiffness and viscous damping
- Linear stiffness and Coulomb damping
- Linear stiffness and  $V^2$  damping
- Viscous damping and zero stiffness

Only the bilinear case will be mentioned here. Figure 3.63a shows the envelope of the spectra for the elasto-plastic case when the maximum amplitude of displacement is  $4\Delta$  and when the damping is either zero or 10 percent of the critical viscous, i.e.,  $0.1 (2 k m)^{1/2}$ . Figure 3.63b also shows the envelope of the spectra for the bilinear, stiffening Case,  $k$ , and  $2k$ , when the maximum amplitude of displacement is  $4\Delta$  and when the damping is either zero or 10 percent of critical.

Example 3.20

Reconsider Example 3.19, but assume that the system allows elasto-plastic action to take place as shown in Figure 3.63a.

Extending the upper envelope for the undamped spectra for  $T/T_I = 10$ , it is seen that  $V/V_I$  is about 5.7. Accordingly, the plastic action will increase the maximum velocity to 570 inches per second, or almost 60 percent.

Example 3.20 (continued)

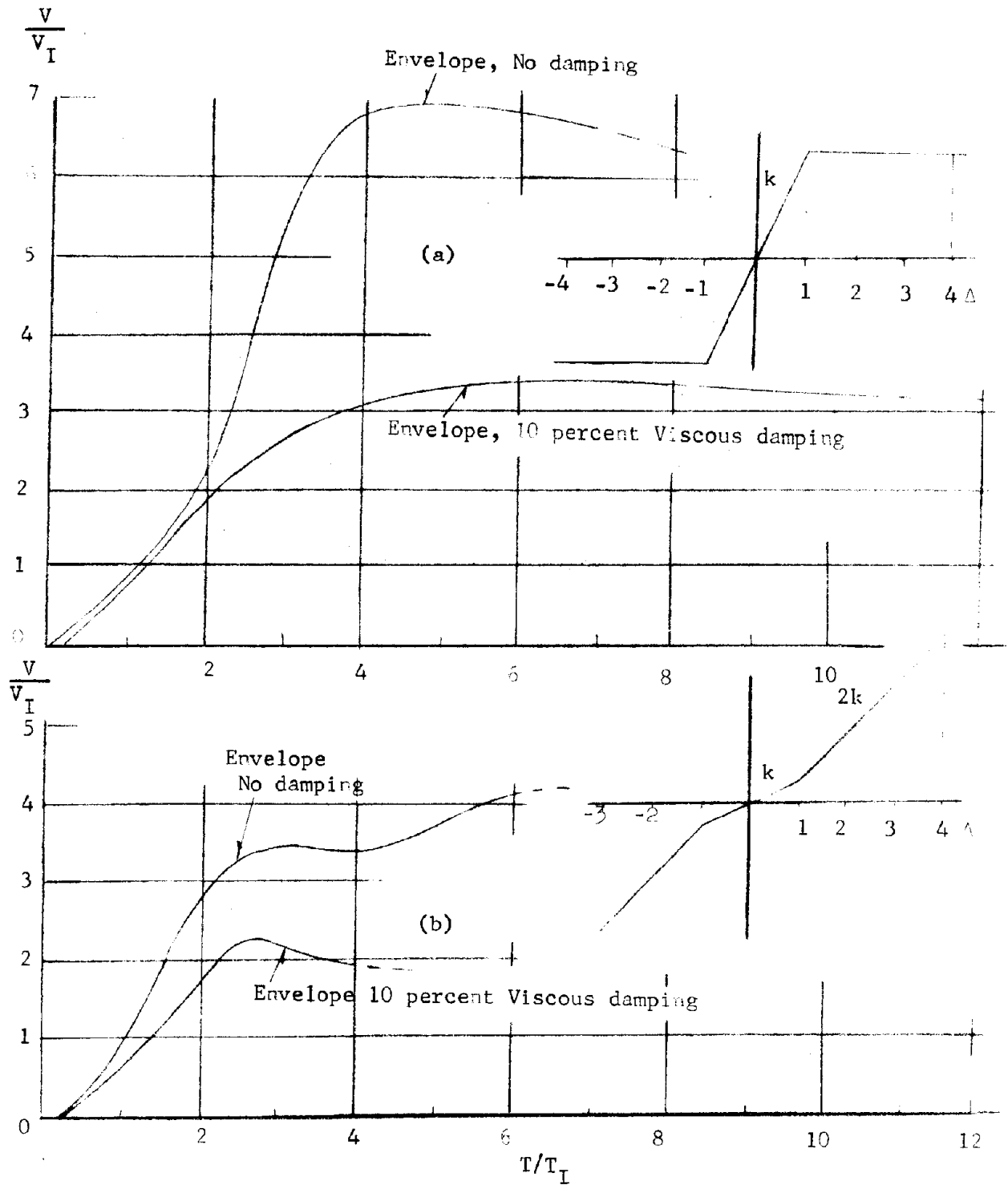


FIGURE 3.63: SUMMARY OF SPECTRA FOR 27 COMBINATIONS OF TYPE I AND TYPE II WAVEFORMS ACTING ON NONLINEAR SYSTEMS

Example 3.20 (continued)

However, in this case the simple harmonic motion relationships between velocity and acceleration and between velocity and displacement cannot be used. Thus the maximum acceleration,  $A_{\max}$ , will be considerably smaller than

$$A_{\max} < V_{\max} \omega$$

and the maximum displacement,  $D_{\max}$ , will be larger than

$$D_{\max} > V_{\max} / \omega$$

If a 10 percent viscous damping is assumed to act in the system, Figure 3.63a gives  $V/V_I \approx 3.2$ , so that  $V_{\max}$  is about 320 inches/second. This is about 73 percent larger than the corresponding value for the 10 percent damping assumption of Example 3.19.

It can be concluded that plastic action in shock mounts may be of slight advantage in reducing the transmitted acceleration, but this small advantage must be balanced against higher transmitted velocity and displacement values.

## SECTION 4: STRUCTURAL ENCLOSURES

### 4.1 Introduction

This section will discuss the influence of structures that are interposed between the free-field and equipment placed within the structures. The structures themselves are designed for the free-field pressures and ground motions and design procedures for protective structures may be found in many references. It is beyond the scope of this report to cover these procedures. In this section, various types of protective structures will be postulated, and their influence on items within the structure enclosures will be evaluated.

Aboveground structures will be exposed to the direct air-blast loading plus ground motions. The free-field pressure-time relationships (see Reference 2.9) together with the ground motions described in Section 3 define the dynamic loading. The dynamic response of the structures influences the motions of the supports of the internal items that must be protected from shock. Fully buried structures, designed to withstand much higher overpressures than aboveground structures, are protected from the direct effect of the air blast, but are generally subjected to much larger ground motions than the foundations of aboveground structures. In fact, in the case of aboveground structures, the predominant motions are due to the direct impact of the air blast, and soil-structure interaction is usually considered to be a less significant factor.

It has been generally assumed in the past that fully buried structures move with the ground. In some cases, structural influence factors have been used to attenuate high frequency accelerations for fully buried monolithic concrete structures, as well as for floor slabs not exposed to the direct air blast.

Recently many studies and model tests have been performed to determine the behavior of a structure in soil media exposed to dynamic loads. Most investigations have as their goal the analysis of the coupling between soil and structure in order to obtain dynamic loads for the design of



underground structures. Since theoretical studies have not as yet resulted in general procedures for design application, it is necessary to represent the behavior of the structural enclosure in terms of simple concepts. Studies in earthquake effects have been of great use in interpreting the response of structures to ground motions. It has been observed that structural response generally is less severe than the response that could be predicted from the measured ground motions by seismographs. Reference 4.1 has given several possible explanations for this difference:

- (a) Imperfect coupling between the structure and the soil medium.
- (b) Damping within the structure.
- (c) Plastic deformations in the structure.

If a fully buried structure is designed to remain elastic for the postulated weapon effects, then conditions, b and c, can be neglected without too much conservatism. If elastic-plastic behavior is tolerated in the design, then this effect should be considered in reducing the shock response requirement for items rigidly mounted to the structure. One method of allowing for this is to reduce the predicted elastic-response spectra envelope for equipments mounted to the structure based on the amount of yielding of the structure. This will be explained and illustrated in Section 4.4.

The coupling effect between structure and soil cannot be easily assessed. An analytical treatment of this problem is presented in Reference 4.2, in which the rigid body motion and first deformation mode are considered to be significant in predicting structure response. The conclusion is that the structure will follow the soil motion closely, except within the initial period of vibration of the structure. The motion in this initial interval may affect the high frequency response, but will have negligible effect on low frequency systems.

Much research (References 4.3 - 4.8) and testing of small scale models has been done on structures in a soil; but, in all cases, the conclusions are that the structure response cannot be predicted by simple analytical methods. Further research is now in progress.

With the advent of automated techniques using computers, it is now feasible to model the soil medium and the structure in terms of many masses,

springs, and dampers. The free-field motions are applied at the boundary of the model; and input requirements to equipment support points are determined. The model is represented by many hundreds of degrees-of-freedom; but with the use of high speed computers, solutions may be readily obtained. Mathematical models are described in Appendix F, with an example.

Simple concepts will be used in computing the structure motions in this section. Aboveground, earthmounded, shallow buried, and deep underground structures will be considered. Their rigid body and deformational motions will be estimated in terms of peak accelerations, velocities, and displacements. Shock-spectra envelopes will then be defined in terms of the resultant motion of the structure.

## 4.2 Aboveground Structures

Aboveground structures are designed in the low overpressure regions. For overpressure regions much above 25 psi, it is probably more economical to place a facility underground. Yet, where functional needs require an aboveground structure, it is entirely feasible to construct exposed or partly exposed aboveground structures for incident overpressures up to 100 psi. For the higher range of pressures, arched or domed structures usually are required. The dynamic input to the supports of items attached to the structure is related to the direct impact of the air blast on the exposed structure, as well as to the foundation motion induced by the ground. In the region defined by low overpressures, the crater induced motions are generally negligible.

In this section, shock effects on equipment placed inside aboveground structures will be considered by examining the characteristics of four types of structures: 3 windowless structures of monolithic concrete (single-story rectangular, two-story and domed); and a multi-story steel framed windowless structure.

4.2.1 Shock spectra method. The air blast impinging directly on the exposed structure excites two significant types of response modes: a rigid body mode and several deformational modes. The rigid body mode will affect low

frequency, as well as high frequency items mounted to the structure; whereas the deformational response will have a significant effect primarily on high frequency systems. In the shock-spectra method, only the first deformational mode will be considered. Peak response (acceleration, velocity, and displacement) in each mode will be determined graphically or by approximate analytical expressions. (The response effect of higher deformation modes may be considered by the normal mode technique described in Appendix A, and combined with the rigid body and first deformation mode to obtain a resultant of all the modes.)

The air blast induced ground motion has been defined empirically in Section 3.5; and ground motions, in terms of peak ground displacement ( $d$ ), velocity ( $v$ ), and acceleration ( $a$ ) of the ground, have been presented. The foundation of the structure is coupled with the ground; and the peak displacement and velocity of the structure can be assumed to follow the ground closely. The structure acceleration, however, may be significantly reduced; as has been seen in the response of structures during earthquakes, where measured data have indicated that ground accelerations were greater than the calculated structure response accelerations. It has been the practice in blast-resistant design of aboveground structures for low overpressures to neglect ground accelerations, since their effect is normally very small compared with the dynamic forces due to air blast. In the analysis of shock effects on components attached to the structure, however, outrunning conditions (a random but oscillatory ground motion) may exist, which may result in a phased combination of ground motions and air-blast slap, that yields a critical response condition. A dynamic analysis may be required for this special case; and the method, outlined in Appendix F, must be used to consider adequately the phasing of the air blast impact on the structure with the outrunning ground motion.

When the shock spectra method is used, the peak response in each mode may be estimated separately: (1) rigid body mode response due to air blast impact on the structure, (2) deformation mode response due to air blast impact on the structure, and (3) rigid body response due to the primary component of the air-blast-induced ground motion.

By combining the peak motions either as the algebraic sum of their absolute values or as the square root of the sum of the squares of each value, an upper bound of the response may be obtained. A study of such approximations (see Reference 4.9) shows that the sum of the absolute values always gives conservative (sometimes ultraconservative) results; whereas the square root of the sum of the squares is generally conservative, but could be unconservative under special conditions. In designing for weapons effects, the square root of the sum of the squares is considered to be adequate, since the errors (probably less than  $\pm 20$  percent) in this approximation fall within the uncertainty of the input data. A direct application of the shock spectra method using the resultant peak displacement, velocity, and acceleration will then consist in applying the amplification factors recommended in Section 2.,

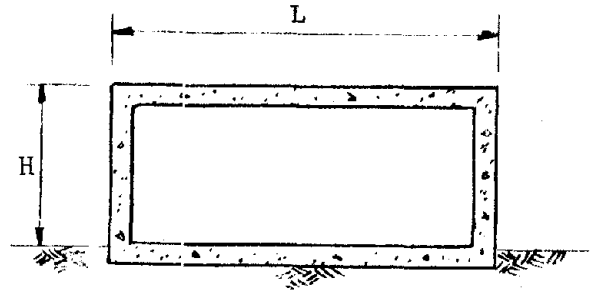
$$D = d$$

$$V = 1.5 v$$

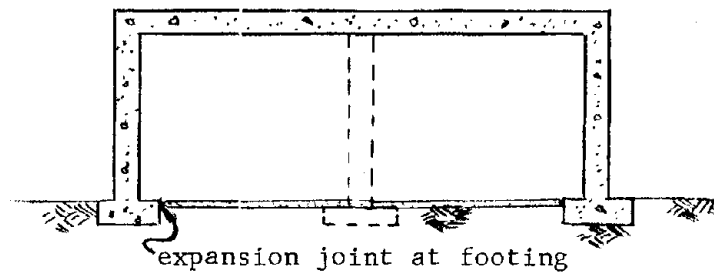
$$A = 2.0 v$$

to obtain the shock spectra envelope for design response for equipments attached to the structure. In this approximate method, the main effort consists in obtaining the rigid body and deformational modes of the structure due to the direct effect of the air blast. (The empirical relationships of Section 3.5 can be used for the input due to ground motion.) The following subsections describe typical aboveground structures and the motions which become input parameters for defining a shock spectra envelope.

4.2.2 Single story structures of rectangular shape. Typical structures are shown in Figure 4.1. These are windowless reinforced concrete structures (usually of monolithic construction) with walls as well as top and bottom slabs 12 to 24 inches thick. The structures are economical up to the 25 psi overpressure region.



(a) Monolithic Flat Slab Construction



(b) Separate Floor Slab Construction, Shear Walls with or without Interior Columns

FIGURE 4.1

(1) Rigid body motions due to air blast on the exposed structure.

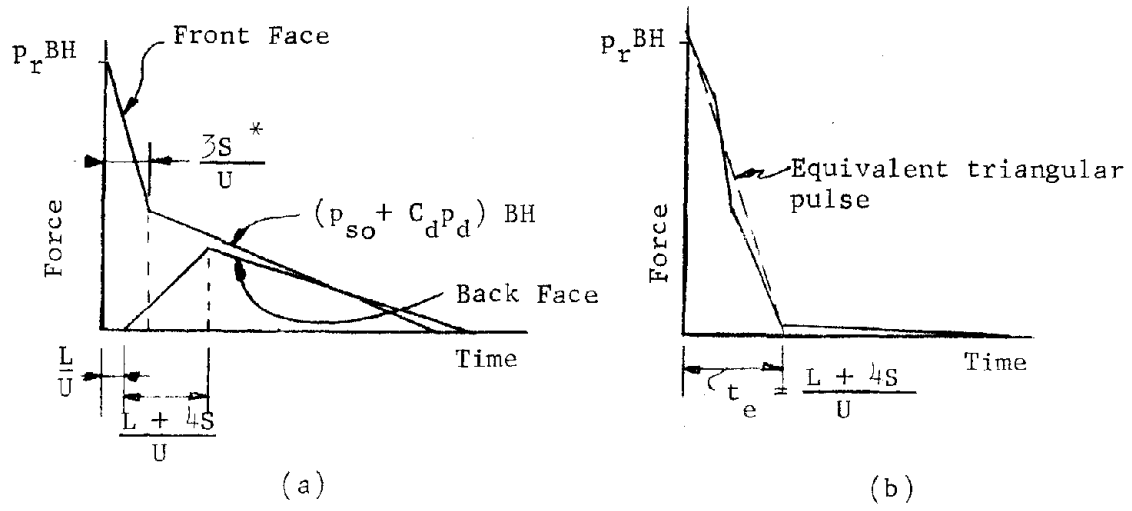
(a) Horizontal. The idealized time history of the net horizontal force on the structure is shown in Figure 4.2. In Figure 4.2a the front and back face load is shown, and Figure 4.2b shows the net time history load and an equivalent triangular load with duration,  $t_e$ . The maximum acceleration of the structure acting as a rigid body will occur during the initial response and is given by the expression:

$$a'_h = (P_{\max} - R_i) / m \quad (4.1)$$

The prime in the symbol  $a'_h$  refers to the peak rigid body sliding motion.

Here,

- $P_{\max}$  = maximum net horizontal force  $p_r \times B \times H$   
 $R_i$  = initial resistance to horizontal sliding motion  
 =  $W C_f$  where  $W$  = weight of structure  
 $C_f$  = coeff. of friction between footing slab and soil.



where

- L = Length of structure parallel to moving shock front (feet)
- U = Shock front velocity (fps)
- S = Clearing height, taken as the full height of the front face (H) or half of its length (B) whichever is smaller.
- B = Length of structure normal to moving shock front (feet)
- $p_r$  = Peak reflected pressure (psi)
- $p_{so}$  = Overpressure (psi)
- $p_d$  = Dynamic pressure (psi)
- $C_d$  = Drag coefficient (dimensionless).

FIGURE 4.2

\*The clearing time,  $3S/U$ , is based on recommendations in "Effects of Nuclear Weapons". The OCE Manual 413 (Reference 4.19) defines the clearing time as  $3S/c_{refl}$ , where  $c_{refl}$  is the velocity of sound in the reflected region. The velocity  $c_{refl}$  is defined analytically in OCE 413 and is significantly less than  $U$  at all overpressure levels. The value of  $3S/U$  is used in this report to illustrate a procedure, realizing the clearing time may be questionable.

The resistance,  $R$ , increases at later times when the overpressure acts on the roof.\*

A maximum value,

$$R_{\max} = (W + p_{so} BL) C_f \quad (4.2)$$

is attained at time  $L/U$ , where  $L$  = length of the structure,  $B$  is the width, and  $U$  = shock front velocity in free-air,

The peak velocity and displacement of the structure can be obtained by graphical integration (called the beam analogy in Reference 4.10). The method is represented in Figure 4.3, in which, on an acceleration-time coordinate system, the accelerating effect of the applied force and the decelerating effect of the resistance to motion at the structure foundation are plotted.

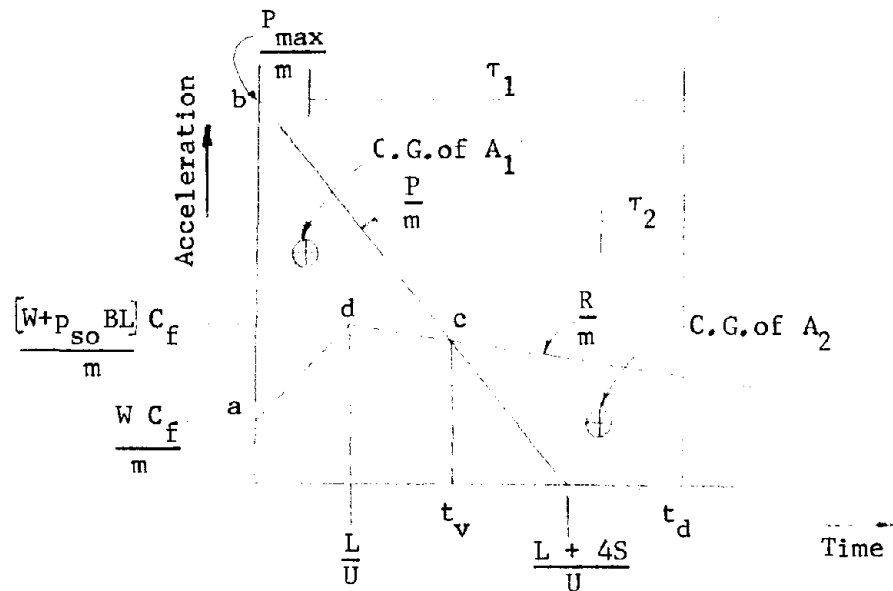


FIGURE 4.3: ACCELERATION VS. TIME

\*The overpressure is a transient pressure pulse across the structure as described in Reference 4.19. This study considers the overpressure acting as a uniform pressure on the roof slab as a function of time. The transient pulse across the structure introduces secondary rotation effects, which are small compared to motions of the structure due to the uniform pressure pulses assumed. These may be included by using the methods of Reference 4.10.

It is seen from the figure that the maximum velocity,  $v'_h$ , occurs at time,  $t'_v$ , and is equal to the area abcd,  $A_1$ , in the plot of acceleration vs. time. The maximum horizontal displacement,  $d'_h$ , occurs at time,  $t'_d$ . Time,  $t'_d$ , is found by equating the area cefg,  $A_2$ , to area abcd,  $A_1$ . The expression for maximum horizontal displacement can then be written simply as:

$$d'_h = A_1 \tau_1 - A_2 \tau_2 \quad (4.3)$$

The rigid body rotation of the structure, due to the net horizontal loading, influences the translation motion of the structure to some degree. This is more significant for a taller structure; and the modified equations are given in Sub-section 4.2.3 for the two-story structure. For structures with small height to length ratios, i.e.,  $H/L < 0.5$ , the rigid body rotation effect on the horizontal and vertical motions is small compared to the rigid body sliding motion.

(b) Vertical. The vertical rigid body motion due to the slap of the air blast on the housing will depend on the soil stiffness. If the soil mobilizes resistance as fast as the load is applied, there will be negligible initial acceleration of the structure. Since the air blast is also loading the adjacent ground surface, the vertical displacement of the structure is essentially the same as the ground displacement at the surface. To determine the initial peak acceleration and velocity, the structure can be represented as a rigid body on a group of springs with the stiffness characteristics of the soil (see Figure 4.4).

Empirical relationships are available for spring rates applying to various types of soils (see Reference 4.11). For most top soils the  $k_s$  value will range from 50 to 300 psi per inch deflection. The frequency is given by:

$$f = \frac{1}{2 \pi} \sqrt{\frac{K}{m_{\text{structure}}}} \quad \text{cps} \quad (4.4)$$

In which:

$$K = k_s BL$$



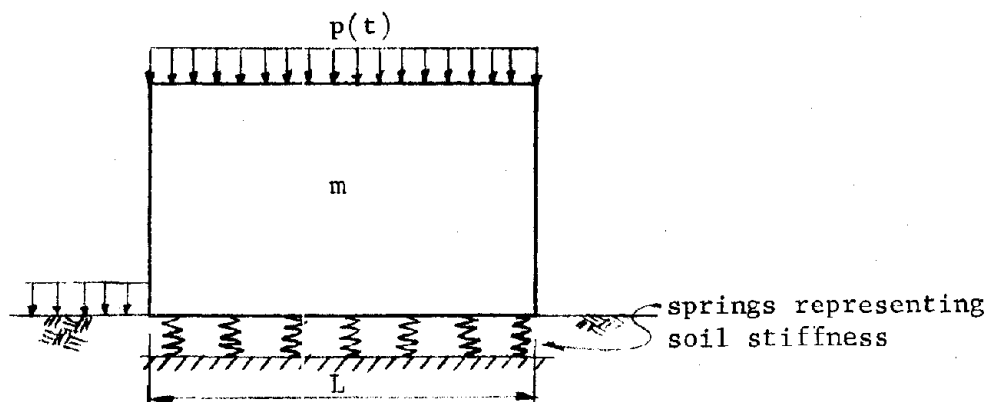


FIGURE 4.4

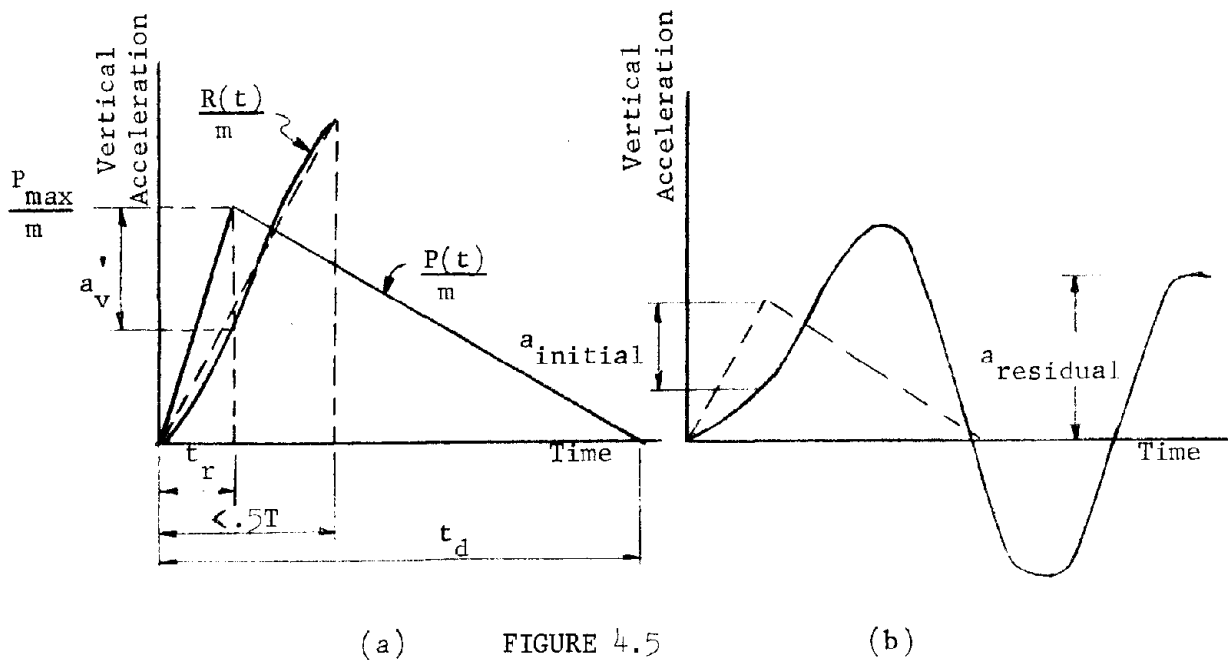
The vertical loading on the roof of the structure may be idealized to a uniform pressure, for the purpose of determining rigid body motions. This pressure varies with time, having a rise time,  $t_r$ , equal to the transit time of the shock front across the width or length of the structure. Thus,

$$t_r = \frac{L}{U} ; L = \text{length of structure}$$

$U = \text{shock front velocity.}$

The initial response of the structure can be estimated from the acceleration-time history as shown in Figure 4.5a. In the acceleration-time coordinate system, the applied load divided by the mass of the structure is readily obtained from the air blast characteristics and the transit time. A triangular equivalent acceleration load has been used in the example of Figure 4.5a.  $\frac{R(t)}{m}$ , the acceleration resistance curve, may be approximated by assuming elastic behavior, i.e., assume the time to reach maximum response is equal to one half the natural period,  $T/2$ ; the peak acceleration amplitude,  $R_{\max}/m$ , is equal to  $2 P_{\max}/m$ ; and the shape of the curve is a sine function. The maximum initial acceleration,  $a'_v$ , can then be determined from the figure. As a conservative assumption, the response in the time period,  $t_r$ , may be neglected, giving:

$$a'_v = \frac{P_{\max}}{m} \quad \text{where } P_{\max} = BLp_{so} \quad (4.5)$$



It is noted here that, if the pulse duration,  $t_d$ , is short compared to the period,  $T$ , ( $t_d \leq T$ ) and if the response is purely elastic with negligible damping in the system, the maximum acceleration at a later time can be as high as twice the peak initial acceleration (see Figure 4.5b). In a real situation, however, damping will usually reduce the residual maximum acceleration to less than the initial maximum acceleration. For large weapon yields, the time duration,  $t_d$ , in most cases will be much greater than the period,  $T$ , and, therefore, the response will approach that of a rectangular step pulse. For this pulse, the peak velocity can be related to  $a_v'$  by the fundamental circular frequency  $\omega$ :

$$v_v' = \frac{a_v'}{\omega} \quad (4.6)$$

(2) Deformational motions due to impact of air blast.

Walls. The air blast induces bending of each element of walls, roof slab and bottom slab. Figure 4.6 shows the idealized pressure-time history on the front wall. It should be assumed that the blast may come from any direction, and that any one of the 4 walls may be exposed to the reflected pressure. The resistance curve is also shown as a linear rise

to the yield resistance; this approximation is acceptable for fast systems.

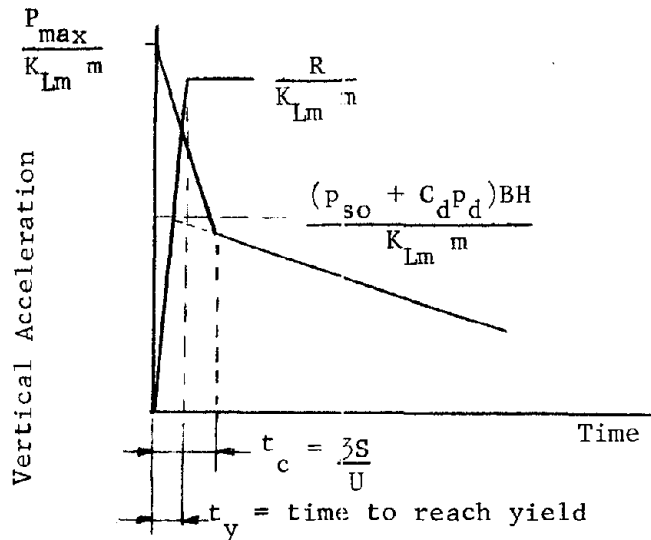


FIGURE 4.6

Figure 4.6 shows an instantaneous rise time for the peak pressure that is considered to be reasonably accurate for pressures less than 25 psi and greater than 200 psi. For intermediate pressure regions, a finite rise time may have to be assumed (see Reference 4.12). For the case with an instantaneous rise, the maximum horizontal acceleration is:

$$a''_h = \frac{P_{\max}}{K_{Lm} m} ; (R = 0) \quad (4.7)$$

where

- $P_{\max}$  =  $BHp_r$
- $P_r$  = max. reflected pressure
- $m$  = mass of the wall
- $K_{Lm}$  = load-mass factor  $\approx 3/4$  for a one-way slab

The double prime in the symbols refer to peak deformational motions. The maximum response elastic displacement and response (pseudo) velocity are related to the maximum acceleration by the common harmonic relationships:

$$d''_{\text{elastic}} = \frac{a''}{\omega^2} \quad (4.8)$$

$$v''_{\text{max}} = \frac{a''}{\omega} \quad (4.9)$$

The graphical method previously described can be used to determine peak velocity and displacement (as an alternate method).

If the wall element yields under the air blast pressure, the ductility factor,  $\mu$ , is determined from available response charts for triangular pulses applied to single-degree-of-freedom systems (References 4.10 and 4.13), and then the maximum response displacement is computed from

$$d''_{\text{max}} = \mu d''_y \quad (4.10)$$

where  $d_y$  = the yield deflection, as calculated from the properties of the slab element.

Roof Slab. As previously noted, the shock front travels across the structure in a time,  $t_r$ , equal to the length of the structure divided by the shock front velocity, and the idealized pressure-time history on the roof can be assumed to be a uniform distributed pressure rising to the peak overpressure value in time,  $t_r$  (see Figure 4.5). However, the roof slab's dynamic response as well as its design is generally based on an instantaneous pressure rise as a conservative assumption. The inertia response of the roof slab (peak response acceleration, velocity, and displacement) may be determined by the method already described for the wall element.  $P_{\text{max}}$  is now taken as a function of the overpressure and not of the reflected pressure.

Bottom Slab. The bottom slab of a monolithic concrete structure has a response similar to that of the roof slab. The overpressure applied to the roof slab is resisted by the supporting walls, which in turn load the bottom slab as the impulse is transferred to the soil. The loading-time history on the bottom slab will be a relatively slowly applied load, due to

the finite time of the loading and roof deformation process; but for design, the soil loading-time history on the bottom slab is assumed to be the same as the idealized loading on the roof slab. This assumption results in a response of the bottom slab equal to the roof slab for equal masses and stiffnesses.

(3) Rigid body motions due to air blast on surrounding soil.

(a) Foundation slab is monolithic with superstructure (see Figure 4.7).

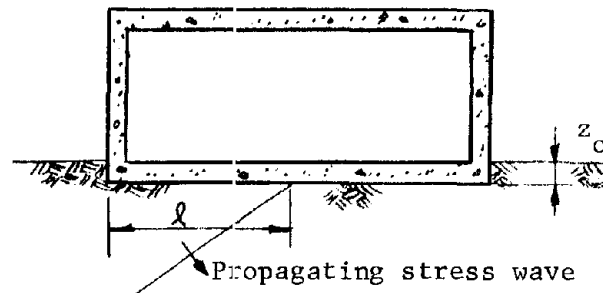


FIGURE 4.7

If the foundation slab is buried to a depth,  $z_0$ , it replaces an equivalent soil mass with a relatively rigid mass. The structure will then have essentially the same displacement and velocity as the ground, i.e.,

$$\begin{aligned}
 d_v''' &= d_{v(\text{ground})} & \text{at depth } z_0 \\
 d_h''' &= d_{h(\text{ground})} \\
 v_v''' &= v_{v(\text{ground})} \\
 v_h''' &= v_{h(\text{ground})}
 \end{aligned}
 \tag{4.11}$$

The triple prime in the symbols refer to the ground induced motions. Under subseismic conditions, the initial acceleration (horizontal and vertical) due to the air blast on the structure may be additive, with the air blast induced outrunning ground acceleration. The acceleration caused by the shock wave impinging directly on the structure will often predominate. In the special cases (for layered soil characteristics) where outrunning conditions may occur in phase with the direct air blast effect, a pulse type

analysis may be warranted (see Appendix F).

(b) Floor slab separated from superstructure. In structures where the floor slab is separated from the main structure (see Figure 4.1b), the acceleration motion of the floor slab will be significantly reduced, due to the shielding from the direct air blast. The only motion that will influence the slab is that of the surrounding soil. In this case, the peak displacement and velocity can be taken as equal to the ground displacement and velocity. The peak acceleration of the slab will, however, be significantly less than the surface ground acceleration, since the acceleration attenuates very rapidly even at small depths below the ground surface. For example, the peak ground acceleration at 10 foot depth will decrease to 25 percent of the surface peak acceleration by the equations given in Section 3. The attenuation of acceleration with depth is based on the rise time of the stress wave increasing with depth; it is often assumed equal to one-half the vertical transit time  $z/2c$ .

In order to obtain a reasonable estimate of the rise time of the stress wave across the soil below the foundation, a similar assumption may be made by equating the rise time to one-half the length of the foundation slab divided by the peak stress effective seismic velocity of the soil (see Figure 4.7).

$$t_r = \frac{\lambda}{2 c_p}$$

where  $\lambda$  = length (L) or width (B) of the structure in feet. Using the same assumptions in deriving Equation (3.18) for peak acceleration from the peak velocity Equation (3.21), namely,  $a = 2 v_p / t_r$ , the acceleration of the slab can be estimated, using the rise time given above:

$$a_v''' = a_h''' = 5 p_{so} / \lambda \quad (4.12)$$

where  $a_v$  and  $a_h$  are the peak horizontal and vertical accelerations of the slab.

#### Example 4.1

Assume that a 25 psi overpressure blast wave from a 20 MT burst acts on the one story reinforced concrete box structure shown in Figure 4.8.

Example 4.1 (continued)

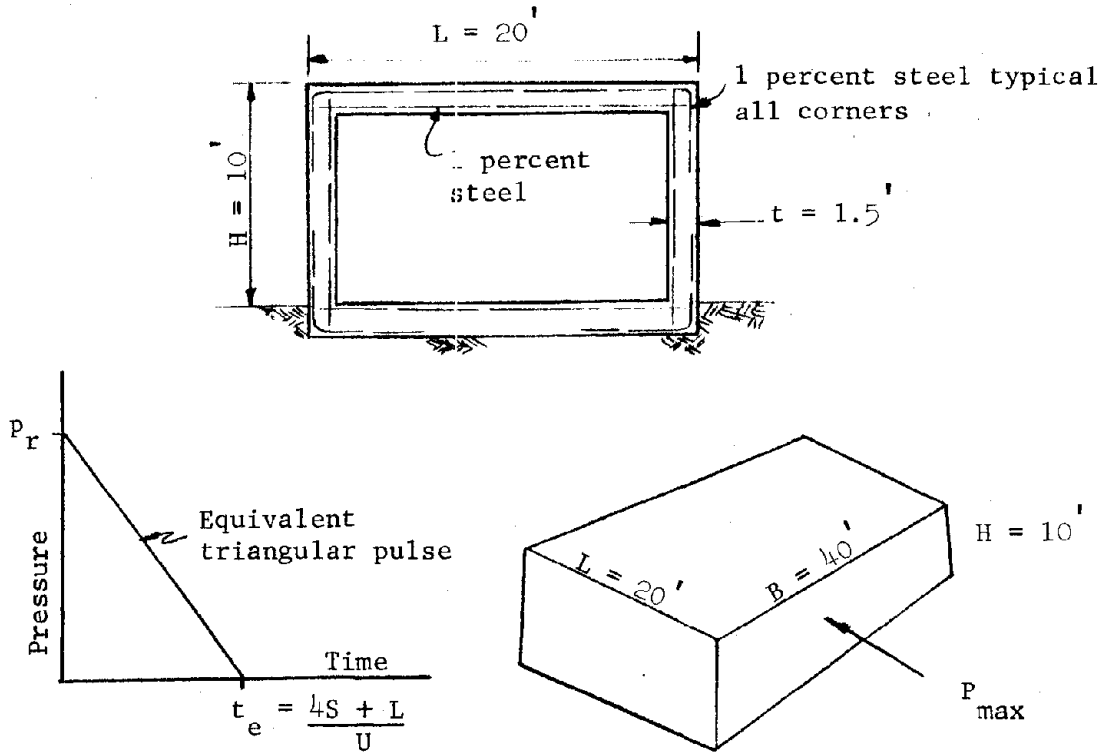


FIGURE 4.8

It is desired to find the motions of the walls as well as of the roof and floor slabs. Case (a) assumes that the roof and floor slab are similarly deformed (floor slab monolithic with superstructure); Case (b) assumes that the floor slab is independent of the superstructure (a thin floor slab is separated from the wall footings). The rigid body rotational motion is assumed to be negligible.

The necessary blast wave constants are

$$p_{so} = 25 \text{ psi}$$

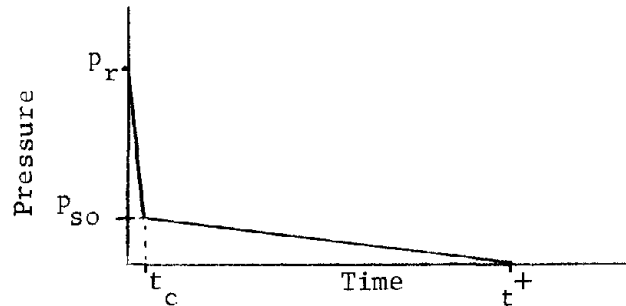
$$D_p^+ = \text{Positive duration of overpressure} = 3.3 \text{ sec}^*$$

\*From Brode, Reference 3.1

Example 4.1 (continued)

$$\begin{aligned}
 t^+ &= \text{Duration of effective triangular overpressure distribution} &= 2.0 \text{ sec} \\
 p_r &= \text{Reflected pressure} = 3.3 \times 25 &= 82.5 \text{ psi} \\
 U &= \text{Shock front velocity} &= 1800 \text{ fps} \\
 t_c &= \text{Clearing time of reflected pressure} = \frac{3S}{U} = \frac{3 \times 10}{1800} &= .017 \text{ sec}
 \end{aligned}$$

The average pressure vs time curve for the front face of the structure is shown below



Dimensional factors for the structure are given in Figure 4.8. The weight of the structure is

$$W = 5.78 \times 10^5 \text{ lbs} = m g$$

and the assumed coefficient of friction (concrete to soil) is

$$C_f = 0.5$$

The duration of the net horizontal triangular load ( $t_e$ ) is

$$t_e = (4H + L)/U = 0.033 \text{ sec}$$

The blast front transit time across the structure is

$$t_r = \frac{L}{U} = .011 \text{ sec}$$

The motion of the structure is made up of three parts

- (1) rigid body motion, denoted by one prime ( $a'$ ,  $v'$ ,  $d'$ )
- (2) deformational motion, denoted by two primes ( $a''$ ,  $v''$ ,  $d''$ )
- (3) ground motion, denoted by three primes ( $a'''$ ,  $v'''$ ,  $d'''$ )



Example 4.1 (continued)

The horizontal and vertical motions are distinguished by using subscripts, h and v.

Case a. Floor slab monolithic with superstructure. Peak structure motions in the horizontal direction will first be computed.

(1) Rigid body horizontal motion. Horizontal forces acting on structure are

$$P_{\max} = 144 p_r B H = 4.75 \times 10^6 \text{ lbs}$$

$$R_i = W C_f = 2.89 \times 10^5 \text{ lbs}$$

$$R_{\max} = (W + 144 p_{so} B L) C_f = 1.73 \times 10^6 \text{ lbs.}, \text{ for } t > t_i$$

Accordingly,

$$P_{\max}/m = \frac{4.75 \times 10^6}{5.78 \times 10^5} g = 8.22 g$$

$$R_i/m = \frac{2.89 \times 10^5}{5.78 \times 10^5} g = 0.50 g$$

$$R_{\max}/m = \frac{1.73 \times 10^6}{5.78 \times 10^5} g = 3.00 g$$

The peak horizontal acceleration is therefore

$$a_h^* = (8.22 - 0.5) g = 7.72 g$$

Figure 4.9 shows the corresponding acceleration diagram in which  $t_v$  is found by simple proportion to be 0.0212 sec. The four indicated areas (dimensions in g x sec) must obey the relation

$$A_1 + A_2 = A_3 + A_4$$

Making use of this fact, it is found that the values of the areas and the time locations of their centroids are:

$$A_1 = 0.0553 \text{ g x sec, and } t_1 = 0.0071 \text{ sec}$$

$$A_2 = 0.0139 \quad t_2 = 0.0037$$

$$A_3 = 0.0182 \quad t_3 = 0.0293$$

$$A_4 = 0.0510 \quad t_4 = 0.0418$$

Example 4.1 (continued)

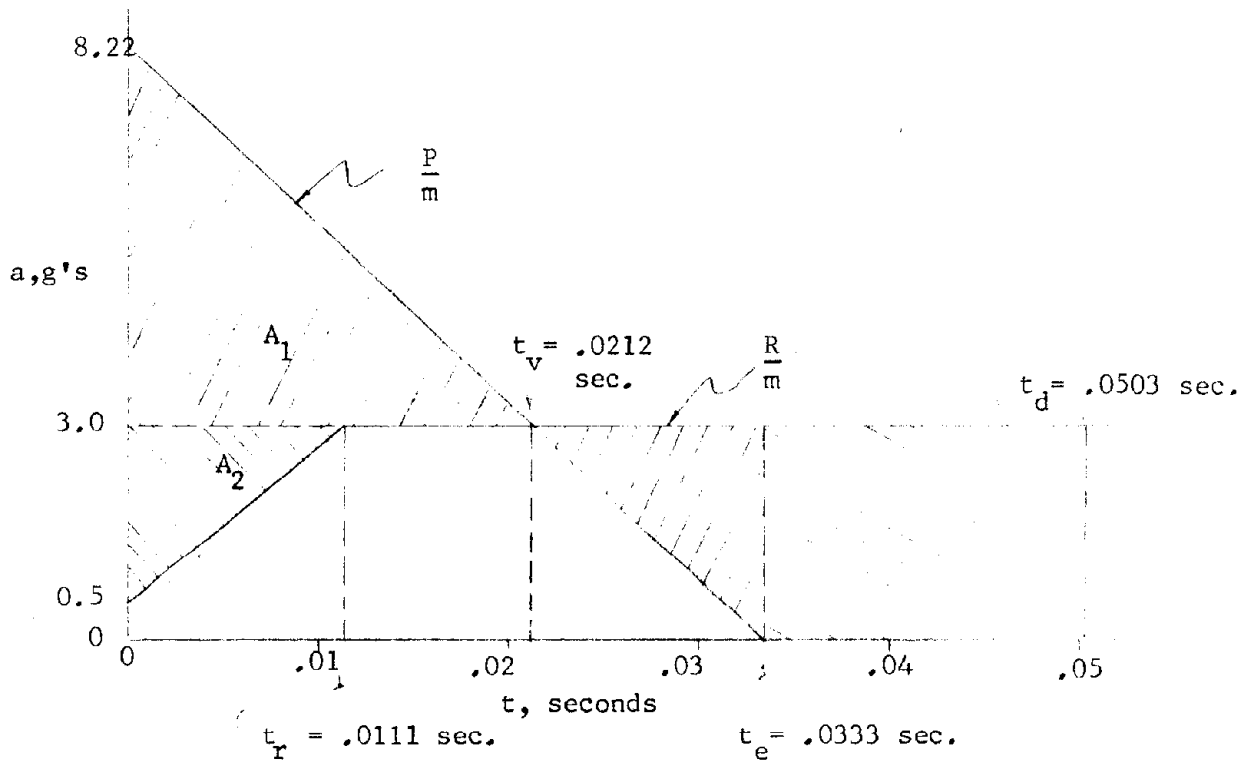


FIGURE 4.9

The peak horizontal velocity is then,

$$v'_h = A_1 + A_2 = 0.0692 \text{ g} \times \text{sec} = 26.7 \text{ in/sec}$$

The sum of the moments of all four areas about the time,  $t_d$ , Equation (4.3), will give the maximum horizontal displacement for rigid body motion, thus,

$$A_1 \tau_1 = 0.0553 \times 0.0432 = 23.90 \times 10^{-4}$$

$$A_2 \tau_2 = 0.0139 \times 0.0466 = 6.48 \times 10^{-4}$$

$$A_3 \tau_3 = 0.0182 \times 0.0210 = 3.82 \times 10^{-4}$$

$$A_4 \tau_4 = 0.0510 \times 0.0085 = 4.34 \times 10^{-4}$$

$$d'_h = A_1 \tau_1 + A_2 \tau_2 - A_3 \tau_3 - A_4 \tau_4 = 22.3 \times 10^{-4} \text{ g sec}^2$$

$$= \underline{0.86 \text{ inches}}$$

Example 4.1 (continued)

(2) Deformational horizontal motion. The deformational motions of the wall located normal to the direction of blast, with dimensions  $B = 40'$  and  $H = 10'$ , will be considered. The weight of the wall is  $9 \times 10^4$  lbs. If an equivalent load mass factor of  $3/4$  is used the wall's equivalent load mass will be

$$K_{Lm} = 6.75 \times 10^4 / g$$

Consequently,

$$a''_h = P_{\max} / K_{Lm} = \frac{4.75 \times 10^6}{6.75 \times 10^4} g = 70 g$$

The wall's resistance to horizontal normal forces will be based on the assumptions that

- a) The pressure is uniformly distributed
- b) The wall is a one-way slab spanning between roof slab and bottom slab with equal fixity at each support
- c) The fundamental period of transverse vibration of the wall is obtainable

The resistance force  $R$  is calculated from Equation (B-5) of Appendix

B.

$$R = .075 (\phi + \phi_s) f_y \times B \times d^2 / H$$

in which

$$\begin{aligned} \phi &= \phi_s &= 1 \text{ percent} \\ f_y &= 5.2 \times 10^4 \text{ psi} \\ B &= 40 \text{ ft} \\ d_{\text{effective}} &= 1.33 \text{ ft} \\ H &= 10 \text{ ft} \end{aligned}$$

Accordingly,

$$R = 8 \times 10^6 \text{ pounds}$$

The natural period of the wall,  $T$ , is based on equal moment capacity at the center and at the edges, Equation (B-16) Appendix B, and is given by:

$$T = \frac{1}{7200} \left( \frac{H}{d} \right) \frac{H}{\sqrt{\phi}} = 0.01 \text{ sec}$$

Example 4.1 (continued)

$$\omega = 2\pi/T = 628 \text{ rad/sec}$$

By means of the response chart of Reference 4.10 and the polygonal loading-time curve method outlined in Reference 4.12, the ductility ratio,  $\mu$ , can be found in terms of the front face loading parameters

$$\frac{t_c}{T} = \frac{.017}{.01} = 1.7$$

$$\frac{P_R - P_{SO}}{R} = \frac{57.5 \times 144 \times 40 \times 10}{8 \times 10^6} = .415$$

$$\frac{t^+ - t_c}{T} = \frac{1.83}{.01} = 183$$

$$\frac{P_{SO}}{R} = \frac{25 \times 144 \times 40 \times 10}{8 \times 10^6} = .18$$

The value of  $\mu$  is found from the chart to be 1.2.

The yield deflection of the wall is expressed by (defined in Appendix B)

$$d_{\text{yield}} = \frac{1}{7600} \frac{H^2}{d} = 0.10 \text{ inches}$$

Therefore

$$d_h'' = \mu d_{\text{yield}} = 0.12 \text{ inches}$$

Moreover, the wall's horizontal pseudo-velocity is

$$v_h'' = \frac{a_h''}{\omega} = \frac{70 g}{628} = 43 \text{ in/sec}$$

(3) Ground motion in horizontal direction. To calculate the horizontal ground motions, it is first necessary to calculate the vertical ground motions. From Section 3 Equations (3.19), (3.21), and (3.22) for the vertical ground motions read

$$a_{vz} = 5 \times 10^{-3} p_{SO} z^{-1} \alpha_z \text{ in g's}$$

$$v_{vz} = 0.5 p_{SO} c^{-1} \alpha_z \text{ in inches/sec}$$

Example 4.1 (continued)

$$d_{vse} = 0.9 p_{so}^{1/2} c^{-1} W^{1/3} \quad \text{in inches}$$

(The residual displacement is assumed to be negligible.)

If the seismic velocity,  $c$ , in kft/sec and the attenuation factor,  $\alpha_z$ , are taken as unity, the above expressions, for  $p_{so} = 25$  psi and for a depth of  $z = 0.005$  kft., will give

$$a_v = 25 \text{ g} \quad ; \quad v_v = 12.5 \text{ in/sec} \quad ; \quad d_v = 12.2 \text{ inches}$$

Assuming that definite relationship exists between vertical and horizontal motions and that it is,

$$a_h = a_v \quad ; \quad v_h = 2 v_v / 3 \quad ; \quad d_h = d_v / 3$$

the peak horizontal ground motions are,

$$a_h = 25 \text{ g} \quad ; \quad v_h = 8.3 \text{ in/sec} \quad ; \quad d_h = 4.1 \text{ inch}$$

The air blast loading on the structure accounts for the maximum rigid body acceleration of the structure except in an outrunning condition. The outrunning condition is neglected in this example. The ground induced peak velocity and displacement are assumed to be the same as the ground motions, Equation (4.11). Accordingly,

$$a'''' = 0$$

$$v_h'''' = 8.3 \text{ in/sec, and}$$

$$d_h'''' = 4.1 \text{ inch}$$

Resultants of the peak horizontal motions are given in the summary tables at the end of this example.

Vertical Motions: The peak motions in the vertical direction will now be calculated.

(1) Rigid body vertical motion. In order to compute the initial acceleration and velocity, assume the vertical stiffness,  $k$ , of the subgrade,

$$k = 100 \text{ lbs/in}^3$$

The calculated vertical ground displacement accounts for the total vertical displacement.

Example 4.1 (continued)

Then the total foundation stiffness,  $K$ , is given by,

$$K = 144 k B L = 11.5 \times 10^6 \text{ lb/in}$$

The up and down fundamental circular frequency,  $\omega_v$ , of the structure on the ground is approximately,

$$\omega_v = \sqrt{\frac{K g}{W}} = \sqrt{\frac{11.5 \times 10^6}{5.78 \times 10^5}} g = 87.7 \text{ rad/sec}$$

This neglects an effective mass of soil.

The maximum downward blast load on the roof of the structure is

$$P_{\max} = 144 p_{so} B L = 2.88 \times 10^6 \text{ lbs}$$

Therefore, a peak downward acceleration of,

$$a'_v = \frac{P_{\max}}{m} = \frac{2.88 \times 10^6}{5.78 \times 10^5} = 5.0 \text{ g}$$

will result.

The peak pseudo-velocity is

$$v'_v = \frac{a'_v}{\omega} = 22 \text{ in/sec}$$

(2) Roof deformations. The resistance force,  $R$ , of the roof slab is calculated by Equation (B-5) Appendix B, assuming the roof slab to be a one-way slab with equal fixity at the wall supports.

$$R = 4 \times 10^6 \text{ lbs}$$

The natural period,  $T$ , of the roof is calculated by Equation (B-16) Appendix B.

$$T = 0.0416 \text{ sec}$$

Therefore,

$$\omega = 2\pi/T = 151 \text{ rad/sec}$$

Consequently the two parameters needed for use in the response chart Reference 4.10, are

$$\frac{t^+}{T} = \frac{2.0}{0.0416} = 48 \quad ; \quad \text{and} \quad \frac{P_{\max}}{R} = \frac{2.88 \times 10^6}{4 \times 10^6} = 0.72$$

Example 4.1 (continued)

For these values the chart gives  $\mu = 1.8$ .

The yield deflection,  $d_{\text{yield}}$ , is calculated (equation to be defined in Appendix B).

$$d_y = 0.472 \text{ inches}$$

Therefore,

$$d_v'' = \mu d_{\text{yield}} = 0.85 \text{ inches}$$

Since, the equivalent mass,  $K_{Lm}$ , of the roof is

$$3/4 W/g = 1.35 \times 10^5 \text{ lbs/g}$$

the roof's initial acceleration will be

$$a_v'' = \frac{P_{\text{max}}}{K_{Lm}} = \frac{2.88 \times 10^6}{1.35 \times 10^5} \text{ g} = 21.3 \text{ g},$$

and the roof's peak pseudo-velocity is, therefore,

$$v_v'' = \frac{a_v''}{\omega} = \frac{21.3 \text{ g}}{151} = 54.5 \text{ in/sec.}$$

It is usually assumed that, when the floor slab is monolithic with the superstructure, its deformation motions are similar to those of the roof slab.

(3) Ground motions in the vertical direction have already been obtained when the horizontal ground motions were calculated. The structure induced motions are

$$a_v''' = 0 \quad ; \quad v_v''' = 12.5 \text{ in/sec} \quad ; \quad d_v''' = 12.2 \text{ inches}$$

If an outrunning condition is considered, the ground induced acceleration is considered in combination with the air slap on the structure.

Resultants of the vertical motions are shown in the summary tables at the end of this example.

Case b. Floor slab separated from superstructure (Figure 4.1b). The superstructure is treated in the same manner as Case (a), except that the mass of the floor slab is not included in the calculations. Moreover, the size of the footings determine the  $K$  of the rigid body vertical motions. The peak values will be slightly different in this case, as the summary table

Example 4.1 (continued)

indicates. The floor itself is subject only to motions due to the effect of the ground motion, and the following results are obtained:

$$a_h'''' = a_z'''' = a_{\text{ground}}$$

at an equivalent travel length of  $\ell = B/2$  or  $L/2$  whichever is smaller

$$L = 20 \text{ ft. (} B = 40 \text{ ft.} > L)$$

Therefore,

$$\ell = 10 \text{ ft.}$$

and from Equation (4.12)

$$a_h'''' = a_z'''' = p_{\text{so}}/\ell = 12.5 \text{ g}$$

Velocities and displacements are obtained as before.

Results of Example 4.1. Summary of results for the rectangular structure considered in Example 4.1 are shown in Tables 4.1, 4.2 and 4.3 and plotted in Figures 4.10, 4.11 and 4.12.

The shock spectra from the peak values of acceleration, velocity and displacement are obtained from the following relationships:

$$D = d_{\text{max}}$$

$$V = 1.5 v_{\text{max}}$$

$$A = 2.0 a_{\text{max}}$$

The peak response values are summarized in Table 4.3, and the shock spectra are plotted in Figures 4.10, 4.11, and 4.12.



Example 4.1 (continued)

TABLE 4.1: INDIVIDUAL COMPONENTS

<u>Vertical</u>	Item	Acceleration (g)			Velocity (in/sec)			Displacement (in)		
		a'	a''	a'''	v'	v''	v'''	d'	d''	d'''
Case a Floor slab monolithic with super- structure	Roof	5	21.3	0	22	4.53	12.5	0.85	12.2	
	Wall	5	0	0	22	0	12.5	0	12.2	
	Base	5	21.3	0	22	54.5	12.5	0.85	12.2	
Case b Floor slab separated from super- structure	Roof	6.8	21.3	0	29.5	54.5	12.5	0.33	0.85	12.2
	Wall	6.8	0	0	29.5	0	12.5	0.33	0	12.2
	Floor	0	0	12.5	0	0	12.5	0	0	12.2

<u>Horizontal</u>	Item	Acceleration (g)			Velocity (in/sec)			Displacement (in)		
		a'	a''	a'''	v'	v''	v'''	d'	d''	d'''
Case a Floor slab monolithic with super- structure	Roof	7.7	0	0	27.0	0	8.3	0.86	0	4.1
	Wall	7.7	70	0	27.0	43.0	8.3	0.86	0.12	4.1
	Base	7.7	0	0	27.0	0	8.3	0.86	0	4.1
Case b Floor slab separated from super- structure	Roof	10.7	0	0	36.0	0	8.3	1.27	0	4.1
	Wall	10.7	70.3	0	36.0	45.0	8.3	1.27	0.14	4.1
	Floor	0	0	12.5	0	0	8.3	0	0	4.1

Example 4.1 (continued)

TABLE 4.2\*: ROOT-MEAN SQUARE RESULTS

Vertical	Item	Acceleration (g) $a_{max}$	Velocity (in/sec) $v_{max}$	Displacement (in) $d_{max}$
Case a	Roof	22	60	12
	Wall	5	24	12
	Base	22	60	12
Case b	Roof	23	62	12
	Wall	7	36	12
	Floor	13	12	12

Horizontal	Item	Acceleration (g) $a_{max}$	Velocity (in/sec) $v_{max}$	Displacement (in) $d_{max}$
Case a	Roof	8	24	4
	Wall	71	48	4
	Base	8	24	4
Case b	Roof	11	36	4
	Wall	71	60	4
	Floor	13	8	4

\*The values are rounded off to the nearest whole number

Example 4.1 (continued)

TABLE 4.3: PEAK RESPONSE PARAMETERS

Vertical	Item	A (g)	V (in/sec)	D (in)
Case a	Roof	44	90	12
	Wall	10	36	12
	Base	44	90	12
Case b	Roof	46	93	12
	Wall	14	54	12
	Floor	26	18	12

Horizontal	Item	A (g)	V (in/sec)	D (in)
Case a	Roof	16	36	4
	Wall	142	72	4
	Base	16	36	4
Case b	Roof	22	54	4
	Wall	142	90	4
	Floor	26	12	4

Example 4.1 (continued)

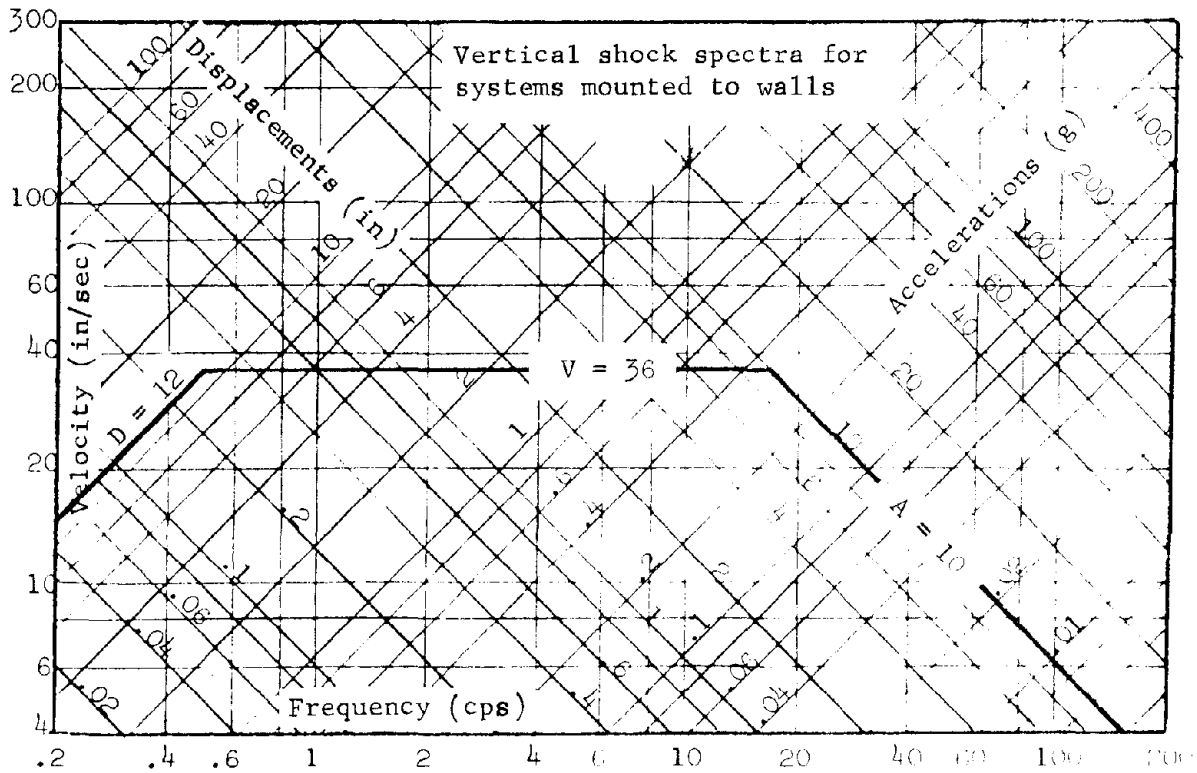
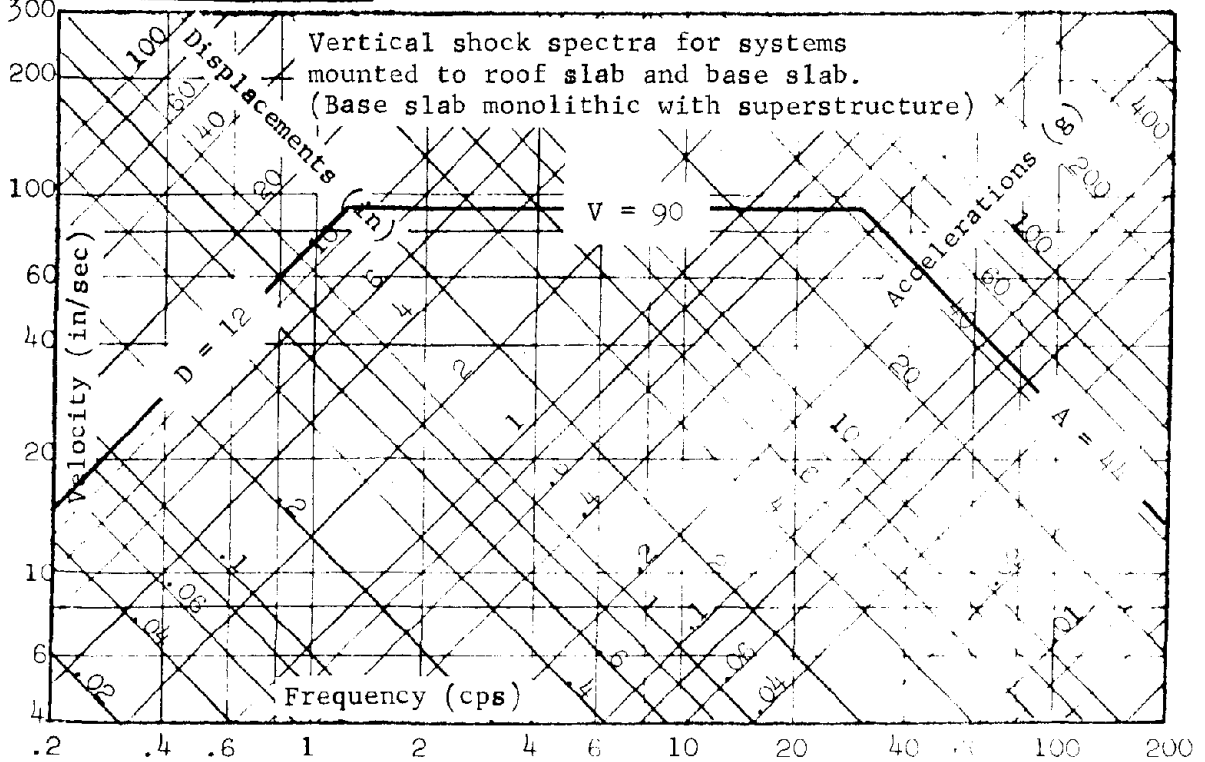


FIGURE 4.10

Example 4.1 (continued)

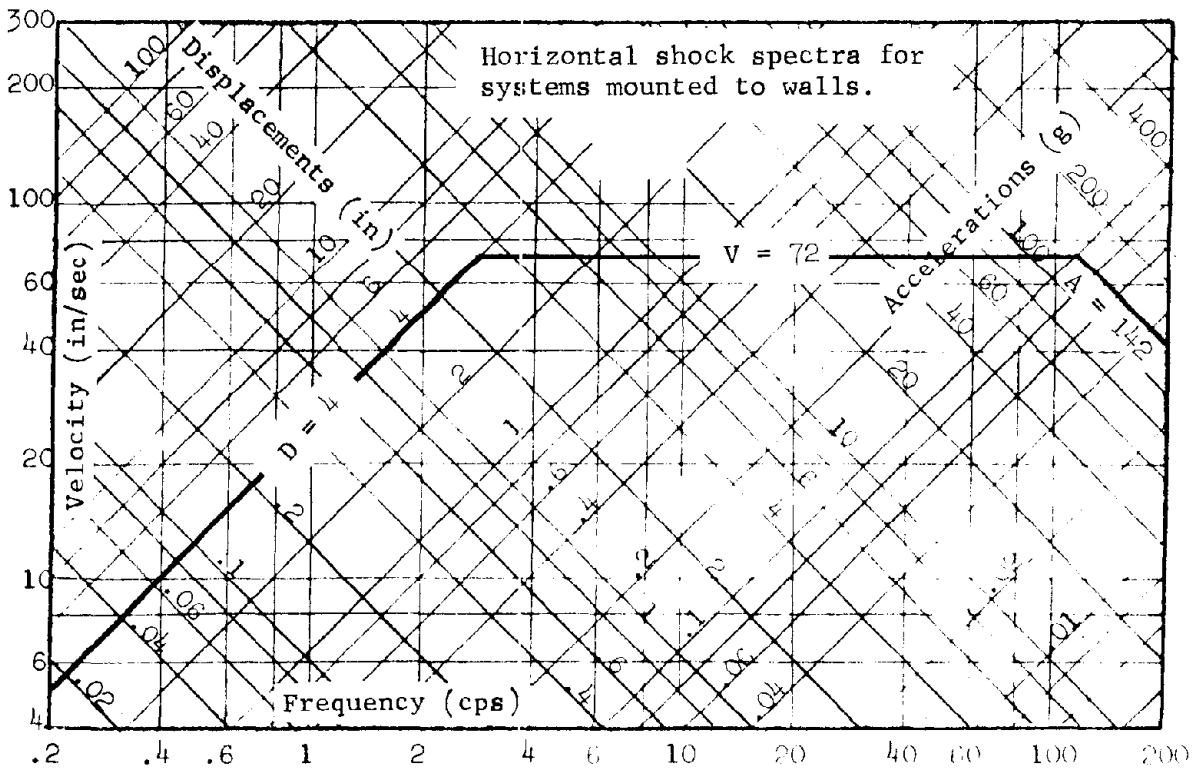
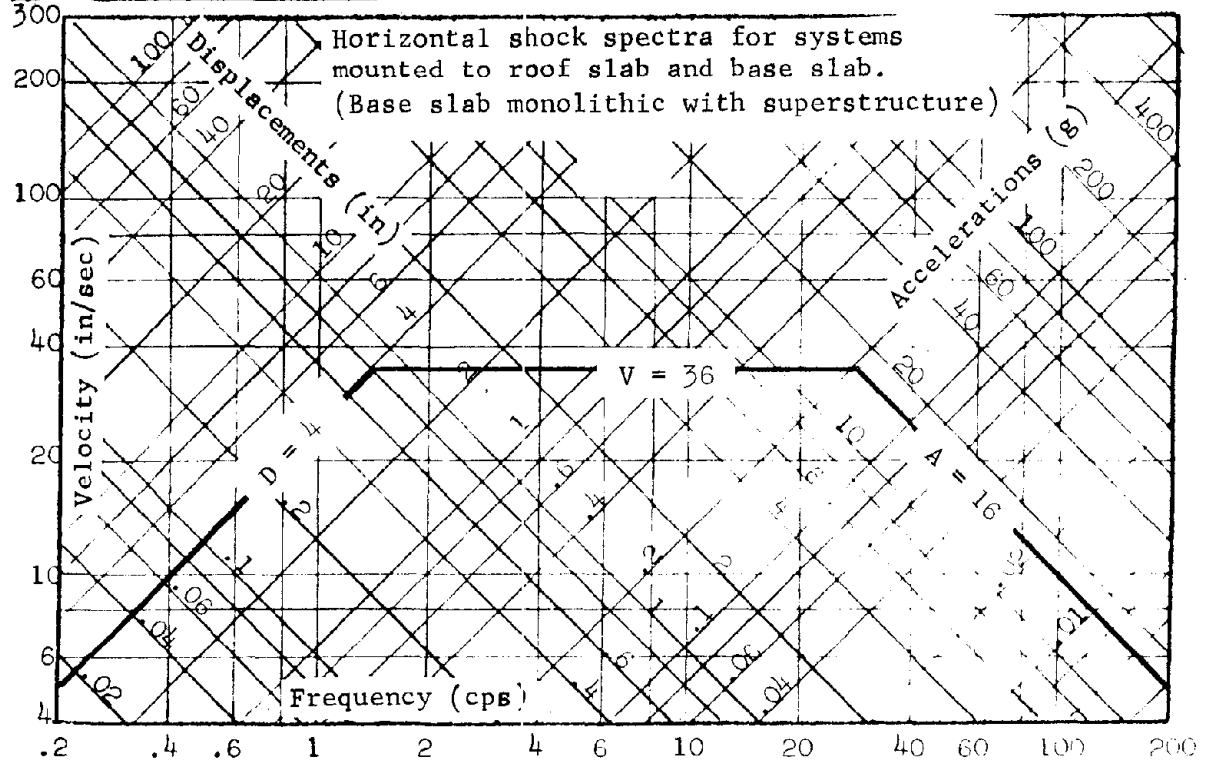


FIGURE 4.11

Example 4.11 (continued)

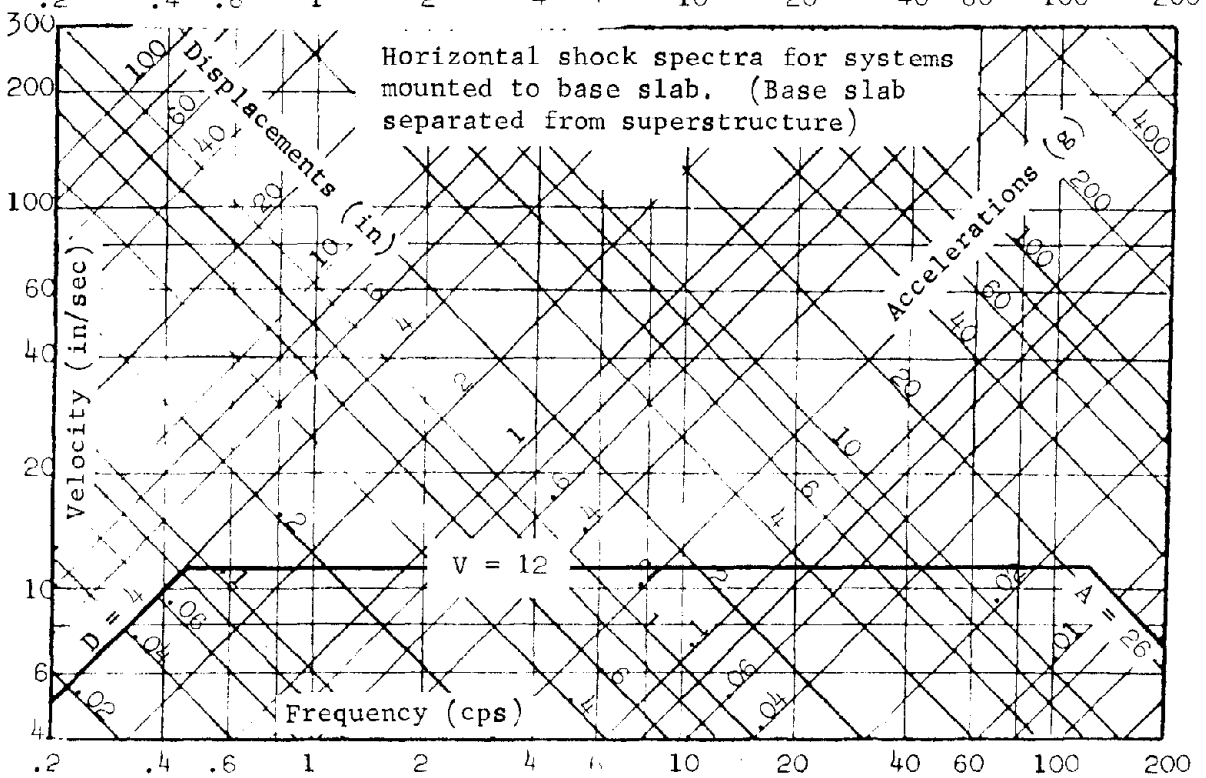
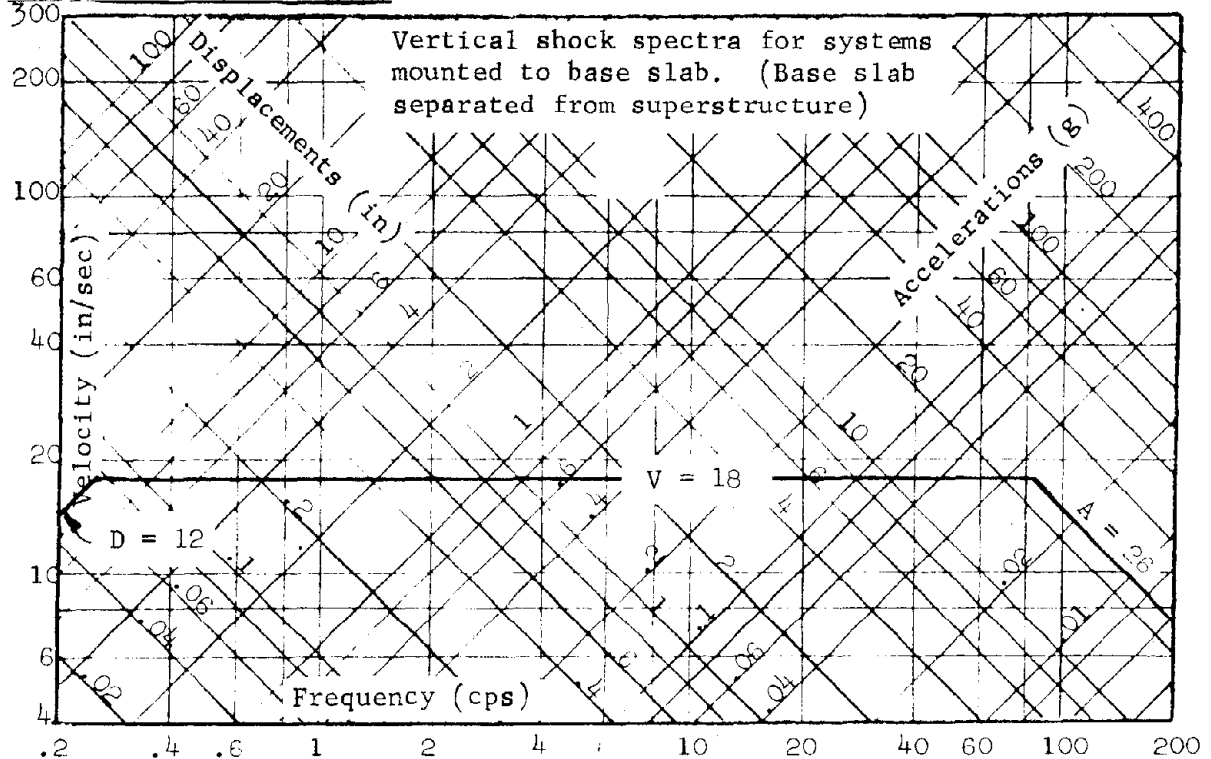


FIGURE 4.12

#### 4.2.3 Two-story reinforced concrete windowless shear wall structures

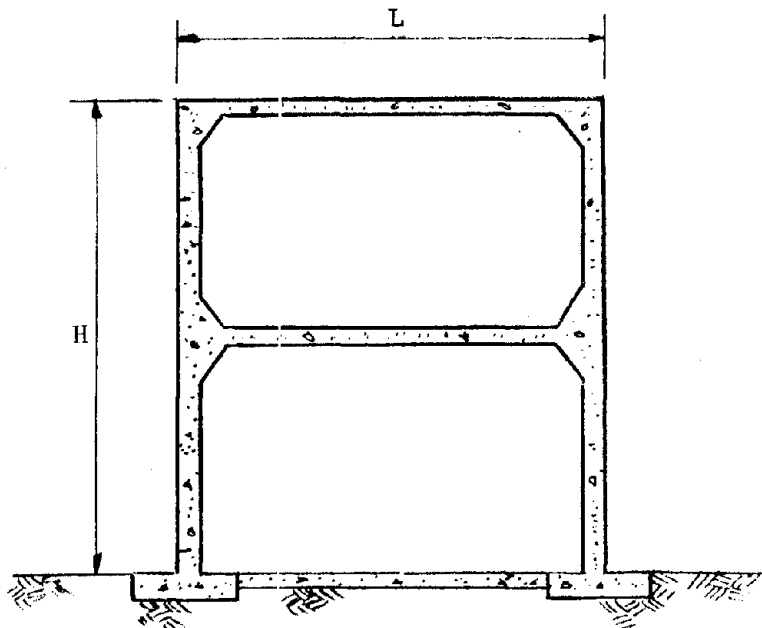
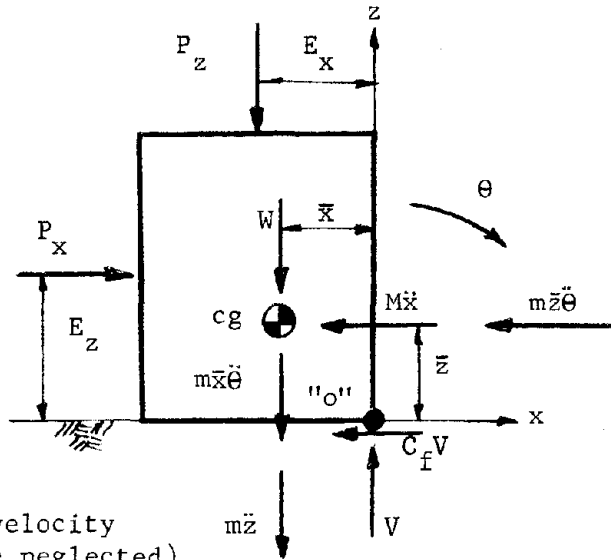


FIGURE 4.13: TWO-STORY STRUCTURE

The structure shown in Figure 4.13 is a monolithic reinforced concrete structure consisting of slabs and shear walls. Its construction may be feasible in the 10 psi overpressure region. The important motions to be considered are the same as those for a one-story structure, with two additional effects: (1) the rigid body rotation is now assumed also to affect the rigid body translation and (2) the second-story floor slab will have a separate vertical response.

(1) Rigid body translation with rotation. The rotation was neglected in a one-story structure. As the height to length ratio,  $H/L$ , increases, the rotational effect becomes more significant. A two-story structure may have a ratio of  $H/L$  as high as 1, and at this ratio, the rotation may alter the translational motion.



(Note: Angular velocity terms are neglected)

FIGURE 4.14: FORCES ACTING ON A RIGID BODY

The free-body diagram in Figure 4.14 shows the important forces to be considered. The equations of motion are

$$\begin{aligned}
 P_x - C_f V - m\ddot{x} - m\bar{z}\ddot{\theta} &= 0 \\
 V - P_z - m\bar{x}\ddot{\theta} - m\ddot{z} - W &= 0 \\
 P_x E_z - P_z E_x - (m\ddot{x} + m\bar{z}\ddot{\theta}) \bar{z} - (m\ddot{z} + m\bar{x}\ddot{\theta} + W) \bar{x} - J_{cg} \ddot{\theta} &= 0
 \end{aligned}
 \tag{4.13}$$

where,

- $P_x$  and  $P_z$  = blast loading forces
- $V$  = vertical reaction at assumed pivot point "o"
- $W$  = structure weight
- $J_{cg}$  = mass moment of inertia about C.G.

All dimensions are shown on Figure 4.14 or have been previously defined.

The magnitude of the rotation amplitudes may be obtained in an approximate manner by ignoring the vertical motion acceleration,  $\ddot{z}$ . (This approximation is suggested in Reference 4.10.) Equations (4.13) reduce to



the following:

$$P_x - C_f V = m\ddot{x} + m\bar{z}\ddot{\theta} \quad (4.14a)$$

$$V - P_z - W = m\bar{x}\ddot{\theta} \quad (4.14b)$$

$$P_x E_z - P_z E_x - W\bar{x} = J_o \ddot{\theta} + m\bar{x}\ddot{z} \quad (4.14c)$$

where,  $J_o = J_{cg} + m\bar{z}^2 + m\bar{x}^2$

By eliminating the force, V, between Equations (4.14a) and (4.14b) and substituting the resulting value of  $m\ddot{x}$  from Equation (4.14a) into (4.14c), we obtain the following equation for  $\ddot{\theta}$ :

$$\ddot{\theta} = \frac{P_x(E_z - \bar{z}) - P_z(E_x - C_f \bar{z}) - W(\bar{x} - C_f \bar{z})}{J_o - C_f m \bar{x} \bar{z} - m \bar{z}^2} \quad (4.15)$$

The lateral acceleration,  $\ddot{x}$ , including the effect of rotation coupling, is obtained from Equations (4.14a) and (4.14b), in terms of the external forces and rotation response,  $\ddot{\theta}$ , given by Equation (4.15),

$$\ddot{x} = \frac{P_x - C_f (P_z + W)}{m} - (\bar{z} + C_f \bar{x}) \ddot{\theta} \quad (4.16)$$

The above equations can then be plotted as a function of time to compute graphically the peak rotation response,  $\theta$ , and the displacement response,  $x$ , when both occur simultaneously. Figure 4.15 represents typical plots of both  $\ddot{\theta}$  and  $\ddot{x}$ . The figure demonstrates the graphical procedure in computing the maximum rotation and displacement. Example 4.2 will further illustrate the computational procedure.

The maximum horizontal acceleration of the C.G. may now be obtained as a function of both  $\ddot{x}$  and  $\ddot{\theta}$  as follows:

$$a'_h = \ddot{x} + \ddot{\theta} \bar{z}$$

For other locations on the structure, the acceleration due to  $\ddot{\theta}$  response will vary according to the vertical moment arm distance from point "o".

It must be noted, that the model postulated in Figure 4.14 is applicable for an initial positive  $\theta$  response. When  $\ddot{\theta}$  calculated from Equation (4.13) is negative for all time periods, overturning is not possible, since the stabilizing moments are larger than the overturning moments. For this condition, overturning rotation can be neglected.

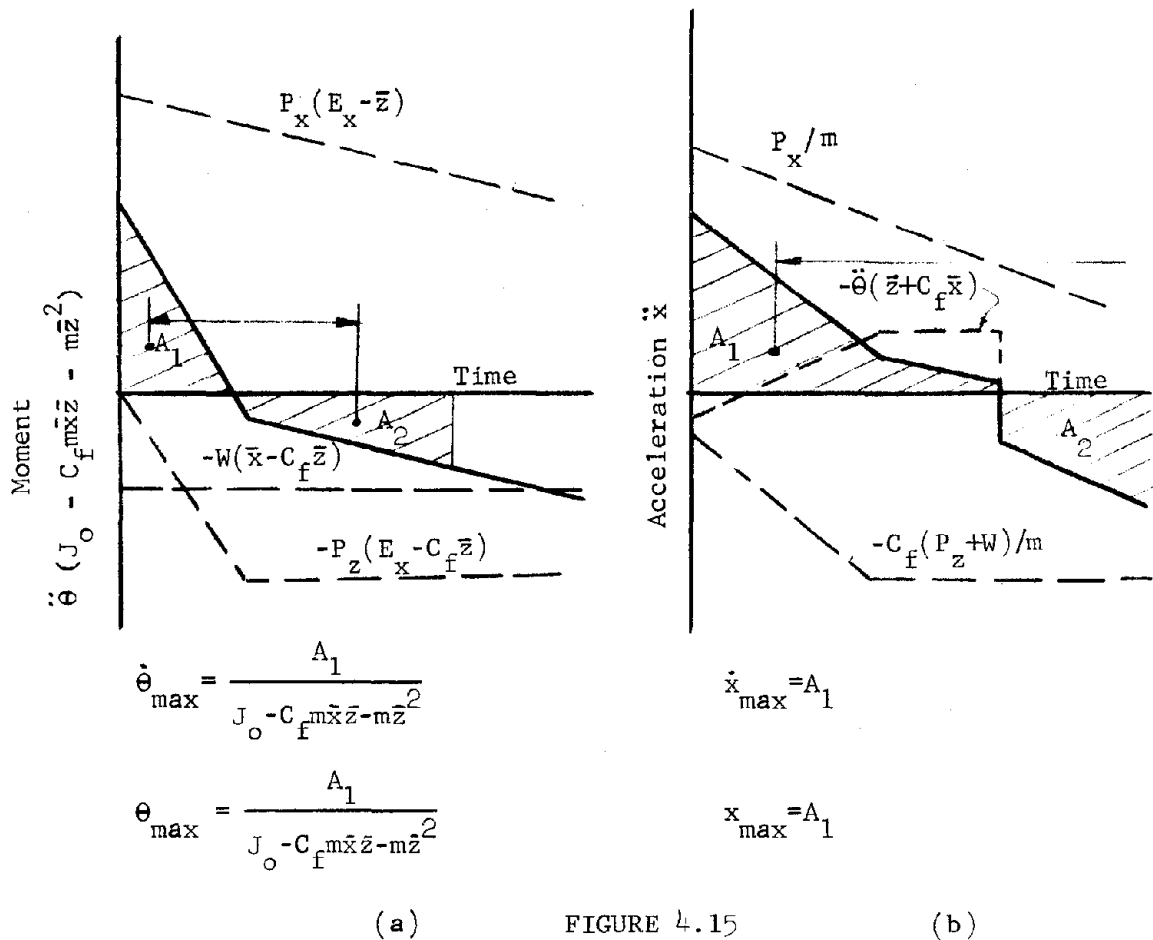


FIGURE 4.15

(2) Vertical response of second story floor slab. Equipment mounted on the second story floor slab has an input that is strongly influenced by the response of the floor slab. If the slab weight is considerably greater than the equipment weight, so that the equipment response on its mounts will not significantly alter the response of the slab, then the response of the slab as a single-degree-of-freedom system may be used as an input to the equipment mounts. The method proposed in Section 2 for constructing a spectra envelope for the second mass,  $m_2$ , for a two-mass system, may be applied in deriving a vertical shock spectra envelope for the equipment mounted to the slab. The vertical input to the slab is then essentially the rigid body motion of the structure in the vertical direction. The rotation response,  $\ddot{\theta}$ , calculated by the method described in the previous subsection may be used to estimate the magnitude of any additional vertical rigid body

acceleration due to rotation, i.e.  $\bar{x}\ddot{\theta}$ . After computing the first mode frequency of the slab, the peak response acceleration, velocity and displacement are obtained from the vertical shock spectra envelope for the idealized SDOF system for  $m_1$ . These peak values are  $D_0, V_0, A_0$ . The vertical response spectra envelope is then defined by the 3-straight lines;

$$D' = D + D_0$$

$$V' = V + 1.5 V_0$$

$$A' = 2 A_0$$

where  $D, V,$  and  $A$  are spectra bounds for the vertical response of the slab, and  $D', V',$  and  $A'$  are the spectra bounds for the vertical response of items mounted to the slab.

#### Example 4.2

Assume that a 10 psi overpressure blast wave, due to a 20 MT burst, acts on the two-story reinforced concrete structure shown in Figure 4.16. (It is noted that, for purposes of illustration, a heavy base slab, cast monolithically with the structure, is specified.) It is desired to find the motions of the walls, roof and floor slabs. As in Example 4.1, the motion of the structure is considered to be divided into three parts, namely,

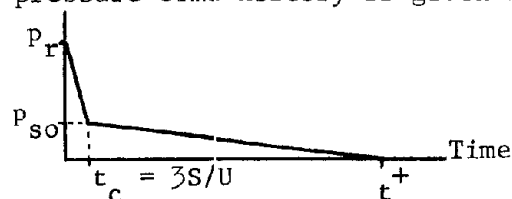
- (1) rigid body motion, denoted by one prime
- (2) deformational motion, denoted by two primes
- (3) ground motion, denoted by three primes.

The necessary blast wave data are

$$p_{so} = 10 \text{ psi}, \quad \begin{array}{c} \text{Overpressure} \\ D_p^+ = 4.3 \text{ sec}, \end{array} \quad t^+ = 3.5 \text{ sec}$$

$$p_r = 2.6 \times 10 \text{ psi} = 26 \text{ psi}, \quad U = 1400 \text{ fps}, \quad \begin{array}{c} \text{Reflected Pressure} \\ t_r^+ = .043 \text{ sec}, \end{array}$$

where the front face pressure-time history is given by



Example 4.2 (continued)

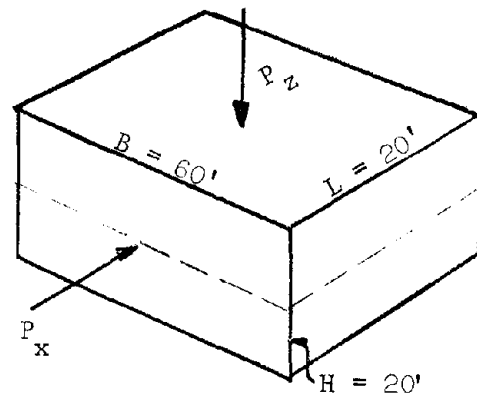
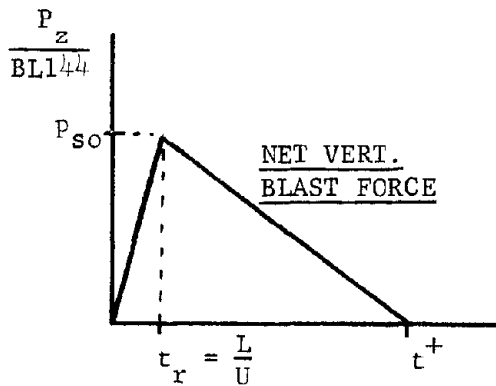
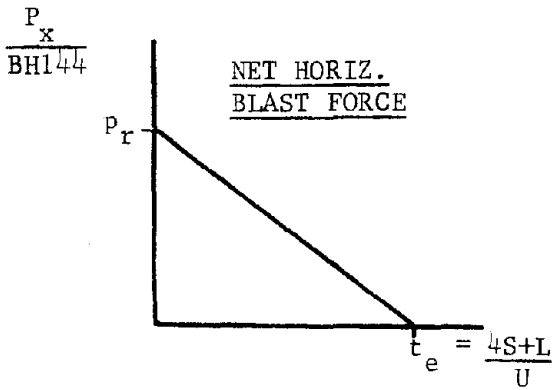
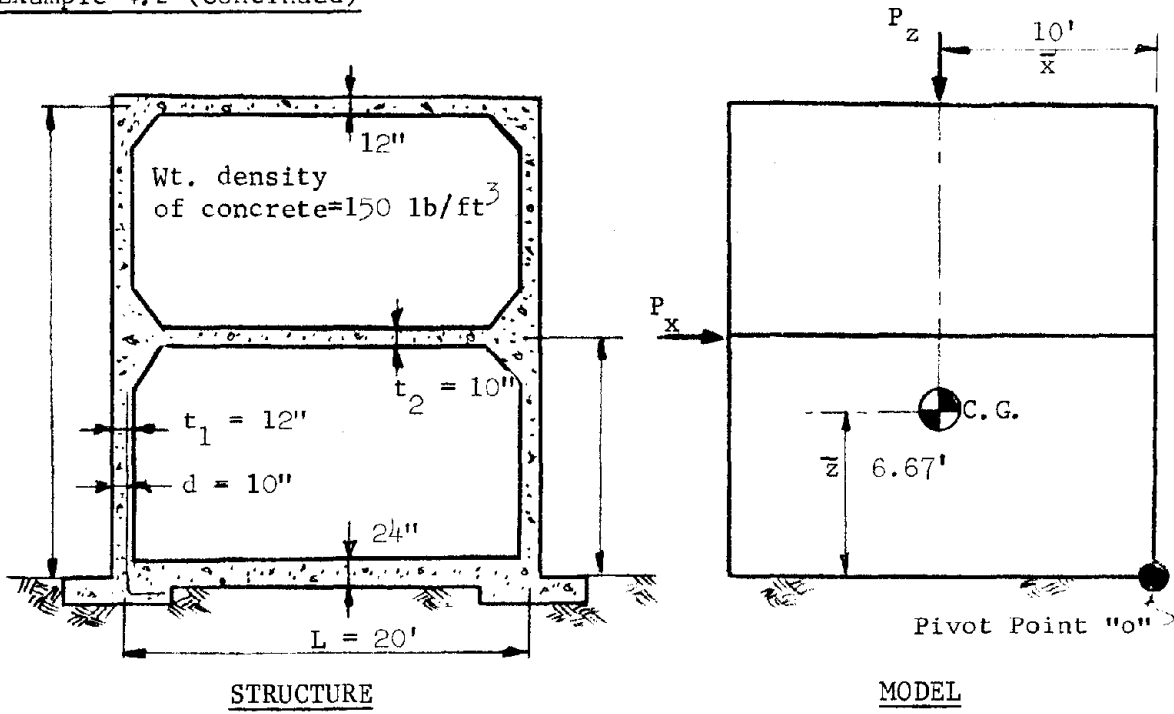


FIGURE 4.16: EXAMPLE 4.2  
192

Example 4.2 (continued)

Pertinent structural dimensions are given in Figure 4.16. The total weight of the structure and the weight moment of inertia of the structure about the assumed pivot point "o" are

$$W = 1.17 \times 10^6 \text{ lbs}$$
$$J_o = 3.31 \times 10^8 \text{ lb-ft}^2$$

The net vertical and horizontal blast force-time histories are as shown in Figure 4.16. The coefficient of friction at the soil-structure interface is assumed to be 0.5.

a. The horizontal motions are first calculated.

(1) Rigid body horizontal motion with rotation. The angular acceleration is calculated, using Equation (4.15) and the graphical method shown in Figure 4.15a. The resulting acceleration is shown in Figure 4.17. Using Equation (4.16) and the results of Figure 4.17 the resultant horizontal center of gravity acceleration is obtained, as shown in Figure 4.18.

The maximum horizontal accelerations are

Roof slab	$a'_h = \ddot{x} + z\ddot{\theta} = 3 + 20 \times .03 = 3.6 \text{ g}$
2nd floor slab	$a'_h = 3 + 10 \times .03 = 3.3 \text{ g}$
Base slab	$a'_h = 3 + 0 = 3.0 \text{ g}$
Side walls	$a'_h = 3 + 10 \times .03 = 3.3 \text{ g}$

The maximum overturning angular velocity is equal to the area,  $A_1$ , shown in Figure 4.17;  $\dot{\theta} = \frac{.03 \times .07}{2} 32.2 = .034 \text{ rad/sec}$ . The maximum translational velocity of the C.G. is equal to the area,  $A_1$ , shown in Figure 4.18;

$\dot{x} = 29.4 \text{ in/sec}$ . The peak horizontal velocity of the structure can be no greater than the sum of these two components, namely,

Roof slab	$v'_h = 29.4 + 240 \times .034 = 37.6 \text{ in/sec}$
2nd Floor slab	$v'_h = 29.4 + 120 \times .034 = 33.5 \text{ in/sec}$
Base slab	$v'_h = 29.4 + 0 = 29.4 \text{ in/sec}$
Side walls	$v'_h = 29.4 + 120 \times .034 = 33.5 \text{ in/sec}$

Example 4.2 (continued)

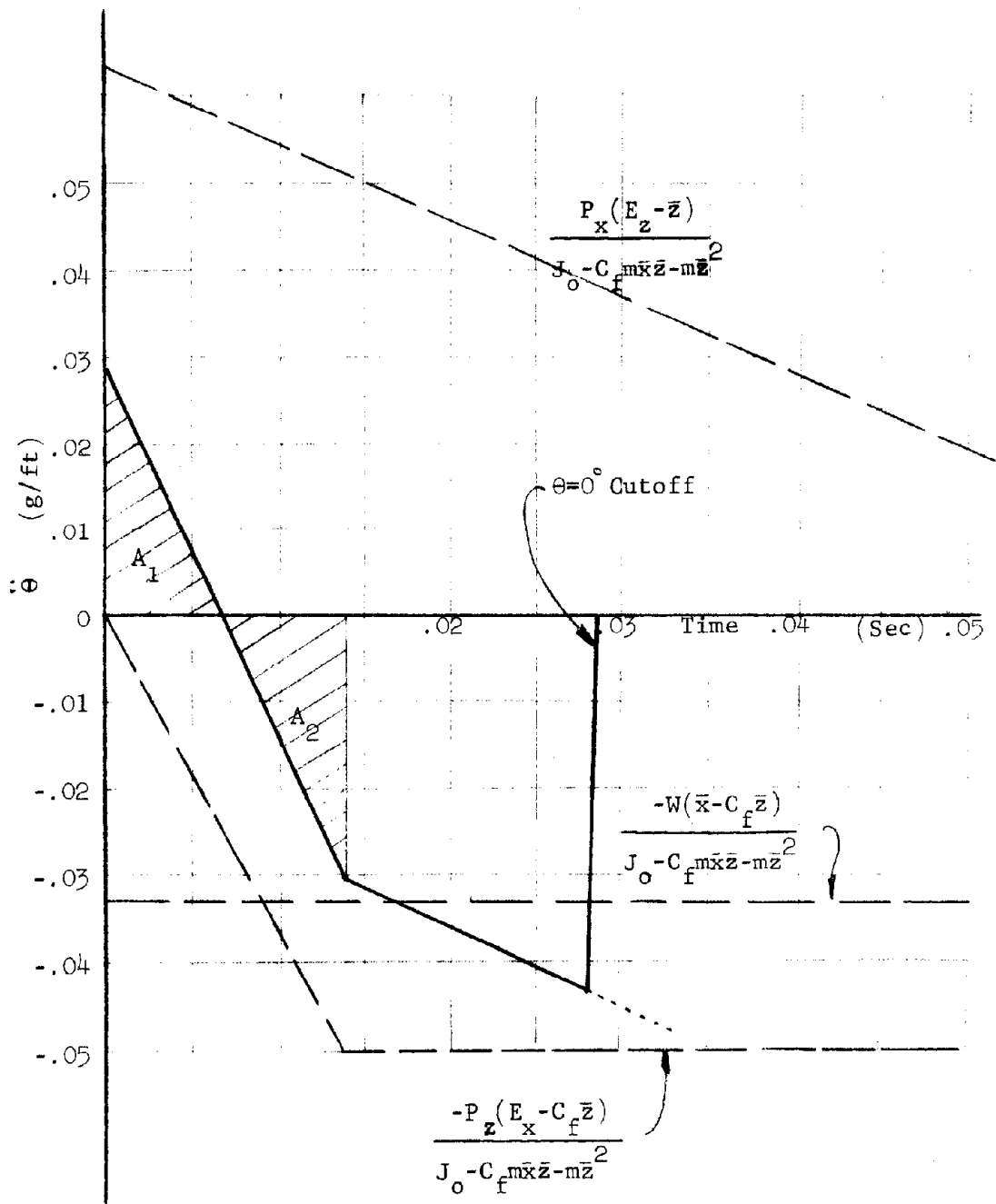


FIGURE 4.17

Example 4.2 (continued)

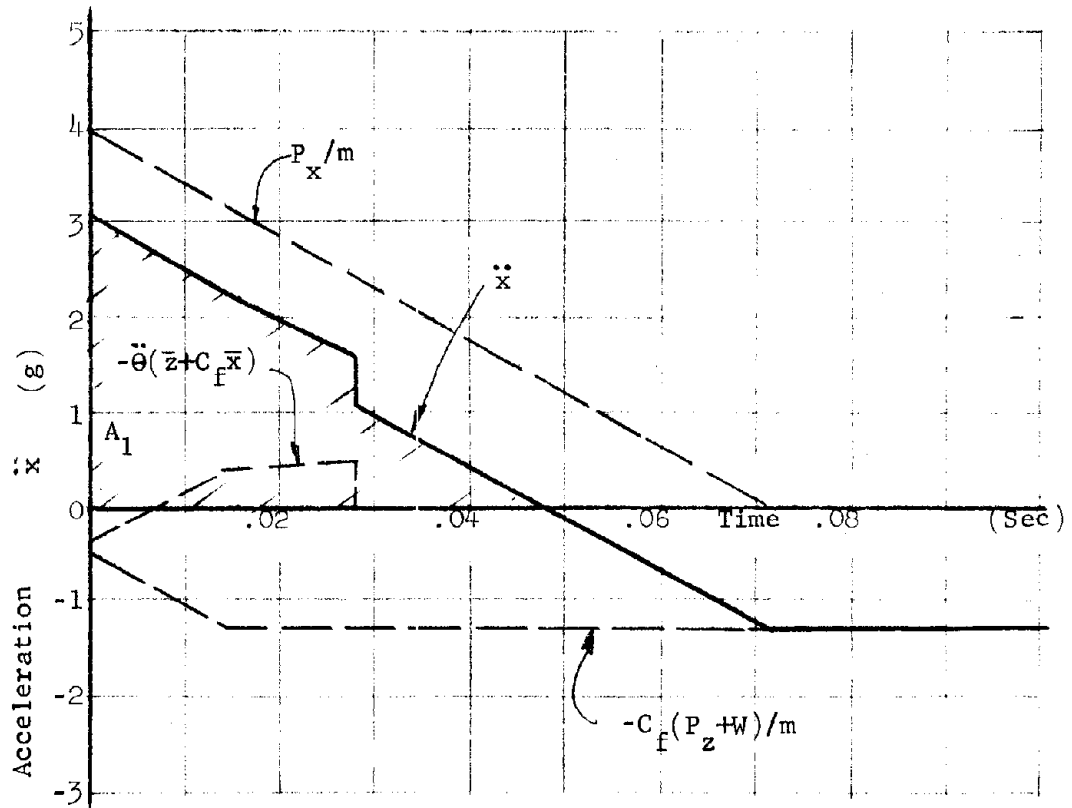


FIGURE 4.18

Example 4.2 (continued)

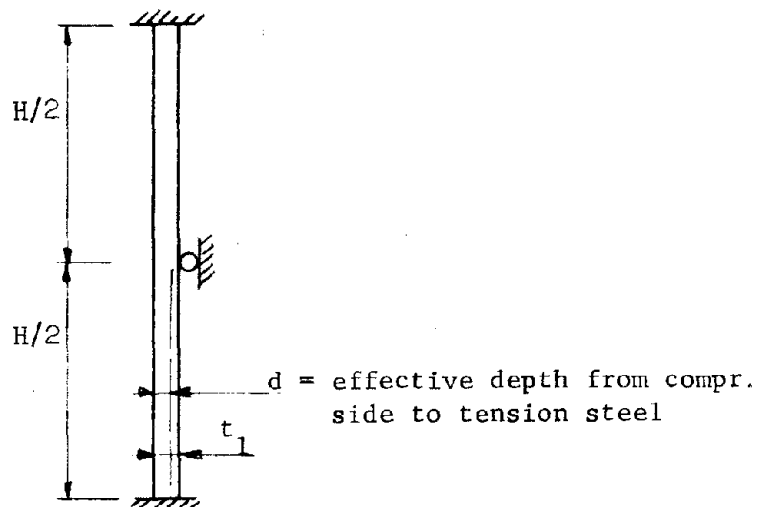
The maximum overturning angular displacement is equal to  $\theta = A_1 \tau$ , where  $\tau$  is the time between the centroids of areas,  $A_1$  and  $A_2$ , of Figure 4.17, namely,  $\theta = .034 \times .01 = 3.4 \times 10^{-4}$  rad. The translational displacement of the C.G. is calculated in a similar manner to be:  $x = 29.4 \times .076 = 2.2$  in. The peak horizontal displacements of the structure can be no greater than the sum of these two components:

Roof slab	$d'_h = 2.2 + 240 \times 3.4 \times 10^{-4} = 2.3$ in.
2nd floor slab	$d'_h = 2.2 + 120 \times 3.4 \times 10^{-4} = 2.2$ in.
Base slab	$d'_h = 2.2 + 0 = 2.2$ in
Side walls	$d'_h = 2.2 + 120 \times 3.4 \times 10^{-4} = 2.2$ in.

It is noted that  $d'_h = 1.9$  in., when the rotation is neglected.

(2) Horizontal deformation response of the walls. The horizontal motions of the wall located normal to the direction of the blast, with dimensions,  $B = 60'$ ,  $H = 20'$  and  $t_1 = 12''$ , will be calculated.

The top and bottom ends of the front wall are considered fixed; and due to the relatively small  $E I$  of the middle slab, a simple support at the intermediate floor level is assumed as shown below.





Example 4.2 (continued)

The natural frequency is given by (as defined in Appendix B)

$$T = .407 (H/\ell)^2 \sqrt{\frac{A\gamma}{EIg}}$$

$$\gamma = \text{weight density} = 150 \text{ lbs/ft}^3$$

$$A = \text{area per unit length} = B t_1 = 60 \text{ ft}^2$$

$$EI = \text{flexural rigidity} = 18.8 \times 10^4 B d^3 \phi \text{ lb-in}^2 = 13.3 \times 10^{10} \text{ lb-in}^2$$

we obtain

$$T = .023 \text{ sec}$$

An approximate value of the flexural resistance of the wall may be obtained (see Appendix B) by considering it as a beam with one fixed support and one hinged end,\*

$$R_f = .075 \left( \phi + \frac{\phi_s}{2} \right) \frac{f_c B d^2}{H/2}$$

where the values of the various parameters have been given previously

$$R_f = .075 (1.5) \frac{5.2 \times 10^4 \times 60 \times 12 \times (10)^2}{10 \times 12} = 3.51 \times 10^6 \text{ lbs.}$$

The total load for the half-span  $H/2$  is

$$P_{\max} = \frac{4.49 \times 10^6}{2} = 2.25 \times 10^6 \text{ lbs.}$$

The yield deflection is given in Appendix B as

$$d_y = \frac{1}{5430} \frac{H/2^2}{d} = 0.26 \text{ in.}$$

The ductility ratio,  $\mu$ , can be found from the parameters

$$\frac{t_r^+}{T} = \frac{.043}{.023} = 1.9$$

$$\frac{P_r - P_{so}}{R} = \frac{16 \times 144 \times 20 \times 60}{2 \times 3.51 \times 10^6} = .39$$

\*Except for the frequency, other parameters are calculated based on this assumption.

Example 4.2 (continued)

$$\frac{t_r^+ - t_r^-}{T} = \frac{3.46}{0.23} = 150$$

$$\frac{P_{so}}{R} = \frac{10 \times 144 \times 20 \times 60}{2 \times 3.51 \times 10^6} = .25$$

using the polygonal loading-time curve method outlined in Reference 4.12 and the response chart of Reference 4.10. Accordingly,  $\mu = 1.2$ .

Therefore,

$$d_h'' = \mu d_y = 0.31 \text{ inches}$$

Using a load mass factor of 3/4,

$$a_h'' = \frac{4}{3} \frac{P_{max}}{m} = \frac{4}{3} \times \frac{2.25 \times 10^6}{9 \times 10^4} \text{ g} = 33.3 \text{ g}$$

and

$$v_h'' = \frac{a_h''}{\omega} = \frac{33.3}{275} \text{ g} = 47 \text{ in/sec}$$

(3) Horizontal ground motions. The ground motions are calculated from the equations given in Section 3.5 (based on a 5 feet burial depth).

$$a_h = a_v = 5 \text{ g}$$

$$v_h = 2/3 v_v = 3.33 \text{ in/sec}$$

$$d_h = \frac{1}{3} d_z = 2.6 \text{ in}$$

The induced structure horizontal motions are

$$v_h''' = 3.33 \text{ in/sec} \quad d_h''' = 2.6 \text{ in.}$$

If the base is separated from the main structure, the base slab ground induced acceleration is

$$a_h''' = a_v''' = 2.5 \text{ g for an equivalent transit distance} = 10' \\ \text{(similar to Figure 4.1b)}$$

b. The vertical motions are now calculated.

(1) Rigid body motions. For footings 5 feet wide and assuming a soil stiffness  $k_z = 100 \text{ lbs/in.}$ , the total stiffness of the soil is

$$K = 11.5 \times 10^6 \text{ lbs/in}$$

Example 4.2 (continued)

The natural frequency is therefore

$$\omega = \sqrt{\frac{K}{m}} = \sqrt{\frac{1.15 \times 10^7 \times 386}{1.17 \times 10^6}} = 62 \text{ rad/sec}$$

The peak force applied to the roof of the structure is

$$P_{\max} = p_{so} L B = 1.73 \times 10^6 \text{ lbs}$$

The maximum acceleration is given by

$$a'_v = \frac{P_{\max}}{m} = \frac{1,730,000}{1.17 \times 10^6} g = 1.5 g$$

and the pseudo-velocity is

$$v'_v = \frac{a'_v}{\omega} = \frac{1.5 \times 386}{62} = 9.4 \text{ in/sec}$$

(2) Roof slab deformation response. Similar to the case of the one-story building, the natural period  $T$  is obtained from

$$T = \frac{1}{7200} \frac{L}{d} \frac{L}{\sqrt{\phi}} = \frac{1}{7200} \frac{20 \times 12}{10} \frac{20}{1} = 0.0667 \text{ sec.}$$

Accordingly,

$$\omega = \frac{2\pi}{T} = 94.2 \text{ rad/sec.}$$

Since the effective positive phase duration is

$$t^+ = 3.5 \text{ sec.}$$

$$\frac{t^+}{T} = \frac{3.5}{0.0667} = 53$$

The resisting force is

$$\begin{aligned} R &= .075 \times 2 \times \frac{5.2 \times 10^4 \times 60 \times 12 \times 10^2}{20 \times 12} \\ &= 2.34 \times 10^5 \text{ lbs} \end{aligned}$$

and the peak applied load is as previously calculated

$$P_{\max} = 1.73 \times 10^6 \text{ lbs}$$

Therefore

$$\frac{P_{\max}}{R} = \frac{1.73}{2.34} = 0.74$$

Example 4.2 (continued)

The ductility ratio is found (from the dynamic response chart of Reference 4.10) to be  $\mu = 2$ .

The yield deflection is calculated based on equal fixity at each support (defined in Appendix B).

$$d_y = \frac{1}{7600} \frac{L^2}{d} = 0.75 \text{ in}$$

Therefore the peak displacement is

$$d_v'' = \mu d_y = 1.5 \text{ in}$$

The initial peak acceleration is

$$a_v'' = \frac{1}{K_{Lm}} \frac{P_{\max}}{m} = \frac{4}{3} \frac{1.73 \times 10^6}{1.8 \times 10^5} \text{ g} = 12.8 \text{ g}$$

and the maximum pseudo-velocity is

$$v_v'' = \frac{a_v''}{\omega} = \frac{12.8 \text{ g}}{94.2} = 52.5 \text{ in/sec}$$

(3) Vertical ground motion. The vertical ground acceleration, velocity and displacement have been previously calculated and are:

$$a_v = 10 \text{ g}, \quad v_v = 5 \text{ in/sec}, \quad d_v = 7.7 \text{ in}$$

The structure induced motions are:

$$v_v''' = 5 \text{ in/sec}, \quad d_v''' = 7.7 \text{ in}$$

For the base slab separated, the vertical acceleration for an effective length  $\ell = 10$  feet is  $= 2.5 \text{ g}$ .

The components of the horizontal and vertical ground motions are summarized in Table 4.4.

Example 4.2 (continued)

TABLE 4.4

	Item	Acceleration (g)			Velocity (in/sec)			Displacement (in)		
		a'	a''	a'''	v'	v''	v'''	d'	d''	d'''
Vertical	Roof	1.5	12.8	0	9.4	52.5	5	0	1.5	7.7
	Wall	1.5	0	0	9.4	0	5	0	0	7.7
	2 <sup>nd</sup> Floor	(See page 206)								
	Base	1.5	0	0	9.4	0	5	0	0	7.7
Horizontal	Roof	3.6	0	0	37.6	0	3.3	2.3	0	2.6
	Wall	3.3	33.3	0	33.5	47	3.3	2.2	.31	2.6
	2 <sup>nd</sup> Floor	3.3	0	0	33.5	0	3.3	2.2	0	2.6
	Base	3.0	0	0	29.4	0	3.3	2.2	0	2.6

Example 4.2 (continued)

The root-mean-square results are given in Table 4.5.

TABLE 4.5

	Item	Acceleration g	Velocity in/sec	Displacement in.
Vertical	Roof	13	54	9
	Wall	2	11	8
	2 <sup>nd</sup> Floor	(See page 206)		
	Base	2	11	8
Horizontal	Roof	4	38	5
	Wall	34	58	5
	2 <sup>nd</sup> Floor	3	35	5
	Base	3	30	5

The above values are rounded off to the nearest whole number.

Example 4.2 (continued)

It is a direct and simple step from the calculated results of Table 4.5 to the peak response values leading to the shock spectra.

Using the relationships,

$$D = d_{\max}$$

$$V = 1.5 V_{\max}$$

$$A = 2.0 \max$$

the peak response values are summarized in Table 4.6. The shock spectra are plotted in Figures 4.19 and 4.20.

TABLE 4.6

	Item	Acceleration (g)	Velocity (in/sec)	Displacement (in)
Vertical	Roof	26	81	9
	Wall	4	17	8
	2 <sup>nd</sup> Floor	(See page 206)		
	Base	4	17	8
Horizontal	Roof	8	57	5
	Wall	68	87	5
	2 <sup>nd</sup> Floor	68	87	5
	Base	6	45	5

Example 4.2 (continued)

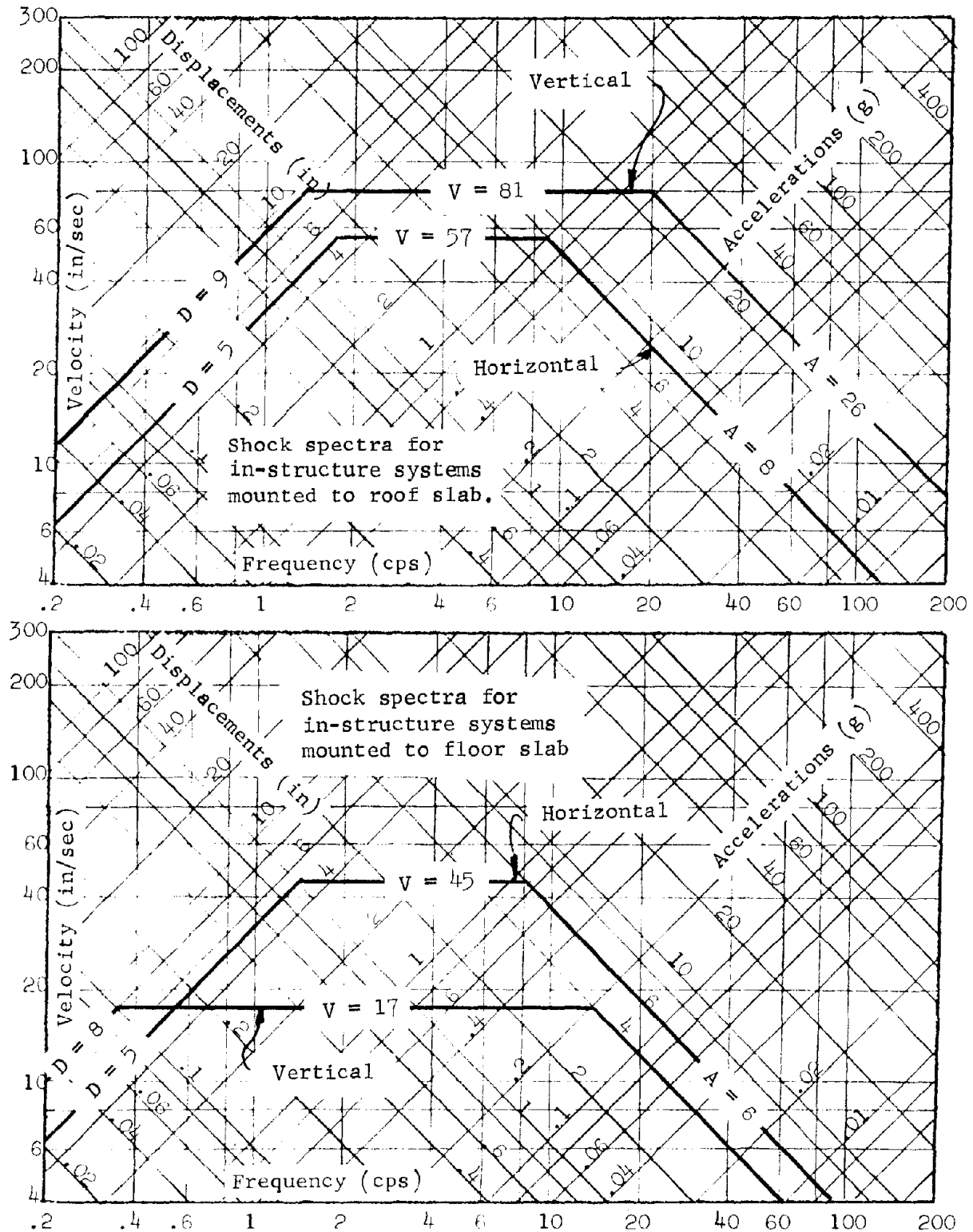


FIGURE 4.19



Example 4.2 (continued)

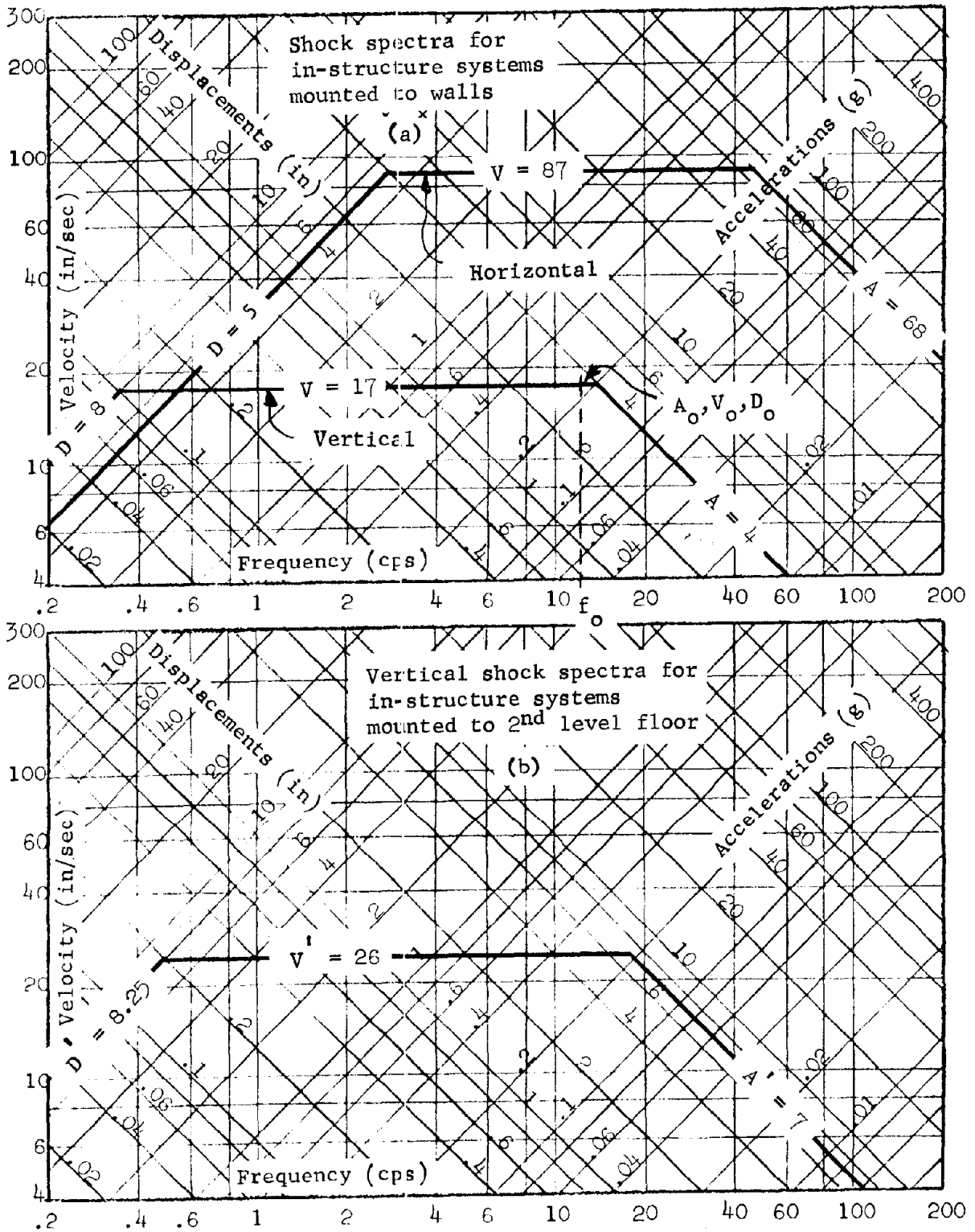


FIGURE 4.20  
205

Example 4.2 (continued)

The second floor level response can now be calculated. The natural frequency of the second floor is

$$\omega = \frac{2\pi}{T} = 94.2 \times \frac{10}{12} = 78.5 \text{ rad/sec}$$

where 94.2 is the frequency of the roof slab, and  $\frac{10}{12}$  is the thickness ratio of middle slab to roof slab, accordingly,

$$f_o = 12.5 \text{ cps}$$

The 2<sup>nd</sup> level floor slab may be considered as a mass that is mounted to the walls; and the vertical response of the floor may be obtained from the critical shock spectra of the walls. (See Figure 4.20a.)

Reading the vertical response from the shock spectra of Figure 4.20a,

$$A_o = 3.5 \text{ g}$$

$$V_o = 17 \text{ in/sec}$$

$$D_o = 0.25 \text{ in.}$$

The upper bound of the vertical response for items mounted to the floor slab are (see description of method in Section 2)

$$A' = 2 A_o = 7 \text{ g}$$

$$V' = 43 \text{ in/sec}$$

$$D' = 8.25 \text{ in.}$$

Figure 2.20b is the plot of the shock spectra bound (vertical component) for equipment mounted to the second level.

The horizontal response of items mounted to the second floor is assumed to be a function of the rigid body motion of the structure.

4.2.4 Dome shaped structures. Dome shaped surface structures of monolithic concrete construction may be feasible in regions where the peak overpressure is less than 75 psi. The streamlined shape reduces the effects of the reflected and the dynamic pressures. As a result, at higher overpressures a dome shaped structure is more economical than a rectangular.

The simplified loading for domes, recommended in Reference 4.13, is used to estimate the motions of the structure due to the direct impingement of the air blast. The loading is divided into a uniform compression mode and a nonuniform flexural mode as shown in Figure 4.21. For any particular time, the compression mode loading is uniform over the dome, and the flexural mode loading varies as  $\sin(\beta - \psi) \cos\theta / \sin\beta$ .

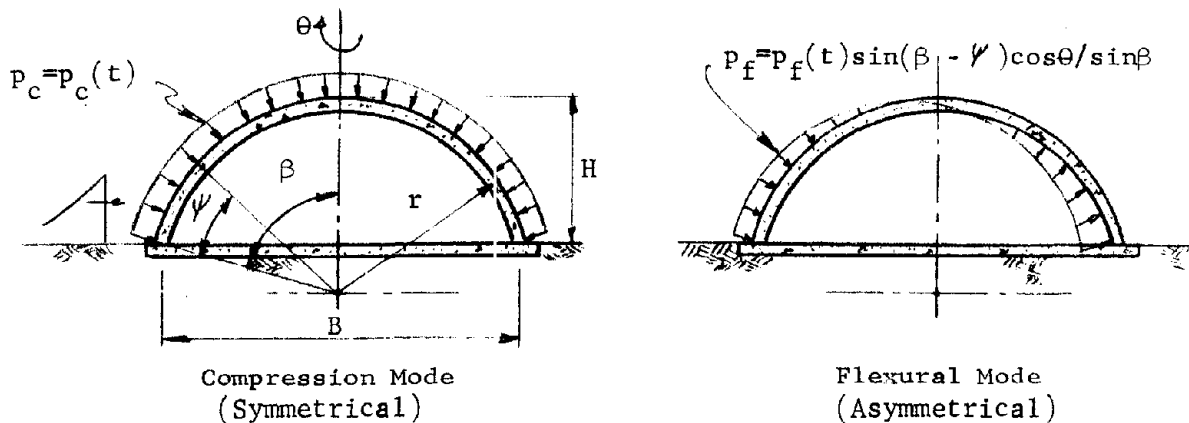
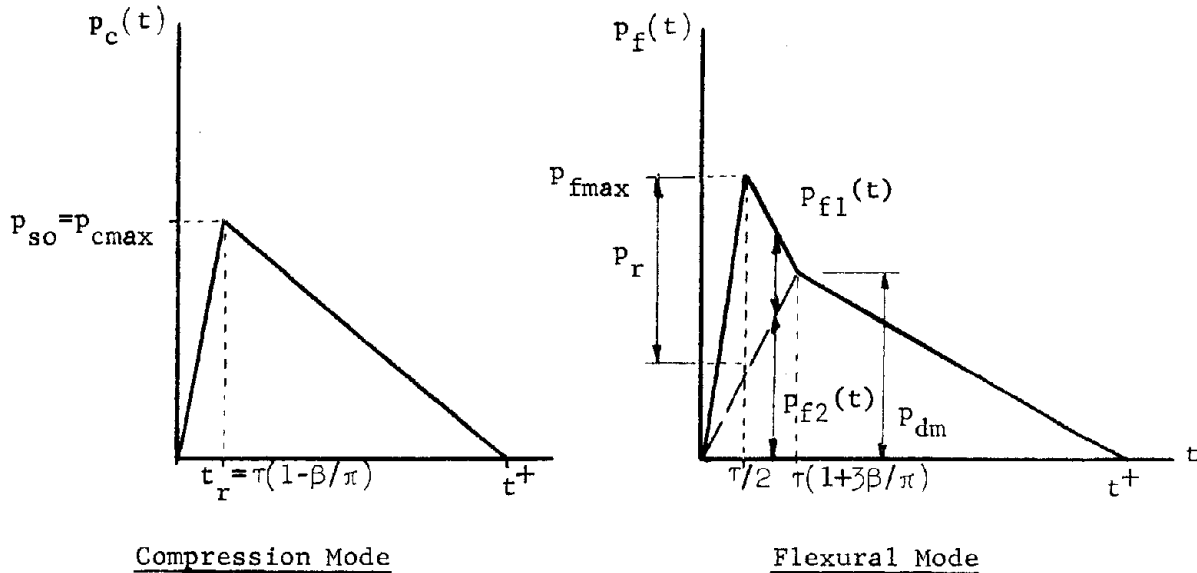


FIGURE 4.21

The pressure-time history for each mode is shown in Figure 4.22. The compression mode loading rises linearly to a value  $p_{s0}$  in the time  $t_r = (1 - \beta/\pi)\tau$ , where  $\tau = B/U$ , and decays linearly to zero at the time  $t^+$ , where  $t^+$  is the duration of the single-triangle representation of the free-field overpressure,  $p_{s0}$ . The flexural mode loading, at the springline,  $p_f(t)$ , is divided into an initial component,  $p_{f1}(t)$ , and a drag component,  $p_{f2}(t)$ , as shown in Figure 4.22. The maximum value of  $p_{f1}(t)$  is equal to the maximum reflected pressure,  $p_r$ , on the windward side of the dome, and the maximum value of  $p_{f2}(t)$  is equal to  $p_{dm} = (\beta/\pi) C_d p_{d0}$ , where  $C_p$  is the

drag coefficient consistent with the dome angle at the springline and  $p_{do}$  is the peak free-field dynamic pressure. Also,  $t^+$  is the duration of the single-triangle representation of  $p_{do}$ .



PRESSURE-TIME HISTORY AT SPRINGLINE AND  $\theta=0^\circ$

FIGURE 4.22

(1) Rigid body motion due to air blast.

Horizontal

The horizontal component of the unsymmetrical loading creates a net horizontal force which may cause a translational motion of the domed structure. This motion is resisted by the friction forces developed at the foundation-soil interface, due to the vertical component of the compression mode and the weight of the dome. The acceleration-time history of this motion is shown in Figure 4.23. Using the graphical procedure outlined in Section 4.2.2, the maximum acceleration, velocity, and displacement are obtained in a manner similar to that outlined for a rectangular structure.

Vertical

The vertical motion can be estimated by taking the vertical component of the compression mode loading and applying it as a driving force on the

structure with a resisting force represented by the soil spring stiffness. The peak response is then obtained as described in Section 4.2.2.

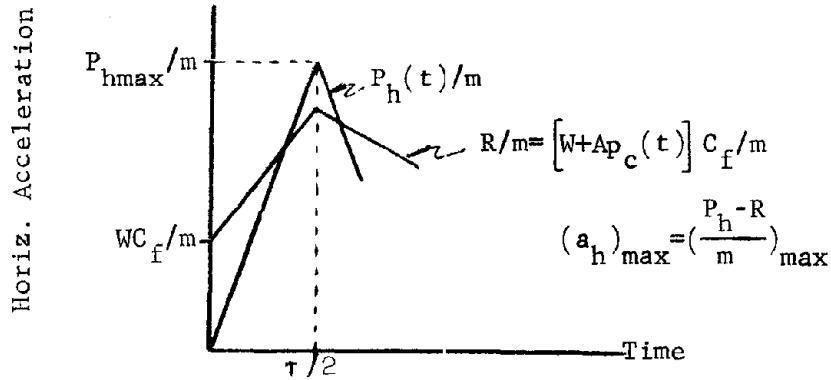


FIGURE 4.23

(2) Deformation motion due to air blast impact on the structure. The sketch of Figure 4.21 shows a compression mode and a flexure mode. The shell deformation peak response can be obtained for each mode separately. The two maxima will not occur at the same point on the shell; but an upper bound response for any point on the shell can be obtained by adding the absolute values of the peak motion in each mode, and considering this to be the resultant of the horizontal and vertical components

$$\begin{aligned}
 a_z'' &= a_h'' = .707 (a_1' + a_2'') \\
 v_z'' &= v_h'' = .707 (v_1' + v_2'') \\
 d_z'' &= d_h'' = .707 (d_1' + d_2'')
 \end{aligned}
 \tag{4.17}$$

where  $a_1'$ ,  $v_1'$ ,  $d_1'$  are the peak response motions normal to the shell in the compression mode

and  $a_2''$ ,  $v_2''$ ,  $d_2''$  are the peak response motions normal to the shell in the flexure mode.

The peak acceleration again is assumed to occur during the initial loading and is approximated by the peak pressure divided by the mass of the shell times an appropriate load-mass factor. In the compression mode

$$\begin{aligned}
 a_1 &= \frac{P_{cmax}}{m K_{Lm}} & K_{Lm} &\approx 1 \\
 v_1 &= \frac{a_1}{\omega_c} & \omega_c &= \text{circular frequency in} \\
 & & & \text{the compression mode}
 \end{aligned} \tag{4.18}$$

$$d_1 = \mu d_y$$

Similarly in the flexure mode

$$\begin{aligned}
 a_2 &= \frac{P_{fmax}}{m K_{Lm}} & K_{Lm} &\approx 3/4 \\
 v_2 &= \frac{a_2}{\omega_f} & \omega_f &= \text{circular frequency in} \\
 & & & \text{the flexure mode}
 \end{aligned}$$

$$d_2 = \mu d_y$$

The resistance force,  $R$ , and the period,  $T$ , must be calculated to solve for  $\mu$ . The yield displacement can be calculated from shell deformation theory, or an order of magnitude accuracy can be obtained from the approximation  $d_y = a/\omega^2$  for each mode.

The procedure is further explained and illustrated in the example at the end of this section.

(3) Rigid body motion due to ground motion. The discussion of ground motion effect for rectangular structures in Section 4.2 is also applicable for the dome type structure.

#### Example 4.3

A dome structure will be considered for a design overpressure of 75 psi. Assumed weapon yield is 20-MT. Figure 4.24 represents a typical dome.

Example 4.3 (continued)

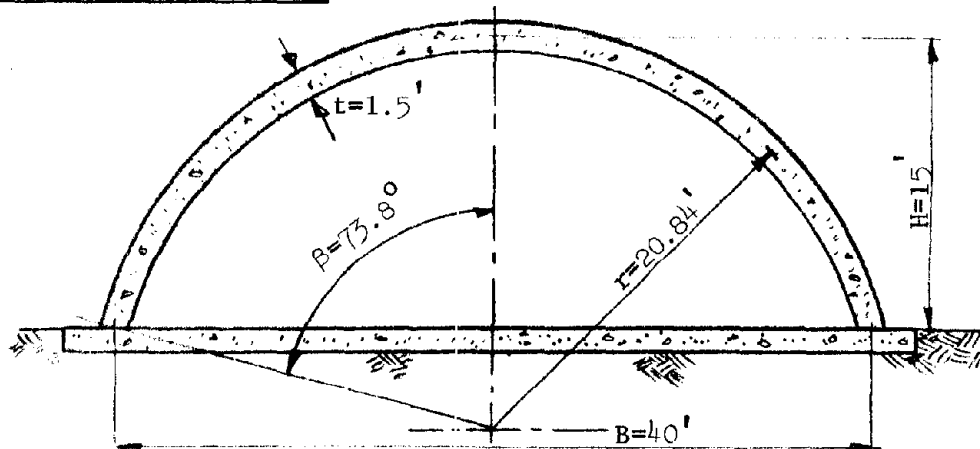


FIGURE 4.24

The necessary blast wave constants are (from Brode, Reference 3.1):

Overpressure

$$p_{so} = 75 \text{ psi} \quad D_p^+ = 2.4 \text{ sec} \quad t^+ = 1.3 \text{ sec.}$$

Dynamic pressure

$$p_{do} = 180 \text{ psi} \quad D_u^+ = 7.9 \text{ sec} \quad t^+ \approx 0.6 \text{ sec.}$$

Reflected pressure at the spring line

$$p_r = 4.5 \times 75 = 337 \text{ psi}$$

Dimensional factors for the structure are given in Figure 4.24. The weight of the structure is

$$W = 724,000 \text{ lbs}$$

The motion of the structure consists of three parts

1. Rigid body motion
2. Deformation responses of shell in the compression mode and flexural mode, and
3. Ground motion.

The response spectra for items mounted to the shell will be developed in this example. The base response is obtained as demonstrated for a rectangular structure.

Example 4.3 (continued)

The compression mode load characteristics are shown in Figure 4.25. The rise time ( $t_r$ ) to peak pressure  $p_{cmax}$  is

$$t_r = \left(1 - \frac{\beta}{\pi}\right) \frac{B}{U}$$
$$= \left(1 - \frac{73.8}{180}\right) \frac{40}{2550} = 0.00925$$

The peak pressure  $p_{cmax}$  is assumed to be equal to the peak overpressure  $p_{so} = 75$  psi.

The total time duration is the overpressure equivalent triangular pulse duration,

$$t^+ = 1.3 \text{ sec.}$$

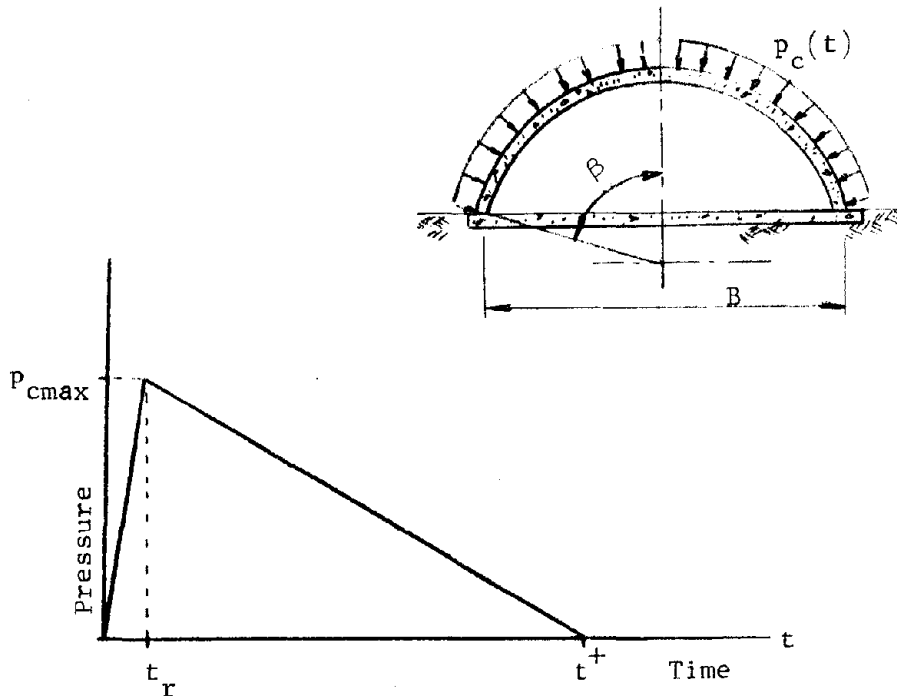


FIGURE 4.25



Example 4.3 (continued)

The flexural mode load characteristics are shown in Figure 4.26. The rise time to peak pressure is one half the transit time of the shock front across the structure:

$$\tau = \frac{B}{U} = \frac{40}{2550} = 0.0157$$

$$\frac{\tau}{2} = 0.00785$$

The clearing time for the reflected pressure is

$$\left(1 + 3 \frac{\beta}{\pi}\right) \tau = \left(1 + 3 \times \frac{73.8}{180}\right) 0.0157 = 0.035$$

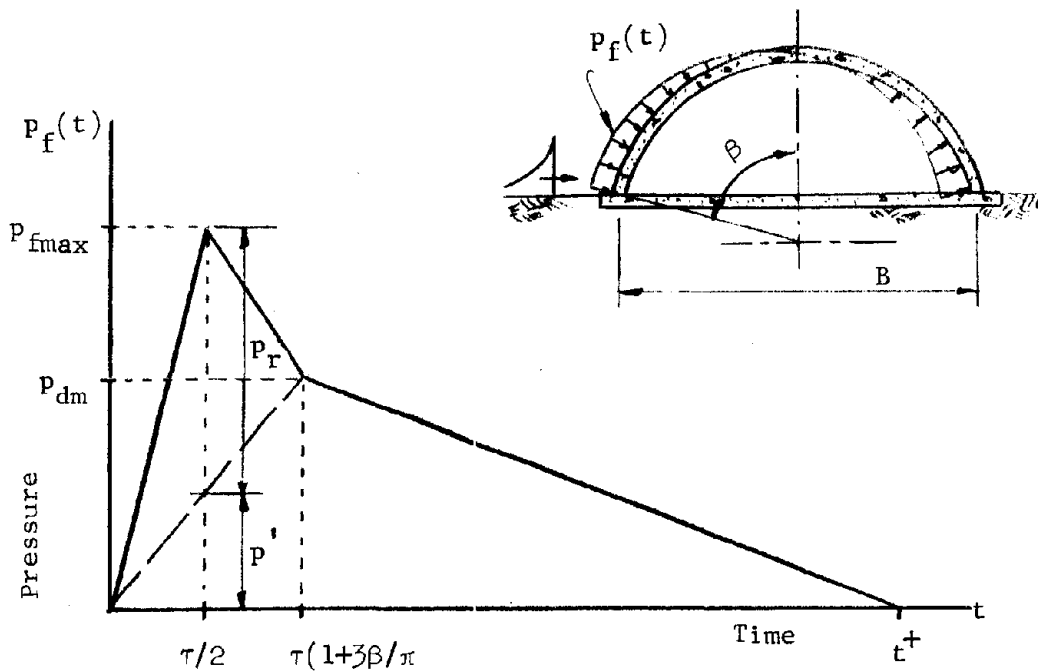


FIGURE 4.26

The maximum pressure at the clearing time (from Reference 4.13) is

$$p_{dm} = \frac{\beta}{\pi} C_d p_{do}$$

Example 4.3 (continued)

where

$$C_d = \text{drag coefficient} = 0.9 \text{ at the base of the windward side (assumed)}$$

$$\text{Thus, } P_{dm} = \frac{73.8}{180} \cdot 0.9 \times 180 = 66.4 \text{ psi}$$

The peak pressure at the springline is

$$\begin{aligned} P_{fmax} &= P_r + p' \quad (p' \text{ is shown in Figure 4.26}) \\ &= 337 + 66.4 \frac{0.00785}{0.035} = 337 + 14.9 \\ &= 352 \text{ psi} \end{aligned}$$

Accordingly, the flexural mode loading varies as

$$P_f = p_f(t) \sin(\beta - \psi) \cos \theta / \sin \beta$$

where  $p_f(t)$  is represented by the pulse shown in Figure 4.26.

The total time duration is the dynamic pressure equivalent triangular pulse duration  $t^+ = 0.6 \text{ sec.}$

(1) Horizontal rigid body motion: The acceleration-time history for the load and resistance is shown in Figure 4.27.

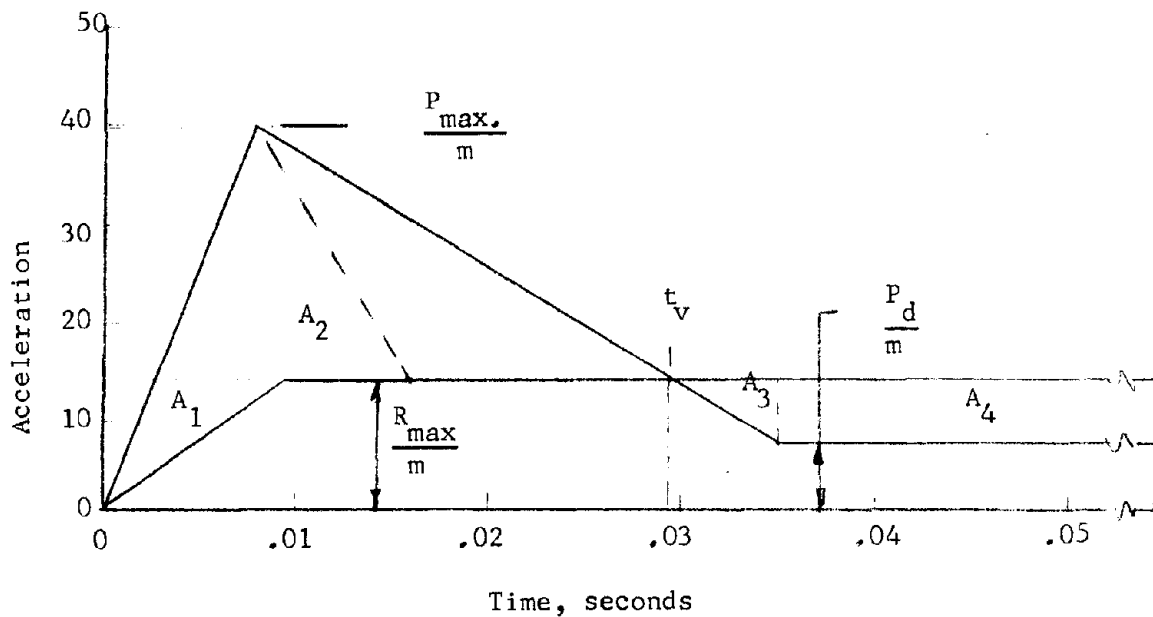


FIGURE 4.27

Example 4.3 (continued)

Only the flexural mode contributes a horizontal force and its maximum value is given by

$$\begin{aligned} P_{\max} &= \frac{P_{f\max} r^2}{\sin \beta} \int_0^{\psi = \beta} \int_0^{\theta = 2\pi} \sin^2(\beta - \psi) \cos^2 \theta \, d\theta \, d\psi \\ &= \frac{P_{f\max} r^2 \pi}{2 \sin \beta} (\beta - \sin^2 \beta) \\ &= \frac{352 \times 20.84^2 \times 144 \pi}{2 \times \sin 73.8^\circ} (1.29 - \sin 147.6^\circ) \\ &= 2.84 \times 10^7 \text{ lbs.} \end{aligned}$$

The maximum resistance is a function of the weight of the structure and the vertical component of the pressure, namely

$$\begin{aligned} R_{\max} &= (W + p_c A) C_f \\ &= (7.24 \times 10^5 + 1.36 \times 10^7) 0.7 \\ &= 1.003 \times 10^7 \text{ lb} \end{aligned}$$

The coefficient of friction  $C_f$  is assumed to be 0.7.

The maximum force at the clearing time of 0.035 sec is

$$P_{dm} = \frac{P_{dm}}{P_{f\max}} P_{\max} = \frac{66.4}{352} \times 2.84 \times 10^7 = .536 \times 10^6 \text{ lbs}$$

The peak forces in terms of acceleration are:

$$\frac{P_{\max}}{m} = \frac{2.84 \times 10^7}{7.24 \times 10^5} \text{ g} = 39.2 \text{ g}$$

$$\frac{R_{\max}}{m} = \frac{1.003 \times 10^7}{7.24 \times 10^5} \text{ g} = 13.9 \text{ g}$$

$$\frac{P_{dm}}{m} = \frac{.536 \times 10^6}{7.24 \times 10^5} \text{ g} = 7.4 \text{ g}$$

$$\frac{W}{m} C_f = 0.7 \text{ g}$$

Example 4.3 (continued)

By inspection of the acceleration-time curve, the maximum acceleration is

$$a'_h = \left( \frac{P-R}{m} \right)_{\max}$$

$$= (39.2 - 11.2) g = 28g$$

at time  $\frac{\tau}{2} = .00785$  sec.

The maximum velocity occurs at  $t_v = 0.0293$  sec and is obtained from

$$v'_h = A_1 + A_2 = 17.5 + 129.5 = 149 \text{ in/sec}$$

The maximum displacement occurs at  $t_d$

where  $A_1 + A_2 = A_3 + A_4$

Accordingly

$$A_1 = 17.5 \text{ in/sec and } t_d - t_1 = 0.085 \text{ sec}$$

$$A_2 = 130 \text{ in/sec and } t_d - t_2 = 0.076$$

$$A_3 = 7.5 \text{ in/sec and } t_d - t_3 = 0.056$$

$$A_4 = 141.5 \text{ in/sec and } t_d - t_4 = 0.027$$

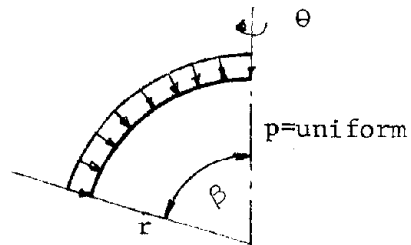
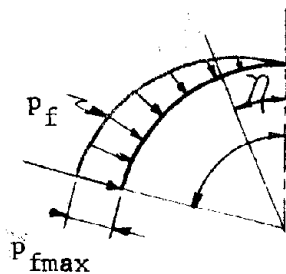
Therefore,

$$d'_n = \sum A_i \times \text{moment arm about } t_d = 0.089$$

$$= (1.49 + 9.85 - 0.42 - 3.82)$$

$$= 7.1 \text{ in.}$$

(2) Horizontal and vertical deformation response of the shell. An equivalent uniform radial pressure for each quadrant of the shell can be derived to simplify the calculation of the flexure mode response (see below).



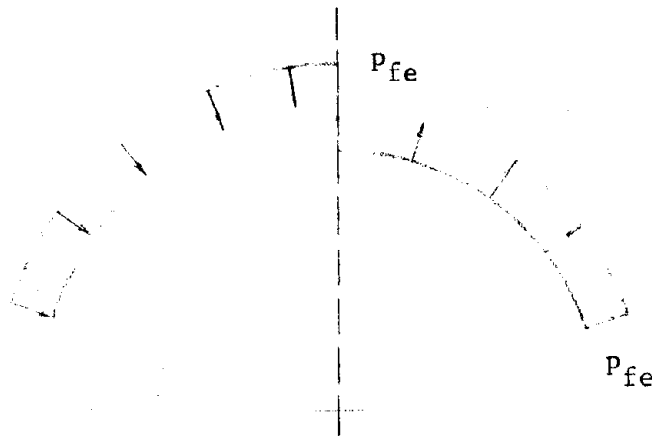
$$p_f = p_{fmax} \frac{\sin \eta \cos \theta}{\sin \beta}$$

Example 4.3 (continued)

Summing up the pressure over 1/4 the surface and equating it to a uniform pressure, the following equivalent pressure,  $p_{fe}$ , is obtained

$$P_{fe} = 0.47 P_{f(max)}$$

$$P_{fe} = 0.47 \times 352 = 165 \text{ psi}$$



The compression mode resistance is given by

$$q_c = 2 \left[ 0.85 f'_{cd} + 0.009 (\phi_t) f_y \right] \frac{t_c}{r}$$

and the flexural mode resistance is

$$q_f = \left[ 0.85 f'_{cd} + 0.009 (\phi_t) f_y \right] \frac{t_f}{r}$$

The terms in the equations are defined in Appendix B, Equations (B-9 and B-10)

$$f'_{cd} = 4 \text{ ksi} ; f_y = 52 \text{ ksi} ; \phi_t = 1 \text{ percent}$$

$t_c$  and  $t_h$  are the required shell thicknesses in each mode.

The quantity in brackets in the above two equations is

$$\begin{aligned} \left[ 0.85 \times 4000 + 0.009 \times 1 \times 52000 \right] &= (3.4 + .47) \times 10^3 \\ &= 3.87 \times 10^3 \text{ psi} \end{aligned}$$

Example 4.3 (continued)

Equating  $q_c$  to  $p_{so}$  and  $q_{fe}$  to  $1.25 p_{fe}$  the required thicknesses are:

$$t_c = \frac{p_{so} \times r}{2 \times 3.87 \times 10^3} = \frac{7.5 \times 2.50 \times 10^3}{7.74 \times 10^3} \approx 2.5 \text{ in.}$$

$$t_f = \frac{1.25 p_{fe} \times r}{3.87 \times 10^3} = \frac{1.25 \times 1.65 \times 25.0 \times 10^3}{3.87 \times 10^3} = 13.5 \text{ in.}$$

$$t_{\text{total}} = t_c + t_f = 16 \text{ in.}$$

The shell thickness used is 18 inches.

The actual resistances are then proportional to the ratio of the actual thickness to the required thickness.

$$q_c = \frac{18}{15.7} \times 75 = 86 \text{ psi} \qquad \frac{p_c}{q_c} = \frac{75}{86} = 0.82$$

$$q_f = \frac{18}{15.7} \times 1.25 \times 165 = 236 \text{ psi} \qquad \frac{p_{fe}}{q_f} = \frac{165}{236} = 0.7$$

The peak accelerations in each mode are:

Compression mode

$$a_1'' = \frac{p_{c\max}}{m} = \frac{75}{1.5 \times 150/144} = 48 \text{ g}$$

Flexural mode

$$\text{Using load - mass factor } K_{Lm} = \frac{3}{4}$$

$$a_2'' = \frac{165}{1.5 \times 150/144} \times \frac{4}{3} = 140 \text{ g}$$

The natural period of vibration (compression mode and flexure mode) is given by the approximation:

$$T = \frac{r}{2500} = \frac{20.84}{2500} = 0.00835 \text{ sec}$$

Therefore,

$$\omega_c = \omega_f = \frac{2\pi}{T} = 753 \text{ rad/sec}$$

Example 4.3 (continued)

Accordingly, the peak pseudo-velocities are

$$v_1'' = \frac{48 \times 386}{753} = 24.6 \text{ in/sec}$$

$$v_2'' = \frac{140 \times 386}{753} = 72 \text{ in/sec}$$

The pseudo elastic (or yield) displacements are:

$$d_{y_1}'' = 24.6/753 = .033''$$

$$d_{y_2}'' = 72/753 = .096''$$

The ratio of the pulse durations to the periods are high (greater than 10). Therefore the ductility ratios are determined from the response chart of Reference 4.10 to be:

in compression

$$\mu = 2.5$$

flexure

$$\mu = 1.8$$

$$d_1'' = .083 \text{ inch} \quad d_2'' = .173 \text{ inch}$$

These displacements are negligible compared to the ground induced displacements.

The max. resultant horizontal and vertical acceleration and velocity, from Equation (4.17); are:

$$a_v'' = a_h'' = .707 (48 + 140) = 133 \text{ g}$$

$$v_v'' = v_h'' = .707 (24.6 + 72) = 69 \text{ in/sec}$$

(3) Horizontal and vertical ground motions. Using the equations in Section 3.5, the peak ground motion intensities are computed at a 5 feet burial depth:

$$a_v = a_h = 75 \text{ g}$$

$$v_v = 37.5 \text{ in/sec} \quad v_h = 25 \text{ in/sec}$$

$$d_v = 21.25 \text{ inch} \quad d_h = 7.1 \text{ inch}$$

Example 4.3 (continued)

Accordingly, the induced motion to the structure are

$$v_v''' = 37.5 \text{ in/sec} \quad v_h''' = 25 \text{ in/sec}$$

$$d_v''' = 21.25 \text{ in} \quad d_h''' = 7.1 \text{ inch}$$

The vertical rigid body motion is now calculated.

This motion is a result of the compression mode loading. The idealized model is shown in Figure 4.28.

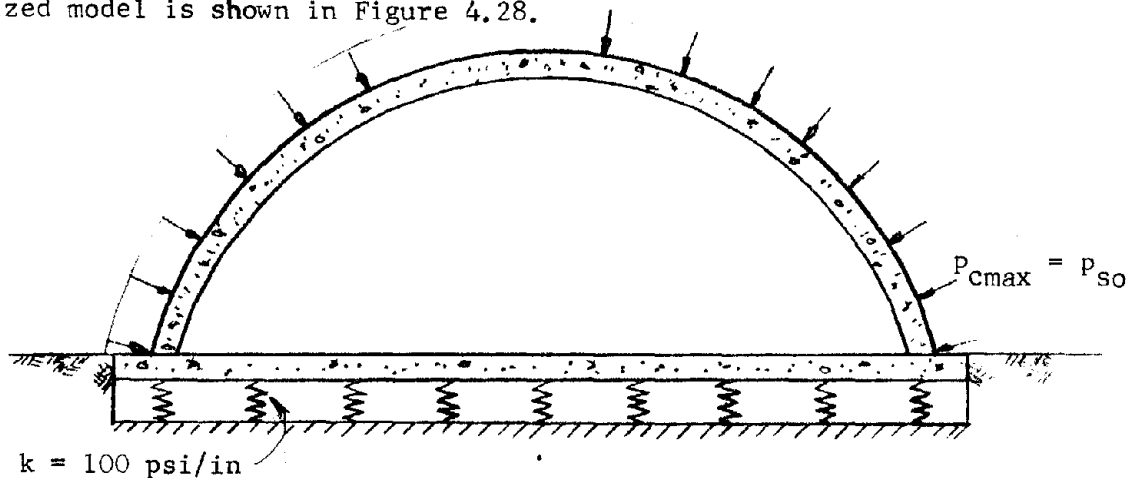


FIGURE 4.28

The total normal force is

$$\begin{aligned}
 P_{\max} &= P_{c\max} \int_0^{\beta} \cos(\beta - \psi) 2\pi r^2 \sin(\beta - \psi) d(\beta - \psi) \\
 &= \pi r^2 P_{c\max} \cos 2(\beta - \psi) \Big|_0^{73.8} \\
 &= \pi (20.84 \times 12)^2 75 \frac{1}{2} (1.845) = 1.36 \times 10^7 \text{ lb}
 \end{aligned}$$

The peak acceleration is:

$$a_v' = \frac{P_{\max}}{m} = \frac{1.36 \times 10^7}{7.24 \times 10^5} g = 18.8 g$$



Example 4.3 (continued)

Total stiffness of the soil

$$K = 144 \text{ k} \pi \left(\frac{B}{2}\right)^2 = 1.81 \times 10^7 \text{ lb/in}$$

Natural frequency

$$\omega = \sqrt{\frac{K}{m}} = \sqrt{\frac{1.81 \times 10^7 \times 386}{7.24 \times 10^5}} = 98.3 \text{ rad/sec}$$

The peak pseudo-velocity is

$$v_{\text{pk}} = \frac{a}{\omega} = \frac{18.8g}{98.3} = 73.8 \text{ in/sec} = 6.3 \text{ fps}$$

The separate responses that must be combined to envelope the response for items mounted to the shell are given in Table 4.7 and the root mean square resultants are given in Table 4.8.

Table 4.7

	Acceleration g			Velocity in/sec			Displacement in		
	a'	a''	a'''	v'	v''	v'''	d'	d''	d'''
Vertical	19	133	0	74	69	38	0	0	21
Horizontal	28	133	0	149	69	25	7	0	7

Table 4.8

	Acceleration g	Velocity in/sec	Displacement in
Vertical	135	108	21
Horizontal	135	166	10

The spectra bounds are (based on the amplification factors used previously in this report)

Vertical

- A = 270 g
- V = 162 in/sec
- D = 21 inch

Horizontal

- A = 270 g
- V = 250 in/sec
- D = 10 inch

The horizontal and vertical shock spectras are plotted in Figure 4.29.

Example 4.3 (continued)

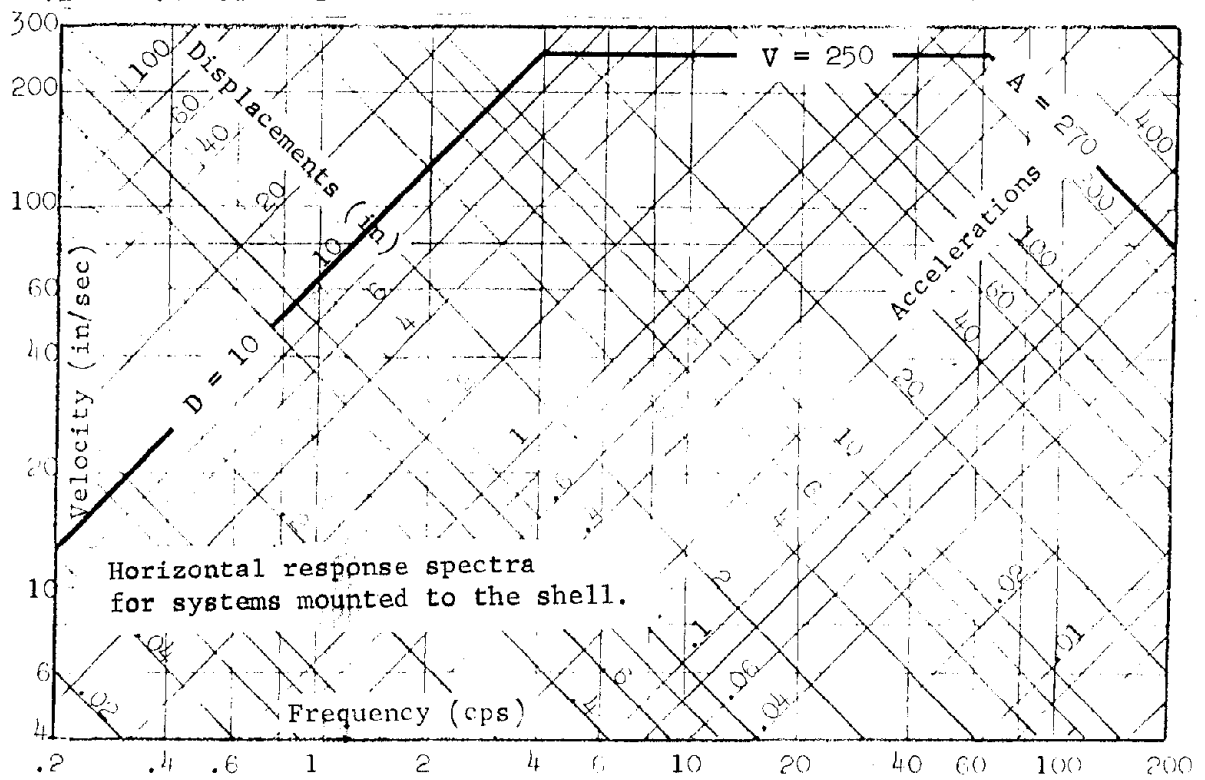
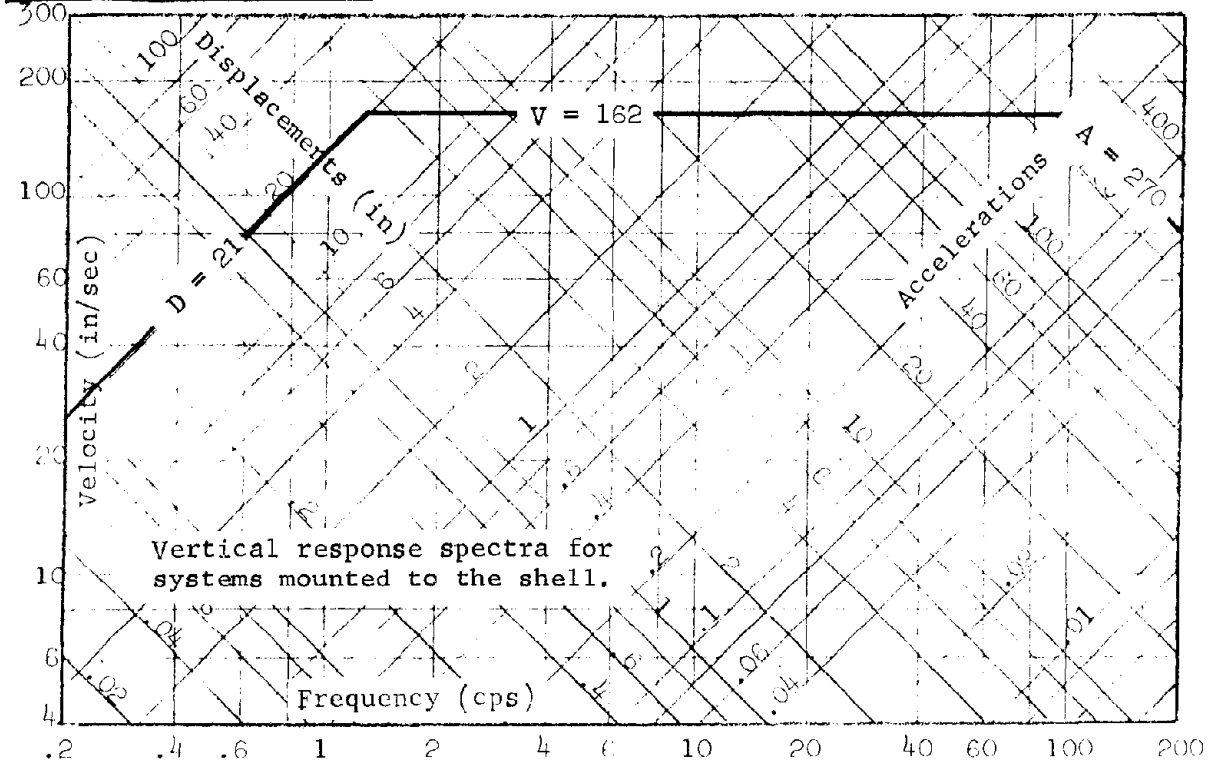


FIGURE 4.29  
222

4.2.5 Two-story steel frame structure. A steel framed structure can be designed to survive only low overpressure levels. The peak values of acceleration, velocity, and displacement, due to rigid body motion, are obtained in the same way as in the case of concrete structures. The horizontal deformation mode of importance is the flexible frame instead of the wall element. An example of a two-story framed structure will be used to illustrate how the peak frame deformation response can be obtained in an approximate manner for use in plotting shock spectra for systems attached to the structure.

Example 4.4

In the example of Figure 4.30, the structure is assumed to be designed to survive a 5 psi environment due to a 20-MT contact surface burst. The lateral loads are transmitted to the foundation by moment resisting frames on 8 feet centers. The two-mass system's horizontal deformational response will be analysed by the normal mode method. The blast wave constants are (from Brode, Reference 2.9)

Overpressure;

$$p_{so} = 5 \text{ psi} \quad D_p^+ = 6.8 \text{ sec} \quad t^+ = 6 \text{ sec}$$

Reflected Pressure:

$$p_r = 2.3 \times 5 = 11.5 \text{ psi}$$

Dimensional and inertia factors for the structure are given in Figure 4.30. Assumptions:

(1) Consider a two-story symmetrical frame structure as a lumped two-mass system with the weights of the columns evenly distributed at the two floors.

(2) The uniformly distributed pressure forces are, therefore, applied as concentrated horizontal forces at each floor level.

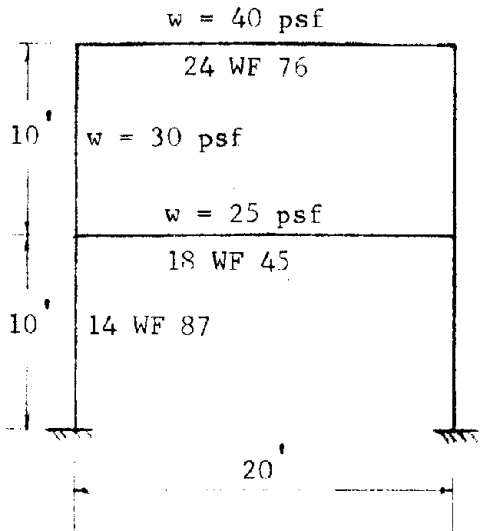
Total horizontal force carried by a column is

$$11.5 \times 8 \times 12 = 1104 \text{ lbs/in height}$$

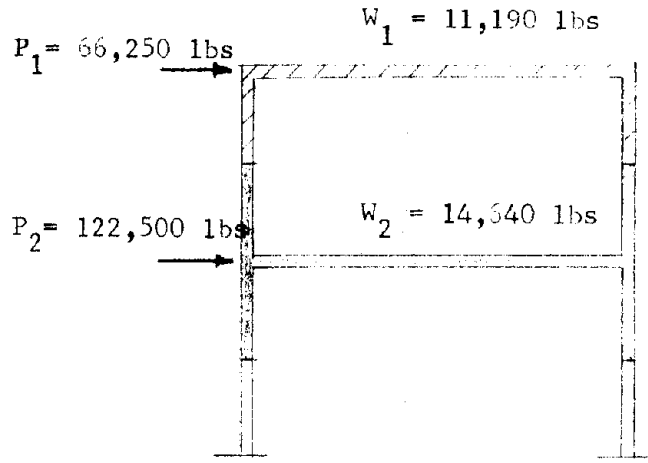
If the girder stiffnesses are very large compared to those of the columns, the appropriate column stiffnesses are given by:

$$k_{11} = k_{21} = k_{12} = 24 EI/L^3 \quad ; \quad k_{22} = 48 EI/L^3$$

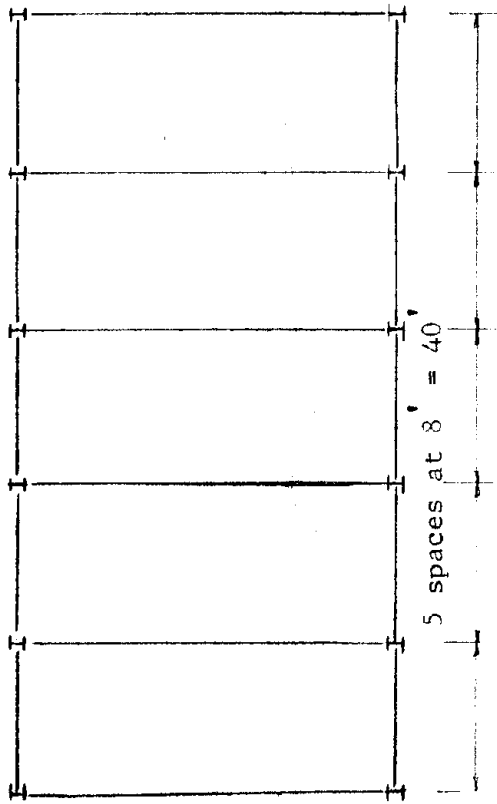
Example 4.4 (continued)



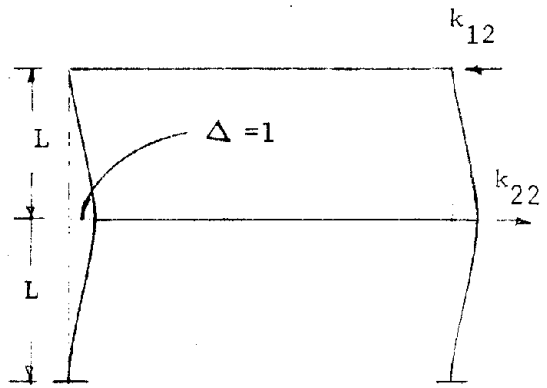
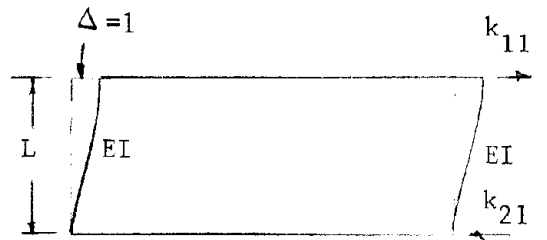
(a) Section



(c) Equivalent Loads



(b) Plan



$$k_{11} = \frac{24 EI}{L^3} = -k_{21} = -k_{12}$$

$$k_{22} = \frac{-48 EI}{L^3}$$

(d) Equivalent Stiffnesses

FIGURE 4.30

Example 4.4 (continued)

where the stiffness notation is as follows:

$k_{11}$  = stiffness reaction at level 1 due to a unit displacement at level 1 (no rotation permitted)

$k_{21}$  = stiffness reaction at level 2 due to unit displacement at level 1 (no rotation permitted)

and a harmonic response in frequency,  $\omega$ , of the two mass system's horizontal motion is governed by\*

$$\omega^2 \begin{bmatrix} m_1 & 0 \\ 0 & m_2 \end{bmatrix} \begin{pmatrix} x_1 \\ x_2 \end{pmatrix} - \begin{bmatrix} k_{11} & k_{12} \\ k_{21} & k_{22} \end{bmatrix} \begin{pmatrix} x_1 \\ x_2 \end{pmatrix} = 0$$

Solving for the frequency eigenvalues,  $\omega_1^2$  and  $\omega_2^2$ , from the characteristic determinant, we find that

$$(\omega^2)_{1,2} = \frac{12 EI}{L^3} \left\{ \frac{(2 m_1 + m_2)}{m_1 m_2} \pm \sqrt{\frac{(2 m_1 + m_2)^2}{(m_1 m_2)^2} - \frac{4}{m_1 m_2}} \right\}$$

Using the numerical values,

$$\left. \begin{array}{l} E = 30 \times 10^6 \text{ psi} \\ \frac{I}{L} = 8 \text{ in}^3 \end{array} \right\} \begin{array}{l} \frac{EI}{L^3} = \frac{30 \times 10^6 \times 8}{120^2} = 1.67 \times 10^4 \text{ lbs/in} \\ k_{12} = 4.0 \times 10^5 \text{ lbs/in}, \quad k_{22} = 8.0 \times 10^5 \text{ lbs/in} \end{array}$$

$$\left. \begin{array}{l} m_1 = 26.8 \text{ lbs sec}^2/\text{in} \\ m_2 = 33.5 \text{ lbs sec}^2/\text{in} \end{array} \right\} \begin{array}{l} m_1 m_2 = 900 \\ 2 m_1 + m_2 = 87 \end{array} \quad \frac{2 m_1 + m_2}{m_1 m_2} = 0.097$$

The two eigenvalues or natural circular frequencies become

$$\omega_1 = 72 \text{ rad/sec}$$

$$\omega_2 = 182 \text{ rad/sec}$$

\* The matrix method is described in Appendix A.

Example 4.4 (continued)

If the girder flexibilities had been included, the calculated frequencies would have been

$$\omega_1 = 44 \text{ rad/sec}$$

$$\omega_2 = 162 \text{ rad/sec}$$

It is seen that the errors in  $\omega_1$  and  $\omega_2$  are not negligible when the girders are treated as rigid. The somewhat more involved analysis, in which girder flexibility has been included, is described in Reference 4.14. In this example, the purpose is to illustrate the method of developing shock spectra for the structure mounted systems, and the simpler assumptions of stiff girders are therefore used. The normal mode amplitudes or eigenvectors  $\begin{pmatrix} x_1 \\ x_2 \end{pmatrix}$  can now be obtained by substituting the frequencies or eigenvalues into the characteristic determinant, and we obtain

$$\omega^2 m_1 x_1 - 4 \times 10^5 (x_1 - x_2) = 0$$

Normalizing this expression by placing  $x_1 = 1$  unit, we find

$$x_2 = \frac{4 \times 10^5 - \omega^2 m_1}{4 \times 10^5}$$

Since,  $\omega_1^2 = 5200$ , and  $m_1 = 26.8$ ,

$$x_2 = \frac{4 \times 10^5 - .52 \times 2.68 \times 10^5}{4 \times 10^5} = 0.65 \text{ unit}$$

Also for  $\omega_2^2 = 33,000$ ,

$$x_2 = \frac{4 \times 10^5 - 3.3 \times 2.68 \times 10^5}{4 \times 10^5} = 1.2 \text{ units}$$

The normalized amplitudes or eigenvectors are then described by the modal matrix,  $\beta$

$$\beta = \begin{bmatrix} 1 & 1 \\ 0.65 & -1.2 \end{bmatrix}$$

Example 4.4 (continued)

The normal mode responses can now be obtained from the normal mode equations (See Appendix A and Reference 4.14).

$$[\beta]^T [m] [\beta] (\ddot{\eta}) + [\beta]^T [k] [\beta] (\eta) = [\beta]^T \begin{pmatrix} P_1 \\ P_2 \end{pmatrix}$$

The generalized mass is

$$[M] = [\beta]^T [m] [\beta] = \begin{bmatrix} 41 & 0 \\ 0 & 74 \end{bmatrix}$$

The generalized force is

$$(N) = [\beta]^T \begin{pmatrix} P_{1\max} \\ P_{2\max} \end{pmatrix} = \begin{pmatrix} 146,250 \\ -83,750 \end{pmatrix}$$

At time  $t = 0$ , the normal mode accelerations are ( $[k] = 0$  at  $t = 0$ )

$$\begin{bmatrix} 41 & 0 \\ 0 & 74 \end{bmatrix} \begin{pmatrix} \ddot{\eta}_1 \\ \ddot{\eta}_2 \end{pmatrix} = \begin{pmatrix} 146,250 \\ -83,750 \end{pmatrix}$$

$$\ddot{\eta}_1 = \frac{146,250}{41} = 3580 \text{ in/sec}^2 = 9.3 \text{ g}$$

$$\ddot{\eta}_2 = \frac{-83,750}{74} = -1130 \text{ in/sec}^2 = -2.93 \text{ g}$$

Transferring back to the coupled coordinate system

$$\ddot{\mathbf{x}} = [\beta] (\ddot{\eta}),$$

it is found that

$$\begin{pmatrix} \ddot{x}_1 \\ \ddot{x}_2 \end{pmatrix} = \begin{bmatrix} 1 & 1 \\ 0.65 & -1.2 \end{bmatrix} \begin{pmatrix} \ddot{\eta}_1 \\ \ddot{\eta}_2 \end{pmatrix}$$

Accordingly,

$$\ddot{x}_1 = \ddot{\eta}_1 + \ddot{\eta}_2$$

$$\ddot{x}_2 = 0.65 \ddot{\eta}_1 - 1.2 \ddot{\eta}_2$$

Example 4.4 (continued)

Substituting the values for  $\ddot{\eta}_1$  and  $\ddot{\eta}_2$

$$\ddot{x}_1 = 9.30g - 2.93g = 6.37 g$$

The upper bound values are:

$$\underline{12.23}$$

$$\ddot{x}_2 = 0.65 (9.3)g - 1.2 (-2.93)g = 9.55g$$

$$\underline{9.55}$$

The peak pseudo-velocity and displacement can be approximated by the following expressions:

The upper bound values are:

$$\dot{x}_1 = \frac{\ddot{\eta}_1}{\omega_1} + \frac{\ddot{\eta}_2}{\omega_2} = \left(\frac{3580}{72}\right) + \left(\frac{-1130}{182}\right) = 50 - 6.2 = 43.8 \quad \underline{56.2 \text{ in/sec}}$$

$$\dot{x}_2 = \frac{0.65 \ddot{\eta}_1}{\omega_1} - \frac{1.2 \ddot{\eta}_2}{\omega_2} = 32.5 + 7.5 = 40 \text{ in/sec} \quad \underline{40 \text{ in/sec}}$$

$$x_1 = \frac{\ddot{\eta}_1}{\omega_1^2} + \frac{\ddot{\eta}_2}{\omega_2^2} = 0.7 - .034 = 0.66 \text{ inches} \quad \underline{0.73 \text{ in.}}$$

$$x_2 = \frac{0.65 \ddot{\eta}_1}{\omega_1^2} - \frac{1.2 \ddot{\eta}_2}{\omega_2^2} = 0.45 + .04 = 0.49 \text{ inches} \quad \underline{0.49 \text{ in.}}$$

If the girder flexibilities had been taken into account, the peak acceleration response would not have been significantly different, but the peak displacement response would have been much greater. Repeating the steps above for the flexible girder case with

$$\omega_1 = 43 \text{ rps} \quad \text{and} \quad \omega_2 = 162 \text{ rpd}$$

$$\ddot{\eta}_1 = \frac{127,500}{35.2} = 3630 \text{ in/sec}^2 = 10.3 g$$

$$\ddot{\eta}_2 = \frac{-139,500}{90} = 1550 \text{ in/sec}^2 = -4.0 g$$



Example 4.4 (continued)

and

	<u>Upper bound values are:</u>
$\ddot{x}_1 = 6.3 \text{ g}$	<u>14.3 g</u>
$\ddot{x}_2 = 11.65 \text{ g}$	<u>11.65 g</u>
$\dot{x}_1 = 75.5 \text{ in/sec}$	<u>94.5 in/sec</u>
$\dot{x}_2 = 58 \text{ in/sec}$	<u>58 in/sec</u>
$x_1 = 1.94''$	<u>2.06''</u>
$x_2 = 1.1''$	<u>1.1''</u>

The results of the above analyses are compared with the exact solution, Case III.

	<u>Case I</u>	<u>Case II</u>	<u>Case III</u>
	Girders stiff peak response based on acceleration at time $t = 0$ (absolute values)	Girders flexible peak response based on acceleration at time $t = 0$ (absolute values)	Girders flexible peak response calculated
Peak Acceleration			
$\ddot{x}_1$	12.23 g	14.3 g	9.0 g
$\ddot{x}_2$	9.55 g	11.65 g	10.5 g
Peak Velocity			
$\dot{x}_1$	56.2 in/sec	94.5 in/sec	25 in/sec
$\dot{x}_2$	40 in/sec	58 in/sec	34.5 in/sec
Peak Displacement			
$x_1$	0.73 in	2.06 in	2.5 in
$x_2$	0.49 in	1.1 in	1.4 in

#### Example 4.4 (continued)

From this summary, it can be concluded that Case I gives acceptable values for peak acceleration and velocity, but peak displacements are too low. Case II gives acceptable values for all three response parameters (within 20 percent of the calculated values shown for Case III).

The horizontal rigid body motions may be combined with the above motions by the root mean square procedure. The horizontal shock spectra for items mounted to the roof and to the top of the columns would be based on motions of mass,  $m_1$ , combined with rigid body motion; for items mounted to the 2<sup>nd</sup> floor level and to intermediate heights of the columns, the horizontal shock spectra would be based on the motion of  $m_2$  combined with rigid body motion.

The deformation response of the girders in the vertical direction is obtained in the same manner as previously explained for concrete structures.

#### 4.3 Partially Buried Structures

Partially buried structures have earth mounds on all sides of the structure, and are distinguished from shallow buried structures by the amount of cover over the structure and the slope of the mound. Figures 4.31 and 4.32 show the required coverage for fully buried rectangular structures and dome structures, as well as normal coverage for partially buried structures.

The structure motions will be a combination of the rigid body motion and deformation motions of the parts of the structure exposed to the direct air blast.

As a general guideline, rectangular structures may be considered partially buried, if as a minimum they have a mound of 1 to 2 slope beginning at the  $H/2$  level. Flatter slopes beginning above  $H/2$  will result in earth cover conditions approaching those of shallow-buried structures (see Figure 4.34). Also, for domed structures, a nominal cover over the

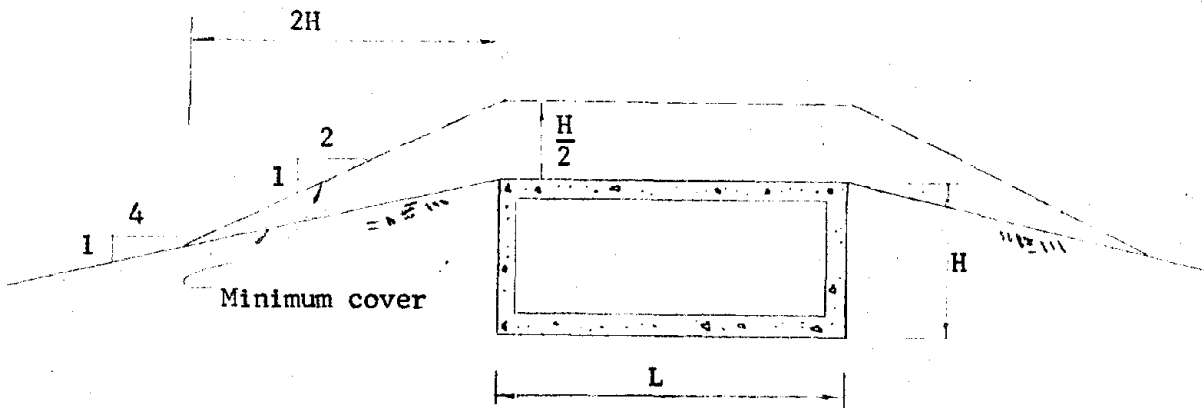


FIGURE 4.31

crown and a mound slope of 1 to 2 as a minimum will constitute a partially buried condition.

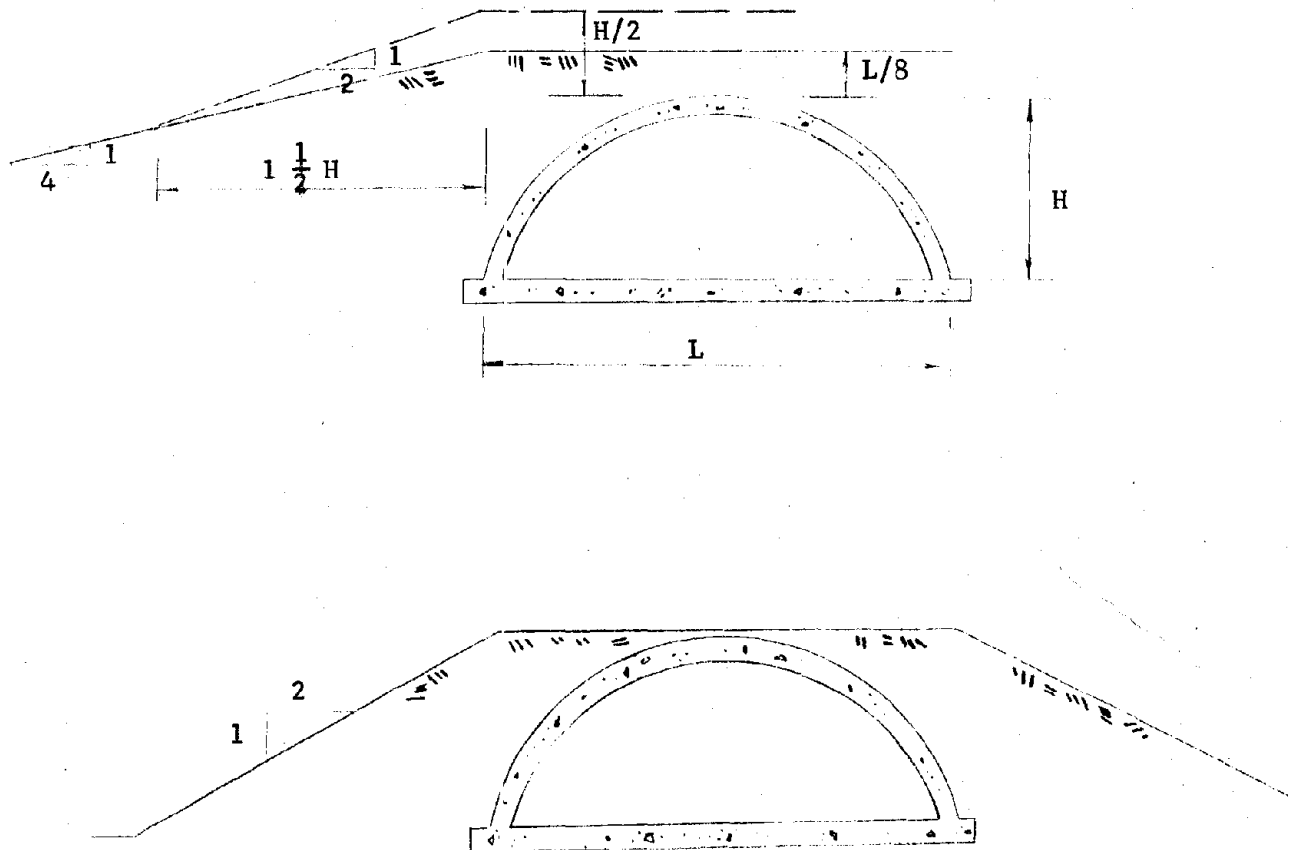


FIGURE 4.32

#### 4.3.1 Mounded rectangular structures (Figure 4.31)

(1) Rigid body motion. For very flat slopes (greater than 1 to 2), the rigid body motion of the structure relative to the ground is negligible. The mound and structure may be assumed to have a dome shape as shown in Figure 4.33, moving together in the horizontal direction, due to the horizontal component of the air blast on the mound. The procedure described in Section 4.2.4 is, therefore, applicable for calculating rigid body motion of the structure and the earth mound.

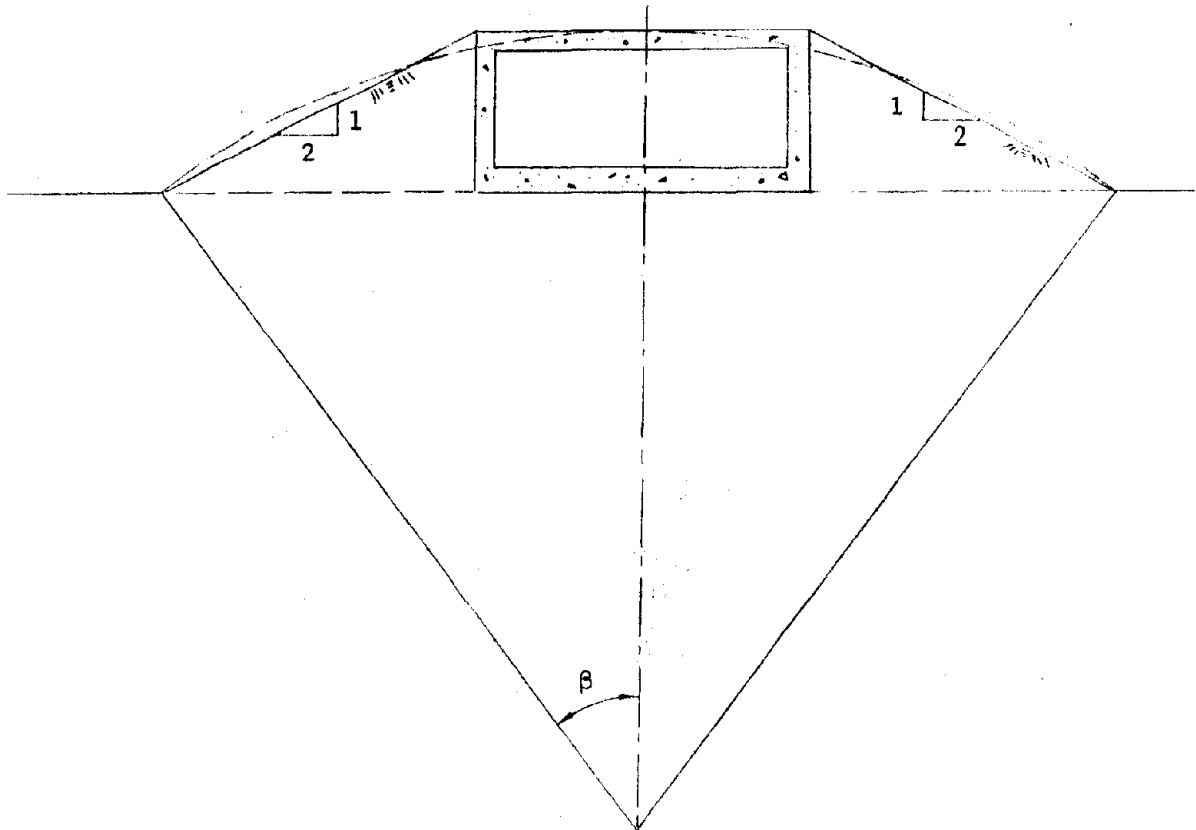


FIGURE 4.33

If it is justified to assume that the structure's overall properties (compressibility, etc.) are roughly similar to those of the soil, the structure's motions can be taken as the peak ground motions at the average depth of the structure. (This assumption will be more fully discussed in Subsection 4.4, Shallow Buried Structures.)

(2) Deformation response due to air blast

Wall: The reflected pressure on the wall is reduced by a factor dependent on the mound angle (angle of incidence). For a slope of 1 to 2, the reflection factor is:

$$\frac{P_r}{P_{so}} < 2 \text{ for all overpressure levels}$$

By use of the method described in Section 4.2.2, the motion of the wall can be determined for the revised reflected pressure.

Roof Slab: The roof slab deformation motion is the same as the deformation motion for the aboveground structures (Section 4.2.2).

Base Slab: The base slab deformation motion due to the slap of the air blast on the roof cannot be distinguished from the ground induced motion. An assumption that the structure moves with the ground will account for the total inertia load to parts of the structure not exposed to the direct air blast.

(3) Rigid body motion due to ground motion. The direct air blast induced ground motion is accounted for under heading (1) of this subsection. If the air blast is superseismic, then the shock spectra based on peak motions described in (1) and (2) above is adequate. For the outrunning condition, a ground induced motion of the structure may take place slightly ahead of the air blast induced motions, thus, resulting in an increase in the shock response of the items mounted to the structure. (Section 4.4 on Shallow Buried Structures will define motions due to outrunning that should be added to motions under headings (1) and (2) above, for plotting the shock spectra envelope).

4.3.2 Mounded dome structures. The stream-line shape of the dome and earth mound will minimize the relative motions of the structure with respect to the ground; and it may be assumed that the structure will move with

the ground. The effective load on the dome will have a small increase in rise time due to the earth mound; and the motions of the partially buried dome may be considered to be the same as that of a shallow buried structure.

#### 4.4 Shallow Buried Structures

The minimum soil coverage shown in Figures 4.31 and 4.32 define the minimum soil mound for the classification of shallow buried structures. The depth of earth cover, at which structures are no longer considered shallow buried, but deep buried, is in the order of 100 feet.

Air-blast-induced and crater-induced ground motions are both important considerations. If the soil is layered, the underlying media will often be hard strata that will serve as wave guides for the crater induced motions. In overpressure regions of 100 psi to 1000 psi and for weapon yields greater than 1 MT, the motions of a shallow-buried structure will be the result of:

- (1) Air blast induced dilatation and shear waves through the soil directly above the structure, blast slap.
- (2) Crater induced motions through the hard layers.
- (3) Air blast induced refracted-reflected waves in the layered soil.

These effects are discussed in Section 3. The complete ground motion history, when shock spectra techniques are being used, can be described by a shock spectra envelope that involves larger amplification factors to account for outrunning motions, that may have been critically phased with the air blast slap motions. In Section 3 on Input Motions, these factors, as well as pulses to be used as input waveforms, have been discussed; they should be used in the design of in-structure shock isolation systems.

4.4.1 Shock spectra approach. Three basic types of structures will be considered; a rectangular structure with very little earth cover over the roof slab, a cylindrical structure with substantial earth cover, and a cylindrical silo with its top flush with grade.

The shock spectra method will assume that the structure motion is the same as the ground motion, i.e., the flexibility of the structure is neglected. Most structures designed to survive the high stresses induced by the air blast will be stiffer than the soil media; and, therefore, in some cases this assumption may not be conservative. The more specific method will use the free-field motions in the form of pulses (defined in Section 3) that are applied to a soil - structure model, a model that will include the flexibility of the structure. When the structural enclosure is designed to yield at a specified overpressure level, the high frequency response of its in-structure systems will be attenuated significantly, if the structural enclosure's frequency in its first deformational mode lies in the intermediate frequency region. (A shallow buried rectangular structure may fall in this category). In this case, the shock spectra for the in-structure systems will be modified to account for flexibility and yielding of the structural enclosure. Most shallow buried structures will be in a soft soil layer with a hard underlying layer. Therefore, response spectra for in-structure systems should normally be based on the assumption that the structure is located in a layered media (unless specific soil data is available indicating a relatively homogeneous media to a large depth below the structure).

4.4.2 Rectangular buried structures. This type of structure is normally feasible at moderately low overpressure levels (less than 100 psi) and at shallow burial depths. The rigid body motion of the structure can be taken as approximately equal to the ground motion predicted at the average depth of the structure (see Figure 4.34).

Since the roof slab is usually close to the ground surface, it will respond to the impingement of the air blast, in addition to the rigid body motion of the structure. The rigid body motion may be considered as an input to the bottom slab communicated by the downward motion of the walls, and it may be taken equal to the initial ground motion. The response of the roof slab will then be an initially upward deformation. If this deformation is in phase with the air blast effect, which results in an initially downward deformation of the roof slab, the combined effect

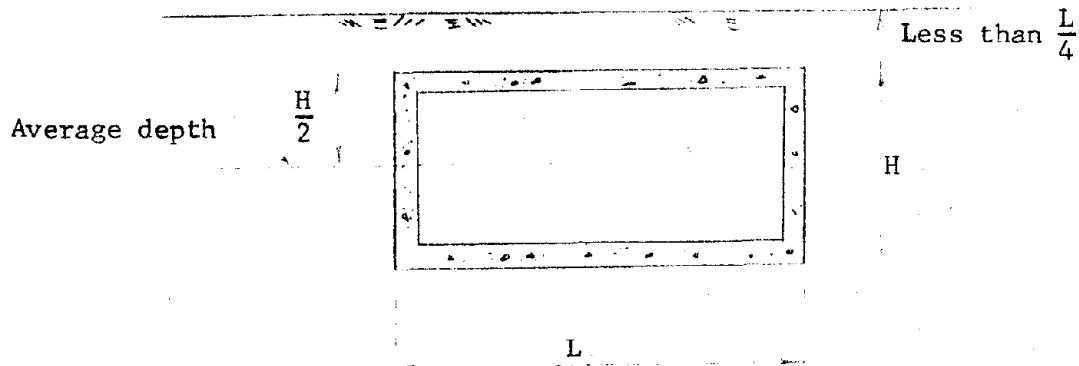


FIGURE 4.34

will be less than the larger of the two effects. The peak vertical acceleration may, therefore, be taken conservatively as

either

$$a = \frac{p_{so}}{m K_{Lm}}$$

where  $m$  = mass of the roof slab  
 $K_{Lm}$  = load mass factor for roof slab

or

$$a = a_v$$

where  $a_v$  = peak vertical ground acceleration at the average depth

whichever is greater.

The peak vertical pseudo-velocity is

either

$$v = \frac{a}{\omega} ;$$

$\omega$  = circular frequency of the roof slab

or

$$v = v_v ;$$

$v_v$  = peak vertical ground velocity at the average depth

whichever is greater.

The peak vertical displacement,  $d$ , can be taken as the ground displacement, since the roof slab response displacements are negligible compared to the ground displacements.

The above method will be a reasonable approximation when the air blast wave is superseismic with respect to the waves traveling through the ground.



In an outrunning condition, however, the initial ground motion may be upward and may slightly lead the arrival of the air blast on the roof slab, thus, inducing a combined response which may exceed the separate responses. An upper bound for this condition is the algebraic sum of the two peak values; the vertical shock spectra for items mounted to the roof slab are often based on this combined value.

(a) Elastic response of the structure. It is usually assumed that a buried structure moves as a rigid body with intensities of displacement, velocity and acceleration (at all points on the structure) equal to the free-field ground motions at some effective depths. The flexible elements of the structure, such as beams, slabs, or shell segments, may be excited at their natural frequencies during this rigid body motion. To assess the complete effect of flexibility of the structure in altering the input motion to systems attached to the structure, the numerical methods outlined in Appendix F would have to be used.

The flexibility of the structure will influence primarily the peak acceleration input to rigid mounted systems. Let us consider a buried rectangular structure with equipment mounted to the bottom slab as shown in Figure 4.35a. The bottom slab is usually designed to resist the ground

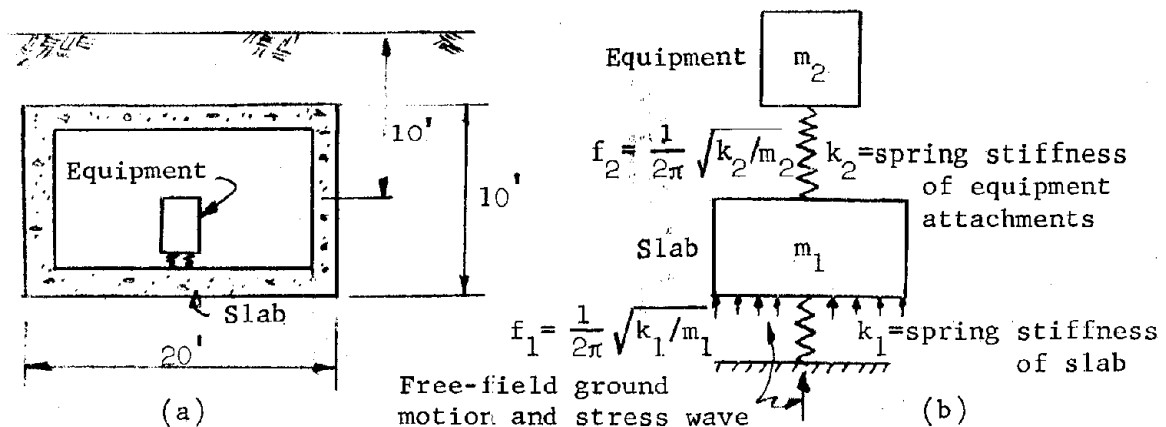


FIGURE 4.35

motion vertical stress wave based on response in the fundamental frequency mode. If the equipment mass is small relative to the structure bottom slab

mass, then the slab can be assumed to be an SDOF system with a response bounded by the shock spectra envelope defined in Section 3.7. Consequently, the two-mass model shown in Figure 4.35b can be considered as a simplified model of the equipment attached to the structure slab in Figure 4.35a and the method suggested in Section 2.4.2 may be used to derive a spectra bound for designing the equipment attachment mounts. The following example illustrates this technique.

Example 4.5

We consider the structure in Figure 4.35a at a 25 psi overpressure location (weapon yield 10 MT). An equipment is hard mounted at the center of the slab; and the assumed characteristics of this equipment and mount give a frequency,  $f_2 = 40$  cps. The natural frequency of the bottom slab,  $f_1$ , as an equivalent single-degree-of-freedom element, is equal to 13 cps. A shock spectra envelope for an SDOF system responding to the free-field vertical ground motions is assumed to be bounded by the two straight lines,  $V = 18$  ips and  $A = 25g$ , in the mid-frequency and high frequency region. This envelope is based on the free-field ground motion at a depth of 10 feet. In this shock spectra envelope, plotted in Figure 4.36, neglecting the equipment weight, the vertical response of the slab is found to be

$$A_1 = 3.8 \text{ g}$$

$$V_1 = 18 \text{ in/sec}$$

These peak values may be assumed to constitute the input to the equipment attachments. The response of  $m_2$  in the high frequency region is then bounded by the straight line

$$A_2 = 2 A_1 = 7.6 \text{ g}$$

as given by the procedure summarized in Section 2.4.2.

In this example, the figure shows that the peak acceleration response,  $A_2$ , of the equipment at  $f_2 = 40$  cps is

$$A_2 = 7.6 \text{ g}$$

instead of the 13 g's given by the shock spectra envelope based on free-field ground motion peak intensities.

Example 4.5 (continued)

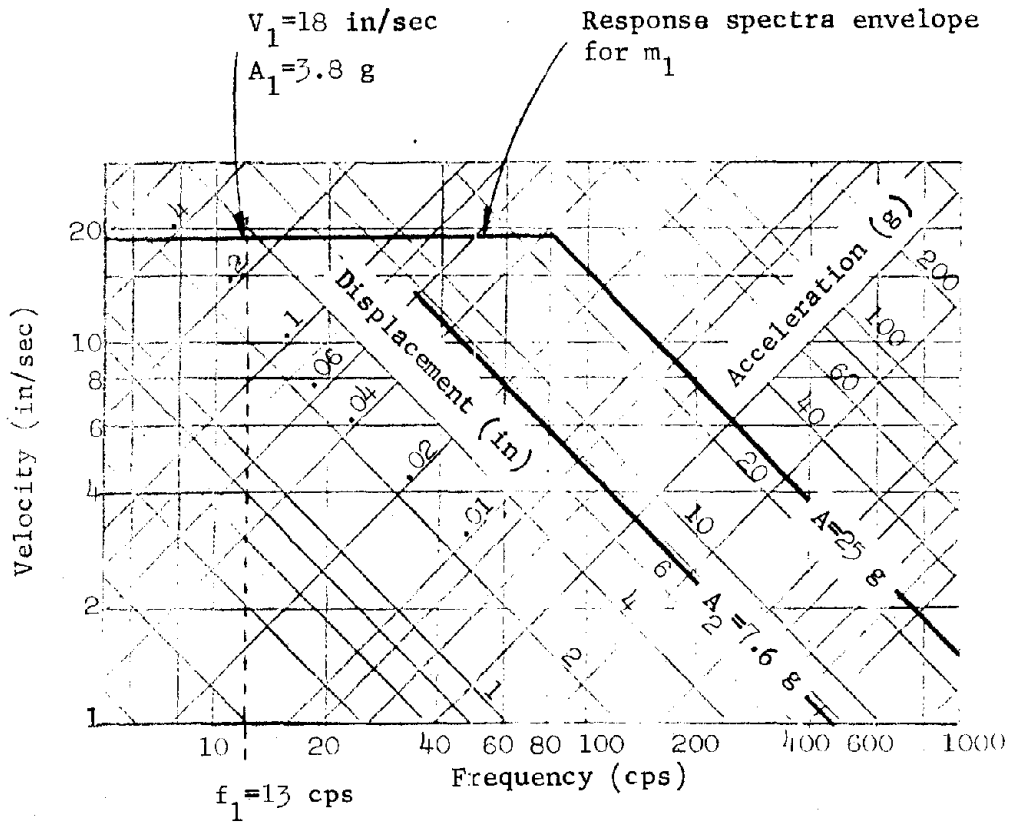


FIGURE 4.36

(b) Elastic-plastic behavior of the structure. If the structure yields at the specified overpressure region, then the acceleration response of items mounted to the structure will be less than the corresponding acceleration response for a non-yielding structure. In the model shown in Figure 4.35b, the spring element representing the slab is now idealized to represent an elastic-plastic hysteretic spring. It is seen in Reference 4.20 that yielding in the first spring will reduce the maximum deformation in the second spring, especially when  $f_2/f_1 = 1$  (for  $m_2/m_1 \ll 1$ ). The reduction factor is not constant, but varies with the ratio of  $f_2/f_1$  for a particular  $m_2/m_1$  ratio. Therefore, general conclusions cannot be drawn

Example 4.5 (continued)

about the response bound on  $m_2$  (the equipment) when the first spring,  $k_2$  (the slab), is elastic-plastic. However, when  $f_2/f_1 > 1$ , and  $m_2/m_1 \ll 1$ , we can bound the acceleration response of  $m_2$  in the following way:

- (1) Construct the elastic-plastic shock spectra envelope from the elastic-spectra bound by the method suggested in Section 2.4.3 for the  $\mu$  value used for design of the structure element that supports the equipment.
- (2) At the frequency of the first spring system,  $f_1$ , determine the acceleration response,  $A_1$ , of the first mass.
- (3) The relative response of the mass,  $m_2$ , (the equipment) in the region,  $f_2/f_1 > 1$ , will be bounded by the constant acceleration line,  $A' = 2 A_1$

When a more precise analysis is warranted, the more correct models and numerical analyses described in Appendix F should be used.

Example 4.6

If in the previous Example 4.5, for the 25 psi overpressure location, the structure bottom slab is designed to yield to a  $\mu$  of 5, the natural frequency of the roof slab (within the elastic range) will be less than the value of 13 cps obtained in the example, namely, 10.5 cps. (The slab is assumed to be a one-way reinforced concrete slab; and the frequency is calculated from Equation B-16 in Appendix B.) Then the elastic-plastic spectra envelope in the high frequency region is defined by the straight lines

$$V_{ep} \text{ (at } \mu = 5) = \frac{18}{5} \text{ in/sec} = 3.7 \text{ say } 4 \text{ in/sec.}$$

$$A_{ep} \approx \left(\frac{5}{10 - 1}\right) 25 = 14 \text{ g}$$

This is shown in Figure 4.37;

at  $f_1 = 10.5$  cps,  $A_1 = 0.7$  g

The shock response envelope for the equipment when  $f_2/f_1 > 1$  will be bounded by the straight line

$$A' = 2 A_1 = 1.4 \text{ g}$$

Therefore, at  $f_2 = 40$  cps,  $A_2 = 1.4$  g for design of the equipment mounts.

Example 4.6 (continued)

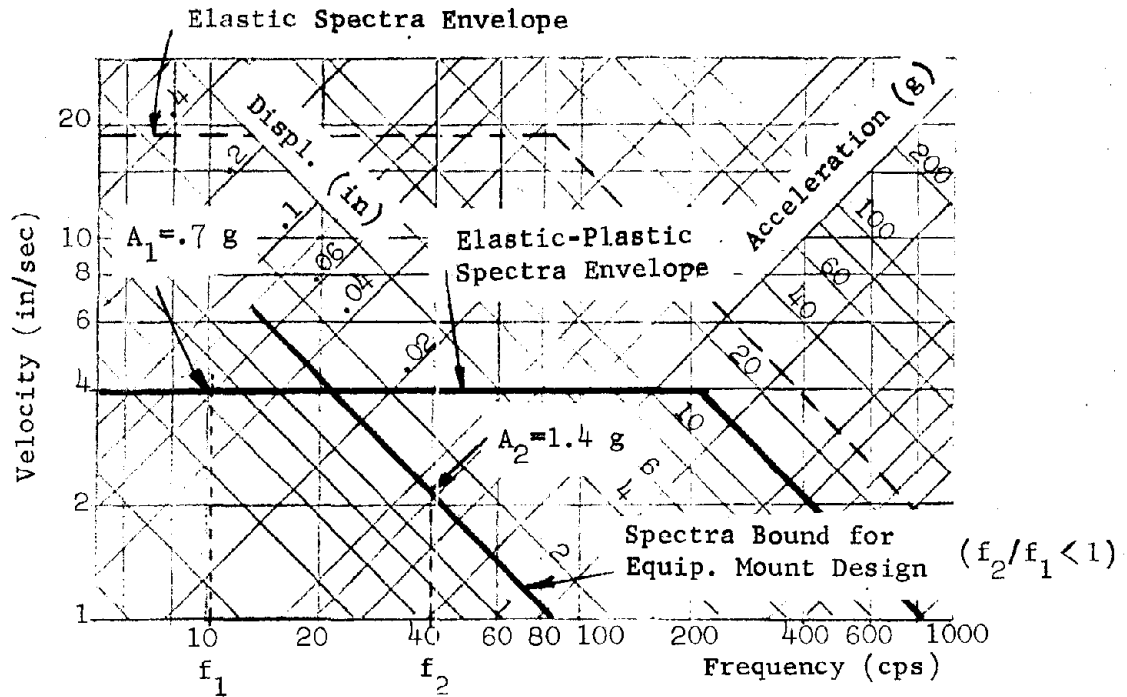


FIGURE 4.37

4.4.3 Cylindrical shaped structures. This type of structure is feasible at high overpressure regions in the order of 1000 psi. Figure 4.38 shows a normal condition.

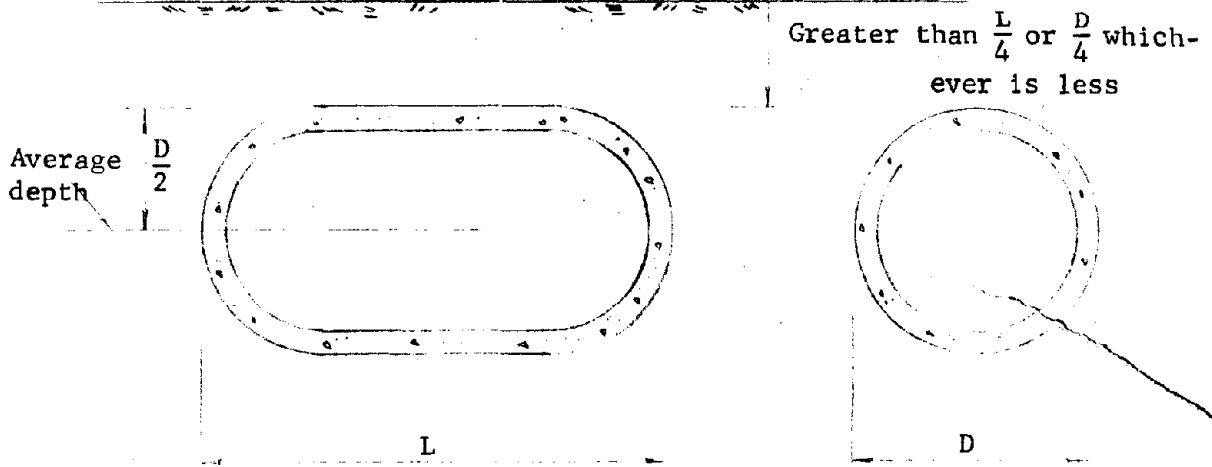


FIGURE 4.38

The walls are usually of very thick reinforced concrete, so that the primary loading induces compressive stresses in the cylinder. The cylinder is usually designed to remain in the elastic region.

The deformation frequencies of cylindrical structures are high compared to those of rectangular structures; and in relatively soft soils the rigid body mode is usually the only significant mode. Therefore, the peak structure motions are assumed to be the peak ground motions at the average depth in both the horizontal and vertical directions; and all points on the structure are assumed to have the same motion. The amplification factors for deriving the shock spectra envelope are given in Section 3.7.

4.4.4 Vertical silos. The protective design of a vertical silo is feasible in overpressure regions of the order of 500 psi. Construction is usually in reinforced concrete; and a heavy cover at the surface protects the interior equipment. Silo structures have been used as missile launchers and retractable antenna enclosures. (See Figure 4.39.)

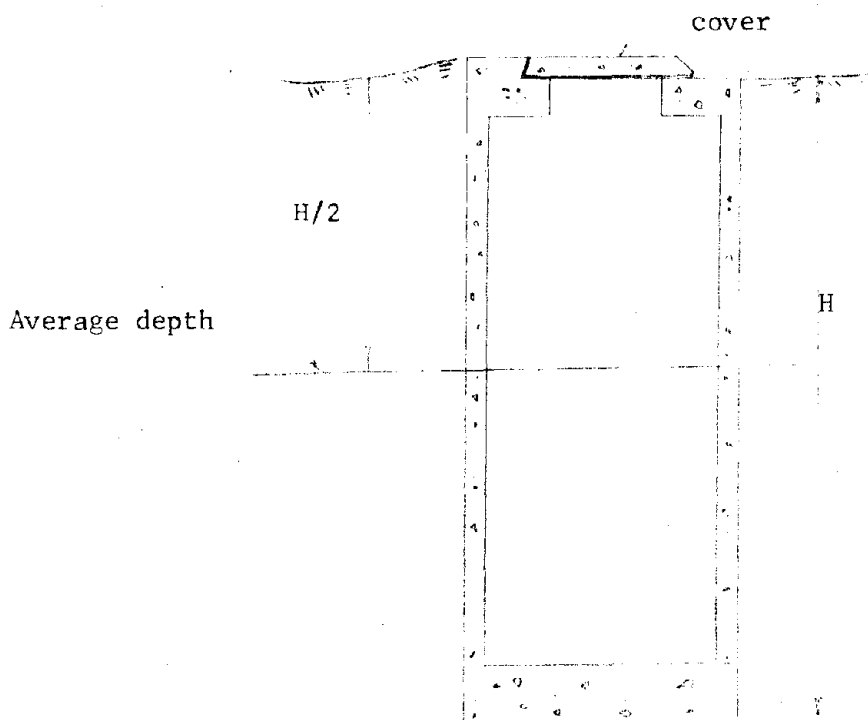


FIGURE 4.39

It is very difficult to assess the significance of the deformation response of the silo, as it influences the response of systems attached to the structure. For low frequency systems, the effect may be negligible, whereas for high frequency systems it may be important. For shock isolation systems located in the silo, the deformation responses of the structure may be neglected in deriving a shock spectra envelope.

The vertical motion of the silo is initially downward if the air blast is superseismic, but an initially upward motion may be expected for an outrunning condition. For the superseismic case, the vertical motion of the silo is the same as the ground motion at depth,  $H$ . For the outrunning case, the vertical ground motion predicted at the average depth,  $\frac{H}{2}$ , is probably more applicable; although this distinction cannot always be justified rationally because of the complexity of the wave propagation history for outrunning conditions.

The horizontal ground motion may induce some tilting as well as translational motion of the silo, especially if the silo penetrates through several soil layers.\* The magnitude of the tilting motion will usually be small compared to the translation; and in the shock spectra envelope approach the silo tilt motion is usually neglected. The horizontal motion of the silo will be assumed equal to the horizontal ground motion at the average depth,  $\frac{H}{2}$ .

The silo roof slab and closure will also feel the impingement of the air blast. The acceleration and velocity response in this area may be amplified under certain conditions of phasing of ground shock and overpressure. The roof slab and closure will have modified motions, which are treated in the same manner as those defined for the roof slab of rectangular structures (Section 4.1.1), if the shock spectra technique is used.

---

\* The tilt effect may be important for missile silos and antenna structures under certain operational requirements. The lumped parameter model of the silo shown in Appendix F may be used for an estimate of the tilt.

#### 4.5 Deep Buried Cavity Liners

Cavity liners are designed to be placed in deep underground locations, when they are required to survive direct or near miss hits from large yield weapons. A high degree of invulnerability is achieved by placing the system in a cavity in competent rock, where full advantage may be taken of the strength of the rock. The principal input to the liner is due to the transmitted shock wave from the crater in a direct radial path; since at great depth and at close-in locations, the crater-induced ground shock will be more important than the air-blast induced pressure. (See discussion in Section 3 on Ground Motions.) The survival requirements for the rock cavity itself and its liner are not within the scope of this report. The present discussion will be concerned only with the influence of a cavity liner on the transmission of ground shock. Figure 4.40 shows one type of

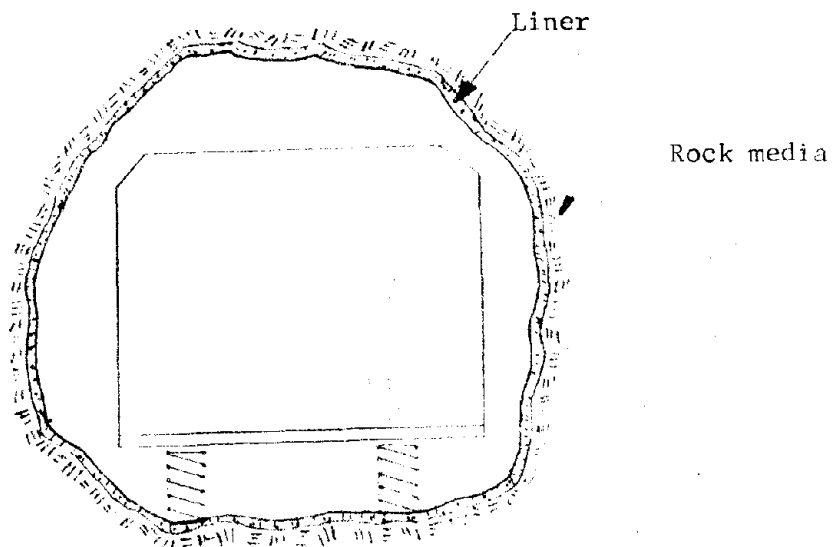


FIGURE 4.40: ROCK CAVITY INSTALLATION

rock cavity installation. In this simple case, a liner or filler material intervenes between the rock medium and any internal system.

In some cases, the liner may consist of nothing more than a steel plate to protect the internal systems from rock spallation. In other cases,



a concrete liner may be poured directly against the rock. Such a liner does not significantly affect the free-field input at the boundary of the cavity. In order to increase the survivability of a liner in the rock cavity, crushable fillers are often placed between the rock and the liner.

Test data (see References 4.15 and 4.16) indicate that some attenuation of the free-field stress wave is due to this crushable material. The emphasis in the tests has been to evaluate the effect of the filler material on the stress level in the structure liner. Filler materials that exhibit energy absorbing properties while at the same time preserving their shape stability under static conditions, have been used in the tests. Foamed plastics (such as rigid polyurethane) and lightweight concretes (such as cellular vermiculite) are examples of materials tested.

Some semi-quantitative estimates may be made from model tests reported in Reference 4.15, where tests were performed on model cylinders by using rigid Polyurethane as a filler with a yield value of less than 100 psi. Various ratios of foam thickness,  $F$ , to liner radius,  $R$ , were tested ( $0 \leq \frac{F}{R} \leq 0.5$ ) for dynamic loads; and it was found that the stress in the liner was significantly reduced when the  $F/R$  ratio was greater than 0.2. The rigid body displacement of the liner was not reduced appreciably when the foam was added. Accelerations were not measured. Therefore, from these tests, it can be concluded that the crushable filler will not affect the shock response of internal systems in the low and intermediate frequency region, but it may reduce the high frequency response.

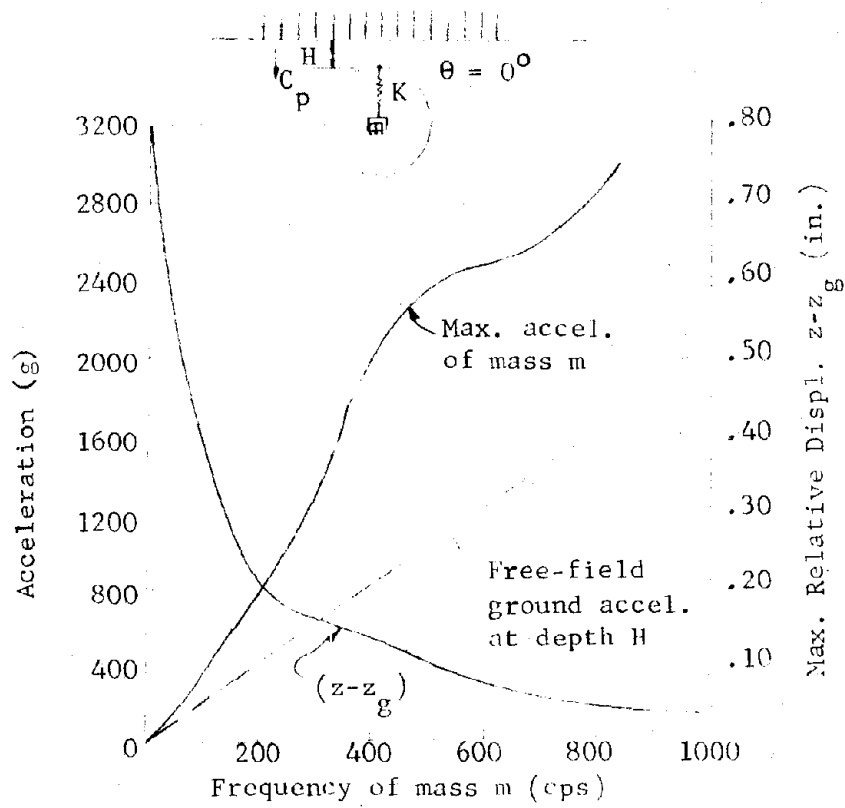
Other investigators have looked into the advantages of crushable fillers, primarily for tunnel liners in rock at very high stress levels (see References 4.1 and 4.17). The filler definitely protects the liner from total collapse, but it has only a negligible effect in reducing the peak displacement, velocity, and acceleration imparted to the liner (the accelerations may have a reduction up to a factor of 2).

Therefore, based on available test data, it can be concluded that a crushable filler is not an efficient method of attenuating the shock input, although it may be an advantage to the liner design itself.

The location of the attachment to the liner (or cavity) with respect to the direction of the stress wave is of importance to the response of the

internal system. Figure 4.41a, taken from Reference 4.18 shows the amplified acceleration at the zero degree boundary point that experiences a full reflection; whereas the  $180^{\circ}$  boundary point, Figure 4.41b, shows an attenuation of acceleration below that of the free field. These differences from the free-field acceleration are of importance in the high frequency region. In the very low frequency range associated with the natural frequencies of shock isolated in-structure systems, the calculated difference is not marked.

Shock spectra based on free-field motions are applicable for any point on the cavity boundary in the low frequency (constant displacement and constant velocity) region. In the high frequency region, unconservative results will be obtained if the support points are located at the upper portion of the cavity where the direct stress wave impinges first. Therefore, the shock spectra envelope can be based on the free-field motions, except in the case of high frequency systems mounted in the upper half of the cavity. The response amplification factors can be based on stress wave propagation in homogeneous media using ground displacement pulses with a full ground return (see Section 3.6).



$p_0$  = peak pressure at the surface  
 = 6500 psi

$C_p$  = propagation velocity of  
 dilatational wave

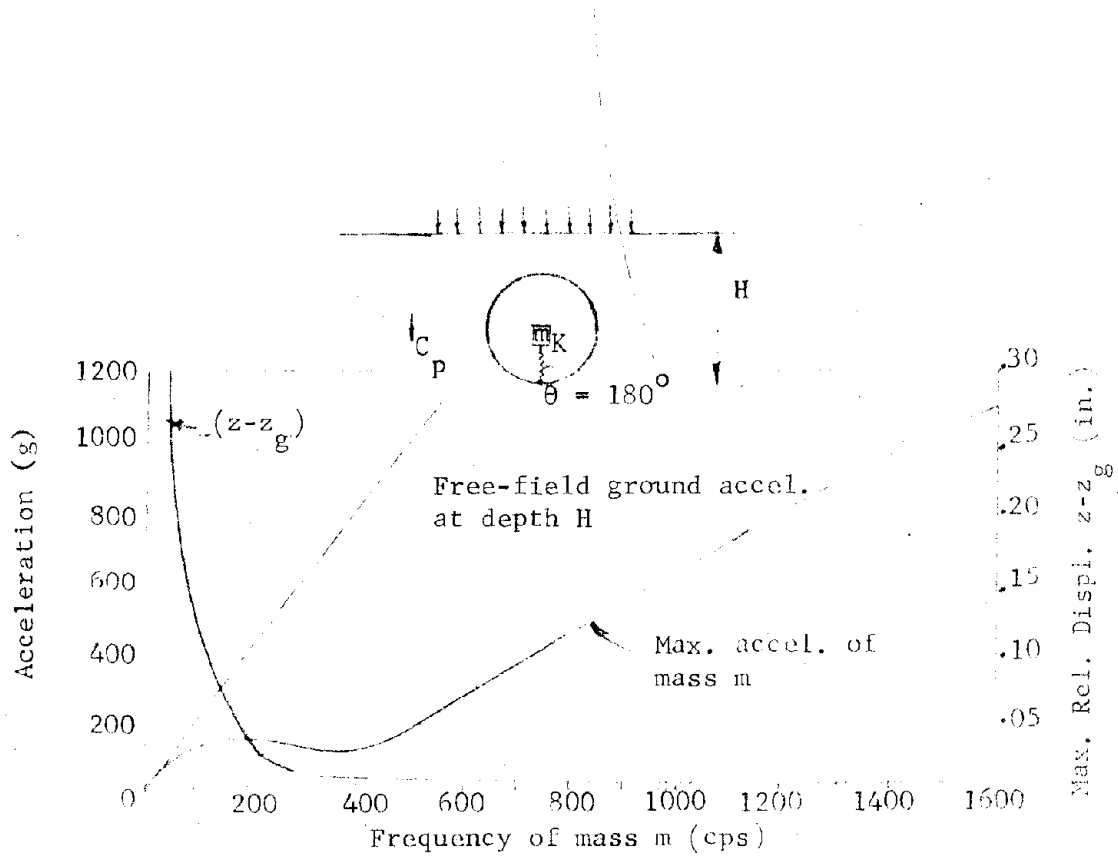
= 17,500 ft/sec

$a$  = cavity radius

= 17.5 ft

(a) Shock Spectra for the motion of mass  $m$   
 attached at the boundary point,  $\theta=0^\circ$

FIGURE 4.41a



$p_o = 6500$  psi  
 $C_p = 17,300$  ft/sec  
 $a = 17.5$  ft

(b) Shock spectra for the motion of mass m attached at the boundary point,  $\theta = 180^\circ$

FIGURE 4.41b

## SECTION 5: SHOCK ISOLATION SYSTEMS

### 5.1 Introduction

Hard mounted systems may be considered as partially shock isolated if their shock response is reduced due to inherent flexibility or yielding of the supporting structure. If deliberately designed flexible components are interposed between the shock sensitive equipment and the structure, the system is called soft mounted or shock mounted. Stiffness of hard-mounted or soft-mounted systems may be described as being linear, non-linear, and/or elastic-plastic for various ranges of response. Damping is sometimes important in the design of shock isolation systems, and may be described as a constant force resisting motion (Coulomb) or a force proportional to velocity of distortion (viscous).

In this section, types of shock isolation systems will be described, and examples of design for weapon effects will be given. The types of springs suitable for the various configurations and ranges of response will also be specified.

It will also be assumed that, using the data and procedures of Sections 2, 3, and 4, the reader has determined the motions of the supports of the hard or soft mounted system. This information may be either an elastic shock response spectra envelope and/or specific input motions of the structure in terms of motion-time histories.

The design of the shock isolation system will start with the following given data:

- (1) Preliminary weight and C.G. location data of the equipments to be supported.
- (2) Tolerable acceleration or velocity responses of equipment and/or personnel to be protected during the attack mode.
- (3) A space envelope of the internal system and an available rattle-space.

The designer then has the task of developing a soft mounted system, or relying upon a hard mounted system such that relative displacements

between supported items and the structure may be accommodated within the available rattlespace while tolerance response magnitudes are not exceeded.

## 5.2 Symmetrical Spring Systems

A symmetrical system is nearly always preferable since it is an optimum system. In that case the center of rigidity will be coincident with the center of mass when the system is in its static equilibrium position. Consider the four-spring system of Figure 5.1 and the two-spring system of Figure 5.2 with their respective equivalent eight and four horizontal and vertical spring components.

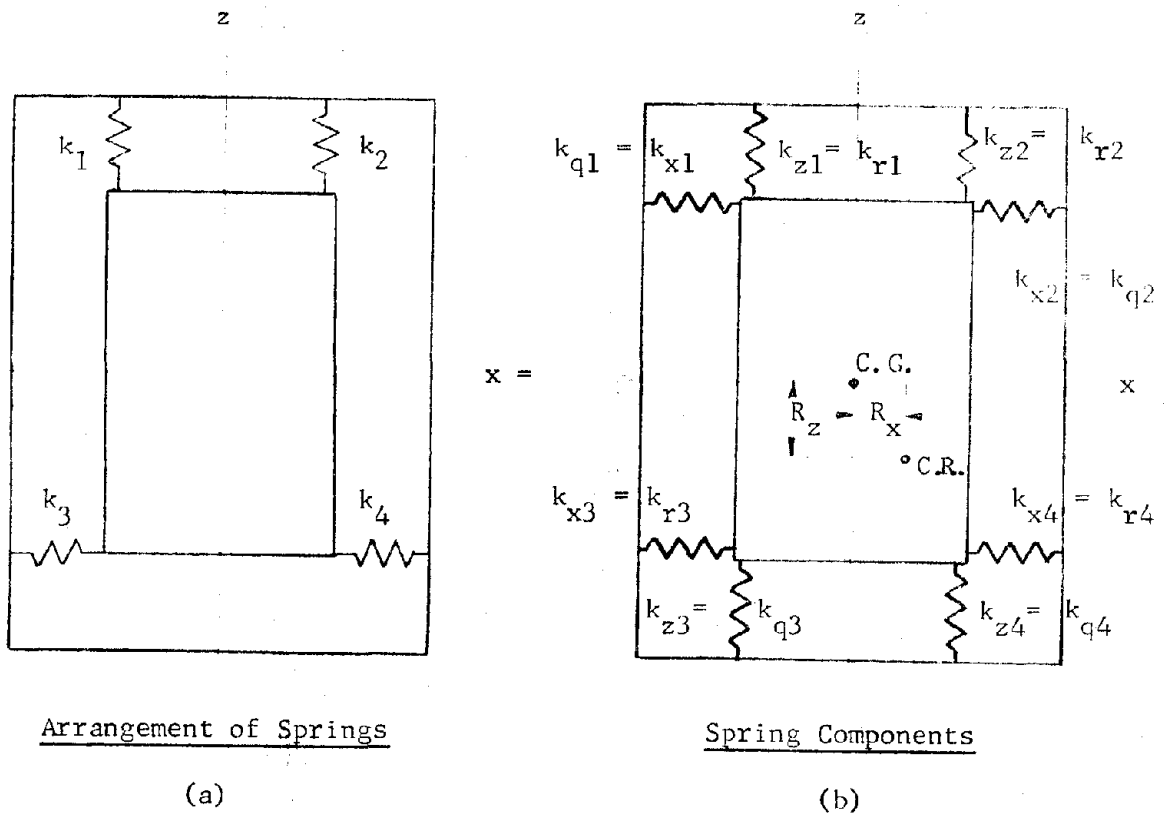


FIGURE 5.1; SPRINGS PARALLEL TO PRINCIPAL AXIS

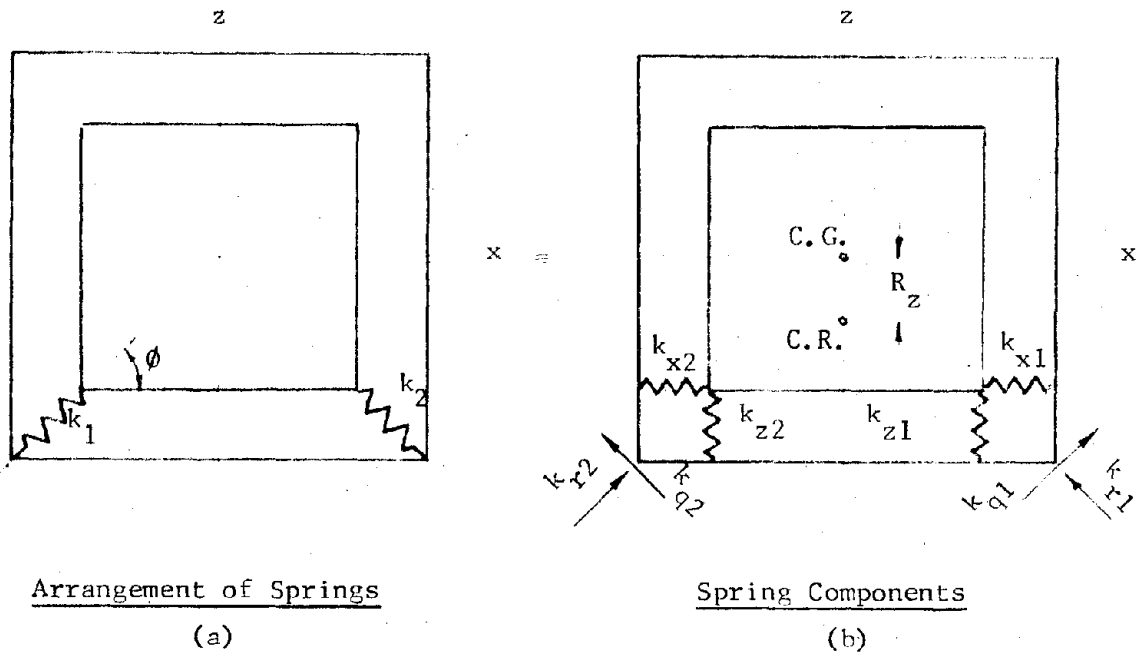


FIGURE 5.2: INCLINED SPRINGS

The definition of spring symbols in Figures 5.1 and 5.2 are:

- $k_1, k_2, \dots$  : Spring number designation
- $k_{r1}, k_{r2}, \dots$  : Spring rate in axial direction for the specific numbered spring (lbs/inch)
- $k_{q1}, k_{q2}, \dots$  : Spring rate in transverse direction for the specific numbered spring (lbs/inch)
- $k_{z1}, k_{z2}, \dots$  : Spring rate component along vertical principal axis for the specific numbered spring (lbs/inch)
- $k_{x1}, k_{x2}, \dots$  : Spring rate component along horizontal principal axis for the specific numbered spring (lbs/inch)

The center of rigidity is defined as the point on the mass where a force must be applied if the mass is required to displace only in translation, i.e., without any rotation. Conversely, if a moment is applied about an axis through the center of rigidity (C.R.), the mass will be displaced only in rotation without any translation. Restricting the C.R. to coincide with the C.G. will enable the designer to simplify the dynamic problem mathematically by decoupling the natural modes, and to make an optimum design from the point of view of required rattlespace and minimum transmitted acceleration and/or velocity.

A discussion of spring rates will be necessary for understanding how to calculate locations of centers of rigidity or stiffness.

5.2.1 Spring lateral stiffnesses. Assume linear, weightless springs and small deformations; moreover the spring ends are either simply hinged or fixed as shown in Figure 5.3a and 5.3b respectively.

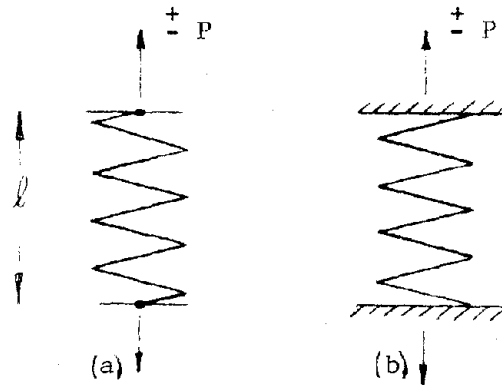


FIGURE 5.3

Denote the axial direction by  $r$  and the transverse by  $q$ . Buckling is critical when the axial load is in compression.

If the static load is zero, spring (a) in Figure 5.3 will have no transverse stiffness, but due to its end fixity, spring (b) will have one, denoted by  $k_q$ ; its magnitude will depend on the spring's dimensions and on its degree of end fixity. If a tensile load,  $P$ , acts, spring (a) as well as spring (b) will have transverse stiffnesses. If a compressive load,  $-P$ , acts, spring (a) will have a negative transverse stiffness, and spring (b) will have a positive transverse stiffness, unless the load is large enough to cause buckling. It is, therefore, seen that the value of  $P$  will enter into the expressions for the transverse stiffnesses of springs (a) and (b). The simplified relationships are:

$$(k_q)_a = + \frac{P}{l} \quad \text{and} \quad (k_q)_b^* = (k_q)_0 + \frac{P}{l} \quad (5.1)$$

\*The lateral spring rate for fixed-ended coil springs is here assumed to be a function of two independent terms,  $(k_q)_0$  and  $P/l$ , to illustrate the significance of the axial load on the lateral spring rate.



This relation is schematically shown in Figure 5.4 for spring (a) and for negligible variation in  $k_r$  (based on small angle approximation).

$$(k_q)_a = \frac{+P \sin \theta}{\Delta q}$$

$$\Delta q = \ell \sin \theta$$

$$k_q = \frac{+P}{\ell}$$

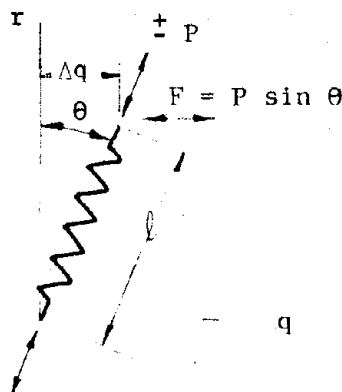


FIGURE 5.4

For compressive loads, buckling criteria (not considered here) will limit the value of  $P$  in both cases. Since the operational spring length,  $\ell$ , is related to the unstressed spring length,  $\ell_o$ , it follows that  $(k_q)_a$  and  $(k_q)_b$  are numerically larger for compression than for tension. Thus,

$$(k_q)_a = \frac{+P}{\ell_o + \frac{+P}{k_r}} = f(P) \text{ and } (k_q)_b = (k_q)_o + f(P) \quad (5.2)$$

### Example 5.1

This example will show the effect of an axial load, both tension and compression, on the lateral spring rate. Let

$$k_r = 4000 \text{ lbs/in}; \quad (k_q)_o = 1000 \text{ lbs/in}; \quad \ell_o = 40 \text{ in};$$

$$(k_q)_a = \frac{+P}{40 + \frac{+P}{4000}} = f(P); \quad (k_q)_b = 1000 + f(P)$$

The Figure 5.5(a) of load,  $P$ , versus spring component,  $(k_q)_a$ , shows that the lateral stiffness is negative\* for all compressional loads, and is

\* A negative spring rate means that instead of tending to restore a configuration to its static equilibrium the spring tends to oppose such a restoration.

Example 5.1 (continued)

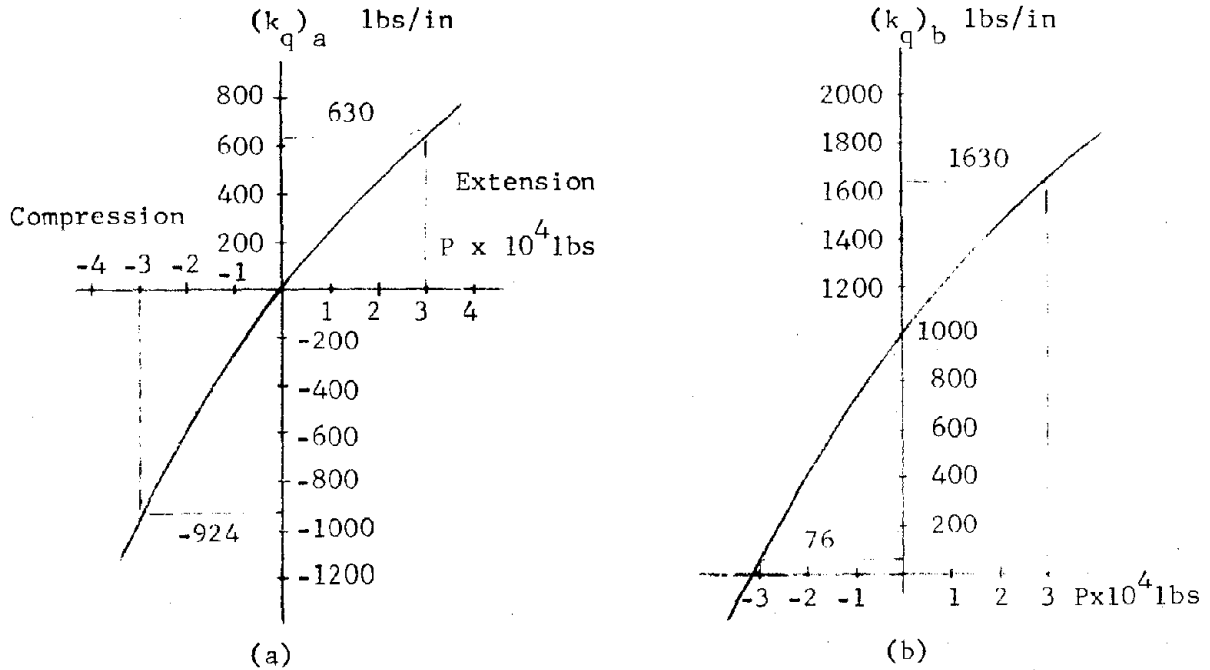


FIGURE 5.5

numerically higher than for extensional loads. Thus, for  $P = 3 \times 10^4$  lbs, i.e., for a deflection of  $\Delta r = 7.5$  inches,

$$(k_q)_a = \begin{cases} 630 \text{ lbs/in for extension} \\ -924 \text{ lbs/in for compression} \end{cases}$$

Figure 5.5(b) shows that for  $(k_q)_b$  the negative stiffness does not occur until the compressional load is slightly larger than  $3 \times 10^4$  lbs;

$$(k_q)_b = \begin{cases} 1000 + 630 = 1630 \text{ lbs/in for extension} \\ 1000 - 924 = 76 \text{ lbs/in for compression} \end{cases}$$

These values are indicated in Figure 5.6. If it is assumed that a linear variation in  $(k_q)_o$  occurs due to the lengths being 47.5 and 32.5 inches instead of 40 inches, the assumed constant value of 1000 lbs/in will be changed so that:

Example 5.1 (continued)

$$(k_q)_b = \begin{cases} 842 + 630 = 1472 \text{ lbs/in for extension} \\ 1230 - 924 = 306 \text{ lbs/in for compression} \end{cases}$$

Figure 5.6 shows the two springs in the extended and in the compressed conditions.

The above variations for  $k_q$  as a function of the axial load or displacement are important considerations in designing a system composed of a group of springs for combined vertical and lateral displacements. This will be shown in Subsection 5.2.3 and 5.2.4.

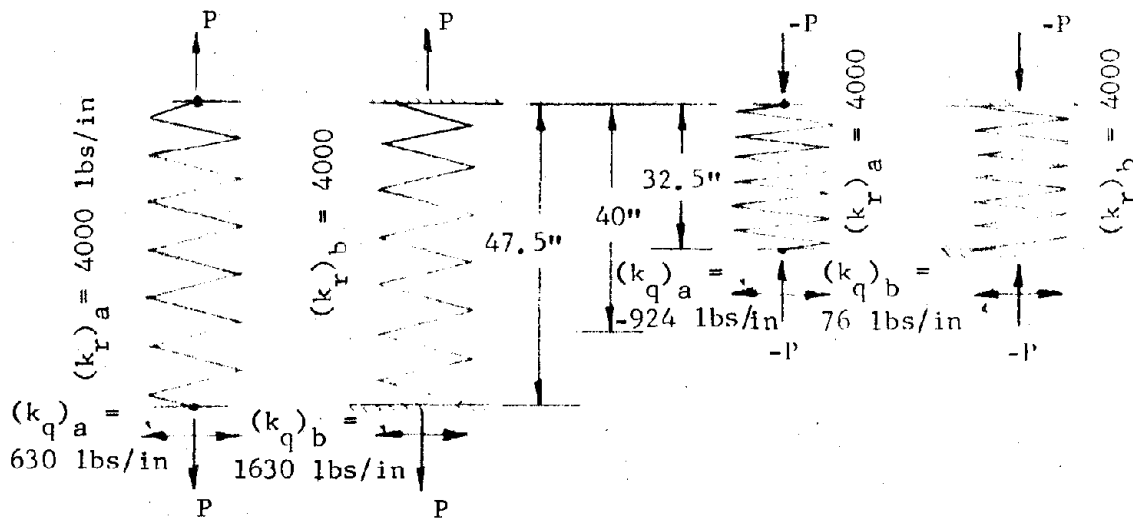


FIGURE 5.6

5.2.2 Spring systems that are parallel to the principal axes of the mass.

It was stated in the Introduction that the spring arrangement (Figure 5.1) for decoupling can be determined by making the resultant horizontal spring force and the resultant vertical spring force pass through the mass center or C.G.. The number of springs in each direction will depend on the capability of the spring elements. If the C.G. is centrally located within the mass, a number of additional springs may be more desirable than to vary the spring rates of initially assumed springs so as to achieve the desired symmetry.

Referring to Figure 5.7a, a plate is acted upon by four coiled springs. Each spring has an axial  $k_r$  as well as a transverse  $k_q$  stiffness. Let the application point coordinates be denoted by  $b_i$  and  $h_i$ , respectively. Figure 5.7b shows the eight component stiffnesses. Assume that the center of rigidity is located by the coordinates  $R_x$  and  $R_z$ . Then for a small horizontal-x displacement only four of the stiffness components will be active. Since the sum of the moments about the CR must be zero,

$$0 = (-h_1 - R_z) k_{r1} + (h_2 - R_z) k_{q2} + (h_3 - R_z) k_{q3} + (h_4 - R_z) k_{r4}$$

giving at once:

$$R_z = \frac{-h_1 k_{r1} + h_2 k_{q2} + h_3 k_{q3} + h_4 k_{r4}}{-k_{r1} + k_{q2} + k_{q3} + k_{r4}} \quad (5.3)$$

Similarly, a vertical-z displacement must result in zero moment of the springs about the CR, giving the coordinate

$$R_x = \frac{b_1 k_{q1} + b_2 k_{r2} - b_3 k_{r3} - b_4 k_{q4}}{k_{q1} + k_{r2} - k_{r3} - k_{q4}} \quad (5.4)$$

The resultant translatory spring stiffnesses are

$$(k_x) = k_{r1} + k_{q2} + k_{q3} + k_{r4}$$

$$(k_z) = k_{q1} + k_{r2} + k_{r3} + k_{q4}$$

and the resultant torsional stiffness,  $k_\theta$ , about the C.R. can be obtained by considering all stiffness component contributions of the same sign;

$$k_\theta = k_{r1} (h_1 + R_z)^2 + k_{q1} (b_1 - R_x)^2 + k_{r2} (b_2 - R_x)^2 + \quad (5.5)$$

$$k_{q2} (h_2 - R_z)^2 + k_{r3} (b_3 + R_x)^2 + k_{q3} (h_3 - R_z)^2 + k_{r4} (h_4 - R_z)^2 + k_{q4} (b_4 - R_x)^2$$

Therefore, a coincidence of the C.G. and the C.R. can always be achieved from Equations (5.3) and (5.4), i.e.,  $R_z$  and  $R_x$  can be reduced to zero, if two or more additional springs can be applied or if the existing spring locations and spring rates are revised.

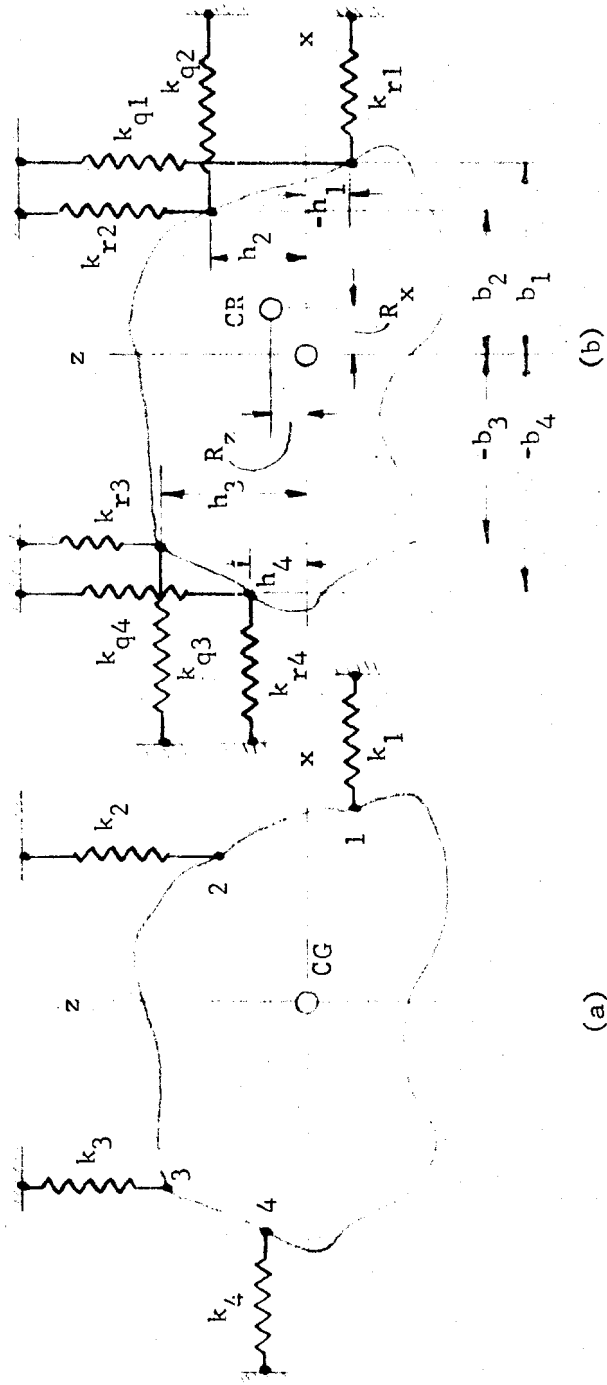


FIGURE 5.7

5.2.3 Spring systems that are inclined to the principal axes of the mass.

A typical inclined spring base mounted system is shown in Figure 5.2. In this case the static axial load in the spring is in compression. An inclined tension mounted system is shown in Figure 5.8 where the static

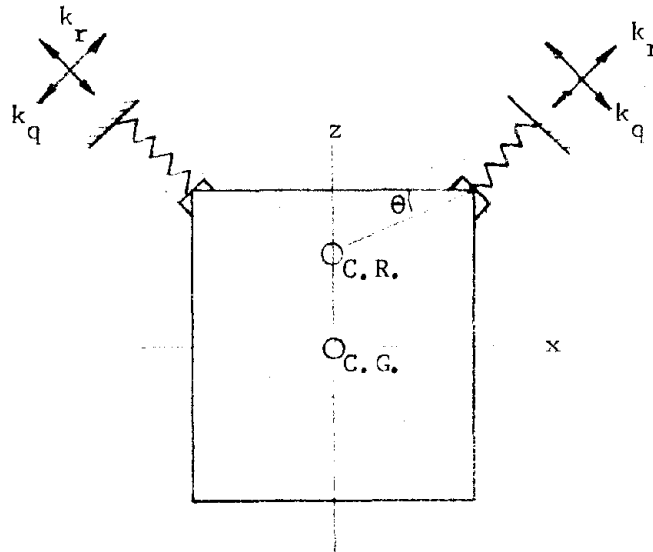


FIGURE 5.8

axial loads in the springs are now in tension. The analysis applying to springs in tension will also apply to springs in compression, provided that their compressive loads,  $-P$ , are not so large as to make the transverse stiffnesses,  $k_q$ , approach zero (see Section 5.2.1). Ordinarily base mounted systems use springs with end fixity, so that the fixity will always provide a restoring spring rate,  $k_q$ , for the motions postulated.

a. Stiffnesses along arbitrary axes of inclined coiled springs. Assume small deformations, and that  $k_r$  and  $k_q$  are the spring's axial and transverse stiffnesses, respectively, assumed to be constant over the range of small deformations.

Referring to Figure 5.9 a spring with  $k_r$  and  $k_q$  stiffnesses is shown inclined at an angle  $\phi$  to the horizontal. If a horizontal displacement of  $\Delta x$  is assumed in Figure 5.9a, the spring shortens the amount  $\Delta r$  in the axial direction, and the spring lengthens  $\Delta q$  in the transverse direction.

The two forces exerted by the spring will, therefore, be as indicated in Figure 5.9b. and will amount to

$$F_r = k_r \Delta r = k_r \cos \phi \Delta x \quad (\text{in the axial direction})$$

$$F_q = k_q \Delta q = k_q \sin \phi \Delta x \quad (\text{in the transverse direction})$$

The equivalent spring reactions in the horizontal-x and in the vertical-z direction are shown in Figure 5.9c. They are expressed by

$$F_x = -k_r \cos^2 \phi \Delta x - k_q \sin^2 \phi \Delta x$$

$$F_z = -k_r \cos \phi \sin \phi \Delta x + k_q \sin \phi \cos \phi \Delta x$$

Accordingly, the equivalent stiffnesses of the spring in the x and in the z direction due to the displacement  $\Delta x$  will be

$$k_{xx} = k_r \cos^2 \phi + k_q \sin^2 \phi \tag{5.6}$$

$$k_{zx} = (k_r - k_q) \sin \phi \cos \phi$$

Similar reasoning relating to an assumed displacement  $\Delta z$  is illustrated in Figure 5.10 a, b, and c, and results in equivalent stiffnesses in the z and in the x direction due to the displacement  $\Delta z$  expressed by

$$k_{zz} = k_r \sin^2 \phi + k_q \cos^2 \phi \tag{5.7}$$

$$k_{xz} = (k_r - k_q) \sin \phi \cos \phi$$

It can, therefore, be seen that the inclined spring's resultant equivalent stiffnesses in the x and in the z direction as functions of displacement  $\Delta x$  and  $\Delta z$  are respectively

$$(k_x) = k_{xx} + k_{xz} \frac{\Delta z}{\Delta x} \quad \text{in the x direction (a)} \tag{5.8}$$

$$(k_z) = k_{zz} + k_{zx} \frac{\Delta x}{\Delta z} \quad \text{in the z direction (b)}$$

The differential quotients will vary for arbitrary displacements in the xz plane; when decoupling is assumed they will be zero.

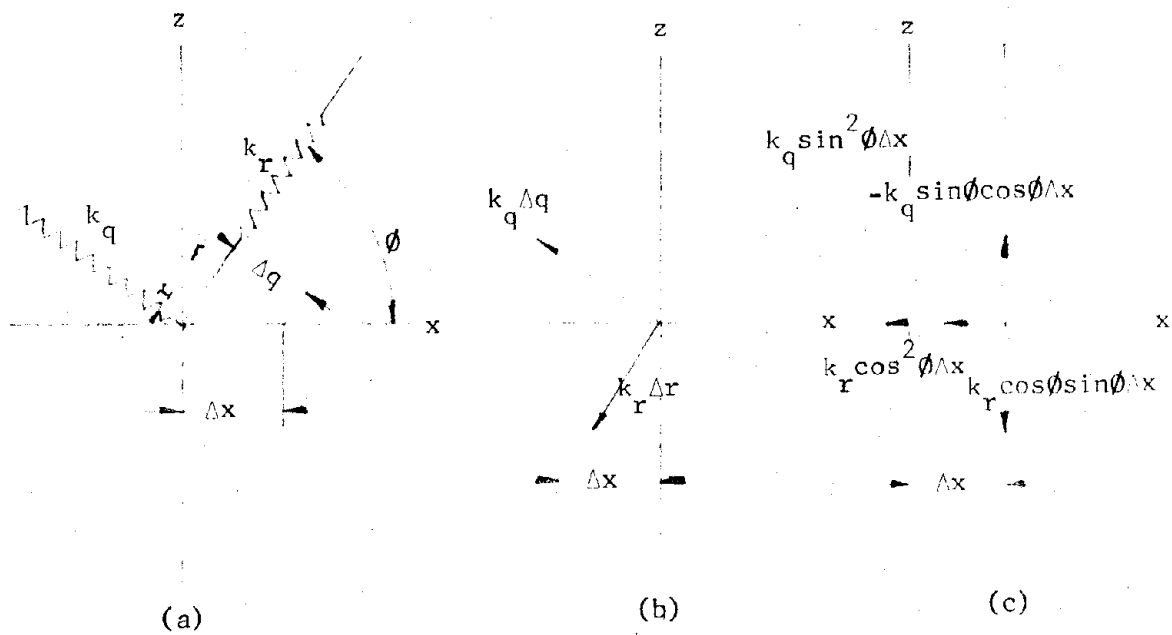


FIGURE 5.9

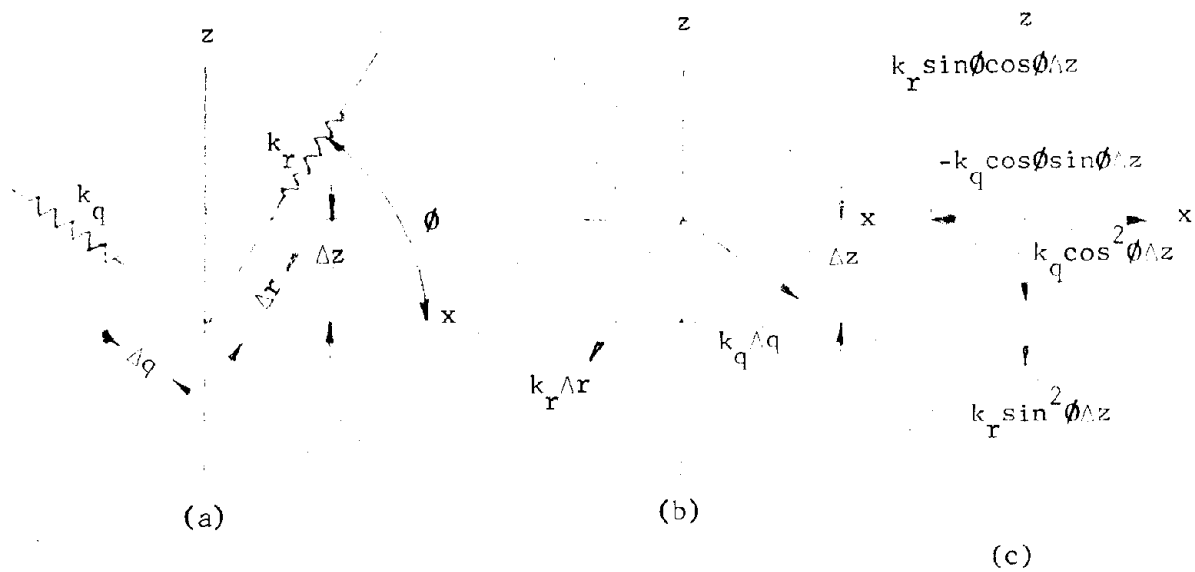
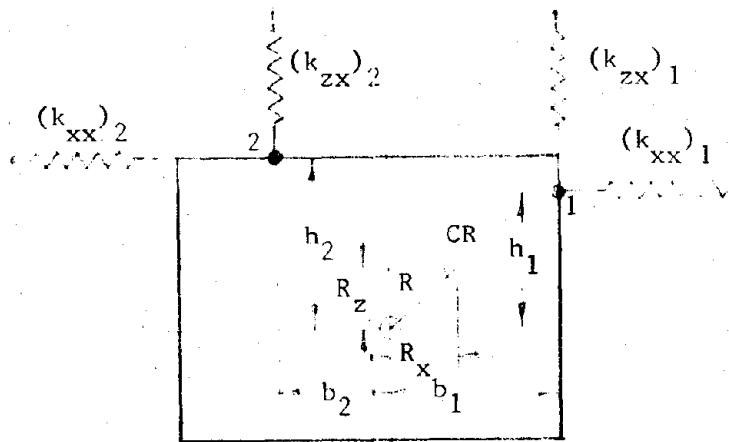


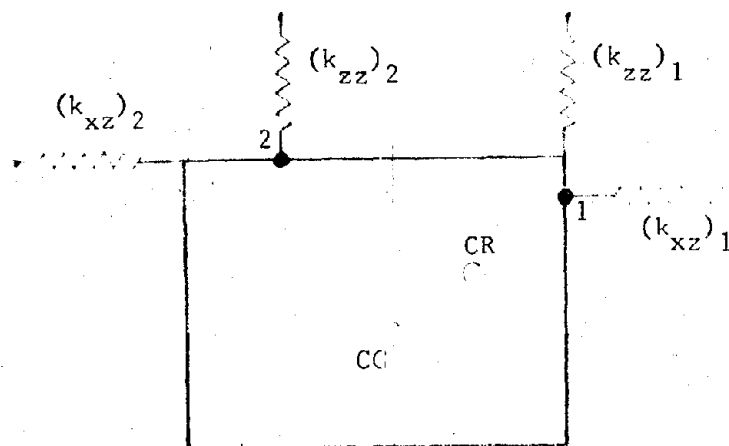
FIGURE 5.10



b. Calculation of location of center of rigidity of inclined coiled spring system. The point of action of a spring on a mass is of great importance in locating the center of rigidity of two or more springs. Figure 5.11a shows a three-degree-of-freedom plate (as shown in Figure 5.8) suspended by two inclined springs, 1 and 2, acting at the points with coordinates  $h_1, b_1$  and  $h_2, -b_2$ , with respect to the axes of the center of mass, C.G. The diagram shows the spring components for a horizontal displacement; and the center of rigidity is assumed to be located at the point CR at the distance  $R$  from the C.G. with the coordinates  $R_x$  and  $R_z$ . In Figure 5.11 b, the inclined spring components for a vertical displacement



(a)



(b)

FIGURE 5.11

are shown. The center of rigidity coordinates,  $R_x$  and  $R_z$ , are then determined by two conditions, requiring that an arbitrary translation  $\Delta x$  as well as an arbitrary translation  $\Delta z$  must not produce spring induced moments about the C.R. This gives two equations, from which  $R_x$  and  $R_z$  can be determined.

$$(h_1 - R_z)(k_{xx})_1 + (h_2 - R_z)(k_{xx})_2 = (b_1 - R_x)(k_{zx})_1 + (b_2 - R_x)(k_{zx})_2$$

for the displacement  $\Delta x$ , and (5.9)

$$(h_1 - R_z)(k_{xz})_1 + (h_2 - R_z)(k_{xz})_2 = (b_1 - R_x)(k_{zz})_1 + (b_2 - R_x)(k_{zz})_2$$

for  $\Delta z$

It is obvious that the above expressions may be generalized to include  $n$  springs by writing

$$\sum_{i=1}^n [(h_i - R_z)(k_{xx})_i] = \sum_{i=1}^n [(b_i - R_x)(k_{zx})_i] \quad (5.10)$$

$$\sum_{i=1}^n [(h_i - R_z)(k_{xz})_i] = \sum_{i=1}^n [(b_i - R_x)(k_{zz})_i]$$

with 
$$R^2 = R_x^2 + R_z^2$$

It is clear that  $R$  may be made equal to zero if  $R_z = R_x = 0$ , and this can always be accomplished if it is possible either to change stiffnesses and/or locations of existing springs or to add one more spring in the  $x$  direction and one more in the  $z$  direction.

Assume two identical springs with

$$k_r/k_q = m ; h_1 = h_2 = h ; b_1 = -b_2 = b \quad \phi_1 = \pi - \phi_2 = \phi$$

which is the normal case when inclined springs are used. From Equations

$$\begin{aligned} (5.6) \text{ and } (5.7) \quad (k_{xx})_1 &= (k_{xx})_2 = k_r (\cos^2 \phi + \frac{1}{m} \sin^2 \phi) \\ (k_{zx})_1 &= -(k_{zx})_2 = k_r (1 - \frac{1}{m}) \sin \phi \cos \phi \\ (k_{zz})_1 &= (k_{zz})_2 = k_r (\sin^2 \phi + \frac{1}{m} \cos^2 \phi) \\ (k_{xz})_1 &= -(k_{xz})_2 = k_r (1 - \frac{1}{m}) \sin \phi \cos \phi \end{aligned} \quad (5.11)$$

Equations (5.9) become

$$(h - R_z) 2 k_r (\cos^2 \phi + \frac{1}{m} \sin^2 \phi) = 2 h k_r (1 - \frac{1}{m}) \sin \phi \cos \phi$$

for locating  $R_z$  ( $R_x = 0$  due to symmetry).

Accordingly

$$\begin{aligned} R_z &= h - b \frac{(1 - \frac{1}{m}) \sin \phi \cos \phi}{\cos^2 \phi + \frac{1}{m} \sin^2 \phi} \\ &= h - b \frac{(1 - \frac{1}{m}) \tan \phi}{1 + \frac{1}{m} \tan^2 \phi} = h - b\psi \end{aligned} \quad (5.12)$$

with

$$\psi = \frac{(1 - \frac{1}{m}) \tan \phi}{1 + \frac{1}{m} \tan^2 \phi} \quad (5.13)$$

and for a CG-CR concentric system,  $R_z \rightarrow 0$ ,  $h/b = \psi$

A plot of  $\psi$  from Equation (5.13) is shown in Figure 5.12 for values of  $m = k_r/k_q$  ranging from 1 to infinity.

**Example 5.2:** Location of the center of rigidity of two inclined springs.

Figures 5.13a and 5.13b show two equivalent diagrams of a rectangular plate of width,  $2b$ , and height,  $2h$ , suspended by two identical springs inclined 45 degrees with the horizontal. If it is assumed that  $k_r/k_q = m = 3$ , Figure 5.12 gives  $\psi = 0.5$ , and accordingly Equation (5.12) defines the  $z$  coordinate of C.R. as

$$R_z = h - b\psi = h - 0.5b$$

From inspection, it is obvious that  $R_x = 0$ . Therefore,

$$R = R_z = h - 0.5b$$

and

$$h - R = 0.5b$$

Moreover,

$$r = \left[ b^2 + (h - R)^2 \right]^{1/2} = 1.23b$$

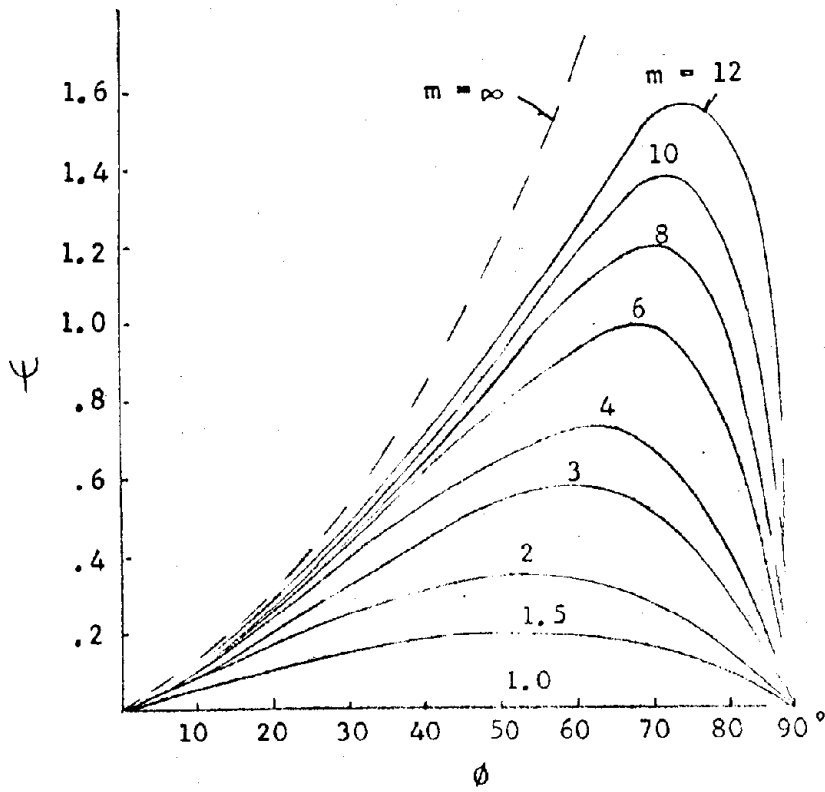


FIGURE 5.12

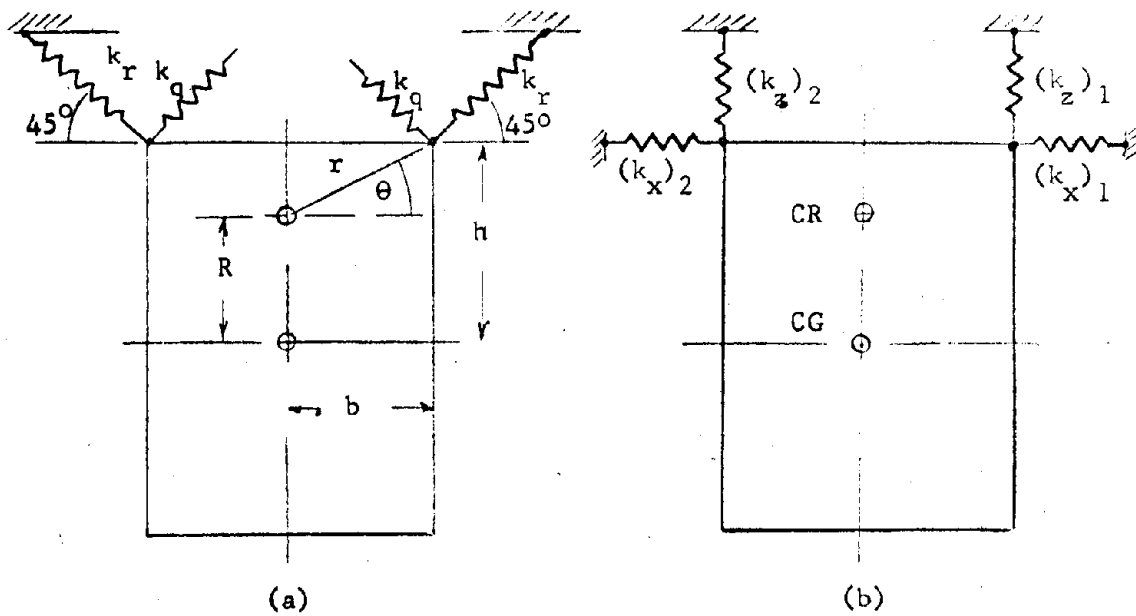


FIGURE 5.13

Example 5.2 (continued)

For a concentric system,

$$h/b = 0.5 \text{ when } k_r/k_q = 3$$

c. Rotation stiffness evaluation of system with two inclined springs.

The arbitrary displacements  $\Delta z$ ,  $\Delta x$ , and  $\Delta \theta$  are related by

$$\begin{aligned}\Delta z &= r \cos \theta \Delta \theta \\ \Delta x &= -r \sin \theta \Delta \theta\end{aligned}\tag{5.14}$$

for pure rotation motion about the CR.

Accordingly,

$$\frac{\Delta x}{\Delta z} = -\tan \theta \text{ and } \frac{\Delta z}{\Delta x} = -\cotan \theta$$

Referring to Figure 5.13a, it is seen that

$$\text{Spring (1)} \quad \frac{\Delta x}{\Delta z} = -\frac{h-R}{b} \text{ and } \frac{\Delta z}{\Delta x} = -\frac{b}{h-R}\tag{5.15}$$

$$\text{Spring (2)} \quad \frac{\Delta x}{\Delta z} = \frac{h-R}{-b} \text{ and } \frac{\Delta z}{\Delta x} = \frac{-b}{h-R}$$

However, only positive values of  $\frac{\Delta x}{\Delta z}$  and  $\frac{\Delta z}{\Delta x}$  are to be used in Equations (5.8).

Equations (5.6) and (5.7) give for identical springs and for

$\phi_1 = \pi - \phi_2 = \phi$  the following stiffnesses

$$\begin{aligned}(k_{xx})_1 &= (k_{xx})_2 = k_r \left( \cos^2 \phi + \frac{1}{m} \sin^2 \phi \right) \\ (k_{zz})_1 &= (k_{zz})_2 = k_r \left( \sin^2 \phi + \frac{1}{m} \cos^2 \phi \right) \\ (k_{zx})_1 &= (k_{zx})_2 = k_r \left( 1 - \frac{1}{m} \right) \sin \phi \cos \phi \\ (k_{xz})_1 &= (k_{xz})_2 = k_r \left( 1 - \frac{1}{m} \right) \sin \phi \cos \phi\end{aligned}\tag{5.16}$$

Accordingly, the component equivalent stiffnesses in the x and in the z

Example 5.2 (continued)

direction, as given by Equations (5.8) will be

$$\begin{aligned}(k_{x\theta})_1 &= \left[ k_r \cos^2 \phi + \frac{1}{m} \sin^2 \phi + \left(1 - \frac{1}{m}\right) \sin \phi \cos \phi + \frac{b}{h - R} \right] \\(k_{z\theta})_1 &= \left[ k_r \sin^2 \phi + \frac{1}{m} \cos^2 \phi + \left(1 - \frac{1}{m}\right) \sin \phi \cos \phi + \frac{h - R}{b} \right] \\(k_{x\theta})_2 &= \left[ k_r \cos^2 \phi + \frac{1}{m} \sin^2 \phi + \left(1 - \frac{1}{m}\right) \sin \phi \cos \phi + \frac{b}{h - R} \right] \\(k_{z\theta})_2 &= \left[ k_r \sin^2 \phi + \frac{1}{m} \cos^2 \phi + \left(1 - \frac{1}{m}\right) \sin \phi \cos \phi + \frac{h - R}{b} \right]\end{aligned}\tag{5.17}$$

and finally for a unit rotation  $\Delta\theta$  the resultant translational stiffnesses become

$$\begin{aligned}(k_{x\theta})_{1,2} &= 2k_r \left[ \cos^2 \phi + \frac{1}{m} \sin^2 \phi + \left(1 - \frac{1}{m}\right) \frac{b}{h - R} \sin \phi \cos \phi \right] \\(k_{z\theta})_{1,2} &= 2k_r \left[ \sin^2 \phi + \frac{1}{m} \cos^2 \phi + \left(1 - \frac{1}{m}\right) \frac{h - R}{b} \sin \phi \cos \phi \right]\end{aligned}\tag{5.18}$$

From Figure 5.13 b, the rotational stiffness  $k_\theta$  about the C.R. is seen to be

$$(k_\theta)_{1,2} = b^2 (k_{z\theta})_{1,2} + (h - R)^2 (k_{x\theta})_{1,2}\tag{5.19}$$

Example 5.3:

This example shows the application of the above equations in solving for  $k_\theta$ .

Assume that  $\frac{k_r}{k_q} = 3$  and that  $\phi = 45^\circ$ , then from Equation (5.18),

$$(k_{x\theta})_{1,2} = 2 k_r \left[ \frac{1}{2} + \frac{1}{6} + \frac{2}{3} \times 2 \times \frac{1}{2} \right] = \frac{8}{3} k_r$$

$$(k_{z\theta})_{1,2} = 2 k_r \left[ \frac{1}{2} + \frac{1}{6} + \frac{2}{3} \times \frac{1}{2} \times \frac{1}{2} \right] = \frac{5}{3} k_r$$

and from Equation (5.19)

$$(k_\theta)_{1,2} = 2 k_r \left[ b^2 \times \frac{5}{3} + \frac{1}{4} b^2 \frac{8}{3} \right] = \frac{14}{3} b^2 k_r$$

5.2.4 Shock isolation system design using shock spectra. A decoupled 3-degree-of-freedom system can be treated as three undamped single-degree-of-freedom systems, involving vertical translation and horizontal translation as well as rotation. The shock spectra are then directly applicable for calculating the peak responses in the horizontal and vertical directions, but rotation inputs are normally neglected. The peak response is ordinarily assumed to occur in each translation mode simultaneously, thereby, resulting in an upper bound of the maximum response.

The step-by-step design procedure is as follows:

- (1) Describe the input in terms of vertical and horizontal shock spectra by the methods of Section 3.6.
- (2) Determine the mass and C.G. of the system. Note that, in order that the system may be treated as a rigid mass on springs, the internal stiffnesses of the mass system may have to be estimated, so as to be certain that the interconnecting elements of the mass have much higher stiffnesses than those required for the isolation system.
- (3) State the allowable accelerations of the mass. If  $A_a$  is the given allowable acceleration in any direction, then the resultant of the horizontal and vertical peak response must not exceed this value,

and

$$\sqrt{A_z^2 + A_x^2} \leq A_a$$

Sometimes the allowable horizontal and vertical accelerations may be specified separately as  $A_z$  (vertical) and  $A_x$  (horizontal). If these two allowable values are equal, then

$$A_z = A_x = .707 A_a$$

- (4) Enter the shock spectra (Figure 5.14) at the tolerable accelerations to determine the frequency requirements ( $f_z$  and  $f_x$ ) and the peak displacements ( $z_{\max}$  and  $x_{\max}$ ).
- (5) Select an arrangement of springs (and types) that will give adequate performance requirements of the frequency and the displacement determined by Figure 5.14. (See Section 5.9 for feasible spring arrangements for specific requirements. The arrangement must be symmetrical.) Either Step 6a, immediately following, or Step 6b, page 275, may then be performed.

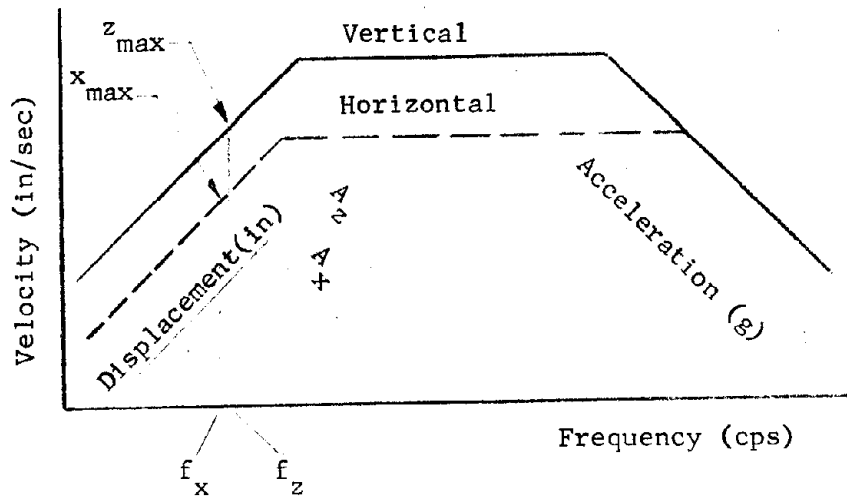


FIGURE 5.14: SHOCK SPECTRA CRITERIA

(6a) Horizontal and vertical springs (springs act in tension and compression only, i.e., no end fixity). See Figure 5.15.

VERTICAL MOTION

HORIZONTAL MOTION

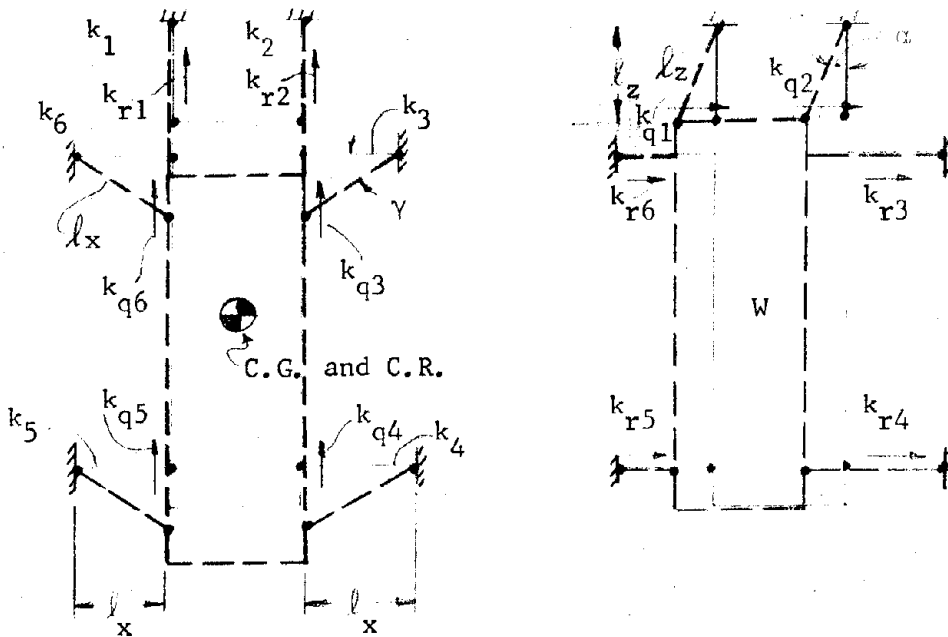


FIGURE 5.15: VERTICAL AND HORIZONTAL DISPLACEMENTS



Calculate maximum allowable spring rates,  $\Sigma k_z$  and  $\Sigma k_x$ , from the fundamental equation:

$$k = 4 \pi^2 f^2 m$$

Establish support points based on given envelope. Calculate angles,  $\gamma$  and  $\alpha$ , (see Figure 5.15) at peak dynamic response. If  $\gamma$  and  $\alpha$  are small, linear independent behavior in horizontal and vertical directions may be assumed. (For large angles greater than approximately  $15^\circ$ , the non-linear response accelerations may be significantly higher than the predicted response based on linear behavior, but the displacements will not be affected if the response is in the constant displacement region of the shock spectra. A more refined dynamic analysis may be required for such a situation.)

The axial spring rates are estimated by the following method.

First calculate maximum allowable  $\Sigma k_z$  and  $\Sigma k_x$ .

$$k_z = 4 \pi^2 f_z^2 m \quad k_x = 4 \pi^2 f_x^2 m$$

(The summation symbol is dropped since individual spring stiffnesses have a number designation.)

$$k_z = k_{r1} + k_{r2} + k_{q3} + k_{q4} + k_{q5} + k_{q6}$$

$$k_x = k_{r1} + k_{r2} + k_{r3} + k_{r4} + k_{r5} + k_{r6}$$

The total allowable axial spring rates are

$$k_{r1} + k_{r2} = k_z - \left( \frac{P_{pl1}}{l_x} + \frac{P_{pl2}}{l_x} + \frac{P_{pl3}}{l_x} + \frac{P_{pl4}}{l_x} \right)$$

$$k_{r3} + k_{r4} + k_{r5} + k_{r6} = k_x - \frac{W}{l_z}$$

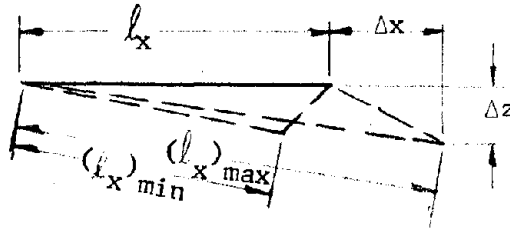
where  $P_{pl}$  = Preload in horizontal springs

$W$  = Weight of suspended mass

$l_x$  and  $l_z$  = Spring lengths in the static position.

The individual axial spring rates are determined by choosing the constants in the system so that Equations (5.3) and (5.4) result in zero eccentricities, i.e.,  $R_x = R_z = 0$ .

The peak axial dynamic spring displacements per spring are calculated from the combined displacements in the geometry shown below:



$$\Delta r = \begin{cases} (l_x)_{\max} - (l_x) \\ (l_x) - (l_x)_{\min} \end{cases}$$

The system design for this specific system is now complete with the three basic requirements established:

- (a) Axial spring rate per spring,  $k_{ri}$
- (b) Peak axial dynamic displacement,  $\Delta r$ , in each spring. It must be remembered that  $\Delta r$  will be greater than  $x_{\max}$  and  $z_{\max}$  because of the combined excursion,
- (c) Rattlespace requirements  $x_{\max}$  and  $z_{\max}$ , peak displacements, occurring in any phasing as shown in Figure 5.16.

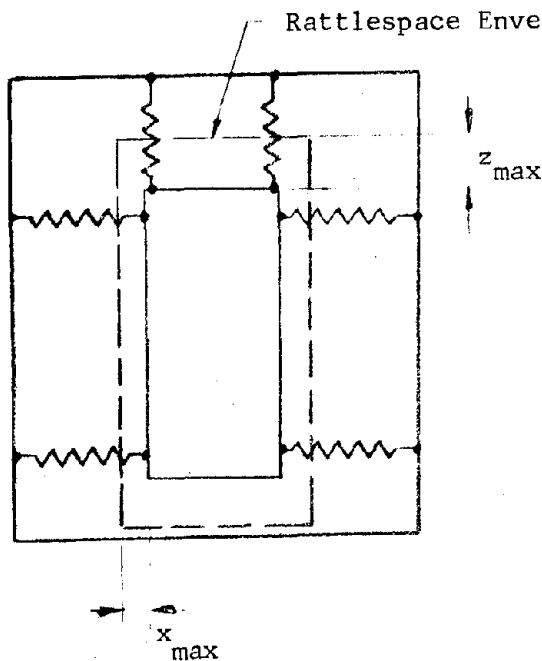


FIGURE 5.16: RATTLESPACE ENVELOPE

Design Example 5.4

Step 1: The input in terms of a shock spectra is specified in Figure 5.17.

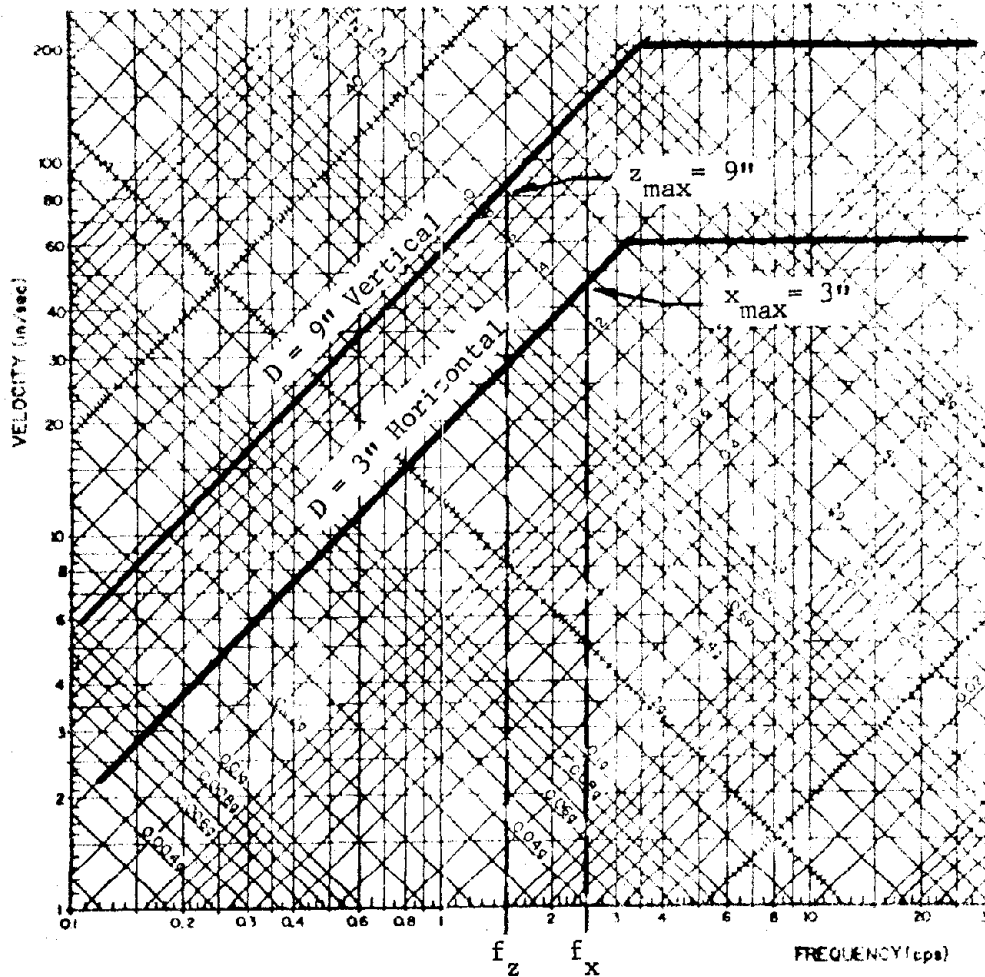


FIGURE 5.17: SHOCK SPECTRA CRITERIA

Steps 2 and 3: An equipment module weighing 3860 lbs is to be supported so that the peak dynamic acceleration response is less than 3 g's. The mass has approximately uniform distribution and the mass C.G. is assumed to be at the geometrical C.G.

Step 4: From Figure 5.17 for a resultant response, A less than 3 g's, the horizontal and vertical response allowables are:

$$A_z = 2g \quad , \quad A_x = 2g$$

Design Example 5.4 (continued)

Peak dynamic displacements are:  $x_{\max} = 3$  inches,  $z_{\max} = 9$  inches.

Limiting frequencies are:

$$f_z \leq 1.5 \text{ cps} \quad f_x \leq 2.5 \text{ cps}$$

Step 5 Design Configuration: Vertical and horizontal springs are positioned so that the resultant horizontal and vertical spring rates are symmetrical with the C.G., i.e., the center of rigidity is coincident with the C.G., in the static (1 g) condition as shown in Figure 5.18. The two vertical springs will have equal spring rates; and horizontal spring rates at each level are equal.

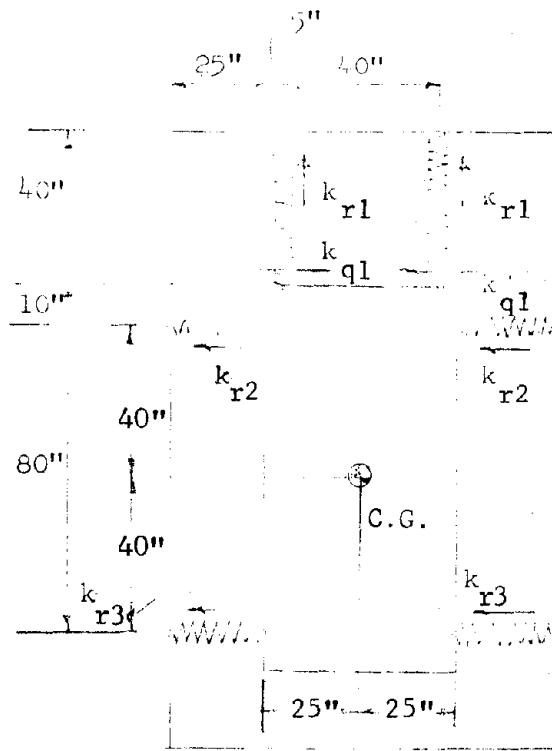


FIGURE 5.18

Step 6a: The resultant spring rate requirements are:

$$k_z = 4 \pi^2 (1.5)^2 (10) = 900 \text{ lb/in}$$

$$k_x = 4 \pi^2 (2.5)^2 (10) = 2500 \text{ lb/in}$$

Design Example 5.4 (continued)

Assume that the horizontal springs will all have a tension preload

$$\begin{aligned}
 P_{p\ell} &= 100 \text{ lbs} \\
 2k_{r1} &= 900 - \frac{4(100)}{25} \\
 k_{r1} &= 442 \text{ lbs/in} \\
 2k_{r2} + 2k_{r3} &= 2500 - \frac{3860}{40} = 2403 \text{ lbs/in}
 \end{aligned}$$

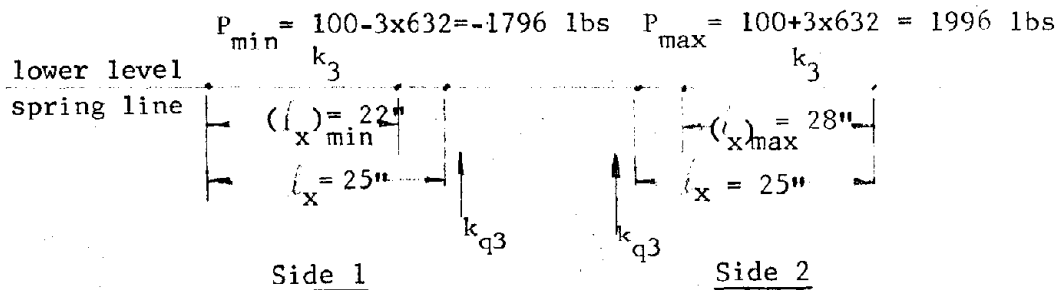
From Equation (5.3), for  $R_z = 0$

$$2k_{r3}(40) - 2k_{r2} 40 - 97 \times 50 = 0$$

$k_{r2}$  and  $k_{r3}$  are then calculated from the above two equations

$$k_{r2} = 570 \text{ lbs/in} \quad k_{r3} = 632 \text{ lbs/in}$$

The increase of lateral spring rates at peak dynamic response will now be checked. First, consider the two horizontal springs at the lower level. On one side the spring is in tension, and on the other side the spring acts in compression.

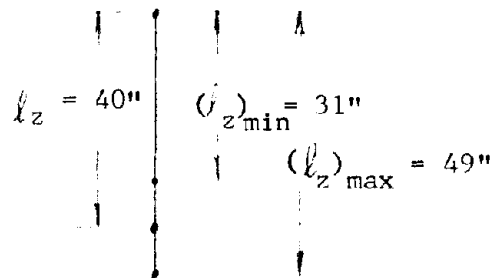


on Side 1 :  $(k_{q3})_{\min} = -1796/22 = -82 \text{ lbs/in}$

on Side 2 :  $(k_{q3})_{\max} = 1996/28 = +71 \text{ lbs/in}$

The lateral spring rate of the vertical springs at peak dynamic response is:

Design Example 5.4 (continued)



$$(k_{q1})_{\max} = \frac{3860/2 + 442 \times 9}{49} = 120 \text{ lbs/in}$$

$$(k_{q2})_{\min} = \frac{3860/2 - 442 \times 9}{49} = -42 \text{ lbs/in}$$

The above maximum lateral spring rates can be compared with the axial spring rates in their respective translation modes. For example, in the horizontal mode:

$$(k_{q1})_{\max} \cong 10 \text{ percent } (2 k_{r2})$$

$$(k_{q1})_{\min} \cong 5 \text{ percent } (2 k_{r2})$$

in the vertical mode

$$(k_{q3})_{\max} \text{ and } (k_{q3})_{\min} \cong 15 \text{ percent } (k_{r1})$$

The maximum and minimum lateral spring rates of the horizontal springs can be reduced significantly by lowering the horizontal frequency to well below the allowable. For example,

$$\text{let } f_x = 0.5 \text{ cps}$$

The relative response displacement remains 3 inches from the shock spectra envelope of Figure 5.17, but the horizontal stiffness is significantly reduced

$$k_x = 100 \text{ lbs/in}$$

whereas, at  $f_x = 2.5 \text{ cps}$ ,  $k_x$  was 2500 lbs/in. Therefore, by inspection the lateral spring rates of the horizontal springs now become insignificant compared to  $k_{r1}$ .

(6b) Inclined Spring System: From the geometry of the system and the characteristics of the spring, i.e., ratio,  $k_r/k_q$ , to be used, determine inclination angle,  $\phi$ , from Figure 5.12 so that the C.G. and C.R. are concentric from Equations (5.12) and (5.13). Calculate maximum allowable vertical and horizontal rates,  $k_z$  and  $k_x$ , from frequency equation as shown in Step (6a). Calculate the axial spring rates of each individual spring from Equation (5.8 a,b) neglecting the non-linear term. Both equations must be satisfied.

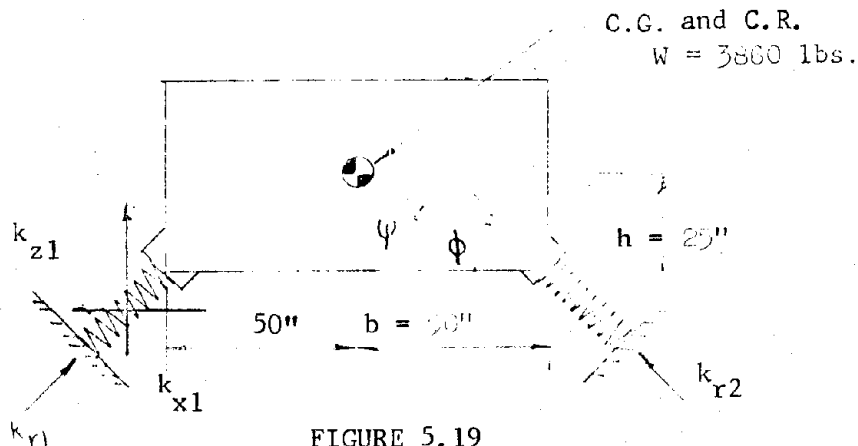
Design Example 5.5

Steps 1 - 4: An equipment module with mass and geometrical properties is specified in Figure 5.19. The shock spectra envelope in the low frequency region is defined by constant displacement lines of  $D = 6''$  for vertical relative response and  $D = 2''$  for horizontal relative response. The acceleration response is to be less than 3 g. The maximum allowable responses determined from the shock spectra envelope defined by the given criteria are:

$$A_z = A_x \leq 2g ; f_z \leq 1.7 \text{ cps} ; f_x \leq \text{cps} ; x_{\text{max}} = 2''$$

$$z_{\text{max}} = 6''$$

Step 5 Design Configuration: Use inclined springs at the base with an inclination angle,  $\phi$ , and spring rate ratio,  $k_r/k_q$ , to make the C.R. coincide with the C.G.



Design Example 5.5 (continued)

Step 6b: From Equation (5.12) for C.R. to be coincident with C.G. by

$$\psi = h/b = 25/50 = 0.5$$

Let  $\phi = 45^\circ$  and from Figure 5.12 the required ratio,  $m = k_r/k_q$ , is found to be:

$$m = \frac{k_r}{k_q} = 3$$

The allowable vertical spring rate is calculated from the frequency equation:

$$k_z = 4 \pi^2 (1.7)^2 10 = 1140 \text{ lb/in}$$

From Equation (5.8b) (Due to symmetry,  $k_{r1} = k_{r2}$ ,  $k_{q1} = k_{q2}$ .)

$$k_{r1} \sin^2 45^\circ + \frac{k_{r1}}{3} \cos^2 45^\circ = \frac{1140}{2}$$

$$k_{r1}/2 + k_{r1}/6 = 1140/2$$

$$k_{r1} = 855 \text{ lbs/in}$$

$$k_{q1} = 855/3 = 285 \text{ lbs/in}$$

The allowable horizontal spring rate is:

$$k_x = 4 \pi^2 (3)^2 (10) = 3540 \text{ lbs/in}$$

Using the calculated values for  $k_{r1}$  and  $k_{q1}$ , the horizontal spring rate is, from Equation (5.8a)

$$k_x = 2(k_r \cos^2 \phi + k_q \sin^2 \phi)$$

$$= 2(855/2 + 285/2) = 1140 \text{ lbs/in}$$

which satisfies the horizontal spring rate requirement,  $k_x \leq 3540$  lbs/in. The spring capability must be considered in providing the required ratio of  $k_r/k_q$ . Coil springs are the type springs that have this capability. Design factors and limitations are given in Section 6.



### 5.3 Near Symmetrical Systems.

Most practical shock isolation systems will not be true symmetrical systems, where the resultant of the spring forces is coincident with the center of gravity. The weight distribution and C.G. location are usually assumed during preliminary design, when the arrangement of springs is established. The final weight may be greater or less than the assumed weight; and the C.G. will shift as a result of different weight distributions. Therefore, the system design must account for variations in weight and C.G. location.

This section will cover systems with small eccentricities between the C.G. and C.R.

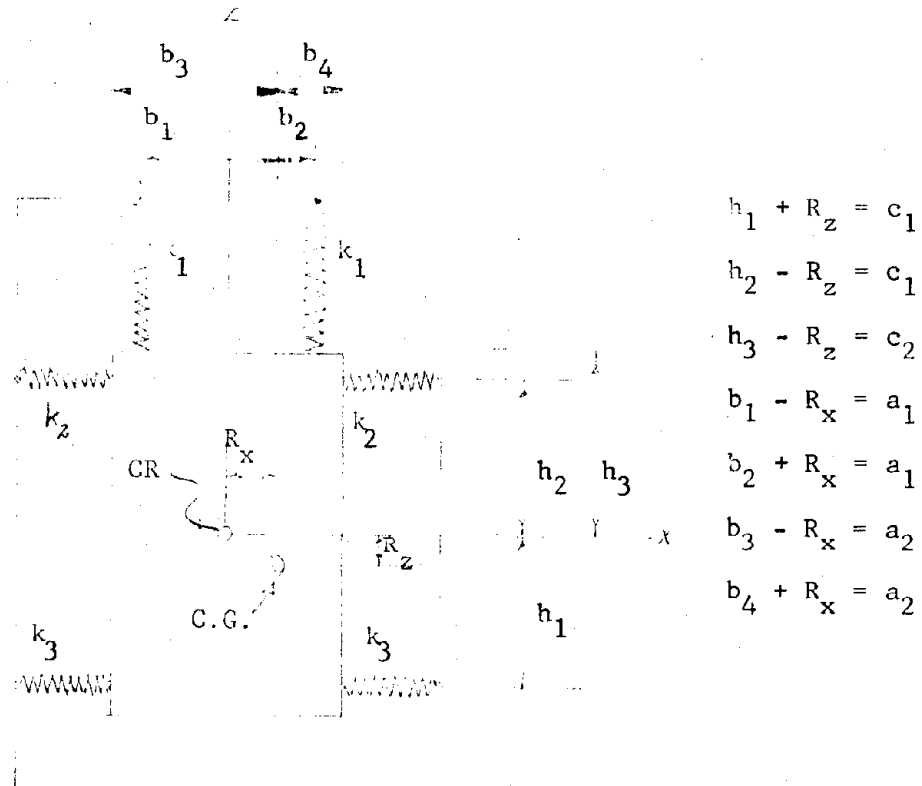


FIGURE 5.20: NEAR SYMMETRICAL SYSTEM

Consider the design shown in Figure 5.20 where the spring system arrangement was based on the C.G. being at the geometrical center. The design must now be verified based on the final C.G. being displaced from the C.R. by eccentricities,  $R_x$  and  $R_z$ . Assuming linear behavior at the spring

attachment points and small angle rotations where  $\sin \theta = \theta$  and  $\cos \theta = 1$ , the three equations describing the undamped free vibration of the system are:

$$m\ddot{z} + k_z z + k_z R_x \theta = 0 \quad (5.20)$$

$$m\ddot{x} + k_x x + k_x R_z \theta = 0 \quad (5.21)$$

$$J\ddot{\theta} + (k_\theta + k_x R_z^2 + k_z R_x^2) \theta + k_z R_x z + k_x R_z x = 0 \quad (5.22)$$

where

$$k_z = 2k_{r1} + 2k_{q2} + 2k_{q3}$$

(no preload in horizontal springs)

$$k_x = 2k_{q1} + 2k_{r2} + 2k_{r3}$$

$$k_\theta = 2b_3^2(k_{r2} + k_{r3}) + 2c_2^2(k_{q1}) + 2a_1^2(k_{r1}) + 2a_2^2(k_{q2} + k_{q3})$$

The ground motion is specified as a vertical and horizontal displacement of the support points. The above equations then become

$$m\ddot{z} + k_z z + k_z R_x \theta = k_z z_s \quad (5.20a)$$

$$m\ddot{x} + k_x x + k_x R_z \theta = k_x x_s \quad (5.21a)$$

$$J\ddot{\theta} + (k_\theta + k_x R_z^2 + k_z R_x^2) \theta + k_x R_z x + k_z R_x z = k_x R_z x_s + k_z R_x z_s \quad (5.22a)$$

Introducing a coordinate transformation so that the relative displacement response can be obtained, let

$$z = z - z_s \quad \ddot{z} = \ddot{z} - \ddot{z}_s$$

$$y = x - x_s \quad \ddot{y} = \ddot{x} - \ddot{x}_s$$

$$\theta = \theta \quad \ddot{\theta} = \ddot{\theta}$$

Equations (5.20), (5.21), (5.22) become

$$m\ddot{z} + k_z z + k_z R_x \theta = -m\ddot{z}_s \quad (5.20b)$$

$$m\ddot{y} + k_x y + k_x R_z \theta = -m\ddot{x}_s \quad (5.21b)$$

$$J\ddot{\theta} + (k_\theta + k_x R_z^2 + k_z R_x^2) \theta + k_x R_z y + k_z R_x z = 0 \quad (5.22b)$$

The coupled frequencies are calculated from the homogeneous portion of the equations and are based on harmonic response. (See Appendix A for derivation.)

The resulting frequency equation is:

$$\begin{aligned} \omega^6 - \omega^4 \left[ \left( \omega_z^2 + \omega_x^2 + \omega_\theta^2 \right) + \frac{1}{\rho^2} \left( R_z^2 \omega_x^2 + R_x^2 \omega_z^2 \right) \right] \\ + \omega^2 \left[ \left( \omega_x^2 \omega_z^2 + \omega_z^2 \omega_\theta^2 + \omega_x^2 \omega_\theta^2 \right) + \frac{\omega_x^2 \omega_z^2}{\rho^2} \left( R_x^2 + R_z^2 \right) \right] \\ - \omega_x^2 \omega_z^2 \omega_\theta^2 \end{aligned} \quad (5.23)$$

where  $\omega_z$ ,  $\omega_x$ , and  $\omega_\theta$  are the uncoupled frequency parameters given by

$$\omega_z^2 = \frac{k_z}{m} \quad \omega_x^2 = \frac{k_x}{m} \quad \omega_\theta^2 = \frac{k_\theta}{J}$$

and  $\rho^2 = J/m$  (radius of gyration).

The frequency equation is a cubic equation in  $\omega^2$ . The roots of the equation are the three coupled frequencies,  $\omega_1^2$ ,  $\omega_2^2$ ,  $\omega_3^2$ ; and are expressed in terms of the uncoupled frequencies,  $\omega_z$ ,  $\omega_x$ ,  $\omega_\theta$ , the eccentricities  $R_x$ ,  $R_z$ , and the physical parameters of the rigid mass,  $m$ ,  $J$ ,  $\rho$ . A computer solution is given in Appendix A for the three roots of the frequency equation for numerical values assigned to the shock isolated system characteristics.

Two cases will be treated here; (a) coupling negligible, and (b) coupling significant. The significance of the coupling can be roughly estimated if the coupled frequencies are known for comparison with the uncoupled frequencies. The response of the coupled system will be close to the single-degree-of-freedom response (uncoupled) when the coupled frequencies are close to the uncoupled frequencies. This will be the case when the eccentricities,  $R_x$  and  $R_z$ , are small compared to the radius of gyration,  $\rho$ , and when the uncoupled pitch frequency,  $\omega_\theta$ , is much greater than the translation frequencies,  $\omega_z$  and  $\omega_x$ .

(a) Negligible coupling. Consider first a two-degree-of-freedom system with one translation mode and a pitch mode. It has been shown in Reference 2.6, and it appears in Figure 5.21 that for

$$\frac{R}{\rho} < 1/2 \text{ and } \frac{\omega_{\theta}}{\omega_t} > 1.5$$

the coupled frequencies,  $\omega_1$  and  $\omega_2$ , are within 9 percent of the uncoupled frequencies,  $\omega_{\theta}$  and  $\omega_t$ . In the above relationships

$$\rho = \sqrt{\frac{J}{m}}, \text{ the radius of gyration}$$

$$R = \text{eccentricity between C.G. and C.R.}$$

$$\omega_{\theta} = \text{pitch frequency, uncoupled.}$$

$$\omega_t = \text{translation frequency } (\omega_x \text{ or } \omega_z), \text{ uncoupled}$$

For example: for  $\omega_{\theta}/\omega_t = 1.5$ ,  $\omega_1/\omega_t = 0.9$ ;  $\omega_1 = 0.9 \omega_t$

$$\omega_2/\omega_t = 1.6; \omega_2 = 1.6/1.5 (\omega_{\theta}) = 1.07 \omega_{\theta}$$

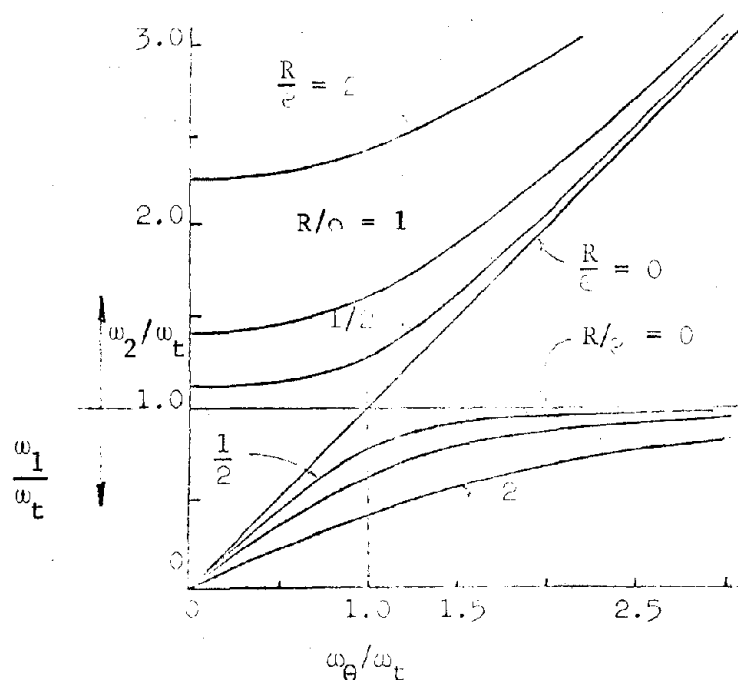


FIGURE 5.21

Consider next a three-degree-of-freedom system that has two translation modes and one pitch mode. An estimate of the significance of  $R_x$  combined with  $R_z$  can be obtained by assuming that the interaction of the two translation modes with pitch can be approximated by an equivalent two-degree-of-freedom system in which the equivalent  $R$  and  $\omega_t$  values relating to the two eccentricities and two translational frequencies are given by

$$R = \sqrt{R_x^2 + R_z^2} \quad \text{and} \quad \omega_t = \sqrt{\omega_x^2 + \omega_z^2}$$

The limiting criteria may, therefore, be written as:

$$R = \sqrt{R_x^2 + R_z^2} < 1/2 \sqrt{\frac{J}{m}} \quad (5.24)$$

and

$$\omega_\theta > 1.5 \sqrt{\omega_x^2 + \omega_z^2} \quad (5.25)$$

A coupled three-degree-of-freedom linear system may be treated as an uncoupled linear system if the above relationships are satisfied, and the response predicted by shock spectra, horizontal and vertical peak displacements and accelerations is a satisfactory measure of the dynamic behavior of the shock isolated system.

#### Example 5.6

In the dynamic model shown in Figure 5.20 the following numerical values are assumed for the physical characteristics of the system.

$$\begin{aligned} m &= 10 \text{ lbs sec}^2/\text{in} \\ k_z &= 1000 \text{ lbs/in} \\ k_x &= 10,000 \text{ lbs/in} \\ R_x &= 3 \text{ in} \\ R_z &= 2 \text{ in} \\ J_{C.G.} &= 800 \text{ in-lbs sec}^2 \\ k_\theta &= 5.6 \times 10^6 \text{ in-lbs} \end{aligned}$$

Example 5.6 (continued)

The frequency parameters are:

$$\omega_x^2 = \frac{k_x}{m} = 1000 \text{ 1/sec}^2$$

$$\omega_z^2 = \frac{k_z}{m} = 100 \text{ 1/sec}^2$$

$$\omega_\theta^2 = \frac{k_\theta}{J} = 7000 \text{ 1/sec}^2$$

The radius of gyration is:

$$\rho = \sqrt{\frac{J}{m}} \cong 9 \text{ in}$$

The equivalent R and  $\omega_t$  are:

$$R = \sqrt{3^2 + 2^2} = 3.6 \text{ in}$$

$$\omega_t = \sqrt{1000 + 100} = 32 \text{ 1/sec}$$

The limiting ratios defined by Equations 5.24 and 5.25 are:

$$\frac{R}{\rho} = 3.6/9 = 0.4 \quad \frac{\omega_\theta}{\omega_t} = 83.7/32 = 2.62$$

which are within the limits where the peak response may be predicted directly from the shock spectra without appreciable error.

(b) Significant coupling. The system shown in Figure 5.22 is a

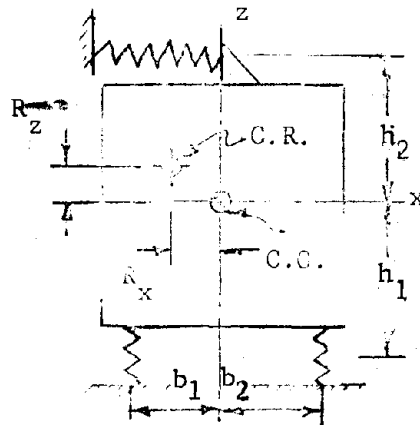


FIGURE 5.22

typical equipment isolation system, where  $R_x$  and  $R_z$  may be relatively small, but the pitch frequency,  $\omega_\theta$ , is close to the translation frequencies,  $\omega_x$  and  $\omega_z$ . Consequently, the pitch response,  $\theta$ , may be significant, and it may introduce additional displacements at the equipment corners and spring support points. Additional rattlespace and spring travel capability are thus required, but the response accelerations are not significantly amplified.

This situation is treated here by the normal mode method and an upper bound to the response is obtained.

For the three-degree-of-freedom system shown in Figure 5.22, the equations of relative motion are defined by Equations (5.20b), (5.21b), and (5.22b). The solution to these equations is given in Appendix A where the coupled equations are written as uncoupled equations in the normal coordinate system. In the normal coordinate system, the equations are of the same form as the equation of a single-degree-of-freedom system, and peak responses for each mode may be obtained directly from the shock spectra.

For the particular case illustrated, the upper bound on the maximum rotation response is given by (see Appendix A for derivation)

$$\begin{aligned} \theta_{\max} = & \left| \beta_{31} \left[ \frac{m \beta_{11} D_{11} + m \beta_{21} D_{21} + J \beta_{31} D_{31}}{m \beta_{11}^2 + m \beta_{21}^2 + J \beta_{31}^2} \right] \right| \left| \beta_{31} \right| \quad (1) \\ & + \left| \beta_{32} \left[ \frac{m \beta_{12} D_{12} + m \beta_{22} D_{22} + J \beta_{32} D_{32}}{m \beta_{12}^2 + m \beta_{22}^2 + J \beta_{32}^2} \right] \right| \left| \beta_{32} \right| \quad (2) \\ & + \left| \beta_{33} \left[ \frac{m \beta_{13} D_{13} + m \beta_{23} D_{23} + J \beta_{33} D_{33}}{m \beta_{13}^2 + m \beta_{23}^2 + J \beta_{33}^2} \right] \right| \left| \beta_{33} \right| \quad (3) \end{aligned} \quad (5.26a)$$

where

- $D_{11}$  = vertical response spectra displacement at frequency 1
- $D_{21}$  = horizontal response spectra displacement at frequency 1
- $D_{31}$  = 0 (no rotational input)
- $D_{12}$  = vertical response spectra displacement at frequency 2
- $D_{22}$  = horizontal response spectra displacement at frequency 2

$$\begin{aligned}
D_{32} &= 0 \text{ (no rotational input)} \\
D_{13} &= \text{vertical response spectra input at frequency 3} \\
D_{23} &= \text{horizontal response spectra input at frequency 3} \\
D_{33} &= 0
\end{aligned}$$

and  $\beta_{ij}$  are amplitude ratios in each mode (defined in Appendix A).

The upper bound translation displacements of the C.G. are:

Relative horizontal displacement

$$(y)_{\max} = \beta_{21} [(1)] + \beta_{22} [(2)] + \beta_{23} [(3)] \quad (5.26b)$$

where the terms in the bracket are defined in Equation (5.26a).

Relative vertical displacement

$$(z)_{\max} = \beta_{11} [(1)] + \beta_{12} [(2)] + \beta_{13} [(3)] \quad (5.26c)$$

The following numerical example illustrates the procedure in solving Equation (5.26).

#### Example 5.7

An equipment module weighing 1800 lbs is isolated from shock with a spring support arrangement as shown in Figure 5.22. The shock spectra in Figure 5.23 represent the peak relative response envelope of the vertical and horizontal motions if there was no coupling. Determine the upper bound response when coupling is considered if the properties of the isolation system are:

$$\begin{aligned}
\text{Weight} &\sim 1800 \text{ lb} \\
\text{Moment of inertia} &\sim 1300 \text{ in-lb sec}^2 \\
k_x &= 2540 \text{ lb/in} \\
k_z &= 3320 \text{ lb/in} \\
R_x &= 2.5 \text{ in} \\
R_z &= 1.38 \text{ in} \\
k_\theta &= 2.287 \times 10^6 \text{ in-lb}
\end{aligned}$$



Example 5.7 (continued)

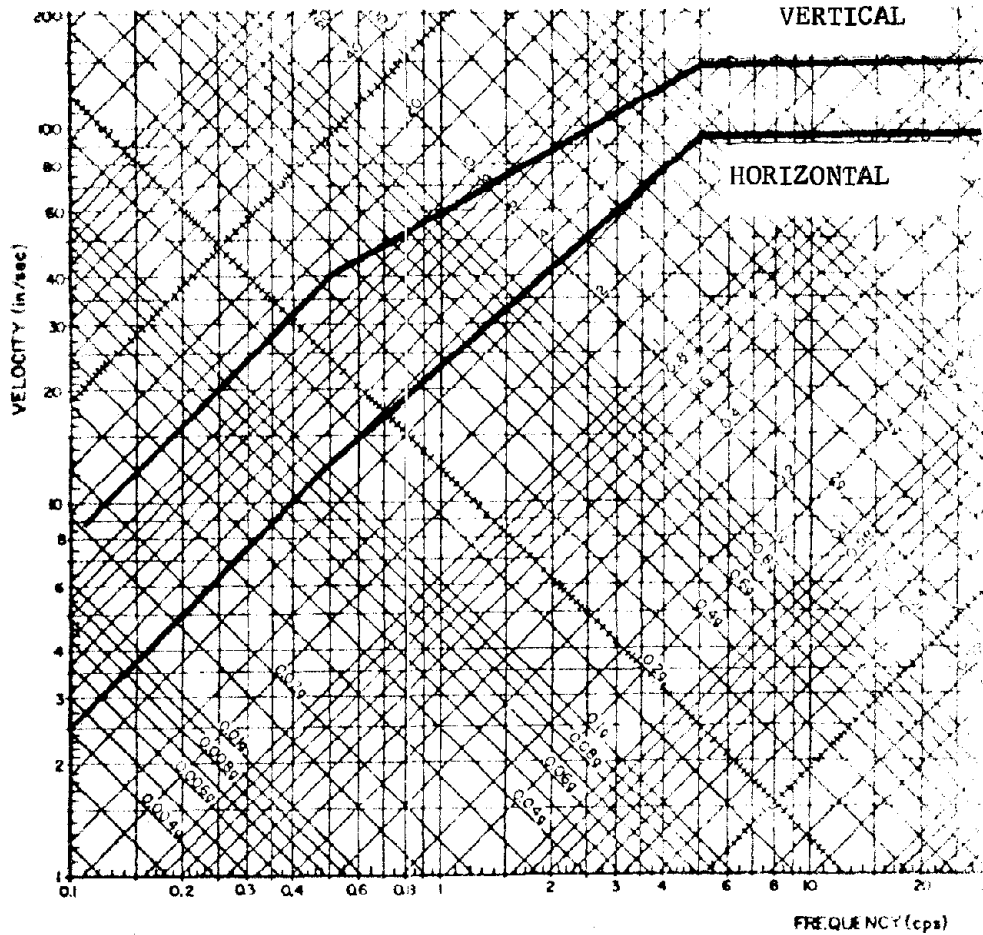


FIGURE 5.23

Step 1: Compute uncoupled natural frequencies

$$f_x = \frac{1}{2\pi} \sqrt{\frac{2540}{4.66}} = 3.7157 \text{ cps}$$

$$f_z = \frac{1}{2\pi} \sqrt{\frac{3320}{4.66}} = 4.2481 \text{ cps}$$

$$f_\theta = \frac{1}{2\pi} \sqrt{\frac{2.287 \times 10^6}{1300}} = 6.6755 \text{ cps}$$

Step 2: From the solution of Equation (5.23) by the procedure used in Appendix A, compute coupled frequencies

Example 5.7 (continued)

$$f_1 = 4.2169 \text{ cps}$$

$$f_2 = 3.7098 \text{ cps}$$

$$f_3 = 6.7356 \text{ cps}$$

Step 3: From the following equations which are derived in Appendix A, compute the modal matrix elements

$$\beta_{1n} = \frac{\frac{\omega_n^2}{z^2} R_x}{\frac{\omega_n^2}{x^2} R_z} \cdot \frac{\omega_n^2 - \omega_x^2}{\omega_n^2 - \omega_z^2}$$

$$\beta_{2n} = 1 \quad n = 1, 2, 3$$

$$\beta_{3n} = \frac{\omega_n^2 - \omega_x^2}{\frac{\omega_n^2}{x^2} R_z}$$

and the resulting matrix is:

$$\beta = \begin{bmatrix} -35.6160 & 0.0243 & 2.7354 \\ 1 & 1 & 1 \\ 0.2086 & -0.0023 & 1.6565 \end{bmatrix}$$

Step 4: From the shock spectra of Figure 5.23 and using the nomenclature of Equation (5.26), compute the peak translational vertical and horizontal response at the three coupled natural frequencies.

$$D_{11} = 4.8 \text{ in. from the vertical spectra envelope at frequency } f_1 = 4.2 \text{ cps}$$

$$D_{12} = 5.2 \text{ in. from the vertical spectra envelope at frequency } f_2 = 3.7 \text{ cps}$$

$$D_{13} = 3.4 \text{ in. from the vertical spectra envelope at frequency } f_3 = 6.7 \text{ cps}$$

$$D_{21} = 3.1 \text{ in. from the horizontal spectra envelope at frequency } f_1 = 4.2 \text{ cps}$$

$$D_{22} = 3.2 \text{ in. from the horizontal spectra envelope at frequency } f_2 = 3.7 \text{ cps}$$

$$D_{23} = 2.3 \text{ in. from the horizontal spectra envelope at frequency } f_3 = 6.7 \text{ cps}$$

Example 5.7 (continued)

$$D_{31} = 0$$

Since translation motions are only provided by the

$$D_{32} = 0$$

shock spectra, a rotation input is not considered.

$$D_{33} = 0$$

Step 5: Solve Equation (5.26) and take the absolute value of the result.

$$\theta_{\max} = \left| .20865 \left( \frac{-780.5}{5971.3} \right) \right| + \left| -.0023 \left( \frac{15.49}{4.669} \right) \right| + \left| 1.6565 \left( \frac{47.86}{3599.46} \right) \right|$$

$$\theta_{\max} = 0.057 \text{ rad}$$

$$y_{\max} = |0.13| + |3.32| + |0.013|$$

$$= 3.46''$$

$$z_{\max} = |4.7| + |0.08| + |0.035|$$

$$z_{\max} = 4.82''$$

Step 6: Compute the translational contribution of the rotation at the corners of the module and add to the translational response.

$$y_{\max} + \theta_{\max} h = 3.46 + (27.4 \text{ in})(.057 \text{ rad}) = 5.01''$$

$$z_{\max} + \theta_{\max} b = 4.82 + (13.0 \text{ in})(.057 \text{ rad}) = 5.56''$$

If the coupling effect had been neglected, the peak horizontal and vertical response would have been taken directly from the shock spectra (and rotation neglected) giving the following magnitudes

$$y_{\max} = 3.2'' \text{ at } f_x = 3.7 \text{ cps}$$

$$z_{\max} = 4.8'' \text{ at } f_z = 4.2 \text{ cps}$$

Therefore, it can be seen that the rattlespace at the corners and the spring travel capability will have to be increased to conservatively account for the coupled response.

## 5.4 Base Mounted Spring Mass Systems

5.4.1 Introduction. Usually, an attempt is made to achieve spring mass symmetry in the design of shock isolation systems; but frequently, circumstances require that an asymmetric system of one form or another be considered. This may be due in part to the rather elaborate support structure required to achieve symmetry if the protected structure is to be located above ground, or to the limited space available if the structure is to be located below ground level. The type of structure may also suggest a particular isolation technique which is more convenient to use than any other, for instance, the pendulous system currently used in silo housed missiles. Certain "off the shelf" equipments will have their mounting points established; and to rearrange the method of support will be costly.

In any case, the types of isolation systems which have been asymmetrically arranged are more often encountered than symmetrical cases. It may thus be assumed that this trend will continue since a system, whatever its type, can be considered to be satisfactory if it performs according to specification and is economically attractive.

The most serious objections to an asymmetrical system is the difficulty in predicting its transient response. The system may have many parameters which, when varied, profoundly alters the response of the system. The engineer is, therefore, interested in a parametric study of the effects of changes in system constants so that he may optimize the design. However, if certain parameters may vary during the normal use of the system, it is important that these changes do not markedly affect the response characteristics.

Before the advent of automatic computational methods, the amount of labor required to study the effects of parametric variations would allow only a cursory look at the system. Today it is fairly easy to write a computer program and obtain the dynamic response solutions for a large number of parametric variations. What is needed is a concise easily understood analysis which will allow the designer to evaluate his proposed design quickly and with a reasonable degree of accuracy. This section

concerns itself with establishing workable methods for evaluating the general response of asymmetric spring mass.

Base mounted systems are here considered as shown in Figure 5.24.

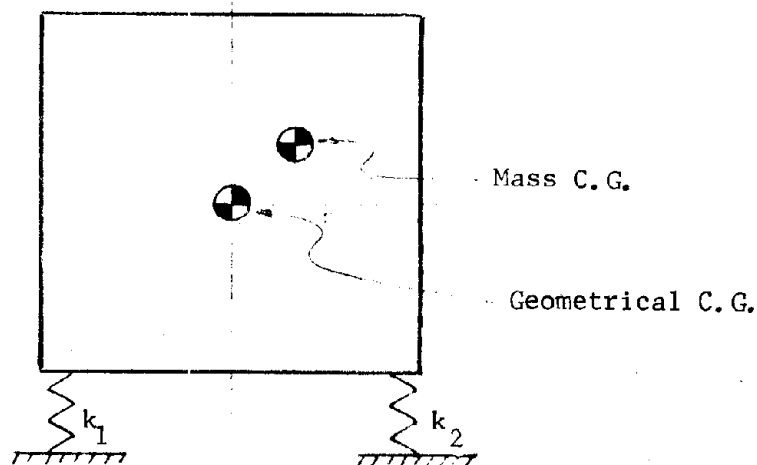


FIGURE 5.24

Vertical springs with end fixity are placed between the equipment or platform and the structure foundation. It was seen in Section 5.1 that the shock isolation system could be designed quickly and with sufficient accuracy by using shock spectra techniques, provided that the system was symmetrical, i.e., C.G. and C.R. are nearly coincident, and the shock disturbances were limited to occur along orthogonal axes.

The shock spectra techniques may also be applied to the base mounted system, except that certain allowances should be made to account for its more complex response motion. Whereas, in the symmetrical system, angular responses are not excited, these modes of response are always present in the asymmetrical system, and their severity can be estimated or determined by the degree of asymmetry or coupling present.

In general, the shock response of an isolated elastic structure will consist of three rigid body translations, three rigid body rotations, and an indeterminate number of deformational responses of the structure itself with all modes more or less coupled together. Obviously, a rigorous investigation of the complete motion is difficult, time consuming and often

unnecessary with proper precautions.

The rigid body equations of motion in a vertical plane x-z for small displacements of the base mounted system illustrated in Figure 5.24 are given by

$$m\ddot{x} + 2k_q \left[ x - x_s - R_z \theta \right] = 0 \quad (5.27)$$

$$m\ddot{z} + 2k_r \left[ z - z_s - R_x \theta \right] = 0 \quad (5.28)$$

$$\begin{aligned} J\ddot{\theta} + 2k_q \left[ \left( R_z^2 + R_x (x - x_s) \right) \theta - R_z (x - x_s) \right] + \\ 2k_r \left[ \left( b^2 + R_x^2 - R_z (z - z_s) \right) \theta - R_x (z - z_s) \right] - m g R_z \theta + \\ \left( 2k_q \left[ R_x (x - x_s) \right] + 2k_r \left[ b^2 - R_z (z - z_s) \right] - m g R_z \right) \beta_o - \\ m g R_x = 0 \end{aligned} \quad (5.29)$$

$$\beta_o = \frac{m g R_x}{2b^2 k_r - m g R_z}$$

where

- m = mass of structure
- J = mass moment of inertia about y axis through C.G.
- $x_s$  = displacement of foundation in x direction
- $z_s$  = displacement of foundation in z direction
- $k_q$  = spring rate in x direction lb/in per side
- $k_r$  = spring rate in z direction lb/in per side
- $\beta_o$  = angle of list due to asymmetrical load
- $R_z$  = (h + e) as shown in Figure 5.25a.

The spring components and idealized characteristics of the system are shown in Figure 5.25a. These equations are similar in form to Equations (5.20), (5.21) and (5.22) of Section 5.3, except that the spring rates have been

stated explicitly, and the static listing and foundation displacements have been accounted for.

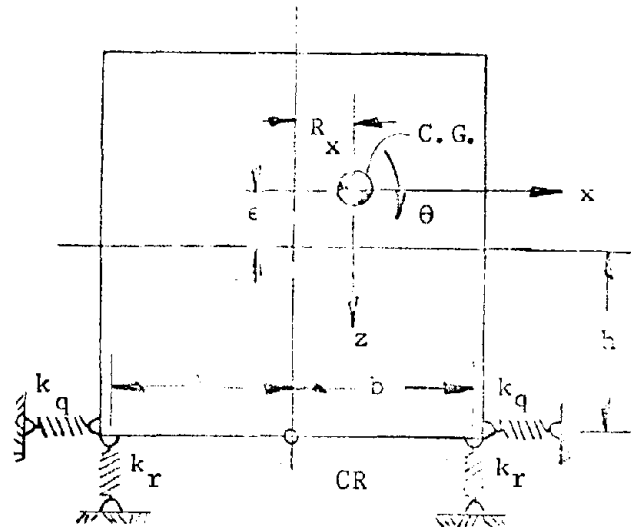


FIGURE 5.25a

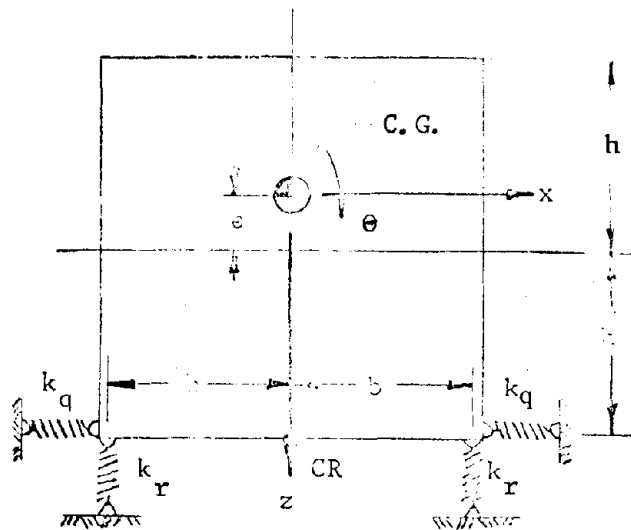


FIGURE 5.25b

If the placement of the mass is confined to the vertical center line.  $R_x = 0$ , the listing angle,  $\beta_0$ , vanishes, the system acquires onefold symmetry. and considerable simplification of Equations (5.27) and (5.29) will occur (see Figure 5.25b). For many systems the horizontal location of the C.G. is adjusted by ballast weights so as to keep the structure level.

Additional simplification is achieved by dropping the dynamic coupling terms and the pendulum term,  $mgR_z \theta$ .

The reduced equations are:

$$m\ddot{x} + 2k_q \left[ x - x_s - R_z \theta \right] = 0 \quad (5.27a)$$

$$m\ddot{z} + 2k_r (z - z_s) = 0 \quad (5.28a)$$

$$J\ddot{\theta} + 2k_q \left[ R_z^2 \theta - R_z (x - x_s) \right] + 2k_r b^2 \theta = 0 \quad (5.29a)$$

The effect of dropping these terms will change the total response of the system on the order of 5 percent for a high C.G. placement and imperceptibly for a very low C.G. location. These errors, therefore, are usually considered acceptable for analysis.

It is to be noted that Equations (5.27a), (5.28a) and (5.29a) describe a rigid body motion confined to a vertical plane. This restriction is a common one, and is justified on the basis that many structures are usually more responsive or critical in one direction than in another. If these assumptions cannot be justified, a more complete set of equations involving additional degrees-of-freedom must be considered. Additional terms describing viscous and friction damping forces could also have been included, but they are neglected on the assumption that their effect is small on peak acceleration and displacement response.

Shock spectra solutions similar to those discussed for symmetric and near symmetric systems (Sections 5.2 and 5.3) are a starting point (or preliminary design phase) of a base mounted system. The stiffness requirements and rattlespace requirements predicted from the shock spectra must now be modified to account for the significant coupling response. The following section (5.4.2) provides conservative guidelines for this preliminary design with recommended factors for modifying the shock spectra response requirements for a base mounted system.

The design is finally verified by solving the equations of motion by numerical methods for the specified input in terms of a velocity pulse. In this phase, the system is investigated for a range of all the parameters of importance, i.e., small shifts in C.G. location, weight variations, phasings of the horizontal and vertical components of the input pulse, etc., to



verify the adequacy of the design within the anticipated or specified variations in the magnitudes of these parameters. Section 5.4.3 demonstrates this final analysis phase with a numerical example illustrating the step by step procedure.

5.4.2 Preliminary analysis. Investigation has shown that for a physical system with a rectangular shape, as shown in Figure 5.24, the single-degree-of-freedom (SDOF) shock spectra can be modified to account for the effects of amplified response which occurs as the result of asymmetry in a base mounted system. This modification is stated as follows:

$$\left\{ \frac{V'_v}{V_v}, \frac{V'_h}{V_h}, \frac{D'_v}{D_v}, \frac{D'_h}{D_h} \right\} = 2 \quad (5.30)$$

where the primed symbols indicate amplified response and the unprimed symbols indicate SDOF shock spectra response. This modification factor of 2 will bound the response at all points on the periphery for practical systems defined by the following range of physical characteristics

$$0.2 < \frac{R_z^2}{\rho^2} < 2$$

$$0.8 < (f_\theta/f_z)^2 < 3$$

where

$$\rho^2 = \frac{J}{m}, \quad f_\theta = \frac{1}{2\pi} \sqrt{\frac{2k_q R_z^2 + 2k_r b^2}{J}}, \quad f_z = \frac{1}{2\pi} \sqrt{\frac{2k_q}{m}}$$

and

$$(f_\theta/f_z)^2 = \frac{1}{\rho^2} \left[ \frac{R_z^2}{2} + b^2 \right]$$

for the special case when the horizontal spring stiffness of the isolation system is close to half the vertical spring stiffness.

#### Example 5.8.

Assume that the equipment illustrated in Figure 5.22 is a square box with  $b = h = 10$  feet. Further assume that the equipment is placed in a shallow buried structure and that the foundation depth is 40 feet. The equipment must survive a 1 MT nuclear surface burst in the 300 psi over-pressure region. The soil is assumed uniform with a seismic velocity of 3000 ft/sec. The equipment must be isolated to the extent that its response

Example 5.8 (continued)

acceleration will not exceed 1 g either horizontally or vertically.

From the above data it is immediately possible to determine the peak shock ground motions and pulse shapes using Equations (3.19), (3.21) and (3.26) in Section 3.5.3. At the 40 foot depth, the peak downward acceleration, velocity and displacement are, respectively:

$$\begin{aligned}a_{vz} &= 28 \text{ g} \\v_{vz} &= 37.5 \text{ in/sec} \\d_v &= 5.2 \text{ in}\end{aligned}$$

In the horizontal direction, it is assumed that

$$\begin{aligned}a_h &= a_v = 28 \text{ g} \\v_h &= 2/3 v_v = 25 \text{ in/sec} \\d_h &= 1/3 d_v = 2 \text{ in}\end{aligned}$$

From the peak ground motions, the SDOF shock spectra of Figure 5.23 are constructed for the following response accelerations and rattlespaces:

$$\begin{aligned}A_v &= A_h = 2 a_v = 2 a_h = 56 \text{ g} \\V_v &= 1.5 v_v = 56.2 \text{ in/sec} \\V_h &= 1.5 v_h = 37.5 \text{ in/sec} \\D_v &= d_v = 6 \text{ in.} \\D_h &= d_h = 2 \text{ in.}\end{aligned}$$

The expressions of Equation (5.30) allow the shock spectra envelope to be modified, as illustrated in Figure 5.26 where the modified spectra envelope is indicated by the dashed lines.

Assume that the shape of a multistory platform is a rectangular box and behaves as a rigid body. The system is described by Figure 5.24,  $b = h = 120''$ , and for a platform length of 8 feet weighing 35 kips, it is found that

Example 5.8 (continued)

$$m = 91 \frac{\text{lb sec}^2}{\text{in}}$$

$$J = 1.14 \times 10^6 \text{ in lb sec}^2$$

$$e = -21.6 \text{ in}, \quad R_z = 120 - 21.6 = 98.4 \text{ in}$$

$$\rho^2 = \frac{J}{m} = 1.25 \times 10^4 \text{ in}^2$$

$$\frac{R_z^2 m}{J} = \frac{(98.4)^2 91}{1.14 \times 10^6} = .722$$

Enter the amplified shock spectra envelope of Figure 5.25 at the intersection of the 1 g vertical and horizontal response, and find the required frequencies

$$f_x = 1.6 \text{ cps horizontally}$$

$$f_z = 0.9 \text{ cps vertically}$$

Recalling that for a SDOF system  $f^2 = \frac{1}{4\pi^2} \frac{k}{m}$ , the translation spring rates are determined as

$$k_x = 4\pi^2 m f_x^2 = 4\pi^2 (91)(1.6)^2 = 9170 \text{ lb/in}$$

$$k_z = 4\pi^2 m f_z^2 = 4\pi^2 (91)(0.9)^2 = 2900 \text{ lb/in}$$

Assuming that coil springs are used, they usually are stiffer vertically than horizontally in the order of  $k_r/k_q \approx 2$ . Thus, if  $k_z = 2k_r = 2900 \text{ lb/in}$ , then  $k_x = 2k_q = 1450 \text{ lb/in}$ . In this case, the vertical frequency remains unchanged, but the horizontal frequency must now be

$$f_x = \frac{1}{2\pi} \sqrt{\frac{1450}{91}} = 0.6 \text{ cps}$$

The corresponding shock responses predicted in this preliminary study are from Figure 5.26 at the natural frequencies,  $f_z$  and  $f_x$ :

$$\ddot{x}_{\text{max}} = 0.15 \text{ g} \quad (x - x_s)_{\text{max}} = 4 \text{ inches}$$

$$\ddot{z}_{\text{max}} = 1 \text{ g} \quad (z - z_s)_{\text{max}} = 12 \text{ inches}$$

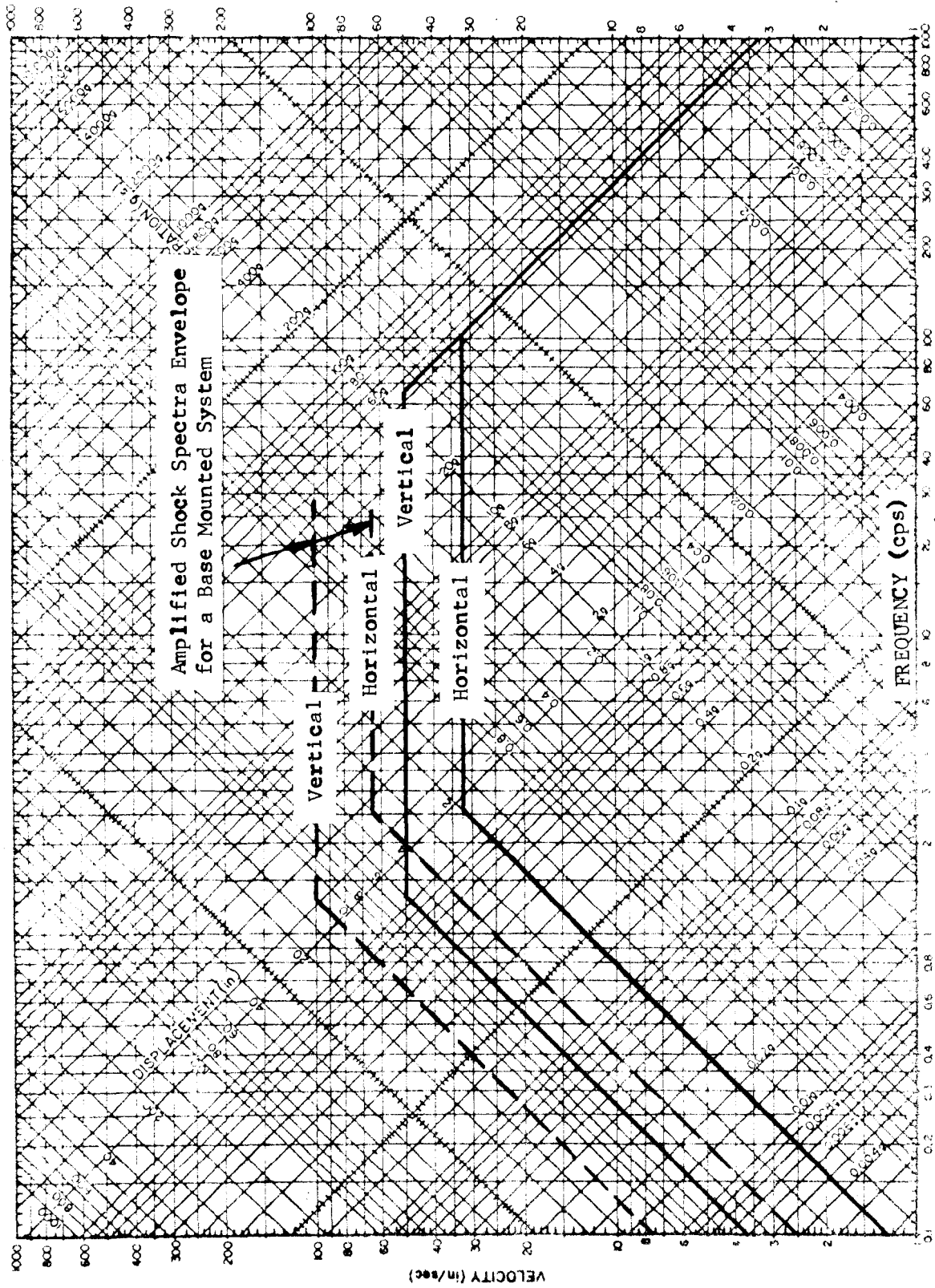


FIGURE 5.26

### Example 5.8 (continued)

It should be noted that this method for determining the peak response of the system is to be considered as an upper bound. Other methods are available for obtaining the response of the system such as the approximate one discussed in Section 5.3 and 5.7.

5.4.3 Analysis for waveform input. A reliable measure of the dynamic response of the system can be obtained by solving the equations of motion, (Equations (5.27a), (5.28a), (5.29a)) for the final design and evaluation. Since the input and physical parameters are seldom invariant, all anticipated variations in these parameters must be considered, and the design of the shock isolation system must be made adequate under the range of parameter variations considered.

The procedure is demonstrated by a numerical example with the necessary discussion.

### Example 5.9.

The system discussed (with a Preliminary Design Example 5.8) in Subsection 5.4.2 is to be analyzed by solving the equations of motions for a shock pulse consistent with the peak ground motion values specified. As a starting point, the unamplified SDOF shock spectra of Figure 5.26 is used to calculate preliminary spring characteristics.\*

For 1 g response,

$$f_x = 2.2 \text{ cps}$$

$$f_z = 1.3 \text{ cps}$$

and the resultant spring rates are

$$k_z = 4\pi^2 m f_v^2 = 4\pi^2 (91)(1.3)^2 = 6050 \text{ lb/in} \quad (k_r = 3025 \text{ lbs/in})$$

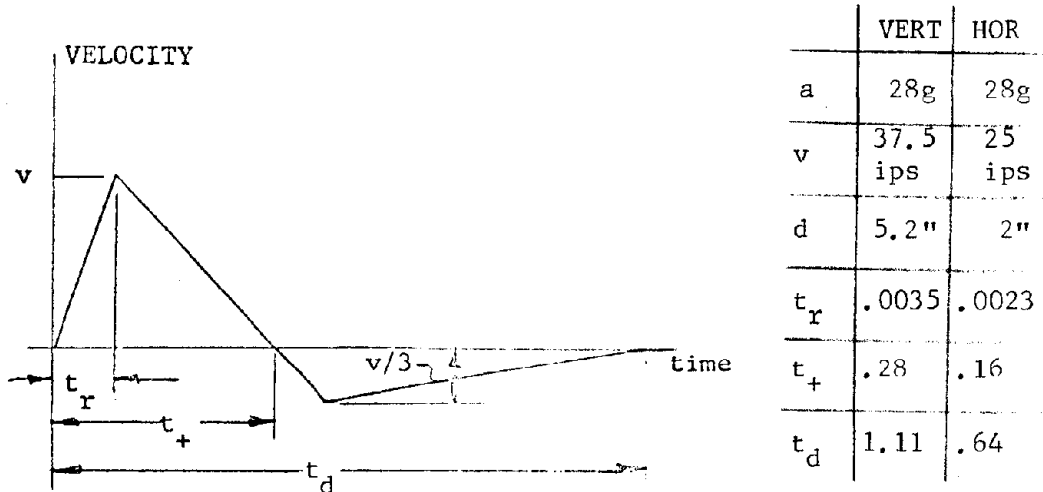
$$k_x = \frac{1}{2} k_z = 3025 \text{ lb/in} \quad (k_q = 1512 \text{ lbs/in})$$

---

\* If the objective of the dynamic analysis is only to verify adequacy of the preliminary design (of Example 5.8), then the spring rates calculated in the preliminary design should be used as a starting point. If the objective of the dynamic analysis is to converge onto a less conservative design, then the spring rates based on the shock spectra envelope for an SDOF system are used as a starting point. This latter approach is adopted in this example.

Example 5.9

Before the equations of motion can be solved, it is necessary to assume the vertical and horizontal pulse shapes. Triangular velocity pulses satisfying the peak values of acceleration, velocity and displacement (calculated in Example 5.8) are illustrated in the following sketch.



A velocity pulse with full ground return motion is assumed with peak negative velocity equal to 1/3 peak positive velocity. Pulse shapes are discussed and defined in Section 3.7. The critical durations are given by

$$t_r = \frac{v}{a}$$

$$t_+ = \frac{2d}{v}$$

Assume that  $t_d = t_+ + \frac{6d}{v} = 4 t_+$

Equations (5.27a), (5.28a), and (5.29a) have been written for numerical solution using the one-step integration method described in Section 2.6, and results were obtained by the electronic computer (Appendix C gives the step-by-step procedure for the solution). The response of the system has been determined for the case where the horizontal and the vertical components of the shock are in phase. The maximum values of absolute acceleration and relative displacement at the corners of the

Example 5.9 (continued)

structure are tabulated in Table 5.2, labeled as Case 1. It is noted that there is approximately a 50 percent increase in the vertical acceleration (shock spectra figures in parenthesis).

The springs will now be resized to fulfill the requirements of 1 g vertical acceleration by entering Figure 5.26 at the intersection of 1.3 cps and 1.54 g and proceeding along a constant displacement line to the intersection of 1 g. The corresponding frequency is seen to be 1 cps. Then, the new spring rate is

$$k_z = 4\pi^2 m f_z^2 = 4\pi^2 (91)(1) = 3580 \text{ lb/in, } (k_r = 1790 \text{ lb/in})$$

from which

$$k_x = 0.5 k_z = 1790 \text{ lb/in } (k_q = 895 \text{ lb/in})$$

The computed results, Case 2, Table 5.2, indicate that the vertical acceleration is 11 percent too high. The springs will now be sized again in exactly the same manner as before, thereby reducing the frequency to 0.9 cps and requiring spring rates of

$$k_z = 4\pi^2 (91)(0.9) = 2900 \text{ lb/in, } (k_r = 1450 \text{ lb/in})$$

$$k_x = 0.5 (k_z) = 1450 \text{ lb/in } (k_q = 725 \text{ lb/in})$$

Case 3 of Table 5.2 indicates that specifications in regard to 1 g acceleration have been met. This case is henceforth referred to as the index case to which further studies will be referenced. It should be noted that the vertical rattlespace of 11.2 inches is almost twice the one given by the original spectra envelope and the horizontal rattlespace is more than 1.5 times the spectral value. These are within the limits recommended by the modification factor of Equation 5.30.

Variation of parameters. It is now possible to determine the effects produced by assumed variations of the more important parameters in comparison with the index case.

a. Variation of mass. If the total mass of the system is varied by as much as  $\pm$  50 percent without disturbing any other properties of the system, the percentage change in response of the index case is tabulated in

### Example 5.9 (continued)

Table 5.1 as Cases 4 through 7 and plotted in Figure 5.27. It can be seen that the acceleration response is very sensitive to changes in mass, and the displacements are less sensitive, in general, but the variation is very non-linear.

b. Variation of moment of inertia. If the mass moment of inertia is increased by as much as 100 percent and decreased by as much as 90 percent, the changes in responses are tabulated as Cases 8 through 11 in Table 5.1 and plotted in Figure 5.28. The acceleration response and vertical displacement response are insensitive to small changes in moment of inertia (less than 25 percent), but the horizontal displacement response is sensitive to small changes in moment of inertia.

c. Location of center of mass. If the center of mass is displaced vertically upwards by 30 inches and vertically downwards by 10 inches, the computer results appear as Cases 12 and 13 in Table 5.1 and in Figure 5.29.

d. Phase lag/lead of horizontal shock pulse. To determine the effects of a phase change between the vertical and horizontal shock pulses, the horizontal pulse has been assumed either to lag or to lead the vertical pulse by one half of the horizontal pulse period equivalent to 0.32 seconds. The computer results appear as Cases 14 and 15. The effect is seen to be very small.

## 5.5 The Symmetrical Pendulum Systems

5.5.1 Description. Large multistory systems may be suspended vertically from springs attached at their sides with arms that extend to enclosure support points located above the C.G. of the system. The springs may be inclined and/or auxiliary horizontal springs may be provided to give additional horizontal stiffness and damping. Two alternative configurations are shown in Figure 5.30. A qualitative comparison of these schemes will first be made, followed by a numerical solution for one of the schemes.

(a) Dynamic response. Spring characteristics and support point locations can be chosen for both pendulum configurations so that maximum



TABLE 5.1

Case Number	Maximum Vertical Acceleration g units		Maximum Horizontal Acceleration g units		Maximum Vertical Rattlespace inches		Maximum Horizontal Rattlespace inches	
	g units	% change	g units	% change	inches	% change	inches	% change
1 Shock Spec.	1.54	(1.0)	0.41	(0.18)	8.4	(6.0)	3.8	(2.0)
2 1st corr.	1.11		0.25		10.4		3.3	
3 2nd corr.	0.95		0.19		11.2		3.1	
4 +10% mass	0.90	-5.3	0.18	-5.3	11.2	0	3.0	-3.2
5 -10% mass	1.02	+7.4	0.21	+9.0	10.8	-3.5	3.1	0
6 +50% mass	.73	-23.0	.10	-15.2	12.1	+8.4	2.9	-6.8
7 -50% mass	1.35	+41.1	.32	+69.5	8.4	-25.0	2.6	-14.9
8 +50% J	.91	-4.1	.17	-12.1	11.2	0	2.5	-20.0
9 +100% J	.67	-8.1	.14	-27.1	11.0	-1.8	2.2	-29.4
10 -50% J	1.08	+13.7	.33	+51.2	11.3	+0.9	3.4	+8.7
11 -90% J	1.45	+52.6	.80	+361.0	10.7	-4.0	3.0	-2.3
12 C.G. 3" up	0.96	-3.2	.27	+40.5	10.9	-2.9	2.5	-18.1
13 C.G. 1" dn.	0.92	-2.6	.19		11.8	-3.5	3.3	+5.3
14 0.36 leg	0.90	+1.0	0.18	-3.5	11.3	+1.0	2.9	-6.5
15 0.36 lead	0.90	-1.0	0.19	+1.5	11.0	-2.0	3.1	0

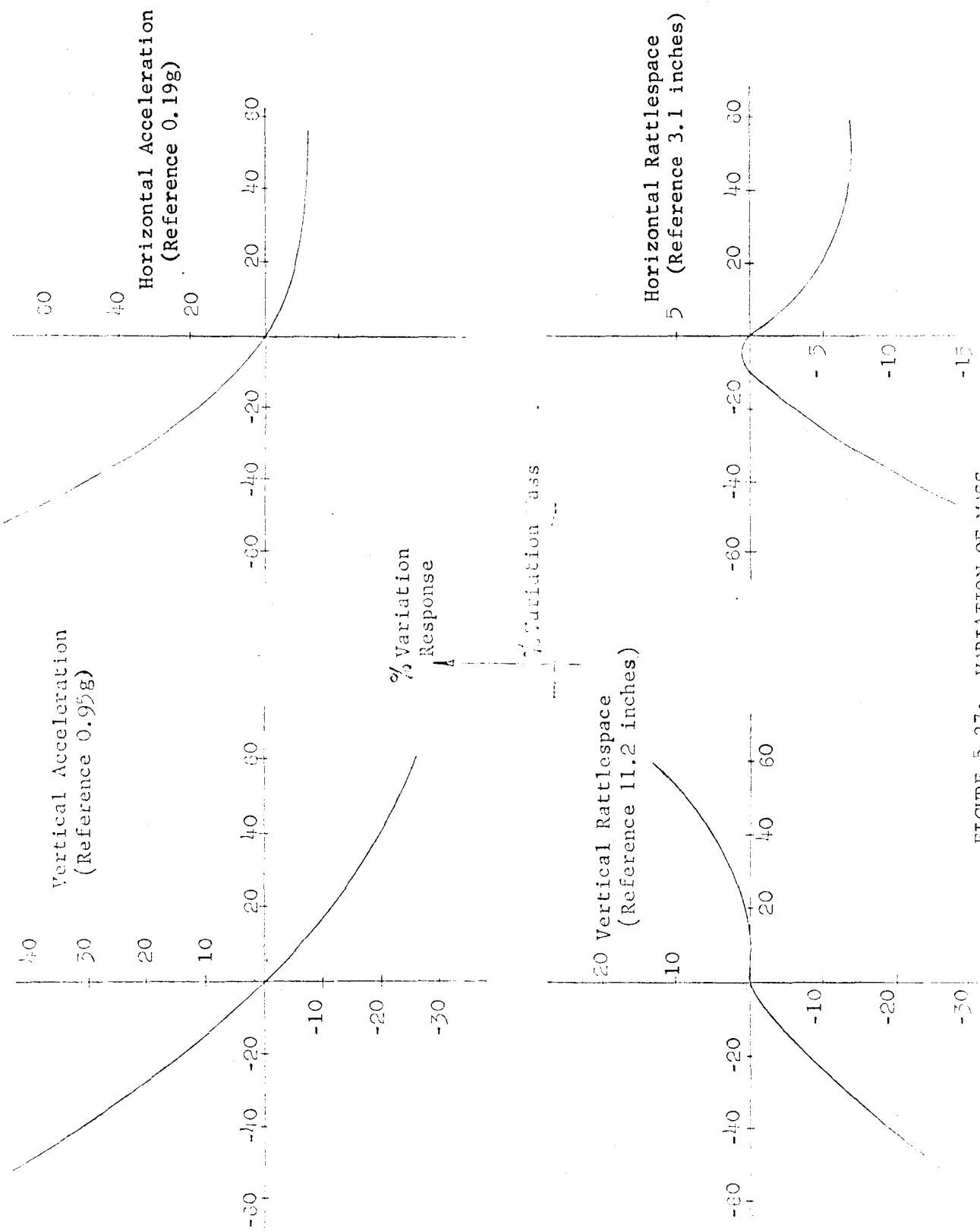
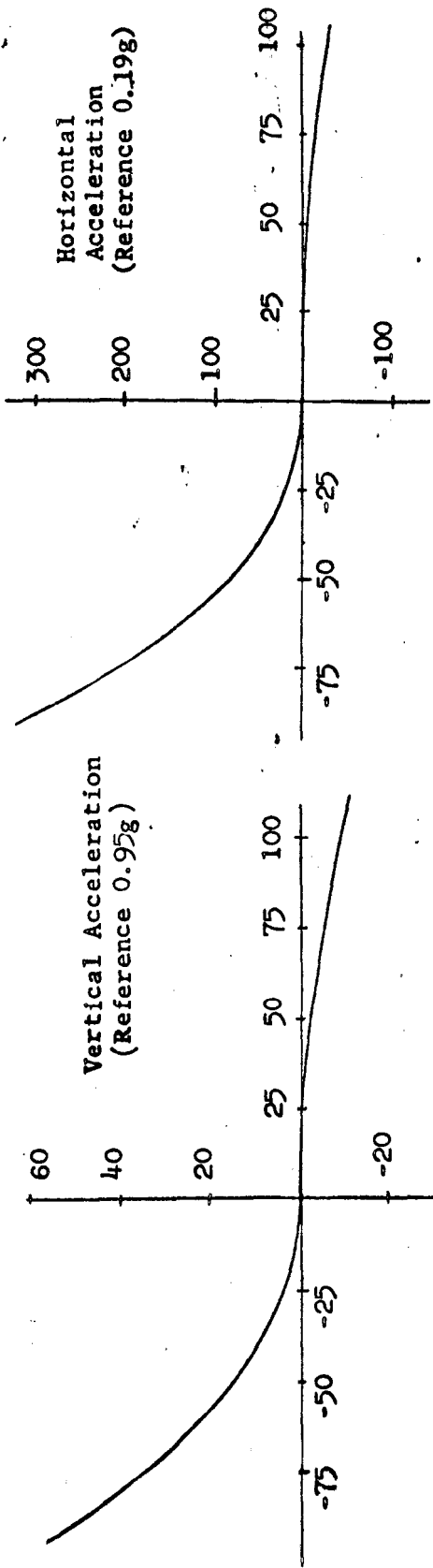


FIGURE 5.27: VARIATION OF MASS



1% Variation  
Response

% Variation J

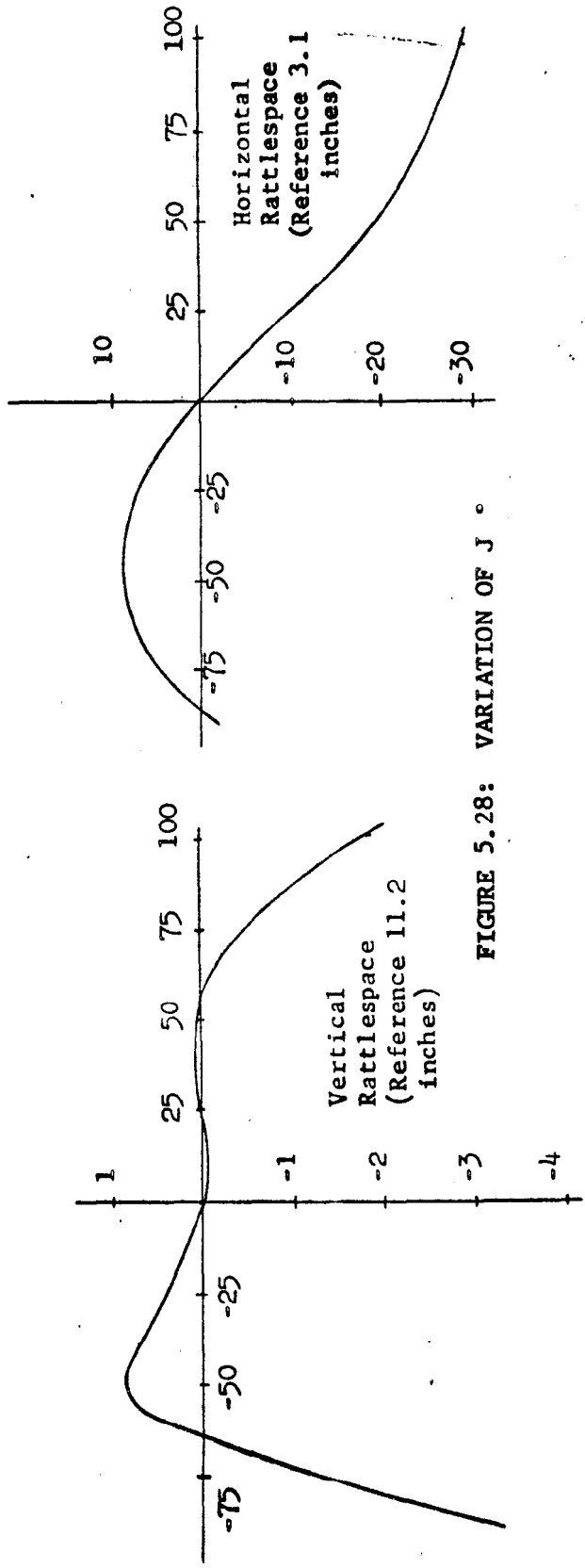


FIGURE 5.28: VARIATION OF J °

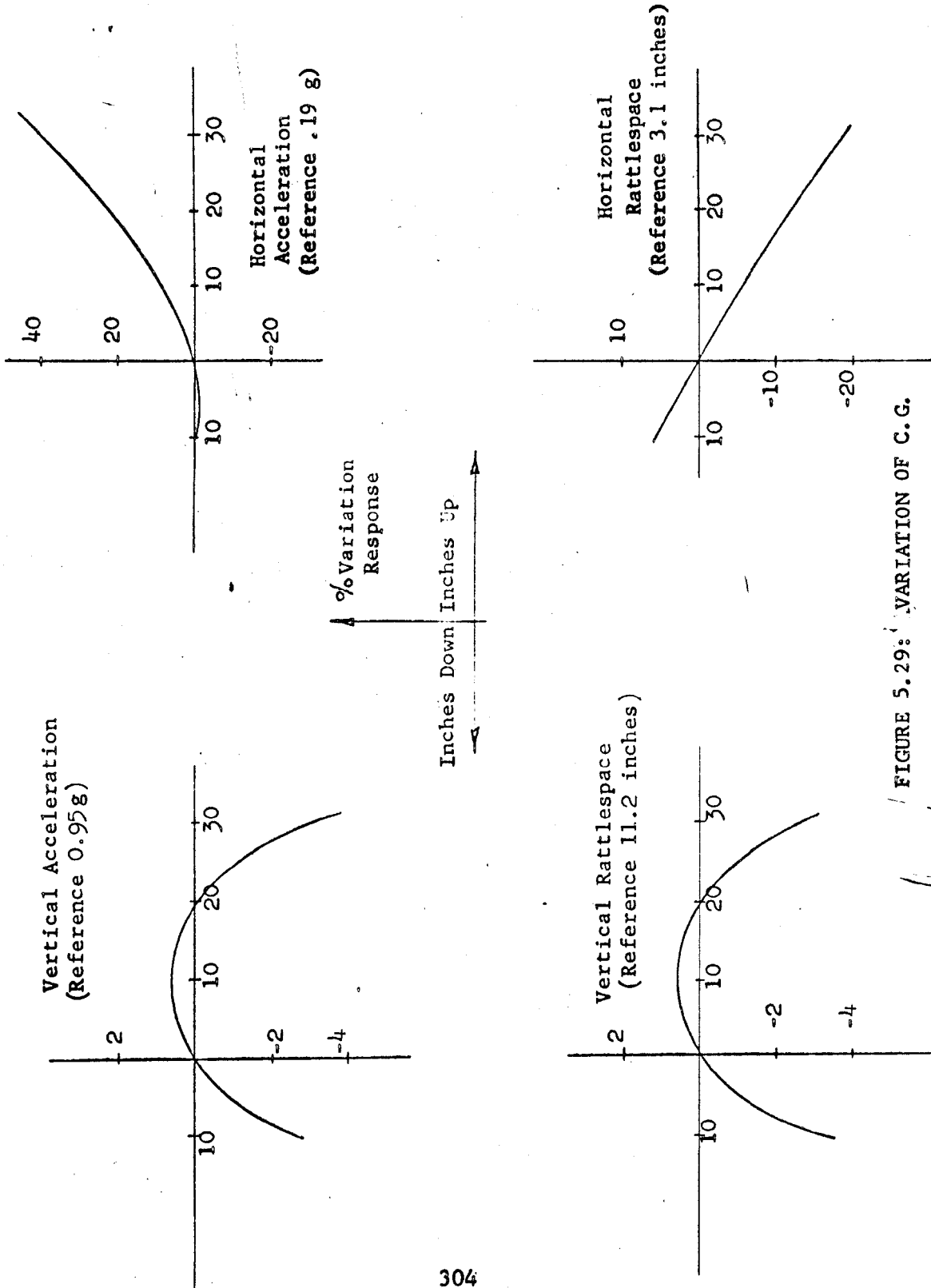


FIGURE 5.29: VARIATION OF C.G.

stability and minimum coupling between the modes is achieved during dynamic response. In a parametric study in Reference 5.1, it is concluded that the double inclined pendulum has the advantage of being relatively insensitive to shifts in location of the center of gravity. However, coupling in Configuration 1 may also be made negligible if the eccentricity "R" is kept small with respect to  $h_3$  and  $h_4$  (see Figure 5.30a). Both systems have two or more levels of support that provide increased stability over a single level suspension system.

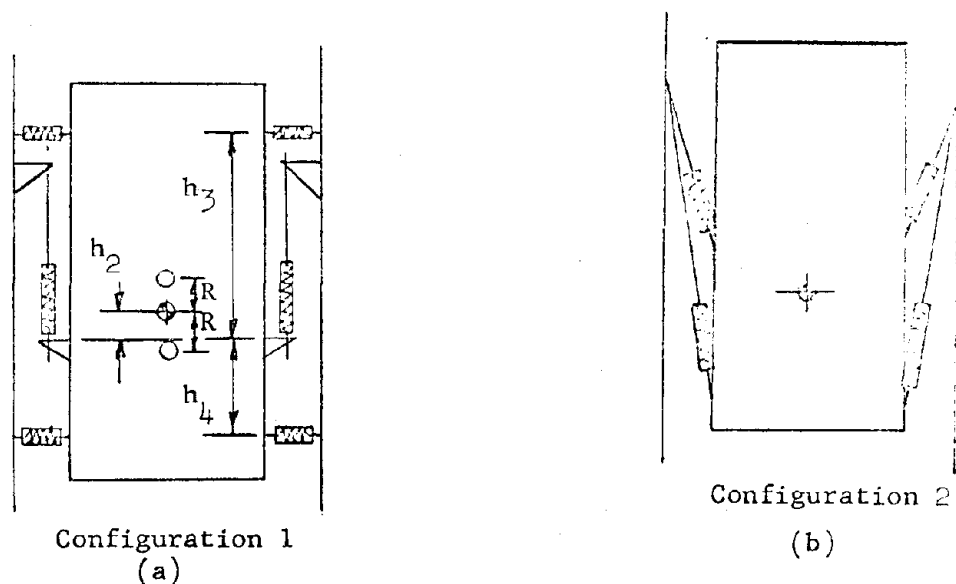


FIGURE 5.30

Therefore, both pendulum configurations will minimize the effects of dynamic coupling.

The equations of motion for Configuration 1 become highly non-linear during large vertical displacements. The horizontal springs during peak displacement will be rotated significantly, thereby, giving appreciable vertical components of spring forces to be added to the main vertical spring forces. This situation will increase the accelerations of the supported mass. Therefore, during design the spring rate of the vertical isolators will have to be decreased so as to give an acceptable resultant vertical effect.

(b) Hardware space requirements. Space requirements are a significant factor because the hardware for both pendulum systems will be situated in the space between the instructure system and the enclosure. The space needed for vertical isolators, including bracketry, in Configuration 1 will be larger than that required for the inclined isolators as shown schematically in Figure 5.31. If the lower level of the double inclined pendulum configuration is fastened to the bottom of the structure, this situation will require an increase in rattlespace in the lower region of the facility (see Figure 5.31).

However, the lower level of horizontal springs shown in Configuration 1, will also increase the rattlespace requirements resulting in approximately equal space requirements for both systems at the bottom of the facility. Therefore, it is concluded that the inclined pendulum system will need a smaller overall space for hardware.

(c) Static equilibrium due to C.G. shift. Possible horizontal C.G. shifts will affect the two systems differently. In Configuration 1, a horizontal shift in C.G. will rotate the instructure system so that either a change in the vertical spring rates or in the pendulum lengths will bring the system back to its original level position without any horizontal displacement. For an inclined pendulum system, Configuration 2, a horizontal C.G. shift will result in a horizontal displacement of the structure. This will add to the overall rattlespace requirement.

(d) Damping requirements. A factor that must be considered in a final design is the damping requirements of the pendulum mode. This will have considerable bearing on the selection of a configuration. If the motion must be damped in a few cycles, a system with horizontal springs (damping type) may be more functional than inclined springs since for the inclined pendulum system a large inclination angle may be required to provide a horizontal component of significant damping. A large inclination angle means increased rattlespace which affects the cost. In general, if the damping requirement is nominal, 2 to 6 percent of equivalent viscous damping, the inherent damping in the system will be sufficient to damp the free vibration motion. A general discussion of damping effects is presented in Section 5.9.

Configuration 1

Configuration 2

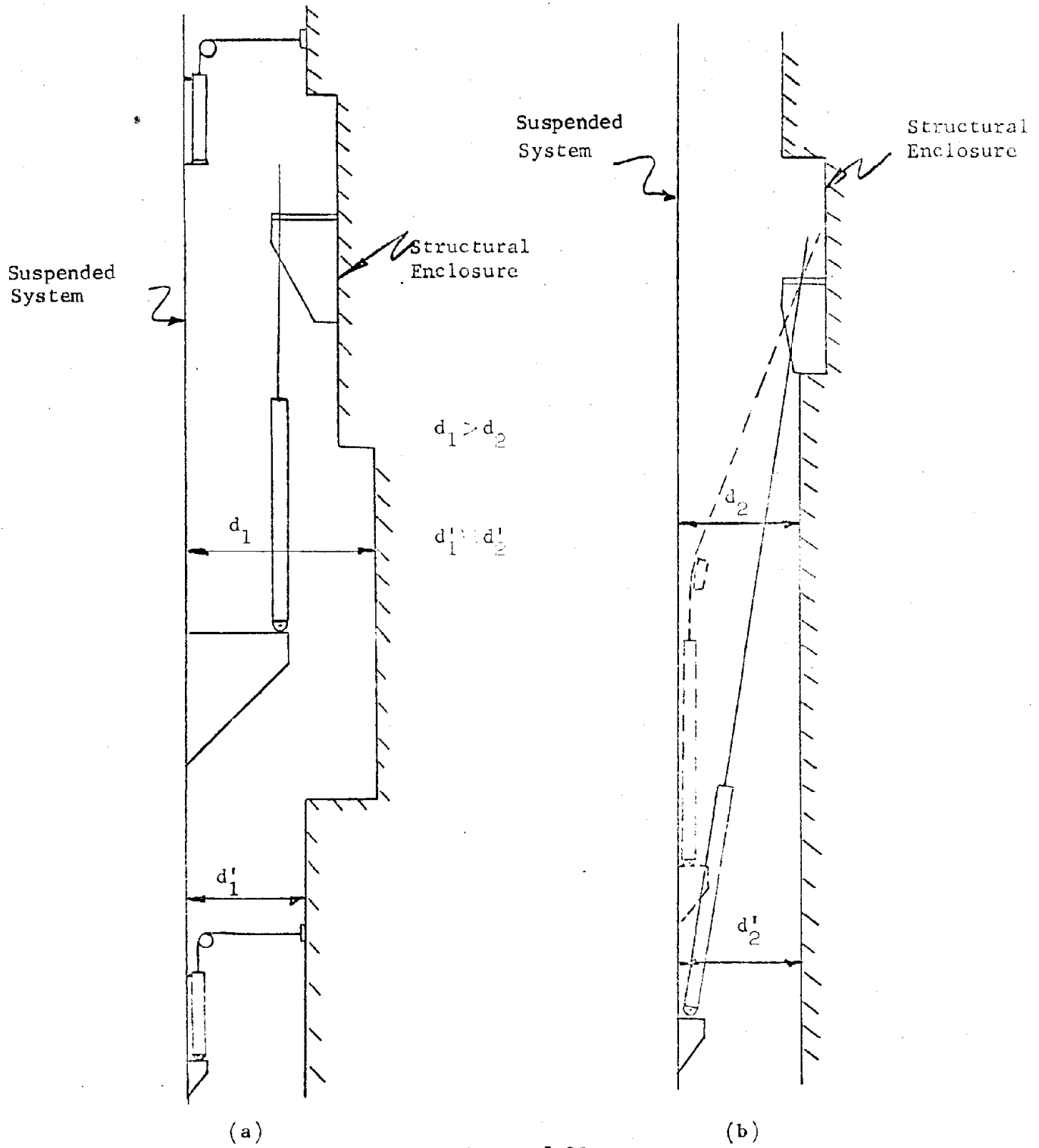


FIGURE 5.31

5.5.2 Inclined pendulum system model. The inclined pendulum system is selected for further discussion in this and the following subsections, and an example is given to illustrate the advantage of the system. This isolation system is desirable when a large instructure mass must be isolated from ground motions with large displacement amplitudes by attenuating the response to very low accelerations (approximately 0.5 g). Some assumptions may be made for the analysis of such a system.

The instructure system is assumed to be a rigid body. This is a good assumption since the isolator frequencies required to attenuate the shock to an acceptable level are very low and the lowest structural frequency ordinarily will be much greater than the isolator frequency. Therefore, the rigid body motion will be ineffective for exciting vibrations of the isolated structure itself.

A six-degree-of-freedom suspension system may be reduced to a three-degree-of-freedom vertical planar system. The motions considered are vertical, horizontal, and pitching about a horizontal axis. Since a primary objective of a design is to determine rattlespace requirements, this simplification is usually acceptable. In plan, the structure is made symmetrical and any rotational motion about a vertical axis will not affect the horizontal rattlespace.

The spring characteristics are idealized to have linear behavior. This assumption would have to be verified after the spring characteristics are known. See Section 6, which discusses spring characteristics and applications.

The small-angle approximation, i.e.,  $\sin \phi = \phi$  rad,  $\cos \phi = 1$ , will generally result in negligible errors in a simple pendulum system if the  $\phi$  angles are less than 15 degrees (0.26 radians). The pendulum system configuration generally will have small-angle excursions during dynamic response. In addition, the isolators are inclined in the static position, and these angles are also small. (If the instructure system is cylindrical, the isolators will be positioned radially around the structure, each with a different inclination angle with regard to a pitching motion.) The vertical excursions are large, but during peak response the inclination angles are still small. Therefore, the small angle approximation is



considered acceptable.

(a) Equations of motion. In Reference 5.1, the equations of motion for a shock isolated system using inclined pendulum cables have been derived for a three-degree-of-freedom system based on assumptions similar to those listed here. The relative vertical, horizontal, and pitching mode displacements were expressed in terms of  $\gamma$ , the vertical motion of the C.G. of the rigid mass,  $\phi$ , the angle of the equivalent pendulum having a point of support directly above the C.G., and  $\theta$ , the rotation about a horizontal axis through the C.G. and normal to the plane of the three-degree-of-freedom system. These three coordinates and other geometric and physical parameters of the isolation system are shown in Figure 5.32.

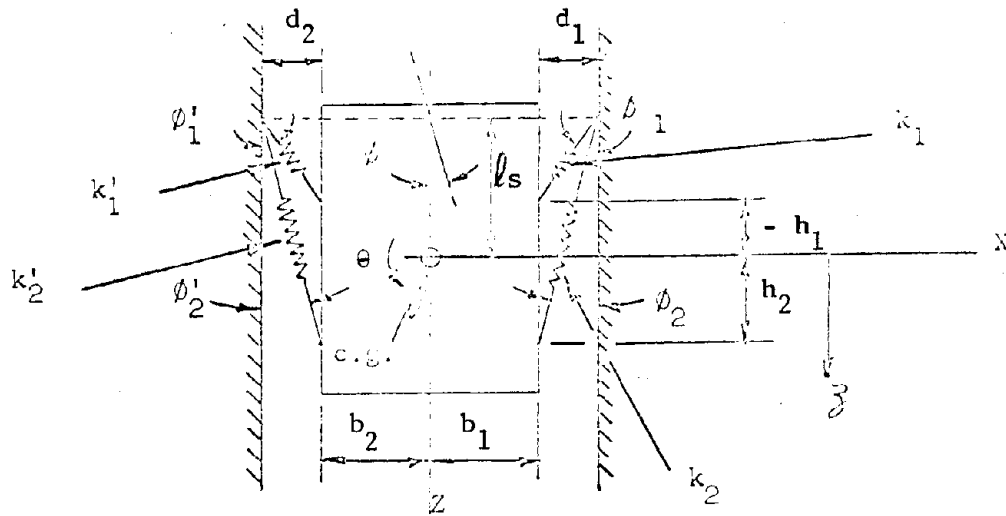


FIGURE 5.32

The equations of motion are

$$\ddot{\gamma} + D_0 \dot{\gamma} = - \ddot{z}_s \quad (5.31)$$

$$\ddot{\phi} + \phi (D_1 \dot{\gamma} + D_2) + \theta (D_3) = - \frac{\ddot{x}_s}{l_s} \quad (5.32)$$

$$\ddot{\theta} + \phi (D_1' \dot{\gamma} + D_2') + \theta (D_3') = 0 \quad (5.33)$$

where

$\ddot{z}_s$  and  $\ddot{x}_s$  = the ground accelerations in the vertical and horizontal directions, respectively

$l_s$  = length of the equivalent pendulum in the static condition when supporting the weight of the structure.

$D_0, D_1, D_2, D_3, D_1', D_2',$  and  $D_3'$  = constants in terms of the system characteristics when the structure is in its static position.

Reference 5.1 gives the values of these constants for the symmetrical case when  $r_1 = r_2$ ,  $k_1' = k_1$ ,  $k_2' = k_2$  in Figure 5.32. It is important to consider the more general case when  $b_1 \neq b_2$  and  $k_1' = k_1$ ,  $k_2' = k_2$  (eccentric location of the C.G.). The expressions are then:

$$D_0 = \frac{2(k_1 + k_2)}{m} \sec^2$$

$$D_1 = \frac{1}{m} \left[ \frac{k_1 + k_1'}{l_s - h_1} + \frac{k_2 + k_2'}{l_s + h_2} - \frac{k_1 + k_2 + k_1' + k_2'}{l_s} \right] \sec^2 / \text{length}$$

$$D_2 = \frac{1}{m} \left[ \frac{k_1 \Delta r_{1s} + k_1' \Delta r_{1s}'}{l_s - h_1} + \frac{k_2 \Delta r_{2s} + k_2' \Delta r_{2s}'}{l_s + h_2} \right] \sec^2$$

$$D_3 = \frac{1}{m l_s} \left[ k_1 \phi_1 (b_1 - a_1 \phi_1) + k_2 \phi_2 (b_1 + h_2 \phi_2) + k_1' \phi_1' (b_2 - h_1 \phi_1') + k_2' \phi_2' (b_2 + h_2 \phi_2') \right] \sec^2$$

$$D_1' = \frac{l_s}{m \rho^2} \left[ \frac{k_1 (-h_1 - b_1 \phi_1)}{l_s - h_1} + \frac{k_2 (h_2 - b_1 \phi_2)}{l_s + h_2} + \frac{k_1' (-h_1 - b_2 \phi_1')}{l_s - h_1} + \frac{k_2' (h_2 - b_2 \phi_2')}{l_s + h_2} \right] \sec^2 / \text{lgth}$$

$$D_2' = \frac{l_s}{m \rho^2} \left[ \frac{k_1 \Delta r_{1s} (-h_1 - b_1 \phi_1)}{l_s - h_1} + \frac{k_2 \Delta r_{2s} (a_2 - b_1 \phi_2)}{l_s + h_2} + \frac{k_1' \Delta r_{1s}' (-h_1 - r_2 \phi_1')}{l_s - b_1} + \frac{k_2' \Delta r_{2s}' (h_2 - b_2 \phi_2')}{l_s + h_2} \right] \sec^2$$

$$D_3' = \frac{1}{m \rho^2} \left[ k_1 (b_1 - h_1 \phi_1)^2 + k_2 (b_1 + h_2 \phi_2)^2 + k_1' (b_2 - h_1 \phi_1')^2 + k_2' (b_2 + h_2 \phi_2')^2 \right] \sec^2$$

\* In many cases the C.G. will not coincide with the geometrical vertical centerline. To maintain a symmetrical system, i.e., C.G. and C.R. coincident,  $R_x = 0$ , the spring rates must be adjusted accordingly. These expressions are simplified when the C.G. is on the vertical centerline.

where

$m$  = mass of the rigid body

$\rho^2 = J/m$ , the square of the radius of gyration;  $J$  is the mass moment of inertia about a horizontal axis through the C.G.

Other terms denote spring rates ( $k_1, k_2$ , etc.), axial static deflections ( $\Delta r_{2s}, \Delta r'_{2s}$ , etc.), and dimensions of the system at static equilibrium ( $h_1, h_2, \phi_1, \phi_2, d_1, d_2$ , etc.). Refer to Figure 5.32 and to the nomenclature for these dimensions.

In the case,  $b_1 = b_2$ , the characteristics are symmetrical, and  $\phi_1 = \phi_1', k_1' = k_1$ , etc. are directly obtainable. With an eccentric C.G.,  $b_1 \neq b_2$ , the unknown variables,  $\phi_1, \phi_2, \phi_1', \phi_2'$ , must be determined in terms of the known variables from the geometry of the system, during static equilibrium. The derivation and the results are given below:

From the geometry of the system (Figure 5.33), the following two equations can be written (for  $\phi < 15^\circ$ )

$$d_1 + d_2 = \phi_1 (l_s - h_1) + \phi_1' (l_s - h_1)$$

$$d_1 + d_2 = \phi_2 (l_s + h_2) + \phi_2' (l_s + h_2)$$

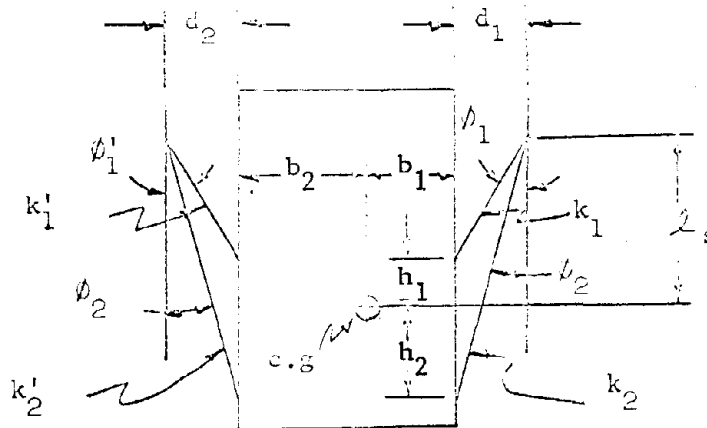


FIGURE 5.33

Taking a free body of the supported structure (Figure 5.34), the equations that satisfy static equilibrium are: (small angle approximation is made)

$$\Sigma F_x = 0: k_1' \Delta r_{1s}' \phi_1' = k_1 \Delta r_{1s} \phi_1$$

$$\Sigma M_A = 0:$$

$$k_2' \Delta r_{2s}' \phi_2' = k_2 \Delta r_{2s} \phi_2$$

$$Wb_2 = (k_1 \Delta r_{1s} + k_2 \Delta r_{2s})(b_1 + b_2)$$

$$\Sigma F_z = 0: k_1' \Delta r_{1s}' + k_2' \Delta r_{2s}' + k_{1s} \Delta r_{1s} + k_2 \Delta r_{2s} = W$$

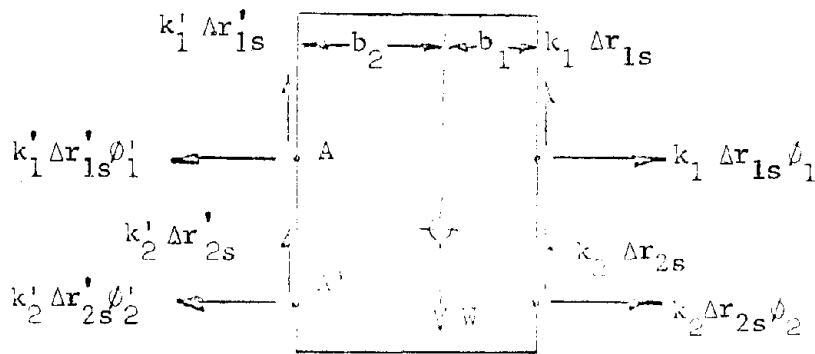


FIGURE 5.34

From the above equations and chosen ratios of  $k_1/k_2$ ,  $k_1/k_1'$ ,  $k_2/k_2'$ , the static condition characteristics,  $\Delta r_{si}$ ,  $\phi_i$ , can be determined for use in the expressions for  $D_0, D_1$  - - - .

It is shown in Reference 5.1 that coupling can be minimized and stability can be assured if the following inequalities are numerically minimized for the case when  $b_1 = b_2 = b$ . As a starting point for design,

$$(1) \frac{k_1}{k_2} \times \frac{h_1}{h_2} \times \left(\frac{\phi_1}{\phi_2}\right)^2 \times \frac{b - h_1 \phi_1}{b + h_2 \phi_2} \rightarrow 1 \quad \left\{ \begin{array}{l} \text{To minimize } D_3, \text{ reduce} \\ \text{coupling between trans-} \\ \text{lational and rotational} \\ \text{modes} \end{array} \right. \quad (5.34)$$

$$(2) \frac{k_1}{l_s - h_1} + \frac{k_2}{l_s + h_2} - \frac{k_1 + k_2}{l_s} \rightarrow 0 \quad \text{To minimize } D_2 \quad (5.35)$$

$$(3) \frac{k_1(-h_1 - b\phi_1)}{l_s - h_1} + \frac{k_2(h_2 - b\phi_2)}{l_s + h_2} \rightarrow 0 \quad \text{To minimize } D_1' \text{ and } D_2' \quad (5.36)$$

The above equations can be used to locate  $h_1$  and  $h_2$  by using the average  $b$  distance, i.e., let  $b = (b_1 + b_2)/2$ . All the necessary equations and conditions are thus developed, and a numerical solution of the dynamic response equations for given input conditions will determine the relative displacements between the suspended mass and the structure enclosure as well as the attenuated accelerations that the system will experience.

#### Example 5.10

A large structure, cylindrical in shape, is to be isolated from ground motions due to weapon effects. The assumed structure properties and requirements are:

- (1) Weight and mass moment of inertia:

$$W = 3.0 \times 10^6 \text{ lbs} \quad J \text{ (C.G.)} = 10 \times 10^7 \text{ ft-lbs-sec}^2$$

Overall dimensions are given in Figure 5.35.

Mass C.G. is assumed to lie on the vertical centerline.

- (2) Tolerable acceleration levels:

Horizontal: 0.2 g

Vertical : 0.5 g

- (3) The motions at the support points are described by the velocity pulses shown in Figures 5.36 and 5.37. The pulse in Figure 5.36 is for a soil (or rock) which remains elastic for the predicted ground motions (100 percent ground return), and the pulse in Figure 5.37 is for a soil that has some plastic deformation (80 percent ground return). (See Section 3.5.)

Example 5.10 (continued)

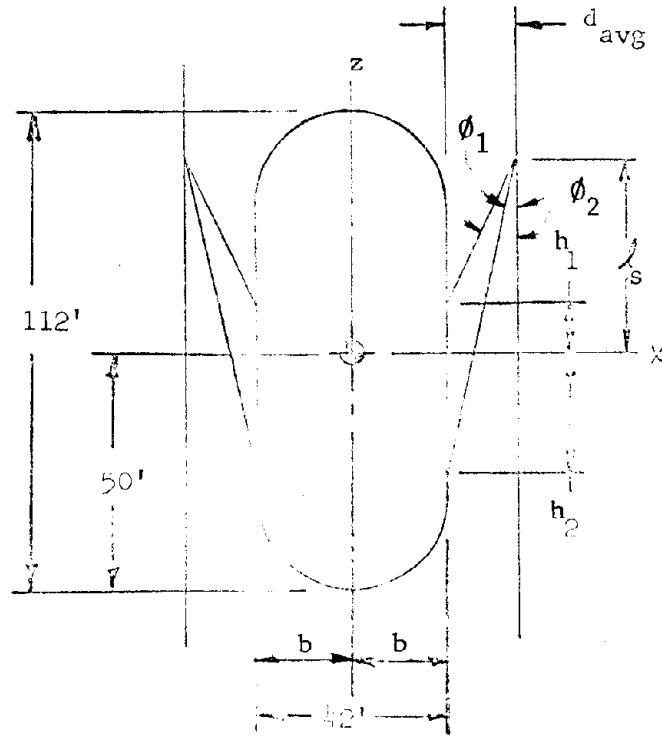
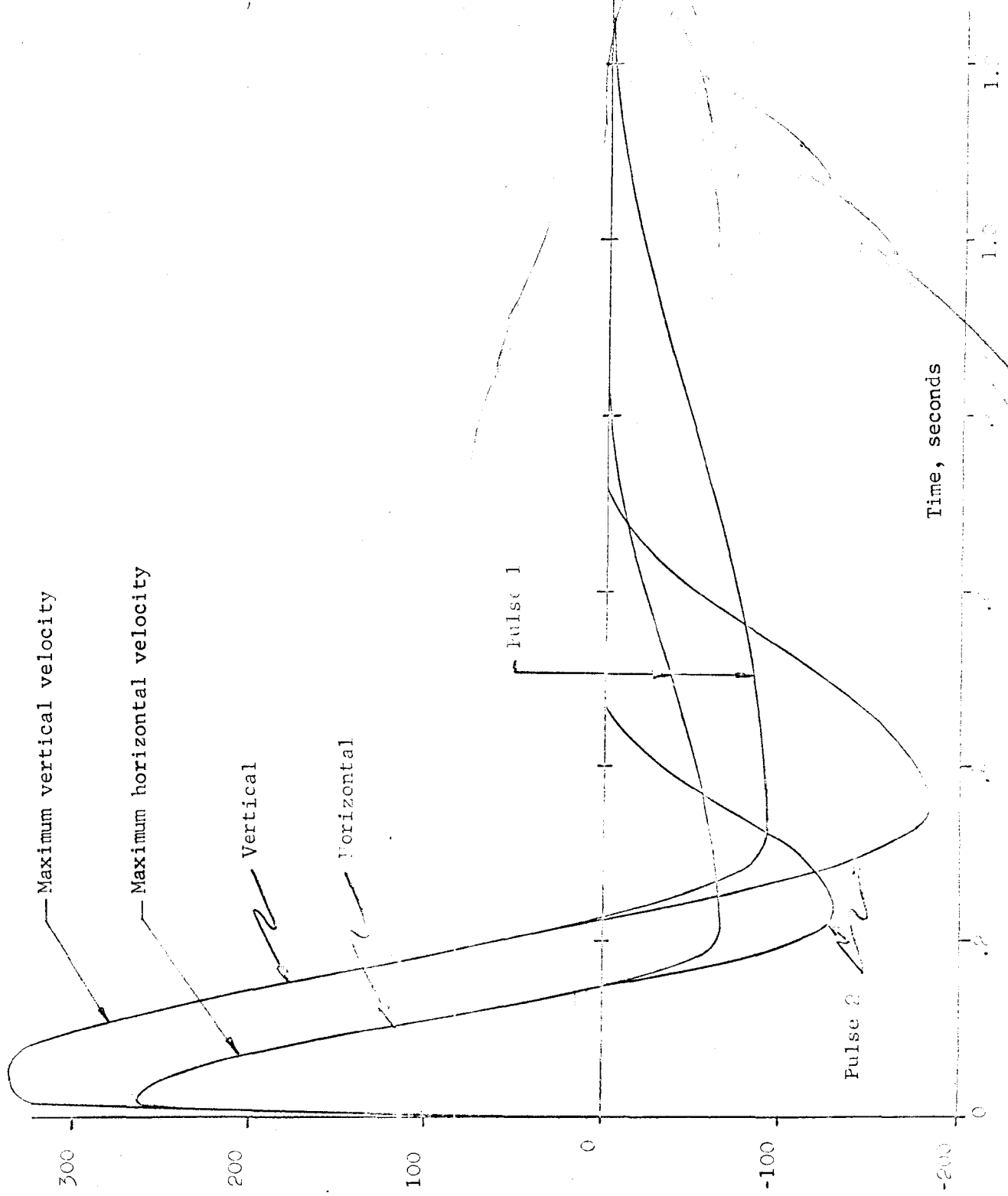


FIGURE 5.35

(4) Peak ground motion intensities are given for five hypothetical conditions, A through E.

Input Cond.	$a_v$ (g)	$a_h$ (g)	$v_v$ (ft/sec)	$v_h$ (ft/sec)	$d_v$ (inch)	$d_h$ (inch)
A	170	170	70	45	85	30
B	165	165	61	51	70	45
C	60	60	33	22	55	20
D	60	60	31	23	50	25
E	24	24	17	11	35	15

The pendulum dimensions are first determined by minimizing the inequalities of Equations (5.34), (5.35) and (5.36) in order to start the design with a stable system that has minimum coupling among the three modes. This is done by trial as shown in Table 5.2. The four springs are chosen to have equal spring rates,  $k_1 = k_2 = k_1' = k_1'$ .



Velocity, inches/second

FIGURE 5.36 BASE VELOCITY

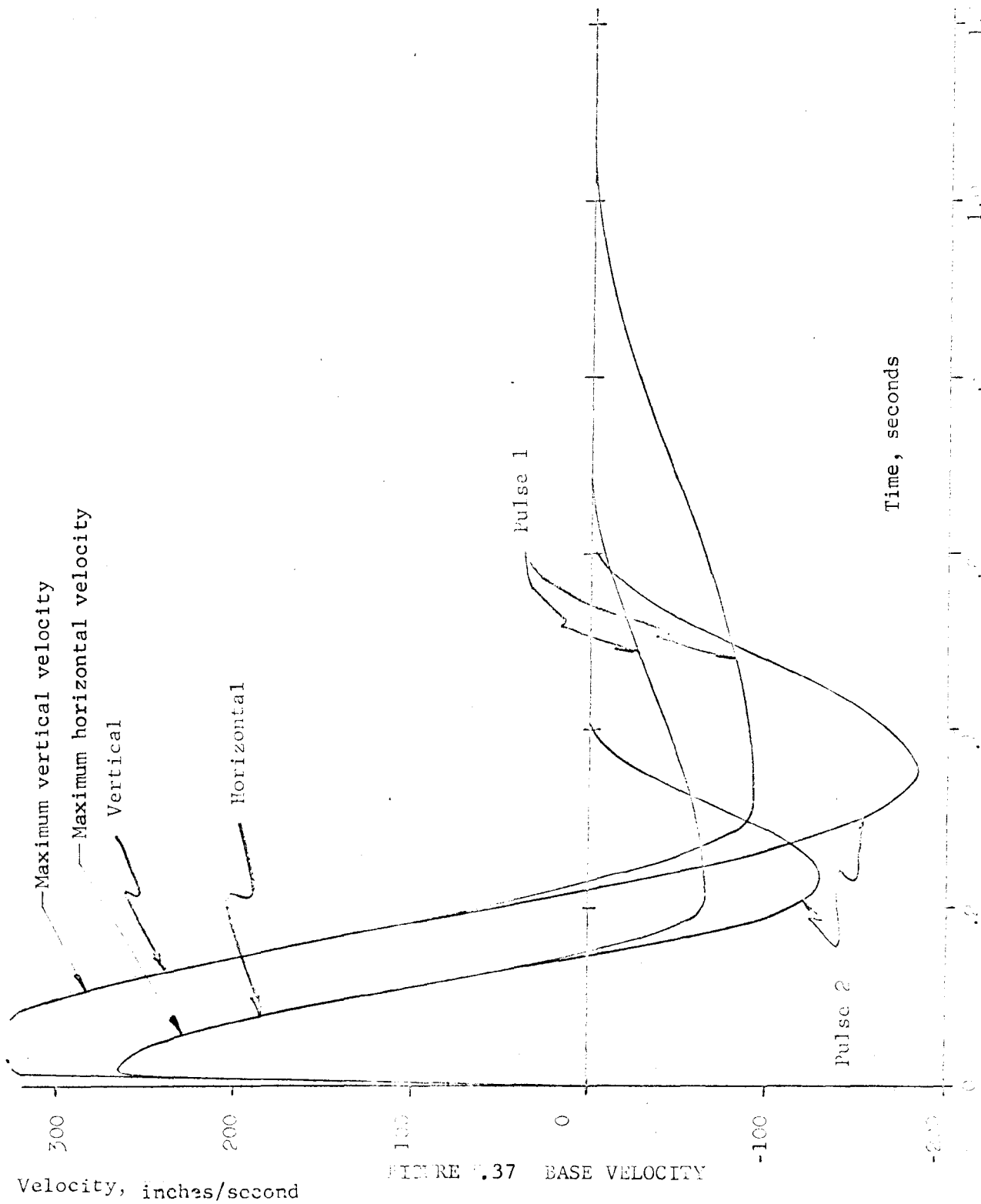


FIGURE 8.37 BASE VELOCITY



Example 5.10 (continued)

TABLE 5.2

d	$l_s$	$h_1$	$h_2$	$\phi_1$	$\phi_2$	$\frac{h_1}{h_2}$	$\left(\frac{\phi_1}{\phi_2}\right)^2$	Eq. 5.34	Eq. 5.35	Eq. 5.36
6'	42.5	7.5	25	.171	.089	.3	3.7	.94	-.004	.0344
6'	40	5	27.5	.171	.089	.182	3.7	.57	small	small
6'	45	10	23.5	.171	.089	.425	3.7	1.33	small	small
6'	45	7.5	30	.16	.08	.25	4.0	.84	small	small
6'	47.5	10	27.5	.16	.08	.365	4.0	1.20	small	small
6'	46.25	8.75	28.25	.16	.08	.31	4.0	1.02	Nominal Position	

The final dimensions  $l_s$ ,  $h_1$ , and  $h_2$ , are:

$$l_s = 46.25 \text{ ft}$$

$$h_1 = 8.75 \text{ ft}$$

$$h_2 = 28.25 \text{ ft}$$

Spring rates. Initially, spring constants are calculated based on the given allowable accelerations of the suspended mass:

Vertical : 0.5 g (static 1 g is not included)

Horizontal : 0.2 g

and by assuming uncoupled single-degree-of-freedom response in the vertical and pendulum modes (the spectra response envelope in the low frequency region is assumed to be bounded by a straight line at constant displacement equal to the peak ground displacement). The required maximum frequencies and resulting vertical spring rates are:

<u>Input Condition</u>	$\frac{f_z}{\text{cps}}$	$\frac{f_x}{\text{cps}}$	$\frac{k_z}{\text{lbs/in}}$
A	0.23	0.2	$1.6 \times 10^4$
B	0.26	0.18	$2.02 \times 10^4$
C	0.30	0.32	$2.72 \times 10^4$
D	0.33	0.28	$3.28 \times 10^4$
E	0.37	0.35	$4.2 \times 10^4$

Example 5.10 (continued)

Approximate horizontal frequencies were calculated from the term  $D_2$  in Equation (5.32).  $D_2$  is the natural frequency expression for the uncoupled pendulum mode.

$$\omega^2 \cong \frac{1}{m} \left[ \frac{k_{z1} \Delta r_s}{l_s - h_1} + \frac{k_{z2} \Delta r_s}{l_s + h_2} \right]$$

where  $k_{z1}$  = vertical spring rate of isolators in upper row

$k_{z2}$  = vertical spring rate of isolators in lower row

$\Delta r_s$  = static deflection

When the spring rates  $k_{z1}$  and  $k_{z2}$  are equal, we obtain the simple case of

$$\omega^2 = \frac{g}{2} \left[ \frac{1}{l_s - h_1} + \frac{1}{l_s + h_2} \right]$$

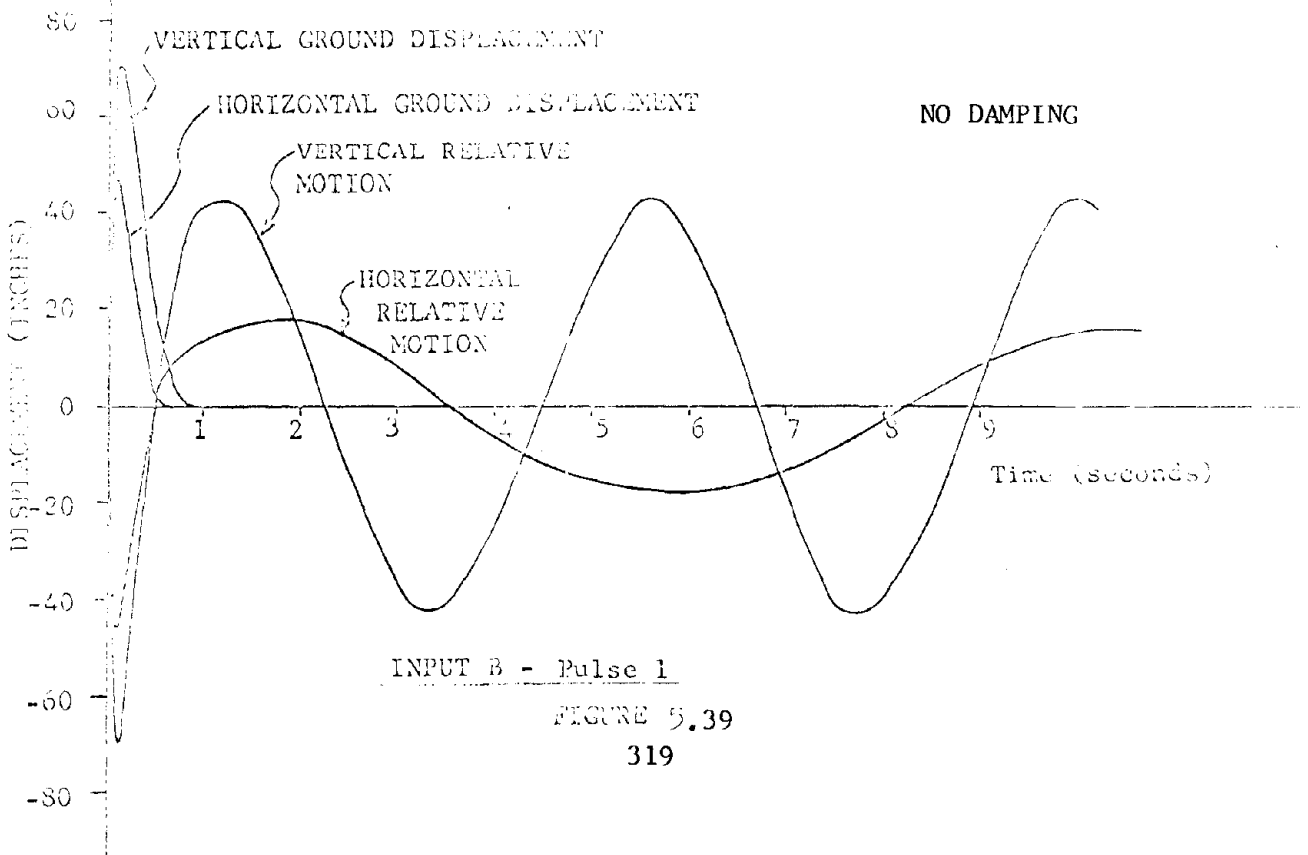
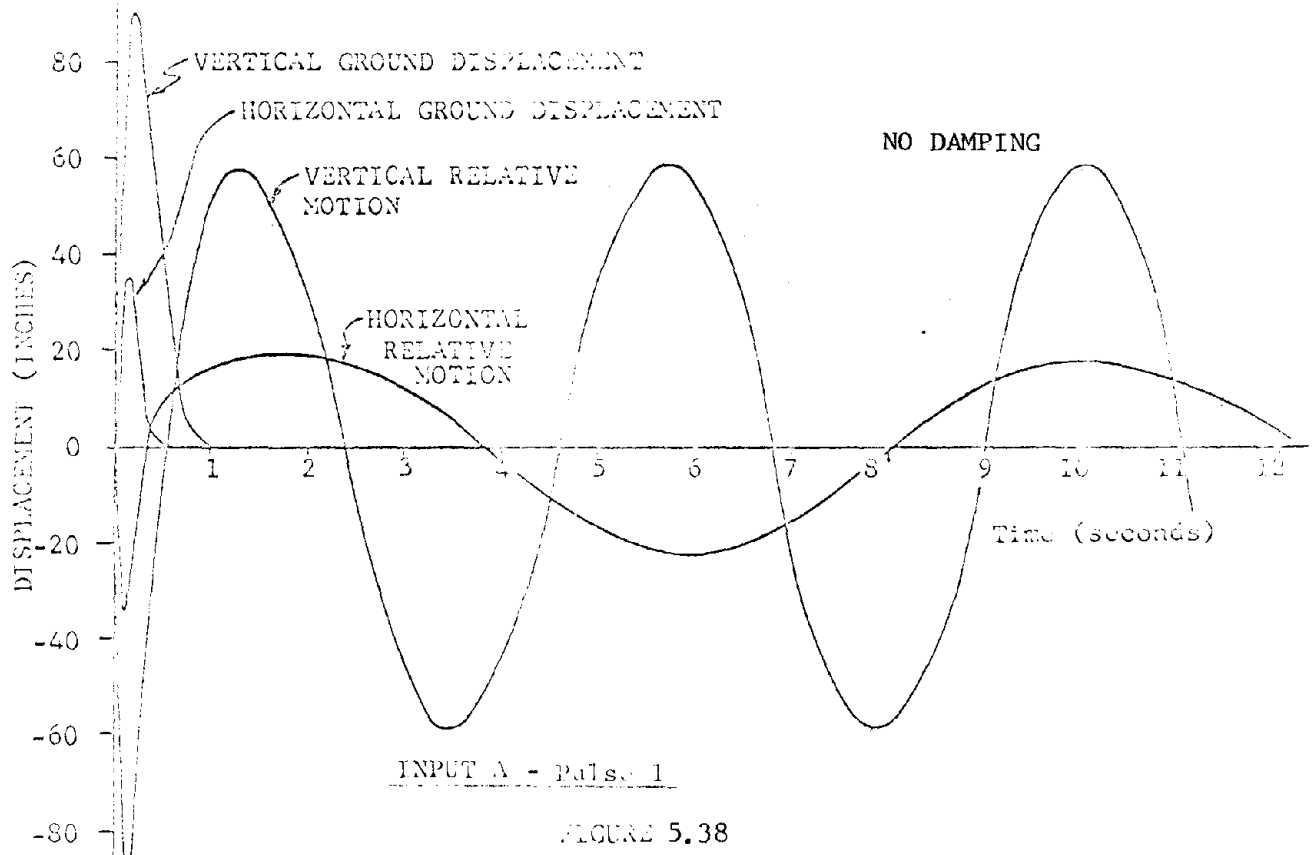
$$\omega^2 = \frac{386}{2} \left[ \frac{1}{37.5 \times 12} + \frac{1}{74.5 \times 12} \right] \cong 0.65$$

$f = 0.13$  cps - - - which is acceptable.

The above analysis was performed to estimate the pendulum frequency and to determine spring rates for preliminary design of the springs.

Computer analysis. A computer response analysis for this system is described in Appendix D. Typical system response for the pulses considered (pulse 1 and pulse 2) with variations in peak intensities (Inputs A, B, C, D, and E) are shown in Figures 5.38 through 5.42.

In reviewing the plots, it is seen that the maximum horizontal relative motion occurs in the initial half cycle of motion and is slightly less than the ground motion. The reason for this is that the ground return time is very short with respect to the period of the horizontal mode. In other words, the ground has returned to its original position before there is any significant absolute motion of the supported mass. Figure 5.43 illustrates this condition. The magnitude of the residual vibration response (the response after the loading function has diminished to zero) is governed by the energy stored in the spring at the time when the ground



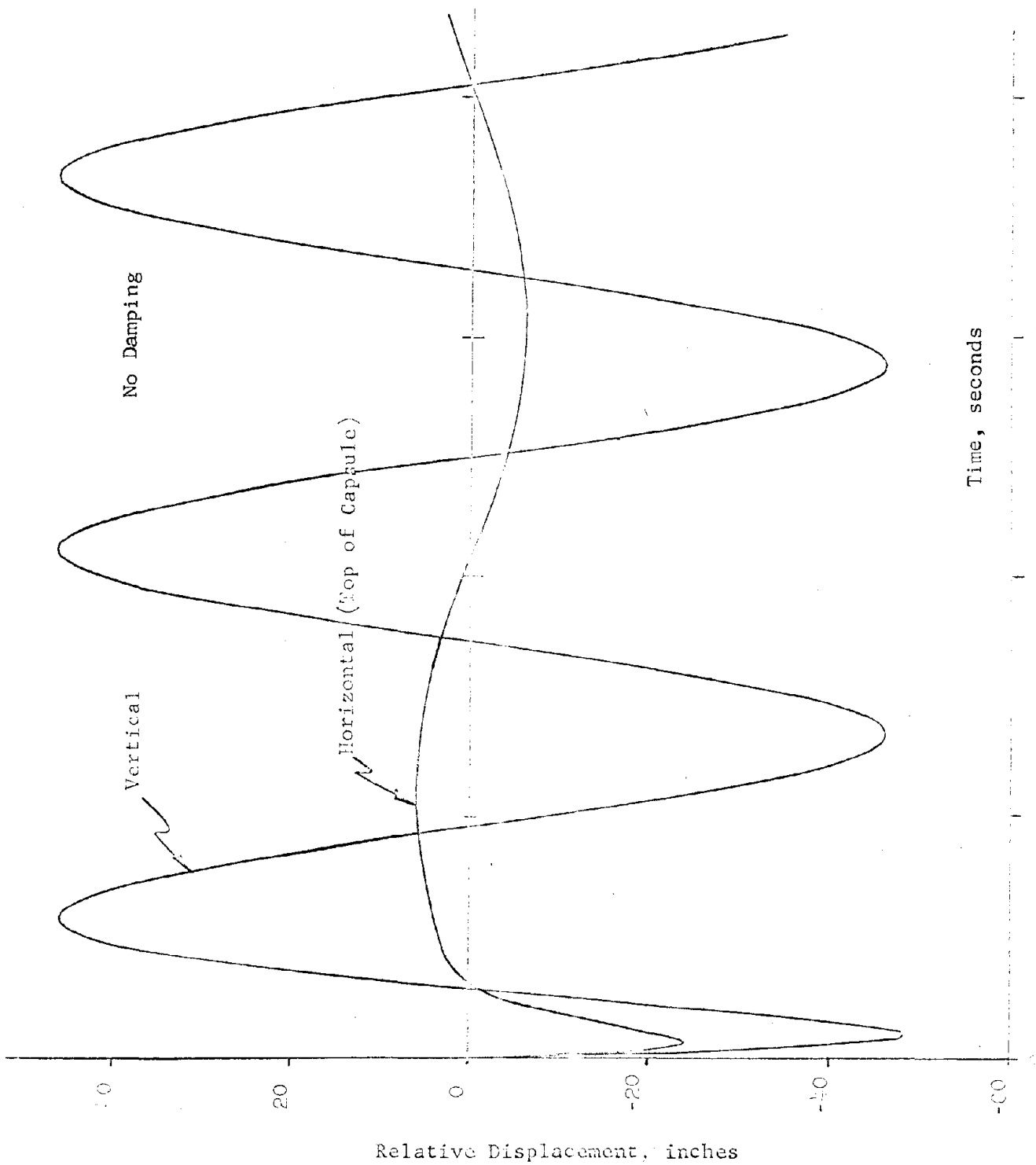
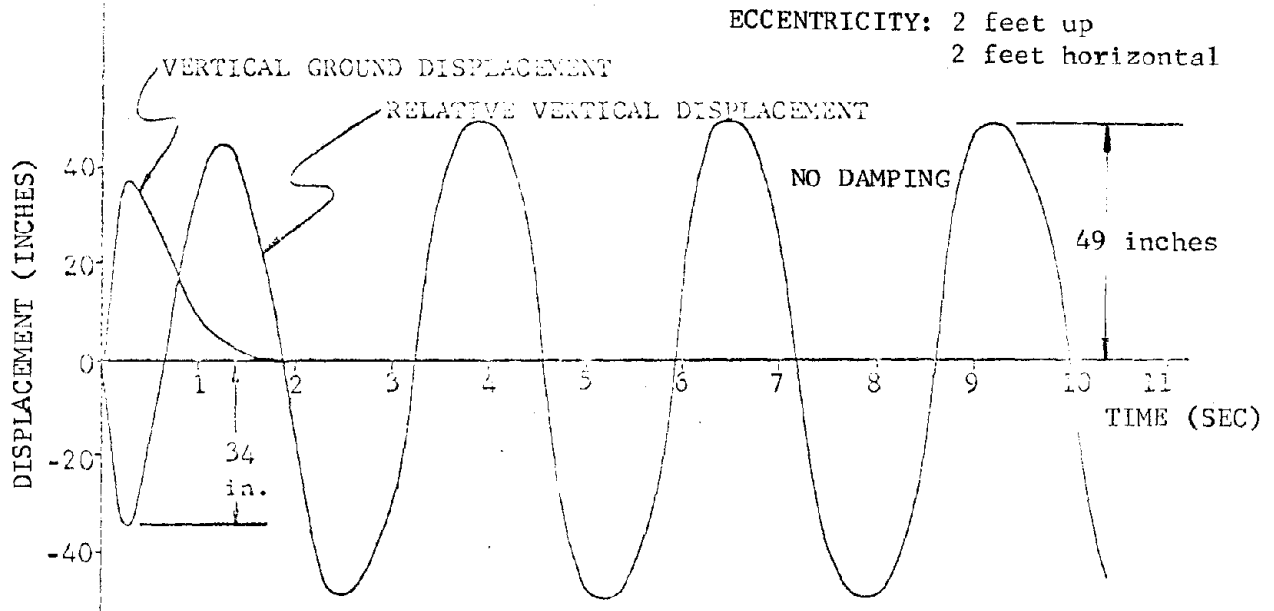
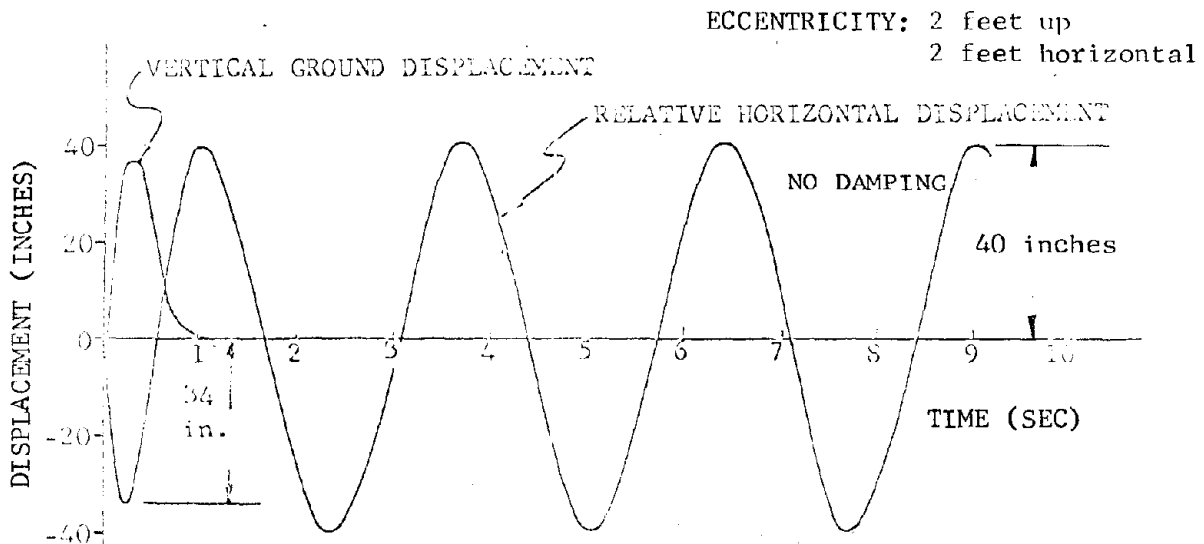


FIGURE 1.40 INPUT C - PULSE 1



INPUT E - PULSE 1

FIGURE 5.41



INPUT E - PULSE 2

FIGURE 5.42

HORIZONTAL MOTION

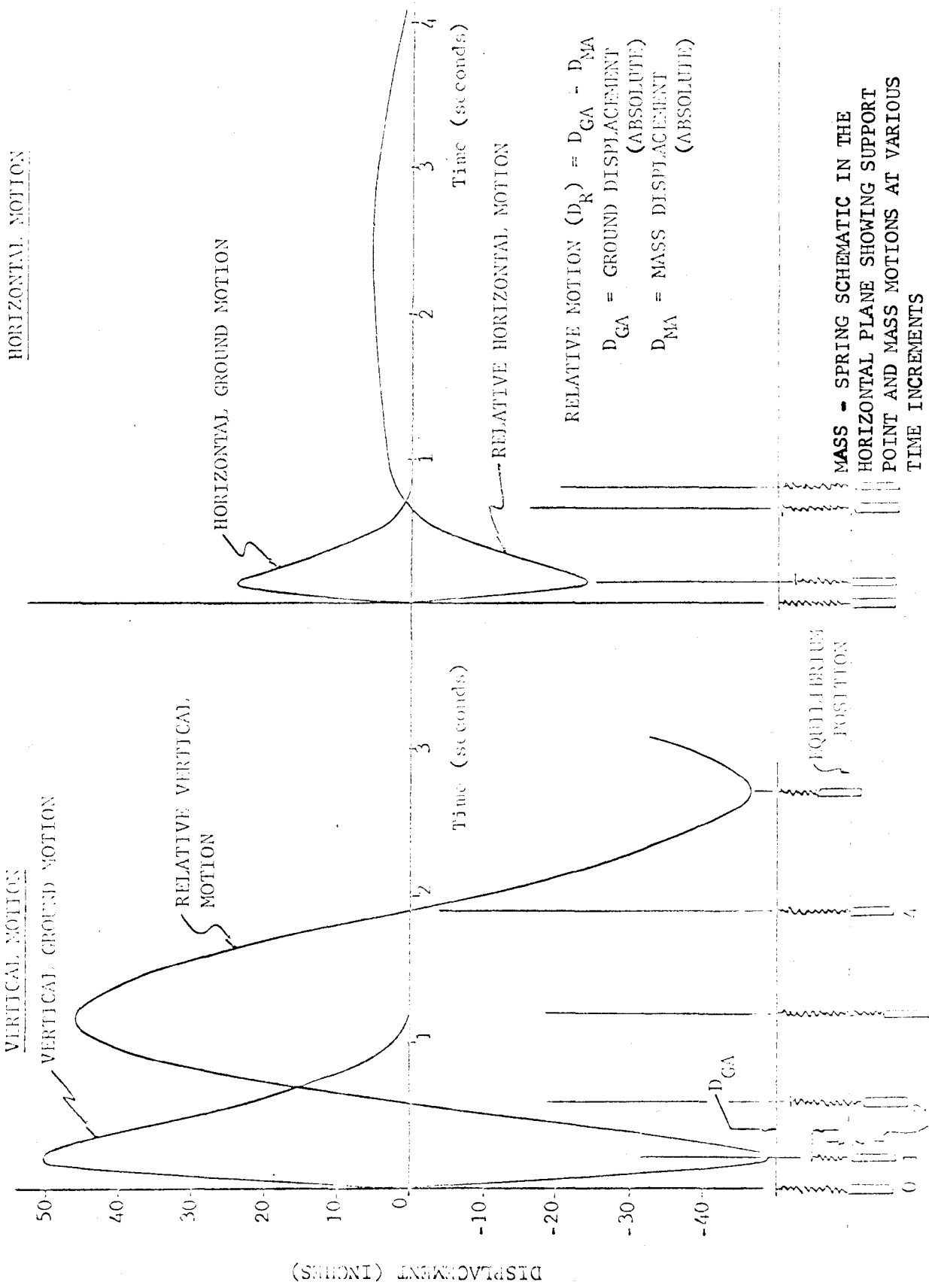


FIGURE 5.43

#### Example 5.10 (continued)

motion has ceased. Since there is very little absolute motion of the mass during this initial period, there is very little energy in the spring system to induce large residual vibration amplitudes.

The natural frequency in the horizontal mode is very low (approximately 0.12 cps which compares favorably with the preliminary design frequency of 0.13 cps). Since it is doubtful that the time duration of the input pulse will ever be long enough to produce appreciable residual vibration amplitudes, it can be concluded that for the configuration analyzed, the peak horizontal relative response will not exceed the peak ground displacements even for reasonable shifts in C.G. location.

The duration of the input pulse, within reasonable limits, has significant effect on the residual vibration response in the vertical mode. The maximum relative vertical displacement can be as large as the peak ground displacement; and if there is no damping in the system, there can be even a slight amplitude buildup due to a partial resonance condition (see Figure 5.41 for Input E). In this case, the natural period of the vertical isolators is about three times the duration of the ground displacement. Consequently, there is appreciable absolute motion of the supported mass during this initial period; and, therefore, large displacements in the residual vibration era are induced.

#### 5.6 High C.G. Pendulum System

The practical applicability of the high center of mass suspension system has been confined almost exclusively to silo-housed missile suspension platforms. A typical but specific system is shown in Figure 5.44.

Considering the supported structure to be a rigid body, the general equations of motion for six-degrees-of-freedom can be written and solved for a particular forcing function. These equations, even when limited to a vertical  $x - z$  plane movement, i.e., three-degrees-of-freedom, are quite complex and tedious in their derivation.

Instead, an equivalent dynamical system has been constructed in

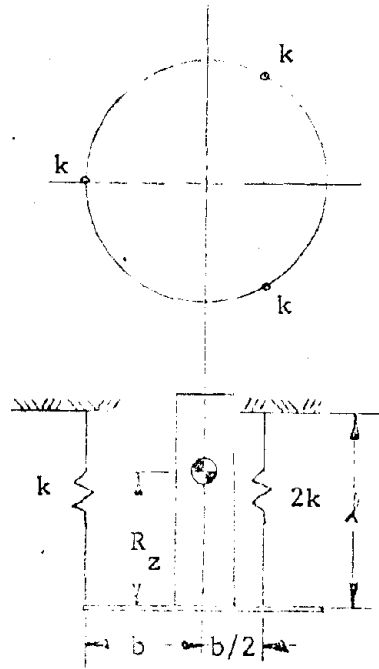


FIGURE 5.44

Reference 5.2 which lends itself to simpler analysis. From Figure 5.45, the equivalent system is seen to consist of two translational springs and one torsional spring. The equivalent spring rates in terms of the original

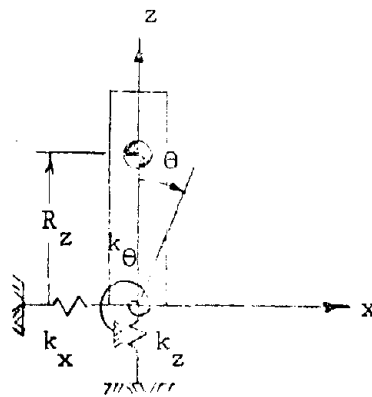


FIGURE 5.45



specific system are

$$\begin{aligned} k_x &= \frac{W}{l} \\ k_z &= 3k \\ k_\theta &= \frac{3k b^2}{2} \end{aligned}$$

Then the equations for motion at the base of the equivalent system, are given by

$$\ddot{x} + R_z \ddot{\theta} + \omega_x^2 x = \omega_x^2 x_s \quad (5.37)$$

$$\ddot{z} + \omega_z^2 z = \omega_z^2 z_s \quad (5.38)$$

$$\ddot{\theta} + \omega_\theta^2 \theta + \frac{R_z \ddot{x}}{\rho^2} = \frac{R_z \ddot{z} \theta}{\rho^2} \quad (5.39)$$

in which small motions are postulated and

$$\omega_x^2 = \frac{k_x}{m} = \frac{g}{l}$$

$$\omega_z^2 = \frac{k_z}{m}$$

$$\omega_\theta^2 = \frac{k_\theta - WR_z}{J_b}$$

$$\rho^2 = \frac{J_b}{m}$$

where

$m$  = mass of missile and platform

$J_b$  = mass moment of inertia of  $m$  about the base

and  $x_s$  and  $z_s$  are foundation shock pulses in the  $x$  and  $z$  directions, respectively. It is assumed that Equation (5.38) is unaffected by motions along the other axes but is itself coupled into the moment equation. It is customary to treat the motion described by this equation as a residual sinusoidal oscillation originating from a shock pulse in the  $z$  direction. The remaining two equations are then solved simultaneously with the response,  $z$ , acting as a forcing function.

5.6.1 General discussion of the system. As an adjunct to understanding the characteristic problems associated with this type of system, a general discussion of its probable response behavior is desirable. In a system of this type, the base dimension,  $b$ , of the supporting platform may be on the order of one half or less than the vertical dimension from the base to the center of mass,  $R_z$ . It can be seen that the pitch stiffness,  $k_\theta = 3k b^2/2$ , is determined by the base dimension and the vertical spring stiffness. Normally, the base dimension is limited by the inner diameter of the silo; and the vertical spring stiffness is determined by the necessity to protect the mass,  $m$ , against a vertical shock pulse. It is not hard to visualize the case where insufficient stiffness exists about the pitch axis to prevent the missile and platform from tipping when a finite angular displacement is introduced about the base. Thus, one of the problems inherent in the high C.G. pendulum suspension is its tendency toward static instability where the equation

$$k_\theta > WR_z$$

cannot be satisfied.

Somewhat more difficult to visualize is the condition where the statically stable system may still be dynamically unstable so that oscillation amplitudes will grow to unexpectedly large values as the result of a transient disturbance. Such a system is said to be parametrically excited, and its dynamic instability is therefore a potential problem of the high C.G. pendulum. (Dynamic stability criteria are defined and further discussed in the following Subsection 5.6.2.)

Finally, even when static and dynamic stability exist the dynamic response of these systems can only be obtained by solution of the coupled equations of motion. For most high C.G. pendulum systems, the vertical response can be determined with good accuracy from the shock spectra. The horizontal accelerations are usually very low; and, therefore, any acceleration amplification due to coupling is negligible. Pendulum and pitching response may combine to give horizontal displacements which exceed shock spectra values.

The following design sequence is recommended:

- (1) Define the input in terms of shock spectra and waveforms
- (2) Establish the geometry of the system to suit the operation requirements
- (3) Determine vertical spring rates assuming uncoupled response in the vertical mode (shock spectra SDOF response values)
- (4) Check static stability. The pitch stiffness should be at least 1.5 times greater than the tipping moment, i.e.,  $k_{\theta}/WR_z \geq 1.5$ . If the pitch stiffness is inadequate, specify auxiliary pitch stiffeners to meet this requirement.
- (5) Check dynamic stability: (see Subsection 5.6.2)
- (6) Using the waveform inputs, compute time-history response for the primary purpose of finding maximum horizontal displacement (see Appendix C for the recommended numerical method of solution). If the system is well within the dynamically stable region, the coupling terms on the right side of Equation (5.39) can be neglected (see Subsection 5.6.2).

5.6.2 Dynamic stability. From Equations (5.37), (5.38), and (5.39) and the discussion in 5.6.1, it was noted that Equation (5.38) has a solution

$$x = z_o \cos \omega_z t$$

which is the residual oscillation after the transient shock displacement,  $z_s$ , has terminated. In practice, the amplitude,  $z_o$ , can be determined from the shock spectra corresponding to the characteristics of the specified disturbance,  $z_s$ , i.e.,  $z_o = (z - z_s)_{\max}$ .

Thus Equations (5.37) and (5.38) reduce to

$$\ddot{x} + R_z \ddot{\theta} + \omega_x^2 x = \omega_x^2 (x_s)$$

$$\ddot{\theta} + \omega_{\theta}^2 \theta + \frac{R_z \ddot{x}}{\rho^2} = - \frac{m R_z z_o \omega_z^2 \theta \cos \omega_z t}{J_b}$$

These differential equations contain periodic coefficients; and the stability criterion, i.e., the solution is unstable when the response becomes unbounded with time, for systems described by equations with

periodic coefficients has been derived by Liapounov (Reference 5.3). As expressed for the pendulous system being analyzed here, the limits of the stable region are defined by very complex relationships between the uncoupled natural frequencies and the physical parameters of the isolated structure. Approximate relationships (see Reference 5.2 for its derivation) in which these parameters are implicitly related are given as follows:

$$4(a_2 - 2) < a_1^2 < 1/4(a_2 + 2)^2 \quad (5.40)$$

The function,  $a_2$ , must also satisfy the condition

$$- 2 < a_2 < 6 \quad (5.41)$$

In these inequalities,  $a_1$  and  $a_2$  have the following values:

$$a_1 = 2 \cos \sqrt{\mu_1} + \cos \sqrt{\mu_2} - \frac{2\pi^2}{R_z^2} \left[ \frac{J_b}{J_o} - 1 \right]^2 z_o^2 \dots \text{higher order terms are neglected}$$

$$a_2 = \frac{1}{2} \left[ a_1^2 - f(a_1) \right]$$

where

$$\left. \begin{array}{l} \mu_1 \\ \mu_2 \end{array} \right\} = \frac{\omega_x^2 + \omega_\theta^2 + \sqrt{\left[ \omega_x^2 + \omega_\theta^2 \right]^2 - 4\omega_x^2 \omega_\theta^2 \frac{J_o}{J_b}}}{\frac{\omega_z^2}{2\pi^2} \frac{J_o}{J_b}} \quad (5.42)$$

$$\text{and } f(a_1) = 2 \cos 2 \sqrt{\mu_1} + \cos 2 \sqrt{\mu_2} - \frac{2\pi^2}{R_z^2} \left[ \frac{J_b}{J_o} - 1 \right]^2 z_o^2 \dots$$

The resulting equations are described in Reference 5.2 as "reasonably accurate approximations".

If the arguments of the trigonometric terms in Equation (5.42) are written in the form

$$\left. \begin{array}{l} \mu_1 \\ \mu_2 \end{array} \right\} = \frac{\left( \frac{\omega_x}{\omega_z} \right)^2 + \left( \frac{\omega_\theta}{\omega_z} \right)^2 + \sqrt{\left[ \left( \frac{\omega_x}{\omega_z} \right)^2 + \left( \frac{\omega_\theta}{\omega_z} \right)^2 \right]^2 - 4 \left( \frac{\omega_x}{\omega_z} \right)^2 \left( \frac{\omega_\theta}{\omega_z} \right)^2 \frac{J_o}{J_b}}{\frac{1}{2\pi^2} \frac{J_o}{J_b}}$$

then the boundaries between stability and instability in the Equations (5.40) and (5.41) can be conveniently plotted for various values of  $R_z$ ,  $z_0$  and the ratio  $J_0/J_b$ .

For example, for the ratio  $J_0/J_b = 0.6$  and the vertical distance to the center of mass is  $R_z = 300$  inches and for specified values of the vertical peak amplitudes  $z_0$ , the stable and unstable regions plot as in Figure 5.46.

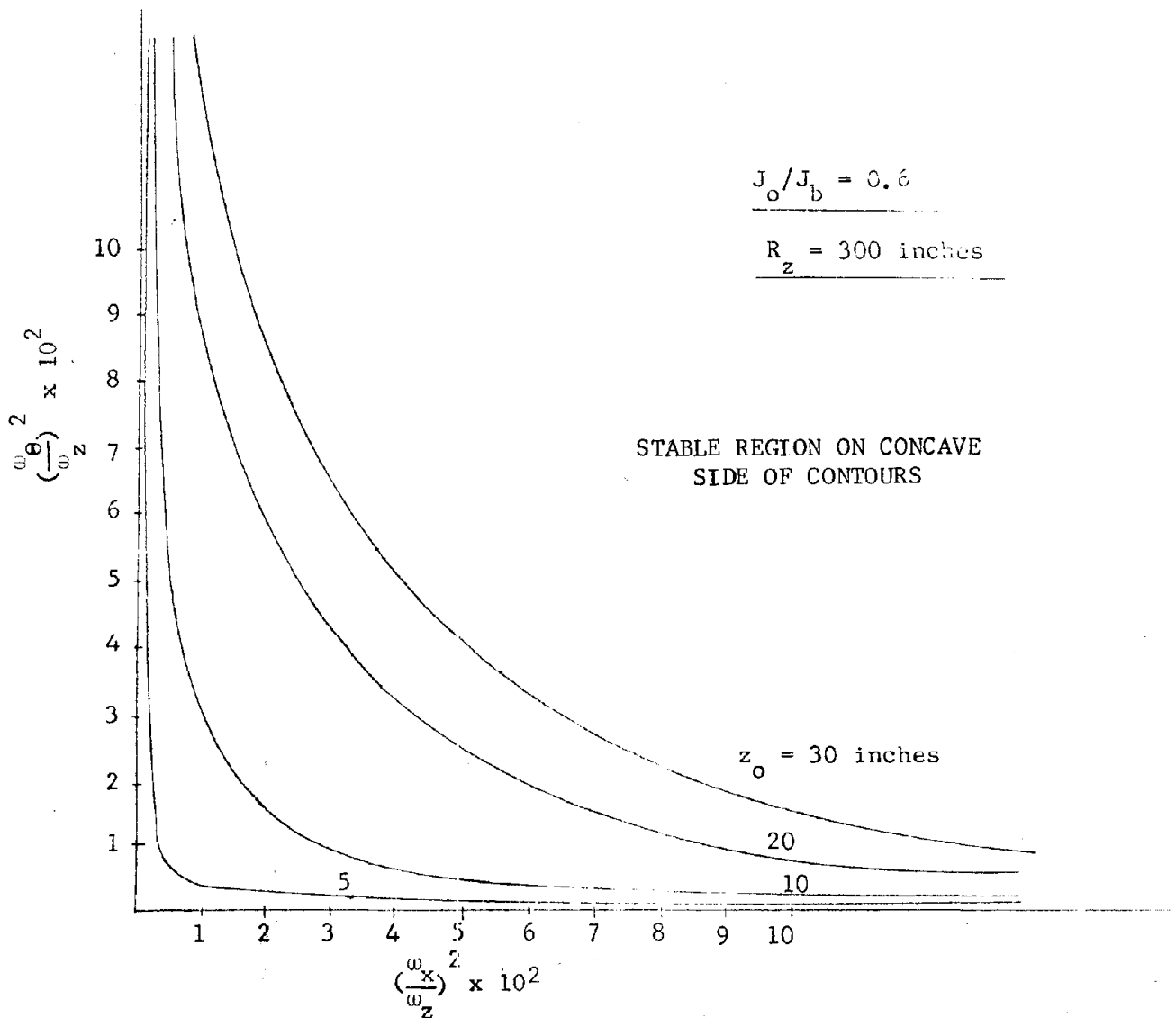


FIGURE 5.46

Obviously, a table of values for  $J_o/J_b$  and  $R_z$  would completely describe the range of stability for Equations (5.37), (5.38) and (5.39). A high C.G. system will have a small ratio of  $(\omega_x/\omega_z)^2$ ; and it can be seen from Figure 5.46 that the unstable region extends even into areas with large values of  $(\omega_\theta/\omega_z)^2$ . This clearly indicates the potential, critical design situation for high C.G. systems.

Example 5.11

A missile illustrated in Figure 5.44 is to be housed in a silo. The suspension system must be capable of reducing the shock effects to a value below 1 g. The pertinent data is:

$$W \text{ (missile and platform)} = 30 \times 10^4 \text{ lb.}$$

$$J_b \text{ (missile and platform)} = 1.65 \times 10^8 \text{ in lb sec}^2$$

$$b = 70 \text{ inches} \quad R_z = 300'' \quad , \quad \ell = 800'' \quad \omega_x^2 = .482/\text{sec}^2$$

Input criteria. The shock spectra envelope is defined by the three straight lines on the shock spectra

$$A_h = 300 \text{ g} \qquad A_v = 300 \text{ g}$$

$$V_h = 50 \text{ in/sec} \qquad V_v = 75 \text{ in/sec}$$

$$D_h = 2 \text{ inches} \qquad D_v = 5 \text{ inches}$$

Vertical spring rate. For design purposes, a vertical spring rate is chosen which corresponds to 0.8 g acceleration in the vertical direction. This corresponds to a frequency of 1.2 cps on the spectra bound constant displacement line of 5 inches.

$$k_z = \frac{4\pi^2 f^2 W}{g} = 4\pi^2 (1.2)^2 \frac{300000}{386} = 44,100 \text{ lb/in} ; \omega_z^2 = 56.9/\text{sec}^2$$

$$k_\theta = \frac{k_z b^2}{2} = \frac{44100 b^2}{2} \text{ lb in/rad}$$

for  $b = 70 \text{ inches} \quad k_\theta = 10.8 \times 10^7 ; \quad \omega_\theta^2 = .272/\text{sec}^2$

Example 5.11 (continued)

Static stability. In order to satisfy static stability

$$\frac{k_{\theta}}{WR_z} = \frac{10.8 \times 10^7}{9 \times 10^7} = 1.2 > 1.0, \text{ but}$$

this does not provide sufficient margin for static stability. Therefore, increase pitch stiffness,  $k_{\theta}$ , to  $13.5 \times 10^7$ .

A statically stable system is achieved by increasing the pitch stiffness,  $k_{\theta}$ , without changing any other parameter of the system. This may be accomplished by the installation of a system of torsion bars at the base of the platform in such a way that the horizontal and vertical frequencies remain unchanged.

Dynamic stability. The following ratios are calculated,

$$\left(\frac{\omega_{\theta}}{\omega_z}\right)^2 = .0048 \quad ; \quad \left(\frac{\omega_x}{\omega_z}\right)^2 = .0085 \quad ; \quad z_o = 5 \text{ inches}$$

For the above parameters and looking at Figure 5.46, the system is close to the unstable region. If the pitch stiffness is increased by a factor of 2, i.e.,  $(\omega_{\theta}/\omega_z)^2 = .01$ , the system is well within the stable region.

5.7 Low C.G. Pendulum System

5.7.1 Introduction. Occasionally, low center of gravity systems are shock isolated by suspending them in a manner similar to Figure 5.47. In many respects, these systems display dynamic behavior identical to base mounted systems or, if the C.G. is very low, to quasi-symmetrical spring systems. An inherent advantage with this method of isolation is the independence of the vertical and horizontal spring rates, and the ability to isolate to very low frequencies.

The equations of small motion for the platform supported symmetrically about the centerline of Figure 5.47 are

$$m\ddot{x} + \frac{W}{\ell} (x - x_s - R_z \theta) = 0 \quad (5.43)$$

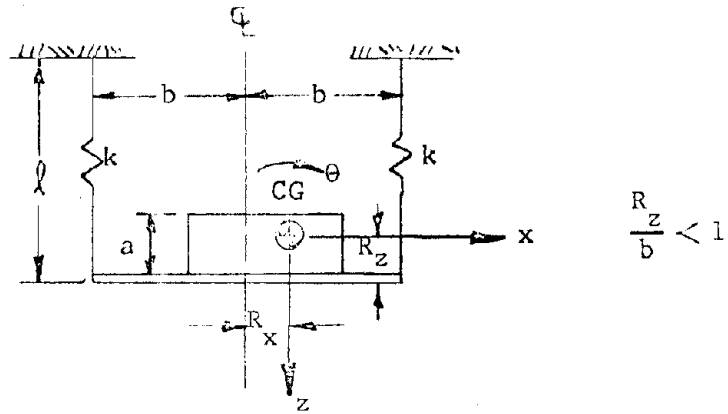


FIGURE 5.47

The spring constant,  $k$ , refers to the total spring rate of all the springs at each pendulum line in a planar system,

$$m\ddot{z} + 2k(z - z_s - R_x\theta) = 0 \quad (5.44)$$

$$J\ddot{\theta} + \frac{W}{l} \left\{ \left[ R_z^2 + R_x(x-x_s) \right] \theta - R_z(x-x_s) \right\} + 2k \left\{ \left[ b^2 + R_x^2 - R_z(z-z_s) \right] \theta - R_x(z-z_s) \right\} - WR_z\theta + \left\{ \frac{WR_x}{l} (x-x_s) + 2k \left[ b^2 - R_z(z-z_s) \right] - WR_z \right\} \beta_0 - R_x W = 0 \quad (5.45)$$

where  $\beta_0$  is the listing angle due to asymmetrical static loading:

$$\beta_0 = \frac{WR_x}{2b^2k - WR_z}$$

The similarity between these equations and those derived for the base mounted system (5.27, 5.28 and 5.29) should be noted.

$m = W/g =$  mass of load and platform

$J =$  mass moment of inertia of platform and load about the C.G. and

$x_s$  and  $z_s$  are the horizontal and vertical support motion inputs.

If the eccentricities,  $R_x$  and  $R_z$ , are very small in comparison to the base dimension,  $b$ , and the radius of gyration is larger than  $\frac{a+b}{8}$ , then the equations of motion can be considered to be essentially uncoupled so



that the shock spectra may be used directly to determine peak accelerations and rattlespaces. The quantities,  $a$  and  $b$ , are the two primary dimensions of the structure, i.e., height and width. In that case, the Equations (5.43, 5.44, and 5.45) reduce to:

$$m\ddot{x} + \frac{W}{l} (x - x_s) = 0$$

$$m\ddot{z} + 2k (z - z_s) = 0$$

$$J\ddot{\theta} + 2kb^2\theta = 0$$

where the third equation drops out if no initial angular disturbances are present; a condition which usually prevails.

The analysis using a waveform input as described in Section 5.4.3 is also applicable for this system. This analysis may be necessary for final design either to better define rattlespace requirements or to verify the rattlespace provided in the preliminary design. The following subsection demonstrates a preliminary design procedure.

5.7.2 Preliminary design. During the preliminary design phase, a systematic method for determining conservative response accelerations and rattlespaces may be appropriate. Consider as the foundation for such a method the rewriting of Equations (5.43, 5.44, 5.45) as follows:

$$m\ddot{x} + \frac{W}{l} (x - x_s - R_z\theta) = 0 \quad (5.43a)$$

$$m\ddot{z} + 2k (z - z_s - R_x\theta) = 0 \quad (5.44a)$$

$$J\ddot{\theta} + mR_z\ddot{x} + mR_x\ddot{z} + \frac{WR_x(x - x_s)}{l} (\theta + \beta_o) - 2kR_z(z - z_s)(\theta + \beta_o) - WR_z(\theta + \beta_o) + 2kb^2\theta - R_xW = 0 \quad (5.45a)$$

If in the two force equations, the quantities,  $R_z\theta_{\max}$  and  $R_x\theta_{\max}$ , are relatively small in comparison to  $(z - z_s)_{\max}$  and  $(z - z_s)_{\max}$ , then the responses,  $x_{\max}$  and  $z_{\max}$ , will be influenced predominantly by the rattlespaces  $(x - x_s)$  and  $(z - z_s)$ . When the isolation systems are very soft, i.e., low natural frequencies, the rattlespaces will be maxima as illustrated by the shock spectra. Moreover, when the moment of inertia is large in comparison to the mass, i.e., large radius of gyration, the

angular response will be small. Then if the eccentricities,  $R_x$  and  $R_z$ , are small, the angular component of displacement in the force equations can be neglected.

In near symmetrical systems, these requirements are often met. However, in many systems, the degree of asymmetry may be considerable with the result that a significant error may be introduced by neglecting the terms,  $R_x \theta$  and  $R_z \theta$ . Still, errors on the order of 25 percent may be acceptable during the preliminary design phase, but if greater conservatism is required, an iterative procedure should be adopted which will allow a convergence to an upper bound solution. The procedures to be followed are developed below.

Dropping the terms,  $R_x \theta$  and  $R_z \theta$ , from Equations (5.43a and 5.44a) yields the equations

$$m\ddot{x} + \frac{W}{\ell} (x - x_s) = 0 \quad (5.43b)$$

$$m\ddot{z} + 2k (z - z_s) = 0 \quad (5.44b)$$

whose bounded response can be obtained directly from the shock spectra.

Then, rewriting Equation (5.45) in terms of these maximum translational responses results in:

$$J\ddot{\theta} + \left[ mR_z \ddot{z} - mR_x \ddot{x} - WR_z + 2kb^2 \right] \theta = m\ddot{x} (R_x \beta_o - R_z) - m\ddot{z} (R_z \beta_o + R_x) + W (R_z \beta_o + R_x) \quad (5.45b)$$

After the transient shocks have passed, Equations (5.43b, 5.44b) indicate that the system will oscillate with residual orthogonal sinusoids whose maximum amplitudes can be no greater than the values obtained from the shock spectra.

That is,

$$\ddot{x} = gA_x \cos (\omega_x t + \phi_1)$$

$$\ddot{z} = gA_z \cos (\omega_z t + \phi_2)$$

where  $A_x$  and  $A_z$  are the horizontal and vertical shock spectra accelerations in g's for an SDOF system at the frequencies  $\omega_x$  and  $\omega_z$ , respectively.

The translational responses above are introduced into (5.45b) and the resultant equation of angular motion is

$$\begin{aligned}
 J\ddot{\theta} + \left[ WR_z A_z \cos(\omega_z t + \phi_2) - WR_x A_x \cos(\omega_x t + \phi_1) - WR_z + 2kb^2 \right] \theta = \\
 WA_x \cos(\omega_x t + \phi_1)(R_x \beta_o - R_z) - WA_z \cos(\omega_z t + \phi_2)(R_z \beta_o + R_x) \\
 + W(R_z \beta_o + R_x)
 \end{aligned} \tag{5.45c}$$

which is insolvable in closed form due to the periodic coefficients of  $\theta$ . But if

$$\left[ |WR_z A_z| + |WR_x A_x| \right] \ll \left[ 2kb^2 - WR_z \right] \tag{5.46}$$

then Equation (5.45c) reduces to\*

$$\begin{aligned}
 J\ddot{\theta} + (2kb^2 - WR_z) \theta = W \left[ A_x (R_x \beta_o - R_z) \cos \omega_x t + A_z (R_z \beta_o + R_x) \right. \\
 \left. \cos \omega_z t + (R_z \beta_o + R_x) \right]
 \end{aligned} \tag{5.45d}$$

where the phase angles are dropped; since the unrelated frequencies,  $\omega_x$  and  $\omega_z$ , must eventually be  $180^\circ$  out of phase, thereby, resulting in an algebraic summation of the three responses for the maximum response.

Equation (5.45d) is a linear ordinary differential equation with harmonic forcing functions and the constant term,  $W(R_z \beta_o + R_x)$ . From the definition of  $\beta_o = WR_x / (2b^2 k - WR_z)$ , the constant term reduces to  $2b^2 k \beta_o$ . A particular solution of Equation (5.45d) corresponding to the constant term is taken in the form

$$\theta = At^2 + Bt + C$$

where A, B, and C are constants. Substituting the assumed solution into Equation (5.45d), where the harmonic forcing functions are neglected temporarily, the coefficients are computed to be:

$$\begin{aligned}
 A &= 0 \\
 B &= 0 \\
 C &= \frac{2b^2 k}{WR_x} \beta_o^2
 \end{aligned}$$

\* When doubt of the inequality, LHS  $\ll$  RHS, exists, see Section 5.7.3.

so that the particular solution to this part of the problem is

$$\theta = \frac{2b^2k}{WR_x} \beta_o^2$$

which can be neglected since  $\beta_o^2 \ll 1$  and  $\frac{2b^2k}{WR_x} \beta_o^2$  are much less than the values for harmonic solutions.

The steady state solutions corresponding to the harmonic inputs can be obtained from classical vibration theory where the transmissibility function for undamped systems is very useful (see Reference 5.4),

$$T = \frac{1}{1 - \left(\frac{\omega}{\omega_n}\right)^2}$$

where  $\omega$  = forced frequency

$\omega_n$  = natural frequency

In this application the forced frequency is  $\omega_x$  and  $\omega_z$  and the natural frequency is  $\omega_\theta$ . Therefore, the transmissibility function defines the ratio of the unknown pitch response to the known translation response as a function of frequency ratios. It is plotted in Figure 5.48 and may be used directly knowing the frequency ratios,  $\omega_x/\omega_\theta$  and  $\omega_z/\omega_\theta$ , where  $T_x$  is a function of  $\omega_x/\omega_\theta$ , and  $T_z$  is a function of  $\omega_z/\omega_\theta$ .

Also

$$\omega_\theta = \sqrt{\frac{(2kb^2 - WR_z)}{J}}, \quad \omega_x = \sqrt{\frac{g}{\ell}}, \quad \omega_z = \sqrt{\frac{2k}{m}}$$

Thus, the maximum angular acceleration is

$$\ddot{\theta} = \frac{W}{J} \left[ \left| T_x A_x (R_x \beta_o - R_z) \right| + \left| T_z A_z (R_z \beta_o + R_x) \right| \right] \quad (5.47)$$

The maximum angular velocity is

$$\dot{\theta} = \frac{W}{J} \left[ \left| \frac{T_x A_x}{\omega_x} (R_x \beta_o - R_z) \right| + \left| \frac{T_z A_z}{\omega_z} (R_z \beta_o + R_x) \right| \right] \quad (5.48)$$

and the maximum angular excursion is

$$\theta = \frac{W}{J} \left[ \left| \frac{T_x A_x}{\omega_x} (R_x \beta_o - R_z) \right| + \left| \frac{T_z A_z}{\omega_z} (R_z \beta_o + R_x) \right| \right] \quad (5.49)$$

TRANSMISSIBILITY CHART

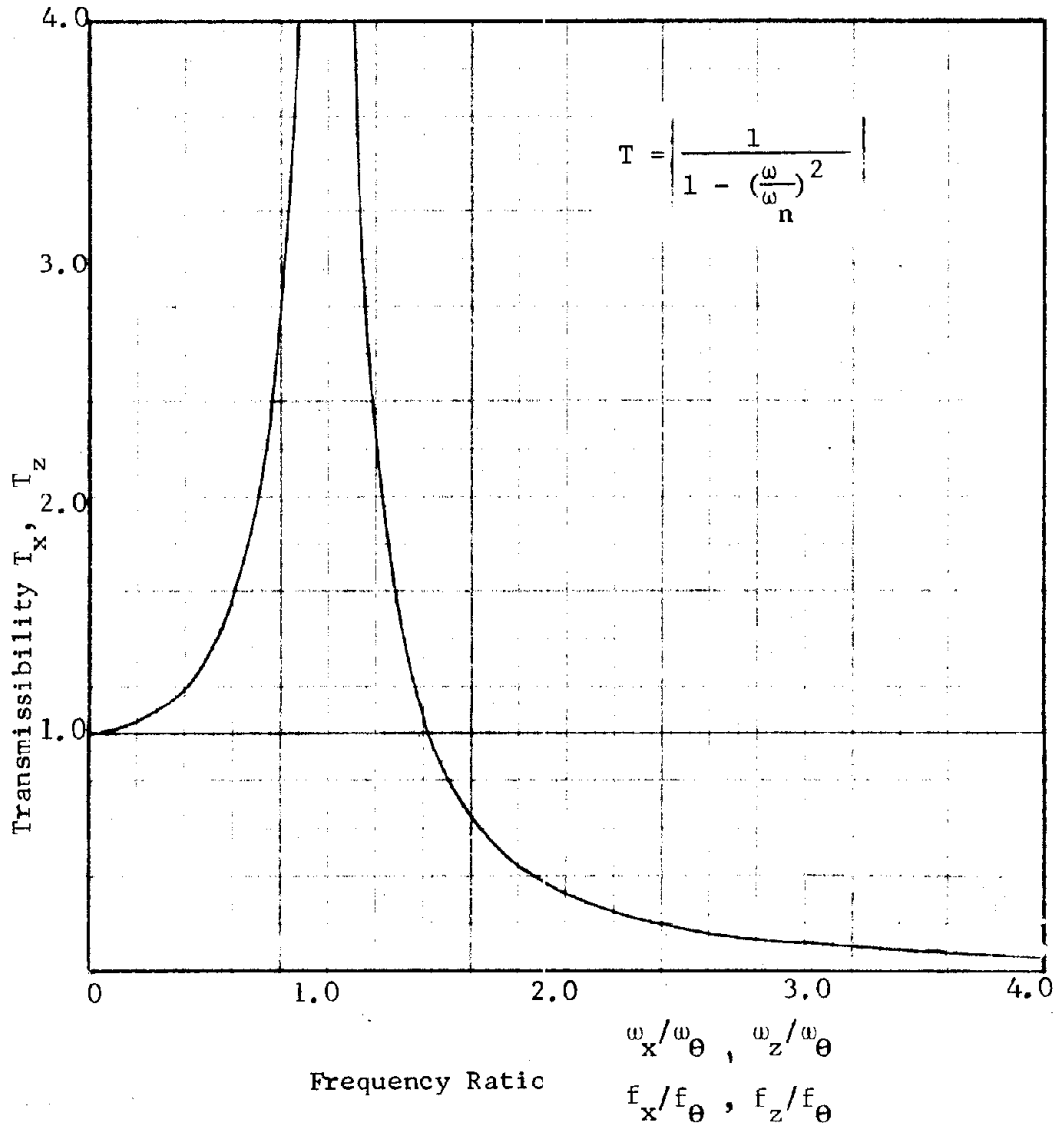


FIGURE 5.48

The total approximate maximum amplitudes at any point on the platform are obtained by adding the translational and rotational components of the shock response from the equations

$$\begin{aligned}
 A'_z &= A_z + \frac{(b + R_x)}{g} \ddot{\theta} & A'_x &= A_x + \frac{R_z}{g} \ddot{\theta} \\
 V'_z &= V_z + (b + R_x) \dot{\theta} & V'_x &= V_x + R_z \dot{\theta} \\
 D'_z &= D_z + (b + R_x) \theta & D'_x &= D_x + R_z \theta
 \end{aligned}
 \tag{5.47a}$$

For the case of no coupling ( $R_x = R_z = 0$ ), the values obtained reduce to the SDOF shock spectra values.

General analysis procedure. The general analysis consists of two major parts:

- (a) An uncoupled frequency analysis to determine the general characteristics of the isolation system and a gross idea of the system response.
- (b) A coupled frequency analysis to confirm the analysis of (a) or to gain a more refined upper bound on the total system response.

The procedure is summarized below:

- (1) From the nuclear explosion data compute the peak ground motions as outlined in Section 3.5.
- (2) Construct the shock spectra from the peak motions as specified in Section 3.6.
- (3) Compute the preliminary SDOF isolation system spring rates from the shock spectra.
- (4) Find the angular response of the system from Equations (5.47) through (5.49) in terms of the translational shock response.
- (5) Determine the peak response of the system due to translation and rotation. If the response is acceptable, i.e., meets the peak acceleration and rattlespace requirements, proceed to the coupled frequency analysis; otherwise decrease the spring rates, and repeat Steps 4 and 5.
- (6) Compute the three coupled frequencies.

- (7) Find the angular response of the system from Equations (5.47) through (5.49) in terms of the translational responses at the coupled natural frequencies.
- (8) Determine the peak response of the system due to translation and rotation.
- (9) Refine the results by accounting for the angular coupling in the force Equations (5.43a) and (5.44a).

Example 5.12

To illustrate the technique, consider the following problem:

A pendulously supported platform carries a weight of 150,000 lbs. The suspension system is arranged symmetrically about the center line as illustrated in Figure 5.47. The constant parameters for the system are

$$\begin{aligned}
 b &= 185 \text{ inches} \\
 R_x &= 10 \text{ inches} \\
 R_z &= 50 \text{ inches} \\
 J &= 7.3 \times 10^6 \text{ in lb sec}^2
 \end{aligned}$$

The pendulum arms are to be attached to the roof of an underground structure which is to be located 20 feet below ground level. The entire system is subject to a 10 MT blast;  $p_{so} = 150$  psi; and soil seismic velocity is 2500 ft/sec.

The structure is to be protected to an acceleration level of 3.5 g or less vertically, and 1 g or less horizontally.

Uncoupled frequency analysis.

Step 1. From Section 3.5.3.1, the peak input disturbances are estimated to be

$$\begin{aligned}
 a_v &= a_h = 37.5 \text{ g} \\
 v_v &= 30 \text{ in/sec} & v_h &= 20 \text{ in/sec} \\
 d_v &= 10 \text{ in} & d_h &= 3.3 \text{ in}
 \end{aligned}$$

Step 2. The SDOF translational response or shock spectra are therefore computed to be

$$A_v = A_h = 2a_v = 75 \text{ g}$$

$$V_v = 1.5 v_v = 45 \text{ in/sec} \quad V_h = 30 \text{ in/sec}$$

$$D_v = d_v = 10 \text{ in} \quad D_h = 3.3 \text{ in}$$

which is modified in the frequency range  $1/2t_d < f < 2/t_d$ , both vertically and horizontally to account for amplification due to resonance. (See Sections 3.6 and 3.7.)

From Section 3.61,  $t^+ = \frac{2d}{v}$ , the vertical and horizontal positive displacement times are:

$$t_v^+ = \frac{20}{30} = 0.66 \text{ sec}$$

$$t_h^+ = \frac{6.6}{20} = 0.33 \text{ sec}$$

Hence, the positive phase durations are:

$$t_{dv} = 4t_v^+ = 2.64 \text{ sec}$$

$$t_{dh} = 4t_h^+ = 1.32 \text{ sec}$$

The horizontal and vertical shock spectra may now be constructed and are included in Figure 5.49.

Step 3. The preliminary spring rates and the approximate general response of the system are determined from the allowable response accelerations. From the shock spectra, Figure 5.49, in order to maintain vertical accelerations below 3.5g, a vertical natural frequency less than 4.5 cps is required. Let

$$f_z = 3 \text{ cps}$$

So that

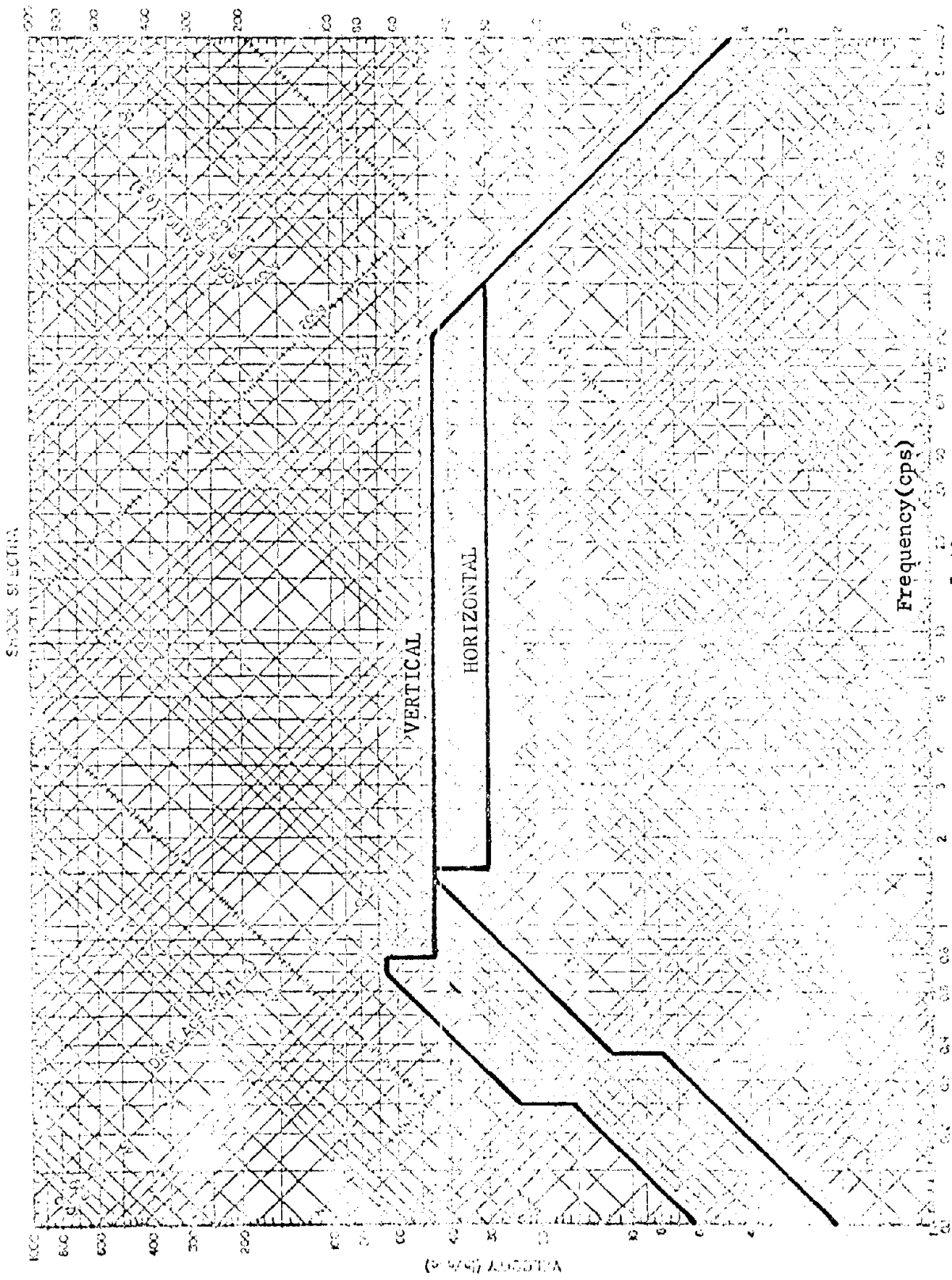
$$k_z = 4 \pi^2 m f_z^2 = 138,000 \text{ lb/in}$$

$$A_z = 2.2 \text{ g}$$

$$D_z = 2.4 \text{ in}$$

Similarly, to remain below 1g horizontally, a natural frequency less than 2 cps is required





Frequency (cps)

FIGURE 5.49

$$f_x \leq 2 \text{ cps}$$

$$k_x = \frac{W}{l} \leq 4 \pi^2 m f_x^2$$

$$l \geq 2.45 \text{ in}$$

Therefore, the pendulum length can be made any convenient length greater than 2.5 inches. In other words, in this example, the choice of the pendulum length is determined by practical limitations rather than the requirement of peak acceleration response attenuation.

Step 4. The effects of the angular response must be checked to assure that peak accelerations and rattlespaces remain within bounded limits. The inequality of (5.46) must be satisfied in order to use Equations (5.47, 5.48 and 5.49).

$$\left[ |WR_{zA_z}| + |WR_{xA_x}| \right] \ll \left[ 2kb^2 - WR_z \right]$$

Let

$$l = 150 \text{ inches}$$

so that

$$f_x = \sqrt{\frac{g}{4\pi^2 l}} = 0.255 \text{ cps}$$

and from the shock spectra of Figure 5.49

$$A_x = 0.022 \text{ g}$$

$$D_x = 3.3 \text{ in.}$$

Substituting the appropriate values in (5.46) yields the result  $1.52 \times 10^7 \ll 4.71 \times 10^9$ . Since the left hand side of the inequality is less than 1 percent of the right hand side, Equation (5.46) is satisfied. The pitch frequency is:

$$f_\theta = \frac{1}{2\pi} \sqrt{\frac{2kb^2 - WR_z}{J}} = 4.04 \text{ cps}$$

and the frequency ratios are:

$$f_x/f_\theta = 0.063$$

$$f_z/f_\theta = 0.742$$

From the transmissibility chart, Figure 5.48,

$$T_x = 1.0$$

$$T_z = 2.2$$

Finally, the angular responses can be computed from Equation (5.47)

$$\ddot{\theta} = 1.02 \text{ rad/sec}^2$$

and from Equation (5.49)

$$\theta = 0.0116 \text{ rad}$$

Step 5. The total peak accelerations and displacements at any point on the platform are approximated by:

$$A_z' = A_z + \frac{(b + R_x)}{g} \ddot{\theta} = 2.2 + 0.514 = 2.71g$$

$$A_x' = A_x + \frac{R_z \ddot{\theta}}{g} = 0.022 + 0.132 = 0.15g$$

$$D_z' = D_z + (b + R_x) \theta = 2.4 + 2.26 = 4.66 \text{ inches}$$

$$D_x' = D_x + R_z \theta = 3.3 + 0.58 = 3.88 \text{ inches}$$

It will be recalled that the foregoing analysis was based on:

(1) Discarding the coupling terms  $R_z \theta$  and  $R_x \theta$  in Equations (5.43a) and (5.44a) to find the translational responses  $\ddot{x}_{\max}$  and  $\ddot{z}_{\max}$  and  $(x - x_s)_{\max}$  and  $(z - z_s)_{\max}$  from the shock spectra.

(2) Treating the translational responses as inputs into the moment equation to obtain the rotational response.

It is of interest to compare the coupling terms,  $R_z \theta$ , and  $R_x \theta$ , with relative rigid body displacements,  $(x - x_s)_{\max}$  and  $(z - z_s)_{\max}$ , to gain insight into the reasonableness of assumption (1) above.

$$\left. \begin{array}{l} R_x \theta_{\max} = 0.116 \text{ in.} \\ (z - z_s)_{\max} = 2.4 \text{ in.} \end{array} \right\} 5 \text{ percent}$$

$$\left. \begin{array}{l} R_z \theta = 0.58 \text{ in.} \\ (x - x_s)_{\max} = 3.3 \text{ in.} \end{array} \right\} 18 \text{ percent}$$

Thus, neglect of coupling in the force equations may, for some very preliminary analyses, be acceptable. However, it should be noted that the results are not conservative and that a more refined technique may be

required to obtain results which more nearly describe a bound on the response amplitudes. The results of extending the analysis are illustrated in the following steps where the coupled frequencies are used to compute the initial magnitudes of  $A_x$  and  $A_z$ .

Coupled frequency analysis.

Step 6. The three coupled natural frequencies are determined from Equations (5.43a, 5.44a, and 5.45a) where the dynamic coupling terms, the ground motions, and the pendulum term are dropped for simplicity. The frequency determinant is found by the method outlined in Appendix A and is:

$$\text{DET} \begin{vmatrix} a_{11} & 0 & a_{13} \\ 0 & a_{22} & a_{23} \\ a_{31} & a_{32} & a_{33} \end{vmatrix} = 0$$

where

$$a_{11} = m\omega^2 - \frac{W}{l} \quad \text{lbs/in}$$

$$a_{13} = \frac{WR_z}{l} \quad \text{lbs}$$

$$a_{22} = m\omega^2 - 2k \quad \text{lbs/in}$$

$$a_{23} = 2k R_x \quad \text{lbs}$$

$$a_{31} = m R_z \omega^2 - \frac{WR_x \beta_0}{l} \quad \text{lbs}$$

$$a_{32} = m R_x \omega^2 + 2k R_z \beta_0 \quad \text{lbs}$$

$$a_{33} = J \omega^2 - 2k b^2 + W R_z \quad \text{lbs-in}$$

When solved, this equation yields three real positive roots which are the coupled natural frequencies (see Appendix A for Fortran program).

$$\omega_1 = 1.6 \text{ rad/sec} \quad f_1 = 0.254 \text{ cps}$$

$$\omega_2 = 19.2 \text{ rad/sec} \quad f_2 = 3.05 \text{ cps}$$

$$\omega_3 = 25.1 \text{ rad/sec} \quad f_3 = 4.00 \text{ cps}$$

The coupled natural frequencies may be associated with their uncoupled counterparts usually by inspection. The justification for associating coupled frequencies with a particular mode of response is that (for the kind of systems considered here) practically all of the response at each of the coupled natural frequencies is derived from the input motion along that axis.

	FREQUENCIES	
	Coupled	Uncoupled
Horizontal translation	0.254	0.255
Vertical translation	3.05	3.00
Pitching	4.00	4.04

Step 7. The method of solution using coupled frequencies is identical with the procedure specified for the uncoupled system analysis. From the shock spectra, Figure 5.49 using the coupled frequencies  $f_z = f_2$  and  $f_x = f_1$  above:

$$\begin{array}{ll}
 f_z = 3.05 \text{ cps} & f_x = 0.254 \text{ cps} \\
 A_z = 2.2g & A_x = 0.022g \\
 D_z = 2.4 \text{ in.} & D_x = 3.3 \text{ in.}
 \end{array}$$

The frequency ratios are

$$\begin{aligned}
 f_x/f_\theta &= \frac{0.254}{4.00} = 0.064 \\
 f_z/f_\theta &= 3.05/4.00 = 0.762
 \end{aligned}$$

from which the transmissibilities are determined (Figure 5.48)

$$\begin{aligned}
 T_x &= 1.00 \\
 T_z &= 2.32
 \end{aligned}$$

Solution of the angular responses  $\ddot{\theta}$  and  $\theta$  are found to be

$$\begin{aligned}
 \ddot{\theta} &= 1.07 \text{ rad/sec}^2 \\
 \theta &= 0.0117 \text{ rad}
 \end{aligned}$$

Step 8. The peak acceleration and rattlespace amplitudes at any point on the platform are determined from Equations (5.47a) as:

$$\begin{aligned}
A'_z &= 2.2 + 0.54 = 2.74g \\
D'_z &= 2.4 + 2.28 = 4.68 \text{ in} \\
A'_x &= 0.022 + 0.139 = 0.16g \\
D'_x &= 3.3 + 0.585 = 3.88 \text{ in}
\end{aligned}$$

A comparison of the results for the coupled and uncoupled system analysis at any point on the platform yields:

	AMPLITUDES	
	Coupled	Uncoupled
$A'_z$	2.74g	2.71g
$D'_z$	4.68 in	4.66 in
$A'_x$	0.16g	0.15g
$D'_x$	3.88 in	3.88 in

Step 9. As in Step 5 the quantities  $R_{x \max} \theta$ ,  $R_{z \max} \theta$ ,  $(x - x_s)_{\max}$  and  $(z - z_s)_{\max}$  are evaluated and compared.

$$\left. \begin{aligned}
R_{x \max} \theta &= 0.117 \text{ in} \\
(z - z_s)_{\max} &= 2.4 \text{ in}
\end{aligned} \right\} 5 \text{ percent}$$

$$\left. \begin{aligned}
R_{z \max} \theta &= 0.585 \text{ in} \\
(x - x_s)_{\max} &= 3.3 \text{ in}
\end{aligned} \right\} 18 \text{ percent}$$

The effect of neglecting the coupling terms in the force equation is seen to be of the same magnitude as in the uncoupled analysis (Step 5).

If the analysis were to terminate at this point, it would be best to assume the maxima of the uncoupled and coupled frequency analyses from Step 8,

$$\begin{aligned}
A'_z &= 2.74 \text{ g} \\
D'_z &= 4.68 \text{ in.} \\
A'_x &= 0.16 \text{ g} \\
D'_x &= 3.88 \text{ in.}
\end{aligned}$$

However, the results are not conservative; and the following procedure is recommended to establish an upper bound.

### First Iteration

The angular coupling  $R_z \theta$  and  $R_x \theta$  is fed back into the force Equations (5.43a and 5.44a) without regard to sign since the phase relations between the translations and rotations are not known. Thus,

$$(x - x_s)_{\max} + R_z \theta_{\max} = 3.3 + 0.585 = 3.89 \text{ in}$$

$$(z - z_s)_{\max} + R_x \theta_{\max} = 2.4 + 0.117 = 2.52 \text{ in}$$

These quantities may be thought of as new peak relative displacements at the C.G. of the system. The corresponding accelerations at the C.G. taken at the coupled frequencies would then be:

$$A_z = \frac{\omega_z^2 D_z}{g} = \frac{(19.2)^2 (2.52)}{386} = 2.41 \text{ g}$$

$$A_x = \frac{\omega_x^2 D_x}{g} = \frac{(1.6)^2 (3.89)}{386} = 0.026 \text{ g}$$

Substituting these values into Equations (5.47 and 5.49), where the frequencies and the transmissibilities remain unchanged from the previous case, yields:

$$\ddot{\theta} = 1.18 \text{ rad/sec}^2$$

$$\theta = 0.0136 \text{ rad}$$

The peak accelerations and rattlespaces are then determined from Equations (5.47a).

$$A_z' = 2.41 + 0.596 = 3.01 \text{ g}$$

$$D_z' = 2.52 + 2.65 = 5.17 \text{ in}$$

$$A_x' = 0.026 + 0.153 = 0.18 \text{ g}$$

$$D_x' = 3.89 + 0.68 = 4.57 \text{ in}$$

### Second Iteration

The procedures under the first iteration are repeated for the new values of  $\ddot{\theta}$  and  $\theta$ .

$$(x - x_s)_{\max} + R_z \theta = 3.3 + 0.68 = 3.98 \text{ in}$$

$$(z - z_s)_{\max} + R_x \theta = 2.4 + 0.136 = 2.54 \text{ in}$$

$$A_z = \frac{\omega_z^2 D_z}{g} = \frac{(19.2)^2 (2.54)}{386} = 2.42 \text{ g}$$

$$A_x = \frac{\omega_x^2 D_x}{g} = \frac{(1.6)^2 (3.98)}{386} = 0.026 \text{ g}$$

$$\ddot{\theta} = 1.18 \text{ rad/sec}^2$$

$$\theta = 0.0136 \text{ rad}$$

$$A_z' = 2.42 + 0.596 = 3.02$$

$$D_z' = 2.54 + 2.65 = 5.19 \text{ in}$$

$$A_x' = 0.026 + 0.153 = 0.18 \text{ g}$$

$$D_x' = 3.98 + 0.68 = 4.66 \text{ in}$$

The maximum accelerations and rattlespaces at any point on the platform are tabulated below for the uncoupled and coupled frequency analyses.

	(1) Uncoupled	(2) Coupled	(3) Coupled 1st Iteration	(4) Coupled 2nd Iteration
$A_z'$	2.71 g	2.74 g	3.01 g	3.02 g
$D_z'$	4.66 in	4.68 in	5.17 in	5.19 in
$A_x'$	0.15 g	0.16 g	0.18 g	0.18 g
$D_x'$	3.88 in	3.88 in	4.57 in	4.66 in

It may, therefore, be concluded that the system has an upper bound response with peak acceleration values of 3.0 g, vertically, and 0.2 g, horizontally, and peak relative displacements at the corners of 5.2 in, vertically, and 4.7 in, horizontally.

5.7.3 Stability considerations for low C.G. pendulous systems. There may be times when it is not possible to satisfy the inequality of Equation (5.46), i.e., instead of having the LHS << RHS, the real situation may have the LHS only slightly less than the RHS. Then, a test for stability using Equation (5.45c) may not be possible. It is also noted that, if the LHS > RHS, instability should be expected to occur.



Equation (5.45c) will be investigated by an intuitive approach based on available analyses. The equation is simplified by dropping the phase angles, static tilt angle, and the constant term.

$$\ddot{\theta} + \left[ WR_{z z} A_z \cos \omega_z t - WR_{x x} A_x \cos \omega_x t - WR_z + 2kb^2 \right] \theta = \\ - WA_{z x} R_x \cos \omega_z t - WA_{x z} R_z \cos \omega_x t$$

Stability considerations are sought from the homogeneous equation so that

$$\ddot{\theta} + \left[ \frac{(2kb^2 - WR_z)}{J} - \left( \frac{WR_{x x} A_x}{J} \cos \omega_x t - \frac{WR_{z z} A_z}{J} \cos \omega_z t \right) \right] \theta = 0$$

If the amplitude of one of the periodic terms is significantly larger than the other, that is, either

$$\frac{WR_{x x} A_x}{J} > \frac{WR_{z z} A_z}{J}$$

or

$$\frac{WR_{z z} A_z}{J} > \frac{WR_{x x} A_x}{J}$$

then the moment equation reduces to the form

$$\ddot{\theta} + \left[ a + 2q \cos \omega t \right] \theta = 0$$

For low C.G. pendulous systems,  $A_z$  is usually much greater than  $A_x$ . Therefore, the second inequality above will normally be satisfied for this system.

The above equation is recognized as the Mathieu Equation, where

$$a = \frac{2kb^2 - WR_z}{J} \quad \text{sec}^{-2} \\ 2q = \frac{WR_{x x} A_x}{J}, \quad \frac{WR_{z z} A_z}{J} \quad \text{sec}^{-2}$$

The regions of instability are plotted in Figure 5.50 in terms of the parameters,  $a$  and  $q$ .

For further investigation of stability considerations, reference may be made to the work of Liapounov (Reference 5.3).

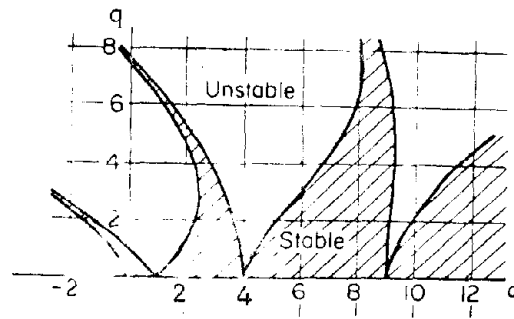


FIGURE 5.50

5.7.4 Effects of platform flexibility. In a spring mounted system such as a platform supported at its corners, as shown in Figure 5.47, the flexibility of the platform is an important consideration. If the deformation modes are excited, equipment which is rigidly attached to the platform will feel a high frequency motion as well as the low frequency rigid body motions. The platform may be activated due to two possible causes:

Case (1) The rigid body motion frequencies may not be significantly lower than the platform frequency. Thus, the rigid body motion is an important forcing vibration input to the platform structure.

Case (2) The isolators may surge and chatter and consequently excite a deformation mode of the platform.

Case (1) The effect in Case (1) can be overcome by designing a platform with a lowest mode frequency that is much higher than the highest rigid body frequency. For example, in the low C.G. system considered in Example 5.12, Subsection 5.7.2, the three rigid body frequencies are calculated as

$$f_x = 0.255 \text{ cps}$$

$$f_z = 3 \text{ cps}$$

$$f_\theta = 4.04 \text{ cps}$$

In this case, the pitch and vertical motions are the most likely to excite a deformation mode of the platform. The vertical mode is particularly important, as it could excite the symmetrical or lowest deformation mode

frequency. Referring to Section 2.4.2 where the two-mass system is considered, Equation (2.28), given as

$$\ddot{x}_2 = \left| \frac{f_2^2}{f_2^2 - f_1^2} \right| A_1 + \left| \frac{f_1^2}{f_1^2 - f_2^2} \right| A_2$$

defines the acceleration of the second mass when  $m_1 \gg m_2$ . Let  $f_1$  be the vertical rigid body frequency ( $f_2 = 3$  cps) and  $f_2$  the lowest platform deformation mode frequency. Then the above equation can be used to find the frequency,  $f_2$ , for which the response,  $\ddot{x}_2$ , is not significantly greater than  $A_1$ . For example, using the spectra envelope of Figure 5.49 and  $f_1 = 3$  cps, and trying  $f_2 = 6 f_1$ ,

$$A_1 = 2.2 \text{ g}$$

$$A_2 = 13 \text{ g}$$

$$\ddot{x}_2 = \left| \frac{324}{324 - 9} \right| 2.2 + \left| \frac{9}{9 - 324} \right| 13 \cong 2.6 \text{ g}$$

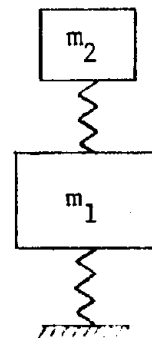
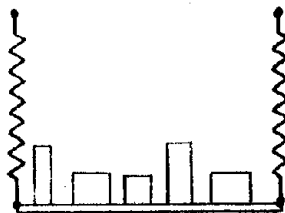
$$\frac{\ddot{x}_2}{A_1} \cong 1.2$$

Therefore, in this example the equipment acceleration would be amplified by 20 percent for the particular case,  $m_2 \ll m_1$  and  $f_2 = 6 f_1$ . A stiffer platform would further reduce this amplification.

The assumption that  $m_2 \ll m_1$  is very conservative for platforms that support heavy equipment. For example, consider a platform and its equipment weighing 60000 pounds. Let the weight distribution approximately be:

Equipment : 40000 pounds

Platform structure: 20000 pounds



Assume the mass,  $m_1$ , to represent about half the mass of the platform and some of the equipment in the vicinity of the isolators. Mass,  $m_2$ , is the equipment mass near the center plus part of the platform mass. Consequently the mass ratio,  $m_2/m_1$ , in the 2-mass model is not very small.

For a less conservative approach in lieu of Equation (2.28), the actual mass ratios must be used. A dynamic analysis must then be performed in order to determine a lower limit on the platform stiffness so that the rigid body assumption is made meaningful. For equipment platforms of the type discussed in this subsection, frequencies on the order of 3 times the pendulum vertical frequency have been specified in the past as being adequate for negligible platform case deformations.

Case (2). High frequency vibrations in the platform due to chatter and surging of the isolators should be minimized during the design phase of the isolators. An analysis and a test are both usually required to determine the magnitude of these accelerations. The procedures that were adopted for the Minuteman System are discussed in Section 9.5; they are recommended when high frequency accelerations may be detrimental to the platform supported equipment.

## 5.8 Effect of Damping

A consideration of damping during both the forced vibration era and during the residual or free vibration era of the shock response should be envisaged in the design of a shock isolation system. Thus, during the forced vibration era an undue amount of damping may generate significant forces acting on the system in addition to the spring forces, while the subsidence of vibrations in the residual or free vibration era is usually desirable so as to minimize energy transfer from one mode to another and to bring the system back to its static condition in a reasonably short time.

5.8.1 Types of damping. Since damping is a process whereby energy is dissipated as heat, the physical mechanisms performing the dissipation are usually manifold; and their action cannot be described a priori by rigorous mathematical relationships, as for instance, existing among mass, acceleration,

and inertia force. Heat dissipation can occur within a material as a result of the deformation and/or the deformational speed of the material, and it always occurs in a gas undergoing non-adiabatic changes. Heat dissipation may also occur due to minute slippage at joints or interfaces of material objects.

Since a damping or friction force is a passive force and cannot dissipate energy without acting over a displacement, its incorporation within a differential equation must be considered in the light of its passivity. Thus, for a single-degree-of-freedom system with a coordinate,  $u$ , mass,  $m$ , and spring stiffness,  $k$ , a constant friction force or Coulomb friction force,  $F_c$ , will appear in the differential equation of force equilibrium as  $\pm F_c$  in the sense that it will always tend to oppose the motion. An equivalent and more explicit way of introducing  $F_c$  into the equation is to write  $(\text{sgn } \dot{u}) F_c$ , read (signum velocity)  $F_c$ , since this implies a change of sign when the velocity changes. Thus, the equation

$$m\ddot{u} + (\text{sgn } \dot{u}) F_c + ku = 0$$

or

$$\ddot{u} + (\text{sgn } \dot{u}) \frac{F_c}{m} + \omega^2 u = 0 \tag{5.50}$$

describes the free vibration of a linear mass-spring system with constant damping of  $F_c$  pounds, and circular frequency,  $k/m = \omega^2$ .

If, instead of constant damping, a purely viscous type is present, the viscous damping force will be proportional to the relative velocity,  $\dot{u}$ , between the mass and the anchorage of its spring. In this case, the equation

$$m\ddot{u} + c\dot{u} + ku = 0$$

or

$$\ddot{u} + \frac{c}{m} \dot{u} + \omega^2 u = 0 \tag{5.51}$$

describes the free vibration of the linear system as influenced by the viscous damping force,  $c\dot{u}$ . The dimensions of  $c$  are, therefore, force per unit velocity.

A more general description of a damping force is to express it as the  $n^{\text{th}}$  power of the relative velocity,  $\dot{u}$ , it is

$$(\text{sgn } \dot{u}) c_n (\dot{u})^n, \text{ or } c_n (\dot{u})^{n-1} u \tag{5.52}$$

in this case, the equation assumes the form

$$m\ddot{u} + (\text{sgn } \dot{u}) c_n (\dot{u})^n + ku = 0$$

or

$$\ddot{u} + (\text{sgn } \dot{u}) \frac{c_n}{m} (\dot{u})^n + \omega_u^2 u = 0 \quad (5.53)$$

It should be pointed out that Equation (5.53) reduces to Equation (5.50) if  $n = 0$ , and it also reduces to Equation (5.51) if  $n = 1$ . Accordingly, Equation (5.53) is able to describe many types of damping. The dimensions of  $c_n$  are, therefore, force per unit relative velocity raised to the  $n^{\text{th}}$  power.

A further generalization of Equation (5.53) can be made by assuming that the damping is expressed by several damping forces proportional to different powers,  $n_1, n_2, \text{ etc.}$ , of the relative velocity,

$$(\text{sgn } \dot{u}) \left[ c_{n_1} (\dot{u})^{n_1} + c_{n_2} (\dot{u})^{n_2} + \dots c_{n_j} (\dot{u})^{n_j} \right] \quad (5.54)$$

describes the friction forces in terms of  $j$  different powers of the relative velocity,  $\dot{u}$ .

5.8.2 Damping during forced loading. In general, the forced vibration era of a soft mounted, damped isolation system will experience larger transmitted forces than the identical but undamped system. A precise determination of the damping forces will involve, not only the parameters of the system itself, but also the shape and magnitude of the velocity input. So as to get a very rough idea of the relative magnitudes of the maximum damping forces and maximum spring force during the forced vibration era, an extremely simplified example will be presented.

#### Example 5.13

Assume that a triangular velocity pulse, Figure 5.51a, acts on a soft mounted frictionless system of weight, 32 kips, with spring stiffness,  $k = 500$  pounds/inch. If the undamped natural frequency of the system is 0.4 cps, the deformation of the spring will occur so rapidly that the absolute motion of the spring mounted mass will be negligible, and the relative maximum displacement of the mass, or the maximum compression of

Example 5.13 (continued)

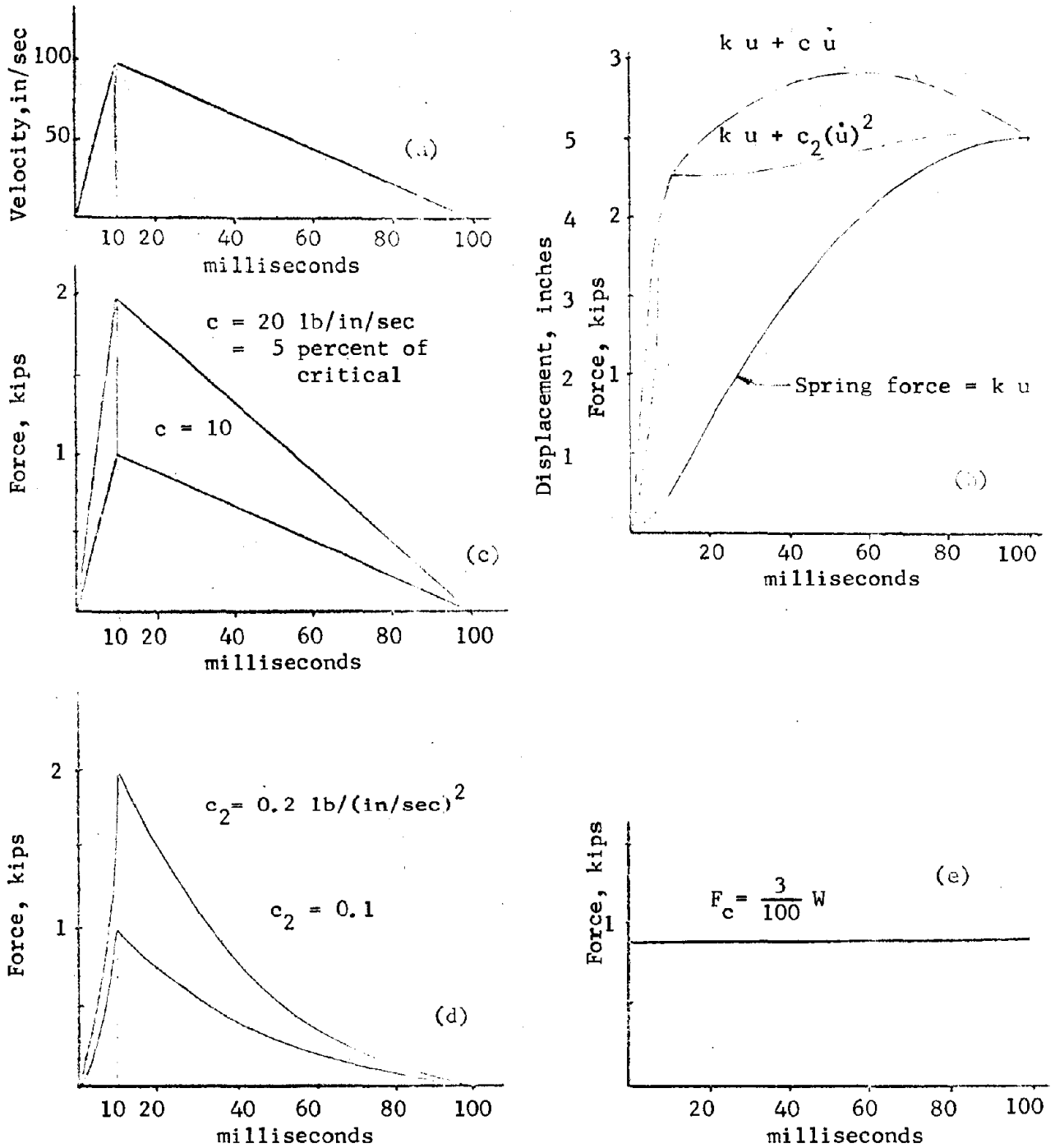


FIGURE 5.51

Example 5.13 (continued)

the spring will be approximately

$$\int_0^t \dot{u} dt = \frac{100}{2} 0.1 = 5 \text{ inches}$$

and, accordingly, the maximum spring force will be

$$k u_{\max} = 500 \times 5 = 2.5 \text{ kips}$$

Figure 5.51b shows the time-displacement or the time-spring force by the solid line curve.

Assuming that the maximum free vibration amplitude is 5 inches, the maximum undamped free vibration velocity,  $\dot{u}_{\max}$ , at a frequency of 0.4 cps will be

$$2\pi \times 0.4 \times 5 = 12.6 \text{ inches/sec}$$

Consequently, the maximum damping forces will be

$$c \dot{u}_{\max} = 20 \times 12.6 = 252 \text{ pounds for viscous damping}$$

$$c_2 (\dot{u}_{\max})^2 = 0.2 \times 12.6^2 = 31.7 \text{ pounds for quadratic damping}$$

$$F_c = 960 \text{ pounds for Coulomb damping}$$

These values should be compared to the maxima damping force values of 2000, 2000, and 960 pounds for the forced vibration era, as seen in Figures 5.51 c, d and e.

If a pure, viscous damping force is present in the system, Figure 5.51c shows its time variation for damping coefficients of 20 and 10 pound seconds per inch, corresponding to 5 and 2.5 percent of critical damping; and Figure 5.51b shows the resultant of the spring force and the larger damping force by the dash-dot line curve.

If a quadratic velocity damping force is present in the system, Figure 5.51d plots the time variation of the damping force curve for coefficients of 0.2 and 0.1 pound/(inches per second)<sup>2</sup>, and Figure 5.51b, indicated by the dotted line curve, gives the resultant of the spring and the larger damping force.



Example 5.13 (continued)

A constant or a Coulomb damping force of 3 percent magnitude of the 32,000 pound shock isolated mass represents a force of 960 lbs. This is shown in Figure 5.51e, and it obviously will translate the spring force curve of Figure 5.51b upward by that amount.

It is seen that the effect of friction in the forced vibration era is to increase the time integral or impulse transmitted to the shock mounted mass and, consequently, to increase the transmitted acceleration and velocity of the mass.

A comparison of the maximum forces of damping origin acting on the isolated mass during the free or residual vibration era and during the forced vibration era can now be made for the three specific cases of assumed damping values.

The following subsection considers the free vibration era, and provides simple expressions for estimating the subsidence duration as a function of the damping characteristics.

**5.8.3 Solution of the damped free vibration:** The subsidence of vibrations in the residual or free vibration era may be dealt with in a relatively simple way if considerations are limited to a single mass system with one or more decoupled degrees of freedom. Equations (5.50) and (5.51) can be solved readily, but Equation (5.53) and (5.54) obviously require special methods if  $\dot{u}$  is different from either zero or unity.

A free vibration with initial amplitude,  $u_0$ , and governed by Equation (5.50) will vibrate at the circular frequency,  $\omega$  rad/sec, and its amplitude will decrease the amount

$$\frac{2F_c}{k} \text{ per half cycle or } \frac{4F_c}{k} \text{ per cycle}$$

The attenuation, therefore, follows a straight line with a slope of

$$-\frac{4F_c \omega}{k 2\pi} = -\frac{2F_c}{\pi \sqrt{km}}$$

Accordingly, in  $\tau$  seconds from the start of free vibrations the amplitude,  $u_\tau$ , will be

$$u_\tau = u_0 \left( 1 - \frac{2F_c \tau}{\pi \sqrt{km}} \right) \quad (5.55)$$

If the free vibration with initial amplitude,  $u_0$ , is governed by Equation (5.51), it will vibrate at the circular frequency,  $p$  rad/sec, and its displacement amplitude at time,  $\tau$ , will be given by

$$u_\tau = u_0 e^{-\nu p \tau} \quad (5.56)$$

in which

$$\nu = \frac{c}{2 \sqrt{km}} = \frac{c}{c_{cr}}$$

and

$$p = \omega \sqrt{1 - \nu^2} \quad (5.57)$$

Since the value of  $\nu$  is usually less than 1/4, the value of  $p$  may be replaced by  $\omega$ , and Equation (5.56) assumes the form

$$u_\tau \approx u_0 e^{-\nu \omega \tau} \quad (5.56a)$$

If the free vibration is governed by Equation (5.53), a graphical solution can be obtained readily by the phase plane delta method, Reference 5.5, by numerical methods, or for a few special integer values of  $u$  in closed form solution.

The concept of equivalent viscous damping is not directly applicable to free vibration since it postulates a steady state of vibration, i.e., a constant amplitude and a constant frequency. However, if the damping is very small so that the attenuation is very slow and the natural frequency changes exceedingly slowly, the concept of an equivalent value of  $\nu$  can be applied stepwise, i.e., for block values of  $\Delta u$  and  $\Delta \omega$ . Since in nearly all practical shock mountings a fair degree of damping is desirable, it is concluded that the equivalent viscous damping concept generally is not applicable.

Viscous damping calculations: Figure 5.52 shows a single mass, three-degree-of-freedom, decoupled system with coordinates,  $x$ ,  $z$ , and  $\theta$ . Assume that the CG and CR coincide. Consider all 8 springs unstressed, and

neglect their transverse stiffnesses. Accordingly, the system's transitory circular undamped frequencies are

$$\omega_x = \sqrt{\frac{4k_x}{m}}$$

$$\omega_z = \sqrt{\frac{4k_z}{m}}$$

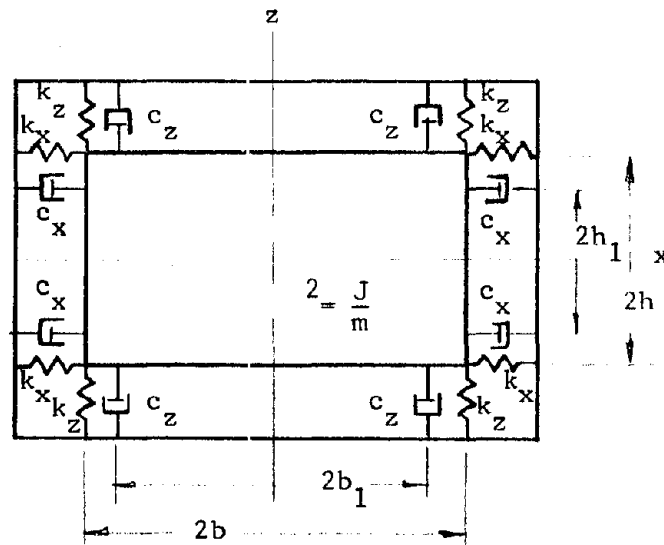


FIGURE 5.52

and the rotational circular undamped frequency is given by

$$\omega_\theta = \sqrt{\frac{4k_x h_1^2 + 4k_z b^2}{2m}}$$

The viscous damping forces are then

$$4c_x \dot{x} \text{ and } 4c_z \dot{z}$$

and the viscous damping moment is

$$4c_x h_1^2 \dot{\theta} + 4c_z b_1^2 \dot{\theta}$$

accordingly, the three differential equations will be

$$\begin{aligned}
 m\ddot{x} + 4c_x \dot{x} + 4k_x x &= 0 \\
 m\ddot{z} + 4c_z \dot{z} + 4k_z z &= 0 \\
 m\rho^2 \ddot{\theta} + 4(c_x h_1^2 + c_z b_1^2) \dot{\theta} + 4(k_x h^2 + k_z b^2) \theta &= 0
 \end{aligned} \tag{5.58}$$

and the values of  $\nu$  from Equation (5.57) are expressed by

$$\begin{aligned}
 \nu_x &= \frac{4c_x}{2\sqrt{4k_x m}} = \frac{c_x}{\sqrt{k_x m}} \\
 \nu_z &= \frac{2c_z}{2\sqrt{4k_z m}} = \frac{c_z}{\sqrt{k_z m}} \\
 \nu_\theta &= \frac{4(c_x h_1^2 + c_z b_1^2)}{2\sqrt{4(k_x h^2 + k_z b^2)}\rho^2 m} = \frac{c_x h_1^2 + c_z b_1^2}{\rho\sqrt{(k_x h^2 + k_z b^2)}m}
 \end{aligned}$$

Assume that the viscous damping becomes effective in reducing the maximum residual amplitudes,  $x_o$ ,  $z_o$ , and  $\theta_o$ , when  $\tau$  is zero, then from Equation (5.56)

$$\begin{aligned}
 x_\tau &= x_o e^{-\nu_x \omega_x \tau} \\
 z_\tau &= z_o e^{-\nu_z \omega_z \tau} \\
 \theta_\tau &= \theta_o e^{-\nu_\theta \omega_\theta \tau}
 \end{aligned}$$

Accordingly, if the attenuation requirements are such that in time,  $\tau$ , the ratios,  $x/x_o$ ,  $z/z_o$ , and  $\theta/\theta_o$ , must be  $1/n_x$ ,  $1/n_z$  and  $1/n_\theta$ , the required values of  $\nu_x$ ,  $\nu_z$  and  $\nu_\theta$  are given by:

$$\begin{aligned}
 \nu_x &= \frac{\log_e(n_x)}{\omega_x \tau} \\
 \nu_z &= \frac{\log_e(n_z)}{\omega_z \tau} \\
 \nu_\theta &= \frac{\log_e(n_\theta)}{\omega_\theta \tau}
 \end{aligned} \tag{5.59}$$

The following numerical example will demonstrate the use of the above equations in calculating subsidence times versus viscous damping coefficients.

Example 5.14.

Let:  $k_x = k_z = k$ ;  $b = \frac{3}{2} h$ ;  $b_1 = \frac{3}{2} h_1$ ;  $b = 2b_1$ ; and  $\rho^2 = \frac{b^2 + h^2}{12}$ , for the configuration shown in Figure 5.52.

If  $n_x = n_z = 10$ , at  $\tau_x = \tau_z = \tau_\theta = \tau$ , find  $c_x$ ,  $c_z$  and  $n_\theta$ .

The uncoupled frequencies are

$$\omega_x = \omega_z = 2 \sqrt{\frac{k}{m}} \text{ rad/sec}$$

$$\omega_\theta = 2 \sqrt{\frac{\frac{k}{m} \frac{4}{9} b^2 + b^2}{b^2 + \frac{4}{9} b^2}} 12 = 2 \sqrt{12 \frac{k}{m}} \text{ rad/sec}$$

From Equation (5.59)

$$v_x = v_z = \frac{\log_e(10)}{2 \sqrt{\frac{k}{m}} \tau} = \frac{2.3026}{2 \sqrt{\frac{k}{m}} \tau} = 1.15 \sqrt{\frac{m}{k\tau^2}}$$

From Equation (5.57)

$$c_x = c_z = 1.15 \sqrt{\frac{m}{k\tau^2}} \cdot \sqrt{km} = 1.15 \frac{m}{\tau} \text{ lbs/inch/sec}$$

which are the required damping coefficients to attenuate the peak translation response to 1/10 the peak amplitudes in time,  $\tau$ . Using these values of  $c_x$  and  $c_z$ , we can now calculate the attenuation factor for rotation amplitude,  $n_\theta$ , in the time period,  $\tau$ ,

$$\begin{aligned} v_\theta &= \frac{1.15 \frac{m}{\tau} (h_1^2 + b_1^2)}{\rho \sqrt{km(h^2 + b^2)}} = \frac{1.15 \frac{m}{\tau} (b_1^2 + h_1^2)}{\sqrt{\frac{km}{12}} (b^2 + h^2)} \\ &= 1.15 \sqrt{\frac{12m}{k\tau^2}} \cdot \left[ \frac{\frac{1}{4} b^2 + \frac{1}{4} \times \frac{4}{9} b^2}{b^2 + \frac{4}{9} b^2} \right] = \sqrt{\frac{m}{k\tau^2}} \end{aligned}$$

Example 5.14 (continued)

From Equation (5.59),

$$\begin{aligned}\log_e (n_\theta) &= \omega_\theta \tau_\theta \\ &= 2 \sqrt{12 \frac{k}{m}} \cdot \tau \cdot \sqrt{\frac{m}{k\tau^2}} = 6.92\end{aligned}$$

Accordingly,

$$n_\theta = 1020$$

It is seen that the rotational attenuation in this case is about 100 times that of the translational. If, however, the spring and dashpot location dimensions,  $b$ ,  $b_1$ ,  $h$ , and  $h_1$ , are reduced to one half of their former values while the mass dimensions,  $b$  and  $h$ , are kept as before, it is found that  $\omega_x$ ,  $\omega_z$ ,  $\nu_x$ ,  $\nu_z$ ,  $c_x$  and  $c_z$  are unchanged, and that

$$\begin{aligned}\omega_\theta &= 2 \sqrt{3 \frac{k}{m}} \\ \nu_\theta &= \frac{1.15 \frac{m}{\tau} \frac{1}{4} (b_1^2 + h_1^2)}{\rho \sqrt{km} \frac{1}{4} (h^2 + b^2)} = 0.5 \sqrt{\frac{m}{k\tau^2}}\end{aligned}$$

so that,

$$\log_e n = 3.46 ; \text{ giving } n_\theta = 32$$

In this case, the rotational attenuation therefore is only about three times that of the translational. Similarly, if the spring and dashpot location dimensions had been divided by 1/3, the rotational frequency,  $\omega_\theta$ , and  $\nu_\theta$  must be divided by three so that

$$\log_e (n_\theta) = 2.31 ; \text{ giving } n_\theta = 10$$

Consequently, for this case  $n_x = n_z = n_\theta = 10$ , or all three initial free vibration amplitudes will decrease to 1/10 of their initial values in the same time,  $\tau$ . If the mass weighs 32,000 lbs and the required time,  $\tau$ , is 3 seconds, the dashpot constants,  $c_x$  and  $c_z$ , must be such as to produce a viscous friction of

$$c_x = c_z = 1.15 \frac{m}{\tau} = 1.15 \frac{32,000}{386 \times 3} = 32 \text{ lbs/in/sec}$$

## 5.9 Hard Mounted Systems

Hard mounted systems are used when the functional equipments are ruggedized to survive the shock environment. These systems will have some inherent flexibility and ductility that can cause some attenuation of the high input accelerations.

Typical hard mounted systems are shown in Figure 5.53.

(a) A piece of equipment directly attached to the structure enclosure is shown in 5.53a. Very little flexibility exists in this type of mounting. The shock spectra envelope in the high frequency region defined by a line parallel to the constant acceleration line on the four-log graph paper is conservatively assumed to be the response acceleration of the equipment.

(b) Figure 5.53b shows an equipment module attached to a vertical structural member. This member provides significant flexibility in the horizontal mode, but very little in the vertical mode.

(c) A two-dimensional structural grid, shown in 5.53c, provides flexibility in both horizontal modes and vertical mode, and it may attenuate the combined vertical and horizontal acceleration response of the equipment.

(d) In Figure 5.53d, a multistory structure is housed within a structural enclosure, and is supported at the base. The multistory structure is a moment resisting frame with significant horizontal flexibility. Vertical flexibility is achieved by the floor beam spans.

Design procedures for each system are given in the following subsections.

5.9.1 Equipment mounted directly to the structure. After it is established that the equipment can survive a specified shock level defined by the shock spectra envelope, the attachments to the supporting structure must be designed. The step-by-step procedure is as follows:

Step 1: Assume the response acceleration of the equipment at its C.G. is equal to the resultant of the horizontal and vertical accelerations given by the constant acceleration region of the shock

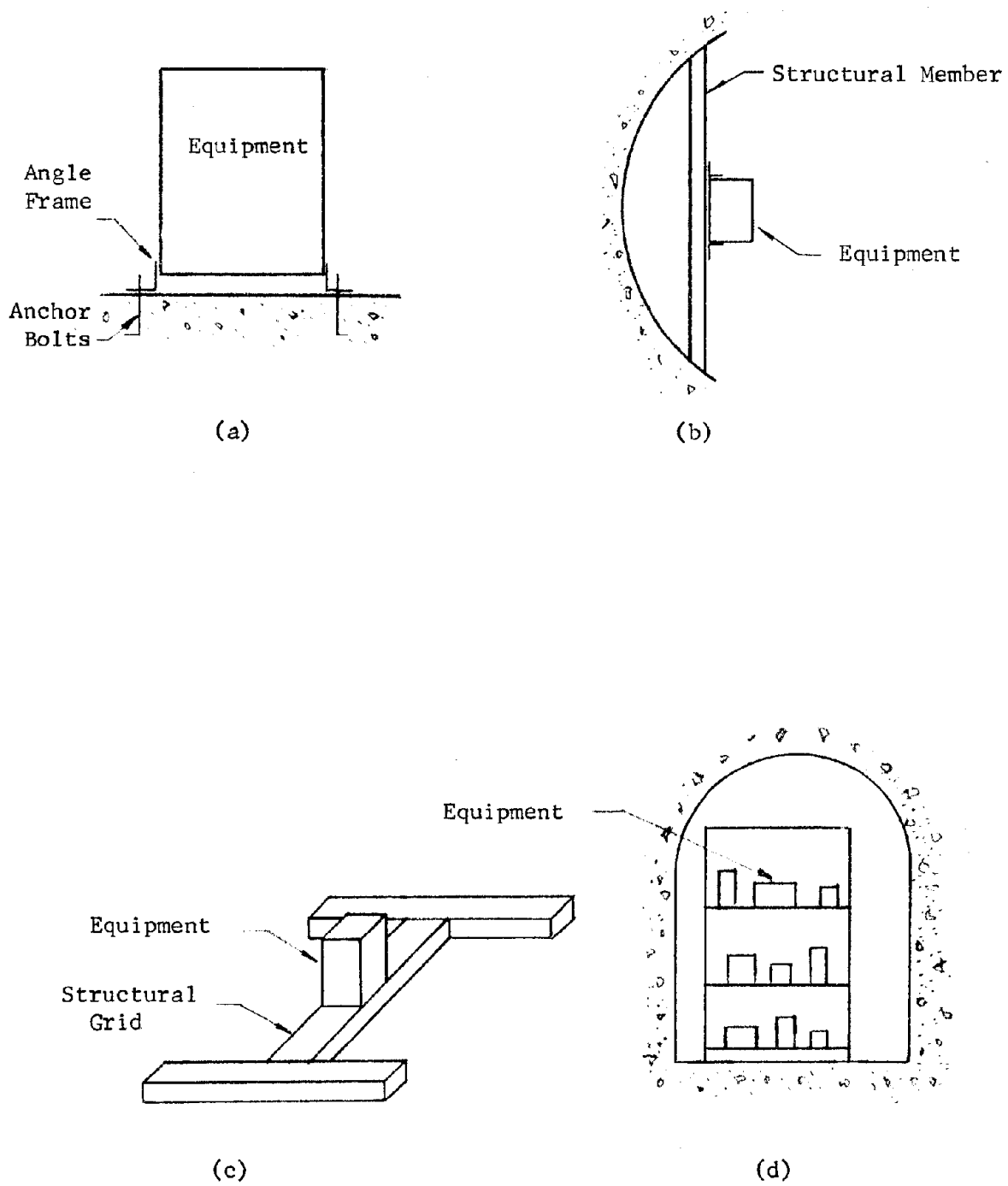
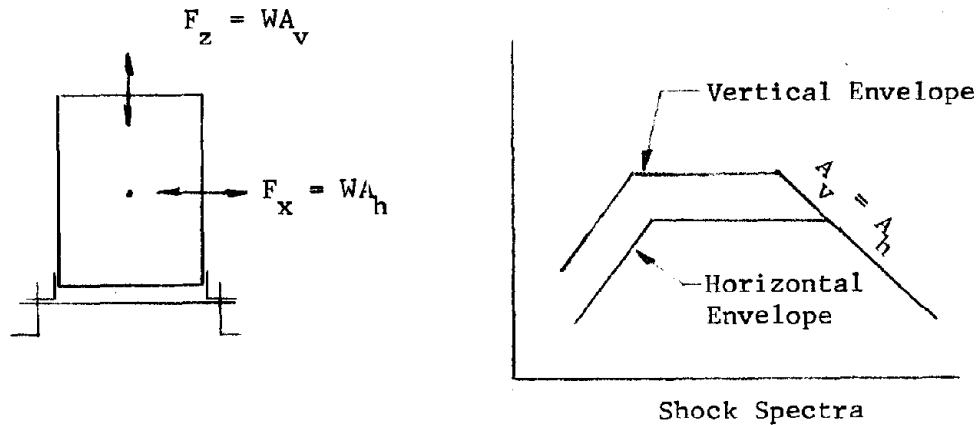


FIGURE 5.53

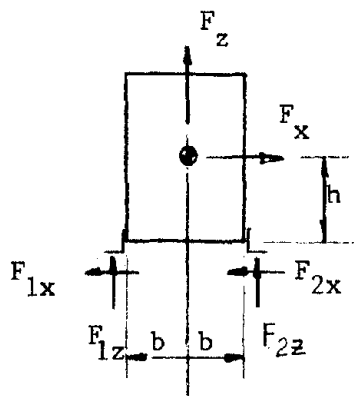


spectra envelope.



These accelerations applied to the equipment weight are the forces used for design of the supports.

**Step 2:** Consider the forces determined in Step 1 to be either in phase or out of phase, and determine the case which causes maximum reactions at the support points. For example, in the symmetrical system, the maximum reaction is:



$$(F_{1z})_{\text{tension}} = \frac{F_z}{2} + \frac{F_x h}{2b}$$

$$F_{1x} = \frac{F_x}{2}$$

**Step 3:** Design the anchors to remain elastic (up to yield) for the combined reactions (worst case) determined in Step 2. If yielding of the anchors or attachment pieces is acceptable, i.e., a ductility ratio of  $\mu > 1$  is allowed for the attachment elements, the design may

be modified accordingly, based on elastic-plastic shock spectra (see Section 2.4.3). The reactions are based on the modified forces:

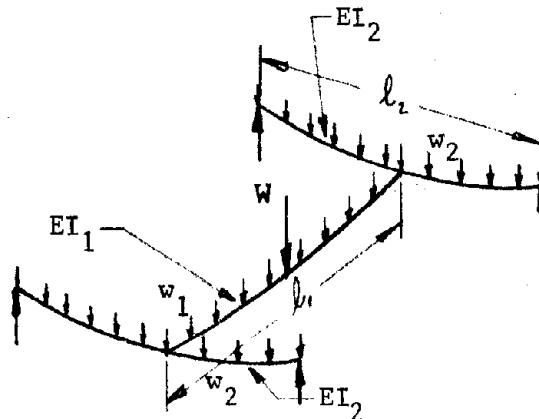
$$F_z = WA_V \left( \frac{\mu}{2\mu - 1} \right) ; F_x = WA_x \left( \frac{\mu}{2\mu - 1} \right)$$

5.9.2 Equipments mounted to structural framework. The mountings in Figure 5.53b and 5.53c represent conditions where either a single member or a group of resilient members support the equipment. Approximate lowest mode frequencies can be determined in each translation mode based on the resiliency of the structural members. From the frequencies calculated, the peak horizontal and vertical response may be determined from the specified shock spectra envelope. The procedure will be illustrated in the following steps for the system shown in Figure 5.53c.

Step 1: Compute lowest mode vertical frequency. A reasonable approximation is to compute the static deflection at equipment location, and assume that the lowest mode frequency is given by:

$$f_z = \frac{1}{2\pi} \sqrt{\frac{g}{\Delta z_{st}}}$$

where  $\Delta z_{st}$  = vertical static deflection at the equipment.



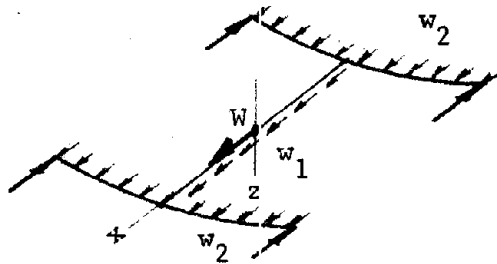
Consider the schematic shown above in order to calculate the static deflection. Assume simple beam connections

$$\Delta z_{st} = \frac{W l_1^3}{48 EI_1} + \frac{5 w_1 l_1^4}{384 EI_1} + \frac{(W + w_1 l_1) l_2^3}{96 EI_2} + \frac{5 w_2 l_2^4}{384 EI_2}$$

where  $W$  = equipment weight

$w_1, w_2$  = weight per unit foot of respective beams

**Step 2:** Compute lowest mode horizontal frequency. Use again the static deflection approximation.

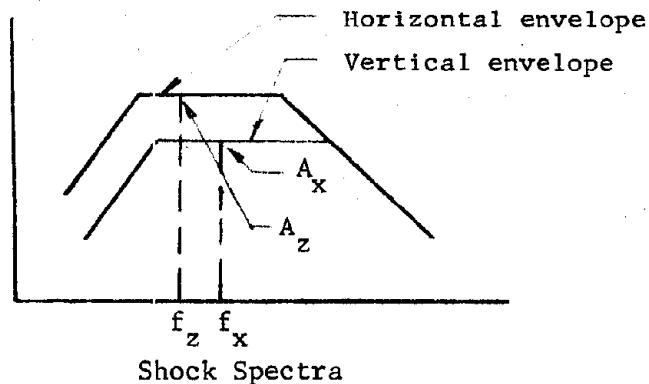


Consider the horizontal mode in the schematic shown above

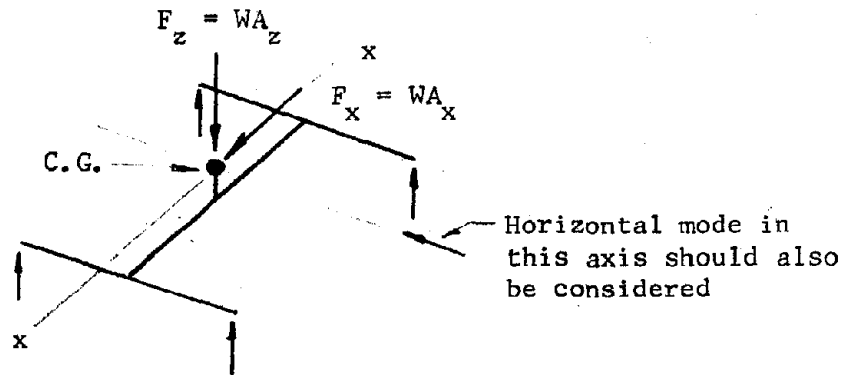
$$\Delta x_{st} = \frac{(W + w_1 l_1) l_2^3}{96 EI_2} + \frac{5 w_2 l_2^4}{384 EI_2}$$

The moment of inertia,  $I_2$ , is now about the vertical axis or the nominally weak axis for WF sections.

**Step 3:** Compute the peak response of the equipment from the shock spectra envelope for an SDOF system at the two frequencies calculated in Steps 1 and 2.



**Step 4:** Design equipment attachments and structural members for the simultaneous application of the peak accelerations at equipment C.G.



The other critical horizontal mode shown above should also be combined with the vertical response to determine the critical stresses in the members and the connections.

5.9.3 Multistory structures. A multistory structure within a hardened structure enclosure is used to support equipment and personnel as shown in Figure 5.53 d. The shock input at the base of the structure will excite both horizontal and vertical vibration modes. We will assume here a symmetrical multistory frame structure with moment resisting connections as shown in Figure 5.54.

The vertical shock motion will excite the beam elements at each floor level; their vertical frequencies and the resulting vertical acceleration response of the equipment may be approximately determined by the procedure given in the previous Subsection 5.9.2.

The horizontal response is a function of the flexibility of the moment resisting frames. Each frame may be isolated as a planar frame system exposed to the horizontal shock motion at the base. Let the mass be concentrated at each floor level thus reducing the planar frame to an n-degree-of-freedom system for horizontal response, where n equals the number of levels above the first level at the foundation. The normal mode technique can then be used to calculate the peak horizontal response at each level by either bounding the response using the given shock spectra envelope for SDOF systems, or performing a dynamic analysis for arbitrary acceleration pulses at the supports. The normal mode technique will be illustrated in the following step-by-step procedure. (The notation is defined in Appendix A.)

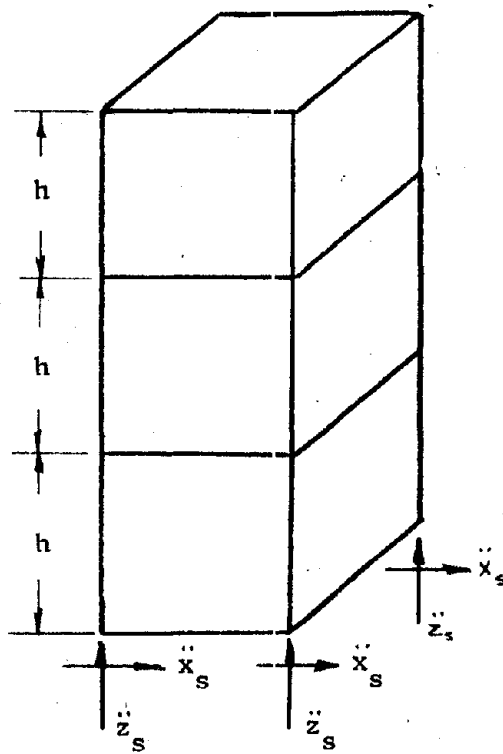
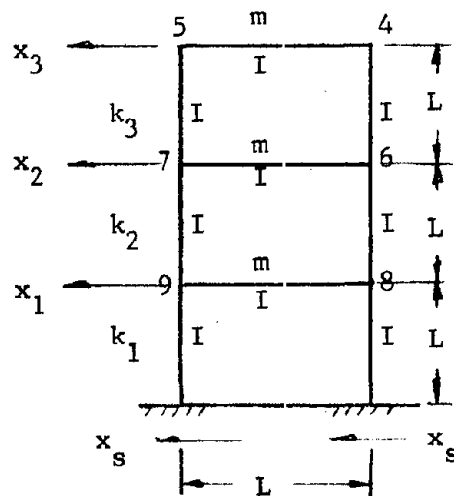


FIGURE 5.54

**Step 1:** Perform preliminary design to estimate mass and stiffness characteristics of main frames. Assume the following 3 level structure with the mass and stiffness ratios noted. (The lowest floor level is assumed to be rigid and to move with the free-field unaffected by any flexibility.)



$$y_1 = x_1 - x_s$$

$$y_2 = x_2 - x_s$$

$$y_3 = x_3 - x_s$$

The equations of motions for a horizontal input at the base are:

$$\begin{bmatrix} m & 0 & 0 \\ 0 & m & 0 \\ 0 & 0 & m \end{bmatrix} \begin{Bmatrix} \ddot{y}_1 \\ \ddot{y}_2 \\ \ddot{y}_3 \end{Bmatrix} + \begin{bmatrix} (k_1 + k_2) & -k_2 & 0 \\ -k_2 & (k_2 + k_3) & -k_3 \\ 0 & -k_3 & k_3 \end{bmatrix} \begin{Bmatrix} y_1 \\ y_2 \\ y_3 \end{Bmatrix} = -m \begin{Bmatrix} \ddot{x}_s \\ \ddot{x}_s \\ \ddot{x}_s \end{Bmatrix} \quad (5.60)$$

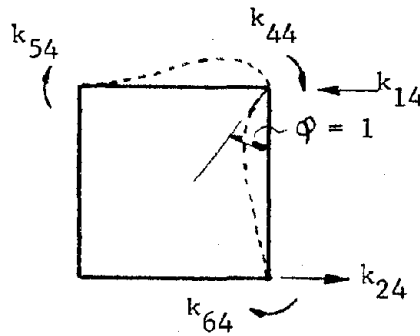
where the stiffness parameters, defined in the notation of Example 4.4 are:

$$k_1 + k_2 = k_{11} = 48 EI/L^3 \quad k_2 = k_{12} = k_{21} = 24 EI/L^3$$

$$k_2 + k_3 = k_{22} = 48 EI/L^3 \quad k_3 = k_{23} = k_{32} = 24 EI/L^3$$

and are based on the assumption that the girders are infinitely stiff. The method of finding the stiffness matrix when accounting for the flexibility of the girders is given in Step 1a.

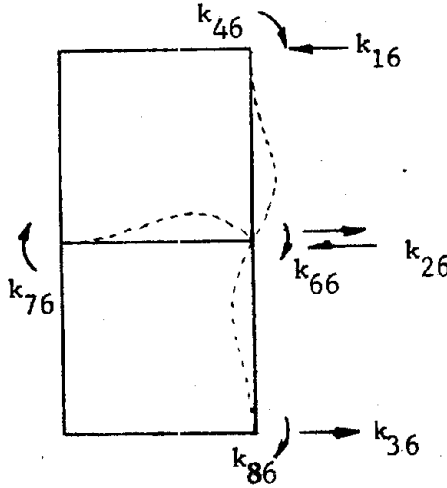
Step 1a: Compute stiffness matrix. First the stiffness matrix is expanded to include the joint stiffness by applying a unit rotation at each joint. The derivation is shown below.



$$k_{44} = \frac{8EI}{L} \quad k_{54} = \frac{2EI}{L} \quad k_{64} = \frac{2EI}{L} \quad k_{24} = \frac{6EI}{L^2} \quad k_{14} = -\frac{6EI}{L^2}$$

Similarly,

$$k_{55} = \frac{8EI}{L} \quad k_{45} = \frac{2EI}{L} \quad k_{75} = \frac{2EI}{L} \quad k_{25} = \frac{6EI}{L^2} \quad k_{15} = -\frac{6EI}{L^2}$$



$$k_{66} = \frac{12EI}{L} \quad k_{46} = k_{76} = k_{86} = \frac{2EI}{L} \quad k_{16} = \frac{-6EI}{L^2} \quad k_{26} = 0 \quad k_{36} = \frac{6EI}{L^2}$$

Similarly,

$$k_{77} = k_{88} = k_{99} = \frac{12EI}{L} \quad k_{68} = k_{98} = \frac{2EI}{L} = k_{57} = k_{67} = k_{97} = k_{79} = k_{89}$$

$$k_{17} = k_{29} = -\frac{6EI}{L^2} \quad k_{37} = \frac{6EI}{L^2} \quad k_{39} = 0$$

The expanded matrix is now a 9 x 9 matrix.

$$[k] = \frac{2EI}{L} \begin{bmatrix} 12/L^2 & -12/L^2 & 0 & -3/L & -3/L & -3/L & -3/L & 0 & 0 \\ -12/L & 24/L^2 & -12/L^2 & 3/L & 3/L & 0 & 0 & -3/L & -3/L \\ 0 & -12/L^2 & 24/L^2 & 0 & 0 & 3/L & 3/L & 0 & 0 \\ \hline -3/L & 3/L & 0 & 4 & 1 & 1 & 0 & 0 & 0 \\ -3/L & 3/L & 0 & 1 & 4 & 0 & 1 & 0 & 0 \\ -3/L & 0 & 3/L & 1 & 0 & 6 & 1 & 1 & 0 \\ -3/L & 0 & 3/L & 0 & 1 & 1 & 6 & 0 & 1 \\ 0 & -3/L & 0 & 0 & 0 & 1 & 0 & 6 & 1 \\ 0 & -3/L & 0 & 0 & 0 & 0 & 1 & 1 & 6 \end{bmatrix}$$

Partition the above matrix as noted, and write the static equilibrium relation:

$$\begin{bmatrix} [k]_{11} & | & [k]_{12} \\ \hline [k]_{21} & | & [k]_{22} \end{bmatrix} \begin{Bmatrix} \{y\} \\ \hline \{\phi\} \end{Bmatrix} = \begin{Bmatrix} \{F\} \\ \hline \{M\} \end{Bmatrix} \quad (5.61)$$

Since there are no rotation inputs, set  $\{M\} = 0$ . Performing the matrix multiplication in the above equation gives

$$\left( [k]_{11} - [k]_{12} [k]_{22}^{-1} [k]_{21} \right) \{y\} = \{F\}$$

The resultant stiffness term in parenthesis is now a 3 x 3 matrix (given the notation  $[\bar{k}]$ ) which includes the flexibility effects of the girders. (See Reference 4.14 for a complete treatment of this procedure.)

In this example, the stiffness matrix is:

$$[\bar{k}] = \frac{EI}{L^3} \begin{bmatrix} 45.72 & -23.68 & 1.27 \\ -23.68 & 45.72 & -17.01 \\ 1.27 & -17.01 & 16.55 \end{bmatrix}$$

whereas, if the girders are assumed to be rigid, the stiffness matrix is, as previously calculated,

$$[k] = \frac{EI}{L^3} \begin{bmatrix} 48 & -24 & 0 \\ -24 & 48 & -24 \\ 0 & -24 & 24 \end{bmatrix}$$

Step 2: Compute the frequencies and mode shapes

$$\omega_1 = 2.44 \sqrt{\frac{EI}{m L^3}} ; \quad \omega_2 = 5.4 \sqrt{\frac{EI}{m L^3}} ; \quad \omega_3 = 8.33 \sqrt{\frac{EI}{m L^3}}$$

$$\beta = \begin{bmatrix} .338 & -1.31 & 2.92 \\ 0.626 & -.893 & -3.16 \\ 1.0 & 1.0 & 1.0 \end{bmatrix}$$



Step 3: Compute the mode participation factors. The generalized mass is:

$$[M] = [\beta]^T [m] [\beta] = \begin{bmatrix} 1.51 & 0 & 0 \\ 0 & 3.52 & 0 \\ 0 & 0 & 19.52 \end{bmatrix}$$

The generalized forcing function is:

$$[N] = [\beta]^T [m] = m \begin{Bmatrix} 1.96 \\ -1.2 \\ .76 \end{Bmatrix}$$

The participation factors,  $\Gamma$ , are

$$\Gamma_1 = \frac{N_1}{M_1} = \frac{1.96}{1.51} = 1.3$$

$$\Gamma_2 = \frac{N_2}{M_2} = \frac{-1.2}{3.52} = -.341$$

$$\Gamma_3 = \frac{N_3}{M_3} = \frac{.76}{19.52} = .039$$

Step 4: The upper bound absolute acceleration response of each mass is calculated.

$$\begin{aligned} (\ddot{x}_1)_{\max} &= |\beta_{11} \Gamma_1 A_1| + |\beta_{21} \Gamma_2 A_2| + |\beta_{31} \Gamma_3 A_3| \quad (5.62) \\ &= |.338 \times 1.3 \times A_1| + |-1.31 \times (-.341) \times A_2| + |2.92 \times .039 \times A_3| \\ &= .44 A_1 + .45 A_2 + .114 A_3 \end{aligned}$$

$$(\ddot{x}_2)_{\max} = .81 A_1 + .305 A_2 + .123 A_3$$

$$(\ddot{x}_3)_{\max} = 1.3 A_1 + .341 A_2 + .039 A_3$$

The above values define the peak horizontal accelerations to be applied at the C.G. of equipment at the respective levels. Design of attachments and framing members should consider these accelerations in combination with the peak vertical acceleration motions which were discussed in Subsection 5.9.2.

### Example 5.15:

Numerical values are assumed for the three level structure considered in this subsection as follows:

$$\begin{aligned} \text{Let } L &= 225 \text{ inches} & E &= 30 \times 10^6 \text{ psi} & I &= 430 \text{ in}^4 \\ m &= 20,000 \text{ lb/386} & &= 52.0 \text{ lb-sec}^2/\text{in} \end{aligned}$$

Assume that the horizontal shock spectra envelope of Figure 5.26 defines the response requirements of an SDOF system.

From Step 2 the frequencies are:

$$\sqrt{\frac{EI}{m L^3}} = \sqrt{\frac{(30 \times 10^6)(430)}{52 (225)^3}} = 4.66$$

$$\omega_1 = 2.44 \times 4.66 = 11.4 \quad \omega_2 = 25.2 \quad \omega_3 = 39$$

$$f_1 = 1.8 \text{ cps} \quad f_2 = 4 \text{ cps} \quad f_3 = 6.2 \text{ cps}$$

Compute the peak acceleration from Step 4. From Figure 5.26 the acceleration amplitudes,  $A_1$ ,  $A_2$ , and  $A_3$ , are:

$$A_1 = 0.7 \text{ g} \quad A_2 = 2.1 \text{ g} \quad A_3 = 3.3 \text{ g}$$

$$(\ddot{x}_1)_{\max} = .44 (.7) + .45 (2.1) + .114 (3.3) = 1.63 \text{ g}$$

$$(\ddot{x}_2)_{\max} = .81 (.7) + .305 (2.1) + .123 (3.3) = 1.61 \text{ g}$$

$$(\ddot{x}_3)_{\max} = 1.3 (.7) + .341 (2.1) + .039 (3.3) = 1.75 \text{ g}$$

### 5.10 Arrangement of Springs

In Sections 5.2 through 5.7, the design aspects of typical shock isolation systems were discussed, and design examples were given for typical ground shock conditions. These systems represent spring arrangements that are commonly used in shock mounting.

Table 5.3 a, b, c, summarizes the comparison of the isolation systems considered, showing the relative merit of each system for the factors listed. A foam type isolator is also included for comparison. The feasibility ranges

TABLE 5.3a

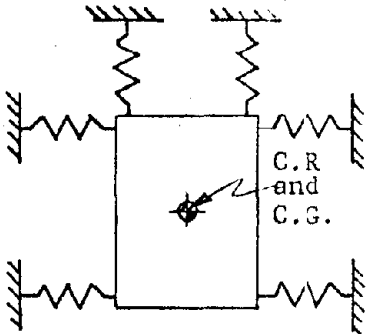
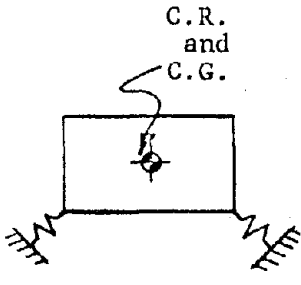
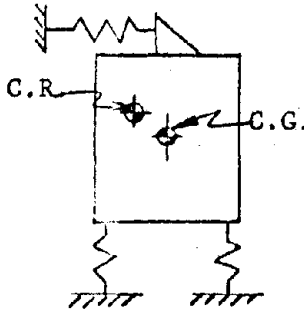
	 <p>Symmetrical: Horizontal and Vertical Springs - Pinned Ends</p>	 <p>Symmetrical: Inclined Isolators</p>	 <p>Near Symmetrical</p>
Feasibility Range	For equipment isolation at low frequency and large relative displacements	For equipment, isolation at mid-range frequency and small relative displacements	For equipment isolation at low and mid-range frequency and low and moderate relative displacements
Dynamic Coupling	Negligible	Negligible	Small pitch response induced
Rattlespace Requirements	Shock spectra values (large horizontal space required for hardware)	Shock spectra values	Shock spectra values are amplified due to pitch response
Dynamic Stability	Not critical	Not critical	Not critical
Static Stability	Not critical	Not critical (but spring stability must be considered)	Not critical, (but spring stability must be considered)
Non-linear Effect	Very significant for acceleration response and rattlespace	Not critical	Not critical

TABLE 5.3b

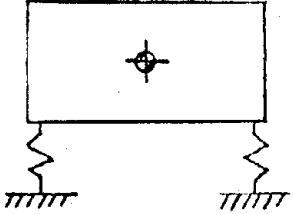
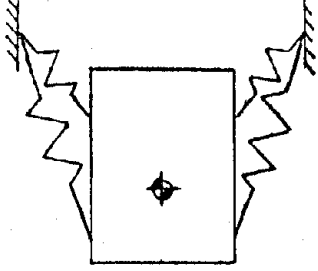
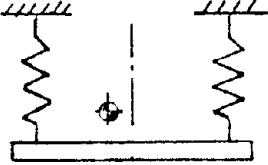
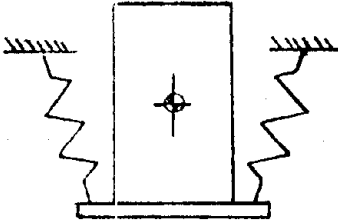
	 Base Mounted System	 Inclined Pendulum	 Pendulum - Low C.G.
Feasibility Range	For equipment and total structure isolation at low and mid-range frequency and small to moderate relative displacements	For total structure isolation at low frequency and large relative displacements	For equipment and personnel platforms at low frequency and large relative displacements
Dynamic Coupling	Very significant for acceleration and displacement response	System characteristics can be selected to minimize coupling	Significant pitch response induced
Rattlespace Requirements	Shock spectra values are amplified due to pitch response (minimum space required for hardware)	Shock spectra values are acceptable when the geometry optimized for minimum coupling	Shock spectra are amplified due to pitch response
Dynamic Stability	Not critical	Not critical when optimized	May be critical
Static Stability	May be critical (spring stability must be considered)	Not critical when optimized	May be critical
Non-linear Effect	Not critical	Some effect on acceleration response	May affect acceleration response and rattlespace

TABLE 5.3c

	 <p>Pendulum - High C.G.</p>
<p><b>Feasibility Range</b></p> <p><b>Dynamic Coupling</b></p> <p><b>Rattlespace Requirements</b></p> <p><b>Dynamic Stability</b></p> <p><b>Static Stability</b></p> <p><b>Non-Linear Effect</b></p>	<p>For missile mounts at low frequency and moderate relative displacements</p> <p>Very significant</p> <p>Shock spectra values are amplified due to pitch response</p> <p>Very critical</p> <p>Very critical</p> <p>Significant effect on acceleration response and rattlespace</p>

(frequency and relative displacement) are further defined as follows:

Frequency ranges

- (1) low frequency: less than 1 cps
- (2) mid-range frequency: 1 to 10 cps

Displacement ranges

- (1) large relative displacement: up to 40 inches vertically and 14 inches horizontally (combined)
- (2) moderate relative displacement: up to 15 inches vertically and 5 inches horizontally (combined)
- (3) small relative displacement: up to 6 inches vertically and 2 inches horizontally (combined)

Non-linear effect refers to the significance of the error in assuming linear behavior when the actual behavior is non-linear.

5.11 Component Isolation Versus Platform Isolation

During the design concept phase of a hardened system, the shock isolation system designer must tentatively decide on the method of supporting the survival essential equipment. Two alternative layouts are: (1) group all the essential equipment together, and support them with a platform or multilevel structure; provide isolators to attenuate the response of the platform to a level determined by the equipment fragility; (2) support each piece of equipment separately, and provide isolation for each piece of equipment to the degree required. The following two subsections provide a few considerations for choosing between the two alternatives.

5.11.1 Component isolation. Component isolation offers the advantage of using simple (and sometimes commercially available) isolator elements. Each piece of equipment is shock isolated only to the level required. Also, some pieces of equipment may need no special isolators if proper framing and ductility is provided to the supporting brackets.

Component isolation will be feasible when only a few pieces of equipment in a group require special shock isolation. Instead of providing isolation for the group in general, each piece of equipment is isolated as

required, and no isolation is provided when hard mounting is acceptable for ruggedized equipment.

5.11.2 Platform isolation. When the shock input level exceeds the resistance capability of all the equipments (and/or personnel survival requirements), a platform isolation system will be feasible. The equipment is rigidly attached to a platform or structure, and either the platform or special isolators provide the necessary flexibility for isolation. Very fragile electronic equipment will almost always be grouped together, and supported on a platform at very low frequency. Therefore, when shock isolation is required for all the equipment and personnel protection, platform isolation is most feasible.

## SECTION 6: SPRINGS

### 6.1 Introduction

6.1.1 Scope of the discussion: The purpose of this section is to provide the engineer with a ready source of information for preliminary designs with respect to the types and size ranges of springs most likely to be of use in the shock isolation of instructure systems housed by primary hardened structural enclosures. In general the small, light weight springs and shock mounts used for the protective mounting of small to medium weights and sizes of equipment are available as standard commercial items in great variety. The choice of shock mounts for such equipment is usually a matter of selection rather than design. Consequently very limited space is allocated here to design methods applicable specifically to these smaller units. It should also be noted that many relatively heavy duty springs and shock mounts are standard items stocked for specific commercial and industrial applications such as, for example, standard railroad car truck and coupling springs. Wherever the design data indicates that such standard springs or mounts may be applicable to a specific installation both procurement time and costs will usually be reduced by their use.

For the analytical basis of the design data presented and for discussions of the many specialized variations of springs in common use but not presented here, the reader is referred to the extensive literature in this field; several of these references are listed at the end of this section.

6.1.2 Considerations in the selection of spring types for specific applications. The major considerations in the selection of the type of spring or shock mount to be used in any specific installation are usually: a) suitability for the intended application, b) cost, and, c) procurement time; although not necessarily in that order. With regard to both cost and procurement time such factors as the space and accessory requirements of the complete installation are considerations which often outweigh the direct cost of the spring. Consequently all generalization must be applied with



reservations. With this limitation in mind, however, it can be said that the order of preference, as influenced by cost and procurement, is mechanical springs, pneumatic springs, liquid (or hydraulic) springs, and finally, combinations of these with external or integral control and damping systems. Table 6.1 provides some very general comparisons of the characteristics which influence choice of spring type.

As treated in this discussion the classification, "Mechanical Springs" includes Helical Coil Springs, Torsion Bars, Bellville Washer Assemblies, and Rubber Springs (or "shock mounts"). In general this group is characterized by a very wide range of application, relatively low cost, simple installation, and good service life. Of these the helical coil springs, including helical compression and extension springs in that order, are by far the most widely used and in terms of direct spring cost, are usually the most economical type of spring available for most applications.

## 6.2 Mechanical Springs

### 6.2.1 Helical coil springs

6.2.1.1 Compression versus extension springs: For purposes of design and function there is little basic difference between helical coil extension and helical coil compression springs. Extension loading may offer appreciable advantage in convenience of suspension and end attachment, and axial extension loading has no tendency to cause the lateral buckling which can occur in helical springs under compression. However, simple extension spring end attachments are usually possible only at the expense of substantial stress concentrations at the attachment points. Stability against buckling is largely offset by a lack of an inherent limit to axial deformation and "fail safe" characteristics. In other words, if the spring itself is the only link between end anchorages, an overload can permanently stretch the spring. Also, if the spring fails, a major collapse of the supported assembly can occur. A properly designed helical compression spring and mounting assembly, on the other hand, although it is designed not to "bottom" under maximum design loading, can bottom under overload without

TABLE 6.1: COMPARISON OF SPRING TYPES

Spring Type	Linear Range	Limitations	Practical Usage	Stiffness Control	Damping	Cost
Coil Springs	Almost full	Large space	Almost universal	None	Separate System	Low to Moderate
Torsion Bar Springs	Almost full	Space for moment arm	Reduction of Rattlespace	None	Separate system	Moderate
Belleville Springs	Very limited to almost full	Small displacements	Limited space	None	Inherent, non-linear	Low to moderate
Rubber Springs	Limited to Very limited	Temperature solvents "aging"	Almost universal	None	Inherent non-linear	Low to moderate
Pneumatic Springs	Limited for direct load	Leakage and static position	Non-linear leveling	Readily made	Readily augmented	Moderate to high
Liquid Springs	Small load changes	Leakage and static position	Large displacement	Readily made	Readily augmented	Generally high

damage to the spring. In case of permanent set or failure of a helical compression spring under long time and repeated loading the maximum displacement of the top of the spring and of the supported assembly is usually limited (by the mounting design) to approximately the solid height of the spring. Additionally, in a correctly designed compression spring and mounting, the operating range and proportions of the spring are such that either buckling will not occur, or the spring is guided to prevent buckling. The cost of extension spring end connections and mounting details to provide performance and safety factors comparable to those of well designed compression spring installations will usually cancel out their limited advantages. For these reasons most heavy duty helical spring installations use compression springs, and the discussion of helical coil springs that follows is largely confined to compression springs. Further, round bar and wire spring stock, only, will be considered as the disadvantages of square and rectangular stock exceed its advantages in most applications.

6.2.1.2 Spring loading and installation configurations: In shock isolation the typical case involves both axial and lateral relative displacements of the ends of the isolation assemblies. Depending on the isolation system design and the configuration of the spring installation, the springs may be required;

- (a) To resist static loads applied axially and dynamic loads and deflections both coincident with, and normal to, the spring axis,
- (b) To resist combined static and dynamic axial loading accompanied by changes in axial orientation.

In nearly all cases the permissible displacements of the supported assembly with respect to the surrounding enclosure, and hence of one end of any specific isolator assembly with respect to the other end, will be limited by the available "rattlespace". For purposes of spring and mounting design for condition (a), above, it is desirable to fix the ends of the spring at the mounting surfaces as in Figure 6.1, as this sharply increases resistance to buckling. In general this type of installation is used in compression to support relatively large static loads but the primary

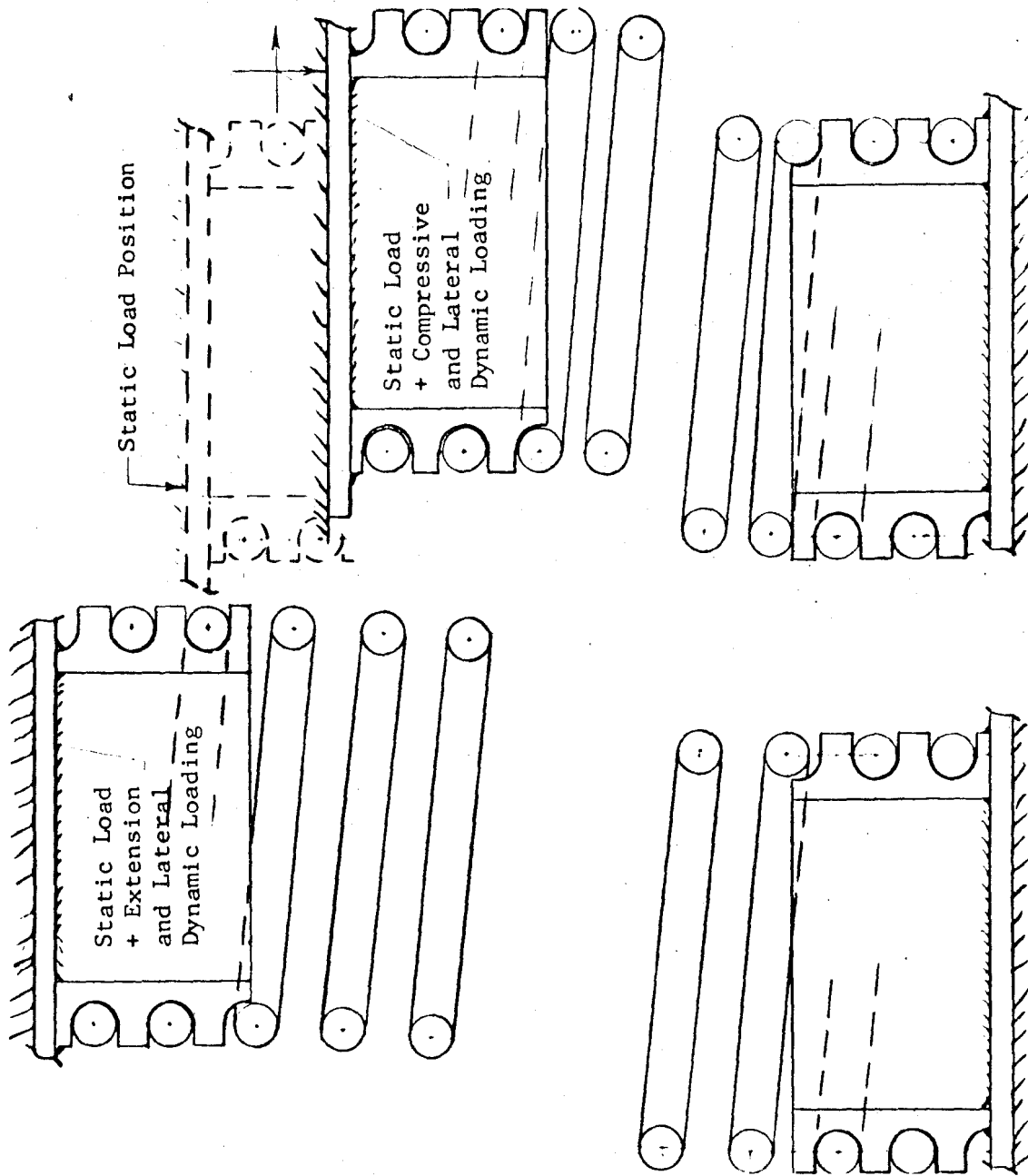


FIGURE 6.1: FIXED ENDED SPRING SUBJECT TO STATIC AND DYNAMIC LOADING

function is shock isolation. The end anchorage permits such isolators to be used in tension as well, for the reasons discussed in 6.2.1.1 above, however, it is preferable that these isolators not be used in tension to support static loads.

Where co-occurrence of the center of mass and the center of rigidity of the supported assembly is important (Reference Section 5.2) it is often desirable to reduce to a minimum the stiffness of shock isolation assemblies normal to their principal axes. We then have the condition of (b), above. Pivot mounting of spring assembly ends as shown in Figure 6.2 will accomplish this purpose. The spring may be guided internally or externally by a telescoping mounting which can be terminated in ball or universal joints to permit angular displacement of the assembly in any direction. This type of isolation assembly is readily adaptable to either extension or compression loading, or both, while using the springs in compression in all cases.

Figure 6.2 illustrates a universal-joint mounted, double acting shock isolation assembly incorporating two, counter wound, nested, helical compression springs. It can be used in any position to resist both extension and compression loading. The housing can be simplified and reduced in length where compression only, or extension only, is required. Nesting of two or more compression springs permits greater energy storage per unit volume of the isolator and is another advantage of compression loading versus extension loading. Counter winding helps prevent "interleaving" of the coils of nested springs, although the housing configuration shown provides guiding for each of the two nested springs. In addition, the basic configuration shown, by control of air venting between ends of the spring housing or from the inside of the housing to outside, can be modified to include air damping or an air spring acting in conjunction with the mechanical spring system.

#### 6.2.1.3 Axially loaded helical compression springs for shock isolation - design considerations.

- a. Design criteria: High combined normal operating and shock loadings together with relatively large deflection requirements

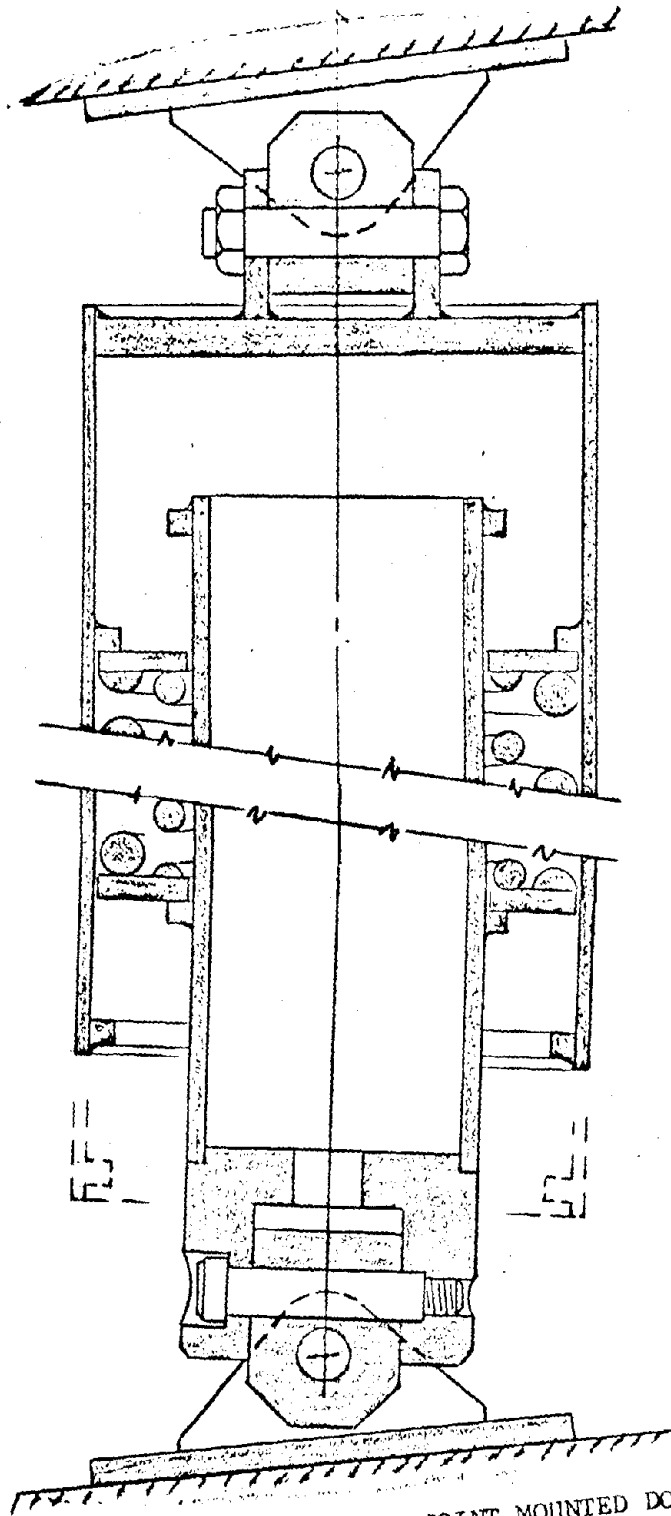


FIGURE 6.2: UNIVERSAL JOINT MOUNTED DOUBLE ACTING  
(TENSION-COMPRESSION) SHOCK ISOLATOR

and limited available space are frequent design parameters for isolators using helical compression springs. Consequently, use of high design stresses is often desirable. The design criteria commonly permit consideration of very high stresses for a limited number of shock loading cycles.

(b) Relaxation and fatigue: Under shock conditions, spring fatigue is unlikely to be a problem, and special surface finishes, shot peening and similar measures to improve fatigue resistance are usually unnecessary.

(c) End finish, the Wahl effect and presetting: Among the design features and fabrication practices for standard heavy industrial springs, that remain important for shock isolation springs, are the use of squared and ground ends to minimize secondary bending stresses, and presetting to offset the Wahl effect. The Wahl effect is essentially a departure of the torsional shear stress from a straight line function. It is caused primarily by the secondary stresses introduced by the bar curvature. The Wahl factor,  $W$ , expresses this effect in terms of the ratio of the maximum torsional shear stress at the inside of the coil,  $\tau_i$ , to the average stress,  $\tau$ , computed by straight line theory, as:

$$W = \frac{\tau_i}{\tau} = \frac{4 \frac{D}{d} - 1}{4 \frac{D}{d} - 4} + \frac{.615}{\frac{D}{d}} \quad (6.1)$$

where  $D$  is the mean coil diameter and  $d$  is the bar diameter. This factor varies from about 1.2 to 1.6 for the more commonly used values of  $D/d$ . The function is plotted in Figure 6.3a. If  $W$  is neglected in design the result is excessive relaxation (i.e. creep) under high static load and a tendency toward brittle fracture under shock loading. Pre-setting to maximum stresses beyond the elastic limit increases the elastic limit (Figure 6.3b) and also introduces permanent pre-stress in the outer fibers of the spring which are opposite and roughly proportional to the maximum stresses under load before pre-setting. Consequently the maximum stresses under applied load after presetting follow more closely those predicted by straight line theory.

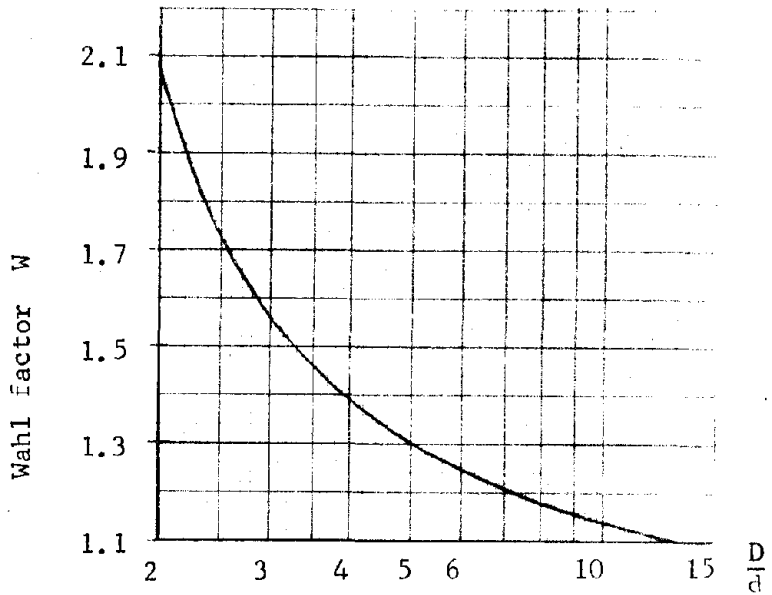


FIGURE 6.3a: EFFECT OF CURVATURE OF COIL

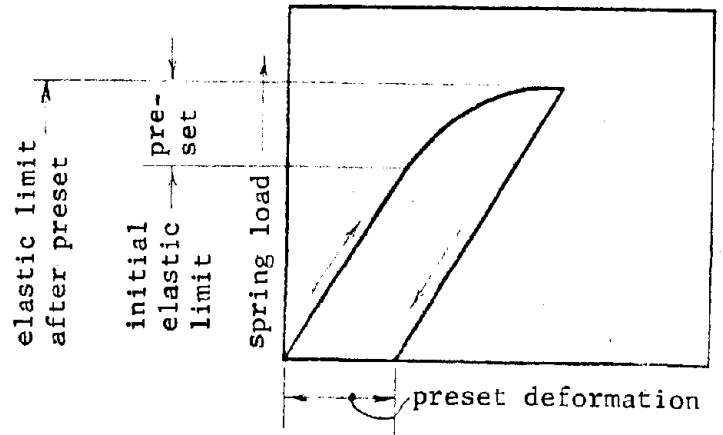


FIGURE 6.3b: EFFECT OF PRESET ON HELICAL COMPRESSION SPRINGS

In pre-set springs at the normal operating stress, load reductions to allow for the Wahl effect can be less severe and are often neglected for values of  $W$  less than 1.3. Presetting is also a useful inspection measure, since failures due to flaws in the metal or unsatisfactory heat treating are likely to occur during presetting rather than in service. One of the very considerable advantages of compression over extension springs lies in the fact that it is not feasible to



preset extension springs. Consequently, extension springs are more susceptible than compression springs to relaxation under normal operating static loads and failure under shock load.

(d) Critical buckling ratio: A compression spring is essentially a composite column and as such may become unstable with respect to lateral buckling. This characteristic is commonly expressed in terms of the critical ratio of axial deflection to effective free height,  $(\Delta_r/H_e)_{cr}$ , at which springs having specific ratios of free height to mean diameter  $H_e/D$ , become unstable in buckling. The relation is illustrated graphically in Figure 6.4, but the values for case (a) (both ends of the spring fixed against both rotation and translation)

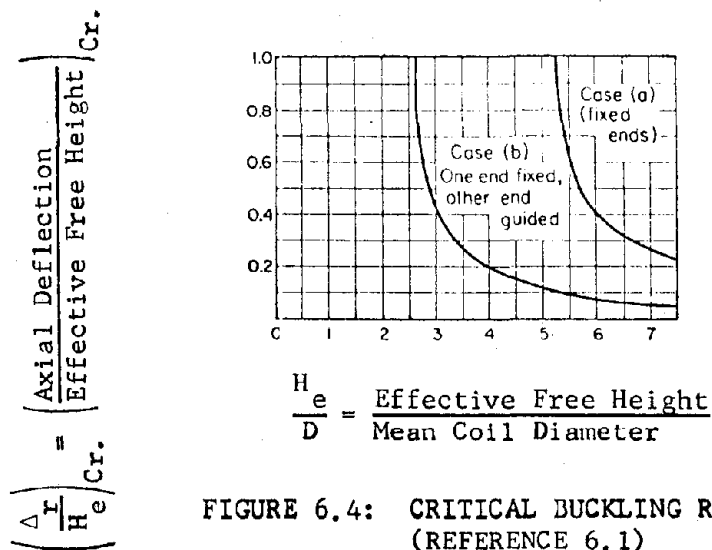


FIGURE 6.4: CRITICAL BUCKLING RATIO (REFERENCE 6.1)

should be applied with caution since the end fixity implied is not always obtained in practice. Heavy compression springs for shock isolation are usually designed on the basis of the maximum allowable stress when compressed to solid height. To maintain the validity of this design basis the critical buckling ratio of total axial deflection to effective free height must not be less than the ratio of

total solid height axial deflection to effective free height<sup>(1)</sup> (i.e.  $\Delta_r/H_e \rightarrow \Delta_{rs}/H_e$ ), or the spring must be guided to prevent buckling. Since avoidance of the critical buckling range by changes in spring dimensions often leads to undesirably large spring diameters D; confining springs against buckling by guiding is often a convenient solution in the type of application under consideration. Mounting end details which maintain spring ends parallel to each other and perpendicular to the spring axis (see Figure 6.2) also minimize secondary stresses due to incipient buckling in guided springs.

(e) Materials: For heavy springs both cost and availability of materials are important considerations. For moderate sizes of springs and where spring size, bar size and available space are not important problems SAE-1095 steel is almost universally used and will usually be found both economical and readily available in stock sizes up to about three inches in diameter. Among the low alloy spring steels SAE 5160H, SAE 8655H, SAE 8660H, SAE 4160M and SAE 9260H are widely used and readily available. The costs (per pound) for springs of these alloys is on the order of 20 percent to 60 percent higher than that for 1095, but higher allowable working stresses can result in smaller springs or smaller numbers of springs at less total weight for corresponding loads and deflections. Savings in the costs of spring housings and in space requirements may also be significant, so that the higher material costs may be largely or entirely offset by other considerations. Both 6150H and 4160M are often economical in springs requiring the larger bar sizes (say upwards of two inches in diameter). SAE 9260H is used chiefly in applications where its superior mechanical properties at low temperature are desired.

f. Costs: The basic prices of large, heavy duty springs of any of the more commonly used spring steels are, within limits, almost direct functions of weight. However the differences in per pound costs between "stock" and "special" springs are significant. Many sizes of

---

<sup>(1)</sup> Not including the closed end turns, usually 1.5 to 2.

heavy springs, up to 40,000 pounds in solid capacity, 2 1/4" bar diameter, 14" outside diameter, and 50" or more in free height and having spring constants from 100 to 16,000 pounds per inch are available as stock designs or stock items. Prices on such stock springs, F.O.B. factory, will usually fall in the range of 18 cents to 30 cents per pound even in small lots. Non-stock sizes in the same materials will usually range from 35 cents to 60 cents per pound or more and the costs will also be heavily influenced by the quantities ordered. Unusually long springs will require special set ups with the resultant higher than normal manufacturing costs. The larger bar diameters (in excess of about 1 1/2") tend to increase costs due both to higher manufacturing costs and to lower allowable design stresses necessitated by the fact that the larger bar sizes are difficult to heat treat to the maximum mechanical properties that can be obtained in smaller sizes.

Maximum spring diameters and bar diameters can often be reduced, with resulting reduction in costs and space requirements as well, by nesting two or more springs in a single assembly. A combination of a stock spring for the outside, and heavier springs, with a smaller, special, spring, counter wound, and nested inside, will often be still more advantageous. Since long compression springs must usually be guided to prevent buckling, it is sometimes economical to use two or more standard springs in series separated by steel disc spacers in place of a single special spring of greater length. Finally, it should be recognized that, as in any other manufactured product, unnecessarily close tolerances will increase costs.

g. Mechanical properties of spring steels: If it is assumed that the temperature and corrosion environment are not severe the principal mechanical properties of interest in spring steels as applied to helical compression spring design are: the torsional modulus of elasticity, or modulus of rigidity  $G$ , the ultimate strength in torsional shear  $\tau_u$ , the elastic limit in torsional shear  $\tau_e$ , the maximum design torsional shear stress at solid height  $\tau_s$ , and the allowable normal (non shock)

working shear stress in torsion  $\tau_w$ . The basic modulus of rigidity for straight high carbon spring steels such as SAE 1095 is approximately  $1.05 \times 10^4$  ksi and for the low alloy spring steels about  $1.15 \times 10^4$  ksi, and these values are commonly used in spring design. However, the effective modulus of rigidity is appreciably, and somewhat indeterminately, reduced both by presetting and by the thin layer of partially decarburized metal produced on the bar surface by hot forming and heat treating in uncontrolled atmospheres. Because these changes are relatively limited and rather indeterminate they are often neglected in spring calculations and allowed to appear as part of the tolerances in the spring characteristics of the finished product. Both effects become more pronounced as bar diameter increases, however, and some attempt to account for this reduction in rigidity will result in more accurate predictions of deflection. A rule of thumb sometimes applied is a reduction in G of 1/2 percent each, for presetting and surface decarburization, for each 1/4 inch of bar diameter beyond one inch.

The ranges of ultimate strength in torsion (or modulus of rupture) and torsional elastic limit for commonly used spring steels are available in numerous handbooks (see Reference 6.3). These are usually expressed as stress ranges because of the considerable variations that occur as a result of the small variations in chemical composition between heats and larger variations which result from differences in, and accuracy in control of, heat treating. Also, the maximum average heat treated properties will vary considerably with bar diameter. The smaller bar sizes will have received both more thorough rolling action during manufacture and more complete and uniform penetration of heat treatment effect than large diameter bars. Unless actual test data and the concurrence of the spring manufacturer are obtained, values near the lower ends of the commonly listed ranges of  $\tau_e$  should be the maximum solid height stress values considered in design.

For preset springs that are designed for a combination of normal static load plus a limited number of cycles of weapons effect shock loading, the minimum handbook values of  $\tau_e$  may be used as the maximum

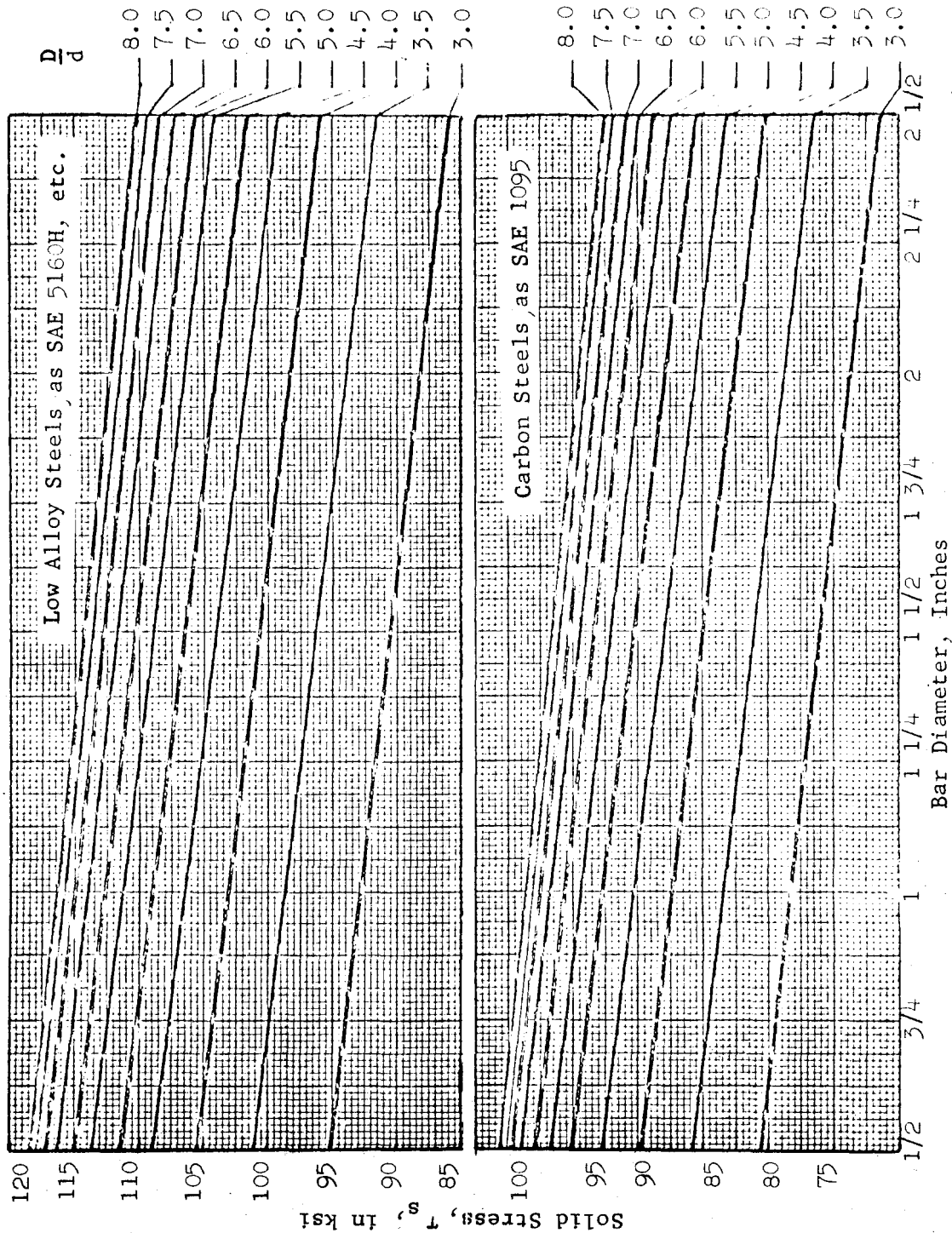


FIGURE 6.5: RECOMMENDED MAXIMUM SOLID STRESSES FOR HELICAL SPRINGS NORMALLY SUBJECT TO DYNAMIC LOADING (REFERENCE 6.5)

design stress at solid height,  $\tau_s$ , provided that this value does not exceed 80 percent of the modulus of rupture:

$$\text{or } \tau_s = \tau_e \leq .8 \tau_u$$

(this allowable is applicable for ordinary conditions where  $D/d > 4$ . Consult manufacturer's recommendations for allowable  $\tau_s$  when  $D/d < 4$ .) For non-preset springs the design stress at solid height,  $\tau_s$ , should be divided by the Wahl factor. In either case the maximum design working stress,  $\tau_w$ , due to combined static and dynamic loading, and corresponding axial deflection should not be greater than 75 percent of the values at solid height.

Springs designed for total working loads which include a large component (25 percent or more) of vibratory loading should be preset in all cases and should be designed for maximum solid height stresses consistent with the values in Figure 6.5. The maximum working stresses should not exceed 75 percent of the solid height stresses.

6.2.1.4 Axially loaded helical compression springs; design procedures and examples: To simplify the discussion and provide a convenient reference, Table 6.2 lists and defines the symbols employed in the formulae used in this subsection. Figures 6.6 and 6.7 have been prepared to simplify preliminary design calculations.

Figure 6.6 is a plot of  $\delta$ , the spring deflection per inch of effective solid height, versus the mean coil diameter  $D$  for various bar diameters  $d$  plotted for the conditions that  $G = 1.05 \times 10^4$  ksi at the torsional shear stress  $\tau$  of 100 ksi. Since  $\delta$  varies directly with the shear stress,  $\tau$ , and inversely with  $G$ , the values of  $\delta_1$  corresponding to values of  $G_1$  and  $\tau_1$ , other than those upon which the table are based, will be determined as:

$$\delta_1 = \frac{105 \tau_1}{G_1} \delta \quad (6.2)$$

It will be noted that values of  $\delta$ , determined for any combination of  $\tau$  and  $G$  will be constant for any bar diameter,  $d$ , or mean coil diameter,  $D$ , as long as the spring index,  $D/d$  remains constant. The bar diameters shown are expected to cover the major range of interest. Since many intermediate

TABLE 6.2: SYMBOLS USED IN SECTIONS 6.2, 6.3 and 6.4

A	: Cross sectional area
$A_b$	: Bonded area, rubber to metal in rubber springs
$A_p$	: Unrestrained peripheral area normal to loaded area of rubber compression springs
$C_\ell$	: Correction factor for stiffness ratio $k_r/k_q$ for helical springs
$C_\delta$	: Correction factor for deformation effect on modulus of rubber compression springs.
$C_s$	: Compressibility constant in liquid springs, static
$C_d$	: Compressibility constant in liquid springs, dynamic
D	: Mean coil diameter in helical springs
$D_o$	: Outside diameter in helical springs
$D_i$	: Minimum clear inside diameter for helical compression spring housings
d	: Bar diameter in helical springs and torsion bars
E	: Modulus of elasticity in tension or compression
F	: Lateral load
G	: Torsional modulus of elasticity (or modulus of rigidity)
H	: Total free height of helical springs and Belleville springs
$H_e$	: Effective free height of helical springs, (less closed end turns)
$h_o$	: Effective height of helical compression springs at working load
$h_w$	: Effective height of helical compression springs at static load
$K_1, K_2, K_3$	: Design coefficients for Belleville Springs
$K_s$	: Shape factor for rubber compression springs
k	: Spring rate
$k_r$	: Spring rate in axial direction
$k_q$	: Spring rate in lateral direction
h	: Solid height of helical springs

TABLE 6.2: SYMBOLS USED IN SECTIONS 6.2, 6.3 and 6.4

$M$	: Modulus of elasticity	Rubber
$M_s$	: Modulus of elasticity static	"
$M_d$	: " " " dynamic	"
$M_t$	: " " " static, tangent, tension	"
$M_c$	: " " " " , " , compression	"
$M_r$	: " " " " , " , shear	"
$N$	: In helical springs, the total number of coils	
$N_e$	: In helical springs, the number of active coils	
$P$	: Axial load in helical springs, load in general	
$P_s$	: Solid height load in springs, static load in general	
$P_f$	: Load at flat position of Belleville springs	
$P^*$	: Max load uncorrected for Wahl effect	
$p$	: Pitch of active coils in helical springs or pressure in air and in liquid springs	
$R$	: Outside radius of Belleville springs	
$r$	: Inside radius of Belleville springs	
$T$	: Torsional moment or torque	
$t$	: Thickness of Belleville springs or in rubber springs	
$V$	: Volume in air and in liquid springs	
$W$	: Wahl factor in helical springs	
$\Delta$	: Deflection in general	
$\Delta_r$	: Axial deflection in helical springs	



TABLE 6.2: SYMBOLS USED IN SECTIONS 6.2, 6.3 and 6.4

$\Delta_q$	:	Lateral deflection in helical springs
$\Delta_{rs}$	:	Axial deflection in helical springs solid
$\Delta_{rw}$	:	" " " " " static
$\Delta_{rd}$	:	" " " " " dynamic
$\delta$	:	" " per inch of effective solid height
$\mathcal{E}$	:	Strain in rubber springs
$\sigma_c$	:	Direct compressive stress, static
$\tau$	:	Shear stress in general
$\tau_i$	:	Max. shear stress inside coil of helical spring
$\tau_e$	:	Elastic limit shear stress
$\tau_u$	:	Ultimate shear stress
$\tau_r$	:	Shear stress due to axial load only
$\tau_s$	:	Shear stress at solid height of helical springs
$\tau_o$	:	Shear stress at working height of helical springs
$\tau_w$	:	Allowable shear stress
$\tau_{qr}$	:	Shear stress due to loads F and F

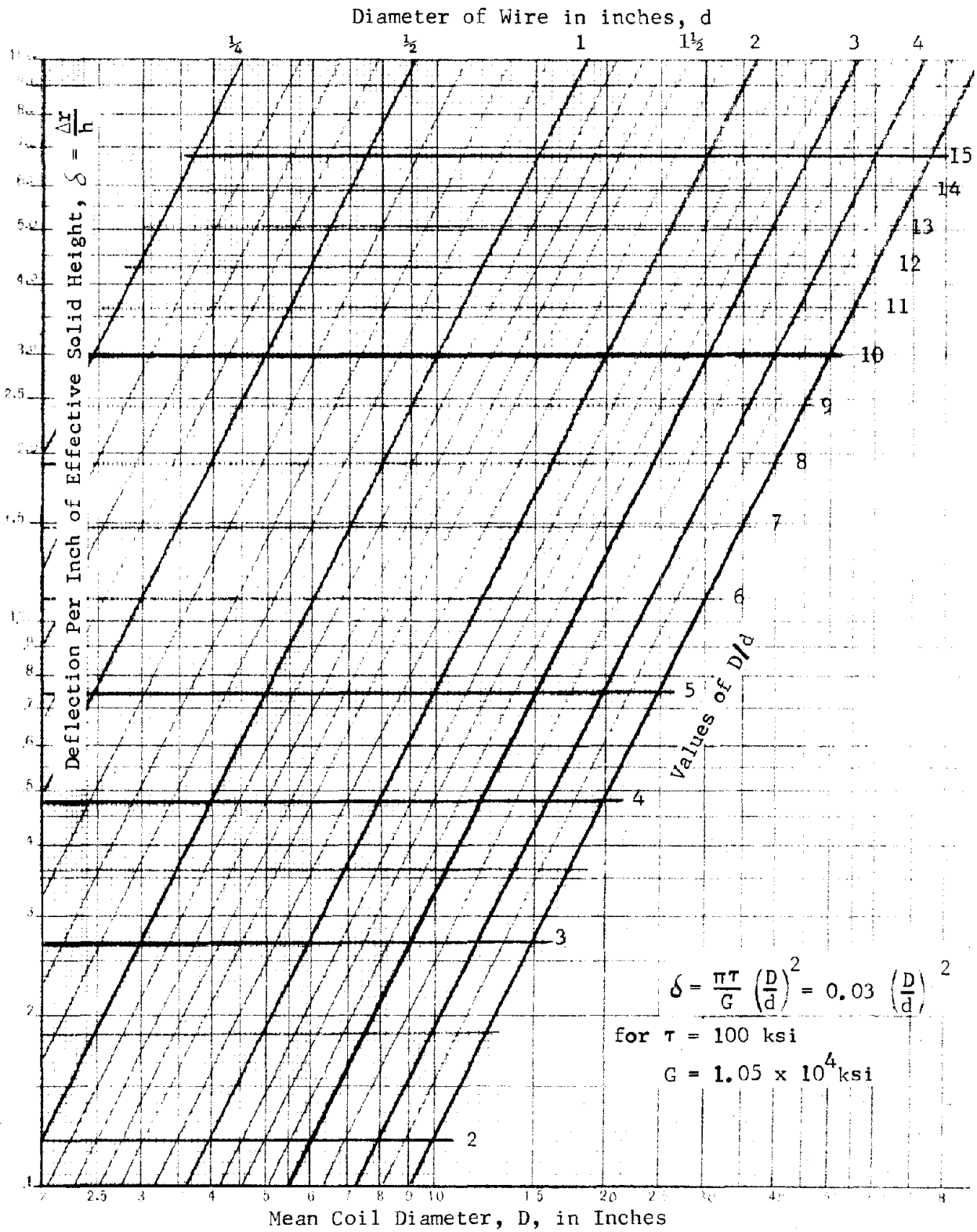


FIGURE 6.6: DEFLECTION OF HELICAL COIL SPRINGS OF ROUND WIRE

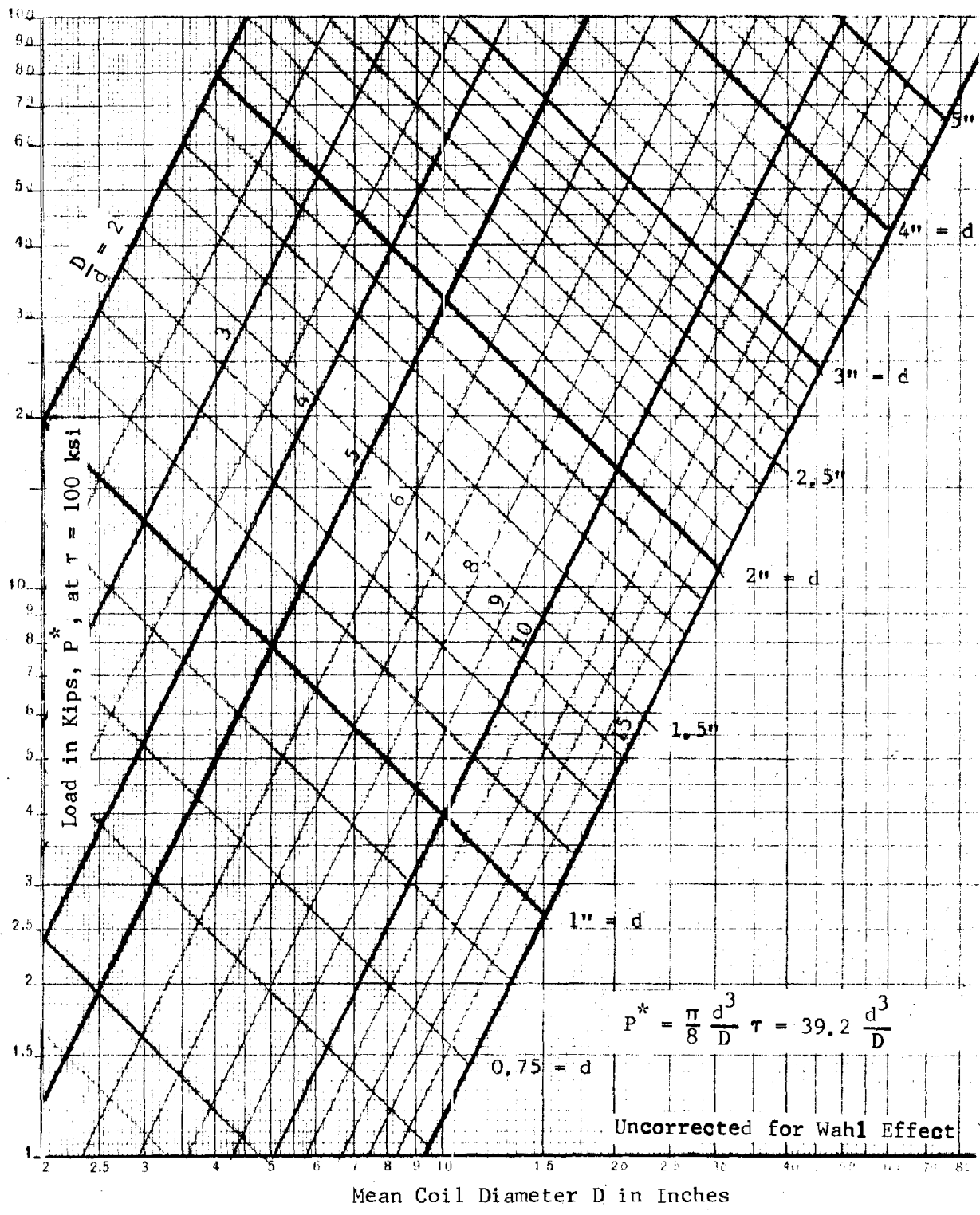


FIGURE 6.7: LOAD FACTORS FOR HELICAL COIL SPRINGS OR ROUND BAR

diameters are available as stock sizes Figures 6.6 and 6.7 may be applied to these by interpolation. Values of D/d and bar diameters larger than those commonly considered in such charts have been included here to cover the many unusual spring problems arising in shock isolation for weapons effects.

The spring allowable load chart gives values of  $P^*$ , uncorrected for coil curvature or Wahl Effect, and Figure 6.7 is based on an allowable shear stress,  $\tau = 100$  ksi. When entering the chart with an actual working load,  $P_w$ , based on any value of working stress,  $\tau_w$  an effective load value,  $P_e$  which is proportional to the ratio  $100/\tau_w$  must be used

$$P_e = 100 P_w / \tau_w \quad (6.3)$$

The above relation also applies to specific combinations of d and D.

After establishing an apparently satisfactory set of spring dimensions the result must be checked for proximity to the critical buckling ratio (see Figure 6.4) and, if buckling is likely, either the spring dimensions must be revised or the spring must be guided. If the spring is to be guided the minimum inside diameter of the guide must be established at a value that will prevent jamming as the spring expands under compressive load. Standard tolerances on the "as fabricated" outside diameter of the spring and on inside diameters of standard pipe and tubing used as housings are available in various handbooks. The spring's diametral expansion under compression from free to solid height may be expressed approximately as:

$$\Delta D = (p^2 - 0.8pd - 0.2d^2)/10D \quad (6.4)$$

where p is the pitch of the active coils at total free height or

$$p = H_e / N_e$$

and  $N_e$  is the number of effective coils.

The most convenient actual design procedures will vary somewhat with the specified parameters which, in addition to loading conditions will usually include one or more of the following limitations; minimum and maximum deflection under a specific shock loading, spring constant, maximum height, maximum outside diameter, specific safety factors for working stresses, and specific safety factors against "bottoming" under maximum combined

normal and shock loading conditions. However the following examples are taken from actual cases and may be considered representative.

Design Example 6.1, below, considers the design specifications for a shock isolation system example given in Section 8 and presents a typical procedure for the design of the helical springs required.

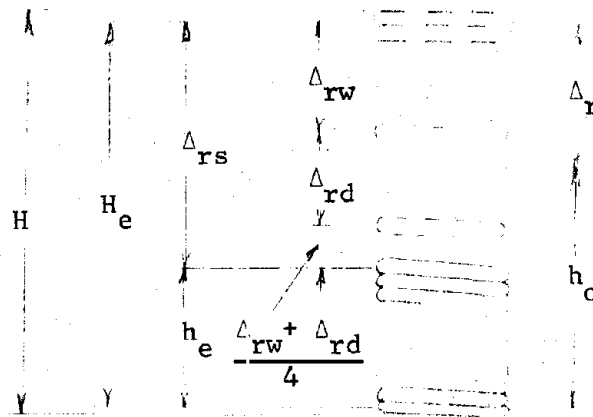


FIGURE 6.8

Example 6.1

Given:  $k_r = 25 \text{ lb/in};$

$\Delta_{rw} = 40 \text{ in}; \Delta_{rd} = \pm 35 \text{ in}.$

- (1) From above: the maximum combined load deflection,  $\Delta_{rw} + \Delta_{rd} = 75$  inches.
- (2) and maximum combined load,  $P = 75 \times 25 = 1875 \text{ lb}.$
- (3) The total load at solid height at  $\Delta_{rs} = 1.25 \times 75 = 94''$   
is  $P_{rs} = 1875 \times 1.25 = 2340 \text{ lb}.$
- (4) Since this is a relatively light spring assume SAE 1095 material and 100 ksi solid stress,  $\tau_s$ . The spring will be pre-set and  $P_{rs} = P^*$  (in Figure 6.7). The spring is to be housed and guided so that it will be stable against lateral buckling. Assume that  $D/d = 6$  to  $7$ . From Figure 6.7, for  $P^* = 2.34 \text{ kips}$  and for  $D/d = 6$  to  $7$ , select  $d = 5/8''$ . Accordingly  $D$  will be about  $4''$ , and  $D_o$  will be about  $4.6''$ .

Example 6.1 (continued)

- (5) If  $G$  is assumed as  $1.05 \times 10^4$  ksi (without reduction) Figure 6.6 gives  $\delta = 1.3$  inch/inch of effective solid height for  $D = 4$ ".
- (6) The effective solid height,  $h_e = 94/1.3 = 72$  inches.
- (7) The number of effective coils,  $N_e = 72/.625 = 115$ , and the total number of coils,  $N = N_e + 2 = 117$ .
- (8) Effective free height,  $H_e = 94 + 72 = 166$  inches  
total free height,  $H = H_e + 2d = 167$  inches
- (9) Pitch of effective coils,  $p = 166/115 = 1.443$  inches
- (10) Minimum clear inside length of spring housing with 4" of spring pre-stress,  $167 - 4 = 163$  inches
- (11) Minimum inside diameter of housing:
- (a) see Equation (6.4) for spring expansion under compression
- $$\Delta D = (p^2 - .8pd - .2d^2)/10D$$
- $$= (1.443^2 - .8 \times 1.443 \times .625 - .2 \times .625^2)/40 = .032 \text{ inch.}$$
- (b) manufacturing tolerance on diameter, about .25 inch.
- (c) minimum clearance, assume .10 inch.
- (d) minimum clear inside diameter of housing,
- $$D_i = 4.625 + .032 + .25 + .10 \cong 5.0 \text{ inches.}$$
- (12) For a value of  $D/d = 4/0.625 = 6.4$ , the stress increase due to the curvature effect of the coils, the Wahl factor  $W$ , as seen from Figure 6.3a, will be about 1.12. This would mean that for the maximum or solid height load of  $P_{rs} = 2.34 \text{ kips} = P^*$ , the stress in the spring would be  $100W$  or 112 kips; however, it is not customary to consider this extreme load when making correction for the curvature effect of the coils; moreover the pre-set will take care of the Wahl effect.

6.2.1.5 Helical compression springs subject to combined axial and lateral loading. When helical springs are required to resist both axial and lateral loading (see Figure 6.1) it is desirable to determine at the design stage the total axial and lateral deflections of one end with respect to the other, the maximum combined stresses in the spring, and the stability against buckling at the two maximum deflections. Under this type of loading springs

become rather inefficient, moreover stresses and deflections are largely indeterminate unless the ends are essentially fixed against rotation, and, even with assumed end fixity, much uncertainty still remains. This discussion applies only to springs having ideal end fixity, and, as previously noted, only round bar stock is considered.

In determining the axial deflection,  $\Delta_r$ , under combined axial load,  $P$ , and lateral load,  $F$ , the axial spring rate,  $k_r$ , is little affected by the lateral deflection  $\Delta_q$  within usual load ranges. For any given spring, then  $P = k_r \Delta_r$ . The lateral spring rate  $k_q$ , however, is materially affected by axial deflection. Moreover  $k_q$  is decreased by axial compressive deformation of the spring and increased by axial extension of the spring. Since the lateral deflection  $\Delta_q$  of the spring is resisted by both torsional and flexural stresses in the metal as well as by other less determinate factors, it is open to question as to whether it is feasible to write a rigorous expression for the value of lateral spring rate  $k_q$ .

The expressions for  $k_r$  and  $k_q$  as given by Equations (5.1b) in Section 5 are considerably idealized, but they will nevertheless be used for design purposes in this section. An idea of the transverse, approximate stiffness  $k_q$  can be expressed analytically for zero axial load by the following simplified formulae, Reference (6.14).

$$(k_q)_0 \approx \frac{12 BS}{Sh_o^3 + 12 Bh_o} \quad \text{for ideal fixity at both ends} \quad (6.5a)$$

$$(k_q)_0 \approx \frac{3 BS}{Sh_o^3 + 3 Bh_o} \quad \text{for one end fixed and other hinged} \quad (6.5b)$$

in which

$$B = \frac{2 h_o}{\pi N_e D} \frac{1}{\frac{1}{EI} + \frac{1}{GI_T}} \quad (6.6a)$$

$$S = \frac{8 h_o}{\pi N_e D^3} EI$$

In this case  $I$  is the rectangular moment of inertia of the torsion bar's cross section with respect to a transverse plane, and  $I_T$  is the torsional moment of inertia of the bar's cross section. For a circular cross section of the bar

$$I = \frac{\pi d^4}{64} \quad \text{and} \quad I_T = I_p = \frac{\pi d^4}{32}$$

Assuming a circular cross section and that  $E = 2.6 G$ , the values of  $B$  and  $S$  become

$$B = 0.0352 \frac{h_o d^4 G}{N_e D} \tag{6.6b}$$

$$S = 0.324 \frac{h_o d^4 G}{N_e D^3}$$

Expressing  $B$  and  $S$  in terms of the axial stiffness  $k_r$  which is equal to  $d^4 G / 8 N_e D^3$ , it is seen that

$$B = 0.282 h_o D^2 k_r \tag{6.6c}$$

$$S = 2.59 h_o k_r$$

Substituting (6.6c) into (6.5a) and (6.5b), we have

$$\left( \frac{k_q}{k_r} \right)_o = \frac{3.39}{1.31 + \left( \frac{h_o}{D} \right)^2} \quad \text{for ideal fixity of both ends} \tag{6.5c}$$

$$\left( \frac{k_q}{k_r} \right)_o = \frac{0.847}{0.327 + \left( \frac{h_o}{D} \right)^2} \quad \text{for one end fixed and other hinged} \tag{6.5d}$$

Then expressing Equation (5.1b) in ratio form

$$\frac{k_q}{k_r} = \left( \frac{k_q}{k_r} \right)_o + \frac{P}{k_r h_o} = \left( \frac{k_q}{k_r} \right)_o + \frac{\Delta r}{h_o}$$

we have

$$\frac{k_q}{k_r} = \frac{3.39}{1.31 + \left( \frac{h_o}{D} \right)^2} + \frac{\Delta r}{h_o} \quad \text{for both ends fixed} \tag{6.7a}$$



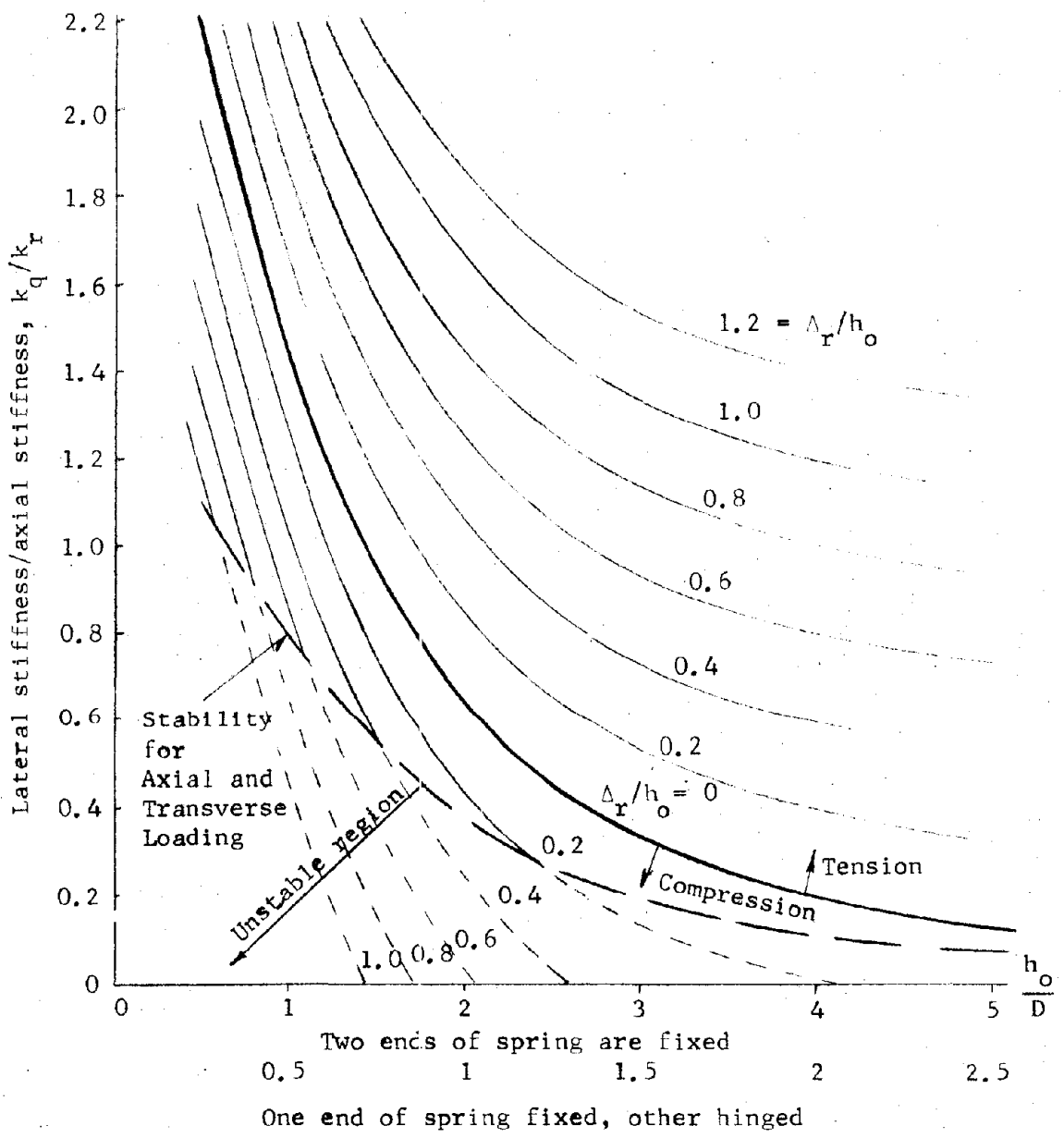


FIGURE 6.9

$$\frac{k_q}{k_r} = \frac{0.847}{0.327 + \left(\frac{h_o}{D}\right)^2} + \frac{\Delta r}{h_o} \quad \text{for one end fixed other hinged} \quad (6.7b)$$

Figure 6.9 shows a plot of Equations (6.7a) and (6.7b), the difference between the two equations appears in the two scales of the abscissa  $h_o/D$ . The family of curves above the  $\Delta r/h_o = 0$  curve refers to tension in the spring, and the family of curves below  $\Delta r/h_o = 0$  refers to compression in the spring. The heavy dashed curve, marked stability, relates to an elastic stability criterion for unspecified ratios of combined axial and lateral loadings that will be presently discussed.

Since helical springs subject to both axial and lateral loading are stable against buckling as long as the potential energy stored in the deflected spring is reduced by a reduction of the lateral deflection and increased by an increase in either lateral deflection or in axial deflection. Any spring, subjected to compressive loads should be checked for such buckling stability; it will be found that this is a very complicated procedure but that it depends greatly on the transverse stiffness  $k_q$  of the spring. The critical buckling ratio of lateral to vertical stiffness according to Reference 6.2 can be expressed empirically by

$$k_q/k_r = 1.2 \Delta_r/h_o \quad (6.8)$$

This approximate equation that excludes specific ratios of axial to lateral loadings is plotted as the straight line in Figure 6.10.

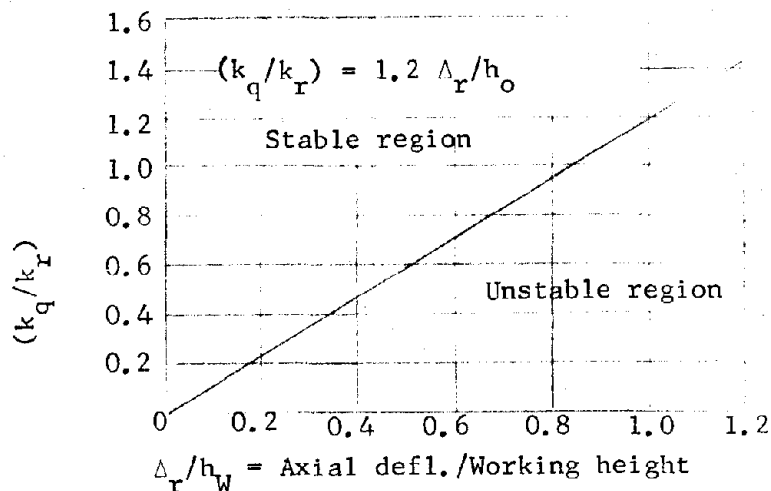


FIGURE 6.10: CRITICAL BUCKLING RATIO (REFERENCE 6.2)

The empirical criterion of Equation (6.8) for combined axial and lateral loadings has been introduced into Figure 6.9 as the marked, dashed line curve. Thus for a spring with both ends fixed and with a working height to spring diameter ratio of  $h_o/D = 2$ , the compressional instability will occur when the  $\Delta_r/h_o$  is almost 0.3. If the  $h_o/D$  ratio had been 3, instability would occur when  $\Delta_r/h_o$  is about 0.14. Moreover if one end of the spring had been fixed and the other end had been hinged, the  $h_o/D$  ratios would have been one half of those for the spring with both ends fixed.

Since axial, and combined axial and lateral loading produce bending as well as shear stresses in helical springs, the relatively higher yield and ultimate strengths of spring steels in flexure, 125 percent to 150 percent of the values in shear, together with the high ratio of shear to bending stresses will normally result in torsional shear being the critical stress under nearly all loading conditions. The total torsional shear stress,  $\tau_{qr}$ , due to the combined axial and lateral loads  $P$  and  $F$ , may be approximated in terms of the axial load stress by

$$\tau_{qr} = \tau_r (1 + \Delta_q/D + Fh_o/P D) \quad (6.9a)$$

where  $\tau_r$  is the shear stress induced by axial load only.

A more useful form of this equation is obtained by identifying  $\tau_{qr}$  with  $P$  and  $F$  and  $\tau_r$  with  $P$  alone so that

$$\frac{\text{Effect of } P \text{ and } F}{\text{Effect of } P} = 1 + \frac{\Delta_q}{D} + \frac{F}{P} \frac{h_o}{D} \quad (6.9b)$$

It will be noted that, since  $\Delta_q = \frac{F}{k_q}$ , the influence of each of the last two terms is to increase the total stress. Consequently, at large ratios of  $F$  to  $P$  the accuracy of results obtained from Equation (6.9) becomes increasingly dependent upon the accuracy with which  $k_q$  is known.

An investigation of the literature indicates that the  $k_q/k_r$  ratios obtained by applying Equations (6.7a) are difficult to check experimentally. Agreement between calculated results and test data has been found to be within 25 percent by some investigators working with small springs. Recent tests (see Reference 6.13) on large springs ( $D = 18.8$ ",  $d = 3$ " and  $h_o = 47.4$ " ), however, have shown disagreements as large as 45 percent between calculated and measured values of,  $k_q/k_r$ , and the plot of this ratio versus  $\Delta_r/h_o$ , in

some cases have had slopes in the opposite direction to that predicted by the theory. These tests were conducted over a range of  $\Delta_r/h_o$  from about .135 to .383. The maximum divergence between test and calculated data occurred at the latter value with the test figure higher than the calculated. The test curve was also concave upward over the range of  $\Delta_r/h_w$  above about .3 resulting in an increasing rate of divergence between test and calculated values beyond this point.

In view of the foregoing, it appears that use of Figure 6.9 will, for large springs, give conservative values of  $\Lambda_q$ , at  $\Delta_r/h_w$  ratios above about .25, when the important objective is the establishment of maximum probable horizontal deflections. However, when the primary purpose is to limit maximum horizontal accelerations and to obtain certain minimum values of horizontal deflection, the calculated ratios of  $k_q/k_r$  should be checked by tests.

A second significant conclusion may be drawn since the large springs used in these tests were specified to have an end finish resulting in a minimum contact arc of  $270^\circ$ , (there is some indication that the actual ground periphery may have been closer to  $290^\circ$ ). Even with this relatively large contact arc, variations in the ratio  $k_q/k_r$  of  $\pm 16$  percent from the mean resulted when the horizontal load was applied at various angles to the centerline of the end bearing area. This suggests that springs subjected to combined horizontal and vertical loading should be fabricated with the longest feasible contact arc even at the expense of squaring more than the usual  $3/4$  turn at each end. Where a number of identical springs are used to support a common load they should be installed with the centerlines of the bearing arcs at various orientations in order to help average out the variations in the  $k_q/k_r$  ratio.

6.2.1.6 Design Example 6.2, helical spring subject to combined axial and lateral loading. The following example illustrates the design steps for a helical spring subject to combined static axial and dynamic axial and lateral loading for which the maximum radial deflection and the two spring rates are specified.

It will be assumed that the empirical stability criterion, Equation (6.8), for unspecified ratios of axial P to lateral F loadings is

sufficiently conservative to take into account operating load ratios up to  $F/P = 1/4$ .

Assume that:

- 1) Spring is fixed at both ends and that  $E = 2.6 G$
- 2) Static axial load  $P_s = 18$  kips
- 3) Axial stiffness  $k_r = 3$  kips/inch
- 4) Lateral stiffness  $k_q = 1.5$  kips/inch
- 5) Dynamic axial deflection  $\Delta_{rd} = 3$  inches
- 6) Max value of  $F/P = 1/4$

Find:

$$\text{Static axial deflection, } \Delta_{rw} = \frac{P_s}{k_r} = 6 \text{ inches}$$

$$\text{Static and dynamic axial deflection} = 9 \text{ inches}$$

$$\text{Operating deflection } \Delta_r^* = \Delta_{rw} + \frac{1}{2} \Delta_{rd} = 7.5 \text{ inches}$$

$$P = k_r \Delta_r = 22.5 \text{ kips}$$

$$F = \frac{P}{4} = 5.63 \text{ kips}$$

$$\Delta_q = \frac{F}{k_q} = 3.75 \text{ inches lateral deflection}$$

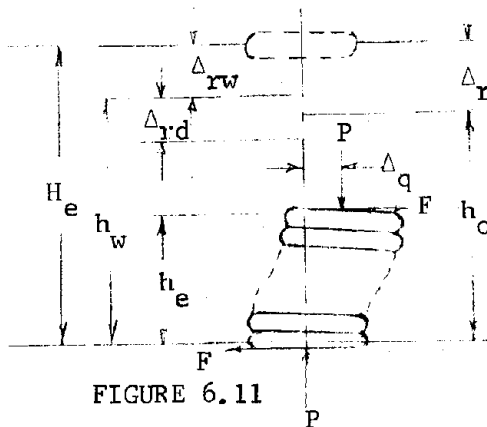


FIGURE 6.11

\* The operating deflection is defined as the maximum axial compressive deflection to occur simultaneously with the maximum lateral deflection.

Accordingly from Figure 6.9 it is seen that:

for  $\frac{k_q}{k_r} = \frac{1}{2}$ , stability demands that  $h_o/D$  is at least 1.6; thus for

$$h_o/D = 1.60 ; \Delta_r/h_o = 0.36 \quad (\text{assumption a})$$

$$= 1.75 ; \quad = 0.20 \quad (\text{assumption b})$$

since  $h_o = H_e - \Delta_r = H_e - 7.5$ , we have on assumption a)

$$H_e - 7.5 = 1.6 D \quad \text{and} \quad 7.5 = 0.36 (H_e - 7.5)$$

giving

$$D = \frac{20.8}{1.6} = 13'' \quad \text{and} \quad H_e = 20.8 + 7.5 = 28.3''$$

If b) is assumed we have

$$H_e - 7.5 = 1.75 D \quad \text{and} \quad 7.5 = 0.20 (H_e - 7.5)$$

giving

$$D = \frac{37.5}{1.75} = 21.4'' \quad \text{and} \quad H_e = 37.5 + 7.5 = 45''$$

Obviously assumption a) is economically preferable if the resulting stress situation is acceptable. To investigate this we use Figure 6.6. It is seen from Figure 6.11 that

$$h_e = H_e - \Delta_{rw} - \Delta_{rd} - \frac{1}{4} (\Delta_{rw} + \Delta_{rd}) = 28.3 - 6 - 3 - 2.25 = 17''$$

and consequently the deflection per inch of solid height is:

$$\delta = \frac{H_e - h_e}{h_e} = \frac{28.3 - 17}{17} = 0.66$$

Figure 6.6 specifies a bar diameter of about  $2 \frac{3}{4}''$  for  $D = 13''$ .

The stress situation is then examined by means of Figure 6.7 which shows that for  $D = 13''$  and for  $d = 2 \frac{3}{4}''$  the allowable load in kips for an assumed value of  $\tau = 100$  ksi is about 73.

Application of Equation (6.9b) with  $\Delta_q/D = 3.75/13 = 0.289$ , with  $F/P = 0.25$ , and with  $h_o/D = 1.60$  gives

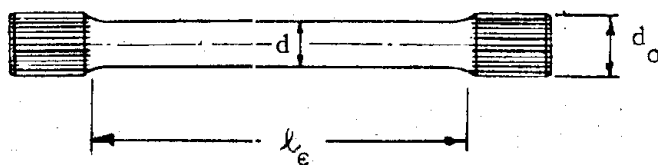
$$\frac{\text{Effect of P and F}}{\text{Effect of P}} = 1 + 0.29 + 0.25 \times 1.6 = 1.69$$

Accordingly the effect of P and F  $\approx 1.69 \times 22.5 = 38$  kips

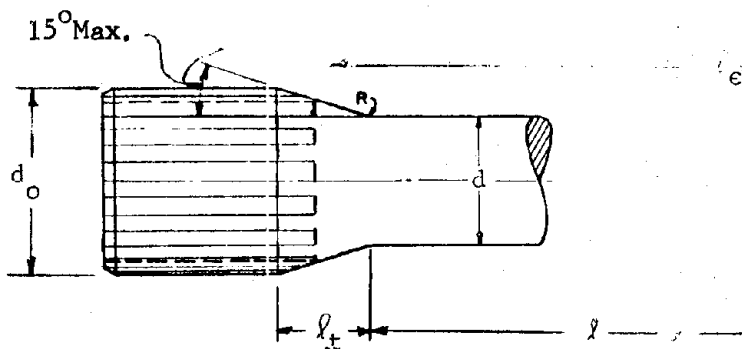
Since the stress increase due to curvature of the coils, the Wahl factor, is about 1.4 for  $D/d = 13/3.25 = 4$ , the corresponding or corrected P and F load will be 38 W kips or 53 kips. This is only about 73 percent of the load at solid height with axial load only.

### 6.2.2 Torsion bar springs

6.2.2.1 Types and applications. Torsion bars, or torsion bar springs, are one of the two most elementary of spring forms (the second being the leaf spring or flat spring subject to simple bending). The most widely used form of torsion bar, and the most applicable in weapons effect shock isolation, is the single bar (Figure 6.12a) although various multiple bar or bar and tube combinations are also used. In order to realize maximum service life torsion bars are usually relieved of bending stress so far as possible by supporting the rotating ends in bearings as illustrated in the isolation system shown in Figure 6.13. Torsion bars are among the most efficient



(a) Single Torsion Bar With Splined Ends



(b) Splined Torsion Bar End

FIGURE 6.12: STANDARD SINGLE TORSION BAR WITH SPLINED ENDS

spring forms from the standpoint of the ratios of both energy storage to weight and energy storage to volume. Their chief disadvantage lies in the stress concentrations which occur at the ends or in the relatively expensive end details necessary to minimize these concentrations. The fact that torsion bars are installed normal to the direction of the loads and displacements they control also tends to increase the cost of end connection hardware but may be a considerable advantage where space is limited in the direction of displacement. In Figure 6.13 a complex combination of bending, direct shear and torsional shear occurs at each support point. The allowable torsional stress and efficiency are accordingly to be watched in design. From the standpoint of increasing the operating stresses and energy storage efficiency, it is possible to machine finish, grind and polish, preset, shot peen and spline anchor torsion bars (see Reference 6.6). While not as wide as that for some types of springs, the useful ranges of sizes and applications of torsion bar springs extend from small valve springs to main suspensions of large masses.

#### 6.2.2.2 Design of steel torsion bars subject to negligible bending stresses.

The essential design formulae for solid round torsion bars, critical for torsion loading only are:

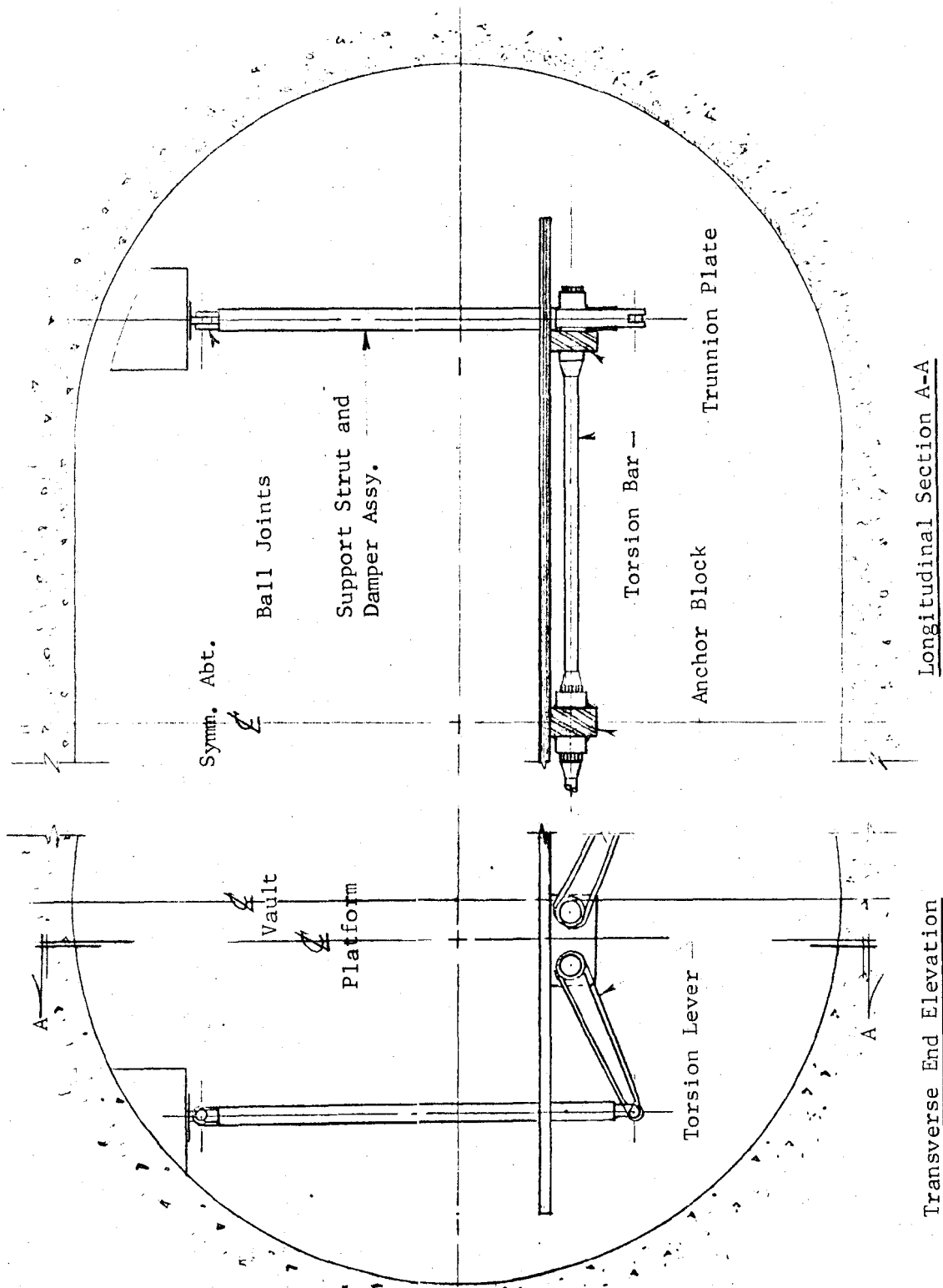
$$\phi = \frac{584 T l_e}{d^4 G} \quad (6.10)$$

$$\tau_{\max} = 16 T / \pi d^3 \quad (6.11)$$

where

- $\phi$  = angular deflection in degrees
- $\tau_{\max}$  = maximum (surface) torsional shear stress
- T = torsional moment
- $l_e$  = effective length of bar
- G = modulus of rigidity
- d = bar diameter





Longitudinal Section A-A

Transverse End Elevation

FIGURE 6. 13: SCHEMATIC: TORSION BAR SHOCK ISOLATION SYSTEM

For torsion bars with splined ends, designed according to the SAE manual (Reference 6.6 and Figure 6.12b), the splined end diameter,  $d_o$ , is recommended to be a minimum of  $1.2d$ . The enlarged ends are faired into the basic bar with a  $30^\circ$  maximum taper and a fillet radius of  $1.3d$ . The recommended value of  $l_e$  for the end design includes part of each tapered end length and is computed as:

$$l_e = l + \frac{2}{3} l_t \left( \frac{1}{d_o} + \frac{d^2}{d_o^2} + \frac{d^3}{d_o^3} \right) \quad (6.12)$$

where

$$l = \text{length of uniform diameter bar}$$

$$l_t = \text{length of tapered portion of bar}$$

**6.2.2.3 Materials, fabrication practices and working stresses.** In general torsion bars are designed as moderately high precision machine parts and are subject to relatively severe treatment in terms of maximum stresses and stress cycling. The uniformly high surface stresses make it important that surface imperfections of all kinds be avoided, and that surface decarburization during heat treatment be eliminated. These ends can usually be accomplished by finish grinding and polishing after machining and by heat treatment in controlled atmosphere furnaces. Shot peening is common practice and has a definitely beneficial effect on fatigue life. Even when fatigue is not a major consideration, the cold working of the surface by shot peening remains desirable as a means of equalizing residual stresses and for the resulting increase in the elastic limit of the surface material. When loading will be in only one direction pre-setting has much the same beneficial effect as it does for helical compression springs. The SAE recommends a pre-setting shear strain of about  $.022$  radian<sup>(1)</sup>. In applications where equal maximum stresses will occur in either direction of twist, pre-setting has no value.

High quality torsion bar springs are commonly fabricated from SAE 8660, SAE 9260, and SAE 9262 low alloy steels. Straight high carbon spring steels

(1) Pre-setting is always performed after shot peening as the shot peening otherwise has a tendency to relieve the pre-stressed surface condition obtained by presetting.

are sometimes used in non-critical applications. Steels having a high sensitivity to minor defects at high heat treats should be avoided. For torsion bars uniformly hardened to 50 or higher on the Rockwell C scale, shot peened and preset the SAE recommends working stresses on the order of 140 ksi for good fatigue life. If preset but not shot peened the working stress should be limited to about 120 ksi, and, if shot peened but not preset, to about 105 ksi.

For torsion bars not subject to a high percentage of cyclic loading the above values are conservative. Where the normal load is largely static and the maximum load includes only a limited number of cycles of shock loading, which comprise 30 percent or more of the design load, 90 percent of the torsional elastic limit of the material can reasonably be used as a maximum working stress.

#### 6.2.2.4 Design Example 6.3: Torsion Bar Spring

(1) Given: the vertical shock isolation system for the platform shown in Figure 6.13 employing four torsion bar suspensions:

- (a) Total load, uniformly distributed,  $W_t = 100$  kips
- (b) The maximum permissible natural frequency is 1 cps
- (c) Vertical dynamic displacement is  $\pm 10''$

(2) The required vertical spring constant,  $k$ , for each isolator is then:

$$k \leq 1/4 (4 \pi^2 f_n^2 m) / 12$$

$$\leq 1/4 (.102 f_n^2 W_t) = 2.55 \times 10^3 \text{ lbs/in}$$

The static load vertical displacement,

$$\Delta_{rs} = 2.5 \times 10^4 / 2.55 \times 10^3 = 9.8'' \quad , \quad \text{Use } 10''$$

(3) Determine deflection angle: Since the displacements are moderate, assume a 20" lever arm\* and equal displacements about a horizontal static lever arm position. Then the total deflection angle,

$$\phi = 2 \sin^{-1} (10/20) = 60^\circ$$

---

\* Using short lever arms, the trunnion plates and anchor blocks will be separate rather than paired as in the sketch.

(4) Determine the required bar diameter "d": the torque at maximum displacement is approximately

$$T \approx 20 \times 2 \times 2.5 \times 10^4 = 10^6 \text{ pound inches}$$

There is to be no reversal of stress (i.e.,  $\Delta_s = \Delta_d$ ), and the torsion bar can be pre-set. Since the bar size will be relatively large the steel selected must be capable of heat treatment to high strength in the larger bar diameters. Assume AISI type 8660H steel, heat treated to Rockwell C/60 to a minimum depth of 1/4 inch, also let

$$G = 1.1 \times 10^7 \text{ psi} ; \tau_e \approx 1.7 \times 10^5 \text{ psi} ; \text{ and use } \tau = 0.9 \tau_e = 1.53 \times 10^5 \text{ psi}$$

Then from Equation (6.11)

$$d = \left[ \frac{16 T}{\pi \tau} \right]^{1/3} = 3.22 \text{ inches}$$

and let

$$d_o \approx 1.3 \times 3.22 = 4.18 \text{ inches}$$

Use SAE 4 1/2 - 16A splined ends with  $d_o = 4.5$  inches

(5) Find required effective length: from Equation (6.10),

$$l_e = \phi d^4 G / (584T) = 122 \text{ inches}$$

(6) Determine overall length and controlling dimensions from SAE recommendations (see Reference 6.6).

### 6.2.3 Coned-disc springs (Belleville Springs)

6.2.3.1 Characteristics, applications and variations. Coned-disc springs, sometimes called Belleville Springs, or Belleville Washers <sup>(1)</sup> are essentially flat spring steel washers <sup>(2)</sup> that have been deformed into a slightly conical shape as schematically shown at the top of Figure 6.14. The spring action occurs when a force is applied tending to force the apex of the cone toward (or beyond) the flat position. Under such loading they exhibit a wide variation in spring rate versus deflection. The manner in which the  $k/\Delta$  ratio

<sup>(1)</sup> After Julian F. Belleville, who obtained the original patent, Paris, 1867.

<sup>(2)</sup> Because of their limited application the radially tapered flat disc spring (having a thickness at any point proportional to the radius to the point) is not discussed here.

varies is controlled largely by the ratio of the "as fabricated" deformation,  $H$ , to the metal thickness,  $t$ . Figure 6.14 illustrates and tabulates dimensions and symbols relevant to this section.

Coned-disc springs are useful chiefly for their ability to support large loads at small deflections with minimum space occupancy in the direction of load, and for applications requiring variable spring rates. In shock mounting systems for hardened structures they should be useful for applications requiring limited shock attenuation at a minimum cost in space and for back up of coil spring systems to reduce shock in case of "bottoming" of the coil springs.

Coned-disc springs may be stacked either in series (to increase total deflections) or in parallel (to increase the load required to produce a specific deflection). Friction damping and breakaway friction in parallel stacked assemblies make their performance less predictable than that of individual springs or series stacks.

The force-deflection characteristic of a coned disc spring depends greatly on the free height  $H$  of its cone frustum and on its thickness  $t$ . Thus for a thick spring with a small ratio of  $H/t$  the spring is essentially linear, up to  $\Delta = 2H$  see Figure 6.14a. For a thinner spring e.g. with  $H/t = 1.41$ , the initial stiffness decreases to zero as  $\Delta$  approaches  $H_1$ ; then, as the deflection passes through the flat shape of the coned disc spring the stiffness commences to increase toward its initial value as  $\Delta$  approaches  $2H$ , see Figure 6.14b. If the ratio  $H/t$  is larger than 1.41, the spring will have a region of negative stiffness before  $\Delta$  has reached  $H$ . This behavior is shown in Figure 6.14c for the specific ratio  $H/t = 2.5$ .

Figure 6.15a illustrates a wide range of the load ratio,  $P/P_f$ , versus deflection ratio,  $\Delta/H$ , obtainable by varying the ratio of  $H/t$ . The load,  $P_f$ , is defined as the load which produces a deflection,  $\Delta$ , equal to the free height,  $H$  or specifically as

$$P_f = K_1 \frac{Ht^3}{R^2} E$$

in which  $K_1$  is to be obtained from Figure 6.16. The curves in Figure 6.15a

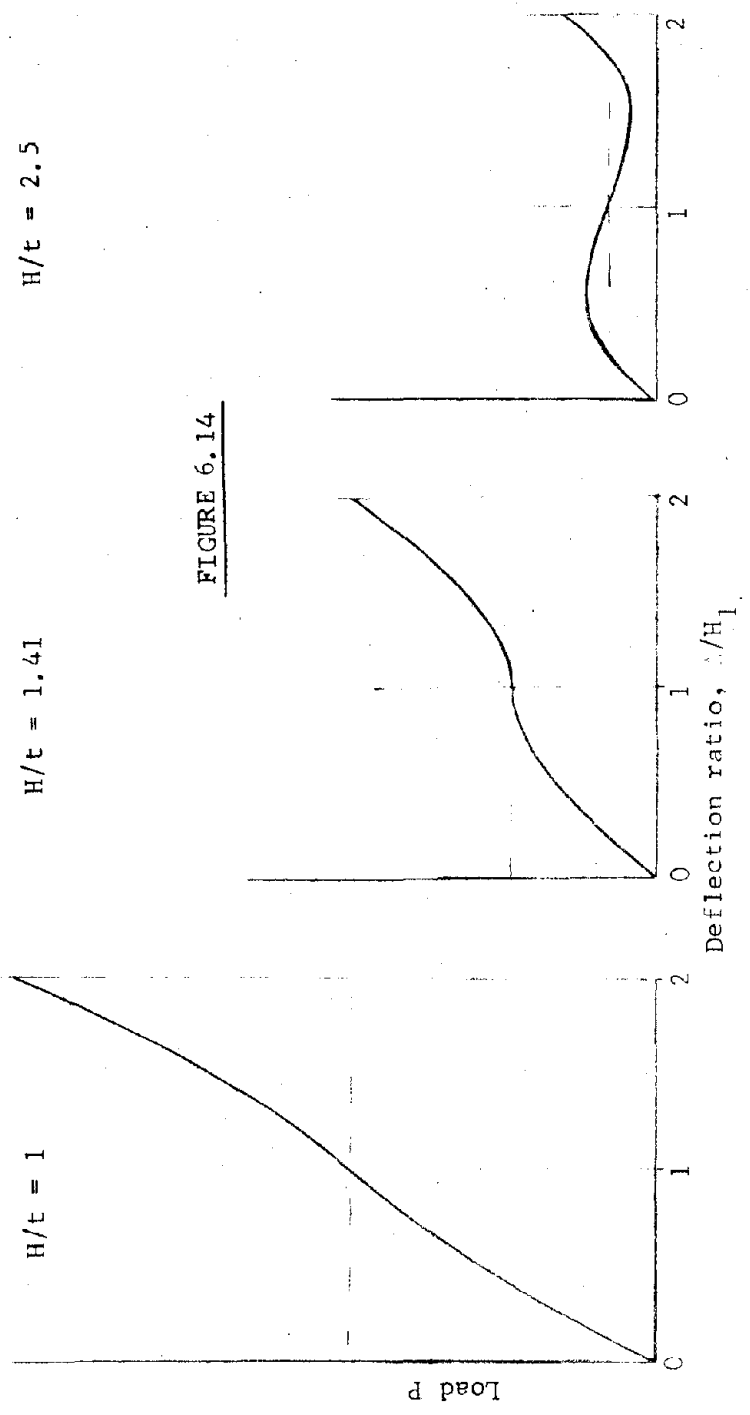
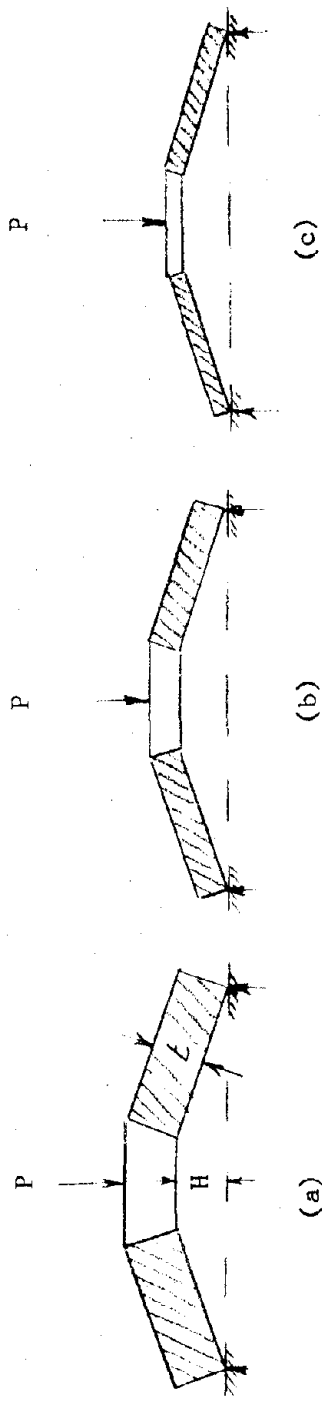


FIGURE 6.14

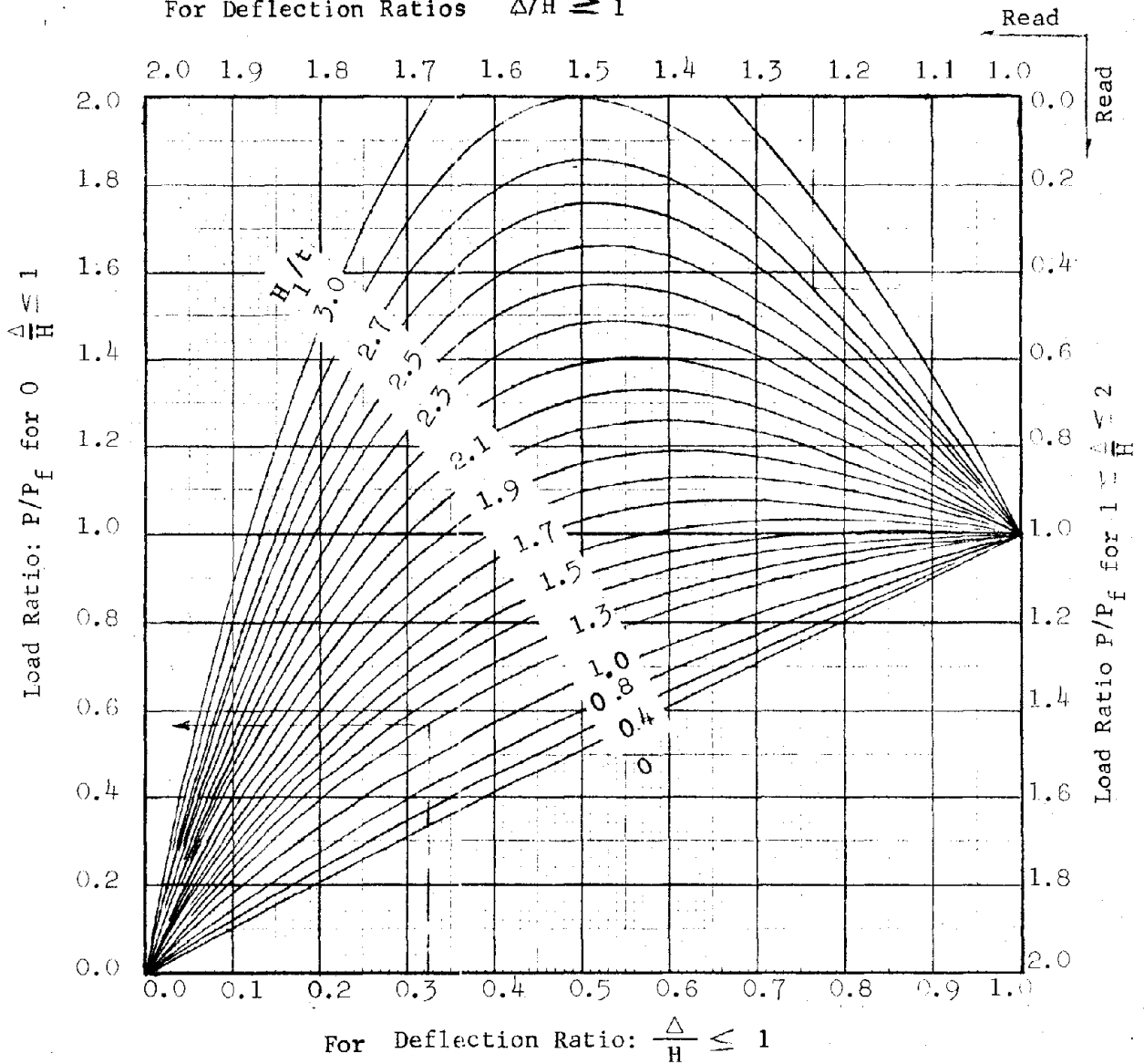
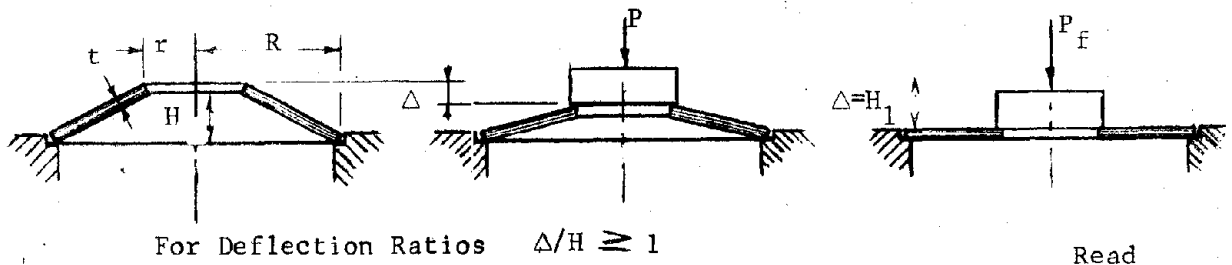


FIGURE 6.15a: LOAD RATIO VERSUS DEFLECTION RATIO AND  $H/t$  RATIO FOR BELLEVILLE SPRINGS

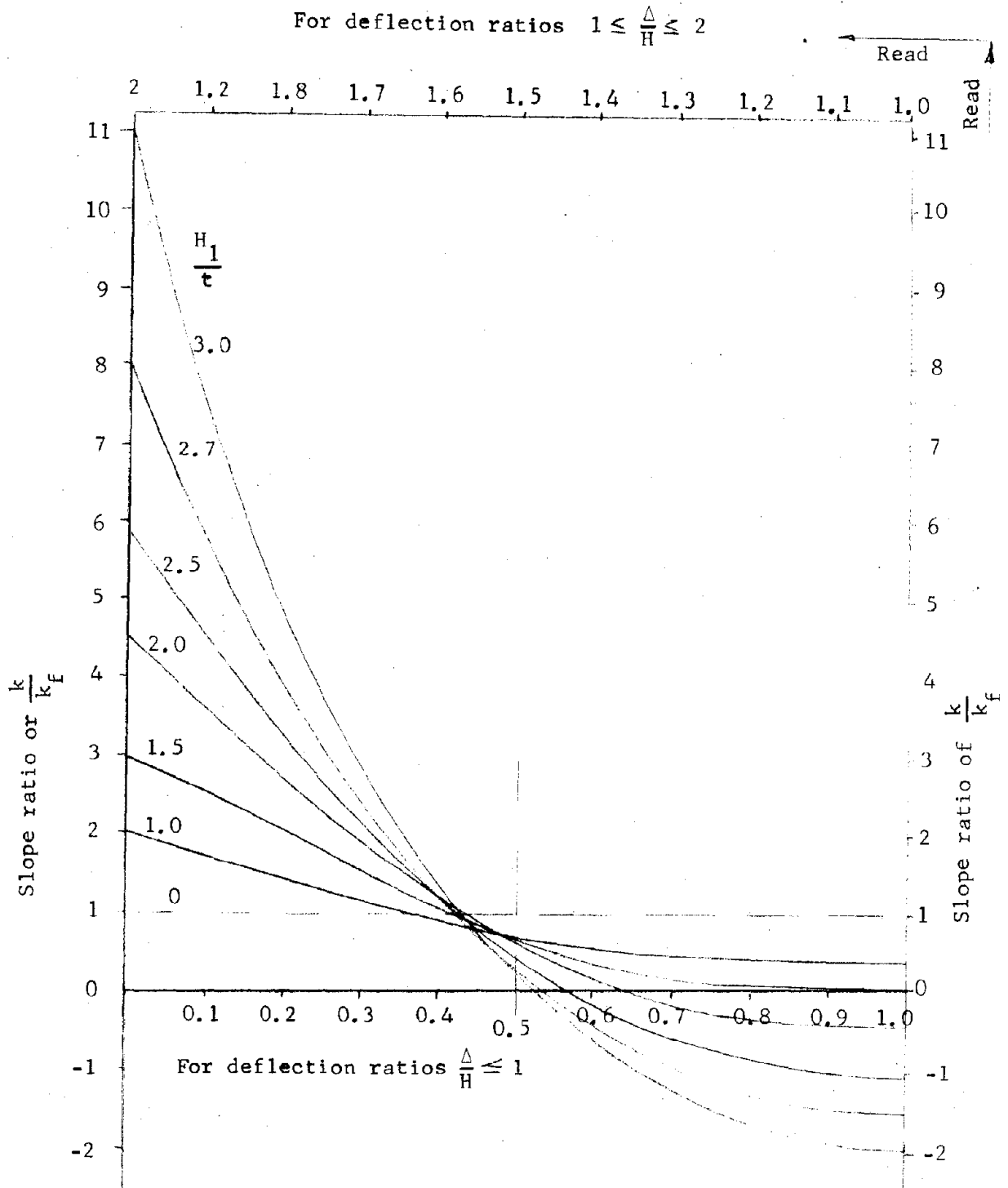


FIGURE 6.15b: SLOPES OR STIFFNESS RATIOS OF FIGURE 6.15a



are characteristic of coned-disc springs loaded at the inner and outer edges. As the H/t ratio increases from very small values the spring rate departs rapidly from a near straight line, with the highest positive values of k occurring at  $\Delta/H = 0$  and 2. At values of H/t below 1.41 minimum k values occur at  $\Delta/H = 1$ . At H/t = 1.41 the spring rate becomes zero for an appreciable interval near  $\Delta/H = 1$ . From H/t = 1.5 to 1.6 the spring rate is seen to be within a few percent of zero from about  $\Delta/H = 0.6$  to 1.4. Springs in this range are commonly called constant force springs and are widely used where it is desired to maintain a constant force over a considerable range of deflection. It can also be seen that, for all H/t ratios greater than 1.41, a negative spring rate range exists, reaching its maximum negative value at  $\Delta/H = 1$ . Series stacked assemblies of coned disc spring elements having H/t ratios greater than 1.6 that are to be operated close to the zero rate loading should consist of reasonably well matched individual elements. Otherwise some of the elements in the stack may transit to their negative spring rate with the effect of producing an erratic load/deflection curve for the assembly. All stacked assemblies must be guided to maintain alignment of individual elements.

Figure 6.15b shows plots of the stiffness ratios  $k/k_F$ , i.e. the positive slopes of several of the curves of Figure 6.15a, within the range of  $0 \leq \Delta/H \leq 2$ .

6.2.3.2 Design formulae. The class of coned-disc springs and the operating ranges of greatest potential value in shock isolation are those pertinent to the support of large loads at small deflections. For simplicity the design discussion will be confined to this area<sup>(1)</sup> of application in which confined springs having H/t ratios of .5 or less are subjected to deflections that are equal to or less than H. For these ranges of spring configuration and deflection and for edge loaded discs the following formulae apply.

$$P = \frac{K_1 \Delta E t^3}{R^2} = \frac{\sigma_c t^2}{K_3} \quad (6.13)$$

(1) For design data on coned-disc springs having large deflections and/or large cone heights the reader is referred to Wahl, "Mechanical Springs", 1963, Reference 6.1.

$$\sigma_c = \frac{K_2 \Delta E t}{R^2} = \frac{K_3 P}{t^2} \quad (6.14)$$

$$\Delta = \frac{P R^2}{K_1 E t^3} = \frac{\sigma_c R^2}{K_1 K_3 E t} \quad (6.15)$$

in which  $\sigma_c$  is the nominal compressive stress at the inside edge of the spring.

The nominal stiffness is given by

$$k = \frac{P}{\Delta} = K_1 \frac{E t^3}{R^2} \quad (6.16)$$

The coefficients  $K_1$ ,  $K_2$  and  $K_3$  vary with the ratio  $R/r$  and are given in graphical form in Figure 6.16.

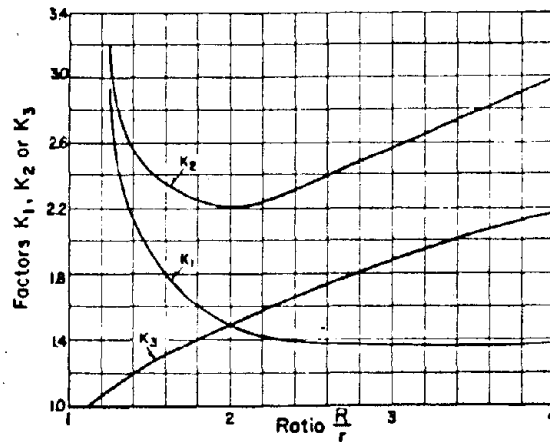


FIGURE 6.16: COEFFICIENTS  $K_1$ ,  $K_2$  AND  $K_3$  VERSUS THE RATIO,  $R/r$  (Reference 6.1)

### 6.2.3.3 Materials, tolerances and design stresses

a. Materials: The maximum stresses in coned-disc springs are the compressive stresses at the inner edge, and the most common uses involve largely static loadings. For these reasons materials are usually somewhat less critical than for most other types of springs. The lighter weights (thinner) springs are commonly blanked and formed from ordinary high carbon steels such as SAE 1074, 1085 and 1095. For the heavier springs and more

severe service applications the low alloy spring steels are used, often as forgings.

b. Tolerances: Standard commercial tolerances on coned-disc spring characteristics and dimensions are closely related. Since the characteristic  $k$  curve is a function of  $H/t$  the tolerances on the thickness of sheet and plate stock from which the washers are blanked have a marked influence. In addition variations in thickness and elastic limit in commercial grade sheet affect the permanent deformation,  $H$ , produced by forming in standard dies. As a result the  $P/\Delta$  values of "commercial grade" springs may vary by  $\pm 20$  percent from the nominal values. "Special grade" springs are fabricated from precision ground stock and more accurately sized and formed. For these the tolerance on  $P/\Delta$  is held to about  $\pm 8$  percent. By testing and selection almost any desired tolerance may be maintained, but costs will increase rapidly with the accuracy specified.

c. Design stresses: When the normal loading will be static or near static (less than about 100 major stress change cycles) for the required life of the spring, or when the maximum design load consists of a near static load plus 30 percent or more of a limited number of cycles of shock loading, and when there is no high temperature creep problem, the maximum stress,  $\sigma_c$ , calculated according to Equation 6.14 may be equal to the compressive elastic limit of the material.

#### 6.2.3.4 Design Example 6.4: Coned Disc Spring Isolator

(1) Given: A piece of equipment weighing 1000 lbs. is to be supported on four vertical coned disc spring isolators. The dynamic displacement is 0.6 inches at 5 cps and the maximum permissible natural frequency of the system is 5 cps.

(2) Required vertical spring rate,  $k \leq 1/4 (.102 \times 5^2 \times 10^3) = 637$  lbs/inch

(3) Design spring rate and displacements: Use  $k = 600$  lbs/inch  
the design frequency is then  $(600/ (.102 \times 250))^{1/2} = 4.85$  cps  
static load displacement,

$$\Delta_{rs} = 10^3 / (4 \times 600) = .416 \text{ inch}$$

and the dynamic displacement at the design frequency is,

$$\Delta_{rd} = (\pm) 637 \times .6/600 = \pm .637 \text{ inch}$$

(4) General considerations: Since the dynamic displacements exceed the static load displacement the isolator must be double acting or it must be designed to resist dynamic uplift as well as combined static and dynamic displacement in the downward direction. To provide approximately linear performance and eliminate the need for spacer rings an H/t ratio of approximately 0.5 will be used, and the deflections of the individual spring washers will be limited to 0.8 H (or to 0.4t). Individual washers must have a load carrying capacity of  $P = (.637 + .416) \times 250 \text{ lbs}/.416 = 630 \text{ lbs}$ . If the material is assumed to be SAE 1095 steel, a maximum design stress of 170 ksi is conservative. Since a considerable choice of stock Belleville spring washers is available with an R/r ratio of 2, this ratio makes a convenient starting point for the design.

(5) Determine t,  $\Delta$ , and H for the spring elements: from Figure 6.16, for R/r = 2,  $K_3 \approx 1.48$ ; and from Equation 6.14,  $t = (k_3 P/\sigma_c)^{1/2}$

It is found that

$$t = (1.48 \times 630/160,000)^{1/2} = .076 \text{ inches}$$

Use the nearest standard gage, No. 15,  $t = .072$

The corresponding stress,  $\sigma_c = 1.48 \times 630/.072^2 = 180 \text{ ksi}$

This is an acceptable stress.

The maximum design deflection,  $\Delta = 0.4 \times 0.072 = 0.029 \text{ inches}$  and

$H = \Delta/0.8 = 0.036 \text{ inches}$ . The overall height is therefore  $H + t$  or 0.108 inches.

(6) Determine the spring element's radii R and r: from Figure 6.16, and for R/r = 2, it is found that  $K_2 = 2.2$ ; and from Equation 6.14, the outside radius is

$$\begin{aligned} R &= (k_2 \Delta Et/\sigma_c)^{1/2} \\ &= \left[ 2.2 \times .029 \times 3 \times 10^7 \times .072 / (1.8 \times 10^5) \right]^{1/2} \\ &= 0.88 \text{ inches} \end{aligned}$$

consequently the inside radius,  $r = .44 \text{ inches}$

(7) Spring rate per element: from Figure 6.16 and for  $R/r = 2$  it is found that  $K_1 = 1.48$ ; and from Equation (6.15) the stiffness of one element is

$$k = K_1 Et^3/R^2 = 1.48 \times 3 \times 10^7 \times .072^3/.88^2 = 21,800 \text{ lbs/inch}$$

(8) Stack assembly:

The minimum number of elements in series to obtain the required vertical spring rate of the stack is  $21,800/600 = 36$ ; use 18 pairs.

(9) Isolator design: A simple approach to the double acting isolator design will incorporate a housing mounted to the equipment frame and isolated by the coned disc spring stack from a center guide which can be mounted to the supporting surface. Numerous variations are practical. A typical design configuration is illustrated in Figure 6.17. The nominal height of the stack is  $.108 \times 36 = 3.89$  inches. This may be reduced to 3.75 inches by a small pre-stress at assembly.

6.2.4 Rubber springs. Rubber springs, commonly called "shock mounts" can be designed to have good weight or volume to energy storage ratios and have inherently good damping characteristics. As a result they have long been used in medium to light duty shock isolation applications. The principal restrictions on their range of application are environmental limitations, performance stability under long term static loading, and a limited thickness of one to two inches for satisfactory curing (for most compounds). The light to medium weight shock mounts are generally available as commercial products, in a complete range of types and sizes, so that their use usually involves selection rather than design. This discussion, consequently, is directed toward larger units which must be custom designed for specific applications.

#### 6.2.4.1 Materials, characteristics and configurations.

a. General material characteristics. Natural and synthetic rubber and rubber compounds have become available in increasing numbers and range of characteristics which are of interest in shock isolation. New compounds have greatly extended the range of temperature and chemical environment within which rubber springs and shock mounts are practical. However, the compounds that have the best environmental resistance are not necessarily

1/2 in. Anchor Bolt  
 Snap Rings  
 Case Hardened Retainer Washer

CONED DISC SPRING  
 (BELLEVILLE WASHER)  
 SHOCK ISOLATOR

Housing

36 Paired Spring Elements 15 Gage  
 1.75 O.D. + .00  
 - .03  
 .88 I.D. + .02  
 - .00  
 Depth of Deformation  
 .036 + .005  
 SAE 1095, H.T. To R/C 60

Mounting Bolts

.64  
 .64

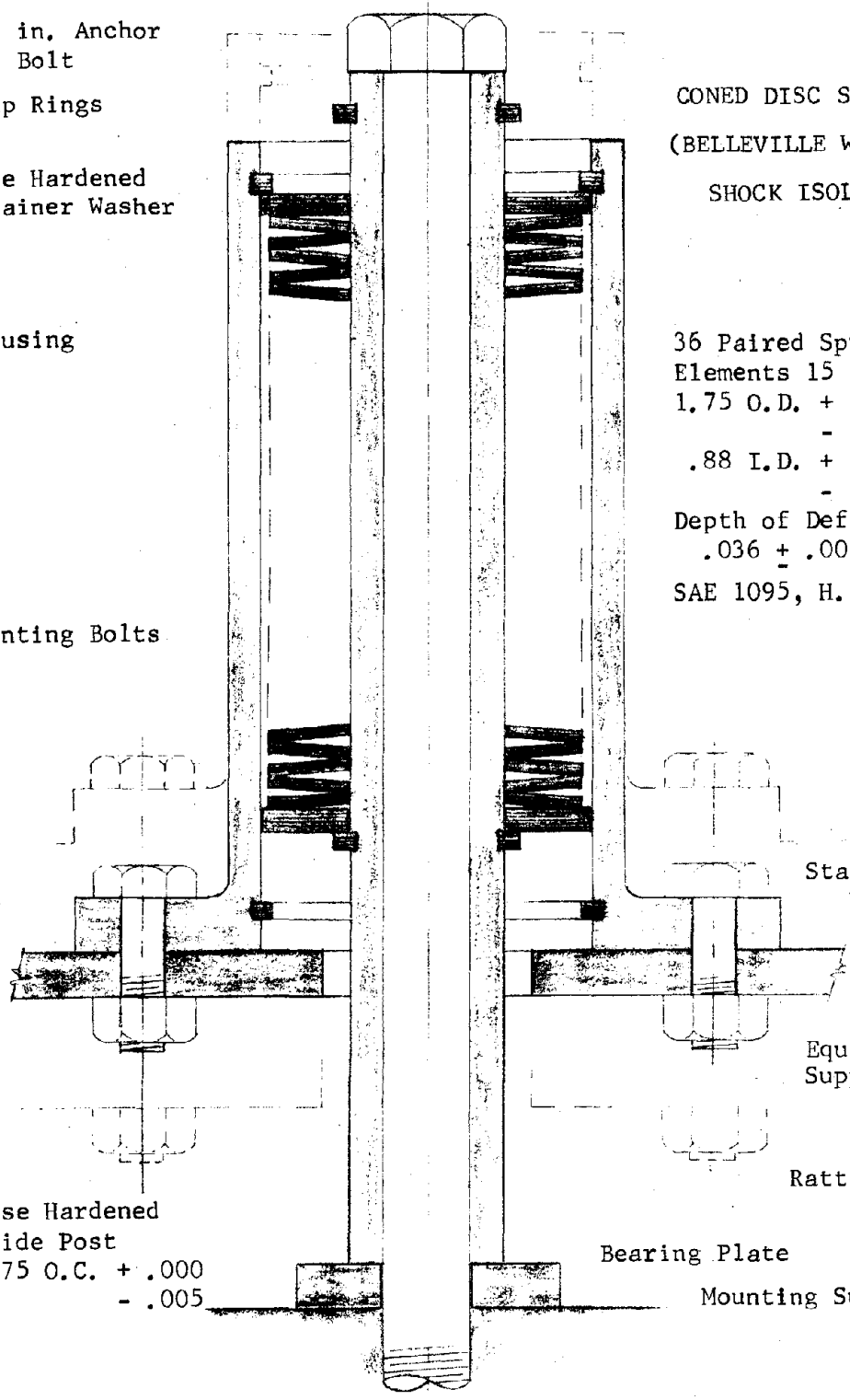
Static Load Position

Equipment Support Frame

Rattlespace

Case Hardened Guide Post  
 .875 O.C. + .000  
 - .005

Bearing Plate  
 Mounting Surface



Design Example 6.4  
 FIGURE 6.17

those with the best characteristics for shock isolation. Natural rubber is, perhaps, still the major elastomeric ingredient in most of the rubber compounds having the best all around characteristics for shock isolators. These characteristics include high tensile and shear strength, good bondability, relatively high energy storage per unit volume, good resistance to permanent set, high damping and capacity for sustaining repeated large deformations with full recovery.

Natural rubber compounds are useful in shock isolators from temperatures of about  $-50^{\circ}$  to  $+150^{\circ}$ F but have poor resistance to solvents, ozone and some other chemicals. Chloroprene (neoprene) and Buna N based compounds have good resistance to petroleum products and have better high temperature resistance than natural rubber as the temperature drops below  $0^{\circ}$ F, but Buna N tends to swell in water. Natural rubber, Chloroprene, and Buna N all show fair resistance to creep under load at moderate temperatures, and Buna N retains this advantage to relatively elevated temperatures. Both Buna N and Chloroprene are more resistant to the "aging" (hardening and cracking) effects of heat, sunlight and ozone than is natural rubber. Silicone rubber compounds have outstanding resistance to the effects of temperature, from  $-70^{\circ}$ F or lower to about  $+400^{\circ}$ F. They also have good resistance to petroleum products and chemicals, but generally have lower tear and abrasion resistance, lower tensile strength, and (except at elevated temperatures) less resistance to permanent set than the previously mentioned elastomers. Some of the newer developments in the field of elastomers such as Viton, Ethylene Propylene rubber, Chlorosulfonated Polyethylene (hypolon) and Polyurethane have properties indicating that they could be compounded to make excellent shock isolator materials but they have had only limited evaluation for that purpose to date. Most shock isolator problems requiring the more specialized elastomers are solved in cooperation with manufacturers. Consequently, the balance of this discussion will be centered around the characteristics of compounds of the widely used natural rubber, Chloroprene and Buna N.

b. Mechanical properties of the materials. The mechanical properties of the rubber compounds which must be considered in the design of rubber

springs are considerably more varied and more variable than those involved in metal spring design. Whereas the useful mechanical properties of metals are linear, and metal springs are designed to operate within the linear ranges; most of the useful mechanical properties of rubber spring materials are nonlinear, but only as functions of stress, but, to a marked degree, as functions of temperature, form and method of loading as well. Compounds of a specific rubber, which differ superficially only in durometer hardness, will vary widely in elastic moduli, tensile and shear strength and usable deformation range. The mechanical properties of a specific rubber compound of a specific durometer hardness will vary appreciably with source of supply and even among production batches from the same supplier. Finally, even durometer hardness, which is the most used single index to which other properties are related, is measured by a method that is somewhat inexact. Measurements on the same specimen may vary by as much as 5 points. Since compounds used in rubber springs cover a range of only about 50 points on the durometer scale (30 to 80) 5 points represents 10 percent of the range of interest, and, in terms of stress/deflection ratio, may represent as much as a 20 percent variation in stiffness.

With the foregoing limitations in mind it is possible to list numerical values or ranges of values for mechanical properties and to evaluate the importance of some of the factors which affect these values. Compared with room temperature characteristics, temperatures up to about 150°F for natural rubber compounds and 250°F for Chloroprene and Buna N have relatively limited effects on the elastic moduli and strength of these products, although aging and creep (permanent set under static load) are accelerated under continuous exposure to these temperatures. At temperatures below 0°F Chloroprene stiffens rapidly (by about 100 percent at - 20°F), and, except for rubbers specially compounded for low temperatures, the normal elastic moduli are unreliable for most rubber compounds below - 20°F.

There are distinct differences in the elastic moduli under static and dynamic loading, with the increased stiffness under dynamic load most apparent in the higher durometer ranges. Only limited data are available upon which to base numerical evaluation of the higher elastic moduli applicable to dynamic loading, but the effect appears to correlate more closely with



durometer hardness than with other parameters. Crede (Reference 6.2) gives values for the ratio of dynamic to static moduli versus durometer hardness that are probably as useful as any available and which may be expressed approximately as:

$$M_d/M_s = 1 + (Dh - 30)/35 \quad (6.17)$$

for the range of 30 to 80 durometer, where;  $M_d/M_s$  is the ratio of dynamic to static moduli and Dh is the durometer hardness number of the compound.

The static tangent moduli  $M_t$  in tension, in compression and in shear versus strain and durometer hardness are plotted for typical shock isolator rubber compounds in Figures 6.18, 6.19 and 6.20. Compressive stress versus deflection for typical compounds is given for a range of shape factors for 40, 50, 60 and 80 durometer hardness in Figures 6.21, 6.22, 6.23, and 6.24. (See Section 6.2.4.2 for definition of shape factors.) Shear stress versus deflection for durometer hardness numbers from 30 through 80 are given in Figure 6.25. Recommended design stress limits are also indicated in Figures 6.21 through 6.25. Although rubber springs are rarely used in tension, and tension loading of rubber to metal bonds is not considered good practice, such loading is sometimes unavoidable in rubber springs subject to combined static and dynamic loading. In such cases the rubber tensile working stresses are usually limited to a value which does not exceed the durometer hardness number of the compound expressed as psi, or 50 psi, whichever is higher. Where rubber to metal bond is in tension the maximum working stress of the bond is usually limited to 50 psi.

c. Basic rubber spring configurations. Nearly all of the numerous configurations of rubber-to-metal-bonded rubber springs in common use are variations of three types. The metal end plates or fittings are usually of steel, and the three basic configurations are:

- (1) The "sandwich" with metal plates bonded to each face of the rubber center slab (Figure 6.26a).

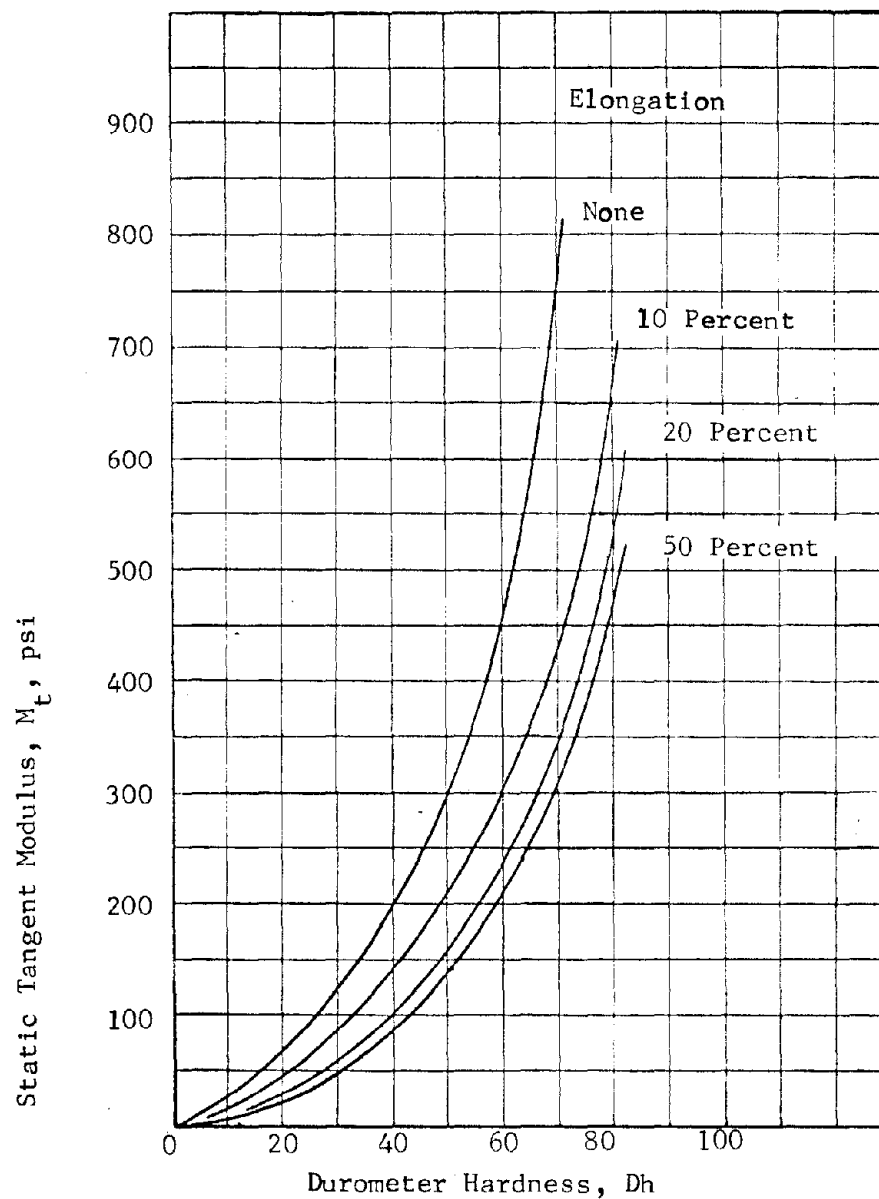


FIGURE 6.18: STATIC TANGENT MODULUS IN TENSION  
 VERSUS  
 DUROMETER HARDNESS AND STRAIN FOR  
 TYPICAL RUBBER SPRING COMPOUNDS  
 (REFERENCE 6.8)

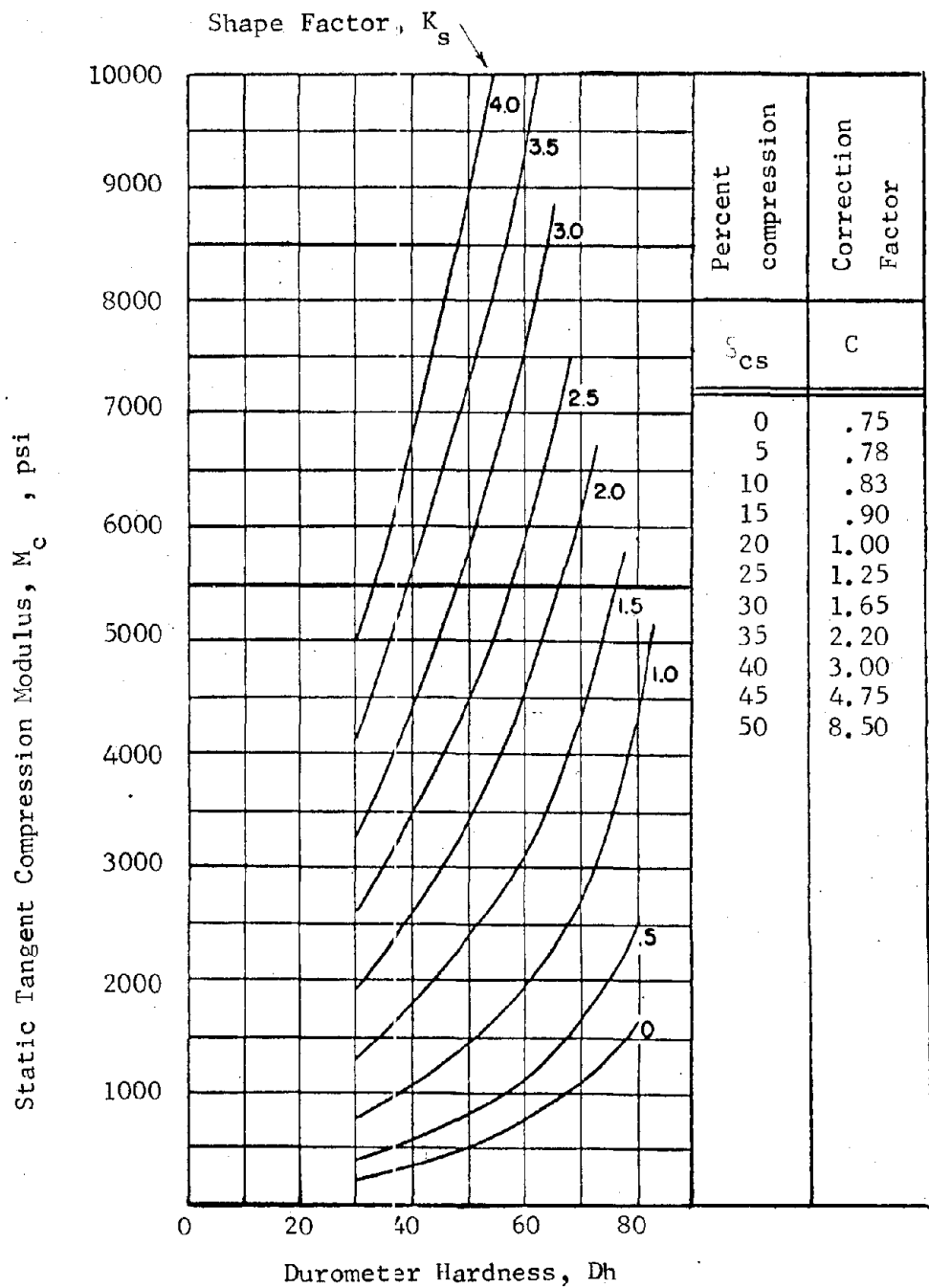


FIGURE 6.19: STATIC TANGENT MODULUS IN COMPRESSION VERSUS DUROMETER HARDNESS AND SHAPE FACTOR FOR TYPICAL RUBBER SPRING COMPOUNDS (REFERENCE 6.8)

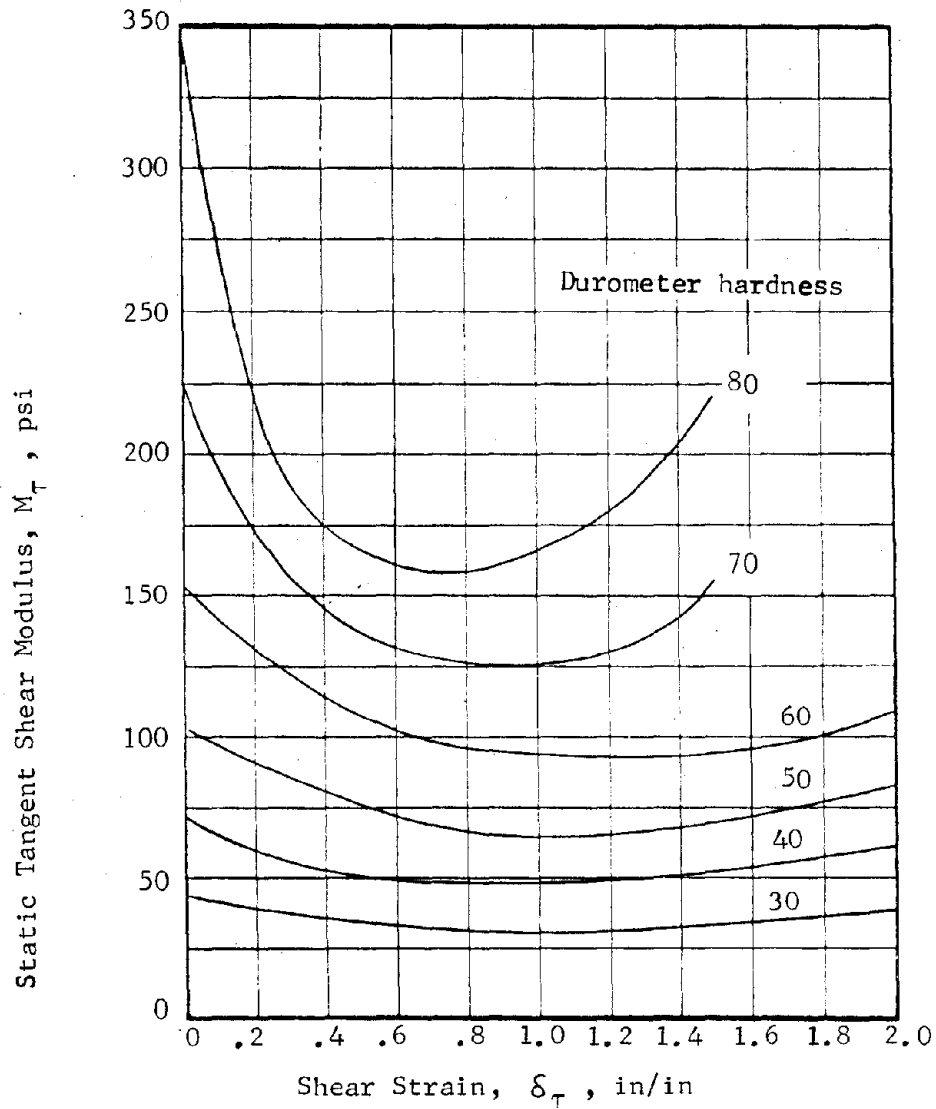


FIGURE 6.20: STATIC TANGENT SHEAR MODULUS VERSUS SHEAR STRAIN AND DUROMETER HARDNESS FOR TYPICAL RUBBER SPRING COMPOUNDS (REFERENCE 6.8)

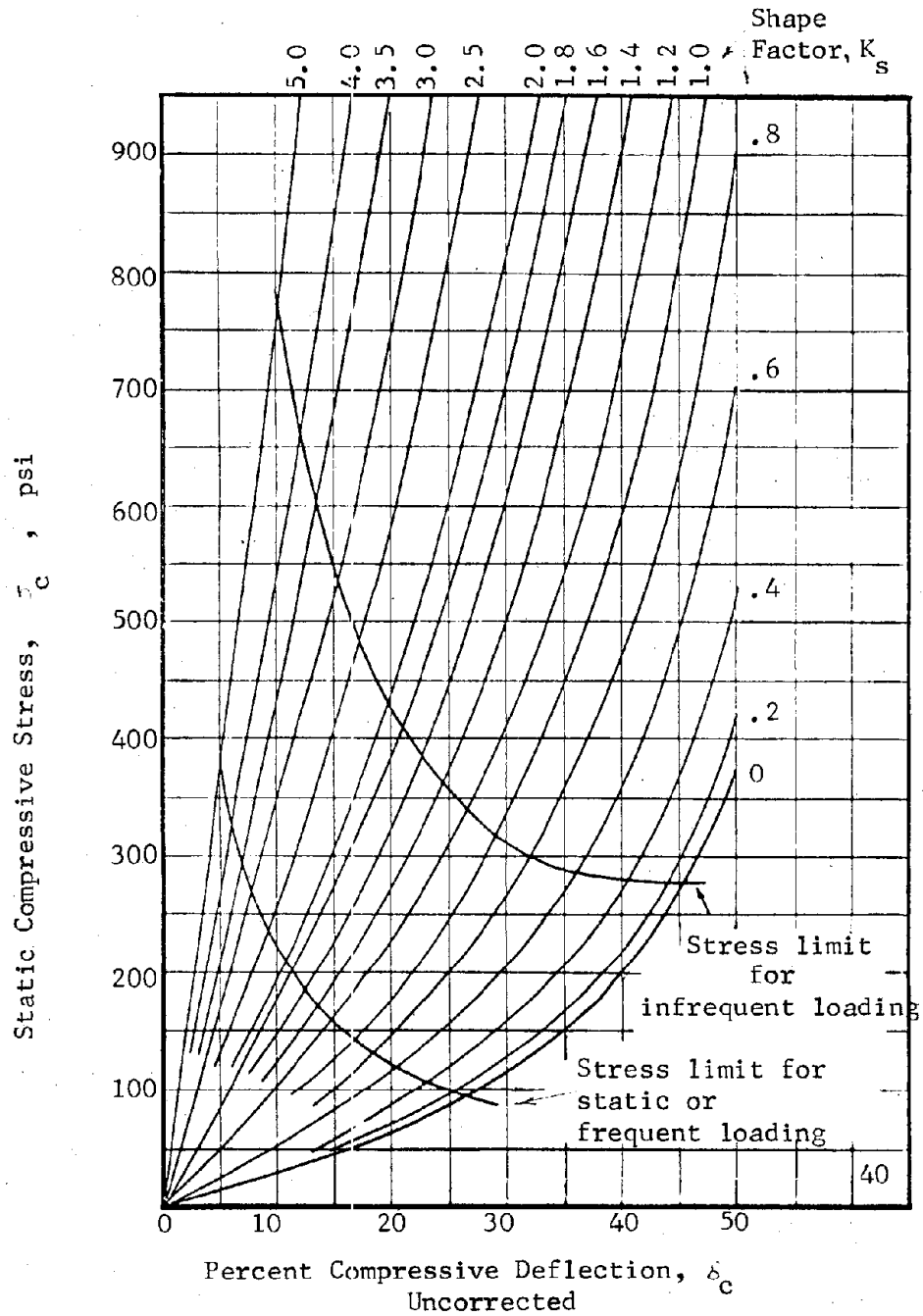


FIGURE 6.21; STATIC COMPRESSIVE STRESS VERSUS SHAPE FACTOR AND UNCORRECTED DEFLECTION FOR TYPICAL 40 DUROMETER RUBBER SPRING COMPOUNDS (REFERENCE 6.8)

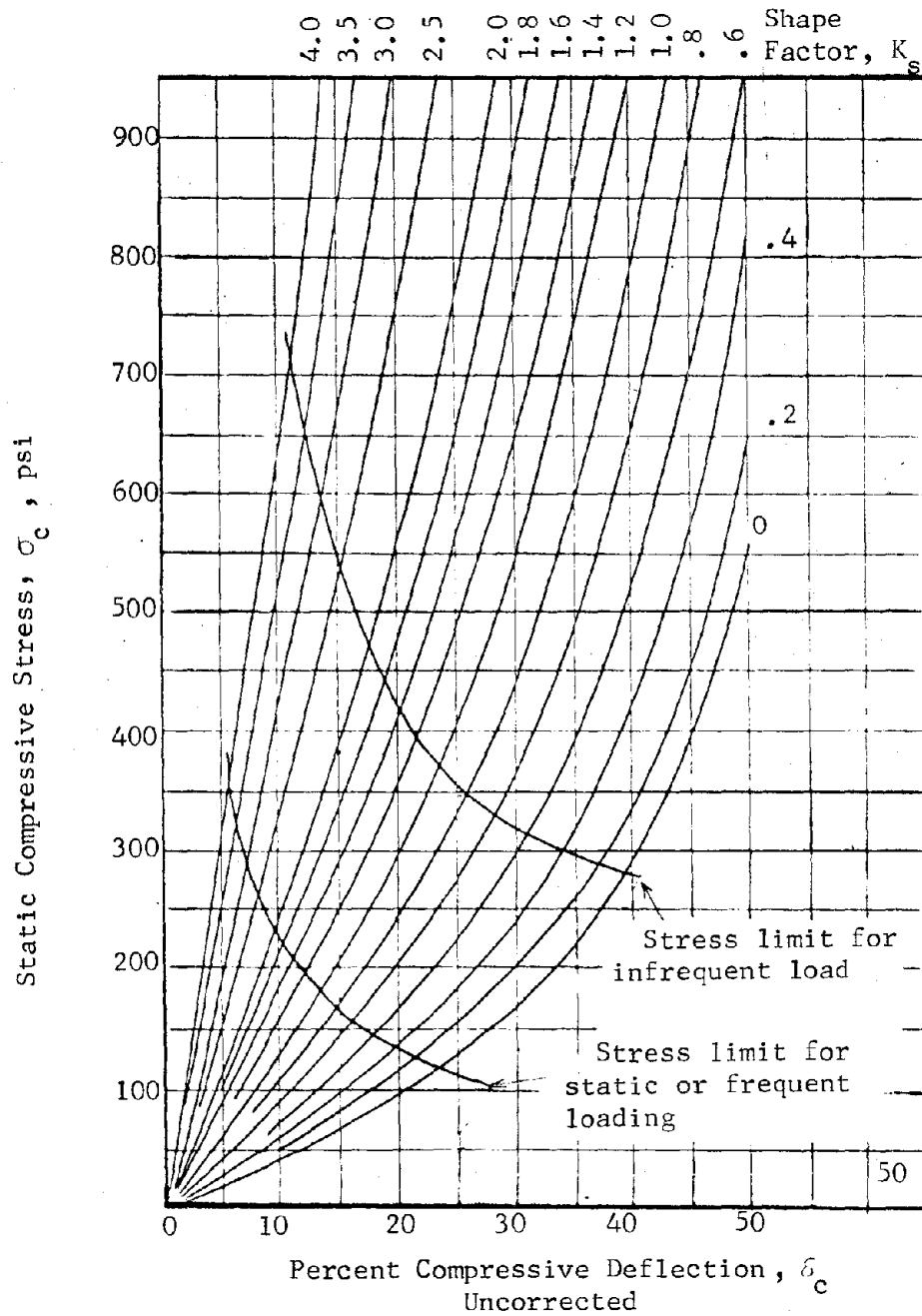


FIGURE 6.22: STATIC COMPRESSIVE STRESS VERSUS SHAPE FACTOR AND UNCORRECTED DEFLECTION FOR TYPICAL 50 DUROMETER RUBBER SPRING COMPOUNDS (REFERENCE 6.8)

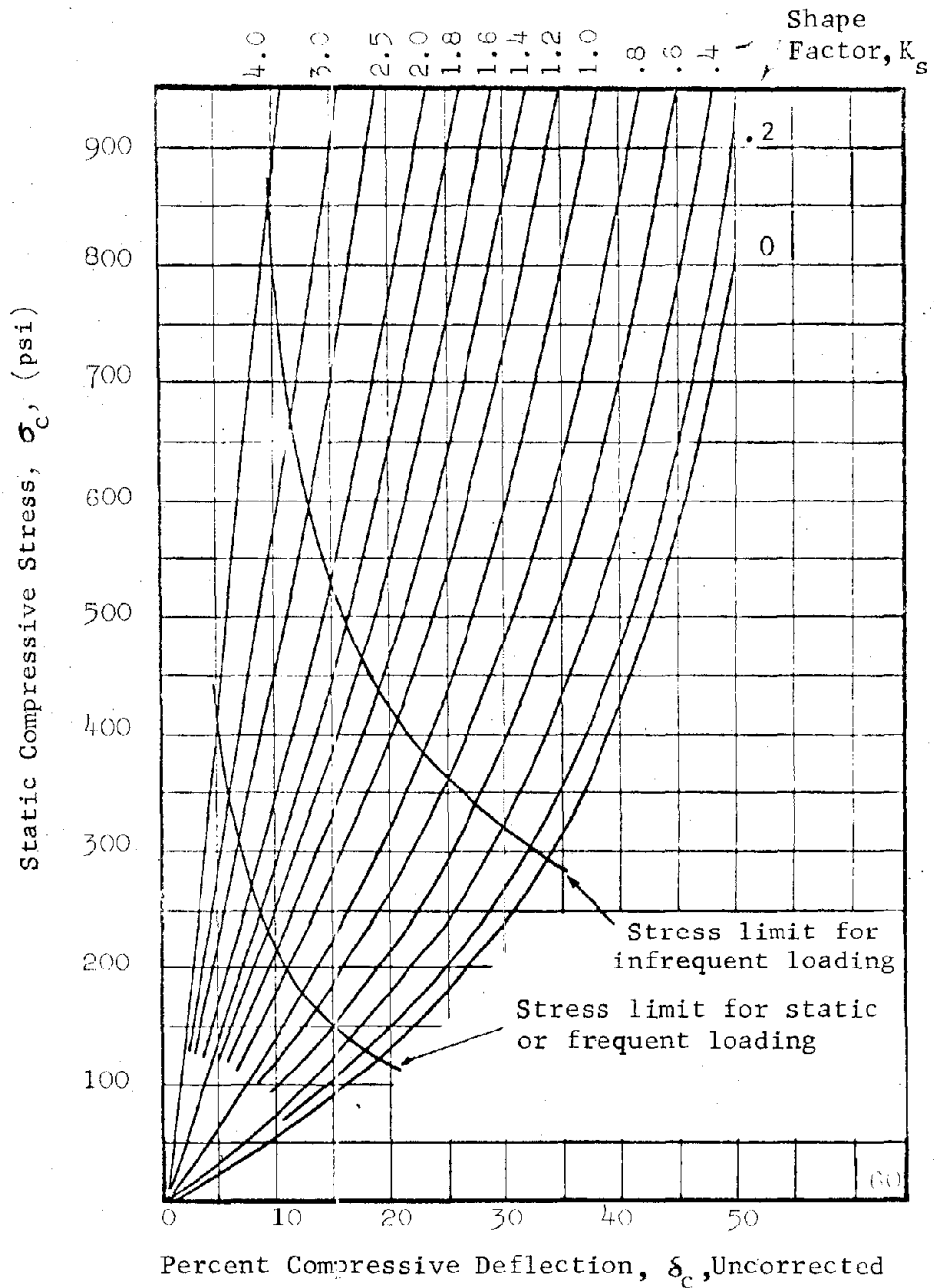


FIGURE 6.23: STATIC COMPRESSIVE STRESS VERSUS SHAPE FACTOR AND UNCORRECTED DEFLECTION FOR TYPICAL 60 DUROMETER RUBBER SPRING COMPOUNDS (REFERENCE 6.8)

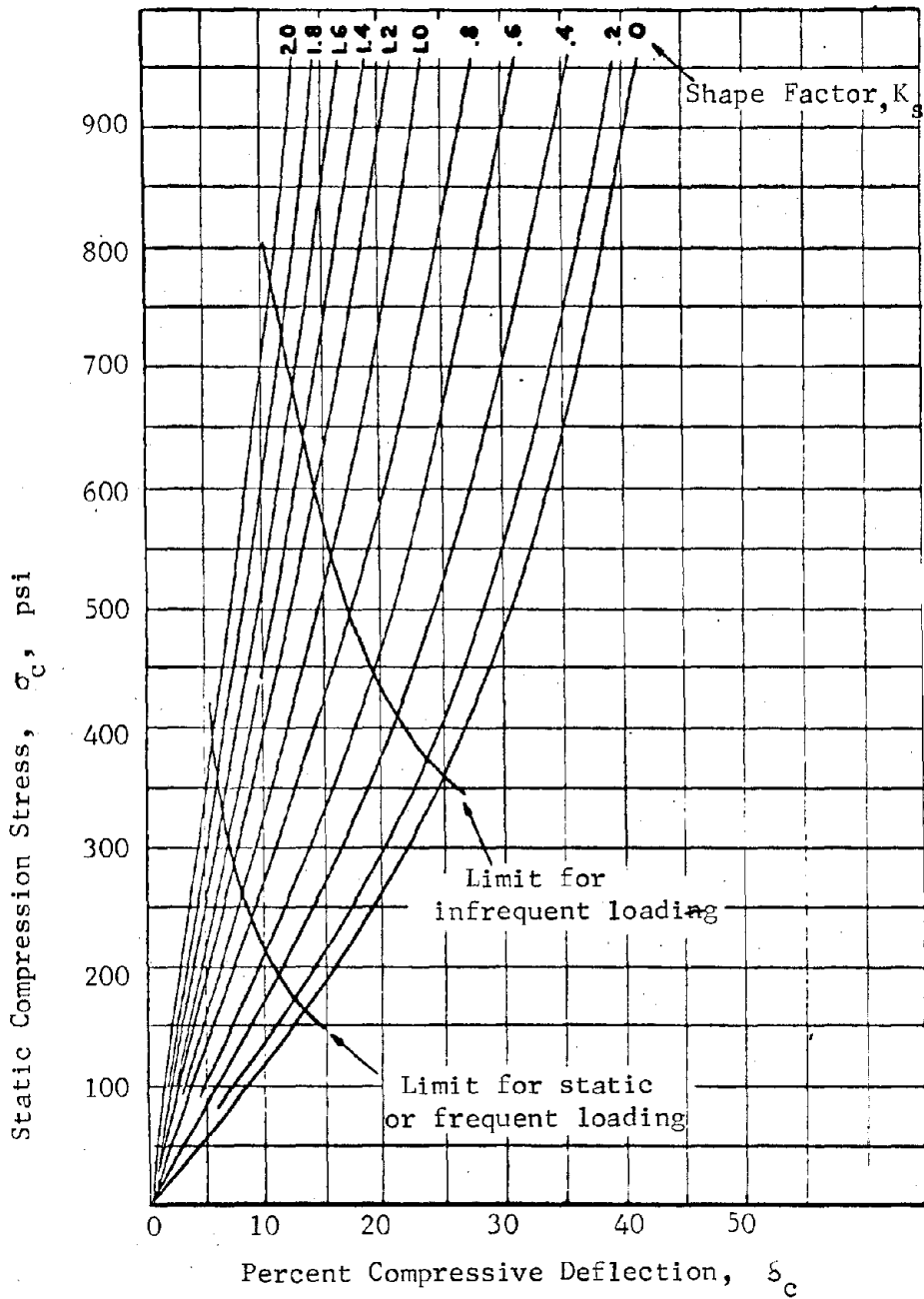


FIGURE 6.24: STATIC COMPRESSIVE STRESS VERSUS SHAPE FACTOR AND UNCORRECTED DEFLECTION FOR TYPICAL 80 DUROMETER RUBBER SPRING COMPOUNDS (REFERENCE 6.8)



Limits for  
 Static or Frequent Loading  
 Limits for  
 Infrequent Loading

Linear Shear Movement

Rotative Shear Moment

Line A-A

Line B-B

Line B-B

Line C-C

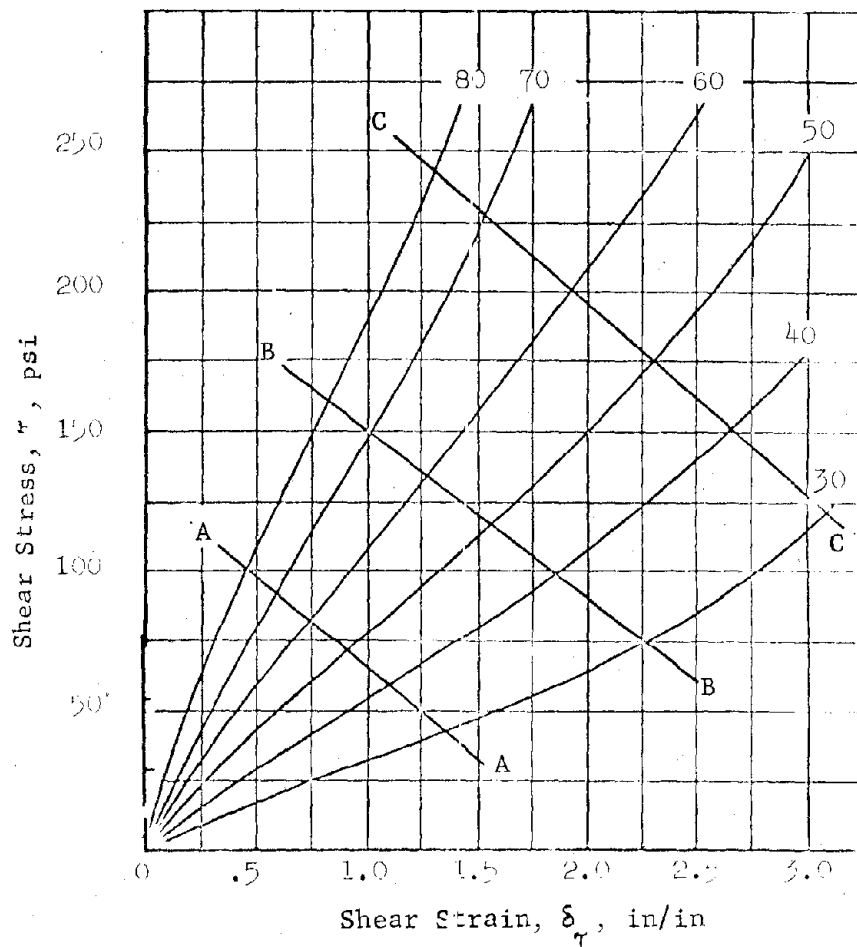


FIGURE 6.25; STATIC SHEAR STRESS VERSUS STRAIN AND DUROMETER HARDNESS FOR TYPICAL RUBBER SPRING COMPOUNDS (REFERENCE 6.8)

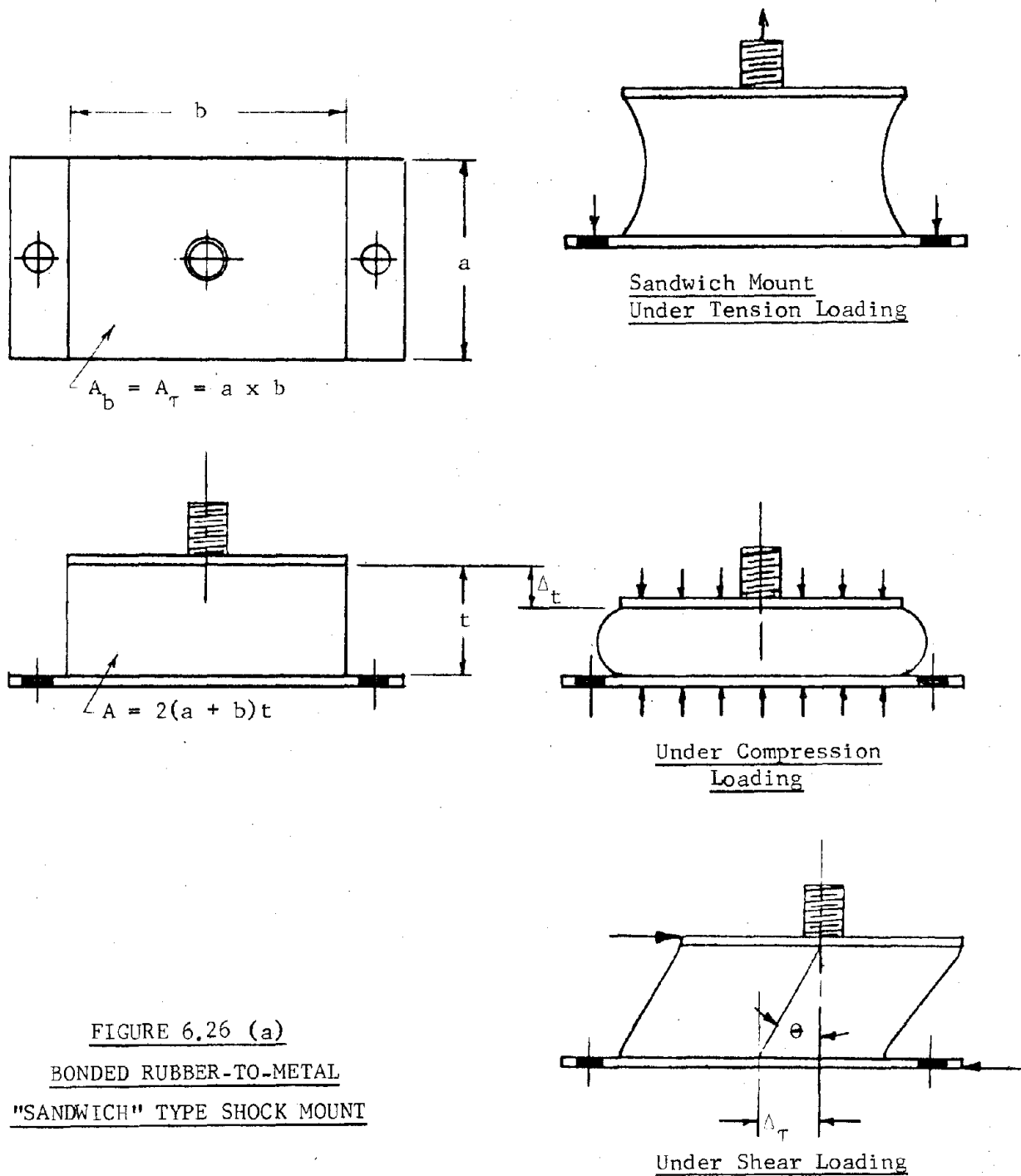


FIGURE 6.26 (a)  
BONDED RUBBER-TO-METAL  
"SANDWICH" TYPE SHOCK MOUNT

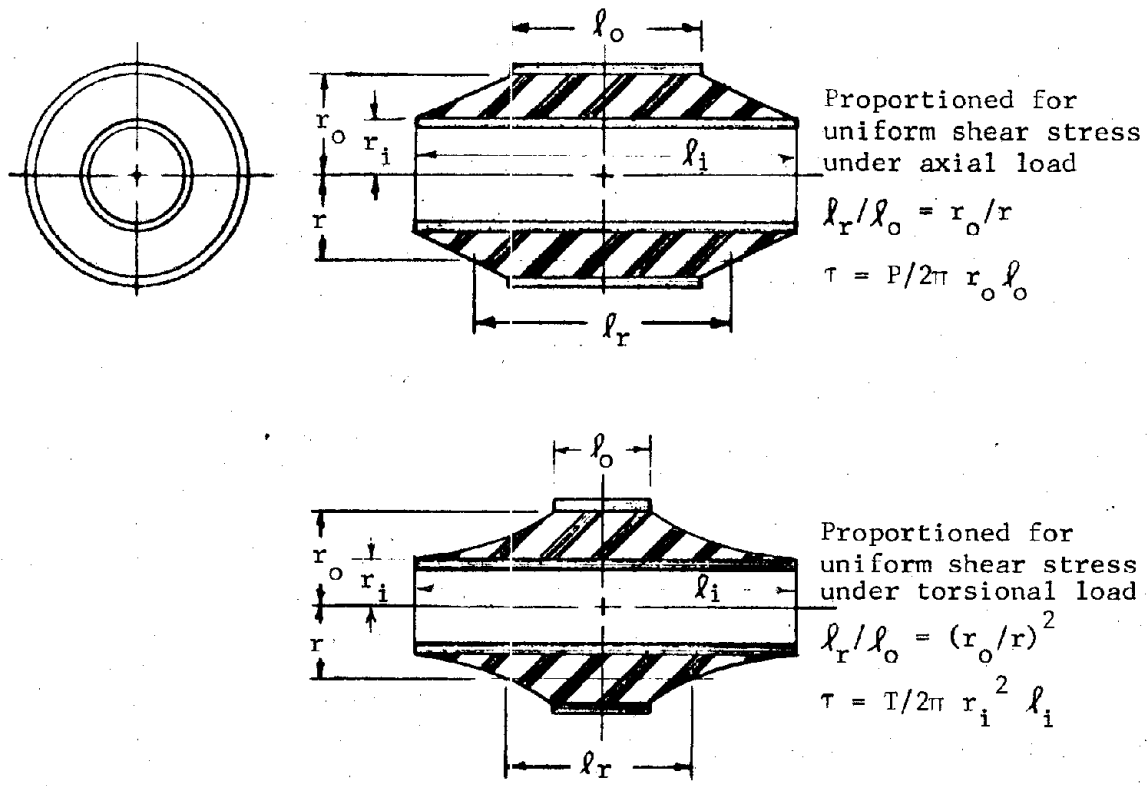


FIGURE 6.26(b): CONCENTRIC BUSHING SHOCK MOUNTS

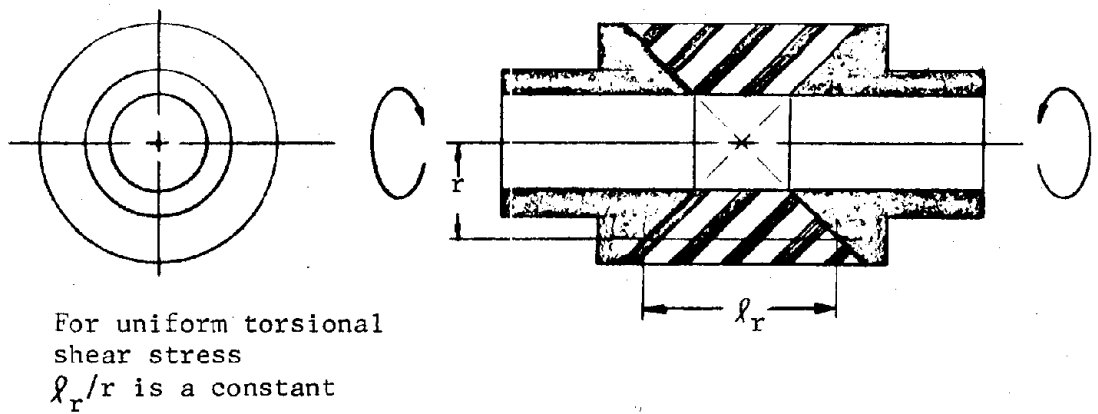


FIGURE 6.26(c): TORSIONAL SHEAR DISC SHOCK ISOLATING COUPLING

- (2) The concentric bushing configuration, in which two concentric metal bushings are separated by, and bonded to, an annular rubber spring (Figure 6.26b).
- (3) The torsional shear disc, or coupling (Figure 6.26c) consisting of two truncated conical metal fittings, co-axially assembled (with the small ends opposed) and bonded to a rubber centerpiece. The torsional shear strain (and stress) in the rubber is equalized by a variation in rubber thickness, parallel to the axis of torsion, so that at any point the axial dimension is approximately proportional to the radial distance.

The "sandwich" type rubber spring is widely used as a heavy duty compression mount, for various combined loadings, and to a limited extent in applications where the major loading is linear shear or tension. The "concentric bushing" is, perhaps, most commonly used under combined axial shear and radial (compression-tension-shear) loading. Typically the axial bond length between rubber and inner bushing is much greater than that along the outer bushing in order to provide approximately equal bond areas and uniform shear stresses. A wide variation in axial to radial spring rate can be obtained by varying the radial to axial proportions of the rubber. Where a high ratio of lateral to axial stiffness is required the circumferential bond length is so much greater at the outer periphery of the rubber than at the center bushing that the necessary outer bond area can often be provided by a plate extending a short distance into the outside diameter of the rubber. Variations of this configuration are widely used for light equipment shock mounting. The "torsional shear disc" rubber springs, as the name implies are used largely to reduce shock and vibration loading transmitted in torsion, as in shaft couplings.

6.2.4.2 Rubber spring design. The large number of variables together with some variation in properties of compounds that are nominally identical make the design of rubber springs a rather inexact procedure and one in which the critical performance characteristics of all designs should be confirmed by test. For this reason all design of prototype rubber springs in which wide latitude of performance is not permissible, must be regarded as preliminary design.

a. Rubber compression springs. Since rubber has a high bulk modulus, relative to its useful stress range, it can be treated, for all practical purposes, as being capable of deformation in the direction of compressive stress only where lateral expansion is also possible. The effective compressive tangent modulus is strongly influenced by the resistance to lateral expansion. Given a slab of rubber of thickness,  $t$ , bonded, loaded area,  $A_b$ , and otherwise unrestrained peripheral surface area,  $A_p$ , normal to the loaded area, it has been found experimentally that the lateral restraint effect of the rubber itself may be expressed as a "shape" factor,  $K_s$ , which is the ratio of the loaded area to the unrestrained peripheral area, or  $K_s = A_b/A_p$ , where  $A_p$  includes the free surface areas of the rubber in all holes through the slab (in the direction of loading) as well as the free peripheral area, and  $A_b$  excludes the cross section areas (normal to the direction of loading) of all such holes. For any specific average compressive stress,  $\sigma_c (= P/A_b)$ , and shape factor,  $K_s$ , Figures 6.21 through 6.24 give the uncorrected static deflection,  $\delta_{cs}$ , as a percentage of  $t$ , for various values of durometer hardness, and Figure 6.19 gives the corresponding, uncorrected static compressive modulus,  $M_c$ . In the inset table on Figure 6.19 the correction factor,  $C_\delta$ , corresponding to  $\delta_{cs}$  can be found. The corrected static compressive modulus,  $M'_c$ , for the specific load, durometer number and rubber configuration is then  $M'_c = C_\delta M_c$ , and the corresponding dynamic modulus  $M'_{cd}$  is found from Equation 6.15 as  $M'_{cd} = M'_c \left[ 1 + (Dh - 30)/35 \right]$ .

Corrected values of percent deflection and spring rates may be computed from the corrected compressive moduli as:

$$\delta'_{cs} = 100 \frac{\sigma_c}{M'_c} \qquad k_c = \frac{M'_c A_b}{t} \qquad (6.18a)$$

$$\delta'_{cd} = 100 \frac{\sigma_c}{M'_{cd}} \qquad k_{cd} = \frac{M'_{cd} A_b}{t} \qquad (6.18b)$$

Corrected values of  $\delta_c$  should not exceed the recommended limits indicated on Figures 6.21 through 6.24. Maximum values of  $\delta'_{cd}$  due to infrequent shock loading can approach the upper limit, but values reflecting static and vibration loadings should not exceed the lower limits. Modifications of existing designs, for larger or smaller loads, or to accommodate new clearances, are facilitated by application of the axiom that "rubber sandwich compression

mounts having the same shape factor and the same average unit compressive stress will deflect the same percentage of their respective thicknesses."

b. Rubber shear spring design. Rubber springs used primarily in shear may be designed in any of the three basic configurations discussed in Section 6.2.4.1 c and illustrated in Figure 6.26. Regardless of configuration the shear strains,  $\delta_\tau$ , will be very large compared to those in metal springs, and the usual assumption in shear formulae that the shear angle  $\theta = \tan \theta$  is not valid. For the present application shear strain is defined as:

$$\delta_\tau = \Delta_\tau/t = \tan \theta$$

where  $\Delta_\tau$  is total shear deformation, or deflection. Recommended limits for working values of  $\delta_\tau$  are given in Figure 6.25. (It will be noted that total strain rather than percentage is used here.)

(1) Analysis of "sandwich" type (Figure 6.26a) rubber springs under shear loading The strains and spring rates for prismatic sandwich type rubber springs under pure shear loading are relatively simpler to compute than under compression loading. Since the shape factor does not enter, the expressions for static loading may be written:

$$\delta_{\tau S} = \tau/M_{\tau S}$$

$$\text{and } k_{\tau S} = M_{\tau S} A_\tau/t \quad (6.19a)$$

where  $\tau$  is the lateral load divided by shear area,  $F/A_\tau$ , and  $M_{\tau S}$  is the static tangent shear modulus for the specific durometer hardness and shear strain,  $\delta_\tau$ . For any given unit stress,  $\tau$ , and durometer hardness a corresponding value of  $\delta_\tau$  may be obtained from Figure 6.25. For the indicated value of  $\delta_\tau$  and Dh,  $M_{\tau S}$  may then be determined from Figure 6.20.  $M_\tau$  for dynamic loading is found by the application of the correction factor defined by Equation 6.16:

$$M_{\tau d} = M_{\tau S} \left[ 1 + (Dh - 30)/35 \right]$$

and consequently:

$$\delta_{\tau d} = \tau/M_{\tau d}$$

$$k_{\tau d} = M_{\tau d} A_\tau/t \quad (6.19b)$$

(2) Concentric bushing rubber springs (Figure 6.26b) under axial loading

Constant stress configuration If a concentric bushing type rubber spring is so proportioned that the length of rubber,  $l_r$ , measured parallel to the axis at any radial distance,  $r$ , is inversely proportional to  $r$ , the cylindrical shear area,  $A_r$ , will be constant for all values of  $r$ , i.e.  $A_r = 2 \pi r l_r$ . The shear stress under a static axial load,  $P$ , is then  $\tau = P/2 \pi r_o h_o$ , where  $r_o$  and  $h_o$  are the outside radius and length, respectively, of the rubber. The total static deflection,  $\Delta_{\tau s}$ , parallel to the axis will be:

$$\Delta_{\tau s} = P (r_o - r_i) \delta_{\tau s} / 2 \pi r_o h_o \tau = (r_o - r_i) \delta_{\tau s}$$

where  $r_i$  is the inside radius of the rubber and  $\delta_{\tau s}$  is obtained from Figure 6.23.  $M_r$  can also be taken from Figure 6.19 and the static spring constant calculated as:

$$k_{\tau s} = P / \Delta_{\tau s} \quad (6.20a)$$

For dynamic loading  $M_{\tau d}$ , and  $\delta_{\tau d}$  are computed as in (1) above, and the dynamic spring constant is:

$$k_{\tau d} = k_{\tau s} M_{\tau d} / M_{\tau s} \quad (6.20b)$$

Constant length configuration Where the length of rubber, parallel to the axis, is constant the shear area and shear stress under axial load will vary inversely with  $r$ . If values of  $\tau$  are computed for successive values of  $r$  varying in small increments from  $r_o$  to  $r_i$  the corresponding values of  $\delta_r$  and  $M_r$  may be obtained from Figures 6.25 and 6.20 respectively. At any value of  $r$  the incremental deflection  $\delta_r = \tau_r / M_r$ , and the total deflection is:

$$\Delta_{\tau} = \int_{r_o}^{r_i} \left( \tau_r / M_r \right) dr$$

Since the values of  $M_r$  do not follow a specific mathematical expression it is necessary to perform the indicated integration graphically, or arithmetically by a finite increment method. Since the values of  $\delta_r$  and  $M_r$  are only approximate, the use of many increments of  $r$  to improve accuracy is probably unwarranted.

(3) Concentric bushing springs (Figure 6.26b) under torsional load

Constant stress configuration The shear stress,  $\tau$ , at a

cylindrical surface at any radius,  $r$ , from  $r = r_i$  to  $r = r_o$ , in a concentric bushing type of rubber spring may be expressed as:  $\tau_r = T/rA_r$ , where  $T$  is the applied torque and  $A_r$  is the area of the cylindrical surface at radius  $r$ . To obtain a constant shear stress, then,  $rA_r$  or  $2\pi r^2 \ell_r$  must be constant, and  $\ell_r$  must vary inversely as  $r^2$ , i.e.  $\ell_r = T/(2\pi \tau r^2)$ . For this configuration  $\ell_r = \ell_i r_i^2/r_o^2$  where  $\ell_i$  is the length of rubber (measured parallel to the axis) bonded to the inner bushing, and

$$\tau = T/(2\pi r_i^2 \ell_i)$$

Using  $\tau$  and the Dh number,  $\delta_{\tau s}$  and  $M_{\tau s}$  may be obtained from Figures 6.25 and 6.19, and the incremental static torsional deflection angle,  $d\theta$ , can be expressed as:

$$d\theta = \frac{dr}{r} \tan \frac{\tau}{M_{\tau}}$$

The angular deflection (in radians) is found to be:

$$\theta = \tan \left[ \frac{T}{2\pi r_i^2 \ell_i M_{\tau}} \right] \ln \left[ \frac{r_o}{r_i} \right]$$

(For derivation see Reference 6.1).

The spring rate is expressed as:  $k_{\theta} = \frac{T}{\theta}$  giving the following equations for the static and dynamic spring rates:

$$k_{\theta s} = \frac{T}{\tan \left[ \frac{T}{2\pi r_i^2 \ell_i M_{\tau}} \right] \ln \left[ \frac{r_o}{r_i} \right]} \quad (6.21a)$$

$$k_{\theta d} = k_{\theta s} \left[ \frac{M_{\tau d}}{M_{\tau s}} \right] \quad (6.21b)$$

(the units are: in - lb/rad.)

Constant length configuration When a torsion load is applied to a concentric bushing spring having a constant length of rubber,  $\ell$ , (measured parallel to the axis) the shear stress on a cylindrical surface at any radius,  $r$ , between  $r_o$  and  $r_i$  varies inversely as the value  $r^2$ . The maximum shear



stress,  $\tau_m$ , will occur at  $r = r_i$ .

$$\tau_m = T/2\pi r_i^2 \ell$$

The shear stress at any radius is then:

$$\tau_r = \tau_m (r_i/r)^2 = T/2\pi r^2 \ell$$

The shear strain,  $\delta_r$ , is obtained from Figure 6.25 for the shear stress calculated above (at any radius  $r$ ) and the shear modulus,  $M_r$ , is then obtained from Figure 6.18. Considering small increments where the stress is essentially constant between two radii ( $r_1$  to  $r_2$ ) the spring rate over the constant length shell of radii  $r_1$  and  $r_2$  is: (see Reference 6.2 for derivation)

$$(k_\theta)_{12} = \frac{4\pi \ell M_r}{\left[1/r_1\right]^2 - \left[1/r_2\right]^2}$$

accordingly the resultant spring rate for  $n$  concentric shells of radii  $r_1$  to  $r_{n+1}$  is:

$$\frac{1}{k_\theta} = \frac{1}{(k_\theta)_{12}} + \frac{1}{(k_\theta)_{23}} + \dots + \frac{1}{(k_\theta)_{n(n+1)}}$$

If the shear modulus does not vary significantly for the stress levels between  $r_i$  and  $r_o$ , then the spring rate can be defined in terms of a constant  $M_r$ . The static and dynamic spring rates are then:

$$k_{\theta s} = \frac{4\pi M_r}{(1/r_i)^2 - (1/r_o)^2} \quad (6.22a)$$

$$k_{\theta d} = k_{\theta s} \left[ \frac{M_{rd}}{M_{rs}} \right] \quad (6.22b)$$

(the units are: in-lbs/rad)

#### 6.2.4.3 Design example 6.5: rubber spring shock isolation system.

##### a. Given:

- (1) Rigid Package (battery) 14" wide, 26" high, 30" long weighing 1400 lbs. c.g. of mass at c.g. of volume.
- (2) Maximum permissible natural frequency of system (a) vertical 10 cps  
(b) horizontal 15 cps

Design example 6.5 (continued)

- (3) Maximum accelerations, vertical (up or down) combined with horizontal (any direction) 25 g's each (35.4 g resultant maximum).
- (4) No rattlespace restrictions.

b. Solution:

- (1) De-couple vertically and horizontal x modes by: (a) separate vertical and horizontal isolation systems, (b) mounting horizontal system symmetrically about c.g. and in horizontal plane of c.g., and (c) using a vertical isolation system symmetrical about vertical axis thru c.g. (see Figure 6.27), (d) design horizontal isolators for minimal stiffness in vertical direction and vertical isolators for minimal stiffness in the horizontal direction, (e) neglect spring constants of mounting frame and battery (i.e. treat as rigid).

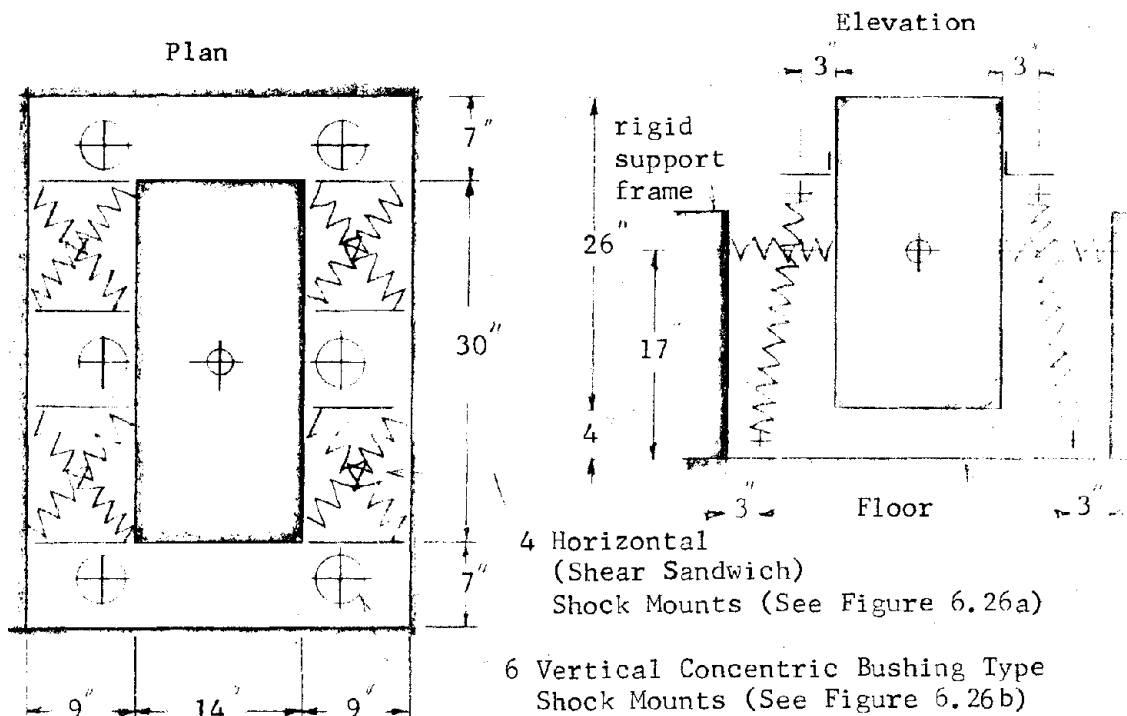


FIGURE 6.27: BATTERY SHOCK ISOLATION SYSTEM SCHEMATIC DESIGN EXAMPLE 6.5

Design example 6.5 (continued)

c. Spring rates and deflections:

(1) Horizontal shear mounts. Assume 40 Dh rubber.

- (a) Maximum permissible average dynamic spring rate with 4 isolators active in any direction.

$$(\text{ave})k_{xd} \leq .102 f_n^2 W/4 = .102 \times 15^2 \times 1400/4 = 8020 \text{ lbs/in}$$

- (b) Dynamic deflection:  $\Delta_{xd} \geq 25 \times \frac{1400}{4 \times 8020} = 1.09''$

- (c) Equivalent static spring rate from Equation 6.17,

$$\begin{aligned} (\text{ave})k_{xs} &\leq k_{xd} / \left[ 1 + (\text{Dh} - 30)/35 \right] \\ &\leq 8020 / \left[ 1 + (40 - 30)/35 \right] = 8020/1.29 = 6200 \text{ lbs/in} \end{aligned}$$

- (d) Equivalent static deflection:  $\Delta_{xs} \geq 25 \times \frac{1400}{4 \times 8020} \geq 1.41''$

(2) Vertical shear mounts. Assume 30 Dh rubber.

- (a) Maximum average dynamic spring rate for 6 isolators

$$k_{yd} \leq .102 \times 10^2 \times 1400/6 = 2380 \text{ lbs/in}$$

- (b) Equivalent static spring rate

$$k_{ys} \leq 2380 / \left[ 1 + (30 - 30)/35 \right] = 2380 \text{ lbs/in}$$

- (c) Static and dynamic deflection

$$\Delta_{ys} = \Delta_{yd} \geq 26 \times \frac{1400}{6 \times 2380} = 2.55''$$

d. Horizontal isolator design:

- (1) From Figure 6.25 the maximum applicable shear strain value for 40 Dh rubber and defined by line B is:

$$\begin{aligned} \delta_\tau &= 1.8 \quad ; \quad \text{the corresponding value of } \tau \leq 100 \text{ psi,} \\ \text{and } M_{\tau s} &= \tau / \delta_\tau = 100/1.8 = 55.5 \text{ psi, which is in agreement with the} \\ &\text{value of } M_{\tau s} \text{ found in Figure 6.20.} \end{aligned}$$

- (2) Slab thickness  $t \geq \Delta_{xs} / \delta_\tau = 1.41/1.8 = .784$ , say .8"

- (3) Bond and shear area at  $\tau = 100$  psi and  $F = 8750$  lbs:

$$A_\tau = 8750/100 = 87.50 \text{ sq. in., say (2) 4" x 11" slabs.}$$

(See Figure 6.28)

Design example 6.5 (continued)

(4) Recheck deflection and spring constant

(a)  $A_T = 2 \times 4 \times 11 = 88 \text{ sq in}$

$\tau_d = 8750/88 = 99.5 \text{ psi}$

$D_h = 40$

(b) From Figure 6.25;

$\Delta_T = 1.87 = \Delta_{XS}/t$

$\Delta_{XS} = 1.87 \times .8 = 1.49''$

$\Delta_{xd} = 1.49/1.29 = 1.16''$  and

$k_{Td} = 8750/1.16$

$= 7540 \text{ lb/in} < 8020 \text{ lb/in, O.K.}$

2, 4" x 11"  
rubber  
slabs  
bonded to  
10 ga. steel  
plate

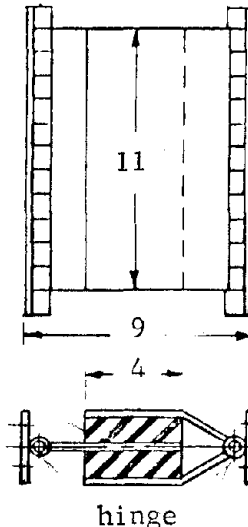


FIGURE 6.28: RUBBER SHEAR SANDWICH TYPE SHOCK ISOLATOR

(5) Deflection clearance: Since both  $M_{TS}$  and  $M_{Td}$  are approximate values, allow space for an average deflection  $\Delta_{CL} = (1.49 + 1.14)/2 = 1.3$ , say

(6) Total rattlespace required by horizontal isolators: 1 3/8"

(a) Each end: 1 3/8 (deflection) + 5/8 clear, say 2"

(b) Each side:  $2 \times 1 \frac{3}{8} + 4 + 2''$  (hardware) = 8 3/4, say 9"

e. Vertical isolator design:  $D_h = 30$ , Concentric Bushing Type, Constant Stress Configuration:  $\Delta_{yd} = 2.55''$ , minimum bottom to floor distance: about 3.0"

(1) From Figure 6.25, maximum useful  $\delta_T = 2.25$

$\tau = 75 \text{ psi}$  and  $M_{TS} = M_{Td} = 75/2.25 = 33.3 \text{ psi}$

(2)  $t \geq \Delta_{ys}/\delta_T \geq 2.55/2.25 \geq 1.13''$

(3) (a) Required shear and bond area =  $6,070/75 = 82.2 \text{ sq. in.}$

(b) If the length of the inner bushing bond length,  $h_i$ , is to be held to about 12 inches, the inner bushing circumference required will be about  $A/\ell = 82.2/12 = 6.83''$  and the bushing  $6.83/\pi = 2.18''$ :  
Use 2" Sched.40 pipe; 2.38" O.D.

Design example 6.5 (continued)

(c) Inside rubber and bond length

$$l_i = 82.2 / 2.38\pi = 11''$$

(d) Inside diameter outer bushing  $2.38 + 2 \times 1.13 = 4.64''$

Use 5" x .12" wall tubing I.D. = 4.76" ;  $t = 1.19''$

Required bond and rubber length at outer bushing

$$l_o = 2.38 \times 1.19 / 4.76 = 5.5''$$

(4) Check spring rate and deflection,  $P_y = 26 \times \frac{1400}{6} = 6070$  lbs

(a)  $A_r = 4.76\pi \times 5.5 = 82.2$  sq. in. ,  $\tau = 6,070 / 82.2 = 74$  psi

from Figure 6.23:  $\delta_r \cong 2.25$  ,  $\Delta_y = 2.25 \times 1.19 = 2.68'' > 2.55''$ , O.K.

(b)  $k_{rs} = k_{rd} = 6070 / 2.68 = 2320 < 2550$  lbs/inch, O.K.

(5) Provide horizontal rattlespace for vertical mounts, 5" outer tube + 1 3/8" response deflection + 5/8" clearance for construction tolerance = 7", total minimum clearance required. (See Figure 6.29.)

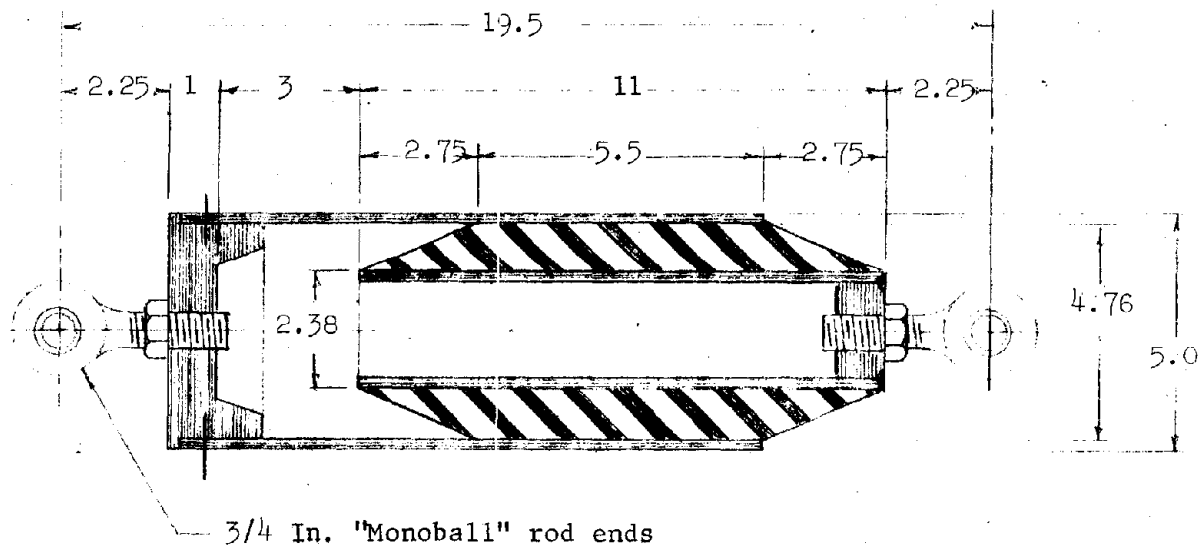


FIGURE 6.29: VERTICAL SHOCK ISOLATOR CONCENTRIC BUSHING TYPE FOR DESIGN EXAMPLE 6.5

## 6.3 Pneumatic Springs

6.3.1 Applications, types and configurations. Pneumatic springs are used in much the same types of applications as coil springs in compression or tension for shock isolation requirements.

There are two major advantages of air springs in general. One of these is their capability of being maintained at a relatively constant length (or height) over a wide range of static loads by varying the absolute air content (and internal pressure) by means of an external source of supply. The other advantage is the feasibility of highly non-linear spring rates and designs that will have relatively low spring rates over a pre-selected, limited, portion of the total displacement range and much higher and selectively non-linear spring rates over the remainder of the displacement range. Their chief disadvantages are relatively fragile construction, higher cost and limited life compared to metal springs.

The principal types of pneumatic springs may be classified, by method of piston seal, as ring sealed or "rolling bellows" sealed; and by the number of sealed compartments as single acting and double acting or "compound" cylinders. Single acting cylinders have only a single sealed compartment between piston and cylinder head. Double acting cylinders are closed at each end.

A variety of effects and system characteristic variations may be introduced by regulation of air flow between the cylinder chamber and a reservoir tank. Some of the system modifications possible are:

- (1) Velocity sensitive damping by use of a fixed orifice between chamber and reservoir.
- (2) Displacement sensitive damping by variable orifice controlled by differential pressure between chamber and reservoir.
- (3) A nearly constant height can be maintained under slowly changing static load by increasing or decreasing system air content using an external air supply and a displacement sensitive servo system controlling inlet and exhaust valves.
- (4) A constant height under widely varying temperature can be achieved by the same system described in (3).

The basic design principles for pneumatic springs are covered in the following two sections. Section 6.3.2 covers the ring sealed cylinder spring type with and without the effects of a reservoir and Section 6.3.3 covers the rolling bellows and air bag spring type concepts.

### 6.3.2 Pneumatic cylinder springs

a. Spring characteristics. A pneumatic cylinder spring obtains its resiliency by the compressibility of the gas contained in a cylinder. The two basic configurations are shown schematically in Figure 6.30 (a)(b).

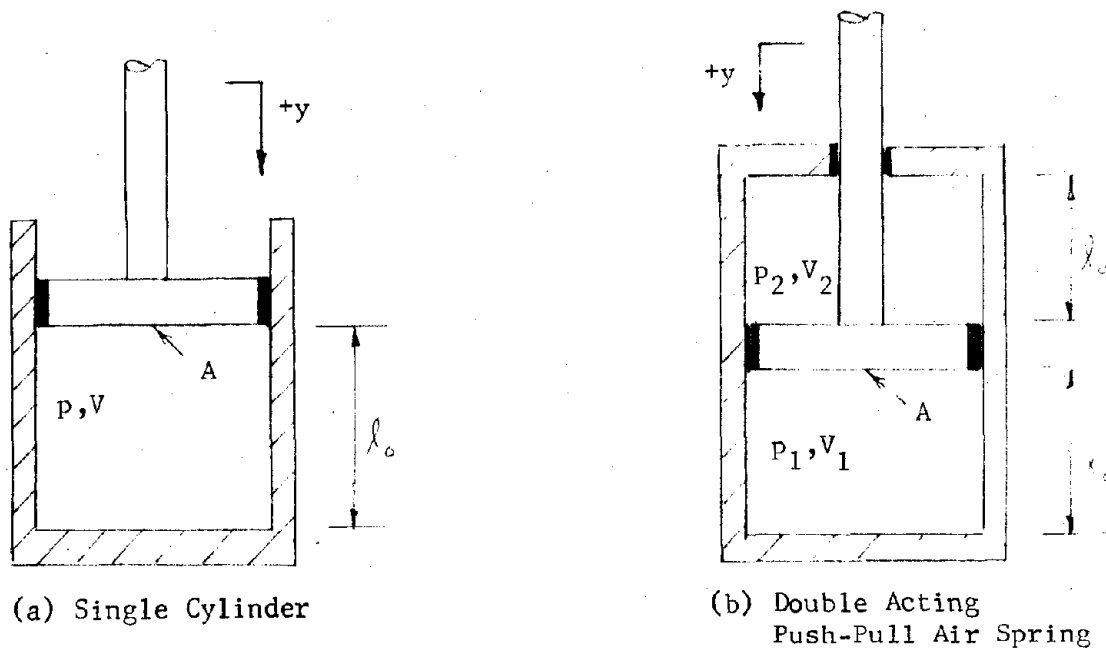


FIGURE 6.30: SCHEMATIC CYLINDER SPRINGS

The spring rates for both configurations are non-linear; the single cylinder increases in stiffness with positive displacement and decreases in stiffness with negative displacement (based on the sign convention shown in Figure 6.30 (a)); the double acting cylinder increases in stiffness with both positive and negative displacements. This is demonstrated in Figure 6.31.

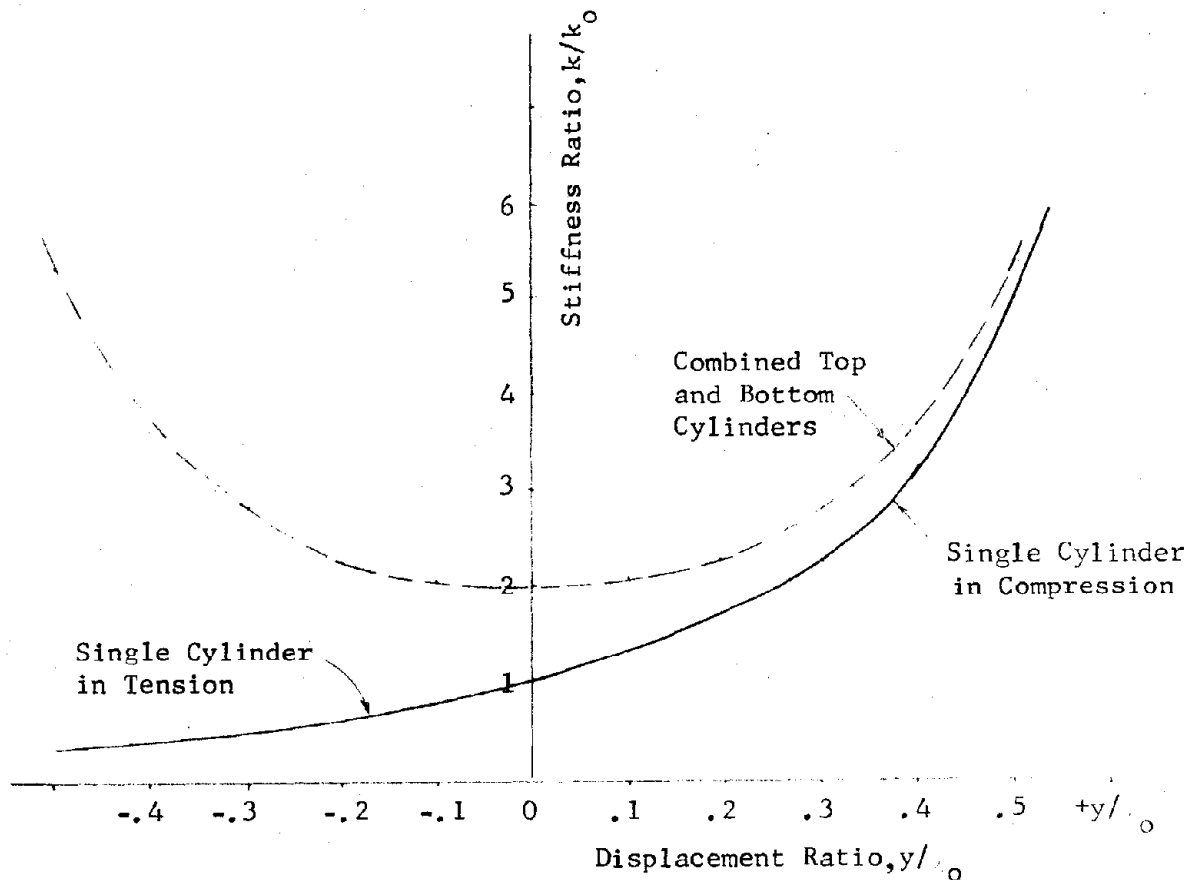


FIGURE 6.31: STIFFNESS VARIATION WITH DISPLACEMENT

Linear behavior can be assumed with negligible error in many design situations when displacements,  $y$ , are small with respect to the cylinder chamber nominal length,  $l_0$ . Reference 6.10 has plotted the variation of frequency ratio  $f_a/f_0$  as a function of the relative displacement for the double acting cylinder spring and this curve is reproduced in Figure 6.32. It can be seen from the figure that for a displacement ratio,  $y/l_0$ , up to 0.3 the maximum change in frequency is 1.2 times the nominal frequency value. Therefore, linear behavior within this displacement ratio can be considered acceptable for design in shock isolation systems.



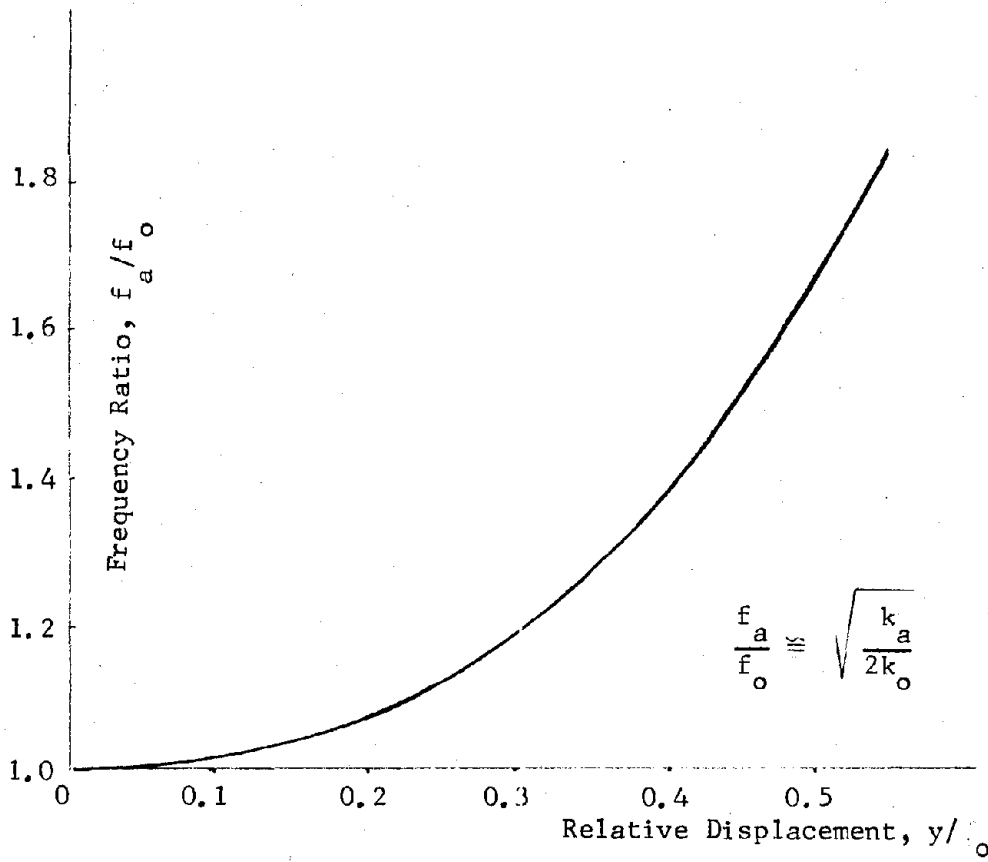


FIGURE 6.32: FREQUENCY RATIO VERSUS RELATIVE DISPLACEMENT

The spring constants for single acting and double acting pneumatic cylinders are derived in References 6.10 and 6.11 resulting in the following equations:

Single Acting Spring (Figure 6.30 a)

$$k_o = n A \frac{p}{l_o} \tag{6.23}$$

where  $k_o$  = spring rate in the neutral position

$n$  = gas constant  $\approx 1.3$  for air

$A, p, l_o$  are defined in Figure 6.30 (a)

$$k_a = k_o \frac{1}{\left[ \frac{l_o - y}{l_o} \right]^{n+1}} \tag{6.24}$$

where  $k_a$  = spring rate at any displacement,  $y$ .

For small displacements  $\frac{y}{l_o} < 0.3$  assume that  $k_a = k_o$ .

Double Acting Spring (Figure 6.28 b)

$$k_o = \frac{n A}{l_o} [p_1 + p_2] \quad (6.25)$$

The stiffness at any displacement ( $k_a$ ) is obtained by using the expressions defined in Equations 6.23 and 6.24 for each chamber (i.e. 2 springs in parallel) with proper regard to size.

For small displacements,  $\frac{y}{l_o} < 0.3$ , it may be assumed that  $k_a = k_o$ .

The use of the above design equations in sizing a pneumatic cylinder and piston near linear characteristics are demonstrated in the following steps:

Given:  $k_{o(max)}$ ,  $y_s$ , and  $y_d$

where  $y_s$  = static displacement

$y_d$  = peak dynamic displacement

- (1) Establish peak pressure(s),  $p_{allow}$  allowed during dynamic response
- (2) Determine required piston area from  $p_{allow}$  and given conditions  $k_o$ ,  $y_s$ , and  $y_d$ .

$$A = \frac{k_o (y_s + y_d)}{p_{allow}}$$

- (3) Determine chamber pressure(s) in static neutral position.

$$P = \frac{k_o y_s}{A}$$

or

$$P_1 = \frac{k_o y_s}{A} + P_2$$

for a double acting cylinder.

- (4) Determine chamber length,  $l_o$ , from Equations 6.23 for single acting cylinder

$$l_o = \frac{k_o}{n A p}$$

and verify near linear behavior from the limiting ratio

$$y_d / l_o < 0.3$$

(5) For a double acting cylinder assume a ratio of  $y_d/\ell_o$  (say 0.3) and calculate:

length  $\ell_o$

$$\ell_o = \frac{y_d}{0.3}$$

pressure  $p_2$

$$p_2 = \left[ \frac{\ell_o}{n} - y_s \right] \frac{k_o}{2A}$$

pressure  $p_1$

$$p_1 = \frac{k_o y_s}{A} + p_2$$

The above calculated characteristics establish a preliminary design configuration.

b. Spring characteristics in a damped pneumatic spring. A damped pneumatic spring is often desirable when the system response must be damped out very rapidly. The damping is usually provided by linking a surge tank to the spring cylinder as shown schematically in Figure 6.33

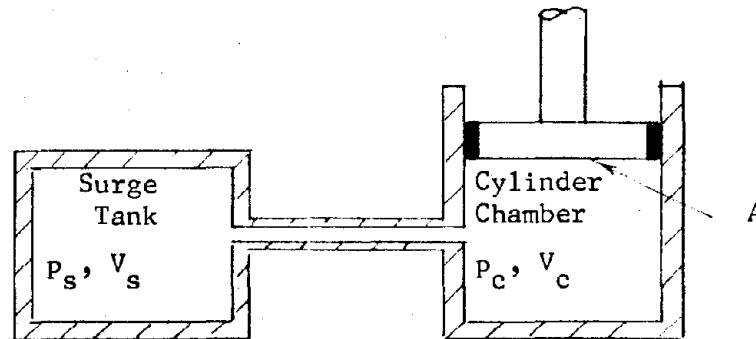


FIGURE 6.33: DAMPED PNEUMATIC SPRING

The gas flow between cylinder chamber and surge tank affects the spring characteristics during dynamic response. This problem is analyzed in depth in Reference 6.11 and only two limiting cases are here defined.

For a very low frequency system the pressure in the chamber and surge tank can equalize and consequently the effective spring rate is a function of the volume of the cylinder and surge tank.

$$k_o = \frac{n p A^2}{V_c + V_s} \quad (6.26)$$

where  $p = p_c = p_s$

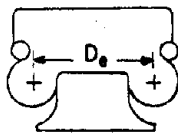
Conversely when the dynamic displacements take place very rapidly (i.e. high frequency systems) there is less time for flow to take place between cylinder and tank. Therefore the spring rate is a function of the cylinder chamber volume only.

$$k_o = \frac{n p_c A^2}{V_c} \quad (6.27)$$

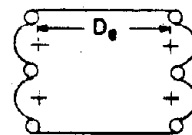
Many damped pneumatic springs will be further complicated by inserting check valves and relief valves that control the flow between cylinder and tank and provide damping in only part of the cycle. For example, damping is not desired during the initial shock input phase, but a large amount of damping is desirable during the residual response. This type of spring of course is non-linear and prototype testing should be performed to determine actual spring and damping characteristics for a dynamic input.

### 6.3.3 Air bags and bellows springs.

a. Configurations. Air bag and air bellows springs function in the same manner, the difference being in the configuration. Air bags consist of a single section or convolution subject to volume change and shape deformation. Air bellows springs are essentially air bags having two or more deformable convolutions. Figure 6.34 shows the two typical configurations.



Air Bag Spring  
(a)



Air Bellows Spring  
(b)

FIGURE 6.34: TYPICAL AIR BAG CONFIGURATIONS

Air bags and bellows are usually constructed of fabric reinforced rubber, capable of withstanding considerable internal pressure and assembled between steel end fittings or plates. The bellows type of construction utilizes one or more annular reinforcing rings to divide the axial length of the bag into several configurations and thus increase the practical ratios of axial length and deflection to diameter.

The so-called "rolling bellows" is actually a positive sealing device which is sometimes used to replace the usual ring type piston seal in air cylinders. The configuration is schematically shown in Figure 6.35.

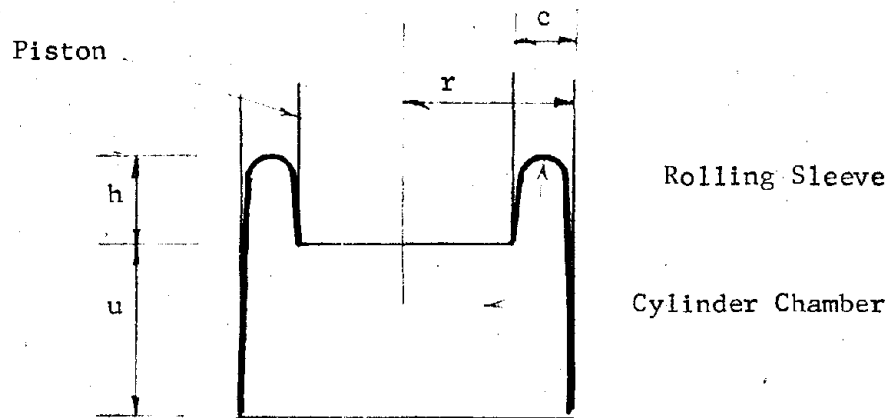


FIGURE 6.35: ROLLING BELLOWS (SLEEVE) CONFIGURATION

The rolling (elastomeric) sleeve is permanently attached both to the piston and to the cylinder wall. The fold in the sleeve moves in the annular clearance between piston wall and cylinder wall during relative motion between these parts.

b. Air bag and bellows springs have very non-linear spring characteristics and design is heavily dependent on application of empirical data. Spring force or load,  $P$ , is a function of internal air pressure and effective area as:

$$P = A_e p_g \quad (6.28)$$

where  $p_g$  is gage pressure. For typical circular cross sections,  $A_e$  is the area circumscribed by a circle having the diameter  $D_e$ . See Figure 6.34.

$D_e$  varies slightly as the spring height,  $h$ , changes. In practice, since both  $A_e$  and  $D_e$  are empirical values, static load versus displacement and pressure are determined experimentally for each specific spring configuration. A typical manufacturers data sheet Figure 6.36 for Firestone "211 A AIRMOUNT" spring gives the internal volume,  $V_s$ , versus the spring height,  $h$ , as well as a family of curves of load versus internal pressure and spring height for various pressure and displacement ranges of the spring.

Since the recommended maximum static operating pressure is usually 100 psi the maximum static load capacity can be taken directly from the 100 psi curve for any desired static load spring height. Conversely, the internal static pressure required to support a specific load at a specific spring height is found from Equation (6.28) as,  $p_g = P/A_e$ , where  $A_e$  is obtained by interpolating between adjacent load curves as;

$$A_e = \Delta P / \Delta p_g$$

It is noted that for the usable range  $A_e$  becomes more linear with increasing compression (decreasing spring height). The pressure versus load values at small spring heights may accordingly be determined with little error by assuming  $A_e$  constant for any specific value of  $h$  for pressures beyond the upper limit of the data sheet curves. The minimum and maximum pressures for which complete load curves are provided in the data sheets are usually 20 psi and 100 psi. Values of  $A_e$  based on these two curves (i.e.,  $A_e = P_{100} - P_{20}/80$ ) will usually be sufficiently accurate for determinations of spring constant for most applications.

For any specific spring and for any specific set of initial, static load, conditions (i.e., spring height, internal volume, internal pressure and load) the characteristic curves and elementary gas law may be used to calculate the dynamic load versus displacement value and spring rate for any spring position. Maximum acceleration and corresponding maximum permissible spring rate,  $k_m$ , are usually governing parameters in weapons effect shock isolation problems, and the maximum spring rate occurs at maximum compressive displacement in the non-linear load-displacement curve of air bag and bellows springs.

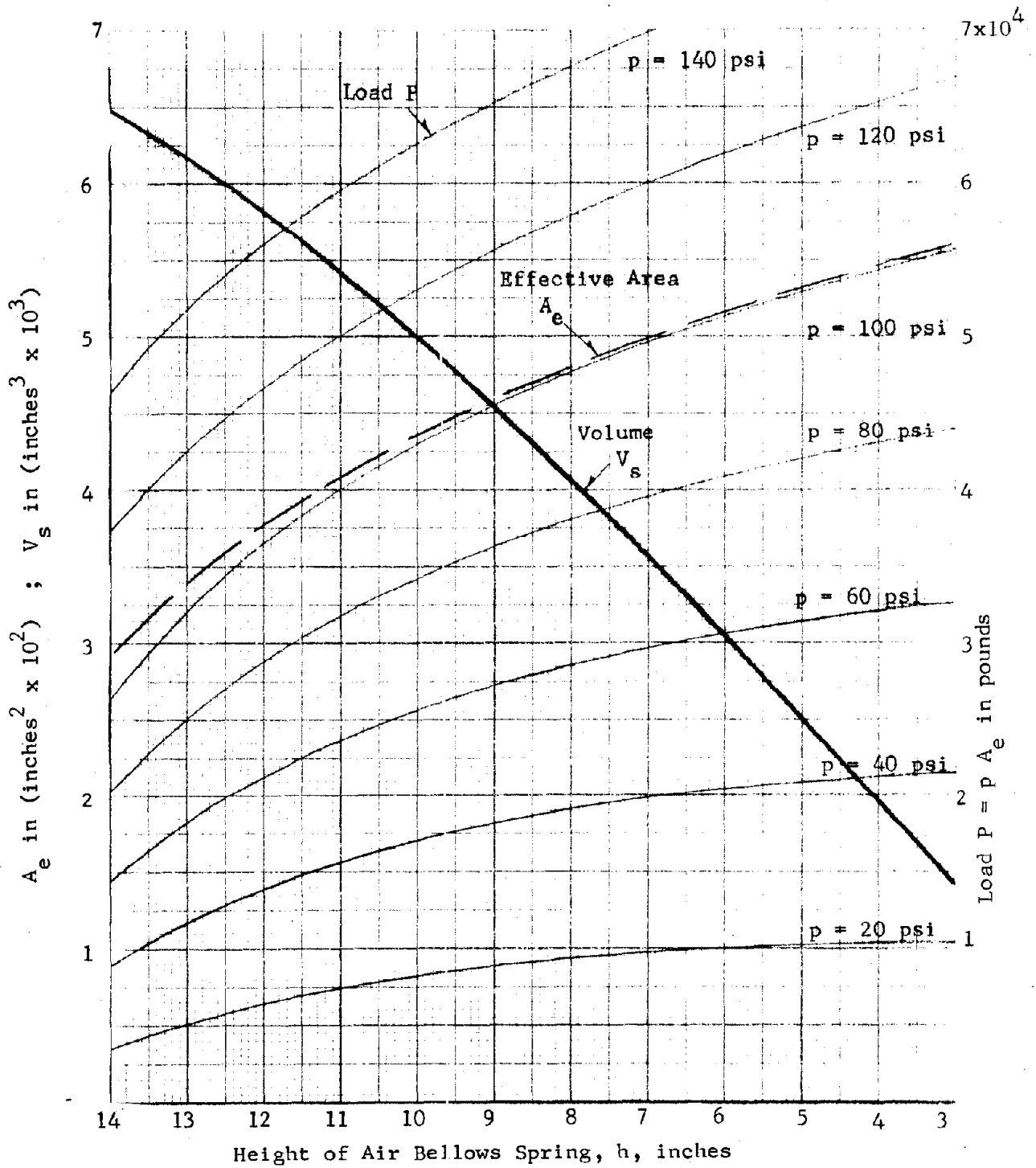


FIGURE 6.36: FIRESTONE "211 A AIRMOUNT" SPRING

It is customary to use the secant rate for the last 20 percent of the design compressive displacement as the measure of maximum spring rate. For this purpose the volumes  $V_{s1}$  and  $V_{s2}$  and  $V_{s2}'$  and the effective areas  $A_{e2}$  and  $A_{e2}'$  corresponding to the initial position,  $h_1$ , maximum dynamic compressive displacement,  $\Delta_{zd}$ , and to  $.8 \Delta_{zd}$  are obtained directly or calculated from the data sheet. The corresponding gage pressures  $p_{2g}$  and  $p_{2g}'$  are then calculated on the basis of volume change from the static position. In terms of internal spring volumes the applicable general gas law is:

$$p_{2a} = p_{1a} (V_{s1}/V_{s2})^n$$

where  $p_{2a}$  and  $p_{1a}$  are absolute pressures at  $V_{s2}$  and  $V_{s1}$  respectively. For the frequency range of air bag springs the value of the exponent,  $n$ , has been found to be about 1.38, and the above expression becomes:

$$p_{2a} = p_{1a} (V_{s1}/V_{s2})^{1.38}$$

or, in terms of gage pressure,

$$p_{2g} = (p_{1g} + 14.7)(V_{s1}/V_{s2})^{1.38} - 14.7$$

For each value of displacement ( $\Delta_{zd}$  and  $.8 \Delta_{zd}$ ), and for calculated value of gage pressure,  $p_{2g}$  and  $p_{2g}'$  the corresponding loads  $P_2$  and  $P_2'$  are determined as:

$$P_2 = p_{2g} A_{e2} \quad , \quad \text{and,} \quad P_2' = p_{2g}' A_{e2}'$$

the secant spring for the last 20 percent of the displacement is then

$$\begin{aligned} k &= (P_2 - P_2') / (\Delta_{zd} - .8 \Delta_{zd}) \\ &= (p_{2g} A_{e2} - p_{2g}' A_{e2}') / \Delta_{zd} \end{aligned} \quad (6.30)$$

If the spring rate of the isolated unit is found to be too high, a "softer" system may be obtained by the addition of a reservoir to increase the total volume. For practical purposes the system characteristics, including the effect of reservoir volume, can be determined from the above expressions by simply substituting the total volume,  $V_t (= V_R + V_s)$ , in each volume term, provided the design insures negligible air flow resistance between spring and reservoir. A suitable reservoir volume can be most



conveniently found by cut and try methods, but the work is expedited if the total volume expression is rewritten in terms of initial gage pressure,  $p_{1g}$ , the volumes,  $V_{t1}$ ,  $V_{t2}$  and  $V'_{t2}$ ; the effective areas  $A_{e2}$  and  $A'_{e2}$ ; and the maximum permissible spring rate,  $k_m$  if we let

$$C_s = \frac{k_m \Delta z d + 14.7 (A_{e2} - A'_{e2})}{5 (p_{1g} + 14.7)} \quad (6.31)$$

$$\text{and } B_t = A_{e2} \left[ \frac{V_{t1}}{V_{t2}} \right]^{1.38} - A'_{e2} \left[ \frac{V_{t1}}{V'_{t2}} \right]^{1.38} \quad (6.32)$$

where  $C_s$  is constant for all combinations of reservoir and spring volume, and  $B_t$  varies with total volume,  $V_t$ . Then  $C_s$  must be greater or equal to  $B_t$ .

c. The spring characteristics for the rolling sleeve can be determined approximately if  $c \ll r$  (see definition of terms in Figure 6.35). The effective piston area is:

$$A_e = \pi r (r - c) \quad (6.33)$$

The volume of gas contained in the cylinder is approximately:

$$V = \pi r (ru + 2 ch) \quad (6.34)$$

For small displacements the spring rate in the equilibrium position is:

$$k_o = \frac{n p \pi r (r - c)^2}{(ru + 2 ch)} \quad (6.35)$$

from substituting Equations (6.33) and (6.34) into Equation (6.27). The rolling sleeve system is more fully described in Reference 6.12 where a concept is discussed which includes a reservoir tank with a throttling device to control the damping period. A schematic of the concept spring is shown in Figure 6.37. This spring-damper system was first developed for the Minuteman Launch Control Center using a conventional pneumatic piston-cylinder configuration (see description in Section 9.5.9). The rolling sleeve concept decreases the leakage and thus reduces the make up air requirement to a minimum.

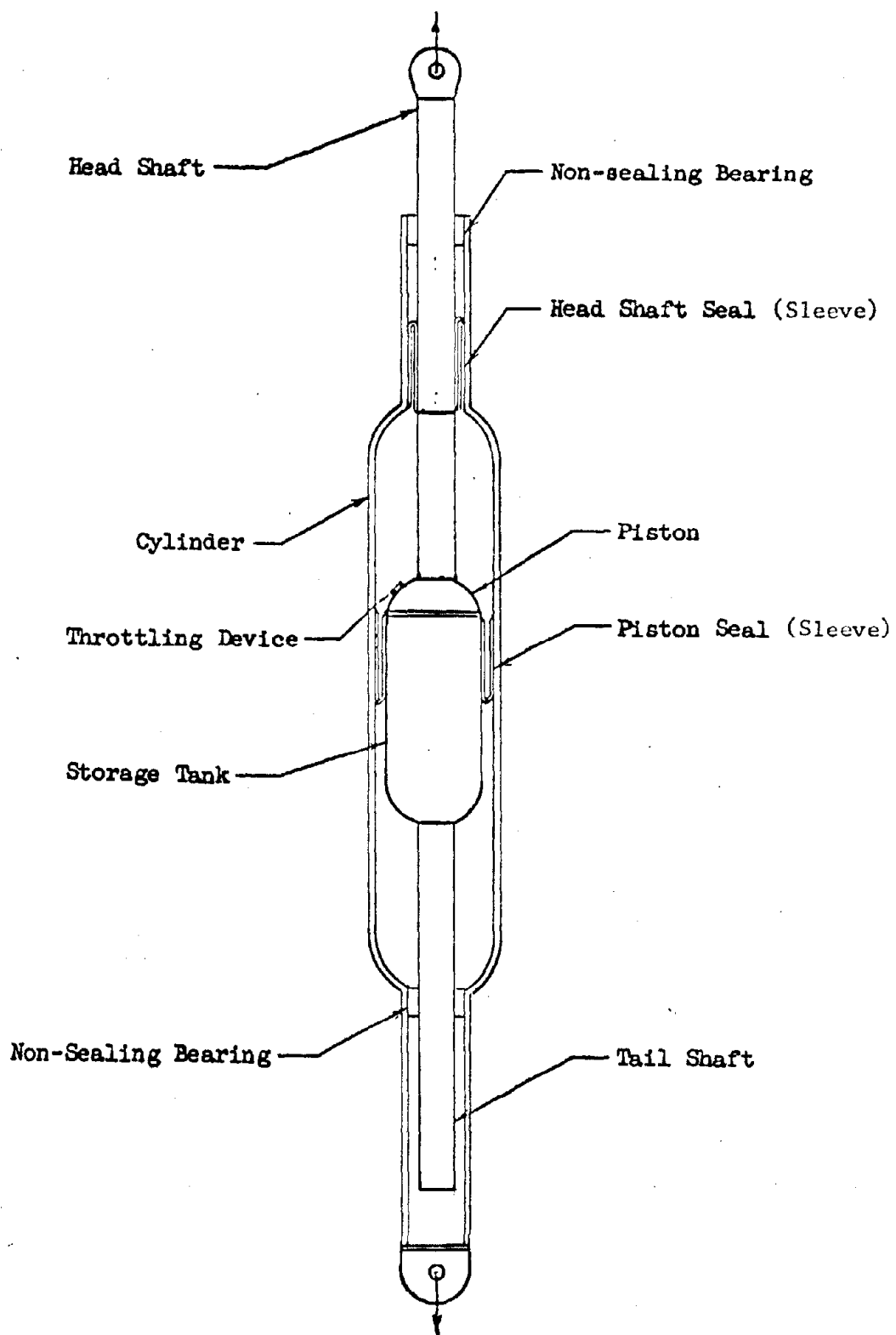


FIGURE 6.37 PNEUMATIC ISOLATOR SCHEMATIC

#### 6.3.4 Design Example 6.6: Air Bellows Shock Isolator

(1) Given: A shock isolation system in the vertical  $z$  direction and employing air bellows springs is to be designed for a maximum static load  $P$  of 25,000 pounds, and a maximum spring rate,  $k_m$  of 2,500 lbs/in. The dynamic displacement,  $\Delta_{zd}$  is  $\pm 10$  inches.

(2) General considerations: The total displacement available should exceed  $2 \Delta_{zd}$  by a minimum of 10 percent to allow some margin of safety. The total required displacement is therefore 22 inches. Since this is beyond the range of standard available single units the design must be based on the use of  $N$  units in series in each isolator assembly. For each unit the minimum required displacement range then becomes,  $\Delta_h = 22/N$  and the maximum system secant spring rate at the  $\Delta_z$  to  $0.8 \Delta_z$  compressive displacement will be  $k_m N = 2500 N$  per unit.

(3) It is judged that the Firestore "No. 211 A AIRMOUNT" (Figure 6.36) will be adequate for both static load and displacement if two units are used in series. The maximum available displacement of each unit is 11.9 inches versus the required  $\Delta_h = 22/2 = 11$  inches, and therefore the spring rate per unit is 5000 lbs/inch.

(4) From Figure 6.36 it is seen that for

$$\text{at } h = 9 \text{ in.}, A_{e1} = 465 \text{ in.}^2 \text{ and } V_{s1} = 4400 \text{ cubic inches}$$

Accordingly it is seen that

-  $\Delta_{zd}$  will correspond to  $h = 4$  in., for which Figure 6.36 gives

$$A_{e2} = 545 \text{ in.}^2 \text{ and } V_{s2} = 1820 \text{ in.}^3$$

Moreover, it is seen that

-  $.8 \Delta_{zd}$  will correspond to  $h = 5$  in., for which

$$A'_{e2} = 531 \text{ in.}^2 \text{ and } V'_{s2} = 2370 \text{ in.}^3$$

(5) The required static load gage pressure from Equation (6.28) is then

$$P_{1g} = 2500/465 \approx 54 \text{ psi}$$

(6) The constant,  $C_s$  from Equation (6.30) is:

$$\frac{5000 \times 5 + 14.7 (545 - 531)}{5 \times (54 + 14.7)} = 73.8$$

(7) For the spring without reservoir  $V_s = V_t$ , and,  $B_s = B_t$ . From Equation (6.31)

$$B_s = 545 \left[ \frac{4400}{1820} \right] 1.38 - 53.1 \left[ \frac{4400}{2370} \right] 1.38 = 596$$

Therefore

$$B_s > C_s \text{ and a reservoir will be required.}$$

(8) By a cut and try method it will be found that the required reservoir volume,  $V_r$ , is about 8000 in.<sup>3</sup>. For this size reservoir,  $V_{t1} = 12,400$  in.<sup>3</sup>,  $V_{t2} = 9820$  in.<sup>3</sup>, and  $V_{t2}' = 10,370$  in.<sup>3</sup>.

Accordingly from Equation (6.31)

$$B_t = 545 \left[ \frac{12400}{9820} \right] 1.38 - 53.1 \left[ \frac{12400}{10370} \right] 1.38 = 69 < C_s$$

Since two springs are used in each assembly the total reservoir volume required will be 16,000 cubic inches.

(9) The Firestone "211 A AIRMOUNT" is a two convolution bellows having a nominal maximum O.D. of 28 inches. The standard unit is supplied with open ends with self sealing flanges and with mounting rings having 24 3/8 inch diameter studs on a 23.5 inch bolt circle at each end. In Figure 6.38 an assembly is shown in which the two units are joined on a 3 inch channel ring having an inside diameter of 22 inches. A similar ring is used to mount the top plate. These rings supply only 2300 in.<sup>3</sup> of the 16000 in.<sup>3</sup> reservoir capacity required. The balance of the reservoir volume is incorporated in a 26 in. 1.0 x 26 in. high base assembly. This type of (series) assembly should be tested for lateral stability and provided with guides to prevent lateral buckling if needed.

## 6.4 Liquid Springs

### 6.4.1 Basic principles and configurations

6.4.1.1 Introduction: Liquid springs have the advantage of being able to provide very high energy absorption and high spring force in very small compact units. Wide variations in spring rate and spring force are possible within a given size envelope, and internal self-damping can be incorporated. Essentially the liquid spring consists of a cylinder, piston rod and a high pressure seal around the piston rod. The cylinder is completely filled with a liquid. The piston rod is pushed into the cylinder,

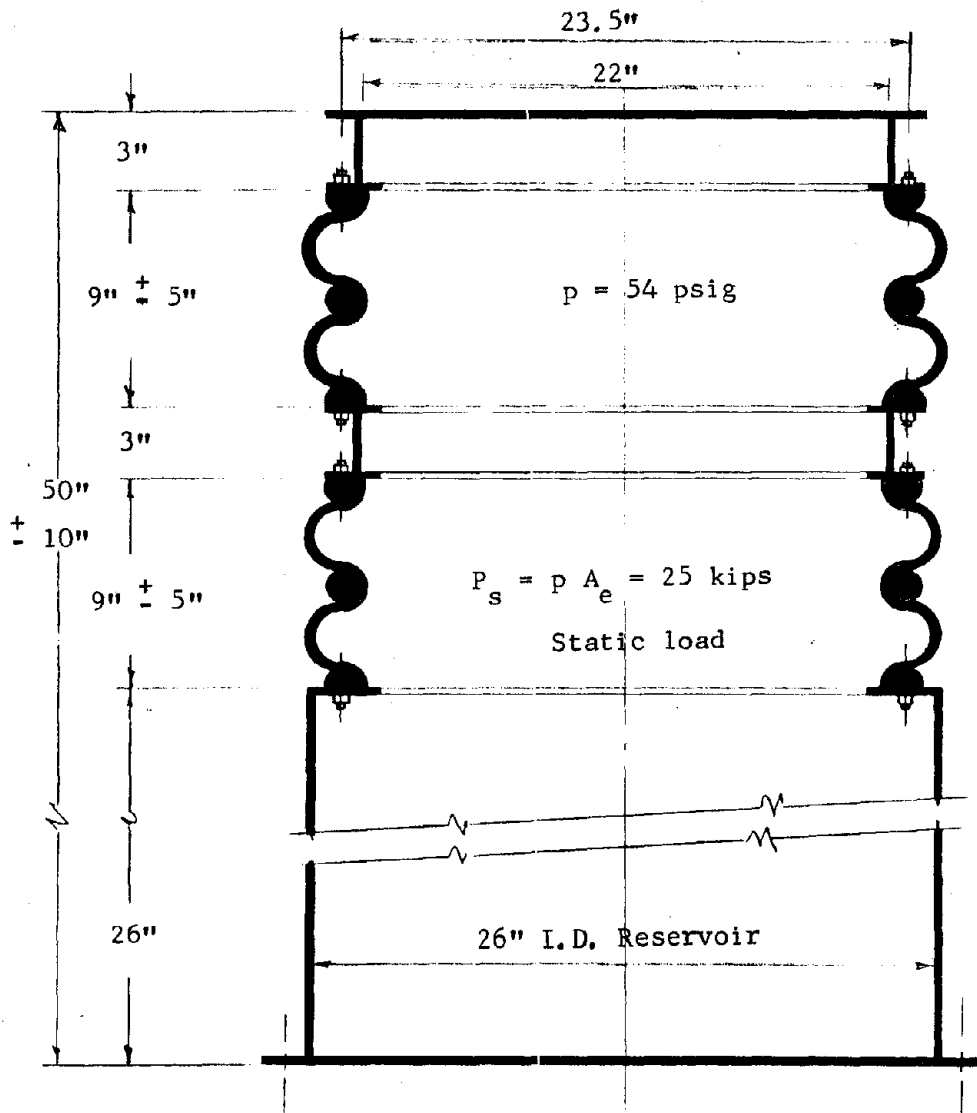


FIGURE 6.38: AIR BELLOWS SHOCK ASSEMBLY

compressing the liquid to high pressures. The force required to push the piston into the cylinder varies nearly linearly with the piston stroke. The slight nonlinearity is due to a small increase in the bulk modulus of the liquid with increasing pressure. Many liquids could be used in liquid springs; however, the smallest spring, for any specific spring rate and stroke requirement, is obtained by using the most compressible liquid available. For this reason, most liquid springs are now filled with some type of silicone oil, some of which will compress nearly 20 percent at 50,000 psi.

6.4.1.2 Development: Practical liquid springs are dependent on dynamic piston rod seals capable of maintaining a fluid tight seal at pressures of 50,000 psi, or more, with reasonable operating life and without undue restraint of piston rod movement.

A seal, developed by Dowty Equipment, Ltd. and known as the Dowty seal (Figure 6.39) utilizes a flat rubber ring sandwiched between two metal rings

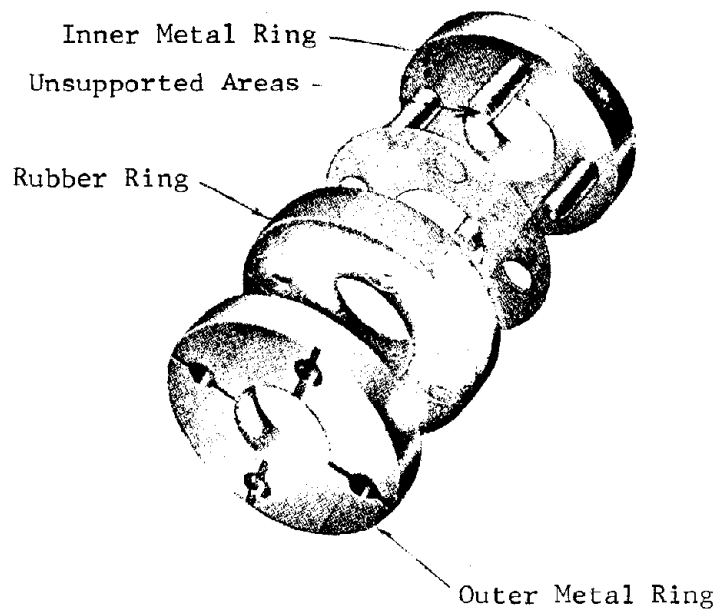


FIGURE 6.39: HIGH PRESSURE SEAL

all closely fitted to the bore of the seal gland and to the piston rod, which passes through the seal instead of pushing the seal ahead of it. Four pins protruding from the inner metal ring pass through close fit holes in the rubber ring and part way through slip fit holes in the outer metal ring. The four

holes through the rubber ring constitute the "unsupported area" of the inner ring. Back-up, or anti-extrusion, rings are used at the inside and outside diameters of the rubber ring. Over a considerable period the Dowty seal has been used in many liquid spring applications, notably in the landing gear shock struts of British aircraft.

The liquid spring using the Dowty seal was introduced in the U. S. by Cleveland Pneumatic Tool Company in 1953, and the seal has since been further modified and improved, notably by the use of teflon at the piston contact surface to reduce friction and wear.

6.4.1.3 Configurations: The three major functional configurations of liquid springs may be classified by manner of loading as: simple compression, simple tension, and compound compression-tension springs. In all cases the fluid is under compression. The required spring rate is obtained by relatively small ratios of volume change to total volume, i.e.  $(V_o - V_d)/V_o$  is small.

a. In simple compression type liquid springs (Figure 6.40) the cylinder is closed at one end and a piston and piston rod of uniform diameter pass through a seal at the other end, a ported piston head on the end of the piston maintaining alignment with the cylinder. Fluid flow through the piston head ports is used to provide damping as the piston moves.

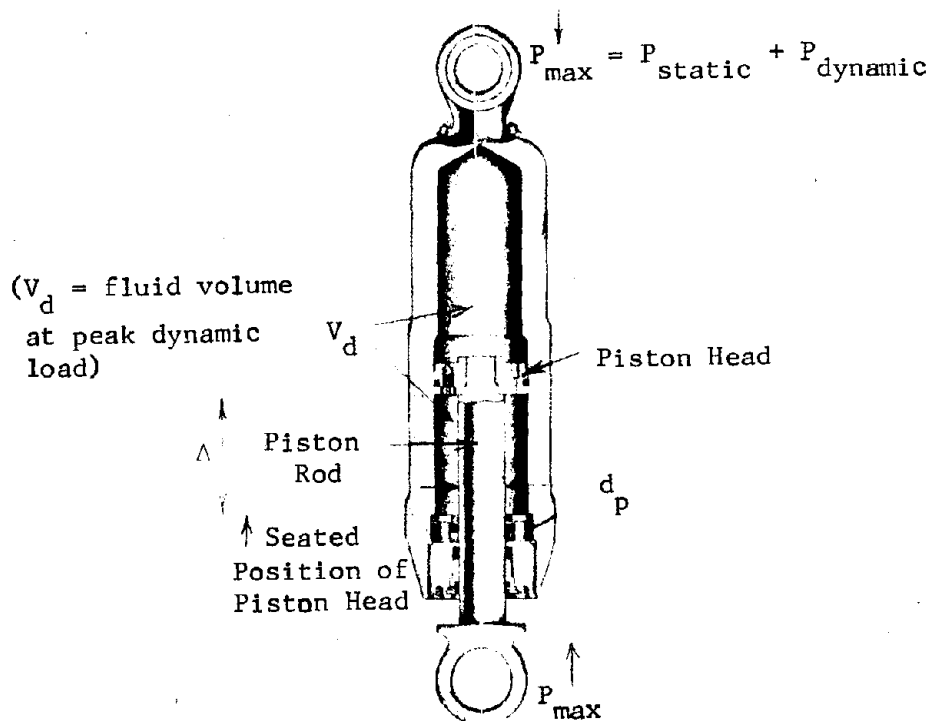


FIGURE 6.40: COMPRESSION TYPE LIQUID SPRING

b. In the typical tension configuration (Figure 6.41) a dual diameter piston passes completely through the cylinder and through seals at each end. Tension loading applied to the small diameter end draws the large diameter end into the cylinder reducing the volume and compressing the fluid. A ported piston head and flow control may also be used here to obtain additional damping.

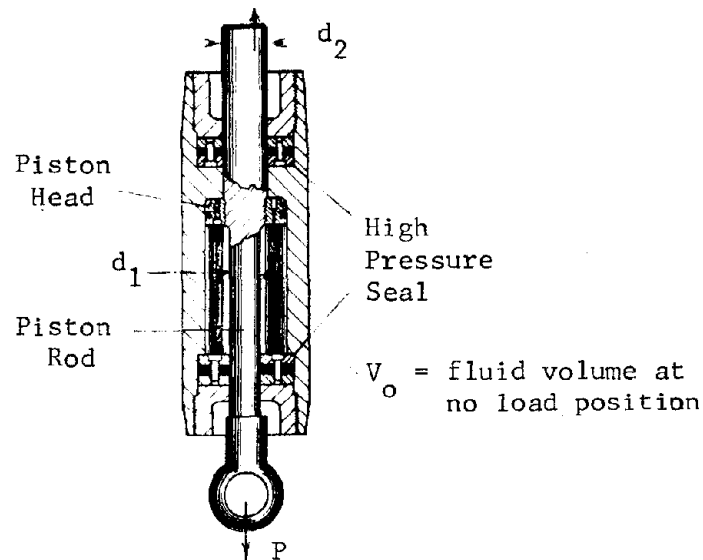


FIGURE 6.41: TENSION TYPE LIQUID SPRING

c. In the compound tension-compression liquid springs a number of arrangements are feasible one of which is illustrated in Figure 6.42. In this arrangement, the compression piston head is guided by the inside diameter of a hollow cylindrical extension on the tension piston head which, in turn, is guided by the inside diameter of the main cylinder. The compression and tension pistons have several inches of axial free travel with respect to each other and are interlocked to restrict this travel distance. In the static pre-load position the tension piston head is bottomed in one end of the main cylinder, and the compression piston head is bottomed against the lock ring in the tension piston head. Under tension load the compression piston and head pull the tension piston into the main cylinder, and under compression load the compression piston enters further into the main cylinder.



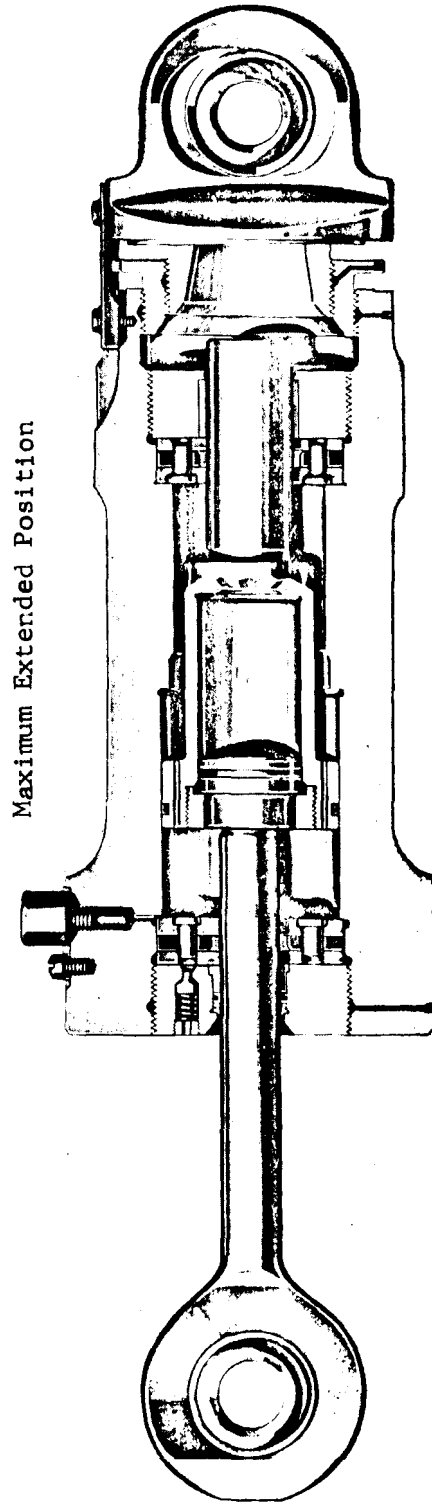
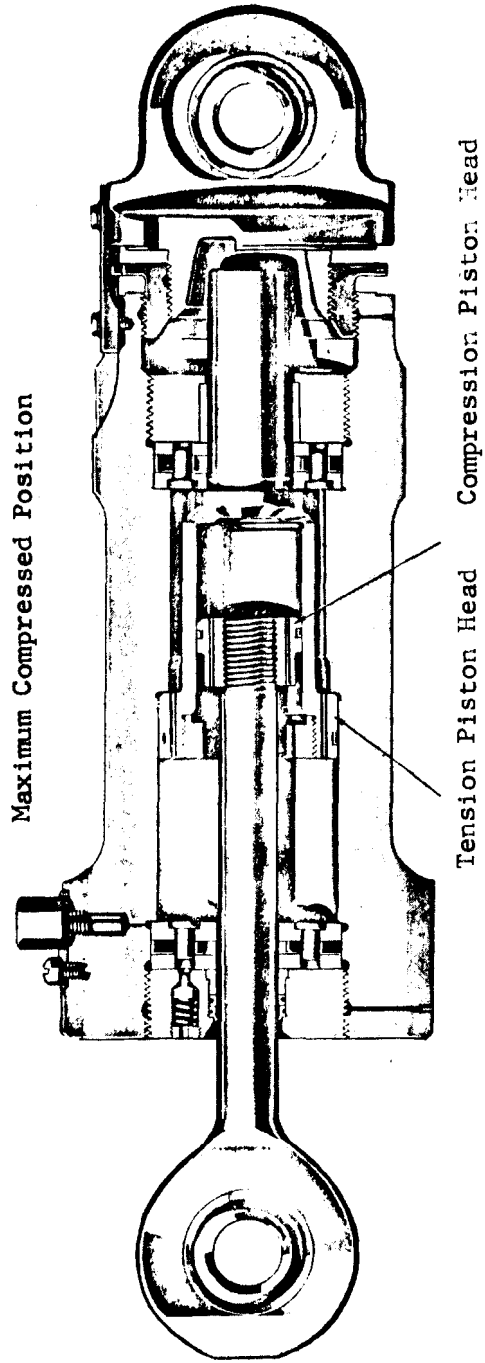


FIGURE 6.42: COMPOUND, COMPRESSION - EXTENSION LIQUID SPRING

## 6.4.2 Miscellaneous parameters.

### 6.4.2.1 Performance modifying influences.

a. Friction and wear: The major life limitation on liquid springs is piston and seal wear. The high sealing pressures inevitably produce friction loading and wear on both piston rod and seal as the rod moves through the seal. Most of the seal improvements in recent years have been in the direction of reduced friction and wear, and tests in excess of 20,000 cycles with negligible leakage indicate that the seals are no longer a major problem. In even the best seals, however, friction provides appreciable damping and increases spring rates from about 2 to 5 percent, and most seals require a minimum preload of 1000 to 5000 psi to insure proper seal function.

b. Cylinder volume change: The high bulk moduli of liquid spring fluids result in a high sensitivity to even small changes in cylinder volume. Cylinder expansion and contraction with both pressure and temperature changes must be taken into consideration in calculating spring rate data.

c. Changes in fluid characteristics with temperature: Temperature changes in liquid spring fluids due either to external influences or to internal heating resulting from load cycling produce distinct changes in spring characteristics. Heating increases the pre-load pressure, or, under fixed load, changes the static load spring length and increases the spring rate. Temperature reduction has the opposite effect. In installations subject to wide variations in ambient temperature, thermostat controlled heating blankets are sometimes used to maintain an approximately constant temperature near the upper end of the anticipated range.

### 6.4.2.2 Safety and cost considerations.

a. Failure damage potential: Liquid spring cylinders are high pressure vessels and are normally pre-loaded to several thousand psi whether or not a static load is supported. Apart from possible damage to the shock isolated equipment, the failure of a liquid spring cylinder can produce hazardous fragmentation. Consequently, the cylinder design should be analyzed thoroughly for all probable combinations of loading and stress. In general the safety factors for all design stresses, based on the elastic limits of the material, should not be less than five.

b. Costs: Liquid spring parts require high quality materials, precision machine work and carefully controlled heat treatment. As a result they are by no means "cheap". However, in terms of energy absorption versus space requirement they are difficult to equal and, as a result, in many applications they may be the most economical shock isolation device available.

#### 6.4.3 Design procedures.

6.4.3.1 Fluid characteristics and basic formulae. The number of shock loading cycles in any short period can be assumed to be very limited in hardened structure shock isolation applications, and the temperature control required to compensate for variation in external ambient temperatures is relatively simple. Accordingly the following discussion will assume isothermal conditions and a specific operating temperature.

For most liquid spring applications the fluids having the best combination of desirable characteristics (high compressibility, temperature and chemical stability and suitable viscosity) are the silicone oils. Of these the most widely used are the General Electric Company's SF96 series, Union Carbide's L.-45 series, Dow Corning's D.C. 210 series, and Dow Corning F4029. All of these have slightly nonlinear stress/strain curves with the bulk moduli increasing with increasing pressure (see Figure 6.43). It will be noted that the highest compressibility is available in the Dow Corning 0.65 centistoke 210 fluid. However the very low viscosity of this fluid may make sealing more difficult, and it is also very volatile compared to the higher viscosity fluids. The D.C. F4029 fluid with nearly as low a bulk modulus and a viscosity of 100 c.s. is usually preferable.

Since all liquid springs, regardless of loading method, operate by varying the volume of, and pressure in, a fixed quantity of fluid which is always under pressure the basic design formulae are applicable to all design variations. The basic parameters are:

Deflection in inches	$\Delta$
Load in pounds	P
Pressure in psi	P
Effective Piston Area in sq. inches	$A_e$
Cylinder Volume in cubic inches	V

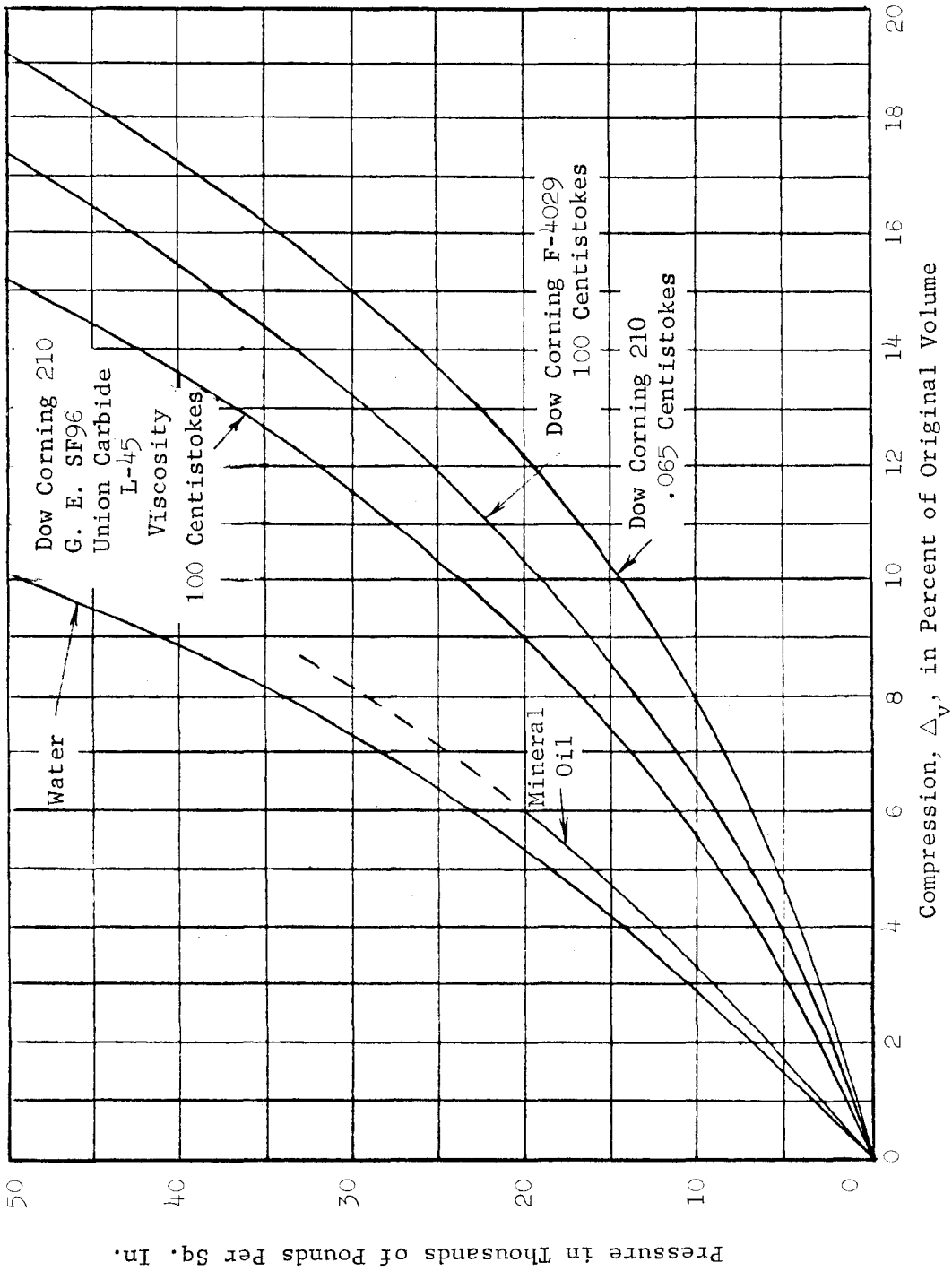


FIGURE 6.43: COMPRESSIBILITY OF FLUIDS

Cylinder volume at no load (or preload)	$V_o$
Fluid System Spring Rate in lbs/in	$k_f$
Cylinder Structure Spring Rate	$k_c$
Preload Pressure in psi	$P_{pl}$
Compressibility of Fluid as a ratio	$C$

Subscripts s and d are used to note the static (1.g) position conditions and peak dynamic response conditions respectively. The other subscripts are self-explanatory or defined when first used.

The basic relationships defining liquid spring fluid characteristics are:

$$P_{max} = P_s + P_d = k (\Delta_s + \Delta_d)$$

$$A_e = \frac{P_{max}}{p_{max}} \quad (6.37)$$

$$P_s = \frac{k \Delta_s}{A_e} + P_{pl} \quad (6.38)$$

The cylinder volume in the static and peak dynamic positions are

$$V_s = V_o - A_e \Delta_s$$

$$V_d = V_o - A_e (\Delta_s + \Delta_d)$$

The compressibilities are defined as:

$$C_s = \frac{V_o - V_s}{V_o} = \frac{A_e \Delta_s}{V_o} \quad (6.39)$$

$$C_d = \frac{V_o - V_d}{V_o} = \frac{A_e (\Delta_s + \Delta_d)}{V_o} \quad (6.40)$$

(The volume change due to breathing of the cylinder is neglected in the above equations. The breathing effect need not be considered in a preliminary design)

Combining the Equations 6.39 and 6.40 results in the simple expression defining the required cylinder volume at a no-load condition.

$$V_o = \frac{A_e \Delta_d}{C_d - C_s} \quad (6.41)$$

The example in the following section shows the use of the above equations.

6.4.3.2 Design example 6.7: Preliminary design of a liquid spring.

a. A liquid spring is required to meet the following criteria. (Reference Section 8 for application.)

(a)  $k = 400$  lbs/in (max. ave.) ;  $\Delta_s = 45$  in. ;  $\Delta_d = \pm 40$  in.

(b) The liquid spring is an integral part of a pendulous shock isolation system with an assumed overall pendulum rod length of 240 inches at static load.

b. For preliminary design assume:

(c)  $k_s/k_f$  is large and  $k = k_f$

(d) Negligible temperature effect

(e) Cylinder volume change negligible compared to fluid volume change

(f) Fluid will be D.C. F-4029

c. Required liquid spring characteristics

(1) Since the required spring rate is low and the deflections are large assume low maximum pressure,  $p_{max} = 25,000$  psi

(2) At  $p_m = 25,000$  psi the compressibility  $C_d = 0.12$  from Figure 6.44 for D.C. F-4029.

(3) Effective piston area required, from Equation 6.37:

$$A_e = \frac{400 (45 + 40)}{25000} = 1.36 \text{ sq. in.}$$

(4) Fluid pressure at static position, from Equation 6.38:

$$p_s = \frac{400 (45)}{1.36} = 13,200 \text{ psi}$$

(5) Compressibility  $C_s$  at the static pressure,  $p_s$ , from Figure 6.44

$$C_s = 0.08$$

(6) Cylinder volume  $V_o$ , from Equation 6.41

$$V_o = \frac{1.36 (40)}{.12 - .08} = 1360 \text{ cu. in.}$$

(7) Piston and cylinder dimensions:

(a) The system is specified as pendulous, so the tension spring

Example 6.7 (continued)

configuration will be required. Since the spring rates are low it will not be necessary to give too much attention to structural stiffness.

- (b) Maximum load (neglecting weight of spring) is  $(40 + 45)$  in.  $\times$  400 lbs/in. = 34000 lbs.

Assume a minimum tensile yield stress of 75 ksi.

$$\text{Use } \sigma_{tw} = \sigma_{ty}/5 = 15 \text{ ksi}$$

Where  $\sigma_{tw}$  = Allowable tensile working stress

$\sigma_{ty}$  = Allowably tensile yield stress

- (c) Tension rod and piston diameters,  $d_1$  and  $d_2$ :

$$\text{Req. tension rod area, } A_1 = 34/15 = 2.26 \text{ sq. in.}$$

$$\text{Req. tension rod dia., } d_1 = 1.70 \text{ in., } A_1 = 2.27 \text{ sq. in.}$$

$$\text{Req. piston area, } A_2 = A_e + A_1 = 1.36 + 2.27 = 3.63 \text{ sq. in.}$$

$$\text{and } d_2 = 2.15 \text{ inches}$$

- (d) Size of cylinder: Min. inside length = 85"

$$\text{Try } l_c = 90 \text{ inches}$$

$$\text{Req. net inside cross section area} = V_o/90 = 1360/90 = 15.1''$$

$$\text{Total inside cross section area} = 15.1 + 2.27 = 17.37 \text{ sq. in.}$$

$$D_c = 4.7 \text{ inches}$$

$$l_c = 90 \text{ inches is adequate}$$

The preliminary design is shown in Figure 6.44.

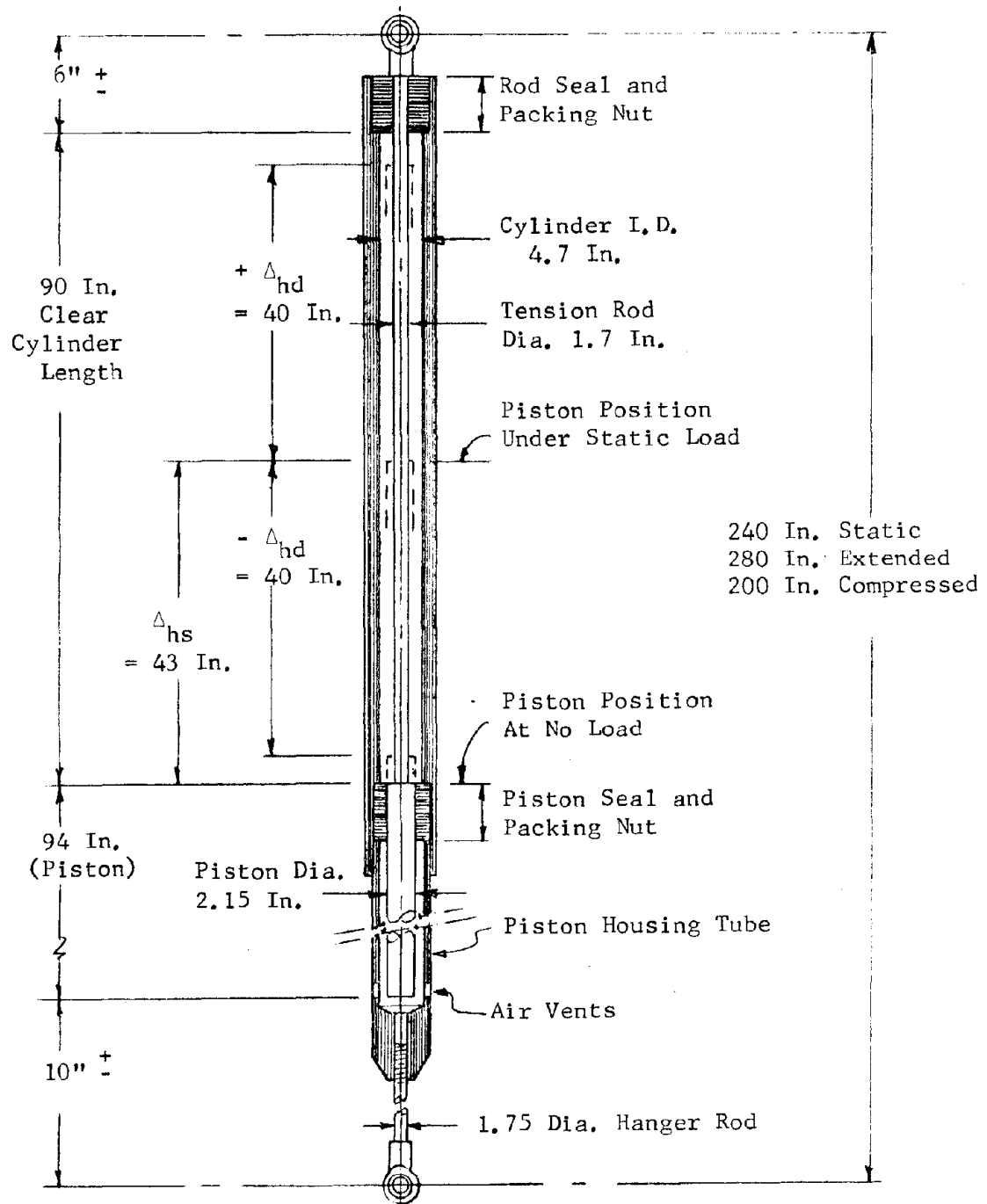


FIGURE 6.44: TENSION TYPE LIQUID SPRING (DESIGN EXAMPLE 6.6)



## SECTION 7: DESIGN OBJECTIVES (TOLERANCES)

### 7.1 Introduction

The criteria that usually establish the degree of shock attenuation and damping required for a hardened facility are the shock and vibration tolerances of man and equipment. It is necessary to know what types of equipment are to be used and whether or not operating personnel will be present and if the operators will be in a restrained position. It is then possible to determine the most critical item from a shock and vibration tolerance standpoint.

The tolerance information presented here will aid the designer in determining the most critical item in a facility and in designing an adequate shock isolation system to protect the item. Human tolerance to shock and vibration is discussed in Section 7.2 and equipment fragility in Section 7.3.

### 7.2 Human Tolerance to Shock and Vibration

Man's tolerance to shock dictates if it is necessary to provide shock isolation as well as the degree of shock attenuation required to protect him from shock injury. Man's tolerance to vibration will also determine the acceptable characteristics of a shock isolation system.

The reference data indicate that man can tolerate relatively large acceleration forces when he is restrained. However, the unrestrained person is subject to loss of balance at relatively low accelerations with the attendant possibility of impact injury. A similar conclusion can be drawn for the effects of vibratory motion on man. Moreover, a man has a low tolerance if vibrations occur near his own natural vibration frequencies.

The human tolerance levels for shock and for vibration are treated separately in the following sections.

7.2.1 Tolerance to shock accelerations. In order to determine whether or not a structure can be considered safe for human occupancy during a nuclear

weapon attack, it is necessary to compare the shock acceleration of the structure with human shock tolerance values. The structure motion may be caused by ground shock or by air blast striking exposed surfaces. A ground shock usually produces a very high initial acceleration with a downward motion, but in an outrunning seismic wave situation the initial motion may be upward. There is usually a horizontal component of the shock motion.

A ground shock motion can affect the unrestrained man directly or indirectly. When a shock is transmitted upward directly to man from the floor or furniture upon which he is situated, he can receive injuries that are dependent on the shock magnitude. On the other hand, if a shock motion moves the floor or other support downward at a very high acceleration, man can receive impact injuries upon termination of his free fall. Even at lower downward or horizontal accelerations of his support, man can lose his balance and receive injuries from impact with other objects or the floor. In cases where a shock motion is transmitted directly to man, it is possible to predict the level of injury for a given shock magnitude. In order to determine the extent of injury from impact occurring when man loses his balance, it is necessary to know the velocity of impact and the part of the body affected.

Restraints are used to avoid free fall and impact injuries. However, it is possible that in some cases restraints can increase injuries by making a man subject to a very high direct downward shock, when he would have received less severe indirect shock injuries if he had not been restrained.

Injuries to man from shock also depend on his position at the time the shock occurs, i.e. standing, seated, and prone. The direction in which the forces are transferred to and through the body relate to the extent and nature of the injury.

The time duration over which the shock forces act and the rate of increase in the force magnitude also affect the extent of injury to man.

From the above it is evident that there are many factors that must be considered in order to predict the extent of injuries possible from the action of ground shocks on man.

Human tolerance to ground shock will be discussed below under the headings that describe his position at the time of the shock transfer.

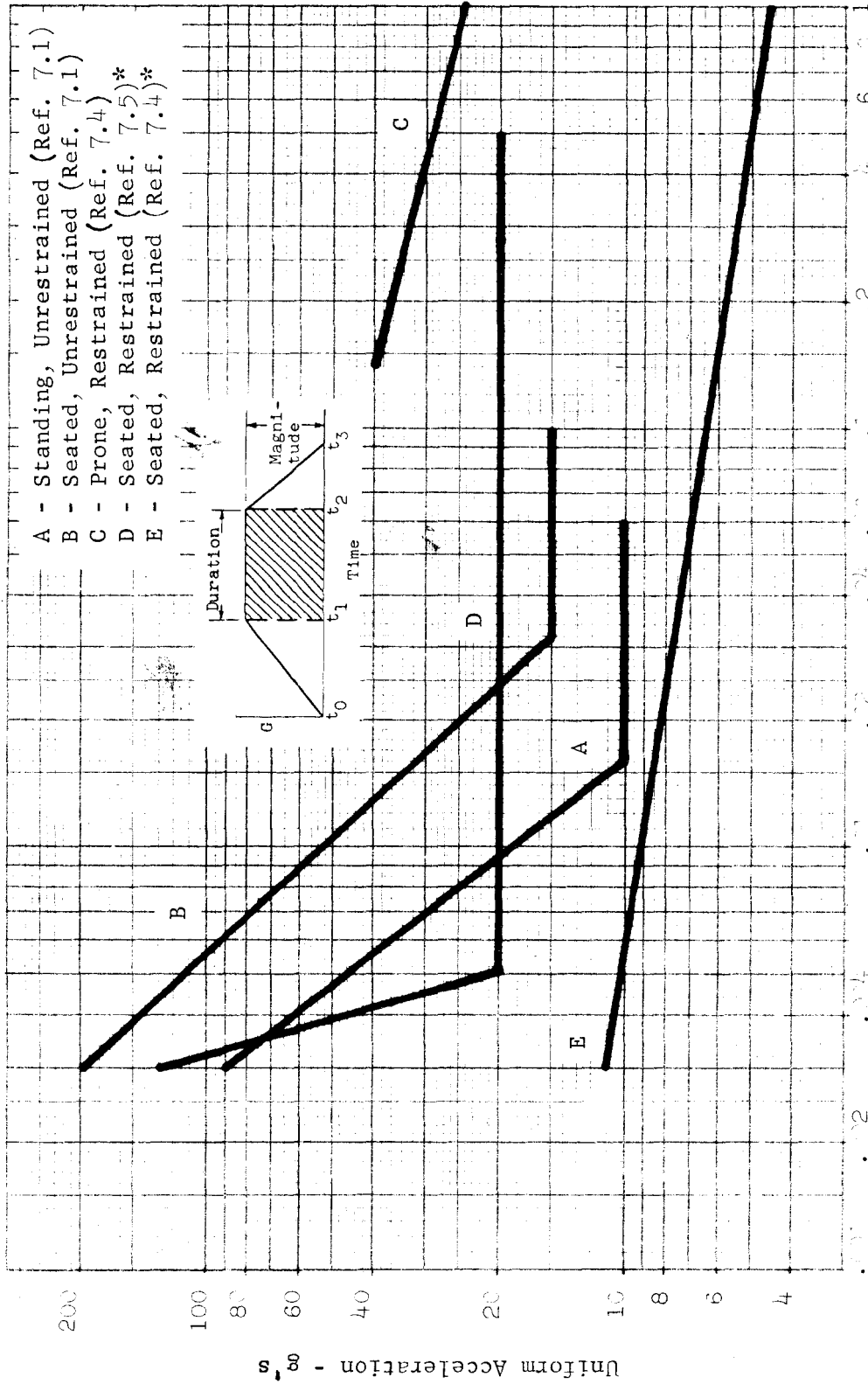
These categories are broken down further for consideration of man's shock tolerance in the restrained or unrestrained condition where data is available.

a. Standing, unrestrained. It is the conclusion of Reference 7.1 that an unrestrained, standing man will respond to a rapidly applied motion or shock delivered upward through the feet, by first going into compression during the interval of application of a positive g load, and then by flying upward. He will receive direct compressive-injuries in the body-supporting bones near the point of load application when the upward floor acceleration exceeds about 20 g during a long-duration shock loading, or at higher accelerations for a short-duration pulse producing floor peak velocities of more than 10 feet per second. He will leave the floor with a kickoff velocity that varies from 60 to 120 percent of the floor peak velocity, depending on the rise time to the floor peak velocity. Curve A in Figure 7.1 represents the above limits reduced by one-half for a man standing on one leg.

During the deceleration phase man may strike overhead objects, lose footing, and fall against objects or the floor. Reference 7.2 indicates that skull fractures occur if the head hits a hard flat surface after a free fall of 5 feet. Head impact with a blunt corner requires only a small fraction of the 5 foot drop for a skull fracture. If the chance of impact injury for the unrestrained operator can be eliminated by the use of protective gear, such as crash helmets, and by providing resilient padding on all exposed corners and projections, the accelerations indicated by Curve A in Figure 7.1 can be used for design maxima.

A conservative design procedure is to attenuate the ground shock to very low accelerations in order to avoid injuries to unrestrained operators. Reference 7.3 indicates that the maximum value for an upward shock motion is 0.75 g to avoid loss of footing and possible impact injury from a fall.

A rapid downward acceleration of the floor causes a man to drop a maximum distance equal to the total downward floor displacement. A drop of only 19 inches is required to obtain a velocity of 10 feet per second, enough to fracture both legs, or a drop of only 5 inches can fracture one leg supporting the entire body weight. In the case of a rapid ground return.



Duration of Positive Uniform Acceleration ( $t_2 - t_1$ ) - Seconds

\* Curve D is an upper comfort limit, above which injury can occur, while Curve E is based on subjective comfort responses to centrifuge tests.

FIGURE 7.1: HUMAN SHOCK TOLERANCE TO PREVENT INTERNAL INJURY  
(IMPACT INJURY NOT CONSIDERED)

the impact load could be even greater than with no ground return. Reference 7.3 indicates that the maximum value for a downward shock motion is 0.5 g to avoid loss of footing and possible impact injury from a fall.

Horizontal accelerations of the floor over 0.5 g can cause loss of balance of a standing man with the attendant impact injury possibilities.

b. Sitting, unrestrained. Reference 7.1 concludes that an unrestrained, seated man subjected to a shock input will receive direct compressive-injuries in the body-supporting bones near the point of load application when the upward floor acceleration exceeds about 15 g during a long-duration shock loading, or at higher accelerations for a short-duration pulse producing peak floor velocities more than 10 feet per second. He will also leave his chair (if it is secured to the floor) with a kickoff velocity which varies from 60 to 120 percent of the peak floor velocity, depending on the rise time to the peak floor velocity. Curve B in Figure 7.1 represents the above acceleration limits for an unrestrained seated man. It should be noted that vertebrae fractures have been produced with long-duration upward acceleration levels of 3 to 4 g for seated subjects with only a lap-belt support (Reference 7.5). If the chance of impact injury for the unrestrained operator could be eliminated by the use of protective gear, such as crash helmets, and by providing resilient padding on all exposed corners and projections, the accelerations indicated by Curve B in Figure 7.1 could be used for design maxima.

A conservative design procedure is to attenuate the ground shock input to very low accelerations in order to avoid injuries to the unrestrained operator. Because of the possibility that an unrestrained man can fall out of his chair, Reference 7.3 recommends a maximum value of 0.75 g for upward accelerations.

A rapid downward acceleration of a chair (if it is secured to the floor) causes an unrestrained man to drop a maximum distance equal to the total downward floor displacement. A fall of only 19 inches is required to obtain a velocity of 10 feet per second, which can injure his spine. Reference 7.3 recommends a maximum value of 1 g to avoid separation of an unrestrained man from his chair.

Horizontal accelerations can cause an unrestrained, seated man to fall off and to impact against the chair or nearby objects, or to suffer whiplash injury. In order to avoid the above possibilities, horizontal accelerations for seated operators have been limited to 1 g in many hardened installations.

c. Prone, unrestrained. The prone position normally applies to hardened facilities with a requirement to provide sleeping quarters for operators. A man is usually partially isolated by resilient material when he is in a prone position. In addition, he is capable of tolerating much higher acceleration loads in the direction transverse to his spinal axis than in the parallel direction. Reference 7.4 presents tolerance levels for centrifuge tests with man in the restrained prone position that agree with data in Reference 7.2 for man falling flat on the back. Curve C in Figure 7.1 presents the centrifuge results for a restrained prone man. If the prone operators were provided with a completely padded enclosure, the accelerations mentioned above could be used for design.

An unrestrained man would leave his bed (if it is secured to the floor) with a kickoff velocity depending on the rise time to the peak floor velocity. Because of the possibility that an unrestrained man can fall out of his bed, a maximum value of 0.75 g has been recommended for the upward acceleration limit.

A rapid downward acceleration of the bed (if it is secured to the floor) causes an unrestrained man to drop a maximum distance equal to the total downward floor displacement. While he may not be injured from landing on a resilient bed, he may also land on the floor and receive impact injuries. A maximum value of 1 g is recommended for downward accelerations to keep a prone man from falling out of his bed.

Horizontal accelerations would not be imparted to an unrestrained man to any extent because he would be free to slide or roll on the bed. A maximum horizontal acceleration of 0.75 g is recommended to prevent a man from rolling off his bed and suffering impact injuries.

d. Sitting, restrained. It should be noted that the term restrained means that the subject is harnessed to a seat so that his limbs and head

move uniformly with his body, i.e. there is no change in alignment of head and limbs. The restrained seated man is not subject to kickoff from his chair after an upward shock motion, and should not impact with the floor or objects in the room. Many tests have been performed to obtain tolerance values for ejection seat design. Curve D in Figure 7.1 is the upper limit reported in Reference 7.5 for design of upward ejection seats. Centrifuge results shown as Curve E in Figure 7.1 include rapid deceleration in the motion, and indicate a somewhat lower tolerance. The latter data are used for longer duration accelerations common to space capsule launches and re-entry. A conservative design approach is to use the latter values for the restrained seated man, since the results include both an acceleration and deceleration phase in the centrifuge pulse.

Reference 7.5 indicates that man's tolerance to downward accelerations in the restrained seated position is about the same as his tolerance to upward accelerations. Therefore, Curve E in Figure 7.1 is recommended for downward acceleration limits for the restrained seated man.

Reference 7.5 indicates that a restrained seated man can tolerate higher forces in the horizontal direction than in the vertical. However, a conservative approach is to use the same limits for horizontal accelerations as are recommended for the vertical accelerations, i.e. Curve E in Figure 7.1.

e. Prone, restrained. The restrained prone man is not subject to falling from his bed, and can tolerate relatively high vertical accelerations, which are indicated by Curve C in Figure 7.1.

Horizontal accelerations for the restrained, prone man induce physical effects similar to those occurring during vertical accelerations of a seated man. Therefore, Curve E in Figure 7.1 is indicated for the horizontal tolerance limits for the restrained prone man.

7.2.2 Summary of human shock tolerance. The variation in man's shock tolerance with the duration of the shock acceleration is shown in Figure 7.1 for several positions. Table 7.1 summarizes the recommended limits of shock accelerations for design in protective structures. It should be noted that the lower of the recommended limits for an unrestrained man are

TABLE 7.1: RECOMMENDED DESIGN VALUES FOR HUMAN TOLERANCE TO SHOCK MOTIONS

- A. Limiting value of acceleration force to prevent internal injury.
- B. Limiting value of acceleration force to avoid possible impact injury.

Shock Direction Posture	Upward	Downward	Horizontal
Standing - Unrestrained	A. 10 g B. 0.75 g	A. 5" at >1 g B. 0.5 g	A. * B. 0.5 g
Sitting - Unrestrained	A. 15 g B. 0.75 g	A. 19" at >1 g B. 1.0 g	A. * B. 1.0 g
Prone - Unrestrained	A. 40 g B. 0.75 g	A. * B. 1.0 g	A. * B. 0.75 g
Sitting - Restrained	A. Curve E, Fig. 7.1 or 15 g	A. Curve E, Fig. 7.1 or 15 g	A. Curve E, Fig. 7.1 or 15 g
Prone - Restrained	A. Curve C, Fig. 7.1 or 40 g	A. Curve C, Fig. 7.1 or 40 g	A. Curve E, Fig. 7.1 or 15 g

\* Displacement limited, i.e. shock displacement must be attenuated to less than the distance between operator and nearest solid object.



conservative to avoid possible impact injury caused by loss of balance.

It is difficult to isolate the effect of the rate of rise to the peak shock acceleration on man. However, Reference 7.5 indicates that a rate of rise equal to 1000 g per second can be tolerated at the shock levels recommended for design.

In designs where vertical and horizontal shock pulse effects are combined, it is recommended that the acceleration vector sum be limited to the lower of the horizontal or vertical limits.

7.2.3 Tolerance to steady-state vibrations. Human tolerance to vibrations is an important consideration in the design of shock isolation systems for structures containing operating personnel, since these systems will continue to vibrate after exposure to the initial shock for periods of time dependent on the degree of damping.

Human tolerance to vibrations has been studied as a function of the vibration frequency, amplitude, duration and subject posture. Reference 7.6 presents the results of short-term vertical vibration tests on man in a restrained seated position. These results are presented in Figure 7.2 in the form of peak acceleration versus frequency of vibration. The duration of the test for each frequency is also noted. These durations may be used to determine the damping requirements for a shock isolation system.

It is interesting to note the dips in the vibration tolerance curve (Figure 7.2) near 4 to 8 cps, which correspond to the natural frequencies of some internal organs. Reference 7.2 describes the various studies of the mechanical impedance of the human body that correlate with vibration tolerance.

Reference 7.7 indicates that standing subjects restrained only at their feet can tolerate higher vertical accelerations than restrained seated subjects. In addition, knee flexing further increases the tolerance level.

A similar tolerance curve for transverse or horizontal vibrations is not available. Reference 7.2 indicates that man can tolerate higher accelerations in the transverse direction than in the direction parallel to his spinal axis. However, head motion of a seated subject is amplified by resonance at a frequency of 2 cps. The head could be restrained to avoid the latter type of response.

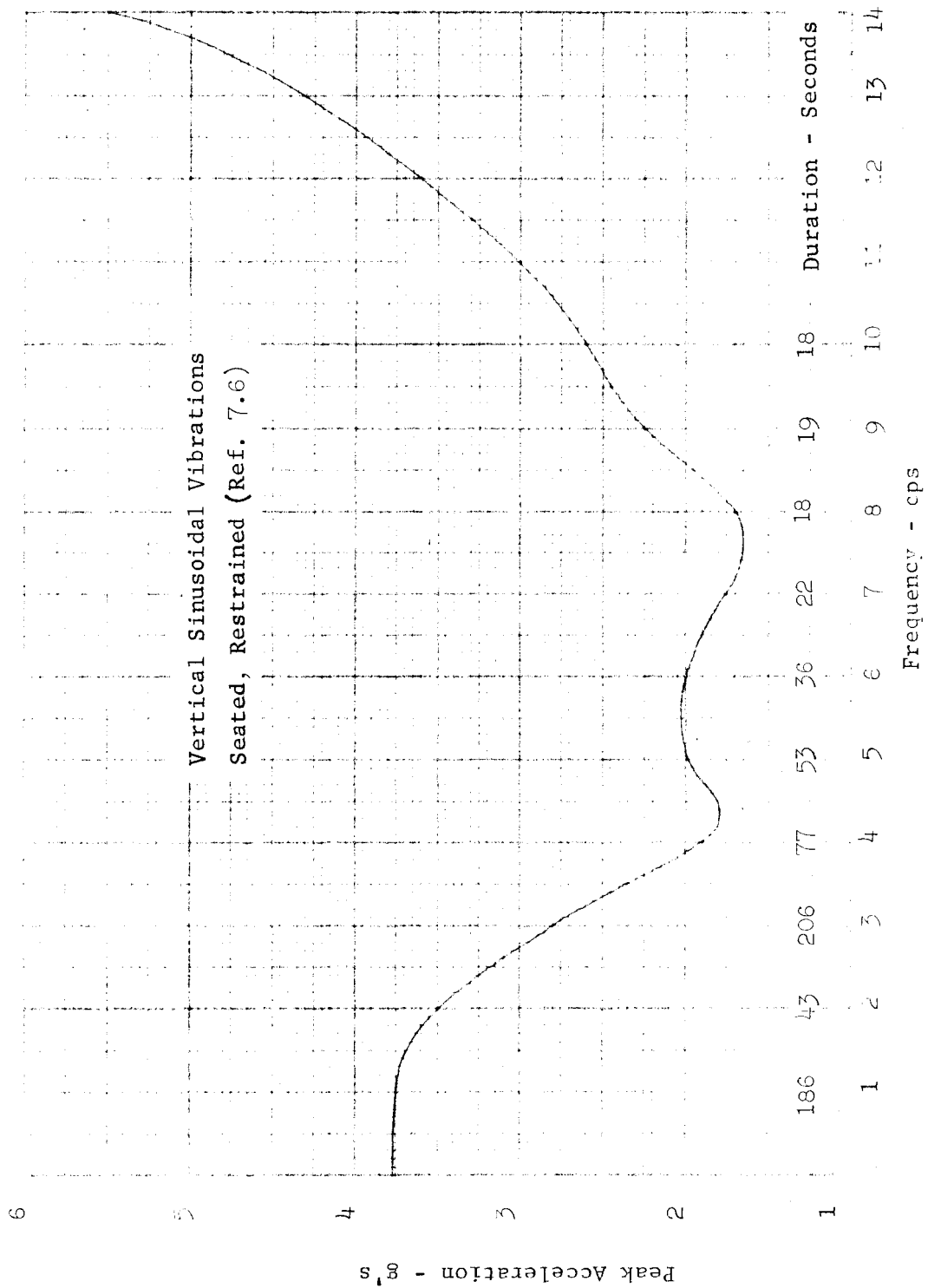


FIGURE 7.2: HUMAN TOLERANCE OF STEADY STATE VIBRATION

Most of the experimental tests on man have been conducted with unidirectional vibration equipment. It is expected that the response of shock isolation systems to ground shock will produce simultaneous vibration in more than one direction, and probably at different frequencies. Careful consideration must be given during the design analysis of the shock isolation system in limiting the combined acceleration from all direction modes to the recommended tolerance values.

In the discussion of shock tolerance, it was mentioned that very low acceleration limits were required to prevent the unrestrained man from falling and suffering impact injuries. Similarly when an unrestrained man is subject to vibratory motions, the floor acceleration must be limited to relatively low values in order to prevent loss of balance and impact injury. The vibration acceleration values recommended for design of shock isolation systems for the unrestrained man are the same as the limiting shock accelerations recommended for the unrestrained man (see Table 7.2).

In the discussion of shock acceleration tolerance, it was mentioned that the unrestrained man could possibly tolerate higher shock levels than those recommended if certain protective measures were used. Similarly, it might be possible to raise the vibration acceleration tolerance for the unrestrained man if he were provided the same protection, and in addition, were provided some form of hand grip restraint to secure himself against the oscillating floor motions. However, it is doubtful that the limiting vibration tolerance for a restrained man could be used, because man cannot secure himself by a hand grip when under an oscillating 3 g load.

The vibration tolerance of a restrained man is discussed below for the seated and prone positions.

a. Sitting, restrained. Figure 7.2 may be used for the vertical vibration tolerance of restrained seated subjects, if the duration of vibration is held within the time limits indicated. It is reasonable to assume that most shock isolation systems are designed with sufficient damping to attenuate the acceleration to negligible levels within one minute. At frequencies below 2 cps the body acts as a unit mass.

If the head is restrained, a seated man can tolerate higher accelerations horizontally than vertically. However, as a conservative design approach, the use of Figure 7.2 is recommended for both the vertical and horizontal vibration tolerance of a restrained seated man. In addition, for cases when the shock isolation system response has vertical and horizontal components the vector sum should be limited to the tolerance values of Figure 7.2.

b. Prone, restrained. The vibration tolerance of man in the restrained prone position has not been reported. However, the tolerance in the prone position should be higher than in the seated position. Therefore, it is recommended that Figure 7.2 be used for the restrained prone position with the limitations discussed for the restrained seated position.

7.2.4 Summary of human vibration tolerance. The vibration tolerance values shown in Figure 7.2 for a restrained seated man are upper limits for total durations of one minute or less. This time restriction should be compatible with the damping characteristics of most shock isolation systems.

Table 7.2 summarizes the recommended vibration tolerance values for the restrained and unrestrained man in various positions. The values recommended for the unrestrained cases are consistent with the limiting shock accelerations recommended for the unrestrained man.

The vector sum of all vibration mode accelerations should be used to determine the shock isolation system limitations.

7.2.5 Design for human tolerance limits. In the design of any hardened facility where human operators are required, it is first necessary to determine whether the shock environment exceeds the human shock tolerance. Section 7.2.1 presents human shock tolerance values for various conditions. When the shock environment exceeds the human shock tolerance, a shock isolation system must be provided. The limiting shock tolerance values in Table 7.1 may be used.

The vibratory response of the shock isolation system must be less than the human vibration tolerance values discussed in Section 7.2.3 and summarized in Table 7.2. Section 8 of this report presents a detailed design procedure for a shock isolation system where human tolerance to shock and

TABLE 7.2: RECOMMENDED DESIGN VALUES FOR HUMAN TOLERANCE TO VIBRATION

- A. Limiting value of acceleration force to prevent internal injury
- B. Limiting value of acceleration force to avoid impact injury.

Vibration Direction Posture	Vertical	Horizontal
Standing - Unrestrained	B. 0.5 g	B. 0.5 g
Sitting - Unrestrained	B. 0.75 g	B. 1.0 g
Prone - Unrestrained	B. 0.75 g	B. 0.75 g
Sitting - Restrained	A. Figure 7.2 or 3 g , $f < 2$ cps 1 minute or less	A. Figure 7.2 or 3 g , $f < 1$ cps 1 minute or less
Prone - Restrained	A. Figure 7.2 or 3 g , $f < 2$ cps 1 minute or less	A. Figure 7.2 or 3 g , $f < 2$ cps 1 minute or less

vibration is considered.

In the two examples discussed below, one facility without shock isolation is reviewed to determine the predicted human tolerance to the shock environment, and another facility with shock isolation is reviewed to determine the predicted human tolerance to the vibration environment.

Example 7.1

The following shock environment is postulated for a structure floor without a shock isolation system:

	<u>Vertical Shock</u>	<u>Horizontal Shock</u>
Peak Acceleration	10 g	10 g
Peak Velocity	30 in/sec	20 in/sec
Peak Displacement	6 inches	2 inches

Peak vertical and horizontal motions may occur simultaneously. Initial motion may be up or down.

Under what conditions can personnel function, and when is shock isolation required?

Each of the possible operator positions is discussed separately below:

Standing, unrestrained. Refer to Figure 7.1, Curve A. An operator standing on two legs would not suffer foot or leg fractures from an upward shock of 10 g. However, if he were walking, it is possible that his foot or leg would be fractured, because his weight could act through one foot or leg. A stiff-legged free-fall following a downward shock motion would not fracture two legs, because he would not reach a velocity of 10 fps. However, if he landed stiff-legged on one leg he could fracture that leg, because his velocity would be over 5 fps.

Referring to Table 7.1, the accelerations are above the limits recommended to prevent loss of balance and impact injury. It is quite likely that an unrestrained standing operator would receive impact injury.

Sitting, unrestrained. Refer to Figure 7.1, Curve B. An operator is not likely to suffer a spine injury from an upward shock, or from free-fall following a downward shock. An upward shock could throw him out of a chair against equipment or to the floor, where he could suffer impact injury. Referring to Table 7.1, the accelerations are above the limits

Example 7.1 (continued)

recommended to prevent loss of balance and impact injury. The unrestrained seated operator could receive impact injury.

Prone, unrestrained. Refer to Figure 7.1, Curve C. It is not likely that an operator in this position would receive a direct shock injury. However, he could be thrown out of his bed. Referring to Table 7.1, loss of balance and impact injury is possible for the unrestrained prone operator.

Sitting, restrained. Refer to Figure 7.1, Curves D and E. Even though the vector sum of the vertical and horizontal motions is above the recommended value (Curve E), it is still well below the limit for ejection seat design (Curve D). It is probable that a well-restrained seated operator could function immediately after the shock impulse.

Prone, restrained. Refer to Figure 7.1, Curves C and E. The vertical shock component is well below the limiting value (Curve C). It is most probable that a restrained prone operator could function immediately after the shock impulse.

Conclusion. If unrestrained operators are present, shock attenuation is required to avoid possible impact injury. If well-restrained operators only are present, no shock attenuation is required.

Example 7.2

A shock isolated platform is designed with the following response characteristics:

	<u>Vertical</u>	<u>Horizontal</u>
Peak Acceleration	1.5 g	0.08 g
Frequency	1.0 cps	0.4 cps
Peak Displacement	15 inches	5 inches

Initial motion may be up or down. Time required to damp response to 1/6 peak value is 30 seconds.

Under what conditions can personnel function?

Refer to Figure 7.2. The vibration tolerance for these frequencies is over 3 g. Therefore, vibration injury to internal organs is not a problem.

### Example 7.2 (continued)

Unrestrained positions. Refer to Table 7.2. The peak vertical acceleration is greater than the recommended values for all unrestrained positions. Therefore, unrestrained operators could receive impact injuries.

Restrained positions. Refer to Figure 7.2. The peak vertical and horizontal vibrations are well below the limiting values for restrained positions. Therefore, restrained operators could function at the end of the indicated damping period.

Conclusion. If unrestrained operators are present, additional attenuation of the response acceleration is required to avoid possible impact injury. If restrained operators only are present, no change in the system is required.

## 7.3 Equipment Fragility

The purpose of this section is to serve as a guide to the designer who must determine the fragility of equipment, in order to know whether or not shock isolation is required, and if so, the degree and form of shock isolation required to prevent an operational failure of the equipment under the maximum anticipated shock input. This section is limited to a discussion of the availability of fragility data, evaluation of test data, and procedures for design and testing for shock and vibration.

7.3.1 Availability of test data. The shock isolation system designer will generally be concerned with equipment which is similar to already procured equipment for corresponding applications, and which has been subjected to shock and vibration tests for acceptance. These test data will usually be found in various government and manufacturer's files. Occasionally, a test report for a particular item is released through a government publication. Although very few summaries of equipment test data have been attempted because of the magnitude of the effort required and the rapid obsolescence of most equipment, Reference 7.8 does contain a summary of test results obtained from a number of government agency reports. It is possible to refer back to the reports cited in Reference 7.8 for more accurate descriptions of the equipment involved. However, it is unlikely that the



above summary of equipment tests would include the models presently on the market. Fortunately, most manufacturers will provide some form of test data on their products, if available.

In the event that test data are not available for the equipment in question or a unique type is required, the usual design schedule does not allow sufficient time to obtain test data before the item is chosen and the facility design fixed. It is then necessary to estimate the fragility of the chosen equipment. The fragility can often be estimated by analysis of the equipment design or by careful comparison with other tested equipment having a similar construction feature. Chapter 42 of Reference 7.9 illustrates the procedures for comparative analysis of equipment structures using equivalent models to determine shock and vibration capabilities.

Several attempts have been made to classify equipment into various categories according to its function and fragility. One example of such a classification is found in Reference 7.10. Only the lowest vulnerability level and equipment frequencies obtained from Reference 7.10 are presented in Table 7.3, because the details of the equipment design and test data are largely unknown. A fair amount of equipment used in a typical facility will fall into one of the categories listed in Table 7.3. Use of the above values will usually lead to conservative shock isolation design requirements.

7.3.2 Interpretation of test data. A word of caution is given to the designer using shock test data so that he will not accept the test data without evaluating the test conditions and failure criteria. In addition to knowing the acceleration response capability it is desirable to know the natural frequencies of the equipment, the directions along which the disturbance was applied, and what were the failure criteria.

Shock spectra have been reported for the standard shock machines for various loadings and modes of operation, which can be used to determine acceleration response capability (see Reference 7.8). Figure 7.3 shows typical shock spectra for several shock testing machines. The natural frequencies of equipment are determined by analysis or by finding resonances with vibration test machines. Therefore if (1) it is known that the equipment or similar equipment has already passed a shock test which produced

TABLE 7.3: ESTIMATES OF FREQUENCY AND VULNERABILITY  
OF TYPICAL EQUIPMENT ITEMS

Item	Lowest Fundamental Natural Frequency cps	Estimated Vulnerability Level g
Heavy Machinery--Motors Generators, Transformers, etc. (> 4000 lb)	5	10
Medium Wt. Machinery-- Pumps, Condensers, Air Conditioning, etc. (1000 to 4000 lb)	10	15
Light Machinery--Fans Small Motors, etc. (< 1000 lb)	15	30
Racks of Communication Equipment, Relays, Rotating Magnetic Drum Units, Large Electronic Equipment with Vacuum Tubes	10	2
Small Electronic Equipment Radios, Incandescent Lamps and Light Bulbs	20	20
Cathode Ray Display Tubes	5	1.5
Transistorized Computers, Fluorescent Lamps and Fixtures, Nuclear Reactors	10	5
Storage Batteries (All Types), Piping, and Duct Work	5	20

a known shock spectrum and (2) if the lowest natural frequency of the equipment is known, then the acceleration response capability can be estimated. For example, if the lowest frequency of an equipment module is 15 cps, and it passed the machine shock test denoted by Curve B in Figure 7.3, then the acceleration response capability is about 20 g's or greater.

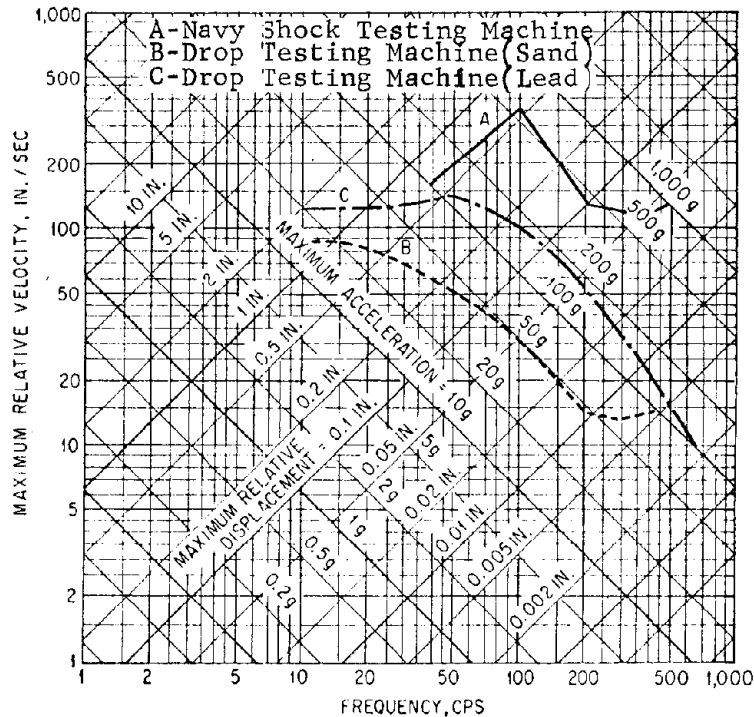


FIGURE 7.3: TYPICAL SHOCK SPECTRA (REFERENCE 7.9)

This approach in defining a fragility level obviously must be used with caution for two reasons:

(a) Since the actual equipment is a multi-mass multi-degree-of-freedom system, then unless it is identical in every respect to the equipment that was tested, there may be higher mode resonant conditions of the internal components which may fail, even though the equipment module at its lowest frequency does have the capability specified by the test machine.

(b) Most tests are performed so that the shock is delivered to the equipment's vertical and horizontal axes separately. In order to duplicate the field input, it is necessary to combine horizontal and vertical

shock inputs by proper orientation of the equipment on the test bed. Therefore, if test data are not available for combined shock loading, it is good practice to assume that the fragility level for the horizontal and vertical component is 0.707 times the rated fragility level in Table 7.3 or that obtained from shock test data.

Modes of failure vary for different equipment and operational requirements. The mode of failure for an air conditioning compressor might be structural, while that for a relay could be purely operational, such as chattering of the contacts under dynamic conditions. With some equipment it will be necessary to know whether it is to be operating at the time of attack, in order to determine the possible ways of failure. In high speed rotating equipment, for instance, gyroscopic moments could be developed and cause a failure which might not otherwise occur. On the other hand, the deformations which would occur in a bearing due to an overload often can be better tolerated if rotation occurs in the bearing than if it is in a static condition.

It is always desirable to know whether the equipment is to be in operation during an attack. Thus, if there are uninsulated conductors that can contact one another during shock, a short circuit could occur. It is apparent, then, that the determination of various failure criteria must be considered when evaluating shock test reports on the equipment to be used.

7.3.3 Design and test for shock. After assessing the equipment fragility level, it is necessary to determine if a resilient element between the structure and equipment module or between the structure and the ground is required to obtain an acceptable acceleration response. If the equipment tolerance level is believed to exceed the given shock-spectra criteria for items mounted directly to the structure, the designer must design equipment anchors to the structure of sufficient strength to resist the inertia forces caused by the acceleration response. He must also write a shock-test specification for the equipment with anchors to validate that the equipment as anchored will indeed survive the shock-spectra criteria.

7.3.3.1 Test specifications. Two methods of specification may be employed in defining a shock test: (1) a specification of the input shock motions

to which the item under test is to be subjected, or (2) a test specification for a particular shock machine whose shock spectrum is known; the method of mounting the test item; and the procedure for operating the machine.

The first method of specification can be used only when the input shock motion can be defined in a reasonably simple manner. (See Section 3 for typical ground motion pulses.)

The second method of specification for a shock test assumes that it is impractical to specify a shock motion because of its complexity; instead, the specification states that the shock test shall be performed in a given manner with a specified shock spectrum or on a particular machine with a known shock spectrum. If a machine is specified, then it should be known that the shock machine will generate appropriate shock response motions. This method avoids a difficulty that arises in the first method in that the undefined input shock motions need not be specified.

An example of the second method of specifying a shock test is presented below (Reference 7.11):

"Equipment to be mounted without individual isolators in structures which are not shock isolated shall be subjected to six shock machine shocks, which produce the shock spectrum specified in Figure 7.4, and shall show no failure, malfunction, or out-of-tolerance performance. Shocks shall be applied at the point of attachment of the equipment to the structure. The shock test shall consist of two shocks in each of three mutually perpendicular directions." In this case the peak acceleration response of 200 g's (Figure 7.4) is the resultant of the horizontal and vertical acceleration components, which is applied as a single component in the six shock tests specified. Since combined horizontal and vertical shock inputs are not usually feasible, the above test of applying a shock input along each axis to produce a response equal to the resultant of the specified criteria values, will induce acceptable critical test conditions. Instead of defining the shock spectrum a specification describing a shock machine with a known shock spectrum and the procedure for operating the machine may be desirable. Military Specifications and Standards which involve the use of

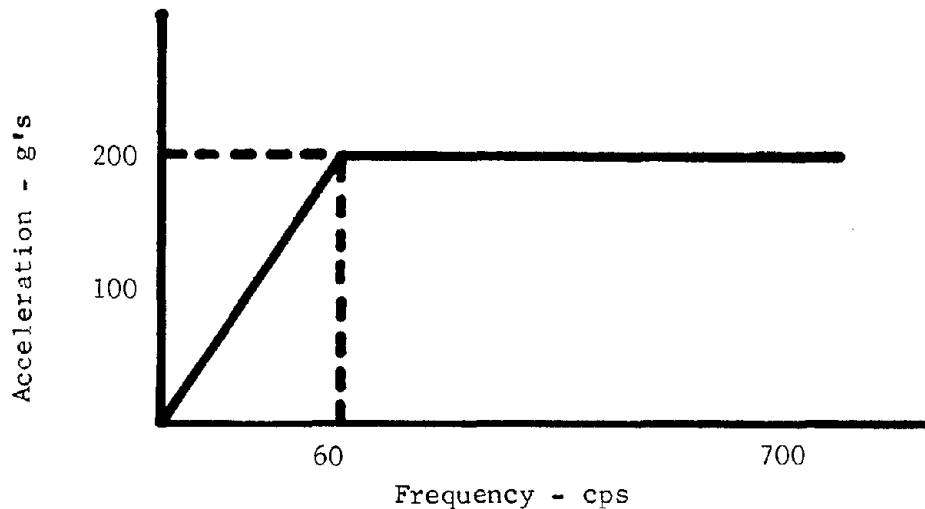


FIGURE 7.4: SHOCK SPECTRUM

standard shock-test machines and procedures are listed below:

MIL-S-901C	High Impact Shock Test Requirements for Shipboard Machinery, Equipment and Systems
MIL-STD-202C	Test Methods for Electronic and Electrical Component Parts

7.3.3.2 Shock-testing machines. A detailed description of shock-testing machines can be found in Chapter 26 of Reference 7.9 and Section 4 of Reference 7.3. The shock machine characteristics, such as the nominal acceleration, velocity change, shock duration and maximum load, have been tabulated. Most important, the limitations and applications of the various machines and methods are discussed.

A number of shock testing machines have been developed for general and for special purposes; they see continued use in the qualification of equipment for military service. Several of these machines produce shock motions whose spectra are generally equivalent to the spectra that define the shock used as a basis for design of equipment for hardened facilities. This is a fortunate circumstance for several reasons:

- (1) The testing machines are available and considerable experience in their use has been accumulated. It is thus possible

to conduct the tests necessary to qualify equipment, using existing test facilities and personnel.

- (2) To the extent that equipment commonly used for military applications will be used, shock tests may have already been conducted and qualification records may be available.

The existing shock machines are limited in their time duration, and therefore only produce the acceleration due to the initial velocity rise of the air slap induced ground motion. The actual motion input to the equipment may be a high frequency random oscillation or a forced transient followed by a free steady-state vibration due to the motions of the supporting structure produced by either induced ground motion or air blast striking an aboveground structure. This oscillating motion may be detrimental to internal components in the equipment, whereas these same components may survive the shock pulse generated by existing shock machines. As the dynamic motions of the soil and structure become better defined, shock machines will undoubtedly be developed to produce oscillatory acceleration motions more closely matching structure response motions.

7.3.4 Design and test for vibration. When a shock isolation system is required, the system will usually be designed for low frequency response. The supported equipment will be exposed to a steady-state vibration instead of the high acceleration shock which will now be filtered by the shock isolation system, but in the process of attenuating the shock, other high frequency low amplitude vibrations may be superimposed upon the steady state vibration due to surging or chattering in the spring isolators themselves.

The equipment fragility level must be verified by a vibration test for low frequency as well as high frequency vibration. Resonant response of both internal components and the equipment as a rigid body will be limiting factors in determining fragility levels. It is recommended that manufacturer's data be consulted and a test specification be written that covers the range of predicted vibrations.

7.3.4.1 Vibration testing specifications. A specification for vibration testing usually includes: (1) a description of the motion, whether it is rectilinear, or elliptical; whether the waveform is sinusoidal or otherwise;

whether the plane of motion is horizontal or vertical; (2) the amplitude of the motion, possibly as a function of the frequency at which the motion should occur; and (3) the duration of the test, possibly the rate of change of frequency or sweep rate. A very good description of environmental testing as related to simulated vibration conditions can be found in Chapter 24 of Reference 7.9.

An example of a vibration specification used and relating to a rack of equipment is presented below (Reference 7.11):

Amplitude

3 g rms (limit to 6 inch double amplitude)

2 to 8 cps (applicable to entire rack at attach points to floor)

2 g rms

8 to 2000 cps (applicable to rack contained equipment and accessories at attach points to rack)

Duration

One sweep at one-half octave per minute both increasing and decreasing in frequency.

Military Specifications and Standards which describe typical vibration tests are listed below:

MIL-STD-202C	Test Methods for Electronic and Electrical Component Parts
MIL-STD-167	Mechanical Vibrations of Shipboard Equipment
MIL-E-5272C	Environmental Testing of Aeronautical and Associated Equipment

7.3.4.2 Vibration testing machines. A detailed description of available vibration testing machines can be found in Chapter 25 of Reference 7.9. The performance characteristics, such as the frequency range, maximum load, acceleration, displacement and frequency cycling period, for various vibration machines have been tabulated.

Vibration testing machines are characterized by the type of drive mechanism employed, such as, direct drive mechanical, reaction-type mechanical, electrodynamic, hydraulic, electromagnetic, piezoelectric and pneumatic.



Testing specifications fall into three categories: low-frequency (1 to 60 cps), intermediate-frequency (5 to 500 cps), and wide-band (5 to 2,000 or 3,000 cps). In general, in the low-frequency category, the mechanical direct-drive and hydraulic vibration machines are suitable for the lowest frequencies and largest displacements. If displacements are less than 1 inch and frequencies above 5 cps, the mechanical reaction-type machine may be considered. All three of these machines can be fitted with large massive tables, simplifying the attachment of the test article to the vibration table. The electrodynamic vibration machine can be used for displacements below 1 inch and frequencies above 3 to 5 cps. However, large, heavy test items in this case may require external flexible supports to avoid forcing the table against its stops. In the intermediate-frequency range, the electrodynamic and hydraulic vibration machines may be used. In the wide-band range, the electrodynamic machine is most widely used.

The above testing machines produce steady-state vibration motions along one axis only. A vibration table to specifically simulate vibration motions resulting from ground shock has been studied in Reference 7.12. The system that is proposed consists of a table supported by horizontal and vertical springs. The spring rates are adjustable so that frequencies can be varied between 1 and 10 cps. The equipment is mounted to the table which is displaced horizontally and vertically (simultaneously) and a quick release mechanism sets the table in motion. This test simulates the low frequency vibration caused by ground shock. However, the effect of surging and chattering of the prototype isolators are not simulated in this test. A second test fixture such as the impact test apparatus used to test Minute-man isolation systems (see Section 9.5) is necessary to simulate the effects of the isolator surging and chattering due to the initial ground acceleration.

## SECTION 8: DESIGN PROCEDURES

### 8.1 Introduction

The shock isolation system(s) is an important element in the overall protective system, and it should perform in a specified manner in an air blast or ground shock environment of a given nuclear weapon. It is important to consider the isolation system through every major phase of the overall system design. Figure 8.1 shows a typical System Design Sequence starting with the broad requirements for the system design and weapon effects criteria, and proceeding through several steps to the final system verification program. It can be seen that the shock isolation problem is a major consideration in every phase.

a. When free-field motions are estimated for a proposed site, the feasibility of an isolation system is an important factor in selecting the facility location. If the input motions exceed the capability of shock isolation systems, alternate sites or greater burial depths must be considered. (The choice of an aboveground structure is primarily dependent on the structure design capability at the specified overpressure level.)

b. During the development of preliminary equipment layout concepts, the equipment fragility levels and personnel functions will influence groupings of various components for proper shock isolation.

c. Shock isolation systems play an important part in the selection of a protective structural enclosure. For example, the feasibility and cost of isolating a large multilevel-platform supporting equipment versus individual isolation of many small equipments is a major consideration in selecting the protective enclosure (or enclosures) necessary to house the overall system.

d. During the preliminary design phase the performance characteristics of a shock isolation system, the optimum arrangement of springs, as well as a preliminary design of the springs must be determined in order that sufficient rattlespace requirements can be established.

e. The isolation system and springs must be designed (after a detailed dynamic analysis if required) in the final phase and the technical

specifications for procurement must be written.

f. A system verification program will involve a dynamic test simulating true operational conditions in order to verify the adequacy of complete system performance (equipment performance as well as isolation system performance).

The step-by-step procedure will be demonstrated in the following section with a numerical example. Only the phases which influence the shock isolation system are considered and where procedures and data given in various sections of this report are used, appropriate references are made to section or equation numbers.

## 8.2 Step-by-step Procedure

### 8.2.1 Step 1 criteria

Step 1 (a) system description: A facility is required to provide power and command functions for a hardened communication system. The facility must be capable of surviving two attack conditions. After the first attack the facility must have a 50-day operational capability wherein a second attack may occur of magnitude equal to the first attack.

Step 1 (b) proposed site: The proposed site for the command and power facility has soil characteristics as follows:

From surface to 300' depth:  $c = 4000$  fps  
Below 300' :  $c = 15000$  fps

Step 1 (c) weapons effects criteria: Two attack conditions are postulated; both may be the result of a contact surface burst with a weapon yield of 1 MT to 20 MT and inducing peak overpressures up to 500 psi at the proposed facility. The blast wave characteristics at the 500 psi overpressure level are from Reference 3.2.

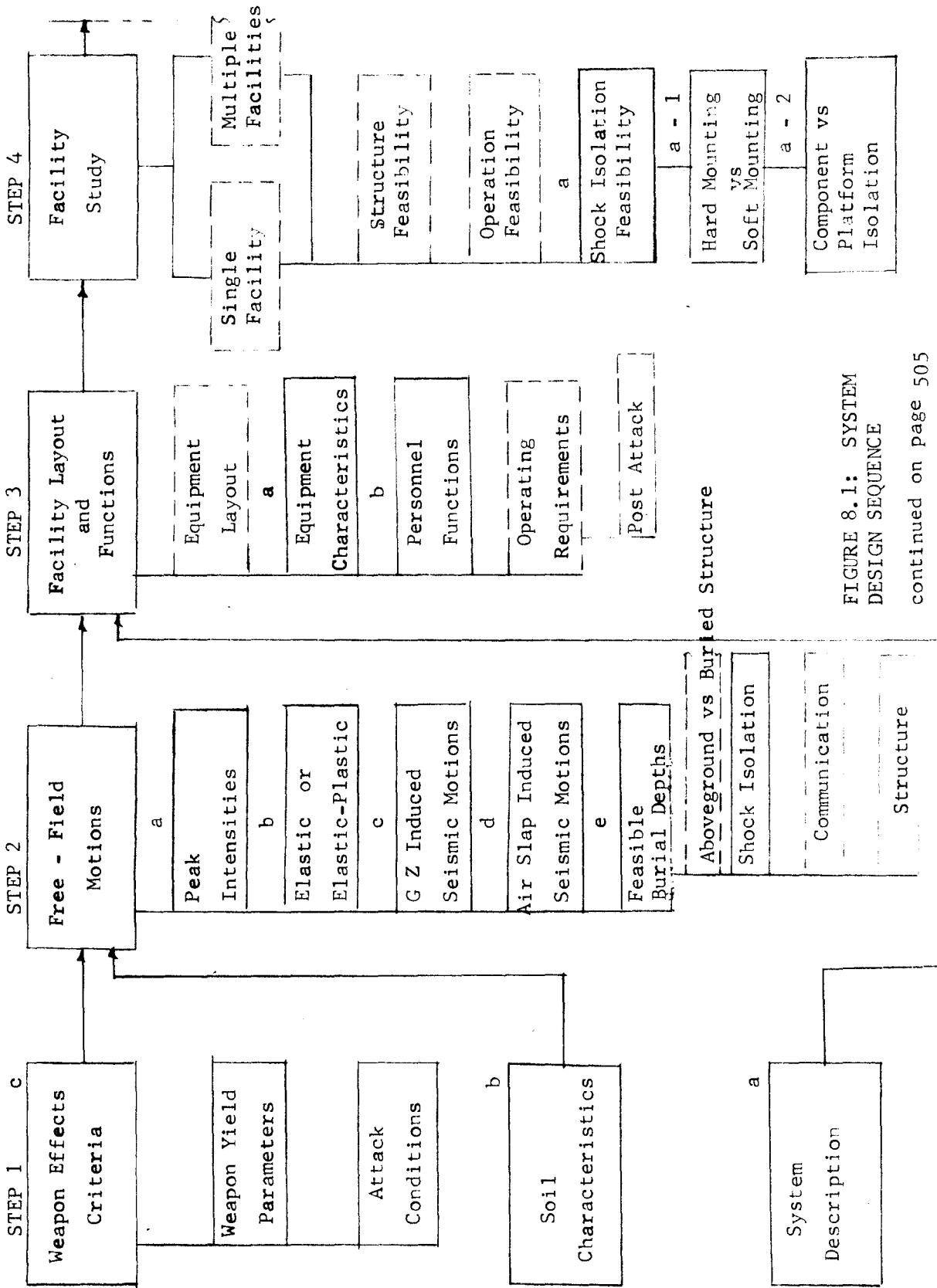


FIGURE 8.1: SYSTEM DESIGN SEQUENCE

continued on page 505

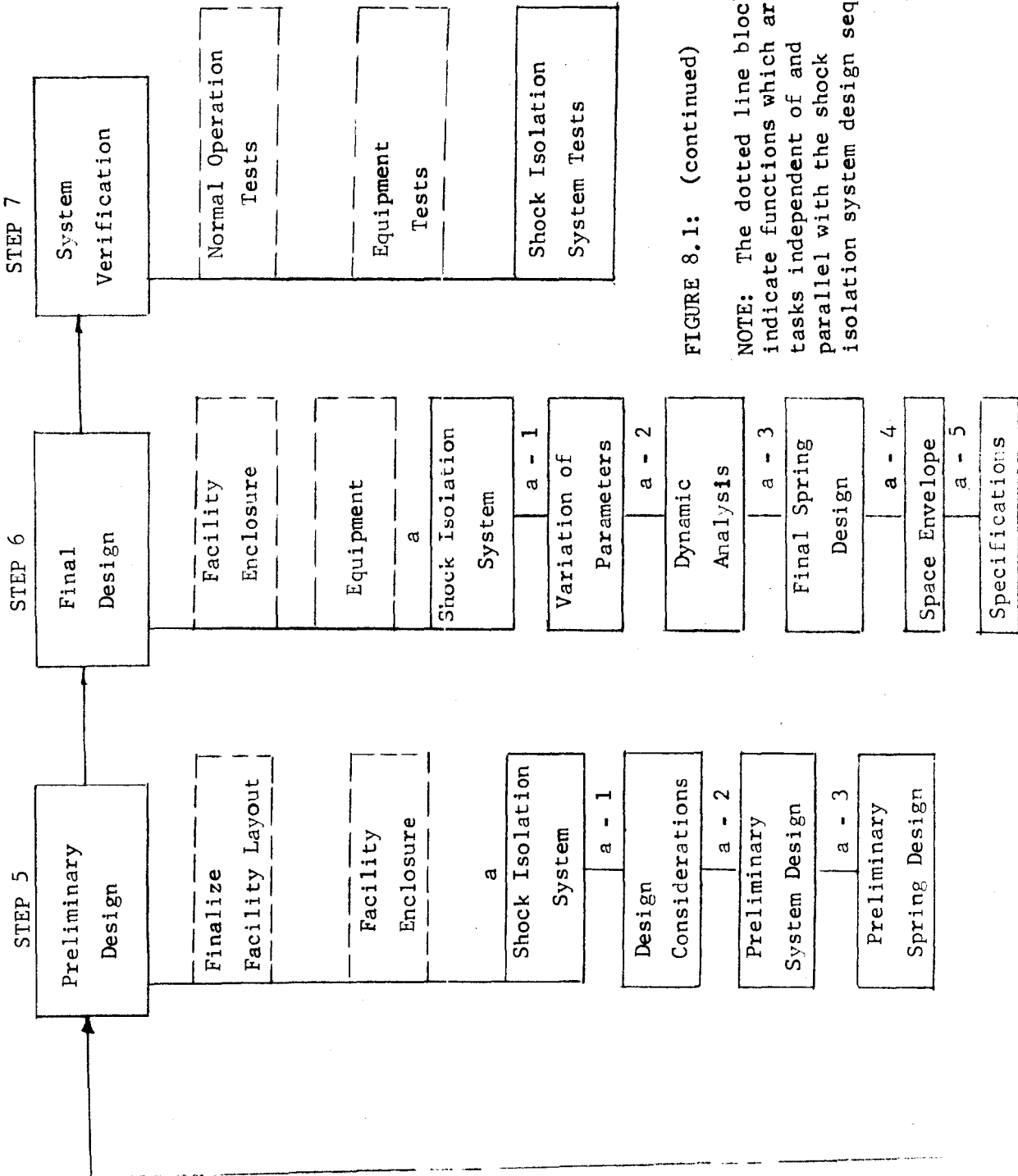


FIGURE 8.1: (continued)

NOTE: The dotted line blocks indicate functions which are tasks independent of and parallel with the shock isolation system design sequence.

continued from page 504

	<u>1 MT</u>	<u>20 MT</u>
$p_{so}$ (peak overpressure)	500 psi	500 psi
$D_p^+$ (positive phase duration - $p_s$ )	1.1 sec	3.0 sec
$t_i$ (equivalent triangular pulse duration - $p_s$ )	0.16 sec	0.435 sec
$q_s$ (peak dynamic pressure)	1000 psi	1000 psi
$D_u^+$ (positive phase duration - $q$ )	2.5 sec	6.8 sec
$t_i'$ (equivalent triangular pulse duration - $q$ )	0.04 sec	0.11 sec
$r_p$ (range from ground zero)	1.9 k-ft	5.2 k-ft
$t_a$ (arrival time)	0.103 sec	0.28 sec

### 8.2.2 Step 2 free-field motions

Step 2 (a) air blast induced motions: The peak ground motion intensities are first calculated for the direct air blast slap at the 500 psi overpressure level. (Seismic motions due to G.Z. induced and air blast induced are considered in steps 2 (c) and 2 (d) respectively). The peak intensities at 0, 25', 50', 75', and 100' burial depth are calculated.

Peak displacements: The elastic displacement at the surface, from Equation 3.22, is

$$d_{vse} = 0.9 P_{so}^{1/2} c_r^{-1} W^{1/3}$$

which is applicable for a homogeneous soil. The postulated condition for this example has a homogeneous layer in the upper 300 feet with seismic velocity  $c = 4000$  fps. Displacements to depths of 100 feet will be calculated from Equations (3.22) through (3.26). The average velocity  $c_r$ , for displacement calculations is assumed to be:

$$c_r = 1/2 (c_p + c_i)$$

Let  $c_i = c = 4000$  fps and  $c_p = 1/2 c_i = 2000$  fps

$$c_r = 3000 \text{ fps}$$

For  $W = 1 \text{ MT}$

$$d_{vse} = \frac{0.9 (500)^{1/2}}{3} = 6.7''$$

For  $W = 20 \text{ MT}$

$$d_{vse} = 18.2''$$

The residual displacement at the surface is given by Equation (3.23).

$$d_{vsr} = \frac{P_{so} - 40}{30} (c_o^{-2}) = \frac{500 - 40}{30 (1.5^2)} = 6.8''$$

The value for  $c_o$  at the surface is assumed to be 1500 fps.

The residual displacements at the other depths are, from Equation (3.24)

$$d_{vzr} \approx d_{vsr} \left(1 - \frac{z^*}{100 \text{ ft}}\right)$$

$z^* = 25'$	$d_{vzr} = 5.1''$
$z^* = 50'$	$d_{vzr} = 3.4''$
$z^* = 75'$	$d_{vzr} = 1.7''$
$z^* = 100'$	$d_{vzr} = 0''$

The elastic component of the relative displacement between the surface and the depths of interest is given by Equation (3.25)

$$d_{vre} = 4.8 \times 10^{-2} P_{so} c_r^{-2} \frac{z^*}{100}$$

For  $z^* = 25'$

$$d_{vre} = \frac{4.8 \times 10^{-2} (500)}{(3)^2} \frac{25}{100} = .67''$$

$z^* = 50'$	$d_{vre} = 1.3''$
$z^* = 75'$	$d_{vre} = 2.0''$
$z^* = 100'$	$d_{vre} = 2.6''$

The peak displacements, elastic plus residual, at the specified depths are:  
(the values are rounded off to the nearest whole number)

			<u>1 MT</u>	<u>20 MT</u>
z =	0'	d <sub>vz</sub> =	14"	25"
z =	25'	d <sub>vz</sub> =	11"	23"
z =	50'	d <sub>vz</sub> =	9"	20"
z =	75'	d <sub>vz</sub> =	6"	18"
z =	100'	d <sub>vz</sub> =	4"	16"

The above values (especially for the 20 MT case) are conservative because Equation (3.22) does not account for attenuation of stress and impulse with depth. A displacement analysis taking small depth increments and adding relative displacements in each increment (as demonstrated in the Air Force Design Manual, Reference 3.2) will give less conservative values. The 20 MT yield gives the maximum displacements.

The horizontal displacement components are taken as 1/3 of the vertical displacements.

Peak velocity: The peak vertical velocity is given by Equation (3.21)

$$v_z = \frac{0.5 p_{so}}{c_p} (\alpha_z) \quad , \quad \alpha_z \text{ is defined in Figure 3.31}$$

<u>z</u>	<u><math>\alpha_z</math> (1 MT)</u>	<u><math>\alpha_z</math> (20 MT)</u>	<u>v (1 MT)</u>	<u>v (20 MT)</u>
0'	1.0	1.0	125 ips	125 ips
25'	0.8	0.91	100 ips	114 ips
50'	0.67	0.83	84 ips	105 ips
75'	0.57	0.79	71 ips	99 ips
100'	0.50	0.72	63 ips	90 ips

A constant value of  $c_p = 2.0$  kfps was assumed in the above calculations for velocity.

The horizontal component of the velocity is taken as 2/3 of the vertical component.

Peak acceleration: The peak vertical acceleration is given by Equation (3.23)

$$a = \frac{5 p_{so}}{z} (\alpha_z) \quad , \quad z \text{ is in feet}$$



<u>z</u>	<u>a (1 MT)</u>	<u>a (20 MT)</u>
5'*	500 g	500 g
25'	80 g	91 g
50'	34 g	42 g
75'	19 g	26 g
100'	13 g	18 g

\* The 5' depth is used in this equation as an indication of the acceleration near the surface.

The horizontal accelerations are assumed to be equal to the vertical accelerations.

It can be seen that the peak intensities are maximum for the highest yield weapon. The displacements are significantly higher, whereas the velocity and acceleration are only slightly higher in varying the yield from 1 MT to 20 MT.

Step 2 (b) idealized velocity pulse due to airblast: It can be seen from the previous calculations for displacement, at the 20 MT level, that the predominant motion is elastic even at shallow burial depths of 25 to 50 feet. Therefore, the ground motion velocity time-history graph will have a negative area which is approximately equal to the positive area. The duration of this velocity pulse is important because of the possible resonance condition for isolation systems with periods near the duration of the ground motion.

A ground motion time history characteristic can be estimated from Equations (3.42) and (3.43) for a triangular velocity pulse. Three depths, 25', 50', and 75', are considered at 20 MT weapon yield only.

$$t_r = \frac{v_{vz}}{a_{vz}} = \frac{114}{91 \times 386}_{25} ; \frac{105}{42 \times 386}_{50} ; \frac{99}{26 \times 386}_{75} ; = (.0032)_{25} ; (.0058)_{50} ; (.01)_{75}$$

$$t^+ = \frac{2d_{vz}}{v_{vz}} = \frac{2 \times 23}{114}_{25} ; \frac{2 \times 20}{105}_{50} ; \frac{2 \times 18}{99}_{75} ; = (.4)_{25} ; (.38)_{50} ; (.36)_{75}$$

Assuming that the duration of the negative velocity is 3 times the positive phase duration,

$$t_d = 4 t^+ = (1.6)_{25} ; (1.52)_{50} ; (1.44)_{75}$$

then the peak negative velocity is 1/3 the peak positive velocity for complete ground return. The pulse shown in Figure 8.2 defines the important characteristics of the velocity pulse due to the direct air slap.

A response amplification due to resonance in the frequency band

$$\frac{1}{2 t_d} \leq f \leq \frac{2}{t_d}$$

$$\frac{1}{2(1.5)} \leq f \leq \frac{2}{1.5}$$

$$0.3 \leq f \leq 1.3$$

must be considered as shown in Figure 3.57.

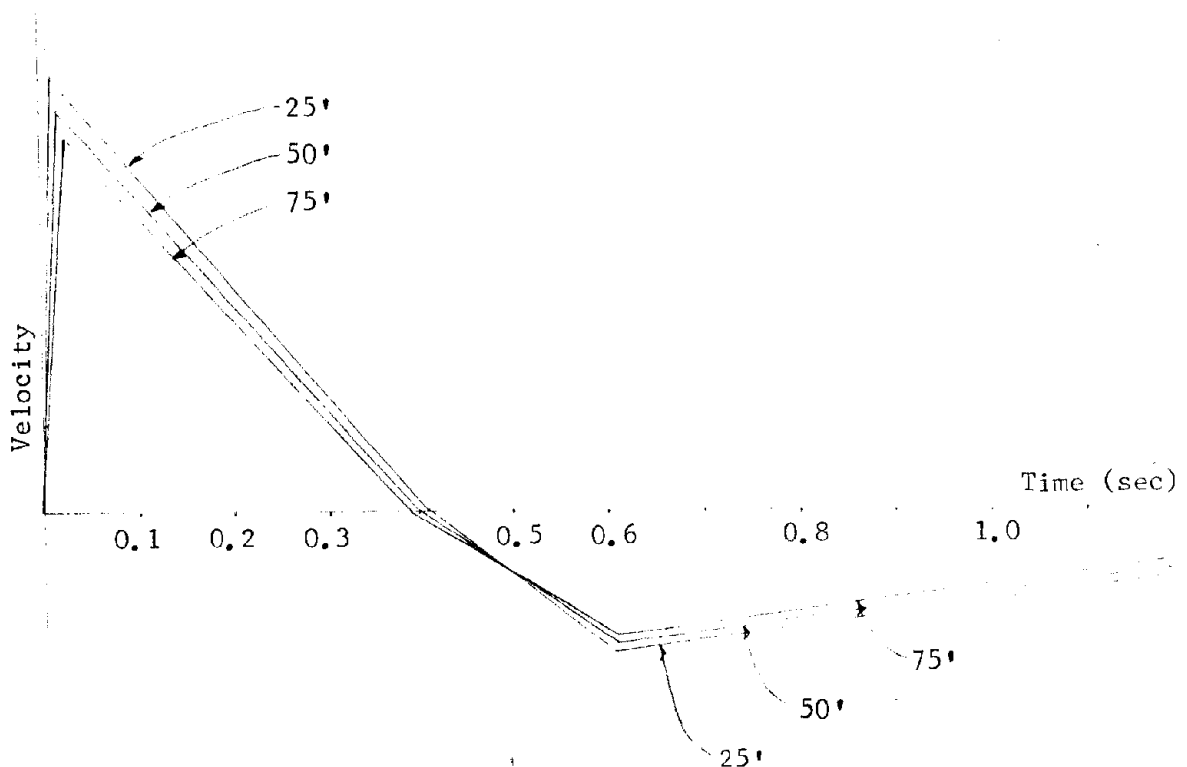


FIGURE 8.2: IDEALIZED VELOCITY PULSE

Step 2 (c) significance of G.Z. seismic induced motion: The G.Z. induced motions are important if the peak intensities are of the same order of magnitude as the motions due to the direct air slap or if G.Z. motion arrives at or near the same time as the direct slap. First the peak intensities are calculated from Equations(3.14.a), applicable for  $R \leq 2.5 W^{1/3} = 7.3 \text{ kft}$

which is greater than R at 500 psi for W = 20 MT. For seismic velocity of 4000 fps and W = 20 MT,

$$a_r = 0.4 W^{5/6} R^{-3.5} c^2 = \frac{0.4(20)^{5/6}}{(5.2)^{3.5}} (4)^2 = .24 \text{ g}$$

$$v_r = 12 W^{5/6} R^{-2.5} c = \frac{12 (24)}{62} = 9.4 \text{ in/sec}$$

$$d_r = 4 W^{5/6} R^{-1.5} = \frac{4 (12)}{11.9} = 4 \text{ inches}$$

The acceleration and the velocity are small compared to the direct slap of the air blast and can be neglected. The displacement may have to be considered.

The hard soil layer at depths of greater than 300' (c = 15,000 fps) may transmit a significant shock pulse with refracted waves into the softer layers near the surface. The peak displacement will be no greater than the 4 inches calculated above but the peak accelerations and velocity may be greater because both acceleration and velocity are functions of seismic velocity. For example at the 500 psi overpressure level distance from ground zero, the peak acceleration and velocity transmitted through the hard layer are:

$$a \cong \left(\frac{15}{4}\right)^2 .24 = 3.4 \text{ g}$$

$$v \cong \left(\frac{15}{4}\right) 9.4 = 35 \text{ in/sec}$$

It is seen that the peak intensities are still small compared to those due to the direct air slap. If the arrival time of the two motions coincide, the combined effect may induce a resultant motion which exceeds the air blast effect separately.

The arrival time of the shock pulse through the hard layer is of importance. Direct G.Z. and air blast induced seismic pulses may be refracted and arrive at the target location near simultaneously with the air blast arrival time (see Figure 8.3). The critical arrival times can be calculated by the method described in Section 3.2.2.4.

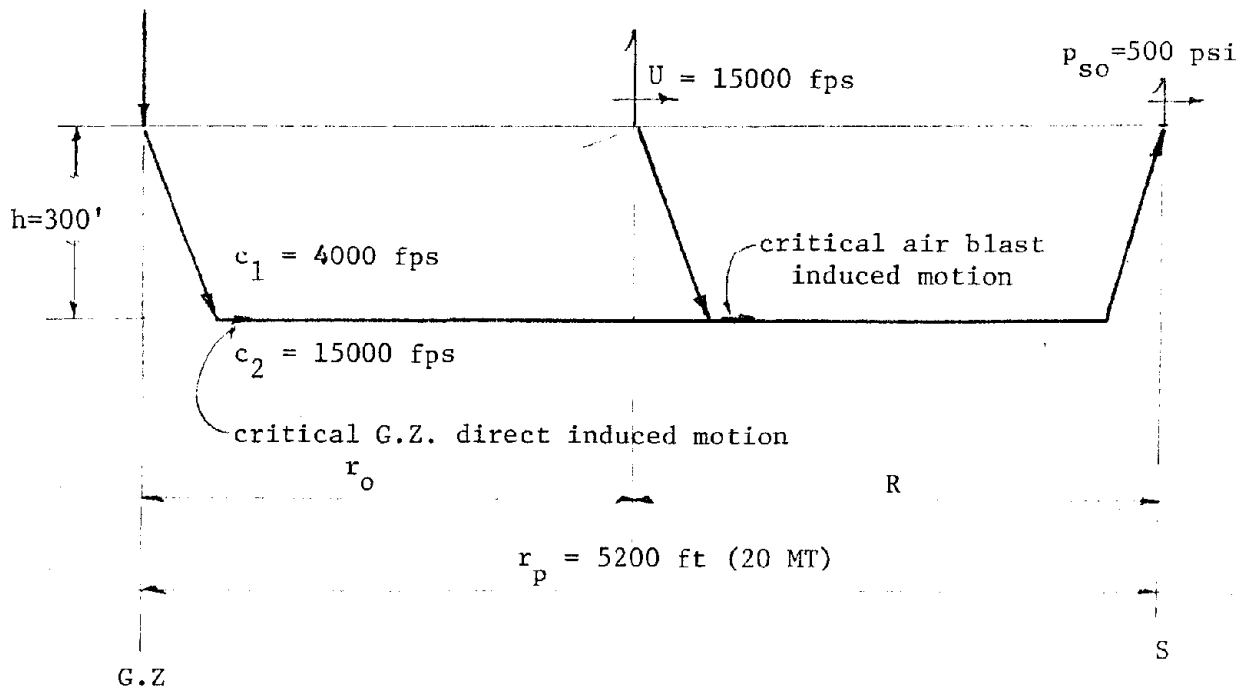


FIGURE 8.3: CRITICAL SEISMIC MOTIONS

The G.Z. direct induced motion arrival time is

$$t_c = \frac{2h}{c_1 c_2} \sqrt{c_2^2 - c_1^2} + \frac{r_p}{c_2}$$

$$t_c = \frac{2(.3)}{4 \times 15} \sqrt{15^2 - 4^2} + \frac{5.2}{15} = .145 + .346 = 0.49 \text{ sec}$$

whereas the arrival time of the air blast at  $r_p = 5200 \text{ ft}$  is  $t_a = 0.28$  seconds. Therefore, the air blast front is superseismic with respect to the G.Z. induced seismic motion (leads by 0.2 seconds). It can be seen that the G.Z. motion (which may have an initial upward vertical component) may occur in phase with the negative portion of the air slap velocity pulse, see Figure 8.2. Let us assume for this particular example the vertical and horizontal components of the motion are equal to the maximum radial motions calculated

$$a_z = a_h = a_r = 3.4 \text{ g}$$

$$v_z = v_h = v_r = 35 \text{ in/sec}$$

$$d_z = d_h = d_r = 4 \text{ inches}$$

The velocity pulse time characteristics are (assuming a systematic pulse)

$$t_r = \frac{35}{3.4 \times 386} = .027 \text{ sec}$$

$$t^+ = \frac{2 \times 4}{35} = 0.23 \text{ sec}$$

$$t_d = 4 \times t^+ = 0.92 \text{ sec}$$

Superimposing this pulse on the air slap pulse shown in Figure 8.2 shows the significance of the G.Z. induced motion. It can be seen from Figure 8.4 that the initial peak acceleration and velocity are not altered. The G.Z. effect is probably insignificant in this particular case for design of the shock isolation systems since the maximum displacement is not significantly altered.

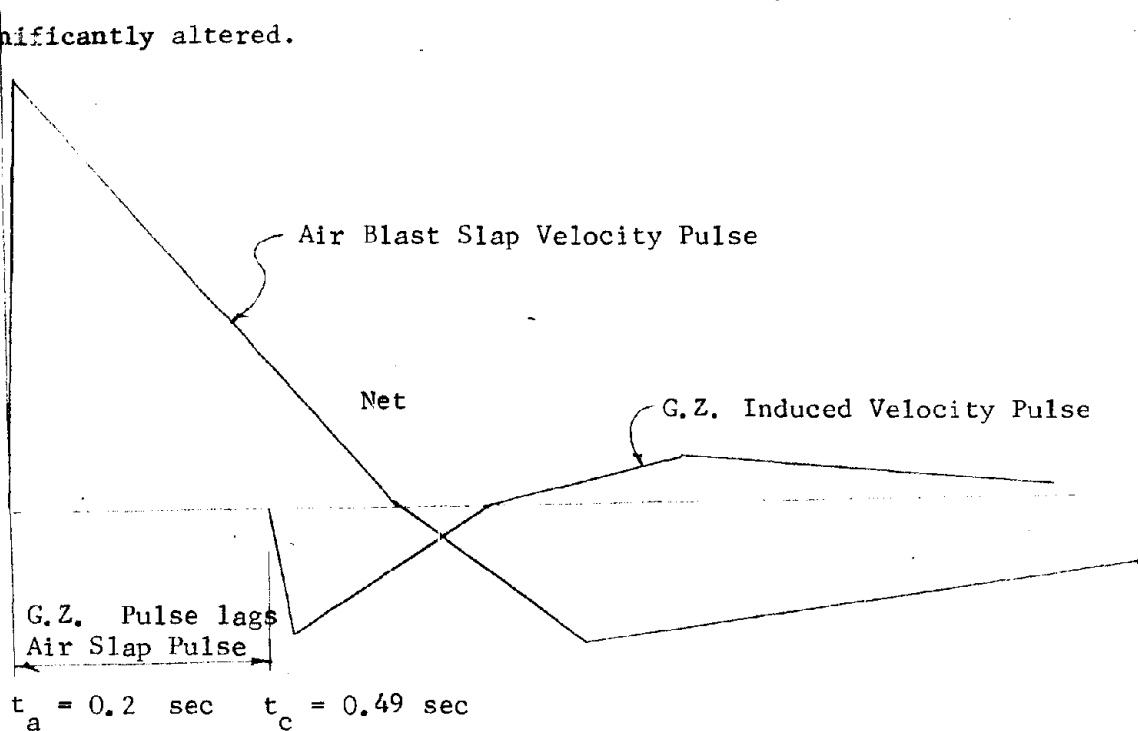


FIGURE 8.4: AIR BLAST PULSE PHASED WITH G. Z. PULSE

Step 2 (d) significance of air slap seismic induced motion: The shock front velocity at the 500 psi overpressure level is 6300 fps. A refracted wave at the layer interface, also shown in Figure 8.3, may lead or lag the direct air blast at the 500 psi location. A refracted wave is induced when the shock front velocity  $U = 15,000$  fps (see Section 3.4). From Reference 3.1 the distance and arrival time of the air blast from G.Z. when  $U = 15,000$  fps are

$$r_o = 2.7 \text{ kft} \quad , \quad t_{ao} = .068 \text{ sec}$$

The distance between this location and the 500 psi location is

$$R = r_p - r_o = 5.2 - 2.7 = 2.5 \text{ kft}$$

The critical time to travel the distance  $R$  through the layer interface is:

$$t_c = \frac{2h}{c_1 c_2} \sqrt{c_2^2 - c_1^2} + \frac{R}{c_2} = .145 + \frac{2.5}{15} = .312 \text{ sec}$$

The time to travel this critical path from G.Z. is

$$t_c + t_{ao} = .312 + .068 = 0.38 \text{ seconds}$$

which lags the direct air slap by 0.10 seconds. The peak intensities will be less than the air blast slap motions (for the superseismic case) and therefore the peak acceleration, velocity, and displacement are not significantly amplified. It has been seen in test data (Reference 3.3) that when seismic induced motions (G.Z. induced or air blast induced) slightly lead the air blast slap (the outrunning condition) then amplified intensities, Equations (3.38) through (3.40), should be considered possible. In this particular case both the G.Z. and air blast induced seismic motions lag the air slap motion at the 500 psi overpressure level.

Step 2 (f) feasible burial depths: The shock isolation requirements must be considered in arriving at a burial depth of the enclosures. An indication of shock response can be seen by plotting a shock spectrum envelope for the burial depths of interest using the standard amplification factors of Equation (3.55) and the relationships of Equation (3.37). The resulting spectrum envelopes are shown in Figures 8.5 and 8.6. It can be seen that the constant displacement and constant velocity bounds are not

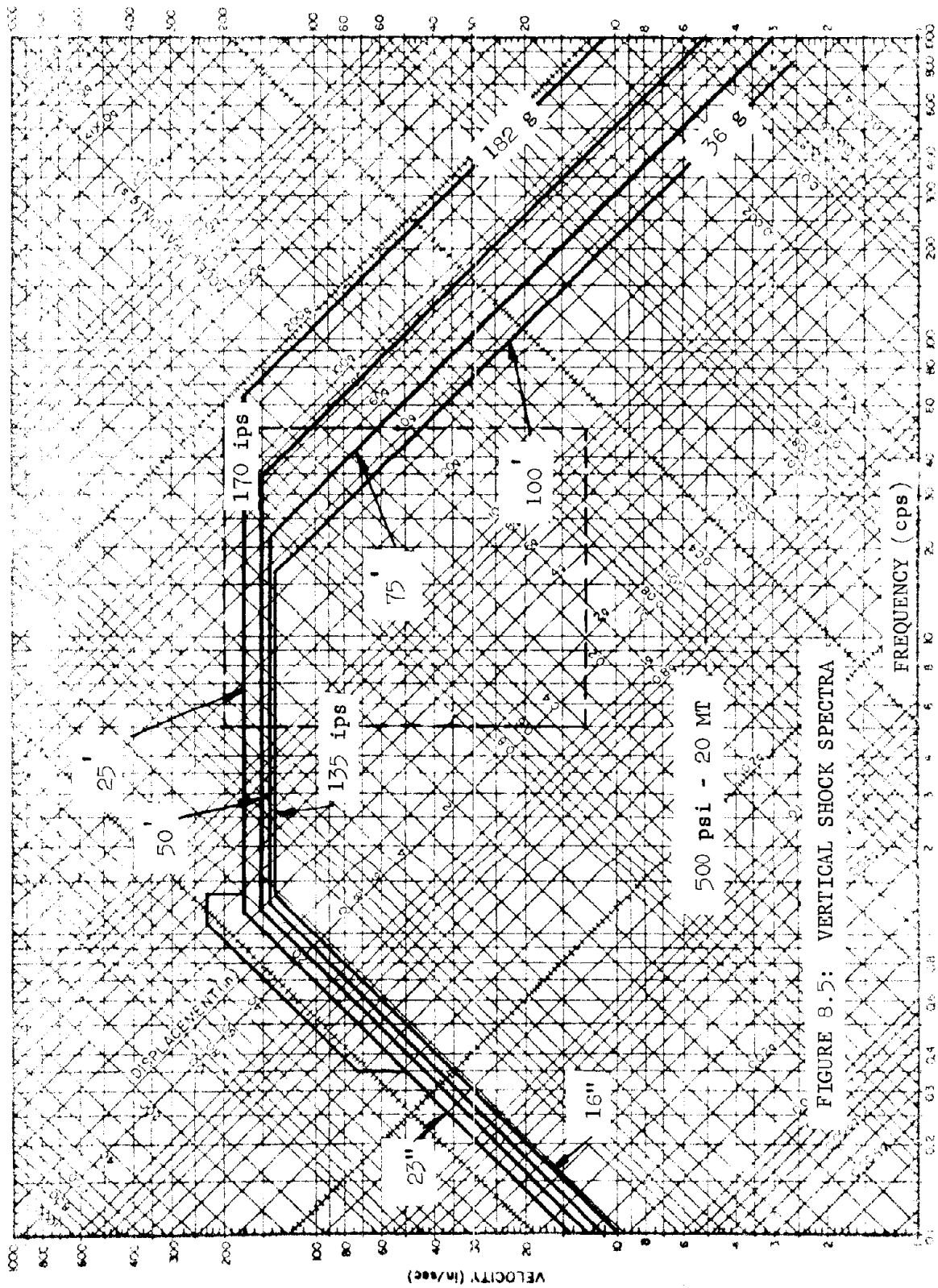


FIGURE 8.5: VERTICAL SHOCK SPECTRA

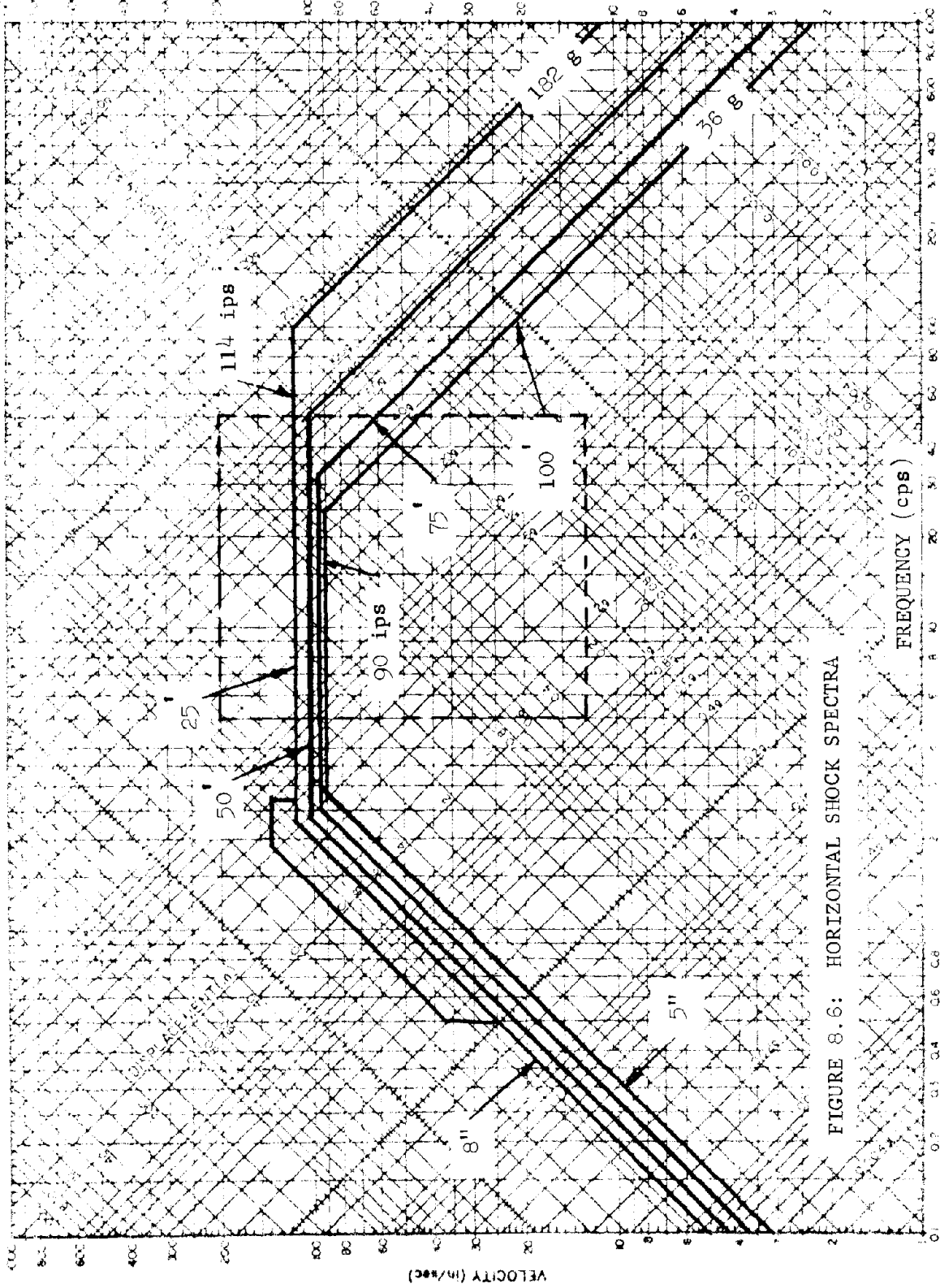


FIGURE 8.6: HORIZONTAL SHOCK SPECTRA



significantly attenuated with increase in burial depth. Also shown on Figures 8.5 and 8.6 is a rectangular envelope encompassing the fragility levels for hard-mounted equipment (see Section 7). This rectangular envelope falls in the constant velocity region indicating that increases in burial depth (up to 100 feet) will not provide enough shock attenuation. Therefore, shock isolating the equipment so that the equipment response frequencies are shifted to the low frequency region of the shock spectra is necessary. The burial depth does not significantly affect the isolation system design in the constant displacement region of the shock spectra. Conversely, if the equipment is ruggedized so that the response falls in the constant acceleration region, significant attenuation is achieved by increasing burial depth.

Both the low frequency and high frequency envelope spectra for average burial depths from 25 feet to 100 feet are within practical design limits for either soft isolation systems or hard-mounting of ruggedized equipment.

### 8.2.3 Step 3: facility layout and functions

Step 3 (a) equipment characteristics: During the facility layout phase, it is important to consider the fragility levels of the equipment as well as the operational functions. Thus, the shock isolation requirements may be an important factor in establishing equipment arrangements. For example, equipments with similar survival operational requirements should be grouped together if possible. Also, it would be desirable to locate equipment with similar fragility levels in the same area.

The equipment is usually classified into two categories:

- (1) System Equipment - electronics, consoles, cables, and operational hardware.
- (2) Facility Equipment - power generation, environmental control, lighting, and support hardware.

The equipment in category (1) is usually a unique design for the specific application at hand and therefore requires a stringent specification for design, fabrication, and test. The equipment in category (2) will usually be selected from commercially available (conventional or ruggedized)

equipment which may or may not have passed military shock tests.

An estimate must then be made of probable fragility levels even though the equipment design or type is not established. The system and facility equipment assumed for this example are listed below with an estimate of the fragility level and lowest mode frequency based on data provided in Section 7. The values shown are considered reasonable for this hypothetical example, and although they may be used as probable values during preliminary design, more specific data should be sought from using agencies or manufacturers when an actual facility is being designed.

The list is arbitrary and incomplete and represents the type of equipment often required in each category. It can be seen that the system equipments have lower fragility levels than the facility equipments. This is generally true for a communication system but may not be true for other systems such as a power plant.

System Equipment

	<u>Wt.</u>	<u>Lowest Freq.</u>	<u>Estimated Fragility Level</u>
Message Authentication System (Rack)	1000 lbs	10 cps	10 g
Signal Data Converter (Rack)	1000 lbs	10 cps	10 g
Data Analysis (Rack)	1000 lbs	10 cps	10 g
Alarm and Monitor Rack	1000 lbs	10 cps	10 g
Radio Rack	1000 lbs	10 cps	10 g
HF Communication Rack	1000 lbs	10 cps	10 g
VHG Communication Rack	1000 lbs	10 cps	10 g
Power and Distribution Rack	1000 lbs	10 cps	10 g
Command Console	3000 lbs	8 cps	6 g
Status Console	1500 lbs	8 cps	6 g
HF Pop-up Antenna	8000 lbs	10 cps	10 g
UHF Fixed Stub Antenna	6000 lbs	150 cps	500 g

	<u>Facility Equipment</u>		<u>Estimated Fragility Level</u>
	<u>Wt.</u>	<u>Lowest Freq.</u>	
Diesel Generator	10000 lbs	30 cps	15 g
Fuel Oil Tank	2000 lbs	60 cps	100 g
Air Compressor	1000 lbs	40 cps	20 g
Air Supply Fan	1000 lbs	40 cps	20 g
Air Exhaust Fan	1000 lbs	40 cps	20 g
Batteries (Emergency Power) 12 reqd	1500 lbs each	60 cps	60 g
Electrical Panels (6 reqd)	500 lbs each	20 cps	10 g
Brine Chiller	8000 lbs	30 cps	15 g
Duct Work		20 cps	20 g
Misc. piping with ruggedized supports		50 cps	100 g
Cable trays with ruggedized supports		50 cps	100 g

Step 3 (b) personnel functions: It is assumed that two people are required to operate the communication system. While on duty the operators will be seated in chairs at the command console and status console. A crew will consist of four people in the hardened facility with duty rotation as required. Two bunks will be necessary for off-duty rest periods.

The personnel fragility factor must be based on three conditions:

- (1) operator seated in chair (strapped in)
- (2) personnel walking in equipment area
- (3) personnel resting on a bunk

It is also customary to assume that the shock motion will occur without any prior warning. For conditions (2) and (3) a low acceleration level (less than 1 g dynamic) of the support platform is required to insure reasonable safety to all personnel. Since there will be two operators in chairs at all times, a higher acceleration (approximately 3 g) level may be tolerated which still represents acceptable safety to the two operators but definitely represents danger to the off-duty personnel. For this example a maximum acceleration of 3 g of the supporting platform will be considered acceptable for personnel safety (see Section 7).

It can be seen that the personnel functions are closely coupled with the system equipment functions and shock isolation will be required for both

system equipment and personnel. Consequently from a shock isolation standpoint it is desirable to arrange the system equipment in a compact area so that a single in-structure platform can support both system equipment and personnel. The trade off studies in step 4 will consider the advantage of the close proximity of the facility equipment with the system equipment.

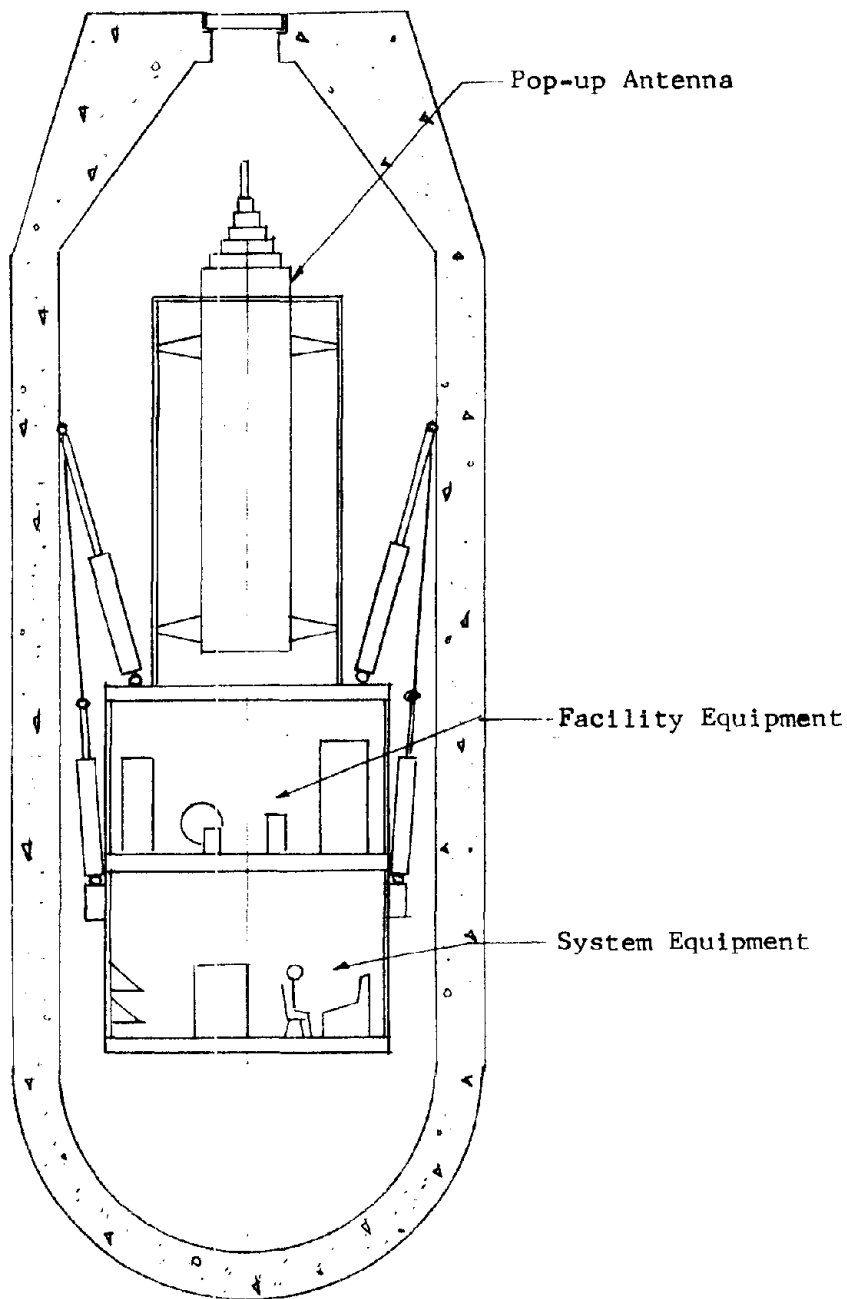
#### 8.2.4 Step 4: facility study

Step 4 (a) shock isolation feasibility: The design of the facility structure(s) must consider the shock isolation requirements as an important factor in adopting the number and size of facility enclosures. Let us consider various concepts which might be proposed by the facility designer and investigate the merit of each concept with respect to shock isolation only. Figure 8.7 shows concept 1 in which the complete system is integrated into one enclosure. Figures 8.8 and 8.9 (concept 2 and 2a) separate the system into three enclosures; one enclosure for the antenna hardware, one enclosure for the system equipment, and one enclosure for the facility equipment. Concept 2a is a variation of concept 2 where the facility equipment is placed in a fairly deep buried enclosure so that possibly the equipment can be hard mounted directly to the foundation slab.

Concept 1 requires a low frequency shock isolation system to support a maximum dead load (estimated to be 250,000 lbs). If a pendulous system can be positioned symmetrically about the mass C.G., the peak dynamic relative displacements will be close to the peak ground displacements (approximately 21" vertically and 7" horizontally). In a pendulous system (with long pendulum rods) it is desirable to attenuate the dynamic acceleration to less than 1 g vertically so that the pendulum rods are tension members only. Liquid springs are feasible for this design.

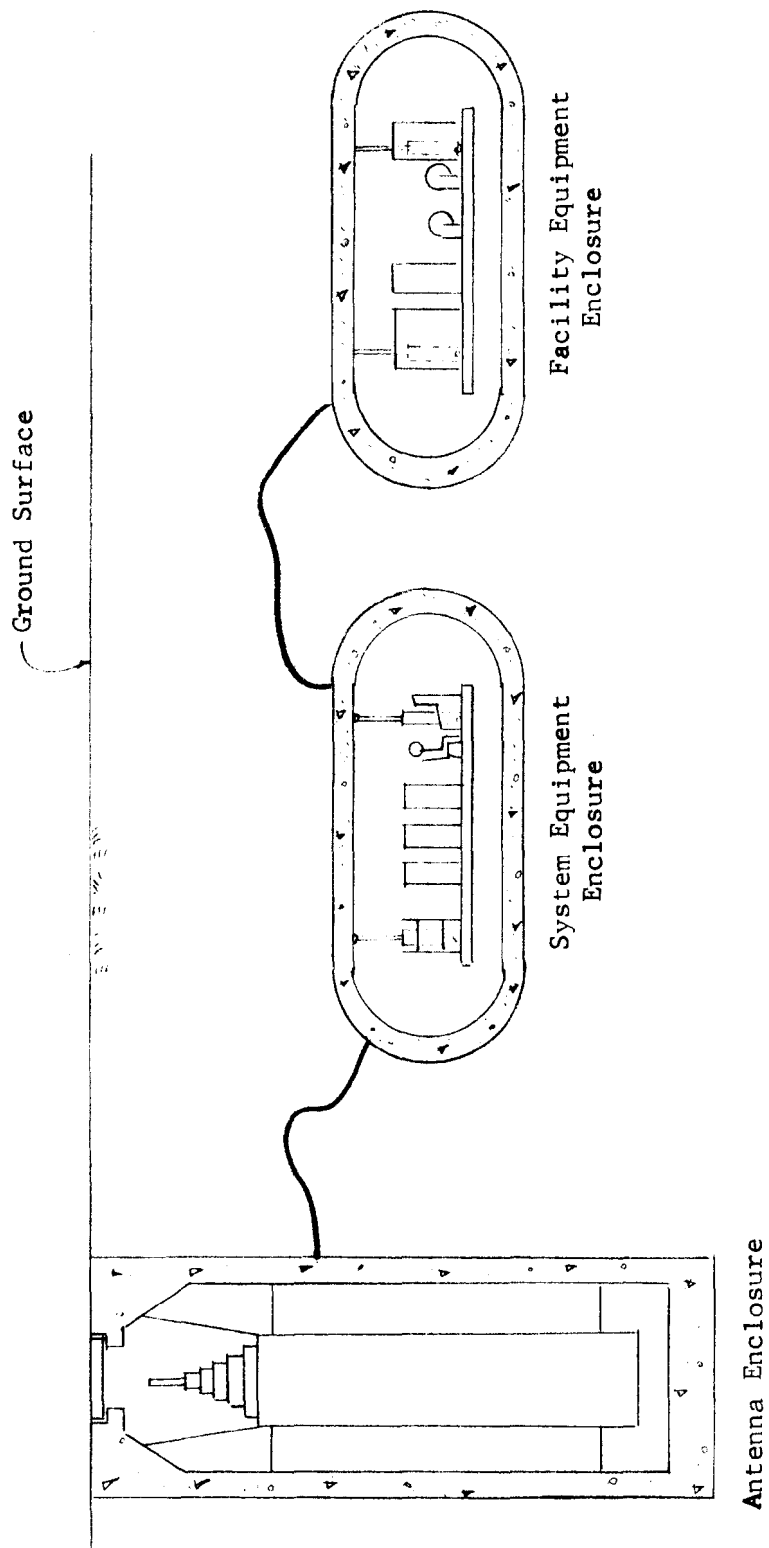
Concept 2 requires 3 separate shock isolation systems: antenna isolation system and 2 equipment platform isolation systems. Smaller spring elements are now required, but more spring elements are necessary. A pendulous system for all three platforms is feasible. Coil spring elements may also be practical, as well as liquid springs and pneumatic springs.

Concept 2a is a modification of concept 2 where the equipment facility is at a burial depth where the shock effect is within the equipment tolerance



Concept 1

FIGURE 8.7: ONE ENCLOSURE FOR OVERALL SYSTEM



Concept 2

FIGURE 8.8: THREE SEPARATE ENCLOSURES

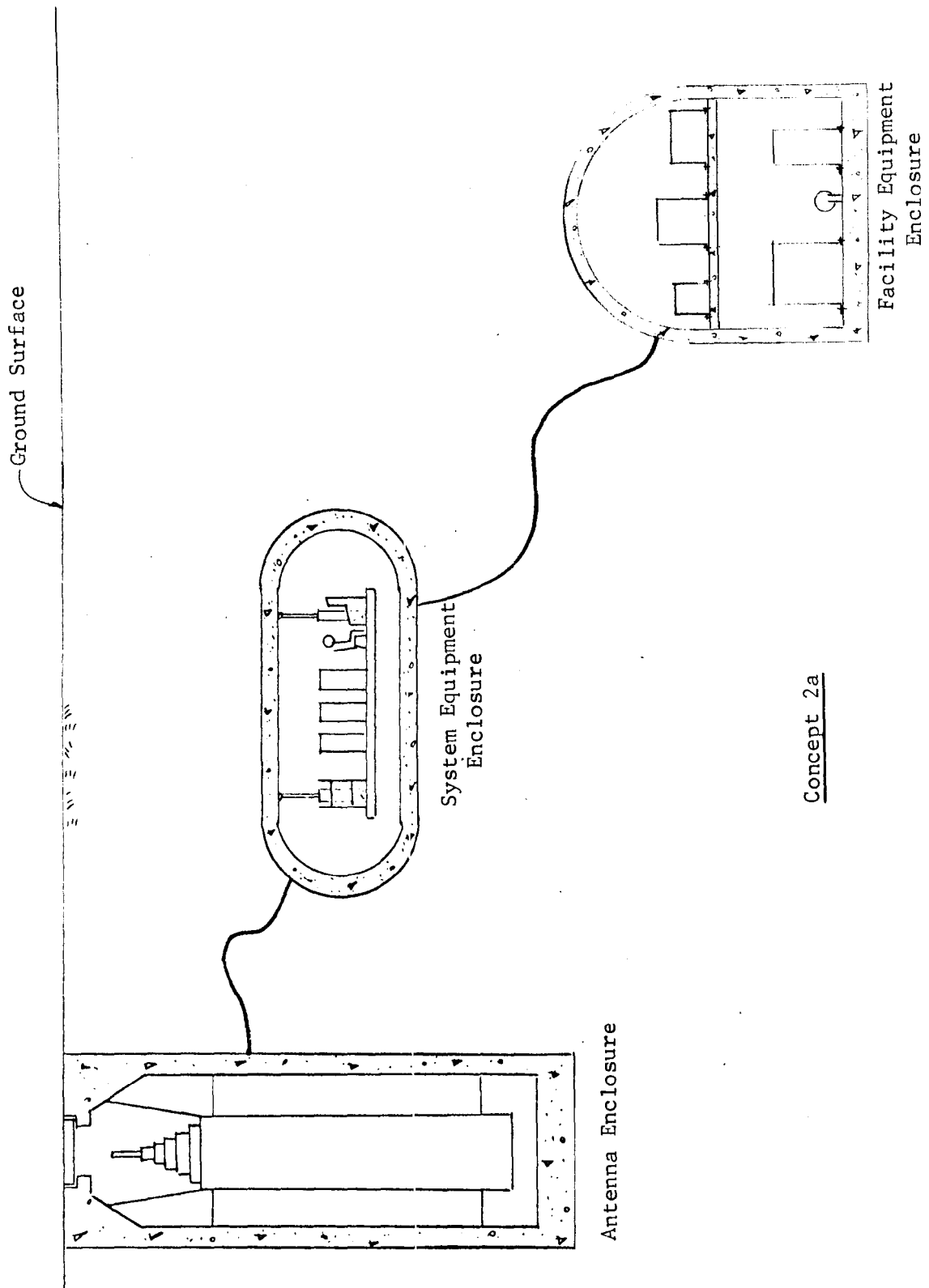


FIGURE 8.9: THREE SEPARATE ENCLOSURES

level. The equipment can be hard mounted to the base slab, thus eliminating the need of a shock isolation system for the equipment facility.

From the above discussion we can conclude that all 3 concepts are feasible for shock isolation. Concept 1 has the advantages of one shock isolation system and minimum total rattlespace. Concept 2 has the advantage of using smaller spring elements, and it is very probable that the isolators required for the two equipment platforms will be identical. Concept 2a minimizes the isolation costs since cost is a function of the required total energy capacity of the isolators.

Consequently concept 2a is preferred as the optimum layout for shock isolating the fragile equipment. Concept 2 is slightly better than concept 1 because there is more flexibility in selecting the type of springs in the isolation system, but it should be pointed out that a trade-off study with costs of structural enclosure and excavation may result in a different conclusion.

#### 8.2.5 Step 5: preliminary design

Step 5 (a) shock isolation system: Concept 2 is now assumed to be the layout chosen for preliminary design.

Step 5 (a-1) design considerations: The three required isolation systems will all be low frequency systems. The flexibility of the structure is therefore not an important factor and the isolation system response is most sensitive to the total ground displacement and peak velocity. (Any high frequency vibration effect due to the initial shock should be considered in the final design.) A response amplification must be considered in the vertical frequency range of  $0.3 \leq f \leq 1.3$  and horizontal frequency range  $0.6 \leq f \leq 2.3$ . This vertical frequency range is definitely in the anticipated design range whereas the horizontal frequency range can be avoided without introducing any disadvantage.

#### Step 5 (a-2) optimum spring arrangement and preliminary system design:

(1) HF antenna system: The erectable antenna is supported in a tall slender frame, approximately 2'-6" square by 24' long. The mass c.g. is at approximately the geometrical c.g. The arrangement of springs must consider



the operational condition of the antenna in the fully erected position (approximately 100 feet above grade). The frame support points in the silo must be capable of restraining the cantilever moments of the antenna in the erected position. Therefore a symmetrical arrangement of vertical and horizontal springs are well suited for this system as shown in Figure 8.10.

The horizontal springs are located at the top and bottom of the antenna frame and provide excellent stability for dynamic response during groundshock and also excellent reaction points for resisting the overturning moment\* when the antenna is in the erected position.

A fragility level of 10g is estimated for the crib and internal components, and moreover the 25 feet depth shock spectra is considered applicable. Because of the amplified vertical response occurring in the 1 g region (35 inches instead of 23.2 inches,) see the vertical shock spectra, (Figure 8.5) it may be judged that a higher g system (approximately 4 g dynamic system) will be more economical than a 1 g system.

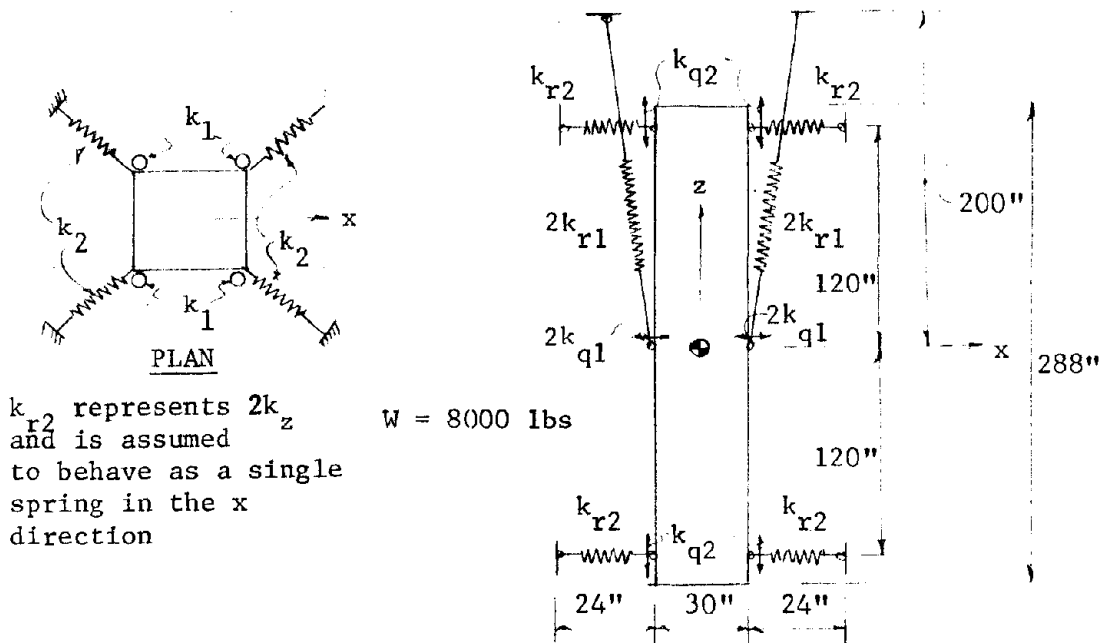


FIGURE 8.10: PROPOSED ANTENNA ISOLATION SYSTEM

\* This factor is included to point out that shock isolation may not be the only consideration in choosing a spring arrangement.

For a 4 g dynamic system vertically (approximately 1.5 cps),

$$\Delta z_d = 16'' \quad \Delta z_s = 4''$$

where  $\Delta z_d$  is the peak dynamic displacement and  $\Delta z_s$  is the static displacement.

The maximum vertical force in the vertical springs is:

$$F_t = (4g + 1g) W = 5 \times 8 = 40 \text{ kips.}$$

The resultant peak stored energy is:

$$U = 1/2 F_t (\Delta z_s + \Delta z_d) = 400 \text{ inch kips}$$

For a 1 g dynamic system (0.55 cps)

$$\Delta z_d = 30'' \quad \Delta z_s = 30''$$

$$F_t = 2 \times 8 = 16 \text{ kips}$$

$$U = 1/2 (16)(60) = 480 \text{ inch kips}$$

Less energy storage capacity is required in the 4 g system, but tension-compression springs are required. In the preliminary design the 1 g system vertically is chosen since this will dictate the maximum rattle space requirements. If negligible coupling between translation vibration modes exists, the vertical rattle space required at the top and bottom for dynamic response is approximately 30 inches.

The horizontal frequency can be selected so that the peak horizontal response displacement is approximately equal to the peak ground displacement (i.e. no amplification due to resonance). An acceleration response of less than 1 g is also desirable so that a simple preloaded compression spring can be used. To get below the amplified response region (Figure 8.6) a frequency of 0.4 cps is required. This will give a dynamic response of less than 0.2g. The peak horizontal response displacement, from shock spectra of Figure 8.6, is less than 8 inches. A preliminary system design will now be performed to establish a space envelope for the antenna system.

The spring rates are first estimated by the method described in Section 5.2.5. The non-linearity of the problem is ignored in this phase of the design.

### Vertical and Horizontal Spring Rates

(The small inclination angle in the vertical springs is ignored)

$$\text{for } f_z = 0.55 \text{ cps and } f_x = 0.4 \text{ cps}$$

$$k_z = 4k_{r1} + 4k_{q2} = 4\pi^2 f_z^2 m = 250 \text{ lbs/in}$$

$$k_x = 4k_{q1} + 4k_{r2} = 4\pi^2 f_x^2 m = 134 \text{ lbs/in}$$

$$4k_{q1} = \frac{W}{\lambda_z} = \frac{8000}{200} = 40 \text{ lbs/in}$$

$$4k_{q2} = \frac{P_{pL}}{\lambda_x} = \frac{0.15 \times 8000}{24} = 50 \text{ lbs/in}$$

where  $p_{pL}$  = preload in horizontal springs.

The above lateral spring rates will vary as a function of dynamic displacement (see Section 5.2.1) but for preliminary design this non-linear effect can be neglected.

Therefore the required axial spring rates are:

$$4k_{r1} = 200 \text{ lbs/in, } 4k_{r2} = 94 \text{ lbs/in}$$

The effect of eccentricity of C.G. with respect to the Center of Rigidity, C.R., is now investigated by the method described in Section 5.3.

The uncoupled frequency parameters are:

$$\omega_z^2 = \frac{k_z}{m} = \frac{250 \times 386}{8000} = 12/\text{sec}^2$$

$$\omega_x^2 = \frac{k_x}{m} = \frac{134 \times 386}{8000} = 6.5/\text{sec}^2$$

$$\omega_\theta^2 = \frac{k_\theta}{J}$$

$$k_\theta = 4(120)^2 \frac{94}{4} + 2(15)^2 \frac{200 + 50}{2} = 1.4 \times 10^6 \text{ in. lbs}$$

$$J = \frac{8000}{386} (288^2 + 30^2) \frac{1}{12} = 13,500 \text{ in. lbs sec}^2$$

$$\omega_{\theta}^2 = \frac{140}{1.35} = 104/\text{sec}^2 ; \quad \omega_{\theta} = 10.2/\text{sec}$$

The radius of gyration is:

$$e = \sqrt{\frac{13500 \times 386}{8000}} = 25.6''$$

The amount of eccentricity, R, and pitch frequency parameter,  $\omega_{\theta}$ , that can be tolerated without significant coupling is given by Equations 5.24 and 5.25

$$R = \sqrt{R_x^2 + R_z^2} < 1/2 \sqrt{J/m} = 12''$$

$$\omega_{\theta} > 1.5 \sqrt{\omega_x^2 + \omega_z^2} = 1.5 \sqrt{12 + 6.5} = 6.5/\text{sec}$$

The value of  $\omega_0 = 10.5$  for the assumed configuration is greater than 6.5. The antenna is symmetrical in plan and therefore very little eccentricity ( $R_x$ ) is expected in the horizontal direction. The distribution of weight in the vertical direction may vary as the hardware design is finalized but it probably will not vary the C.G. location ( $R_z$ ) by more than  $\pm 12$  inches. Therefore pitch response is considered negligible in establishing rattlespace requirements.

Step 5 (a-3) preliminary spring design

The required spring characteristics for the Antenna system based on the preliminary system design are:

$$\text{Vertical Spring Rate } 4k_{r1} = 200 \text{ pounds/inch}$$

$$\Delta z_s = 30 \text{ inches}$$

$$\Delta z_d = 30 \text{ inches}$$

$$\text{Horizontal Spring Rate } 4k_{r2} = 100 \text{ pounds/inch}$$

$$\Delta z_p = 12 \text{ inches}$$

$$\Delta z_d = 8 \text{ inches}$$

where  $z_p$  equals the preload displacement required in the spring.

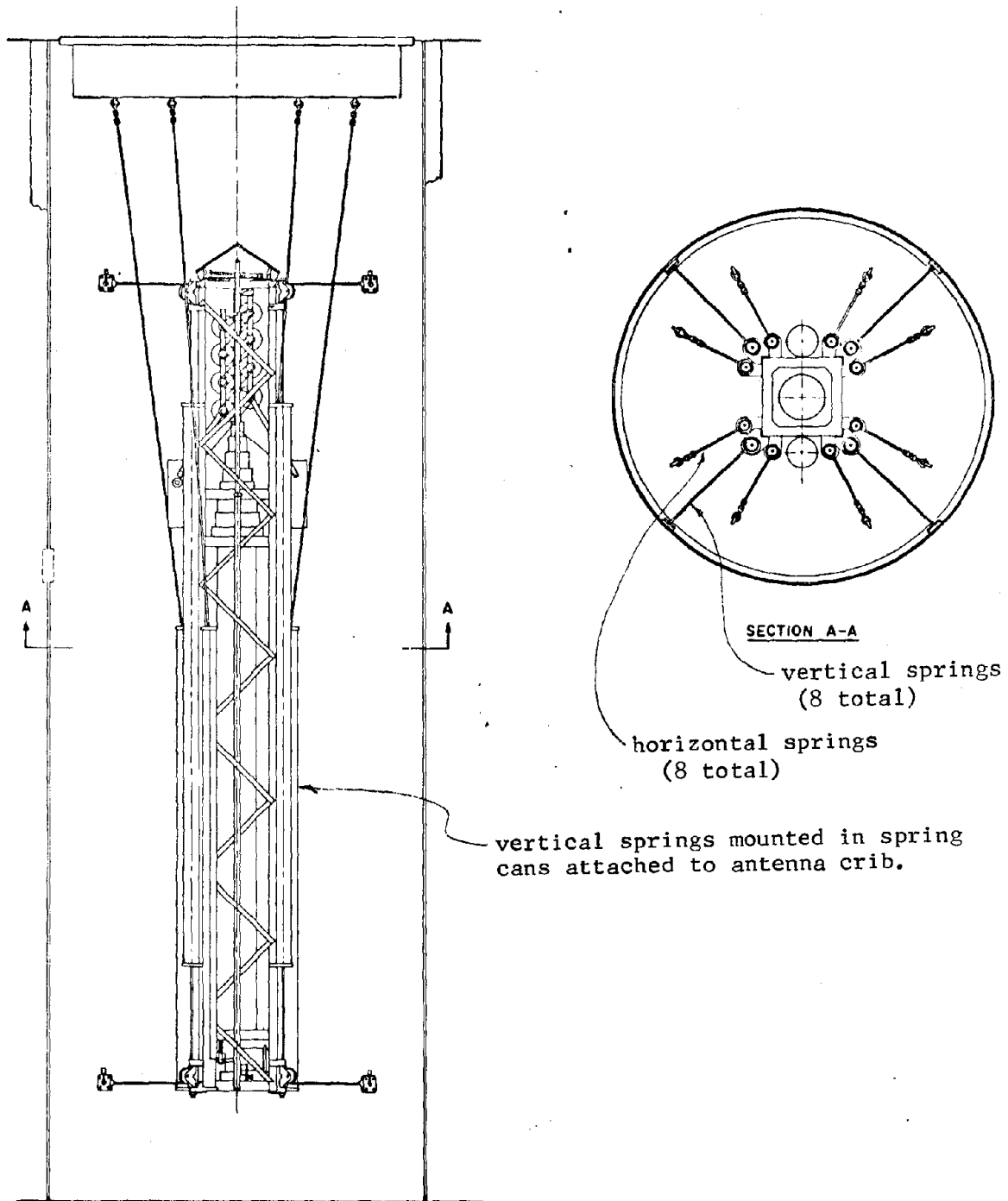


FIGURE 8.11: ANTENNA SHOCK ISOLATION SYSTEM

Four vertical and eight horizontal spring elements have been assumed.

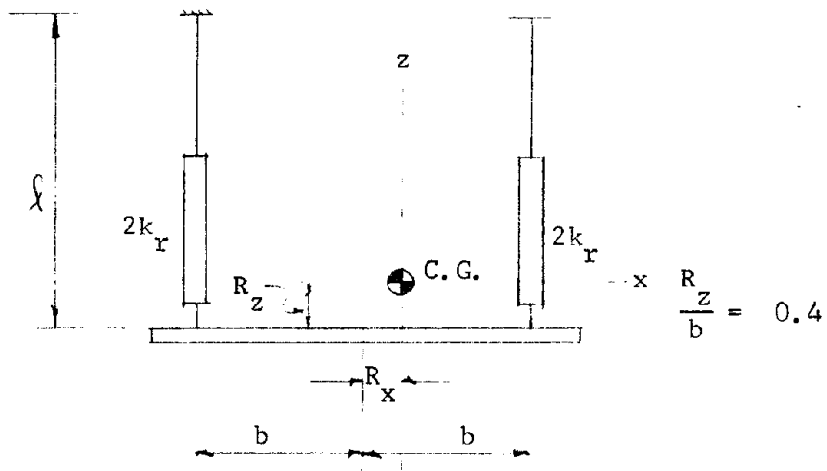
$$k_{r1} = 50 \text{ pounds/inch}$$

$$k_{r2} = 22.5 \text{ pounds/inch}$$

If eight vertical spring elements are used instead of the assumed four,  
 $k_{r1} = 25 \text{ pounds/inch}$ .

Coil springs are feasible for this system, and the springs may be mounted in cans attached to the antenna; cables run from springs to supporting structure, as shown in Figure 8.10. See Example 6.1 in Section 6 for the detailed steps for spring design. The springs are mounted in spring cans and cable suspended from the facility enclosure as shown in Figure 8.11.

(2) System equipment platform: The assumed platform geometry is shown in Figure 8.12. In plan the mass C.G. is assumed to be fairly close to the geometrical C.G. and in elevation the mass C.G. is assumed to be 25 inches maximum from the top of the platform. This geometry is well suited for a pendulous (low C.G.) system. Four point suspension symmetrically placed about the geometrical C.G. position may be feasible. A preliminary design will be performed based on the method described in Section 5.7. Motions in the x - z plane will be considered since this is the weak axis in pitch. The model with assumed characteristics is shown in Figure 8.13.



$$m = 172 \text{ lb sec}^2/\text{in} ; J = 731,000 \text{ lb-in-sec}^2 ; e = 65 \text{ in}$$

$$b = 63 \text{ in} ; \lambda = 240 \text{ in} ; R_{x(\text{max})} = 10 \text{ in} ; R_{z(\text{max})} = 25 \text{ in}$$

FIGURE 8.13: ASSUMED PLATFORM CHARACTERISTICS

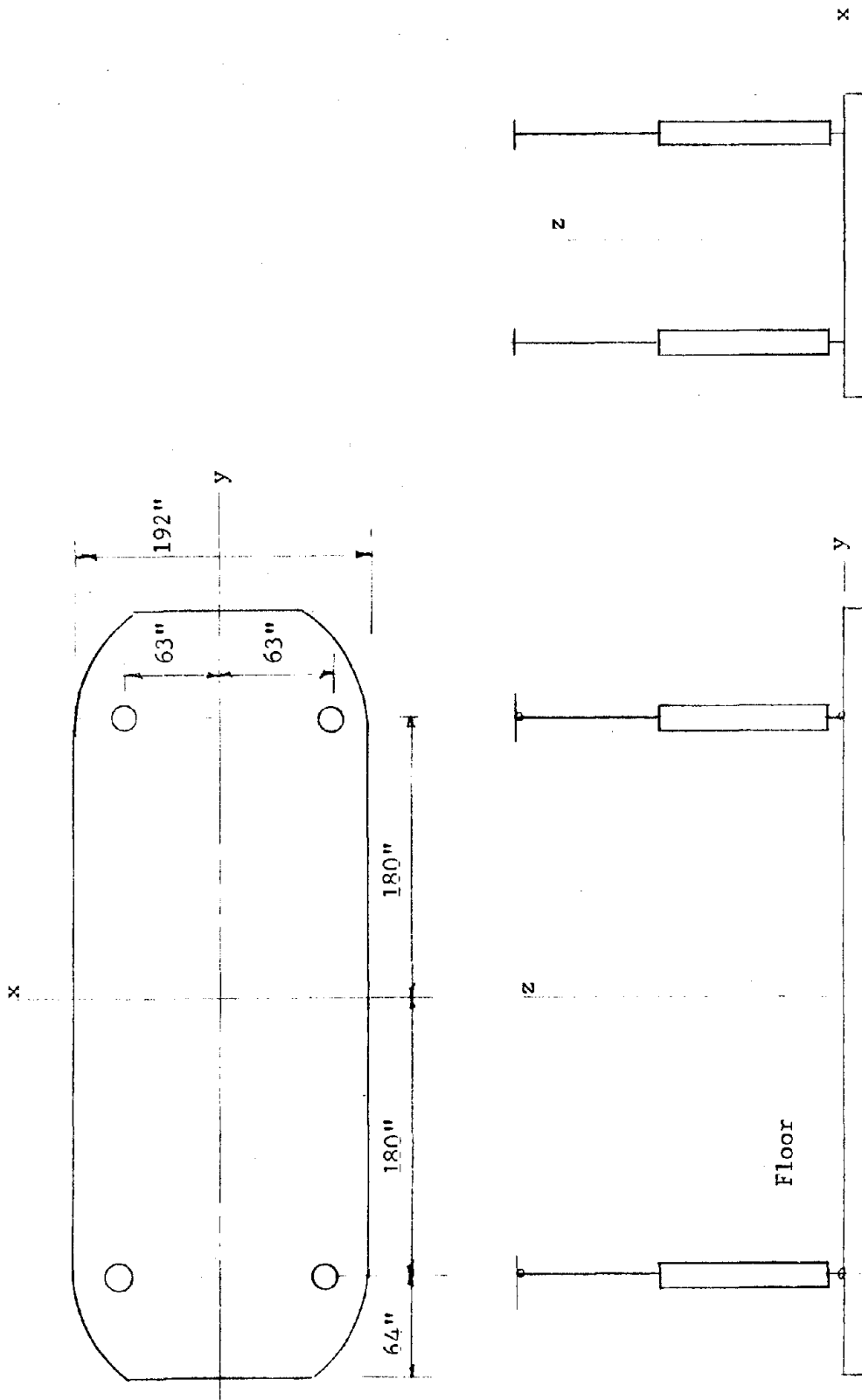


FIGURE 8.12: SYSTEM EQUIPMENT FLOOR GEOMETRY

The design objective is to keep the vertical and horizontal response acceleration to less than 1 g. From shock spectra, Figure 8.5 (50 foot depth level) the vertical frequency is selected based on SDOF response.

$$f_z = 0.5 \text{ cps}, \quad A_z = 0.8 \text{ g}, \quad D_z = 30 \text{ inches}$$

For a pendulum length of 240 inches the uncoupled horizontal frequency and response accelerations are:

$$f_x = \frac{1}{2\pi} \sqrt{\frac{g}{\ell}} = \frac{1}{6.28} \sqrt{\frac{386}{240}} = 0.20 \text{ cps}, \quad A_x = .03 \text{ g}, \quad D_x = 7 \text{ inches}$$

The uncoupled frequency parameters are

$$\omega_x = \sqrt{\frac{g}{\ell}} = 1.3/\text{sec}$$

$$\omega_z = \sqrt{\frac{k_z}{m}} = 3.14/\text{sec} \quad k_{z/2} = 850 \text{ lbs/in} \quad (2k_r = k_{z/2})$$

$$\omega_\theta = \sqrt{\frac{k_z b^2 - WR_z}{J}} = \sqrt{7} \text{ sec}^{-1} = 2.65 \text{ sec}^{-1}$$

The inequality of Equation 5.37 is now checked to make certain that the response can be bounded by this approximate method to ensure that a stable system is obtained.

$$\left[ |WR_z A_z| + |WR_x A_x| \right] \ll \ll \left[ k_z b^2 - WR_z \right]$$

$$1.32 \times 10^6 < 5.1 \times 10^6$$

The inequality is not completely satisfied (i.e. the "much greater than" is not satisfied). Therefore, the dynamic stability must be considered. From the discussion in Section 5.7.3, the expression on the left-hand side of the inequality is related to the constant,  $2q$ , in the stability equation, and the expression on the right-hand side is equal to the constant,  $a$ .

$$\text{Let} \quad a = \frac{5.1 \times 10^6}{.73 \times 10^6} = 7$$



since  $|WR_z A_z| \gg |WR_x A_x|$

$$q \cong \frac{WR_z A_z}{2J} \cong \frac{1.32 \times 10^6}{2 \times .73 \times 10^6} = 0.9$$

From the Ince-Strutt stability chart (Figure 8.14), the point defined by the values  $a = 7$  and  $q = 0.9$  is well within the stable region indicating that the response is bounded. Also  $q$  is relatively small (less than 1) so that as the coefficient  $a$ , varies, the unstable regions are small finite widths (for the variable  $a$  greater than 2). Damping in the system will also eliminate the lower level unstable regions, i.e., for small values of  $q$ , and thus the system is stable for any value of  $a$  when  $q$  is small. Therefore it is concluded that the response bound can be predicted by the method of Section 5.7.2.

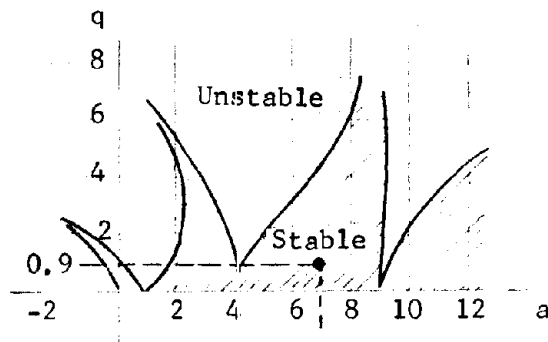


FIGURE 8.14: STABLE REGION OF MATHIEU EQUATION INDICATED BY SHADED AREA. (See Section 5.7.3)

The uncoupled frequency ratios are:

$$\frac{\omega_x}{\omega_\theta} = \frac{1.3}{2.65} = .49$$

$$\frac{\omega_z}{\omega_\theta} = \frac{3.14}{2.48} = 1.26$$

From the transmissibility chart of Figure 5.48

$$T_x = 1.3 \quad T_z = 1.75$$

The angular response is then computed from Equation 5.38 and 5.40

$$\ddot{\theta} = \frac{66400}{731000} \left[ |1.3 \times .030 \times 25| + |1.75 \times 0.8 \times 10| \right]$$

$$\ddot{\theta} = 1.35 \text{ rad/sec}^2$$

$$\theta = \frac{66400}{731000} \left[ \left| \frac{.97}{1.3^2} \right| + \left| \frac{14}{3.14^2} \right| \right]$$

$$\theta = .18 \text{ rad}$$

The peak accelerations and displacements are

$$A'_z = 0.8 + \frac{63 + 10}{386} (1.35) = 1.65 \text{ g}$$

$$A'_x = 0.030 + \frac{25 \times 1.01}{386} = .098 \text{ g}$$

$$D'_z = 30 + (63 + 10) .18 = 44 \text{ inches}$$

$$D'_x = 7 + (25) .18 = 11.5 \text{ inches}$$

The above vertical acceleration is near the tolerable value of 1 g. By looking at Example 5.12, it can be seen that if the coupled frequencies are used in the above calculations the vertical acceleration will be significantly greater but the displacements will not be altered appreciably. Therefore, no further iterations are required at this time to establish displacement rattlespace requirements.

Preliminary spring design. The required spring characteristics for the equipment platform based on the preliminary design are:

$$\text{total vertical spring rate} = 1600 \text{ lbs/in}$$

Assuming a 4 point suspension

$$k_z = 400 \text{ lbs/in (per spring)}$$

The pendulum length in the static position is:

$$= 240 \text{ inches}$$

and static and dynamic deflections recommended for design are:

$$\Delta z_s = 45 \text{ inches}$$

$$\Delta z_d = 40 \text{ inches}$$

$$\Delta x_d = 12 \text{ inches}$$

A liquid spring isolator in the vertical pendulum rod is well suited for this system. For instance, if a lower acceleration response is desired in the final design the force accounting for the increase in static displacement,  $\Delta z_s - \Delta z_d$ , can be obtained by pre-pressurizing the fluid in the no-load position so that no increase in isolator free length is required. The liquid spring design is given in Example 6.7 in Section 6.

#### 8.2.6 Step 6 final design

The equipment layout is now finalized, the facility enclosure dimensions are fixed, and space envelopes are established for each spring isolator. Equipment weights and inertia characteristics are estimated with upper and lower bounds for each item so that the final spring design can now account for the maximum and minimum weight conditions the variation in C.G. location, and required damping characteristics.

The shock isolation system designer must define the platform vibration characteristics for the equipment designer. The vibration requirement may be specified in the form of a specific vibration test to demonstrate adequacy or an analysis may be specified in addition to or in lieu of a test to demonstrate equipment adequacy. It is recommended that the shock isolation system designer be cognizant of the equipment design and test specifications so that resonant conditions (equipment frequency with platform frequency) can be avoided and to make certain that testing or analysis adequately represents the vibration of the platform during ground shock.

Step 6 (a-1) parameter variations: Since equipment and platform weights and center of gravity locations are not accurately known, tolerances will usually be placed on nominal assigned values which will hopefully bound the as-built condition. The weight and center of gravity analysis is an important task and the greater accuracy in the analyses here will enable the shock isolation system designer to assume only nominal variations in the values calculated. For the two isolation systems considered in this section the following parameter variations are reasonable.

(1) Antenna Crib

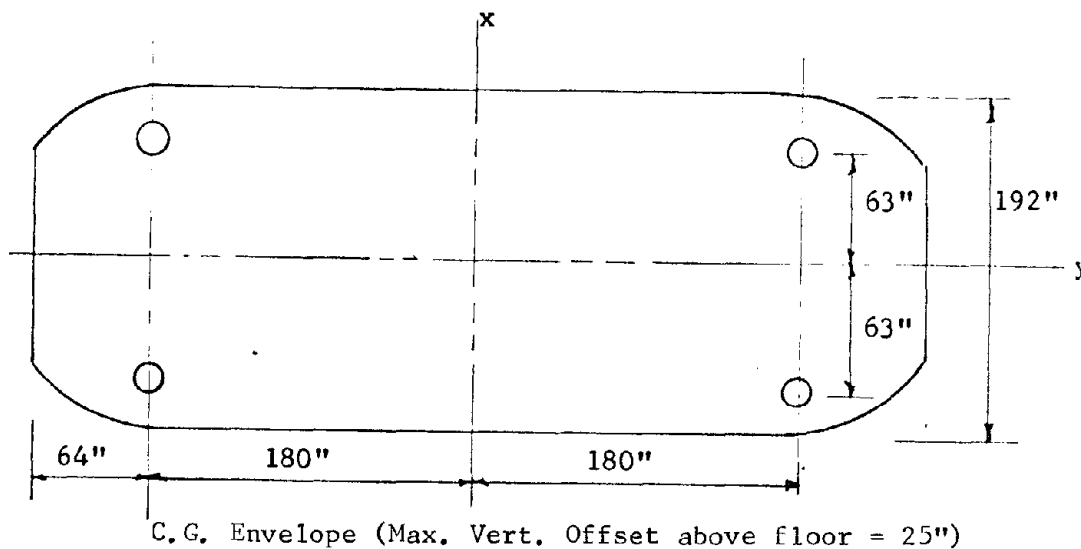
$$W = 8000 \pm 500 \text{ lbs.}$$

$$R_x = \pm 2 \text{ inches}$$

$$R_z = \pm 1 \text{ s inches}$$

(2) System Equipment Platform

Figure 8.15 shows the assumed variations in weight and inertia data.



WEIGHT AND INERTIA DATA

ITEM	MAX. WT. (+10 PERCENT)	NOMINAL WT.	MIN. WT. (-10 PERCENT)	UNITS
WEIGHT	73,000	66,000	60,000	Lbs.
$J_x$	2,800,000	2,500,000	2,300,000	Lb-in-sec <sup>2</sup>
$J_y$	800,000	730,000	660,000	Lb-in-sec <sup>2</sup>
$J_z$	3,300,000	3,000,000	2,700,000	Lb-in-sec <sup>2</sup>

FIGURE 8.15: SYSTEM EQUIPMENT PLATFORM WEIGHT AND INERTIA DATA

Step 6 (a-2) dynamic analysis: A dynamic analysis is usually necessary to adequately demonstrate that the system will respond in a normal manner with variations in ground motion characteristics and system characteristics.

The total ground motion in a layered soil media may result in complex vertical and horizontal velocity wave forms. When these complex wave forms

are applied to a multi-degree-of-freedom system the response may be greater than the values predicted by the approximate methods in the preliminary design. More than one type of velocity wave form may be necessary to account for a range of soil properties. The following conditions should be assumed to account for the range of soil properties:

- (1) Air blast induced velocity pulse with negligible ground return
  - Horizontal and vertical components in phase
  - Horizontal component lead and lag vertical component
- (2) Air blast induced velocity pulse with ground return
  - Horizontal and vertical components in phase
  - Horizontal component lead and lag vertical component
- (3) Superposition of refracted and reflected pulses onto the air blast induced velocity pulses in conditions (1) and (2)
  - Superseismic combination
  - Outrunning combination

For the weapon effects condition assumed for this design example, the outrunning combination was not considered since the analysis in step 2 demonstrated that the conditions cited were superseismic.

The linear undamped isolation system assumed during preliminary design may be adequate for simple symmetrical systems with small displacements. A dynamic analysis is needed to accurately account for (1) variation in weight and inertia properties, (2) non-linear system behavior and spring behavior, and (3) damping effects both viscous and Coulomb. For example, in the antenna system, the weight and center-of-gravity location variation may be insignificant, but the non-linear characteristics may be significant. For the equipment platform isolation system both non-linear behavior and weight and center-of-gravity location variations may be significant. Damping is important as it affects response acceleration, time to damp out the residual motion, and final rest position. The allowable maximum and minimum damping characteristics of the system are determined by varying the damping values in the dynamic analysis until an unacceptable response is obtained.

The above discussion points out situations where a dynamic analysis may be necessary. The two systems considered in this section would require

a dynamic analysis. The equations of motion are similar to Equations (5.27), (5.28) and (5.29) for a three-degree-of-freedom system and the numerical procedure for solving the equations is given in Appendix C. This three-degree-of-freedom system is based on a two-dimensional model. More degrees-of-freedom must be considered when there is significant eccentricity in plan and the isolators are non-linear spring damper systems.

Step 6 (a-3) final spring design: The dynamic analysis provides the final spring properties required for final spring design. In addition to spring stiffness,  $k$ , and static and dynamic displacements, the allowable viscous and Coulomb damping requirements are specified.

The viscous damping factor will usually have an upper and lower allowable. The lower limit is governed by the time required to reduce the residual oscillatory motion to a specified value (see Section 5.8). The upper limit for damping is governed by the dynamic response.

The Coulomb damping will have an upper limit allowable which may be governed by post attack operational requirements or dynamic response. In most cases the amount of damping in an isolator system cannot be determined by analysis but must be determined by prototype testing.

Prototype testing is a very important part of the final spring design phase. Two types of tests are required:

- (1) a shock-displacement test to determine damping characteristics. A twang test is sufficient to evaluate the residual damping properties but a high velocity initial displacement stroke is required to measure damping in the initial stroke which is especially important in liquid springs.
- (2) a shock-displacement test with the isolator suspending an equivalent mass to determine high frequency vibrations of items attached to the suspended mass. The weight of the equivalent mass is based on the tributary load supported in the actual system.

Both tests may influence the final spring design details. If measured values of damping in test (1) are too low, auxiliary dampers (pneumatic dash-pots) may be required. Test (2) may indicate unacceptable high frequency vibrations

caused by chattering or surging of the spring elements. The high frequency vibration response can be minimized by eliminating loose elements in the isolator assembly.

In a system such as the equipment platform isolation system, the isolator assembly is attached to the facility enclosure at one end. The initial shock motion of the facility enclosure is transmitted directly to the isolator facility attachment causing the upper portion of the isolator to be accelerated. Therefore, the isolator rod design must consider the stresses resulting from the horizontal and vertical acceleration components at the facility attachment points. The horizontal acceleration component may induce very high bending stresses in a pendulous hanger rod. This can be attenuated by adding a flexible element such as a chain or cable between the rod and the facility anchor point. The horizontal acceleration motion of the isolator can be assumed to vary linearly from the facility attachment point to the platform attachment point as shown in Figure 8.16.

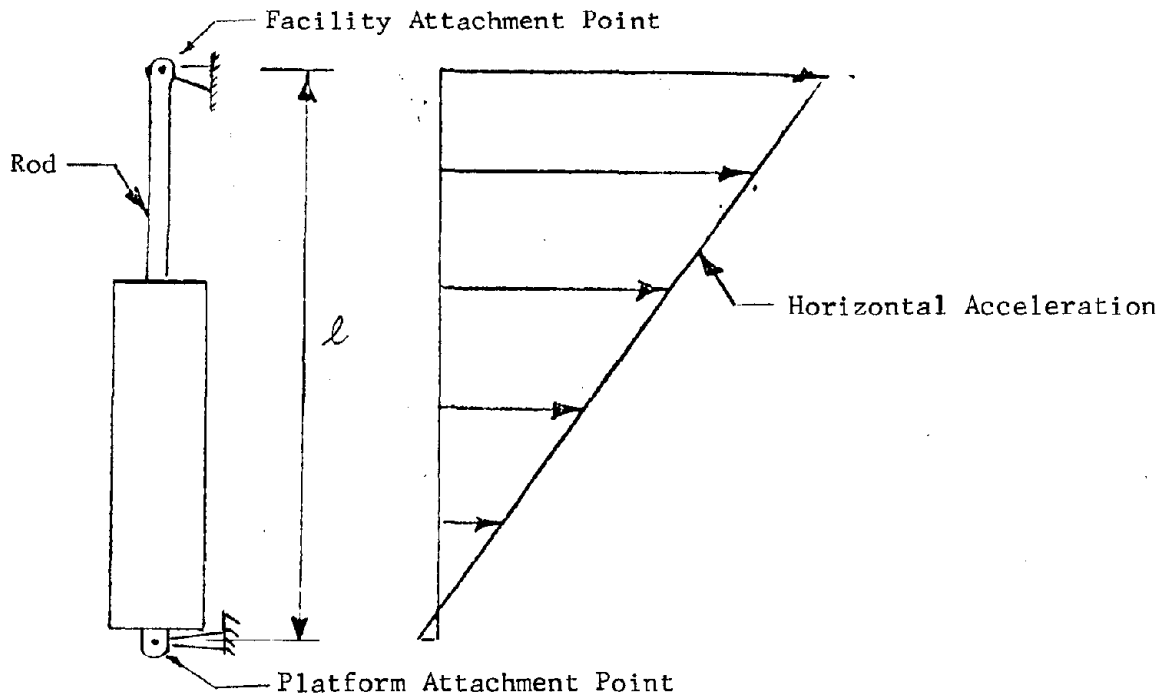


FIGURE 8.16: ASSUMED ACCELERATION MOTION OF PENDULOUS ISOLATORS

The acceleration at the top is the free-field peak acceleration and the acceleration at the bottom is the peak platform acceleration.

Step 6 (a-4) space envelope: As noted above, one end of the isolator is attached to the facility enclosure and the other end is attached to the platform or crib which is suspended. The differential motion between these two points requires that a free space be provided around the isolator or cable. This space envelope must be defined dimensionally and given to the equipment layout designer so that there will not be any encroachment in this space. For example, the space envelope required, including the dimensions of the isolator, around the equipment platform pendulous isolators would be similar to the envelope shown in Figure 8.17.

Step 6 (a-5) specifications: A good design and technical specification will usually result in acceptable production isolators. The final spring design, which includes prototype testing, establishes the required characteristics of the isolator. The specification makes provision for detailed hardware design and production testing to insure that each isolator will perform as specified. The requirements in a specification should include the following:

- (1) Control drawings for detailed hardware design and construction
- (2) Performance
  - (a) Spring rate with tolerance
  - (b) Damping factors with tolerance
  - (c) Static load; upper and lower limits
  - (d) Peak dynamic displacements
  - (e) Operational functioning requirements
- (3) Environments
  - (a) Non-operating (environments encountered in transportation, handling and storage)
  - (b) Operating (environments encountered in the installed condition)
- (4) Performance tests (to verify the characteristics listed in (2)).
- (5) Environmental tests (on preproduction article only).



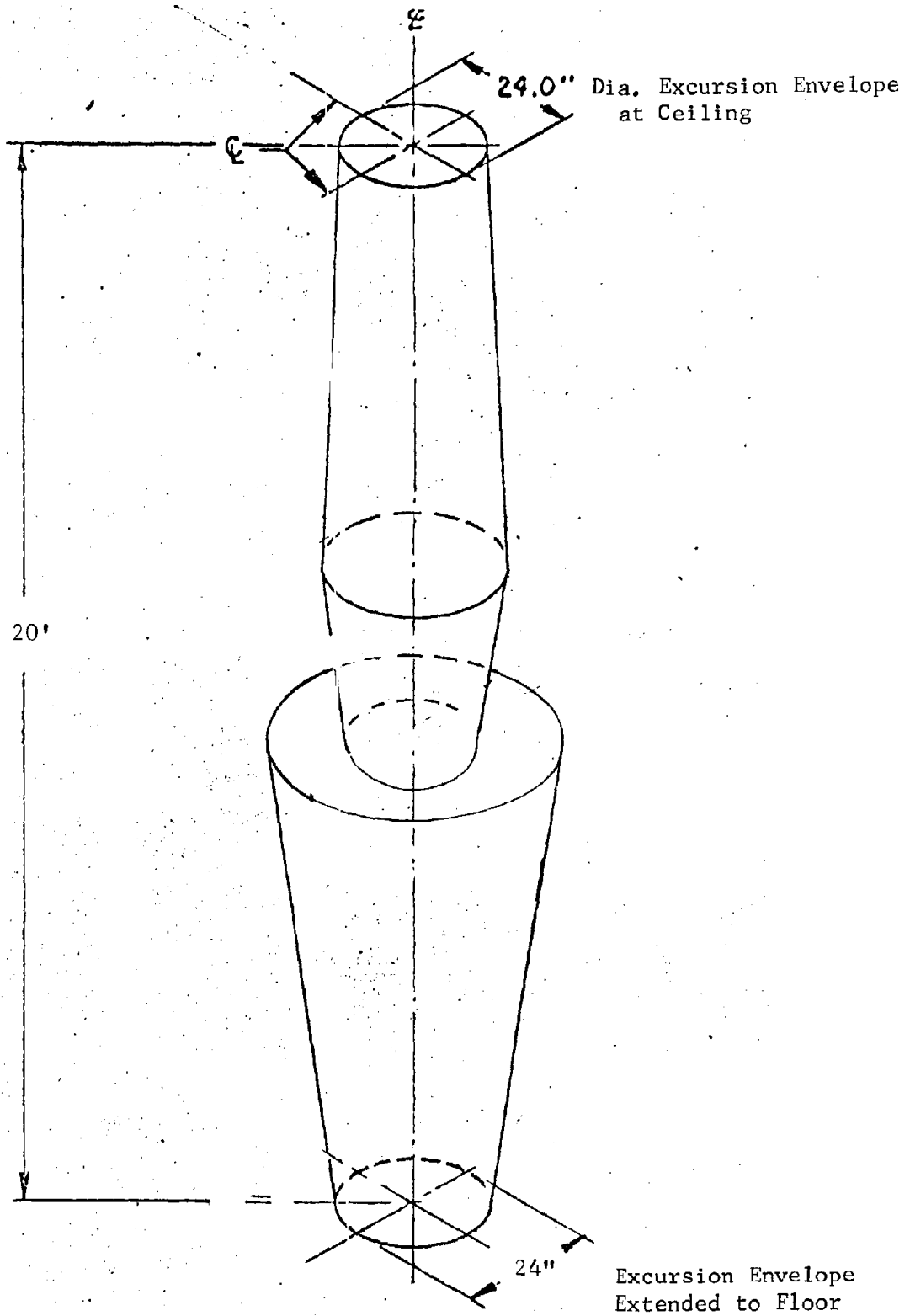


FIGURE 8.17: ISOMETRIC VIEW OF ISOLATOR MAXIMUM DYNAMIC EXCURSION ENVELOPE

8.2.7 Step 7 system verification: After the isolation system is installed and the total system is connected and checked, a complete system verification test program is performed. A dynamic response test is included in this program with the equipment (and personnel) in the operational status.

A true dynamic response test which will simulate the ground shock conditions due to weapon effects can only be achieved by exposing the facility enclosure to the predicted ground motions. Obviously this is not feasible. A twang test is usually an acceptable compromise for soft linear shock isolation systems. The platform or crib is displaced vertically and horizontally to the predicted peak response displacements and a quick release mechanism allows the system to freely oscillate and eventually return to the original position. All the operating functions are monitored during and after the test to verify acceptable performance.

Conclusion: The steps described in this section demonstrate a typical design cycle for a system (in particular a shock isolation system) exposed to a specified weapon effects condition. The steps may slightly deviate from this procedure to suit each particular situation but in general the sequence is considered typical for any major system. The shock isolation system designer may also get involved in other aspects of the overall project such as the preparation of maintenance manuals, preparation of installation procedure, and field supervision for installation and checkout of the shock isolation system. Therefore, it can be conclusively stated that shock isolation systems are an important part of the overall system and shock isolation must be considered in every phase (all 7 steps in this section) of the complete design cycle.

## SECTION 9. SHOCK ISOLATION SYSTEMS USED FOR HARDENED FACILITIES

### 9.1 Introduction

A survey of the shock isolation techniques presently employed in various hardened facilities provides useful information for the engineer who must determine the most appropriate shock isolation design to use in a new facility. This section presents a description of the shock isolation systems used for several ICBM launch facilities and for the NORAD facilities; it is founded on published information, and where available, on unclassified data developed by the cognizant military agencies and design contractors. It is not intended to be a complete documentation of all the features of the shock isolation systems that are discussed.

Information summarized for these examples of shock isolation systems was compiled from many published sources. Cognizant design agencies are: Air Force Systems Command Ballistic Systems Division for the ICBM Systems and Corps of Engineers, Department of the Army for the NORAD Center. Weapon System Contractors and Architect Engineer organizations in key roles were: General Dynamics/Astronautics, Martin-Marietta Company, Boeing, TRW Systems, Bechtel Corporation, Daniel Mann Johnson and Mendenhall, The Ralph M. Parsons Company, and Parsons, Brinkerhoff, Quade and Douglas.

In addition to the descriptions of the shock isolation systems, information on analytical methods used for design, alternate designs considered, test results obtained, and problems encountered, are included when it is available. Table 9.1 lists the various shock isolation systems described in this section.

### 9.2 Atlas F ICBM Facilities

#### 9.2.1 Atlas silo crib

a. Description. The Atlas missile, fuel storage tanks, and accessory equipment are mounted on a structural steel framework; the silo crib is suspended within an underground reinforced concrete silo by a shock

TABLE 9.1

Principal Shock Isolation Systems	Type of Spring System	Isolated Weight	Tolerance Levels	Special Analysis or Tests
<u>ATLAS F</u> Silo Crib Control Center	Pendulous Coil Springs Pendulous Air Springs	1500 tons 25 tons	.4g vert. .1g horiz. 1g vert. 1g horiz.	dynamic analysis - 2 dimensional
<u>TITAN I</u> Launcher Control Center Powerhouse Equip. Terminal Propell. Terminal Antenna	Pendulous Coil Springs Spring Beams Spring Beams Spring Beams Coil Springs: Base Wall Pendulous Coil Springs	500 tons 200 tons 200 tons 50 tons 150 tons 30 tons	.8g vert. .2g horiz. 3g vert/horiz 3g vert/horiz 3g vert/horiz 3g vert/horiz 3g vert/horiz	dynamic analysis - 2 dimensional
<u>TITAN II</u> Missile Mount Control Center Equip. Platforms		150 tons 80 tons 1 to 10 tons	.8g vert. .1g horiz. 1g vert/horiz 3g vert/horiz	Twang test verified stability Twang test showed pneumatic effects Twang test showed coupling
<u>MINUTEMAN</u> Missile Mount Equipment Room Control Center Launcher Equip. Bldg. Control Equip. Bldg. Antenna	Pendulous Coil Springs Pendulous Coil Springs Pendulous air Springs Pendulous liquid Springs Pendulous Coil Springs Pendulous liquid Springs Vert/horiz Coil Springs	40 tons 8/15 tons 40/80 tons 30 tons 30 tons 6 tons	.8g vert. .1g horiz. 3g vert/horiz 3g vert/horiz .5g down 3g vert/horiz 3g vert/horiz 5g vert/horiz	dynamic analysis - 2 dimensional twang test verified stability shock test showed high freq. vibration dynamic analysis - 3 dimensional shock displ. test verified analysis (same as control center) dynamic analysis - 2 dimensional twang test verified analysis/damping
<u>NORAD</u> Main Bldg. and Utility Bldg.	Base Mounted Coil Springs		1g vert/horiz	dynamic analysis - 2 dimensional modal test verified analysis and spring characteristics

isolation system. The fuel tanks and equipment are located on floors at eight different levels within the crib.

The crib is approximately 150 feet high, and is octagonal in plan with a width across the points of 49 feet. The total weight of the crib and its contents is approximately 1500 tons. The missile is the most fragile item supported by the crib, and therefore, the design of the shock isolation system is governed by the peak accelerations, 0.4 g vertical and 0.1 g horizontal, tolerated by the missile.

b. Shock criteria. The ground-shock response spectra envelope at low frequency is in the low-to-moderate displacement region (approximately 6 inches vertical and 2 inches horizontal). The vertical shock spectrum response curve used for design of the shock isolation system is shown in Figure 9.1.

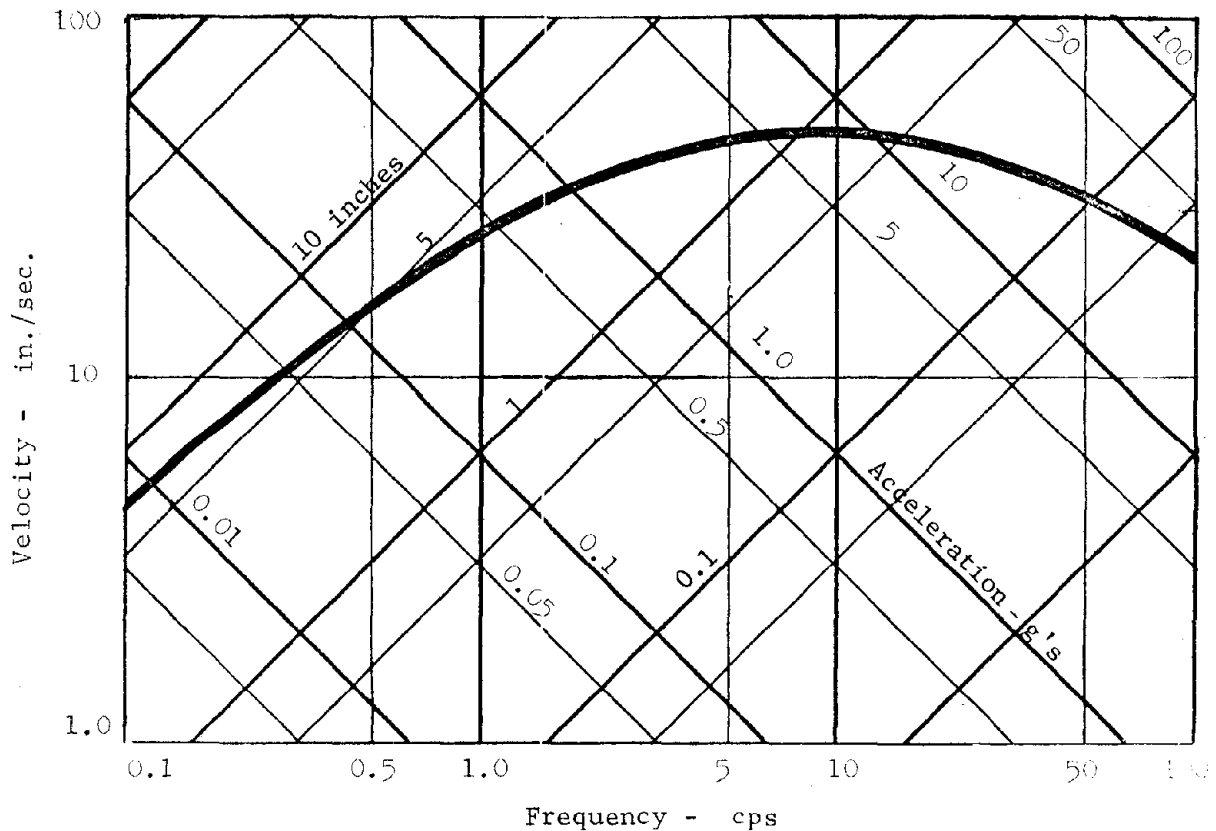


FIGURE 9.1: VERTICAL GROUNDSHOCK SPECTRUM FOR ATLAS F CRIB SUSPENSION DESIGN

c. Shock isolation design. The silo crib is supported and shock isolated by four pendulous springs, referred to as shock struts, which are equally spaced around the periphery of the crib; one end of each strut is attached to the crib a few feet below the center of gravity, and the other end of each strut is attached to the silo wall about 10 feet below the silo roof. Figure 9.2 is a cross-section view of the silo-crib suspension system, which also shows the relative positions of other items in the crib.

Each shock strut is usually composed of seven spring elements mounted in series around a common compression rod. Each spring element contains an inner and outer spring. The outer spring is approximately 2 feet in diameter and is made from a 3 1/2 inch diameter chrome molybdenum spring steel stock.

Vertical shock attenuation is provided by the coil springs, while horizontal attenuation is provided by the pendulum action of the shock struts. Vertical dampers are located on each strut near the top coil springs. Horizontal dampers are located between the silo crib and silo walls at the point of attachment for the shock struts.

An 18 inch rattlespace provides sufficient clearance for the predicted pitch motions and tilt angle of the crib. The change in the silo-crib tilt angle due to shifting of the center of gravity during fueling of the missile amounts to 1/4 degree. Support of the crib near its center of gravity minimizes the pitch motion.

Additional spring connections are provided between the missile launch platform and the silo crib to attenuate the higher frequency vibrations from the ground shock.

Hydraulically operated positioning and locking mechanisms are used to align the crib prior to missile launch.

d. Alternate designs considered. Since the Atlas missile was one of the first ICBM requiring a shock isolation design for the launch facility, considerable study went into the consideration of alternate approaches to the problem of hardening the launch facility.

Development of new equipment that could be hard mounted was discarded because of the cost of the test program required to qualify the equipment.

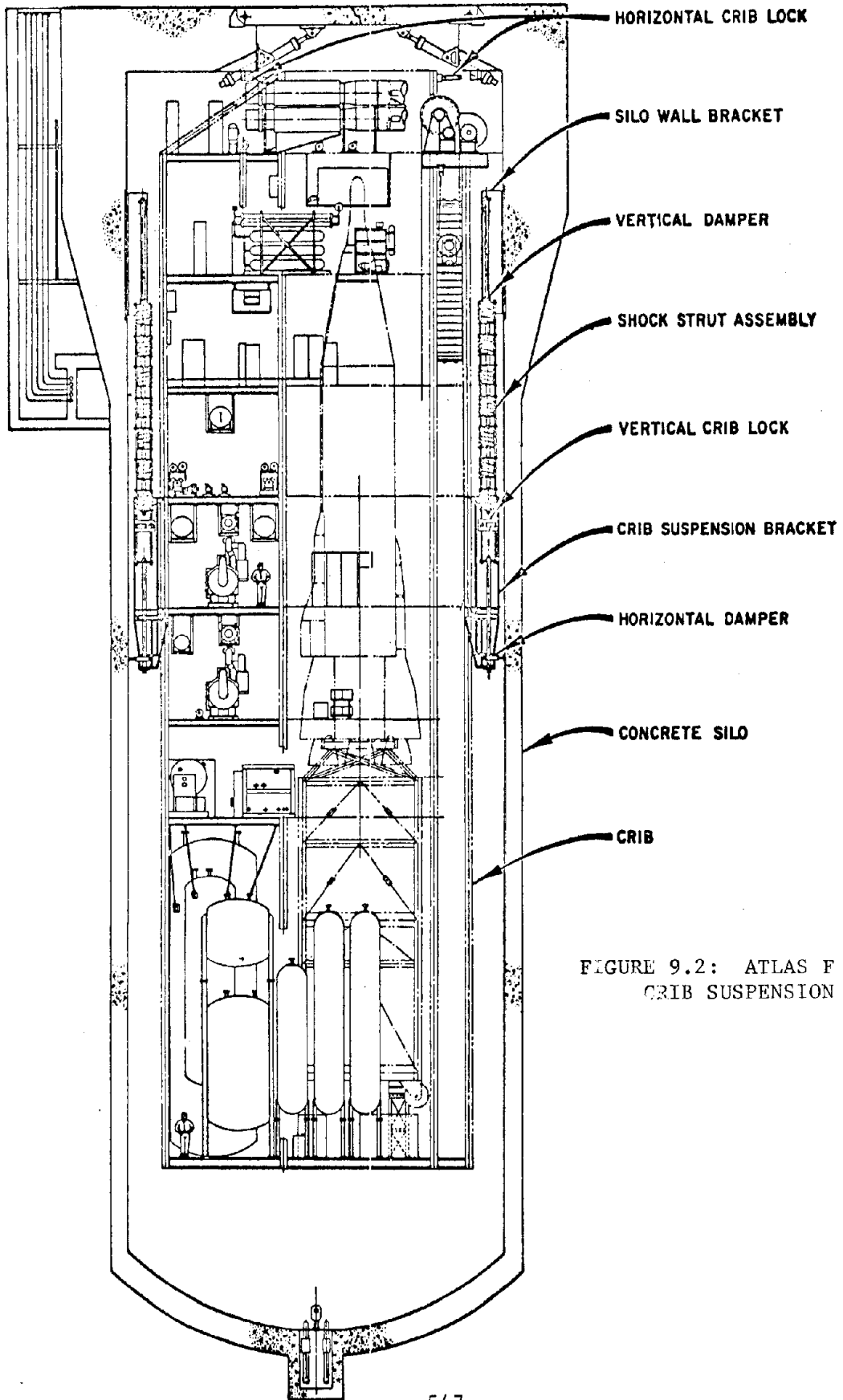


FIGURE 9.2: ATLAS F SILO  
CRIB SUSPENSION SYSTEM

Shock isolation of individual pieces of equipment was discarded because of the large amount of space required to prevent impacting between adjacent pieces of equipment, the need for flexible connections between all items, and other operational problems.

Mounting all the equipment on one shock isolated framework appeared not only to solve the problems mentioned above, but also provided the following advantages:

- (1) Permitted use of standard equipment.
- (2) Reduced number of flexible connections to a minimum.
- (3) Provided a total mass sufficient to insure stable operation of all equipment.
- (4) Protected operating personnel from shock.

Other types of springs were considered, such as hydraulic and pneumatic springs. However, at that time the coil spring design promised the most reliable operation and the lowest maintenance effort.

e. Design analysis. Vertical spring rates and rattlespace requirements were established by the use of shock spectra. A dynamic analysis was used to study the missile response, the critical design element was the pitch motion due to coupling of modes. The model used for this analysis is shown in Figure 9.3.

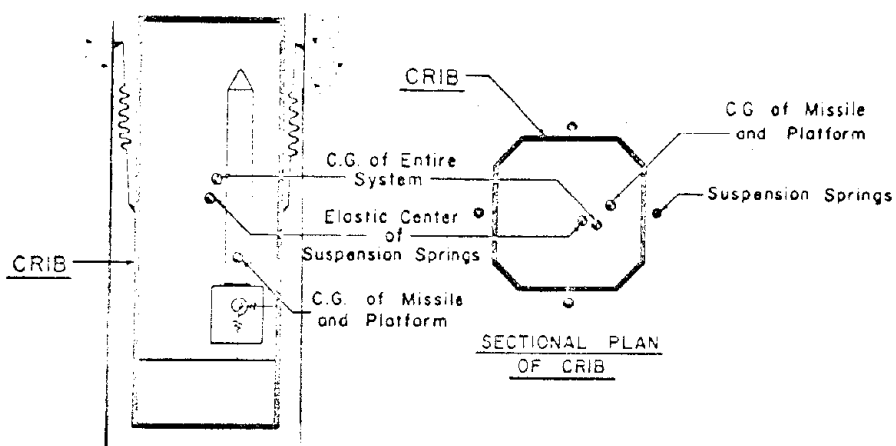


FIGURE 9.3: ANALYTICAL MODEL OF ATLAS F CRIB SUSPENSION SYSTEM



f. Problems encountered. A characteristic of coil springs is that the spring rate cannot be adjusted after installation. Moreover, the adjustment of the spring rate by adding or removing springs in series during installation affects the spring load carrying capability and the system pitch characteristics.

In the Atlas system design, the load capability of the springs was fully utilized; this made it impossible to increase the system weight or shift the center-of-gravity. Spring failures occurred in some of the first installations because of poor quality control during spring manufacture and due to the high stress level under the static load condition.

When a lighter weight alloy was substituted for the fuel tanks, it was necessary to add ballast to maintain the center-of-gravity position. Throughout the assembly of the crib, it was necessary to maintain a close check on the equipment weights, because there was no tolerance in the system's load capability and because the crib tilt angle was very sensitive to changes in weight and center-of-gravity location.

#### 9.2.2 Atlas launch control center (LCC)

a. Description. The equipment and personnel required to control the missile launch operation are located in an underground structure, the launch control center being connected to the missile silo via a tunnel. The equipment is mounted on two floors that are shock isolated from the underground chamber. Figure 9.4 is a cross-section view of the control center, showing the floor and shock isolation system arrangement.

The shock isolated floors are integrally connected by peripheral truss work. The floors are constructed of decking over steel beams, and are approximately thirty-eight feet in diameter. The entire floor system is suspended from the top of the LCC chamber. The total weight supported by the shock isolation system is approximately 25 tons.

The operating personnel, who might be seated, standing, or lying on a bunk, are the critical element in the isolator design and must be isolated from ground shock. A value of 1.0 g for the peak vertical and horizontal floor accelerations was chosen to prevent injury to the operating personnel and malfunction of the fragile operating equipment.

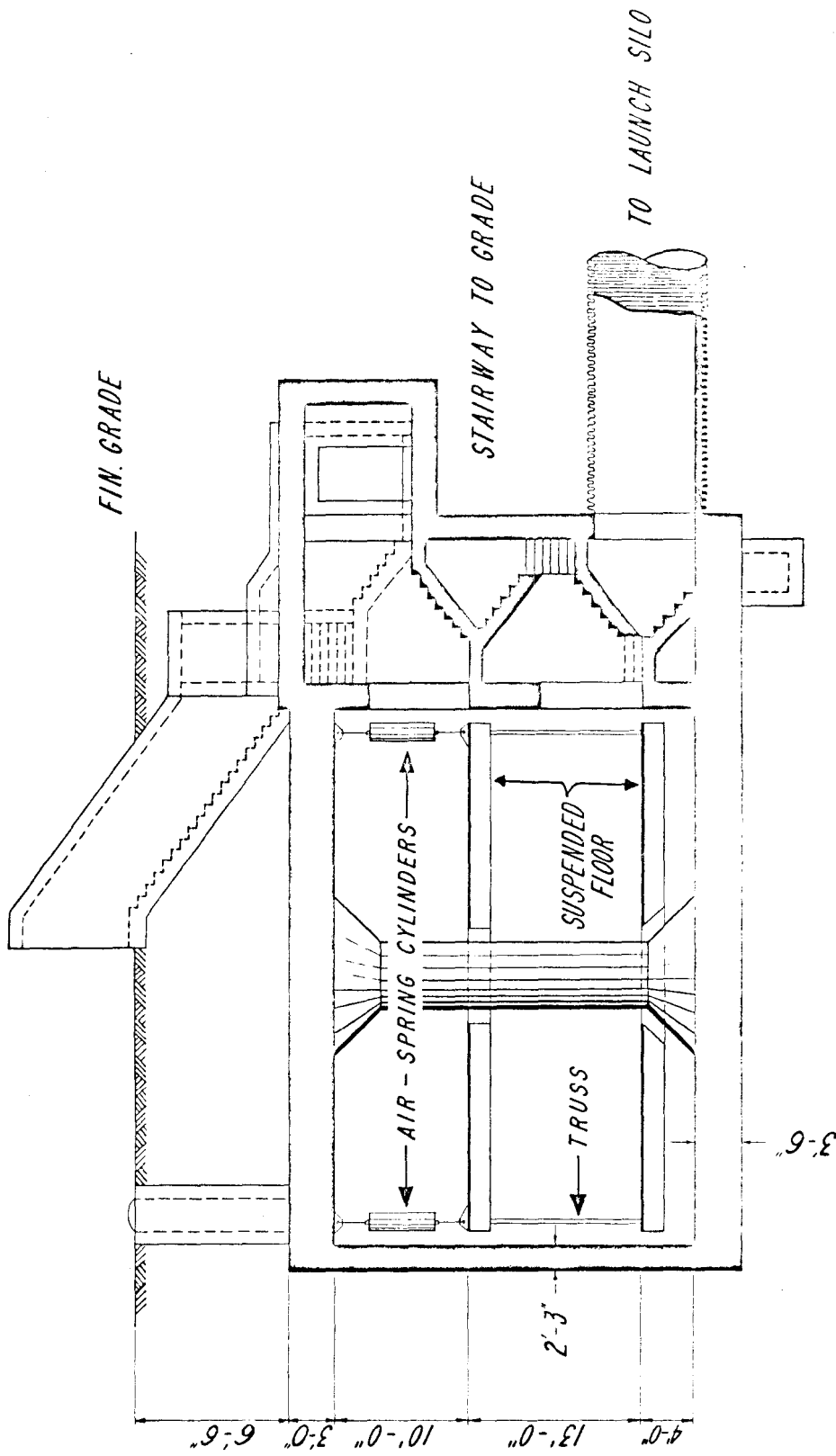


FIGURE 9.4: ATLAS LAUNCH CONTROL CENTER (LCC)

b. Shock criteria. Same as silo crib shock criteria (see Section 9.2.1.b).

c. Shock isolation design. The LCC floor assembly is supported by four pendulous springs spaced evenly around the floor periphery. Pneumatic springs are used for vertical shock attenuation; they are supplied by the compressed air system in the missile silo. Horizontal shock attenuation is provided by the pendulum action of the isolator support rods.

Adequate rattlespace is provided between the isolated floors and the cavity surfaces for the predicted ground shock displacements.

An advantage of this suspension system is that the floors will level themselves with a shift in the center-of-gravity. This feature permitted the design and construction of the LCC to proceed while the weight and location of certain vital control equipment were still under consideration.

d. Alternate designs considered. Pneumatic isolators were chosen over coil springs, because the former can be automatically controlled after installation to maintain a level floor with changes in weight distribution. The presence of operating personnel provides the necessary monitoring to detect failures in the air supply.

e. Design analysis. The design analysis was based on shock spectra. The peak horizontal and vertical response were assumed to occur simultaneously, and the pitch response was considered to be negligible. The non-linear behavior of the spring was considered in the spring design so that the dynamic response would not exceed 1 g.

f. Tests performed. The Atlas site installation at the Operational System Test Facility located at Vandenberg Air Force Base was equipped with special devices to carry out a complete functional test program which would insure compliance with the specified performance standards. The test facility provided a means for displacing the isolated systems to the predicted peak vertical and horizontal response distances simultaneously, prior to a sudden release. However, there are no published reports presenting the results of the dynamic tests.

g. Problems encountered. A pneumatic spring requires a continuous compressed air supply. A leak in a pneumatic system will cause a drop of the supported platform. The LCC has some essential equipment mounted on the

underside of the lower floor level. Therefore a loss of air pressure can cause damage to this equipment. To correct this problem pads were installed at the periphery of the platform so that the resilient pads would mitigate equipment impacts with the chamber floor.

### 9.3 Titan I ICBM Launch Facilities

#### 9.3.1 Missile launcher system

a. Description. The Titan missile and the missile elevator are mounted on a crib structure, which is supported within an underground reinforced concrete silo by a shock isolation system. The total weight isolated is approximately 500 tons. Figure 9.5 is a cross-section view showing the arrangement of the Titan I missile and supporting structure within the silo.

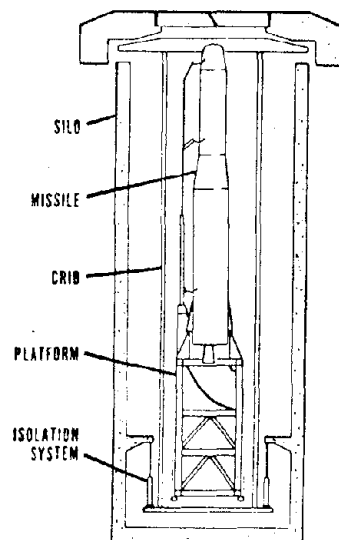


FIGURE 9.5: THE TITAN I LAUNCHER SYSTEM

The missile is the most fragile item supported by the crib, and, therefore, the design of the shock isolation system is governed by the peak accelerations (0.8 g vertical and 0.2 g horizontal) tolerated by the missile.

b. Shock criteria. The ground shock spectra envelope at low frequency was in the low-to-moderate displacement region (approximately 6 inches vertical and 2 inches horizontal).

c. Shock isolation design. The silo crib is supported and shock isolated by four pendulous springs, which are equally spaced around the periphery of the crib; one end of each spring assembly is attached to the base of the crib, and the other end is attached to the side of the silo. The vertical center-of-gravity is above the spring attachment level on the crib, but well below the missile center-of-gravity because of the elevator weight.

Vertical shock attenuation is provided by the spring assemblies, which consist of four coil springs mounted in series around a common compression rod. Horizontal shock attenuation is provided by the pendulum action of the spring assemblies.

d. Alternate designs considered. In preliminary studies it was determined that the launcher facility should be separated into three subsystems in order to use smaller spring elements with simpler shock isolation systems. The three subsystems are: the launcher silo; the equipment terminal; and the propellant terminal. The latter two subsystems are discussed separately (see Sections 9.3.4 and 9.3.5).

Several shock isolation designs were considered for the silo crib. Base mounted and side mounted springs were considered for pitch stability, but were rejected because of the need for a releveling system to compensate for any permanent set of the silo following a ground shock. Pendulous systems offered a simpler solution to the permanent set problem.

It was originally felt necessary to attach the shock isolation system as close to the silo bottom as possible to take advantage of depth attenuation of the shock. However, it was determined later that the entire silo moves as a rigid body.

When the vertical center-of-gravity of the missile and crib structure is higher than the point of attachment of the shock isolation system on the crib, pitch stability is more difficult to attain. Initial studies indicated that it was necessary to cross-couple the vertical springs to obtain pitch stability. Later on reduced ground shock criteria allowed the use of stiffer

springs that did not require cross-coupling for pitch stability. Coil springs were chosen over pneumatic springs, because of their higher reliability.

e. Design analysis. The shock spectra criteria were used in the preliminary design to establish vertical spring rates and rough estimates of the rattlespace required. Velocity pulses were derived based on the given shock spectra and these pulses were used to finalize and verify the design.

f. Problems encountered. Poor quality control in the spring fabrication resulted in spring failures during installation of the first units. Improved specifications corrected this situation.

### 9.3.2 Titan I launch control center

a. Description. The equipment and personnel needed to control the missile launch operation are located in an underground launch control center, which consists of a shock isolated two story structure within a hemispherically shaped chamber. The floors are circular shaped with the lower floor having a diameter of approximately 90 feet. The total weight supported by the isolation system is approximately 200 tons.

The shock isolation system requirement of less than 3 g vertical and horizontal acceleration for the peak floor response was considered acceptable for both personnel and electronic equipment. Some designers have used lower values for personnel who may be unrestrained during ground shock.

b. Shock criteria. Same as silo crib shock criteria (see Section 9.3.1.b).

c. Shock isolation design. The LCC floors are integrally connected via a steel framework and are shock isolated from the LCC chamber by means of a base mounted pendulous spring-beam assembly. Figure 9.6 shows a cross-section view of the LCC structural configuration.

Vertical shock attenuation is achieved by beam flexure, while the horizontal shock attenuation is achieved by the pendulous supports in the spring beam system.

The spring-beam system was considered adequate for the low shock magnitude, because a low frequency system was not required. Coil springs could be used in place of the spring-beam system.

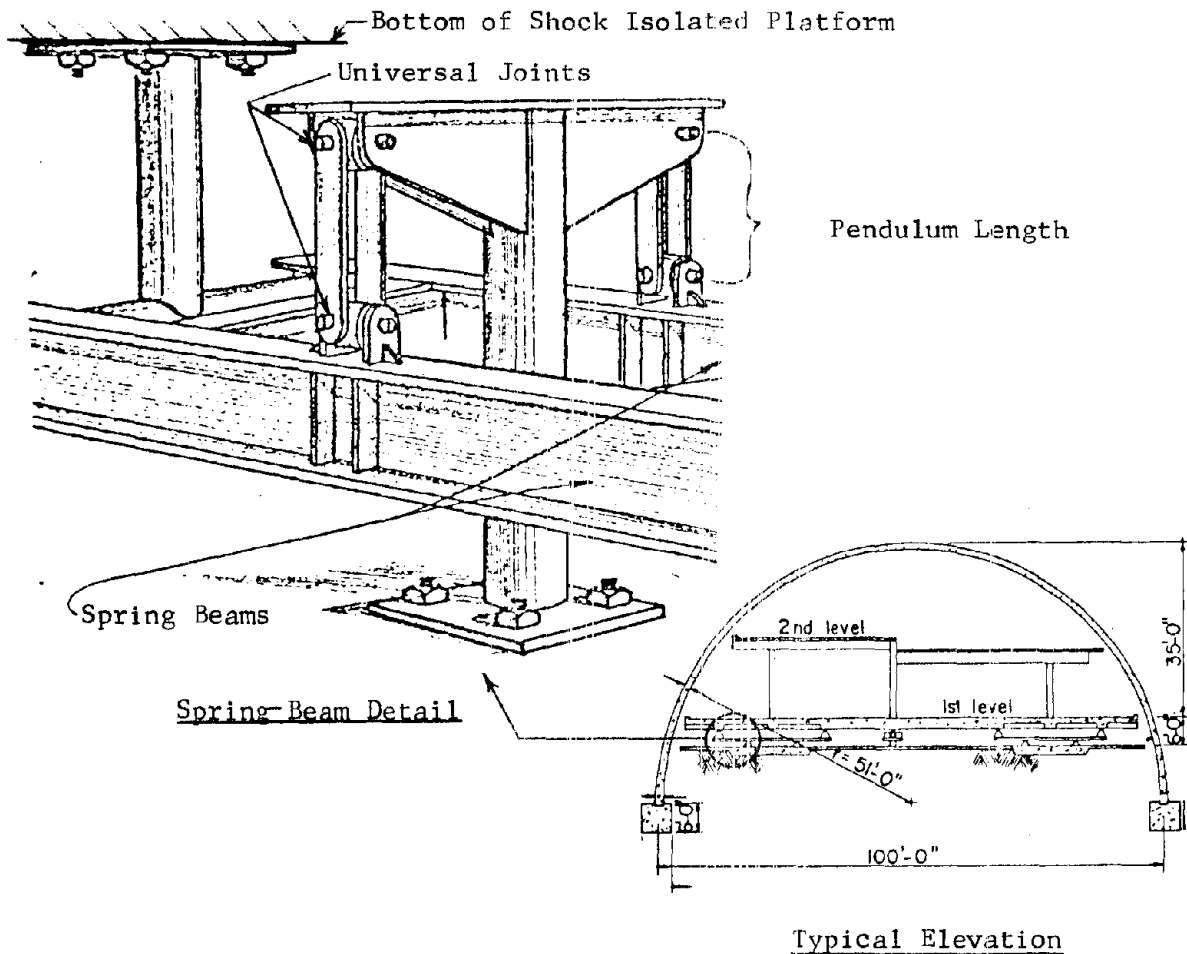


FIGURE 9.6: TITAN I LAUNCH CONTROL CENTER

d. Design analysis. The design analysis was based on shock spectra response. The coupling effect was considered to be negligible.

e. Comments. From an economical standpoint, the use of base mounted coil springs may have been cheaper than the spring-beam system.

### 9.3.3 Titan I powerhouse

a. Description. A housing for all the utilities necessary to sustain the launch facility for a 2 week emergency period is provided by the underground powerhouse, which has a structure very similar to the LCC. The lower floor is approximately 115 feet in diameter. The weight supported by the shock isolation system is approximately 200 tons.

The same shock attenuation criteria were used for the powerhouse as were used for the LCC (see Section 9.3.2.a.).

b. Shock criteria. Same as silo crib shock criteria (see Section 9.3.1.b.).

c. Shock isolation system. The equipment is located on two integrally structured floors, which are shock isolated by a base mounted spring-beam assembly, similar to the one used for the LCC.

Coil springs were placed between the heavy equipment and the platform to prevent the transmission of operating vibrations from the equipment to the platform.

d. Design analysis. Same as LCC design analysis (see Section 9.3.2.d.).

e. Comments. It is possible that the addition of coil spring mounts to the heavy equipment may cause amplification of the relative displacement between equipment and platform due to resonance and coupling of vibration modes during ground shock.

#### 9.3.4 Titan I equipment terminal

a. Description. Various equipment items required for the missile launch operation are separately housed in the underground equipment terminal. The equipment is mounted on four shock isolated circular floors located within a vertical cylindrical chamber.

The same shock attenuation criteria were used for the equipment terminal as were used for the LCC and powerhouse (see Section 9.3.2.a.).

b. Shock criteria. Same as silo crib shock criteria (see Section 9.3.1.b.).

c. Shock isolation system. Spring-beam shock isolation systems, similar to those used for the LCC and powerhouse, were used for the equipment terminal, except that each floor has a separate shock isolation system. The upper three floors are connected by hanger rods to spring-beam assemblies mounted on the chamber wall just below the floor above. Figure 9.7 shows a cross-section view of the equipment terminal.

Additional shock mounts were used for attaching individual equipment items to the floors.

d. Design analysis. Same as LCC design analysis (see Section 9.3.2.d.).

e. Comments. Refer to comments for LCC and powerhouse. (See Sections 9.3.2.e. and 9.3.3.e.)



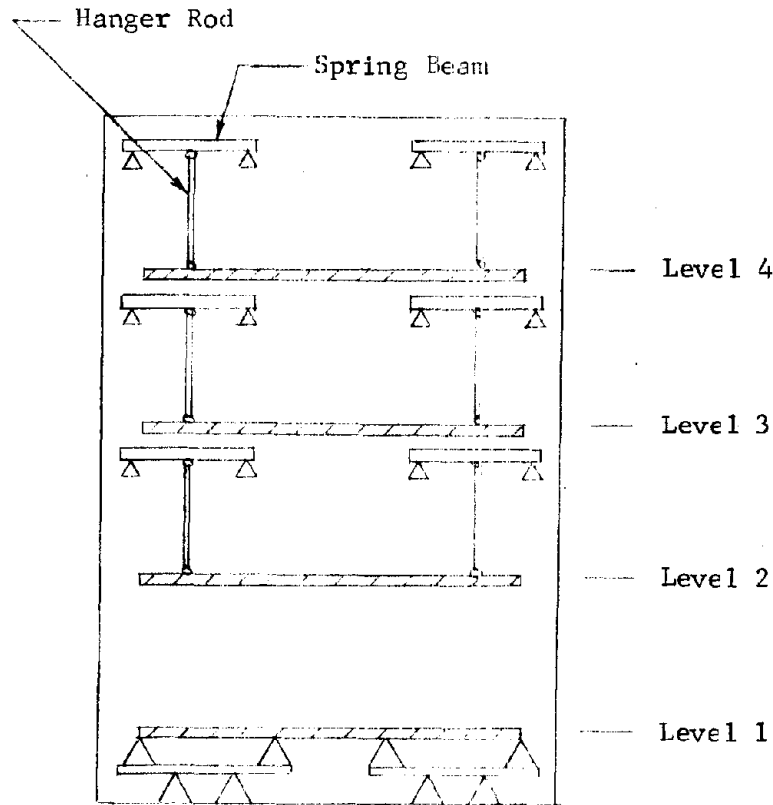


FIGURE 9.7: EQUIPMENT TERMINAL

### 9.3.5 Titan I propellant terminal

a. Description. The LOX propellant is stored in a separate underground chamber called the propellant terminal. The associated equipment and propellant storage tanks are supported by a shock isolated two-level rigid frame structure. The total weight supported by each floor shock isolation system is approximately 150 tons.

The ground shock attenuation requirement for the propellant terminal equipment allowed a peak vertical and horizontal platform response of 3 g's.

b. Shock criteria. Same as silo crib shock criteria (see Section 9.3.1.b.).

c. Shock isolation system. The rigid frame support structure is shock isolated by means of base mounted and wall mounted coil springs for vertical and horizontal shock attenuation, respectively. Universal joint connections

are used at the spring attachment points. Figure 9.8 is a cross-section view of the propellant terminal showing the arrangement of the shock isolation system.

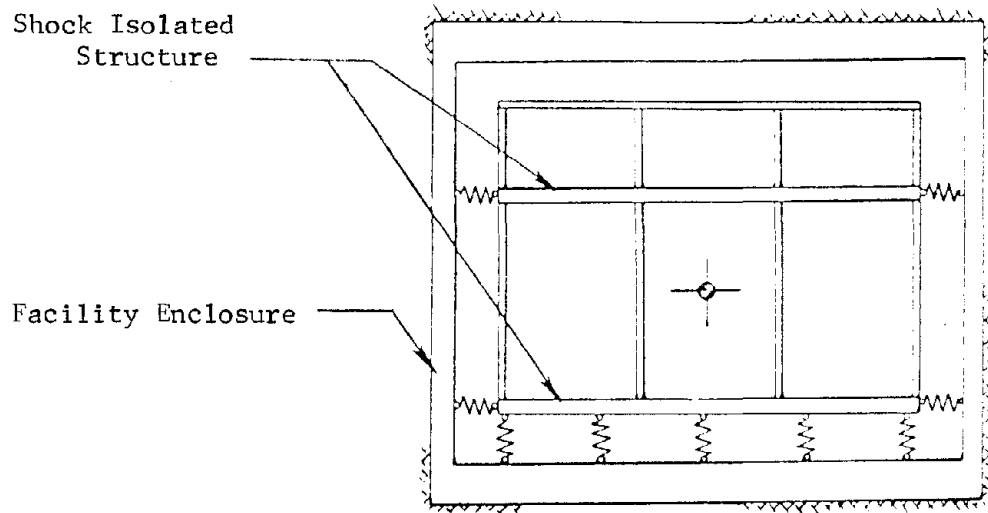


FIGURE 9.8: PROPELLANT TERMINAL

d. Design analysis. Same as LCC design analysis (see Section 9.3.2.d.).

e. Comments. The center-of-rigidity will fall below the vertical center-of-gravity due to the static load on the vertical springs. If the springs are symmetrically located, vertically and horizontally, about the system center-of-gravity, it is possible to have a pitch response (see Section 5.2). It is not known whether or not this was considered for the spring travel and rattlespace requirements.

#### 9.3.6 Titan I antenna system

a. Description. The antenna system is housed in a shallow underground silo and is mounted on a shock isolated crib. The system includes a mechanism for raising the antenna above ground level during the missile launch operation. The total weight supported by the shock isolation system is approximately 30 tons.

A fragility level similar to that for the missile was used for design of the antenna crib shock isolation system (see Section 9.3.1.a.).

b. Shock criteria. Same as silo crib shock criteria (see Section 9.3.1.b.).

c. Shock isolation system. The antenna crib is shock isolated by a pendulous spring system attached to the crib at the vertical center-of-gravity level, in order to minimize pitch response. Coil springs are used to attenuate the vertical ground shock, while the horizontal ground shock is attenuated by the pendulum action of the spring system. Figure 9.9 is a cross-section view of the antenna system.

Results of the missile silo crib shock isolation system design studies were instructive in the design of the antenna crib shock isolation system.

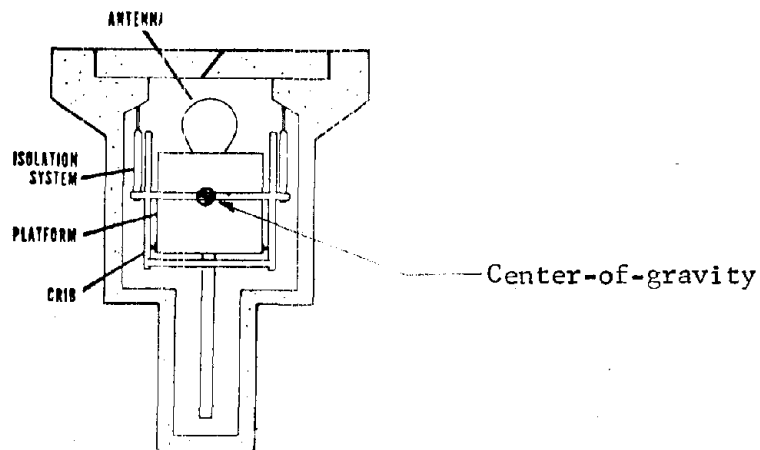


FIGURE 9.9: ANTIENNA SYSTEM

d. Design analysis. Same as for silo crib design analysis (see Section 9.3.1.e.).

## 9.4 Titan II ICBM Launch Facilities

### 9.4.1 Missile launcher system

a. Description. The Titan II missile is supported by a shock isolated thrust mount within an underground silo. The missile is not elevated to the ground surface level prior to launch, but is launched from within the silo. The thrust mount is locked in place prior to the missile launch.

The thrust mount has a circular ring, upon which the skirt of the missile rests prior to launch. The fueled missile weighs approximately 150 tons.

The missile must be shock isolated so that it will experience no rigid body acceleration greater than 0.8 g vertically and 0.1 g horizontally. Oscillations must be damped within 60 seconds to allow lockup for launch. The alignment tolerances for the missile 60 seconds after the ground shock are:

- (1) within  $\pm 0.25$  inch of the vertical neutral position,
- (2) within  $\pm 0.40$  inch of the horizontal neutral position,
- (3) within 0.25 degree from verticality for the missile axis.

b. Shock criteria. The input motion was defined by a shock spectra envelope predicting constant peak response displacements at low frequency in the order of 12 inches vertically and 4 inches horizontally.

c. Shock isolation design. The Titan II missile mount is supported by four pendulous springs equally spaced around the missile periphery. One end of each spring assembly is attached to the silo wall near the mid-point of the missile, and the other end of each spring assembly is attached to the thrust ring. Figure 9.10 is a detailed diagram of the shock isolation system.

Each spring assembly consists of four coil springs mounted in series. The coil diameter is approximately 20 inches and the wire diameter is approximately 3 inches. Vertical and horizontal dampers are attached between the thrust ring and silo wall, in order to subdue oscillations within 60 seconds. A lockup mechanism, which is part of the damper assembly, prevents motion of the thrust mount during missile launch.

The missile center-of-gravity is well above the point of attachment for the shock isolation system; this introduces the possibility of missile pitch motions.

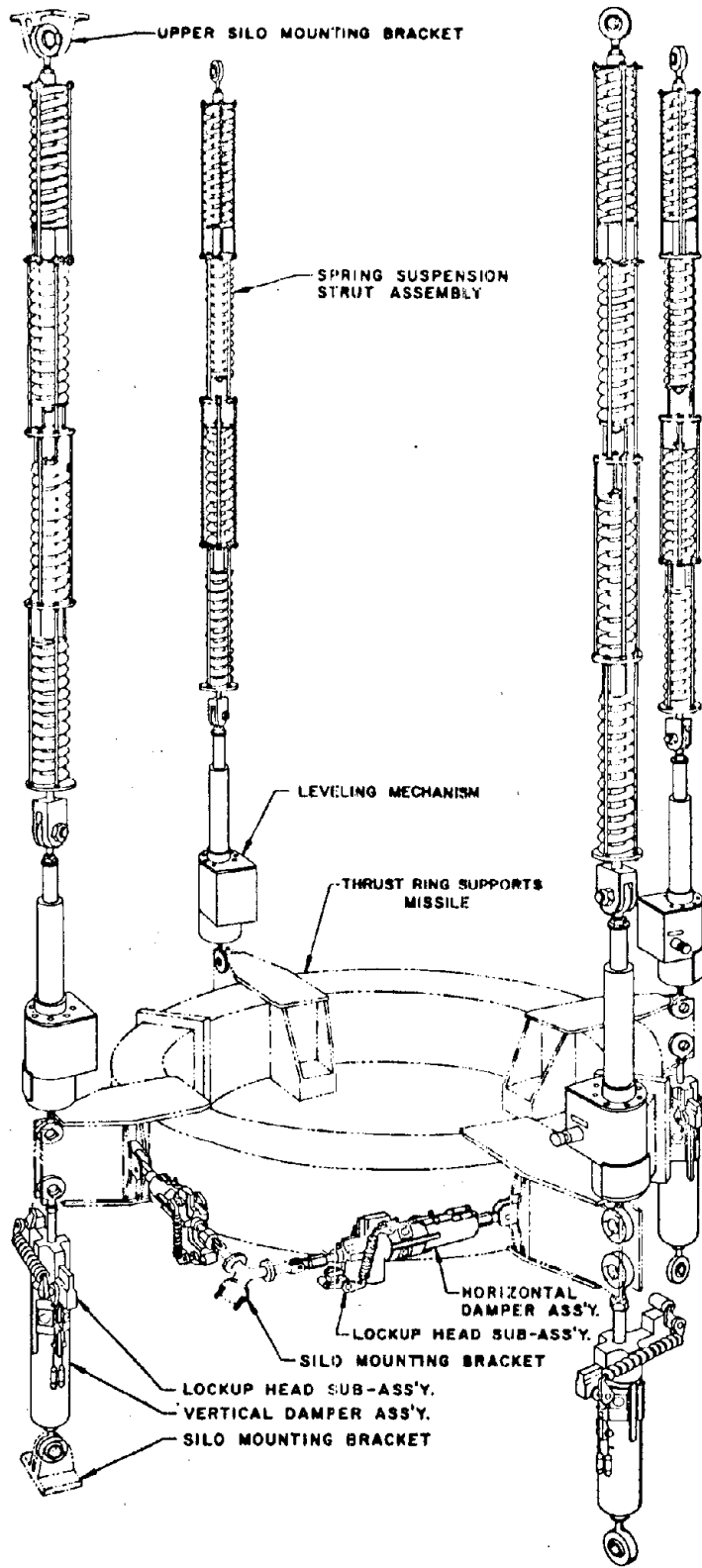


FIGURE 9.10: TITAN II IN-SILO SHOCK ISOLATION SYSTEM

d. Design analysis. The design analysis was very similar to that used for the Titan I missile mount system (see Section 9.3.1.e.).

e. Tests performed. A series of tests was performed at an operational site with a missile ballasted with water. The tests were classified into three categories; Natural Frequency Response Tests, Stickout and Lock-up Demonstration Tests, and Twang (initial displacement and quick release) Response Tests. Each test category will be briefly described with any significant results summarized.

(1) Natural frequency response tests. With the isolation system locked the thrust mount assembly was manually excited by personnel pushing against the re-entry vehicle tip, in order to obtain the first elastic mode frequency of the assembly. The apparent first elastic mode frequency was seen to be 0.40 cps. Evidence of higher modes, at 1.63 cps and 7.7 cps existed in the data. An equivalent viscous damping of 0.47 percent of critical was evident.

(2) Stickout and lock-up demonstration tests. The rotational and translational differences between the position of undamped static equilibrium and the positions of damped static equilibrium are referred to as the amount of "stickout".

A series of static tests were performed where the thrust assembly was displaced with hydraulic jacks. The dampers were unlocked and the damper shoes were engaged. Slow release of the jacking pressure allows the assembly to reach a second position of static equilibrium which could be compared to the initial equilibrium position. The maximum horizontal and vertical stickout measured was 3/32 inch and 1/16 inch, respectively. This was well within the tolerances specified in the criteria.

A series of lockup capability tests was performed to demonstrate that the system can be locked with the dampers at the extreme locking range limits. The tests were successfully accomplished by electrically locking the system with the dampers at various positions within the specified locking range limits.

(3) Twang response tests. The missile-thrust mount assembly was displaced both vertically and horizontally to the predicted single-degree-of-freedom shock spectra response displacements. The assembly was restrained in this position by explosive bolts, which were simultaneously fired to allow the

sudden release and ensuing motion of the assembly. The rigid body vertical (longitudinal) frequency of 0.86 cps was measured, which confirmed the frequency predicted by analysis. The pitch frequency and pendulum frequency were observed at about 0.3 cps and 0.1 cps, respectively. Dynamic instability was not observed in any of these tests.

All perceptible oscillatory motion was terminated 29 seconds after release when the damper shoes were engaged. Also all dampers had returned to within the locking range specified. When the damper shoes were disengaged all perceptible oscillatory motion terminated 67 seconds after release.

#### 9.4.2 Titan II launch control center

a. Description. The equipment and personnel required to control the missile launch operation are located in a shock isolated three level framed structure within an underground cylindrical chamber. The LCC structure, referred to as the cage, has a circular floor plan. The total weight supported by the shock isolation system is 80 tons.

Figure 9.11 shows the layout of the LCC cage and shock isolation system.

The ground shock must be attenuated to less than 1.0 g at the cage in both the vertical and horizontal direction for protection of the operating personnel.

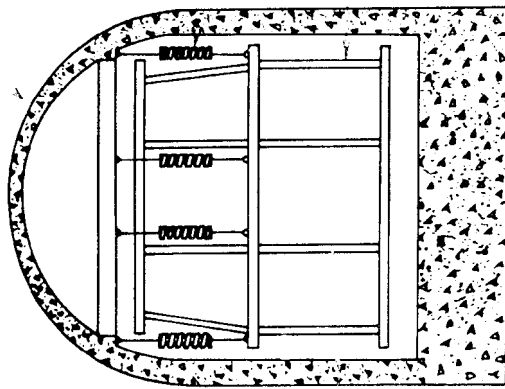
b. Shock criteria. The input motion was defined by a shock spectra envelope predicting constant peak response displacements at low frequency on the order of 12 inches vertically and 4 inches horizontally.

c. Shock isolation design. The LCC cage is supported by eight pendulous spring assemblies evenly spaced around the periphery of the cage. Each spring assembly consists of one coil spring within a cylindrical can. One end of each spring assembly is attached to the LCC chamber roof and the other end is attached to the second floor level of the cage, which is near the vertical center-of-gravity to minimize coupling of modes.

The coil springs provide vertical shock attenuation at a frequency of 0.75 cps. Universal joints at each end of the spring assemblies provide horizontal shock attenuation by pendulum oscillations at a frequency of about 0.3 cps.

The rattlepace provided for ground shock displacements of the LCC chamber is 12 inches at the top and bottom, and is 4 inches around the periphery of the cage.

Concrete  
Enclosure



Level 1

Level 2

Level 3

Coil  
Springs

Rigid Cage with  
Braced Columns

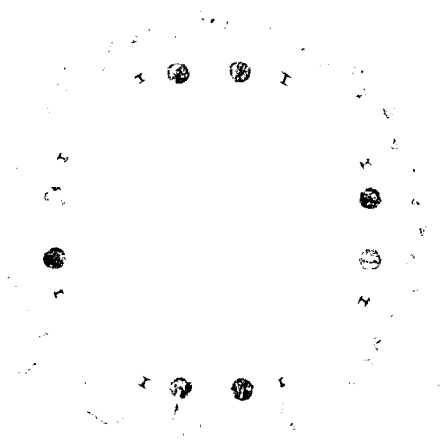


FIGURE 9.11: TITAN II LAUNCH CONTROL CENTER



d. Design analysis. The response predicted by shock spectra was considered adequate for design, because the system symmetry tended to minimize coupling of modes. The Titan I studies indicated the advantage of having the center-of-rigidity located near the center-of-gravity.

e. Tests performed. A series of twang tests was performed at an operational site to verify the design adequacy of the system. In the vertical twang tests horizontal motions were observed. Neoprene sheets had been placed between the LCC chamber wall and three of the first level partition walls and corresponding floors, in order to provide air conditioning for the operating personnel. Figure 9.12 shows the layout plan for the first level

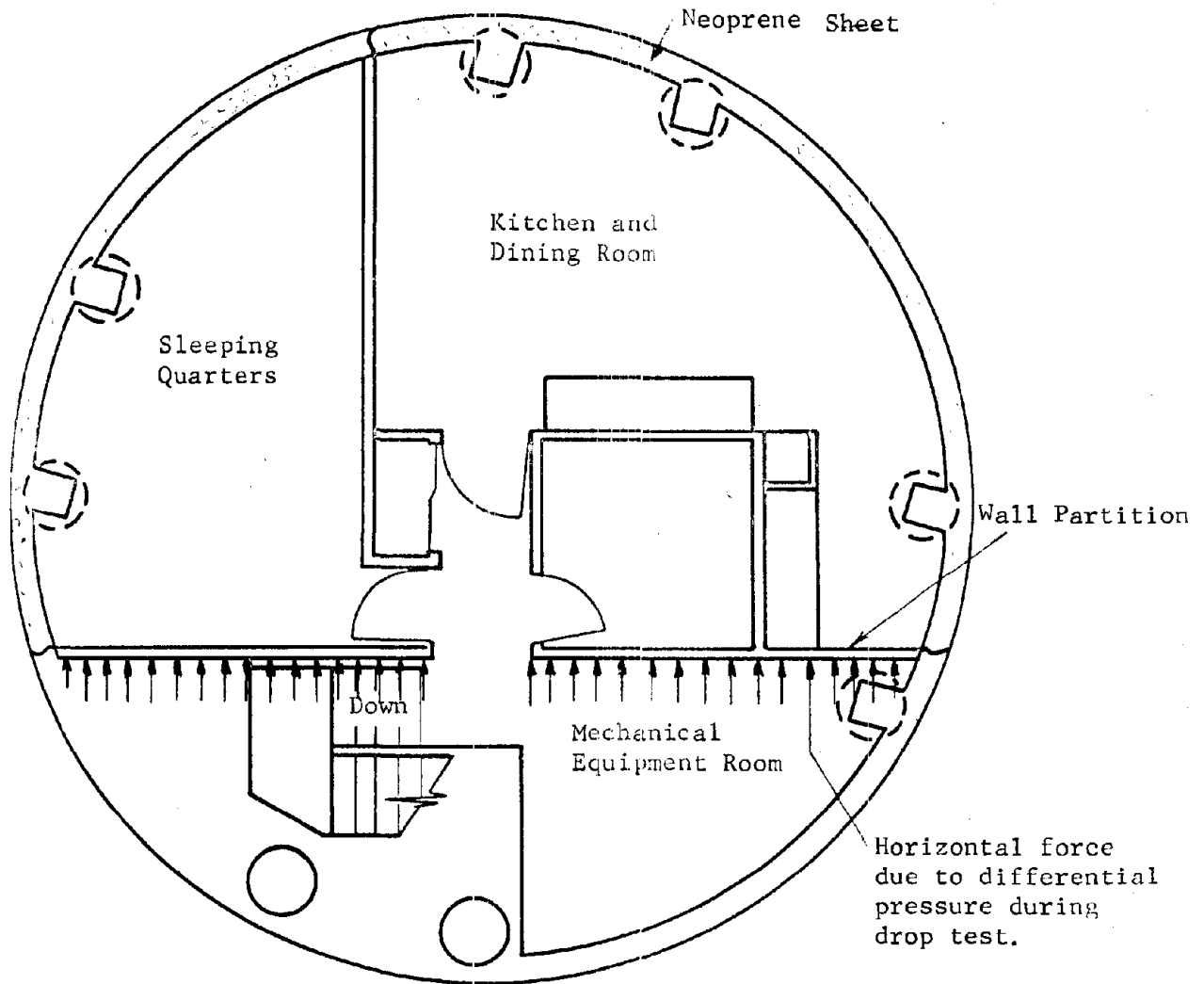


FIGURE 9.12: LCC FIRST LEVEL

of the LCC cage. These sheets caused unsymmetrical air pressures on the floor and walls as the air, above and below the cage, was alternately compressed and expanded by the vertical motion of the cage within the chamber. When the neoprene sheets were opened at three places, the horizontal motion was considerably reduced during subsequent tests.

A pneumatic damping as well as spring effect was also observed during vertical oscillation, damping out the motion after two cycles. The major portion of the damping was due to the viscous effects of the air trapped above the third level. When several floor plates on the third level were removed, the motion was completely damped in three cycles. The pneumatic damping effect did not significantly alter the spring characteristics as the frequency remained close to the calculated value.

f. Problems encountered. The pneumatic effects caused by the neoprene sheets were discussed above under the twang test results.

The rattlespace in some areas was found to be less than the specified 12 inches vertically and 4 inches horizontally.

#### 9.4.3 Titan II equipment platforms

a. Description. There are several equipment items located on platforms in the launch silo adjacent to the launch duct that are supported by individual shock isolation systems.

The equipment tolerance required that the ground shock be attenuated to 3 g vertically and horizontally.

b. Shock criteria. Same as missile silo (see Section 9.4.1.b.).

c. Shock isolation design. All equipment platforms were supported by pendulous spring assemblies. Figure 9.13 shows two arrangements used for supporting the equipment. Coil springs located within cans welded to the supporting structure provide vertical shock attenuation, while horizontal shock attenuation is provided by the pendulum action of hanger rods with universal joints connecting the coil springs to the equipment platform.

d. Design analysis. The vertical and horizontal responses were assumed to be independent single-degree-of-freedom systems predicted by the corresponding shock spectra. Coupling of modes was neglected. Neglecting the combined horizontal and vertical response underestimates the peak stresses at the spring can attachments to the facility.

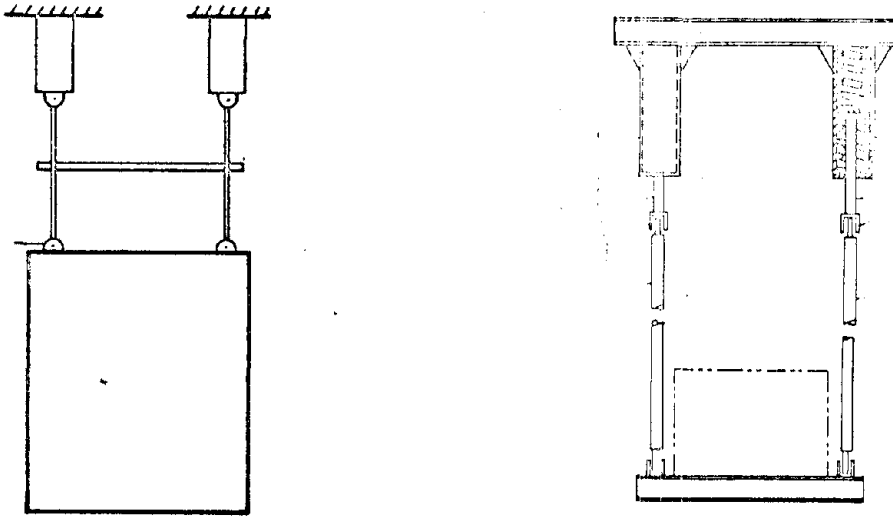


FIGURE 9.13: SCHEMATIC ARRANGEMENT OF ISOLATORS FOR INDIVIDUAL EQUIPMENT

e. Tests performed. Twang tests were performed on all equipment platform isolation systems. The accelerations were within the specified criteria values. During the combined horizontal and vertical twang tests, the horizontal displacements were amplified after a few cycles by about 25 percent over the peak displacements predicted by shock spectra. This clearly indicated the importance of considering the coupling response in a non-symmetrical system. Fortunately the rattlespace was sufficient to accommodate this amplified response.

f. Problems encountered. Coupling of modes amplified horizontal displacements, but the rattlespace was adequate (see discussion of twang tests above).

## 9.5 Minuteman ICBM Launch Facilities

### 9.5.1 Missile mount system (Wing I)

a. Description. The missile is centrally located in the underground launch silo, and rests on a receiver ring with no tie-down between the missile skirt and missile mount. The receiver ring rests concentrically on a support ring, which is attached to a shock isolating support system. The missile is launched directly from the silo. The total weight supported by the shock isolation system is about 83,000 pounds.

The missile fragility determines the maximum allowable system response. The maximum permissible axial loading on the missile skirt is the limiting criteria.

b. Shock criteria. The ground shock spectra envelope used for design of the shock isolation system was in the low frequency region. Originally, the nuclear shock criteria were interpreted as follows:

- (1) Input pulses to fit shock spectra envelope were positive velocity pulses only, i.e., no ground return.
- (2) Vertical and horizontal inputs were in-phase.

Later on the criteria interpretation was revised as follows:

- (1) The missile mount design must assume that the horizontal and vertical ground shock input can occur with any phasing.
- (2) The design must be satisfactory for inputs of any velocity pulse that fits the shock spectra envelope.

In addition to being capable of surviving loads and motions implied by the velocity pulses, it was also required that the system survive the loads and motions implied by a direct application of shock spectra response.

c. Shock isolation design. The shock isolation system is shown in Figure 9.14. It consists of three 100 inches long pendulum rods connecting the missile support ring to one end of rocker arms, the other ends of which are connected via rods to vertical coil springs within cans anchored to the silo wall about 300 inches below the rocker arms. The three pendulum rods have universal joints at each end and are spaced at equal intervals around the missile. The brackets supporting the rocker arm fulcrums are also attached to the silo wall.

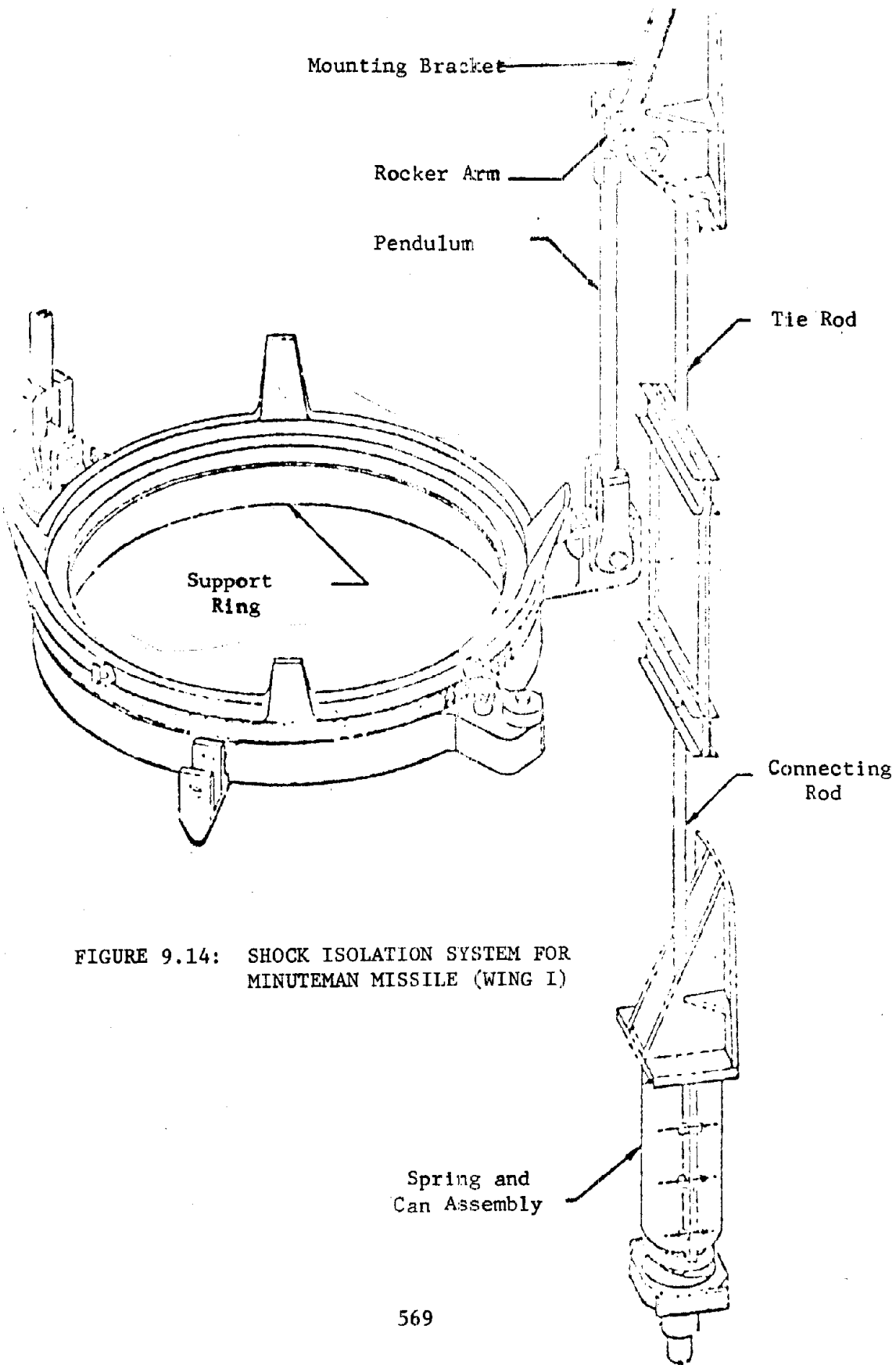


FIGURE 9.14: SHOCK ISOLATION SYSTEM FOR MINUTEMAN MISSILE (WING I)

The vertical, compression loaded coil, springs provide isolation against vertical ground motion and the pendulum rods provide isolation against horizontal ground motion. No additional damping is used, since sufficient damping occurs through the inherent frictional energy losses of the isolation system. The total vertical spring stiffness is 18,000 pounds per inch.

Vertical displacement is limited to 4.3 inches by the rocker arm and snubber block arrangement. Horizontal motion at the mount is limited to 6.0 inches by the rattlespace. Snubbers were added to the rocker arm to prevent support ring movement after the springs were unloaded, in order to avoid impact of the support ring with the missile nozzles during launch.

The support and isolation system hardware was designed for three times the maximum load obtained from the dynamic analysis. The hard mounted structural elements were designed to take the unattenuated shock loads.

d. Design analysis. Design of the missile shock isolation system was based on the following criteria:

- (1) The minimum missile axial load must be greater than 0.2 times the missile weight, and no separation must occur between the missile skirt and the mount under combined axial load and pitch motion.
- (2) Missile and mount displacements must be less than the available rattlespace.
- (3) Eccentric axial loading on the missile skirt must not exceed the allowable bending moment. If this criteria is met the missile will not impact the silo or tip over.
- (4) All oscillations must be damped within the specified time period.
- (5) Factor of safety for the missile structure is 1.5.

After the system is exposed to the specified shock the missile must return to within the following limits of its initial position:

- (1) Verticality. The missile axis shall be within a 15 minute angle from the vertical.
- (2) Lateral positioning. The missile axis shall be within 0.5 inch of the silo centerline in the plane of the missile base.
- (3) Vertical positioning. The missile elevation shall be maintained to within  $\pm 0.25$  inch.

These positioning criteria restrict the amount of Coulomb damping permitted in the isolation system.

In a preliminary design study using 50 inch pendulum arms, the vertical frequency was twice the pitch frequency, so that there was coupling between the vertical mode and pitch mode. The pendulum arms were extended to 100 inches to decouple the two modes.

A two-dimensional analysis model was found to be adequate for establishing final design. The model is characterized by:

- (1) two-dimensions
- (2) three-degrees-of-freedom
- (3) linear springs
- (4) rigid missile
- (5) non-linear motions
- (6) initial tilts and center of gravity offsets
- (7) damping values from test program

The values used for the analysis model are shown in Figure 9.15. Using feed-back from the test program the analytical model was able to predict the test results with a high degree of accuracy. The flow diagram for the design and qualification procedure is shown in Figure 9.16.

The effect of missile bending was found to be negligible in relation to the mount behavior because of sufficient frequency separation. A three dimensional analysis showed that the frequency ratios were such that vertical energy could not be transferred to the missile pitch mode or lateral mode.

It was assumed that horizontal inputs lagged the vertical. A study of input phasing indicated that the minimum margin of safety occurs at zero phasing with 0.5 inch center-of-gravity offset, 0.25 degree initial tilt, and the damping value obtained from system testing.

e. Tests performed. The dynamic characteristics of the missile mount system were determined by testing. Motion was initiated by statically displacing the missile mount to the design shock values, and suddenly releasing it.

Originally, excess friction due to rubbing of the springs and vertical rods, plus friction in the rocker arm bearings, prevented vertical alignment

MODEL DESCRIPTION

Pendulum Length	= 100 in.
Effective Base Radius	= 55 in.
Gross Pitch Stiffness	= $27.225 \times 10^6$ in-lb/rad.
Net Pitch Stiffness	= $11.505 \times 10^6$ in-lb/rad.
Total Vertical Spring Rate	= 18000 lb/in.
Vertical Frequency	= 1.46 cps
Pitch Frequency (Coupled)	= 0.136 cps
Pendulum Frequency (Coupled)	= 0.57 cps

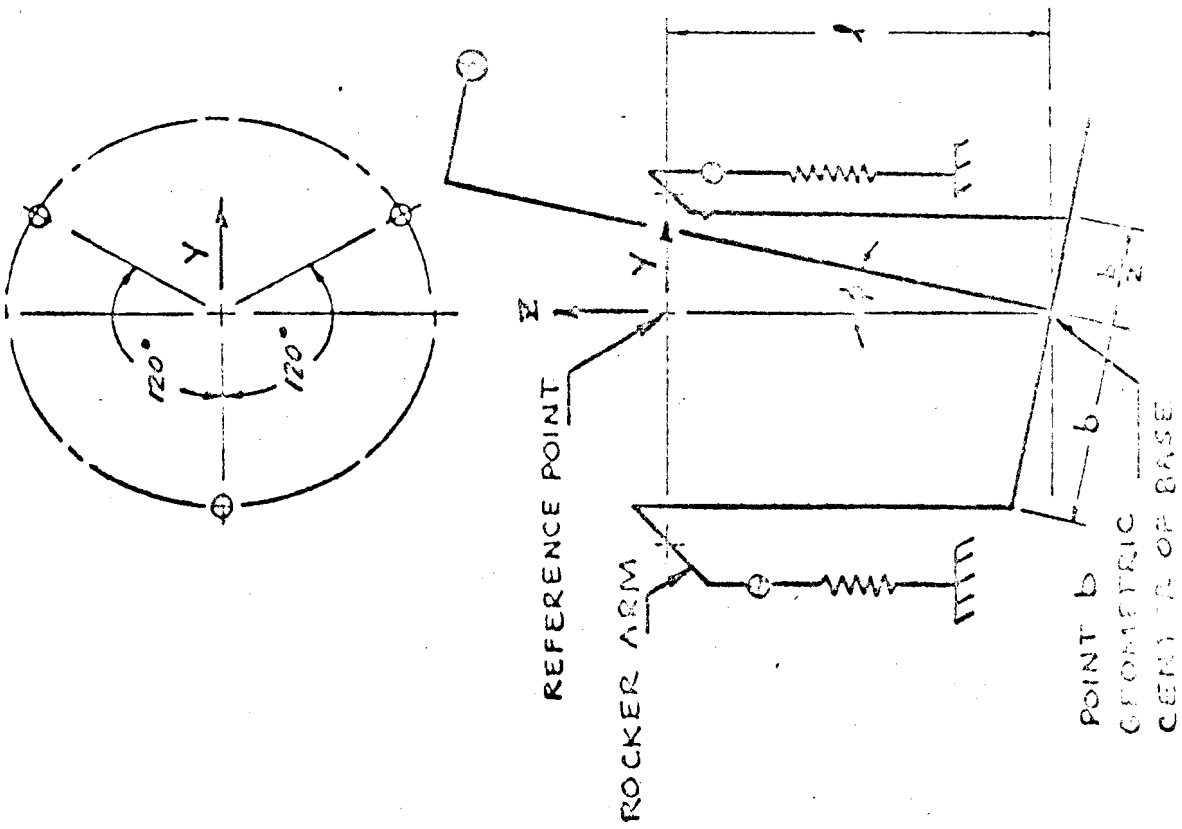


FIGURE 9.15: ANALYSIS MODEL - 2 DIMENSIONAL



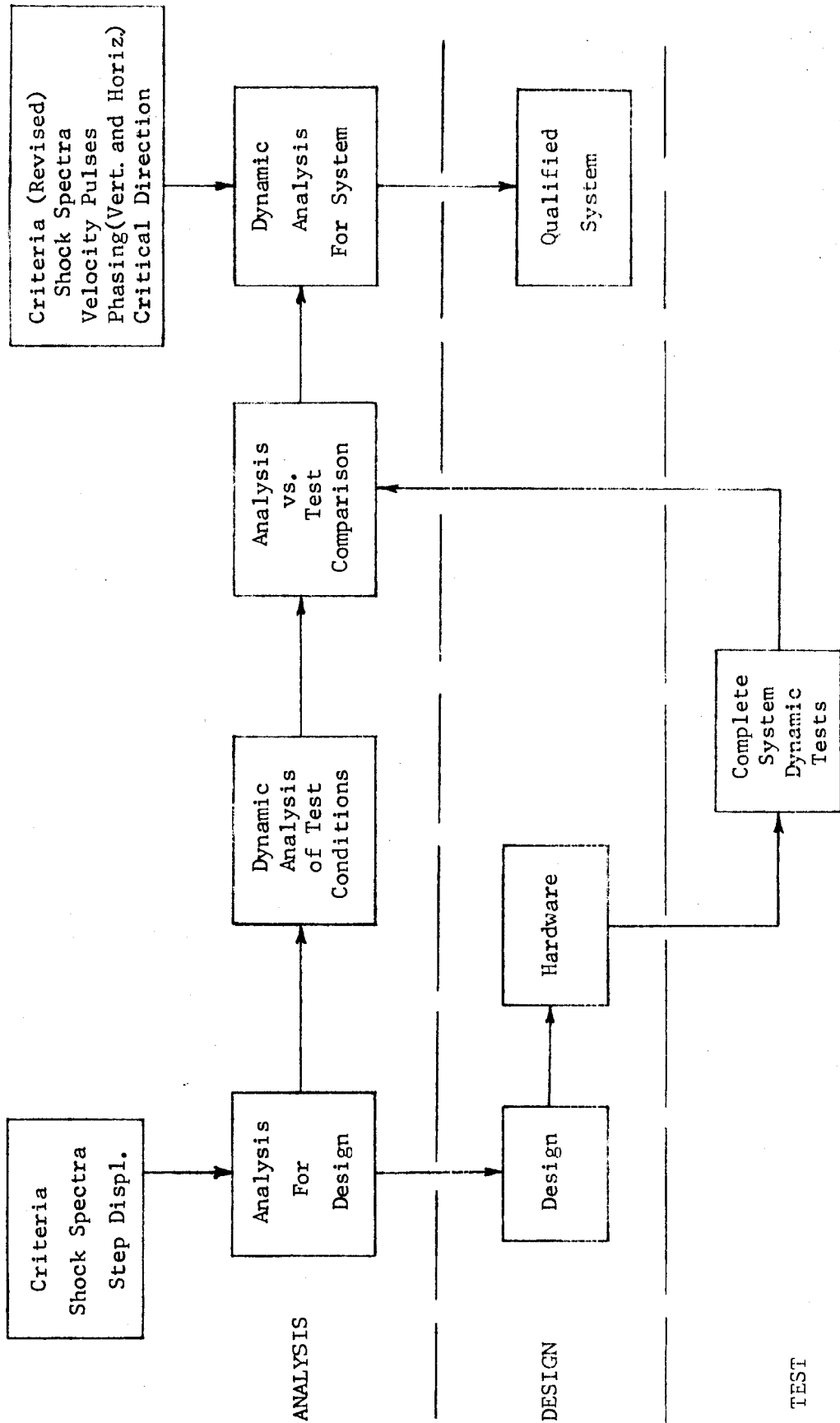


FIGURE 9.16: DESIGN AND QUALIFICATION METHOD

after simulated ground shock. That condition was fixed by relieving binding in the springs, and improving the rocker arm bearings.

Vertical oscillations were damped out in about 6 seconds. Lateral oscillations persisted longer, but were damped within the 5 minute limit. The missile was within verticality limits after oscillations ceased.

The structural capability of the missile skirt under axial loading was not exceeded, and the missile was stable.

f. Comments. The system is displacement limited in the vertical direction to about 4.3 inches because of the rocker arm design.

#### 9.5.2 Missile mount system (Wings II-VI)

a. Description. The Minuteman missile design used for these wings is essentially the same as the missile design used for Wing I. However, the shock isolation system had to be redesigned for higher ground shock requirements.

b. Shock criteria. The ground shock spectra envelope used for design of the shock isolation system was in the intermediate displacement region (see Section 9.5.1.b).

c. Shock isolation design. The rods and rocker arms of the Wing I system are replaced by a cable and pulley arrangement with the same vertical dimensions. The vertical spring stiffness is reduced to 4500 pounds per inch to allow for the higher shock levels. The lower spring stiffness made it necessary to add torsion bars between the springs to increase the net pitch stiffness. The shock isolation system is shown in Figure 9.17.

Vertical displacement is limited to 12.5 inches by snubber cables. Horizontal displacement at the mount is limited to 6 inches by the rattlespace.

d. Alternate designs considered. Liquid springs were given serious consideration for use in place of the coil springs. A shock isolation system design for the Minuteman missile incorporating liquid springs is shown in Figure 9.18. Vertical shock attenuation is achieved by a piston movement, which causes expansion and contraction of the liquid within a cylinder. Horizontal shock attenuation is achieved by the pendulum action of the spring assembly. Three liquid springs are hydraulically interconnected to achieve the required pitch stiffness.

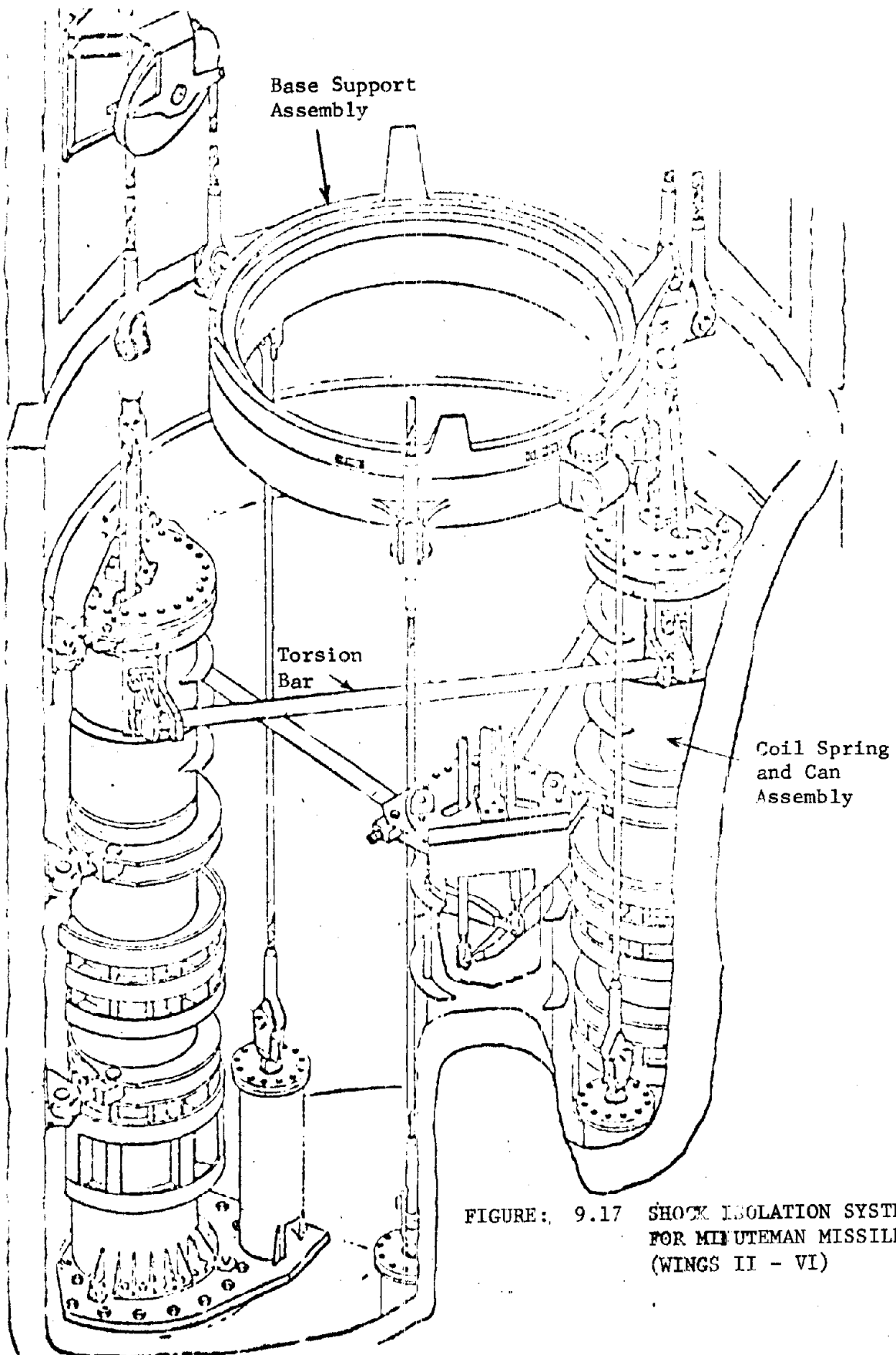
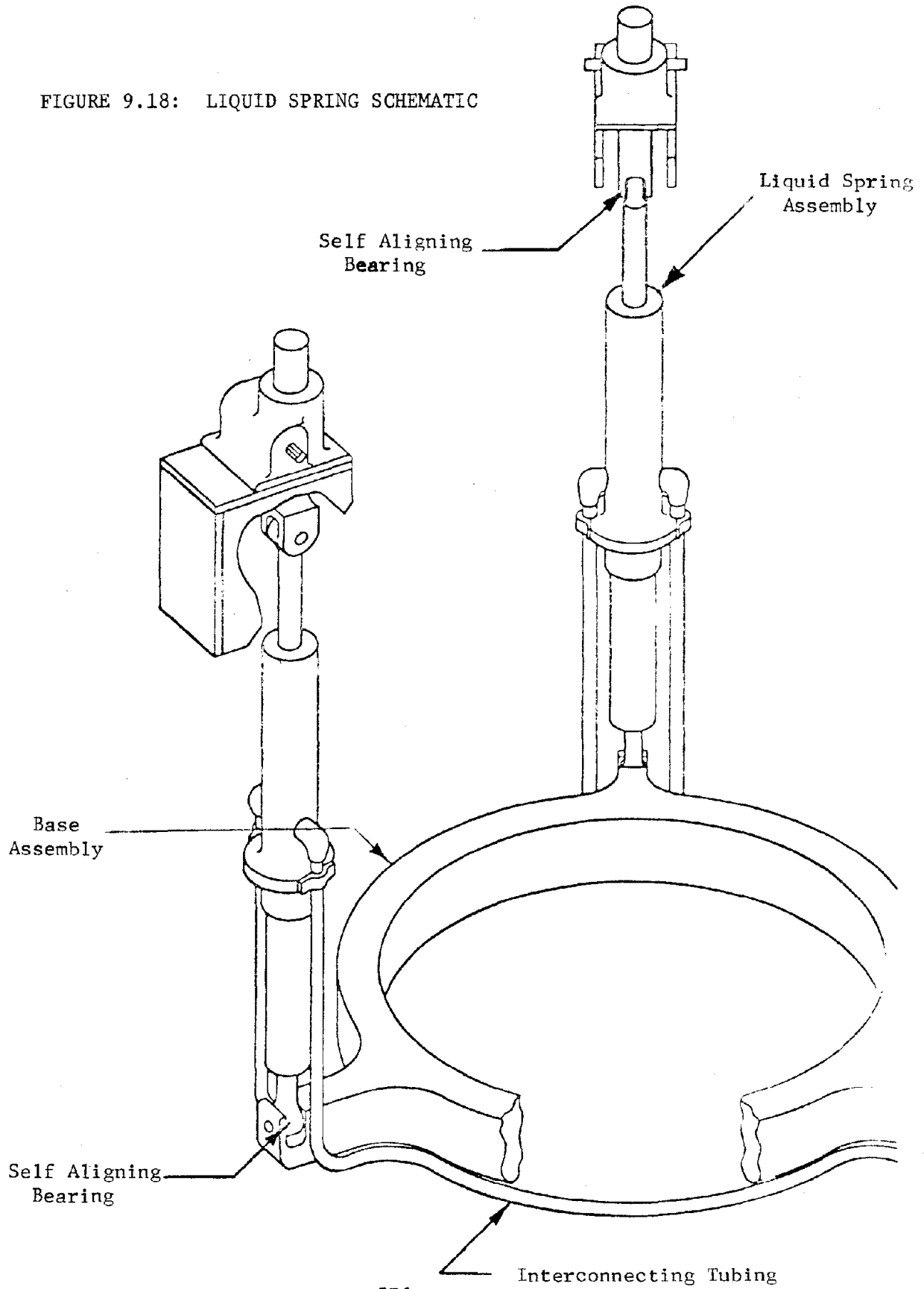


FIGURE: 9.17 SHOCK ISOLATION SYSTEM FOR MINUTEMAN MISSILE (WINGS II - VI)

FIGURE 9.18: LIQUID SPRING SCHEMATIC



It is possible to obtain equivalent spring rates with liquid springs of a smaller diameter than the diameter of the corresponding coil springs. This is important where space is limited.

The liquid spring system for the Minuteman missile mount was shown to have a lower production cost than the coil spring system. However, the liquid spring system was not adopted because of the longer time required to obtain a qualified design.

e. Design analysis. The design criteria for the Wings II - VI missile shock isolation system are the same as the criteria used for the Wing I system except the initial ground shock amplitudes are higher for Wings II - VI. (See Section 9.5.1.d.)

A two-dimensional analysis model was found to be adequate for establishing final design. The values used for the analysis model are shown in Figure 9.19.

The reduction in the vertical spring stiffness required by the larger displacements for Wings II - VI resulted in pitch instability, which made it necessary to add torsional stiffener bars between the vertical compression springs to increase pitch stability.

The support and isolation system hardware was designed for three times the maximum load obtained from the dynamic analysis, except the cables, which are designed to have an ultimate strength six times the static load.

f. Tests performed. The dynamic characteristics of the missile mount system were determined by testing. The system was pulled down because of the larger displacements.

Oscillations were damped out within the specified time period.

g. Comments. The complexity of the coil spring system results in very high production costs (see Section 9.5.2.d).

### 9.5.3 Minuteman launch equipment room (LER)(Wings I-V)

a. Description. Several of the equipment items required for missile launch are mounted on a shock isolated platform in the annular space around the top of the missile silo. The platform has an inner radius of about 7 feet, an outside radius of about 12 feet, extends annularly for approximately 150° of arc, and weighs 17,000 pounds. Plan and section views of the platform are shown in Figure 9.20.



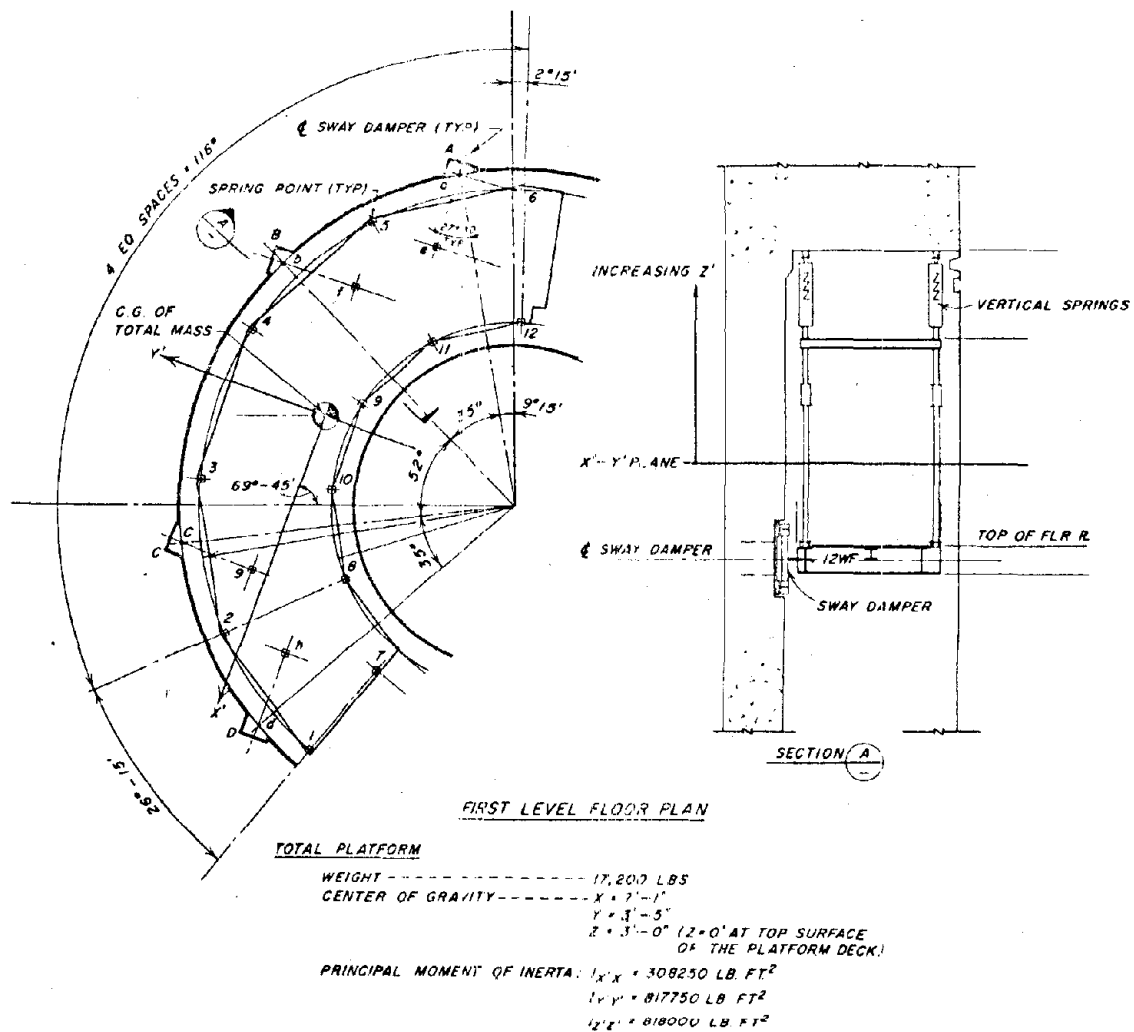


FIGURE 9.20; PLAN AND SECTION VIEWS OF LER PLATFORM

Eight electronic equipment racks are located along the outer periphery of the platform. The shock isolation system was designed to protect the most fragile piece of equipment mounted on the platform, and the design was based on an allowable maximum incremental acceleration load of 3 g's in any direction.

b. Shock criteria. The shock input was given in terms of shock response spectra. Input velocity pulses were derived consistent with the given shock spectra for an evaluation analysis after the design was complete.

c. Shock isolation design. Twelve hanger rod and compression spring assemblies attached to the LER ceiling and uniformly spaced around the edges of the platform, support and isolate the platform. A combination of five spring rates were used in an attempt to obtain dynamic symmetry throughout the platform (i.e. to get the center-of-rigidity to coincide with the center-of-gravity).

The isolators utilize a rod and support can that confine a coil spring; end plates and stops are attached to the rod and can, which cause the spring to be loaded in compression from either axial direction (see Figure 9.21). Transfer of force from one set of plates and stops to the other occurs at the no load position. The spring wire sizes varied from 5/8 to 1 3/8 inches in diameter and mean diameters varied from 4 to 7 5/8 inches in diameter in the different assemblies. The hanger rods are made of 2 inch diameter pipe.

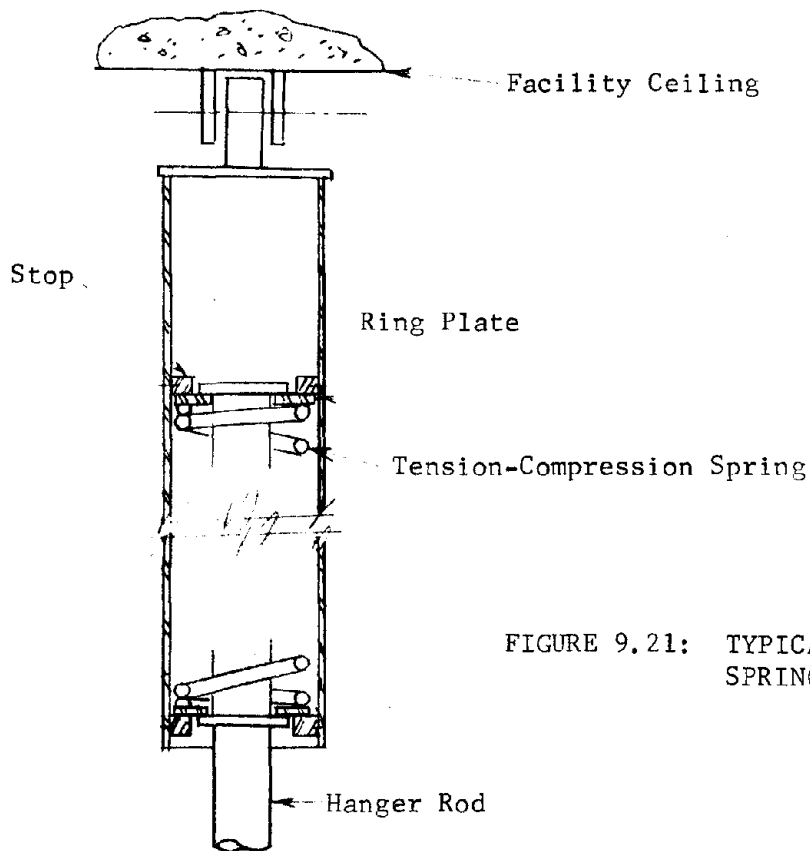


FIGURE 9.21: TYPICAL COMPRESSION SPRING CAN ASSEMBLY



The horizontal rattlespace is 6 inches. Vertical displacement is limited to about 12 inches by the full compression of the springs. Pneumatic sway dampers are attached between the platform and capsule wall for quick post-attack capability.

d. Design analysis. The initial design was based on shock spectra response only. Coupling was assumed to be negligible.

After the system was designed, a dynamic analysis was performed so that the design adequacy or deficiency could be established.

A comprehensive analysis included (1) synthesized wave forms, (2) 5 percent vertical damping, (3) non-linear stiffness curve and viscous damping to represent the sway dampers, (4) horizontal shock inputs from eight directions, (5) different phasing of vertical and horizontal shock inputs, and (6) center-of-gravity eccentricity.

e. Tests performed. The sway damper characteristics were measured at the Air Force Weapons Laboratory (AFWL) shock-displacement test facility at frequencies and displacements used for analysis. The non-linear stiffness and damping factors were then used for a final analysis.

The isolators were also tested at AFWL and found to have less than 5 percent critical damping.

#### 9.5.4 Minuteman launch equipment room (Wing VI)

a. Description. Only the configuration design changes from Wings I-V will be mentioned here. The weight of the LER platform was increased to 29,000 pounds.

b. Shock criteria. The criteria were the same as for Wings I-V (see Section 9.5.3.b).

c. Shock isolation design. The number of isolators was reduced to eight with 3 different spring rates, 625, 1210, and 1940 lbs./in. The rattlespace was increased to 12 inches horizontally and 14 inches vertically. The hanger rods were increased to 5" outside diameter. Sway dampers were removed. Modifications were made in the spring assembly after testing (see Section 9.5.4.e). The double compression springs were replaced by tension-compression springs, and teflon spacers were utilized at the rod-to-can interfaces. (A tension-compression spring is illustrated in Figure 9.21.)

d. Design Analysis. An attempt was made to put a 1 g floor in the LER, but the spring was too large for the available space and the floor became too sensitive to small changes in weight.

A dynamic analysis program was used, which handled 3-dimensional analysis of floors, various combinations of geometry, center-of-gravity location, linear and non-linear isolators, friction damping and shock phasing. A lateral shock analysis of each isolator was conducted to determine bending moments in the isolator rod and lateral acceleration history of the platform. The results were used to size the hanger rods.

e. Tests performed. Tests were conducted to determine high frequency shock transmission of the isolators. The high frequency equipment fragility level was around 10g. A floor segment including two cabinets was suspended by two isolators from the input beam. The input beam was made to move in a prescribed acceleration-time history to create the input environment. A pendulum struck this beam to produce horizontal impact. The pulse was varied by placing rubber pads between the pendulum and beam, foam rubber between the beam and support structure, and by adjusting the pendulum drop height.

The vertical impact was provided by four double acting air jacks that support the beam vertically. Initial air pressure and cavity volume in the jacks plus foam between the beam and support structure shape the vertical pulse. A hydraulic-mechanical quick-release device was used to restrain and release the jacks. The test configuration is shown in Figure 9.22.

Initial tests conducted on the double compression-spring isolators demonstrated that impacting of the isolators internal parts created unacceptable high frequency accelerations at the LER floor equipment tie-down locations.

A modified design utilized tension-compression springs and teflon spacers at the two rod-to-can interfaces. Incorporation of the tension-compression isolator reduced the floor environment during vertical testing approximately 3 times for frequencies above 100 cps, which are induced mainly by internal parts impact (see Figure 9.23). The tension-compression design may aggravate the floor response below 100 cps, due to changes in spring surge frequencies and load path transmission.

The floor environment due to horizontal impact is well within the criteria for the tension-compression design. The teflon spacers between the rod

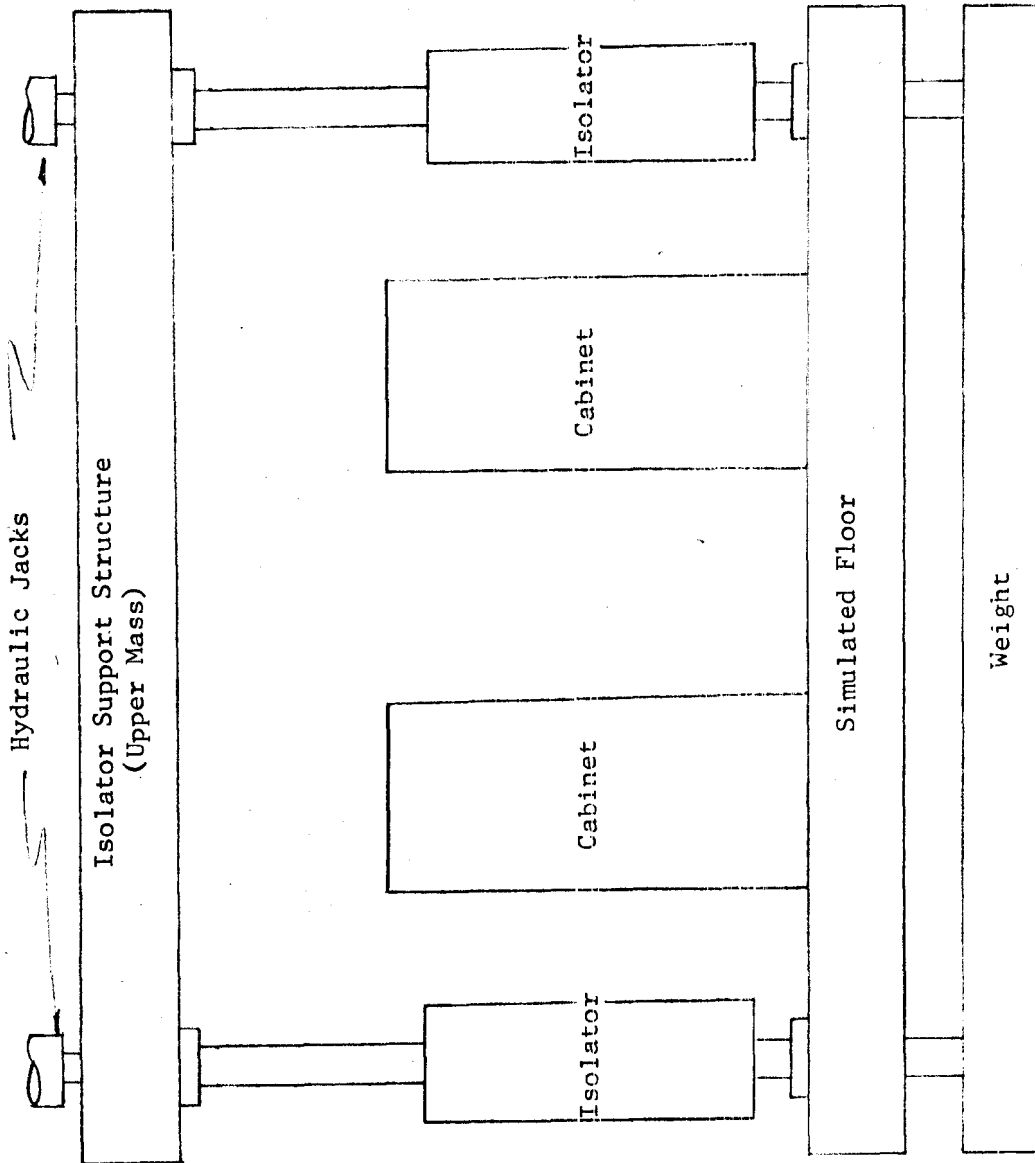


FIGURE 9.22: ISOLATOR TEST FIXTURE

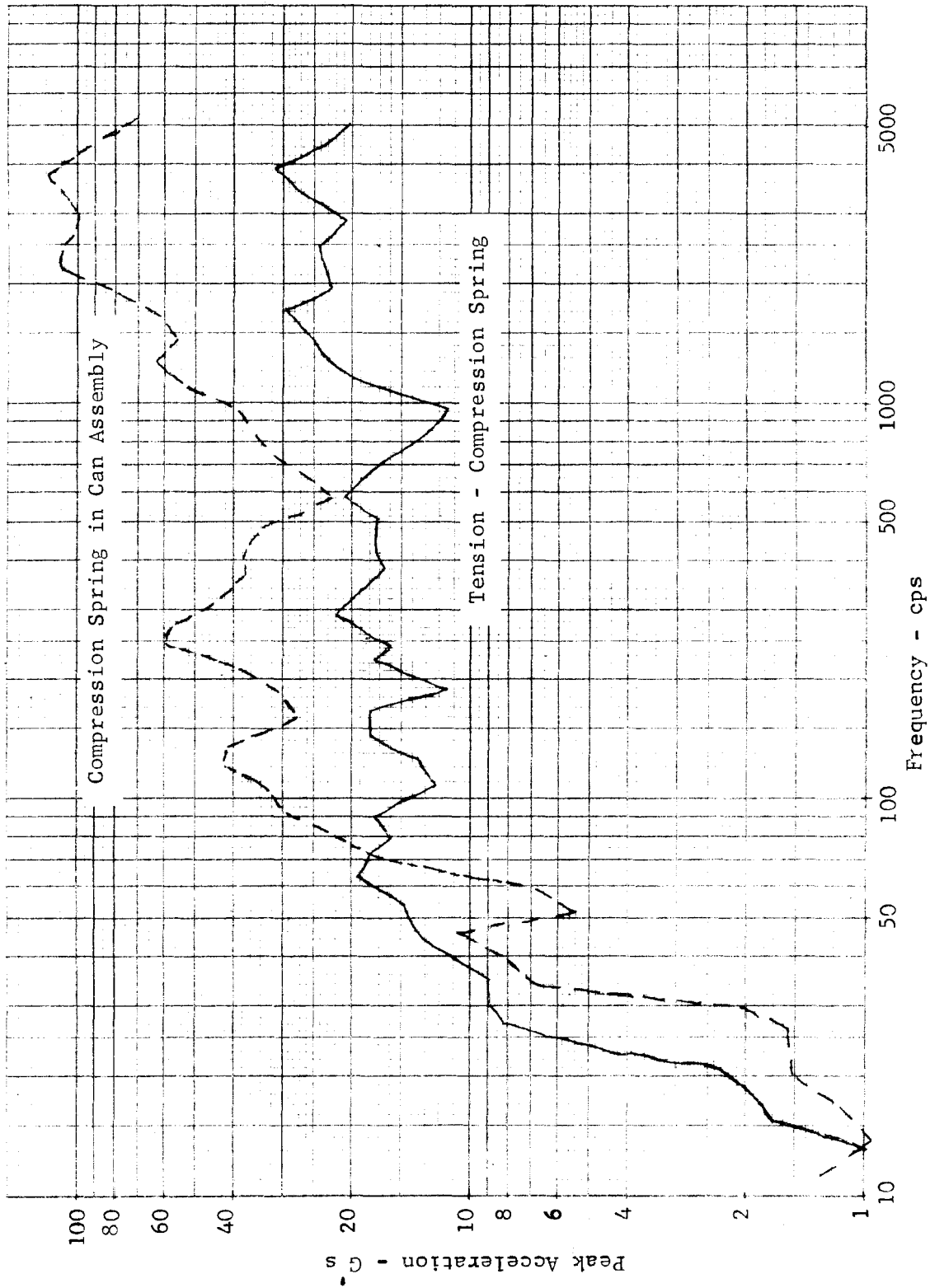


FIGURE 9.23: VERTICAL SHOCK SPECTRA AT CABINET TIE-DOWN

and can were responsible for a reduction in floor acceleration during horizontal testing of approximately 4 times.

Tests with elastomer isolator pads indicated that they are most effective when loaded in shear. However, the equipment environment will be increased at frequencies near the isolated equipment-on-pad frequencies.

#### 9.5.5 Minuteman launch equipment building (LEB) (Wings II-V)

a. Description. The power supply and air conditioning equipment needed for the missile launch facility are located in the underground launch equipment building. The equipment is placed on a rectangular platform approximately 15 by 25 feet in size. The total weight is about 30,000 pounds.

It was necessary for the shock isolation system to attenuate the peak ground accelerations to a level less than 3 g's vertically and horizontally.

b. Shock criteria. The input to the shock isolation system was defined in terms of shock spectra, which were very low.

c. Shock isolation design. The LEB platform is supported by ten vertical spring isolators. Figure 9.24 shows the LEB platform plan and isolator

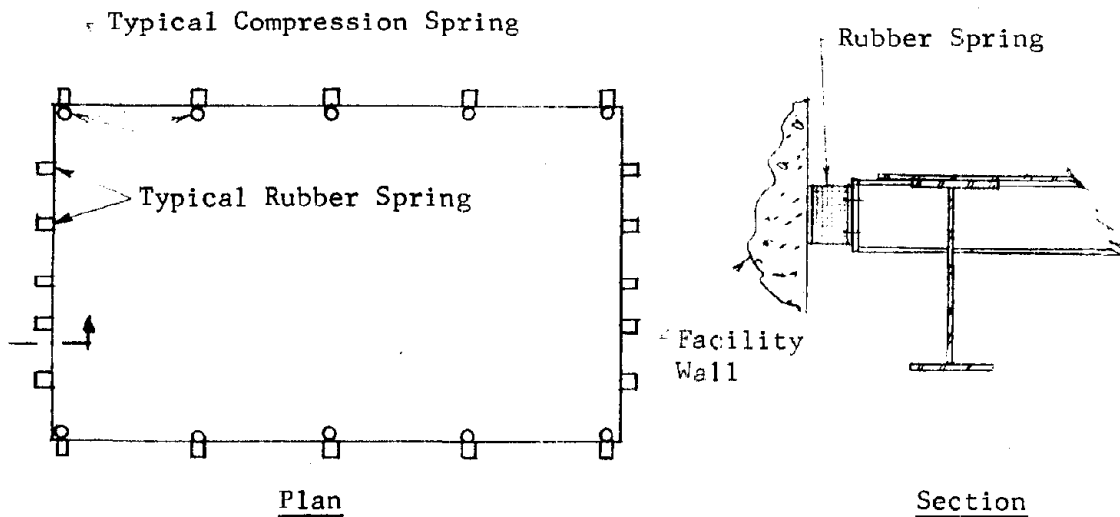


FIGURE 9.24: LEB PLATFORM SHOCK ISOLATION SYSTEM

locations. The basic LEB isolator design utilized a compression spring and support can, similar to LER Wing I-V isolator design (see Figure 9.21). Horizontally there are rubber bumpers between the platform and side walls.

d. Design analysis. The system was assumed to be uncoupled in the vertical and horizontal directions and, thus, shock spectra were directly applicable. A dynamic analysis was not performed.

#### 9.5.6 Minuteman launch equipment building (Wing VI)

a. Description. The loaded LEB platform weight increased to 60,000 pounds for Wing VI. Increased ground shock magnitude made it necessary to re-design the shock isolation system.

The shock attenuation requirement was the same as that for Wings II-V, namely, less than 3 g's vertically and horizontally.

b. Shock criteria. The input was defined in terms of shock spectra, and the input levels are in the moderate to high level region.

c. Shock isolation design. The Wing VI shock isolation system consists of four pendulous spring isolators which support the LEB platform at the corners. It is a low center-of-gravity pendulous system. The isolator design utilized coil springs, compression mounted in a can assembly, and cable supported from the facility roof slab. A schematic of the isolator is shown in Figure 9.25.

d. Design analysis. A comparison study was performed to determine the most economical isolator design. A vertical response of 3 g's versus a vertical response of 1 g was considered. It was found that the 1 g coil spring isolator was most feasible, especially since a flexible cable can be used to support the spring elements. The flexible cable can tolerate the initial horizontal shock without inducing significant bending stresses in the spring can. Conversely a rigid rod would have to be stiff enough to resist elastically the bending due to the high initial horizontal shock.

A dynamic analysis was performed to determine the maximum coupled response. Velocity pulses derived from the given shock spectra were used as inputs at the support points. It was found that the maximum coupled displacement response was about 20 percent greater than the single-degree-of-freedom response, when the horizontal and vertical pulses were in phase. When the vertical pulse leads the horizontal pulse by about 1 second, the horizontal displacement response is amplified by about 75 percent.

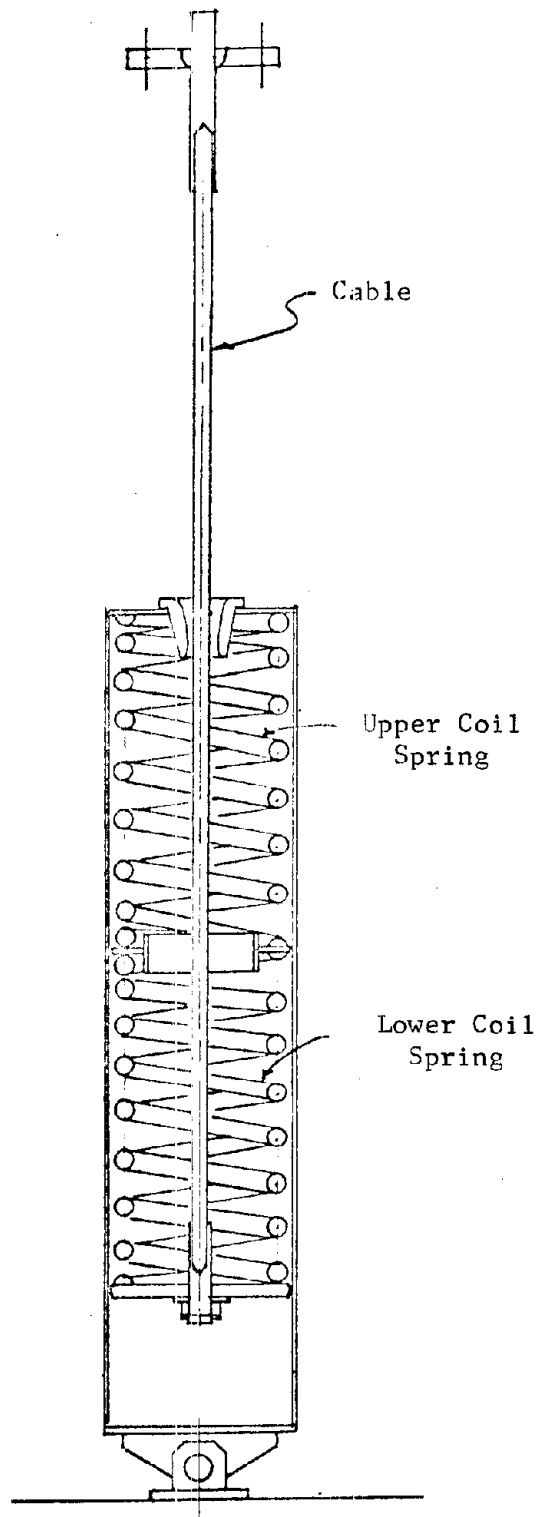


FIGURE 9.25: LEB SHOCK ISOLATOR  
587

e. Tests performed. Impact testing was conducted on the LEB isolator, and data was obtained to determine the adequacy of the isolator for high frequency shock transmissibility characteristics.

Initial testing was conducted when no positive means of attachment had been provided between the three load interfaces within the can; namely the cable-to-bottom coil, coil-to-coil, and top coil-to-can interfaces.

The second series of LEB tests were conducted on isolators modified to include four bolts fixing the top coil-to-can interface.

The third series of LEB tests included a rubber ring on the bottom coil-to-cable interface plate, bolting of this "damping" plate to the bottom coil, banding straps to provide a fixed coil-to-coil interface, and load cells incorporated on the top coil-to-can bolted interface.

The LEB isolator design does not transmit the input accelerations to the floor. The floor vibrations are induced by cable-to-can contact in the horizontal axes, and surging and rubbing in the vertical axis.

The horizontal floor vibrations are within acceptable limits (less than 10 g in the high frequency region) as shown in Figure 9.26. Release of the compressive load in the isolator excites the natural vibration modes of the coil springs. This would occur even if the cable were replaced by a rod and the coil were forced to expand at the input velocity. This rate is high enough to excite the coil spring's inherent modes of response. The floor vibration environment during vertical testing can be attributed to this phenomenon (referred to as surging of the spring) in conjunction with impacting and rubbing of the coil and damping plate on the can. The data shows that the surging amplitudes are high enough to overcome the static compressive load in the spring. The upper coil spring and can recorded loss of contact at 70 milliseconds after time zero, and impact at 150 milliseconds. Figure 9.26 shows the severity of this impact. It is important to note that this floor environment is relatively independent of the ground motion, or input level. To induce spring surging, only a sufficient relative ground - floor velocity is required.

Fixing the upper coil-to-can interface eliminated the impact which occurred at 150 milliseconds. By reducing the floor response resulting from this impact, the spectra in Figure 9.26 indicate that the high frequency vibration levels can be reduced to about one fifth.



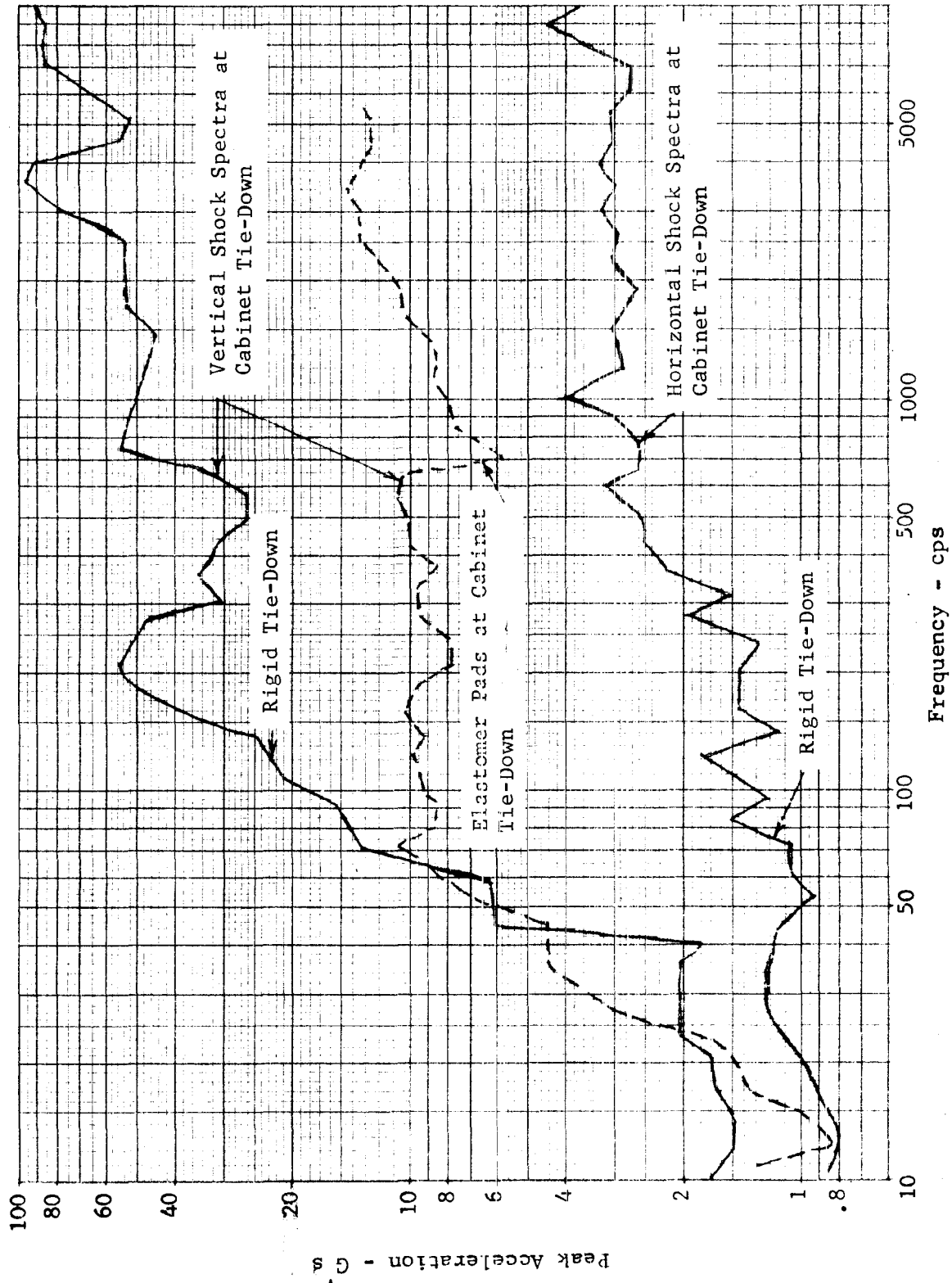


FIGURE 9.26: VERTICAL AND HORIZONTAL SHOCK SPECTRA AT CABINET TIE-DOWN

9.5.7 Minuteman launch control equipment building (LCEB) (Wings I-V)

a. Description. The power supply and air conditioning equipment needed for the launch control center are located in the underground launch control equipment building on an equipment platform, shock isolated within the LCEB enclosure.

The peak acceleration response of the platform must not exceed 3 g's vertically and horizontally.

b. Shock criteria. The shock input was defined in terms of shock spectra in the moderate to high ground motion region.

c. Shock isolation design. The LCEB platform is supported by 12 pendulous spring isolators. Lateral restraint is provided by leaf springs which rub against the side walls of the enclosure. The leaf spring is shown in Figure 9.27. The vertical isolators utilize a coil spring-in-can arrangement very similar to the LER spring design (see Figure 9.21).

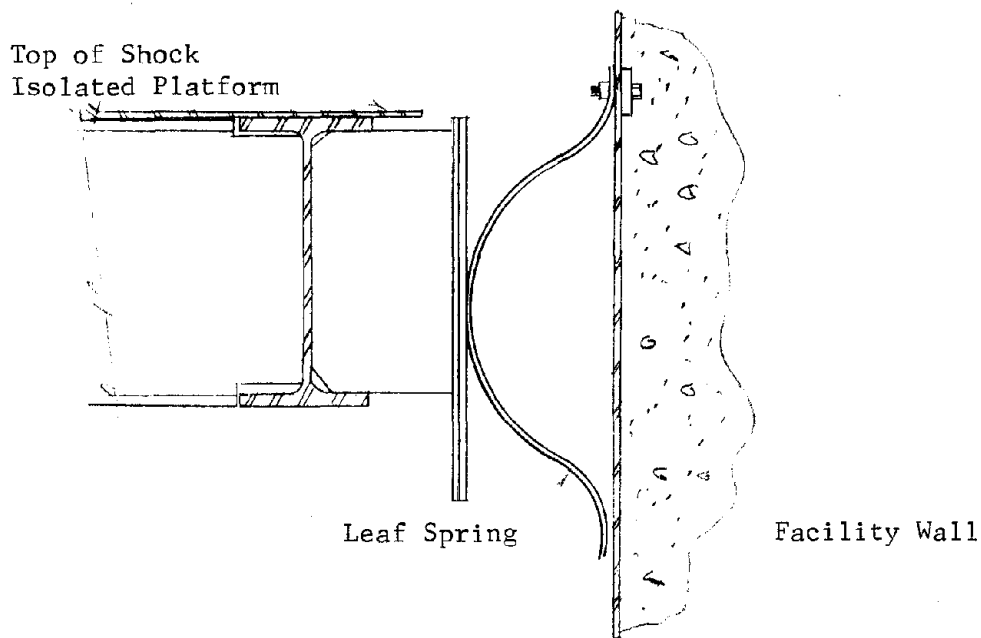


FIGURE 9.27: TYPICAL LEAF SPRING DETAIL

This system seemed desirable based on previous designs, because the vertical and horizontal spring systems were uncoupled for all practical purposes.

d. Design analysis. The isolator system was designed by estimating natural frequencies, assuming the system was uncoupled. Spring forces and stiffness were established on the basis of estimated center-of-gravity location, assuming a single-degree-of-freedom response based on shock spectra. The peak responses were reevaluated after weights and eccentricities had been measured, they were found to be highly stable.

e. Comments. The isolator assembly impact motions induce high frequency vibrations of the platform as were described for the LER platform (see Section 9.5.4.e). The equipment was not sensitive to high frequency vibrations, therefore modifications were not required to eliminate the chatter of the isolator components during dynamic response.

#### 9.5.8 Minuteman launch control equipment building (Wing VI)

a. Description. Increased ground shock criteria required redesign of the shock isolation system. The allowable platform response remained the same.

b. Shock criteria. The shock input was defined in terms of shock spectra in the high ground-motion region. Since the system is not linear, velocity pulses were defined for initial downward and initial upward motion.

c. Shock isolator design. The LCEB platform is supported within its enclosure by four pendulous bilinear liquid spring assemblies. Figure 9.28 is a schematic diagram showing the LCEB shock isolation system layout. Figure 9.29 shows a cross-sectional view of the liquid spring.

The maximum rattlespace of the platform from its static position is 33 inches upward, 11 inches downward, and 20 inches horizontally relative to the enclosure.

In the static position, the isolator acts as a tension spring supporting the platform in space by the action of pressurized liquid in the cylinder.

Two types of ground shock are assumed to be encountered:

- (1) Positive Pulse - During a positive pulse, the enclosure initially moves downward allowing the low rate piston (upper rod) to move down relative to the platform due to the reaction

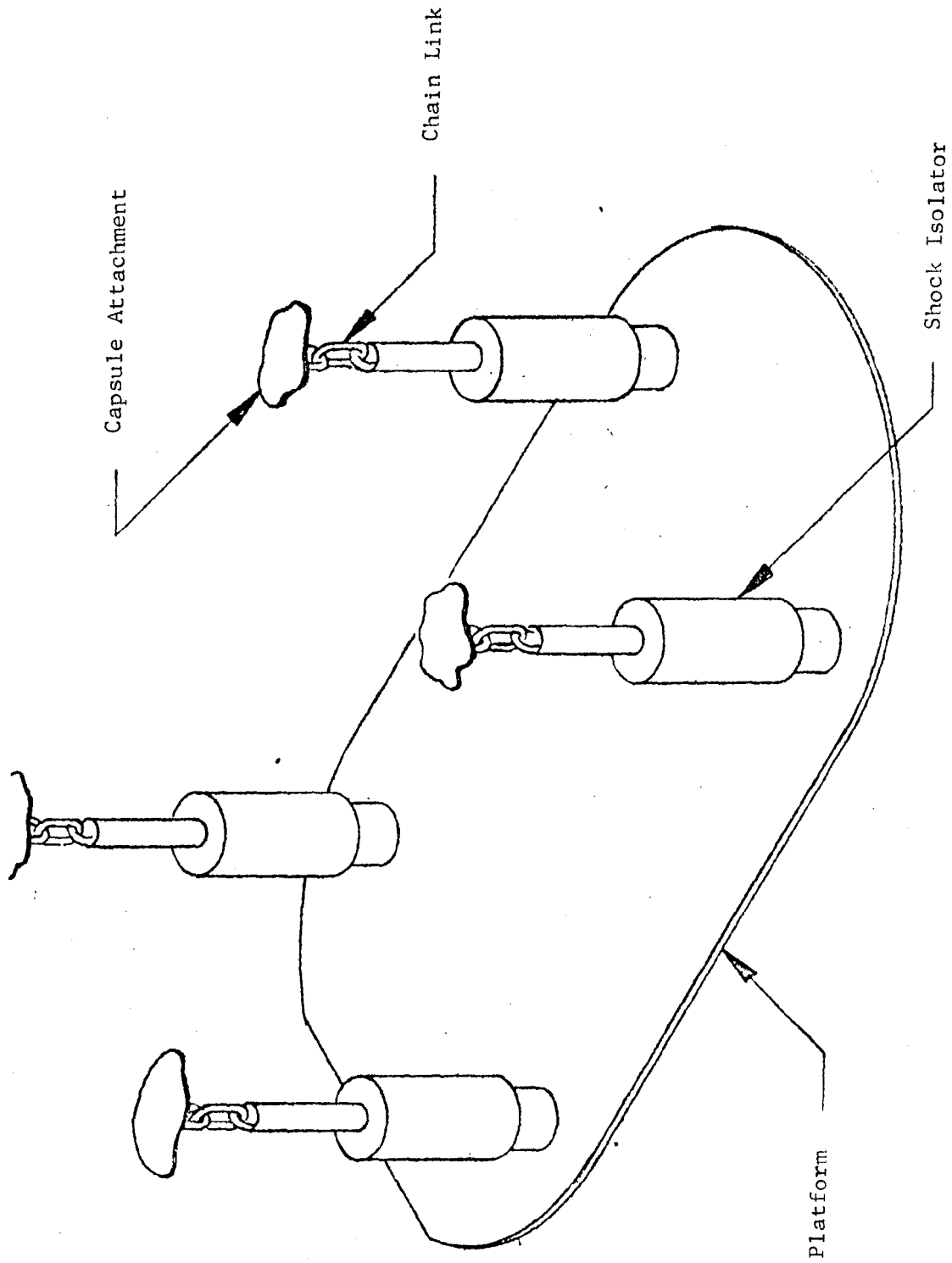
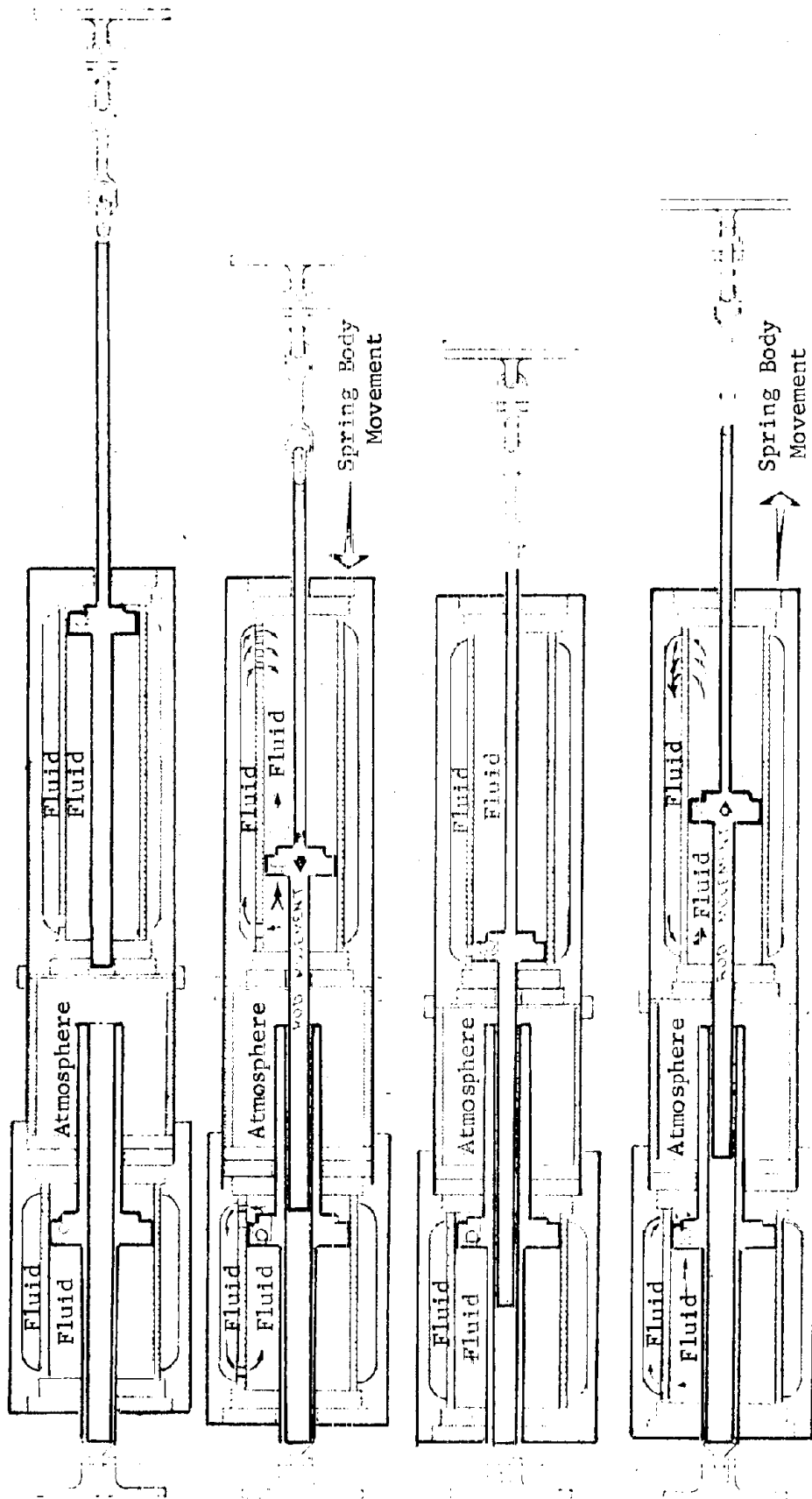


FIGURE 9.28: SCHEMATIC OF LCEB FLOOR SHOCK ISOLATION SYSTEM



Static Retracting Retracted Extending  
 FIGURE 9.29: BILINEAR LIQUID SPRING CONCEPT

of the liquid pressure on the face of the piston. The high rate piston (lower rod) moves up relative to the isolator body.

As the platform returns to, or travels beyond its relative static position, the piston compresses the liquid in the cylinders increasing resistance to the downward movement of the platform.

- (2) Negative Pulse - During a negative pulse the enclosure initially moves upward. This moves the isolator upward relative to the platform, thereby extending the high rate piston. As the piston extends, the liquid in the lower cylinder is compressed tending to return the platform to the relative static position.

d. Design analysis. The system studies (and conclusions) performed for the Minuteman Launch Control Center (see Section 9.5.11) isolation system were the basis for selection of the isolation system for the LCEB.

A 3-dimensional model of the total system was used to establish the design for the rigid body motions (see Figure 9.30). Vertical and horizontal velocity pulses with and without ground return were used and phased within reasonable limits to obtain the maximum response.

A model of a single isolator was also used to evaluate the effect of the isolator component characteristics. This model is shown in Figure 9.31 with definitions of all the symbols.

e. Tests performed. A test program was implemented to verify that the dynamic analysis model (single isolator as shown in Figure 9.31) satisfactorily predicts the dynamic response of the single isolator. Displacement tests were performed by first displacing the floor mass, and then quickly releasing the mass, allowing free oscillations. Satisfactory correlation was obtained. It is interesting to compare the floor acceleration for (1) an initial relative upward displacement of 33 inches (equivalent to an initial downward ground motion) and (2) an initial relative downward displacement of 10 inches (equivalent to an initial upward ground motion) as shown in Figure 9.32. The maximum acceleration for case (1) above is 0.6 g, and for case

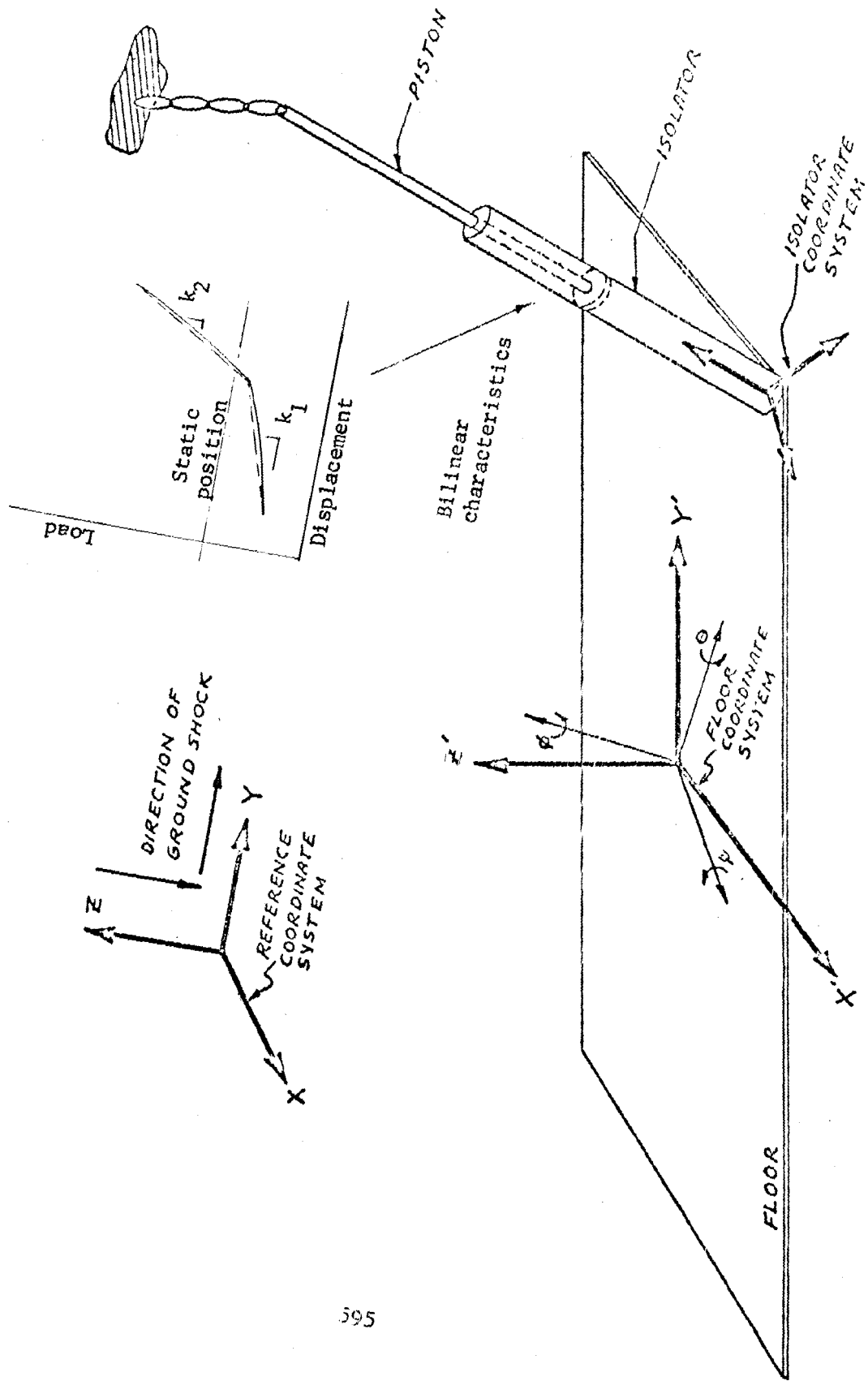
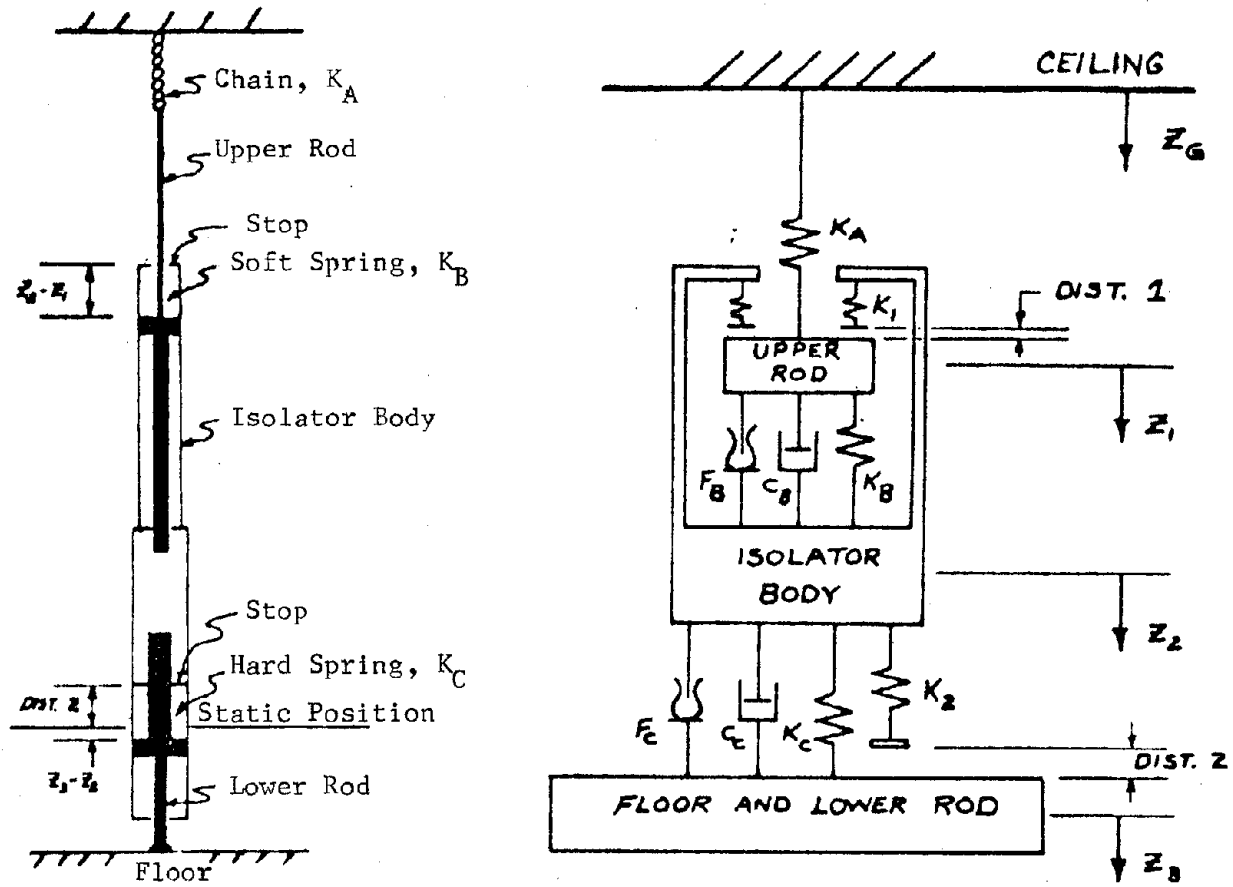


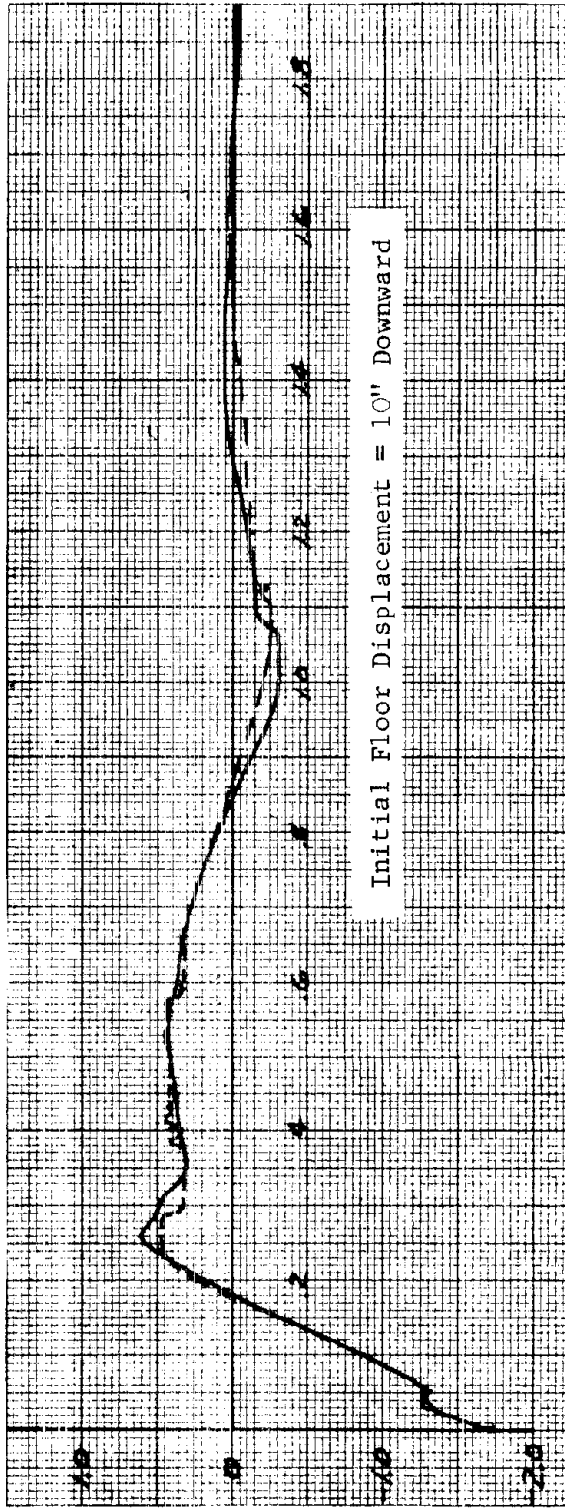
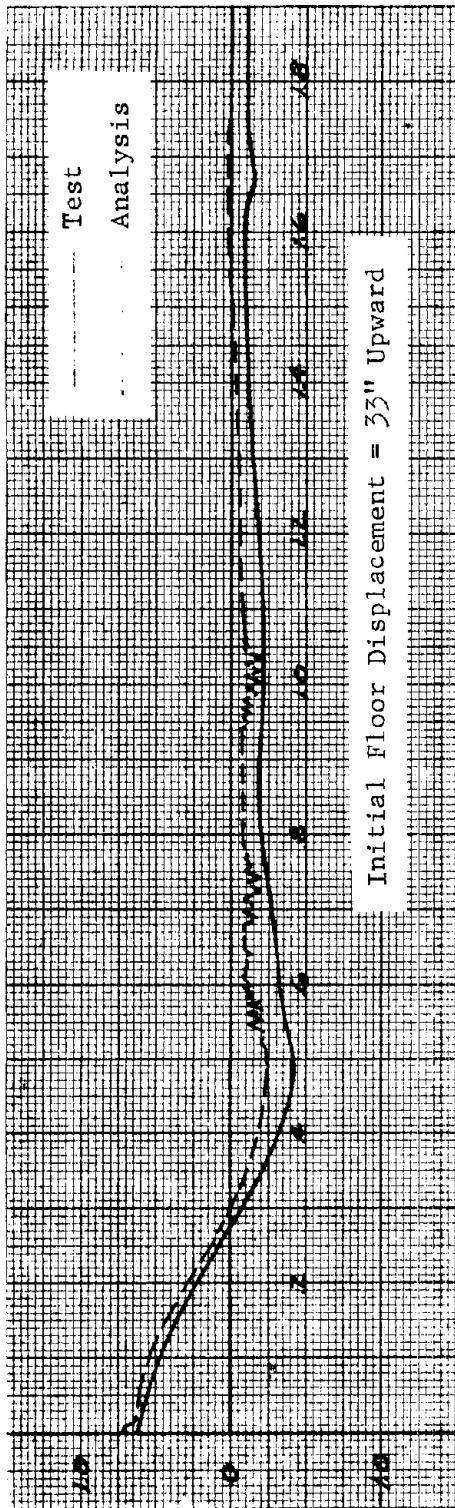
FIGURE 9.30: LCC 3-DIMENSIONAL COORDINATE SYSTEM



- Where
- $K_A$  -- Spring rate of chain
  - $K_B$  -- Spring rate of soft liquid spring
  - $K_C$  -- Spring rate of hard liquid spring
  - $K_1$  -- Spring rate of stop between isolator body and upper rod
  - $K_2$  -- Spring rate of stop between isolator body and lower rod
  - Dist.1-- Distance between upper rod and isolator body stop for static position
  - Dist.2-- Distance between lower rod and isolator body stop for static position
  - $F_B$  -- Friction between upper rod and isolator body
  - $F_C$  -- Friction between lower rod and isolator body
  - $Z_G$  -- Vertical ground displacement
  - $Z_1$  -- Upper rod vertical displacement relative to static position
  - $Z_2$  -- Isolator body vertical displacement relative to static position
  - $Z_3$  -- Floor vertical displacement relative to static position
  - $C_B$  -- Damping coefficient between upper rod and isolator body. Subscripts P and N denote positive and negative damping respectively. Damping coefficient is function of position
  - $C_C$  -- Damping coefficient between lower rod and isolator body

FIGURE 9.31: SINGLE ISOLATOR DYNAMIC MODEL





Floor Acceleration - G's

Time - Seconds

FIGURE 9.32: COMPARISON OF ANALYSIS AND TEST RESULTS

(2) the maximum acceleration is 1.75 g, indicating a lower response acceleration for the platform if the initial ground motion is down. In most practical situations, at high overpressure levels, the significant initial motion is down. Therefore, this design minimizes the total vertical rattlespace by using bilinear characteristics in the isolator design.

#### 9.5.9 Minuteman launch control center (LCC) (Wing I)

a. Description. The launch control center consists of the facility control consoles and associated electronic equipment needed for operational control of the missile site and launch sequence. The platform supporting the above equipment and operating personnel is roughly 12 feet wide by 30 feet long, weighing approximately 80,000 pounds, and is located within the LCC enclosure.

The maximum platform acceleration permitted was 3 g in any direction. However, the downward acceleration was limited to 0.5 g to prevent an unsupported man from falling.

b. Shock criteria. The shock input was defined in terms of shock spectra.

c. Shock isolation design. The LCC platform is supported by 4 pendulous pneumatic shock isolators attached to the LCC enclosure roof. There are 4 pneumatic sway dampers attached horizontally between the platform and enclosure walls. The rattlespace is 34 inches up, 11 inches down, and 11 inches in any lateral direction.

Figure 9.33 is a cross-section view of the pneumatic spring. Each pneumatic shock isolator consists of a piston, cylinder, air storage tank, coil spring, and several check valves and bleed holes. A compressed air supply is connected to each storage tank. The piston rod is attached to the capsule roof, and the bottom of the cylinder to the platform. A neutral position is maintained by the action of the compression coil spring and sliding valve located between the piston and cylinder end plate. In the neutral position, the isolator acts as a conventional pneumatic spring, and platform weight is supported by the pressurized air in the cylinder.

During a ground shock the enclosure moves downward, forcing the piston to move down. Thus, the air pressure in the cylinder is reduced, and air bleeds through the check valves into the cylinder from the storage tank. The

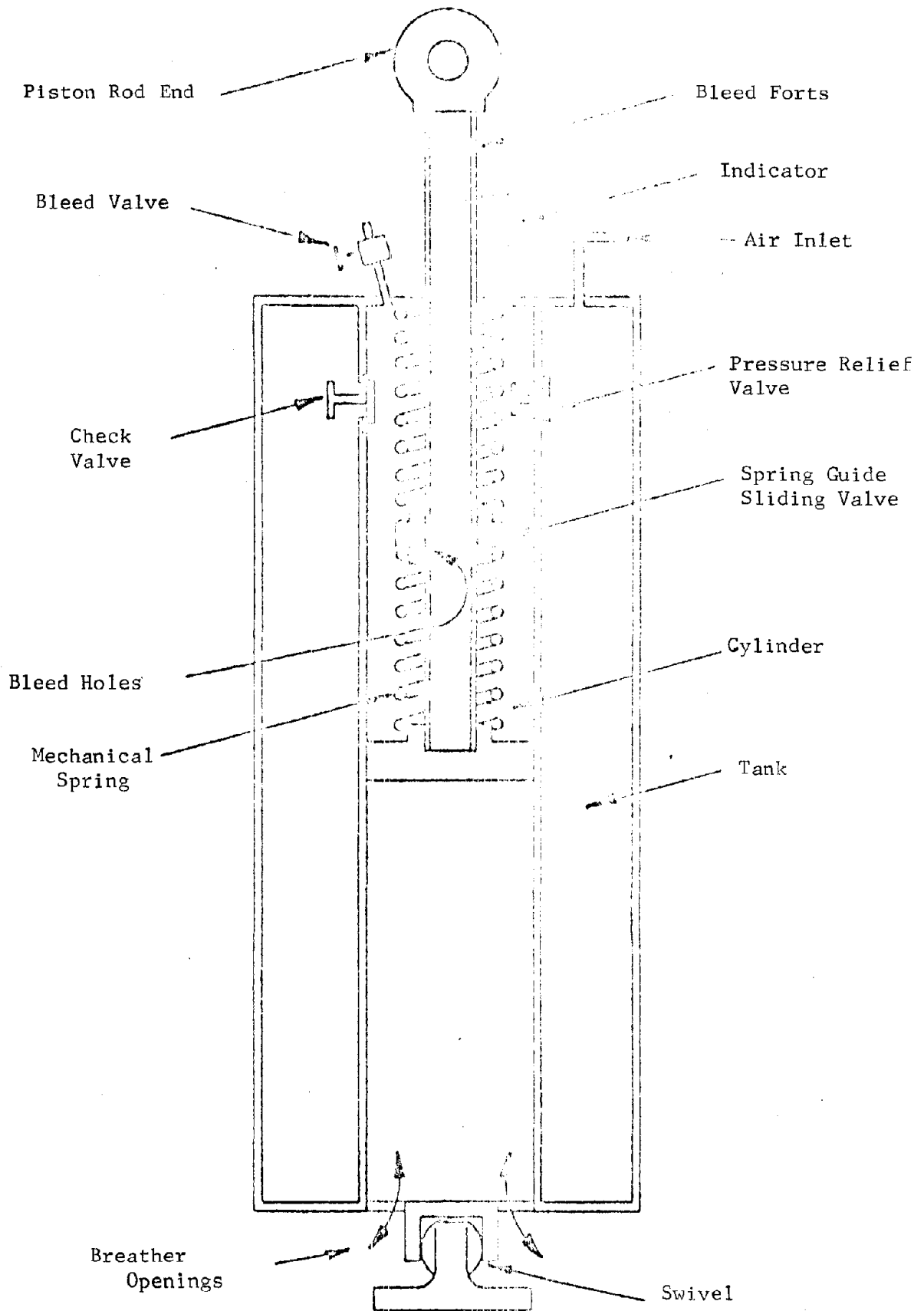


FIGURE 9.33: PNEUMATIC SHOCK ISOLATOR

entering air, together with the air initially in the cylinder, partially supports the weight of the platform, reducing downward displacement and acceleration of the platform. As the enclosure returns toward its initial position, the piston compresses the air in the cylinder, stopping the downward movement of the platform. However, the additional air drawn into the cylinder during the downward stroke of the piston must be released during the upward stroke of the piston, in order to return the platform to the neutral position. Two methods of releasing air are provided: (1) Small orifices in the piston rod release air from the cylinder when the piston is displaced downward from the normal position. (2) A number of pressure relief valves release "excess pressure" in the cylinder into the storage tank and into the LCC enclosure if required, depending upon the magnitude of the initial ground shock.

The pneumatic sway damper utilizes a double acting piston motion in a cylinder, which has bleed holes at either end. Maximum damping occurs under maximum enclosure accelerations, due to friction losses when the air, compressed by the rapidly moving piston, is allowed to bleed out of the cylinder.

d. Alternate designs considered. Coil springs were considered in the preliminary stages of design. However, the space envelope required to accommodate the linear shock spectra response, as well as the spring elements, was considered excessive.

e. Design analysis. Wave forms were derived by matching given shock spectra and used as the input to the isolator support point. A single isolator with a sway damper acting as a two-degree-of-freedom system was the model used for the design analysis. Three combinations of weight and wave forms were used to check the performance of the system under different loading conditions. A separate analysis was also performed to investigate the rotation about the vertical axis. The analysis indicated that there would be no feedback from the rotational mode into the transverse or vertical mode.

f. Tests performed. A test fixture capable of supporting a full-scale LCC floor prototype was built at AFWL. Velocity pulses are applied to simulate ground shock conditions. The tests showed acceptable dynamic response, but correlation of test with analysis was unattainable, because of unknown dynamic characteristics of the internal check valves and relief valves in the isolator.

g. Problems encountered. For a pneumatic system to function satisfactorily, the air leakage must be kept to a minimum. The first units delivered to the installations had excessive leakage, requiring makeup air bottles to be replaced on a daily basis, whereas, the design replacement cycle was 30 days. Design modifications were made on the seals to decrease leakage. An air compressor had to be added to the system, because air leakage could not be reduced to an acceptable value.

Leveling of the floor was a problem in the initial phases of installation, because of imperfect procedures used to adjust the air pressure.

#### 9.5.10 Minuteman launch control center (Wings II-V)

a. Description. The major difference from Wing I design was in the method of attaching the shock isolators to the LCC enclosure. A length of chain was inserted between the ceiling and the piston rod on the pneumatic spring (see Figure 9.34). In addition, the sway dampers were removed from the platforms for Wings IV and V.

b. Design analysis. A three-dimensional rigid-body dynamic analysis was developed in order to verify the design adequacy of the system for various phasing combinations of the vertical and horizontal inputs. This analysis was programmed for computer solution, and acceptable correlation was obtained with the test program at AFWL. Difficulty existed in obtaining good correlation to verify the rattlespace adequacy, because the dynamic characteristics of the check valves and relief valves in the isolator could not be determined with any degree of accuracy.

c. Tests performed. The test facility at AFWL was used to verify the computer analysis of the system performance (see Section 9.5.9.f).

#### 9.5.11 Minuteman launch control center (Wing VI)

a. Description. The shock isolation system had to be redesigned to provide for increased weight on the LCC platform and for higher input shock levels. The platform weight is between 80 and 85 tons.

Vertical platform accelerations are limited to values which produce no more than a 3 g vector sum for the peak vertical and horizontal accelerations together.

b. Shock criteria. The shock inputs were defined in terms of shock spectra, and velocity pulses were defined which produced responses within the given shock spectra (see Section 9.5.8.b).

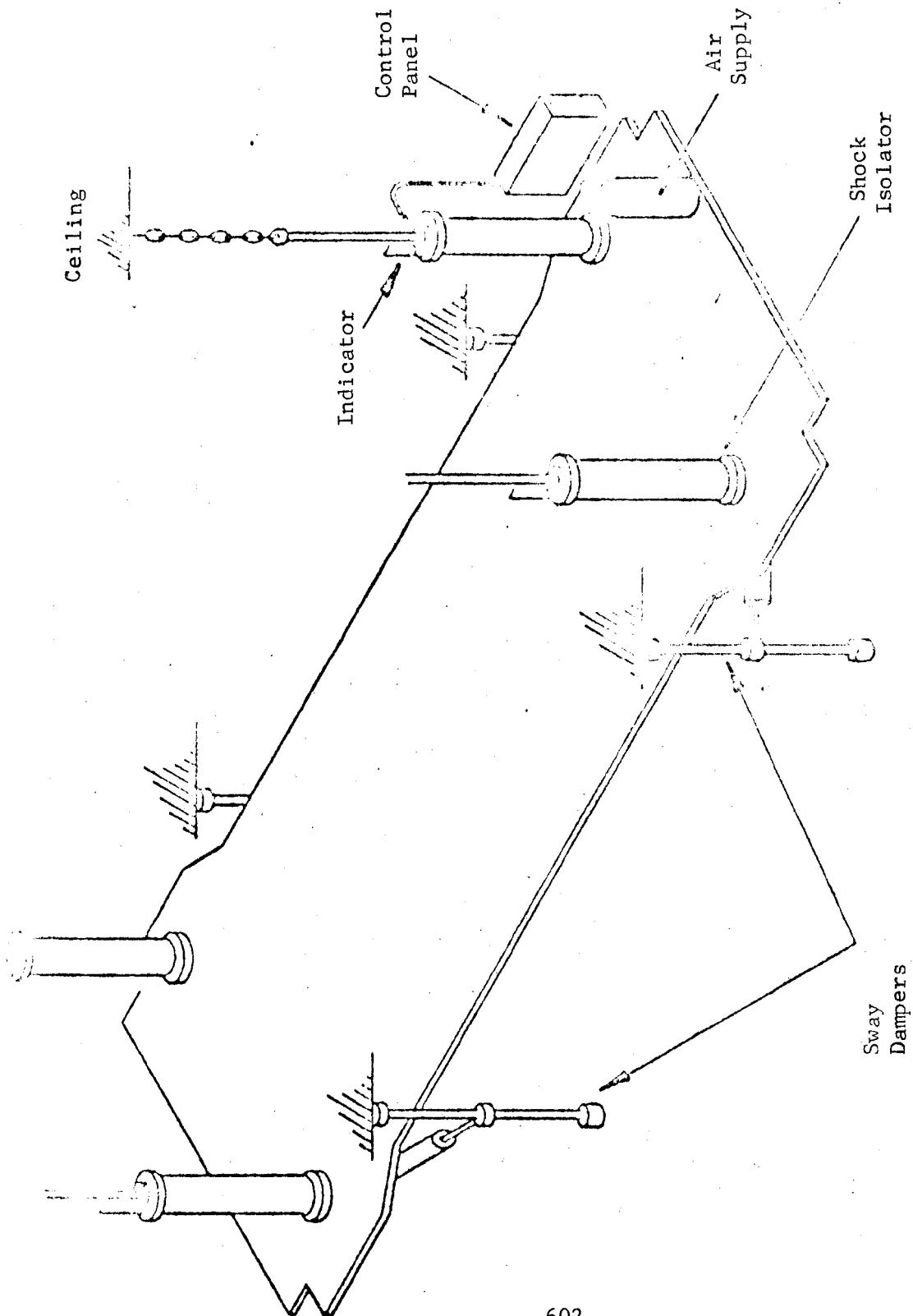


FIGURE 9.34: PNEUMATIC SHOCK ISOLATION SYSTEM, WINGS II AND III

c. Shock isolation design. Four bilinear liquid spring isolators support the LCC platform. The description for the LCEB Wing VI isolation system is also applicable for this system (see Section 9.5.8.c).

d. Alternate designs considered. Preliminary studies were performed to determine the type of isolation systems to be used for Wing VI LCC and LCEB. The first choice was to continue the pneumatic system used for the Wings I - V LCC, in order to eliminate the development cost of a new isolation system. A new design was required when it became obvious that the Wing VI LCC platform weight would be more than twice that of the Wings I - V LCC platform. A special bilinear liquid spring isolator and an air-bag pneumatic isolator were proposed. (A non-linear system was mandatory, since the rattle-space had already been established on the assumption that the Wing I - V non-linear pneumatic isolators would be used. The latter produce a total amplitude response less than that required for a linear system.)

The air-bag pneumatic system operating characteristics were the same as the Wing I - V LCC pneumatic isolators. The rolling sleeve bellows replacing the piston cylinder would reduce air leakage. Figure 9.35 shows a schematic of the air-bag isolator with some of the advantages and disadvantages listed.

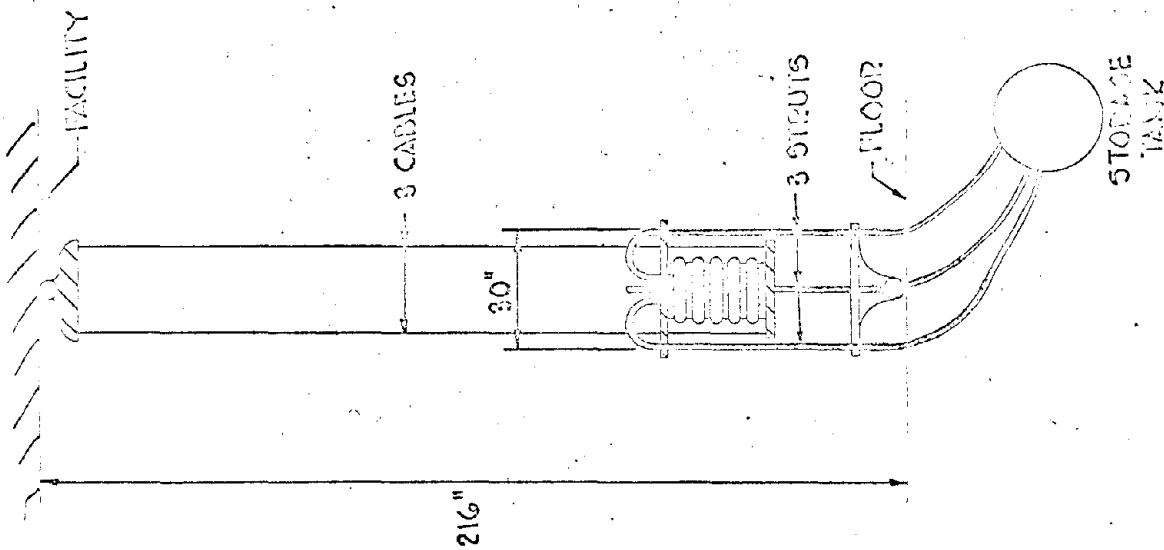
In the liquid spring study it was found that a bilinear passive liquid spring would satisfy the requirements of the system (acceleration attenuation and rattlespace). Also the liquid spring seal design maintained leakage at a negligible amount, and was now within the state-of-the-art. The simplicity of the liquid spring isolator was preferred over the pneumatic system.

e. Design analysis and tests performed. The analyses and tests discussed for the Wing VI LCEB were also performed on this system (see Sections 9.5.8.d and e).

#### 9.5.12 Minuteman antenna system

a. Description. The minuteman antenna is protected from air blast effects through the use of an underground silo. Prior to missile launch the silo cover is removed, and the telescoping antenna is extended above the ground surface level. The antenna is mounted in a structural crib, which is shock isolated within the antenna silo.

The lowest fragility level for the antenna components was found to be 5 to 10 g's at low frequencies.



### ADVANTAGES

1. MINIMUM RATTLE SPACE
2. MINIMUM RESPONSE - THEORETICAL
3. EASY ADJUSTMENT TO ACCOUNT FOR A WEIGHT CHANGE AND/OR C.G. SHIFT -  $\frac{1}{2}$  UNUSUAL FOR EACH ACTUATOR

### DISADVANTAGES

1. HARDWARE DESIGN WEAKNESSES: SEALS, RELIEF VALVES, STABILITY, FLEXIBLE CONNECTIONS
2. HIGH COST TO QUALIFY
3. MAXIMUM SPACE ENVELOPE
4. STORAGE TANK SPACE REQUIREMENT
5. HAND PUMP FOR MAKE-UP AIR

FIGURE 9.35: NON-LINEAR PNEUMATIC AIR BAGS



b. Shock criteria. The input motion was given in terms of shock spectra response levels. Velocity pulses were also defined as input functions. In addition to horizontal and vertical input components, a rotation input was also defined.

c. Shock isolation design. The antenna crib is shock isolated from the silo by means of horizontal and vertical cables attached to the silo at one end and to coil springs mounted on the crib at the other end. Figure 9.36 shows the cable and crib arrangement within the antenna silo. The compression coil springs are mounted within vertical tubes attached to the outside of the crib.

In the neutral position, the vertical springs are compressed 45 inches and the horizontal springs are compressed 20 inches, which allows the springs to remain in compression for all the dynamic motions postulated.

d. Design analysis. The model used for dynamic analysis is shown in Figure 9.37. In order to make a reasonable dynamic analysis of this system the following assumptions were made:

- (1) All the motion is initially in the x-z plane, and due to damping present, only motion on this plane was considered. (This reduces the system to a three-degree-of-freedom system.)
- (2) Vertical, horizontal, and pitch shock pulses in and out of phase should be considered.
- (3) The crib and silo move essentially as a rigid body.
- (4) Rotation of the crib in the x-z plane is about the center-of-gravity.
- (5) The vertical springs are conical and the horizontal springs are truly horizontal at equilibrium.
- (6) All spring attachment points are fixed.
- (7) All the damping forces of each type (friction or viscous) can be combined into one force acting at the center-of-gravity in the direction of the mode.
- (8) Each pair of parallel vertical springs can be considered as one effective spring.



FIGURE 9.36: TRANSMIT ANTENNA  
606

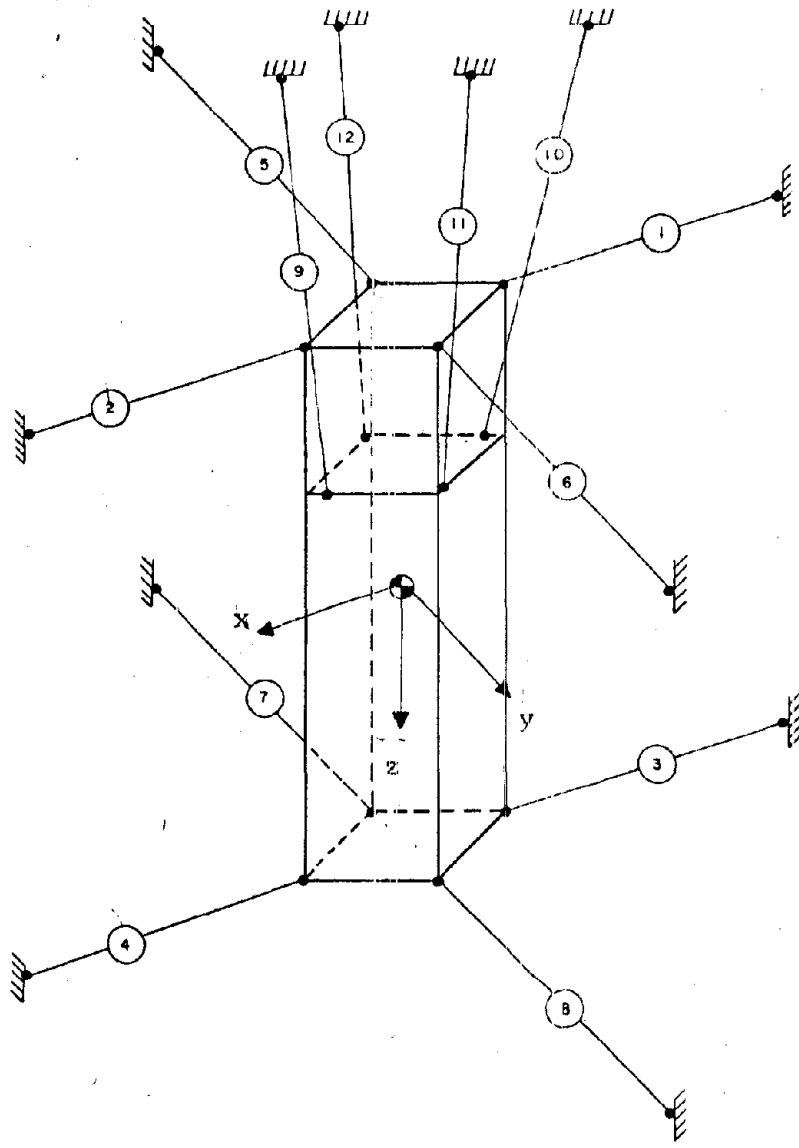


FIGURE 9.37: SUSPENSION SYSTEM SCHEMATIC DIAGRAM

The equations of motion that were developed are three ordinary differential equations, taking into account both the viscous and the friction damping, and the coupling terms containing extreme non-linearities due to the large displacement both in the vertical and horizontal directions. In order to solve the equations, the Runge-Kutta numerical technique was used, and the time increment chosen in the solution was 1/100 second.

The response was found to be less than 1 g (dynamic) vertically and 0.5 g horizontally for all variations of input and practical variations of viscous and friction damping. These factors were verified in a test program. The displacement response slightly exceeded the shock spectra displacements, indicating very little coupling.

e. Tests performed. A prototype antenna was erected in a test fixture where twang tests were performed, i.e. the antenna was given an initial displacement vertically and horizontally, and a quick release allowed free oscillations. From these tests it was concluded that the predominating damping was due to friction, and the viscous damping was small, approximately 5 percent. This same input condition was used in the computer analysis with the measured damping characteristics and excellent correlation was observed, accordingly this test program verified the dynamic analysis.

f. Problems encountered. Some slack in the cable occurs during the initial motion of the silo support points, because the springs are quite soft, and the response is not fast enough to follow the ground surface. Protective guards had to be put over some of the components in the region of the vertical cables, so the cable would not snag on the components.

## 9.6 NORAD Facilities

a. Description. The North American Air Defense Command (NORAD) Combat Operations Center (CDC) consists of a complex of shock isolated buildings located within unlined rock cavities. The building complex consists of 8 three-story buildings and various utility structures. The 8 main buildings measure 41 feet in width, 40 feet in height, and vary in length from 100 to 320 feet. A typical section is shown in Figure 9.38. Utility buildings are one and two story structures somewhat smaller in plan than the main buildings.

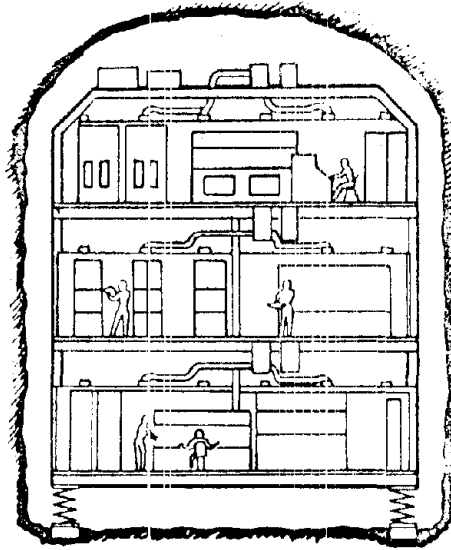


FIGURE 9.38: NORAD FACILITY - TYPICAL SECTION

The shock isolation system was required to limit peak accelerations in any direction to 1 g maximum.

b. Shock criteria. The input motions were given as two sets of ground displacements; ground transmitted, and air induced shock displacements. Peak displacements were considered not to be additive, but a vertical displacement from one source could act with the horizontal displacement from the other source. The input displacements were assumed to be instantaneous.

c. Shock isolation design. A base-mounted shock isolation system is used to attenuate the vertical and horizontal ground shock. Each of the stiff monocoque buildings rests on two rows of relatively soft coil springs. Commercial Coulomb dampers are mounted to the base in order to damp oscillations. The coil spring isolators were fabricated from 3 inch diameter semi-finished hot rolled 4160 M aircraft quality steel wire. The isolator dimensions and properties are as follows:

Vertical stiffness	= 2600 lb/inch
Horizontal stiffness	= 1145 lb/inch

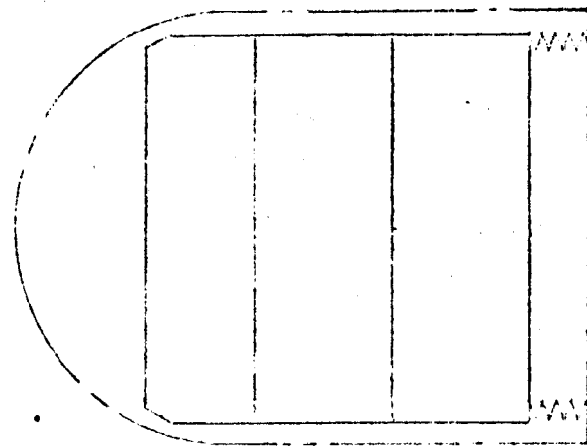
Free height	=	47.4 inches
Coil diameter	=	18.8 inches
Spring static deflection	=	10 inches
Vertical frequency	=	1 cps

d. Alternate designs considered. The preliminary design of the NORAD COC complex called for a free-standing multi-winged building three stories in height. Structurally the building was to act as one unit. Equipment and personnel were to be shock isolated with respect to the structure. However, further study indicated this method of isolation was not feasible, and isolation with respect to the rock chamber should be used. This necessitated the abandonment of the multi-winged construction in favor of a complex of individually isolated buildings.

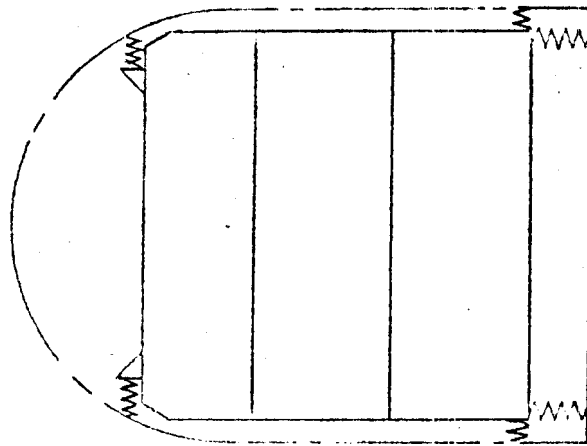
Three schemes of shock isolation were considered: a pendulum system, a center-of-gravity spring system, and a base supported spring system. These three systems are schematically represented in Figure 9.39. The pendulum system was eliminated from consideration because of the large sway space required around the periphery of the buildings. The center of gravity system circumvents this problem, but adds uncertainties to the design, namely, the degree to which a center-of-gravity system can be achieved, and the reliability of side and overhead isolator anchoring details. The base-supported system requires somewhat more rattle space than the center-of-gravity system, but it eliminates the need for overhead and side isolators. This compromise was found to be feasible, and was adopted for the NORAD shock isolation system.

e. Design analysis. Three aspects of the shock isolation system design were of paramount importance,

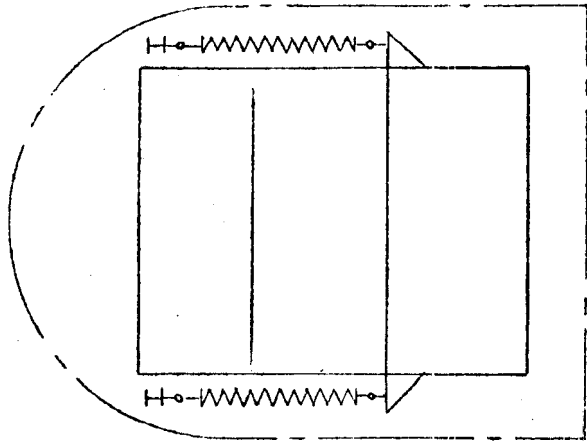
- (1) The natural frequencies of the building, its structural components, and contents must not coincide with the vertical frequency of the springs (1 cps). To insure that resonance would not occur, a minimum natural frequency of 3 cps was specified.
- (2) The loads and load distribution had to be accurately known beforehand. The minimum expected load to be used for **determining** shock attenuation and the maximum load to be used in calculating stress levels in the isolators. The loading was assumed to be symmetrically distributed with its inertia and geometric axes coincident.



BASE MOUNTED SYSTEM



CENTER OF GRAVITY SYSTEM



PENDULUM SYSTEM

FIGURE 9.39: ALTERNATE DESIGNS CONSIDERED

- (3) The behavior of large coil springs under combined vertical and lateral loads had to be established. Experimental data on the behavior of small coil springs was available, but it was questionable whether it was applicable. Design procedures were developed for these large springs, and a test program was established for verification.

The six natural frequencies of the shock isolated system were determined under the following assumptions and conditions:

- (1) minimum expected load acting,
- (2) load uniformly distributed,
- (3) inertia and geometric axes of building coincident,
- (4) building considered as rigid body
- (5) springs uniformly distributed along the longitudinal edges of the building.

The vertical motion and the twisting motion of the building about its vertical axis are uncoupled motions. It was felt that the twisting motion would not occur as a result of nuclear groundshock; therefore, it was deleted from further consideration. Thus, the system reduced to a five-degree-of-freedom system with an uncoupled vertical motion.

The response of the system to a step displacement input pulse was determined with the aid of a digital computer. The following conclusions were made:

- (1) accelerations were less than one g,
- (2) rattle-space provided was adequate,
- (3) twenty percent variations in the minimum expected load did not significantly alter the response,
- (4) response to the maximum expected load was not significantly different from the response to the minimum expected load,
- (5) two foot rectilinear displacements between the inertia and geometric axes did not significantly affect the natural frequencies,
- (6) system will vibrate freely for a period of 70 to 140 seconds after attack.



It was decided to use damping devices to eliminate possible resonance motion during the period of free vibration. Viscous dampers were investigated, and found impractical because expensive and complicated damper layouts were required. Directional Coulomb dampers were then considered, and found to be adequate both in cost and construction. Damping time with Coulomb dampers in place was calculated to be 5 to 12 seconds.

Spring design was based on the underlying assumptions of fixed ends, and the development of an inflection point at mid-height of the spring. The vertical load was assumed to produce the following stress resultants in the coils:

- (1) torsional moment,
- (2) direct shear force,
- (3) bending moment (due to load eccentricity),
- (4) axial force.

The lateral load was assumed to produce a bending moment only. Stresses resulting from these effects were combined for sizing of the springs.

f. Tests performed. Tests were made on three full scale springs, in order to establish the ratio of lateral to vertical spring stiffness, and to verify the design stresses. The following results and conclusions were obtained:

- (1) It is not necessary to secure the end coils to their base plates.
- (2) The end coil stresses are maximum but less than calculated stresses.
- (3) The average value of the lateral to vertical spring stiffness ratio is .44.

A scaled dynamic model was tested at AFWL to verify a dynamic analysis and predicted response. Details of the test with results are described in the Shock, Vibration, and Associated Environments 32nd Symposium, Bulletin No. 32, Part III, December 1963, Test of a Scaled Dynamic Model of the South Building, NORAD Combat Operations Center, by J. E. Johnson and R. E. Crawford.

g. Problems encountered. Erection of the buildings commenced by placing the springs on their foundation in a compressed position, and subsequently erecting the buildings on the compressed springs. Compression was applied by means of four turnbuckle rods per spring. This scheme was to provide a stable foundation for erection. However, considerable side sway of the springs was experienced during the initial stages of construction. This sway was eliminated by bracing the springs against the chamber walls. After erection was completed and the equipment was installed, the bracing and turnbuckle rods were removed, and the structure ballasted to a level position. Once leveling was completed, the Coulomb dampers were installed.

The provision of ballasting is extremely important for systems of this type and scale. Initial tilts ranging from one to two inches were anticipated for the completed buildings. Since these tilts (or tilts resulting from future load growths) cannot be corrected by adjusting the mechanical coil springs, a means of ballasting was provided. Five percent of the minimum expected load was assumed to be ballast. Ballasting is accomplished by placing steel billets along the inside of the exterior walls at the first floor level. (Water ballasting was considered, but proved to be too expensive due to the required plumbing and piping systems.)

## SYMBOLS\*

The following symbols are used in this report. Other symbols not listed below are defined where they are used.

A	Shock spectra acceleration bound in the high frequency region (g's)
$A_o, A_1, A_2$	Subscript refers to a specific point on the four log shock spectra coordinate system
$A_1, A_2, A_i$	Impulse areas in a force-time plot (lbs-sec)
A	Piston head area in a pneumatic spring system (in <sup>2</sup> )
a	Ground acceleration (g's)
$a', v', d'$	The prime notation refers to the air blast induced rigid body motion, air blast induced deformational motion and ground induced rigid body motion, respectively.
$a'', v'', d''$	
$a''', v''', d'''$	
B	Width of structure normal to front face loading (feet)
C	Intercept constant for travel distance-time curves
$C_f$	Coefficient of friction between footing slab and soil
c	Viscous damping coefficient (lbs-sec/in)
c	Seismic velocity of shear waves
$c_a$	Acoustic velocity in air
$c_s$	Seismic velocity of shear waves
$c_R$	Seismic velocity of Rayleigh waves
$c_i$	Seismic velocity of the initial part of the wave front (ft/sec)
$c_p$	Seismic velocity of the peak stress or strain (ft/sec)
$c_{refl.}$	Velocity of sound in the reflected region (fps)
$c_d$	Drag coefficient (dimensionless)
D	Shock spectra displacement bound in the low frequency region (inches)

---

\* The symbols used in Section 6.2 are not included in this list, but are listed separately in Section 6, Table 6.2.

SYMBOLS (continued)

$D_o, D_1, D_2$	Subscript refers to a specific point on the four log shock spectra coordinate system
$D_p^+$	Positive phase duration of the overpressure pulse (sec)
$D_p^-$	Negative phase duration of the overpressure pulse (sec)
$D_2$	Characteristic time (sec)
$d$	Ground displacement (inches)
$d_v, v_v, a_v$	Peak vertical ground displacement, velocity, and acceleration at the surface, respectively
$d_{vz}, v_{vz}, a_{vz}$	Peak vertical ground displacement, velocity, and acceleration at depth z, respectively
$d_{ve}$	Peak vertical elastic displacement at the surface (inches)
$d_{vr}$	Peak vertical residual displacement at the surface (inches)
$d_{vzr}$	Peak vertical residual displacement at depth z (inches)
$d_{vze}$	Peak elastic displacement at depth z (inches)
$d_h, v_h, a_h$	Peak horizontal ground displacement, velocity, and acceleration at the surface, respectively
$d_y$	Yield deflection (inches)
$E$	Modulus of elasticity of medium
$E$	Modulus of elasticity of structural elements (psi)
$EI$	Flexural rigidity: lb-in <sup>2</sup>
$e$	Mass density (lbs-sec <sup>2</sup> /in <sup>4</sup> )
$e_z$	Vertical eccentricity between applied force and mass center of gravity (feet)
$e_x$	Horizontal eccentricity between applied force and mass center of gravity (feet)
$e_p$	Eccentricity between passive pressure force and mass center of gravity (feet)
$f$	Frequency in cps
$f'_{cd}$	Dynamic compressive strength of concrete (psi)
$f_y$	Yield strength of steel
$G$	Modulus of shear of medium
G.Z.	Ground Zero

SYMBOLS (continued)

$g$	Acceleration due to gravity ( $32.2 \text{ ft/sec}^2 = 386 \text{ in/sec}^2$ )
$H$	Height (feet)
$h$	Layer depth (feet)
$h_c$	Depth of crater (feet)
$I_p^+$	Positive impulse of the overpressure pulse (sec)
$J$	Mass moment of inertia ( $\text{in-lbs sec}^2$ )
$K_s$	Total soil spring rate that is effective below a structure foundation ( $\text{lbs/sec}$ )
$K_{LM}$	Load-mass factor (dimensionless)
$k$	Spring rate ( $\text{lbs/in}$ )
$k_i, k_2$	Subscript notation refers to multimass response parameters
$k_p$	Ratio of residual strain to peak strain
$k$	Constant of linearity (dimensionless)
$k_s$	Spring rate of the soil ( $\text{psi/in}$ )
$k_{ij}$	Stiffness coefficient (i.e. $k_{ij}$ equals the force at mass point (or joint) $i$ due to a unit displacement at mass point (or joint) $j$ ).
$L_{eq}$	Equivalent length
$L$	Length of building (feet)
$L_w$	Characteristic length (feet)
$l_n$	Equivalent layer thickness
$l$	Length of pendulum arm in a pendulous isolation system (feet or inches)
$l_o$	Static length of spring or cylinder chamber (inches)
$M_i$	Tangent modulus of deformation at initial stress level (psi)
$M_p$	Secant modulus of deformation at peak stress level (psi)
$M_r$	Unload secant modulus of deformation (psi)
$m$	Mass ( $\text{lbs-sec}^2/\text{in}$ )

SYMBOLS (continued)

$m_1, m_2$	Subscript notation refers to multimass response parameters
$P_{max}$	Maximum force (lbs)
$P_x$	Maximum lateral force on a rigid body (lbs)
$P_z$	Maximum vertical force on a rigid body (lbs)
$P_p$	Force due to passive pressure of soil (lbs)
$p$	Cylinder pressure in a pneumatic spring system (psi)
$p$	Pressure (psi)
$p_{so}$	Peak overpressure (psi)
$p_a$	Ambient pressure in air (psi)
$(p_{so})_o$	Peak overpressure when outrunning begins (psi)
$p_f(t)$	Idealized flexural mode loading pressure on a dome structure (psi)
$p_c(t)$	Idealized compression mode loading pressure on a dome structure (psi)
$p_l$	Horizontal pressure component (psi)
$P_{do}$	Peak dynamic pressure (psi)
$P_d$	Dynamic pressure (psi)
$P_{dm}$	Maximum dynamic pressure at the clearing time (psi)
$P_{fe}$	Equivalent normal uniform pressure for flexure mode analysis for domes (psi)
$P_{refl}$	Reflected shock wave overpressure for angle of incident of zero degrees (psi)
$q_c, q_f$	Resistance capability of a dome in the compression and and flexure mode, respectively (psi)
$R_{n-m}$	Reflected wave from layer n-m
$R$	Slant range from G.Z. (feet)
$R(t)$	Resisting force of a structural or structural element as a function of time (lbs)
$R_i$	Initial resisting force (lbs)
$R_f$	Flexural resistance of a structural element (lbs)
$R$	Eccentricity between center of gravity and center of rigidity (inches)

SYMBOLS (continued)

$r_{cr}$	Critical distance when a direct wave and a reflected-refracted wave arrive simultaneously (ft.)
$r_p$	Distance from G.Z. to blast front in feet (ft)
$r_c$	Radius of crater (feet)
$r_o$	Range from G.Z. at which outrunning begins (feet)
$r$	Radius of a dome or cylindrical structure (ft)
$T$	Period of vibration, $T = 1/f$ (sec)
$T_n$	Transmitted or reflected wave from layer $n$
$TR_{n-m}$	Critically refracted-reflected wave through interface $n,m$
$T_x, T_z$	Transmissibility factor from one mode to another due to a resonant condition (dimensionless)
$t$	Time coordinate (sec or millisecc)
$t_d$	Time duration of the idealized displacement pulse (sec or millisecc)
$t_{cr}$	Critical time when a direct wave and a reflected-refracted wave arrive simultaneously (sec. or millisecc)
$t_r$	Rise time of the pressure, stress or velocity pulse (sec or millisecc)
$t_s$	Arrival time of the blast front at a specific distance from ground zero (sec or millisecc)
$t_i$	Time duration for an equivalent triangular pulse with impulse equal to $I_p^+$ (psi-sec)
$t^+$	Positive phase duration of an idealized air blast induced velocity pulse (sec or millisecc)
$t_t$	Transit time of a G.Z. induced pulse (sec or millisecc)
$t_\theta$	Time phasing between outrunning pulse and air blast induced pulse
$t_o$	Air blast arrival when outrunning begins (sec or millisecc)
$t_v$	Time when maximum velocity occurs (millisecc or sec)
$t$	Thickness of wall, shell, etc (feet or inches)
$t_c$	Required thickness in compression mode for dome structures (inches or feet)
$t_f$	Required thickness in flexure mode for dome structure

$t_c$	Clearing time (sec or millisecc)
$t_e$	Time duration for an equivalent triangular pulse (sec or millisecc)
U	Shock front velocity in air (fps)
V	Shock Spectra velocity bound in the mid-frequency region (inches/sec)
$V_0, V_1, V_2$	Subscript refers to a specific point on the four log shock spectra coordinate system
V	Cylinder volume in a pneumatic spring system (in <sup>3</sup> )
v	Ground velocity (inches/sec)
W	Weapon yield in MT
W	Weight of structure (lbs)
w	Weight per unit length (plf)
$x, \dot{x}, \ddot{x}$	Absolute lateral response displacement, velocity and acceleration respectively (inches, inches/sec, inches/sec <sup>2</sup> )
$x_s, \dot{x}_s, \ddot{x}_s$	Lateral ground or support motion: displacement, velocity, and acceleration respectively (inches, inches/sec, inches/sec <sup>2</sup> )
$x_1, x_2$	Subscript notation refers to multimass response parameters
x	Horizontal distance (ft)
$\bar{x}$	Horizontal distance between mass center of gravity and point of rotation (feet)
$y, \dot{y}, \ddot{y}$	Relative lateral response displacement, velocity, and acceleration (inches, inches/sec, inches/sec <sup>2</sup> )
$y_1, y_2$	Subscript notation refers to multimass response parameters
y	Relative displacement in the lateral direction (inches)
y	Displacement along the axis of the spring (inches)
$y_e$	Yield deflection (inches)
$y_m$	Maximum transient deflection
z	Vertical depth (feet)
z	Relative displacement in the vertical direction (inches)



SYMBOLS (continued)

$\alpha_i, \beta_i$	Angles of incident, reflected and refracted waves at a boundary (in degrees or radians)
$\alpha$	Equivalence factor
$\alpha_z$	Stress attenuation factor as a function of depth
$\beta$	Ratio of recovery displacement to positive displacement
$\beta$	Angle between vertical axis and spring line for a dome structure
$\beta_{ij}$	Amplitude ratios in the normal mode coordinate system
$\beta_0$	Angle of list due to asymmetrical load
$\Delta$	Small increment (dimensionless)
$\epsilon_z$	Strain at depth z (in/in)
$\eta$	Angle from vertical axis to an arbitrary point on the shell (radian or degrees)
$\theta_s, \ddot{\theta}_s$	Angular rotation (radians) and acceleration (g's/ft)
$\theta$	Angle of rotation about the vertical axis and measured from the horizontal plane parallel to the moving shock front
$\theta$	Pitch response in a 3-DOF system (radians)
$u$	Ductility factor, ratio of peak displacement to yield displacement
$\nu$	Poisson's ratio of medium
$\nu$	Viscous damping factor
$\rho$	Mass density of medium
$\sigma_z$	Stress at depth z (psi)
$\tau$	Time characteristic (sec or millisec)
$\phi_t$	Percentage of tensile reinforcing in reinforced concrete
$\psi$	Angle between spring line and any point on the dome for a domed structure
$\omega_1, \omega_2$	Subscript notation refers to multimass response parameters
$\omega$	Natural frequency parameter = $k/m$

## REFERENCES

- 2.1 "Shock and Vibration Engineering", Charles T. Morrow, Wiley, 1963.
- 2.2 "Dynamics of Package Cushioning", R. D. Mindlin, Bell Telephone Laboratories.
- 2.3 "Ground Shock and Missile Response", Millard V. Barton, ASME Colloquium Report, Shock and Structural Response, November 30, 1960.
- 2.4 "Design Procedures for Shock Isolation Systems of Underground Protective Structures", Vol. III: "Response Spectra of Single-Degree-of-Freedom Elastic and Inelastic Systems", A. S. Veletsos and N. M. Newmark, AFWL TDR 63-3096, June 1964.
- 2.5 "Principles and Practices for Design of Hardened Structures", Air Force Manual, AFWL-TDR-62-138, December 1962. AD 295408
- 2.6 "Engineering Vibrations", Jacobsen and Ayre, McGraw-Hill, 1958.
- 2.7 "Numerical Integration for One-Dimensional Stress Waves", R. O. Smith and N. M. Newmark, Technical Report Sponsored by The Office of Naval Research Contract Nonr1834(03), August 1958
- 2.8 "A Review of Numerical Integration Methods for Dynamic Response of Structures", by T. P. Tung and N. M. Newmark, Technical Report Sponsored by The Office of Naval Research Contract N6ori-071(06).
- 2.9 "A Review of Nuclear Explosion Phenomena Pertinent to Protective Construction", H. L. Brode, Rand Report R-425-PR, May 1964. AD 601139
- 2.10 "Shock and Vibration Handbook", Volumes I, II, and III, Harris and Crede, McGraw-Hill, 1961.
- 2.11 "Vibration Theory and Applications", W. T. Thomson, Prentice-Hall, Inc., Revised Edition 1965.
- 3.1 "A Review of Nuclear Explosion Phenomena Pertinent to Protective Construction", H. L. Brode, Rand Report R-425-PR, May 1964.
- 3.2 "Principles and Practices for Design of Hardened Structures", Air Force Design Manual, AFWL-TDR-62-138, December 1962.
- 3.3 "Nuclear Geoplosics", Part IV: "Empirical Analysis of Ground Motion and Cratering", F. M. Sauer, editor, SRI, DASA-1285, May 1964.
- 3.4 "Design Manual - AEC Test Structures", Vol. I: "Nuclear Weapons Effects and Blast Loading", Holmes and Narver, Inc., December 1961.

REFERENCES (continued)

- 3.5 "Ground Displacements Resulting from Air-Blast Loading", S. D. Wilson and E. A. Sibley, Am. Soc. Civil Engineers, 1962.
- 3.6 "Design of Structures to Resist Nuclear Weapons", ASCE Manual 42, 1961.
- 3.7 "Computations of Free-Field Motions and Shock Spectra for Linear and Non-Linear Systems", N. M. Newmark, for Ralph M. Parsons Co., July 15, 1964 (Secret).
- 3.8 "A Guide for the Design of Shock Isolation Systems for Underground Protective Structures", prepared by Ralph M. Parsons Co., for AFWL, AFSWC-TDR-62-64, December 1962.
- 4.1 "Nuclear Geoplosics", Part V: "Effects on Underground Structures and Equipment", F. M. Sauer, editor, SRI, DASA-1285, May 1964.
- 4.2 "Design Procedures for Shock Isolation Systems of Underground Protective Structures", Vol. I: "Structure Interior Motions Due to Air Blast Induced Ground Shock", AFWL-RTD TDR 63-3096, June 1964.
- 4.3 "A Theoretical Study of Structure - Medium Interaction", AFSWC (AFWL) - TDR-62-30, March 1962.
- 4.4 "A Study of Static and Dynamic Resistance and Behavior of Structural Elements", AFWL-TDR-63-3060, December 1963.
- 4.5 "A Study of the Dynamic Soil - Structure Interaction Characteristics of Real Soil Media", AFWL-TDR-63-3075, December 1963.
- 4.6 "The Interaction between a Structural Tube and the Surrounding Soil" AFWL-TDR-63-3109, January 1964.
- 4.7 "A Theoretical Analysis of Stress Wave Interaction in a Model Soil - Further Studies", AFWL-TDR-64-12, April 1964.
- 4.8 "The Response of Buried Cylinders to Quasi-Static Overpressures" AFWL WL TDR 64-13, September 1964.
- 4.9 "Mode Superposition in Multi-Degree-of-Freedom Systems Using Earthquake Response Spectrum Data", H. C. Merchant and D. E. Hudson, Bulletin of the Seismological Society of America, Vol. 52, No. 2 pp 405-416, April, 1962.

REFERENCES (continued)

- 4.10 "Design Manual-AEC Test Structures", Volume II: "Structural Response Characteristics under Dynamic Loads", Holmes and Narver, Inc., December 1961.
- 4.11 "Dynamics of Bases and Foundations", D. D. Barkan, McGraw-Hill Book Inc., New York, 1962.
- 4.12 (Same as Reference 3.6).
- 4.13 (Same as Reference 2.5).
- 4.14 "Dynamics of Structures", Hurty and Rubinstein, Prentice-Hall, Inc., 1964.
- 4.15 "Response of Foam - Isolated Tunnel Linings to Transient Loadings", AFWL-TDR-64-28.
- 4.16 "Preliminary Studies of Aggregates for Shock Isolating Lightweight Concrete", G. F. Smith, E. S. Perry, J. Neils Thompson, SMRL, The University of Texas, August 1962.
- 4.17 "Displacement Spectrum Measurements", STL, Operation Nougat, Shot Hard Hat, Barton and Lindahl, POR-1806, 1963 (Confidential).
- 4.18 "Displacement and Acceleration Spectra for Air-Induced Ground Shock", McCabe, Mow, Baron, Shock, Vibration and Associated Environments Bulletin No. 32, Part II, August 1963.
- 4.19 "Design of Structures to Resist the Effects of Atomic Weapons", Weapons Effects Data, Manuals-Corps of Engineers, EM 1110-345-413, Revised Designation-TM 5, July 1, 1959.
- 4.20 "Design Procedures for Shock Isolation Systems of Underground Protective Structures", Volume IV: "Response of Two-Degree-of-Freedom Elastic and Inelastic Systems", Newmark, et al, AFWL Report RTO-TDR 63-3096, December 1965.
- 5.1 "A Study of the Feasibility of Shock Isolating Very Large Manned Underground Structures", AFWL-TDR 64-53, March 1964.
- 5.2 "Dynamic Stability of Pendulous Missile Suspension Systems, Chobotov, V., STL/TR-60-0000-19386, November 1960.

REFERENCES (continued)

- 5.3 "On the Stability of Motion in a Special Case in the Three Bodies Problem", A. M. Liapounov, *Sobr. Soch. izd. Akad. Nauk, SSSR*, Vol. I, pp 327-401, 1954.
- 5.4 "Mechanical Vibrations", A. H. Church, John Wiley, New York, p 89, 1957.
- 5.5 (Same as Reference 2.6).
- 6.1 "Mechanical Springs", A. M. Wahl, McGraw-Hill Book Co., Inc., 1963.
- 6.2 "Vibration and Shock Isolation", C. E. Crede, John Wiley and Sons, New York, 1951.
- 6.3 "Manual on Design and Application of Helical and Spiral Springs", SAE, New York, TR-9, 1958.
- 6.4 "Handbook of Mechanical Spring Design", Associated Spring Corp., 1964.
- 6.5 "Heavy Duty Coil Springs", Crucible Steel Co., 1960.
- 6.6 "Manual on Design and Manufacture of Torsion Bar Springs", SAE, New York, 1947.
- 6.7 "Manual on Design and Manufacture of Coned Disc or Belleville Springs", SAE, New York, 1955.
- 6.8 "Guide for the Selection and Application of Shock Mounts to Shipboard Equipment", A. B. Burns, Bureau of Ships, Bu Ships Code 423, Index SF 013 10 01, 1961.
- 6.9 "Engineering Guide 850, U. S. Rubber Mountings for Vibration and Shock Isolation", U. S. Rubber, 1960.
- 6.10 "Simulation of the Response of Equipment Located in Underground Installations to Blast Induced Ground Motions", Barry Research and Development, DASA Report 1549, November 1964. AD 608531
- 6.11 (Same as Reference 2.10).
- 6.12 (Same as Reference 5.1).

REFERENCES (continued)

- 6.13 "Design Analysis-Structural and Shock Mounting, NORAD COC", Parsons, Brinckerhoff-Ryan, Corps of Engineers Report, December 1962.
- 6.14 "Die Federn Ihre Gestaltung und Berechnung", Professor Dipl.-Ing. Paul Speer, Special Publication V.D.I.-Verlag, pp. 94-99, 1938.
- 7.1 "Man's Response to Shock Motions" (See Ref. 7.13 for Follow-on), A. E. Hirsch, DTMB Report 1797, January 1964. AD 436809
- 7.2 "The Effects of Shock and Vibration on Man", D. E. Goldman and H. E. VonGierke, NMRI Report 60-3, January 1960. AD 241621
- 7.3 (Same as Ref. 3.8).
- 7.4 "Human Engineering", Chapter 10, E. J. McCormick, McGraw-Hill, New York, 1957.
- 7.5 "Human Tolerance to Rapidly Applied Accelerations: A Summary of the Literature", A. M. Eiband, NASA MEMO 5-19-59E, June 1959.
- 7.6 "Short Time Human Tolerance to Sinusoidal Vibrations", AD 227341 G. H. Ziegenruecker and E. B. Magid, WADC TR 59-391, July 1959.
- 7.7 "Whole-Body Vibration of Standing Subjects", R. E. Chaney, Boeing Report D3-6779, August 1965. AD 472912
- 7.8 "Shock Hardening of Equipment", R. A. Eubanks and B. R. Juskie, 32nd Symposium on Shock, Vibration and Associated Environments, Bulletin No. 32, Part III, pp. 23-73, April 1963.
- 7.9 (Same as Ref. 2.10).
- 7.10 "Vulnerability Handbook for Hardened Installations", Volume I, Chapter 12, (Revised), Newmark, Hansen and Associates, AD 365 316, August 1965, (Confidential).
- 7.11 "WS-133B, Environmental Design Criteria, Minuteman" AFBSD Exhibit 62-51, (Rev. 5), November 1, 1963.
- 7.12 (Same as Reference 6.10).
- 7.13 "Man's Response to Ship Shock Motions", R. M. Mahone, DTMB Report 2135, January 1966. AD 628891

REFERENCES (continued)

- C.1 "Numerische Behandlung von Differential-Gleichungen", L. Collatz, Springer Verlag, Berlin, p. 34, 1951.
- C.2 "Numerical Methods for Scientists and Engineers", McGraw-Hill, 1962.
- C.3 "Efficiency of Predictor-Corrector Procedures", T. E. Hull, A. L. Greemer, J.ACM, 10, 291-301, 1963.
- C.4 "Numerical Methods and Fortran Programming", John Wiley, 1964.
- C.5 "Numerical Methods in Fortran", Prentice-Hall, 1964.
- C.6 "Mathematical Methods for Digital Computers", John Wiley, 1960.
- F.1 "Analytical and Experimental Investigations of Silo and Tunnel Linings", AFWL TDR 63-3085, September 1964.
- F.2 "Seismic Analysis of Bridges on Long Piles", ASCE Journal, Volume 90 No. 3953, June 1964.

## APPENDIX A

### EQUATIONS FOR MULTI-DEGREE-OF-FREEDOM SYSTEMS

In this Appendix, equations of motion of multi-degree-of-freedom systems will be expressed and solved by matrix notation. Recent developments in electronic computer applications have placed great emphasis on the formulation of response equations in matrix notation for convenience in numerical computation. Although for a two-degree-of-freedom system, matrix notation is not as essential as for higher-degree-of-freedom systems, matrix notation will first be applied to a two-mass system as an introduction to the more involved conditions. The two-mass system has been introduced in Section 2. The more involved cases will be discussed in Section 5.

#### 1. Definitions of matrix algebra.

Matrix array: A matrix  $[A]$  is a rectangular array of  $m$  rows and  $n$  columns.

$$[A] = \begin{bmatrix} a_{11} & a_{12} & & a_{1n} \\ a_{21} & a_{22} & & a_{2n} \\ & & a_{ij} & \\ & & & \\ & & & \\ a_{m1} & a_{m2} & & a_{mn} \end{bmatrix} \begin{array}{l} m \text{ rows} \\ n \text{ columns} \end{array}$$

$(m, n) = \text{order}$

$a_{ij}$  = a specific element at row  $i$  and column  $j$ .

#### Equality

$$[A] = [B] \quad \text{if } a_{ij} = b_{ij}$$

#### Addition and subtraction

$$\begin{array}{ccc} [A] & \pm & [B] = [C] \\ (m,n) & & (m,n) \end{array} \quad \text{provided } c_{ij} = a_{ij} \pm b_{ij}$$



Transposition

$$[A] = \begin{bmatrix} a_{11} & a_{12} & a_{1n} \\ a_{21} & a_{22} & a_{2n} \\ a_{m1} & a_{m2} & a_{mn} \end{bmatrix} \quad [A]^T = \begin{bmatrix} a_{11} & a_{21} & a_{m1} \\ a_{12} & a_{22} & a_{m2} \\ a_{1n} & a_{2n} & a_{mn} \end{bmatrix}$$

$[A]^T$  is the transpose of  $[A]$  when the rows and columns are interchanged.

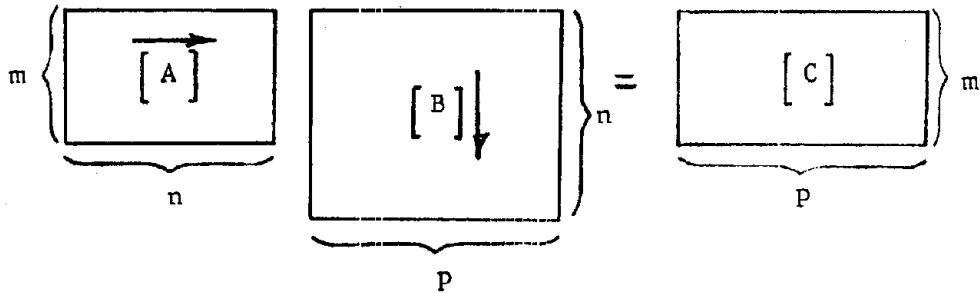
Multiplication

Two matrices are conformable (can be multiplied) if

$$\begin{matrix} [A] & [B] & = & [C] \\ (m,n) & (n,p) & & (m,p) \end{matrix}$$

equal

the number of columns of the first matrix,  $n$ , is equal to the number of rows of the second matrix. Thus



$$c_{ij} = \sum_{k=1}^n a_{ik} b_{kj}$$

For example when  $[A]$  and  $[B]$  are  $3 \times 3$  matrices,

$$c_{32} = a_{31} b_{12} + a_{32} b_{22} + a_{33} b_{32}$$

Unit matrix

$$[U] = \begin{bmatrix} 1 & 0 & 0 \\ 0 & 1 & 0 \\ 0 & 0 & 1 \end{bmatrix}$$

The matrix is a square matrix and the elements on the principal diagonal are unity.

### Inverse matrix

Given  $[A]$  of order  $n$ ,  $n$  (square). Find the reciprocal matrix  $[R]$  such that

$$[A] [R] = [R] [A] = [U]$$

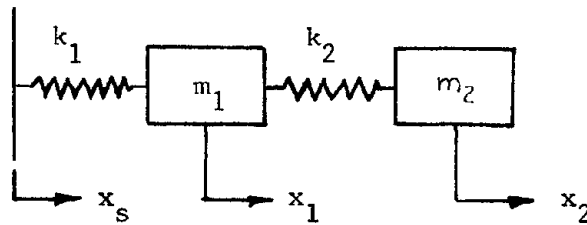
The matrix  $[R]$  is defined as the inverse of matrix  $[A]$  with the following notation

$$\text{Inverse } [A] = [A]^{-1}$$

The bracket notation  $[ ]$  refers to a rectangular (or square) array of elements. The parenthesis notation  $( )$  refers to a single column of elements.

For a complete treatment the reader is referred to the many texts on matrix algebra.

### 2. Derivation of response equation for a two -degree-of-freedom system.



The equations of motion are

$$m_1 \ddot{x}_1 + (k_1 + k_2) x_1 - k_2 x_2 = k_1 x_s \quad (\text{A-1})$$

$$m_2 \ddot{x}_2 + k_2 x_2 - k_2 x_1 = 0 \quad (\text{A-2})$$

where  $\ddot{x}_1$ ,  $x_1$ ,  $\ddot{x}_2$ ,  $x_2$  are the absolute coordinates of the two masses.

Introducing a coordinate transformation,

$$y_1 = x_1 - x_s \quad \ddot{y}_1 = \ddot{x}_1 - \ddot{x}_s$$

$$y_2 = x_2 - x_s \quad \ddot{y}_2 = \ddot{x}_2 - \ddot{x}_s$$

equations (A-1) and (A-2) can be rewritten in terms of the relative displacements  $y_1$  and  $y_2$ , the relative accelerations  $\ddot{y}_1$  and  $\ddot{y}_2$ ,

and the support acceleration  $\ddot{x}_s$ .

$$m_1 \ddot{y}_1 + (k_1 + k_2) y_1 - k_2 y_2 = -m_1 \ddot{x}_s \quad (\text{A-3a})$$

$$m_2 \ddot{y}_2 + k_2 y_2 - k_2 y_1 = -m_2 \ddot{x}_s \quad (\text{A-3b})$$

or simply

$$[m] (\ddot{y}) + [k] (y) = - (m) \ddot{x}_s \quad (\text{A-4})$$

in matrix notation.

a. Normal mode vibrations. Free vibrations of the two-mass system are obtained from the homogeneous solution of Equation (A-4) by postulating harmonic response:

$$\text{writing } y_1 = y_{1\max} \sin \omega t \quad (\text{A-5})$$

$$y_2 = y_{2\max} \sin \omega t$$

and substituting into Equations (A-3a) and (A-3b) we obtain

$$\omega_1^2 m_1 y_1 - (k_1 + k_2) y_1 + k_2 y_2 = 0 \quad (\text{A-6})$$

$$\omega_2^2 m_2 y_2 - k_2 y_2 + k_2 y_1 = 0$$

The natural frequencies (eigenvalues) can be determined by solving the determinant of Equation (A-6).

$$\begin{vmatrix} \omega^2 m_1 - (k_1 + k_2) & k_2 \\ k_2 & (\omega^2 m_2 - k_2) \end{vmatrix} = 0 \quad (\text{A-7})$$

$$\text{or } \omega^4 - \left( \frac{k_1 + k_2}{m_1} + \frac{k_2}{m_2} \right) \omega^2 + \frac{k_1 k_2}{m_1 m_2} = 0$$

Discarding the negative results, we obtain two positive natural frequencies which we denote as  $\omega_1$  and  $\omega_2$ .

The amplitude ratios  $y_2/y_1$  may be found from Equation (A-6) as

$$\frac{y_2}{y_1} = \frac{-k_2}{\omega^2 m_2 - k_2} \quad \text{or} \quad \frac{k_1 + k_2 - \omega^2 m_1}{k_2} \quad (\text{A-8})$$

Substituting the two frequencies  $\omega_1^2$ ,  $\omega_2^2$  into either of Equation (A-8) results in the amplitude ratios in the two modes  $\omega_1$  and  $\omega_2$ . Thus, normalizing  $y_1 = 1$  and at natural frequency  $\omega_1$ ,  $y_2$  is solved from Equation (A-6)

$$y_2 = \frac{-k_2}{\omega_1^2 m_2 - k_2} = \frac{k_1 + k_2 - \omega_1^2 m_1}{k_2} = \beta_{21} \quad (\text{A-9})$$

At natural frequency  $\omega_2$

$$y_2 = \frac{k_2}{\omega_2^2 m_2 - k_2} = \frac{k_1 + k_2 - \omega_2^2 m_1}{k_2} = \beta_{22} \quad (\text{A-10})$$

Either of the two terms defining  $y_2$  in Equations (A-9) and (A-10) may be used to calculate the amplitude ratio.

where

$\beta_{21}$  = amplitude of mass 2 in frequency mode  $\omega_1$  if  
 $y_1 = 1$

$\beta_{22}$  = amplitude of mass 2 in frequency mode  $\omega_2$  if  
 $y_1 = 1$

The above amplitude ratios define an orthogonal set of coordinates that is called the modal matrix  $[\beta]$

$$[\beta] = \begin{bmatrix} 1 & 1 \\ \beta_{21} & \beta_{22} \end{bmatrix} \quad (\text{A-11})$$

With the use of the modal matrix it is possible to express the equations of motion in a coordinate system that will uncouple the original Equations (A-3 and A-4). Let  $\eta$  be the new coordinate system such that  $(y) = [\beta](\eta)$  and  $(\ddot{y}) = [\beta](\ddot{\eta})$  (A-12)

Substitute into Equation (A-4) and pre-multiply by  $[\beta]$

$$[\beta]^T [m] [\beta] (\ddot{\eta}) + [\beta]^T [k] [\beta] (\eta) = - [\beta]^T \begin{pmatrix} m_1 & x_s \\ m_2 & x_s \end{pmatrix} \quad (\text{A-13})$$

where the new set of coordinates  $(\eta)$  are orthogonal and are called the normal mode coordinates.

$$\left. \begin{aligned}
\text{let } [M] &= [\beta]^T [m] [\beta] && : \text{ Generalized Mass (Diagonal)} \\
[K] &= [\beta]^T [k] [\beta] && : \text{ Generalized Stiffness (Diagonal)} \\
[\beta]^T (m) &= (N) && : \text{ Generalized Forcing Function} \\
\frac{K_r}{M_r} &= \omega_r^2 && : \text{ Normal mode frequency} \\
\frac{N_r}{M_r} &= \Gamma_r && : \text{ Mode participation factor}
\end{aligned} \right\} \text{(A-14)}$$

Substitution into Equation (A-13) yields the following

$$\begin{bmatrix} M_1 & 0 \\ 0 & M_2 \end{bmatrix} \begin{pmatrix} \ddot{\eta}_1 \\ \ddot{\eta}_2 \end{pmatrix} + \begin{bmatrix} K_1 & 0 \\ 0 & K_2 \end{bmatrix} \begin{pmatrix} \eta_1 \\ \eta_2 \end{pmatrix} = - \begin{pmatrix} N_1 \\ N_2 \end{pmatrix} \ddot{x}_s$$

where

$$M_1 = m_1 + m_2 \beta_{21}^2$$

$$M_2 = m_1 + m_2 \beta_{22}^2$$

$$K_1 = k_1 + k_2 (1 - \beta_{21})^2$$

$$K_2 = k_1 + k_2 (1 - \beta_{22})^2$$

$$N_1 = m_1 + m_2 \beta_{21}$$

$$N_2 = m_1 + m_2 \beta_{22}$$

Equation (A-13) can now be written in the normal mode coordinate system:

$$\ddot{\eta}_1 + \omega_1^2 \eta_1 = - \Gamma_1 \ddot{x}_s$$

$$\ddot{\eta}_2 + \omega_2^2 \eta_2 = - \Gamma_2 \ddot{x}_s$$

(A-15)

or 
$$(\ddot{\eta}) + (\omega^2 \eta) = - (\Gamma \ddot{x}_s)$$

The displacement response in each mode to the generalized forcing function can then be determined from the convolution integral

$$D_r(t) = -\frac{1}{\omega_r} \int_0^t \ddot{x}_s(\tau) \sin \omega_r(t - \tau) d\tau$$

$$D_r(t) = -\int_0^t \dot{x}_s(\tau) \cos \omega_r(t - \tau) d\tau \quad (A-16)$$

$$D_r(t) = -\frac{d}{dt} \int_0^t x_s(\tau) \cos \omega_r(t - \tau) d\tau$$

$D_r(t)$  = Dynamic Response Factor

where  $\tau$  is a dummy variable of integration and the initial conditions are all zero.

The general solution to Equation (A-15) is then the sum of two harmonic motion components (in terms of  $\omega_1$  and  $\omega_2$ ) and  $D_r(t)$ .

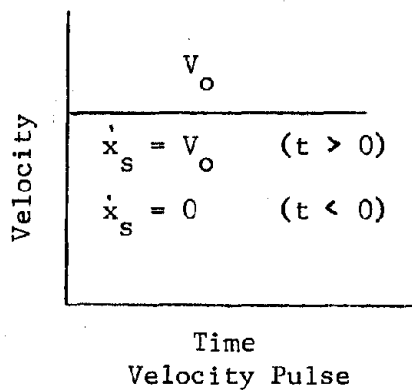
Once the normal mode response is known the transformation back to the coupled coordinate system is made through the relationships

$$(\ddot{y}) = [\beta](\ddot{\eta}) \quad (A-17a)$$

$$(\dot{x}) = (\dot{y}) + (\dot{x}_s) \quad (A-17b)$$

Special Case: Velocity Pulse Input

As an example assume that the ground motion is a step-velocity pulse



The dynamic response factor is calculated from Equation (A-16) as

$$D_r(t) = -\frac{v_o}{\omega_r} \sin \omega_r t$$

and

$$D_{r(\max)} = -\frac{v_o}{\omega_r} \quad (\text{A-18})$$

The peak displacement response in each mode is

$$u_r = \Gamma_r D_{r(\max)} \quad (\text{A-19})$$

This response can now be related back to the coupled system to find the peak absolute accelerations.

$$\ddot{x} = \ddot{y} + \ddot{x}_s = [\beta] \ddot{\eta} + \ddot{x}_s \quad (\text{A-20})$$

For the  $i^{\text{th}}$  mass acceleration

$$\ddot{x}_i = [\beta_{in}] \ddot{\eta} + \ddot{x}_s \quad (\text{A-21})$$

where  $[\beta_{in}]$  is the  $i^{\text{th}}$  row matrix of  $[\beta]$

Rewriting Equation (A-15)

$$\ddot{\eta} = -(\omega^2 \eta) - (\Gamma \ddot{x}_s) \quad (\text{A-22})$$

Substituting Equation (A-22) into (A-21)

$$\ddot{x}_i = [\beta_{in}] \left\{ -(\omega^2 \eta) - (\Gamma \ddot{x}_s) \right\} + \ddot{x}_s \quad (\text{A-23})$$

$$\text{or } \ddot{x}_i = -[\beta_{in}] (\omega^2 \eta) + \ddot{x}_s \left\{ 1 - [\beta_{in}] (\Gamma) \right\} \quad (\text{A-24})$$

But  $[\beta_{in}] (\Gamma) = 1$  from substitution of expressions (A-14).

Therefore Equation (A-24) reduces to

$$\ddot{x}_i = -[\beta_{in}] (\omega^2 \eta) \quad (\text{A-25})$$

\* This expression holds due to orthogonality of normal modes. See paper by Dana Young "Response of Structural Systems to Ground Shock" in Reference 2.3 for justification of this equality.

The response maximum acceleration is then from Equations (A-18) and (A-19):

$$\ddot{x}_{\max} = [\beta] (\Gamma \omega v_o) \quad (A-26)$$

In the case of the two-mass system,

$$\begin{pmatrix} \ddot{x}_1 \\ \ddot{x}_{2\max} \end{pmatrix} = \begin{bmatrix} 1 & 1 \\ \beta_{21} & \beta_{22} \end{bmatrix} \begin{pmatrix} \Gamma_1 \omega_1 v_o \\ \Gamma_2 \omega_2 v_o \end{pmatrix} \quad (A-27)$$

Letting  $\omega_1 v_o = A_1$ , max acceleration response at frequency  $\omega_1$

$\omega_2 v_o = A_2$ , max acceleration response at frequency  $\omega_2$ .

Thus

$$\ddot{x}_{1\max} = \Gamma_1 A_1 + \Gamma_2 A_2 \quad (A-28a)$$

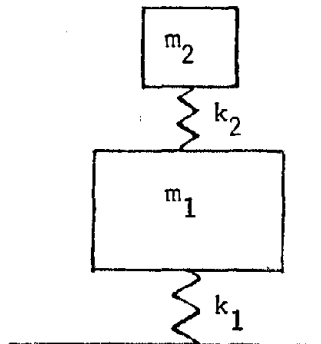
$$\ddot{x}_{2\max} = \beta_{21} \Gamma_1 A_1 + \beta_{22} \Gamma_2 A_2 \quad (A-28b)$$

The peak responses in each mode will not usually occur simultaneously, but an upper bound response can be obtained by adding the absolute values of the peak response in each mode. Thus

$$\begin{aligned} \ddot{x}_{1\max} &= \left| \Gamma_1 A_1 \right| + \left| \Gamma_2 A_2 \right| \\ \ddot{x}_{2\max} &= \left| \beta_{21} \Gamma_1 A_1 \right| + \left| \beta_{22} \Gamma_2 A_2 \right| \end{aligned} \quad (A-29)$$

These are useful general expressions for the peak acceleration response of a two-mass system.

Special case. A special case of great interest occurs when  $m_1 \gg m_2$ . This was discussed in Section 2 as a situation that may describe an element of small mass  $m_2$  mounted on a flexible support as shown below





Let  $m_1 = 10 m_2$

Solving the determinant of Equation (A-7) for the frequencies  $\omega_1^2$  and  $\omega_2^2$  it is seen that

$$\omega_1^2 \approx \frac{k_1}{m_1} ; \quad \omega_2^2 \approx \frac{11 k_2}{m_1} \quad (\text{A-30})$$

where  $k_1 \gg k_2$

The amplitude ratios are

$$\beta_{21} = \frac{-\frac{10}{11}\omega_2^2}{\omega_1^2 - \frac{10}{11}\omega_2^2} \approx \frac{-\omega_2^2}{\omega_1^2 - \omega_2^2} \quad (\text{A-31})$$

$$\beta_{22} = \frac{11\omega_1^2 + \omega_2^2 - 11\omega_2^2}{\omega_2^2} \approx 10 \frac{(\omega_1^2 - \omega_2^2)}{\omega_2^2} \quad (\text{A-32})$$

or in general if  $m_1 \gg m_2$

$$\beta_{22} \approx \frac{m_1}{m_2} \left( \frac{\omega_1^2 - \omega_2^2}{\omega_2^2} \right) \quad (\text{A-33})$$

The modal matrix  $[\beta] =$  
$$\begin{bmatrix} 1 & 1 \\ \frac{-\omega_2^2}{\omega_1^2 - \omega_2^2} & \frac{m_1}{m_2} \left( \frac{\omega_1^2 - \omega_2^2}{\omega_2^2} \right) \end{bmatrix} \quad (\text{A-34})$$

Solving for the generalized mass  $[M]$  and the generalized force

(N) we have

$$[M] = [\beta]^T [m] [\beta] = \begin{bmatrix} m_1 \left\{ 1 + \frac{1}{10} \left( \frac{\omega_2^2}{\omega_1^2 - \omega_2^2} \right)^2 \right\} & 0 \\ 0 & m_1 \left\{ 1 + \frac{10(\omega_1^2 - \omega_2^2)}{\omega_2^2} \right\} \end{bmatrix} \quad (\text{A-35})$$

$$[N] = [\beta]^T (m) = \begin{pmatrix} m_1 \left\{ 1 - \frac{\omega_2^2}{10(\omega_1^2 - \omega_2^2)} \right\} \\ m_1 \left\{ 1 + \frac{(\omega_1^2 - \omega_2^2)}{\omega_2^2} \right\} \end{pmatrix} \quad (\text{A-36})$$

The mode participation factors are:

$$\Gamma_1 = \frac{m_1 \left\{ 1 - \frac{\omega_2^2}{10(\omega_1^2 - \omega_2^2)} \right\}}{m_1 \left\{ 1 + \frac{1}{10} \left( \frac{\omega_2^2}{\omega_1^2 - \omega_2^2} \right)^2 \right\}} = \frac{\omega_1^4 - 2.1 \omega_1^2 \omega_2^2 + 1.1 \omega_2^4}{\omega_1^4 - 2 \omega_1^2 \omega_2^2 + 1.1 \omega_2^4} \approx 1 \quad (\text{A-37})$$

and

$$\Gamma_2 = \frac{m_1 \left\{ 1 + \frac{(\omega_1^2 - \omega_2^2)}{\omega_2^2} \right\}}{m_1 \left\{ 1 + \frac{10}{\omega_2^2} \left( \frac{\omega_1^2 - \omega_2^2}{\omega_2^2} \right)^2 \right\}} = \frac{\omega_1^2 \omega_2^2}{10\omega_1^4 - 20\omega_1^2 \omega_2^2 + 11\omega_2^4} \quad (\text{A-38})$$

$$\approx \frac{\omega_1^2 \omega_2^2}{10(\omega_1^2 - \omega_2^2)^2}$$

Therefore:

$$\left| \beta_{21} \Gamma_1 \right| = \frac{\omega_2^2}{\omega_1^2 - \omega_2^2} \quad (\text{A-39})$$

$$\left| \beta_{22} \Gamma_2 \right| = \frac{10}{\omega_2^2} \frac{(\omega_1^2 - \omega_2^2)}{10(\omega_1^2 - \omega_2^2)^2} \frac{\omega_1^2 \omega_2^2}{\omega_2^2} = \frac{\omega_1^2}{\omega_1^2 - \omega_2^2} \quad (\text{A-40})$$

Therefore, when  $m_1 \gg m_2$ , the peak acceleration of mass  $m_2$  may be written from Equation (A-29) as

$$\ddot{x}_{2\max} = \left| \frac{\omega_2^2}{\omega_1^2 - \omega_2^2} \right| A_1 + \left| \frac{\omega_1^2}{\omega_1^2 - \omega_2^2} \right| A_2 \quad (\text{A-41})$$

which is Equation (2.24) of Section 2 that was derived in a more direct manner.

3. Three-degree-of-freedom systems. The mathematical methods outlined in the previous section of this appendix may be directly applied to higher degree-of-freedom systems without difficulty. The matrix algebra however becomes very lengthy in terms of specific higher order systems and the generalized normal mode expansions of the three-degree-of-freedom system is not formally derived here. Instead, more useful general information is included for two classes of systems i.e., the three mass three-degree-of-freedom system and a one mass three-degree-of-freedom system. The frequency equations, amplitude ratios, and approximate response equations using single-degree-of-freedom shock spectra are derived.

3.1 Three mass system. The homogeneous equations of motion for the

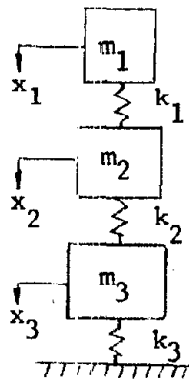


FIGURE A-1

three mass system of Figure A-1 are given by the following equations

$$\begin{aligned} m_1 \ddot{x}_1 + k_1 (x_1 - x_2) &= 0 \\ m_2 \ddot{x}_2 + k_1 (x_2 - x_1) + k_2 (x_2 - x_3) &= 0 \\ m_3 \ddot{x}_3 + k_2 (x_3 - x_2) + k_3 x_3 &= 0 \end{aligned} \quad (\text{A-42})$$

In the usual way, the following solutions are assumed

$$\begin{aligned}x_1 &= x_{1\max} \sin \omega t \\x_2 &= x_{2\max} \sin \omega t \\x_3 &= x_{3\max} \sin \omega t\end{aligned}\tag{A-43}$$

and substituted into the equations of motion to obtain the algebraic equations

$$\begin{bmatrix}k_1 - m_1 \omega^2 & -k_2 & 0 \\-k_2 & (k_1 + k_2 - m_2 \omega^2) & -k_2 \\0 & -k_2 & (k_2 + k_3 - m_3 \omega^2)\end{bmatrix} \cdot \begin{Bmatrix}x_{1\max} \\x_{2\max} \\x_{3\max}\end{Bmatrix} = 0\tag{A-44}$$

The determinant of the square matrix when equated to zero reduces to the frequency equation which after simplification becomes

$$\begin{aligned}\omega^6 - \omega^4 \left[ \omega_1^2 + \omega_2^2 (1 + \lambda_2^2) + \omega_3^2 (1 + \lambda_3^2) \right] + \omega^2 \left[ \omega_1^2 \omega_2^2 (1 + \lambda_2^2 - 1/\lambda_2^2) + \right. \\ \left. \omega_1^2 \omega_3^2 (1 + \lambda_3^2) + \omega_2^2 \omega_3^2 (1 + \lambda_2^2 + \lambda_2^2 \lambda_3^2) \right] - \omega_1^2 \omega_2^2 \omega_3^2 \left[ 1 + \lambda_2^2 \lambda_3^2 + \right. \\ \left. \lambda_2^2 + \lambda_3^2 / \lambda_2^2 \right] = 0\end{aligned}\tag{A-45}$$

$$\text{where } \omega_1^2 = k_1/m_1$$

$$\omega_2^2 = k_2/m_2$$

$$\omega_3^2 = k_3/m_3$$

$$\lambda_2^2 = k_1/k_2$$

$$\lambda_3^2 = k_2/k_3$$

The amplitude ratios are

$$(x_{1\max}/x_{2\max})_n = \frac{k_2}{k_1 - m_1 \omega_n^2} \quad n = 1, 2, 3\tag{A-46}$$

$$(x_{3\max}/x_{2\max})_n = \frac{k_2}{k_2 + k_3 - m_3 \omega_n^2} \quad n = 1, 2, 3 \quad \text{(A-46)}$$

cont'd

where  $\omega_n$  are roots of Equation (A-45)

Thus, normalizing  $x_{2\max} = 1$ , the modal matrix is derived

$$\beta = \begin{bmatrix} \beta_{11} & \beta_{12} & \beta_{13} \\ \beta_{21} & \beta_{22} & \beta_{23} \\ \beta_{31} & \beta_{32} & \beta_{33} \end{bmatrix} = \begin{bmatrix} \frac{k_2}{k_1 - m_1 \omega_1^2} & \frac{k_2}{k_1 - m_1 \omega_2^2} & \frac{k_2}{k_1 - m_1 \omega_3^2} \\ 1 & 1 & 1 \\ \frac{k_2}{k_2 + k_3 - m_3 \omega_1^2} & \frac{k_2}{k_2 + k_3 - m_3 \omega_2^2} & \frac{k_2}{k_2 + k_3 - m_3 \omega_3^2} \end{bmatrix} \quad \text{(A-47)}$$

3.2 One mass system. A typical one mass system taken from Section 5 is repeated in Figure A-2 for convenience

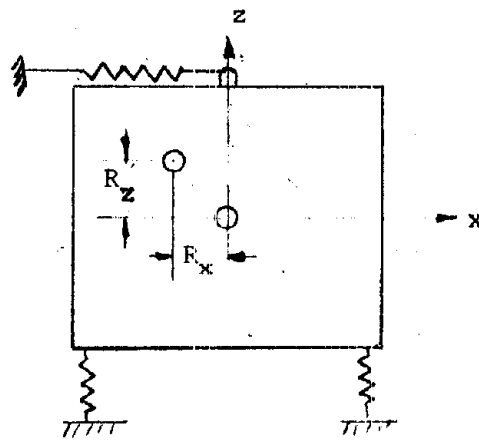


FIGURE A-2

The homogeneous equations of motion as derived in Section 5.3 are

$$\begin{aligned} m\ddot{z} + k_z (z + R_x \theta) &= 0 \\ m\ddot{x} + k_x (x + R_z \theta) &= 0 \\ J\ddot{\theta} + k_\theta \theta + k_x (x + R_z \theta) R_z + k_z (z + R_x \theta) R_x &= 0 \end{aligned} \quad \text{(A-48)}$$

Let

$$z = z_{\max} \sin \omega t$$

$$x = x_{\max} \sin \omega t$$

$$\theta = \theta_{\max} \sin \omega t$$

and substitute into (A-48) to obtain the algebraic equations

$$\begin{bmatrix} \omega_z^2 - \omega^2 & 0 & \omega_z^2 R_x \\ 0 & \omega_x^2 - \omega^2 & \omega_x^2 R_z \\ \frac{\omega_x^2 R_x}{\rho^2} & \frac{\omega_x^2 R_z}{\rho^2} & \omega_\theta^2 - \omega^2 + \frac{\omega_x^2 R_z^2 + \omega_z^2 R_x^2}{\rho^2} \end{bmatrix} \begin{Bmatrix} z_{\max} \\ y_{\max} \\ \theta_{\max} \end{Bmatrix} = 0 \quad (\text{A-49})$$

where

$$\omega_x^2 = k_x/m$$

$$\omega_z^2 = k_z/m$$

$$\omega_\theta^2 = k_\theta/J$$

$$\rho^2 = J/m$$

The frequency equation after simplification becomes

$$\omega^6 - \omega^4 \left[ \omega_x^2 + \omega_z^2 + \omega_\theta^2 + \frac{\omega_x^2 R_z^2 + \omega_z^2 R_x^2}{\rho^2} \right] + \omega^2 \left[ \omega_x^2 \omega_z^2 \left( 1 + \frac{R_x^2 + R_z^2}{\rho^2} \right) + \omega_x^2 \omega_\theta^2 + \omega_z^2 \omega_\theta^2 \right] + \omega_x^2 \omega_z^2 \omega_\theta^2 = 0 \quad (\text{A-50})$$

and the normalized modal matrix is

$$\beta = \begin{bmatrix} \beta_{11} & \beta_{12} & \beta_{13} \\ \beta_{21} & \beta_{22} & \beta_{23} \\ \beta_{31} & \beta_{32} & \beta_{33} \end{bmatrix}$$

$$\begin{aligned}
\text{where } \beta_{1n} &= \frac{\omega_z^2 R_x}{\omega_x^2 R_z} \cdot \frac{\omega_n^2 - \omega_x^2}{\omega_n^2 - \omega_z^2} & n &= 1, 2, 3 \\
\beta_{2n} &= 1 & n &= 1, 2, 3 \\
\beta_{3n} &= \frac{\omega_n^2 - \omega_x^2}{\omega_x^2 R_x} & n &= 1, 2, 3
\end{aligned} \tag{A-51}$$

The non-homogeneous equations of motion corresponding to foundation disturbances are from Section 5.3.

$$\begin{aligned}
m\ddot{\eta} + k_z (\eta + R_x \theta) &= -m\ddot{z}_s \\
m\ddot{y} + k_x (y + R_z \theta) &= -m\ddot{x}_s
\end{aligned} \tag{A-48a}$$

$$J\ddot{\theta} + k_\theta \theta + k_x (y + R_z \theta) R_z + k_z (y + R_x \theta) R_x = 0$$

Let  $(y) = [\beta] (\eta)$

where

$$(y) = \begin{pmatrix} \eta \\ y \\ \theta \end{pmatrix}, \quad (\eta) = \begin{pmatrix} \eta_1 \\ \eta_2 \\ \eta_3 \end{pmatrix}$$

Substituting into (A-48a) and premultiplying by  $[\beta]^T$  produces an equation analogous to (A-13)

$$[\beta]^T [m] [\beta] (\ddot{\eta}) + [\beta]^T [k] [\beta] (\eta) = -[\beta]^T \begin{pmatrix} m\ddot{x}_s \\ m\ddot{z}_s \\ 0 \end{pmatrix} \tag{A-52}$$

where

$$[m] = \begin{bmatrix} m & 0 & 0 \\ 0 & m & 0 \\ 0 & 0 & J \end{bmatrix}$$

$$[k] = \begin{bmatrix} k_z & 0 & k_z R_x \\ 0 & k_x & k_x R_z \\ k_z R_x & k_x R_z & (k_\theta + k_x R_z^2 + k_z R_x^2) \end{bmatrix}$$

Thus

$$[M] (\ddot{\eta}) + [K] (\eta) = -[\beta]^T \begin{pmatrix} m\ddot{z}_s \\ m\ddot{x}_s \\ J\ddot{\theta} \end{pmatrix} \quad (\text{A-53})$$

where

$$\begin{aligned} [M] &= [\beta]^T \begin{bmatrix} m & & \\ & m & \\ & & J \end{bmatrix} [\beta] \\ [K] &= [\beta]^T \begin{bmatrix} k & & \\ & k & \\ & & J \end{bmatrix} [\beta] \\ (N) &= [\beta]^T \begin{pmatrix} m\ddot{z}_s \\ m\ddot{x}_s \\ J\ddot{\theta} \end{pmatrix} \end{aligned}$$

or

$$\begin{aligned} \ddot{\eta}_1 + \omega_1^2 \eta_1 &= -\Gamma_{11} \ddot{z}_s - \Gamma_{21} \ddot{x}_s - \Gamma_{31} \ddot{\theta} \\ \ddot{\eta}_2 + \omega_2^2 \eta_2 &= -\Gamma_{12} \ddot{z}_s - \Gamma_{22} \ddot{x}_s - \Gamma_{32} \ddot{\theta} \\ \ddot{\eta}_3 + \omega_3^2 \eta_3 &= -\Gamma_{13} \ddot{z}_s - \Gamma_{23} \ddot{x}_s - \Gamma_{33} \ddot{\theta} \end{aligned} \quad (\text{A53a})$$

where

$$\begin{aligned} \omega_r^2 &= \frac{K_r}{M_r} \\ M_1 &= m\beta_{11}^2 + m\beta_{21}^2 + J\beta_{31}^2 \\ M_2 &= m\beta_{12}^2 + m\beta_{22}^2 + J\beta_{32}^2 \\ M_3 &= m\beta_{13}^2 + m\beta_{23}^2 + J\beta_{32}^2 \\ \Gamma_{11} M_1 &= m\beta_{11} \\ \Gamma_{21} M_1 &= m\beta_{21} \\ \Gamma_{31} M_1 &= J\beta_{31} \\ \Gamma_{12} M_2 &= m\beta_{12} \\ \Gamma_{22} M_2 &= m\beta_{22} \\ \Gamma_{32} M_2 &= J\beta_{32} \end{aligned}$$



$$\begin{aligned} \Gamma_{13} M_3 &= m\beta_{13} \\ \Gamma_{23} M_3 &= m\beta_{23} \\ \Gamma_{33} M_3 &= J\beta_{33} \end{aligned}$$

Equations (A53a) are recognized as SDOF systems with two input displacements  $\ddot{x}_s$  and  $\ddot{z}_s$  modified by the participation factors  $\Gamma$ . The maximum excursions are therefore:

$$\begin{aligned} \eta_{1\max} &= \Gamma_{11} D_{11} + \Gamma_{21} D_{21} + \Gamma_{31} \cdot 0 \\ \eta_{2\max} &= \Gamma_{12} D_{12} + \Gamma_{22} D_{22} + \Gamma_{23} \cdot 0 \\ \eta_{3\max} &= \Gamma_{13} D_{13} + \Gamma_{23} D_{23} + \Gamma_{33} \cdot 0 \end{aligned} \tag{A-54}$$

where  $D_{ij}$  are the shock spectra responses in the  $j$ th mode due to ground movements in the  $i$ th direction i.e.

- $i = 1$  VERTICAL
- $i = 2$  HORIZONTAL
- $i = 3$  ROTATIONAL

Since  $\begin{bmatrix} y \\ \theta \end{bmatrix} = \begin{bmatrix} \beta \end{bmatrix} \begin{pmatrix} \eta_1 \\ \eta_2 \\ \eta_3 \end{pmatrix}$  (7)

$$\begin{pmatrix} \eta \\ y \\ \theta \end{pmatrix} = \begin{bmatrix} \beta \end{bmatrix} \begin{pmatrix} \eta_1 \\ \eta_2 \\ \eta_3 \end{pmatrix}$$

It follows that

$$\begin{aligned} \eta &= \left| \beta_{11} \frac{m\beta_{11} D_{11} + m\beta_{21} D_{21} + J\beta_{31} \cdot 0}{m\beta_{11}^2 + m\beta_{21}^2 + J\beta_{31}^2} \right| \\ &+ \left| \beta_{21} \frac{m\beta_{12} D_{12} + m\beta_{22} D_{22} + J\beta_{23} \cdot 0}{m\beta_{12}^2 + m\beta_{21}^2 + J\beta_{31}^2} \right| \\ &+ \left| \beta_{31} \frac{m\beta_{13} D_{13} + m\beta_{23} D_{23} + J\beta_{33} \cdot 0}{m\beta_{13}^2 + m\beta_{21}^2 + \beta_{31}^2} \right| \\ &= \left| \beta_{11} \right| \left[ (1) \right] + \left| \beta_{21} \right| \left[ (2) \right] + \left| \beta_{31} \right| \left[ (3) \right] \end{aligned}$$

$$\begin{aligned}
 y &= \left| \beta_{21} \begin{bmatrix} (1) \end{bmatrix} \right| + \left| \beta_{22} \begin{bmatrix} (2) \end{bmatrix} \right| + \left| \beta_{23} \begin{bmatrix} (3) \end{bmatrix} \right| \\
 \theta &= \left| \beta_{31} \begin{bmatrix} (1) \end{bmatrix} \right| + \left| \beta_{23} \begin{bmatrix} (2) \end{bmatrix} \right| + \left| \beta_{33} \begin{bmatrix} (3) \end{bmatrix} \right|
 \end{aligned}$$

3.3 Computer program. As an aid to calculating the coupled natural frequencies for three-degree-of-freedom systems a computer program in Fortran language is included for the direct solution of three mass systems (System 1) and one mass systems (System 2). It is noted that the frequency equation solved is of the form

$$\omega^6 + \alpha\omega^4 + \beta\omega^2 + \gamma = 0 \quad (\text{A-55})$$

Although the computer program is written specifically for the two systems discussed in 3.1 and 3.2 herein, other systems may be handled by an appropriate adjustment of the constants  $\alpha$ ,  $\beta$  and  $\gamma$  in the program.

```

101. = CF PROGRAM CUBIC
102. = CALL COPY(103.,106.)
103. = * READ THE SYSTEM PARAMETERS INTO THE PROGRAM IN THE IN-LB-SEC OR
104. = * ANY OTHER COMPATIBLE SYSTEM OF UNITS
105. = * TO SOLVE FOR THE NATURAL FREQUENCIES OF SYSTEM 1 TYPE START(108.)
106. = * TO SOLVE FOR THE NATURAL FREQUENCIES OF SYSTEM 2 TYPE START(125.)
107. = PAUSE
108. = CALL COPY(109.,110.)
109. = * ENTER THE VALUE OF THE MASSES M1,M2,M3 AND THE SPRING CONSTANTS
110. = * K1,K2,K3
111. = CF READ O,W1,W2,W3,S1,S2,S3
112. = C DEFINITION OF SYSTEM CONSTANTS
113. = OMEGA1=S1/W1
114. = OMEGA2=S2/W2
115. = OMEGA3=S3/W3
116. = AMBDA2=S1/S2
117. = AMBDA3=S2/S3
118. = ALPHA=-(OMEGA1+OMEGA2*(1.+AMBDA2)+OMEGA3*(1.+AMBDA3))
119. = OBETA=OMEGA1*OMEGA2+OMEGA1*OMEGA3*(1.+AMBDA3)+OMEGA2*OMEGA3*(1.+AMB
120. = GAMMA=-(OMEGA1*OMEGA2*OMEGA3)
121. = GO TO 1
122. = 3 CALL COPY(123.,124.)
123. = * ENTER THE VALUE OF THE MASS M, MOMENT OF INERTIA J, SPRING
124. = * CONSTANTS KX,KZ,KO AND THE ECCENTRICITIES RX,RZ
125. = CF READ O,W,W2,SX,SZ,SO,RX,RZ
126. = C DEFINITION OF SYSTEM CONSTANTS
127. = OMEGA1=SX/W
128. = OMEGA2=SZ/W
129. = OMEGA3=SO/W2
130. = RHO=W2/W
131. = ALPHA=-(OMEGA1+OMEGA2+OMEGA3+(OMEGA1*RZ**2+OMEGA2*RX**2))/RHO)
132. = OBETA=OMEGA1*OMEGA2+OMEGA1*OMEGA3+OMEGA2*OMEGA3+OMEGA1*OMEGA2*(RX**
133. = GAMMA=-(OMEGA1*OMEGA2*OMEGA3)
134. = 1 A=1./3.*(3.*BETA-ALPHA**2)
135. = B=1./27.*(2.*ALPHA**3-9.*ALPHA*BETA+27.*GAMMA)
136. = PHI=ARCOS(B/2./SQRT(-(A**3/27.)))
137. = PHI=PHI+3.1415927
138. = C SOLUTIONS TO THE FREQUENCY EQUATION IN CPS
139. = F1=1./(2.*3.1415927)*SQRT(2.*SQRT(-(A/3.))*COS(PHI/3.)-ALPHA/3.)
140. = OF2=1./(2.*3.1415927)*SQRT(2.*SQRT(-(A/3.))*COS(PHI/3.+2.*3.1415927
141. = OF3=1./(2.*3.1415927)*SQRT(2.*SQRT(-(A/3.))*COS(PHI/3.+4.*3.1415927
142. = PRINT 100
143. = 100 FORMAT(3X,9HFREQ NO 1,7X,9HFREQ NO 2,7X,9HFREQ NO 3)
144. = PRINT 101
145. = 101 FORMAT(6X,3HCPS,13X,3HCPS,13X,3HCPS,/)
146. = PRINT 102,F1,F2,F3
147. = 102 FORMAT(3E16.8)
148. = PAUSE
149. = END

```

## APPENDIX B

### USEFUL RELATIONSHIPS IN STRUCTURAL MECHANICS

It is beyond the scope of this report to derive analytical formulae for design of structures exposed to air blast and ground shock; the purpose of the report is to present design procedures for in-structure systems. It is, however, necessary to understand the behavior of structures under dynamic loads in order to consider their effect on the input motions at the support points of the in-structure systems.

This appendix includes some basic relationships in structural mechanics that are useful in calculating structure enclosure resistances and frequencies. They are extracted from existing manuals on protective construction design; moreover, they are used without derivation in Section 4 of this report where the effect of the structural enclosure on input motions is discussed. For background information, the following references are recommended:

- B.1 Corps of Engineer Manuals Em 1110-345-413 to 418 "Design of Structures to Resist the Effects of Atomic Weapons".
- B.2 Design Manual AEC Test Structures, December 1961
  - Volume I: Nuclear Weapon Effects
  - Volume II: Structural Response Characteristics Under Dynamic Loads
  - Volume III: Design of Blast Resistance Structures.
- B.3 Air Force Design Manual - Principles and Practices for Design of Hardened Structures AFWL-TDR-62-138, December 1962.
- B.4 ASCE Manual 42: Design of Structures to Resist Nuclear Weapons Effects, 1961.

Symbols are defined where they first appear in the following subsections. The relationships are based on consistent units.

1. Yield resistance. The yield resistance force  $R$  is defined as the total load (applied statically with uniform intensity) that will make a structural element reach its elastic capacity. Only flexural properties of beams and shells will be considered since most structures are designed to yield in flexure initially.

a. Simply supported beam.

Reinforced Concrete:  $R = .075 \frac{\phi b d^2 f_y}{L}$  (B-1)

where

$\phi$  = percent tension reinforcing steel at beam centerline

b = beam width

d = effective depth

$f_y$  = yield strength of reinforcing steel

L = beam length

Steel:  $R = 8 f_y Z/L$  (B-2)

$R = 9.2 f_y S/L$  for WF sections about stiff axis

where

Z = plastic section modulus

S = section modulus

b. Beam - one fixed support, one hinged

Reinforced Concrete:  $R = .075 (\phi + \phi'/2) f_y b d^2/L$  (B-3)

$\phi'$  = percent tension reinforcing steel at fixed support

Steel:  $R = 12 f_y Z/L$  (B-4)

c. Beam - both ends with equal fixity

Reinforced Concrete:  $R = .075 (\phi + \phi') f_y b d^2/L$  (B-5)

Steel:  $R = 16 f_y Z/L$  (B-6)

d. Two-way reinforced concrete slabs

$$R_2 = C R_1 \quad (B-7)$$

where

$R_1$  = resistance of a one-way slab spanning in short direction (lbs), obtained from beam formulas.

$R_2$  = resistance of two-way slab.

$C$  = correction factor for two-way action

$$C = 1 + \alpha \left[ \frac{1}{6 - 4\alpha} + \frac{3}{2} \frac{\phi_L + \phi'_L}{\phi_s + \phi'_s} \right] \quad (B-8)$$

where

$\alpha$  = ratio of short span to long span

$L, s$  = subscripts; L refers to reinforcing steel parallel to longest dimension, and s refers to reinforcing steel parallel to shortest dimension.

e. Reinforced concrete dome

The yield resistance for a dome is denoted by  $q$ , and is given in load per unit area.

Compression Mode:  $q_c = (1.7f'_c + 0.018 \phi_t f_y) \frac{t_c}{r} \quad (B-9)$

$q_c$  = resistance in terms of uniform radial pressure

$\phi_t$  = total percent reinf. steel on both faces

$f'_c$  = concrete compression strength

$t_c$  = concrete thickness required for compressive mode

$r$  = radius of dome

e. continued

$$\text{Flexural Mode: } q_f = (0.85f'_c + .009 \phi_t f_r) \frac{t_f}{r} \quad (\text{B-10})$$

$t_f$  = concrete thickness required for flexure mode.

$q_f$  = average resistance (in psi) over one quadrant of the dome.

The required thickness is taken as the sum of the above two thicknesses.

$$t_{\text{total}} = t_c + t_f$$

2. Natural periods and load-mass factors. Natural periods in the flexural modes are given for the elements described in Subsection 1 above assuming uniform sectional properties. (For deep beam elements shear deformations must also be considered.)

a. Simply supported beam

Reinforced Concrete: (Based on cracked section)

$$T = \frac{1}{3600(\text{fps})} \frac{L}{d} \frac{L}{\sqrt{\phi}} \quad (\text{B-11})$$

where

T = period of vibration

L = Length of span in feet

d = effective depth (feet)

Steel:

$$\text{WF Section, } T = \frac{1}{26,400(\text{fps})} \frac{L}{\phi} L \quad \text{and} \quad (\text{B-12})$$

$$\text{rectangular section, } T = \frac{L}{t} \frac{L}{6900(\text{fps})} \quad (\text{B-13})$$

2.a continued

where

$\rho$  = radius of gyration in feet

t = thickness in feet

b. Beam-one fixed support, one hinged

Reinforced Concrete:

$$T = \frac{1}{5260(\text{fps})} \frac{L}{d} \frac{L}{\sqrt{\phi}} \text{ sec} \quad (\text{B-14})$$

Steel:

WF Section

$$T = \frac{1}{38600(\text{fps})} \frac{L}{e} L \quad (\text{B-15})$$

c. Beam- both ends with equal fixity

Reinforced Concrete:

$$T = \frac{1}{7200(\text{fps})} \frac{L}{d} \frac{L}{\sqrt{\phi}} \quad (\text{B-16})$$

Steel:

WF Section

$$T = \frac{1}{52,800(\text{fps})} \frac{L}{e} L \quad (\text{B-17})$$

d. Two-way reinforced concrete slabs for simple support all four sides:

$$k = \left(77 + \frac{180}{\alpha^3}\right) \frac{EI}{L^4} \text{ psi/inch} \quad (\text{B-18})$$



2.d continued

where

k = stiffness, (uniform load/area to cause unit center deflection) all other terms have been previously defined.

$$T = 5.3 \sqrt{\frac{m}{k}} \quad (\text{B-19})$$

where

$\alpha$  = short span/long span

m = mass per unit area

Reinforced Concrete Slabs  
For fixed supports all four sides

$$k = \left( 307 + \frac{500}{\alpha^3} \right) \frac{EI}{L^4} \quad (\text{B-20})$$

$$T = 4.5 \sqrt{\frac{m}{k}} \quad (\text{B-21})$$

e. Reinforced concrete dome

In compression mode or flexure mode

$$T = \frac{r}{2500 \text{ fps}} \quad (\text{B-22})$$

where

r = radius in feet

f. Fixed-end beam with middle support



$$T_1 = 0.407 L^2 \sqrt{\frac{A_Y}{EIg}} \text{ seconds (first mode)}$$

$$T_2 = 0.69 T_1 \text{ seconds (second mode)}$$

$$T_3 = 0.25 T_1 \text{ seconds (third mode)}$$

$A_Y$  = weight per unit length

3. Yield Deflections. The yield deflection is defined as the deflection of a structural element when the stress at the critical section reaches the yield stress value for the material used. Some approximate relationships are given below for typical structural elements which have predominately flexure flexibility. The concrete and steel properties are assumed to be:

Concrete dynamic compressive strength and reinforcing steel yield strength;  $f'_{yd} = 4000 \text{ psi}$ ,  $f_y = 50,000 \text{ psi}$ .

Structural steel dynamic yield and modulus;  $f'_{yd} = 42,000 \text{ psi}$ ,  
 $E = 30,000,000 \text{ psi}$ .

a. Simple supported beams

Reinforced Concrete:  $\delta_y = \left(\frac{L^2}{d}\right)/3800$  (B-24)

where

$\delta_y$  = yield deflection

other symbols have been previously defined

Steel:

(WF sections)

$$\delta_y = \left(\frac{L^2}{d}\right)/3000$$
 (B-25)

d = depth of beam

b. Beam-one fixed support, one hinged

Reinforced Concrete:

$$\delta_y^* = \left(\frac{L^2}{d}\right)/5430 \quad (\text{B-26})$$

Steel:

(WF section)

$$\delta_y^* = \left(\frac{L^2}{d}\right)/4290 \quad (\text{B-27})$$

c. Beam-both ends with equal fixity

Reinforced Concrete:

$$\delta_y^* = \left(\frac{L^2}{d}\right)/7600 \quad (\text{B-28})$$

Steel:

(WF section)

$$\delta_y^* = \left(\frac{L^2}{d}\right)/6000 \quad (\text{B-29})$$

---

\*The yield deflections are effective values lying between the yield deflection when yield begins at the supports and the yield deflection when yield begins at the mid-point.

## APPENDIX C

### NUMERICAL METHODS

#### 1. Introduction

The class of problems considered in this section are of the simultaneous ordinary differential equation type with constant or variable coefficients and describe specifically the motion of single-mass three-degree-of-freedom systems which appear in Section 5. Two methods are presented:

- (1) Approximate single-step integration methods (used in Example 5.9).
- (2) More precise predictor-corrector methods.

#### 2. Equations of Motion

A typical set of dynamical equations is taken from Section 5.4 for the base-mounted system and for convenience are reproduced here

$$\begin{aligned}
 m\ddot{x} + 2k_q (x - x_s - R_z \theta) &= 0 \\
 m\ddot{z} + 2k_r (z - z_s - R_x \theta) &= 0 \\
 J\ddot{\theta} + 2k_q \left\{ \left[ R_z^2 + R_x (x - x_s) \right] \theta - R_z (x - x_s) \right\} + 2k_r \left\{ \left[ b^2 + R_x^2 \right. \right. \\
 &\quad \left. \left. - R_z (z - z_s) \right] \theta - R_x (z - z_s) \right\} - mgR_z \theta + \left\{ 2k_q \left[ R_x (x - x_s) \right] \right. \\
 &\quad \left. + 2k_r \left[ b^2 - R_z (z - z_s) \right] - mgR_x \right\} \beta_0 - mgR_x = 0
 \end{aligned} \tag{C-1}$$

It will be recalled that a simpler, less accurate form of these equations was presented in Section 5.4 as follows:

$$\begin{aligned}
 m\ddot{x} + 2k_q (x - x_s - R_z \theta) &= 0 \\
 m\ddot{z} + 2k_r (z - z_s - R_x \theta) &= 0 \\
 J\ddot{\theta} + 2k_q \left[ R_z^2 \theta - R_z (x - x_s) \right] + 2k_r b^2 \theta &= 0
 \end{aligned} \tag{C-2}$$

The second set of equations (C-2) will be solved by the one step method. The first set of equations (C-1) will be solved using the predictor-corrector methods where the accuracy of the numerical technique is compatible with the accuracy of the equations.

#### 3. Solution by One-Step Integration

The second set of equations is transformed into the following equivalent set:

$$\begin{aligned}
\omega_x^2 (y_1 - R_z \theta) &= -\ddot{y}_1 - \ddot{x}_s \\
\omega_z^2 (y_2 - R_x \theta) &= -\ddot{y}_2 - \ddot{z}_s \\
\omega_\theta^2 \theta - \frac{\omega_x^2 R_z}{\rho^2} y_1 &= -\ddot{\theta}
\end{aligned}
\tag{C-3}$$

where

$$\begin{aligned}
y_1 &= x - x_s \\
y_2 &= z - z_s \\
\omega_x^2 &= \frac{2k_q}{m} \\
\omega_z^2 &= \frac{2k_r}{m} \\
\omega_\theta^2 &= \frac{2k_q R_z^2 + 2k_r b^2}{J} \\
\rho^2 &= \frac{J}{m}
\end{aligned}$$

Equations (C-3) may be integrated over a small but finite interval of time and velocity to yield:

$$\begin{aligned}
\int_{t_1}^{t_2} \omega_x^2 (y_1 - R_z \theta) dt &= - \int_{\dot{y}_{11}}^{\dot{y}_{12}} d\dot{y}_1 - \int_{\dot{x}_{s1}}^{\dot{x}_{s2}} d\dot{x}_s \\
\int_{t_1}^{t_2} \omega_z^2 (y_2 - R_x \theta) dt &= - \int_{\dot{y}_{21}}^{\dot{y}_{22}} d\dot{y}_2 - \int_{\dot{z}_{s1}}^{\dot{z}_{s2}} d\dot{z}_s
\end{aligned}
\tag{C-4}$$

$$\int_{t_1}^{t_2} \left( \omega_{\theta}^2 - \frac{\omega^2 R_z}{\rho^2} y_1 \right) dt = - \int_{\dot{\theta}_1}^{\dot{\theta}_2} d\dot{\theta}$$

As a first approximation of the finite integration formulae, the following derivation is presented:

$$dv = a dt$$

$$\int_{v_1}^{v_2} dv = \int_{t_1}^{t_2} a dt$$

Let

$$a = \frac{a_1 + a_2}{2}$$

Hence

$$v_2 = \frac{a_1 + a_2}{2} (t_2 - t_1) + v_1 \quad (C-5)$$

where

a = acceleration

b = velocity

d = displacement

Similarly

$$d_2 = \frac{\Delta t}{2} (v_1 + v_2) + d_1 \quad (C-6)$$

The left hand side of equations (C-4) are the form  $\int_{t_1}^{t_2} F dt$  which are approximated as

$$\int_{t_1}^{t_2} F dt = \frac{F_1 + F_2}{2} (t_2 - t_1) = (F_1 + F_2) \frac{\Delta t}{2} \quad (C-7)$$

Equations (C-4) can therefore be reproduced as the difference equations in matrix notation

$$\begin{bmatrix} \frac{\omega_x^2 \Delta t}{2} + \frac{2}{\Delta t} & 0 & -\frac{\omega_{xz}^2 R \Delta t}{2} \\ 0 & \frac{\omega_z^2 \Delta t}{2} + \frac{2}{\Delta t} & -\frac{\omega_{zx}^2 R \Delta t}{2} \\ -\frac{\omega_{xx}^2 R \Delta t}{2\rho^2} & 0 & \frac{\omega_\theta^2 \Delta t}{2} + \frac{2}{\Delta t} \end{bmatrix} \cdot \begin{Bmatrix} y_{12} \\ y_{22} \\ \theta_2 \end{Bmatrix} =$$

$$\begin{bmatrix} -\frac{\omega_x^2 \Delta t}{2} + \frac{2}{\Delta t} & 0 & \frac{\omega_{xz}^2 R \Delta t}{2} \\ 0 & -\frac{\omega_z^2 \Delta t}{2} + \frac{2}{\Delta t} & \frac{\omega_{zx}^2 R \Delta t}{2} \\ \frac{\omega_{xx}^2 R \Delta t}{2\rho^2} & 0 & -\frac{\omega_\theta^2 \Delta t}{2} + \frac{2}{\Delta t} \end{bmatrix} \cdot \begin{Bmatrix} y_{11} \\ y_{21} \\ \theta_1 \end{Bmatrix} +$$

$$\begin{Bmatrix} 2\dot{y}_{11} + \dot{x}_{s1} - \dot{x}_{s2} \\ 2\dot{y}_{21} + \dot{z}_{s1} - \dot{z}_{s2} \\ 2\dot{\theta}_1 \end{Bmatrix} \quad (C-8)$$

which can be solved simultaneously for the current response values  $y_{12}$ ,  $y_{22}$ , and  $\theta_2$  in terms of the previous values  $y_{11}$ ,  $y_{21}$ ,  $\theta_1$ ,  $\dot{y}_{11}$ ,  $\dot{y}_{21}$ ,  $\dot{\theta}_1$  and the ground motion velocity functions  $\dot{x}_s$  and  $\dot{z}_s$ .

The problem is started by assigning initial conditions usually  $y_{11} = y_{21} = \theta_1 = \dot{y}_{11} = \dot{y}_{21} = \dot{\theta}_2 = 0$ . The relative velocities are calculated from equation (C-6). The absolute accelerations may be determined by direct substitution of the relative displacements in equations (C-2).

It should be noted that the one-step method described herein is to be used to obtain approximate engineering results and, in general, cannot be assumed to be accurate over a large response time. For example, the time step is usually taken as 1/10 to 1/20 of the smallest uncoupled natural period of the system. A comparison of the numerical solution with the exact solution may indicate a drift in as early as the first period of oscillation. The drift may occur in either frequency or amplitude or both. Accuracies can usually be improved by taking a smaller time increment, however, no simple means is available for measuring the error. The general method used to confirm the accuracy is to compare the responses corresponding to successively smaller time steps until no additional improvement in accuracy can be obtained. Even then, instability of the numerical technique may be a problem so that the results obtained may still differ significantly from the time response. For the case where accurate response histories are desired the following method is recommended.

#### 4. Solution By Predictor-Corrector Method

The solution of the equations of motion (C-1) will be obtained by a combination of one-step (Runge-Kutta) and multi-step (Adams-Bashforth) methods which go to make up the predictor-corrector method considered here. The original set of three second-order differential equations are reduced to the following set of first order differential equations:

$$\begin{aligned}
 (1) \quad \dot{x} &= X_1 \\
 (2) \quad \dot{X}_1 &= -\omega_x^2(x - x_s - R_z \theta) \\
 (3) \quad \dot{z} &= Z_1 \\
 (4) \quad \dot{Z}_1 &= -\omega_z^2(z - z_s - R_x \theta)
 \end{aligned}
 \tag{C-9}$$



(C-9)  
continued

$$(5) \quad \dot{\theta} = \theta_1$$

$$(6) \quad \ddot{\theta} = -\omega_{\theta}^2 \theta - \frac{1}{\rho^2} \left\langle \left[ \omega_x^2 R_x (x - x_s) - \omega_z^2 R_z (z - z_s) \right] \theta \right. \\ \left. - \omega_x^2 R_z (x - x_s) - \omega_z^2 R_x (z - z_s) - g R_x + \left\{ \omega_x^2 \left[ R_x (x - x_s) \right] \right. \right. \\ \left. \left. + \omega_z^2 \left[ b^2 - R_z (z - z_s) \right] - g R_z \right\} \beta_0 \right\rangle$$

where

$$\omega_x^2 = \frac{2k_q}{m}$$

$$\omega_z^2 = \frac{2k_r}{m}$$

$$\omega_{\theta}^2 = \frac{2k_q R_z^2 + 2k_r (b^2 + R_x^2) - mg R_z}{J}$$

$$\rho^2 = J/m.$$

It is convenient to make a variable change in the six equations (C-9) to obtain standard notation for the discussion which follows.

Let

$$\begin{Bmatrix} y_1 \\ y_2 \\ y_3 \\ y_4 \\ y_5 \\ y_6 \end{Bmatrix} = \begin{Bmatrix} x \\ X_1 \\ z \\ Z_1 \\ \theta \\ \theta_1 \end{Bmatrix} = \begin{Bmatrix} x \\ \dot{x} \\ z \\ \dot{z} \\ \theta \\ \dot{\theta} \end{Bmatrix} \quad (C-10)$$

and

$$\begin{Bmatrix} f_1 \\ f_2 \\ f_3 \\ f_4 \\ f_5 \\ f_6 \end{Bmatrix} = \begin{Bmatrix} y_2 \\ -\omega_x^2(y_1 - x_s - R_z y_5) \\ y_4 \\ -\omega_z^2(y_5 - z_s - R_x y_5) \\ y_6 \\ \left( -\omega_\theta^2 y_5 - \frac{1}{\rho^2} \left\langle \left[ \omega_x^2 R_x (y_1 - x_s) - \omega_z^2 R_z (y_3 - z_s) \right] y_5 \right. \right. \\ \left. \left. - \omega_x^2 R_x z (y_1 - x_s) - \omega_z^2 R_z x (y_3 - z_s) - g R_x \right. \right. \\ \left. \left. + \left\{ \omega_x^2 R_x (y_1 - x_s) + \omega_z^2 \left[ b^2 - R_z (y_3 - z_s) \right] - g R_z \right\} \beta_0 \right\rangle \right) \end{Bmatrix} \quad (C-11)$$

so that

$$\begin{Bmatrix} \dot{y}_1 \\ \dot{y}_2 \\ \dot{y}_3 \\ \dot{y}_4 \\ \dot{y}_5 \\ \dot{y}_6 \end{Bmatrix} = \begin{Bmatrix} f_1 \\ f_2 \\ f_3 \\ f_4 \\ f_5 \\ f_6 \end{Bmatrix} \quad (C-11a)$$

Equations (C-11a) may be solved directly for the variables of (C-10), (viz.,  $y_i$ ,  $i = 1, 2, \dots, 6$ ) in both the one-step and multi-step modes to be discussed below. It is noted that these solutions correspond to the absolute displacements and velocities in the prime coordinate system. The absolute accelerations can be obtained by substitution into equations (C-11), (viz.,  $f_i$ ,  $i = 2, 4, 6$ ).

### One-Step Method (Runge-Kutta)

The Fourth Order Runge-Kutta Method has become a standard numerical analyses technique particularly when used in conjunction with a predictor-corrector method. Like all one-step methods, no readily obtainable means is available for computing errors so that the Runge-Kutta method is seldom used as an independent means of solving differential equations.\* It is, however, useful in starting or restarting an interrupted predictor-corrector analysis. This usefulness stems from the fact that current values of the variable are dependent only on the immediately preceding value and differentiations (undesirable in numerical analyses) need not be performed.

The Fourth Order Runge-Kutta Method is defined by the equation

$$y_{i,m+1} = y_{i,m} + \frac{h}{6}(k_{i,1} + 2k_{i,2} + 2k_{i,3} + k_{i,4}) \quad (C-12)$$

where

$$k_{i,1} = f_i(t_m, y_{n,m})$$

$$k_{i,2} = f_i\left(t_m + \frac{h}{2}, y_{n,m} + \frac{hk_{n,1}}{2}\right)$$

$$k_{i,3} = f_i\left(t_m + \frac{h}{2}, y_{n,m} + \frac{hk_{n,2}}{2}\right)$$

$$k_{i,4} = f_i(t_m + h, y_{n,m} + hk_{n,3})$$

t = time

h = step size.

The subscript i refers to the ith variable or function; the subscript m refers to the mth time step; and the subscript n refers to the particular variables in the ith variable.

For example, to evaluate the second variable of equations (C-10) (viz.,  $y_2 = \dot{x}$ ) in the first time step, equation (C-12) becomes:

$$y_{2,1} = y_{2,0} + \frac{h}{6}(k_{2,1} + 2k_{2,2} + 2k_{2,3} + k_{2,4})$$

---

\* See References C.2, C.4 and C.5 for a complete treatment of the Runge-Kutta Method.

where

$$k_{2,1} = -\omega_x^2 (-x_s \Big|_{t=t_0} + y_{1,0} - R_z y_{5,0})$$

$$k_{2,2} = -\omega_x^2 \left[ -x_s \Big|_{t=t_0+h/2} + y_{1,0} + \frac{hk_{1,1}}{2} - R_z (y_{5,0} + \frac{hk_{5,1}}{2}) \right]$$

$$k_{1,1} = y_{2,0} \quad k_{5,1} = y_{6,0}$$

$$k_{2,3} = -\omega_x^2 \left[ -x_s \Big|_{t=t_0+h/2} + y_{1,0} + \frac{hk_{1,2}}{2} - R_z (y_{5,0} + \frac{hk_{5,2}}{2}) \right]$$

$$k_{1,2} = y_{2,0} + \frac{hk_{2,1}}{2} \quad k_{5,2} = y_{6,0} + \frac{hk_{5,2}}{2}$$

$$k_{2,4} = -\omega_x^2 \left[ -x_s \Big|_{t=t_0+h} + y_{1,0} + hk_{1,3} - R_z (y_{5,0} + hk_{5,3}) \right]$$

$$k_{1,3} = y_{2,0} + \frac{hk_{2,2}}{2} \quad k_{5,3} = y_{6,0} + \frac{hk_{5,2}}{2}$$

If  $t_0 = 0$  and the system starts from static equilibrium and the ground displacements  $x_s$  and  $z_s$  are at the point of incipient motion there follows:

$$k_{2,1} = 0$$

$$k_{1,1} = 0$$

$$k_{5,1} = 0$$

$$k_{2,2} = \omega_x^2 \left[ -x_s \Big|_{t=h/2} \right]$$

$$k_{1,2} = 0$$

$$k_{5,2} = 0$$

$$k_{2,3} = -\omega^2 \left[ -x_s \Big|_{t=h/2} \right]$$

$$k_{1,3} = -\frac{\omega^2 h}{2} \left[ -x_s \Big|_{t=h/2} \right]$$

$$k_{5,3} = 0$$

$$k_{2,4} = -\omega^2 \left[ -x_s \Big|_{t=h} - \frac{h^2 \omega^2}{2} (-x_s \Big|_{t=h/2}) \right]$$

Hence

$$y_{2,1} = \frac{h}{6} \left\{ \begin{aligned} & -2\omega^2 (-x_s \Big|_{t=h/2}) - 2\omega^2 (-x_s \Big|_{t=h/2}) \\ & -2\omega^2 \left[ -x_s \Big|_{t=h} - \frac{h^2 \omega^2}{2} (-x_s \Big|_{t=h/2}) \right] \end{aligned} \right\}$$

which is the velocity  $\dot{x}$  after the first step  $h$ .

The magnitude of the time increment  $h$  is initially chosen as 1/10 of the smallest uncoupled natural period of the system. Using this step size, the parameters of the Runge-Kutta equation are thus determined. Collatz (Reference C-1) suggests that if

$$\left| \frac{k_{i,2} - k_{i,3}}{k_{i,1} - k_{i,2}} \right| > 0.03$$

then the step size is too large and should be reduced. Each time that the step size is changed, the Runge-Kutta parameters must be re-evaluated. It therefore follows that a change in step size necessitates recalculation of the six response variables in (C-10). Step size changes and Runge-Kutta

restarts are required under the following conditions:

- (1) to satisfy the Collatz criteria
- (2) to satisfy the truncation and error criteria of the predictor-corrector analysis discussed in the following subsection.

#### Predictor-Corrector Method

Predictor-corrector formulae are especially useful because they

- (1) can be made computationally efficient
- (2) provide error magnitudes.

On the other hand, they are not self-starting so that a one-step method is necessary for the initial start or for restarts caused by a step-size change.

Since most of the computation occurs in the predictor-corrector mode, care must be taken that the results obtained are realistic. This is accomplished by placing various restrictions on the calculations. Accuracy and efficiency are maintained by varying the step size  $h$  as the program progresses.

A variety of predictor-corrector formulae are available for computation. Each has certain advantages and disadvantages (see Reference C-2) which make it more or less attractive for certain types of problems. For clarity, one such method is discussed here, the Adams-Bashforth "2/3" method, which is accurate and also insures against instability for most applications.

The predictor equation is:

$$y_{i,m+1} = 2/3y_{i,m-1} + 1/3y_{i,m-2} + \frac{h}{72}(191f_{i,m} - 107f_{i,m-1} + 109f_{i,m-2} - 25f_{i,m-3}) + \frac{707}{2160} h^5 y^{(5)}(\theta) \quad (C-13)$$

The corrector equation is

$$y_{i,m+1} = 2/3y_{i,m-1} + 1/3y_{i,m-2} + \frac{h}{72}(25f_{i,m+1} + 91f_{i,m} + 43f_{i,m-1} + 9f_{i,m-2}) - \frac{43}{2160} h^5 y^{(5)}(\theta) \quad (C-14)$$

It can be seen that initially the first term which can be operated on in the predictor is  $y_{i,4}$  which requires that  $y_{i,3}, y_{i,2}, y_{i,1}, y_{i,0}, f_{i,3}, f_{i,2}, f_{i,1}$  and  $f_{i,0}$  be known. These terms are supplied by the Runge-Kutta Method.

For example, suppose that the variables and functions  $y_{i,m}, f_{i,m}, i = 1, 2, \dots, 6, m=0, 1, 2, 3$  are known from the Runge-Kutta analysis. Then, the predictor  $y_{i,4}, i=1, 2, 3, \dots, 6$  can be evaluated from equation (C-13). This in turn allows the functions  $f_{i,4}, i=1, 2, 3, \dots, 6$  to be computed from Equation C-11). Thenceforth, equations (C-14) and (C-11) can be solved alternately until no perceptible change between succeeding values of  $y_{i,4}, i=1, 2, 3, \dots, 6$  in the corrector equation (C-14) can be obtained.

If  $y_{i,m+1}^j$  is the  $j$ th evaluation of the corrector equation of the  $y_i^{\text{th}}$  variable in the  $m+1$  step then an idea of the convergence of the iteration is obtained from  $|y_{i,m+1}^{j+1} - y_{i,m+1}^j|$ . The iteration can be carried out until the absolute value of the difference is less than some preassigned value. Hull and Creemer (Reference C-3) suggest that the most efficient number of operations on the corrector is two. Therefore, one method of establishing the step size  $h$  is satisfaction of the inequality  $|y_{i,m+1}^2 - y_{i,m+1}^1| \leq \epsilon$  in at most two iterations where  $h$  is varied until the requirement is met. The value of  $\epsilon$  is allowed to vary between  $10^{-7}$  and  $10^{-4}$ .

The assumption of a finite number of terms in the predictor-corrector formulae carries with it inherent truncation errors. The truncation error in the predictor is, from (C-13),  $\frac{707}{2160} h^5 y^{(5)}(\theta)$  and in the corrector it is from (C-14),  $-\frac{43}{2160} h^5 y^{(5)}(\theta)$ . If  $Y_{i,m+1}$  is the true value of variables at  $t = t_{m+1}$ , and  $p_{i,m+1}$  and  $c_{i,m+1}^{j+1}$  are the predicted and corrected values of the variables from the preceding formulae then the following approximate relationships can be asserted

$$Y_{i,m+1} \approx p_{i,m+1} + \frac{707h^5 y^{(5)}(\theta)}{2160}$$

$$Y_{i,m+1} \approx c_{i,m+1}^{j+1} - \frac{43}{2160} h^5 y^5(\theta)$$

Then

$$y^5(\theta) \approx \frac{72}{25h^5} (c_{i,m+1}^{j+1} - p_{i,m+1})$$

so that the absolute truncation error in the corrector  $E_T^c \approx -\frac{43}{2160} h^5 y^5(\theta)$  is given by

$$E_T^c \approx -\frac{43}{750} (c_{i,m+1}^{j+1} - p_{i,m+1})$$

and the relative error is,

$$E_{T,R}^c \approx \frac{-43}{750} \frac{c_{i,m+1}^{j+1} - p_{i,m+1}}{c_{i,m+1}^{j+1}}$$

It is important that the relative error remain bounded within a specified limit throughout the calculations since an expanding or oscillating relative error indicates instability in the solution.

Finally, from the truncation error

$$E_T^c \approx Y_{i,m+1} - c_{i,m+1}^{j+1} = \frac{-43}{750} (c_{i,m+1}^{j+1} - p_{i,m+1})$$

the final value of the corrector can be adjusted to account for the "mop up" error so that

$$y_{i,m+1} \approx \frac{1}{750} (43p_{i,m+1} + 707c_{i,m+1}^{j+1})$$

##### 5. Implementation of the Formulae

The combined utilization of the Runge-Kutta and predictor-corrector methods can be systematized according to the following step-by-step procedure:

- (1) Reduce the original set of differential equations (C-1) into an equivalent set of first order differential equations (C-9).



- (2) Assume a step size  $h$ . As a starting point  $h = \frac{T}{10}$  where  $T$  is the smallest uncoupled natural period of the system.
- (3) Compute variables (C-10) for one or two time steps using the Runge-Kutta formulas (C-13). Check the suitability of the step size from the criteria:

$$\left| \frac{k_{i,2} - k_{i,3}}{k_{i,1} - k_{i,2}} \right| > 0.03.$$

- (4) If the step size is suitable, compute variables and functions for three steps from equations (C-10 and C-11).
- (5) Assume a convergence factor  $\epsilon$  and absolute and relative error bounds  $E_T^C$  and  $E_{T,R}^C$ . These may be allowed to vary in range  $10^{-7}$  to  $10^{-4}$ . Some experimentation may be required.
- (6) Using the step size in the last evaluation of the Runge-Kutta computations, compute one predictor (C-13) and two correctors (C-14) for each of the variables (C-10) and check convergence factors and truncation errors. If the step size is suitable compute the final value of the variables from the "mop up" formula and proceed to next time step repeating the predictor-corrector operation as before.
- (7) If the step size is too large, i.e. convergence and errors are too large (greater than  $10^{-4}$ ), halve the step size and repeat the above procedures beginning with the initial conditions and Runge-Kutta methods. This procedure is repeated until convergence factors and errors are within acceptable limits.

- (8) If the step size is too small i.e., convergence and errors are smaller than desired (less than  $10^{-7}$ ), the step size should be doubled and the Runge-Kutta-predictor-corrector procedures repeated as before.
- (9) With the proper step size, several or many steps may be repeated in the predictor-corrector mode with the convergence and error remaining within specified limits. If and when a step size change becomes necessary it is only necessary to go back to the last acceptable computation, halve or double the step size  $h$ , and begin the Runge-Kutta-predictor-corrector calculations from that point.

Additional background on numerical methods can be found in References C.4 through C.6.

## APPENDIX D

### COMPUTER PROGRAM FOR INCLINED PENDULUM SYSTEM RESPONSE

The inclined pendulum system considered is described in Section 5.5. The equations of motion are defined by Equations 5.18, 5.19, and 5.20 and the configuration is shown in Figures 5.29 and 5.32.

The method of analysis is described in the following subsections and General Flow Diagrams with necessary subroutines are also presented.

(The computer step by step program is available)

## 1.0 INTRODUCTION

THE PURPOSE OF THIS PROGRAM IS TO ANALYZE THE RESPONSE OF A DYNAMIC MODEL TO TIME-DEPENDENT FORCING FUNCTIONS. MATHEMATICALLY THE PROBLEM REDUCES TO THE SOLUTIONS OF SIMULTANEOUS DIFFERENTIAL EQUATIONS. THE RUNGE-KUTTA-GILL METHOD OF NUMERICAL SOLUTION OF FIRST DERIVATIVES IS USED ALONG WITH THE HAMMING METHOD FOR CONTROL OF TRUNCATION ERRORS. PROGRAMMING IS IN THE FORTRAN CODING LANGUAGE AND IS ORGANIZED AS A SET OF SEPARATE SUBROUTINES FOR EACH PHASE OF INPUT, SOLUTION AND OUTPUT. EXTENTIONS AND/OR MODIFICATIONS TO THE PROGRAM MAY READILY BE MADE.

## 2.0 DYNAMIC MODEL

THE DYNAMIC MODEL CONSISTS OF A RIGID MASS SUPPORTED AT FOUR POINTS BY PENDULAR SUPPORTS. THE SYSTEM HAS THREE DEGREES-OF-FREEDOM, HORIZONTAL AND VERTICAL TRANSLATION AND ROTATION ABOUT A HORIZONTAL AXIS THROUGH THE CENTER OF GRAVITY. SUPPORTING LINKS ARE LINEAR SPRINGS IN TENSION OR COMPRESSION IN ADDITION TO PROVIDING PENDULUM ACTION. DAMPING HAS NOT BEEN CONSIDERED IN THIS MODEL. A DIAGRAM OF THE SYSTEM AND EQUATIONS OF MOTION AND EQUILIBRIUM CONDITIONS ARE GIVEN IN SECTION 5.5.

## 3.0 EQUATIONS OF MOTION

FOR SOLUTIONS BY THE RUNGE-KUTTA METHOD THE SECOND ORDER EQUATIONS OF MOTIONS ARE RESTATED AS SIX FIRST ORDER EQUATIONS AS FOLLOWS-

LET V(1)= VERTICAL DISPLACEMENT OF MASS  
V(2)= VERTICAL VELOCITY OF MASS  
V(3)= ROTATION ANGLE OF PENDULUM  
V(4)= ANGULAR VELOCITY OF PENDULUM  
V(5)= ROTATION OF MASS ABOUT A HORIZONTAL AXIS  
THROUGH C.G.  
V(6)= ANGULAR VELOCITY ABOUT C.G.

THE FIRST DERIVATIVE OF THE ABOVE VARIABLES FORM THE EQUATIONS TO BE SOLVED.

F(1)= V(2)  
F(2)= VERTICAL ACCELERATION OF MASS=GIVEN EQUATION  
F(3)= V(4)  
F(4)= ANGULAR ACCELERATION OF PENDULUM=GIVEN EQUATION  
F(5)= V(6)  
F(6)= ANGULAR ACCELERATION ABOUT C.G.=GIVEN EQUATION

AS RESTATED, THESE EQUATIONS CAN BE EVALUATED FOR RATE-OF-CHANGE OVER ANY INTERVAL OF TIME BY KNOWING THE RESULTS OF THE PREVIOUS INTERVAL OF TIME. THIS IS THE BASIS OF THE RUNGE-KUTTA METHOD OF SOLUTION.

#### 4.0 SOLUTION METHOD

THE PROGRAM IS COMPOSED OF FOUR PARTS, INPUT, COMPUTING OF STATIC AND DYNAMIC PARAMETERS, RUNGE-KUTTA SOLUTIONS AND OUTPUT. INPUT AND OUTPUT PHASES ARE DISCUSSED SEPARATELY BELOW. FLOW DIAGRAMS FOR THIS PROGRAM ARE GIVEN IN APPENDIX 2.

#### 4.1 SMALL ANGLE ASSUMPTION

THE ASSUMPTION IS MADE THAT ALL ANGLES ARE SMALL, SO THAT THE SINE OF AN ANGLE EQUALS THE ANGLE IN RADIANS AND THE COSINE OF AN ANGLE EQUALS ONE.

#### 4.2 UNITS

ALL EQUATIONS ARE WRITTEN IN THE UNITS OF INCHES, POUNDS AND SECONDS. UNITS FOR INPUT DATA ARE NOTED ON INPUT FORMS.

#### 4.3 STATIC EQUILIBRIUM

IN CASES WHERE THE C.G. DOES NOT COINCIDE WITH THE GEOMETRIC CENTER OF THE MASS, EQUILIBRIUM IS OBTAINED BY HORIZONTAL TRANSLATION OF THE MASS. THE RESULTING UNEQUAL RATTLE SPACE AND THE ANGLES THE SUPPORTING LINKS MAKE WITH THE VERTICAL MUST BE CALCULATED TO FORM THE STARTING CONDITIONS FOR THE RUN. ALSO, SEVERAL FACTORS USED IN THE EQUATIONS OF MOTION ARE DERIVED FROM STATIC CONDITIONS. EQUATIONS FOR THESE PARAMETERS ARE GIVEN IN APPENDIX 1.

#### 4.4 FORCING FUNCTIONS

BASE VELOCITY/TIME PLOTS ARE USED TO INPUT BOTH HORIZONTAL AND VERTICAL FORCING FUNCTIONS. PLOTS ARE POINT TO POINT IN THE FORM OF TABLES OF TIME VS. VELOCITY. TO OBTAIN BASE DISPLACEMENTS THESE TABLES ARE INTEGRATED, ASSUMING STRAIGHT LINES CONNECT EACH POINT OF THE VELOCITY TABLE. ACCELERATIONS ARE COMPUTED BY CALCULATING THE CHANGE IN VELOCITIES BETWEEN TIME INTERVALS DIVIDED BY THE INTERVAL.

#### 4.5 RUNGE-KUTTA

REFERENCE IS MADE TO 'MATHEMATICAL METHODS FOR DIGITAL COMPUTERS' BY ANTHONY RALSTON OR OTHER TEXTS ON MATHEMATICAL ANALYSIS FOR DETAIL OF THIS NUMERICAL METHOD OF SOLUTION.

## 4.6 SOLUTION TOLERANCE CONTROL

TRUNCATION ERRORS ARE CONTROLLED BY ENTRIES 24 THROUGH 26 OF THE INPUT DATA. EXPERIENCE IN RUNNING THE PROGRAM HAS SHOWN THAT ACCURACY GREATER THAN REQUIRED IS OBTAINED BY USING .0001 FOR THE MAXIMUM TRUNCATION ERROR BEFORE REDUCING ( $H=1/2H$ ) THE TIME INTERVAL AND .00001 FOR THE MAXIMUM TRUNCATION ERROR BEFORE DOUBLING ( $H=2H$ ) THE TIME INTERVAL. MINIMUM TIME INTERVAL SHOULD BE .000001. LARGER NUMBERS MAY REDUCE ACCURACY DEPENDING ON THE CASE. NO FAST RULE CAN BE STATED IN THIS REGARD.

## 5.0 INPUT DATA

THERE ARE THREE INPUT DATA CONFIGURATIONS TO SIMPLIFY THE PREPARATION OF INPUT DATA WHEN RUNNING A SERIES OF CASES IN SUCCESSION.

TYPE 1, NOTED BY A ZERO IN COLUMN 4 OF THE PARAMETER CARD, IS THE BASIC INPUT SYSTEM AND IS USED FOR INPUT OF A SINGLE CASE OR THE FIRST CASE IN A SERIES. INPUT CARDS CONSISTS OF TWO TITLE CARDS, ONE PARAMETER CARD, SIX GENERAL DATA CARDS AND TABLE CARDS AS REQUIRED FOR THE VELOCITY INPUTS. ALL CARDS SHOWN ON PAGES 1 TO 3 AND AT LEAST ONE CARD FROM PAGES 4 AND 5 ARE REQUIRED. A BLANK CARD IS PLACED AT THE END OF THE DATA CARDS FOR THIS TYPE.

TYPE 2, NOTED BY A 1 IN COLUMN 4 OF THE PARAMETER CARD, IS DESIGNED TO RUN ADDITIONAL CASES FOLLOWING A TYPE 1 INPUT. INPUT CARDS SHOWN ON PAGE 1 ARE REQUIRED, HOWEVER, CARDS SHOWN ON PAGES 2 TO 5 ARE OPTIONAL. IN ADDITION SINGLE ITEMS MAY BE CHANGED BY THE USE OF ALTER CARDS, PAGE 6 OF THE INPUT FORMS. TWO BLANK CARDS ARE REQUIRED IN THIS SET OF DATA. ONE AT THE END OF THE PAGE 1 TO 5 INPUT CARDS AND A SECOND ONE AT THE END OF THE ALTER CARDS. USE BOTH BLANK CARDS EVEN IF ONE TYPE OF CARD IS OMITTED.

TYPE 3, NOTED BY A 2 IN COLUMN 4 OF THE PARAMETER CARD, IS USED FOR RUNNING ADDITIONAL CASES WHEN ONLY A FEW ITEMS ARE TO BE CHANGED. INPUT CARDS SHOWN ON PAGE 1 ARE REQUIRED. ALL CHANGES TO DATA FROM THE PREVIOUS CASES ARE MADE BY ALTER CARDS, SEE PAGE 6 OF INPUT FORMS. A BLANK CARD IS PLACED AT THE END OF THE ALTER CARDS.

DATA IS SAVED BY THE PROGRAM FROM CASE TO CASE. ALL CHANGES MADE TO BASE DATA, TYPE 1 CASE, ARE RETAINED AND APPLY TO ALL FOLLOWING CASES.

DATA ENTERED ON THE PARAMETER CARD IS IN FOUR DIGIT FIXED POINT FORMAT, THAT IS, EACH ITEM HAS BEEN ALLOTTED FOUR CARD COLUMNS AND IS PUNCHED RIGHT JUSTIFIED WITHOUT DECIMAL POINTS. ALL OTHER DATA ITEMS ARE FLOATING POINT FORMAT. THIS MEANS THE DATA CAN BE PLACED ANYWHERE WITHIN THE CARD COLUMNS ALLOTTED AND MUST BE SHOWN AND PUNCHED WITH A DECIMAL POINT.

## 6.0 OUTPUT

THE TIME INTERVAL BETWEEN PRINTING AND THE LENGTH OF TIME FOR A RUN IS CONTROLLED BY ENTRIES 19 THROUGH 23 AND 27 OF THE INPUT DATA, SEE PAGE 2 OF THE INPUT FORMS APPENDIX 5. IT WILL BE NOTED THAT THE INTERVAL BETWEEN PRINTING MAY BE VARIED DURING THE RUN. THIS FEATURE PROVIDES A MEANS OF OBTAINING GREATER DETAIL IN THE OUTPUT WHEN THE FORCING FUNCTIONS ARE ACTING AND THEN REDUCING THE FREQUENCY OF PRINTING AND RUNNING FOR LONG PERIODS OF TIME WITH LESS OUTPUT.

IN ADDITION TO LISTINGS, OUTPUT IN THE FORM OF PUNCHED CARDS CAN BE OBTAINED FOR OFF-LINE PLOTTING OF RESULTS. UP TO FOUR VARIABLES CAN BE PUNCHED IN EACH RUN. SELECTIONS ARE MADE BY SUPPLYING ITEM NUMBERS IN LOCATION 6 THROUGH 9 ON THE PARAMETER INPUT CARD. ITEM NUMBERS HAVE BEEN ASSIGNED EACH PRINTED RESULT BASED ON SEQUENCE OF PRINTING, THAT IS, STARTING ON THE FIRST PAGE, MASS HORIZONTAL DISPLACEMENT HAS BEEN NUMBERED 1 AND NUMBERS CONTINUE IN SEQUENCE TO 14 FOR PHI ON THE SECOND PAGE. THE TIME COLUMN IS NOT NUMBERED ON EITHER PAGE.

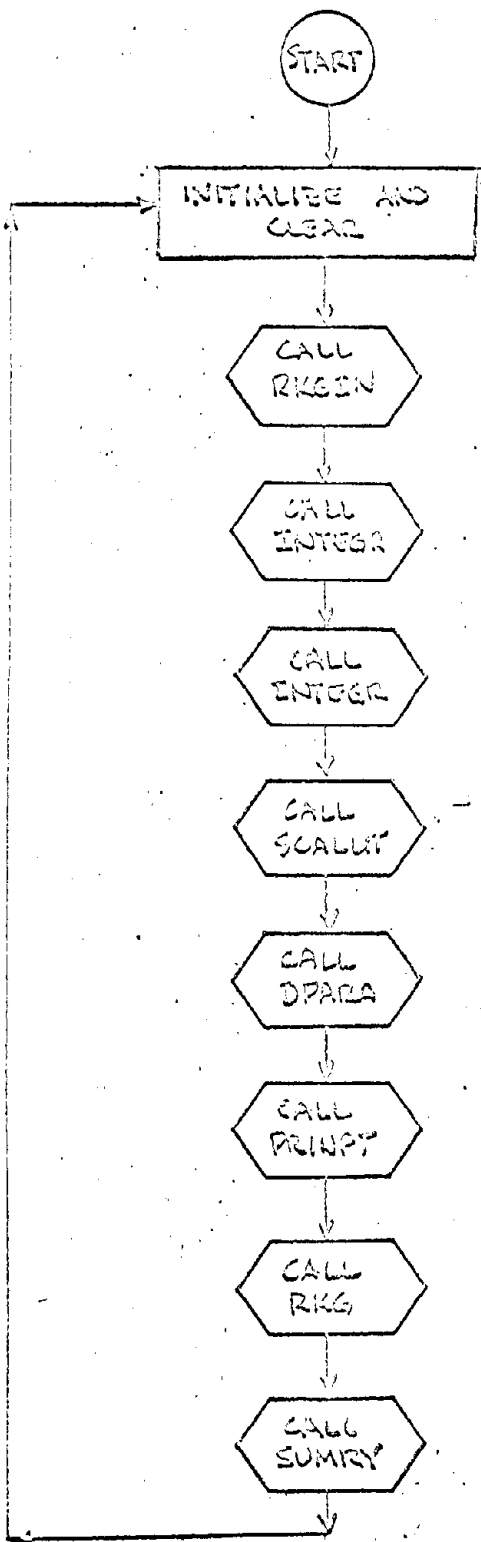
SAMPLE OUTPUT LISTING AND PLOT ARE GIVEN IN APPENDIX 6.

## 7.0 MACHINE REQUIREMENTS

THIS PROGRAM HAS BEEN PREPARED IN TWO FORMS. THE BASIC PROGRAM WAS DEVELOPED AND TESTED ON A IBM 1620 MODEL II COMPUTER EQUIPED WITH A IBM 1311 DISK STORAGE DRIVE, 40K OF CORE STORAGE, INDEX REGISTERS AND FLOATING POINT HARDWARE. A SECOND VERSION WAS PREPARED TO RUN ON A IBM 7094 COMPUTER. INPUT AND OUTPUT ARE IDENTICAL FOR BOTH PROGRAMS.

## 8.0 OPERATING PROCEDURE

STANDARD OPERATING PROCEDURES HAVE BEEN EMPLOYED FOR BOTH MACHINE CONFIGURATIONS. FOR RUNNING ON THE IBM 1620, REFERENCE SHOULD BE MADE TO THE 1620 MONITOR II OPERATING SYSTEM MANUAL. THE STANDARD IBM FORTRAN II MONITOR IS USED FOR THE IBM 7094 PROGRAM VERSION.



GENERAL FLOW

DIAGRAM

SET CONSTANTS, CLEAR INPUT & OUTPUT AREAS

READ INPUT DATA

INTEGRATE VERT VELOCITY/TIME CURVE FOR DISPL/TIME

INTEGRATE HORIZ VELOCITY/TIME CURVE FOR DISPL/TIME

SCALE INPUT DATA TO COMMON UNITS OF INCHES, LBS, SEC

COMPUTE STATIC PARAMETERS

PRINT INPUT DATA AND STATIC PARAMETERS

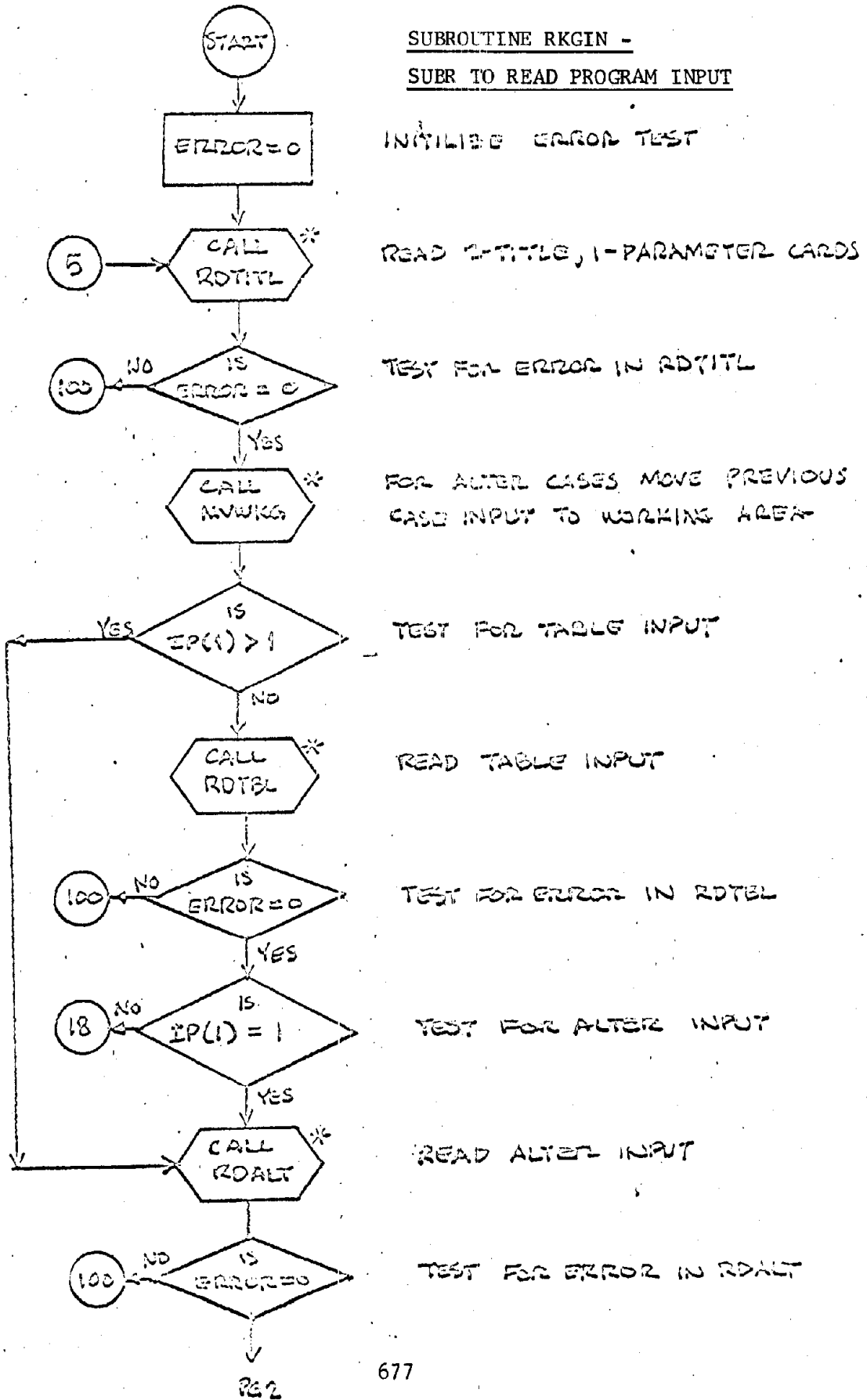
SOLVE TIME DEPENDENT FUNCTIONS OVER TIME PERIOD OF CONCERN

PRINT SUMMARY OF RESULTS

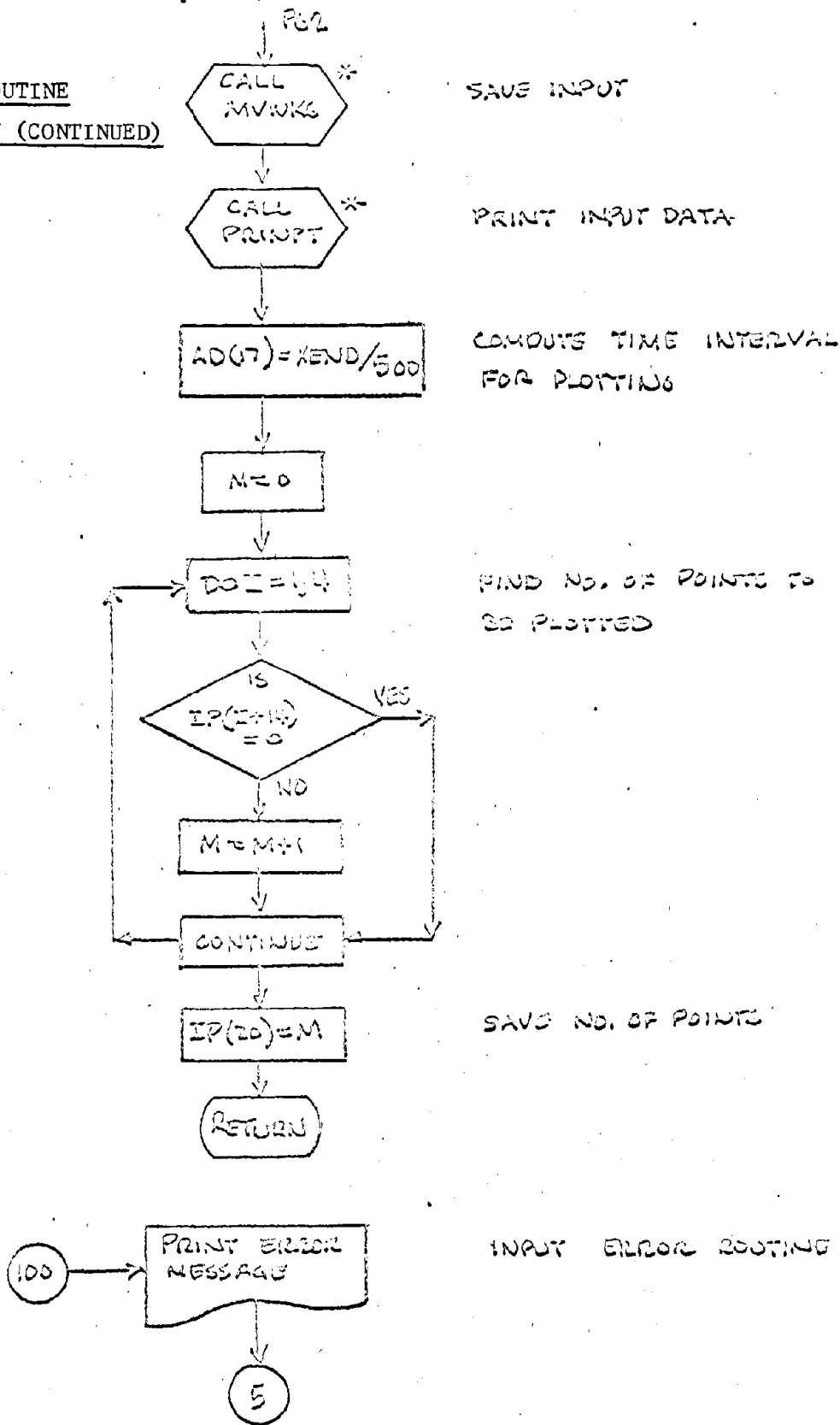
GO BACK FOR NEXT CASE



SUBROUTINE RKGIN -  
SUBR TO READ PROGRAM INPUT



SUBROUTINE  
RKGIN (CONTINUED)



SAVE INPUT

PRINT INPUT DATA

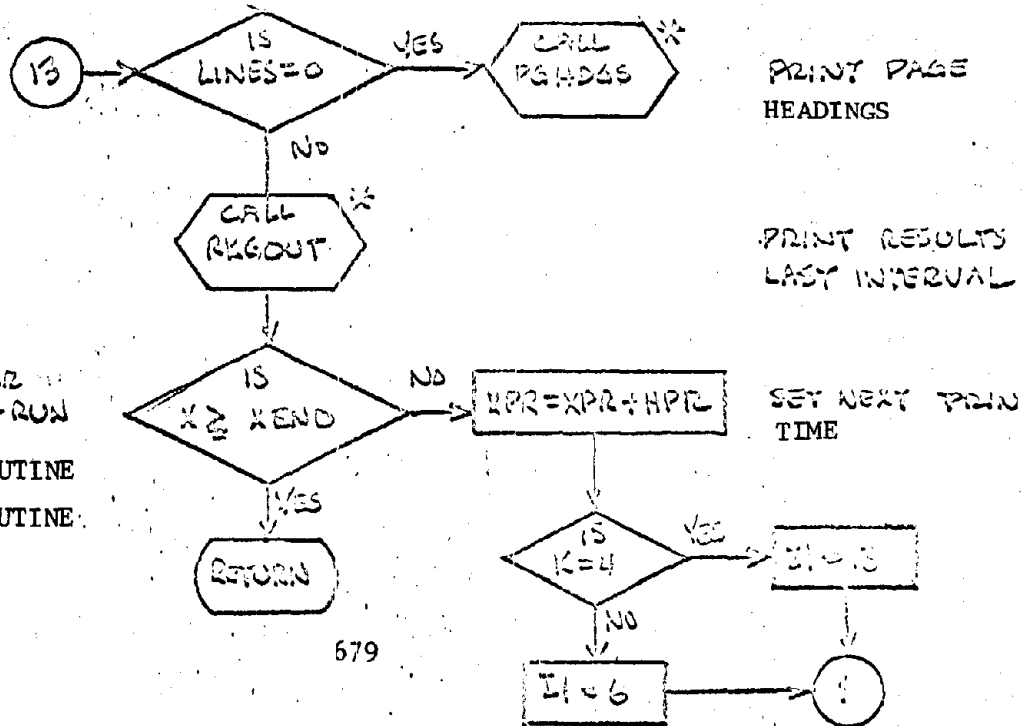
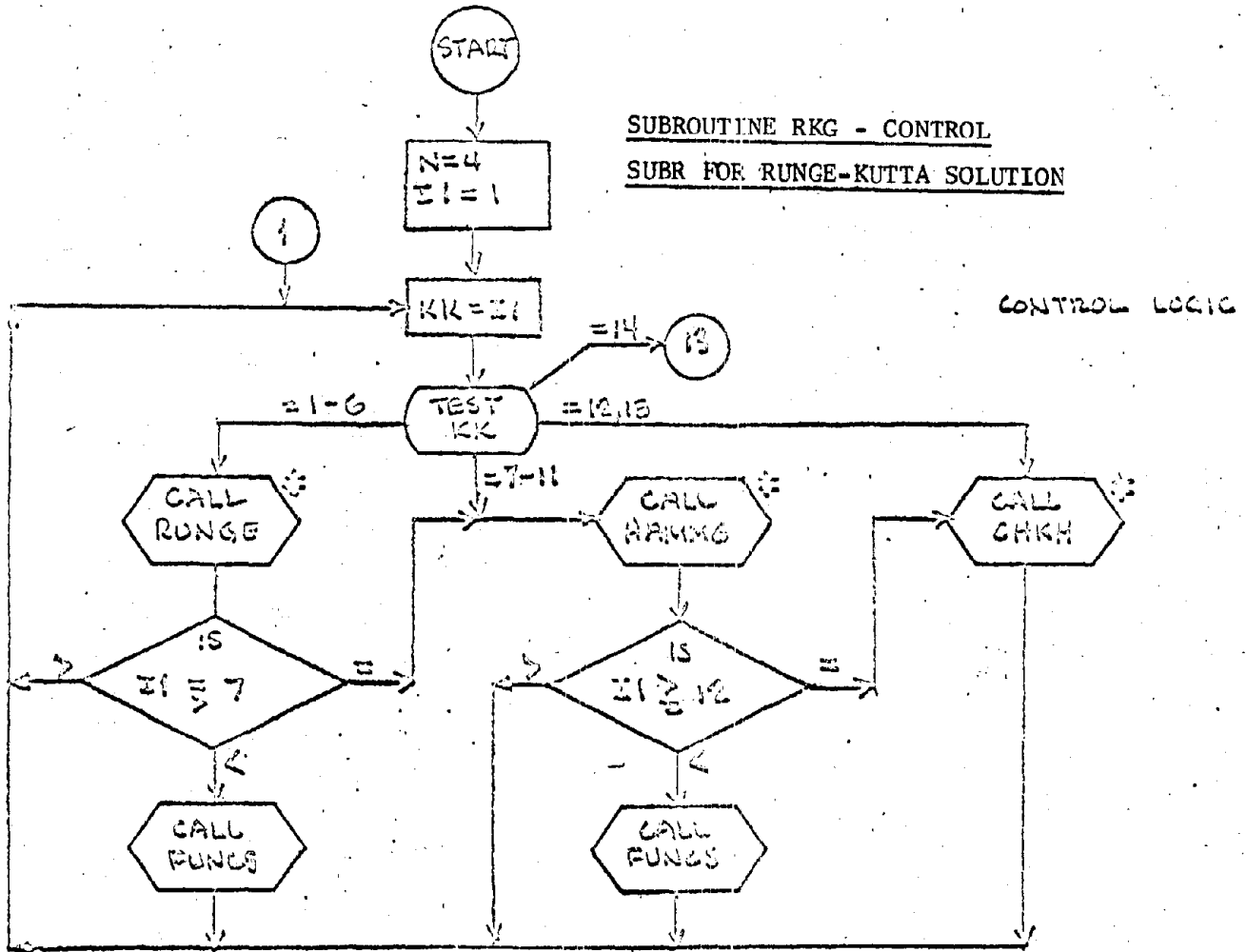
COMPUTE TIME INTERVAL  
FOR PLOTTING

FIND NO. OF POINTS TO  
BE PLOTTED

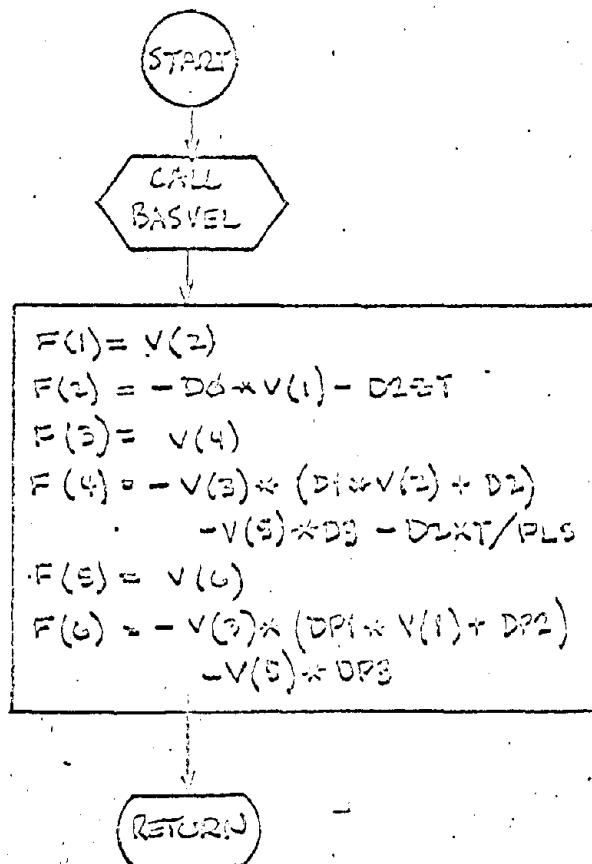
SAVE NO. OF POINTS

INPUT ERROR ROUTINE

SUBROUTINE RKG - CONTROL  
SUBR FOR RUNGE-KUTTA SOLUTION

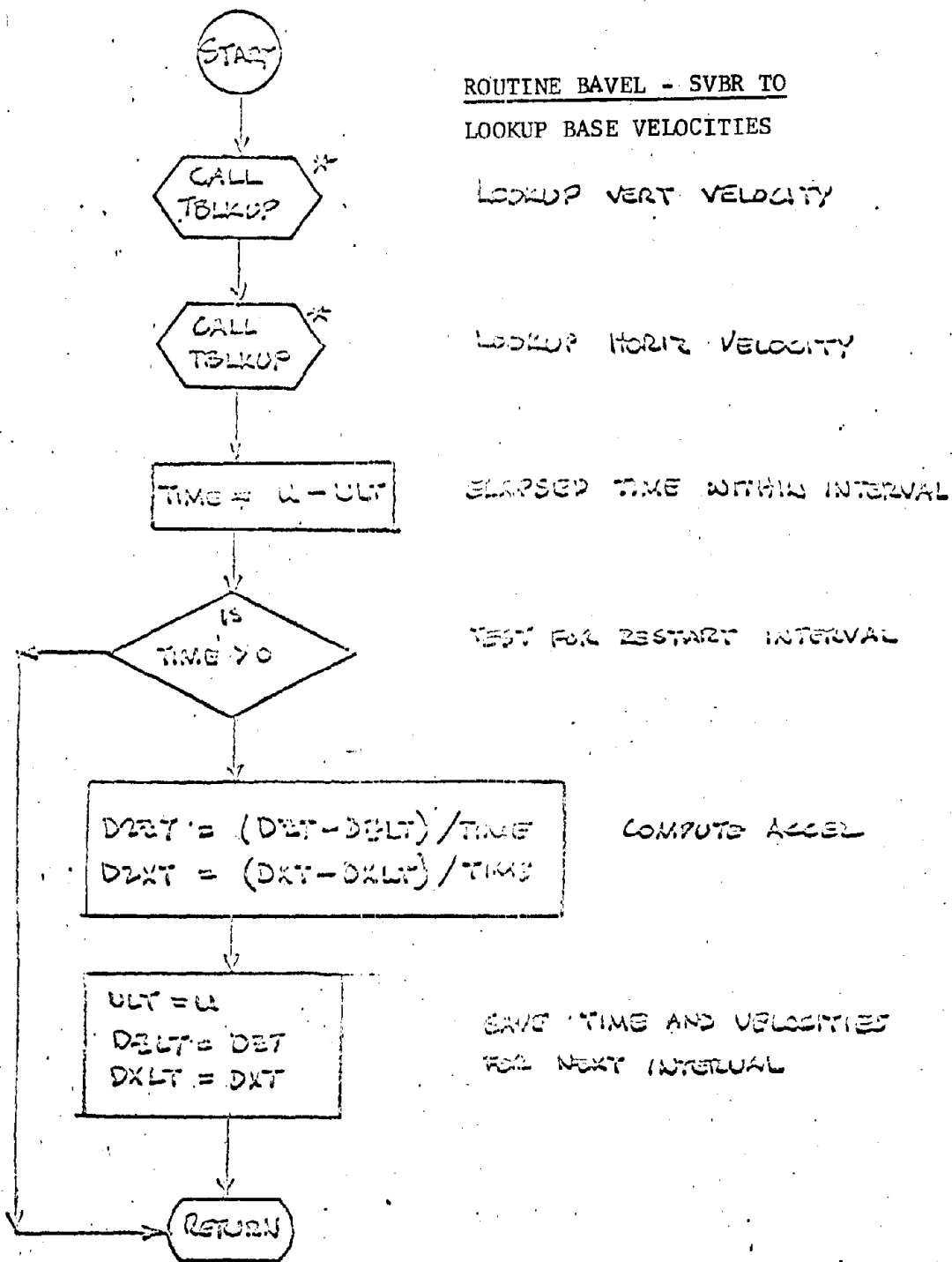


ROUTINE FUNKS - SUBR TO COMPUTE FUNCTIONS  
FOR EACH TIME INTERVAL



LOOKUP BASE VELOCITIES

COMPUTE FUNCTIONS



ROUTINE BAVEL - SVBR TO  
LOOKUP BASE VELOCITIES

LOOKUP VERT VELOCITY

LOOKUP HORIZ VELOCITY

ELAPSED TIME WITHIN INTERVAL

TEST FOR RESTART INTERVAL

COMPUTE ACCEL

SAVE TIME AND VELOCITIES  
FOR NEXT INTERVAL

\* UTILITY ROUTINE - REFER TO FORTRAN

## APPENDIX E

### DISCUSSION OF VERTICAL STATIC STRESS AND DISPLACEMENT

In view of the relatively long duration of overpressure for large yield detonations it is desirable to acquire an understanding of the static aspects of soil deformations subjected to a surface pressure  $p_{so}$  which is assumed to attenuate with depth  $z$  according to the expression

$$p_z = p_{so} \frac{1}{1 + \frac{z}{L}} \quad (E-1)$$

in which  $p_z$  is the vertical pressure at depth  $z$  and  $L$  is a characteristic length that may be a function of  $p_{so}$  as well as of other parameters.

If the soil is assumed to be linearly elastic and if its vertical confined modulus  $M$  is constant, the vertical deformation of a layer of thickness  $dz$  is given by

$$\epsilon dz = \frac{p_z}{M} dz = \frac{p_{so} dz}{M(1 + \frac{z}{L})} \quad (E-2)$$

Accordingly the total deformation of a layer of vertical thickness  $z$  will be

$$d_z = \frac{p_{so}}{M} L \left( n \left( 1 + \frac{z}{L} \right) \right) \quad (E-3)$$

The displacement  $d_z$  is seen to be unlimited if  $z$  approaches infinity.

1. Linear variation of confined modulus  $M$  with depth. If it is assumed that the vertical stiffness of the soil varies with depth so that

$$M_z = f(z) \quad (E-4)$$

it will be found that the total deformation  $d_z$  will be finite only if  $f(z)$  increases with depth.

A simple linear variation of  $M_z$  with depth will now be assumed, namely:

$$M_z = M_o \left( 1 + k' \frac{z}{L} \right) ; \text{ i.e. } k' = \left[ \frac{M_z}{M_o} - 1 \right] \frac{L}{z} \quad (E-5)$$

This means that if the soil density at depth  $z$  is  $\rho_z$  the seismic velocity at that depth will be given by

$$c_z = (M_z/\rho_z)^{1/2} \quad (\text{E-6})$$

In this case Equation (E-2) takes the form

$$c \, dz = \frac{P_{so}}{M_o} \frac{dz}{(1 + \frac{z}{L})(1 + k' \frac{z}{L})}$$

Accordingly

$$d_z = \frac{P_{so}}{M_o} \int_0^z \frac{dz}{(1 + \frac{z}{L})(1 + k' \frac{z}{L})} \quad (\text{E-7})$$

Thus, if  $k' = 1$

$$\begin{aligned} d_z &= \frac{P_{so}}{M_o} \int_0^z \frac{dz}{(1 + \frac{z}{L})^2} \\ &= \frac{P_{so}}{M_o} \frac{z}{1 + \frac{z}{L}} \end{aligned}$$

This is seen to give a limiting value of displacement, namely

$$d_z = \frac{P_{so}}{M_o} L \quad \text{if } z \rightarrow \infty. \quad (\text{E-7a})$$

For all positive values of  $k'$  it can be shown that the solution of (E-7) is given by:

$$d_z = \frac{P_{so}}{M_o} L \frac{2}{k' - 1} \operatorname{arctanh} \left[ \frac{(k' - 1) \frac{z}{L}}{2 + (1 + k') \frac{z}{L}} \right] \quad (\text{E-8})$$

or

$$d_z = \frac{P_{so}}{M_o} (L_{eq})_z \quad (\text{E-8a})$$

and that the limiting value as  $z \rightarrow \infty$  will be

$$(d_z)_\infty = \frac{P_{so}}{M_o} L \frac{2}{k' - 1} \operatorname{arctanh} \left[ \frac{k' - 1}{k' + 1} \right] \quad (\text{E-9})$$

or

$$(d_z)_\infty = \frac{P_{so}}{M_o} (L_{eq}) \quad (E-9a)$$

A plot of  $(L_{eq}/L)_\infty$  is shown in Figure 1 for two  $k'$  scale values ranging from 1 to 8, and, from 5 to 80.

Example E-1

Assume that  $p_{so} = 250$  psi;  $M_o = 10^5$  psi at surface;  $M_z = 10^6$  psi at  $z = 300$  ft; and  $L = 200$  ft. Find the surface displacement. From Equation (E-5), and since the dimensionless

$$k' = \left( \frac{10^6}{10^5} - 1 \right) \frac{200}{300} = 6$$

It is seen from Figure E-1 that

$$\left( \frac{L_{eq}}{L} \right)_\infty = 0.36 ; \text{ or } (L_{eq})_\infty = 0.36 \times 200 = 72 \text{ ft}$$

and from Equation (E-8a) that

$$(d_z)_{z \rightarrow \infty} = \frac{250}{10^5} 72 = 0.180 \text{ ft} \quad 2.16 \text{ inches}$$

It is often desirable to find the relative displacement between the surface and a layer at depth  $z$ . This is given by Equation (E-8) and plotted for the parameter  $k'$  in Figure E-2 for different values of  $z/L$ .

Example E-2

Assume the same data as for Example E-1, but find the relative displacement between the two layers at  $z_1 = 100$  ft and  $z_2 = 300$  ft. From Figure E-2 interpolate for  $k' = 6$  and find for

$$\frac{z_2}{L} = \frac{300}{200} = 1.5 ; \text{ that } \left( \frac{L_{eq}}{L} \right)_2 = 0.28$$

$$\left( \frac{L_{eq}}{L} \right)_{2-1} = 0.07,$$

$$\frac{z_1}{L} = \frac{100}{200} = 0.5 ; \text{ that } \left( \frac{L_{eq}}{L} \right)_1 = 0.21$$



VALUES OF  $\frac{L_{eq}}{L}$  FOR COMPUTING THE BASOLUTE ELASTIC DISPLACEMENT AT SURFACE

$$(d_z) = \frac{P_{so}}{M_o} (L_{eq})$$

for  $P_z = \frac{P_{so}}{1 + \frac{z}{L}}$  and  $M_z = M_o (1 + k \frac{z}{L})$

$$k' = \left[ \frac{M_z}{M_o} - 1 \right] \frac{L}{z}$$

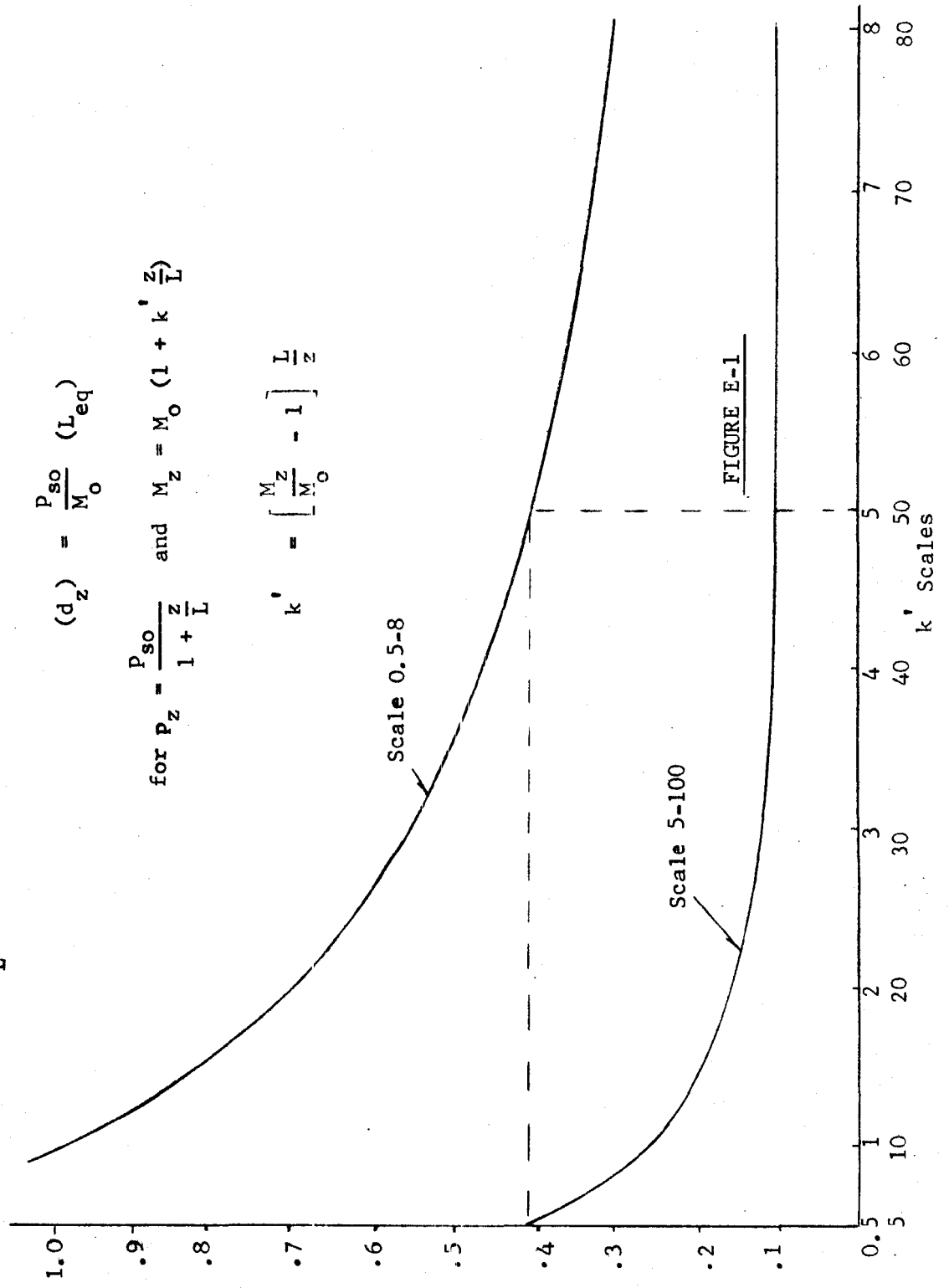
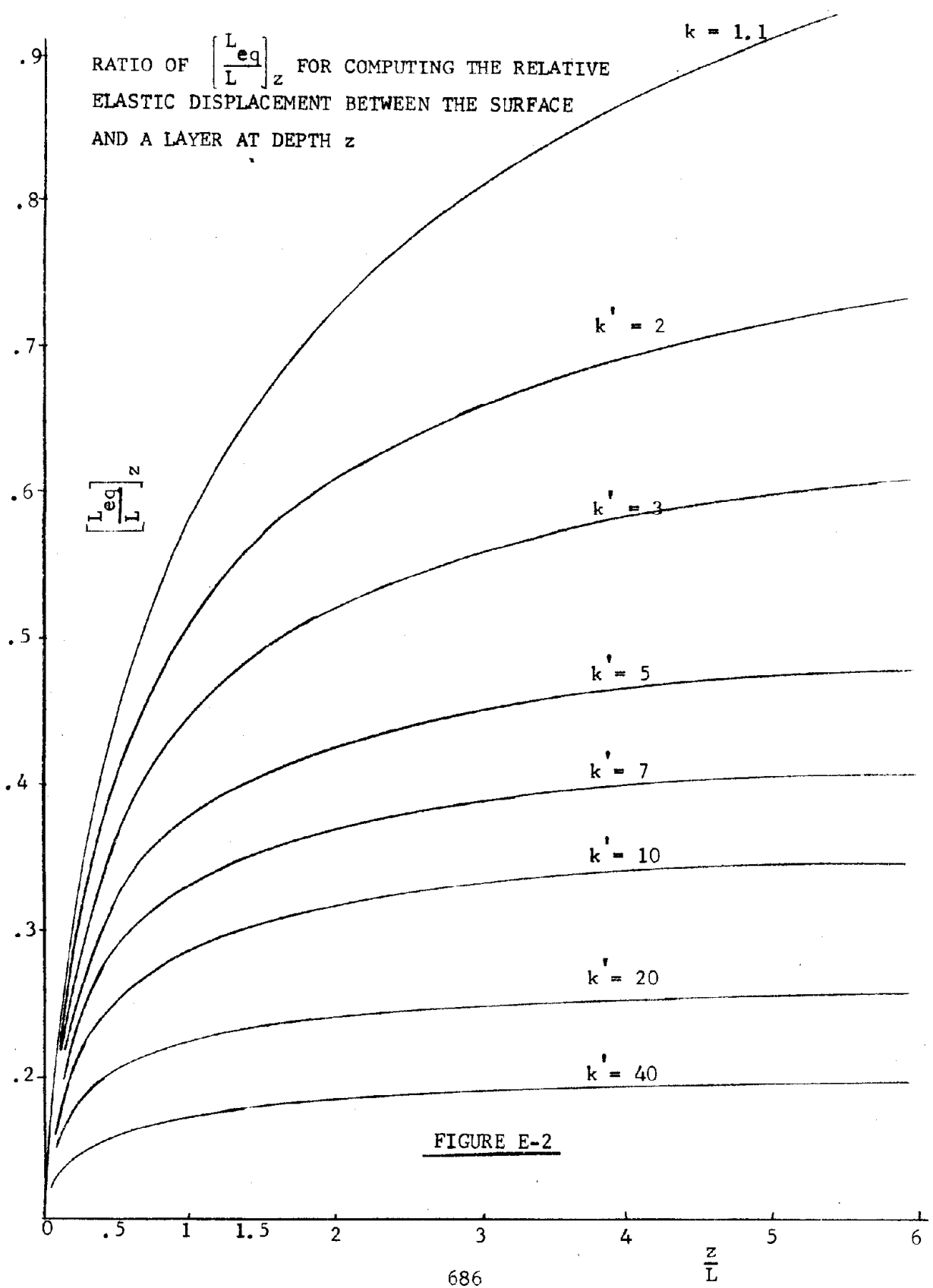


FIGURE E-1



Example E-2 (continued)

$$\text{Accordingly } (L_{\text{eq}})_{2-1} = 0.07 \times 200 = 14 \text{ ft}$$

$$\text{and } (dz)_{2-1} = \frac{250}{10^5} 14 = 0.035 \text{ ft} \approx 0.42 \text{ inches}$$

The absolute displacement of a soil layer located at depth  $z$  is obtained by subtracting Equation (E-8) from Equation (E-9). The results in terms of  $(L_{\text{eq}}/L)_{\text{abs}}$  are plotted in Figure E-3 in terms of  $z/L$ .

Example E-3

Assume the same data as for Example E-1, but find the absolute displacement at  $z = 100$  ft. From Figure E-3 interpolate for  $k' = 6$  and find for

$$\frac{z}{L} = \frac{100}{200} = 0.5 \text{ that } \left(\frac{L_{\text{eq}}}{L}\right)_{\text{abs}} = 0.16$$

accordingly

$$(L_{\text{eq}})_{\text{abs}} = 0.16 \times 200 = 32 \text{ ft}$$

and

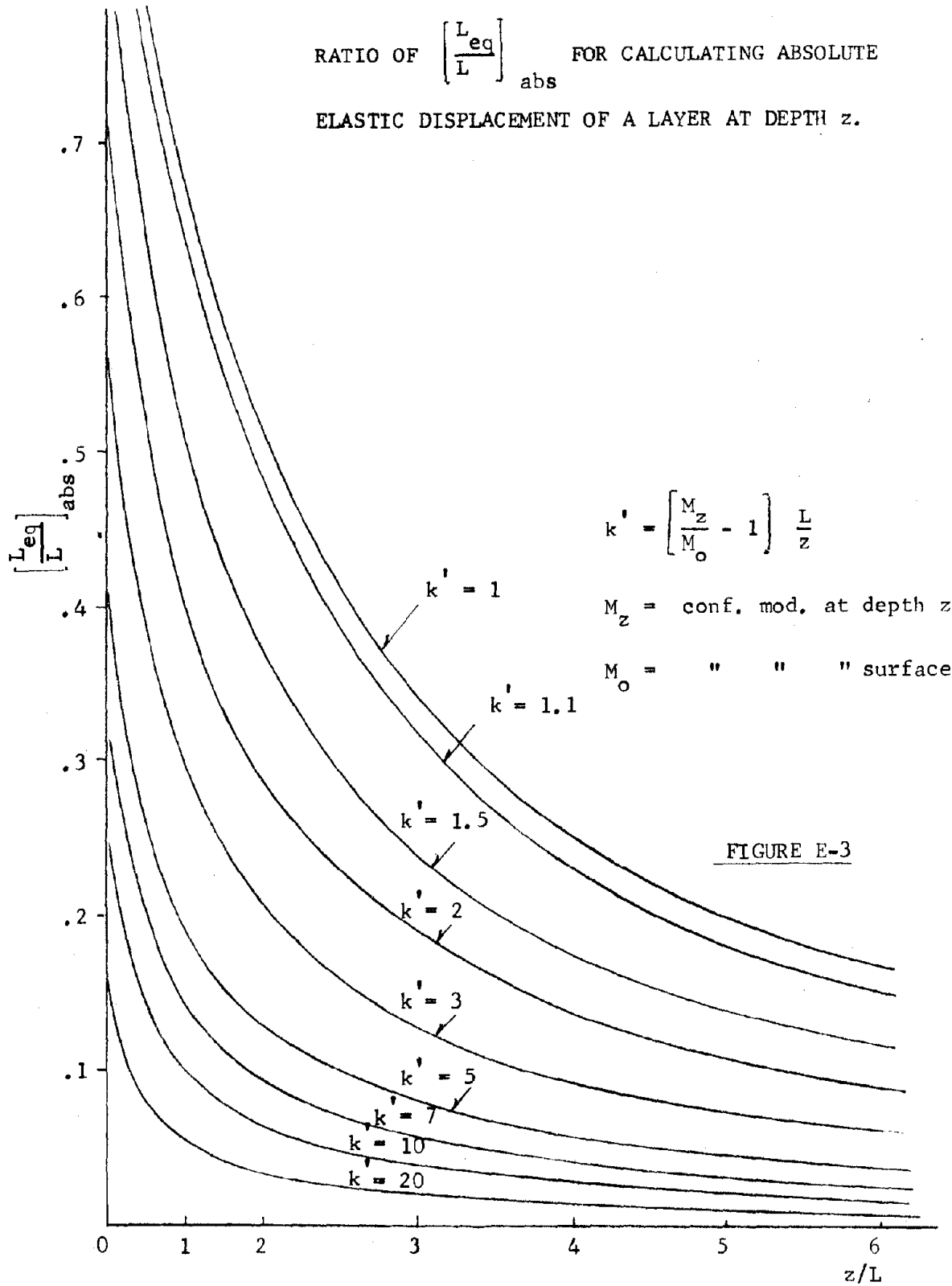
$$(d_z)_{100} = \frac{250}{10^5} 32 = 0.080 \text{ ft} \approx 0.96 \text{ inches}$$

2. Application related to nuclear blasts. The preceding considerations, involving a pressure attenuation with depth, expressed by Equation (E-1), and a stiffness appreciation with depth, expressed by Equation (E-5), can be applied to a pseudo-static soil pressure situation relating to the compressive effect of a nuclear blast. In that case the characteristic length  $L$  in feet may be expressed by Equation (3.17) or by

$$L = C p_{\text{so}}^{-\frac{1}{2}} W^{\frac{1}{3}} \quad (\text{E-10})$$

in which  $C$  is a constant and  $W$  is the yield of the nuclear device. The constant may be taken as 2300 if  $p_{\text{so}}$  is in psi and  $W$  is in megatons. The value of  $k'$  is then defined by the stiffness property  $M$  of the soil at two levels and by the value of  $L$ , see Equation (E-5). Since ordinarily the density  $\rho_z$  of the soil increases with depth, the corresponding seismic velocity at depth  $z$  can be found from Equation (E-6).

RATIO OF  $\left[ \frac{L_{eq}}{L} \right]_{abs}$  FOR CALCULATING ABSOLUTE  
ELASTIC DISPLACEMENT OF A LAYER AT DEPTH  $z$ .



Example E-4

The plots on Figure E-4 show the data for an assumed site, exhibiting linear increases in vertical stiffness and in density of soil. Consequently a parabolic curve for seismic velocity will result. The relationship between the location  $r_p$  and the corresponding overpressure is assumed to be given by equation (3.8), i.e. by

$$r_p = 4.3 \times 10^4 W^{\frac{1}{3}} P_{so}^{-\frac{1}{2}} \text{ ft.} \quad (\text{E-11})$$

The following Table I lists the pertinent computational data.

TABLE E-I

W =		10 KT	100 KT	1 MT	10 MT	100 MT
100 psi	$r_p$ ; Eq (E-11)	920	2000	4300	9300	20,000 ft
	L; Eq (E-10)	49	106	230	500	1070 ft
	$k'$ ; Eq (E-5)	2.0	44	9.5	21	44
	$(L_{eq}/L)$ ; Fig. E-1	.69	.44	.26	.16	.10
500 psi	$r_p$ ; Eq (E-11)	410	895	1920	4160	8950 ft
	L; Eq (E-10)	22	48	103	223	480 ft
	$k'$ ; Eq (E-5)	0.90	2.0	4.2	9.2	20
	$(L_{eq}/L)$ ; Fig. E-1	1.0	.70	.45	.27	.16
1000 psi	$r_p$ ; Eq (E-11)	291	623	1360	2940	6320 ft
	L; Eq (E-10)	16	34	73	158	340 ft
	$k'$ ; Eq (E-5)	0.63	1.4	3	65	14
	$(L_{eq}/L)$ ; Fig. E-1	1.2	.84	.55	.34	.20

$M_z =$	5	10	15	20	$25 \times 10^5$ psi
$\rho_z =$	2	4	6	8	10 slugs/ft <sup>3</sup>
$c_z =$	2	4	6	8	$10 \times 10^3$ fps

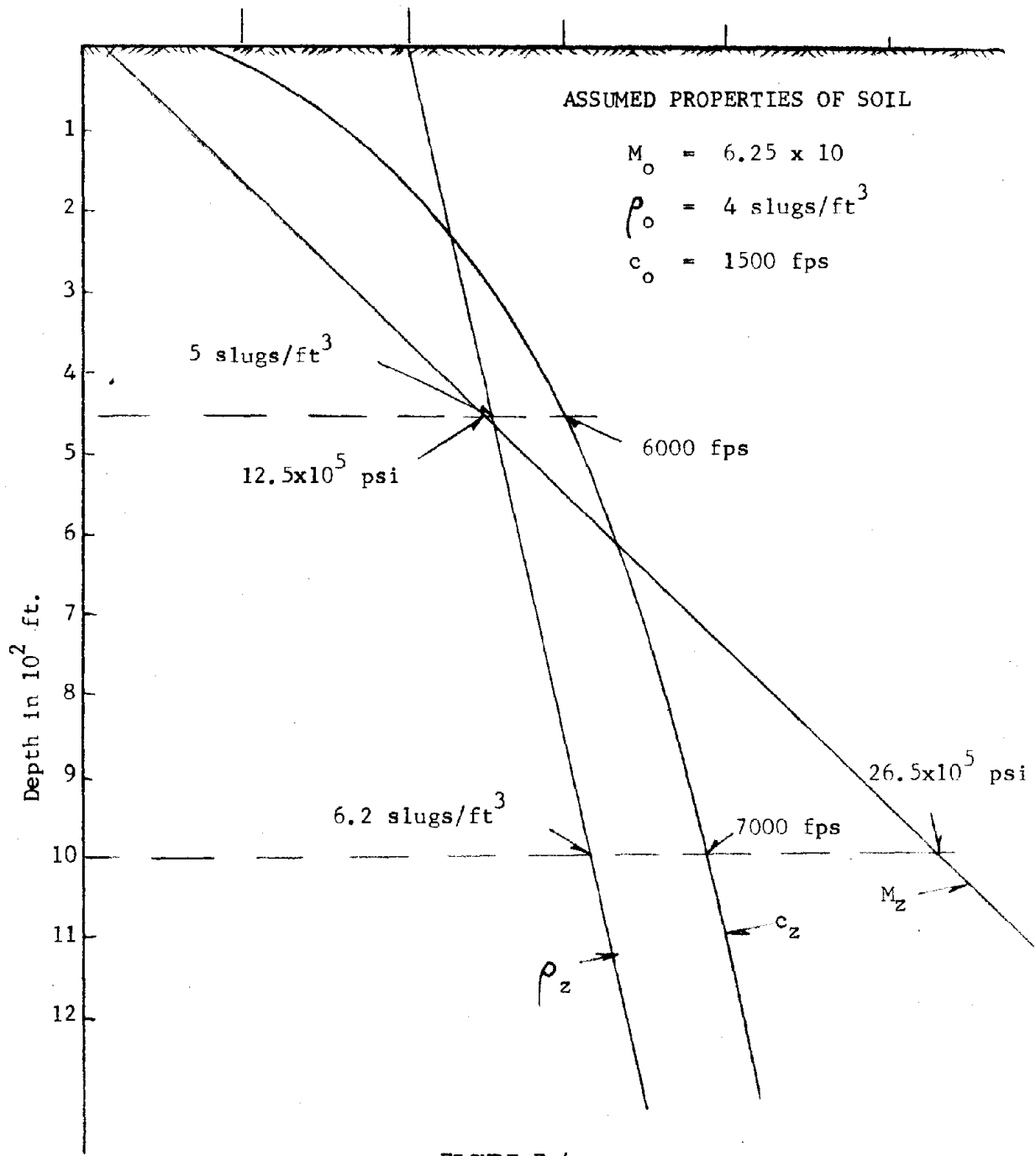


FIGURE E-4

The elastic displacement results for the assumed site are given in Table E-II.

TABLE E-II  
Elastic Displacement at Surface, in inches

	10 KT	100 KT	1 MT	10 MT	100 MT
$p_{so} = 100$ psi	0.65	0.89	1.2	1.5	2.0
= 500	2.2	3.2	4.4	5.8	7.4
= 1000	3.6	5.4	7.7	10.3	13.1

Since the soil was assumed to be linearly elastic no permanent deformation will be established. The results are plotted in Figure E-5.

3. Stratified soil with constant elastic properties for each stratum.  
If it is assumed that the pressure attenuation with depth is still given by Equation (E-1) it is possible to calculate the pressure acting at the top of each stratum. Thus, if the top of the  $n$ th stratum is at level  $z_n$ , then

$$p_{zn} = p_{so} \frac{1}{1 + \frac{z_n}{L}} \quad (E-12)$$

Accordingly the elastic deformation in the  $n$ th stratum will be

$$(d_z)_{n+1} = \frac{p_{zn}}{M_{zn}} (L_{eq})_n \quad (E-13)$$

with the equivalent length given by

$$(L_{eq})_n = L \ln \left[ 1 + \frac{z_{n+1} - z_n}{L} \right] \quad (E-13a)$$

or if

$$z_{n+1} - z_n \ll L,$$

the expression

$$L_{eq} \approx L \left[ 1 - \frac{z_{n+1} - z_n}{2L} \right] \quad (E-13b)$$

ABSOLUTE ELASTIC DISPLACEMENTS AT THE SURFACE  
FOR THE SITE CONSTANTS OF FIGURE E-4 AND FOR  
VARIOUS YIELDS

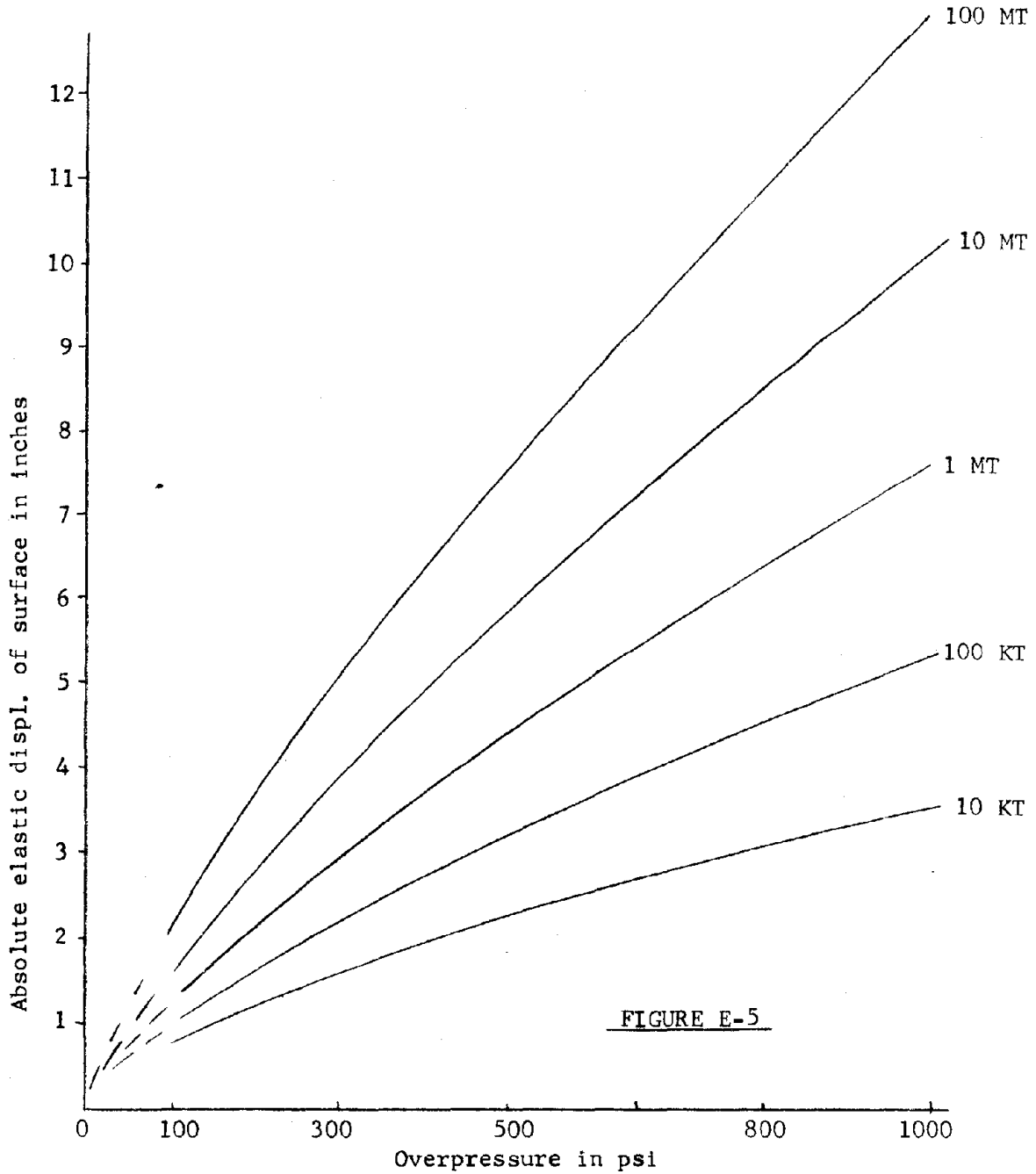


FIGURE E-5



The equivalent length  $L_{eq}$  thus takes into account the attenuation of the pressure  $p_{zn}$  within the nth layer.

Example E-5

Assume a specific site with horizontal layers as listed below

- $z = 0$  to  $z_1 = 60'$ ;  $M_1 = 6.25 \times 10^4$  psi;  $\rho_1 = 4.0$  slugs/ft  $c_1 = 1500$  fps  
 $z = 60$  to  $z_2 = 180'$ ;  $M_2 = 125 \times 10^4$ ;  $\rho_2 = 5.0$   $c_2 = 6000$   
 $z = 180$  to  $z_3 = 780'$ ;  $M_3 = 382 \times 10^4$ ;  $\rho_3 = 5.5$   $c_3 = 10,000$   
 $z = 780$  to  $z_4 = 3780'$ ;  $M_4 = 875 \times 10^4$ ;  $\rho_4 = 5.6$   $c_4 = 15,000$   
 $z = 3780$  to  $z \rightarrow \infty$ ;  $M_5 \rightarrow \infty$

Assume an overpressure  $p_{so}$  of 300 psi and a yield of 10 MT. From Equation (E-10) it is found that:

$$L = 2300 \sqrt[3]{10 / \sqrt{300}} = 287 \text{ ft} \approx 300 \text{ ft}$$

Then, if the pressure attenuates in accordance with Equation (E-12), i.e. regardless of layering,

at  $z_1 = 60'$ ;  $p_1 = 250$  psi  $z_3 = 780'$ ;  $p_3 = 83$   
 $z_2 = 180'$ ;  $p_2 = 187$   $z_4 = 3780'$ ;  $p_4 = 22$

Since within each layer attenuation of pressure occurs in accordance with Equation (E-13), the equivalent thicknesses of the four layers, Equation (E-13a) are

60 ft layer  $\ell_n \ 1.2 = 0.182$ ;  $(L_{eq})_1 = 54.5'$   
 180 ft "  $\ell_n \ 1.4 = 0.336$ ;  $(L_{eq})_2 = 101'$   
 600 ft "  $\ell_n \ 3.0 = 1.100$ ;  $(L_{eq})_3 = 330'$   
 3000 ft "  $\ell_n \ 11.0 = 2.397$ ;  $(L_{eq})_4 = 719'$

Example E-5 (continued)

Accordingly Equation (E-13) will give the results

$$\begin{array}{ll} d_1 = 0.2608 \text{ ft} & d_3 = 0.1620 \text{ ft} \\ d_2 = 0.0202 \text{ ft} & d_4 = 0.0685 \text{ ft} \end{array}$$

Total displacement  $\Sigma d = 0.5115 \text{ ft}$

If the average pressures of 275, 218.5, 135, 52.5 psi had been used for the 60', 120', 600', and 3000' thick strata respectively, the results would have been

$$\begin{array}{ll} d_1 = 0.2645 \text{ ft} & d_3 = 0.2120 \text{ ft} \\ d_2 = 0.0209 \text{ ft} & d_4 = 0.1800 \text{ ft} \end{array}$$

Total displacement  $\Sigma d = 0.6774 \text{ ft}$

giving a result 32 percent larger than those obtained by the use of Equation (E-13). If no attenuation within the four layers had been assumed the total displacement would have been 76 percent larger than the results obtained by using Equation (E-13).

4. Calculations for nonlinear soil stiffness. If data for in situ soil is available at various depths and relate to the situation of zero overpressure at the surface, a question still arises in regard to the effect of the attenuated overpressure on the in situ soil properties. It is desirable to remember that this fact complicates any analysis of the problem.

However, it is generally accepted that for a steadily increasing load the initial nonlinearity of some soils will manifest itself first as a reduction in stiffness, including a transition region of minimum stiffness. When the external loading is removed the return of the soil to a no-load situation is likely to occur along a reasonably straight line whose slope corresponds approximately to that of the initial stiffness except in the "locking" region where the slope of the line is approximately the tangent at the final point of the curve if that tangent slope is larger than the initial slope. A typical soil curve is shown in idealized form in Figure E-6 and the corresponding slopes or stiffnesses of Figure E-6 have been drawn in Figure E-7.

All subsequent considerations of nonlinear soils will be based on the assumption that the typical curves in Figures E-6 and E-6a can be adjusted to apply to soil properties at any depth z by modifying independently the two coordinates, the pressure or stress ratio  $\sigma_z/\sigma_o$  and the stiffness or strain ratio  $\epsilon_o/\epsilon_z$ . In other words the stress ordinates or pressures can be multiplied by a constant s and the corresponding abscissas or strains can then be read off in terms of  $\epsilon_z/\epsilon_o$ . The numerical value of the strain ratio is then assumed to be related to the stiffness factor  $M_o/M_z$ . However the effect of the "hydrostatic" soil pressure

$$p_{pz} = \int_0^z \sigma_z dz = g \int_0^z \rho_z dz \quad (E-14)$$

can only be taken into account empirically by a judicious variation of the ratios  $\sigma_z/\sigma_o$  and  $M_o/M_z$ .

#### Example E-6

Assume a soil with the following properties:

At surface:  $M_o = 10^5$  psi ;  $\sigma_o = 100$  psi ; and  $\rho_o g = 130$  lbs/ft<sup>3</sup>

At 53 ft depth:  $M_z = 3 \times 10^5$  psi ;  $\sigma_z = 150$  psi ; and  $\rho_z g = 140$  lbs/ft<sup>3</sup>

#### At the surface

Referring to Figure E-6 it is seen that the terminal point of linearity or the initial slope of unity, marked (1), coincides with  $\sigma_z/\sigma_o = 1$  which means that if the overpressure  $p_{30}$  ordinate is taken as 100 psi, then the corresponding abscissa,  $\epsilon_z/\epsilon_o = 1$ , will be  $1/M_o = 10^{-5}$  in<sup>2</sup>/lb. Accordingly the strain ratio will be  $10^2/10^{-5} = 10^{-3}$  in/in, and the permanent strain ratio  $(\epsilon_z/\epsilon_o)_o$  will be zero. When an overpressure of 300 psi acts on the surface,  $\sigma_z/\sigma_o = 3$ ; see point (2) and the corresponding abscissa  $\epsilon_z/\epsilon_o$  then is 5. This means that the nonlinear strain ratio is  $5 \times 10^{-3}$  in/in. If the 300 psi overpressure is reduced to zero,  $\epsilon_z/\epsilon_o$  will reduce to 2, and the permanent strain ratio at the surface  $(\epsilon_z/\epsilon_o)_o$  is seen to be  $2 \times 10^3$  in/in. Similarly if the overpressure is increased to 1000 psi at

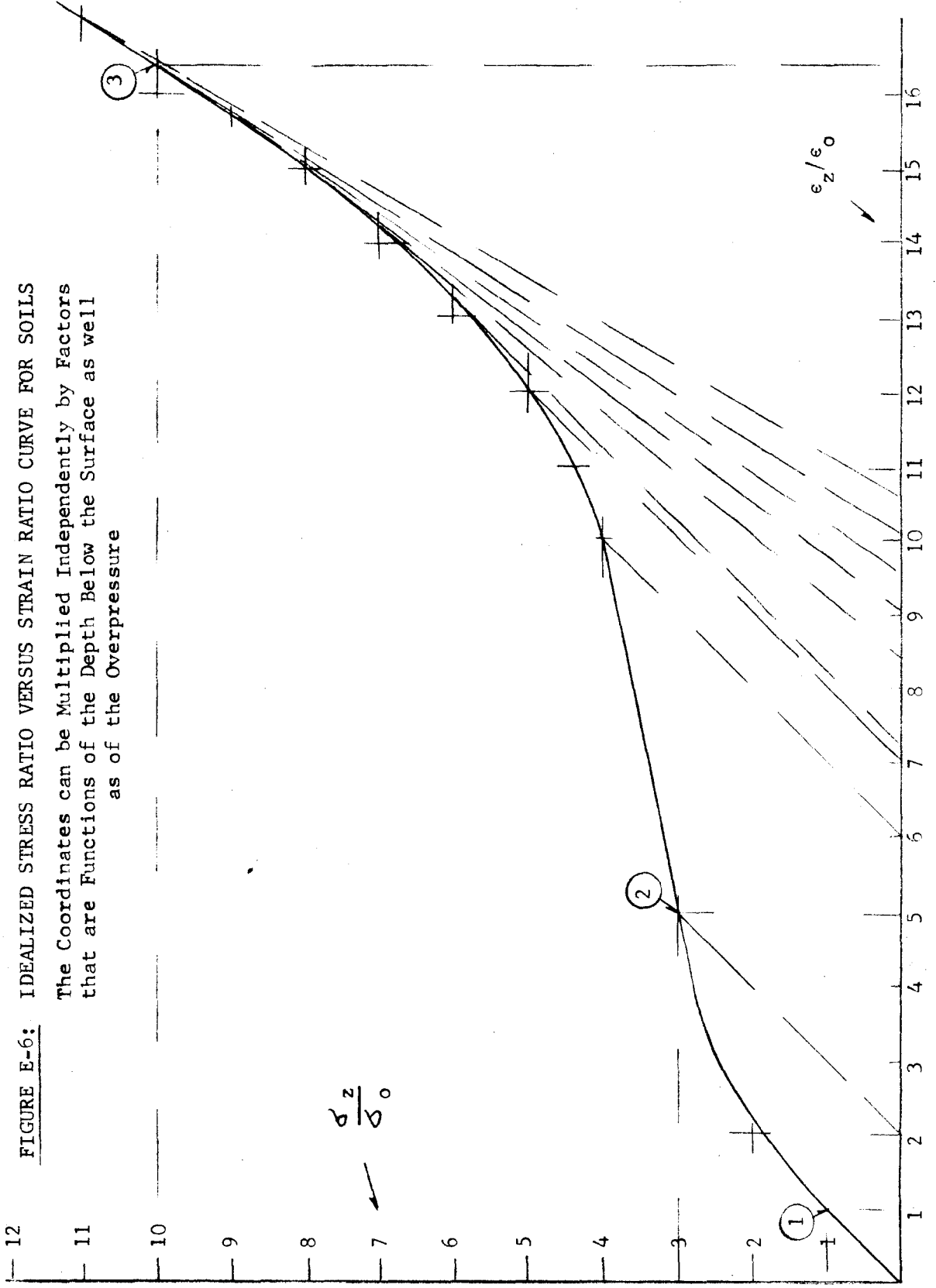


**FIGURE E-6: IDEALIZED STRESS RATIO VERSUS STRAIN RATIO CURVE FOR SOILS**  
 The Coordinates can be Multiplied Independently by Factors  
 that are Functions of the Depth Below the Surface as well  
 as of the Overpressure

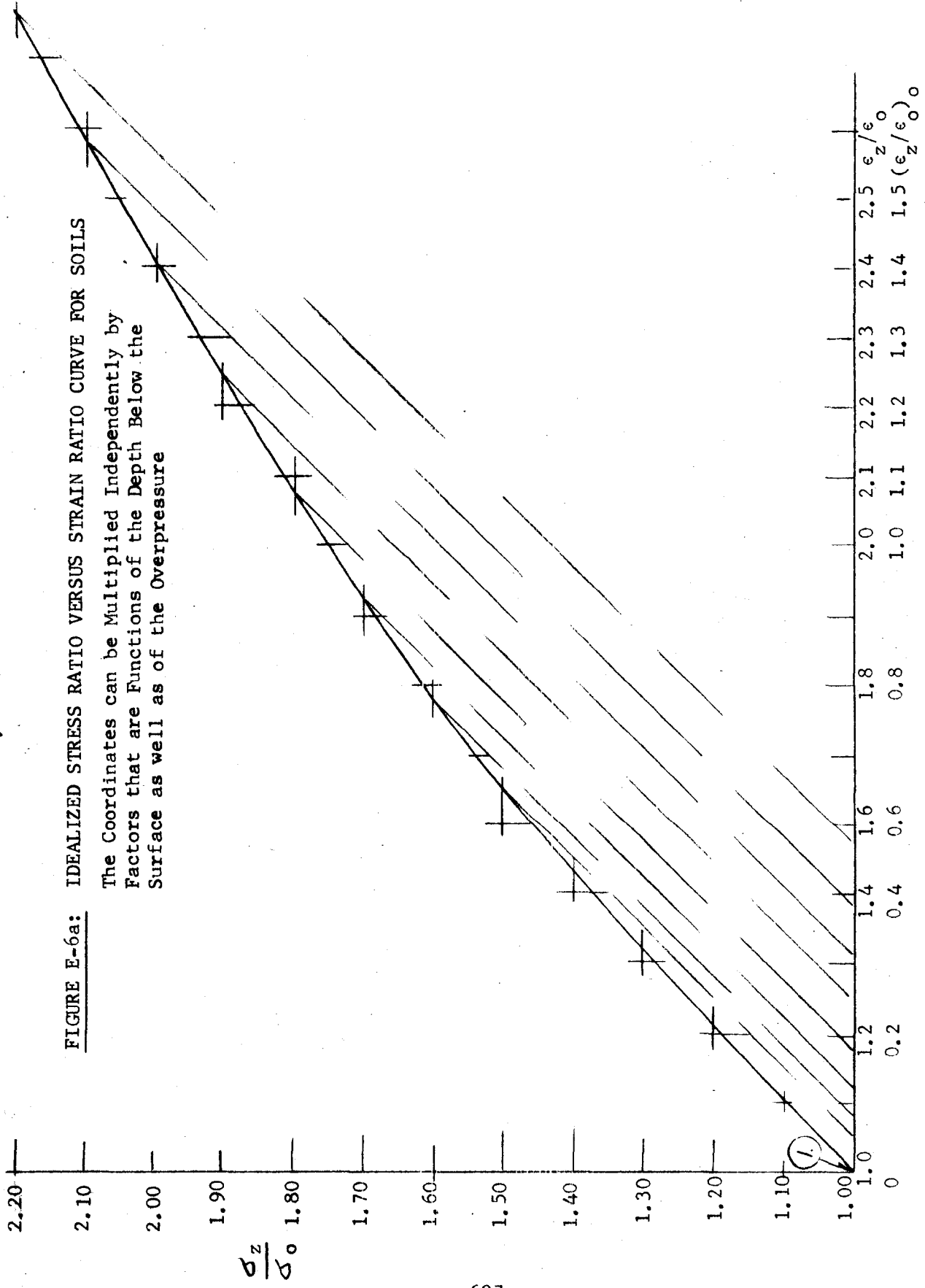
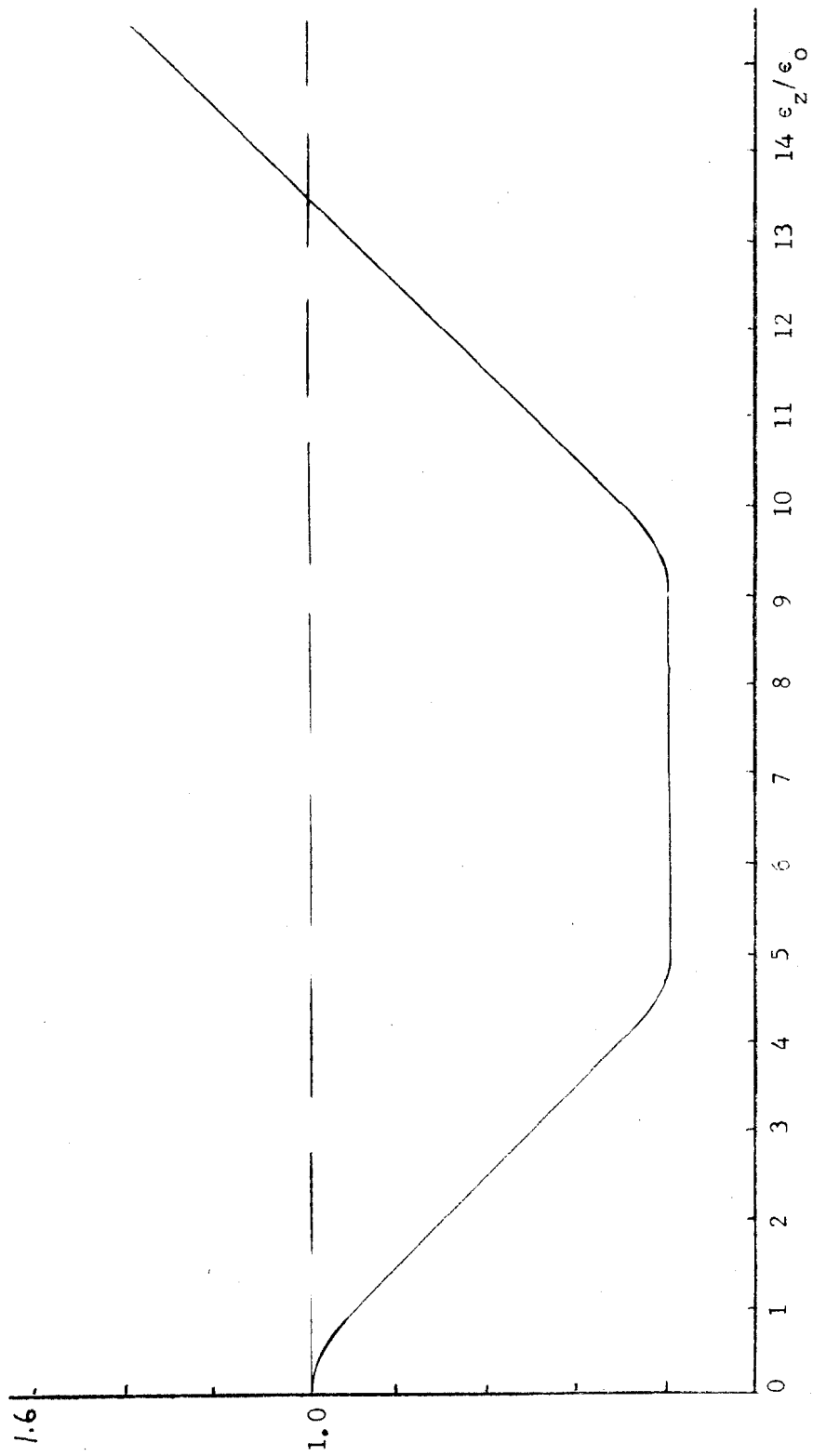


**FIGURE E-6a: IDEALIZED STRESS RATIO VERSUS STRAIN RATIO CURVE FOR SOILS**

The Coordinates can be Multiplied Independently by Factors that are Functions of the Depth Below the Surface as well as of the Overpressure

$$\frac{\frac{\sigma_z}{\sigma_0}}{\frac{\epsilon_z}{\epsilon_0}}$$

FIGURE E-7: SLOPE OF STRESS RATIO - STRAIN RATIO CURVES OF FIGURES 3.40 AND 3.40a



Example E-6 (continued)

the surface  $\sigma_z/\sigma_0 = 10$ ; see point (3), and the corresponding abscissa  $\epsilon_z/\epsilon_0$  is about 16.4; this means that the nonlinear strain ratio is  $16.4 \times 10^{-3}$  in/in. A reduction of the 1000 psi surface pressure to zero will then leave a permanent strain ratio  $(\epsilon_z/\epsilon_0)_0$  of  $10.1 \times 10^{-3}$  in/in at the surface.

At 53 ft depth the hydrostatic pressure is 50 psi

The results obtained for the 100, 300, 1000 psi static overpressure loadings of surface soil corresponding to points (1) (2) and (3) can be arbitrarily related to the soil at the 53 ft depth by multiplying all ordinates of Figure E-6 by  $\sigma_z/\sigma_0$  or 150/100, and all abscissas or strain ratios of Figure E-6 by  $\epsilon_z/\epsilon_0$  or by  $M_0/M_z = 10^5/3 \times 10^5 = 0.333$ . Thus at point (1) the pressure of 150 psi will correspond to a strain ratio of  $10^{-3} \times 0.333 = 0.333 \times 10^{-3}$  in/in. At point (2) the pressure of  $1.5 \times 300 = 450$  psi will correspond to a strain ratio of  $5 \times 10^{-3} \times 0.333 = 1.67 \times 10^{-3}$  in/in and a permanent strain ratio of  $2 \times 10^{-3} \times 0.333 = 0.67 \times 10^{-3}$  in/in. At point (3) a pressure of 1500 psi will correspond to a  $16.4 \times 10^{-3} \times 0.333 = 5.46 \times 10^{-3}$  in/in strain ratio and a permanent strain ratio of  $10.1 \times 10^{-3} \times 0.333 = 1.62 \times 10^{-3}$  in/in.

Summary of Example E-6

At surface			At 53 ft depth			
$P_{so}$	$\epsilon_z/\epsilon_0$	$(\epsilon_z/\epsilon_0)_0$	$P_{so}$	$P_z$	$\epsilon_z/\epsilon_0$	$(\epsilon_z/\epsilon_0)_0$
psi	$10^{-3}$ in/in.		psi		$10^{-3}$ in/in	
100	1	0	100	150	0.33	0
300	5	2	300	450	1.67	0.67
1000	16.4	10.1	1000	1500	2.55	1.62

Procedure for nonlinear soils

The method for finding maximum and permanent strain ratios at a given depth  $z$  in a given soil for a given overpressure  $p_{so}$  and yield  $W$  by means of Figure E-6 is as follows:

Example E-6 (continued)

- (1) Compute the characteristic length  $L$  from Equation (E-10)

$$L = 2300 p_{so}^{-\frac{1}{2}} w^{\frac{1}{3}}$$

- (2) Compute the load pressure  $p_z$  at depth  $z$  from Equation (E-1)

$$p_z = \frac{p_{so}}{1 + \frac{z}{L}}$$

- (3) Compute the "hydrostatic" vertical soil pressure  $p_z$  from Equation (E-14)

$$p_{\rho z} = \int_0^z \rho_z dz$$

- (4) Decide on the value of  $M_z$  at depth  $z$ . If a linear variation with depth is indicated, the expression

$$M_z = M_o (1 + az)$$

can be applied, and the strain ratio will be proportional to  $M_o/M_z$

- (5) By a comparison of  $p_z$  and  $p_{\rho z}$  or by additional knowledge of soil properties decide on a stress ordinate multiplying factor that will be appropriate for depth  $z$ , call this factor  $s$
- (6) Divide the load pressure  $p_z$  by  $s$ ; then for that value find the corresponding abscissa,  $\epsilon_z/\epsilon_o$ , from Figure E-6 and multiply this abscissa by the strain ratio factor  $M_o/M_z$ . This gives the maximum strain ratio at the depth  $z$ . The permanent strain ratio at the depth  $z$  is found by following the appropriate return line in Figures E-6 or E-6a to zero load and then multiplying this strain ratio by  $M_o/M_z$ .
- (7) Having determined the maximum and the permanent strain ratios at a number of judiciously chosen depths, either a numerical or a graphical integration can be used to find the corresponding vertical displacements.



### Example E-7

A practical case will now be considered in which only the soil stiffness is assumed to increase with depth while the  $\sigma_z/\sigma_0$  stress factor remains constant. In other words the "hydrostatic" stress effect as well as other depth effects are neglected in regard to stress level. The case will apply to a 10 MT burst; it will be worked out for overpressure levels of 200, 300, and 1000 psi.

Table E-III lists the attenuated pressures at depths down to 2000 ft. Based on the assumption that at point (1) of Figure E-6 the stress is 100 psi, Figure E-6 in conjunction with Table E-III will give the maximum and permanent strain ratios. These have been recorded in Table E-IV at each level for the three overpressures by taking into account the specific stiffness increase in  $M_z$  as governed by the equation

$$M_z = M_1 (1 + 0.0415z)$$

with  $z$  in feet. Table E-V gives the results of integrating, graphically, with respect to depth the maximum and permanent strain ratios of Table E-IV.

Figures E-8, E-9, and E-10 plot the results of Tables E-IV and E-V for the 200, 300, and 1000 psi overpressure cases respectively, using the two depth scales of 0-100 ft and 100-1000 ft.

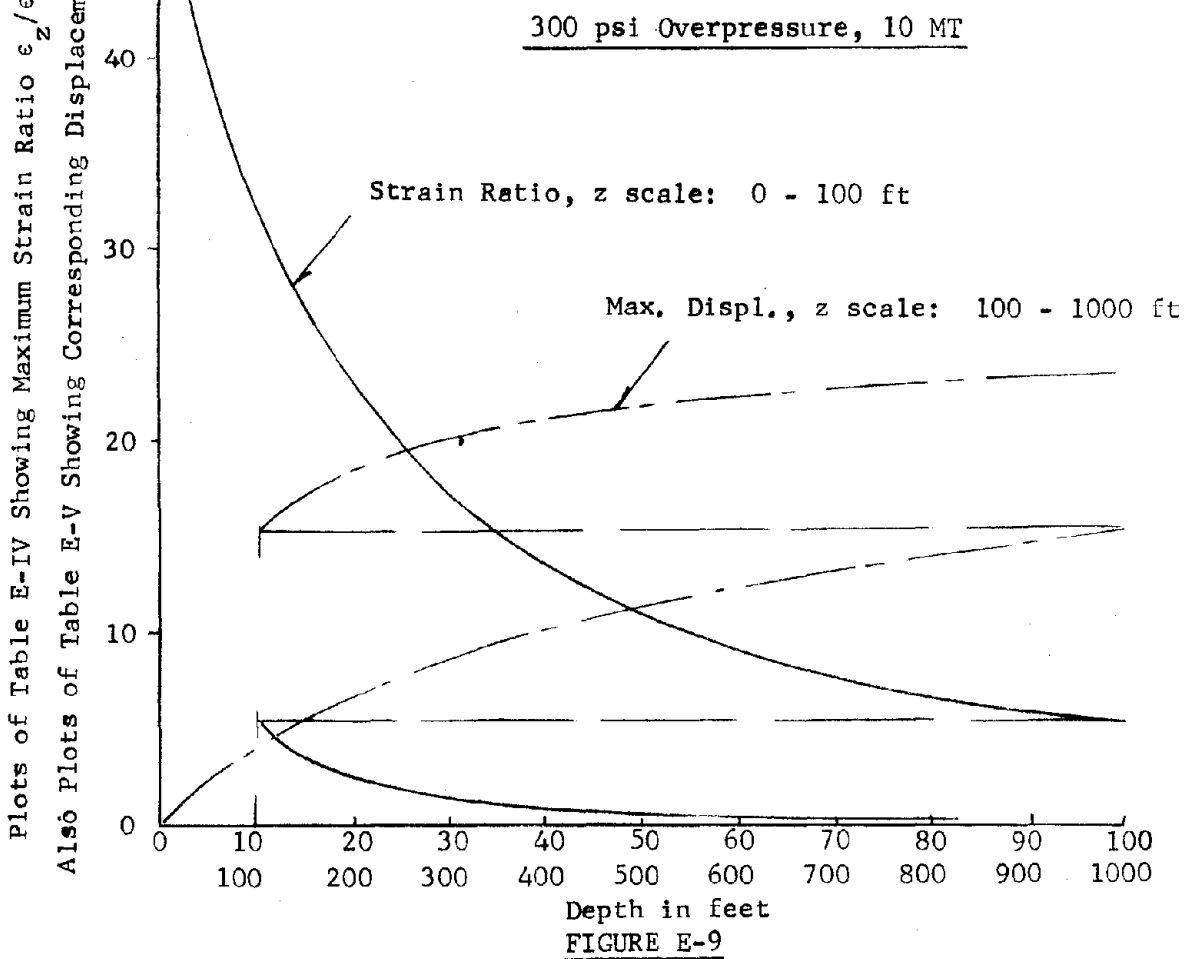
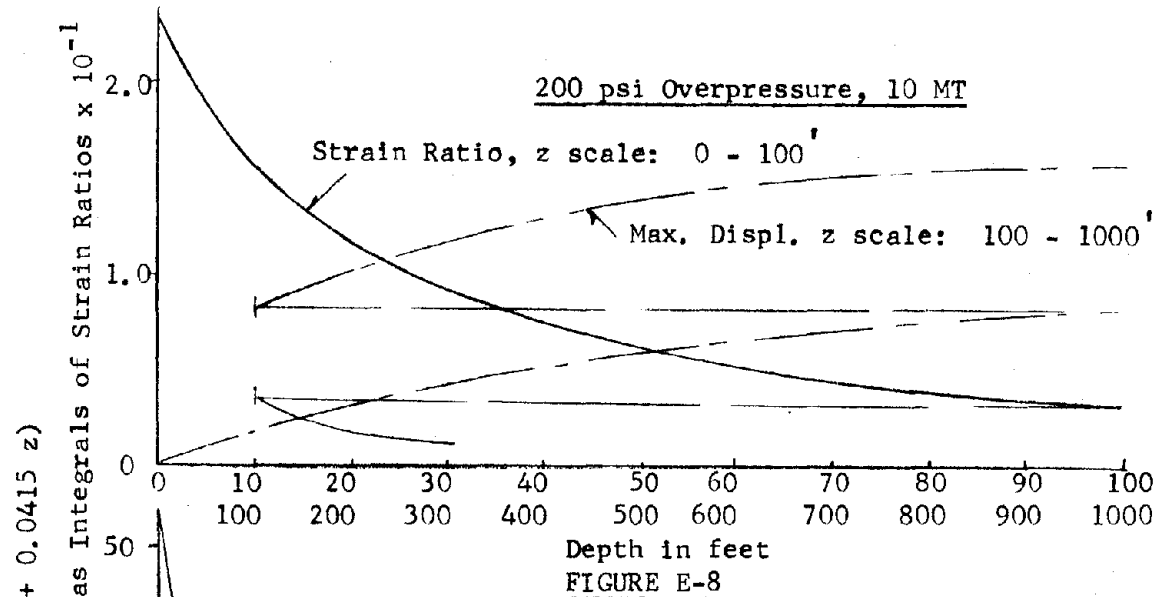
It is seen that the permanent strain ratios become relatively small for depths below 100 ft, and that the maximum strain ratios reduce to one tenth of their surface values at depths between 100 and 160 ft.

Table E-V or Figures E-8 to E-10 can now be used to calculate the displacements for any given value of  $M_0$ . If the same soil constants are chosen as are represented in Figure E-4, the value of  $M_0$  is  $6.25 \times 10^4$  psi. In this case the integrated strain ratios of Table E-V must be multiplied by:

$$\frac{100 \text{ psi}}{M_0} = \frac{100}{6.25 \times 10^4} = 1.6 \times 10^{-3}$$

Accordingly the total and the permanent displacements between the surface and the 2000 ft depth for the 1000 psi overpressure case will be

Max. displacement	$978 \times 1.6 \times 10^{-3}$	$= 1.57 \text{ ft} \approx 18.8 \text{ inches}$
Permanent "	$552 \times 1.6 \times 10^{-3}$	$= .88 \text{ ft} \approx 10.6 \text{ inches}$



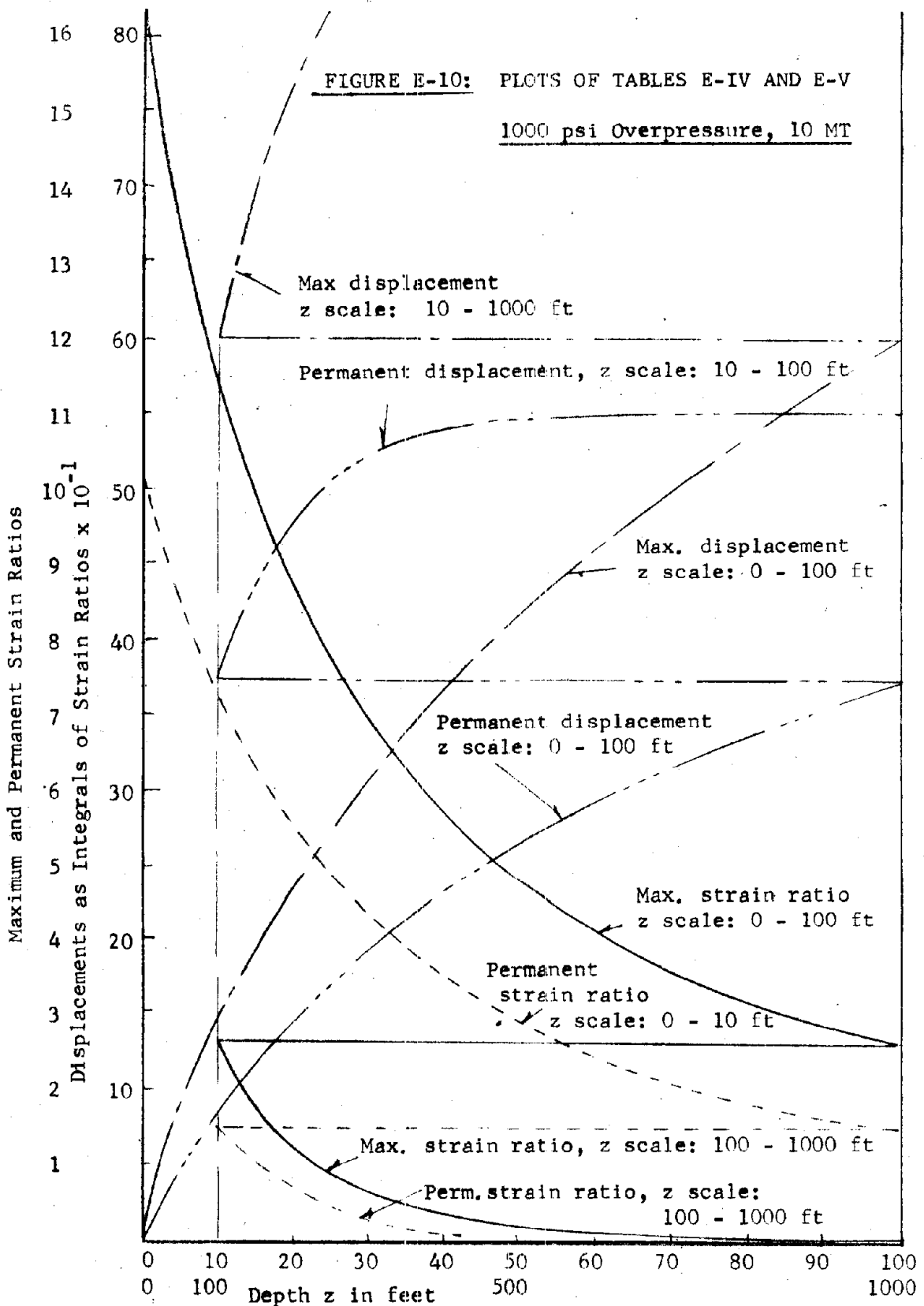


TABLE E-III

Attenuation of Vertical Pressure  $p_z$  with Depth  $z$ 

L	520 ft	368 ft	300 ft	165 ft
Surface $z = 0$ ft	100 psi	200 psi	300 psi	1000 psi
10	98	195	291	943
20	96	190	282	893
30	95	185	273	846
40	93	181	264	806
50	91	176	257	768
60	90	172	250	735
70	88	168	243	702
80	87	164	237	673
90	85	161	231	647
100	84	157	225	623
200	72	129	180	453
300	63	110	150	353
400	56	96	128	292
500	51	85	112	248
800	39	63	82	171
1000	34	54	69	142
2000	21	31	39	76

TABLE E-IV

## Strain Factors at Different Depths

	200		300		1000 psi	
0 depth	2.310	.310	5.20	2.00	16.35	10.5
10 ft depth	1.590	.205	3.24	1.13	11.30	7.2
20	1.170	.137	2.30	.77	8.58	5.53
30	.920	.098	1.69	.44	6.82	4.44
40	.748	.071	1.32	.34	5.67	3.46
50	.625	.055	1.11	.26	4.78	2.92
60	.528	.043	.92	.20	4.14	2.52
70	.456	.031	.79	.17	3.64	2.26
80	.402	.025	.68	.14	3.21	1.89
90	.359	.019	.60	.12	2.87	1.73
100	.316	.013	.53	.10	2.62	1.51
200	.141	.011	.22	.02	1.22	.73
300	.086	0	.12	0	.56	.30
400	.056	0	.08	0	.26	.10
500	.039	0	.05	0	.15	.03
800	.024	0	.03	0	.07	.004
1000	.013	0	.02	0	.03	.001
2000 ft depth	.004	0	.005	0	.01	0

The second factor is for permanent strain ratio

TABLE E-V  
Integrations of Strains

	200 psi		300 psi		1000 psi	
10 ft depth	18.0	2.5	40.0	15.5	135	84
20	31.5	4.2	67.5	24.5	233	147
30	42.0	5.4	87.5	30.1	309	196
40	50.5	6.2	103	33.9	371	235
50	57.5	6.8	115	36.9	423	266
60	63.3	7.3	125	39.4	467	293
70	68.3	7.7	133	41.3	506	317
80	72.8	8.0	140	42.9	540	338
90	76.6	8.2	146	44.2	570	386
100	80.0	9.8	153	45.3	598	372
200	102.7	11.0	186	51.3	768	477
300	119.7	11.5	202	52.3	858	527
400	131.7	11.5	212	52.3	898	547
500	139.7	11.5	218	52.3	918	552
800	144.5	11.5	230	52.3	948	552
1000	153.5	11.5	235	52.3	958	552
2000	157.0	11.5	245	52.3	978	552

The second factor is for permanent strain integral.

TABLE E-VI

Results of Nonlinear Soil Calculations for 10 MT Yield  
Absolute Displacements in Inches

			200 psi	300 psi	1000 psi
Max. displ. at surface			3.02 (2.70)	4.70 (3.70)	18.8 (9.90)
Perm. " " "			0.22	1.00	10.6
Max. " " 50' level			1.80 (0.48)	2.50 (0.70)	11.7 (1.30)
Perm. " " 50' "			0.09	.30	5.3
Max. " " 100' level			1.40 (.029)	1.77 (0.42)	7.3 (1.10)
Perm. " " 100' "			0.03	0.13	3.5

For comparison the displacements obtained by employing the linear theory of soil as obtained by the use of Figures E-1 and E-3 are shown in brackets in the above tabulation. It is seen that for the maximum displacement at the surface the linear theory gives values that are not radically different from those obtained by the nonlinear. This is due to the assumed "locking" action of the soil which as shown in Figure E-6 renders the gross appearance of the curve relatively linear. At the 50 ft and 100 ft depths however the linear and nonlinear theory results are seen to differ considerably, especially for the largest overpressure.

#### Conclusions

The static deformation of a soil is relatively easy to estimate if the soil properties are known at various depths and if the vertical load stress is assumed to attenuate in a given manner. But the dynamic deformation of a soil involves considerable uncertainty, especially in a stratified medium where wave reflections and refractions of dilatational as well as of distortional waves are bound to occur.

## APPENDIX F

### SOIL-STRUCTURE MODELS FOR COMPUTER SOLUTION

1. Simplified models. A mathematical model representing a structure and its surrounding soil may be defined in terms of lumped parameters. Figure F-1 shows a cylindrical structure and the analogous model consisting of lumped masses connected by extensional straight bars (from Reference F.1).

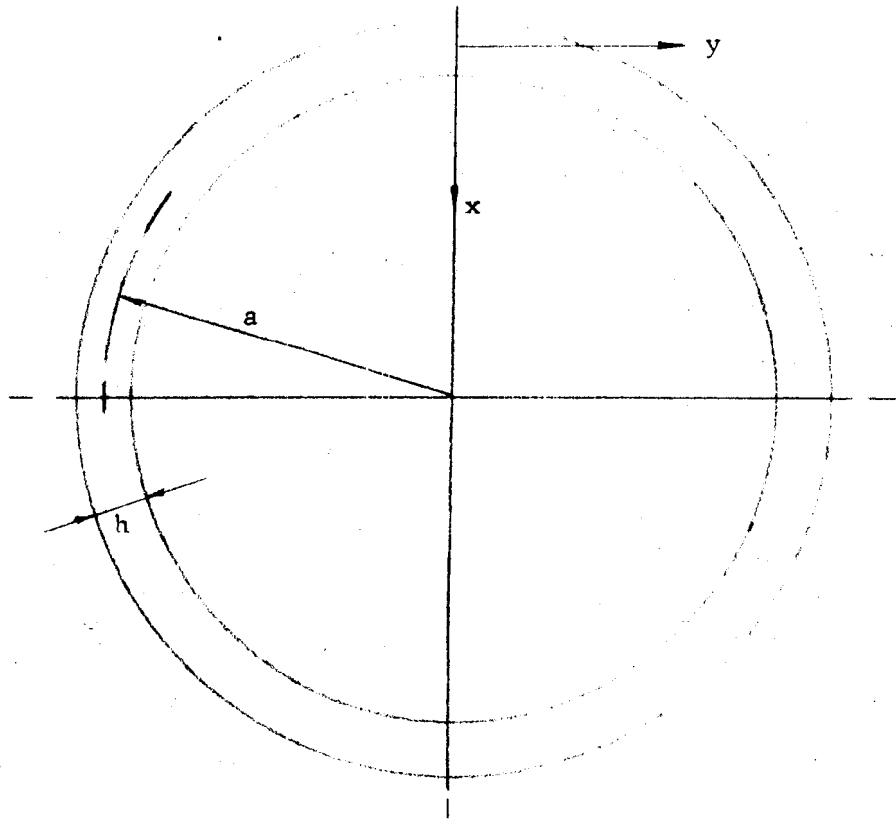
The straight bars are assumed to be massless and rigidly connected to each mass and they are assumed to have bending as well as extensional stiffnesses. Figure F-2 shows a free body diagram for a typical joint where the soil-interface with the structure is represented by a non-linear hysteretic type spring in parallel with a non-linear dashpot. The forcing function is applied at each mass (in a radial direction); it can be defined in terms of the arrival time and the force-time relationship of the stress wave passing through the soil. The model enables the investigator to determine the significance of the radial deformational modes in defining the input to items attached to the structure.

In the reference above and in Reference the bending and shear modes of the structure in its longitudinal direction are also represented by a lumped mass model (see Figure F-3). In the case of a long silo structure the bending and shear modes may be important. The forcing functions are therefore applied at each mass and the soil interface with the structure is defined in terms of springs and dashpots acting between masses. From this analysis the effect of the transverse flexibility of a structure in modifying the input to items attached to the structure may be determined.

2. Generalized model. A more generalized approach than the cited examples may be taken by assuming that the soil and the structure are broken up into a finite number of discrete masses, each mass connected by compression springs and shear springs to adjacent ones. The masses located at the boundary will be acted upon by external forces or by ground velocities. The in-structure systems are treated as a subsystem using as inputs the obtained responses of the structural enclosures.



a) Silo Lining Geometry



b) Analogous Structure

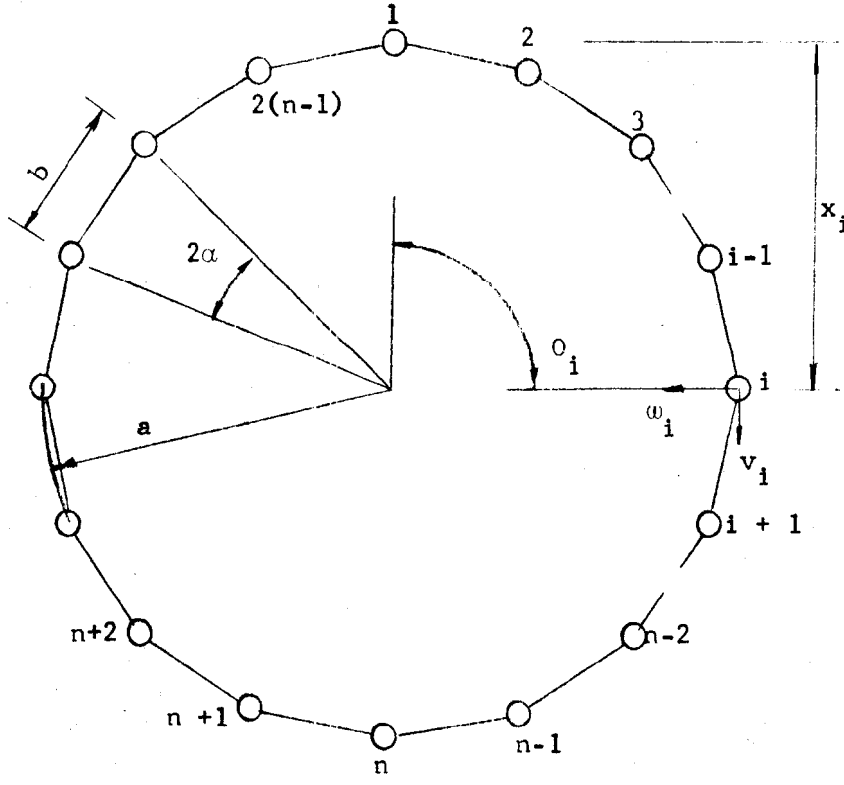


FIGURE F-1: ACTUAL AND ANALOGOUS STRUCTURES

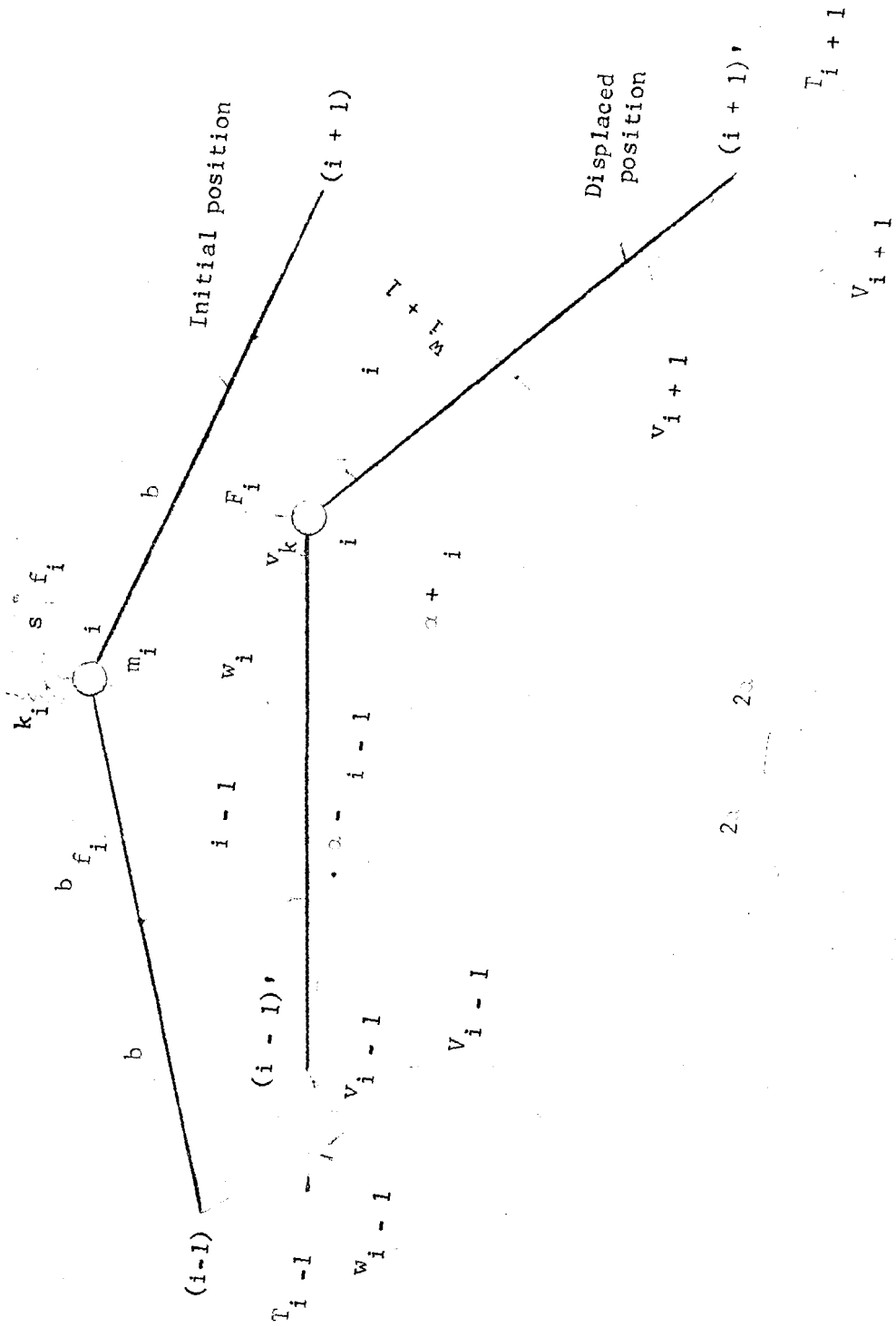


FIGURE F-2: FREE BODY DIAGRAM FOR TYPICAL JOINT

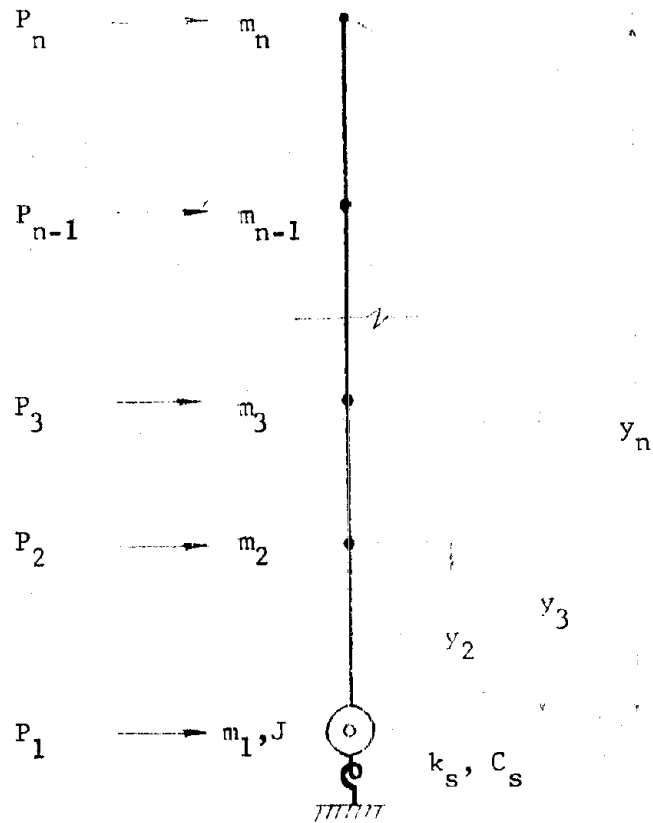


FIGURE F-3: LUMPED PARAMETER MODEL OF SILO

Figure F-4 shows a two dimensional, lumped soil-structure model amenable to computer solution. The absolute horizontal and vertical response-time histories of each mass can be computed as well as the relative displacement history between adjacent masses. The shear springs between adjacent soil masses may exhibit elastic-plastic behavior following an elastic region. Moreover a Coulomb type damping force equal to the yield value of the plastic spring can be made to depend on the normal force or compression between two lumped soil masses.

Any combination of overpressure, vertical ground shock or horizontal ground pulses can be applied at the boundaries of the model at any phasing relationship desired. The response of the six masses representing the structure itself is obtained in terms of displacement, velocity, and acceleration, that are expressed as functions of time. Horizontal and vertical

displacements but no rotations are possible in the simplified model shown in Figure F-5.

The second order equations of motion for the discrete masses are very similar and a typical set for mass No. 9 is given below:

$$(X_4 - X_9)K_{4-9} + (X_{17} - X_9)K_{9-17} + (X_8 - X_9)\tau_{8-9} + (X_{10} - X_9)\tau_{9-10} = M_9 \ddot{X}_9$$

$$(Y_8 - Y_9)K_{8-9} + (Y_{10} - Y_9)K_{9-10} + (Y_4 - Y_9)\tau_{4-9} + (Y_{17} - Y_9)\tau_{9-17} = M_9 \ddot{Y}_9$$

Where by definition:

- $F_1, F_6, \dots, F_{24}$  : each are overpressure force vs time (as a traveling wave)
- $x_1, x_2, \dots, x_5$  : each are horizontal displacement of freefield vs time
- $y_1, y_2, \dots, y_5$  : each are vertical displacement of freefield vs time
- $\tau_{1-2}, \tau_{2-7}, \dots$  : each are shear springs with are represented as coulomb dampers with  $F_{\text{yield}} = \mu \times \text{normal force}$
- $K_{1-2}, K_{2-3}, \dots$  : each are vertical compressive springs which are non-linear but defined by analytical function
- $K_{1-6}, K_{2-7}, \dots$  : each are horizontal compressive springs which are non-linear but defined by analytical function.
- $K_{11-14}, K_{12-15}, \dots$  : are compressive springs of structure (radial)
- $K_{11-12}, K_{12-13}, \dots$  : are compressive springs of structure (longitudinal)
- $\tau_{11-12}, \dots, \tau_{12-13}$  : are shear (and bending) springs of structure

The yield values of the four shear constants ( $\tau_{8-9}, \tau_{9-10}, \tau_{4-9}, \tau_{9-7}$ ) will be a function of the compressions in the longitudinal springs ( $K_{i-j}$ ). The effects of damping may be accounted for in the longitudinal constants ( $K_{4-9}, K_{9-17}, K_{8-9}, K_{9-10}$ ) by assuming that the springs have bilinear force-displacement characteristics with hysteresis.

In this example, since the structure is represented by only six masses with inter-connecting longitudinal and shear springs, it cannot give a very complete representation of the structure's behavior. The horizontal or

Structure (see Figure F-5)

Overpressure Pulse

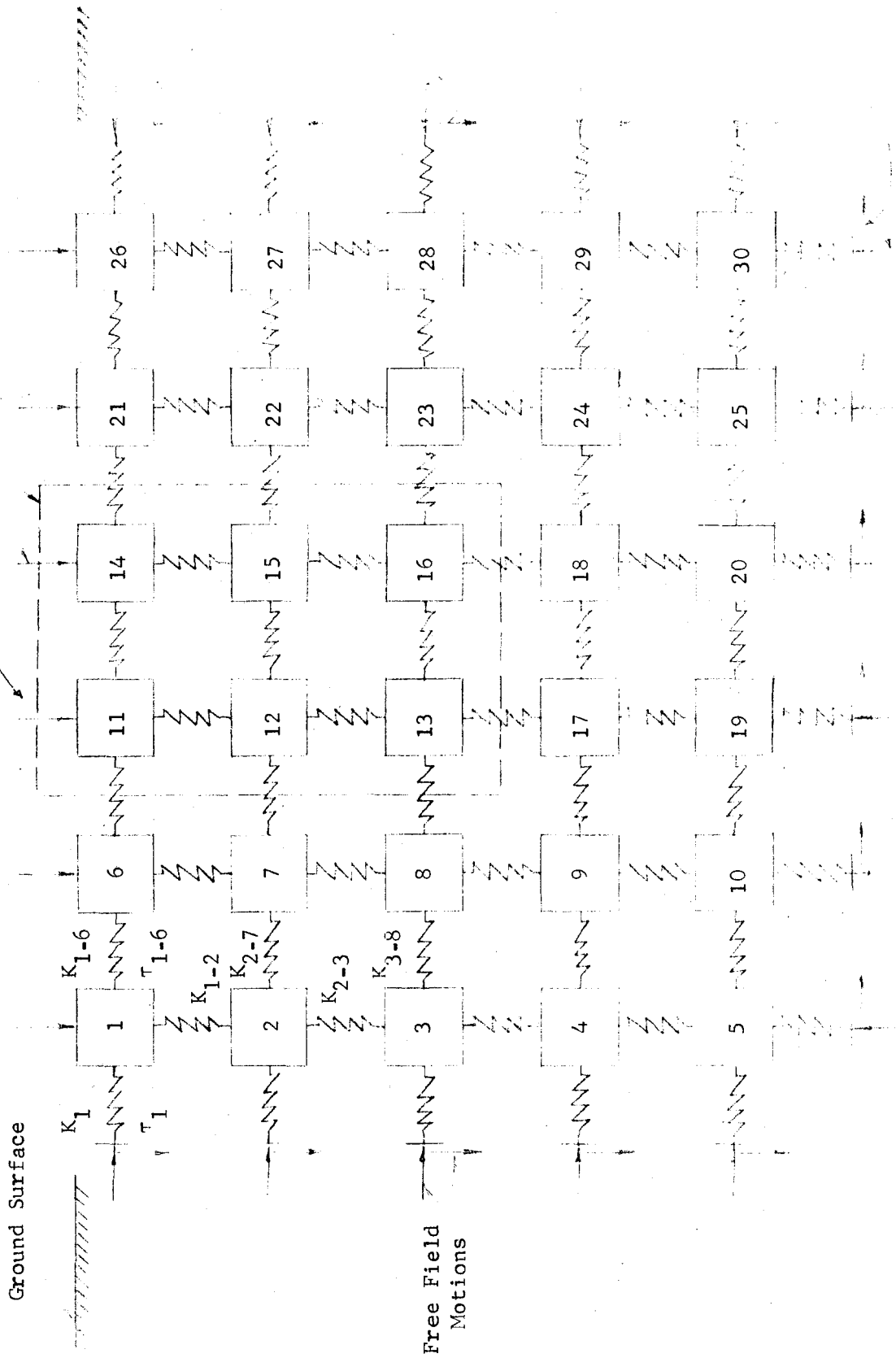
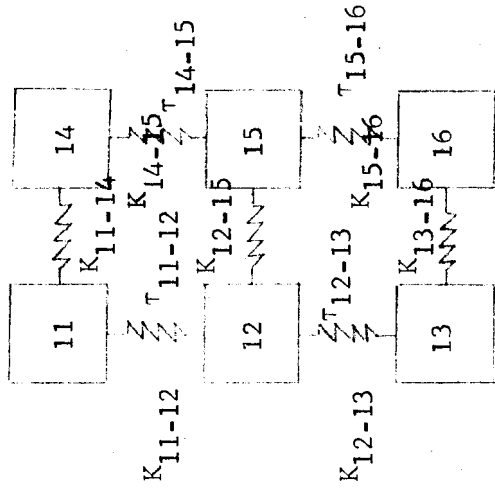
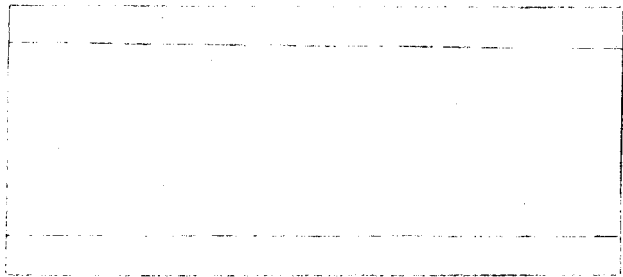
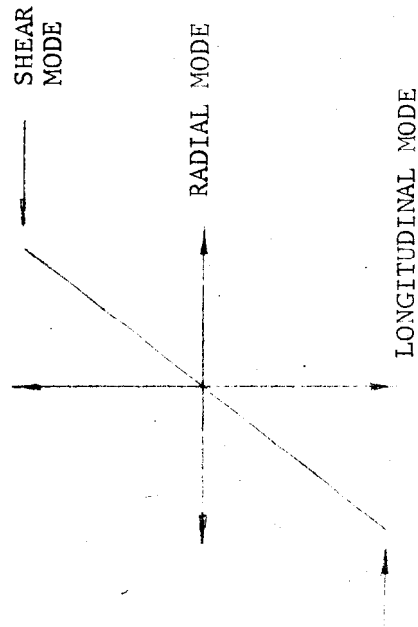


FIGURE F-4: TWO DIMENSIONAL STRUCTURE RESPONSE MODEL



DYNAMIC MODEL



BURIED SILO

FUNDAMENTAL MODES

Model of Structure

FIGURE F-5

"breathing" modes involve the longitudinal springs  $K_{11-14}$ ,  $K_{12-15}$ , and  $K_{13-16}$  as well as the shear springs  $\tau_{11-12}$ ,  $\tau_{12-13}$ ,  $\tau_{14-15}$  and  $\tau_{15-16}$ . The vertical modes involve mainly the longitudinal springs  $K_{11-12}$ ,  $K_{12-13}$ ,  $K_{14-15}$  and  $K_{15-16}$ . If the structure's bending mode is of interest it will be inadequately represented by the indicated spring system, but two additional sets of diagonal springs of relatively high stiffness will introduce "bending" deformations.

The computed relative displacements determine the distortional configurations by which loads and distortions of the structure itself can be inferred.

#### Example

A flush-buried steel reinforced concrete structure is to be investigated for its response which results from a surface blast wave in the 100 psi overpressure region. In Figure F-6 it is assumed that the soil surrounding the structure is less stiff than the structure itself and therefore a frictional force is induced on the vertical walls of the structure due to

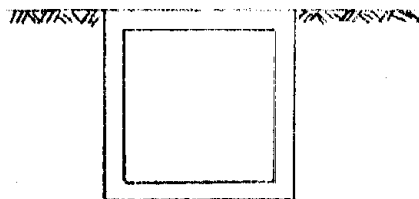
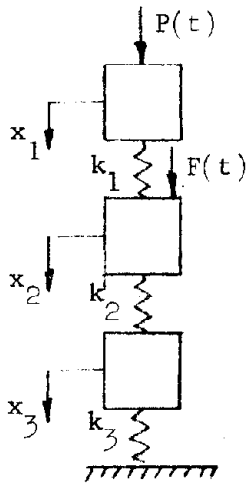


FIGURE F-6

relative movement between the soil and the structure during passage of the blast wave. The frictional force is dependent on the normal stress acting on the vertical slabs which in turn is composed of a hydrostatic stress and an overpressure induced stress. In addition to the friction force, the overpressure pulse acts directly on the top slab tending to drive the entire structure downwards.

The model chosen to represent the vertical motion of the structure is shown in Figure F-7.



- $m_1$  = effective mass of top slab
- $m_2$  = effective mass of vertical slabs
- $m_3$  = effective mass of bottom slab
- $k_1$  = spring constant of top slab
- $k_2$  = spring constant of bottom slab
- $k_3$  = spring constant of soil

FIGURE F-7

The corresponding equations of motion

$$\begin{aligned}
 m_1 \ddot{x}_1 + k_1 (x_1 - x_2) &= P(t) \\
 m_2 \ddot{x}_2 + k_1 (x_2 - x_1) + k_2 (x_2 - x_3) &= F(t) \\
 m_3 \ddot{x}_3 + k_2 (x_3 - x_2) + k_3 (x_3) &= 0
 \end{aligned}
 \tag{F-1}$$

during the impulsive period are given in Equation (F-1). The friction force between side walls and soil which resist motion of the structure has been neglected. These equations may be solved as they stand but for most purposes it is useful to transform them into an equivalent form as follows:

$$\begin{aligned}
 \omega_1^2 y_1 - P/m_1 &= -\ddot{y}_1 - \ddot{y}_2 - \ddot{x}_3 \\
 -\lambda_2^2 \omega_2^2 y_1 + \omega_2^2 y_2 - F/m_2 &= -\ddot{y}_2 - \ddot{x}_3 \\
 -\lambda_3^2 \omega_3^2 y_2 + \omega_3^2 x_3 &= -\ddot{x}_3
 \end{aligned}
 \tag{F-2}$$



where

$$\omega_1^2 = k_1/m_1$$

$$\omega_2^2 = k_2/m_2$$

$$\omega_3^2 = k_3/m_3$$

$$\lambda_2^2 = k_1/k_2$$

$$\lambda_3^2 = k_2/k_3$$

$$y_1 = x_1 - x_2$$

$$y_2 = x_2 - x_3$$

Equation (F-2) may be rewritten in the following impulse-momentum form

$$\int_{t_1}^{t_2} [\omega_1^2 y_1 - P/m_1] dt = - \int_{\dot{y}_{11}}^{\dot{y}_{12}} d\dot{y}_1 - \int_{\dot{y}_{21}}^{\dot{y}_{22}} d\dot{y}_2 - \int_{\dot{x}_{31}}^{\dot{x}_{32}} d\dot{x}_3$$

$$\int_{t_1}^{t_2} [-\lambda_2^2 \omega_2^2 y_1 + \omega_2 y_2 - F/m_2] dt = - \int_{\dot{y}_{21}}^{\dot{y}_{22}} d\dot{y}_2 - \int_{\dot{x}_{31}}^{\dot{x}_{32}} d\dot{x}_3 \quad (F-3)$$

$$\int_{t_1}^{t_2} [-\lambda_3^2 \omega_3^2 y_2 + \omega_3^2 x_3] dt = - \int_{\dot{x}_{31}}^{\dot{x}_{32}} d\dot{x}_3$$

Using Equations (C-5) thru (C-7) of Appendix C allows a system of difference equations to be written

$$y_{12} \left( \frac{\omega_1^2 \Delta t}{2} + \frac{2}{\Delta t} \right) + y_{22} \left( \frac{2}{\Delta t} \right) + x_{32} \left( \frac{2}{\Delta t} \right) = y_{11} \left( \frac{2}{\Delta t} - \frac{\omega_1^2 \Delta t}{2} \right) + y_{21} \left( \frac{2}{\Delta t} \right) + x_{31} \left( \frac{2}{\Delta t} \right) + 2\dot{y}_{11} + 2\dot{y}_{21} + 2\dot{x}_{31} + \frac{P_1 + P_2}{m_1} \frac{\Delta t}{2}$$

$$y_{12} \left( -\frac{\omega_2^2 \Delta t}{2} + \frac{2}{\Delta t} \right) + y_{22} \left( \frac{\omega_2^2 \Delta t}{2} + \frac{2}{\Delta t} \right) + x_{32} \left( \frac{2}{\Delta t} \right) = y_{11} \left( \frac{\omega_2^2 \Delta t}{2} + \frac{2}{\Delta t} \right) + y_{21} \left( \frac{2}{\Delta t} - \frac{\omega_2^2 \Delta t}{2} \right) + x_{31} \left( \frac{2}{\Delta t} \right) + 2\dot{y}_{21} + 2\dot{x}_{31} + \frac{F_1 + F_2}{m_2} \frac{\Delta t}{2} \quad (F-4)$$

$$y_{22} \left( -\frac{\omega_3^2 \Delta t}{2} + \frac{2}{\Delta t} \right) + x_{32} \left( \frac{\omega_3^2 \Delta t}{2} + \frac{2}{\Delta t} \right) = y_{21} \left( \frac{\omega_3^2 \Delta t}{2} + \frac{2}{\Delta t} \right) + x_{31} \left( \frac{2}{\Delta t} - \frac{\omega_3^2 \Delta t}{2} \right) + 2\dot{x}_{31}$$

These equations are to be solved simultaneously for the response values  $y_{12}$ ,  $y_{22}$ , and  $x_{32}$  in terms of the previous values on the right hand side of the equations.

As a numerical example, consider the structure to have a base and height dimension of 20 feet and a length of 60 feet. The walls are 2 1/2 feet thick with 1.3 percent steel reinforcement. The mass of each slab is

$$m = \frac{2.5\text{ft} \times 20\text{ft} \times 60\text{ft} \times 150 \text{ lb/ft}^3}{g} = \frac{45 \times 10^4}{g}$$

The equivalent mass of each slab is, from Equation B-16,

$$m_e = k_{Lm} m = \frac{0.78 \times 45 \times 10^4}{g} = \frac{35 \times 10^4}{g}$$

The natural period of the slabs are (Equation B-16)

$$T = \frac{1}{7200} \frac{L^2}{d \sqrt{\phi}} = \frac{(20\text{ft})^3}{7200 \text{ fps } (2.19\text{ft}) \sqrt{1.3}} = 0.0222 \text{ sec}$$

and the natural frequency is

$$f = \frac{1}{T} = 45 \text{ cps}$$

In the notation of the model of Figure F-7

$$m_1 = m_3 = \frac{35 \times 10^4}{g} \frac{\text{lb sec}^2}{\text{in}}$$

$$m_2 = \underbrace{2 \frac{45 \times 10^4}{g}}_{\text{Longitudinal Slabs}} + \underbrace{2(1-0.78) \frac{45 \times 10^4}{g}}_{\text{Top and Bottom Slabs}} + \underbrace{2 \frac{45 \times 10^4}{g} \frac{20}{60}}_{\text{End Slabs}} = \frac{140 \times 10^4}{g} \frac{\text{lb sec}^2}{\text{in}}$$

$$k_1 = k_2 = (2\pi f)^2 m_1 = 7.25 \times 10^7 \text{ lb/in}$$

The spring  $k_3$  represents the elasticity of the soil

$$k_3 = 100 \text{ lb/in/in}^2 \times 60\text{ft} \times 20\text{ft} \times 144 \text{ in}^2/\text{ft}^2 = 1.728 \times 10^7 \text{ lb/in}$$

Let  $P(t)$  represent the force on the top slab caused by the overpressure pulse in terms of a Brode overpressure function.

$$P(t) = 20\text{ft} \times 60\text{ft} \times 144 \text{ in}^2/\text{ft}^2 \times P_{so} \left(1 - \frac{t}{D_+}\right) \left(Ae - \frac{\alpha t}{D_+} + Be - \frac{\beta t}{D_+} + Ce - \frac{\gamma t}{D_+}\right)$$

which for the 100 psi overpressure region and 1 MT yield results in

$$P(t) = 1.728 \times 10^7 \left(1 - \frac{t}{9}\right) (0.6e^{-2.11t} + 0.4e^{-12.8t}) \text{ lb} \quad t \leq 0.9 \text{ sec}$$

The average hydrostatic pressure acting on the vertical slabs is

$$p = 110 \text{ lb/ft}^3 \times 10 \text{ ft} = 1100 \text{ lb/ft}^2$$

The lateral stress on the soil due to the overpressure is about one-third the Brode overpressure. Therefore the total frictional force\* acting on the structure is

$$F(t) = \frac{2 \times 20 \times 60 \times 144 \times 100 + 2 \times 20 \times 20 \times 144 \times 100}{3} \left(1 - \frac{t}{9}\right) (0.6e^{-2.11t} + 0.4e^{-12.8t}) \\ + 2 \times 20 \times 60 \times 1100 + 2 \times 20 \times 20 \times 1100 \quad f$$

where  $f$  = coefficient of friction, assumed to be 0.5

$$F(t) = 7.7 \times 10^6 \left(1 - \frac{t}{9}\right) (0.6e^{-2.11t} + 0.4e^{-17.8t}) + 1.76 \times 10^6 \text{ lb} \quad t \leq 0.9$$

which is the combination of the overpressure component and the hydrostatic component. Note that the form of  $F(t)$  is  $F(t) = \gamma P(t) + \text{constant}$ .

Substitution of the physical parameters and the forcing functions  $P(t)$  and  $F(t)$  into Equations (F-4) where the initial conditions are zero allows solution of the time history response of the model of Figure F-7. These equations are solved at each increment in time where the solutions of the variables on the left hand side become inputs on the right hand side as time is indexed over one increment. The time increment is usually taken as 1/10 to 1/20 of the lowest uncoupled natural period of the system - in this case 0.002 seconds.

Included herein is a Fortran computer program which solves the difference Equations (F-4) and yields displacement and velocity time histories. The results of the particular problem are plotted in Figures F-8 and F-9 in terms of displacements. For convenience, Figure F-8 represents the response with both the direct air blast and fictional forces acting while in Figure F-9 the frictional component has been neglected. This example only illustrates a method for computing response of a soil-structure model and therefore general conclusions should not be drawn from the results.

---

\* The soil mass adjacent to the structure is assumed to be moving down relative to structure, giving a constant positive soil friction force. This assumption is undoubtedly conservative.

```

01. = CF PROGRAM SSI
02. = C ENTER THE MASSES M1,M2,M3, THE SPRING CONSTANTS K1,K2,K3, THE
03. = C FRICTION CONSTANT, THE TIME INCREMENT, AND THE HYDROSTATIC CONSTANT
04. = CF READ 0,W1,W2,W3,S1,S2,S3,GAMMA,DELT,CONSTF
05. = PAUSE
06. = PRINT 101
07. = 1010FORMAT(10X,13HDISPLACEMENTS,9X,2H**,10X,10HVELOCITIES,11X,2H**,2X,
    44HTIME)
08. = PRINT 103
09. = 1020FORMAT(4X,2HX1,9X,2HX2,9X,2HX3,9X,3HDX1,8X,3HDX2,8X,3HDX3,9X,1HT,/
    4)
10. = PRINT 102
11. = 103 FORMAT(15X,2HIN,30X,3HIPS,20X,3HSEC)
12. = C COMPUTE CONSTANTS
13. = OMEGA1=S1/W1
14. = OMEGA2=S2/W2
15. = OMEGA3=S3/W3
16. = AMBD2=S1/S2
17. = AMBD3=S2/S3
18. = C1=OMEGA1*DELT/2.+2./DELT
19. = C2=2./DELT
20. = C3=2./DELT-OMEGA1*DELT/2.
21. = C4=DELT/2./W1
22. = C5=AMBD2*OMEGA2*DELT/2.
23. = C6=OMEGA2*DELT/2.+2./DELT
24. = C7=2./DELT-OMEGA2*DELT/2.
25. = C8=DELT/2./W2
26. = C9=AMBD3*OMEGA3*DELT/2.
27. = C10=OMEGA3*DELT/2.+2./DELT
28. = C11=2./DELT-OMEGA3*DELT/2.
29. = DELTA=C1*(C6*C10+C9*C2)+C5*(C2*C10+C9*C2)
30. = C INITIAL CONDITIONS
31. = Y11=0.
32. = Y21=0.
33. = X31=0.
34. = DY11=0.
35. = DY21=0.
36. = DX31=0.
37. = C BEGIN PROBLEM SOLUTION
38. = T=0.
39. = P1=FF(T)
40. = F1=GAMMA*P1+CONSTF
41. = 1 T=T+DELT
42. = P2=FF(T)
43. = F2=GAMMA*P2+CONSTF
44. = C SOLVE DE'S
45. = R1=C3*Y11+C2*Y21+C2*X31+2.*DY11+2.*DY21+2.*DX31+C4*(P1+P2)
46. = R2=C5*Y11+C7*Y21+C2*X31+2.*DY21+2.*DX31+C8*(F1+F2)
47. = R3=C9*Y21+C11*X31+2.*DX31
48. = X32=(C1*(C6*R3+C9*R2)+C5*(C2*R3+C9*R1))/DELTA
49. = Y22=(C1*(R2*C10-R3*C2)+C5*(R1*C10-R3*C3))/DELTA
50. = Y12=(R1*(C6*C10+C9*C2)-R2*(C2*C10+C9*C2)+R3*(C2*C2-C6*C2))/DELTA
51. = DY12=2.*(Y12-Y11)/DELT-DY11
52. = DY22=2.*(Y22-Y21)/DELT-DY21
53. = DX32=2.*(X32-X31)/DELT-DX31
54. = PRINT 104,Y12,Y22,X32,DY12,DY22,DX32,T
55. = 104 FORMAT(7E11.4)
56. = P1=P2

```

```
157. = F1=F2
158. = Y11=Y12
159. = Y21=Y22
160. = X31=X32
161. = DY11=DY12
162. = DY21=DY22
163. = DX31=DX32
164. = GO TO 1
165. = END
```

```
1. = FUNCTION FF(T)
   = IF(T-.9)1,1,2
   = 10FF=60.*20.*144.*100.*(1.-T/.9)*(.6*EXP(-(1.9*T/.9))+.4*EXP(-(11.5*
   = 4T/.9)))
   = GO TO 3
105. = 2 FF=0.
106. = 3 RETURN
107. = END
```

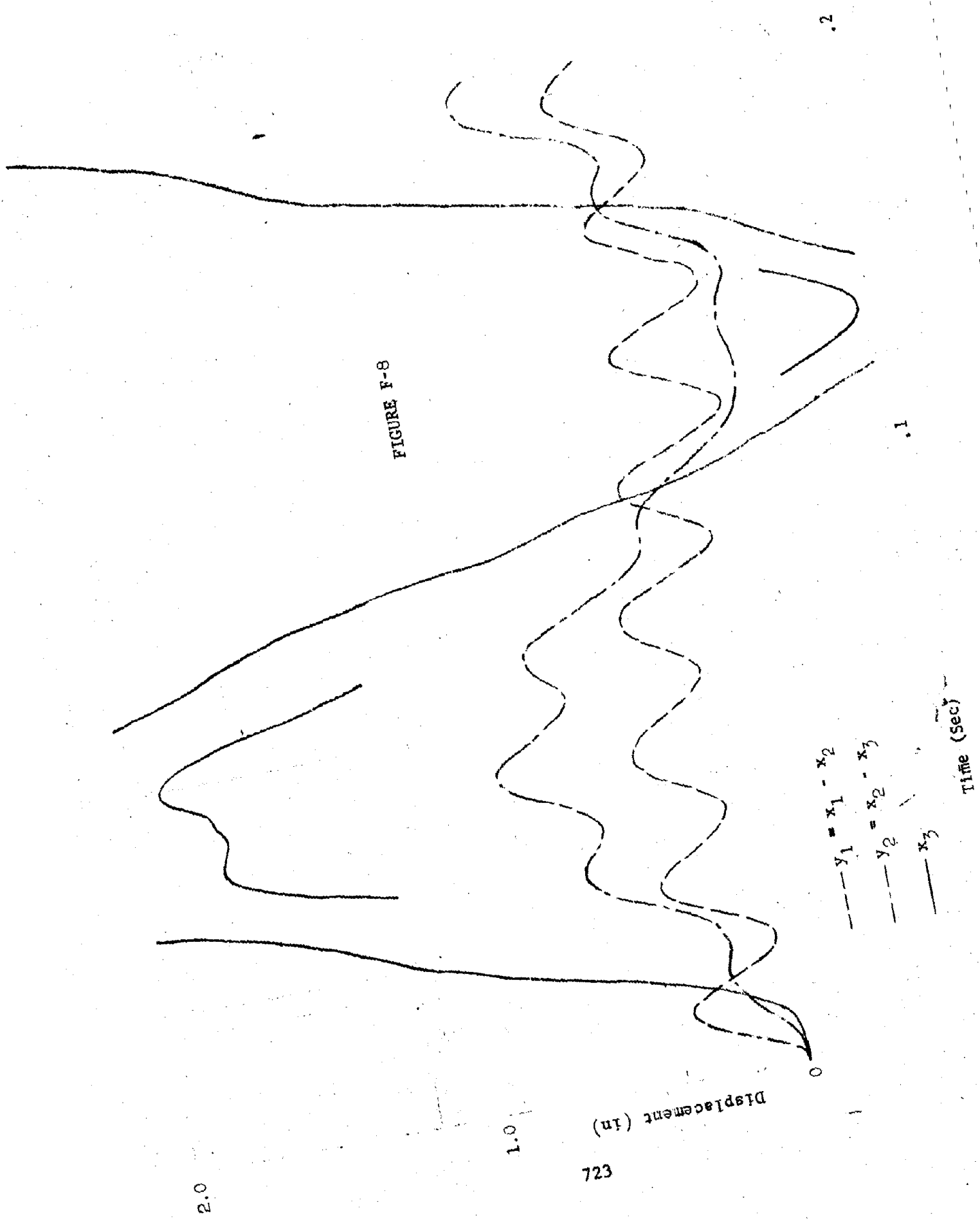


FIGURE F-8

723

FIGURE F-9

